

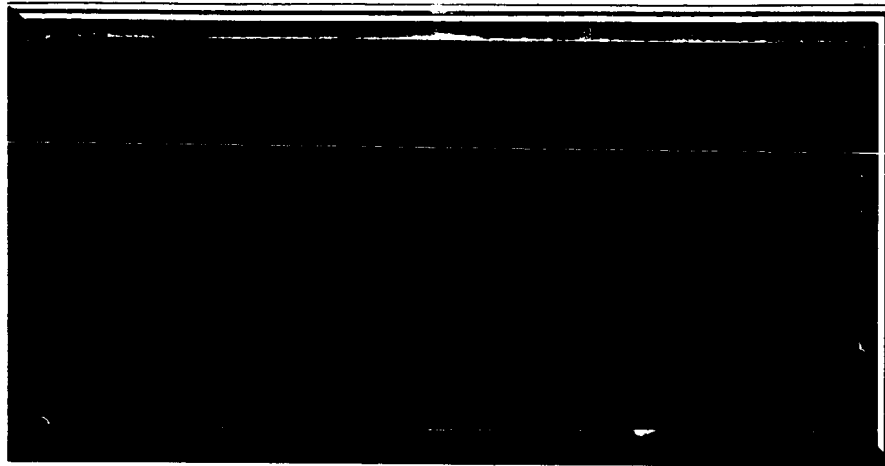
SPACECRAFT

NASA CR71487



DEPARTMENT

MISSILE AND SPACE DIVISION



FACILITY FORM 602

<u>N66-21079</u>	
(ACCESSION NUMBER)	(THRU)
<u>788</u>	<u>1</u>
(PAGES)	(CODE)
<u>CR 71487</u>	<u>31</u>
(NASA CR OR TMX OR AD NUMBER)	(CATEGORY)

GPO PRICE \$ _____

CFSTI PRICE(S) \$ _____

Hard copy (HC) 10.88

Microfiche (MF) 3.50

ff 653 July 65

JULY 30, 1965

NASA CR71487

DIN: 65SD4388

**VOYAGER SPACECRAFT SYSTEM
PRELIMINARY DESIGN
FLIGHT SPACECRAFT PREFERRED
DESIGN**

**G&C, Pwr, Eng'g Mech, Prop
VOLUME A (Book 3 of 4)**

PERFORMED UNDER
CONTRACT NO. 951112

NAS-7-100

for

**CALIFORNIA INSTITUTE OF TECHNOLOGY
JET PROPULSION LABORATORY
4800 OAK GROVE DRIVE
PASADENA, CALIFORNIA**

GENERAL  ELECTRIC

SPACECRAFT DEPARTMENT
A Department of the Missile and Space Division
Valley Forge Space Technology Center
P. O. Box 8555 • Philadelphia, Penna. 19101

TABLE OF CONTENTS

BOOK 3, VOLUME A

<u>Section</u>	<u>CII No.</u>
IV. SUBSYSTEM LEVEL FUNCTIONAL REQUIREMENTS - GUIDANCE AND CONTROL	
Guidance and Control Subsystem	VB234FD101
Spacecraft Attitude Control Subsystem	VB234FD102
Cold Gas Jet Subsystem	VB234FD104
Autopilot Subsystem	VB234FD105
Approach Guidance Subsystem	VB234FD106
Control and Sequencer ①	VB234FD107
Articulation Subsystem ②	VB234FD108
IV. SUBSYSTEM LEVEL FUNCTIONAL REQUIREMENTS - ENGINEERING MECHANICS	
Temperature Control Subsystem	VB235FD101
Spacecraft Structure	VB235FD102
Structural Design Criteria	VB235FD103
Pyrotechnics Subsystem	VB235FD104
Determination Weight, CG&Moments	VB235FD105
Electronic Packaging	VB235FD106
Electronic Harnessing	VB235FD107
Planet Scan Platform	VB235FD108
High Gain Antenna Deployment and Gimbal Mechanism	VB235FD109
Solar Array Structure	VB235FD110
IV. SUBSYSTEM LEVEL FUNCTIONAL REQUIREMENTS - POWER	
Spacecraft Power Subsystem	VB236FD101
IV. SUBSYSTEM LEVEL FUNCTIONAL REQUIREMENTS - PROPULSION	
Retropropulsion and Midcourse Propulsion System	VB238FD101

CII-VR234FD101

GUIDANCE AND CONTROL SUBSYSTEM

INDEX

- 1 **Scope**
- 2 **Applicable Documents**
- 3 **Description**
- 4 **Mission Sequence**

1.0 SCOPE

This document summarizes the function and elements of the Guidance and Control Subsystem. It defines the functions and the equipment make-up of each subsystem forming Guidance and Control. The operation of the subsystem is described in the context of the mission.

2.0 APPLICABLE DOCUMENTS

VB220SR101	Design Characteristics
VB220SR102	Design Restraints
VB220SR103	Maneuver Accuracy
VB220FD101	Standard Trajectories
VB220FD103	Spacecraft Component Design Parameters
VB220FD111	Maneuver Execution Accuracy
VB220FD112	Flight Sequence
VB234FD102	Spacecraft Attitude Control Subsystem
VB234FD104	Attitude Control Cold Gas Jet Subsystem
VB234FD105	Autopilot Subsystem
VB234FD106	Approach Guidance
VB234FD108	Articulation Subsystem

3.0 DESCRIPTION

The Guidance and Control Subsystem is comprised of five equipment subsystems:

1. Attitude Control
2. Cold Gas Jet
3. Autopilot
4. Articulation
5. Approach Guidance

The relation between these five is depicted in Figure 3-1. The electronic assembly of this subsystem is depicted in Figure 3-2.

These subsystems maintain the spatial attitude of the Voyager Spacecraft and articulated devices during the four major mission phases:

1. Cruise
2. Maneuver
3. Guidance correction
4. Orbital.

During the approach phase the subsystems also perform measurements of the angles between the Spacecraft line of sight to Mars and the Sun and Canopus. These are used in the orbit determination system to supplement the DSIF measurements.

3.1 ATTITUDE CONTROL

The attitude control subsystem acquires and stabilizes the Spacecraft to the external attitude references from any initial attitude and rates up to three degrees per second. It then maintains the Spacecraft attitude relative to these references to less than 3/4 degree during the heliocentric cruise and Mars orbital phases. It also maneuvers the spacecraft, by sequential rotations, to any arbitrary spatial attitude necessary to perform velocity change or capsule separation maneuvers.

The attitude control subsystem consists of: optical sensors (Sun sensors in pitch and yaw and star sensor in roll) to determine attitude deviations from the references; gyroscopes which provide rate signals during acquisition of references and position signals during maneuvers; and electronic circuitry which processes the sensor signals to operate the appropriate solenoid valves of the Cold Gas Jet Subsystem.

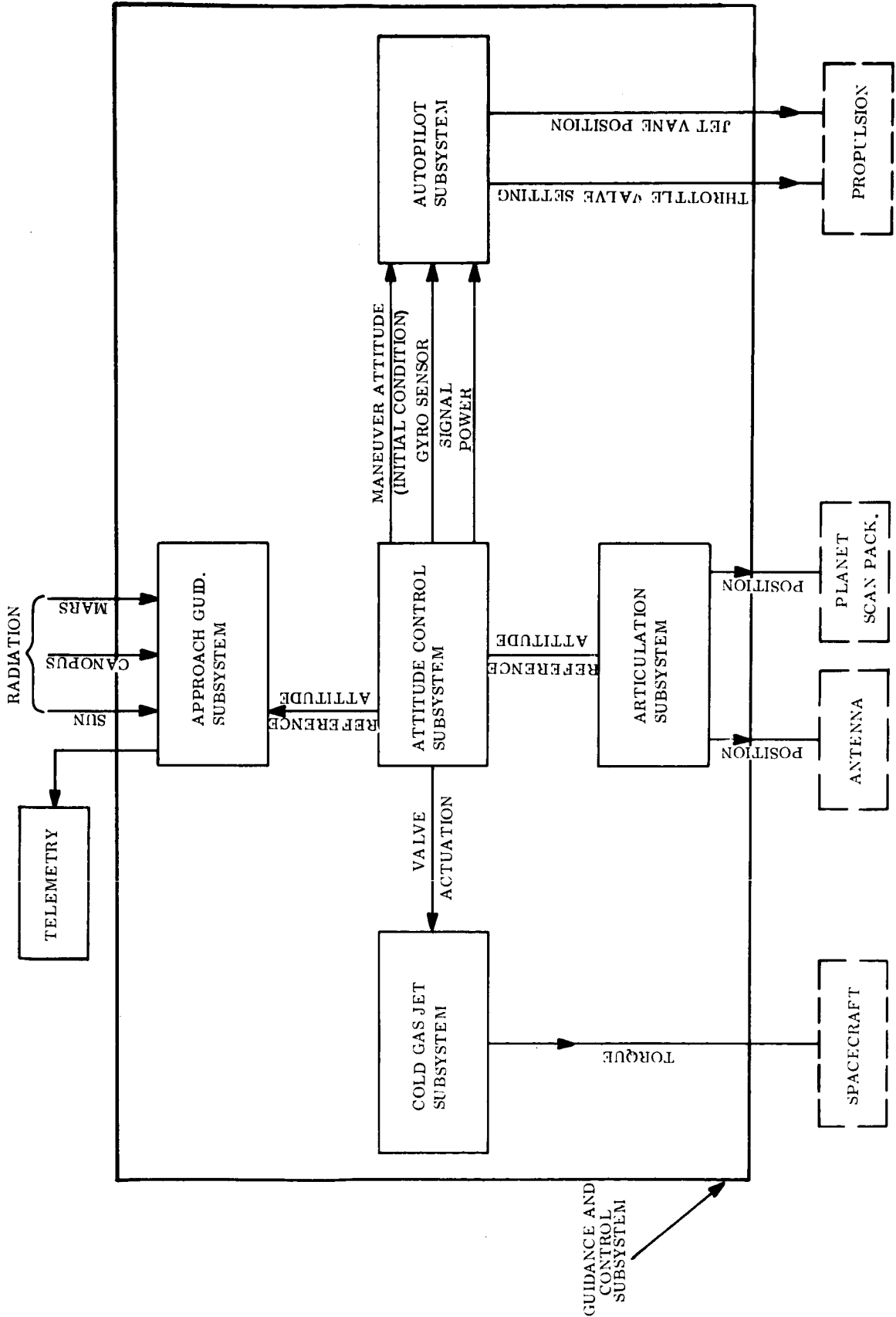


Figure 3-1. Guidance and Control Subsystem

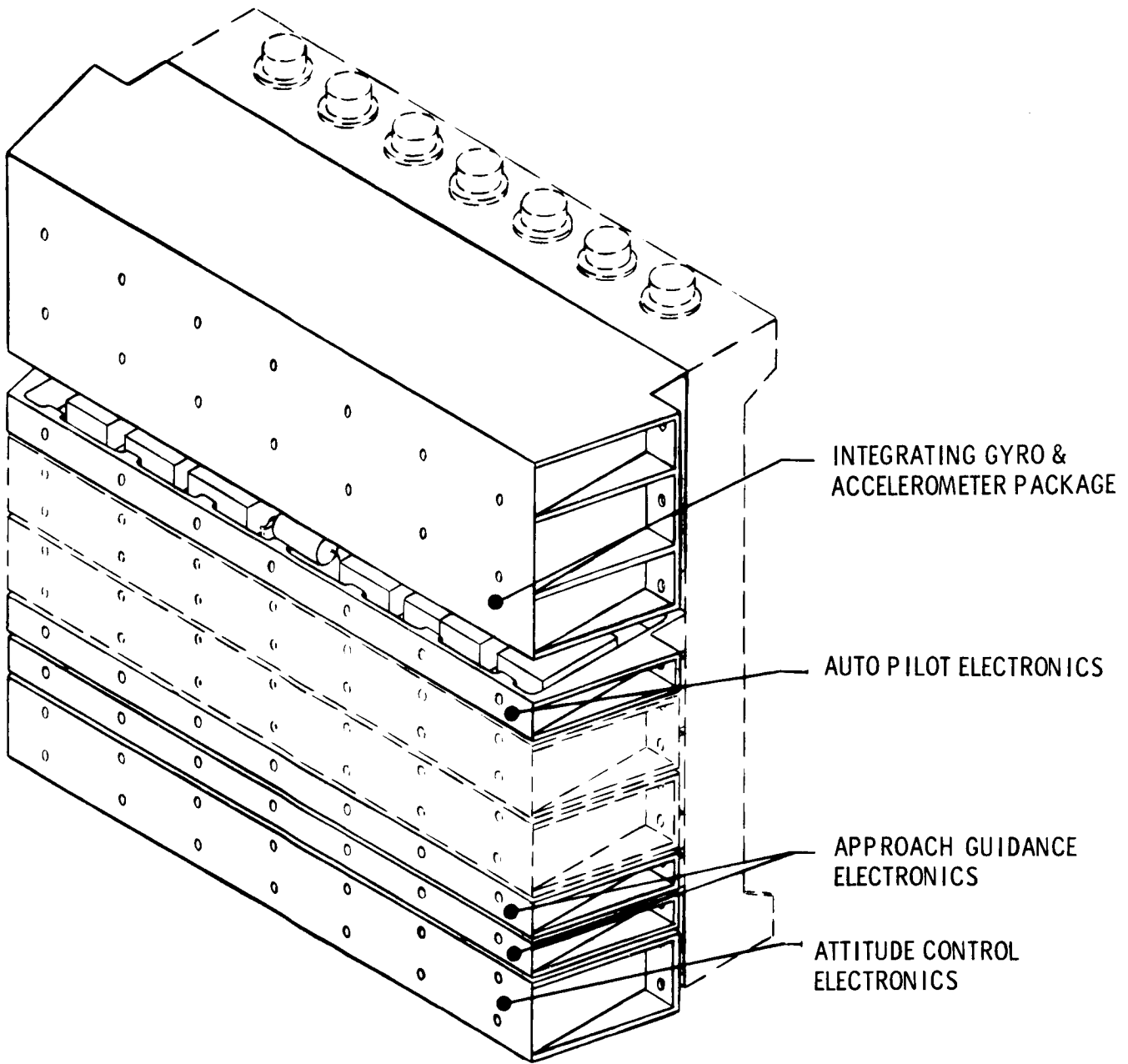


Figure 3-2 Electronic Assembly 12 Guidance & Control

The subsystem has three basic functions or modes of operation:

1. Acquisition mode
2. Cruise mode
3. Maneuver (or inertial) mode

In the acquisition mode the roll star sensor is initially locked out, wide field of view sun sensors are used in pitch and yaw, and rate signals are provided by the gyroscopes. The system acquires the sun reference in two axes in less than 20 minutes from the start of acquisition. After this the narrow field of view cruise sun sensors are switched in, the Canopus sensor enabled and the vehicle is made to roll about the sun line in search of Canopus. When the star comes in the field of view of the sensor, acquisition is completed. The Canopus search and acquisition can take up to 70 minutes.

In the cruise mode the cruise (narrow field of view) sun sensors are controlling pitch and yaw axes and the Canopus sensor the roll axis. The gyros are off and damping is obtained by passive means such as derived rate.

In the maneuver mode the optical sensors are replaced by the gyros operating in position mode. Gyros are torqued in sequence to produce a vehicle rate about the desired axis. The time the gyros are torqued is controlled to yield the desired rotation. This same basic mode is employed during an inertial hold except that the gyro torquers are not energized.

3.2 GAS JET SUBSYSTEM

The Cold Gas Jet subsystem applies torques to the Spacecraft as required by the attitude control system to perform its function of acquiring and holding its references and to maneuver the spacecraft to desired attitudes. This subsystem also imparts a small velocity to the spacecraft after capsule separation. This velocity increment is normal to the capsule separating direction and assures that the capsule will not impact the spacecraft after the application of the capsule deflection impulse.

The Gas Jet Subsystem consists of: tanks which contain the propellant (Freon); regulators, filters, fill valves, solenoid valves and nozzles. The electrical signal which actuates the solenoid valves is provided by the attitude control system.

3.3 AUTOPILOT

The Autopilot maintains the inertial attitude of the vehicle during propulsion thrusting and shuts off the rocket engines when the desired velocity has been achieved.

Functionally this subsystem consists of: gyroscopes, signal processing electronics, jet vane and throttle valve actuators, velocimeter and switching logic. The mutual operation of these components perform the autopilot function. The gyroscopes and the velocimeter

are functionally a part of the autopilot. Physically they are in the attitude control system and described as part of that subsystem. The jet vane and throttle valve actuators are physically a part of the rocket engines and as such provided by the propulsion system. The specification and design of these actuators are dictated by the autopilot subsystem.

The gyroscopes generate signals proportional to spacecraft angular position. These signals are processed by lead networks and amplifiers in the autopilot electronics. The amplified signals actuate throttle valve actuators to result in pitch and yaw control torques. In the roll loop the signals operate jet vane actuators.

3.4 ARTICULATION SUBSYSTEM

The articulation subsystem points the high gain antenna to Earth and the planet scan platform package to Mars.

This subsystem consists of stepper motors, a horizon sensor, and circuitry to actuate the stepper. The physical gimbals and bearings are part of the Engineering Mechanics subsystem VB235FD108 and VB235FD109.

The articulation subsystem employs the attitude stabilized characteristic of the spacecraft and the known ephemerides of the spacecraft, Earth and Mars to operate the gimbals open loop, that is by programmed or commanded steps. The outboard gimbal of the planetary scan platform is operated closed loop employing an IR horizon sensor.

3.5 APPROACH GUIDANCE

The Approach Guidance subsystem measures the angles between the spacecraft, the Sun, Canopus and Mars and telemeters this data to Earth for use in the orbit determination system. The equipment consists of optics, an image forming tube and appropriate circuitry.

The function of the Approach Guidance Subsystem is one of data taking and not of calculating, inasmuch as the data is used to supplement the radio tracking data in the orbit determination program on Earth.

4.0 MISSION SEQUENCE

The operation of the Guidance and Control subsystem can be summarized in the context of the mission sequence.

Shortly after separation from the Launch Vehicle, the Attitude Control Subsystem is energized. It goes into its acquisition mode and stabilizes the spacecraft to Sun and Canopus. It is then in the cruise mode until the first mid-course maneuver which occurs several days after separation from the Launch Vehicle. At this point the attitude control subsystem is put into the maneuver mode and the spacecraft is rotated to the desired attitude for execution of the mid-course maneuver. During rocket engine thrusting the maneuver attitude is maintained by the autopilot which also terminates thrust when the proper velocity has been achieved. After termination of thrusting, the attitude control subsystem goes into its acquisition mode and reacquires Sun and Canopus.

The system is then in the cruise mode. During this cruise the articulation subsystem periodically updates the two high-gain antenna gimbal angles to maintain pointing to the Earth. Cruise continues until the second mid-course maneuver which may occur several weeks or months after the first. The sequence of the first maneuver is then repeated. Cruise continues until about four days before encounter at which time the approach guidance equipment is turned on. Measurements begin about 500,000 km from the planet or two days before encounter and continue for one day. Shortly after the approach guidance measurements have been completed and the data processed, the attitude control system is placed in the maneuver mode and rotated to place it in the appropriate attitude for capsule release. The capsule is then released and a small velocity change applied to the spacecraft normal to the capsule separation direction. After a ten-minute delay to permit spacecraft - capsule separation, the spacecraft, which is still in the maneuver mode, is rotated to put it in the appropriate attitude for the final mid-course correction. At termination of that maneuver Sun and Canopus are reacquired. Cruise proceeds for about a day at which time the maneuver mode is again assumed and the spacecraft is rotated to the appropriate attitude for the orbit insertion maneuver. During orbit insertion as the rocket engines are thrusting the autopilot maintains the attitude of the vehicle and terminates thrust when the desired velocity change has been achieved.

After orbit insertion has been accomplished the attitude control system again reacquires Sun and Canopus and the system is in the steady state cruise or orbit mode.

The planet scan platform is deployed and the articulation subsystem rotates the two inboard gimbals to erect a perpendicular to the orbit plane. A horizon sensor, which controls the outboard gimbal, acquires the planet and then rotates the outboard gimbal to point the science instruments to the local vertical. The two inboard gimbal angles are periodically updated to keep the final axis normal to the orbit plane as it precesses and as Mars progresses around the sun.

Finally during the latter portions of the mission the Sun may be occulted by Mars. In as much as this event is anticipated and accurately predictable in time, the attitude control system will be commanded to go into the inertial mode in the pitch and yaw axes. The gyros then hold position during the occultation.

CII-VB234FD102

ATTITUDE CONTROL SUBSYSTEM

FUNCTIONAL DESCRIPTION

Index

- 1.0 **Scope**
- 2.0 **Documentation**
- 3.0 **ACS Operation**
- 4.0 **ACS Interface Definitions**
- 5.0 **ACS Performance Parameters**
- 6.0 **ACS Physical Characteristics and Operational Constraints**
- 7.0 **Safety Considerations**

1.0 SCOPE

The Voyager 1971 Attitude Control Subsystem controls the angular orientation of the spacecraft at all times, except during "launch-to-initial-turn-on" and rocket motor firing periods.

This functional description presents a delineation of the operation of the preferred design of the Attitude Control Subsystem (ACS). In addition, compilations are presented of all ACS interfaces and pertinent ACS performance parameters. Also presented are defined ACS physical characteristics and the safety factors given consideration in formulating the ACS operational procedures.

2.0 DOCUMENTATION

The following are supplementary and supporting documents to this functional description.

VB220FD101 Standard Trajectories
VB220FD110 Telemetry Channel Assignments
VB220FD111 Maneuver Execution Accuracy
VB220FD112 Flight Sequence
VB234FD101 Guidance and Control Subsystem
VB264FD104 Attitude Control and Approach Guidance OSE

3.0 ACS OPERATION

The mission requirements of the ACS are:

- a. To acquire external attitude
- b. To stabilize the spacecraft to these references for the purposes of providing
 - Efficient solar power conversion
 - Antenna earth-pointing reference
 - Planet Scan Platform Mars-pointing reference
- c. To provide self-contained inertial references, for the purposes of maneuvering the spacecraft to any spatial orientation, and maintaining that orientation for guidance and capsule separation purposes

The external references chosen for Voyager ACS are the Sun and the star Canopus.

The following sections of this paragraph describe the mechanization of the ACS to achieve these objectives, the pertinent subsystem performance characteristics, the ACS operational modes and sequences, and those modes that enhance the ACS functional reliability.

3.1 MECHANIZATION

The three ACS objectives are illustrated in Figure 3-1. Solar panel orientation is accomplished by pointing the panel surfaces normal to the Sun's radiation. (The spacecraft negative roll axis is pointed at the center of the Sun.) Holding a fixed orientation to the Sun and the star Canopus is accomplished by pointing the spacecraft roll-yaw plane so that Canopus lies in it. The capability of maneuvering the spacecraft to any orientation is provided by the use of three strapped-down gyros (aligned respectively to the spacecraft pitch, yaw and roll axes) which can be switched by command to operate in a position mode and torqued by a precision gyro torquer for a precise time increment. The following is a description of the mechanization of the ACS by component assemblies to perform the required functions.

3.1.1 SOLAR ORIENTATION LOOPS

Solar orientation is accomplished by controlling spacecraft motions about its pitch and yaw axes. Both control loops are identical except for the amount of thrust provided by the cold gas Jet system which is sized in relation to the spacecraft inertias to give equal control angular accelerations about both axes.

The basic components of each of the solar orientation loops are a sun sensor with a spherical field of view to provide an error signal and a Cold Gas Jet system to provide control torque. Auxiliary components to process the error signal and to provide loop compensation for control of the torque, are the threshold detector, the rate gyroscope and the gas jet driver. Interconnection of these components is depicted in Figure 3-2 for the pitch and yaw loops. Correlating this diagram with Figure 3-1, it can be seen how the pitch and yaw loops point the spacecraft at the Sun.

3.1.2 ROLL-YAW PLANE ORIENTATION LOOPS

The roll-yaw plane orientation is accomplished by controlling spacecraft motion about the roll axis while the negative roll axis is pointed at the Sun as previously described.

The basic components of the roll axis control loop are a star sensor with a 4 degree by 32 degree total field of view (selectable in four steps of 4 by 10 degrees) to provide an error signal, a rate gyroscope for acquisition rate control, and a Cold Gas Jet system to provide control torque. A threshold detector and a gas jet driver process the error signal to control the torque. Their interconnection is depicted in Figure 3-3. Correlating this diagram with Figure 3-1, it can be seen how the roll loop, in conjunction with the solar orientation loops, orients the spacecraft to Canopus. The spacecraft negative yaw axis will not necessarily point directly at the star, since the spacecraft-Canopus line is not perpendicular to the spacecraft-Sun line at all points along the heliocentric orbit. The negative yaw axis will point perpendicular to the spacecraft-Sun line, such that Canopus will lie in the spacecraft roll-yaw plane.

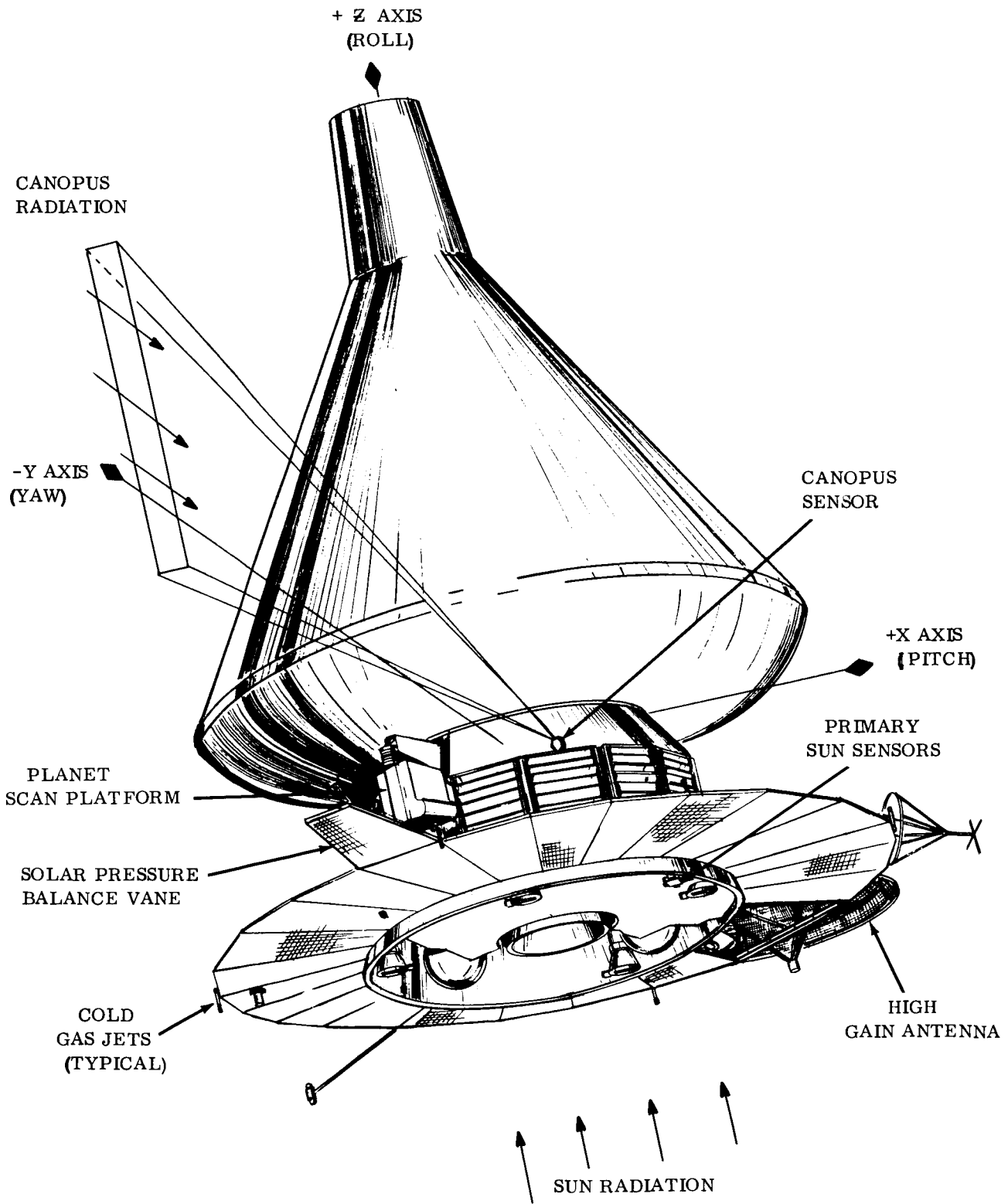


Figure 3-1. Voyager 1971 External Configuration

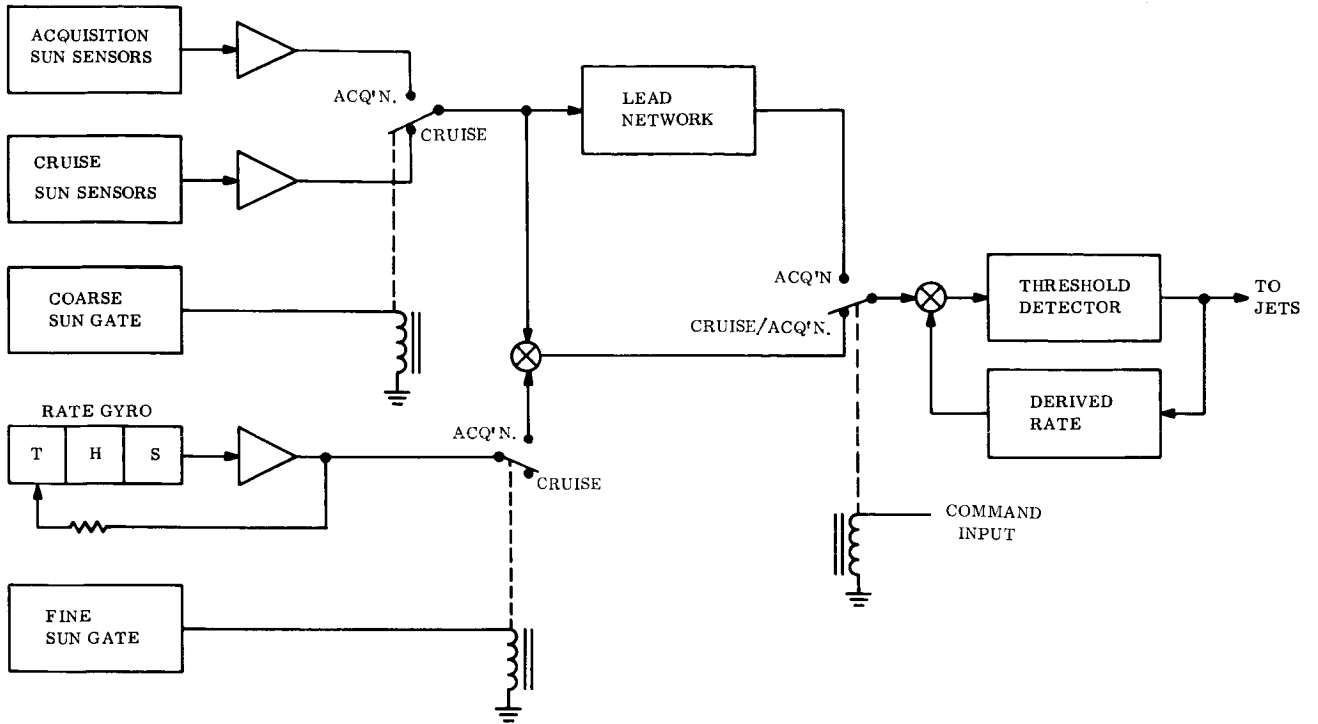


Figure 3-2. Pitch or Yaw Acquisition and Cruise Modes - Simplified Block Diagram

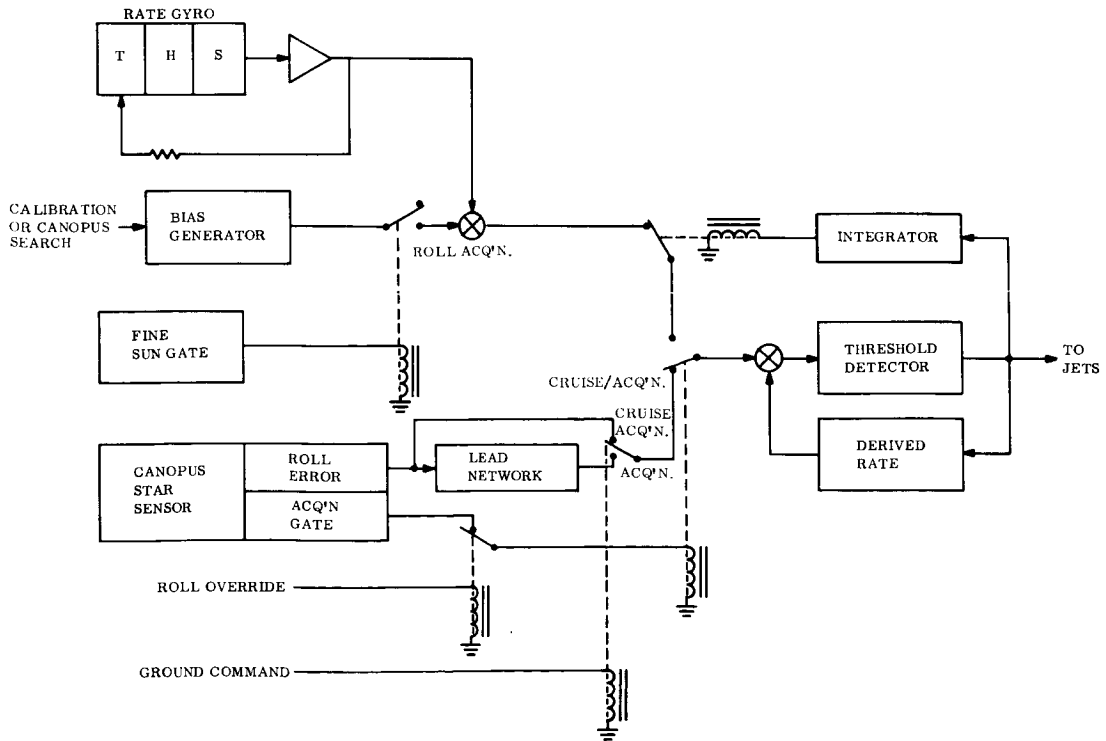


Figure 3-3. Roll Acquisition and Cruise Modes - Simplified Block Diagram

3.1.3 COMMANDED ORIENTATION LOOPS

Maneuvering the spacecraft to any orientation desired is accomplished by switching the control loops to the gyros, which are in position mode, and then commanding a specific angle of turn for each axis sequentially. All the axes operate in the same manner.

The basic components of each of the commanded orientation loops are a gyro to provide an error signal referenced to the spacecraft's position at the time of switching and a Cold Gas Jet system to provide control torque. Auxiliary components to torque the gyro and process the error signal are: the torquer current generator; the gyro output amplifier, demodulator and torquer amplifier; the gyro buffer amplifier; the threshold detector; and the gas jet driver. The interconnection of these components is depicted in Figure 3-4. By commanding rotations of the spacecraft through precalculated angles about any of the spacecraft axes, any desired spacecraft orientation can be obtained in an optimum sequence.

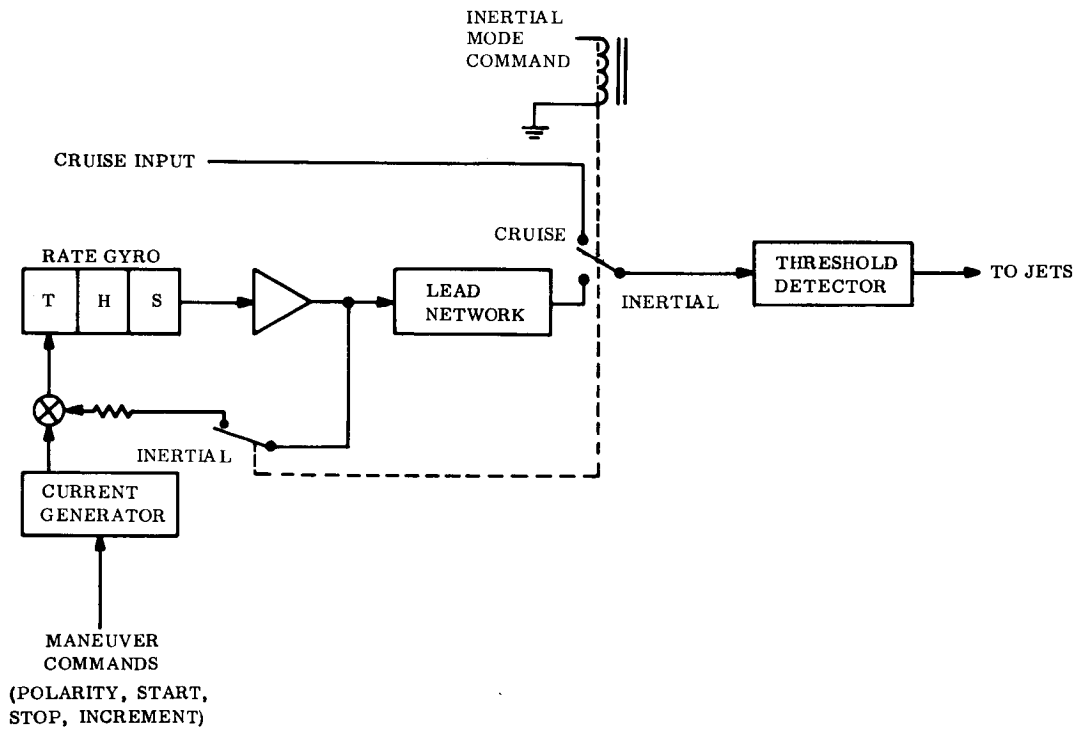


Figure 3-4. Inertial/Maneuver Modes, Typical Pitch, Yaw, Roll - Simplified Block Diagram

3.1.4 COMPLETE MECHANIZATION OF THE ACS

Figure 3-5 is a diagram of the complete ACS mechanization. The previous block diagrams are simplified descriptions of the individual control loops abstracted from Figure 3-5. All component assemblies depicted in this diagram are considered a part of the ACS except for the Gas Jet Subsystem. (See VB234FD104.) Also, the accelerometer and its associated electronics within the Gyro and Accelerometer Package are functionally a part of the Auto-pilot Subsystem. The accelerometer was packaged with the gyros because these components have similar mounting and alignment requirements and can possibly be obtained from one vendor source. All other significant components within the ACS which have not been discussed thus far, are covered in paragraphs 3.3, Modes and Sequences, and 3.4, Functional Reliability.

3.2 PERFORMANCE CHARACTERISTICS

The following pertinent performance characteristics indicate subsystem performance capability, rather than all subsystem parameters.

- a. Pointing Accuracy - The control dead-band is plus or minus eight milliradians and the null-offset is no greater than four milliradians about each of the control axes.
- b. Maneuver Rate - The controlled angular rate for commanded turns is 3.14 milliradians per second about each axis.
- c. Search Rates - The control angular rates about the roll axis for Canopus search and magnetometer calibration are 1.7 and 3.9 milliradians per second respectively, with a rate dead-band of 0.4 milliradians per second for both.
- d. Acquisition Time - It takes no longer than 20 minutes to stabilize to the Sun and no longer than 70 minutes to stabilize to Canopus after the Sun has been acquired.
- e. Transfer Functions - Significant component transfer functions are depicted in Figure 3-5 for individual blocks. See paragraph 3.5 for detailed functional descriptions of all the ACS component assemblies.

3.3 MODES AND SEQUENCES

The following is a description of the ACS in each of its modes of operation. The automatic sequencing of the ACS is initiated by the logic control unit. Based on digital information received from the three control loops, the sun gate sensors, the Command Decoder, and the Computer and Sequencer, the logic control unit makes decisions as to the ACS situations and sends digital signals to the loops to change component interconnections. In this manner the ACS is sequenced through the following modes of operation to fulfill its mission of controlling the angular orientation of the spacecraft:

- Cruise Mode

- Pitch and Yaw Acquisition Mode
- Roll Calibration Mode
- Roll Acquisition Mode
- Reacquisitions
- Maneuver Mode
- Occultations

3.3.1 CRUISE MODE

This mode applies to the operating condition of the ACS when the components of the individual loops are interconnected as indicated in Figures 3-2 and 3-3. (Normally, this condition exists when the celestial references have been acquired.) When the cruise mode interconnections are changed, the ACS will be performing in either the acquisition or maneuver mode. The roll calibration and roll override situations are just particular phases of the acquisition mode. The cruise mode also pertains to normal operating conditions of the spacecraft in orbit about Mars as well as during the interplanetary cruise phase.

3.3.2 ACQUISITION MODE

In this mode the ACS rotates the spacecraft from any arbitrary attitude, to accomplish the acquisition of the basic celestial references by the three controlled axes.

For normal acquisition, the components are interconnected for cruise mode operation and the gyros are at operating temperature. Upon receipt of power to turn on the ACS at separation of the spacecraft from the booster, the following connections are made under the direction of the logic control unit: the acquisition sun sensors are switched in and the cruise sun sensors out of the pitch and yaw loops; the gyros are switched to their rate mode and connected to their respective control loops; and the Canopus sensor is deenergized. The pitch and yaw loops drive the spacecraft negative roll axis toward pointing at the Sun. When the negative roll axis is within 10 degrees of the sun line, the coarse sun gate signals the logic control unit and the acquisition sun sensors are switched out while the cruise sun sensors are switched into the pitch and yaw loops. When the negative roll axis is within two degrees of the sun line, the fine sun gate signals the logic control unit and the Canopus sensor is energized simultaneously with applying a search rate bias of 1.7 milliradians per second from the roll bias generator to the roll loop. During this previous activity the roll loop has no controlling position signal, and the gyro serves to limit roll rotation rates to plus or minus 0.2 milliradians per second. The pitch and yaw gyros also serve to limit rates about their respective axes in acquiring the Sun. Under the influence of the roll bias signal the spacecraft rotates at 1.7 milliradians per second about its roll axis. When the star Canopus or any other star of sufficient brilliance comes within the star sensor's field of view, the star sensor signals the logic control unit and the gyros are switched out of the loops. The ACS is now operating in the cruise mode.

Confirmation that the star acquired by the Canopus sensor is indeed Canopus is based on proper performance of the Communication loop pointing in the high gain antenna for peak performance. (While it is recognized that the high gain antenna gimbal arrangement defined in the recommended Articulation Subsystem does not allow the high gain antenna to point toward the earth prior to the first mid-course correction, a change in gimbal order as recommended in document VB234AA108, Articulation Subsystem Tradeoffs, Volume B, will provide for proper confirmation early in the mission.)

If, after the cruise mode has been established, it is determined that the star sensor has erroneously identified and locked onto a celestial object other than Canopus, a roll override command may be sent. Upon receipt of the command, the logic control unit will turn the gyros back on in the rate mode and connect them to their respective loops. Roll search rate bias is then applied and the remainder of the normal acquisition sequence takes place, terminating in the cruise mode.

After stabilizing on the sun in the initial acquisition sequence, a stored command in the Controller and Sequencer subsystem will inject a roll calibration procedure unless it is inhibited from the ground. This procedure is used to calibrate instruments in the Science Package and is the same as the Canopus search except that the rate is 3.9 milliradians per second and the star sensor is left deenergized. Upon completion of this roll calibration procedure, the Controller and Sequencer signals the logic control unit and acquisition is resumed at the point of energizing the star sensor and applying the roll search bias.

3.3.3 REACQUISITION SEQUENCES

Part or all of the automatic acquisition sequence will occur in the following situations:

- a. With the spacecraft stabilized to the Sun and Canopus, any non-catastrophic disturbance that results in the loss of either of these references will cause the logic control unit to automatically turn on the gyro heaters. When the gyros are up to temperature they are turned on in their rate mode and the logic control unit re-directs the necessary portions of the acquisition sequence to return the ACS to the cruise mode.
- b. With the spacecraft operating in the maneuver mode, the signal to switch to the cruise mode will cause the logic control unit to immediately redirect acquisition as the gyros will already be at their operating temperatures. This same condition applies to reacquisitions after occultations of the Sun or Canopus in orbit about Mars.

(NOTE: It is not recommended that gyros be energized prior to being brought up to normal operating temperature. However, if the Spacecraft power status warrants emergency procedures, the gyros will provide degraded rate information for use in reacquisition. The possibility exists, under these conditions, of permanently degrading gyro performance.)

3.3.4 OCCULTATION DURING ORBIT MODE

Since unanticipated occultations of the sun or Canopus will not occur in Mars orbit, the following command sequences together with automatic reacquisition sequences will provide control during occultation periods.

Sixty minutes before the anticipated onset of an occultation, a command is given the ACS to turn on gyro heaters. Thirty minutes later the required gyros are turned on (roll gyro for Canopus occultation; pitch and yaw gyros for Sun occultation). Virtually all probable orbits, however, do not encounter a Canopus occultation. Just prior to occultation, the affected axes are switched to inertial mode, and maintained so until completion of the event, when the ACS is commanded to re-acquire references. Automatic reacquisition and turn-off of gyros results. (The command system is set up so that either all gyros may be energized or deenergized by a single command; or just pitch and yaw gyros, by a second command. A similar situation exists in switching the ACS to cruise versus inertial modes. Thus, in order to achieve a situation wherein only the roll gyro is energized and only the roll loop is in inertial mode, a sequence of all gyros on - all axes to inertial mode - pitch and yaw axis to cruise mode - pitch and yaw gyros off - is required. This is presumably the optimum switching sequence, since the use of only the roll gyro is an unlikely situation.)

3.3.5 MARS LIMB AND NATURAL SATELLITE INTERFERENCES

The Canopus sensor may be caused to lose track of its target star if either excessive light from the Mars limb enters the sensor shield, or if one of the natural Mars Satellites passes through the sensor's field of view. It is shown in VB220FD101 that the minimum Canopus - Orbiter-near-limb angle is greater than 35 degrees for the 1971 Satellite design orbit, which indicates that interference from this source should not be a problem. The orbits and phases of the natural Satellites are known, and therefore possible passes through the sensor's field of view can be predicted. Since such passes would cause loss of tracking of Canopus, the ACS will be commanded to either a roll drift mode or a roll inertial hold mode during those periods when such interference is anticipated.

3.3.6 MANEUVER MODE AND SEQUENCE

In this mode the Controller and Sequencer (C&S) takes direct control of the attitude control logic functions in maneuvering the spacecraft to a precalculated attitude in space for the purposes of trajectory corrections, capsule separation or orbit insertion.

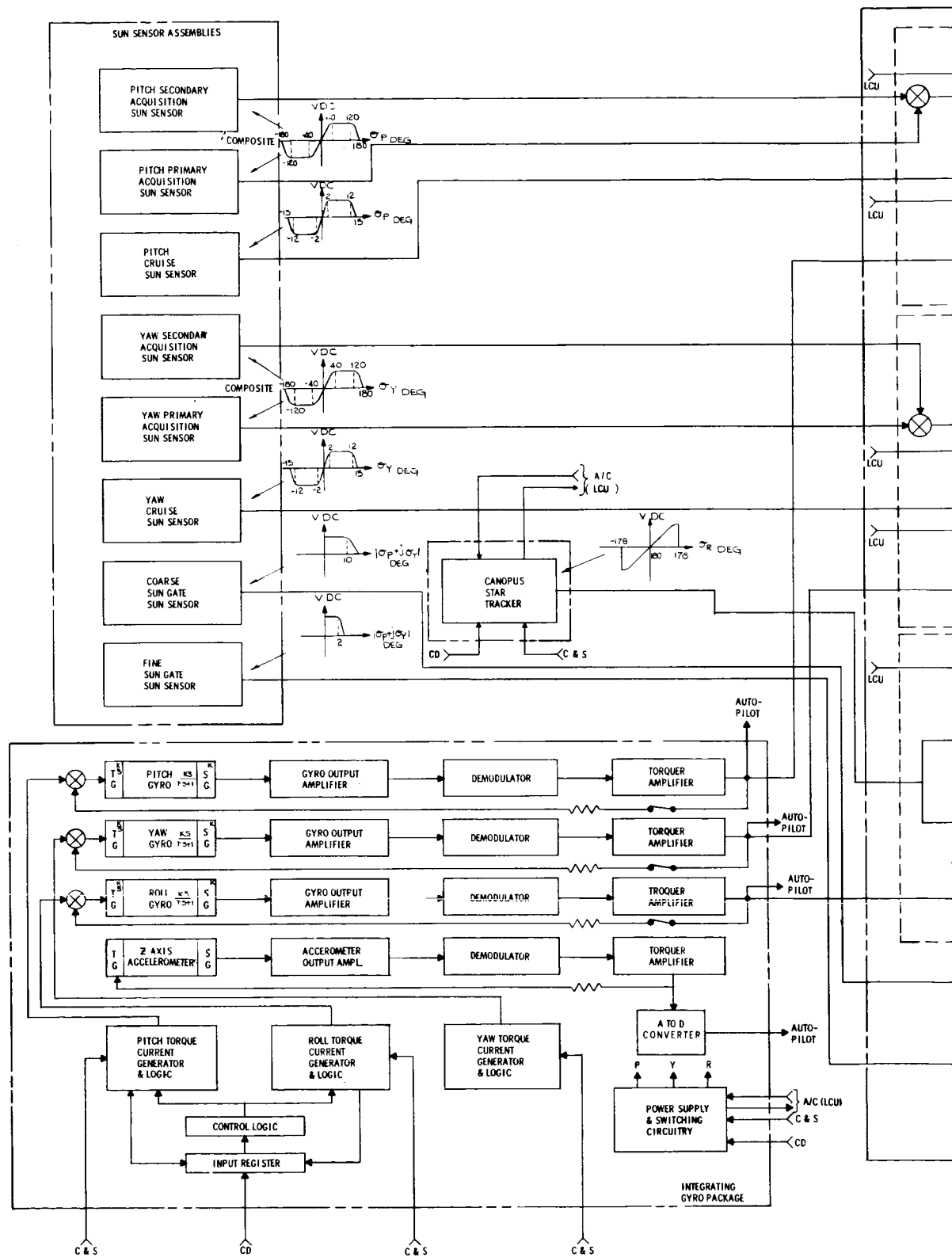
Initially the components are interconnected for cruise mode operation. Before the start of maneuvers the following preparations are made: sixty minutes before, the gyro heaters are turned on; thirty minutes before, all three gyros are turned on; and ten to six minutes before, the high gain communication antenna is reoriented to its expected final position. Just prior to initiating the first turn, the three control loops are switched to the inertial mode (gyro in position mode as input to the loop). The C&S signals the torquer current generators in the Integrating Gyro Package to torque their respective gyros for a predetermined time increment. This is done for one axis at a time in any combination of axes for one to three turns. At the completion of the final turn, forty minutes are allowed for Earth communication to verify the maneuver. Then the intended event is performed while the spacecraft

remains in this inertial mode. At the completion of the event the C&S relinquishes control of the attitude control logic functions to the logic control unit by the command to switch to the normal (cruise) mode of spacecraft control. At this point reacquisition of the celestial references is obtained as described previously under "Reacquisition Sequences." When the spacecraft attitude has been stabilized in the cruise mode, the high gain communication antenna reorientation is initiated.

3.4 FUNCTIONAL RELIABILITY

The following is a description of those items which contribute to the reliable performance of the ACS functions:

- a. Attitude Control Gas Jet Subsystem - (See Figure 3-5.) Coupled pairs of gas jets are used on each axis with two valves controlling each jet. These valves are connected in parallel electrically and in series pneumatically. The jets of each couple are supplied from separate tanks and regulators. Two single, particular valves must fail in the primary failure mode (leakage) before excessive loss of gas occurs. In this case, control angular acceleration is cut to half its existing value, which is toward the nominal value in the orbit phase of the mission. (See paragraph 3.5.4 for a description of redundant valve drivers.)
- b. Lead Network Back-up - Each control loop contains a lead network which may be used in the position signal path with some success during acquisition in case of a gyro failure. While it is recognized that three-axis acquisition with lead networks applied to position signals from sensors having limited linear range is unlikely to be successful, settling with a single gyro failure holds some promise of success. In addition, the lead networks may be used as back-up for derived rate networks. Trade offs will be required during the next phase to determine whether compatibility exists, and the emphasis required.
- c. Command Turn Back-up - A gyro turn control unit is included in the Integrating Gyro Package which can store magnitude and polarity for a maneuver consisting of a roll-pitch-roll sequence, based on inputs from the Command Decoder in case of a C&S failure. Decrementing of the storage register, is obtained from digital reset integrators which monitor the integrated current passing through the gyro torquer windings.
- d. Roll Search Inhibit Logic - In the event of a failed roll gyro (provided the output is near zero), the roll search bias will be removed after a slightly greater than normal jet firing time. This prevents spin-up and allows other back-up measures to be invoked by ground command.
- e. Roll Back-up Mode - In case of a Canopus sensor failure, the roll gyro can be invoked to provide attitude control of the roll axis. Incremental adjustments (positive or negative) of the roll axis may be obtained by ground command.
- f. AC Electronics Reliability - See paragraph 3.5.4.2 for discussion.



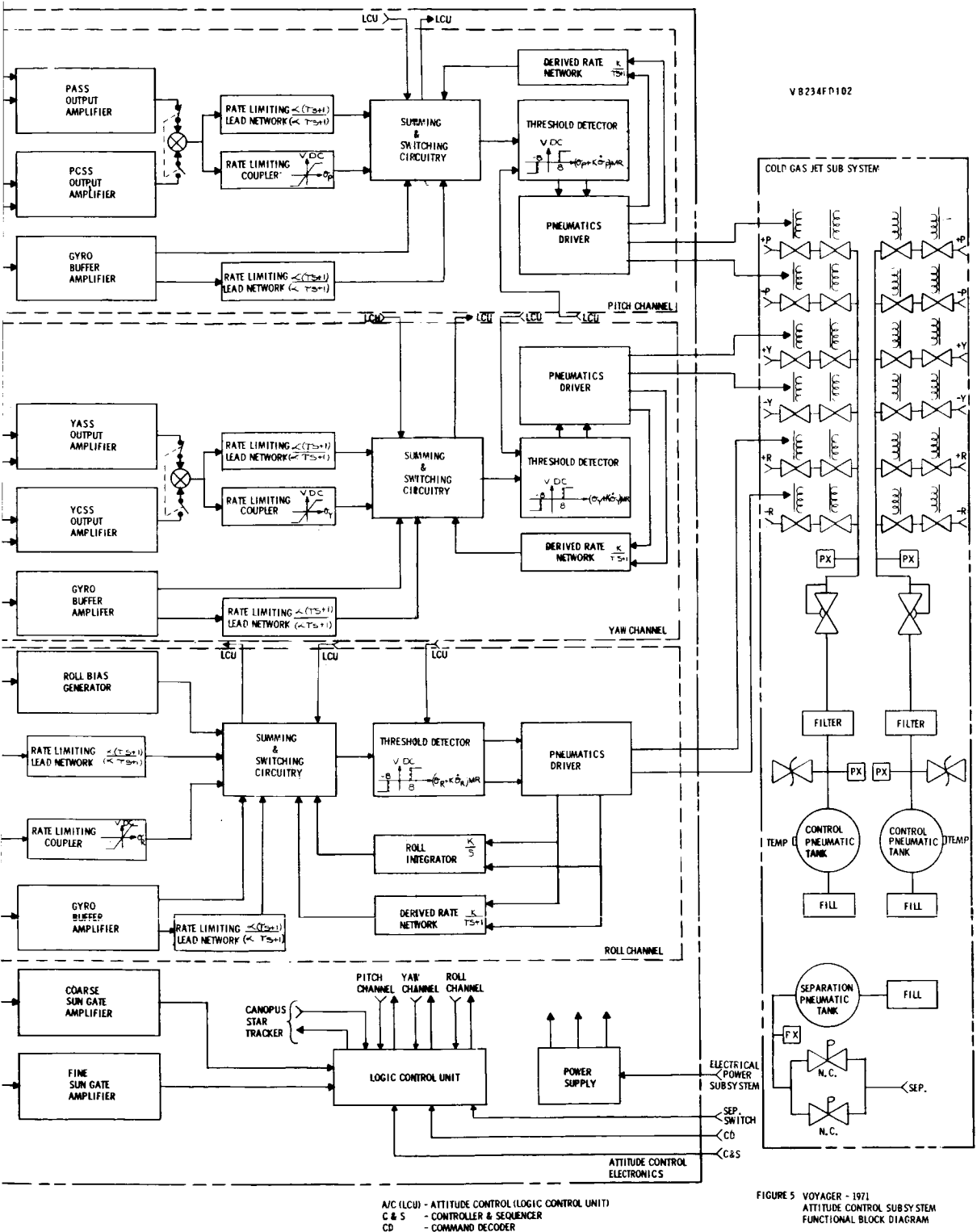


Figure 3-5. Voyager 1971 Attitude Control Subsystem Functional Block Diagram

3.5 COMPONENT DESCRIPTIONS

Although Phase IA study is a system design study, the following paragraphs are included to indicate some approaches to component design which will be considered, and to provide preliminary information on selection of vendor supplied components. It is naturally not intended to show results of formal design effort, or firm decisions on purchased parts and components.

Figure 3-6 is an isometric view of the Guidance and Control Electronics Assembly, Bay XII, showing the ACS Gyro and Accelerometer Package and the Attitude Control Electronics Package.

3.5.1 VOYAGER SUN SENSORS

The sun sensor consists of a series of photoelectric angle detectors (hereafter called eyes) placed about the vehicle to provide a 4π steradian field of view. It has two output control axes. This type of sensor is space proven on vehicles such as OSO, Aerobee, and is being used on future missions such as OAO & LOS. The sensing element in these detectors is a silicon solar cell. The eyes themselves are made by the Ball Brothers Research Corp. in Boulder, Colorado. Materials used in the manufacture of the eyes are selected for long-term operation in a space environment. These sensors have been fully qualified to withstand the temperature, vibration and shock normally expected in satellite applications. The lens which is placed in front of the silicon cell is made of Borosilicate Crown with Serium Oxide added to protect against radiation browning.

For the Voyager application 8 acquisition eyes, 4 cruise eyes and 2 gating eyes (a total of 14 detectors) constitute a complete 2-axis sun sensor. The acquisition eyes provide a rough indication of the location of the Sun within the field of view. These sensors provide a signal that determines the direction of the angle through which the spacecraft should be rotated to bring the Sun within the field of view of the cruise eyes. There is an unstable null located 180 degrees from the true system sensor null. If the Sun is on either side of this null, the vehicle is commanded to rotate away from this point. The unstable null is only a small region and any spacecraft movement will cause the sun direction to shift from this point.

The cruise sun sensor is composed of four solar cells each of which consists of a lens, a cutoff plate and a silicon cell. The lens focuses the light beam and provides the means of interrupting the beam with the cutoff plate as the angle of the light beam is varied. The field of view of the combined cruise sun sensor is 15 degrees half angle, and is conical. The acquisition eyes will each have an angular range of ± 90 degrees (hemispherical). Figures 3-7 and 3-8 illustrate the positions of the sensor eyes.

The acquisition eyes at the +Z side of the paddles (secondary sensors) are placed on four separate mounts, while the primary sensor (eyes located on the negative Z side of the paddles) may all be placed on the same mounting plate or pad.

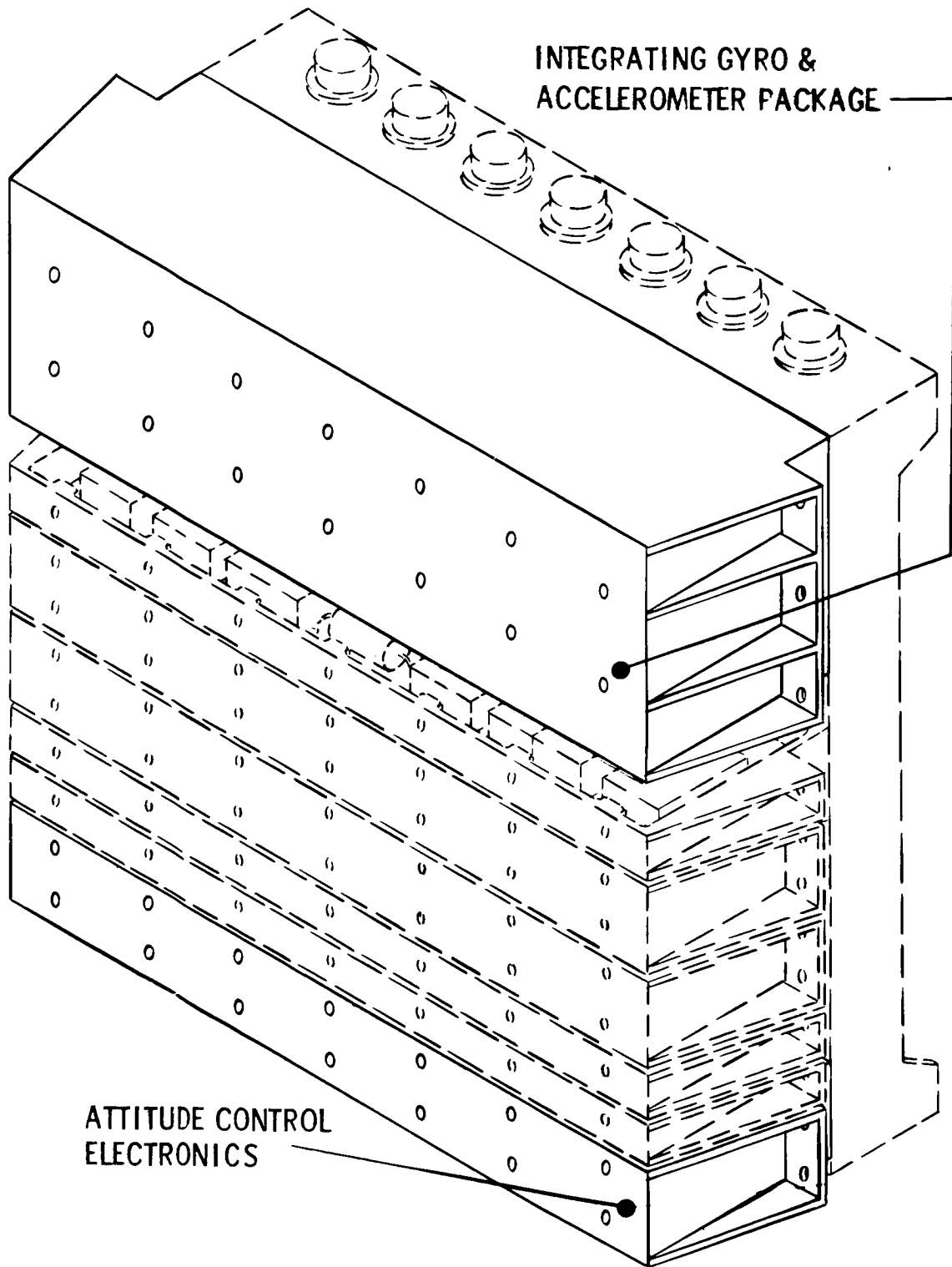


Figure 3-6. Isometric View - Guidance and Control Electronics Assembly, Bay X111

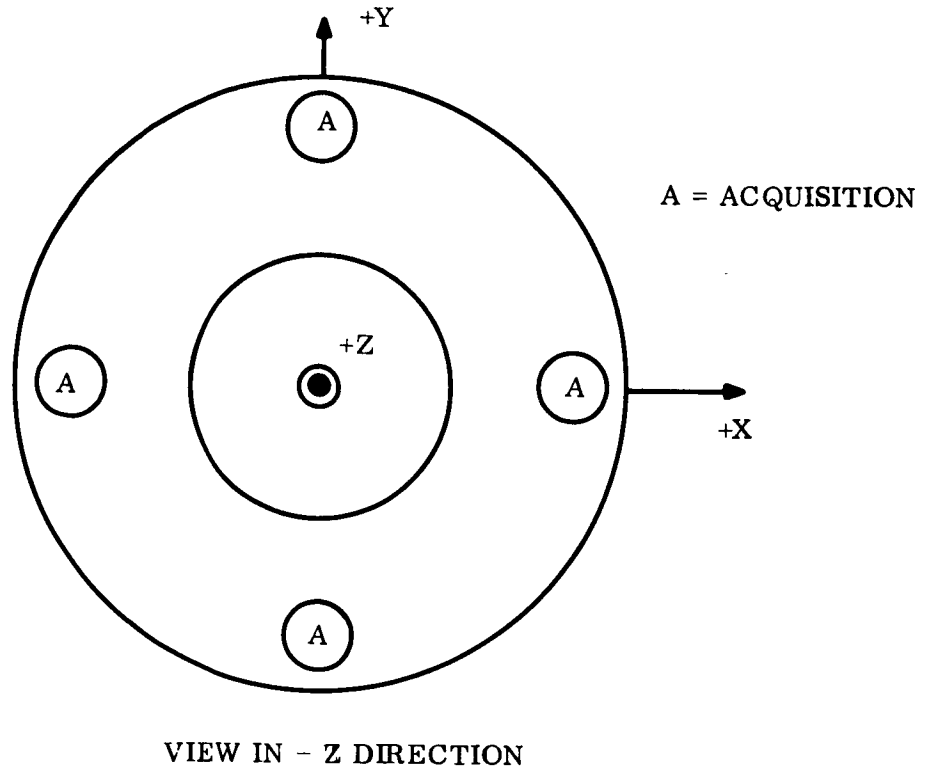


Figure 3-7. Secondary Acquisition Sun Sensors

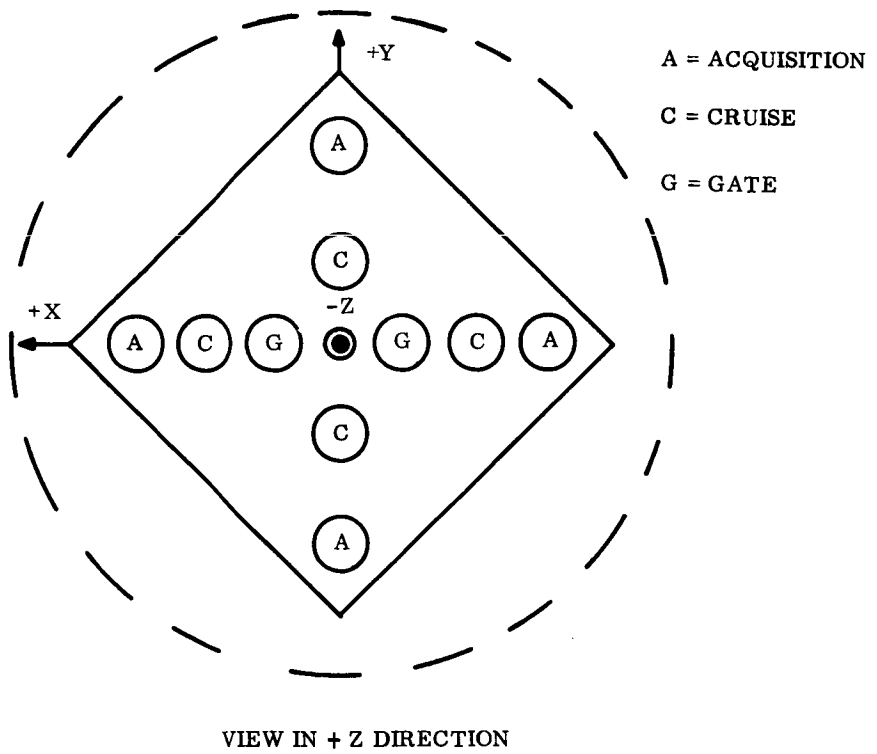


Figure 3-8. Primary Sun Sensors

In Figure 3-8, the two eyes marked "G" are gating eyes. One gate provides indication that a null has been achieved, for sequencing purposes, while the other gate provides a logic signal for switching out the acquisition eyes when the sun is in the field of view of the cruise eyes. The field of view of the null-sensing eye will be a 1 or 2 degree half angle conical detector while the logic eye will have a field of view based on the possible albedo problem of Mars but will be less than 12 degrees half angle.

Tables 3-1 and 3-2 show the performance characteristics of the acquisition and cruise sun sensors, for a distance of 1 AU.

Table 3-1
Acquisition Sun Sensors

Field of View	360 ^o (single axis)
Linear Range	+ 40 degrees
Accuracy	+ 1.0 degrees (anti-null)
Sensitivity	11.0 Ma/degree (anti-null)
Cross Coupling	8% of Max. output (anti-null)
Power	None
Reliability	0.9996 1 year life
Weight	≈ 1.2 lb.

Table 3-2
Cruise Sun Sensors

Field of View	+ 15 degrees
Linear Region	+ 1 degree
Accuracy Null	0.05 degrees at 1 sigma
Sensitivity	1.0 ma/degree Peak ≈ 1.7 Ma
Linearity	+ 5% of 1 ^o output
Cross Coupling	2 minutes for 1 ^o travel
Power	None
Weight	≈ 1.2 lb.

Figures 3-9 and 3-10 are the transfer functions of acquisition and cruise eyes.

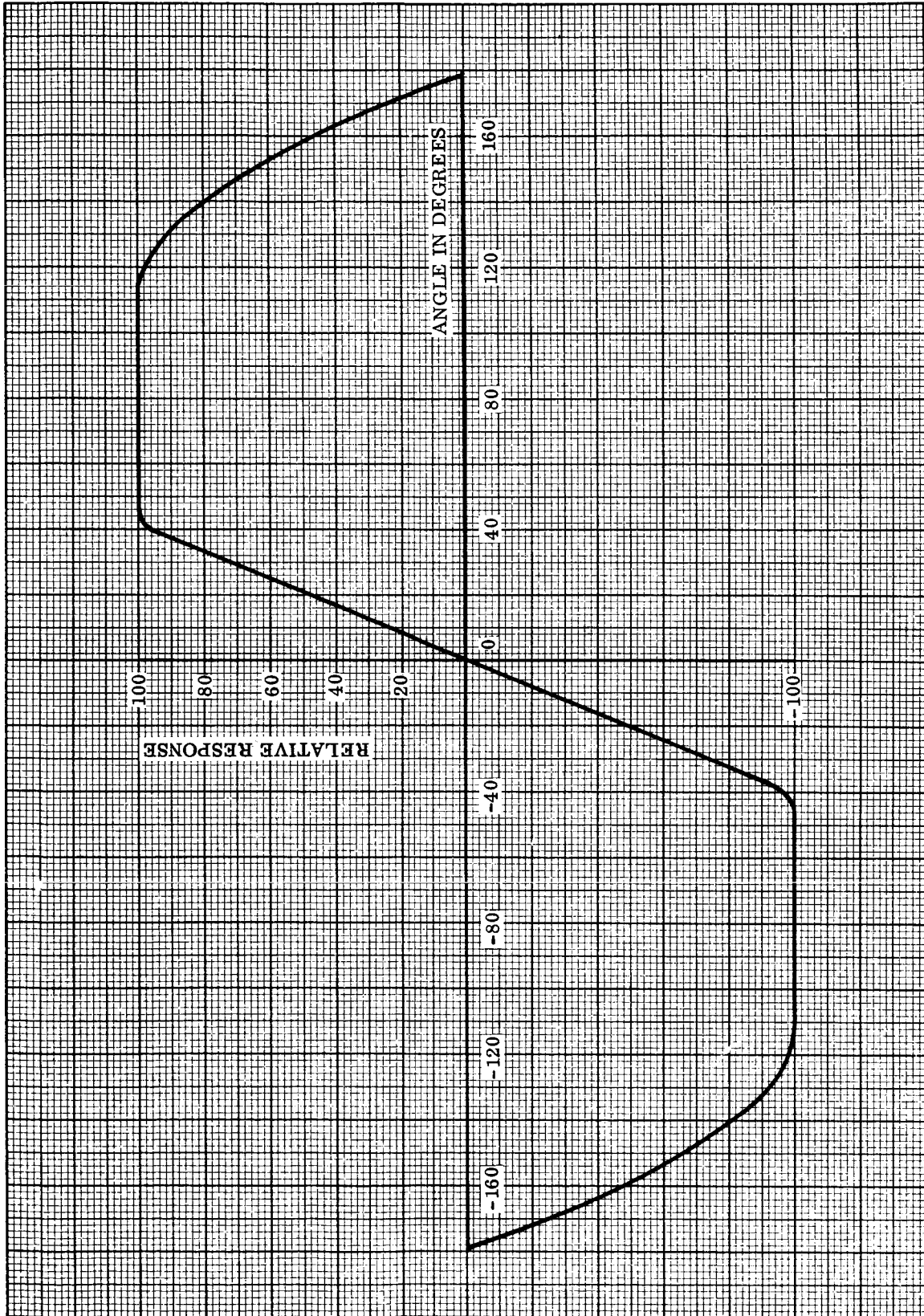


Figure 3-9. Acquisition Sensor Relative Response Characteristic

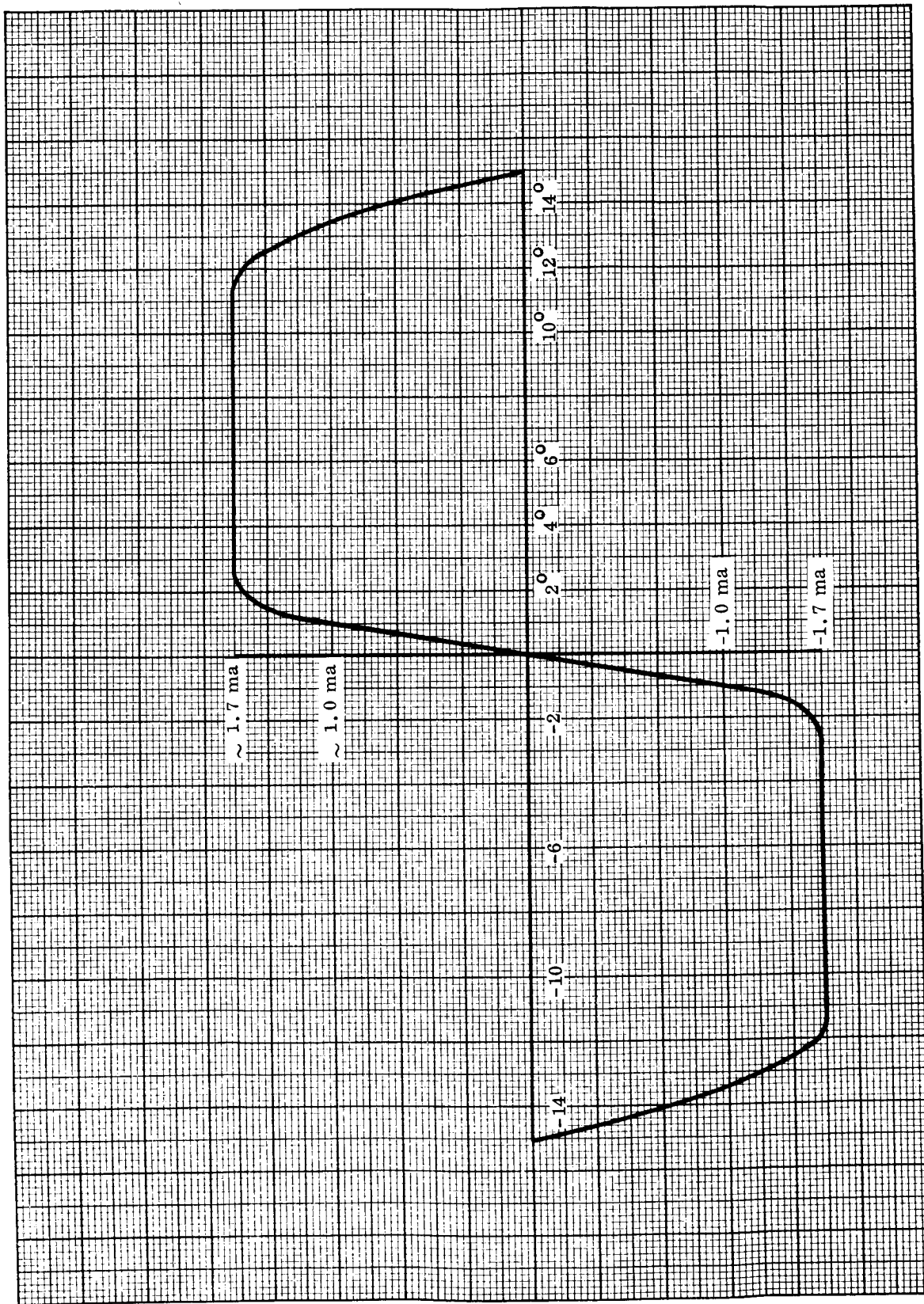


Figure 3-10. Cruise Eyes Transfer Function

3.5.2 CANOPUS SENSOR

The Canopus Sensor is essentially that flown by JPL on the Mariner Spacecraft. It is recognized that it may be desirable to improve certain characteristics of this sensor, based on JPL experience. The characteristics cited below are based on the "System Description and Performance of a Canopus Star Tracker", by the Barnes Engineering Company.

3.5.2.1 BRIEF DESCRIPTION

This sensor incorporates an electrostatically focussed and deflected version of the image dissector tube, similar to CBS Laboratories Type CL-1147. It has a slit aperture defining an instantaneous field of view which can be electronically scanned across the sensor view field. In operation the slit view field is caused to oscillate or dither in short strokes in a direction orthogonal to the long axis of the slit. Also, by program or command, the slit field of view can be shifted along its long axis to any of a series of fixed, overlapping positions.

The sensor is mounted on the spacecraft such that the dither motion of the instantaneous field will detect Canopus direction changes due to roll, but the length of the slit permits some change in pitch without effect. During the relatively long Voyager mission, however, Canopus will gradually move toward the end of the slit field. Therefore, periodically the field is electronically stepped to the next fixed position, restoring Canopus to near the center of the field.

A roll axis null error signal is generated by a phase sensitive demodulator and a dc bipolar output is supplied to the ACS.

3.5.2.2 PERFORMANCE PARAMETERS

1. S/N Canopus	greater than 100/1
2. Field of View	$\pm 2^\circ$ roll x $\pm 16^\circ$ pitch
3. Instantaneous Field of View	0.86° roll x 10° pitch
4. Optical Resolution	0.05°
5. Gimbaling and Scan	All Electronic
6. Roll Scan	1000 cps sinusoidal
7. Pitch Deflection	6 positions (4.6° overlap)
8. Star Acquisition	Between 1/4 and 4 times Canopus brightness

3.5.2.3 PHYSICAL CHARACTERISTICS AND CONSTRAINTS

1. Size	Approximately 4 x 5 x 11 inches
2. Weight	Approximately 6.25 lb.
3. Power	Approximately 1.75 watts

3.5.3 GYRO AND ACCELEROMETER PACKAGE

This unit is physically a part of the ACS, and electrically a part of both the ACS and the autopilot. The accelerometer is electrically a part of the autopilot. Since it is physically in the ACS it is described herein.

3.5.3.1 CONFIGURATION SELECTION

The technique selected for Voyager application is shown in Figure 3-11. This approach has the capability of rate or position information with rate-plus-position information being generated by the means of lead networks which are included as part of the attitude control and autopilot electronics.

3.5.3.2 PACKAGE DESCRIPTION - GENERAL

The package contains three rate integrating gyroscopes, one force balance accelerometer, gyro and accelerometer loop electronics, gyro temperature controls, torque generators (precision current supplies), logic circuitry, relays, relay drivers, regulated dc power supply and gyro torquing control unit (back-up maneuver electronics).

Upon receipt of a "gyros on" command, unregulated dc and 400 cycle power is applied to the temperature controls. The 400 cycle power sets the "nominal" frequency of the pulse width modulated temperature controller.

When the gyros reach temperature, a signal from the temperature controls is sent to a logic circuit which, when combined with a "roll on" and/or "pitch and yaw on" supplies 400 cycle wheel power and 2400 cycle power to the gyro, gyro electronics and the regulated dc power supply. This function is capable of being obtained separately, as a back up, from a ground command override. The gyro portion of the package is now ready for operation and is capable of furnishing rate or position information depending on the state of the cage/uncage command.

When a command is received for autopilot mode, 2400 cycle and regulated dc power is applied to the accelerometer and accelerometer electronics. Figure 3-11 shows the accelerometer power switches in series, because the gyros are on in either autopilot or attitude control, but the accelerometer is on in only the autopilot mode. The analog output of the accelerometer is converted to digital information which in turn is sent to the autopilot where it is counted to form velocity information. Since the normal failure mode of the accelerometer loop is an open, a clock in the autopilot can serve as a velocity control back-up.

Each gyro loop is capable of supplying vehicle maneuver signals from receipt of positive on, negative on, and off commands via the torque generator and logic circuits. These circuits then apply a precision current to the gyro torque motors to obtain a new vehicle position.

The roll torque generator is also capable of receiving positive or negative incremental commands which are converted to incremental gyro commands.

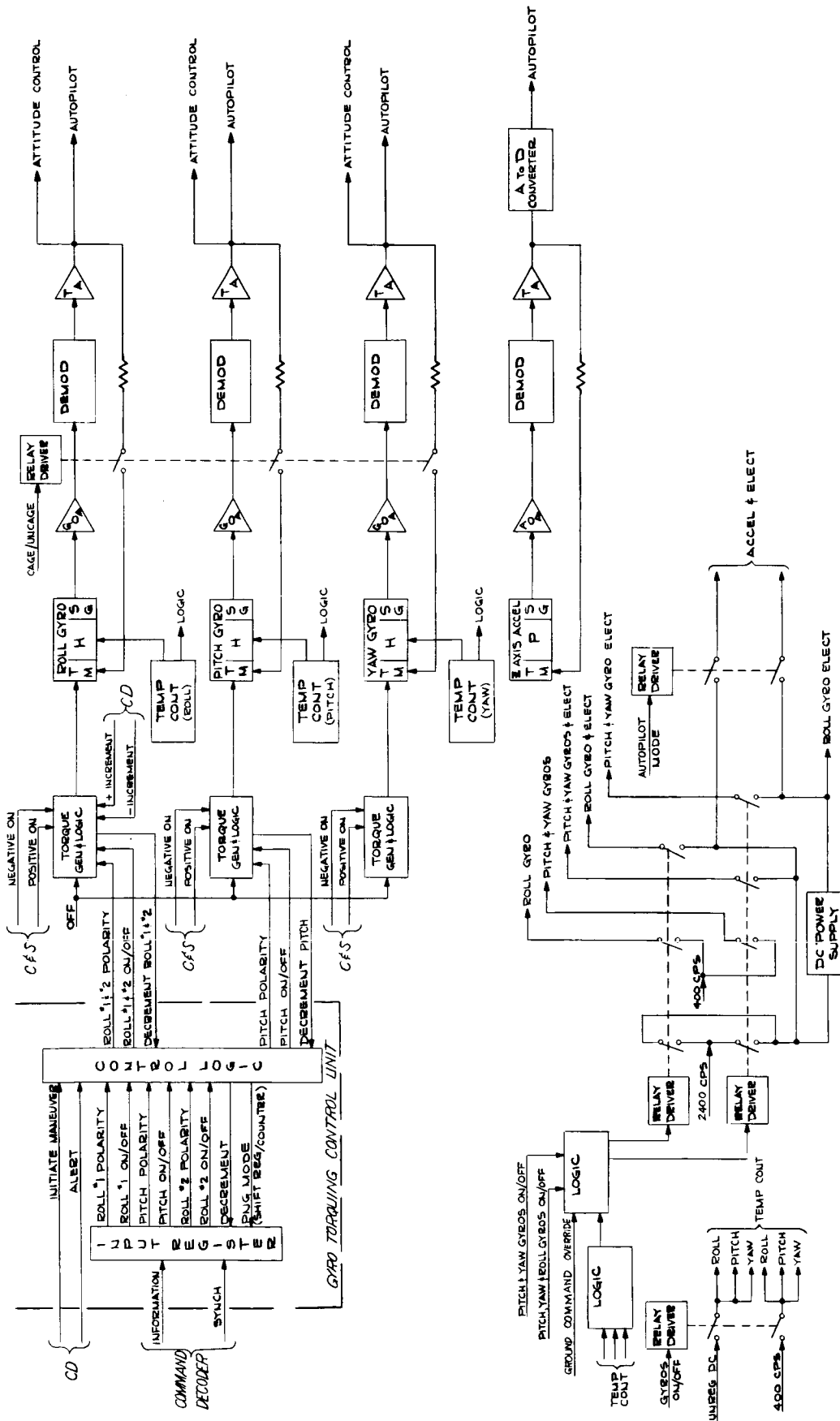


Figure 3-11. Gyro and Accelerometer Package

The gyro torquing control unit (back-up maneuver capability) is similar in function except that it contains integral registers and control logic, and that it operates independently of the computer and sequencer.

3.5.3.3 THERMAL CONSIDERATIONS

All three gyros and the accelerometer are thermally connected. Each gyro has an individual temperature control, each of which has the capability to temperature control the entire sensor block. This capability adds redundancy, in that the package can operate without degradation after loss of two temperature controls. In addition, each gyro contains an over-heat thermostat to prevent temperature run-away in case of a full-on controller failure. The accelerometer does not have a heater or temperature controller, but because of thermal connection to the gyros, it is thermally stabilized.

It is presently planned to operate the gyros at approximately 100°F. This will tend to minimize operating heater power and warm-up time as well as not causing any great difficulty in selecting the proper thermal resistances.

3.5.3.4 ANALOG TO DIGITAL CONVERTER

It is necessary to employ analog to digital converters to supply digital acceleration information and to form the decrement pulses from the torque generator to the control logic when the gyro torquing control unit is in use.

The analog to digital converter is an integrator that is reset by a capacitance discharge. The input to the converter is integrated by a Miller integrator. When the output of the integrator reaches a prescribed level, it triggers a delay multivibrator that resets the integrator and delivers an output pulse. Thus, the device is a voltage-to-frequency converter whose sum of output pulses is the integral of the input voltage. This device has the capability to deliver 10,000 pulses per second.

3.5.3.5 GYRO TORQUING CONTROL UNIT

The GTCU, shown in Figure 3-12 is a midcourse maneuver system designed to operate from the command decoder independent of the computer and sequencer. It is composed of an input register designed to operate as a serial shift register and "psuedo-noise generator" counter, control logic to generate the proper sequencing for the maneuver, and a current monitor to control the integrated torque applied to each gyro.

Receipt of an "alert" command clears the finite maneuver flip-flops causing the input register to operate as a serial shift register. Some arbitrary time later, coded steering commands are gated into the input register via the INFO and SYNC lines. Thirty-six bits of information are required to accommodate sign and magnitude commands for a roll-pitch-roll maneuver. The information is maintained in the input register until receipt of initiate maneuver command.

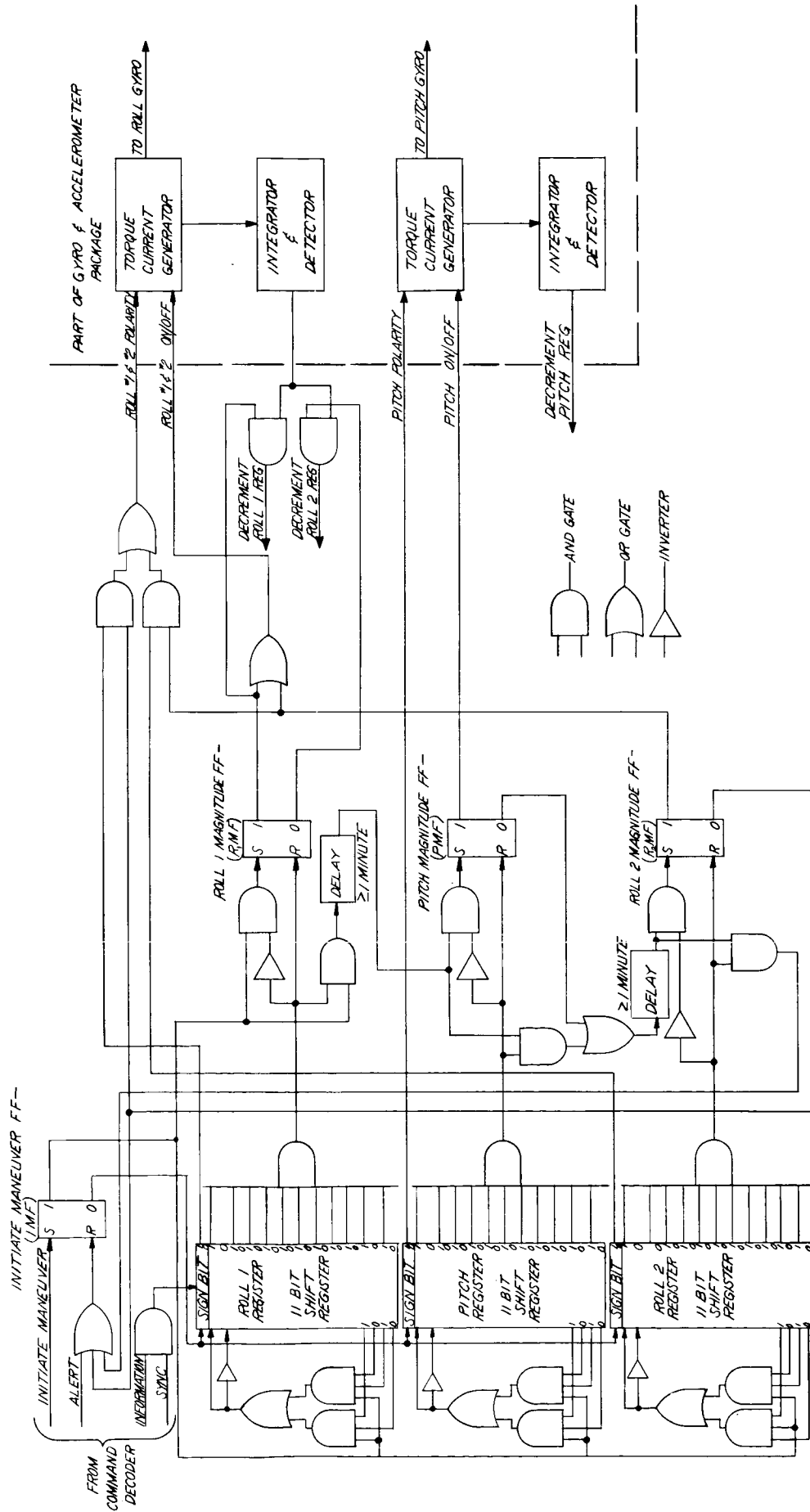


Figure 3-12. Gyro Torquing Control Unit

Initiate maneuver command sets the initiate maneuver flip-flop (IMF) in the "one" state which allows the input register to function as a pseudo-noise generator counter. IMF is also gated with the contents of the eleven magnitude bits of the Roll-1 section of the input register. If Roll-1 section contains any information other than a zero roll command the R_1 MF flip-flop is set. Accordingly the roll torque current generator is turned on and allowed to remain on until the R_1 MF flip-flop is reset. The integrator and detector (analog to digital converter) monitors the torque generator and generates decrement pulses according to the amount of current delivered to the gyro torquer. Each decrement pulse will step the input register converter section appropriate to the Roll-1 magnitude until a zero command code has been reached. This will cause the R_1 MF flip-flop to be reset stopping the torquing action.

At the same time a delay is triggered allowing the roll control to settle before continuing with the maneuver.

If the contents of the Roll-1 section of the input register had been a zero command at the receipt of the initiate maneuver, the roll maneuver would have been omitted and the delay triggered directly. At the end of the delay the pitch maneuver is initiated. This operates exactly as the Roll-1. Completion of the pitch maneuver or a zero pitch command causes the triggering of the delay which starts the Roll-2 maneuver, completion of the Roll-2 maneuver clears the IMF causing all action to cease.

3.5.3.6 GYRO SELECTION

The Kearfott Alpha Ball Bearing Gyro has been selected as the most suitable considering all the Voyager requirements. The following table compares the key features of the alpha gyro to the Voyager specifications.

Table 3-3. Key Features of the Alpha Gyro

	Voyager Spec.	Alpha Gyro
Input angular freedom	+ 6 deg	+ 6.1 deg
"G" Insensitive drift	< 0.25 deg/hr	< 0.25 deg/hr
Controlled temperature	100°F	100°F
Motor excitation frequency	400 cps	400 cps
Motor Power	> 1.5	2.5
Torquer scale factor	< 400 deg/hr/ma	134/deg/hr/ma
Torquer Linearity	0.1 %	0.02 %

3.5.3.7 ACCELEROMETER SELECTION

For the Voyager Gyro and Accelerometer package, the Bell VII B Force Balance Accelerometer has been chosen. Since all accelerometers investigated met the accuracy requirements, final selection was based on lowest size, weight and input power.

3.5.3.8 MECHANICAL CONFIGURATION

The gyro and accelerometer package are contained in a single unit having a physical size of 6.45 inches by 6.0 inches by 20 inches.

Due to its location in the vehicle (Bay 12), the package requires an off axis alignment of 7.5 degrees for the pitch and yaw gyros.

3.5.4 ATTITUDE CONTROL ELECTRONICS

3.5.4.1 DESCRIPTION

Circuitry for the pitch and yaw axes are identical. Inputs are provided by the acquisition and cruise sun sensors, and the rate gyros. Separate amplifiers are employed for the acquisition and cruise sun sensors, with gains controlled by signals from the Logic Control Unit (LCU) of the Control Electronics to adjust for decreasing sun intensity as the vehicle-sun distance increases. As control passes from the acquisition to the cruise sun sensors, power is removed from the acquisition sun sensor amplifiers, thereby disabling this signal path and preventing reflections from the vehicle or the albedo of Earth, Moon, or Mars from producing null offsets.

A buffer amplifier is provided in the rate gyro signal path to split the input signals into redundant paths and to facilitate switching in a lead network during slewing maneuvers.

The outputs of the gyro amplifier and the sun sensor amplifiers are summed by a third amplifier. The sun error signal is coupled to the summing amplifier through a resistor network which limits the position signal at a desired level and through a lead network having a time constant on the order of 1 to 2 seconds. In the transition from acquisition to cruise modes, the gyro signal is disabled by means of switch S2. The derived rate network functions during all modes, with the charge and discharge time constants set to different values by R1 and R2. The charge time constant is of the order of 20 to 30 seconds.

The derived rate network shown in Figure 3-13 is one possible implementation. When the threshold of either detector is exceeded, an analog switch connects the RC network to either a positive supply or a negative supply initiating the "derived rate" feed-back signal. Minimum solenoid "on" time would be controlled by the analog switches. Because of the long time constant, the analog switch leakage must be low. One possible implementation of this switch would employ field effect transistors.

Following the summing amplifier are threshold detectors, which are triggered when the combined rate and position inputs exceed the limits defined by the switching line equations.

Denoting the three channels as A, B, C, the logic circuits following the threshold detectors perform the function: $F = M_{AJ}(A, B, C) = AB + AC + BC$. Parallel majority voter circuits, connected to each threshold detector output, drive a series-parallel redundant output stage.

- NOTES
1. CHANNELS B AND C ARE IDENTICAL TO A.
 2. DIFFERENTIAL SIGNALS.
 3. SOLENOID COUPLE - EACH HALF IN SERIES ELECTRICALLY, CONNECTED IN PARALLEL MECHANICALLY.
 4. SIGNALING TO THE SOLENOID COUPLES, WHICH OPEN SOLENOIDS IN PARALLEL, ONLY ONE WIRE IN AND ONE GATE FORM.
 5. RELEASED SWITCH - THESE MAY BE CHANGE OF CHANNELS WITHIN PHASE OR SWITCHING TRANSFORMER.

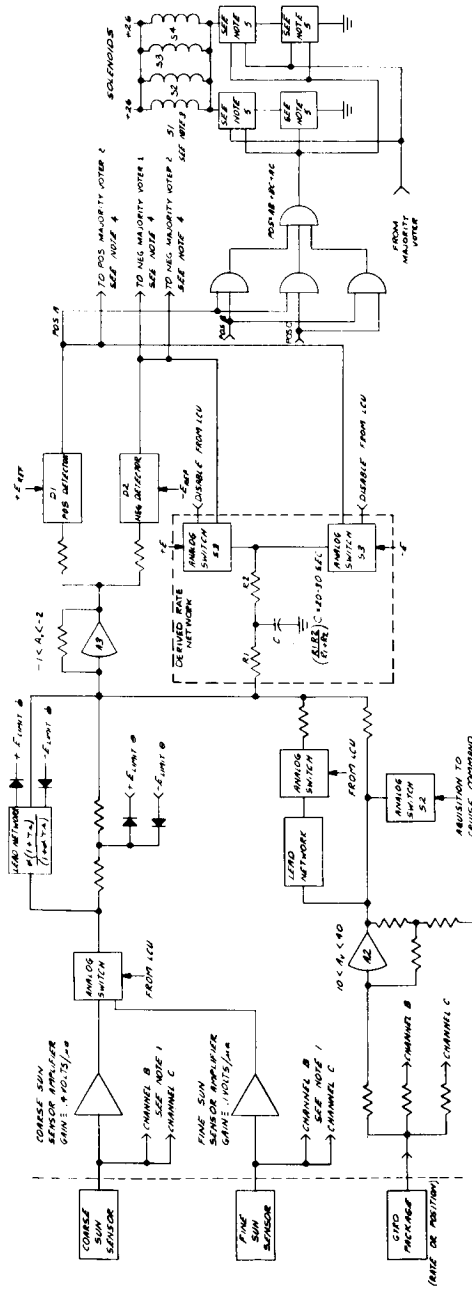


Figure 3-13. Single Axis of Attitude Control Electronics

Roll Channel

The inputs of the roll channel are the Canopus Sensor signal, the gyro and the roll bias, which generates the roll search after sun acquisition. In addition to the derived rate feedback, a roll integrator limits solenoid firing in the event of gyro failure during roll search. The remaining portions of this axis are identical to the pitch and yaw axes.

Logic Control Unit

The Logic Control Unit (LCU) processes commands from the C and S system and the Command Decoder, and handles the automatic sequencing of the control subsystem logic.

Power Supply

Power at several voltage levels at one percent and three percent regulation is required. These voltages are obtained by transforming the 2400 cps, 50 volt input, rectifying, filtering, and in some cases regulating the filtered output. The voltage levels are ± 12 volts and ± 6 volts. The use of a transformer-rectifier-regulator supply within the Attitude Control Electronics provides isolation of the circuitry from disturbances emanating from other components. Conversely, transients generated within the Attitude Control Electronics will be attenuated.

Components and Circuits

Figure 3-13 illustrates a possible approach to implementing the control functions. The component types mentioned in the following section are under active consideration. A final choice of parts will be made during the next design phase. The summing amplifiers, sun gates and threshold detectors may be integrated differential amplifiers. In the Biosatellite Jet Controller the T. I. SN522 is being used both as a summing amplifier and as a threshold detector. Figure 3-14 shows the circuit configuration employing the SN522 in the Biosatellite Jet Controller. Over a -30° to 150° F temperature range, changes in threshold points are less than ± 2.5 percent and can be further improved by temperature and load compensation of the reference voltages. During a 1000 hour test, variations in triggering points and hysteresis were less than 0.5 percent. Figure 3-15 shows another configuration employing the TI SN524. During temperature tests over a range of -30° to 150° F, triggering point variations of this circuit were less than one percent.

Logical functions will be performed by integrated DTL NAND gates and J-K flip flops. A single "family" of commercially available circuits will be utilized. It is anticipated that most switching will be done with solid state devices rather than relays.

Solenoid drive will be provided by either conventional transistors or compound-connected (Darlington) transistors in single packages.

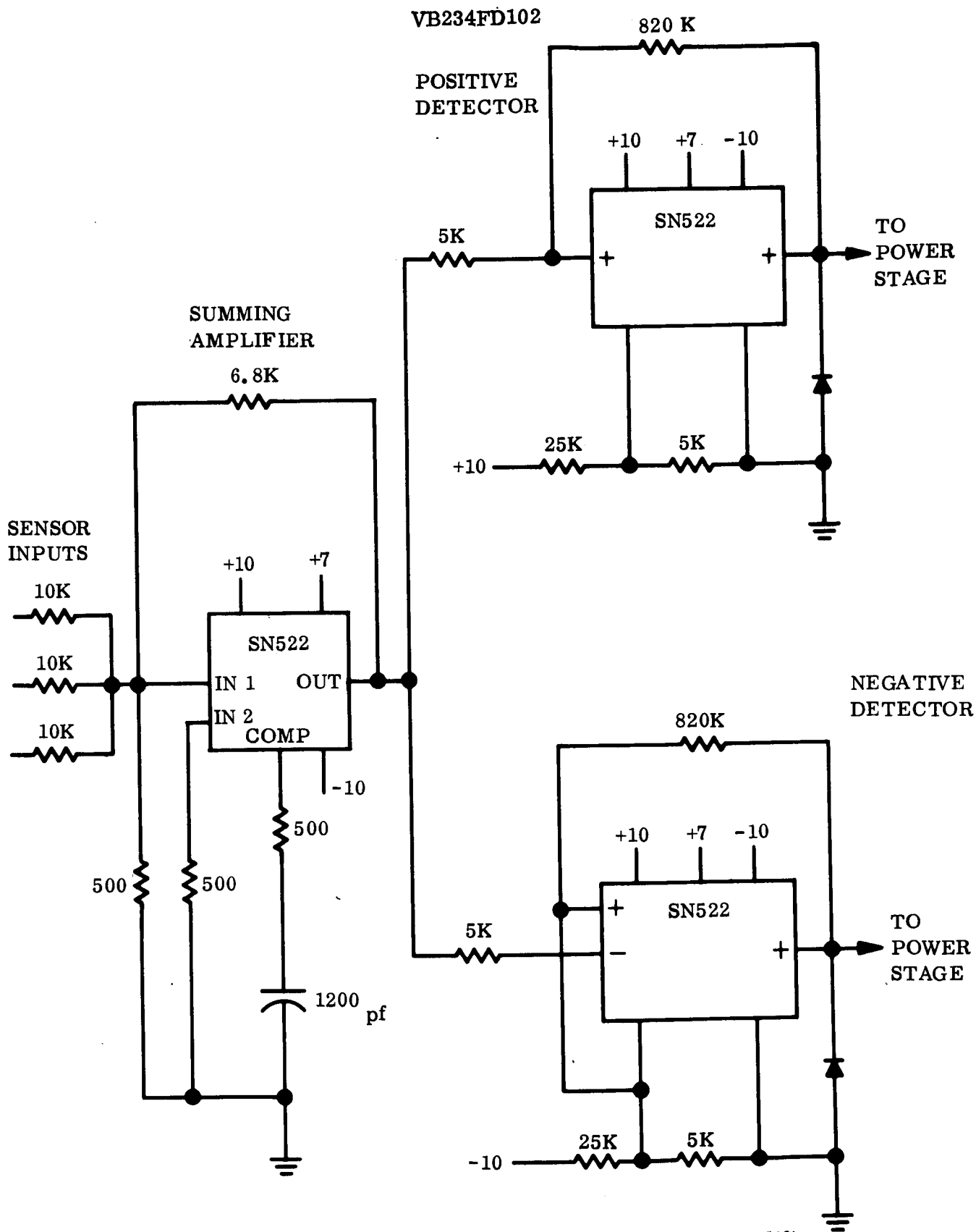


Figure 3-14. Biosatellite Jet Controller Summing Amplifier and Threshold Detectors

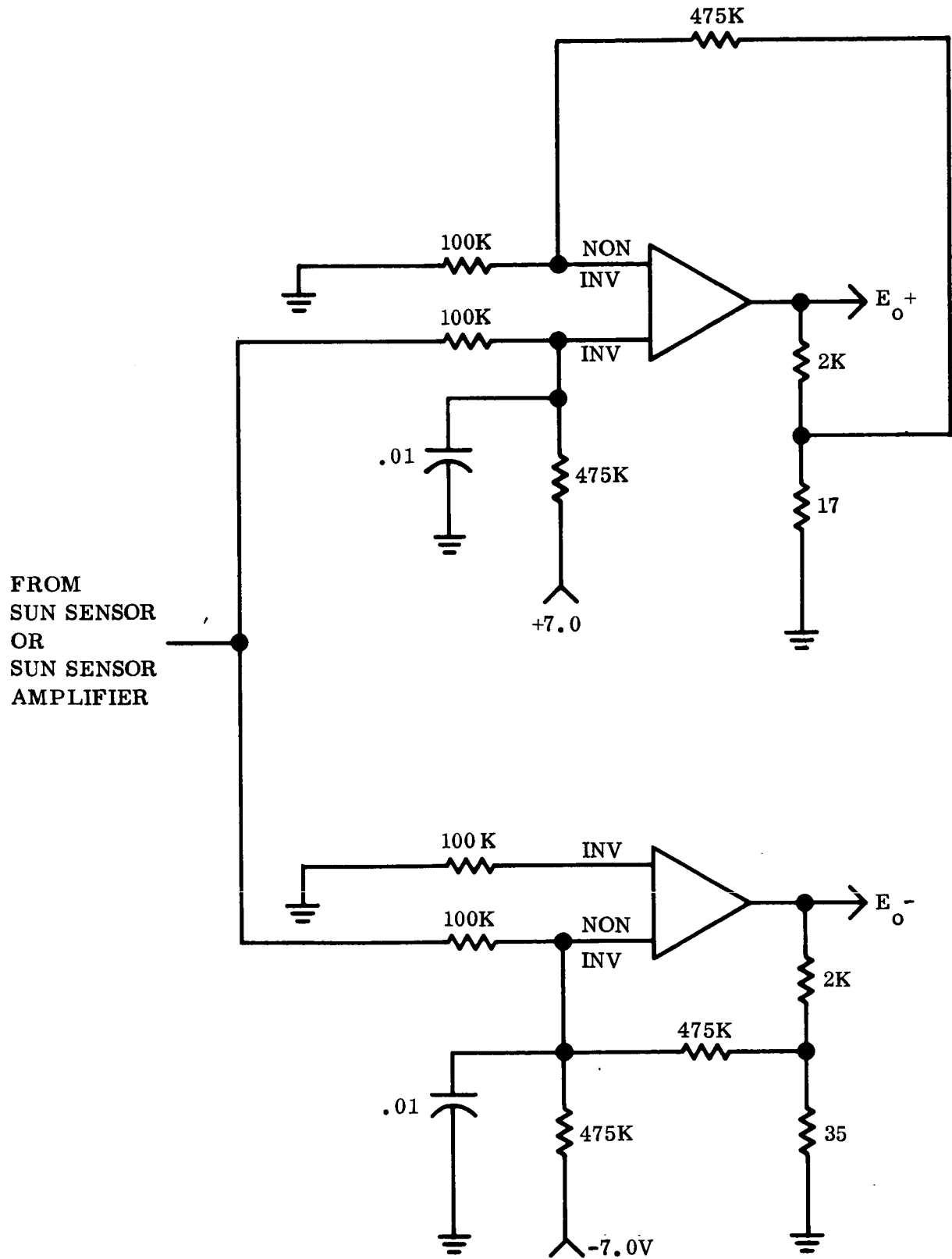


Figure 3-15. Threshold Detectors Using SN 524's

3.5.4.2 USE OF REDUNDANCY TECHNIQUES TO IMPROVE COMPONENT RELIABILITY

To achieve the highest possible reliability of the electronics subsystems extensive use of redundancy and voting techniques has been made. Because of the availability of integrated linear and digital circuits, the weight-power-size penalty incurred by the use of redundant circuitry is much more reasonable than that which would be incurred using conventional piece parts. Figure 3-16 illustrates the redundancy-voting technique for the Attitude Control Electronics. The desired result of this configuration is that no single component failure will degrade performance.

Each control axis consists of three identical channels from the sensor outputs to the output of the threshold detectors. At the output of the threshold detectors a pair of voters produces a solenoid drive signal whenever two of the three channels indicate their position-rate threshold has been exceeded. The solenoid valves are in parallel electrically. The driver stages are connected in a series-parallel arrangement. Either majority gate can provide sufficient power to all four driver stages to fire the solenoids. The driver stages consist of two switching transistors in series. In the event of a failure of one of these transistors by shorting, the series arrangements prevent a solenoid from being held on and depleting the gas supply.

The solenoid power is supplied by the three battery busses in an "or" arrangement, permitting the loss of two supply lines. The diodes shown in Figure 3-16 would be located at the Power Supply Panel.

Logic Control Units

Each sun gate null is available to the LCU on three separate lines. Commands from C&S or CD to the LCU, and outputs from the LCU to the C&S, and the Canopus sensor are single lines. The form of the LCU will be DTL NAND logic, with logical functions being generated in triplicate and voted. The majority voting will most likely be done with NAND gates rather than majority gates because of the absence of commercially available majority logic integrated circuitry.

Power Supply

Two independent transformer-rectifier filter systems are provided in the power supply. Standby redundancy will be used with the failure of one supply causing the second system to be switched in place of the failed system.

Summary

1. A failure in the sensor output to threshold detector chain does not affect performance because of the voting gates following this chain.
2. A failure in either of the majority gate networks does not affect system performance because either circuit can drive all solenoids.
3. A failure in a driver transistor (either open or short) does not prevent solenoid firing since a second driving stage remains.

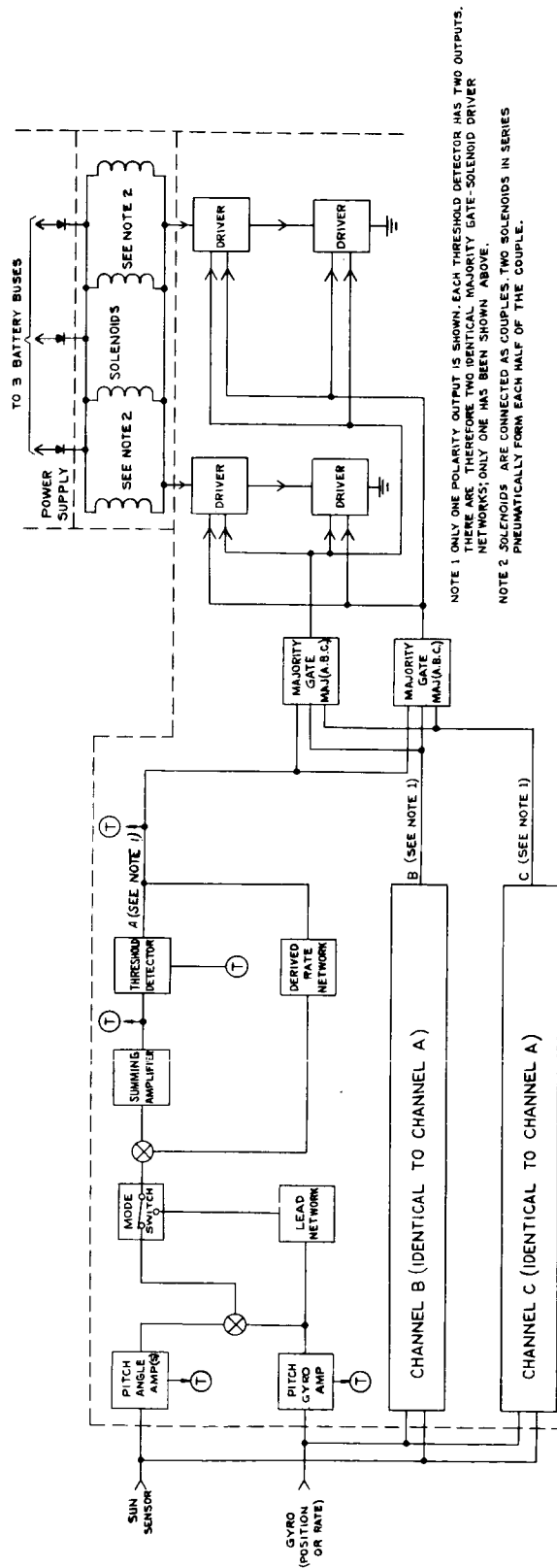


Figure 3-16. ACS Reliability Block Diagram (Single Axis)

Testing Redundant Circuitry

The use of voting techniques permits operation of a component despite a failure of one channel. While this quality improves reliability, it does complicate component testing.

In order to test each of the individual channels, provisions for testing individual channels must be provided. Test points on each channel must be provided after circuits having calibrated or adjustable gain or trigger level.

In testing any axis of the Attitude Control Electronics, the following steps are taken to test both the individual channels, and the functioning of the voting logic:

1. Each of the individual channels is tested, simulating the gyro and sensor inputs, one channel at a time. Gain and threshold levels are measured using test points after each of the amplifiers and detectors. (These points are marked (T) on Figure 3-16.)
2. The voting and solenoid drives are tested by energizing each channel individually, then each combination of 2/3 channels and finally all three channels. It should not be possible to energize a solenoid with a single channel. The combination of 2/3 and all three channels should energize the proper solenoids at the required position and rate thresholds.

4.0 INTERFACE DEFINITIONS

The overall functional boundaries of the ACS are the radiation inputs to the celestial sensors and spacecraft motion to the inertial sensors, and the output torques applied to the spacecraft by the gas jets. In addition to these functional boundaries, mechanical and electrical interfaces with other subsystems exist. The various interfaces are defined below, with sources and destinations identified.

4.1 INPUTS TO ACS

4.1.1 DIRECTLY SENSED INPUTS

- a. Solar radiation to the acquisition, cruise and sun gate sun sensors. Solar intensity varies as the square of distance to Sun (1 to 1.67 AU when the entire Mars orbit is considered).
- b. Canopus radiation to the Canopus sensor.
- c. Spacecraft body rates about the three control axes as inputs to the Gyro and Accelerometer Package.

4.1.2 INPUTS FROM OTHER SUBSYSTEMS

- a. Power Subsystem - The ACS receives power from three power sources:

2400 cps square wave, 50 V RMS
 400 cps square wave, 3 phase
 Unregulated DC, 30-44 VDC

Table 4-1. ACS COMMAND INPUTS

QC	CODE			NOMENCLATURE	SOURCE		COMMENTS
	EC	DC	SC		PRIMARY	BACK-UP	
		1		Change Attitude Control State (Inhibit/Enable)	Sep. Sw C&S	C.D.	Controls the operational status of the ACS
			1	Change Canopus High Gate State (Override/Normal)	C.D.		Allows Canopus Sensor to recognize stars brighter than normally
			2	Change Canopus Low Gate State (Override/Normal)	C.D.		Allows Canopus Tracker to recognize stars dimmer than normally
			3	Change Roll Search Auto Mode (On/Off)	C.D.		In combination, DC 3 and DC 4 provide for either automatic (ACS LCU) initiation of roll rate mode, or commanded on or commanded off states
			4	Change Roll Search Auto Bypass Mode (On/Off)	C.D.		
			2	Change Roll Turn Mode (Calibration/Search)	C&S	C.D.	Input to LCU as to next roll turn rate magnitude required
			5	Change Canopus Sensor Auto Mode (On/Off)	C.D.		In combination, DC 5 and DC 6 provide for either automatic (ACS LCU) control of Canopus Sensor Power, or commanded on or commanded off states
			6	Change Canopus Sensor Auto Bypass Mode (On/Off)	C.D.		
			7	Roll Override	C.D.		Provides for rejection of acquired star and re-initiation of roll search
1				Load Canopus Sensor Cone Angle Register and Execute	C.D.		Provides direct command of Canopus Sensor cone angle, by magnitude
	11			Step Canopus Sensor Cone Angle (+)	C&S	C.D.	These two signals (EC 11 and EC 12) provide for incrementing Canopus Sensor cone angle in either direction
		12		Step Canopus Sensor Cone Angle (-)	C&S	C.D.	
		10		Change Gyro and Accelerometer Heater Auto Mode (On/Off)	C.D.		In combination, DC 10 and EC 3 provide for either automatic (ACS LCU) control of heater power state, or commanded on or commanded off states
	3			Change Gyro and Accelerometer Heater Auto Bypass Mode (On/Off)			
		11		Change Gyros (All Axes) / Gyro Electronics Auto Mode (On/Off)	C.D.		In combination, DC 11 and EC 4 provide for either automatic (ACS LCU) control of gyro operating power, or commanded on or commanded off states
			4	Change Gyros (All Axes) / Gyro Electronics Auto Bypass Mode (On/Off)	C&S	C.D.	
		5		Change Spacecraft Control Mode (Inertial/Cruise) (All Axes)	C&S G&C	C.D.	In combination, EC 5 and EC 6 provide for either automatic (ACS LCU) control of signal interconnections and gyro rate/position mode to provide inertial or cruise/acquisition operating mode, or commanded inertial or commanded cruise/acquisition mode
		6		Change Spacecraft Control Mode (Inertial/Cruise) (Pitch and Yaw Axes)	C&S	C.D.	
2				Load Turn Register		C.D.	Provides magnitudes and polarities of CD initiated maneuver turns
		12		Initiate Maneuver Register Turns		C.D.	Initiates ACS maneuvering after storage of magnitudes and polarities
			6	Initiate Positive Pitch Turn	C&S		
			7	Initiate Negative Pitch Turn	C&S		
			8	Initiate Positive Roll Turn	C&S		
			9	Initiate Negative Roll Turn	C&S		
		13		Roll Negative Increment	C.D.		These (DC 13 and DC 14) provide for incrementing roll attitude in inertial mode
		14		Roll Positive Increment	C.D.		
			10	Initiate Positive Yaw Turn	C&S		
			11	Initiate Negative Yaw Turn	C&S		
			12	Stop Pitch, Roll and/or Yaw Turns	C&S		
	7			Change Derived Rate State (Cruise/Orbit)	C&S	C.D.	Provides for changing derived rate network parameters (if advantage accrues from such changes)
	9			Change Sun Sensor Amplifier Gain State (High/Medium)	C&S	C.D.	EC 9 and EC 10 provide three steps in Sun Sensor Amplifier gain to compensate for reduced sun intensity
	10			Set Sun Sensor Amplifier Gain State Low	C&S	C.D.	
		15		Change Yaw Lead Network State (Derived Rate/Lead Network)	C.D.		DC 15, 16, 17 provide for insertion of lead networks operating on Sun or Canopus error signals, in case of gyro or derived rate network failures
		16		Change Pitch Lead Network State (Derived Rate/Lead Network)	C.D.		
		17		Change Roll Lead Network State (Derived Rate/Lead Network)	C.D.		

- b. Separation Switch - An input from the booster separation switch initiates attitude control performance.
- c. Command Decoder and Computer & Sequencer Subsystems - The ACS receives commands from both the CD and the C&S. Table 4-1 which is an excerpt from VB220FD112, Flight Sequence Functional Specification lists the commands, identifies each with an alpha-numeric code, and indicates source and priority of each. A "comments column clarifies the operation resulting from each command. Four classifications are assigned: QC - Quantitative Command, all of which originate in the Command Decoder; EC - Either Command, discrete commands which originate in the C&S normally, with CD back-up; DC - Discrete Command; which originate in the CD only, and SC - Stored Commands, which originate in the C&S with no CD back-up.

4.2 OUTPUTS OF THE ACS

ACS outputs include driver signals to the 24 cold gas jet solenoid valves, telemetry, test points and thermal outputs.

4.2.1 DRIVER SIGNALS

The ACS generates appropriate signals which drive the redundant, coupled cold gas jet subsystem solenoid valves as required to perform the specified control functions.

4.2.2 TELEMETRY

Various points in the ACS will deliver information for telemetry to Earth, for operational and diagnostic purposes. Table 4-2 is an excerpt from the overall Voyager telemetry list, presented with additional detail in Document VB220FD110, Telemetry Channel Assignments.

Table 4-2. ACS Telemetry

Pitch Cruise Sun Sensor
 Yaw Cruise Sun Sensor
 Pitch Acquisition Sun Sensor
 Yaw Acquisition Sun Sensor
 Pitch Gyro Output
 Yaw Gyro Output
 Roll Gyro Output
 Threshold Detector Inputs Pitch
 Threshold Detector Inputs Yaw
 Threshold Detector Inputs Roll
 Canopus Sensor Error
 Canopus Sensor, Pitch Angle
 Accelerometer Output
 Gyro Torquer Input, Pitch
 Gyro Torquer Input, Yaw
 Gyro Torquer Input, Roll
 Canopus Sensor Intensity
 Fine Sun Gate

Table 4-2. ACS Telemetry (Cont)

Coarse Sun Gate
 Canopus Acquisition Complete
 Attitude Control Logic Status
 Gyro Loop Status
 Gyro Temperature, Pitch
 Gyro Temperature, Yaw
 Gyro Temperature, Roll
 Canopus Sensor Temperature
 Coax Sol. Valve Temp. #1
 Coax Sol. Valve Temp. #2
 Coax Sol. Valve Temp. #3
 Coax Sol. Valve Temp. #4
 Pitch Acq'n Sun Sensor Temp.
 Pitch Acq'n Sun Sensor Temp.
 Yaw Acq'n Sun Sensor Temp.
 Yaw Acq'n Sun Sensor Temp.

4.2.3 TEST POINTS

The following test points (Table 4-3) will be available by direct access for system testing after assembly of the spacecraft.

Table 4-3. ACS Test Points

Attitude Control Electronics:

Acquisition Sun Sensor Simulation Inputs	3 per 2 axes	6
Cruise Sun Sensor Simulation Inputs	3 per 2 axes	6
Canopus Simulation Inputs	3 per 1 axis	3
Threshold Detector Outputs	6 per 3 axes	18
Majority Gate Outputs	4 per 3 axes	12
Solenoid Drive Current	4 per 3 axes	12
Roll Integrator Output		1
Sun Gate Amplifier Output		2

Gyro Accelerometer Package

Gyro Output Amplifier	1 per 3 axes	3
Accelerometer Output Amplifier		1
Accelerometer Torque Input		1
Gyro Logic Circuits		7
Accelerometer Logic Circuits		2

4.2.4 THERMAL OUTPUTS

The thermal interfaces of the various components will be designed to remove the heat in excess of that required for proper temperature control; or will (in the case of several of the pneumatics components) provide additional heat inputs to the components where such is required. (Ref. VB220FB103, Spacecraft Component Design Parameters.)

5.0 ATTITUDE CONTROL PERFORMANCE PARAMETERS

5.1 CONTROL ANGULAR ACCELERATION

The nominal value of control angular acceleration at booster separation will be 0.225 m rad/sec² each axis. Failure of a single nozzle of a couple reduces this value to 0.1125 m rad/sec². Use of expendables, and lander separation, will reduce moments of inertia such that control angular acceleration will be increased by factors of 3.86, 7.38, and 2.15 for the X, Y and Z axes respectively, during the orbit phase.

5.2 CONTROL DEADBAND

The nominal control "deadband" is ± 8 m rad from the nominal zero position about each of the three control axes in all operation modes. Since the radiation intensity from the Sun decreases during transit phase by a factor of from 0.525 to 0.37, depending on Mars position at arrival date, the deadband will vary by the inverse of the applicable factor. Command-generated gain changes (3 increments) incorporated in the Attitude Control Electronics (pitch and yaw channels) provides capability to compensate for the gain changes of the cruise sun sensor, in order that the deadband variation be minimized.

5.3 COMMANDED ANGULAR RATE

The angular rate during commanded turns is 3.14 m rad/sec for each axis.

5.4 ACQUISITION TURN RATES

Limited acquisition rates in pitch and yaw axes during sun acquisition are nominally 17.5 m rad/sec. Roll rate during sun acquisition is limited to approximately 0.2 m rad/sec. During magnetometer calibration the commanded roll turn rate is 3.9 m rad/sec. with a rate deadband of 0.4 m rad/sec. During Canopus search the roll turn rate is 1.7 m rad/sec with a deadband of 0.4 m rad/sec.

5.5 LIMIT CYCLE RATE

The nominal limit cycle rate is 3.375×10^{-6} rad/sec.

5.6 NULL OFFSET

Alignment errors, null offsets and drifts in sensors and electronics, etc. results in a shift of the mean value of the pointing direction of each axis of not more than 4 m rad for each axis.

5.7 FREQUENCY - SHAPING NETWORKS

Three networks are indicated for each control axis: derived rate network, lead for gyro control compensation, and a lead which is used as a back-up for gyro failure during acquisition, or for derived rate network failure during cruise mode. While none of the

time constants have been specifically identified, the lead networks have lead time constants on the order of 10 sec, corresponding to a rate/position gain ratio of 10.

5.8 MANEUVER ACCURACY

While a complete maneuver error analysis has not been accomplished, maneuver accuracy for three maneuvers (typical large mid-course correction maneuver, lander separation followed by final midcourse correction maneuver, and orbit insertion maneuver) has been determined on the basis of the more significant error contributors. For details, see Document VB220FD111.

Large Midcourse Maneuver

Per axis error, total through verification:

Roll 7.04 milliradians, 1 σ

Pitch 7.51 milliradians, 1 σ

Yaw 7.51 milliradians, 1 σ

Half-cone angle, roll axis to desired direction:

11.4 milliradians, 68% probability

Lander Separation

Per axis error, total through maneuver verification:

Roll 20.44 milliradians, 3 σ

Pitch 23.25 milliradians, 3 σ

Yaw 20.44 milliradians, 3 σ

Half-cone angle, roll axis to desired direction:

23.25 milliradians, 99% probability

26.75 milliradians, 99.7% probability

Final Midcourse Correction (immediately after Lander Separation):

Per axis error, total through verification:

Roll 7.33 milliradians, 1 σ

Pitch 9.07 milliradians, 1 σ

Yaw 7.33 milliradians, 1 σ

Half-cone angle, roll axis to desired direction:

13.6 milliradians, 68% probability

Orbit Injection

Per axis error, total through verification:

Roll 7.04 milliradians, 1 σ

Pitch 7.51 milliradians, 1 σ

Yaw 7.51 milliradians, 1 σ

Half-cone angle, roll axis to desired direction:

11.4 milliradians, 68% probability

5.9 RELIABILITY

The reliability of the ACS calculated from expected failure rates is given below for the various phases of the mission, and for the total mission (through 30 days in Mars orbit).

Phase 1 (Injection) 1 Hour	Phase 2 (Transit) 178 Days	Phase 3 (Orbit Inj.) 2 Days	Phase 4 (Mars Orbit) 30 Days	Mission 210 Days
0.999	0.989	0.999	0.996	0.984

6.0 ACS PHYSICAL CHARACTERISTICS AND OPERATIONAL CONSTRAINTS

The first part of this section defines the physical characteristics of the complete ACS, which is composed of the component assemblies as previously defined and depicted in the Functional Block Diagram, Figure 3-5. The second part of this section defines the operational constraints placed on the ACS, which have evolved from the design effort.

6.1 ACS PHYSICAL CHARACTERISTICS

The estimated weight, and power input and dissipation for the various ACS components are indicated in Table 6-1.

Table 6-1. ACS Component Physical Characteristics

<u>Component</u>	<u>Weight, LBS</u>	<u>Power In, W</u> (Average)	<u>Power Dis, W</u> (Average)
Secondary Sun Sensors (4 total)	1.2	-	-
Cruise Sun Sensor Assembly (Includes all primary sun sensors)	1.2	-	-
Canopus Sensor	6.25	1.75	1.75
Gyro Accelerometer Package	14.5	27.0	27.0
AC Electronics	8.6	7.8	7.6
TOTAL ACS	31.75	36.55	36.35

6.2 ACS OPERATIONAL CONSTRAINTS

The following constraints, which have either evolved from the design of the Spacecraft and the ACS, or which are estimated to evolve from proposed configurations are imposed on the overall system.

6.2.1 TURN LIMITS

- a. In normal operation, as commanded by the C&S, maneuvers of up to 180 degrees magnitude, either polarity, about all three control axes, in any sequence may be performed.
- b. In the back-up configuration, as commanded by the CD, maneuvers of up to 180 degrees in either polarity about the roll and pitch axes, may be made. The sequence of turns in this mode is restricted to roll-pitch-roll.

6.2.2 TIME TO COMPLETE STABILIZATION

Stabilization to the Solar reference will be accomplished within 20 minutes after initiation, including reduction of initial rates as high as 3 degrees per second.

Acquisition of a guide star by the Canopus sensor will be accomplished with an additional 70 minutes, if no calibration turn maneuver is required. Calibration turn requires an additional 32 minutes per 360 degree turn.

6.2.3 INITIAL RATES

The ACS is anticipated to be able to control from initial rates of greater than 5 degrees per second without degradation of performance.

6.2.4 ENVIRONMENTAL CONDITIONS

Canopus Sensor - This sensor must be mounted in the vehicle, and vehicle structure and appendages must be located such that no light is reflected into the shield of the sensor.

Sun Sensor - Reflected light impingement on the Solar sensors must be prevented. Albedo inputs to the acquisition sensors have not been determined, but are estimated to be such that on the order of 8 degrees pointing error will be introduced until the acquisition sensors are switched out. The alignment of the various acquisition sensors must be such as to minimize the effect of albedo.

6.2.5 SEPARATION MANEUVER NOZZLE

This nozzle shall be aligned, and the thrust controlled, such that the angular torque developed due to misalignment and center of gravity location error shall not exceed 25 percent of the control torque available from ACS control gas jets.

7.0 SAFETY CONSIDERATIONS

The following are the factors concerning the ACS that were considered in the formulation of operational procedures to ensure the safety of personnel and equipment:

- a. Internal damage to the gyros by not warming them up before turning them on
- b. Damage to the Canopus Sensor's sensitive element by exposure to intense light
- c. Damage to the optical surfaces of celestial sensors by improper handling.

The operational procedures that were formulated concerning the above components are located in Document VB264FD104.

CII-VB234FD104

ATTITUDE CONTROL
COLD GAS JET
SUBSYSTEM

Index

- 1 Scope
- 2 Applicable Documents
- 3 Functional Description
- 4 Interface Definition
- 5 Performance Parameters
- 6 Physical Characteristics and Constraints
- 7 Safety Consideration

1.0 SCOPE

This document describes the function of the Attitude Control Cold Gas Jet Subsystem, its functional boundaries, performance parameters, physical characteristics, component design and safety considerations.

2.0 APPLICABLE DOCUMENTS

VB234FD101	Guidance and Control Subsystem
VB234FD102	Spacecraft Attitude Control Subsystem
VB220SR101	Design Characteristics
VB220SR102	Design Restraints

3.0 FUNCTIONAL DESCRIPTION

The cold gas jet subsystem will perform the following functions:

- a. Apply torques to the spacecraft upon receipt of electrical signals - See Figure 3-1.
- b. Provide translatory force to impart lateral velocity to spacecraft following capsule separation - See Figure 3-2.

3.1 ATTITUDE CONTROL COLD GAS JET SUBSYSTEM

The attitude control pneumatic subsystem consists of two separate subassemblies, as used on Mariner each containing about 28 pounds of Freon 14.

These 28 pounds of Freon-14 consist of:

- 15.70 pounds - basic requirement (this corresponds to 7595 ft-lb-sec of angular impulse, the amount required to complete mission).
- 2.80 pounds - for leakage and crosscoupling effect due to nozzle misalignment.
- 9.50 pounds - to offset the effect of catastrophe leakage through one nozzle.

Each subassembly contains six reaction jets, one in each axis-direction. The corresponding reaction jets of the two subassemblies comprise a couple, i.e., the pitch jet of one subassembly and the pitch jet of the other subassembly are positioned on opposite sides of the vehicle such that when they are actuated pure torque is exerted on the vehicle about the pitch axis. Command to operate control solenoid valves will be generated by jet drivers which are part of attitude control electronics.

In case of failure of either jet to operate, (e.g., if a valve fails to open) the remaining jet will be able to carry on the function alone. The torque exerted will then be halved, and

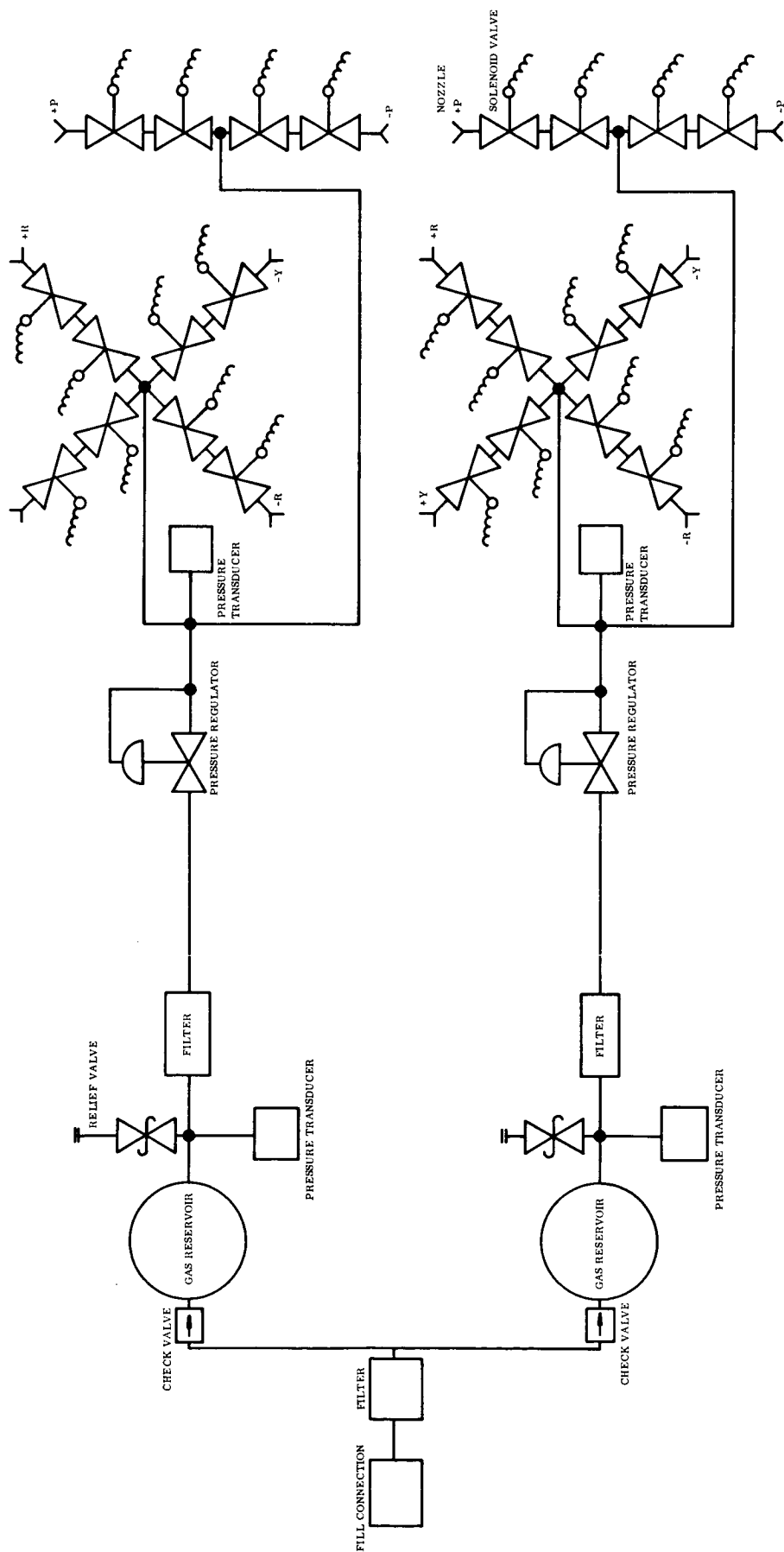


Figure 3-1. Cold Gas Jet Subsystem Schematic

the vehicle will also be subjected to linear as well as angular acceleration. To minimize the effect of excessive seat leakage or failure of any of the solenoid valves to close, two solenoid valves are used in series with each nozzle. In addition pressure regulators having two seats in series, are used to minimize the most common regulator failure - seat leakage. Thus it is seen that the chance of catastrophic failure occurring has been greatly reduced.

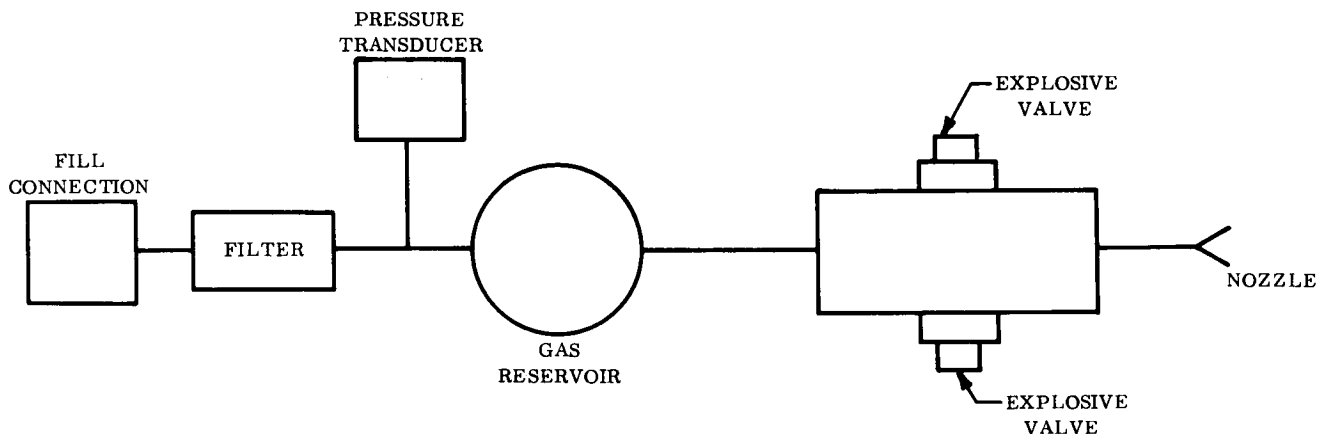


Figure 3-2. Separation Propulsion Schematic

3.2 SPACECRAFT SEPARATION PROPULSION

The Separation Propulsion portion of the subsystem is used to accelerate the spacecraft in a direction perpendicular to the roll axis, in order that the lander will not impact the spacecraft during the lander trajectory deflection.

The Separation components consist of a gas storage reservoir containing 0.52 pound of gaseous nitrogen stored in a titanium container at 525 psia, two normally closed explosively actuated valves in parallel and one nozzle. A pressure transducer to monitor nitrogen pressure is also included. See Figure 3-2. The Separation Propulsion imparts a velocity of about 0.2 ft/sec to the spacecraft. At the end of 15 minutes the separation distance between the capsule and spacecraft is 160 feet. The thrust generated by the escape subsystem decays exponentially from a peak value of 0.45 pound. At the end of 240 seconds 90 percent of the

stored mass is expelled, while the pressure decays to below four percent of original value. Gas temperature at this condition will be below 220°R.

The actuating fluid is assumed to have a specific impulse of 58 seconds, under the conditions of continuous blowdown and minimum heat transfer from surrounding areas.

3.3 COMPONENT DESIGN

Components will be selected based on their suitability for the Voyager mission and compatibility with over-all system requirements (weight, size, power, operating characteristics). Components successfully qualified and used on other programs will be preferred.

3.3.1 GAS STORAGE RESERVOIR

The tanks are made of 6AL-4V Titanium, spherical and heliarc welded about the girth. The burst to operating pressure ratio is 2.2 at ambient conditions based on a boss weld and scratch allowance of 25 percent.

3.3.2 CHECK VALVE

The check valve at the fill connection prevents back-flow and escape of gas while the charging equipment is being disconnected following completion of charging, and before fill fittings are capped. The check valve is constructed of aluminum with a soft elastomer seal at the valve seat.

3.3.3 RELIEF VALVE

The relief valve is constructed of a suitable (magnetically compatible) stainless steel, and titanium. The valve seat is of elastomer or plastic material. The design maintains constant seat load up to the instant of opening. Anti-reaction fittings are used at the outlet of relief valves to avoid generating thrust if the relief valve opens.

3.3.4 PRESSURE TRANSDUCER

The pressure transducer is of the potentiometer type containing a bellows or a bourdon tube pressure sensing element. The applied voltage is 3.2 volts, with power consumption on the order of milliwatts.

Pressure transducers used are in three ranges: 0-50 psi to sense the pressure downstream of pressure regulators, 0-4000 psi to sense the stored gas pressure in the pneumatic attitude control subsystem and 0-600 psi to sense the pressure in the spacecraft Separation Propulsion unit.

3.3.5 FILTERS

Filters are installed to remove any particulate contamination from the gas as it leaves the reservoir. Filtration elements are woven stainless steel wire screens that prevent the passage of particles of a pre-determined size.

3.3.6 PRESSURE REGULATORS

Pressure regulators are single stage units containing two seats in series for redundancy against leakage, the most common failure mode of regulators. Designed for a nominal outlet pressure range of 38 ± 3 psi, the regulator normally utilizes one seat for flow control and lock-up that maintains outlet pressure at 36.5 ± 1.5 psi. If the seat fails, the second seat takes over and maintains outlet pressure in the range of 39.5 ± 1.5 psi.

3.3.7 SOLENOID VALVES

The valves are of the direct acting co-axial type, constructed wherever possible of material compatible with Voyager magnetic constraints. To reduce the magnetic field generated by the valves when energized the following can be done: twist and shield the electrical wires to each solenoid, shield each solenoid valve, arrange pairs of solenoid valves such that their magnetic fields external of the valves mutually cancel each other.

Two types of seat materials will be considered for use in these valves. One is a soft seat (plastic or elastomer) the other is a hard seat (metal to metal). The advantage of the soft seat is that it is more tolerant to contamination, while hard seat valves exhibit better response time characteristics (short and repeatable response action). Although at present hard seat valves are the likely candidates for Voyager, a more careful investigation in this area will be required.

3.3.8 EXPLOSIVE VALVES - See VB235FD104 for details

3.3.9 NOZZLES

The nozzles are made of Titanium having 100:1 area ratios, with 30 degree straight exit cones.

3.4 ASSEMBLY CONSIDERATIONS

To minimize leakage, the interface within system will be hermetically sealed wherever feasible. This will be accomplished by welding of tube and component fittings and soldering or brazing of component body seals. It is planned to use titanium to a large extent in the system. Gas storage tanks, pressure regulators, tubing and fittings made of titanium alloys are already available. The advantages of titanium are its high strength to weight ratio; weldability, machinability, magnetic properties and resistance to corrosion. Other materials will be used, however, as necessary, based on their compatibility with overall Voyager constraints.

Components, wherever possible, will be mounted in clusters. Roll and yaw control solenoids and nozzles, would represent one such cluster, that would be entirely self contained, having one gas inlet connection and one electrical connector, all mounted on a suitable honeycomb bracket with internal interconnecting tubing. Other clusters would consist of pairs of pitch nozzles and corresponding control solenoid valves, regulator,

filter pressure transducer and relief valve assemblies. Each component would first be tested individually for performance, then assembled into the proper cluster. All environmental tests will then be performed on complete clusters.

The tank, tubing and valves are equipped with strip heaters and surrounded with several layers of superinsulation for temperature control.

4.0 INTERFACE DEFINITION

4.1 MECHANICAL

Nozzle Alignment - Mounting Interface with Spacecraft Structure.

4.2 ELECTRICAL

Solenoid Valves - Input: 30 to 45 V from Attitude Control Electronics

Explosive Valve - Input: Pyrocontroller (Capacitor Discharge)

Pressure Transducers - Input: 3.2 V from Attitude Control Electronics
- Output: 0-3.2 V to Data Handling and Storage.

4.3 THERMAL

Stripheaters - Power from Temperature Control Subsystem.

4.4 CAPSULE INTERFACE - Gas from cold gas jet subsystem will not contaminate capsule.

4.5 OSE INTERFACE - The gas jet subsystem shall be charged by the appropriate OSE function as follows:

Attitude Control tanks - Freon-14 @ 2500 psia and 70^oF

Separation Propulsion tanks - Gaseous Nitrogen @ 525 psia and 70^oF.

5.0 PERFORMANCE PARAMETERS

The attitude control cold gas jet subsystem will impart to the vehicle an acceleration $\left(\frac{\text{Torque}}{\text{Inertia}}\right)$ of 0.225 m rad/sec² in each axis. This corresponds to thrust levels per nozzle of 0.0625 pound, 0.0578 pound and 0.0408 pound about the Pitch, Yaw and Roll axis respectively for the spacecraft moments of inertia during cruise, with the nozzles being located on 11 ft. moment arms (cg to thrust center line distance). The angular acceleration increases after capsule separation and expending of retro propulsion fuel. Although the predominant length of valve "on-time" will be 30 ms, the system can tolerate "on-times" as low as 14 ms with good repeatability. Although specific impulse is affected by short "on-times." The decrease of specific impulse occurs because transient (pressure rise and

decay) rather than steady rate conditions, predominate. By making the thrust chamber volume (volume between valve seat and nozzle throat) as small as practically possible, the transient portion of the thrust profile is minimized. Tests at Aerospace Corp. have shown that for pulses of down to 10 ms there was no appreciable decrease in specific impulse.

As shown in Volume B, Section VB234AA104, the reliability of the selected Attitude Control Cold Gas Jet Subsystem and Spacecraft Separation Components is 0.9998 and 0.99967 respectively, based on failure rate data reported in General Electric Reliability Manual TRA873-74 using high-reliability and space application modifiers.

6.0 PHYSICAL CHARACTERISTICS AND CONSTRAINTS

6.1 WEIGHT

Total loaded cold gas jet subsystem weight will be about 102 pounds. Refer to weights table in Section VB220FD103 for weight breakdown by components. The Separation Propulsion Unit will weigh about 3.2 pounds.

6.2 VOLUME

The total volume of the cold gas jet subsystem and Separation Propulsion unit will occupy about 1.75 ft³. Solenoid and relief valve seat leak rate is below 3 scc/hr. Static Seal leakage shall not exceed 1.0 scc/hr.

6.4 POWER CONSUMPTION

Average power consumption is negligible. Peak power required, when three couples are commanded, will be 24 watts.

6.5 CLEANLINESS

Although pneumatic components are not unique in their sensitivity to contamination, their performance characteristics and processing criteria (manufacturing, testing, installation) make contamination the prime hazard to successful performance. Two types of contaminants may be present in the system: 1) those carried in by the actuating gas and contained in the components at assembly and 2) contaminants generated internally by the rubbing, sliding and impact action of component operation.

The amount and size of contaminants carried in and contained in components can be reduced, if not entirely eliminated, by filtration of gas and cleaning components during and after assembly. In addition, precautions shall be taken during every phase of processing, such as inspection, testing and installation, to minimize the possibility of contaminating the components and assembly. The environment in which processing of pneumatics will take place, shall conform to class 10,000 Fed. Std. 209 (10,000 particles per cu. ft. greater than 1/2 micron). Components and assembly shall be protected by filters and shall be

purged and sealed at the end of each stage of processing. To reduce the amount of self-generated contamination will require careful selection of materials in sliding contact with each other and exhaustive determination of surface finishes and forming or machining processes that result in sliding surfaces that are least likely to shed contaminant without exceeding Voyager design constraints or impairing component performance.

7.0 SAFETY CONSIDERATIONS

The pneumatic subsystem as a whole and its individual components, will be extensively proof tested to assure safe operation. Test levels shall be as follows:

<u>Item</u>	<u>Proof Pressure</u>	<u>Burst Pressure</u> (Qual. Unit Only)
Gas Bottle	1-1/2 x oper. press.	2.2 x oper. press.
Components (valves, regulators, etc.)	1-1/2 x oper. press.	2-1/2 x oper. press.
Tubing and Fittings	1-1/2 x oper. press.	4 x oper. press.
Subsystem Assembly	1-1/2 x oper. press.	-

In addition, components using electrical power for actuation or excitation will be subjected to insulation resistance tests at up to 1000 vdc and dielectric strength tests (Hi-Pot) of up to 60 cycles, 1000 vac.

To ascertain personnel safety, proof and burst pressure tests are to be performed in high pressure test cells (Refer to VB291FD105 and VR110VP005 for details).

For loading procedure and handling limitations see VB280FD109 and VB280FD110.

CII-VB234FD105

FUNCTIONAL DESCRIPTION

VOYAGER AUTOPILOT

Index

1. Scope
2. Applicable Documents
3. Functional Description
4. Interface Description
5. Performance Parameters
6. Physical Characteristics and Constraints
7. Safety Considerations

1.0 SCOPE

This document describes the function of the Voyager Autopilot, its functional boundaries, the subsystem performance factors, its interfaces with other subsystems and the physical makeup of the recommended preliminary design.

The function of the Autopilot is to provide control of the velocity increment, both magnitude and orientation, imparted to the vehicle during the propulsion operations of mid-course corrections and of Mars orbit insertion.

A functional block diagram showing the major interfaces and functions of the Autopilot is shown in Figure 1-1.

2.0 APPLICABLE DOCUMENTS

The following documents are applicable to this functional description:

VB220SR101	Design Characteristics
VB220SR102	Design Restraints
VB220SR103	Mid-Course Maneuver Accuracy and Propellant Requirements
VB220FD103	Spacecraft Component Design Para.
VB220FD110	Telemetry Channel Assignment
VB220FD111	Maneuver Execution Accuracy
VB234FD101	Guidance and Control Subsystem

3.0 FUNCTIONAL DESCRIPTION

The Autopilot controls the orientation of the velocity vector to an accuracy of 20 mr 3σ from the position at which autopilot control is started. The magnitude accuracy is less than 1 percent 3σ for velocity increments greater than 1 meter per second and less than 3 percent 3σ in the 0.1 to 1 meter per second range.

The Autopilot receives pitch, yaw, and roll vehicle attitude errors from gyros in the Attitude Control Subsystem from the time that the spacecraft is in proper orientation for propulsion operations until thrust is terminated by a signal generated within the Autopilot. The Autopilot converts the gyro attitude error signals into appropriate flow control commands for the four throttlable midcourse correction engines and to four jet vane actuators for pitch and yaw and for roll control respectively. The magnitude of acceleration is sensed and integrated within the Autopilot Subsystem and is compared with a pre-set desired

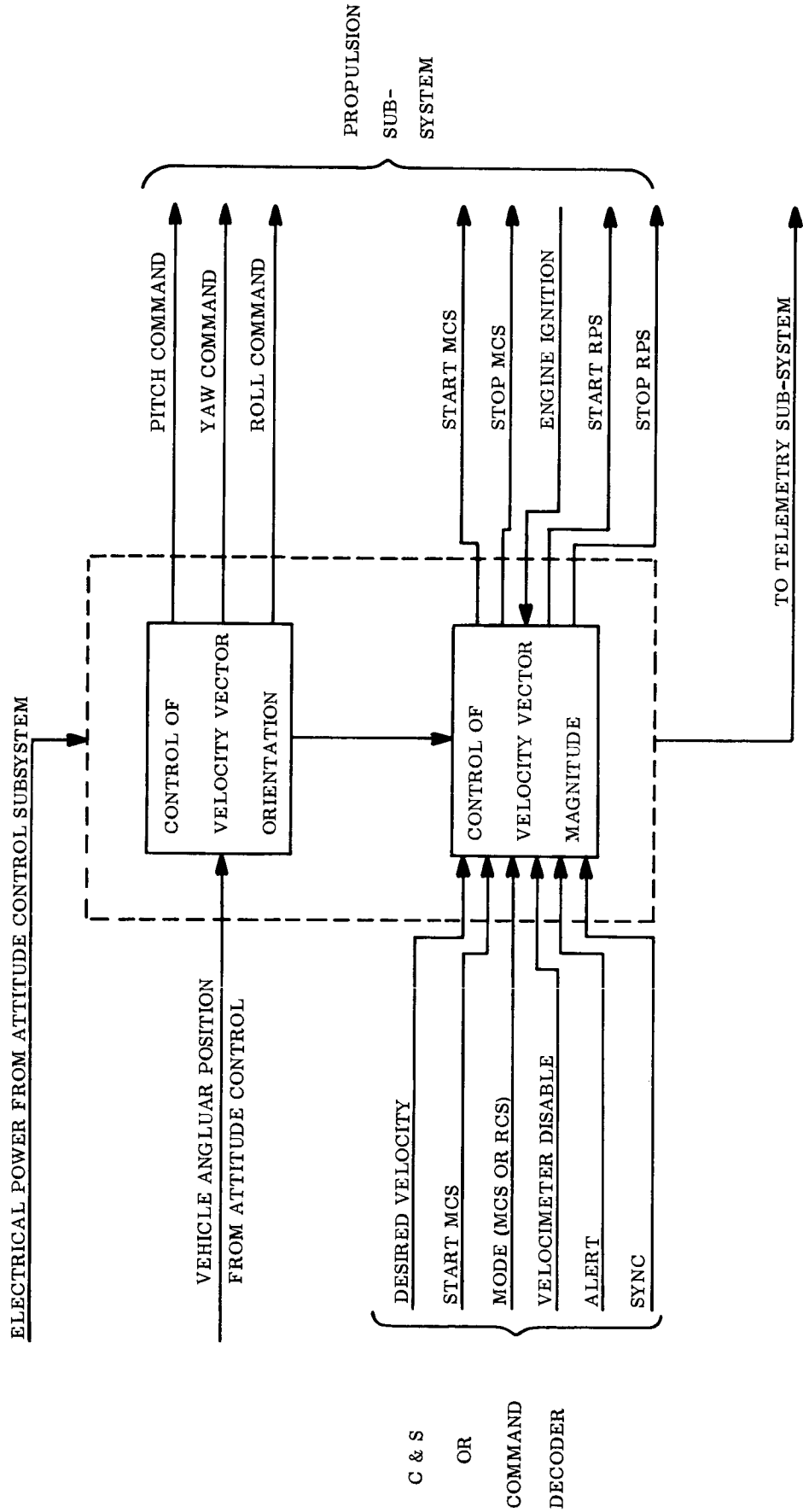


Figure 1-1. Autopilot Functional Diagram

value. When the spacecraft has achieved the desired magnitude of velocity, the Autopilot generates a signal to cause termination of the thrusting. The Autopilot acts in accordance with commands from the C&S or Command Decoder for desired velocity increment, mode (midcourse correction or orbit insertion), engine start and stop commands, and a velocimeter disable command. Diagnostic and status information is provided to the Telemetry Subsystem.

The signal flow diagram of Figure 3-1 shows the implementation of the autopilot. The section dealing with the control of the orientation of the velocity vector increment will be discussed, followed by a discussion of that part which controls its magnitude. The torque for pitch and yaw axis control is generated as shown in Figure 3-2 by differentially throttling pairs of thrusters whose nominal thrust vectors are parallel to the roll axis at a distance of 50 inches and which pass through the pitch and yaw axes. The control loop is designed to have all four engines operating at minimum thrust, 25 pounds, with zero error signal. At saturation actuation signal, 55 pounds thrust is available which is sufficient to offset the disturbance of the Retro Propulsion System 2200 pound thrust-engine with a center of mass uncertainty of location of 0.5 inches. Having the Mid-Course System engines operating at the low end of the throttling range for zero error signal yields least weight when center of mass uncertainties increase with time as happens during RPS engine operation. The amplifiers K_2 of Figure 3-1 contain the lead-lag networks required for pitch and yaw channel servo loop stabilization. The signals for increased thrust are detected and separated by the polarity sensors and are directed to the proper throttle valve amplifiers K_3 . A bias is introduced in each amplifier to insure that a minimum of servo dead zone is present in the pitch and yaw channels of the autopilot. Parallel summing of the control signal and position transducer signal is accomplished in the K_3 amplifiers.

Roll control torques are generated by a single jet vane placed in each of the MCS engines in such a fashion as to develop a lift thrust vector normal to both the engine thrust line and to a line normal to the roll axis passing through the center of lift. The Autopilot receives roll position information from the attitude control subsystem and processes it through the amplifiers K_1 which contain lead-lag networks required for loop stabilization. The amplifiers also have the parallel summing networks for taking the jet vane angle pickoff information to generate the jet vane actuation position error signal. Closed loop control of the jet vane angle then causes roll torque in proportion to roll position and rate.

This mechanization of the control of the orientation of the velocity increment will cause the total force vector applied to the vehicle to pass through the vehicle center of mass

Control of the magnitude of the velocity increment is obtained by sensing the acceleration along the nominal thrust axis, integrating, and comparing the result with the pre-set value to generate a thrust termination signal. The desired velocity is received in pseudo-random pulse code from the command decoder and is shifted into the shift register. The desired velocity is received a second time and as it is shifted into the register, the input pulses are compared with the overflow content and compared. If the overflow is the same as the second word, no alarm is made; if an error is detected, an incorrect velocity alarm is sent to the telemetry subsystem and the process may be repeated.

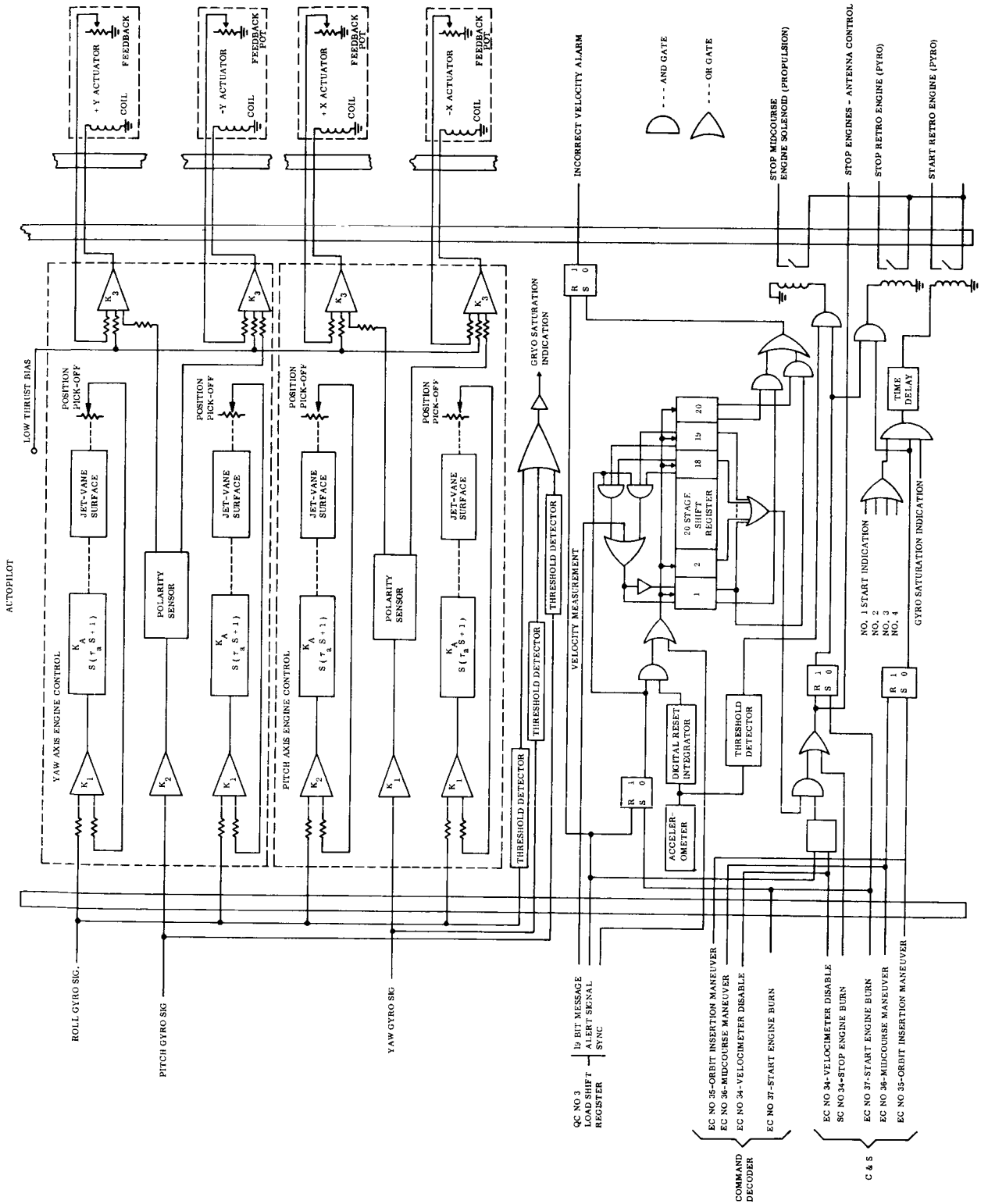
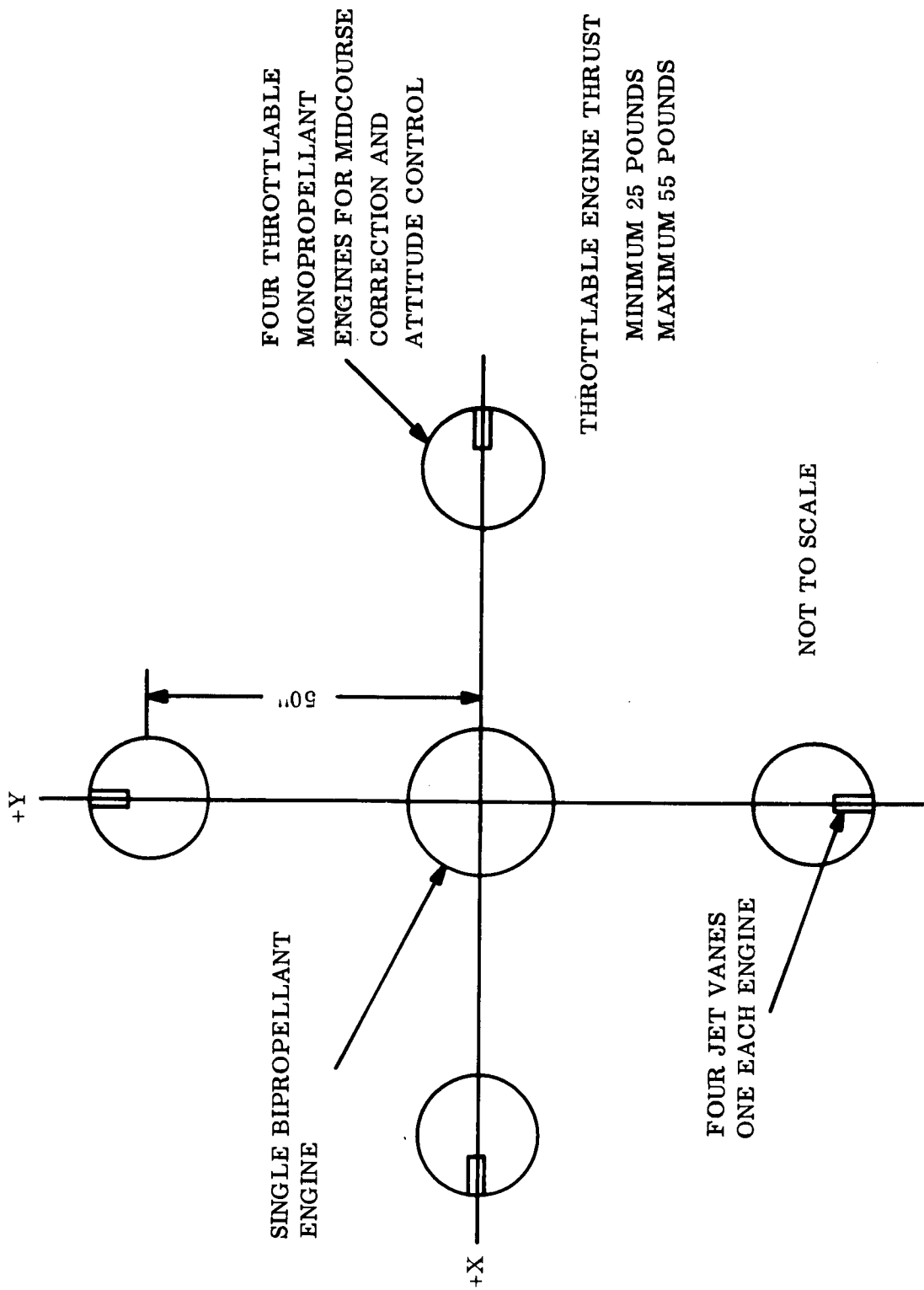


Figure 3-1. Signal Flow Diagram



(LOOKING INTO ENGINE EXHAUST)
Figure 3-2. Engine Configuration

Commands for mid-course corrections mode or retropropulsion mode, engine start and velocimeter disable are received either from the C&S or from the command decoder. Backup engine stop signals from the C&S are processed through the autopilot which will terminate thrust in the event that the velocimeter fails to generate the thrust termination signal. The backup signal is timed to prevent premature shutdown with lowest thrust level expected. In general, this will be 5 percent longer than the nominal time.

Receipt of the engine start signal changes the operation of the shift register to that of a counter. The counter, having been loaded with the 1's complement of the desired velocity, will trigger the logic OR gate when the register indicates all ones. When in the mid-course correction mode, signals are sent to the MCS engine solenoid valves to cause termination of these engines. When in the orbit insertion mode, the engine fire signal causes signals to be sent to the MCS engines and the signal is delayed a sufficient number of seconds before initiating ignition of the RPS engine to cause RPS propellant settling. The outputs of chamber pressure transducers are sent to an OR gate whose output indicates that at least one MCS engine is firing and this output is added with an indication that the gyros are not at their stops in an AND gate. When this logic is satisfied, the vehicle will be under full autopilot control with MCS engines, and RPS engine propellants will have been settled. A signal is then sent to the pyrotechnic subsystem to initiate RPS engine firing. Thrust termination is caused in the same manner as for MCS firing with termination signal going also to the pyrotechnic subsystem for RPS engine. Actual MCS engine shut-off is prevented until the acceleration level indicates RPS engine has terminated.

The sequence of operation of the autopilot is as follows:

Required maneuver velocity is received and stored.

Required maneuver velocity stored is verified.

Autopilot power is received.

Engine start signal is received and sent to MCS engine.

MCS engines start.

RPS engines start, signal sent after time delay (RPS engine mode only).

Stored velocity is achieved.

RPS engine stop signal is sent (RCS engine mode only).

RPS engine thrust terminates (RPS engine mode only).

Sensed acceleration is below threshold value.

MCS engine stop signal sent.

MCS engine thrust terminates.

The autopilot consists physically of 10 operational amplifiers, compensation network, a 20 stage shift register and associated logic circuitry located in Bay 12 and also four jet vane actuators located in the expansion cones of each MCS engine. Micro electronics is used in redundant fashion where voltage and power levels will permit. The jet vane actuators are limited rotation brushless DC torque motor with position feedback transducers.

4.0 INTERFACE DEFINITION

4.1 FUNCTIONAL INTERFACE

The Autopilot has major interfaces with the Attitude Control Subsystem, the Propulsion Subsystem, the vehicle configuration and structure, C&S and command decoder.

The autopilot receives DC signals proportional to roll, pitch, and yaw vehicle attitude error from the Attitude Control Subsystem. The signal must be capable of being processed by the lead lag network of the Autopilot to derive the rate information required for autopilot loop stabilization. In turn, the Autopilot must prevent input axis rotations under disturbance from reaching 50 percent of the linear range of the gyro or about 2 degrees. Further, due to voltage saturation in the Autopilot, vehicle angular rate should be limited. The Propulsion Subsystem interface with the autopilot includes engine start and stop signals, control signals for each of the four MCS throttleable engines and jet vane shaft angle positions. Also, the dynamic properties of the fuels and oxidizer in the tanks affect the Autopilot. Autopilot signals operate directly the MCS start and stop solenoid valves. Fuel flow command signals are sent directly to the MCS flow control valves. Jet vanes actuators provide a shaft angle position in proportion to the autopilot generated error signals which causes roll control torques through the lift action of jet vanes of the propulsion subsystem attached to the actuator shaft.

The vehicle configuration and structure affect the autopilot through the location of principal axes, sensor axes, and control axes. Design philosophy requires that the lowest natural frequency of the structure be above 10 cps which will be above any frequency of interest in the autopilot control loop or that lower frequencies be well damped and constant over the propulsion operation conditions. Higher frequency phenomena during propulsion operation may affect gyro performance, particularly through the effect of the lead networks. When these modes are uncovered in test, they will be filtered electronically or altered mechanically such that autopilot control is not affected.

The nominal alignment of the principal axes, sensor axes and control axes is possible with the recommended configuration. This eliminates the needs for any uncoupling circuitry within the autopilot

An autopilot interface exists between the Command Decoder and the C&S. The command decoder provides the alert signal, sync signal, and the 19-bit message for loading the velocimeter in the primary mode and, in event of C&S failure, further provides signals to start engines, change from MCS to RPS mode, engine start, velocimeter disable and engine stop signals.

The Autopilot is turned on by receipt of power from the Attitude Control Subsystem in two categories: 1) those functions related to the velocimeter which require activation a long period of time prior to use and 2) those remaining parts of the Autopilot which require activation just prior to propulsion operations.

4.2 MECHANICAL INTERFACES

The jet vane actuators mate mechanically with the MCS engines and also with the jet vanes. The Autopilot mechanical interface with the vehicle structure consists of the vehicle mass, moments and products of inertia, center of mass location and uncertainties, and structural resonance phenomena. The structural interface also includes alignment of sensors and rocket motors which affect autopilot operation.

4.3 ELECTRICAL INTERFACES

Gyro outpost signals are received from the Attitude Control Subsystem. Actuation signals generated by the Autopilot are sent to the MCS throttle valves and the signals proportioned to throttle valve position are received by the Autopilot. The MCS start solenoid valves are controlled by the Autopilot. Start and stop signals for the RPS are generated by the Pyrotechnics Subsystem from standard pulses generated by the Autopilot. Basic power for the Autopilot is supplied from within the Attitude Control Subsystem. Commands are accepted from the C & S and also directly from the Command Decoder. Hardwire test points are incorporated for system checkout. Properly buffered signals are provided to the Telemetry Subsystem for transmission.

4.4 AUTOPILOT INPUT INTERFACES

A. Attitude Control Subsystem

Roll, Pitch, and Yaw Attitude Error Signals

Scale Factor 5.3 mv/mr

Linear Range $\pm 4^{\circ}$

Stops $\pm 6^{\circ}$

B. Propulsion Subsystem

MCS Pitch and Yaw Control Torque 125-ft pounds at saturation input

MCS Roll Control Torque 21-ft pounds at saturation input

Misalignment $-.625^{\circ}$ and $.1875$ inch

MCS Engine Firing Indications (4)

MCS Throttle Valve Position (4)

C. Engineering Mechanics

Moments of inertia as below:

MOMENTS OF INERTIA SLUG-FT²

	Roll		Pitch		Yaw	
	Min.	Max.	Min.	Max.	Min.	Max.
MCS operation	3728	3750	5203	5243	4771	4811
RPS operation	1358	1789	971	1311	634	878

Center of Mass location uncertainties as below:

<u>Condition</u>	<u>Uncertainty</u>		
	X Axis	Y Axis	Z Axis
MCS Operations	+ .126 in.	+ .133 in.	+ .741 in.
RPS Start	+ .110	+ .120	+ .761

No structural resonance below 10 CPS unless well damped and possessing invariant characteristics

D. C & S Command Decoder

<u>Source</u>	<u>Command Designation</u>	<u>Function</u>
Command Decoder	QC 3	Alert
		SYNC Pulses
		Velocity Set Command
	EC 35 & EC-36	Mode
	EC-37	MCS Start
	EC-34	Velocimeter Disable

C&S	EC 35 & EC-36	Mode
	EC-37	MCS Start
	EC-34	Velocimeter Disable
	SC-34	MCS Stop

4.5 AUTOPILOT OUTPUT INTERFACES

Propulsion Subsystem

MCS Solenoid Valves

Voltage 30 VDC nominal

Current 1.3A initial

0.3A holding

Opening time 12 MS

Closing time 8 MS

MCS Throttle Valves

Power 1 Watt

Pyrotechnic Subsystem

Standard Pulse Errors Engine Start & Stop

Antenna pointing Subsystem

Standard Pulse At Thrust Termination

Check out and Telemetry

Checkout

<u>Function</u>	<u>Test Point</u>
MCS Engine Control	8 error signals 8 feedback signals
Velocimeter	Engine Cutoff

Telemetry

<u>Function</u>	<u>Channel</u>
Accelerometer Temperature	M701
Pitch Lead Network Output	C11
Yaw Lead Network Output	C12
Roll Lead Network Output	C13
Accelerometer	A5
Velocimeter	A6

5.0 PERFORMANCE PARAMETERS

Under these interface conditions, the Autopilot, having attitude control loop gains of about 6.25 will contribute a pointing error of about $20 \text{ mrad } 3\sigma$ and velocity magnitude error of less than 1 percent 3σ down to velocity corrections of slightly less than 1 meter per second. For a ΔV of 0.1 meter per second a 3 percent 3σ error will result. The closed loop band pass of the pitch and yaw channels of the autopilot is approximately 3.5 rad/sec and for roll, about 1.5 rad/sec.

6.0 PHYSICAL CHARACTERISTICS AND CONSTRAINTS

The autopilot electronics are located in Bay 12 Guidance and Control Equipment Bay. (See Figure 3-6 VB234FD102.) Input power is 6.9 watts average and 14.5 watts peak while dissipated power is 6.7 watts average and 6.9 watts peak.

For purpose of this study, the jet vane actuators are considered a part of the autopilot and these actuators are located on the expansion section of each MCS engine with a total weight for the four of 8 pounds. They consume 14 watts average and 16 watts peak.

7.0 SAFETY CONSIDERATIONS

The only way that the autopilot could present a safety hazard would be a premature engine firing in that the firing signals are processed by the autopilot. MCS engine firing is prevented by not having power available for application to the solenoid valves until ready for use.

The RPS engine cannot be fired prematurely due to safety provisions in the pyrotechnic subsystem.

VB234FD106

VB234FD106

APPROACH GUIDANCE SUBSYSTEM

Index

- 1 **Scope**
- 2 **Applicable Document**
- 3 **Functional Description**
- 4 **Interface Definition**
- 5 **Performance Parameters**
- 6 **Physical Characteristics**
- 7 **Safety Considerations**

1.0 SCOPE

This section describes the Approach Guidance Subsystem, the function of which is to provide precise navigational measurements during the planetary approach phase of the interplanetary trajectory. These data, together with the radio guidance data from the Deep Space Instrumentation Facility (DSIF), will allow a more accurate determination of the required bus orbital insertion and capsule deflection maneuvers than DSIF data alone can provide. As a result, the accuracy of the capsule landing site and the bus orbit will be improved.

2.0 APPLICABLE DOCUMENTS

VB234FD101	Guidance and Control Subsystem
VB220SR101	Design Characteristics
VB220SR102	Design Restraints
VB220FD110	Telemetry Channel Assignments
VB220FD112	Flight Sequence

3.0 FUNCTIONAL DESCRIPTION

The Spacecraft Approach Guidance Subsystem consists of on-board angle measuring and data-processing equipment. The sensor measures the direction of a vector from the spacecraft to Mars with respect to a celestial coordinate system. This measurement is independent of spacecraft attitude as long as the sensor field-of-view limitations are not exceeded. The measured angles are used in the orbit determination program to improve the estimate of impact parameter vector.

The DSIF measures range and range-rate between Earth and the spacecraft. These measurements, combined with the ballistic constraints of free fall through space, determine the velocity and the three components of spacecraft position to a reasonable accuracy. If DSIF provides a dispersion of 350 km in the impact parameter, a single on-board sensor measurement taken just before capsule separation will reduce this dispersion to about 35 km.

The Approach Guidance Sensor is a modification of the "Optical Inertial Space Sextant."¹ It has covers to protect the optics during the launch and transit modes. These covers are jettisoned 4.5 days prior to Mars encounter. Power is applied to the sensor 4 days prior to encounter, at a distance of approximately 1,000,000 km from Mars. Measurements are taken over a range of 500,000 km to 200,000 km from Mars which covers a time period of approximately 2 to 0.8 days to encounter.

The sensor contains three optical assemblies which, by means of fiber optics, present a non-overlapping field array to a single vidicon image tube as shown in Figure 3-1. The optical assemblies simultaneously view Mars, Canopus and the Sun. Although Mars and the Sun will provide considerably brighter images than Canopus, their brightness is reduced to approximately that of Canopus by the use of smaller apertures and optical filters. No electrical compensation is required when passing from one field to the next.

¹ See NASA Contractor Report No. CR-133, "Optical Inertial Space Sextant for an Advanced Space Navigation System" by W. D. Foley, et al, of the Armament Control Product Section of the General Electric Company under contract No. NA52-1087 from the Ames Research Center of NASA.

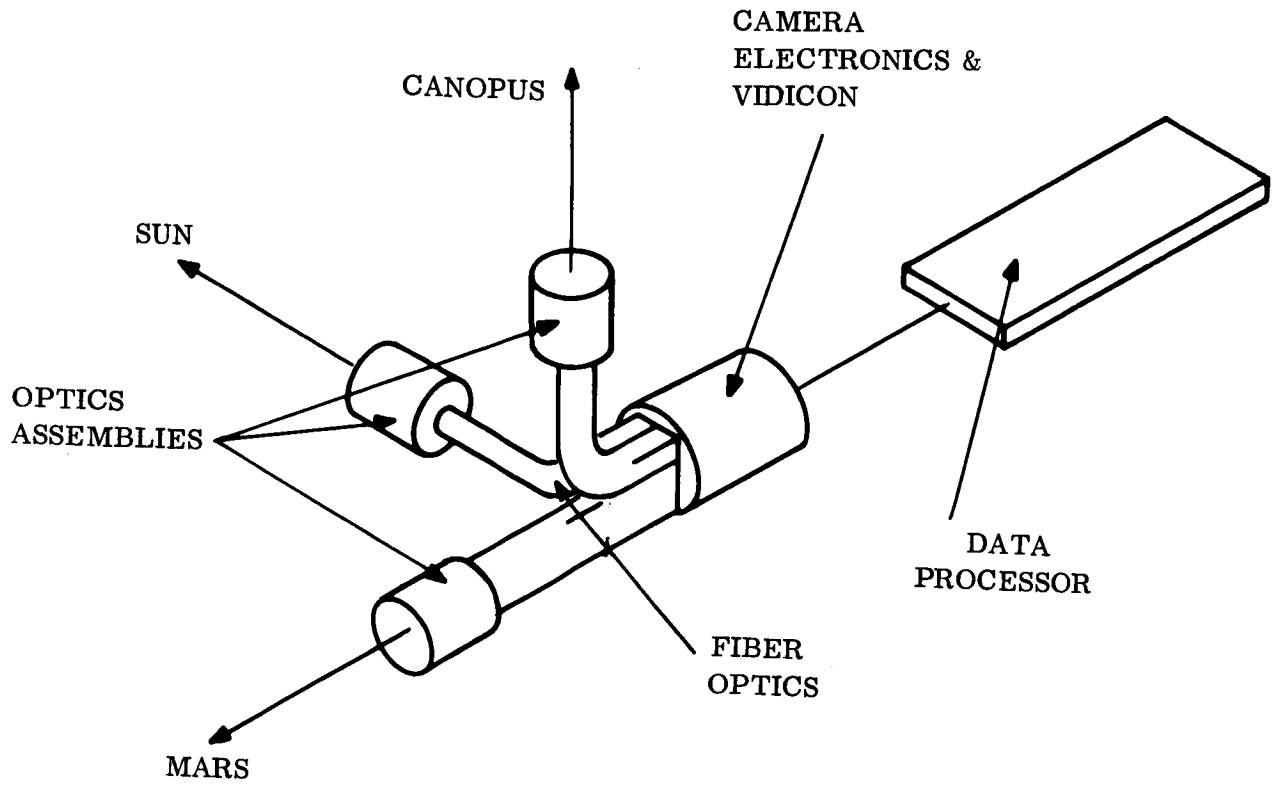


Figure 3-1. System Concept

The vidicon, which has an integral reticle pattern to initialize and linearize the sweeps, serves as the primary sensing element. The video output of the vidicon is amplified by a chain of camera electronics. Pulse center-detection circuits generate pulses which define the Canopus and solar disc centers, as well as the planet edge crossings. These signals are provided to a digital data processor which relates them to pulses obtained from the reticle pattern and provides the image plane coordinates of these points as output words. The data is read out of the processor serially to the Telemetry Subsystem and transmitted in real time. During readout the processor is inhibited from updating the data. A full frame of data includes the address of the center of Canopus, the address of the center of the Sun and the addresses of six points on the horizon of Mars. Figure 3-2 is a block diagram of the sensor, while Figure 3-3 shows the field array.

The field-of-view is made narrow to obtain the best accuracy. The fields of view indicated in Figure 3-3 have been chosen to account for the target size, the target motions during the approach phase of the trajectory from 500,000 km to 200,000 km, the spacecraft attitude control errors, and sensor misalignments. They are not large enough, however, to account for the variations in approach geometry due to the various possible launch and arrival dates. Thus, pre-launch adjustments of the sighting directions are required for the Mars and Canopus optics. Since the integrity of the spacecraft shroud cannot be violated, this adjustment is done remotely. Two possibilities are under consideration. The first is to take advantage of the flexibility of the fiber optics and actually deflect the optics, while the second possibility would be to rotate an optical wedge assembly in front of the optics. Further study is required in this area before the appropriate technique may be chosen.

4.0 INTERFACE DEFINITION

4.1 MECHANICAL

The sensor reference axes will be parallel to the attitude control axes to within ± 0.05 degrees.

4.2 ELECTRICAL POWER

The sensor will operate from 50 VRMS, 2400 cps power and consume approximately 20 watts. Power will not be supplied during the cruise mode, but will be applied four days prior to Mars encounter.

4.3 PYROTECHNICS

The pyrotechnic subsystem shall remove the Approach Guidance Sensor covers 4.5 days prior to Mars impact.

4.4 TELEMETRY SUBSYSTEM

The Approach Guidance data (160 bits) will be provided on a single output line. The Telemetry Subsystem will provide sync pulses which will be used to establish the readout rate and a voltage level which will be used to inhibit updating of the data.

4.5 LCE

Four hardwire lines will be provided for remotely adjusting the sensor orientation.

5.0 PERFORMANCE PARAMETERS

Range of Operation - the design range is 500,000 to 200,000 km from Mars.

Accuracy - the sensor measurements will allow ground calculation of the true center of Mars with respect to celestial references to within at least 0.3 milliradians.

Angular Motion of Mars - the Mars clock angle variation will be approximately one degree maximum while the Mars cone angle variation is approximately 1.5 degrees maximum during the planetary approach phase.

Angular Motion of Canopus - the Canopus cone angle will vary less than 1 degree during the approach phase

Target Size - the angle subtended by the Sun is approximately 0.35 degrees, while the Mars subtended angle will vary from 0.766 to 1.94 degrees over the range of operation.

Vehicle Stability - the vehicle must be stabilized to a Sun-Canopus reference to within ± 0.75 degrees, with slew rates not exceeding 0.03 degrees/second.

Fields-of-View - the Sun field is 2.0 x 2.0 degrees, the Canopus field is 3.5 x 2.0 degrees, and the Mars field is 5.5 x 5.5 degrees.

Optical Apertures - the aperture for the Canopus optics will be one inch. The Sun and Mars optical apertures will be smaller and depend upon the efficiency of the optical filters chosen to reduce the brightness of their images.

Focal Length - the focal length of the combined field is 4.34 inches.

Quantization - the composite field-of-view will be quantized into 1024 parts in both the x and y directions.

Output Word Length - the address of each data point consists of a 20-bit word, with 10 bits defining the x position and 10 bits defining the y-position. A total of 20 eight-bit words will be transmitted per observation defining the addresses of the Sun, Canopus and six points on the Mars limb.

Frame Rate - the frame rate is four frames/second.

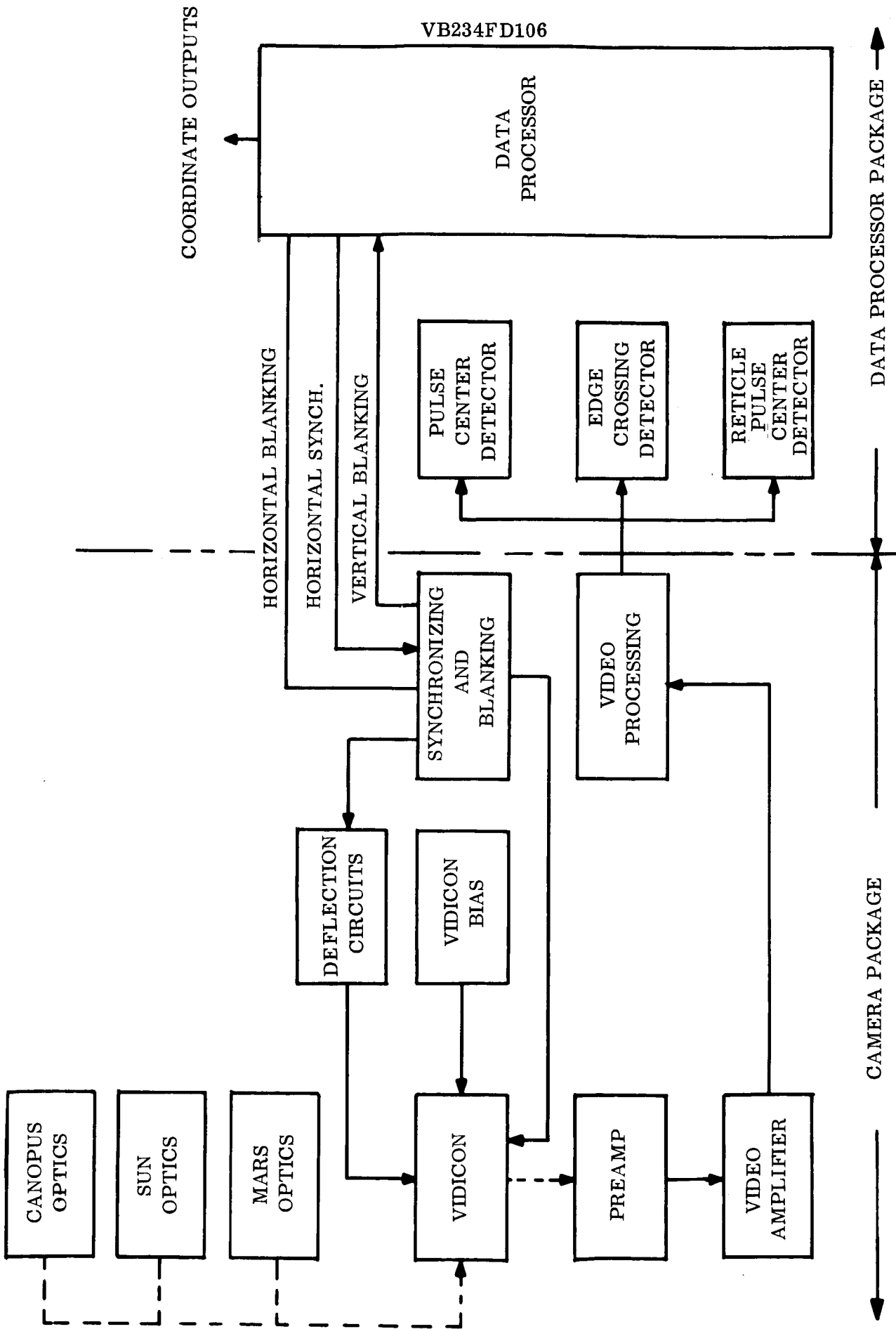


Figure 3-2. System Block Diagram

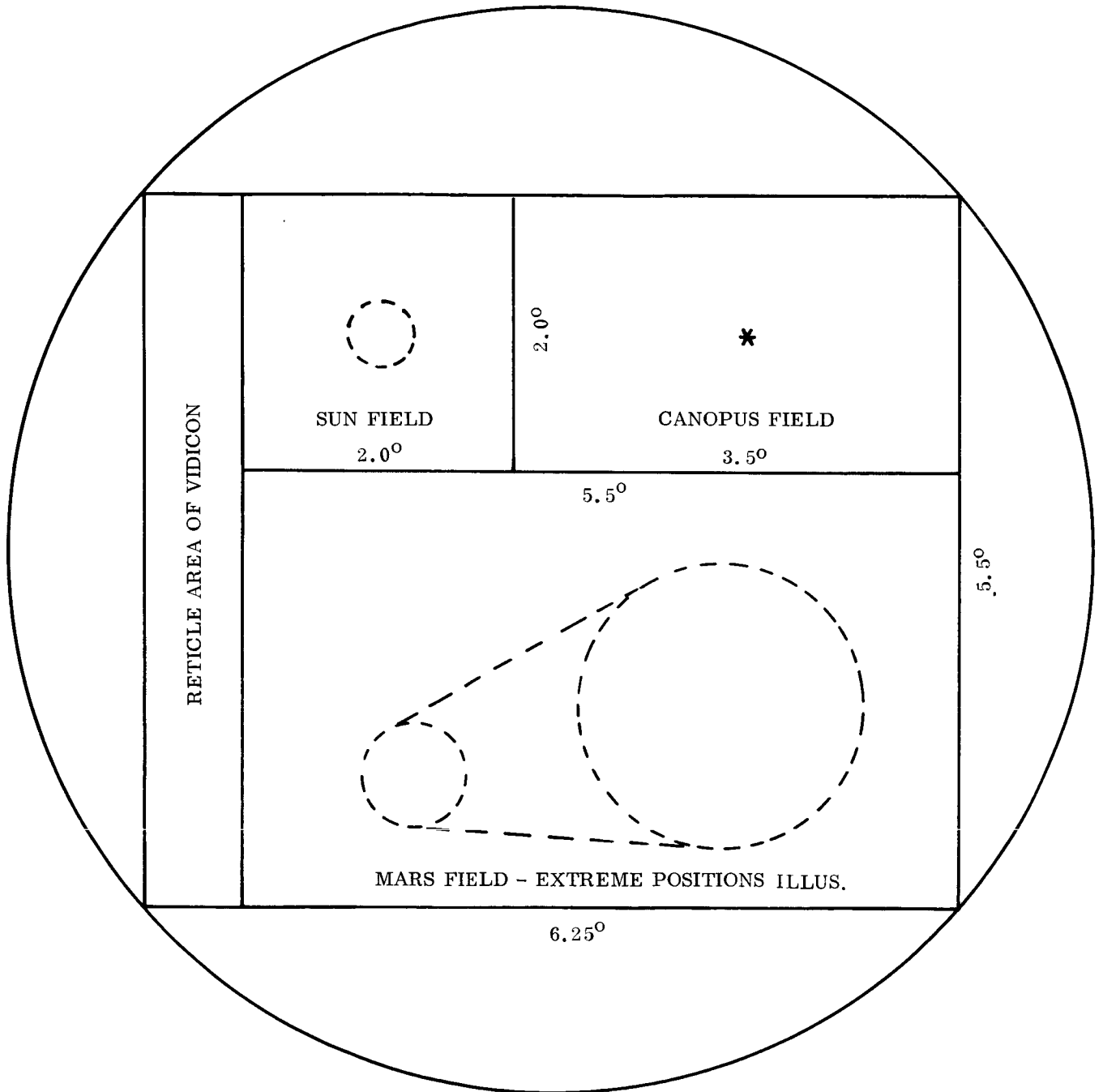


Figure 3-3. Combined Fields of View

6.0 PHYSICAL CHARACTERISTICS

The size, weight and power for the sensor is as follows:

	Size (in)	Weight (lbs.)	Power (watts)
Optics/Vidicon Camera Assembly	10 x 10 x 16	19	15
Data Processor	<u>2.5 x 6 x 20</u>	<u>6</u>	<u>5</u>
Totals	1900 cu. in.	25 lbs.	20 watts

7.0 SAFETY CONSIDERATIONS

The Approach Guidance Subsystem presents no pre-launch safety hazards to personnel, equipment, or facilities.

CII - VB234FD107

CONTROLLER AND SEQUENCER SUBSYSTEM

Index

- 1 Scope
- 2 Applicable Documents
- 3 Controller & Sequencer Functional Description
- 4 Interfaces
- 5 Performance Parameters
- 6 Physical Characteristics & Restraints

*Note: CBS shall have
ability to send many controls
to Earth via telemetry to assist in
condition*

1.0 SCOPE

A functional description of the Controller & Sequencer; and definitions of interfaces, performance parameters, and physical characteristics and restraints therefor are contained in this document.

2.0 APPLICABLE DOCUMENTS

- VB220SR101 - Design Characteristics
- VB220SR102 - Design Restraints
- VB220FD112 - Flight Sequence
- VB233FD103 - Flight Command Subsystem

3.0 CONTROLLER & SEQUENCER FUNCTIONAL DESCRIPTION

The Controller & Sequencer (C & S) Subsystem receives command data from the Flight Command Subsystem, stores the data in an electrically alterable memory, and reads out at times specified by the data, commands to other subsystems on the spacecraft; and provides cyclic timing and control signals to other spacecraft subsystems. Command execution times are determined by comparing time tags contained in the stored command data words with either the Master Timer, which operates continuously throughout the mission, or the Sequence Timer, which only operates during a maneuver sequence of events or during the orbital phase of the mission when it is recycled once per orbital period. The timer to which each command is keyed is specified by one bit in the stored command data word.

Figure 3-1 is a block diagram of the C & S. The C & S has two modes of operation:

1. The Memory Update Mode is used when new command data are being written into the C & S magnetic core memory
2. The Memory Scan Mode is used when the memory contents are being examined for commands requiring execution.

A pulse appearing on the alert line from the Flight Command Subsystem places the C & S in the Memory Update Mode. The alert pulse is followed by a command data word (described in Figures 3-2 and 3-3). The first ten bits of the command data word are shifted into the Address PNG (pseudo-noise generator) which functions as a simple shift register in the Memory Update Mode. The last 27 bits of the command data word are written serially in the address of the Memory or Memories specified by the bits in the Address PNG. This procedure is repeated each time a pulse appears on the alert line. If two successive alert pulses do not occur within a fixed period (approximately two minutes), the Memory Scan Mode is automatically initiated by the C & S.

In the event that an ^{invalid} bit is detected by the Flight Command Subsystem while a command data word is being relayed to the C & S, an "erase" signal from the former to the latter subsystem results in erasure of the memory address contents if more than ten bits of the command data word have been received by the C & S. Erasure consists of writing all "zeroes" in the address. If ten or fewer bits have been received by the C & S, no action is required because no part of the invalid word has been written in the Memory or Memories.

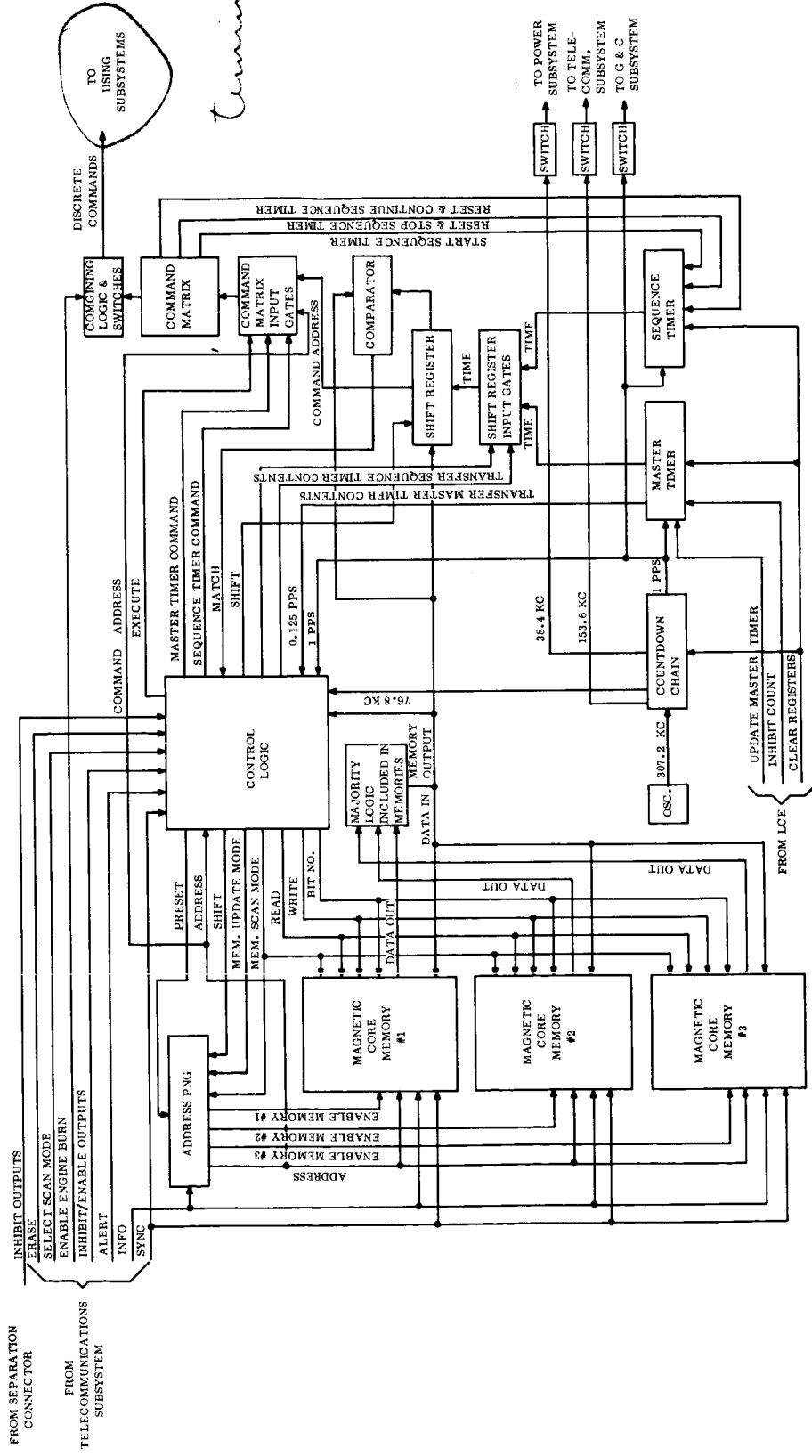
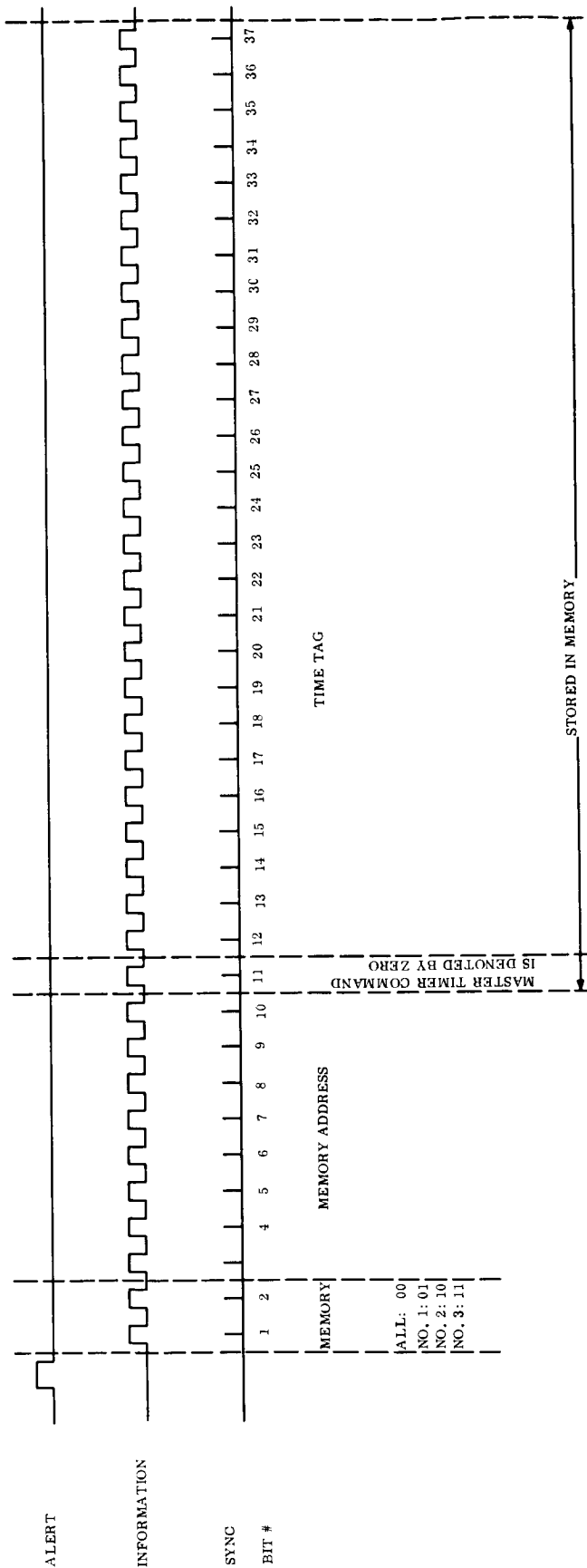


Figure 3-1. Controller and Sequencer

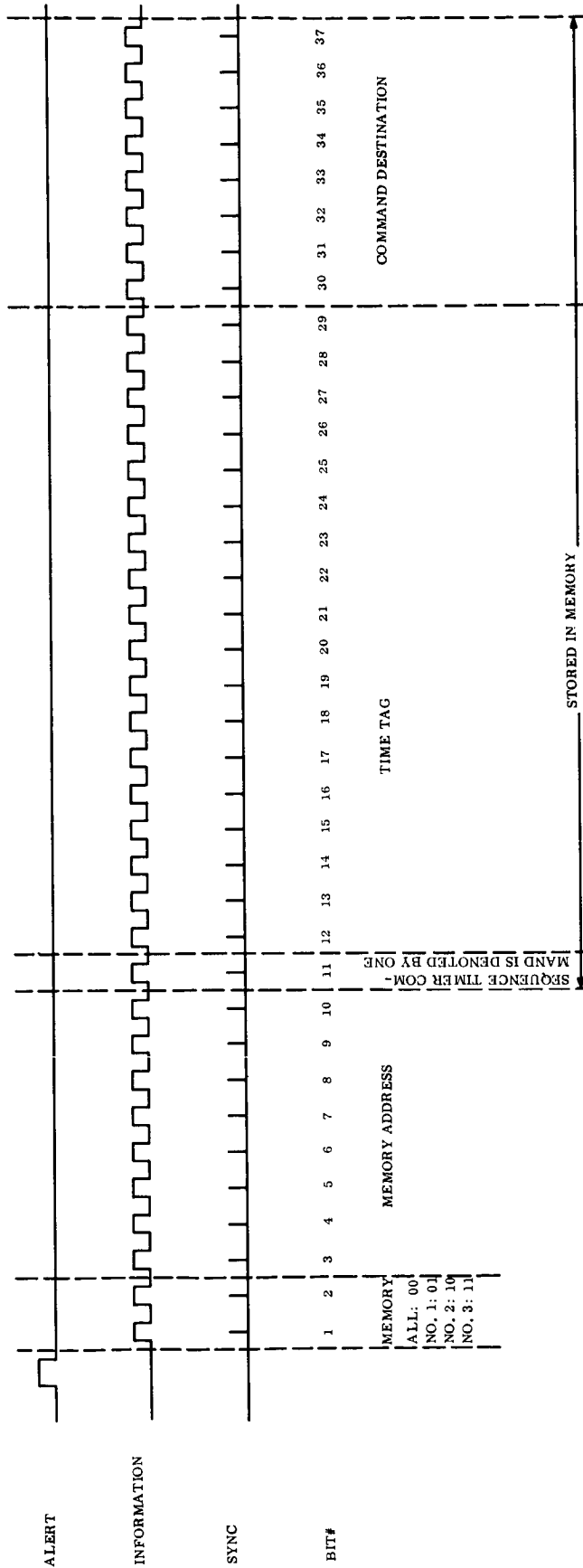


A Master Timer Command data word consists of 37 bits. The first two bits specify the Memory or Memories in which bits 11 to 37 are to be stored. Critical command data words are transmitted three times and stored in a different Memory (but same Memory address) each time. Other command data words are transmitted once and stored in all Memories simultaneously. Bits 3 to 10 specify the memory location in which bits 11 to 37 are to be stored. The memory location of a Master Timer Command also determines the destination of the command. Bit 11 specifies the timer to which the command is related. A "zero" in bit 11 denotes Master Timer; a "one" denotes Sequence Timer. Bits 12 to 37 specify the reading of the Master Timer when the command is to be executed.

A pulse will appear on the alert line prior to any data transfer to the C & S. While the C & S is receiving data no pulses will appear on the alert line.

The 37-bit word will appear on the information line and each bit will bracket a pulse appearing on the sync line.

Figure 3-2. Master Timer Command Data Word Structure



A Sequence Timer Command data word consists of 37 bits. The first two bits specify the Memory or Memories in which bits 11 to 37 are to be stored. Critical command data words are transmitted three times and stored in a different Memory (but same Memory address) each time. Other command data words are transmitted once and stored in all Memories simultaneously. Bits 3 to 10 specify the memory location in which bits 11 to 37 are to be stored. Bit 11 specifies the timer to which the command is related. A "one" in bit 11 denotes Sequence Timer; a "zero" denotes Master Timer. Bits 12 to 29 specify the reading of the Sequence Timer when the command is to be executed. Bits 30 to 37 specify the destination of the command.

A pulse will appear on the alert line prior to any data transfer to the C & S. While the C & S is receiving data no pulses will appear on the alert line.

The 37-bit word will appear on the information line and each bit will bracket a pulse appearing on the sync line.

Figure 3-3. Sequence Timer Command Data Word Structure

In the Memory Scan Mode, the Address PNG, functioning as a pseudo-noise generator, is shifted 255 times following the occurrence of each one-second pulse from the Countdown Chain, thereby generating 255 different memory address numbers. Between Address PNG shifts, the contents of the memory address (in all memories) specified by the PNG are examined for coincidence of command time tag and the time registered by the pertinent timer. The first bit of the word in the memory address is read out and rewritten in its original location. The contents of the timer specified by this bit are transferred in parallel to the Shift Register so that the least significant time bit is contained in the output stage of the register. The second bit of the memory word is read out and rewritten. This bit (the least significant bit of the command time tag) is compared with the number in the output stage of the Shift Register. If a mismatch is detected, readout of the memory address is discontinued and the Address PNG is shifted. If a match is detected, the Shift Register is shifted once placing the next least significant time bit in the output stage of the register and the memory output in the input stage. The third bit of the memory word is read out (and rewritten) and compared with the number in the Shift Register output stages. Once again, if no match is detected, readout of the address is discontinued. If a match is detected, the Shift Register is shifted and the next bit of the memory word is read out and rewritten.

The readout of time tag bits from the memory and comparison with time bits continues until a mismatch occurs or a complete match of time tag and time is found to exist. When the time tag of a Master Timer Command matches the time registered by the Master Timer, an execute signal is immediately conveyed to the destination determined by the Command Matrix and Combining Logic from the number in the Address PNG. When the time tag of a Sequence Timer Command matches the time registered by the Sequence Timer, the last eight bits (command destination) of the memory word are read out (and rewritten) and shifted into the Shift Register. An execute signal is then conveyed to the destination determined by the Command Matrix and Combining Logic from the eight destination bits contained in the Shift Register. Whenever an execute signal is generated, scanning of the memory contents is suspended until the start of the next one-second interval.

Unless a complete match is detected and an execute signal generated, the time tag of every command stored in the memory is examined once a second for coincidence with the time registered by the pertinent timer. Examination of one memory word requires from 150 to 490 microseconds. One complete scan cycle, therefore, requires from 38 to 125 milliseconds, approximately. Thus, the memory is dormant during a large portion of each one-second interval.

The Master Timer is a 26-stage counter which counts pulses occurring once per second. It is started shortly before launch and continues to operate throughout the mission. Commands which are keyed to the Master Timer are, for the most part, predictable as to timing of execution.

The Sequence Timer is an 18-stage counter which also counts pulses occurring once per second. Commands pertaining to maneuver or orbital events are keyed to the Sequence Timer. The timer is started by a Master Timer Command to initiate a maneuver sequence or orbital operation. At the completion of a maneuver sequence the timer is reset and halted by a Sequence Timer Command. During orbital operation, the timer is in continuous operation but is reset to zero once per orbit by a Sequence Timer Command.

Most of the Master Timer Commands and those Sequence Timer Commands which pertain to maneuver events and are predictable with respect to the start of a maneuver sequence are loaded into the Memory from the LCE via the Flight Command Subsystem prior to launch. Other commands are loaded at appropriate times after launch by ground command via the Flight Command Subsystem. Words containing "all ones" or "all zeroes" are written into all memory addresses not occupied by active commands.

Prior to launch, a voltage level change on the "inhibit count" line from the LCE inhibits the 1-pps signal from the Countdown Chain to the Master Timer. A few seconds after initiation of the inhibit signal, the Countdown Chain and the Master Timer are preset, and the Sequence Timer is stopped (if counting) and cleared by a pulse on the "clear registers" line from the LCE. The Master Timer is then updated by pulses on the "update pulses" line from the LCE. The timer is started by removing the inhibit voltage level. The inhibit signal is restored during "holds" in the pre-launch procedure to maintain synchronism of the timer with launch time.

All C & S outputs except telemetry and cyclic outputs are inhibited by a circuit using the spacecraft-booster separation connector. At separation, the circuit is interrupted and the inhibit removed.

3.1 COMPONENT FUNCTIONS

Detailed functional logic of the C & S components is shown in the accompanying figures and described briefly in the following paragraphs. Redundancy approaches are also described. In general, redundancy is applied wherever a failure can disable several or all of the C & S functions. Redundancy is not applied to the individual command outputs. Logic symbols used herein are identified in Figure 3-4.

3.1.1 ADDRESS PNG

Figure 3-5 is a functional logic diagram of the Address PNG. The Address PNG receives shift pulses, preset pulses, and signals denoting operating mode from the Control Logic, and information pulses from the Flight Command Subsystem. It provides enable signals to the three Memories, and eight-bit memory address numbers to the three Memories, to the Control Logic, and to the Command Matrix Input Gates.

Shifting or presetting of the Address PNG is triggered by the trailing edge of a positive pulse appearing on the "shift Address PNG" or "Preset Address PNG" line, respectively. In the Memory Update Mode, it functions as a simple shift register. The first ten bits of each command data word are shifted into the register. The contents of stages 9 and 10 are decoded to determine the Memory or Memories which shall store the last 27 bits of the command data word. The contents of stages 1 to 8 specify the memory address in which the 27 bits are to be written.

In the Memory Scan Mode, all Memories are enabled regardless of the contents of stages 9 and 10. Stages 1 to 8 function as a pseudo-noise generator. The outputs of stages 1 and 8 are combined in an "exclusive OR" to form the input of stage 1. Each shift pulse applied to

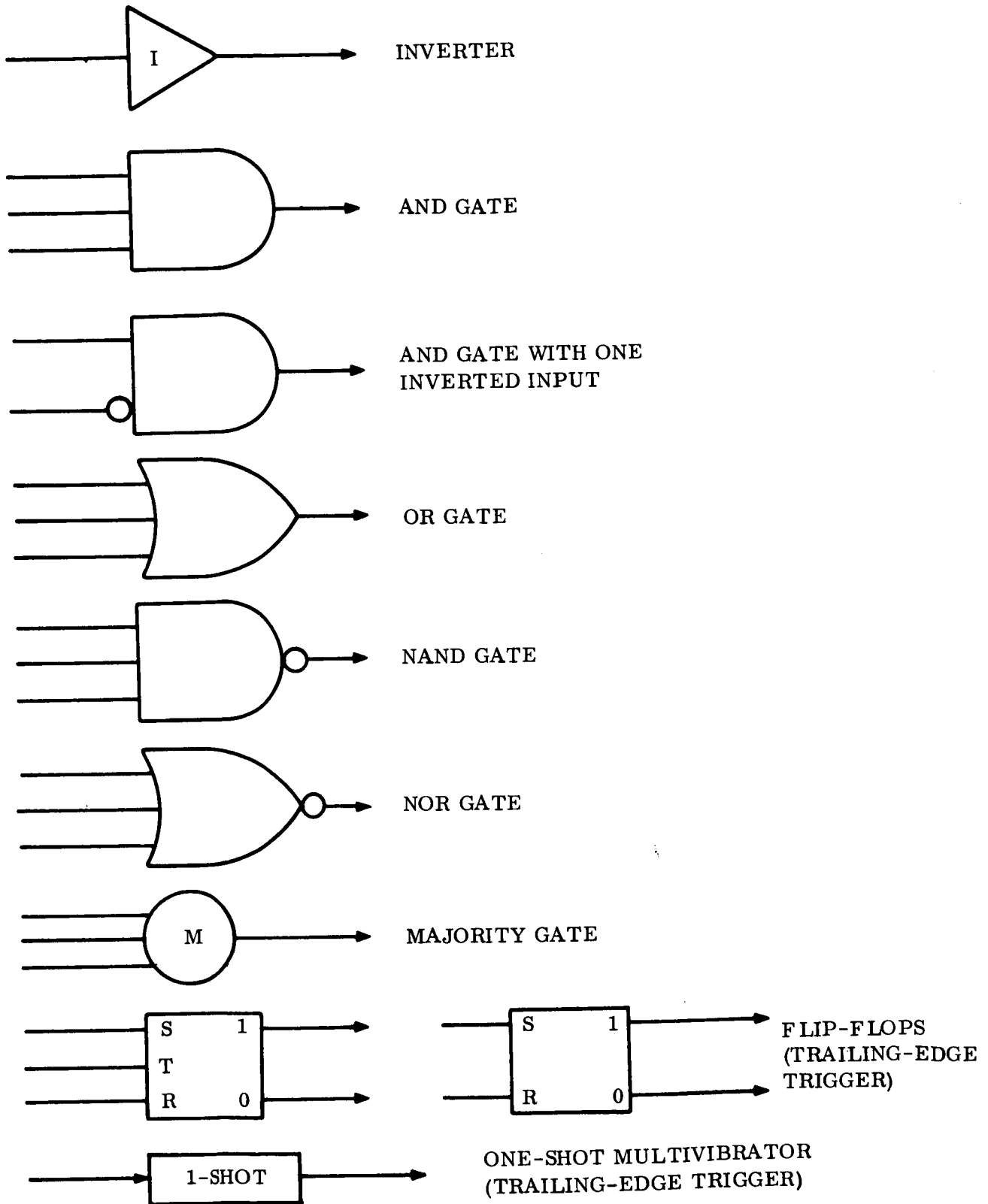


Figure 3-4. Logic Symbols

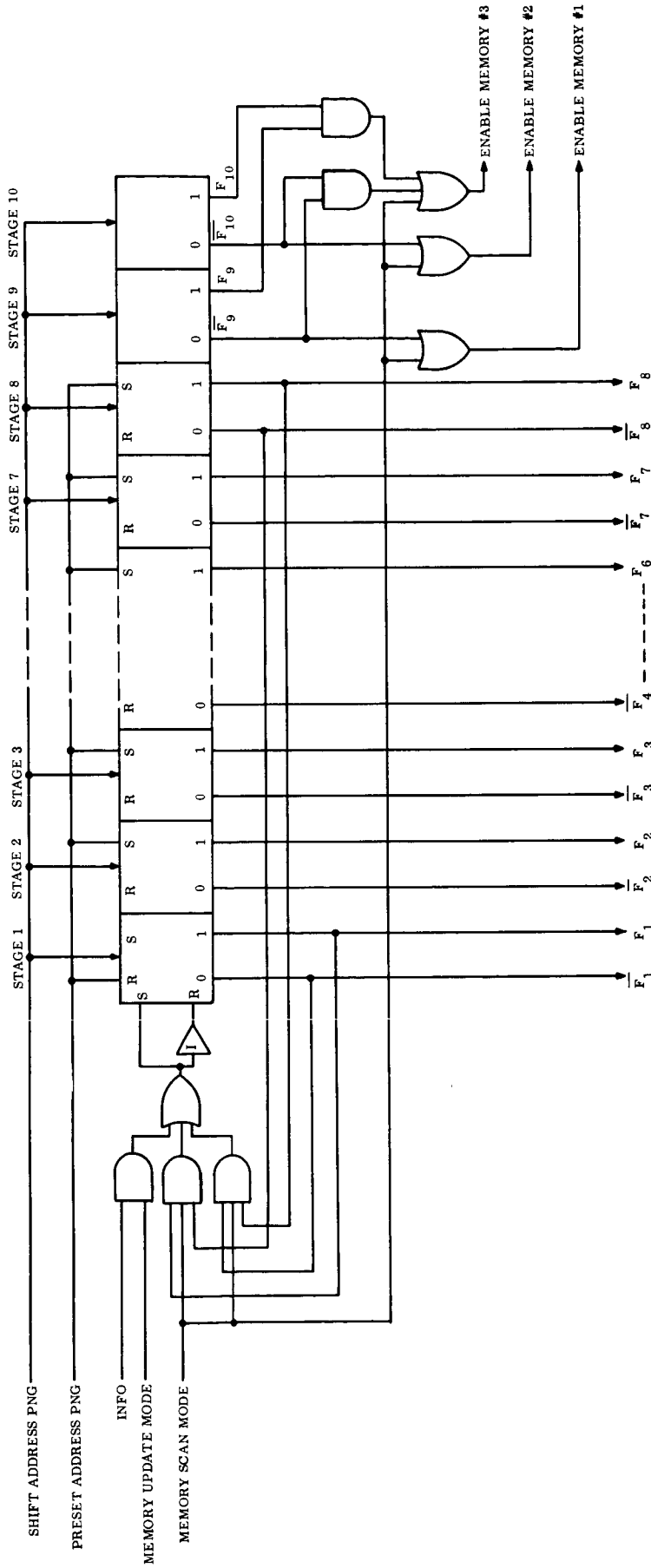


Figure 3-5. C & S Address PNG

the Address PNG produces a different state of stages 1 to 8. All possible states of stages 1 to 8 except the "all-zeroes" state can be generated in this way. Thus, 255 different memory addresses can be specified by the Address PNG.

Redundancy approaches are shown in Figures 3-6 and 3-7. Three complete Address PNG's are used with voting in triplicate between stages 3 and 4 and stages 7 and 8. The majority gates and inverters used for this internal redundancy also provide the redundant outputs from stages 3 and 7. Voting in triplicate is performed on the three sets of outputs of stages 1, 2, 4, 5, 6, and 8 to provide the redundant outputs of these stages. Voting in triplicate is also performed on the three sets of outputs of the logic connected to stages 9 and 10 to provide the redundant memory enable signals.

3.1.2 MEMORY

Figure 3-8 is a block diagram of the Memory. Each Memory is composed of a core matrix, read and write word selector switches, read and write bit selector switches, diode matrix, word and bit number decoder gates, current stabilizers, sense amplifier, and output flip-flop and associated gates.

The core matrix is arranged in 255 words with 27 bits per word. That is, 255 word lines (X-lines) each thread 27 cores, and 27 bit lines (Y-lines) each thread 255 cores. The total number of cores is 6885. A single sense winding threads every core in the matrix.

The cores are addressed serially. A core is read out (or placed in the "zero state") by coincidence of aiding half-select read currents in the X-line and the Y-line which intersect at the core. A "one" is written by coincidence of aiding half-select write currents (opposite in polarity to read currents) in the X- and Y-lines. A "zero" is written (i. e., the core is left in the "zero" state) by omitting the half-select write current in the Y-line.

Figures 3-9 and 3-10 indicate the selection of X- and Y-lines, respectively. Closure of two switches is required to provide half-select current in an X-line. One of the switches is selected by decoding four bits of an 8-bit word contained in the address PNG. The second switch is selected by decoding the other four bits of the 8-bit word. Closure of one switch is required to provide half-select current in a Y-line. The switch is selected by decoding a 6-bit number in the 6-stage counter of the control logic.

In the Memory Update Mode. the output flip-flop is set by a "one" information bit in conjunction with a sync bit. The core being addressed is then read out. Sense amplifier output is inhibited in this mode so that the flip-flop is unaffected by readout (or clearing) of a core. The content of the flip-flop is then written into the core being addressed and the flip-flop is reset by the trailing edge of the write pulse.

In the Memory Scan Mode, the sense amplifier output is not inhibited. The output flip-flop is set by readout of a "one" from the core being addressed. The content of the flip-flop is then rewritten in that core and the flip-flop is reset by the trailing edge of the write pulse.

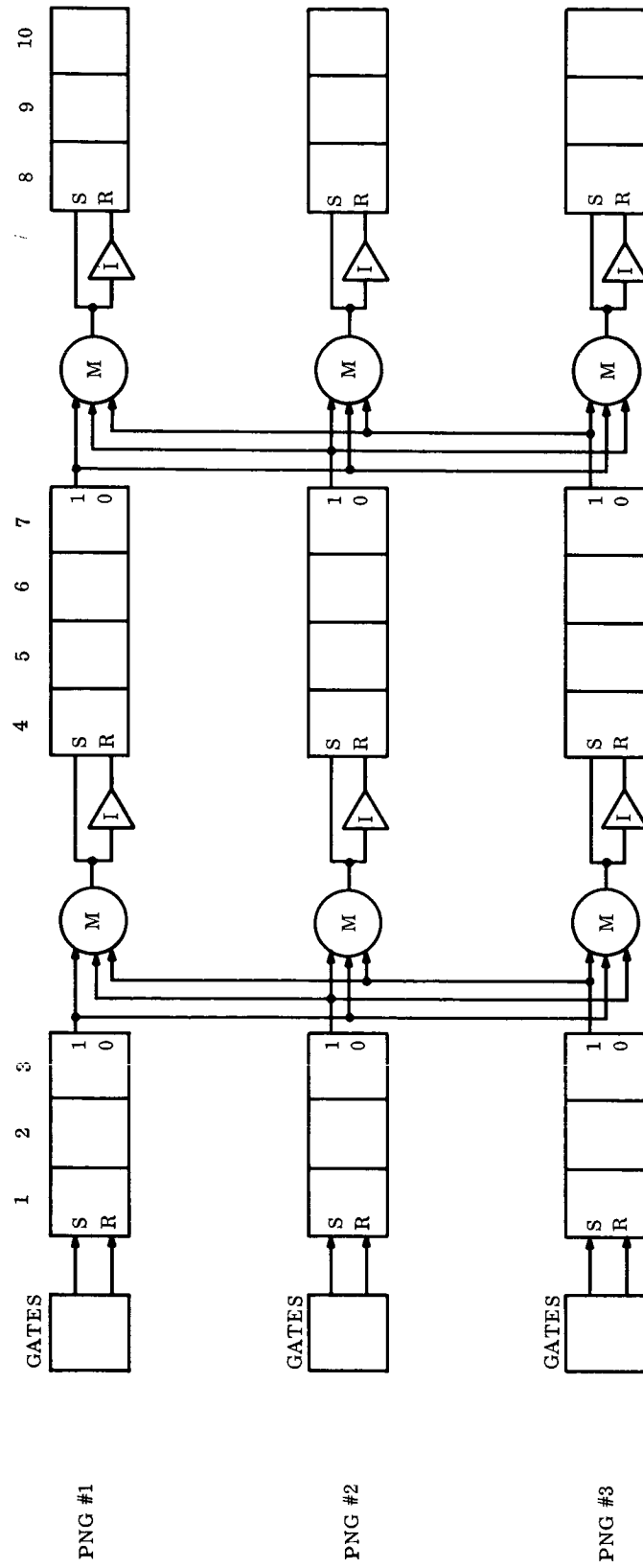


Figure 3-6. C & S Address PNG Internal Redundancy

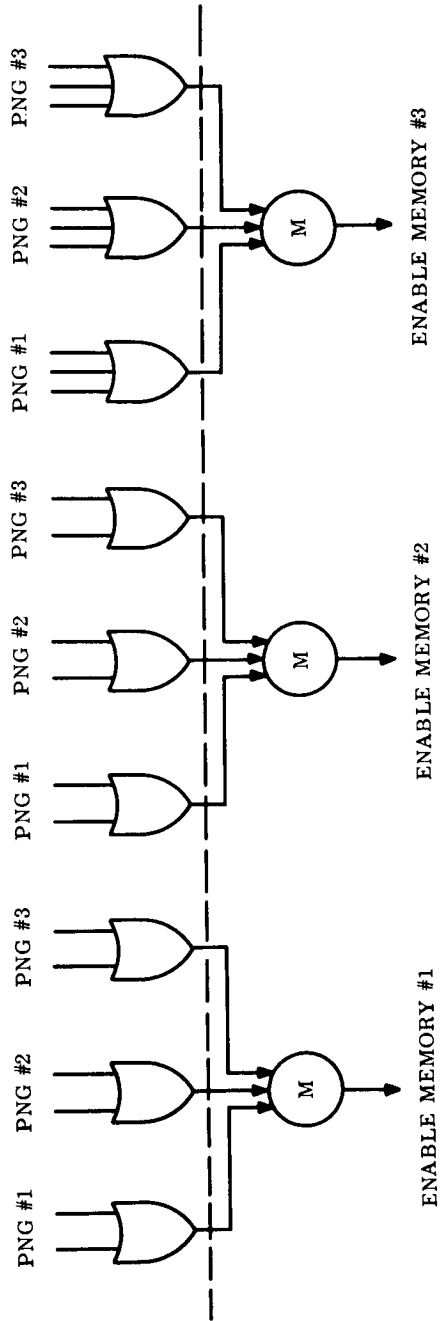
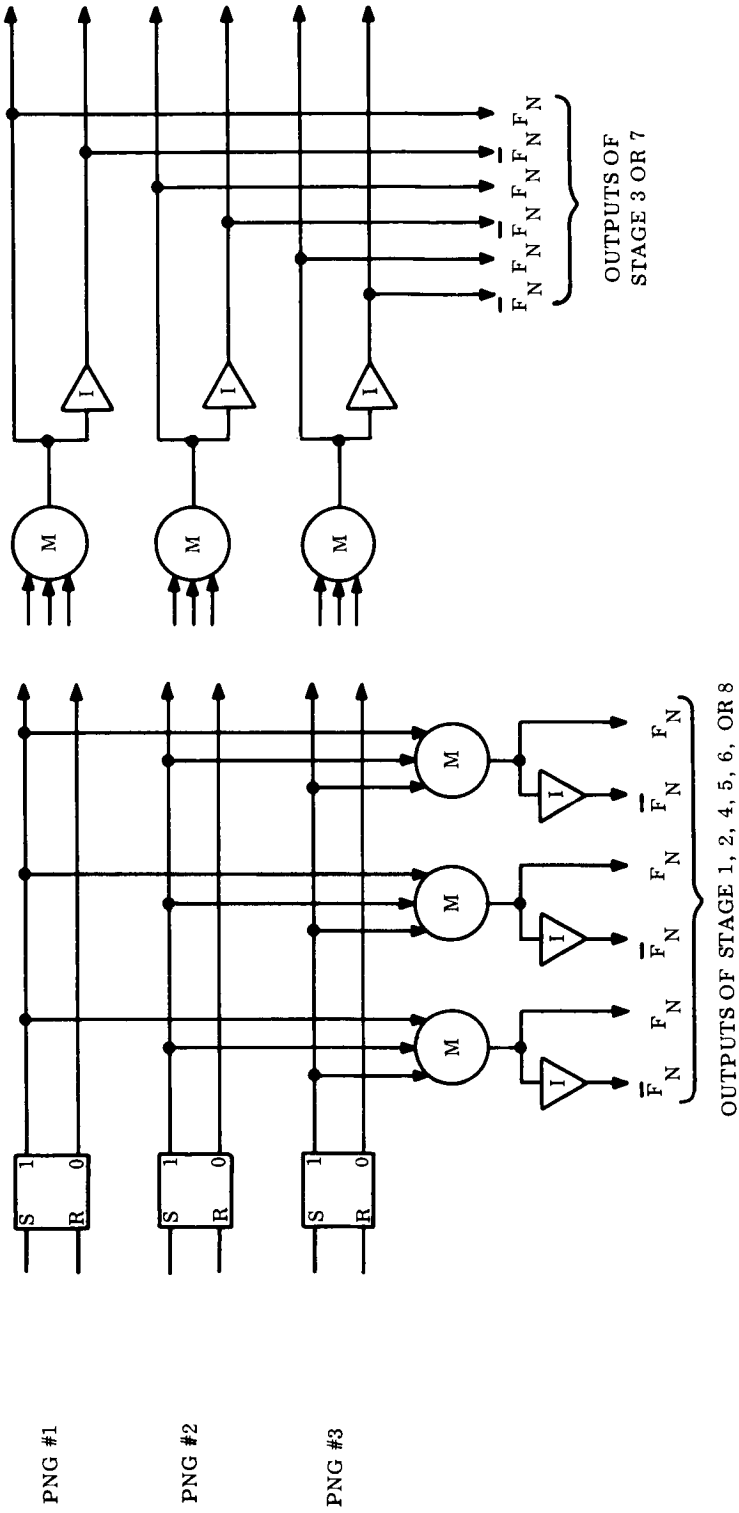


Figure 3-7. C & S Address PNG Output Redundancy

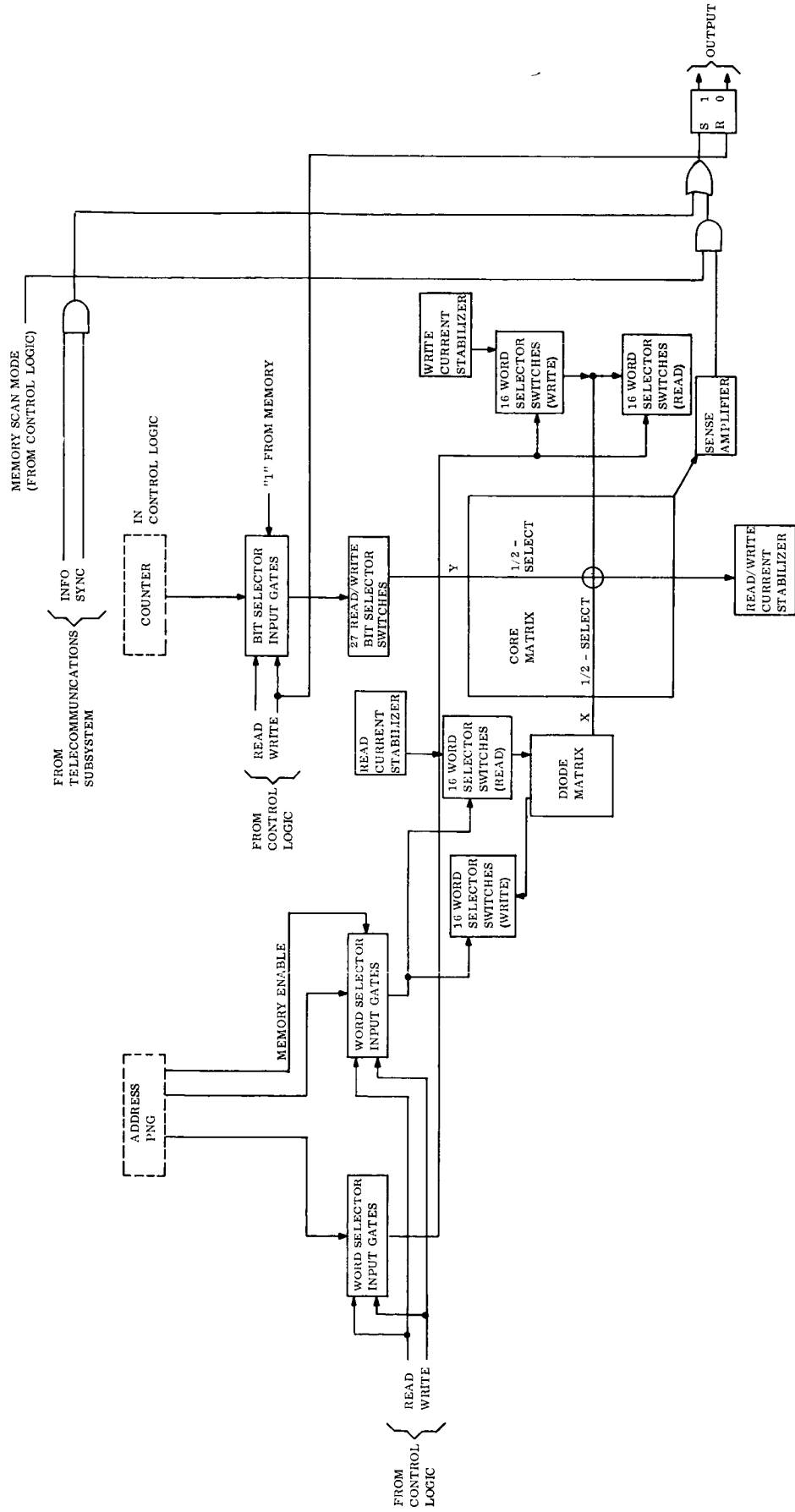


Figure 3-8. C & S Memory

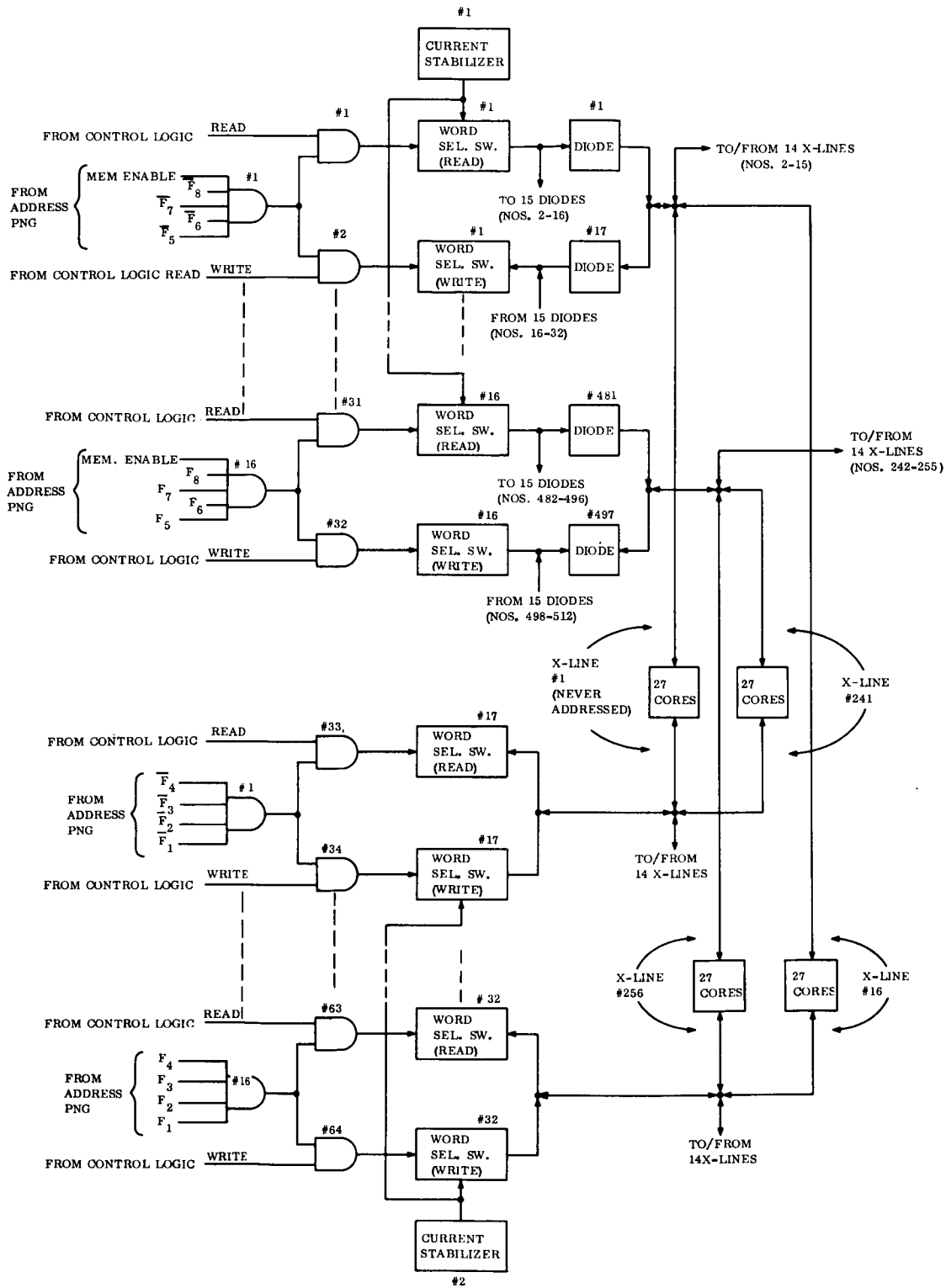


Figure 3-9. C & S Memory X-Line Selection

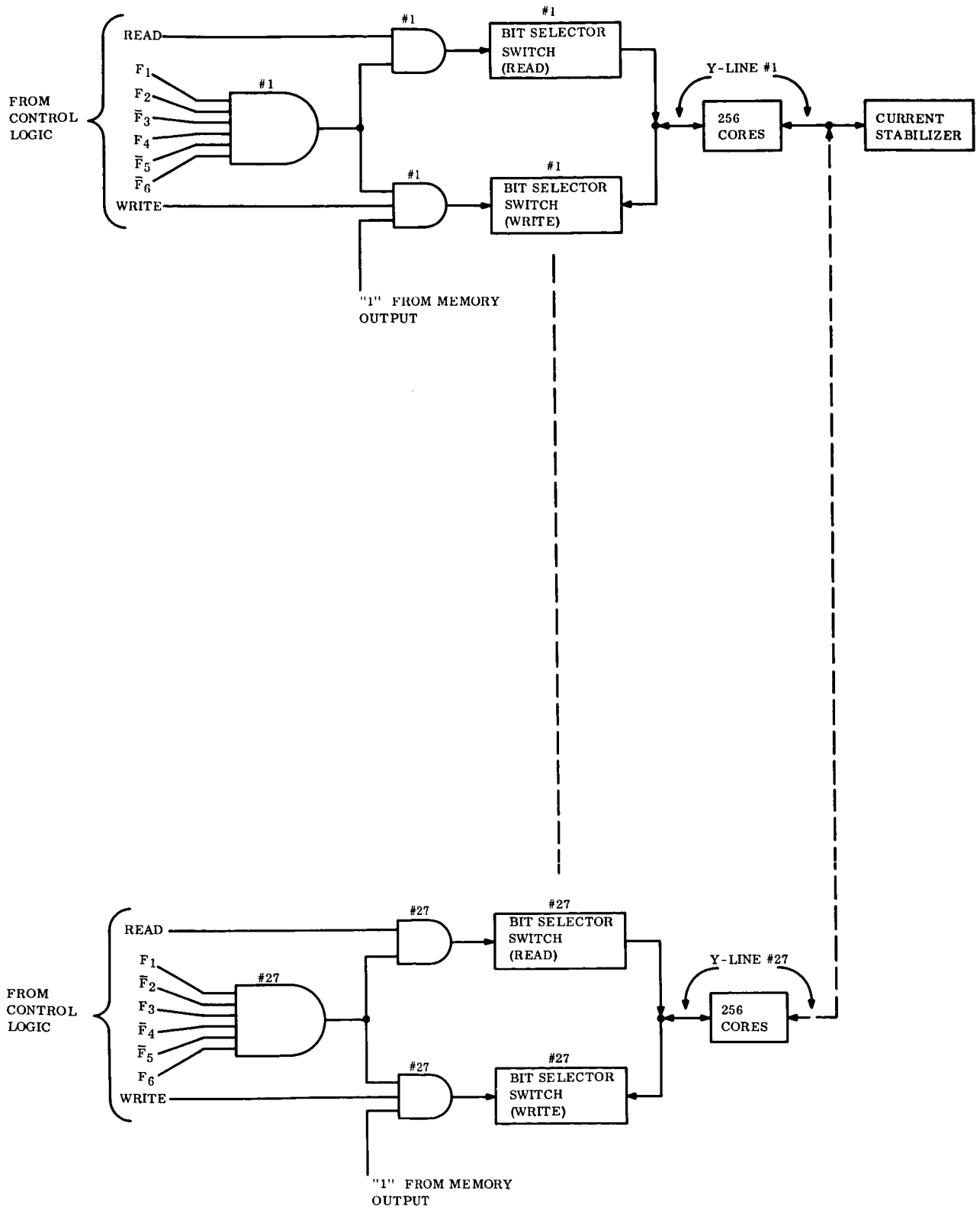


Figure 3-10. C & S Memory Y-Line Selection

Three complete memories are used with voting in triplicate on the contents of the output flip-flops as shown in Figure 3-11. The three memories can be loaded independently or simultaneously in the Memory Update Mode but are read out simultaneously in the Memory Scan Mode. Critical commands are transmitted three times and loaded in a different Memory (but in the corresponding address in each Memory) each time. Unless an error occurs in the corresponding bit positions of at least two of the three words, errors will be corrected by the voting at the outputs of the memories.

Non-critical commands are transmitted once and loaded in three memories simultaneously.

3.1.3 CONTROL LOGIC

Figures 3-12 and 3-13 are functional logic diagrams of the Control Logic. The Control Logic receives alert and synchronization pulses and commands to inhibit or enable C & S command outputs, to erase invalid command word data and to initiate the Memory Scan Mode (backup for automatic function) from the Telecommunications Subsystem; 76.8 Kc, 1 pps, and 0.125 pps timing signals from the Countdown Chain and Master Timer; indications of match or lack of match of time tag and timer bits from the Comparator; 8-bit memory address numbers from the Address PNG; and Memory output signal. It provides preset and shift pulses, and C & S operating mode signals to the Address PNG; read and write timing pulses, C & S operating mode signals, and bit selection numbers to the Memories; shift pulses to the Shift Register; enable pulses to the shift Register Input Gates; and enable and execute signals to the Command Matrix Input Gates.

The timing (see Figures 3-14 and 3-15) of all Control Logic output signals is controlled by a 6-stage binary counter which is stepped by the trailing edges of sync, timing, or erase pulses. The counter contents, in conjunction with the Address PNG contents, also determine which memory cores are being addressed. The Memory Update Mode is initiated when the 6-state counter contents equal zero if an alert pulse is present. A 4-stage counter begins counting pulses occurring every eight seconds. Overflow of the 4-state counter initiates the Memory Scan Mode. The counter is recycled if an alert pulse is received before overflow occurs.

In the Memory Update Mode the first ten sync pulses are used as Address PNG shift pulses. The tenth sync pulse changes the 6-stage counter contents from binary 9 to binary 10. This resets a flip-flop which prevents further shifting of the Address PNG and enables an erase operation if an erase command is received from the Telecommunications Subsystem. The next 37 sync pulses trigger read and write pulses to the memories. A delay of four microseconds between the trailing edge of each sync (or timing) pulse and the leading edge of the read pulse allows transition of the 6-stage counter contents to occur before any memory core is addressed. The 6-stage counter is then reset by a succeeding alert pulse or by a pulse which presets the Address PNG in the Memory Scan Mode.

Should an erase command be received by the C & S while in the Memory Update Mode, the 6-stage counter is stepped by the erase pulses until another alert pulse is received or the C & S returns to the Memory Scan Mode automatically. The result is the writing of "all zeroes" into the memory address.

VB234FD107

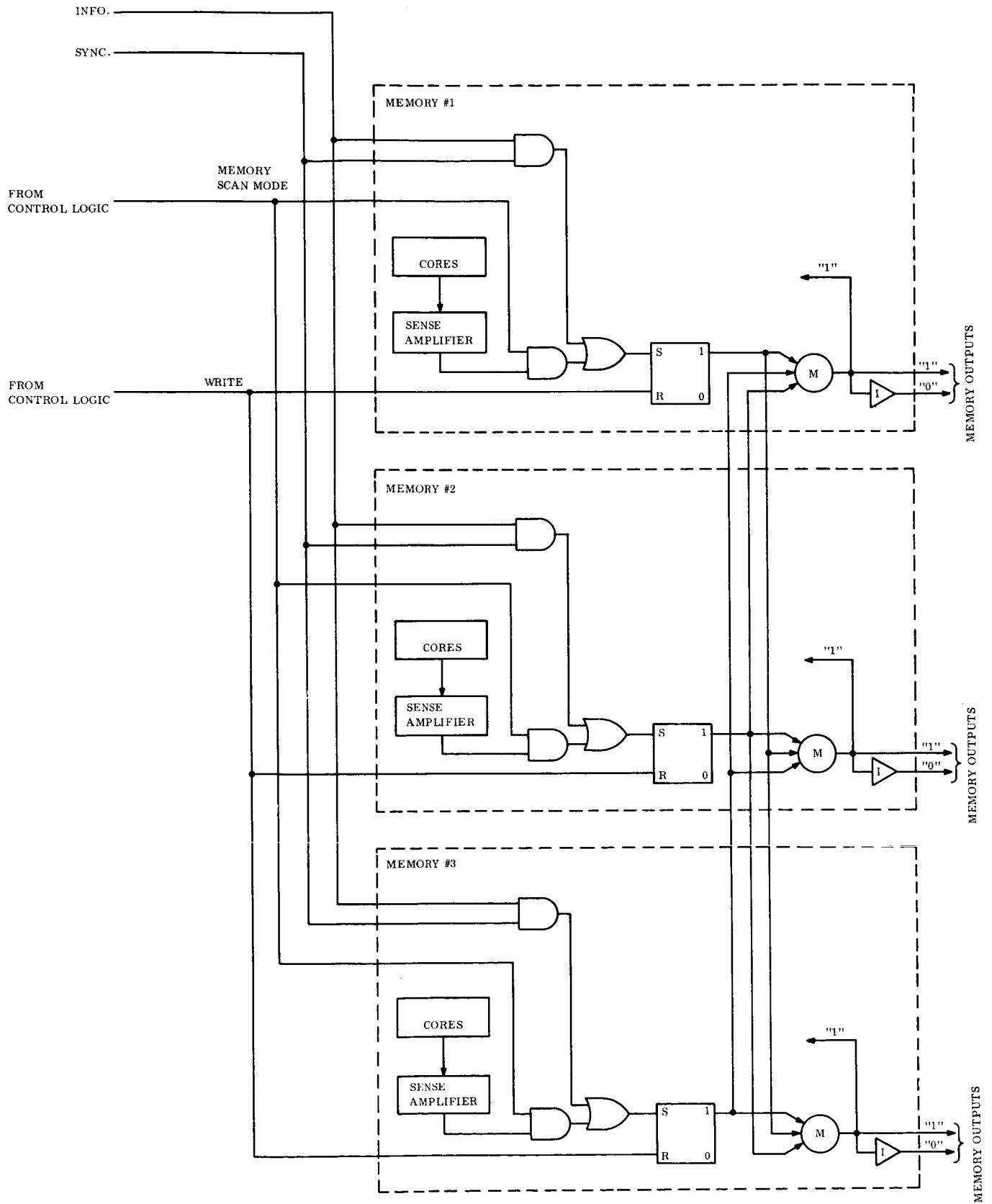


Figure 3-11. C & S Memory Input/Output

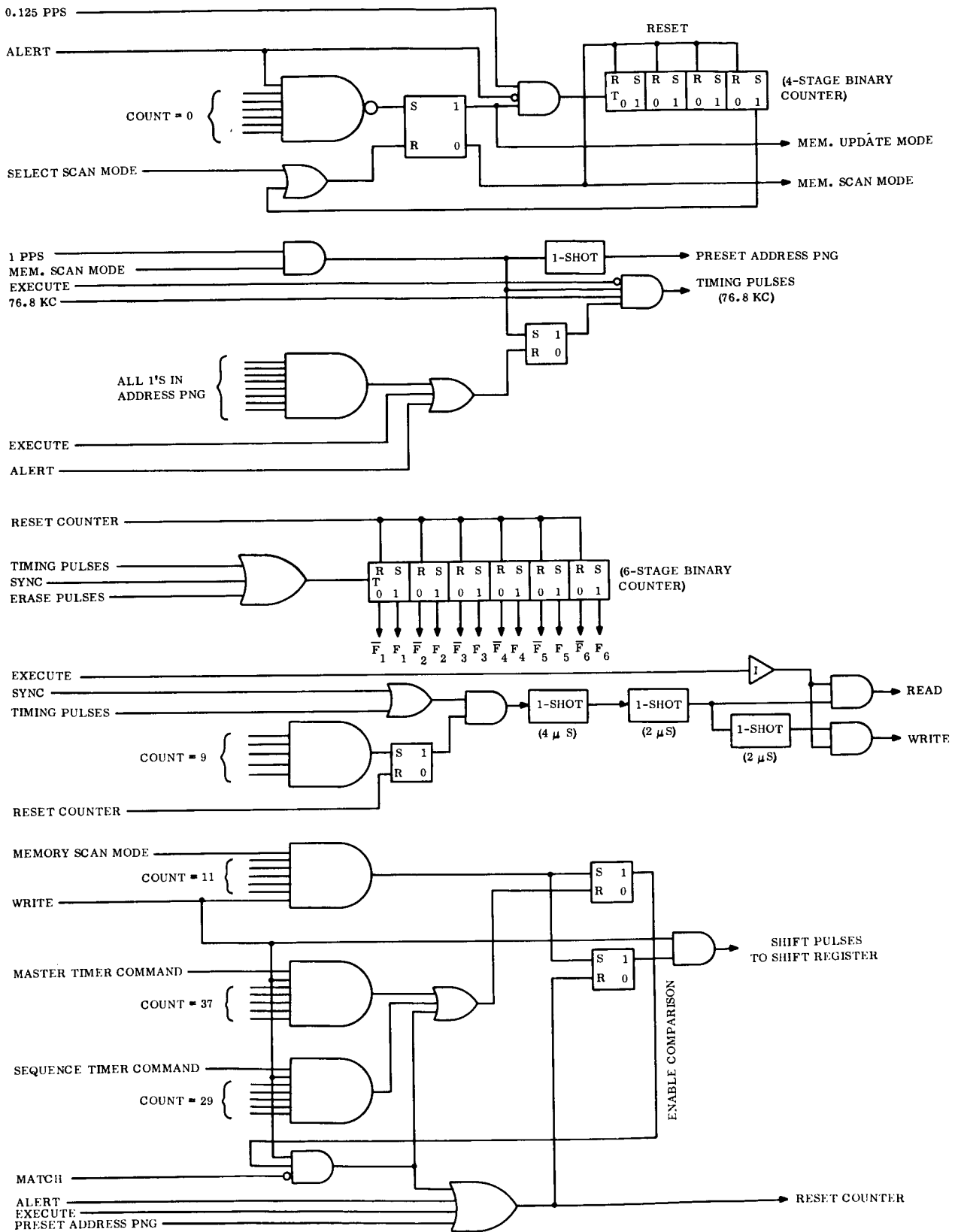


Figure 3-12. C & S Control Logic

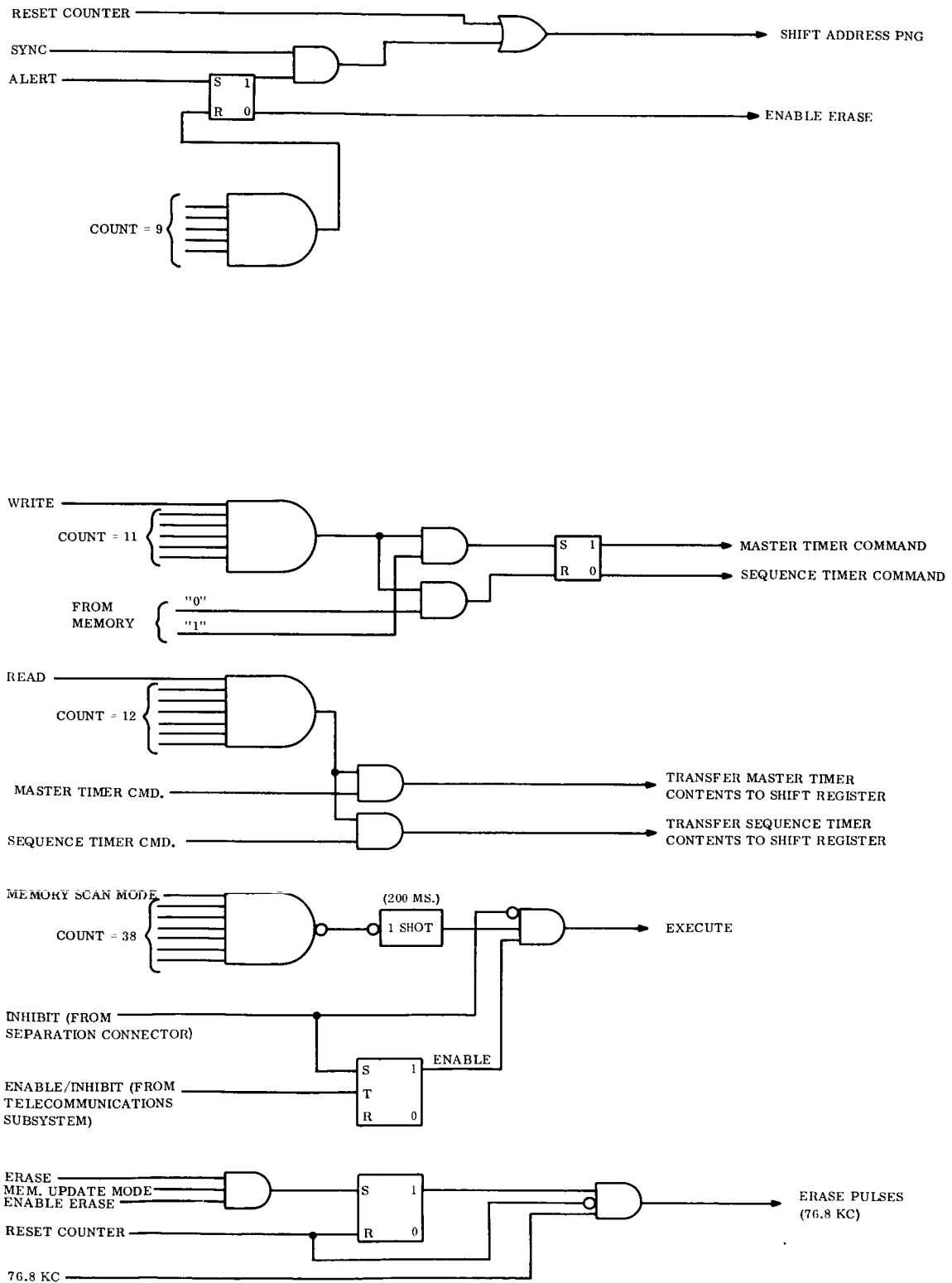


Figure 3-13. C & S Control Logic

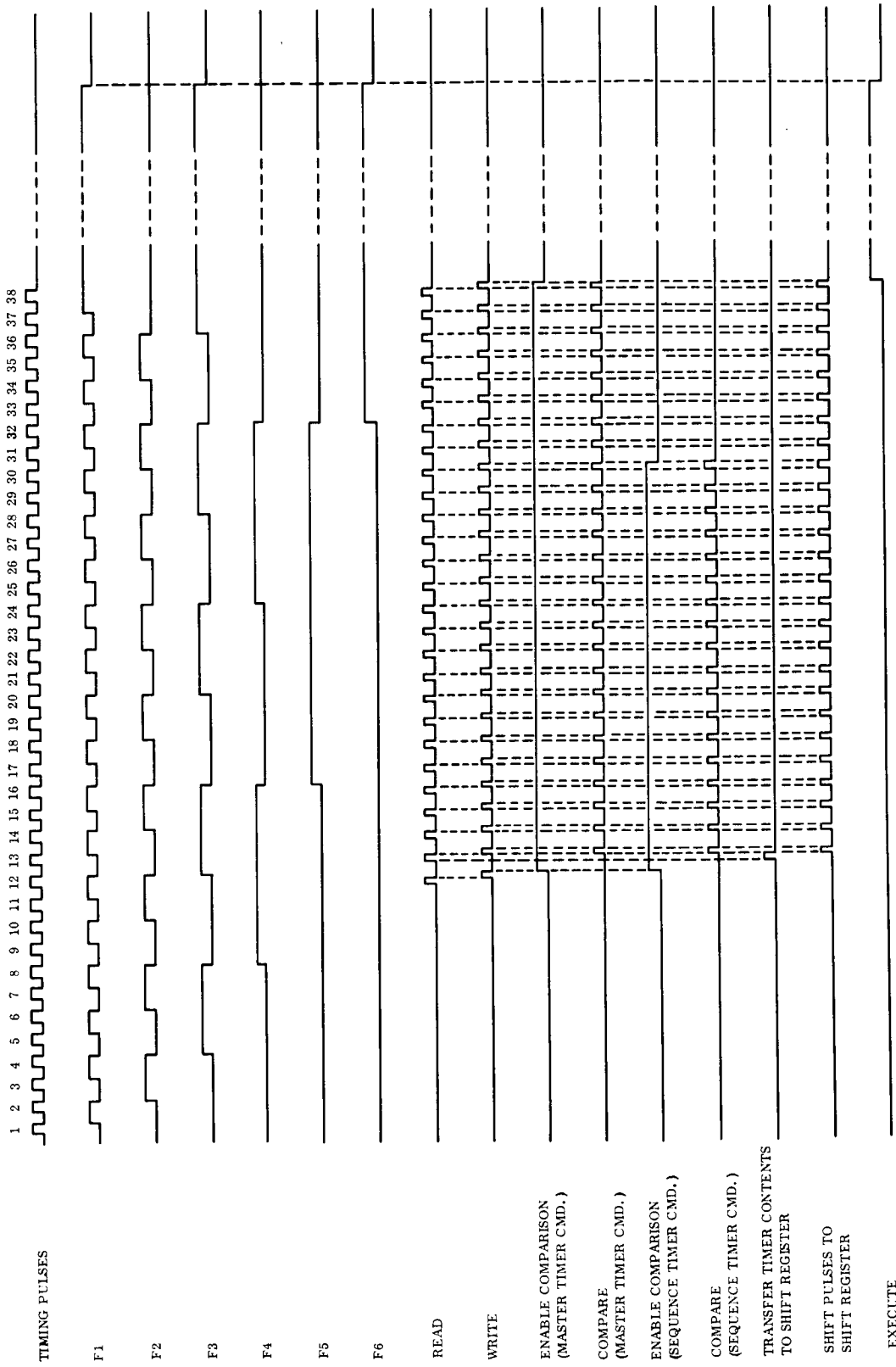


Figure 3-14. Memory Update Mode Timing

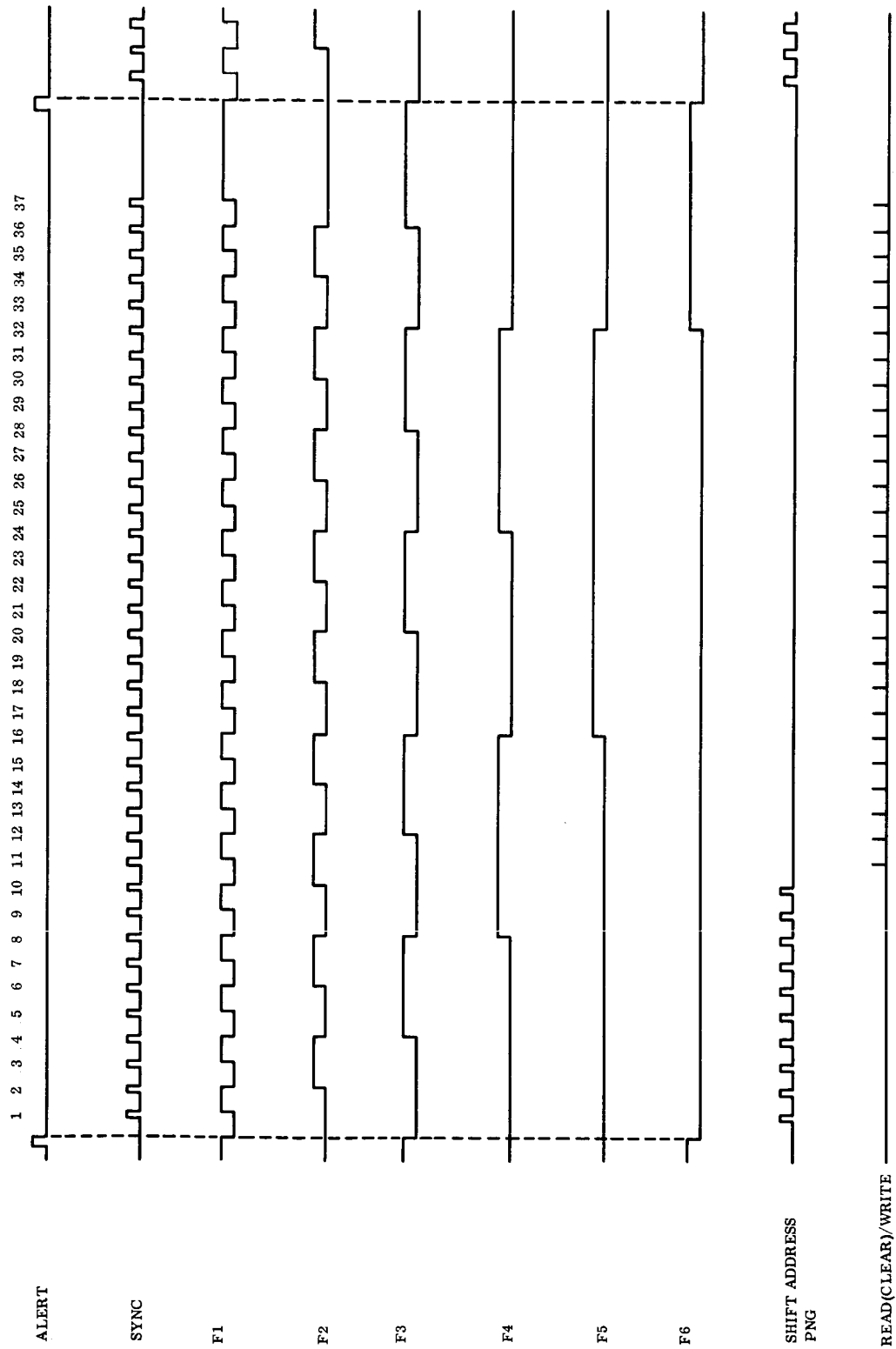


Figure 3-15. Memory Scan Mode Timing

In the Memory Scan Mode, the Address PNG is preset and the 6-stage counter reset by the trailing edge of a pulse occurring once per second. A train of timing pulses is initiated by the leading edge of the next one-second pulse. The tenth timing pulse changes the 6-stage counter contents from binary 9 to binary 10, which sets a flip-flop to enable the eleventh and succeeding timing pulses to trigger read and write signals to the Memories.

When the contents of the 6-stage counter equal binary 11, the trailing edge of the write pulse sets or resets a flip-flop depending on the output of the Memories to indicate whether the command under scrutiny is a Master Timer or Sequence Timer Command.

The twelfth timing pulse changes the 6-stage counter contents from binary 11 to 12, setting flip-flops which enable checking of the output of the Comparator whenever the write pulse occurs and shifting of the Shift Register by the trailing edge of each write pulse. The read pulse occurring while the counter contents equal 12 produces a signal to the Shift Register Input Gates to store Master Timer or Sequence Timer contents in the Shift Register.

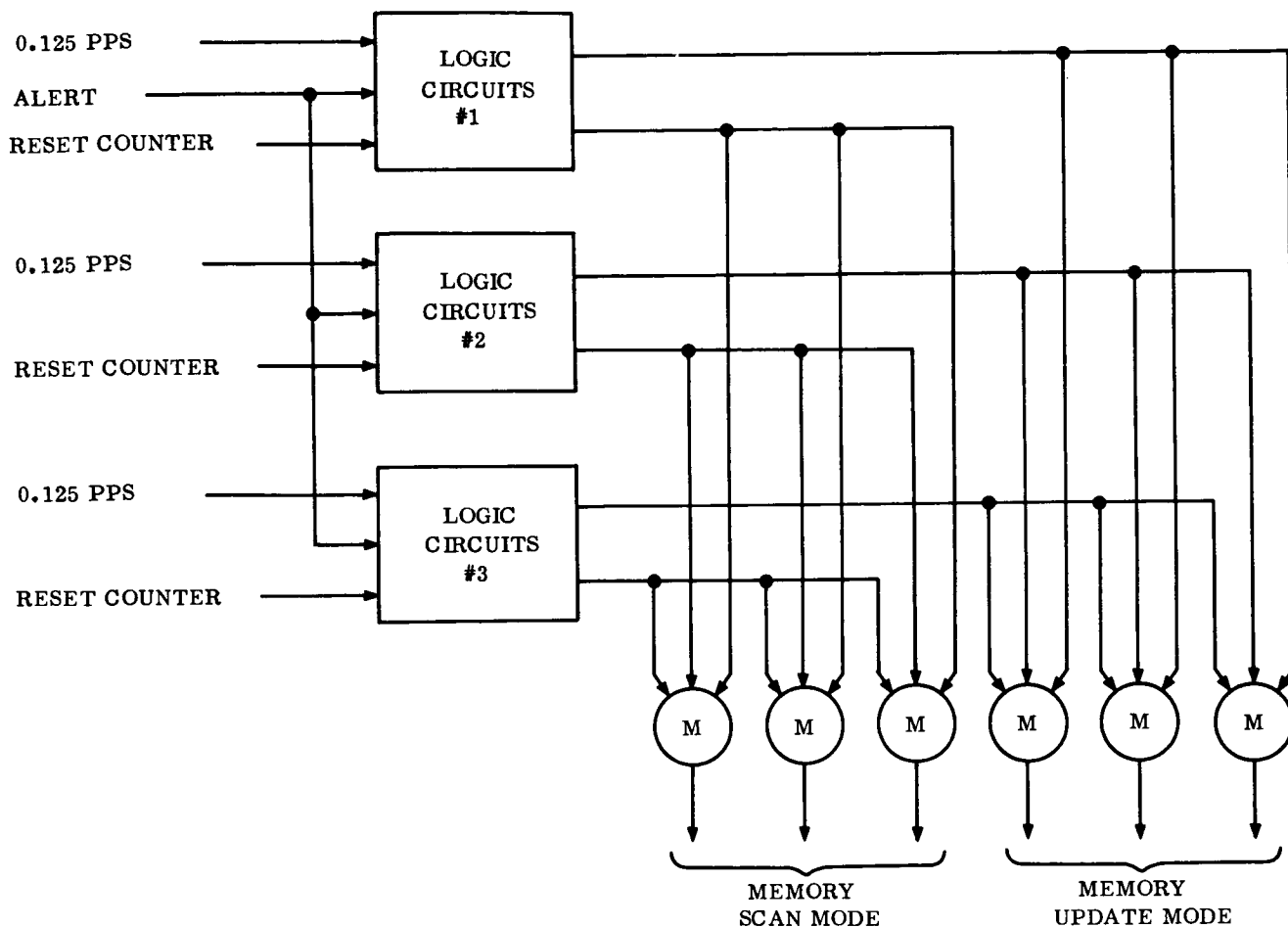
The 6-stage counter is reset either by the trailing edge of the write pulse when comparison is enabled and a mismatch is indicated by the Comparator or by the trailing edge of the execute signal. The Address PNG is shifted each time the 6-stage counter is reset.

Unless disabled earlier by a mismatch indication, comparison of command time tag and timer bits continues until occurrence of the write pulse trailing edge when 6-stage counter contents equal 29 for a Sequence Timer Command or 37 for a Master Timer Command.

The execute signal (200 milliseconds duration) is initiated when the 6-stage counter contents change from 37 to 38 which occurs only when a complete match exists between command time tag and timer contents. Timing, read, and write pulses are disabled for the duration of the execute signal. The 6-stage counter and the flip-flops enabling timing, read, and write pulses are reset by the trailing edge of the execute signal.

Stepping and resetting of the 6-stage counter and shifting of the Address PNG continue until an execute signal has been generated or until the contents of the Address PNG change from "all ones" to the next state indicating that all stored commands have been scanned once. Operation then ceases until the start of the next one-second interval. When an alert pulse occurs, during a memory scan cycle, the Memory Scan Mode is replaced by the Update Mode only when the 6-stage counter contains "all zeroes". This prevents loss of stored information as a result of changing Memory address information before a bit has been rewritten in the Memories.

Redundancy approaches are indicated in Figure 3-16 and 3-17. Three complete sets of logic elements are used with voting in triplicate on the output signals. In addition, voting in triplicate is performed on the outputs of the one-shot multivibrators used to generate the read and write pulses.



REDUNDANCY OF FOLLOWING SIGNALS IS SIMILAR TO THAT SHOWN ABOVE.

- RESET COUNTER
- PRESET ADDRESS PNG
- SHIFT ADDRESS PNG
- SHIFT PULSES TO SHIFT REGISTER
- MASTER TIMER COMMAND
- SEQUENCE TIMER COMMAND
- TRANSFER MASTER TIMER CONTENTS TO SHIFT REGISTER
- TRANSFER SEQUENCE TIMER CONTENTS TO SHIFT REGISTER
- EXECUTE
- TIMING PULSES
- ERASE PULSES
- COUNTER OUTPUTS \overline{F}_1 , F_1 , \overline{F}_2 , F_2 , etc.

Figure 3-16. C & S Control Logic Redundancy

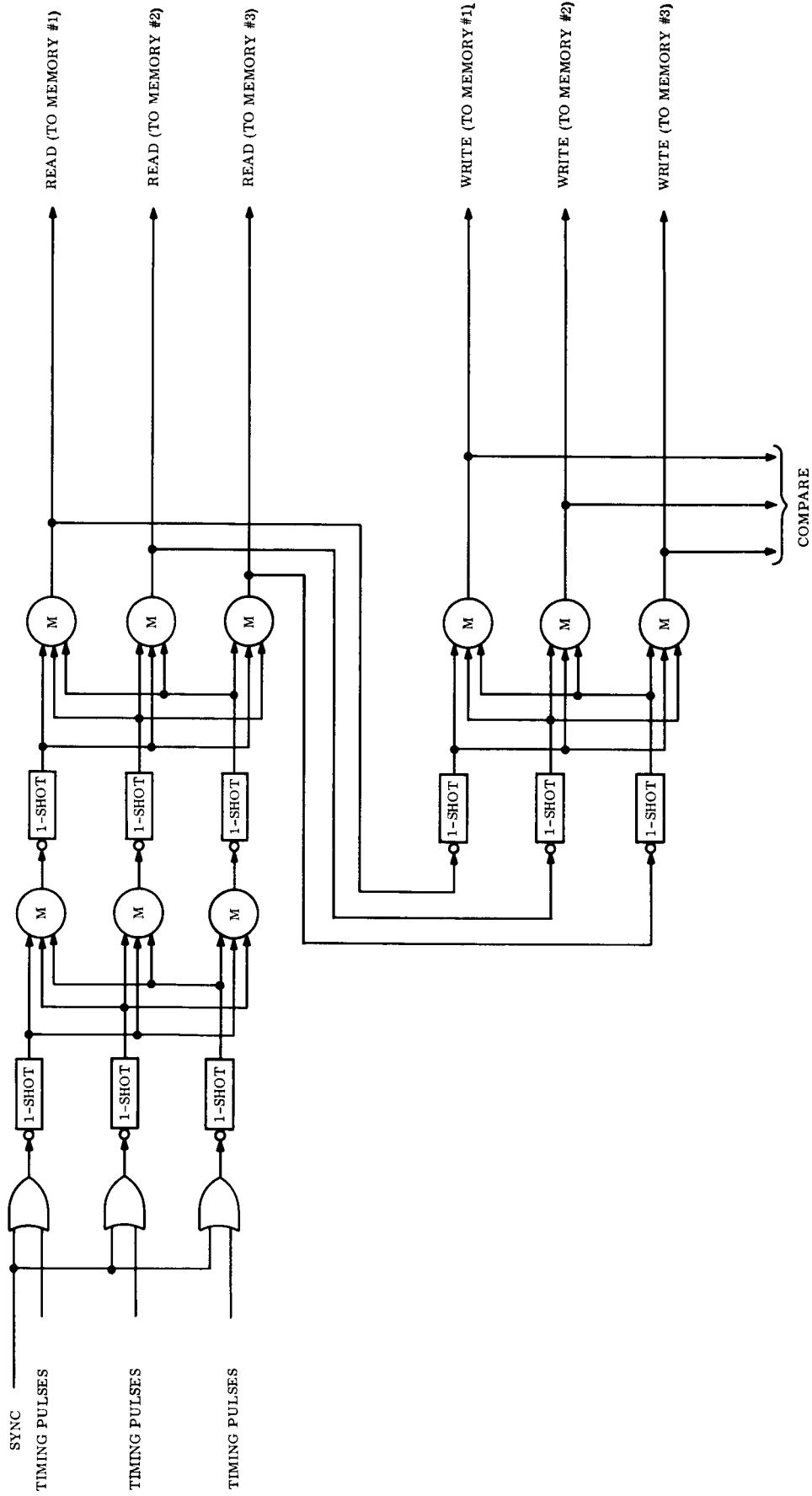


Figure 3-17. C & S Control Logic Redundancy

3.1.4 OSCILLATOR

The crystal oscillator provides 307.2 Kc pulses to the countdown chain. Alternate redundancy approaches are shown in Figure 3-18. In one case, the voltage drop developed across the capacitor when one oscillator is functioning is used to bias off the other oscillator. In the other case, the voltage drop is applied to digital logic to inhibit the output of one oscillator when the other is functioning.

3.1.5 COUNTDOWN CHAIN

Figure 3-19 is a functional logic diagram of the Countdown Chain. The chain consists of a series of frequency dividers which provide 153.6 Kc, 76.8 Kc, 38.4 Kc, and 1 pps cyclic outputs. Stages 1 to 3 and 11 to 19 each perform division by two. Division by three is performed by Stages 4 and 5 and associated gates; and division by 25, by Stages 6 to 10 and associated gates. Provision is made for presetting the Countdown Chain by a "clear registers" pulse from the LCE to insure that all redundant elements are synchronized with one another.

Countdown Chain redundancy approaches are shown in Figures 3-20 and 3-21. Three complete chains are used with voting in triplicate performed within the input logic and between Stages 2 and 3, 5 and 6, 8 and 9, 10 and 11, 14 and 15, and 18 and 19. Voting elements used between Stages 2 and 3 also provide the outputs of Stage 2 to the Control Logic. Single majority gates provide the outputs of Stages 1, 3, and 19 to other spacecraft subsystems. Voting in triplicate is performed on the outputs of Stage 19 to the Control Logic and the Master and Sequence Timers.

3.1.6 MASTER TIMER

The functional logic of the Master Timer is shown in Figure 3-22. The timer is a 26-stage binary counter which counts Countdown Chain output pulses occurring once per second. Means are provided for presetting, inhibiting, and updating of the timer prior to launch by signals from the LCE. The outputs of the 26 stages are connected to input terminals of the Shift Register Input Gates.

Operation of the Master Timer is initiated by the following sequence of events prior to launch. An "inhibit count" signal (voltage level) from the LCE inhibits counting of the one-second pulses by the timer. The start of the inhibit signal is followed shortly by a "clear registers" pulse from the LCE which presets all counter stages to a coarse initial value. A train of "update pulses" then presets the timer to the desired initial value. Counting of one-second pulses is resumed upon removal of the inhibit signal. During "holds" in the launch sequence, the inhibit signal is restored to maintain synchronism of the timer with launch time.

Master Timer redundancy approaches are shown in Figures 3-23 and 3-24. Three complete timers are used with voting in triplicate occurring within the input logic and between stages 2 and 3, 6 and 7, 10 and 11, 14 and 15, 18 and 19, and 22 and 23. The voting elements used for this internal redundancy also provide the output signals for Stages 2, 6, 10, 14, 18, and 22. Voting in triplicate is performed on the output signals of Stages 1, 3 to 5, 7 to 9, 11 to 13, 15 to 17, 19 to 21, and 23 to 26.

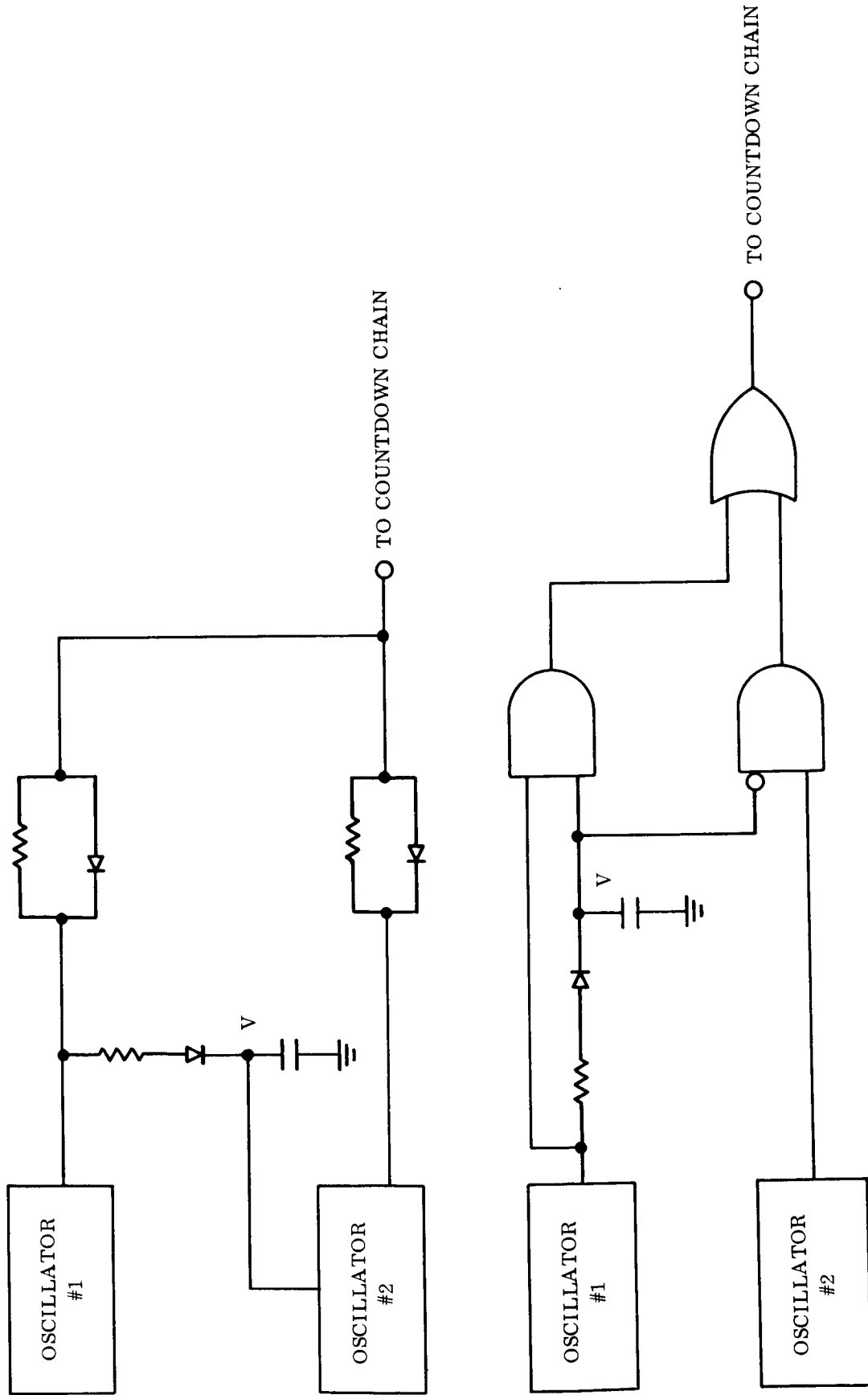


Figure 3-18. Approaches to Oscillator Redundancy

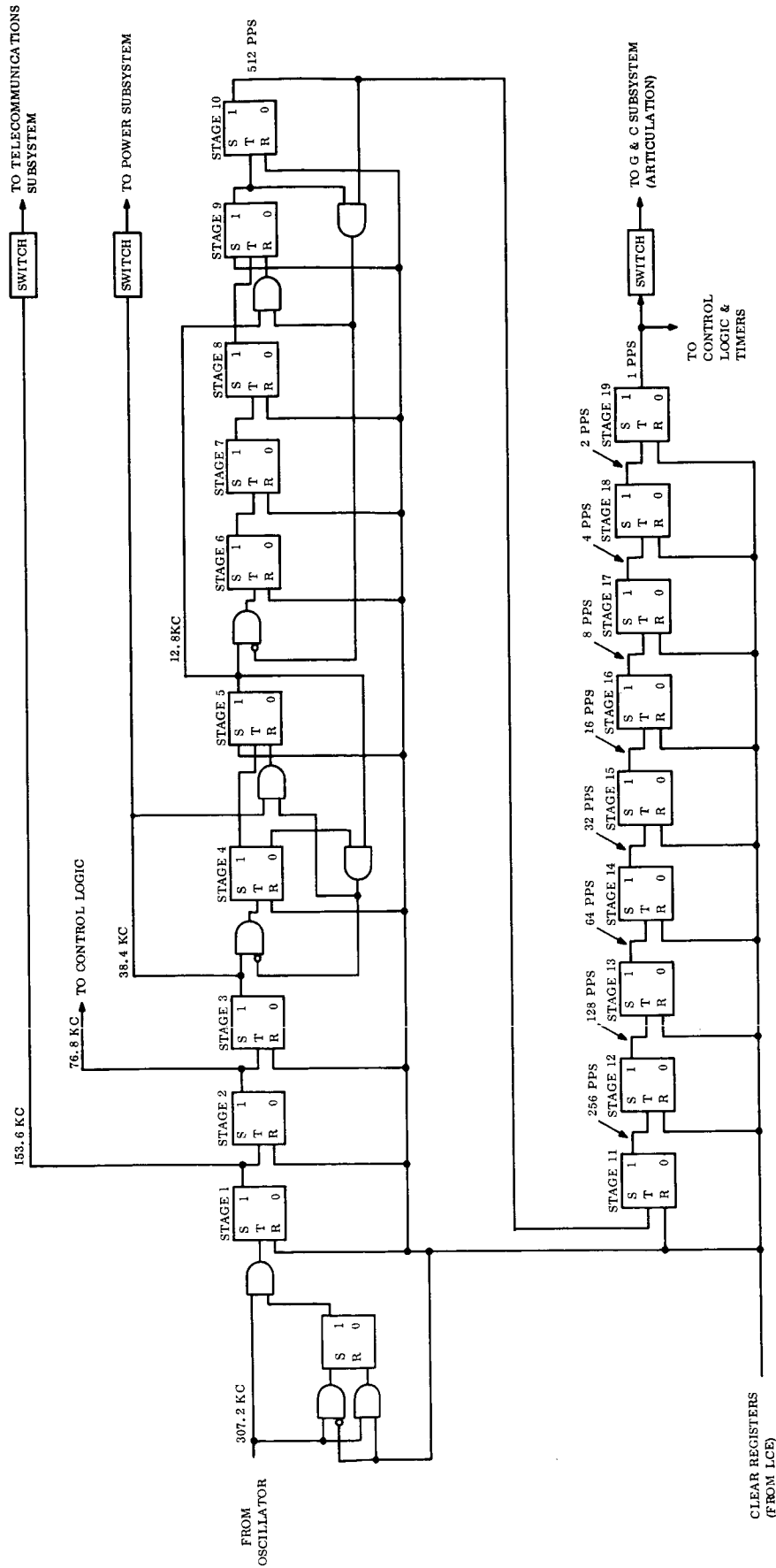


Figure 3-19. C & S Countdown Chain

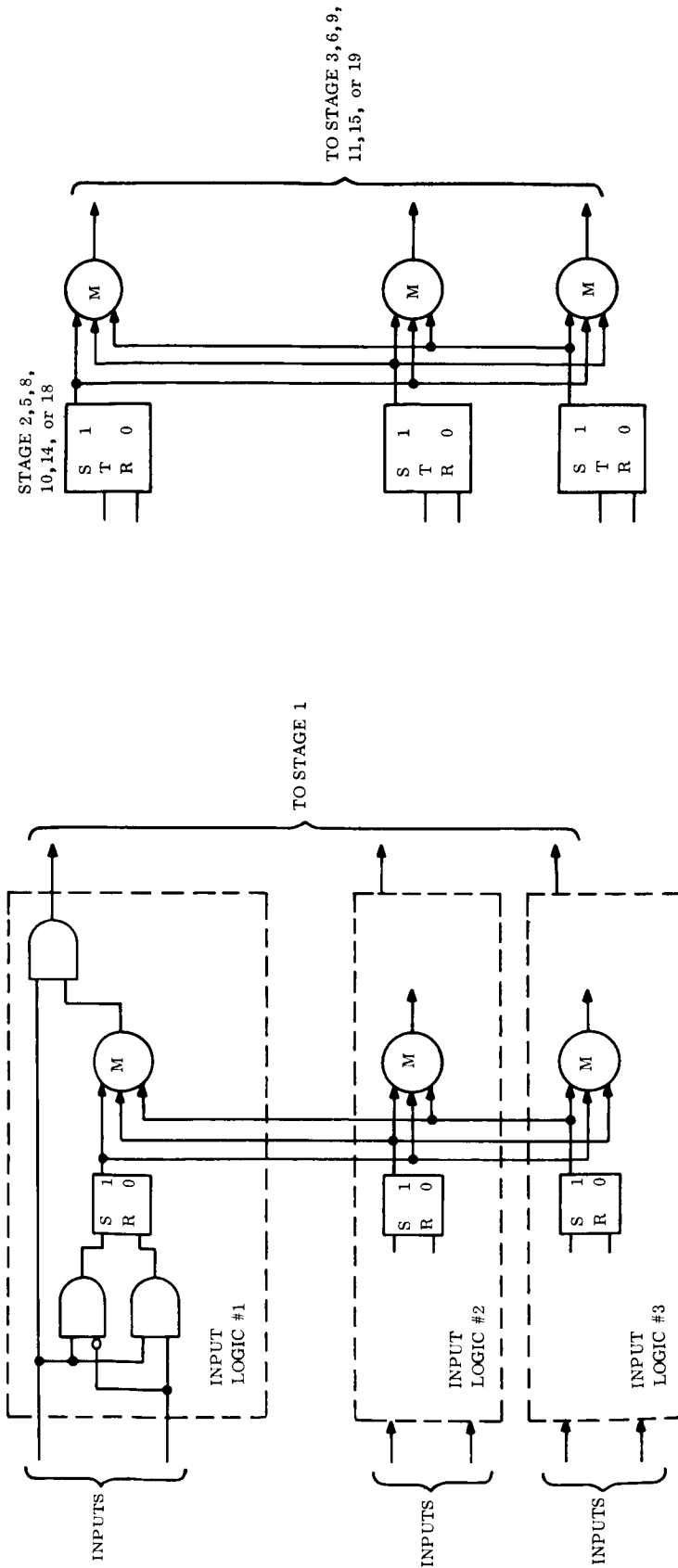


Figure 3-20. C & S Countdown Chain Internal Redundancy

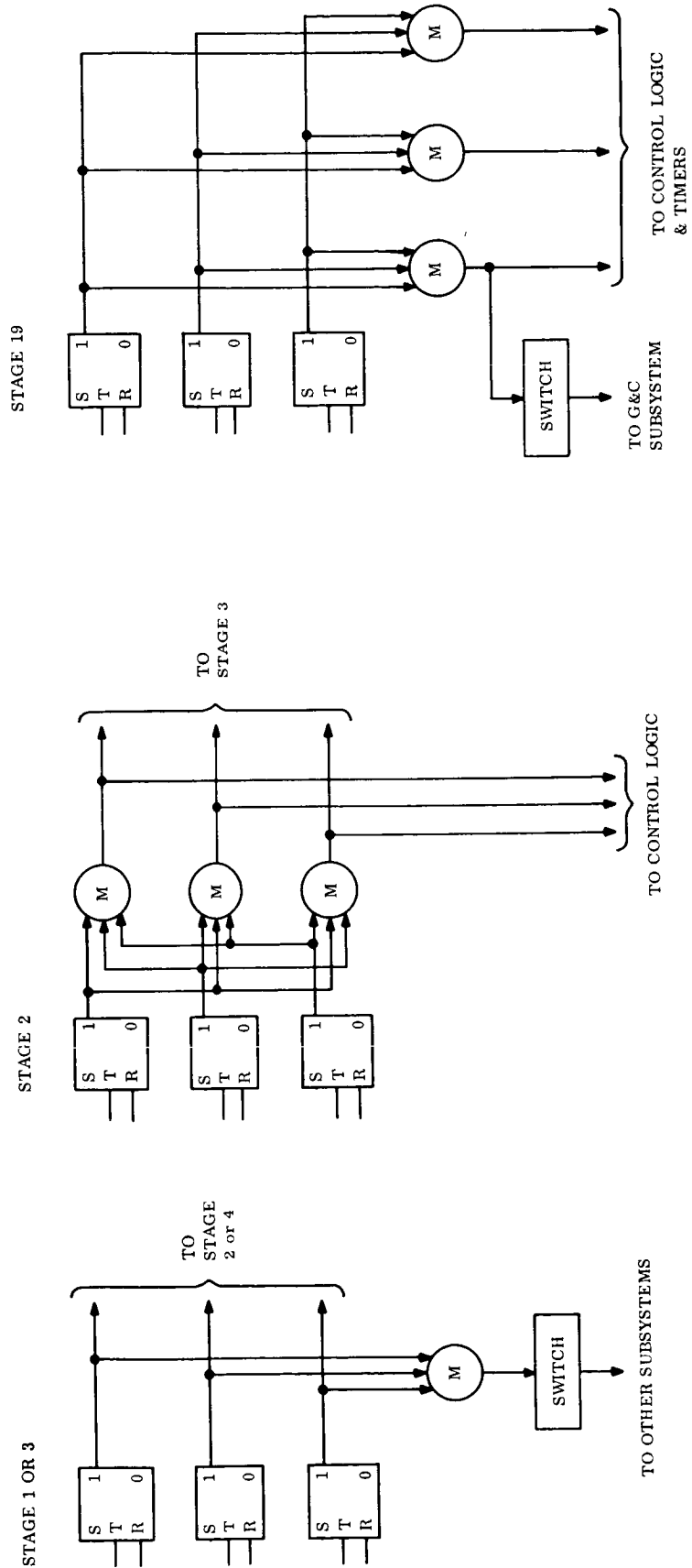


Figure 3-21. C & S Countdown Chain Output Redundancy

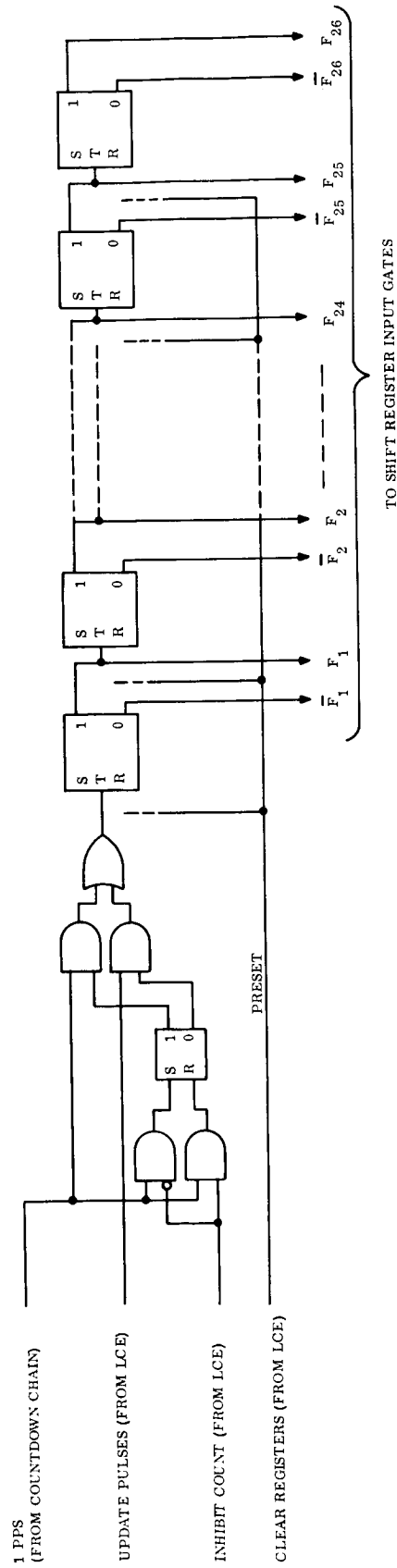


Figure 3-22. C & S Master Timer

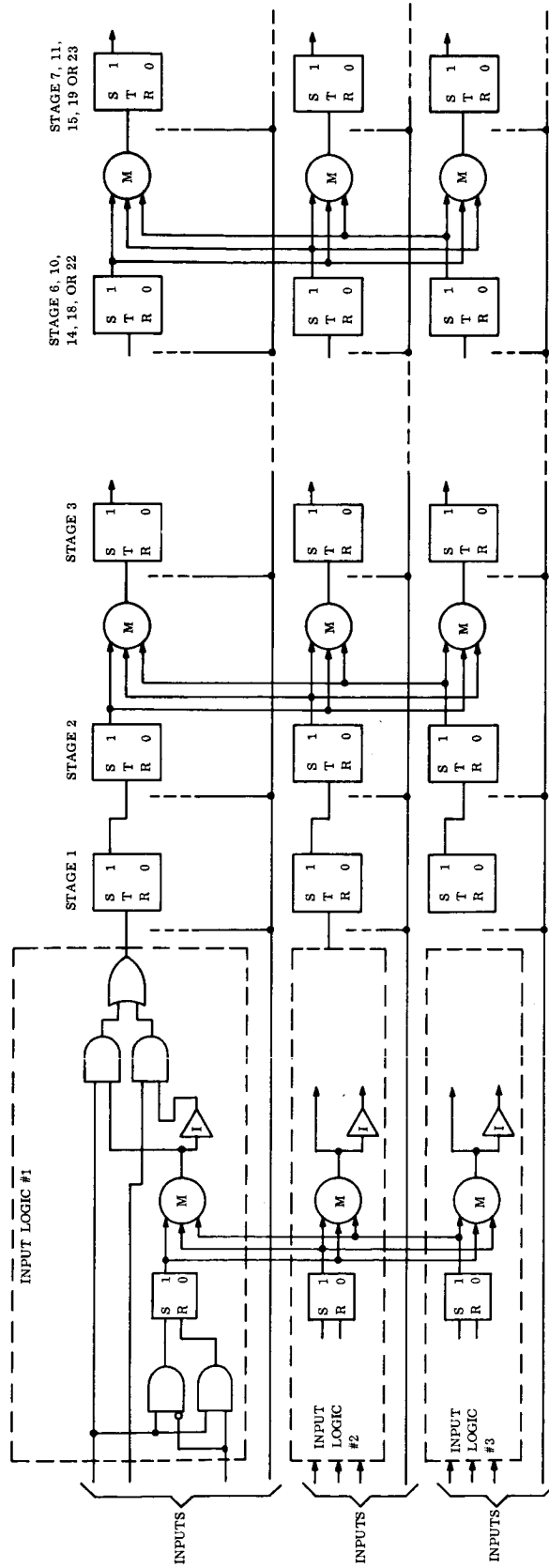


Figure 3-23. C & S Master Timer Internal Redundancy

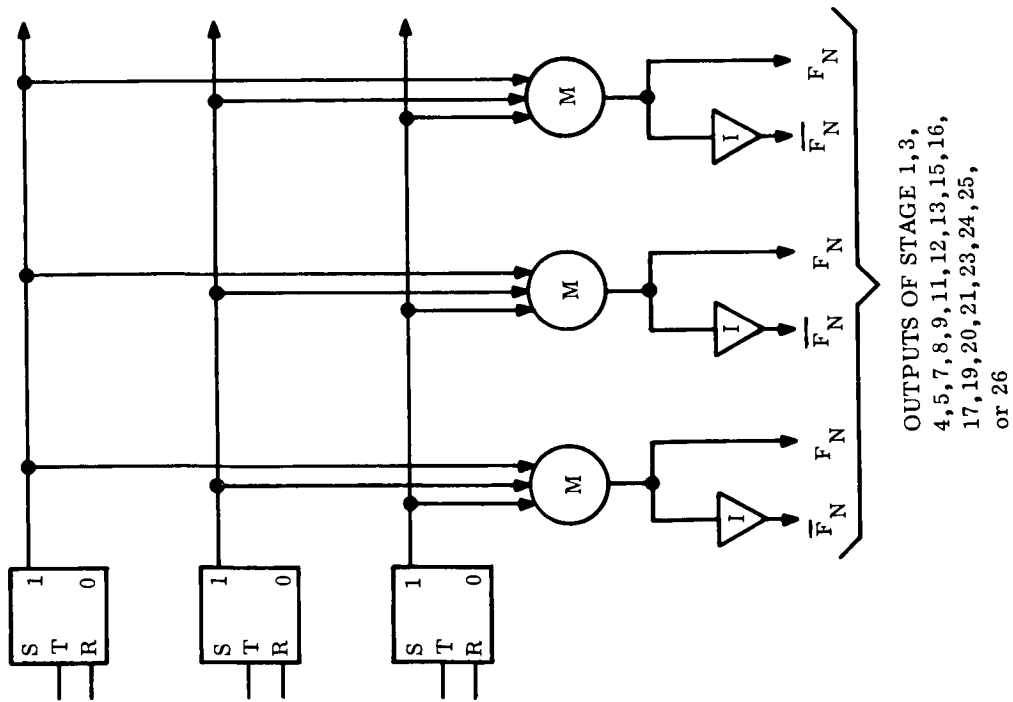
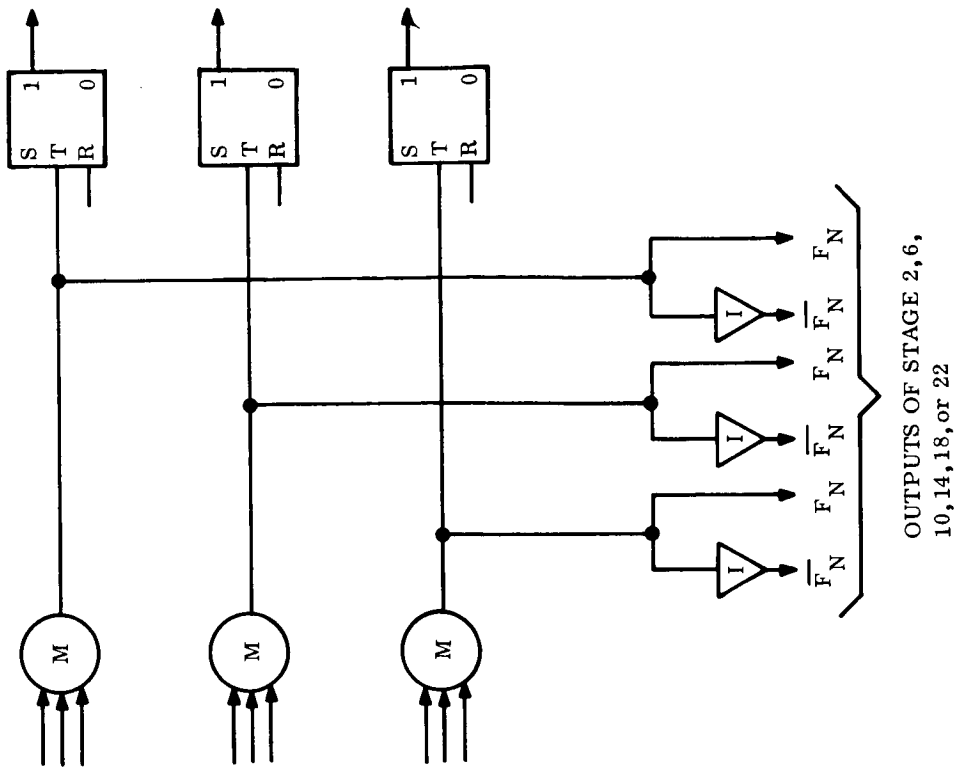


Figure 3-24. C & S Master Timer Output Redundancy

3.1.7 SEQUENCE TIMER

The functional logic of the Sequence Timer is shown in Figure 3-25. The timer is an 18-stage binary counter that counts pulses occurring once per second. Means are provided for starting, resetting and stopping, or resetting and continuing timer operation by C & S stored commands; and for clearing the timer by a pulse from the LCE. The outputs of the 18 stages are connected to input terminals of the Shift Register Input Gates.

Prior to launch, a pulse on the "clear registers" line stops the timer if it has been counting and resets every stage to "zero".

Sequence Timer redundancy approaches are shown in Figure 3-26 and 3-27. Three complete timers are used with voting in triplicate performed between Stages 2 and 3, 6 and 7, 10 and 11, and 14 and 15. These voting elements also provide the output signals for Stages 2, 6, 10, and 14. Voting in triplicate is performed on the outputs of Stages 1, 3 to 5, 7 to 9, 11 to 13, and 15 to 18.

3.1.8 SHIFT REGISTER INPUT GATES

The functional logic of the Shift Register Input Gates is shown in Figure 3-28. When a "transfer Master Timer contents" pulse is received from the Control Logic, the contents of the Master Timer are presented to Shift Register Stages 1 to 26 for the duration of the pulse. The most significant time bit is presented to Shift Register Stage 1 and the least significant bit to Stage 26. When a "transfer Sequence Timer contents" pulse is received, the contents of the Sequence Timer are presented to Shift Register Stages 9 to 26. The most significant time bit is presented to Stage 9 and the least significant bit to Stage 26. Three complete sets of gates are used with no internal or output voting performed.

3.1.9 SHIFT REGISTER

The Shift Register functional logic is shown in Figure 3-29. The various stages are preset by pulses appearing on the set or reset lines from the Shift Register Input Gates. The Shift Register is shifted by pulses received from the Control Logic. Whenever shifting occurs, memory output information is shifted into Stage 1 of the register. The outputs of Stages 1 to 8 are presented to the Command Matrix Input Gates. The output of Stage 26 is presented to the Comparator.

Shift Register redundancy approaches are shown in Figures 3-30 and 3-31. Three complete registers are used with voting in triplicate performed between Stages 4 and 5, 8 and 9, 12 and 13, 16 and 17, 20 and 21, and 24 and 25. The voting elements used for the internal redundancy also provide the output signals for Stages 4, 8, 12, 16, 20 and 24. Voting in triplicate is performed on the outputs of Stages 2, 3, 5, 6, 7, and 26. No voting is performed on Stage 1 outputs.

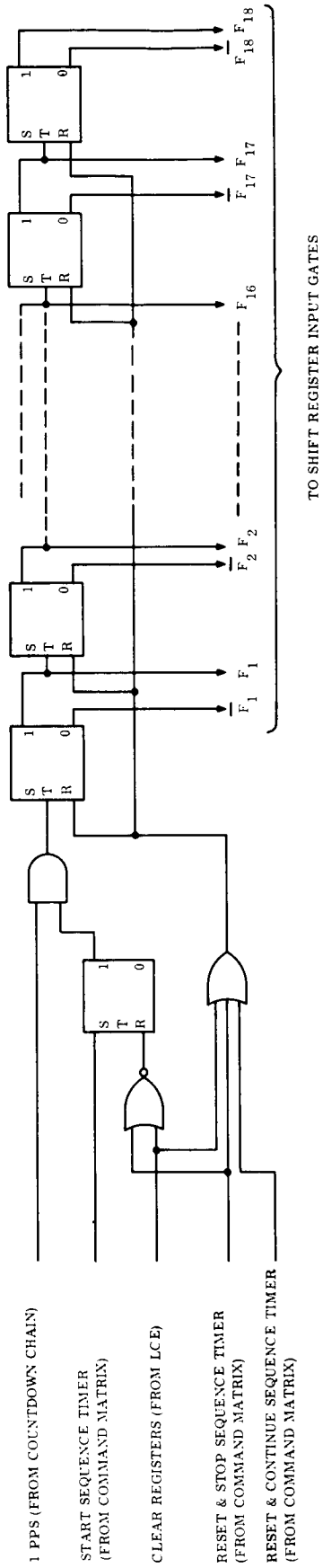


Figure 3-25. C & S Sequence Timer

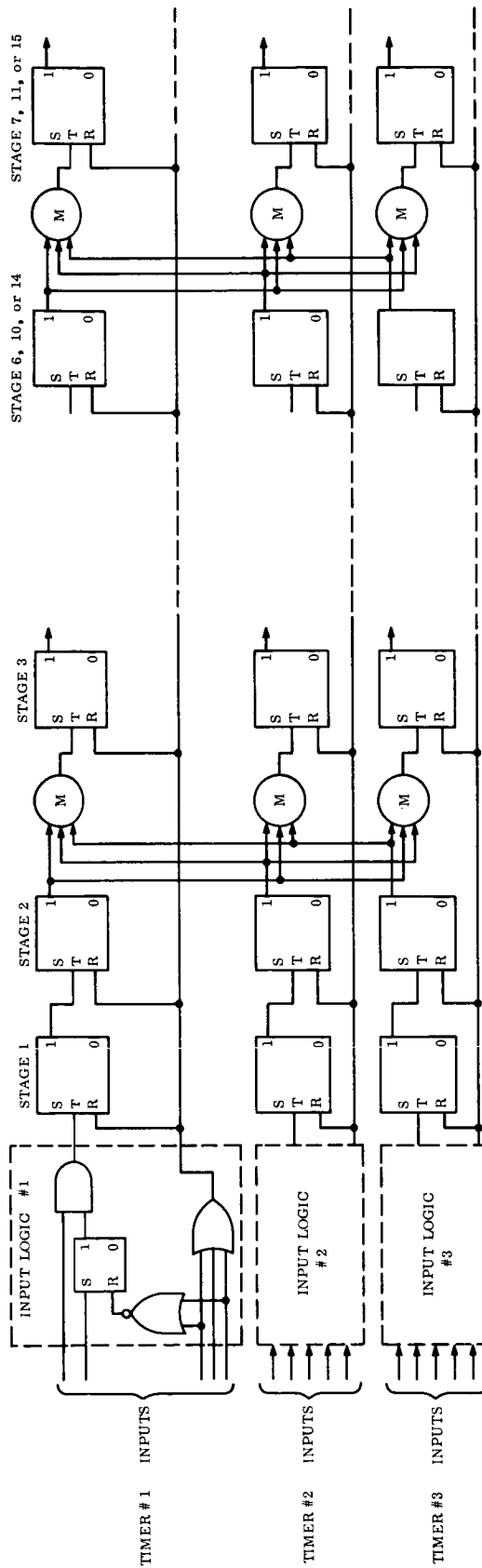
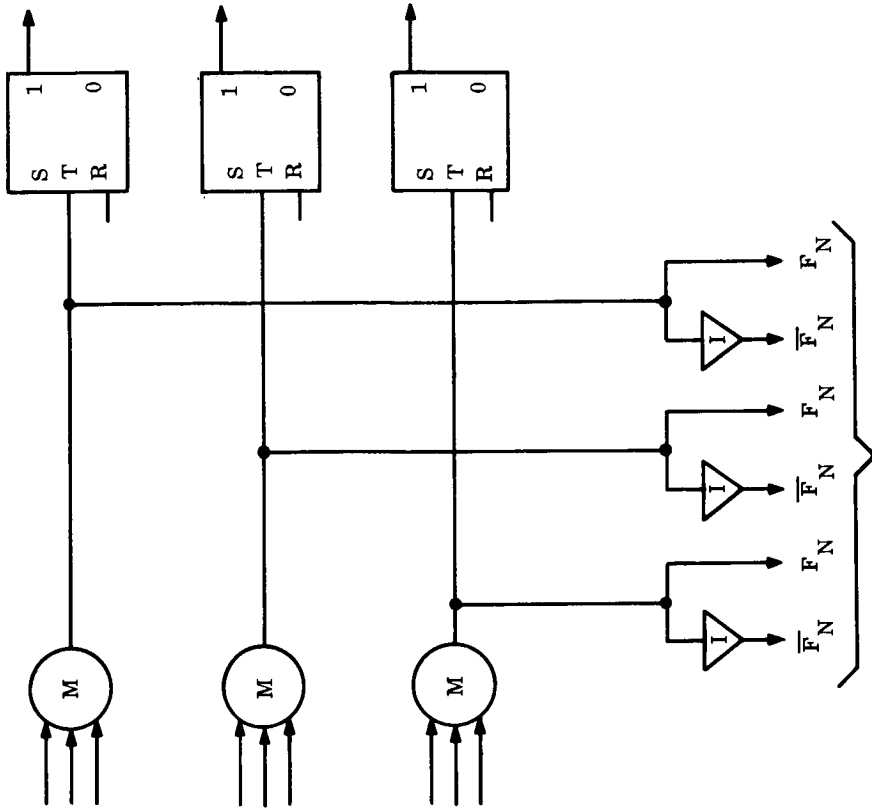
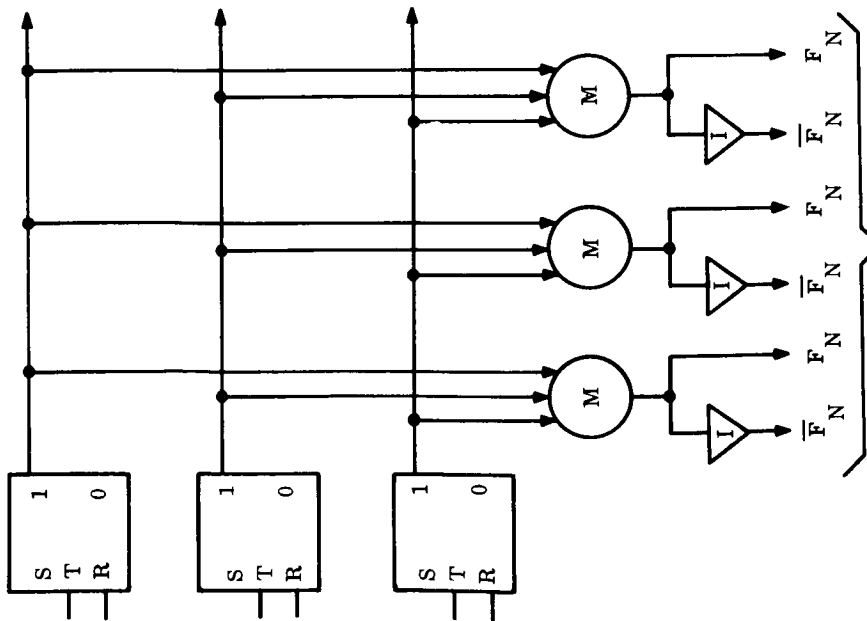


Figure 3-26. C & S Sequence Timer Internal Redundancy



OUTPUTS OF STAGE 2, 6,
10, or 14



OUTPUTS OF STAGE 1, 3,
4, 5, 7, 8, 9, 11, 12, 13, 15, 16
17, or 18.

Figure 3-27. C & S Sequency Timer Output Redundancy

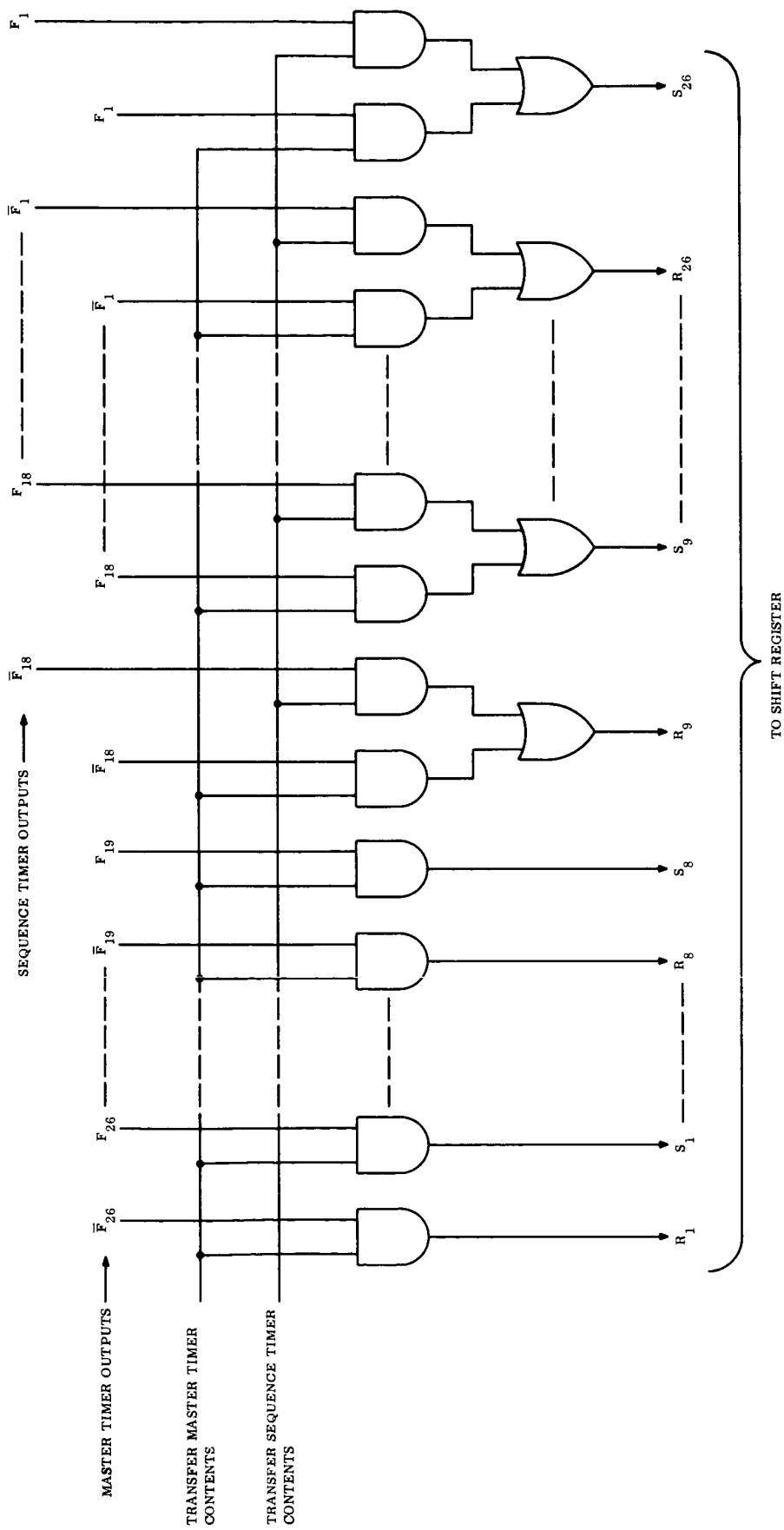


Figure 3-28. C & S Shift Register Input Gates

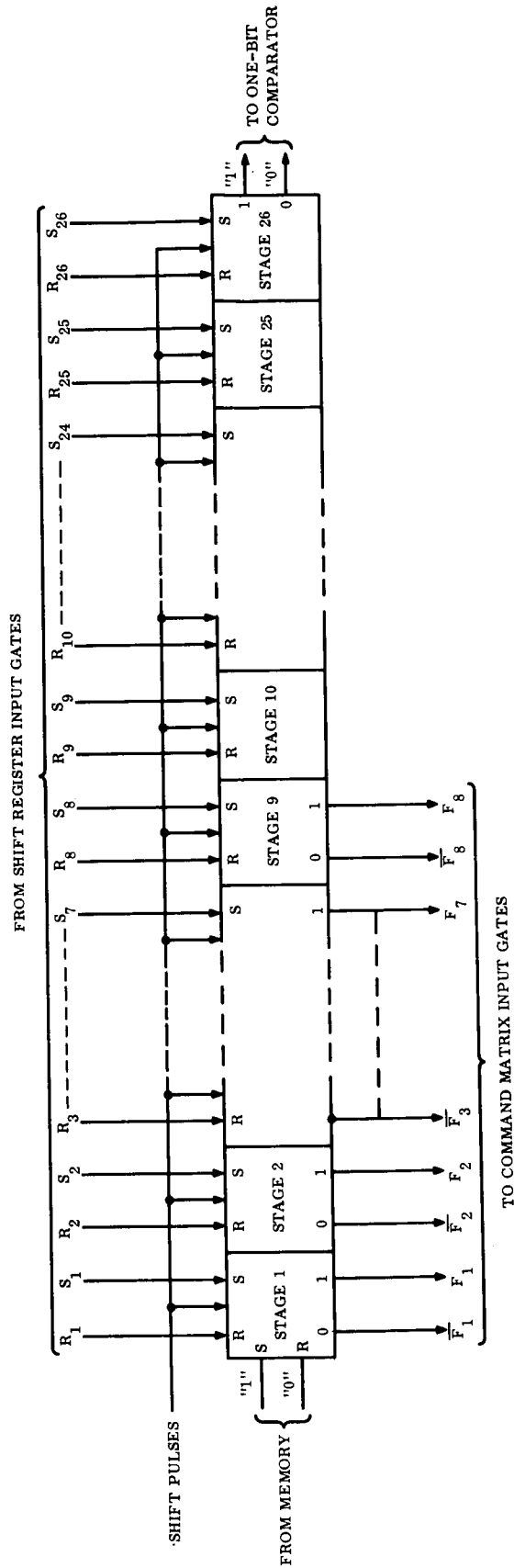


Figure 3-29. C & S Shift Register

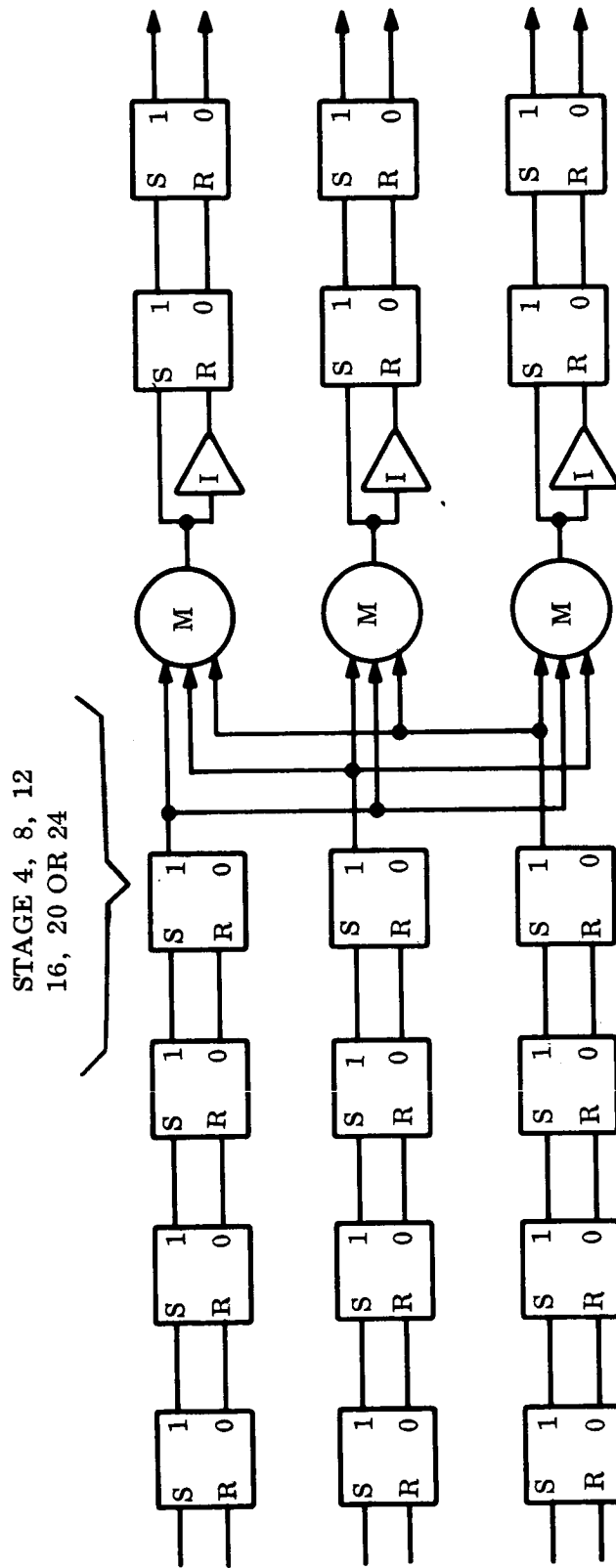


Figure 3-30. C & S Shift Register Internal Redundancy

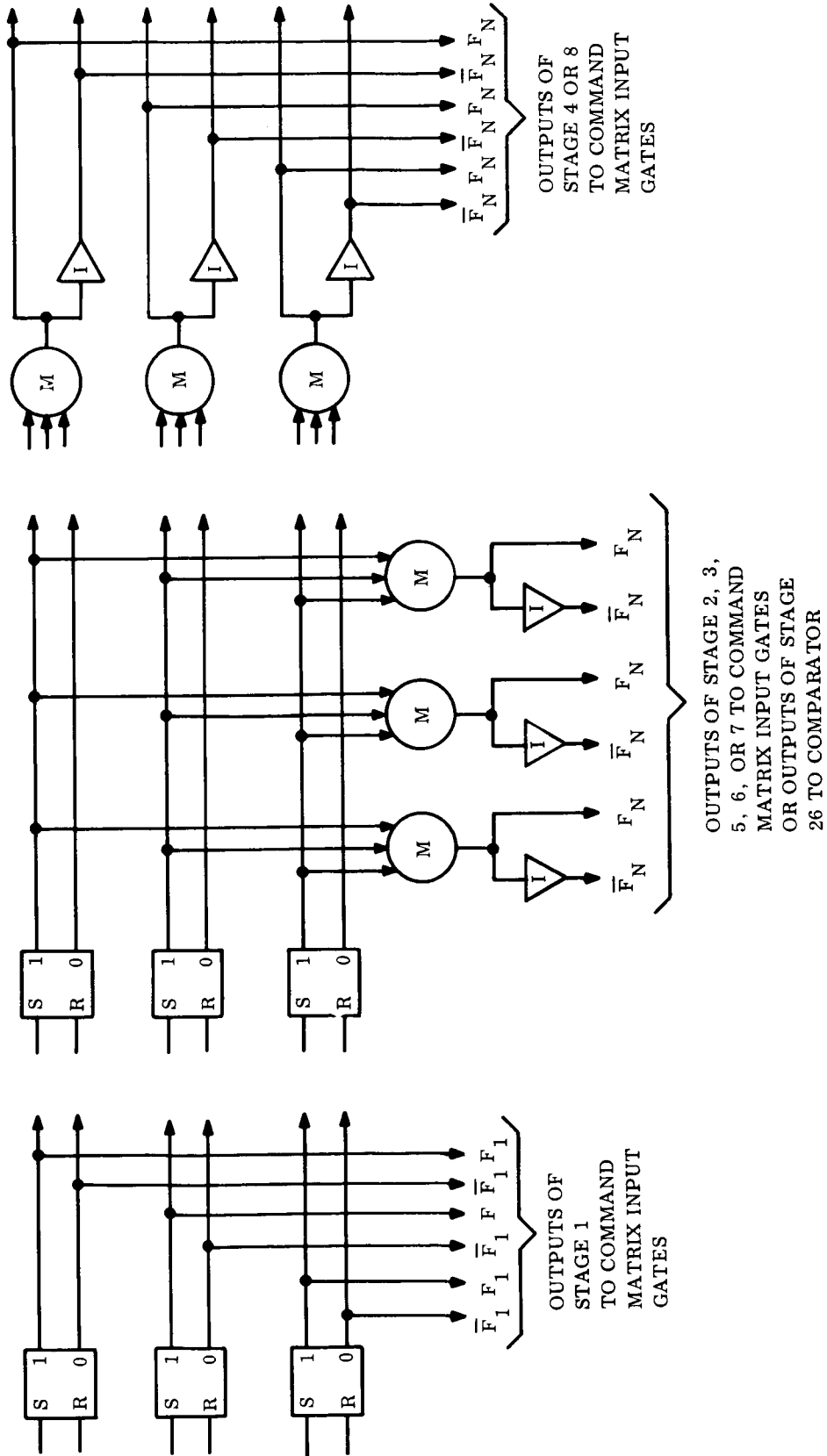


Figure 3-31. C & S Shift Register Output Redundancy

3.1.10 COMPARATOR

Figure 3-32 shows the functional logic of the Comparator. The Comparator receives voltage level signals from the Memories and the Shift Register. It provides to the Control Logic voltage levels indicating match or lack of match of input voltage levels. That is, if both inputs are logical "ones" or both are logical "zeroes", the Comparator provides a logical "one" output level. Otherwise, a logical "zero" output is provided.

Three complete Comparators are used. Each is connected to a different set of input lines and provides a separate output. No internal or output voting is performed.

3.1.11 COMMAND MATRIX INPUT GATES

The functional logic of the Command Matrix Input Gates is shown in Figure 3-33. When a Master Timer Command indication and an execute signal are received simultaneously from the Control Logic, the contents of Address PNG Stages 1 to 8 are presented to the Command Matrix when a Sequence Timer Command indication and an execute signal occur simultaneously. Three complete sets of gates are used. No internal or output voting is performed.

3.1.12 COMMAND MATRIX

Command Matrix logic is shown in Figure 3-34. The Command Matrix decodes a maximum of 255 different stages of an 8-bit word presented to it by the Command Matrix Input Gates. Matrix outputs are connected to the Combining Logic and Output Switches. The Command Matrix redundancy approach is shown in Figure 3-35. Single voting is performed between the second and third logic levels of the matrix. Three complete sets of first and second logic level elements and a single set of third level elements are used.

3.1.13 COMBINING LOGIC & OUTPUT SWITCHES

The Combining Logic and Output Switches component receives inputs from the Command Matrix and provides command signals to the using subsystems. Examples of the various component functions are shown in Figure 3-36. Example (a) occurs where two or more memory addresses are allotted to a Master Timer Command so that two or more time tags can be stored simultaneously. Example (b) is a case of commands to two or more destinations always occurring simultaneously. A single command data word in the Memories is sufficient to initiate output signals to two or more destinations. Example (c) is the common case of a single input signal from the Command Matrix being routed to a single destination. Example (d) is the unique case of stored engine-burn commands requiring enable commands from the ground prior to execution time. Engine burn is a maneuver sequence event. Should inhibiting of engine burn be necessary, commanding of the succeeding events of the sequence will normally be required. Therefore, special provision is made for inhibiting only the engine-burn commands.

Output switches provide closures of approximately 200 milliseconds to the using subsystems. A pulse transformer is incorporated in the circuit configuration to provide isolation of the using subsystems from the C & S. No redundancy is provided in the Combining Logic & Output Switches.

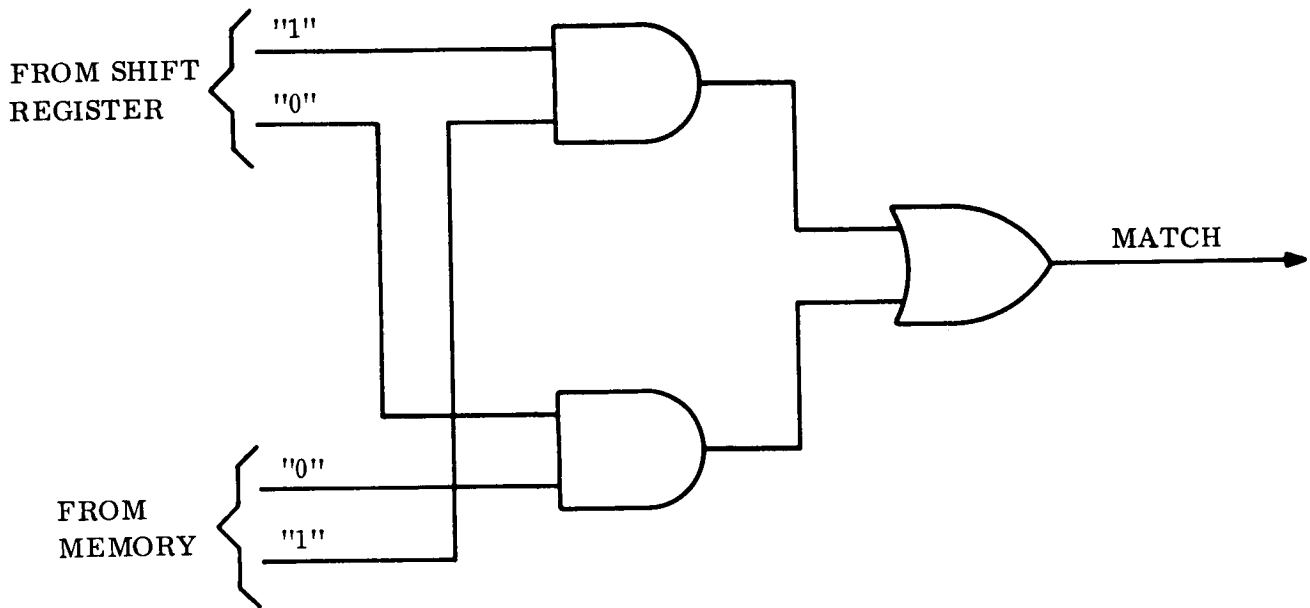


Figure 3-32. C & S Comparator

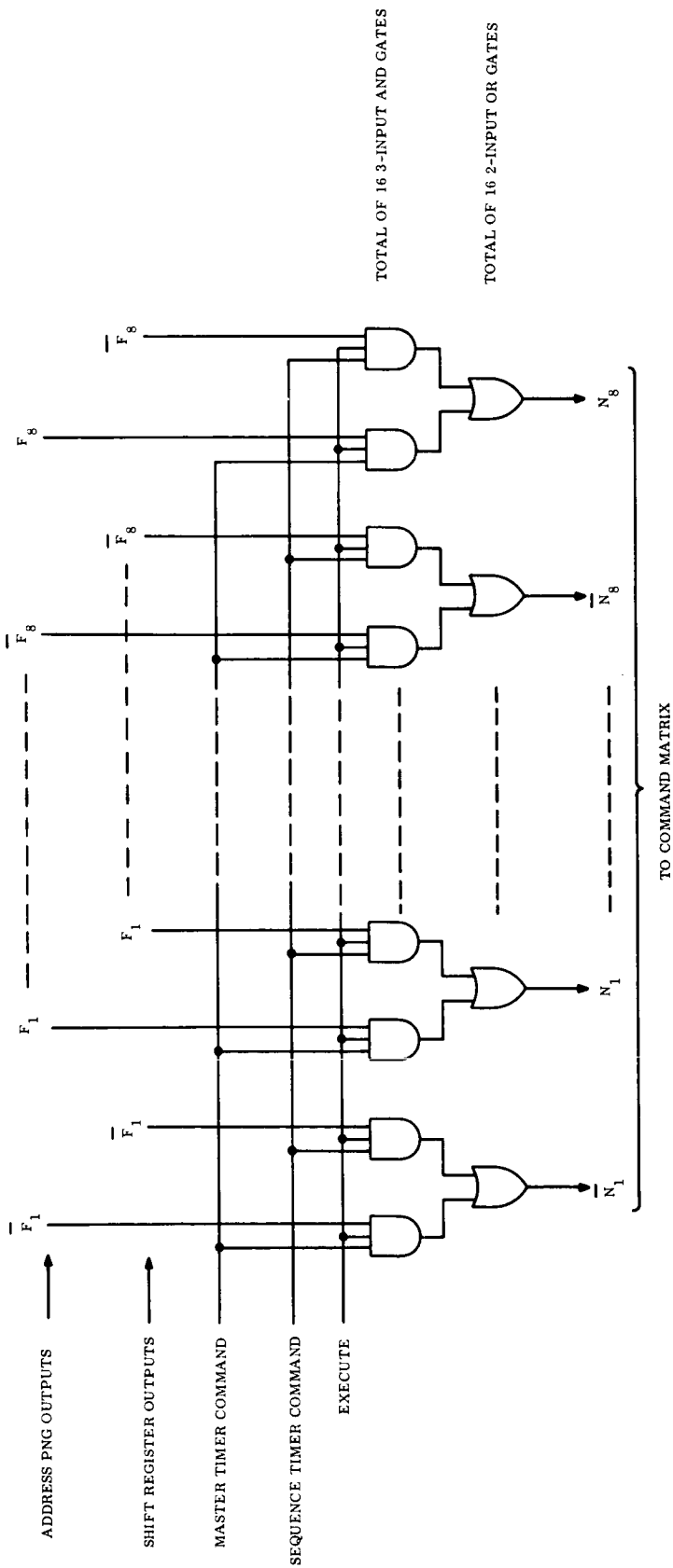


Figure 3-33. C & S Command Matrix Input Gates

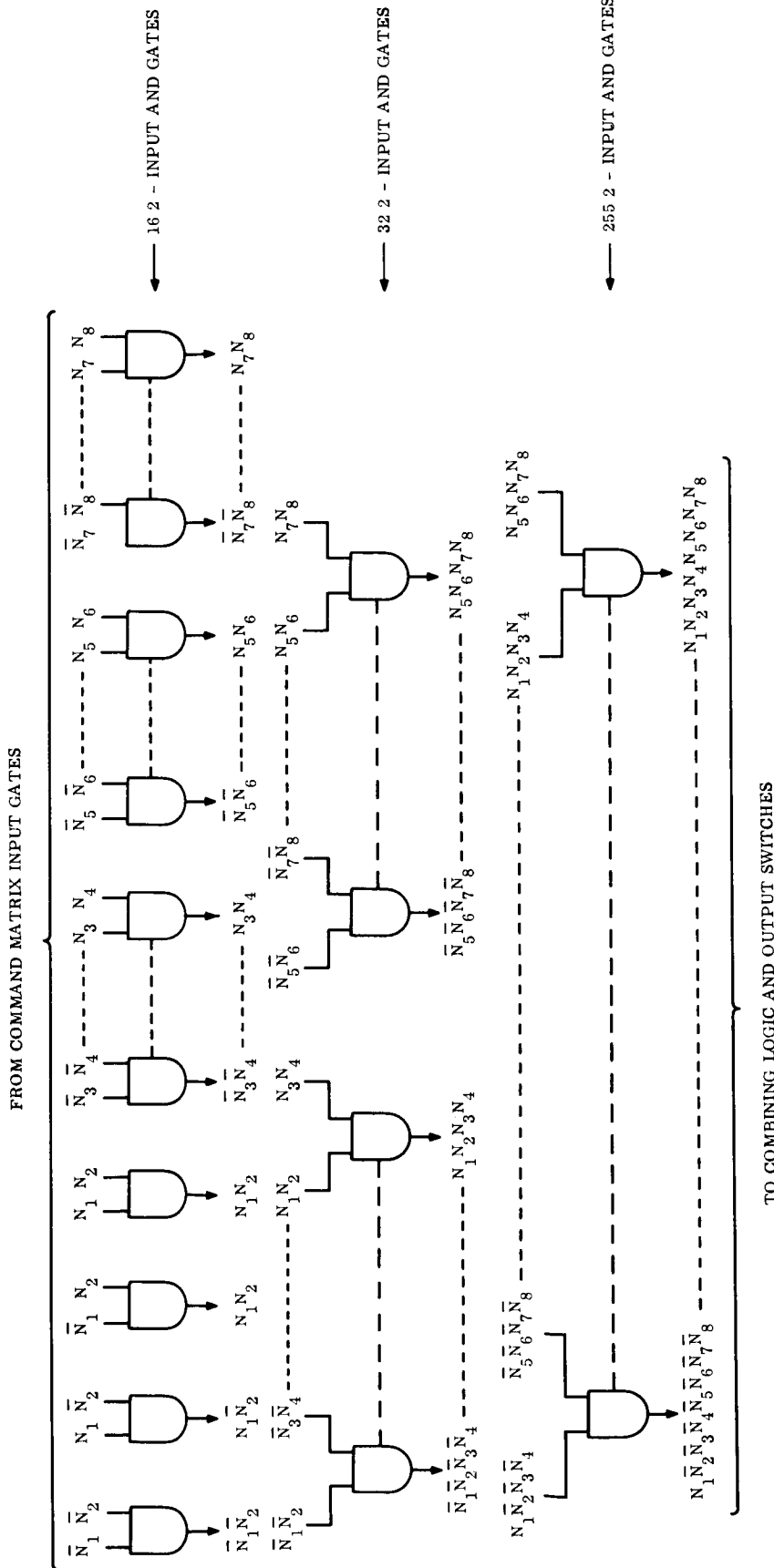


Figure 3-34. C & S Command Matrix

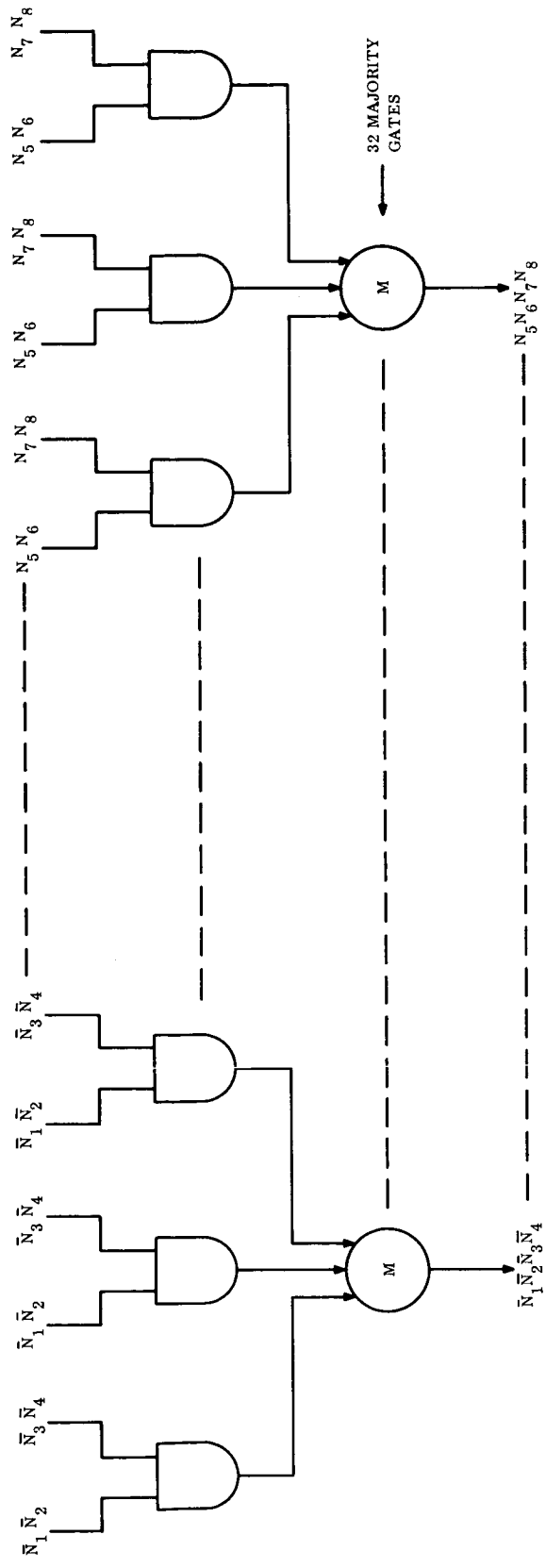


Figure 3-35. C & S Command Matrix Redundancy

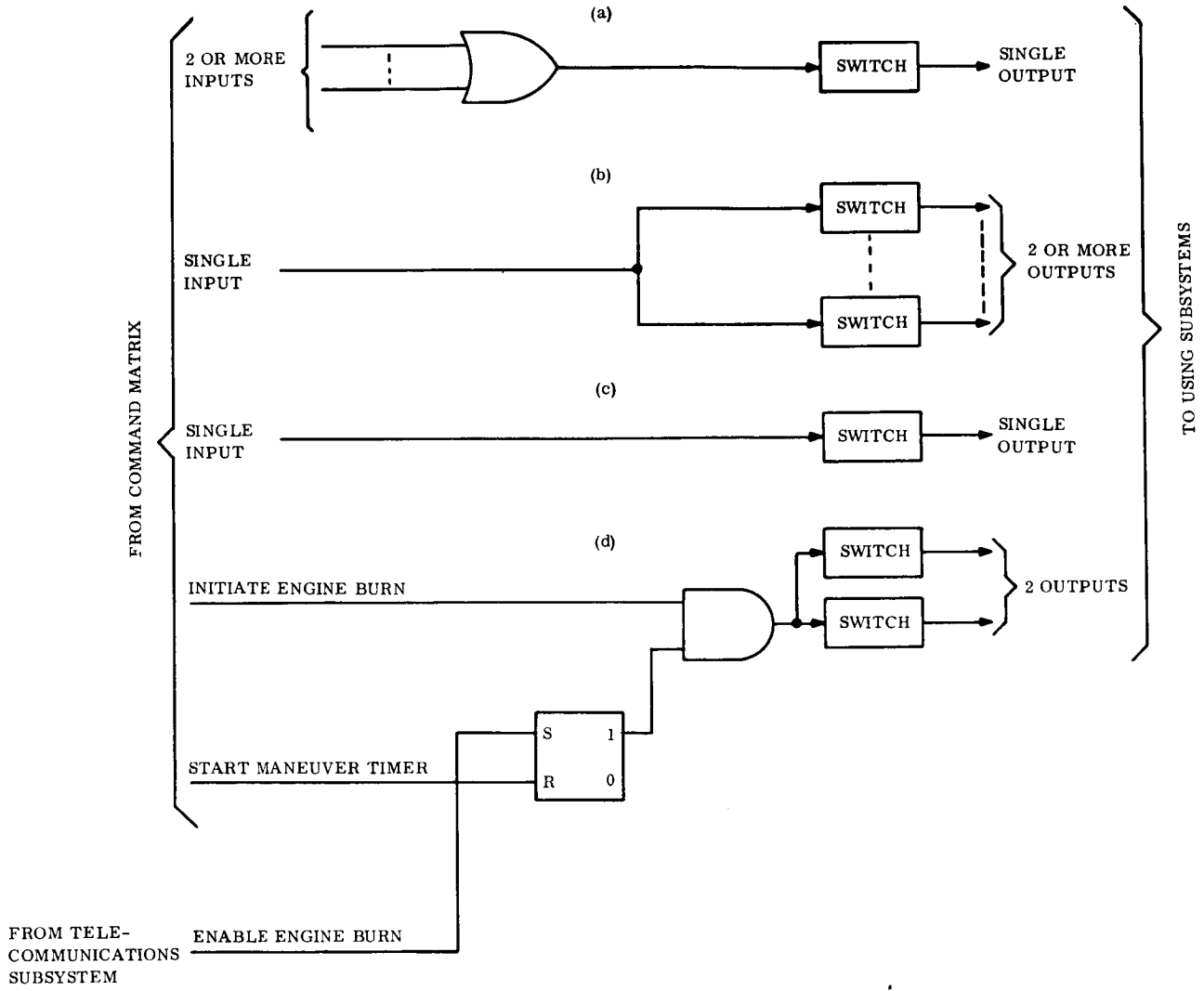


Figure 3-36. Examples of Combining Logic and Output Switches

3.1.14 POWER SUPPLY

The Power Supply input is 50v, 2.4 kc square-wave primary power, from the Electrical Power Subsystem with transformer isolation at the interface. The outputs are + 15, + 6, + 3, and - 3 vdc.

Three complete Power Supplies are used. Each provides power to one set of those C & S components which are triply redundant. Decoupling networks are used at the output of each Power Supply and at a number of points in the Components comprising the load of each supply to protect against short circuits in the load. The location of these networks to most advantage requires a thorough failure-mode analysis as does any approach to providing power to the Oscillators and the non-redundant elements of the C & S.

The use of redundant supplies provides a means of checking operation of all circuits in the triply redundant area of the C & S. If the output of one supply is interrupted, the C & S should continue to operate normally only if all circuits in the loads of the other two supplies are functioning properly. All circuits can be checked by interrupting the outputs of only two power supplies, one at a time.

4.0 INTERFACES

4.1 BOUNDARY DEFINITIONS

4.1.1 INPUT BOUNDARIES

Input boundaries of the C & S are the lines carrying 50v, 2.4 kc square-wave primary power; discrete and quantitative command signals from the Flight Command Subsystem; pre-launch operations signals from the LCE; and C & S output inhibit from the spacecraft-booster separation connector.

4.1.2 OUTPUT BOUNDARIES

Output boundaries of the C & S are solid-state switch closures or interruptions of circuits provided by the using subsystems.

4.2 INTERFACE DEFINITIONS

4.2.1 INPUTS

From LCE:

- a) Step changes in voltage level to inhibit or enable counting of one second pulses by the Master Timer.
- b) Pulses to preset the Countdown Chain and Master Timer and reset and stop the Sequence Timer.

- c) A train of pulses to up-date the Master Timer.
- d) Power supply output inhibits

From Electrical Power Subsystem:

50v, 2.4 kc square-wave primary power with transformer isolation at the interface. Power consumption will be essentially constant throughout the mission.

From Flight Command Subsystem:

- a) A discrete command to inhibit or enable C & S outputs.
- b) A discrete command to select the Memory Scan Mode.
- c) A discrete command to erase an invalid word from the Memory or Memories.
- d) A discrete command to enable engine burn.
- e) Command data words (quantitative commands) described in Figures 2 and 3. A portion of each command data word is stored by the C & S for later read out to control sequencing of other spacecraft subsystems and of the C & S Sequence Timer.

From Spacecraft-Booster Separation Connector:

An inhibit on C & S discrete command outputs which is removed at separation.

4.2.2 OUTPUTS

To LCE:

Quantitative commands as they are received from the Flight Command Subsystem by the C & S.

To Guidance & Control Subsystem:

- a) Discrete commands listed in VB220FD112. These are 200-millisecond closures of circuits supplied by the G & C Subsystem.
- b) A 1 pps square-wave signal to control antenna and scan platform articulation. This is an alternating closure and interruption of a circuit supplied by the G & C Subsystem.

To Pyrotechnic Subsystem:

Discrete commands listed in VB220FD112. These are 200-millisecond closures of circuits supplied by the Pyrotechnic Subsystem.

To Electrical Power Subsystem:

- a) Discrete commands listed in VB220FD112. These are 200-millisecond closures of circuits supplied by the Electrical Power Subsystem.
- b) A 38.4 kc square-wave signal to control power output frequency. This is an alternate closure and interruption of a circuit supplied by the Electrical Power subsystem.

To Telecommunications Subsystem:

- a) Discrete commands listed in VB220FD112. These are 200-millisecond closures of circuits supplied by the Telecommunications Subsystem.
- b) A 153.6 kc square-wave signal to control telemetry data rates. This is an alternating closure and interruption of a circuit supplied by the Telecommunications-Subsystem.
- c) An "event" indication each time a C & S command is issued. This is a 200-millisecond closure of a circuit supplied by the Data Handling & Storage Subsystem.
- d) An indication of the C & S operating mode (Memory Scan or Memory Update). This is a closure or interruption (maintained for the duration of the mode) of a circuit supplied by the Data Handling & Storage Subsystem.
- e) An indication of the state (enabled or inhibited) of the C & S command outputs. This is a closure or interruption (maintained for the duration of the state) of a circuit supplied by the Data Handling & Storage Subsystem.
- f) Indications of the states of all Master and Sequence Timer stages. These are closures or interruptions (maintained for the duration of each state) of circuits supplied by the Data Handling & Storage Subsystem.

To Capsule:

Discrete commands listed in VB220FD112. These are 200 millisecond closures of circuits supplied by the Capsule.

To Data Automation Equipment:

Discrete commands listed in VB220FD112. These are 200-millisecond closures of circuits supplied by the Data Automation Equipment.

5.0 PERFORMANCE PARAMETERS TIMING ACCURACY

C & S basic timing tolerance is \pm one part in 10^4 or 0.01 percent over a temperature range of 40° to 90° F. Spacecraft power frequencies and event initiation are subject to this tolerance.

6.0 PHYSICAL CHARACTERISTICS AND RESTRAINTS

The C & S receives 50v, 2.4 kc square-wave primary power. Power required is 200 watts.

The weight of the C & S is 16 pounds.

Volume of the C & S is 600 cubic inches packaged in two double (300 cubic inches) modules.

Umbilical lines are required for the following signals:

To the LCE from the C & S:

Alert, information, and sync signals as these are received from the Flight Command Subsystem by the C & S.

From the LCE to the C & S:

Inhibit power supply outputs, inhibit count, clear counters, and up-date Master Timer signals to C & S components.

Figure 6-1 is an isometric drawing of the C & S.

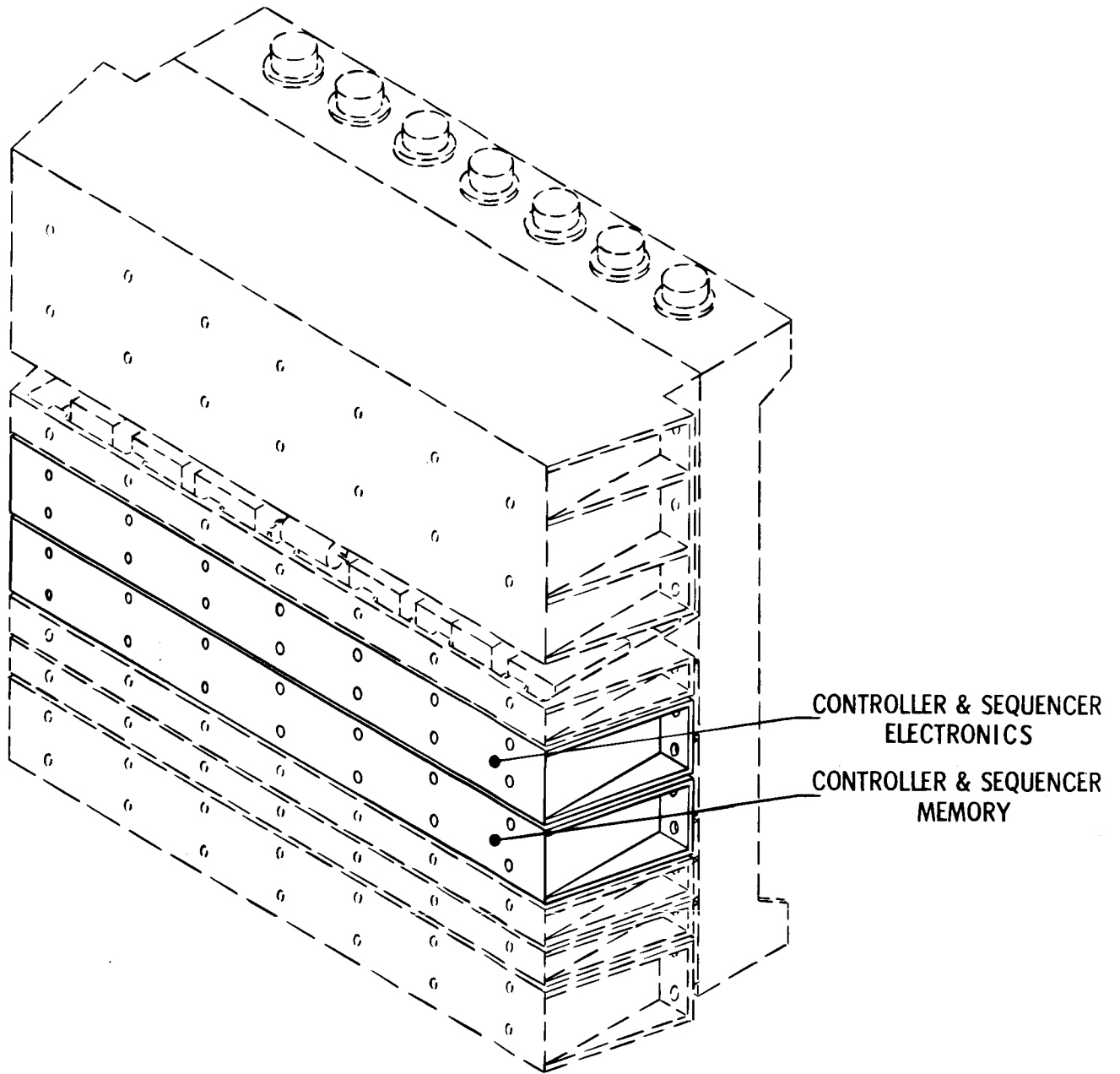


Figure 6-1. Isometric View of Control and Sequencer

CII-VB234FD108

ARTICULATION SUBSYSTEM

Index

1	Scope
2	Applicable Documents
3	Functional Description
4	Interfaces
5	Performance Parameters
6	Physical Characteristics
7	Safety Considerations

1.0 SCOPE

This section describes the articulation subsystem, which orients the High Gain Antenna (HGA) and the Planetary Science Package (PSP). The description covers gimbal requirements, actuation, and control. A discussion of bearings, housings, and supporting structure associated with the gimbals is contained in the Engineering Mechanics section.

2.0 APPLICABLE DOCUMENTS

VB220SR101	Design Characteristics
VB220SR102	Design Restraints
VB220FD110	Telemetry Channel Assignments

3.0 FUNCTIONAL DESCRIPTION

3.1 HIGH GAIN ANTENNA ORIENTATION

The HGA is oriented to the Earth throughout the mission except during slewing of the antenna or the spacecraft, or if the communication distance is less than 15 million kilometers. When the communication distance is less than 15 million kilometers another antenna (rigidly mounted to the spacecraft) is used.

3.2 PLANETARY SCIENCE PACKAGE ORIENTATION

The orientation requirements of the PSP are defined by the following constraints:

- a. In order to preserve image orthogonality, the zenith angle should be less than 30 degrees. The zenith angle is defined as the angle between the instrument line of sight and the local vertical of the observed point on the surface. The zenith angle is 0 when the observed point is the sub-spacecraft point.
- b. The region of planetary surface which is of interest consists of the sunlit side and that portion of the dark side that is within 10 degrees of the terminator.

3.3 SPACECRAFT ORIENTATION

Since the orientation of the HGA and PSP is referenced to the orientation of the spacecraft, it is appropriate at this time to briefly describe the orientation of the spacecraft. The reference coordinate system has its origin at the spacecraft center of mass and consists of the following right-hand triad:

Z axis: The Z axis is parallel to the spacecraft - sun line and is directed away from the Sun.

Y axis: The Y, Z plane contains the guide star, Canopus, with the Y axis directed away from Canopus.

X axis: The X axis completed the right-hand triad, where the order is X, Y, Z.

During midcourse correction maneuvers, the Z axis of the spacecraft is oriented in the direction of the desired ΔV . During separation of the lander, the spacecraft Z axis is pointed in the direction of lander separation. During all the above maneuvers, orientation about the Z axis is used to augment the HGA gimbal.

At all times other than during maneuvers, the spacecraft in its normal cruise attitude. In the cruise attitude, the spacecraft X, Y, and Z axes are oriented to the reference coordinate subsystem X, Y, and Z axes respectively.

3.4 HIGH GAIN ANTENNA GIMBAL ARRANGEMENT

The High Gain Antenna is mounted to the spacecraft through a 2-axis gimbal. Figure 3-1 depicts the gimbal arrangement. At gimbal null the antenna is oriented to the sun. The inboard gimbal (A) rotates the axis of the outboard gimbal (B) about the spacecraft - X axis. The outboard gimbal (B) rotates the antenna about the spacecraft intermediate Y axis. The gimbal ranges are the following

$$-25 \leq A \leq +15$$

$$-50 \leq B \leq +206$$

These gimbal ranges are adequate for Earth orientation of the antenna for all conditions specified in Section 3.1.

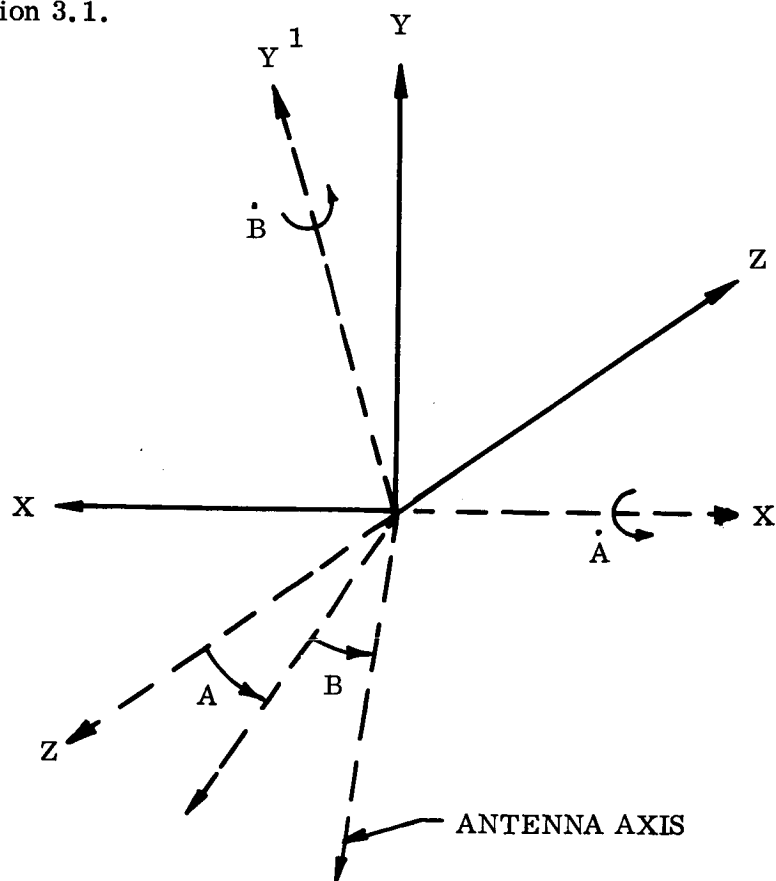


Figure 3-1. Antenna Gimbal Arrangement

In the normal cruise attitude both gimbals are used to orient the antenna. In maneuver attitudes gimbal A is set to 0. Gimbal B and orientation about the Z axis of the spacecraft are used to orient the antenna to the Earth.

The time history of gimbal angles in the cruise mode are given in Figures 3-2, 3-3, 3-4, and 3-5. These figures represent extreme conditions which arise from the earliest and latest possible launch dates for both the 1971 and 1973 missions. Actual conditions will be somewhere between these extremes.

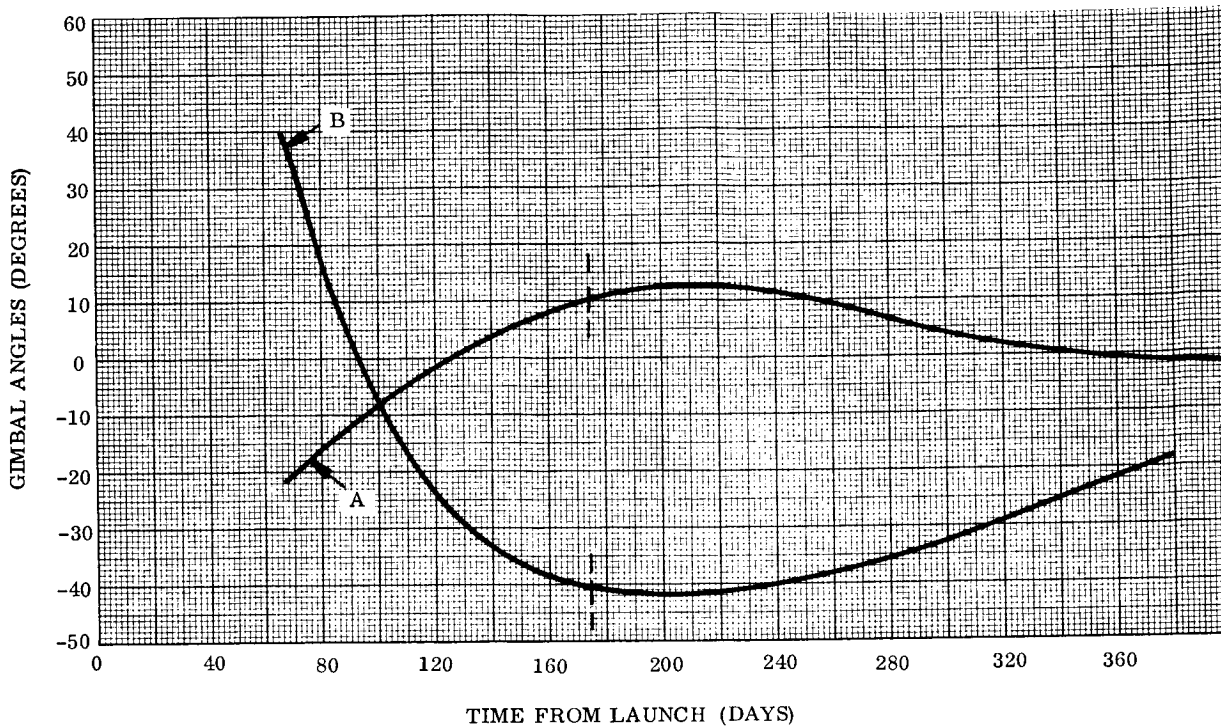


Figure 3-2. Antenna Gimbal Angles, May 3, 1971 Launch

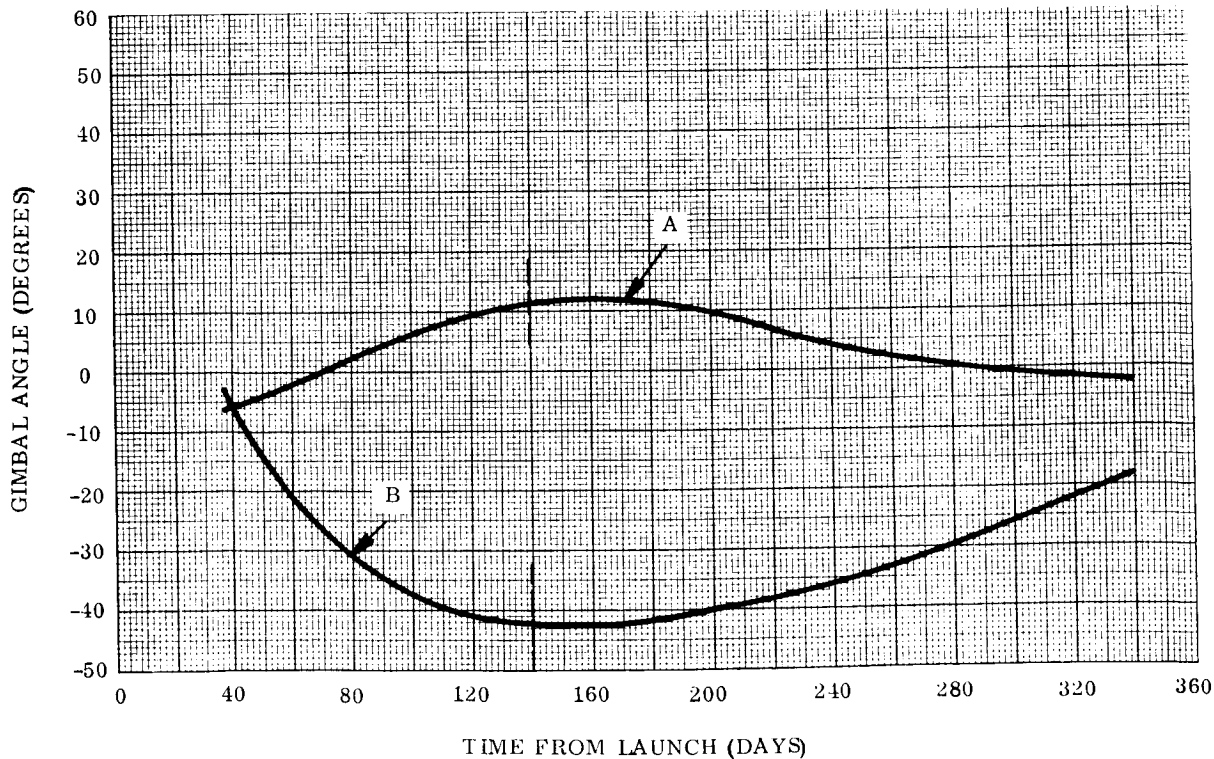


Figure 3-3. Antenna Gimbal Angles, June 22, 1971 Launch

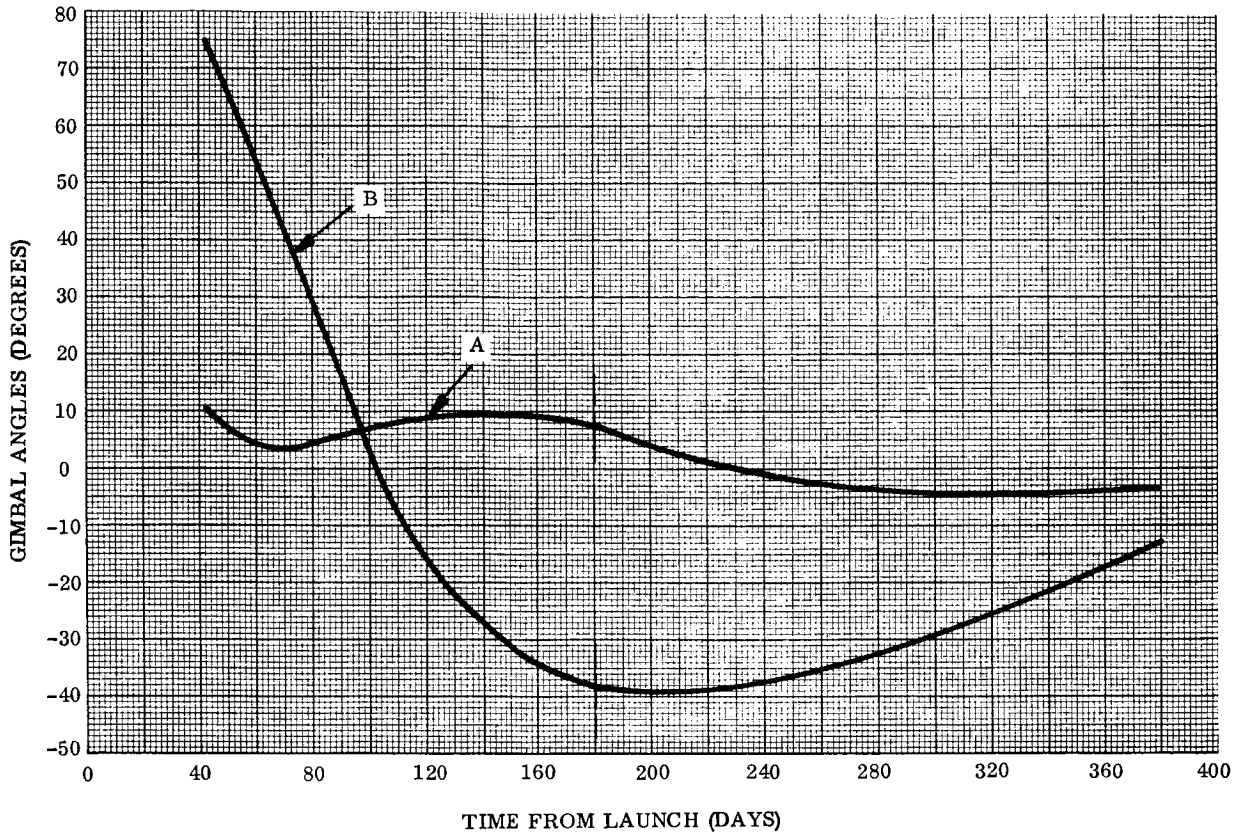


Figure 3-4. Antenna Gimbal Angles, June 8, 1973 Launch

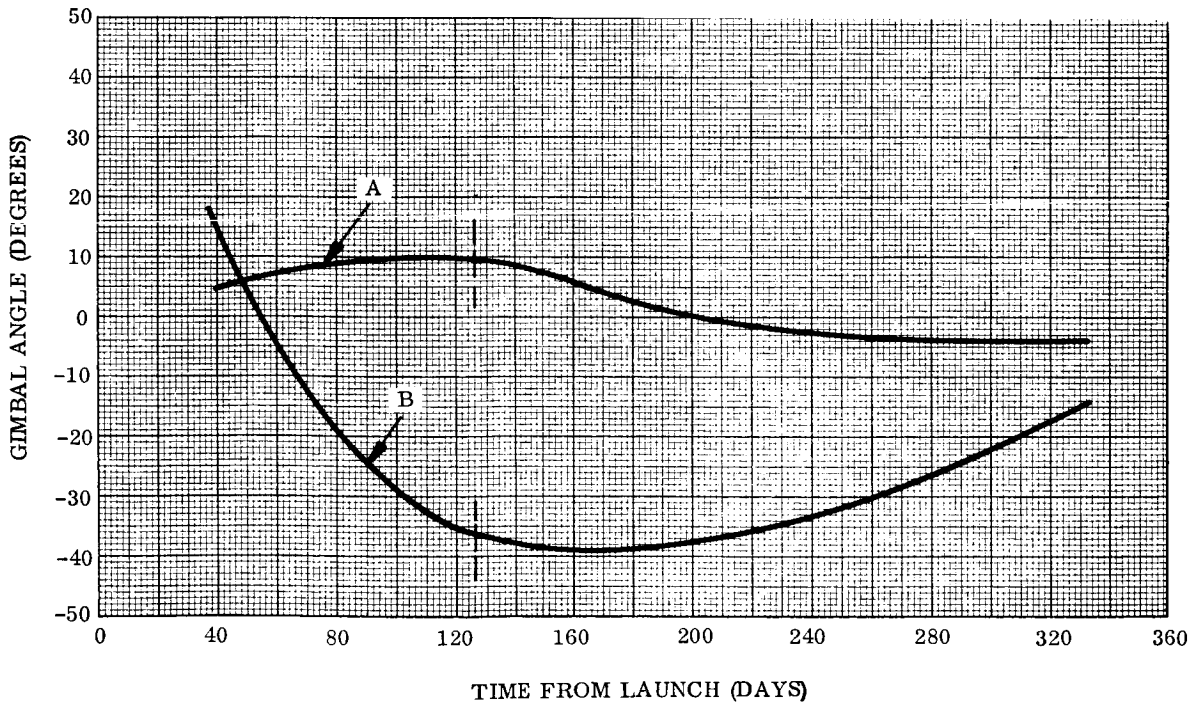


Figure 3-5. Antenna Gimbal Angles, August 15, 1973 Launch

3.5 PLANETARY SCIENCE PACKAGE GIMBAL ARRANGEMENT

The Planetary Science Package (PSP) is mounted to the spacecraft through a 3-axis gimbal. Figure 3-6 depicts the gimbal arrangement. Two axes of this gimbal erect a perpendicular (W) to the plane of the orbit. The third axis rotates the instruments about this perpendicular in such a way that the line of sight of the instruments (L) is parallel to the local vertical. L is maintained parallel to the local vertical throughout the portion of the orbit where the subspacecraft point is on the sunlit side and on the dark side within 10 degrees of the terminators. At gimbal null, W is along the +Y axis of the spacecraft and L is along the -X axis of the spacecraft. The inboard gimbal (C) is a rotation about the +Z axis. The intermediate gimbal (D) is a rotation about the +X' axis. W is at an angle D from the +Y' axis. The outboard gimbal (E) rotates L about W. Thus, L is at an angle E from -X'.

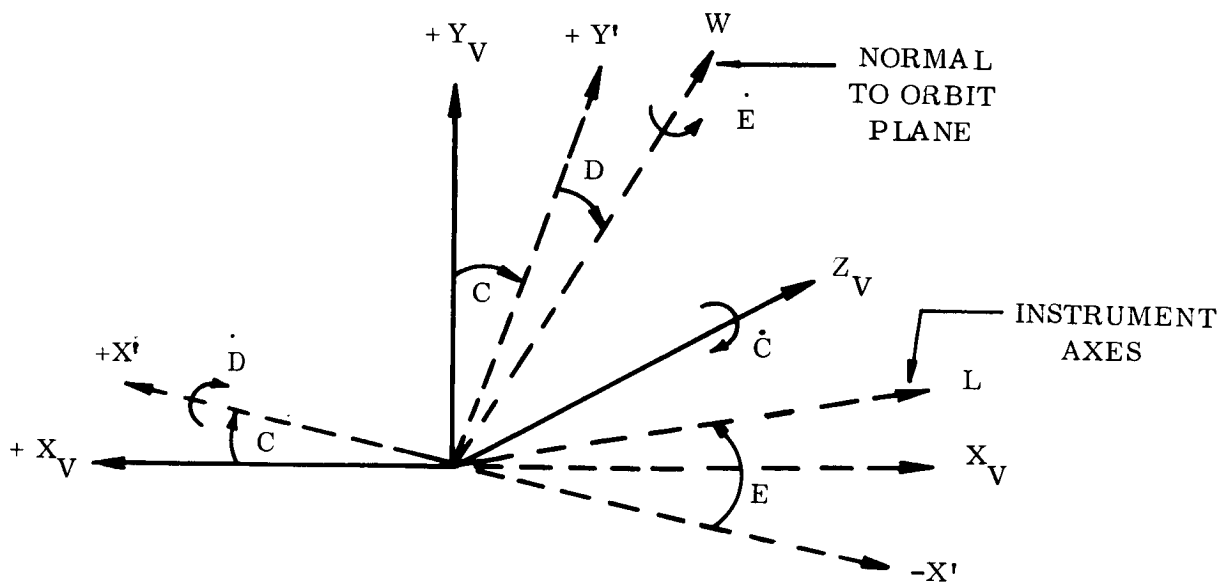


Figure 3-6. Planetary Science Package
Gimbal Arrangement

The gimbal ranges are functions of orbit parameters. For the selected orbit of 3000 kilometers periapsis, 25,000 kilometers apoapsis, and 40 degrees inclination the ranges are as follows:

$$-23 \leq C \leq +53$$

$$-57 \leq D \leq +6$$

$$-10 \leq E \leq +190$$

The time history of gimbal angles for the selected orbit are given in Figures 3-7, 3-8, 3-9, and 3-10.

3.6 GIMBAL ANGLE CONTROL

The primary mode for controlling HGA gimbals A and B and PSP gimbals C and D is through the C & S. Backup mode for these gimbals is directly from the command decoder. Either mode is available at all times.

The primary mode for controlling PSP gimbal E is closed loop through a horizon sensor. Backup mode for this gimbal is through the C & S.

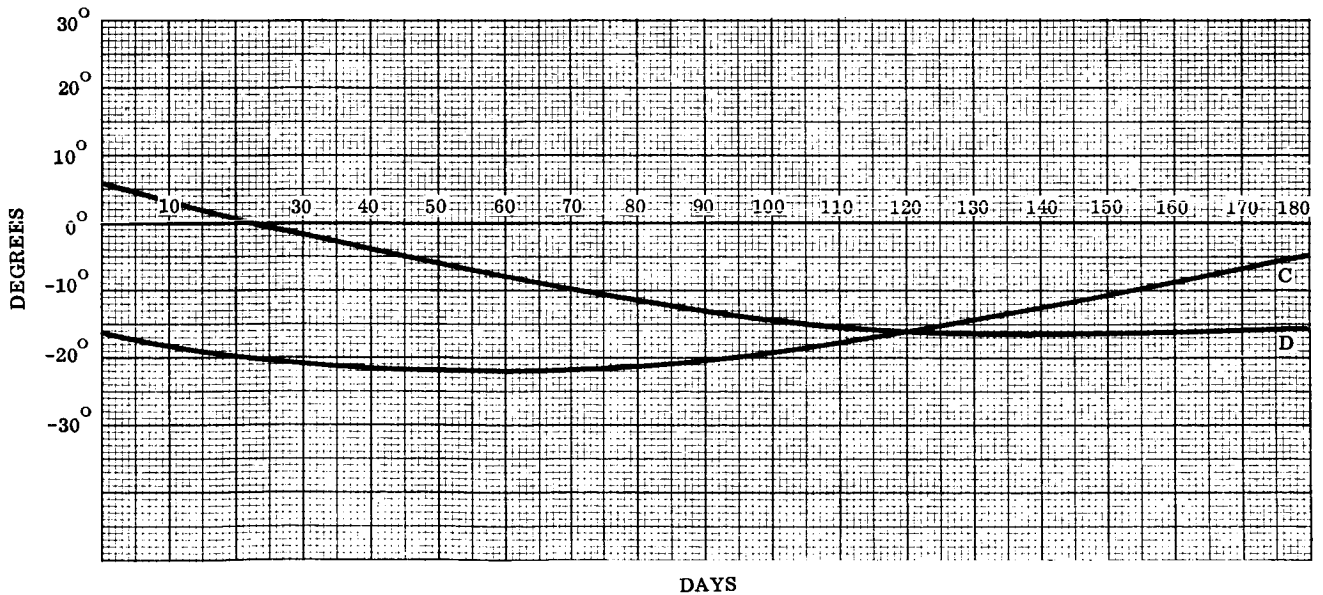


Figure 3-7. PSP Gimbal Angles C & D as a Function of Time
(Nov. 13, 1971 Arrival)

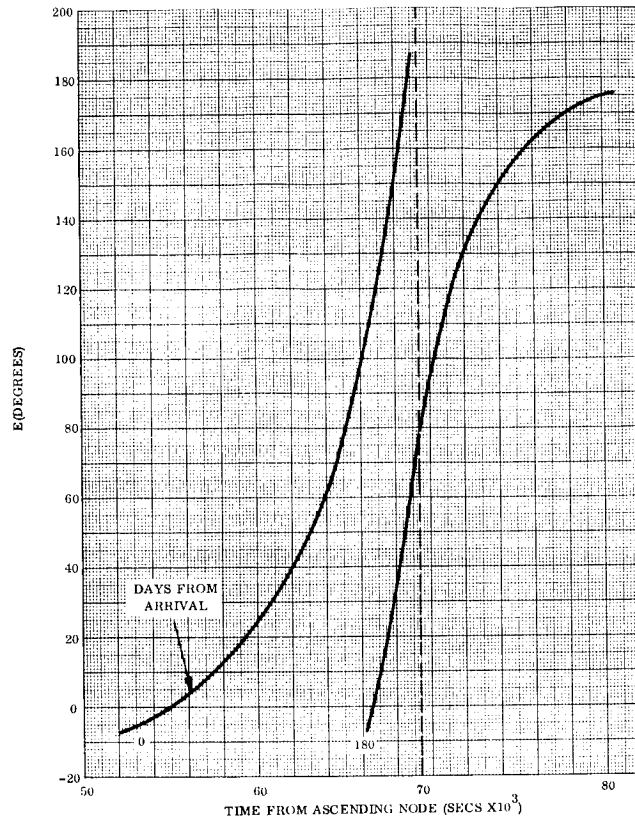


Figure 3-8. PSP Gimbal Angle E as a Function of Time (Nov. 13, 1971 Arrival)

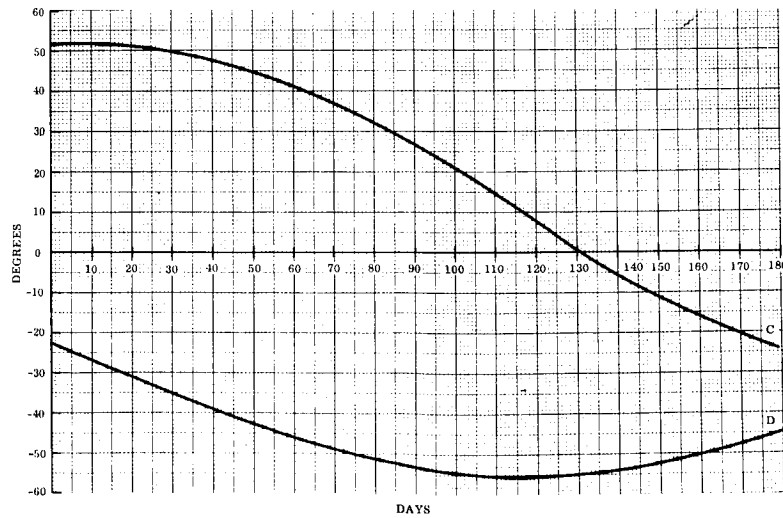


Figure 3-9. PSP Gimbal Angles C & D as a Function of Time (Jan. 25, 1974 Arrival)

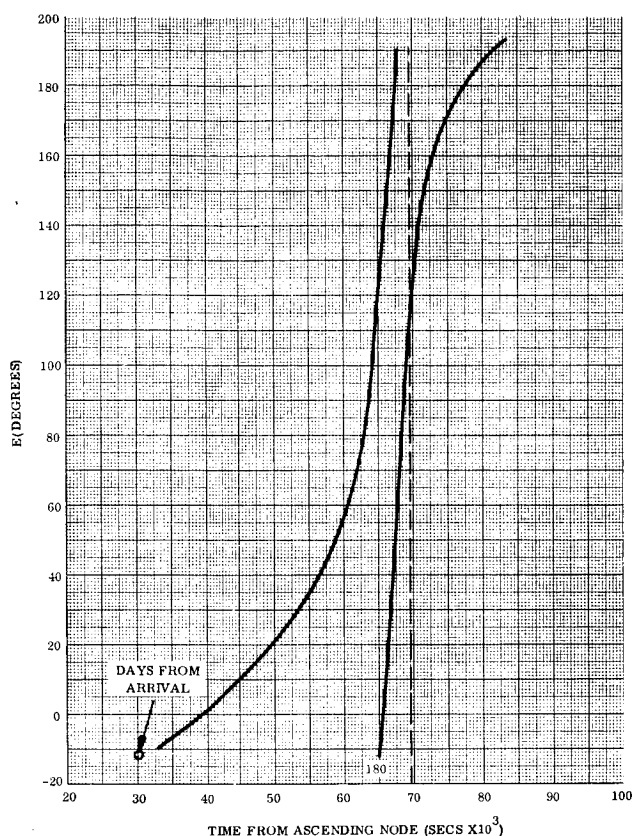


Figure 3-10. PSP Gimbal Angle E as a Function of Time
(Jan. 25, 1974 Arrival)

The block diagram for the gimbal drives is shown in Figure 3-11. All gimbal drives are identical except for components set off in dotted lines. Gimbal angles A, B, C, and D in either mode may be changed one positive or negative increment per command.

A "step 1+" or "step 1-" command from either the C & S or the command decoder is applied at the input of a stepper motor. The motor executes 90-degree steps in the desired direction. These steps are geared down to 1/4 degree at the gimbal.

In the C & S mode all gimbals may be commanded to slew in a positive or negative direction at a rate of one increment (1/4 degree) per second. A C & S command to start positive or start negative slew is used to set a flip-flop. The output of the flip-flop is combined with a clock signal from the C & S. The resulting train of pulses is applied at the input of the stepper motor. Slewing may be stopped by a C & S command. If gimbal stop is encountered, slewing stops automatically.

Gimbal E of the PSP can be commanded to change from the primary to the backup mode (and vice versa) by either the C & S or the command decoder.

During engine firing the stepper motors for gimbals A and B are energized in such a way that they are stalled. Thus, stall torque is available to prevent the gimbals from moving due to engine acceleration.

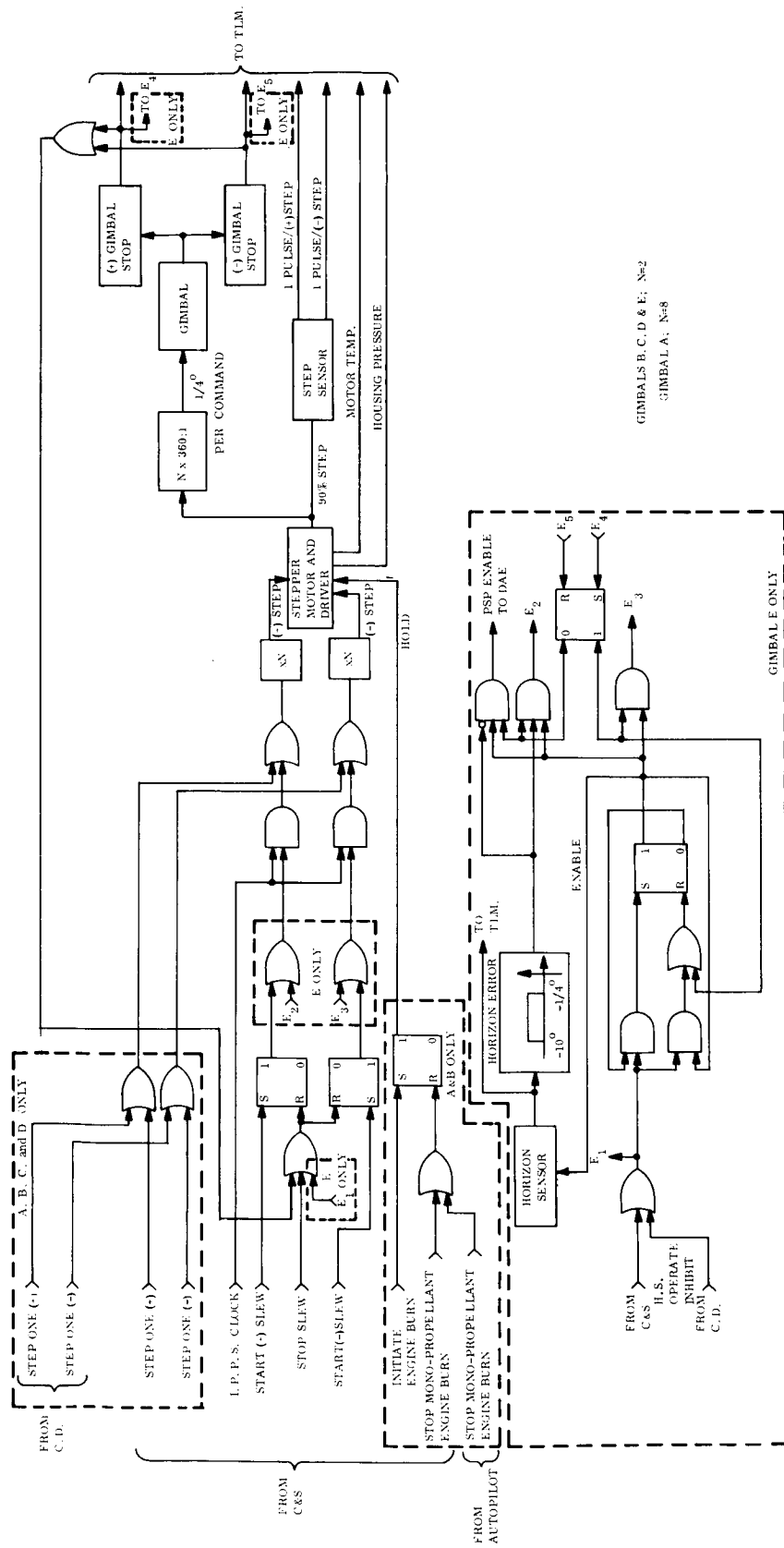


Figure 3-11. Gimbal Drive Block Diagram

When E is in the primary mode the gibal attitude error is sensed by an IR horizon scanner. If the error is less than $-1/4$ degree but greater than -10 degrees and the positive gibal stop is not encountered, gibal E is advanced at a rate of $+1/4$ degree per second. When E is in the primary mode and the positive gibal stop is encountered (10 degrees beyond the evening terminator) the gibal automatically slews at a rate of $-1/4$ degree per second until the negative gibal stop is encountered. Gibal E is then in the proper position for operation at the morning terminator. After slewing to the sunrise position the gibal is automatically switched into the backup mode. The C & S returns the gibal to the primary mode just prior to the start of operation at sunrise.

Gibal pickoff is accomplished by means of a step sensor on the output shaft of the stepper motor. The step sensor drives a reversible counter. The counter is located in the telemetry subsystem. Each time negative gibal stop is encountered the counter is set to zero. Thereafter the counter is made to count up the positive steps and count down the negative steps that are sensed by the step sensor. The output of the counter provides a direct indication of gibal angle. This output is telemetered to the ground along with the positive gibal stop indicator output.

3.7 GIBAL DRIVE COMPONENTS

The following is a functional description of the key components that make up the gibal drive. Such standard components as flip-flop, "and" gates, "or" gates, etc., are not described.

3.7.1 STEPPER MOTOR

A stepper motor is used to drive the gimbals. The motor is the IMC Magnetics Corp. Model Number 020-800, which has the following key characteristics:

Input Voltage	28 volts
Running Energy	.33 watts-second per step
Stall Power	30 watts
Stepping Torque	8 oz. in.
Stall Torque	25 oz. in.
Detent Torque	0.8 oz. in.
Rotor Inertia	15.4 gm cm ²
Weight	26 ozs.

The controller for this motor is the IMC Model No. 1905-103 modified in that it is hermetically sealed.

The operation of this motor and controller are such that for a positive or negative pulse at the input of the controller, the motor executes a positive or negative 90 degree-step of its rotor.

The motor can be put in a "stalled mode." In this mode the motor is energized and acts like a brake. The available holding torque is equal to the stall torque. If the motor is not energized it has some residual holding torque. This torque is referred to above as detent torque.

The output of the motor is geared down to provide the required running or holding torque (whichever is greater) at the gimbal. In general, the required gear ratio is greater than 360 to 1. Therefore, the gimbal will advance less than 1/4 degree per pulse at the input of the controller. The gimbal resolution required is 1/4 degree. An interface component at the input of the motor controller will provide the necessary number of pulses to the controller for every input command, so that the gimbal will execute a 1/4 degree change for every input command to the interface component.

During engines operation the motors that drive gimbals A and B are energized in the stall mode. The resulting stall torque prevents motion of the high gain antenna gimbals due to thrust induced angular acceleration.

3.7.2 STEP SENSOR

A step sensor is provided for each gimbal to monitor 1/4 degree steps of the gimbal. The sensor is basically comprised of a pair of magnetically actuated switches positioned in such a manner that the time sequence of their closure will indicate the occurrence and direction of each step change in angle. The switches are mounted parallel to the axis of a rotating shaft in the drive mechanism and are actuated by one more more equally spaced bar magnets attached to a shaft. In each actuator drive the number of magnets, the number of switched pairs, and the gear ratio of the shaft carrying the magnets, are selected so as to provide one pulse pair for each 1/4 degree step of the outboard end of the gimbal. Table 3-1 specifies the above parameters for the various gimbals.

3.7.3 GIMBAL STOP SENSOR

Limit sensors are provided to detect full positive and full negative angular displacement of each gimbal. The sensors consist of a pair of hermetically sealed snap action switches (e.g., Microswitch 1 HM 1). These switches require a differential travel of .006 in. maximum and therefore can be operated to sense 1/4 degree shaft motion at a radius of 1.5 in.

3.7.4 HORIZON SENSOR

A dither type horizon sensor, made by Advanced Technology Division of American Standard, is used for the horizon sensor. In this sensor, the projected fields of view of 2 thermistor bolometers are made to oscillate (or dither), across the horizon - space interface, at diametrically opposed points on the planetary disc. The action of the sensor causes the center of each dither field to lie close to the horizon edge. The two dither fields are independently controlled to track the horizon edges. The local vertical is determined by bisecting the angle between the dither fields. The local vertical can be determined to within 0.10 degree. The valid error range of this horizon sensor is a function of altitude. At all altitude of interest range is at least ± 45 degrees.

Table 3-1. Step Sensor Parameters

DEVICE	AXIS	STEPPER-TO-LOAD REDUCTION	MOTOR STEPS / .25 degrees LOAD	STEPPER-TO-MAGNET- SHAFT RATIO	NO. OF MAGNETS	NO OF SWITCH PAIRS	K (see note)
HIGH GAIN ANTENNA	A	2880:1	8	2:1	1	1	1
	B	720:1	2	1:1	2 or 1	1 or 2	2
PLANETARY SCIENCE PACKAGE	C	720:1	2	1:1	2 or 1	1 or 2	2
	D	720:1	2	1:1	2 or 1	1 or 2	2
	E	720:1	2	1:1	2 or 1	1 or 2	2

NOTE: Wherever an optional number of switchpairs and magnets is given, the product of the number of magnets and number of switch pairs shall equal K.

4.0 INTERFACES

The following is a definition of the key interfaces between the articulation subsystem and the various other subsystems.

4.1 MECHANICAL INTERFACES

4.1.1 ATTITUDE CONTROL INTERFACE

The gimbals in the articulation subsystem are referenced to the spacecraft coordinate system. Therefore, the articulation subsystem is dependent on the attitude control for orientation of the gimbal references.

4.1.2 ENGINEERING MECHANICS INTERFACE

The articulation subsystem is dependent on the engineering mechanics for rigid alignment of the gimbal references to the spacecraft coordinate system. Bearings, housings, and mechanism sealing is also provided by engineering mechanics.

4.1.3 PYROTECHNICS

Both the HGA and PSP are caged in the launch configuration. The articulation subsystem is dependent on the pyrotechnics for uncaging and deploying the HGA and the PSP.

4.2 ELECTRICAL INTERFACES

4.2.1 C & S INTERFACE

Primary controls for gimbals A, B, C, and D and backup control for gimbal E are derived from signals provided by the C & S. Gimbal E switching from primary to backup mode and vice versa is also derived from the C & S.

The gimbal angle control signals from the C & S to each of the gimbals are as follows:

Step 1 (+): (all but gimbal E)	This signal is used to advance the gimbal +1/4 degree (E. C. 20, 22, 24, 26)
Step 1 (-): (all but gimbal E)	This signal is used to advance the gimbal -1/4 degree (E. C. 21, 23, 25, 27)
Start (+) Slew:	This signal is used to start the gimbal slewing at a rate of +1/4 degree per second. (S. C. 18, 20, 23, 25, 27)

Start (-) Slew:	This signal is used to start the gimbal slewing at a rate of $-1/4$ degree, per second (S. C. 19, 21, 24, 26, 29)
Stop Slew:	This signal is used to stop all gimbal slew. (S. C. 22, 28)
One Plus Per Second Clock:	This signal is used as the stepping rate during gimbal slewing. It is provided to the gimbal drive at all times.

In addition to the above signals, Gimbal E derives the following signal from the C & S:

Change Gimbal E Mode:	This signal is used to change gimbal E from the primary mode to the backup mode or vice versa.
-----------------------	--

In addition to the above commands, gimbals A and B derive the following commands from the C & S:

Initiate Engine Burn:	This signal is used to energize the stepper motors in a stall mode (E. C. 37)
Stop Mono-Prop Engine Burn:	This signal is used to turn off the stepper motor stall mode (S. C. 34)

All of the above signals are pulses with a trailing edge transient suitable for triggering a flip-flop.

If the C & S is used to drive the gimbals while the spacecraft is in the cruise mode, the drive requirements are as depicted in Figures 3-2, 3-3, 3-4, 3-5, 3-7, 3-8, 3-9, and 3-10.

The number of C & S commands required to drive the various gimbals while in the cruise mode are given in Table 4-1.

4.2.2 INTERFACE WITH THE COMMAND DECODER

Backup control for all gimbals (except E) is derived from the command decoder. The gimbal angle control signals from the command decoder to each of the gimbals (except E) are as follows:

Step 1 (+):	This signal is used to advance the gimbal $+1/4$ degree.
Step 1 (-):	This signal is used to advance the gimbal $-1/4$ degree.

Gimbal E receives the following signal from the decoder:

Change gimbal E mode:	This signal is used to change gimbal E from the primary mode to the backup mode or vice versa.
-----------------------	--

Table 4-1. Number of Commands Required to Drive Gimbals (Cruise Attitude)

	May 3, 1971 Launch		June 22, 1971 Launch		July 8, 1973 Launch		August 15, 1973 Launch	
	15 MKM to Encounter	Orbit	15 MKM to Encounter	Orbit	15 MKM to Encounter	Orbit	15 MKM to Encounter	Orbit
A	128	60	72	56	60	56	28	52
B	324	88	80	68	452	92	216	76
C				92				304
D				100				176
E				1600 per Orbit				1600 per Orbit

Horizon Error:

This signal is an indication of the error output of the horizon sensor. The signal ranges from -1.6 to +1.6 Volts DC.

4.2.4 POWER SUBSYSTEM INTERFACE

Electrical power for operation of the articulation subsystem is derived from the power subsystem. The required power is 50 volts at 2400 cycles per second square wave. Power switching for the articulation subsystem is contained in the power subsystem.

4.2.5 INTERFACE WITH THE DATA AUTOMATION EQUIPMENT (DAE)

Gimbal E, in the horizon sensor mode provides a logic signal to the DAE. Logical 1 indicates that gimbal E is properly aligned and is not undergoing a step change in attitude.

All of the above signals are pulsed with a trailing edge transient suitable for triggering a flip-flop. If the command decoder is used to drive the gimbals during the cruise mode, the drive requirements are as depicted in Figures 3-2, 3-3, 3-4, 3-5, 3-7, 3-8, 3-9, and 3-10.

The number of commands required to drive the various gimbals while in the cruise mode is given in Table 4-1, Section 4.2.1.

4.2.3 INTERFACE WITH THE TELEMETRY SUBSYSTEM

All gimbals have the following interfaces with the telemetry subsystem:

+ Step Sensor
(-Step Sensor):

These signals are provided to the telemetry subsystem as an indication of a change in gimbal angle. The signals are pulses suitable for driving a flip-flop. The differences between the number of + step signals and - step signals received is accumulated in a reversible counter located in the telemetry subsystem. The state of the counter is telemetered to the ground.

+ Gimbal Stop
(-Gimbal Stop):

These signals are provided to the telemetry subsystem to indicate that positive or negative gimbal stop has been encountered. When negative gimbal stop is encountered the reversible counter in the telemetry subsystem is set to zero. When positive gimbal stop is encountered, an indication of this fact is telemetered to the ground. Gimbal stop signals are in the standard logic level format.

Motor Temperature:

This signal is an indication of the gimbal motor temperature. The signal range is 0 to 100 millivolts DC.

Housing Pressure:

This signal provides an indication of the pressure in the gimbal actuator housing. The signal ranges from 0 to +3.2 volts DC.

In addition to the above signals gimbal E provides the following signals to the telemetry subsystem:

5.0 PERFORMANCE PARAMETERS

The following is a description of performance parameters for the various components which make up the articulation subsystem. In addition to these performance parameters, there is provided in this section an error budget for the HGA and PSP orientation.

5.1 STEPPER MOTOR PARAMETERS

The critical parameters of the stepper motor are as follows:

Stepper Torque/Speed:

The torque/speed characteristics of the motor is such that it can drive the gimbal load in a zero-G field at a speed of 1/4 degree per second.

Holding Torque:

For gimbal A and B the holding torque is sufficiently high to prevent motion of the gimbal during firing of the retro-engine. During retro engine firing, the gimbal motors are energized so that the full stall torque holds the gimbals. For gimbals C, D, and E the detent torque is sufficiently high to prevent motion of these gimbals (during) firing of the attitude control jets.

5.2 STEP SENSOR PARAMETERS

The step sensor senses the occurrence of each 90-degree change in motor shaft angle for any speeds from 0 to 2 steps per second.

5.3 GIMBAL STOP SENSOR PARAMETERS

The gimbal stop sensor detects the occurrence of gimbal stop with an accuracy of 1/4 degree.

5.4 HGA ERROR BUDGET

The following is an error budget for all of the elements of the systems which affect the orientation of HGA:

	Cruise	Maneuver
Antenna Beam Alignment to Antenna Geometry	0.1	0.1
Antenna Geometry Alignment to Gimbal	0.05	0.05
Gimbal Alignment to Spacecraft	0.05	0.05

	Cruise	Maneuver
Attitude Control Sensor Error (2 axis RSS)	0.18	0.32
Gimbal Backlash (2 axis RSS)	<u>0.07</u>	<u>0.07</u>
RSS	0.23	0.35
Attitude control Error (2 axis RSS)	0.67	1.4
Gimbal Quantization (2 axis RSS)	0.18	0.18
C & S Error	<u>nil</u>	<u>nil</u>
ARITHMETIC SUM	1.08	1.93

5.5 PSP ERROR BUDGET

The following is an error budget for all of the elements of the system which affect the orientation of the PSP:

Instrument Alignment to Structure	0.10
Structure Alignment to Gimbal	0.05
Gimbal Alignment to Spacecraft	0.05
Spacecraft Attitude Control Sensor Error (2 axis RSS)	0.18
Gimbal Backlash (2 axis RSS)	0.07
Horizon Sensor Error	0.10
Horizon Sensor Alignment	<u>0.05</u>
RSS	0.27
Spacecraft Attitude Control Error (2 axis RSS)	0.67
Gimbal Quantization Error (2 axis RSS)	0.18
C & S Error	nil
Gimbal E Control Error	<u>0.10</u>
ARITHMETIC SUM	1.22

6.0 PHYSICAL CHARACTERISTICS

The following are the key physical characteristics for the components which make up the articulation subsystem:

COMPONENT	QUANTITY	WEIGHT	POWER
Stepper Motor	5	1.6 lbs	30 watts* .3 W avg.
C & S and C.D. Interface Electronics	5	.5 lbs	(included above)
Mars Vertical Sensor (Control and Horizon Sensor	1	6.5 lbs	4.4 W avg.
SUBSYSTEM TOTALS		8.6 lbs	5.9 W avg.

* During Engine Burn, Gimbals A & B only.

The following is the estimated reliability of the articulation subsystem during the various phases of the mission:

MISSION PHASE	DURATION	RELIABILITY	
		HGA	PSP
Separation and Acquisition	1 hr.		
Transit	178 days	.976	
Orbit Injection	2 days	.999	
Orbit	30 days	.996	.977
TOTAL MISSION	210 days	.971	.977

7.0 SAFETY CONSIDERATIONS

7.1 OPERATOR SAFETY

There are no operator safety hazards in the articulation subsystem.

7.2 EQUIPMENT SAFETY

The equipment shall be designed with the following equipment safety considerations:

- a. There will be no damage to the equipment if stepper motors are commanded to drive while the gimbals are caged or against gimbal stop.
- b. There will be no damage to equipment if the gimbals are driven, by an external torque applied to the outboard end of the gimbal, at less than 10 degrees per second. If the gimbals are uncaged in a one-G field, care must be taken to prevent unrestraining motion of the outboard end of the gimbals.

CII-VB235FD101

TEMPERATURE CONTROL SUBSYSTEM FUNCTIONAL DESCRIPTION

Index

- 1 Scope
- 2 Applicable Documents
- 3 Functional Description
- 4 Interface Definition
- 5 Performance Parameters
- 6 Physical Characteristics and Constraints
- 7 Thermal Subsystem Safety Considerations

1.0 SCOPE

This functional description describes the method of Flight Spacecraft temperature control for all mission phases along with an identification of the associated subsystem boundaries, performance parameters, physical characteristics, constraints and safety considerations.

2.0 APPLICABLE DOCUMENTS

1. VB220SR101 - Design Characteristics
2. VB220SR102 - Design Restraints
3. VB220FD103 - Spacecraft Component Design Parameters
4. VB220FD113 - Layout and Configuration
5. VB220FD105 - Launch Vehicle Interface
6. VB220FD106 - Flight Capsule Interface

3.0 FUNCTIONAL DESCRIPTION

3.1 INTRODUCTION

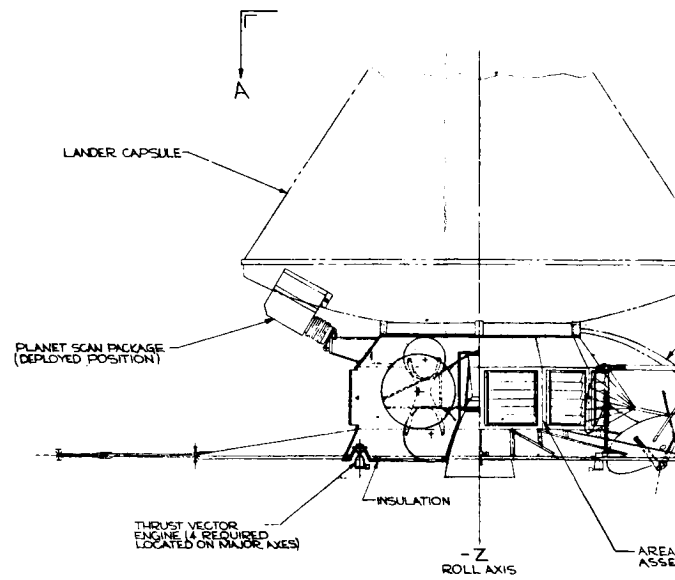
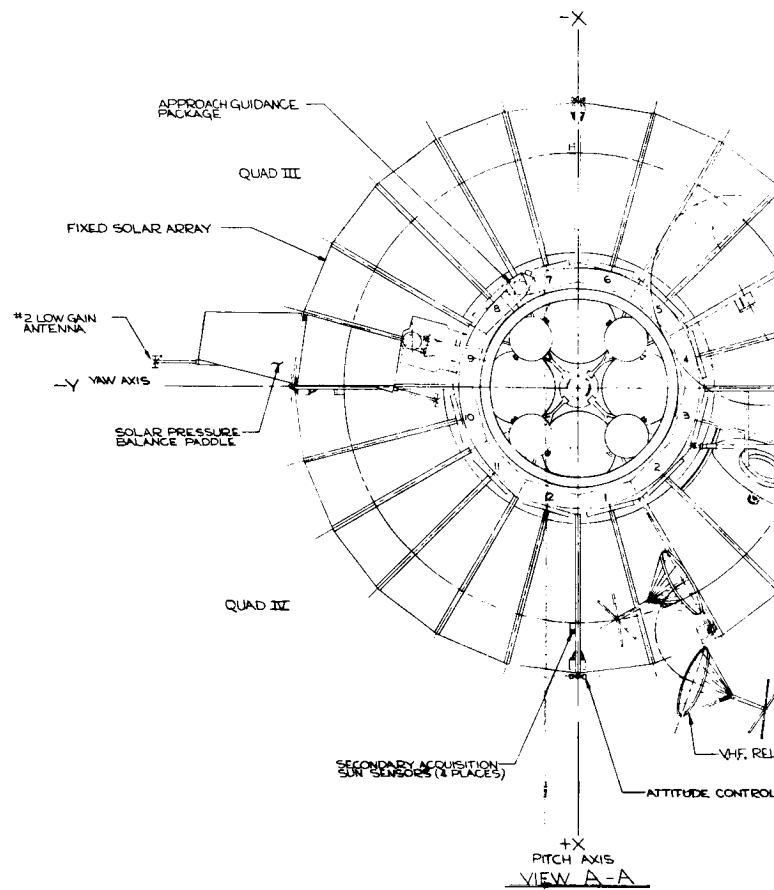
The purpose of the temperature control subsystem is to maintain all equipments within specified temperature ranges to enhance and maintain operational reliability. The Ag-Cd batteries must be maintained between 40° and 80°F. The monopropellant (hydrazine) must be kept above 35°F. The biopropellants should be held between 40° and 80°F with a maximum temperature difference between them of 10°F. The Freon gas must be maintained between 40° and 100°F. Therefore, the average temperature of all assemblies is maintained between 40° and 70°F thereby allowing for a 10°F difference between sub-assemblies and their mounting panels. It is recognized that local temperatures beneath some high dissipating sub-assemblies (the power amplifier, power supply in the radio subsystem for example) will measurably exceed 80°F. These exceptions are not detrimental to sub-assembly performance. Practical temperature limits for all equipment are listed in the Thermal Balance Drawing, (Figure 3-1).

The methods of thermal control employed for various parts of the vehicle for the several mission phases are described below.

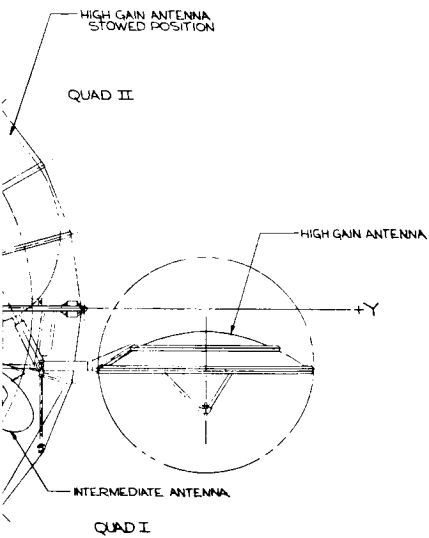
3.2 GROUND TEMPERATURE CONTROL

3.2.1 GROUND TRANSPORT

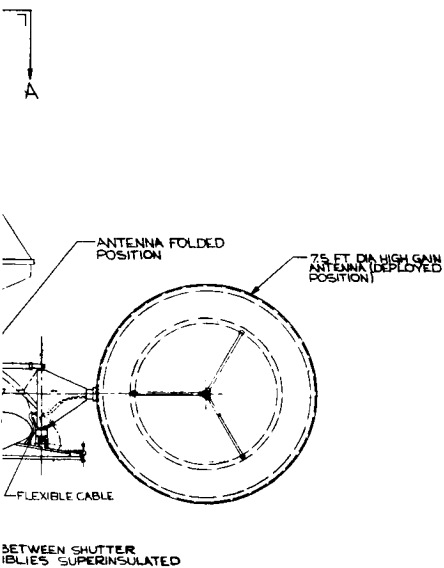
The ground transport spacecraft container is covered with an insulated blanket to reduce solar heat loads or nocturnal cooling effects. Temperature and humidity conditioned air are also supplied to the transportation container.



4-①



Y ANTENNA
NOZZLES



BETWEEN SHUTTER
BLINDS SUPERINSULATED

NOTES

1. BAY TO BAY CONDUCTION CONDUCTANCE = 0.73 BTU/HR/FT²
2. PLACE SILICONE GREASE ON MOUNTING SURFACES OF ALL ELECTRONIC SUBASSEMBLIES IN BUS SECTION.
3. SUPERINSULATION THICKNESS = 1/4 INCH ON NORMALLY NON-ILLUMINATED SURFACES. 25 LAYERS OF 1/4 MIL MYLAR, ALUMINIZED ON BOTH SIDES WITH AN OUTER LAYER OF 2 MIL ALUM. FOIL, ATTACHED WITH VELCRO FASTENERS AND STAINLESS STEEL THREAD. SUPERINSULATION AROUND ALL 100' XFT. ENGINEERS TO CONSIST OF 3 MIL STAINLESS STEEL FOIL (OUTER LAYER) BACKED WITH 3 PPS 0.1" FELT & 1 MIL STAINLESS STEEL FOIL, WITH 25 LAYERS 1/4 MIL ALUMINIZED MYLAR AS INNERMOST LAYERS IN AN OVERALL THICKNESS OF 0.6 INCH.
5. FLEXIBLE CABLES TO SCAN PLATFORM (HIGH GAIN ANTENNA WRAPPED WITH 25 LAYERS 1/4 MIL ALUMINIZED MYLAR WITH AN OUTER LAYER OF 2 MIL AL FOIL TO APPROXIMATE 1/4 INCH THICKNESS.
6. FREON LINES CONTAINED IN SUPERINSULATED CONDUIT (1/4 INCH THICKNESS OF 25 LAYERS OF 1/4 MIL ALUMINIZED MYLAR, AND OUTER LAYER OF 2 MIL AL FOIL.
7. SUPERINSULATION THICKNESS = 0.4 INCH ON NORMALLY ILLUMINATED SURFACES. OUTER LAYER IS 3 MIL AL FOIL BACKED BY 3 PPS. OF 1 MIL AL FOIL, 1/2 MIL TISSULAS, WITH 20 INNERMOST LAYERS OF 1/4 MIL AL MYLAR.
8. ALL BLANK SPACES ON THIS DRAWING WILL BE FILLED IN AS PART OF PHASE I B EFFORT.

41 (7)

COMPONENT	MISSION PHASE	AVG. THERMAL DISSIPATIONS															TEMP LIMITS					EXPECTED TEMPERATURE																					
		ON PAD		ASCENT		PARKING ORBIT (EARTH)		ACQUISITION		CRUISE		MID-COURSE MANEUVER		APPROACH		REFROPRE		ILLUM MARES ORBIT		SUN OCCULTER MARES ORBIT		WEIGHT POUNDS		THERMAL RANGE (LET/UF)		MOUNTING CLEARANCE (ET/UF)		NON OPERATING	OPERATING		ON PAD		ASCENT		PARKING ORBIT (EARTH)		ACQUISITION		CRUISE		MID-COURSE MANEUVER		
		MAX	MIN	MAX	MIN	MAX	MIN	MAX	MIN	MAX	MIN	MAX	MIN	MAX	MIN	MAX	MIN	MAX	MIN	MAX	MIN	MAX	MIN	MAX	MIN	MAX	MIN	MAX	MIN	MAX	MIN	MAX	MIN	MAX	MIN	MAX	MIN	MAX	MIN	MAX	MIN	MAX	
TOTAL BAY #1 (SCIENCE 5/6)		00.00		00.00		00.00		00.00		00.00		00.00		00.00		00.00		00.00		00.00		10.00		2.4		1.0		10.00		10.00		10.00		10.00		10.00		10.00		10.00			
TOTAL BAY #2 (DAS/SCIENCE)		00.00		00.00		00.00		00.00		00.00		00.00		00.00		00.00		00.00		00.00		10.00		5.5		10.3		10.00		10.00		10.00		10.00		10.00		10.00		10.00		10.00	
TOTAL BAY #3 (DATA HANDLING 5/6)		00.00		00.00		00.00		00.00		00.00		00.00		00.00		00.00		00.00		00.00		10.00		58.5		11.7		10.00		10.00		10.00		10.00		10.00		10.00		10.00		10.00	
TOTAL BAY #4 (DATA HANDLING 5/6)		00.00		00.00		00.00		00.00		00.00		00.00		00.00		00.00		00.00		00.00		10.00		42.0		8.4		10.00		10.00		10.00		10.00		10.00		10.00		10.00		10.00	
TOTAL BAY #5 (COMMAND 5/6)		00.00		00.00		00.00		00.00		00.00		00.00		00.00		00.00		00.00		00.00		10.00		44.5		8.9		10.00		10.00		10.00		10.00		10.00		10.00		10.00		10.00	
TOTAL BAY (NORMAL COND.)		00.00		00.00		00.00		00.00		00.00		00.00		00.00		00.00		00.00		00.00		10.00		22.9		4.6		10.00		10.00		10.00		10.00		10.00		10.00		10.00		10.00	
BAY #1 (RADIO 5/6)		00.00		00.00		00.00		00.00		00.00		00.00		00.00		00.00		00.00		00.00		10.00		1.1		0.1		10.00		10.00		10.00		10.00		10.00		10.00		10.00		10.00	
BAY #2 (RADIO 5/6)		00.00		00.00		00.00		00.00		00.00		00.00		00.00		00.00		00.00		00.00		10.00		1.1		0.1		10.00		10.00		10.00		10.00		10.00		10.00		10.00		10.00	
BAY #3 (RADIO 5/6)		00.00		00.00		00.00		00.00		00.00		00.00		00.00		00.00		00.00		00.00		10.00		1.1		0.1		10.00		10.00		10.00		10.00		10.00		10.00		10.00		10.00	
BAY #4 (RADIO 5/6)		00.00		00.00		00.00		00.00		00.00		00.00		00.00		00.00		00.00		00.00		10.00		1.1		0.1		10.00		10.00		10.00		10.00		10.00		10.00		10.00		10.00	
BAY #5 (RADIO 5/6)		00.00		00.00		00.00		00.00		00.00		00.00		00.00		00.00		00.00		00.00		10.00		1.1		0.1		10.00		10.00		10.00		10.00		10.00		10.00		10.00		10.00	
TOTAL BAY #1 (POWER 5/6)		00.00		00.00		00.00		00.00		00.00		00.00		00.00		00.00		00.00		00.00		10.00		7.0		10.1		10.00		10.00		10.00		10.00		10.00		10.00		10.00		10.00	
TOTAL BAY #2 (POWER 5/6)		00.00		00.00		00.00		00.00		00.00		00.00		00.00		00.00		00.00		00.00		10.00		7.0		10.1		10.00		10.00		10.00		10.00		10.00		10.00		10.00		10.00	
TOTAL BAY #3 (POWER 5/6)		00.00		00.00		00.00		00.00		00.00		00.00		00.00		00.00		00.00		00.00		10.00		7.0		10.1		10.00		10.00		10.00		10.00		10.00		10.00		10.00		10.00	
TOTAL BAY #4 (POWER 5/6)		00.00		00.00		00.00		00.00		00.00		00.00		00.00		00.00		00.00		00.00		10.00		7.0		10.1		10.00		10.00		10.00		10.00		10.00		10.00		10.00		10.00	
TOTAL BAY #5 (POWER 5/6)		00.00		00.00		00.00		00.00		00.00		00.00		00.00		00.00		00.00		00.00		10.00		7.0		10.1		10.00		10.00		10.00		10.00		10.00		10.00		10.00		10.00	
TOTAL BAY		00.00		00.00		00.00		00.00		00.00		00.00		00.00		00.00		00.00		00.00		10.00		17.4		10.1		10.00		10.00		10.00		10.00		10.00		10.00		10.00		10.00	

4-3

THERMAL CONTROL - 1/2 TELEMETRY SENSORS

SUBSYSTEM	TYPE SENSOR	SENSOR LOCATION	MISSION PHASE	DATA PRIORITY	SENSOR OUTPUT	SCALE UNITS	SENSOR OPERATING RANGE	MAXIMUM TEMPERATURE	SAMPLING RATE	MODE	WORD FRAME NO.
POWER	TEMP	SOLAR ARRAY	ALL EXCEPT SUN SHUTTER	C	0 TO 100 MV	°F	250° To -100° F	± 5	1 PER SCAN	ABNORMAL	
		SOLAR ARRAY	2 PER EACH BATTERY	A			100° To -350° F		1 PER SCAN	ABNORMAL	
RADIO	TEMP	VCO #1	REC	C			40° To 80° F		1 PER SCAN	ABNORMAL	
		VCO #2					100° To 200° F		1 PER SCAN	ABNORMAL	
STRUCTURE	TEMP	2 PER BAY ON COMPONENT MOUNTING PANEL BAYS 1, 5, 6, 8, 10, 11, 12					0° To 250° F		1 PER SCAN	ABNORMAL	
		2 PER BAY # 2 & 3							1 PER SCAN	ABNORMAL	
	TEMP	FLY CASE TO SCAN PLATFORM					-100° To 200° F		1 PER SCAN	ABNORMAL	
		FLY CASE TO M. GUN ANTENNA					0° To 90°		1 PER SCAN	ABNORMAL	
GUIDANCE & CONTROL	TEMP	ACCELEROMETER					0° To 200° F		1 PER SCAN	ABNORMAL	
		APPROACH GUIDANCE SENSORS					-200° To 200° F		1 PER SCAN	ABNORMAL	
GUIDANCE & CONTROL	TEMP	SUN RATE/TARGET ACQUISITION/CRUISE SENSORS					-200° To 200° F		1 PER SCAN	ABNORMAL	
		1 PER SECONDARY ACQUISITION SUN SENSOR							1 PER SCAN	ABNORMAL	
GUIDANCE & CONTROL	TEMP	COMBAT SCAN TRAILER					-100° To 200° F		1 PER SCAN	ABNORMAL	
		MAR. VERTICAL SENSOR							1 PER SCAN	ABNORMAL	
GUIDANCE & CONTROL	TEMP	SCAN PLATFORM ACTUATOR					-100° To 200° F		1 PER SCAN	ABNORMAL	
		SCAN PLATFORM ACTUATOR							1 PER SCAN	ABNORMAL	
GUIDANCE & CONTROL	TEMP	ANTENNA ACTUATOR					-100° To 200° F		1 PER SCAN	ABNORMAL	
		ANTENNA ACTUATOR							1 PER SCAN	ABNORMAL	
GUIDANCE & CONTROL	TEMP	1 PER SOLENOID CENTER							1 PER SCAN	ABNORMAL	
		2 PER INSTRUMENT ON SCAN PLATFORM							1 PER SCAN	ABNORMAL	
SCIENCE PAYLOAD	TEMP	2 PER INSTRUMENT ON BUS BODY							1 PER SCAN	ABNORMAL	
		1 PER FUEL SYSTEM PRESSURIZATION TANK FOR BIPROPELLANT DATED 5/2					0° To 130° F		1 PER SCAN	ABNORMAL	
SCIENCE PAYLOAD	TEMP	1 PER FUEL & PRESSURIZATION TANK FOR PROPELLANT 5/2							1 PER SCAN	ABNORMAL	
		1 PER FUEL & PRESSURIZATION TANK FOR PROPELLANT 5/2							1 PER SCAN	ABNORMAL	

*Data Priorities:
 A. Real Time Analysis
 B. Near Real Time Analysis
 C. Post Pass/Post Flight Analysis

EXPECTED TEMPERATURES (°F)

ON PNO

ASCENT

PARKING ORBIT (BRTM)

ACQUISITION

CRUISE

WPS COURSE MANEUVER

APPROACH

RETROFIRE

LLUM. MAPS ORBIT

SUN OCCULTED MAPS ORBIT

ALLOWABLE TOLERANCE FOR EACH SENSOR

ON PNO		ASCENT		PARKING ORBIT (BRTM)		ACQUISITION		CRUISE		WPS COURSE MANEUVER		APPROACH		RETROFIRE		LLUM. MAPS ORBIT		SUN OCCULTED MAPS ORBIT		ALLOWABLE TOLERANCE FOR EACH SENSOR	
MIN	MAX	MIN	MAX	MIN	MAX	MIN	MAX	MIN	MAX	MIN	MAX	MIN	MAX	MIN	MAX	MIN	MAX	MIN	MAX	MIN	MAX

HEATER LOCATIONS

ITEM	HEATER CAPACITY (W)	LAUNCH PAD	ASCENT	EARTH ORBIT	ACQUISITION
FRESH TANK #1	2.0*	0.0	0.0	0.0	0.0
FRESH TANK #2	2.0*	0.0	0.0	0.0	0.0
FRESH TANK #3	2.0*	0.0	0.0	0.0	0.0
FRESH TANK #4	2.0*	0.0	0.0	0.0	0.0
FRESH TANK #5	2.0*	0.0	0.0	0.0	0.0
SCAN PLATFORM					
INST A	2.0	1.0	1.0	1.0	1.0
INST B	2.0	1.0	1.0	1.0	1.0
INST C	2.0	1.0	1.0	1.0	1.0
MONOPROPELLANT TANK #1	2.0*	0.0	0.0	0.0	0.0
MONOPROPELLANT TANK #2	2.0*	0.0	0.0	0.0	0.0
MONOPROPELLANT TANK #3	2.0*	0.0	0.0	0.0	0.0
MONOPROPELLANT TANK #4	2.0*	0.0	0.0	0.0	0.0
HIGH GAIN ANTENNA FLEX CABLE	1.0	1.0	1.0	1.0	1.0
SCAN PLATFORM FLEX CABLE	1.0	1.0	1.0	1.0	1.0
GYRO #1	2.0	0.0	0.0	0.0	0.0
GYRO #2	2.0	0.0	0.0	0.0	0.0
GYRO #3	2.0	0.0	0.0	0.0	0.0

HEATER DIM LENGTH x WIDTH (IN) x (IN)

LAUNCH PAD

ASCENT

EARTH ORBIT

ACQUISITION

CONDUCTIVITY (BTU IN/FT HOURS IN) x (IN)

* FOR CONTINGENCY PURPOSES ONLY

MOUNTING PANEL

BAY NO.	THICKNESS (IN)	CONDUCTIVITY (BTU IN/FT HOURS IN) x (IN)	EXPOSED SURFACE (FT ²)
1	0.08	70.0	2.0
2			4.0
3			6.0
4			8.0
5			10.0
6			12.0
7			14.0
8			16.0
9			18.0
10			20.0
11			22.0
12			24.0

62

THERMOSTAT LOCATION						THERMOSTAT SET POINTS (°F)		
TED AVERAGE DISSIPATION (W)						ON	OFF	HIGH LIMIT
MID-COURSE MANEUVERS	APPROACH	RETRO MANEUVER	ILLUM. MARS ORBIT	SUN OCCULTED MARS ORBIT				
0.0	0.0	0.0	0.0	0.0	NEAR TANK MOUNTS			
0.0	0.0	0.0	0.0	0.0	NEAR TANK MOUNTS			
1.0	1.0	1.0	1.0	1.0	ADJACENT TO SOLENOID CLUSTER #1			
1.0	1.0	1.0	1.0	1.0	ADJACENT TO SOLENOID CLUSTER #2			
1.0	1.0	1.0	1.0	1.0	ADJACENT TO SOLENOID CLUSTER #3			
1.0	1.0	1.0	1.0	1.0	ADJACENT TO SOLENOID CLUSTER #4			
0.0	0.0	0.0	0.0	0.0	NEAR TANK MOUNTS			
0.0	0.0	0.0	0.0	0.0	NEAR TANK MOUNTS			
0.0	0.0	0.0	0.0	0.0	NEAR TANK MOUNTS			
0.0	0.0	0.0	0.0	0.0	NEAR TANK MOUNTS			
1.0	1.0	1.0	1.0	1.0	HEAT ALONG CABLE			
1.0	1.0	1.0	1.0	1.0	HEAT ALONG CABLE			
4.0	4.0	4.0	4.0	4.0	INTERNAL			
4.0	4.0	4.0	4.0	4.0	INTERNAL			
4.0	4.0	4.0	4.0	4.0	INTERNAL			

THERMAL CONTROL COATINGS

INTERNAL	OK	E
ALL SURFACES OF BUS/ELECTRONIC COMPONENTS	—	0.9
ALL TANKAGE VALVES, REGULATOR, PLUMBING* (WHEREVER PRACTICAL)	—	0.9
INTERNAL SURFACES OF OUTBOARD MOUNTING PANELS	—	0.9
INTERNAL SURFACES OF INBOARD MOUNTING PANELS	—	0.9
INTERNAL SURFACES OF SUPERINSULATION BLANKETS	—	0.1
EXTERNAL	OK	E
HIGH GAIN ANTENNA	0.3	0.85
LOW GAIN ANTENNA	0.25	0.85
LOW GAIN ANTENNA	0.25	0.85
EXTERNAL SURFACE OF THE OUTBOARD MOUNT PANELS	0.12	0.12
EXTERNAL SURFACE OF LOUVERS	0.12	0.12
EXTERNAL SURFACE OF LEADERS	0.12	0.12
EXTERNAL SURFACE OF ALL ALUMINIZED MYLAR SUPERINSULATION BLANKETS, PERMANENT SPRAYED	0.4	0.4
EXTERNAL SURFACES OF SCAN PLATFORM	0.5	0.15
EXTERNAL SURFACES OF SUPERINSULATION BLANKET, NORMALLY THERMALLY UNCOATED	0.64	0.16
EXTERNAL SURFACE OF THERMOPUS THERMOKER	0.3	0.3
EXTERNAL SURFACE OF ALL SUN SHIELDS	0.3	0.3
EXTERNAL SURFACE OF EARTH SENSOR	0.3	0.3
EXTERNAL SURFACE OF MARS VERTICAL SENSOR	0.3	0.3
EXTERNAL SURFACE OF ALL ROCKET ENGINES	0.4	0.4

SHUTTER BASIC DIMS			ALLOCATION (FLUENT)	
LENGTH IN	WIDTH IN	THICK IN	START	STOP
20.0	4.0	0.256	40	70
20.0	4.0	0.256	40	70

Figure 3-1. Thermal Balance Drawing Sheet 2 of 2

3.2.2 LAUNCH PAD

The preferred method of temperature control with the shrouded flight spacecraft on the launch pad is to duct filtered air directly through a fly-away disconnect in the nose fairing such that the air enters in the area of the thermal control shutters and also flows over the Flight Capsule as illustrated in Figure 3-2. This air should enter the shroud on the side closest to the high heat dissipating radio subsystem. The shutters are capable of normal operation while on the ground. An air flow rate of 10 pounds/minute at 40°F and 50 percent relative humidity (to eliminate moisture condensation within the nose fairing) is sufficient to handle the heating loads of both the Bus section (300 W) and the Flight Capsule (150 W). See appendix for analysis. The external surface of the nose fairing should have a low solar absorptivity to minimize the solar load.

3.3 ASCENT TEMPERATURE CONTROL

A maximum average electronic assembly temperature of 65°F at lift-off ensures tolerable temperatures during the ascent phase. The internal surface of the shroud should have a low emissivity to minimize radiant heat flow from the hot shroud during the powered flight heating interval. After shroud separation the spacecraft experiences a short (a few minutes) transient burst of free molecule heating. The inherent thermal mass of the spacecraft is sufficient to endure this molecular heating transient without detriment.

3.4 SPACE ENVIRONMENT TEMPERATURE CONTROL

3.4.1 SPACECRAFT BUS SECTION

All electronic assemblies, tanks, plumbing and structure are thermally integrated to the maximum extent possible within a superinsulation cocoon (see configuration in Figure 3-1). This thermal coupling is achieved by the use of (1) high emissivity surfaces, (2) an open type internal structure, and (3) silicone grease between heat dissipating sub-assemblies and their mounting plates. Advantage is taken of the Spacecraft's Sun-Canopus orientation during the transit and Mars orbit phases by allowing some solar energy (4.6 watts/ft² near earth, 1.9 watts/ft² in Mars orbit) to penetrate the normally illuminated surface of the Bus superinsulation cocoon to aid in keeping the several enclosed tanks warm. Excess heat is released from within the superinsulated enclosure by means of eleven sets of shutters (one set on the external surface of each electronic assembly except for the bay whose external surface is blocked by the scan platform) which control the emittance of the heat rejection surfaces. Each shutter is actuated by a two phase fluid sensor/bellows/drive rod/return spring arrangement as illustrated in Figure 3-3.

3.4.2 APPENDAGE SUPPORT STRUCTURE

All support structure for appendages such as solar arrays, antennas, the scan platform, retro and mid-course engines, and booms are conductively insulated from the Bus structure.

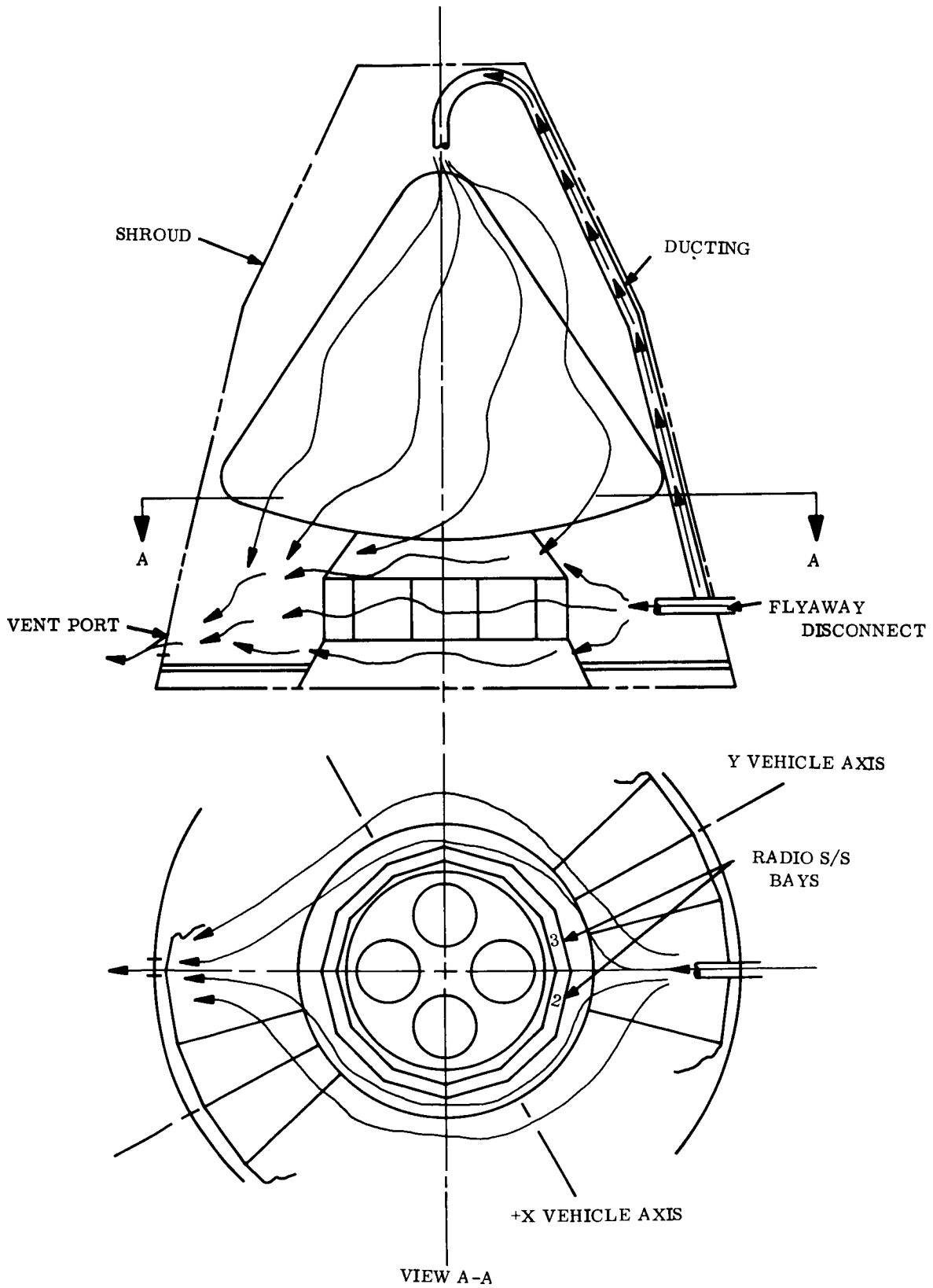


Figure 3-2. Pad Cooling Air Flow Distribution

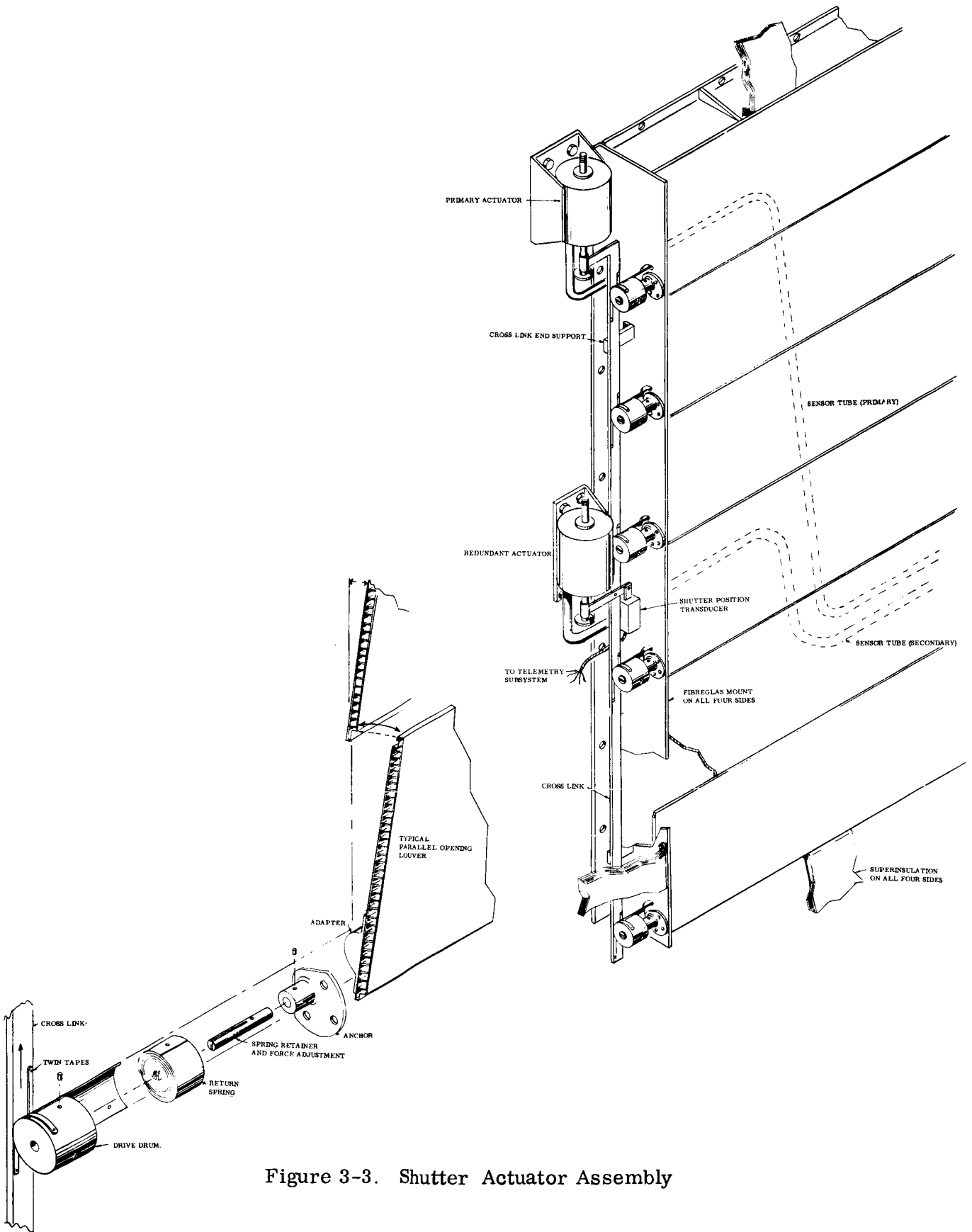


Figure 3-3. Shutter Actuator Assembly

3.4.3 EXTERNAL SENSORS

The various Guidance and Control sensors are mounted in good thermal contact with the Bus section and augmented with coatings and superinsulation as appropriate.

3.4.4 PLANET SCAN PLATFORM

Present knowledge regarding the science instruments and design of the scan platform is insufficient for thermal design purposes. However, the preferred approach is to employ passive temperature control methods (i. e. , coatings, superinsulation blankets, conductively insulated mountings, thermostatically controlled heaters, etc). Should the individual science instruments have markedly different allowable temperature ranges (such as is indicated in the JPL EPD 250 report), each instrument would then be thermally isolated from all others even though they all might be housed within a common structure. Louvers would be used only if a significant advantage could be demonstrated.

3.4.5 FLEXIBLE CABLING & ARTICULATION DEVICES

The movable cables to the High Gain Antenna and to the scan platform are kept warm by means of thermostatically controlled heaters attached to the cables and wrapped with superinsulation.

The articulation devices are wrapped in superinsulation and conductively insulated from their support structure. A very small amount of heater power may be required for the seldom operated stepping motors.

3.4.6 SOLAR ARRAY, ANTENNAS, MAGNETOMETER AND ROCKET ENGINES

These items are passively temperature controlled by means of coatings.

3.4.7 ATTITUDE CONTROL GAS LINES, SOLENOIDS AND NOZZLES

The portions of the Freon lines which are external to the Bus section are wrapped with superinsulation. Thermostatically controlled heaters are attached to the lines along their superinsulated length. These lines are conductively insulated from the solar array.

Conductive heat transfer from the lines to the solenoids assures proper solenoid temperatures. The several nozzle/solenoid assemblies are clustered into four groups to increase their effective thermal mass.

3.4.8 G&C GYROS AND ACCELEROMETER

The three gyros and the accelerometer are thermally integrated as one assembly. Proportional controllers regulate each gyro heater separately. The gyro heaters are commanded on one hour prior to any maneuver sequence. Each heater has the capacity (35W) to accomplish the warm-up without the aid of the other two heaters in a half-hour period

(see appendix for analysis). The thermal resistance between this gyro/accelerometer assembly and its surroundings is fixed such that the gyros do not exceed 100°F during operation.

3.5 SHUTTER DESCRIPTION

3.5.1 MECHANICAL DESIGN

3.5.1.1 ACTUATOR

A two-phase fluid-bellows-piston type actuator has been selected to actuate the ganged shutters. (See Figure 3-3).

The bellows actuator employed is a pressure compensated design such that ambient pressure does not influence piston travel. The control fluid is Ethyl Chloride with its normal operating pressure ranging from 10.8 psia at 40°F to 20 psia at 70°F. The fluid is contained in a beryllium copper bellows that is silver soldered to the housing and to the piston stop. The space between the housing and the bellows is evacuated to approximately 10 microns Hg. No "O" rings or gaskets are employed to contain the fluid.

The louvers, suspended on their inboard faces by supports on either end, open and shut as each drive drum rotates 90 degrees. The method of suspension minimizes envelope requirements and permits a full louver opening even in the face of an individual closed (failed) louver. Due to dimensional limitations, the actuators are offset from the basic drive linkage, by an aluminum crosslink bar, which runs the length of the panel. The actuator piston is connected to the crosslink through an individual sidelink joined to the crosslink to compensate for the offset. The crosslink moves linearly, in response to actuator piston motion, over two end supports and beneath the column of drive drums. It is joined to the drums by twin beryllium copper drive tapes.

Linkage failure including tape drive failure, although remote, is not catastrophic. Hang up of the linkage is prevented by the positive constraints provided by the actuator piston (on one end) and by the drive drums and end supports (above and below). Redundant sidelinks are provided to continue operation in the event of a primary sidelink failure. A tape drive failure results in an individual shutter closing without affecting the other blades.

No conventional bearings are employed. Flexure pivots are employed at the undriven end while torsion springs integral with the drive drums serve as support at the driven end. The flexure pivot has a restraining ring overhang as a lateral stop to prevent reverse load damage. The torsion spring serves as a restraining force (acting against the actuator force) for positioning the louver in the closed position.

All materials employed are non-magnetic.

Support bracketry is fiberglass with hard anodized aluminum fittings. Superinsulation surrounds each assembly up to the fiberglass mounts.

3.5.1.2 TEMPERATURE SENSOR

The aluminum bronze sensing tube is permanently connected to the bellows and is installed snake fashion on the space facing side of an equipment mounting panel to cover potentially hot areas.

3.5.1.3 BLADE DESIGN

The louver blades operate in parallel fashion, as shown in Figure 3-3, and consist of a lightweight phenolic honeycomb bonded between outer and inner surfaces of three-mil aluminum. A 4 percent overlap between blades is provided to achieve a tight radiation seal in the closed position. This is achieved with flush blades and by intermeshing undercut edges between adjacent blades.

In addition, a tooth edge contact is provided to assure a positive radiation seal during closure even under adverse blade warping. There is no metal to metal contact between blades in the closed position or between outer and inner surfaces.

3.5.1.4 ACTUATOR REDUNDANCY

Redundant actuator-sensor tube assemblies are provided for each shutter assembly. An initial adjustment setting at the piston end permits bias control. Should either bellows lose pressure, the secondary bellows assembly, operating in parallel, automatically overcomes the position bias and assumes operation for that heat rejection panel. Thus, the vehicle continues to operate under its normal mode of temperature control.

3.5.1.5 FAIL-SAFE POSITION

The principal fail-safe position for the louvers is the closed position. In the event both actuators lose fluid, all louvers are closed by the force of the return springs.

3.5.2 THERMAL DESIGN

3.5.2.1 CONTROL TEMPERATURE RANGE

The control temperature range of the primary actuators is 40° to 70°F thereby providing for a 10°F temperature difference between the sub-assemblies and the heat rejection surface. The secondary actuators operate in essentially the same temperature range but biased by about 2°F.

3.5.2.2 COATING DESCRIPTION

The internal and external blade surfaces are coated with an electron beam vacuum deposited Al_2O_3 (a GE operational process initially developed by Dr. Hass at Fort Belvoir, Va.) yielding a solar absorptivity of 0.12 and a hemispherical emissivity of 0.12. The heat rejection surface beneath the shutters is coated with ALZAC (a commercial alodine process) to yield $\alpha = 0.16$ with $\epsilon = 0.74$.

3.5.2.3 EFFECTIVE RADIATION PROPERTIES

Figures 3-4 and 3-5 show the effective emissivity and solar absorptivities for a diffuse, parallel-type shutter assembly. The analyses are presented in the appendix.

3.6 THERMOSWITCH CHARACTERISTICS

3.6.1 DESCRIPTION

Klixon type M2S bimetallic thermostats (made by the Metal and Controls Division of Texas Instruments Co.) are preferred for the control of all heaters. Tolerances can be guaranteed as follows: set point $\pm 2^{\circ}\text{F}$, differential 5°F maximum, drift $\pm 2^{\circ}\text{F}$. Normal installation of the heater controllers involves a group of three thermostats, two control temperature thermostats wired in parallel and one over-ride thermostat wired in series.

3.6.2 EMI CONTROL

EMI control of the thermostats for generated or conducted noise is obtained by using a potted module (wired within four inches of the switch) consisting of a capacitor, a resistor and a diode in parallel.

3.7 TELEMETRY CHARACTERISTICS OF TEMPERATURE CONTROL S/S

3.7.1 REQUIREMENTS

The number, location, range and priority of the temperature sensors and shutter position indicators are shown on the Thermal Balance Drawing (Figure 3-1.)

3.7.2 TEMPERATURE SENSOR DESCRIPTION

The transducers for temperature measurement are resistance thermometers. The resistive material is pure, annealed strain-free platinum wire mounted upon an insulating base.

Each temperature sensor is placed in a simple circuit containing, in general, a resistor in parallel connection. The resistor and sensor resistance values are chosen such that the combination provides a net resistance which will vary from 500 to 600 ohms as the temperature varies from the cold end to the hot end of its range. The linearity and temperature sensitivity of the net resistance is negligibly altered from that of the sensor alone if the sensor resistance and its parallel connected resistance are chosen appropriately. A precision one milliamper current provided by the data encoder converts this resistance to a voltage ranging from 0.50 to 0.60 vdc. This one current supply is the only one to be used for all temperature measurements and its current is switched from one sensor to another in the data sampling sequence.

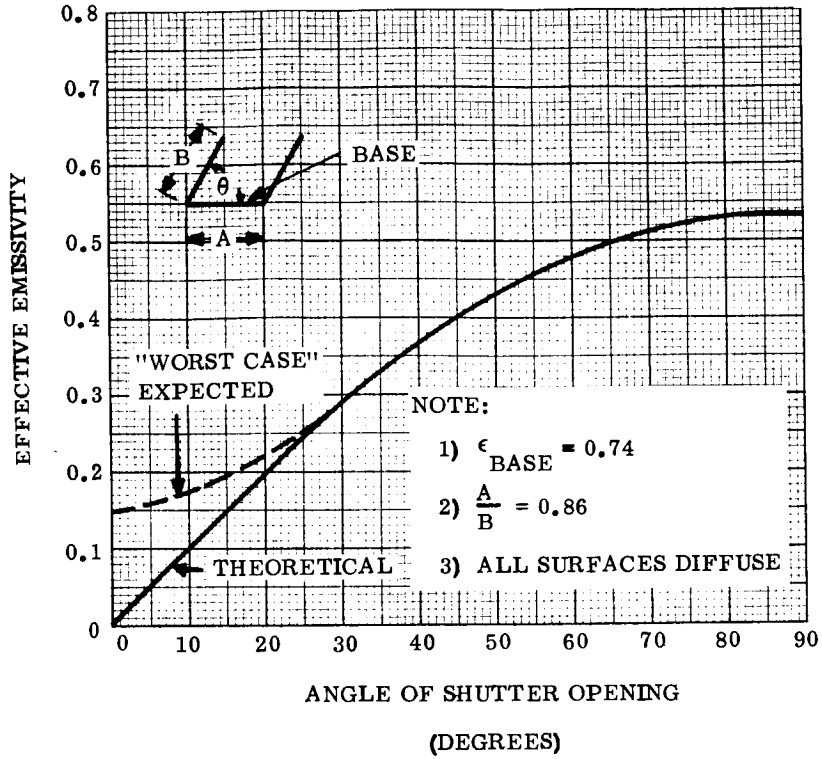


Figure 3-4. Effective Emissivity vs Angle of Shutter Opening

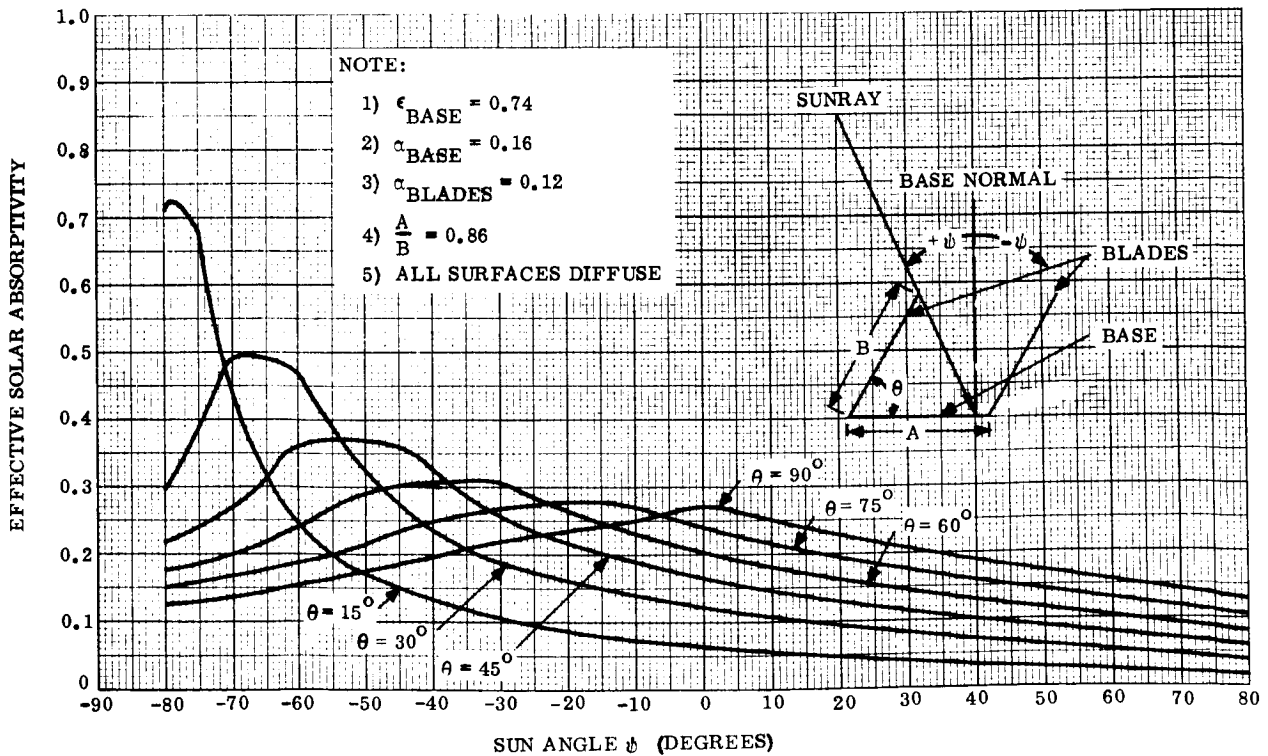


Figure 3-5. Effective Solar Absorptivity vs Sun Angle for Various Shutter Opening Angles

The sensitivity of the measurement may be estimated by considering a temperature band from -100° to 100° F. This 200° F degree range is spread over a voltage range of 100 mv resulting in a sensitivity of 2° F deg/mv. If the smallest voltage change discernible by the encoder is 0.8 mv, then the smallest discernible temperature change is 1.5° F.

3.7.3 SHUTTER POSITION TRANSDUCER DESCRIPTION

The position of the temperature control shutters is measured by a variable reluctance type of linear position transducer, frequently called a linear differential transformer. It is directly connected to the actuator drive rod mechanism such that any motion of the rod results in an identical motion of the transducer shaft.

The linear differential transformer is essentially a transformer with a movable mass of magnetically permeable material which magnetically links the primary and secondary windings. As the transducer shaft and the permeable material move, a voltage is induced in the secondary ranks in the proportion to the distance moved.

4.0 INTERFACE DEFINITION

Thermal interface requirements between the Flight Spacecraft and Flight Capsule, between the Flight Spacecraft and Booster and between the Flight Spacecraft and Shroud are delineated on the Thermal Interface Drawing Figure 4-1.

5.0 PERFORMANCE PARAMETERS

5.1 TEMPERATURE PREDICTIONS

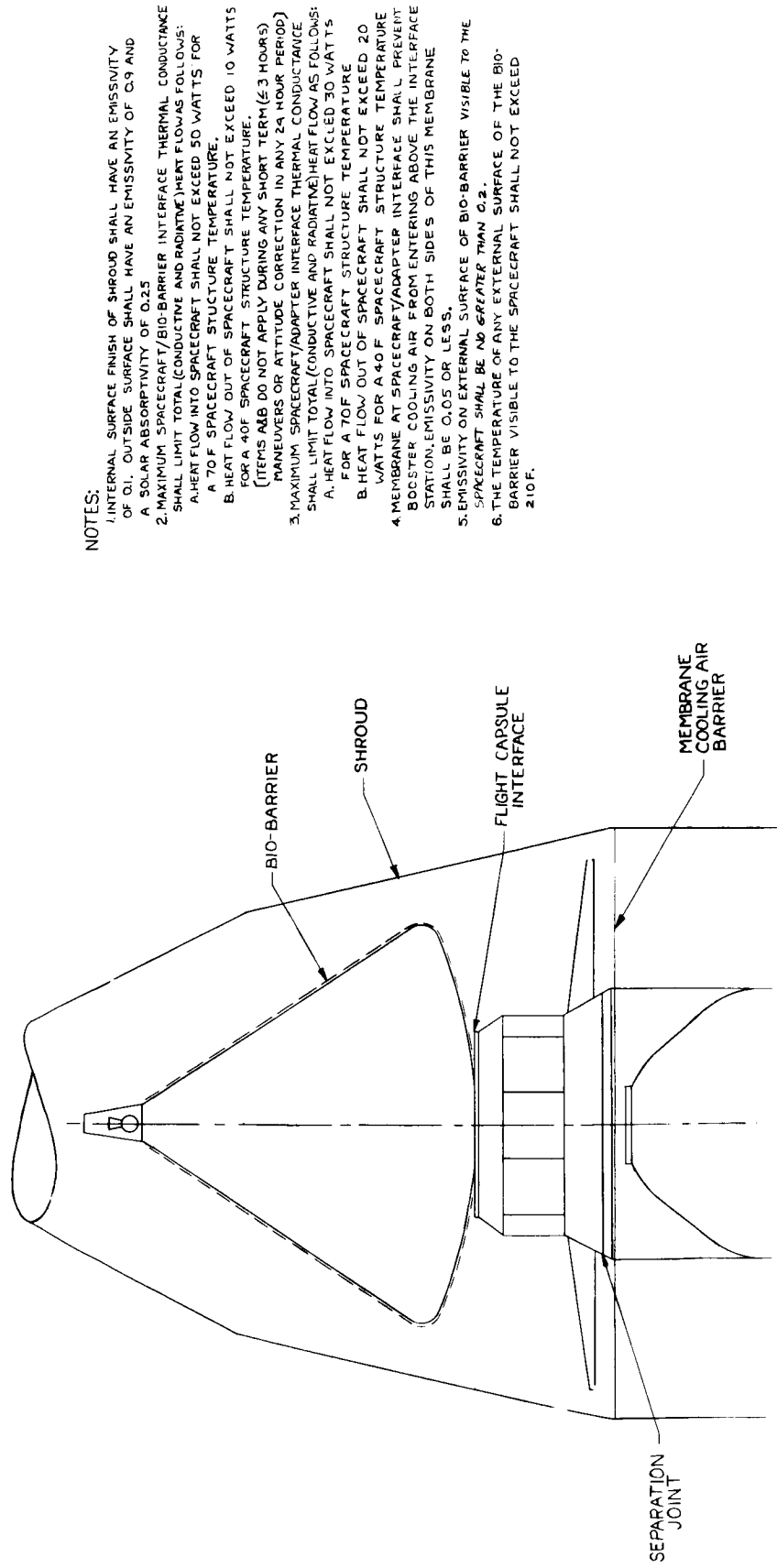
5.1.1 BUS SECTION

All temperatures (both the Bay Averages and the Individual Sub-assembly temperatures) presented herein are based on the equipment assembly locations and dissipations as shown in the Thermal Balance Drawing Figure 3-1. Subsequent to the thermal analysis, some relocation was required to achieve a better location for the spacecraft center of mass with the final arrangement shown in VB220FD113. These changes have not created any thermal problem. Thus the temperatures presented herein can be considered typical.

5.1.1.1 EQUIPMENT ASSEMBLY AVERAGE TEMPERATURES

The average expected temperatures of the various assemblies for the several mission phases are listed in Table 5-1. The midcourse maneuver transient bay temperatures are shown in Figure 5-1.

Bay average temperatures for the abnormal conditions of equipment shutdown (science and radio subsystems) and shutter failure (designed for closed position) are listed in Table 5-2. Any additional temperature rises due to midcourse maneuver sun impingement on a bay with a failed closed shutter assembly are negligible over those temperatures already shown in Table 5-2.



NOTES:

1. INTERNAL SURFACE FINISH OF SHROUD SHALL HAVE AN EMISSIVITY OF 0.1. OUTSIDE SURFACE SHALL HAVE AN EMISSIVITY OF 0.9 AND A SOLAR ABSORPTIVITY OF 0.25
2. MAXIMUM SPACECRAFT/BIO-BARRIER INTERFACE THERMAL CONDUCTANCE SHALL LIMIT TOTAL (CONDUCTIVE AND RADIATIVE) HEAT FLOW AS FOLLOWS:
 - A. HEAT FLOW INTO SPACECRAFT SHALL NOT EXCEED 50 WATTS FOR A 70 F SPACECRAFT STRUCTURE TEMPERATURE.
 - B. HEAT FLOW OUT OF SPACECRAFT SHALL NOT EXCEED 10 WATTS FOR A 40 F SPACECRAFT STRUCTURE TEMPERATURE.
3. MAXIMUM SPACECRAFT/ADAPTER INTERFACE THERMAL CONDUCTANCE SHALL LIMIT TOTAL (CONDUCTIVE AND RADIATIVE) HEAT FLOW AS FOLLOWS:
 - A. HEAT FLOW INTO SPACECRAFT SHALL NOT EXCEED 30 WATTS FOR A 70 F SPACECRAFT STRUCTURE TEMPERATURE.
 - B. HEAT FLOW OUT OF SPACECRAFT SHALL NOT EXCEED 20 WATTS FOR A 40 F SPACECRAFT STRUCTURE TEMPERATURE.
4. MEMBRANE AT SPACECRAFT/ADAPTER INTERFACE SHALL PREVENT BOOSTER COOLING AIR FROM ENTERING ABOVE THE INTERFACE STATION. EMISSIVITY ON BOTH SIDES OF THIS MEMBRANE SHALL BE 0.05 OR LESS.
5. EMISSIVITY ON EXTERNAL SURFACE OF BIO-BARRIER VISIBLE TO THE SPACECRAFT SHALL BE NO GREATER THAN 0.2.
6. THE TEMPERATURE OF ANY EXTERNAL SURFACE OF THE BIO-BARRIER VISIBLE TO THE SPACECRAFT SHALL NOT EXCEED 210 F.

Figure 4-1. Thermal Interface Drawing

TABLE 5-1

AVERAGE BAY TEMPERATURES (°F) VS. MISSION PHASE							
Bay	Subsystem	Earth Orbit	Transit		Mid Course Correction*	Mars Orbit	
			Max.	Min.		Max.	Min.
1	Command	64	48	44	52	56	50
2	Radio	71	48	43	59	54	49
3	Radio	74	62	52	89	65	63
4	Power	65	53	50	68	58	55
5	Power	61	49	45	60	60	48
6	Power	59	58	53	53	61	58
7	G & C	57	48	42	58	56	45
8	C & S	57	45	42	49	54	46
9	Science	62	46	46	47	56	47
10	DAS & Science	62	53	52	54	58	55
11	DH & S	57	45	42	47	54	48
12	DH & S, Relay	55	44	41	45	57	51
Center Tankage		60	50	46	53	58	52

*Maximum temperatures after two hours of direct solar flux (280 Btu/hr ft²) on Bay 3.

TABLE 5-2

AVERAGE BAY TEMPERATURES ($^{\circ}$ F) FOR ABNORMAL CONDITIONS

Bay	Subsystem	Shutter Assembly Failed Closed*	Component Shutdown In Bays 2, 3, & 9**
1	Command	--	31
2	Radio	--	4
3	Radio	102	23
4	Power	82	46
5	Power	75	40
6	Power	92	50
7	G & C	77	36
8	C & S	--	33
9	Science	79	30
10	DAS & Science	71	46
11	DH & S	--	35
12	DH & S, Relay	71	31
Center Tankage		64	40

* Shutter assembly failed on only one bay at a time

** With 6.2 Watts of heater power in center node (on tanks)

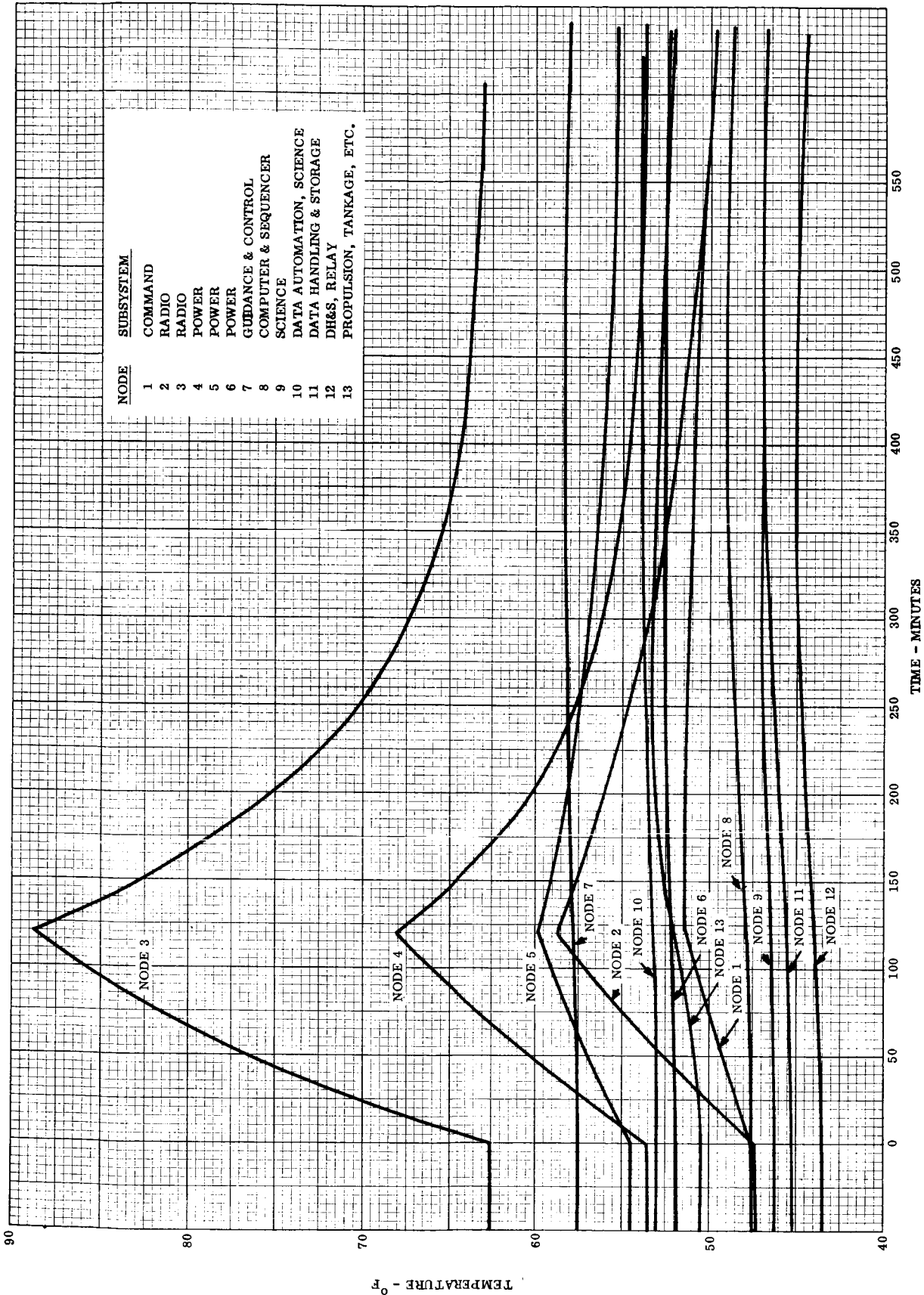


Figure 5-1. Temperature Histories During Midcourse Maneuvers(2 Hour Exposure to $S = 280 \text{ Btu/hr-Ft}^2$)

5.1.1.2 INDIVIDUAL SUB-ASSEMBLIES

The maximum local base temperatures of the individual electronic sub-assemblies (assuming a 60-mil aluminum mounting plate with a conductivity of 70 Btu/hr ft²F) are shown on the thermal balance drawing, Figure 3-1. The mounting panel temperature distributions are shown in the appendix for 30- and 60-mil panel thicknesses.

5.1.2 SOLAR ARRAY

Figure 5-2 shows the radial temperature distribution for a solar panel near earth, at Mars encounter and after bio-barrier ejection. Temperatures versus distance from the Sun are shown in Figure 5-3. The transient cooling curve expected during the Mars shade time is shown in Figure 5-4. Analyses are presented in the appendix.

5.1.3 HIGH GAIN ANTENNA

The expected gross temperature of the dish is shown in Figure 5-5 as a function of distance from the sun. The cooling transient expected for the Mars shade period is given in Figure 5-6. Analyses are presented in the appendix.

5.2 HEATER POWER REQUIREMENTS

A total of 57W of heater power could possibly be used. However, of that amount 30W are for contingency purposes and 12W are estimated for gyro operation. Thus 15W will be a much more realistic mission average value. The locations of the heaters and the predicted wattage required are listed on the Thermal Balance Drawing (Figure 3-1).

5.3 RELIABILITY CONSIDERATIONS

5.3.1 THERMOSWITCH OPERATION

Experience to date with the Klixon thermostats used to control the heaters on a flown GE classified satellite program has shown a failure rate of 0.00001 per 500 cycles. This figure is based on both calculated and operational experience. Acceptance testing of the thermostats (involving about 2000 switches) have shown no rejections. Furthermore, the actual tolerance of the switches is much tighter than the value assigned as a limit (3 or 4^oF range versus an expected 7^oF range).

5.3.2 CONTINGENCY HEATERS

The four monopropellant and two Freon tanks each have a 5-Watt thermostatically controlled heater for contingency purposes, although heaters are theoretically not required.

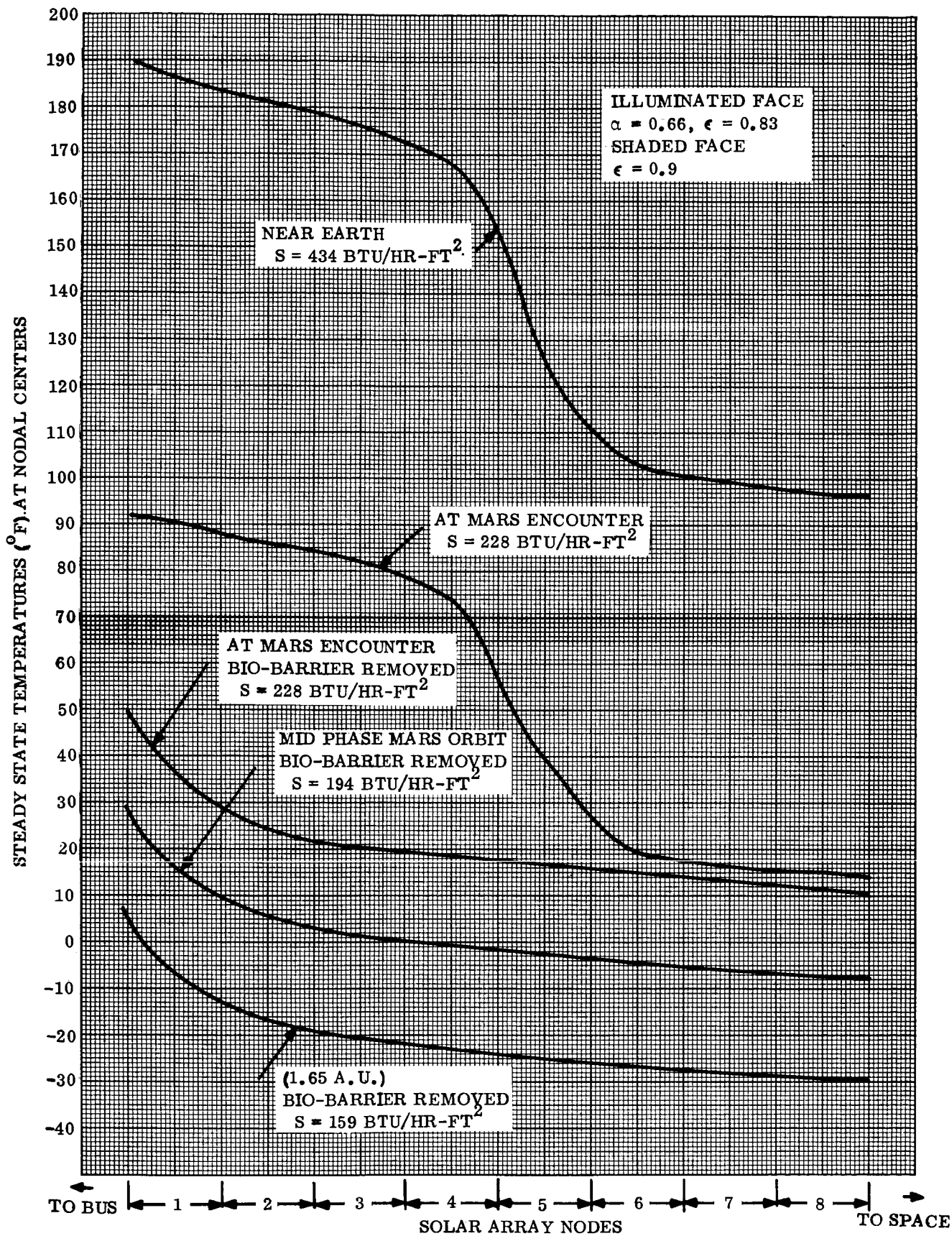


Figure 5-2. Fixed Solar Array Radial Temperature Distribution

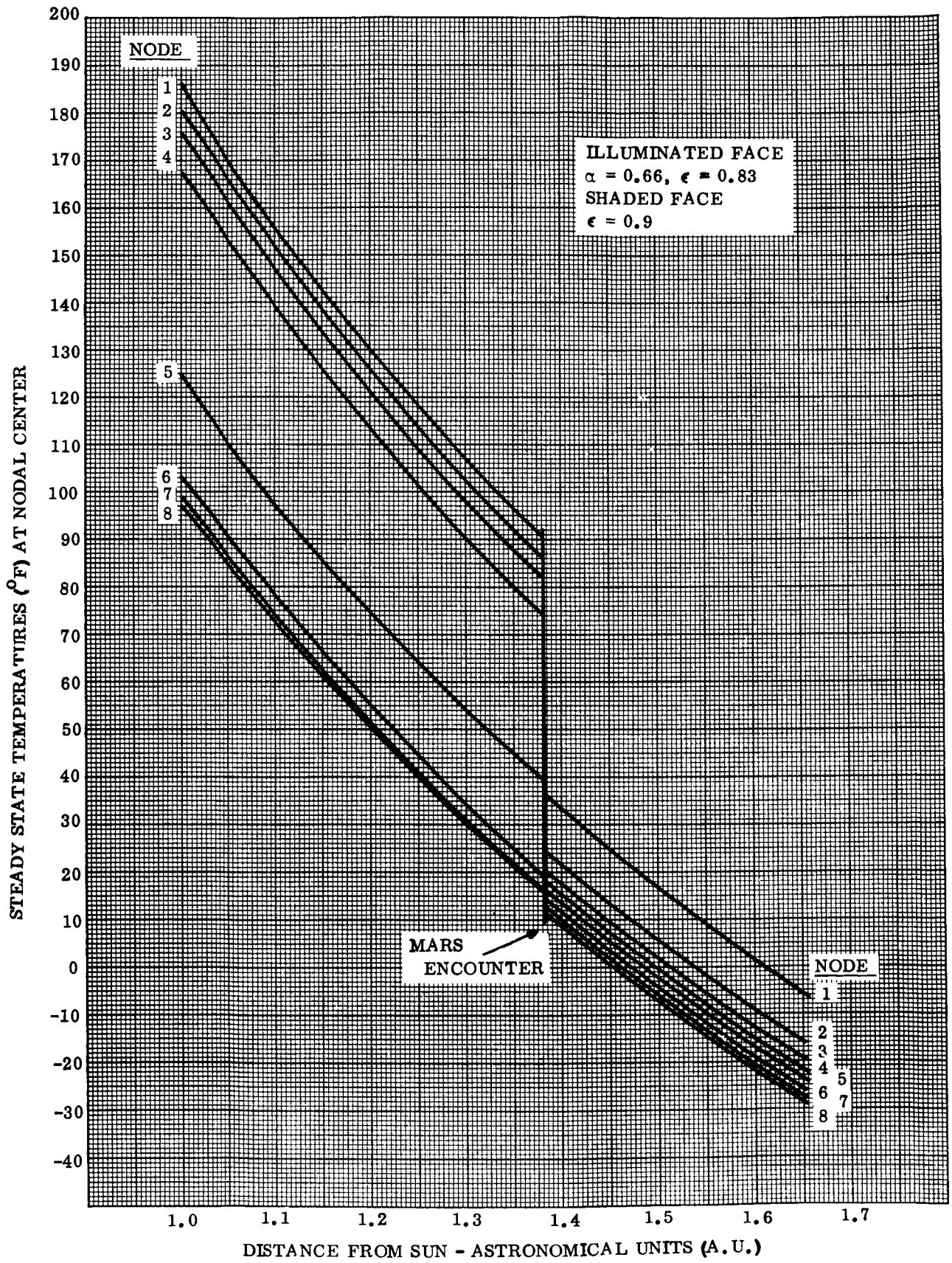


Figure 5-3. Fixed Solar Array Nodal Temperatures vs Distance from Sun

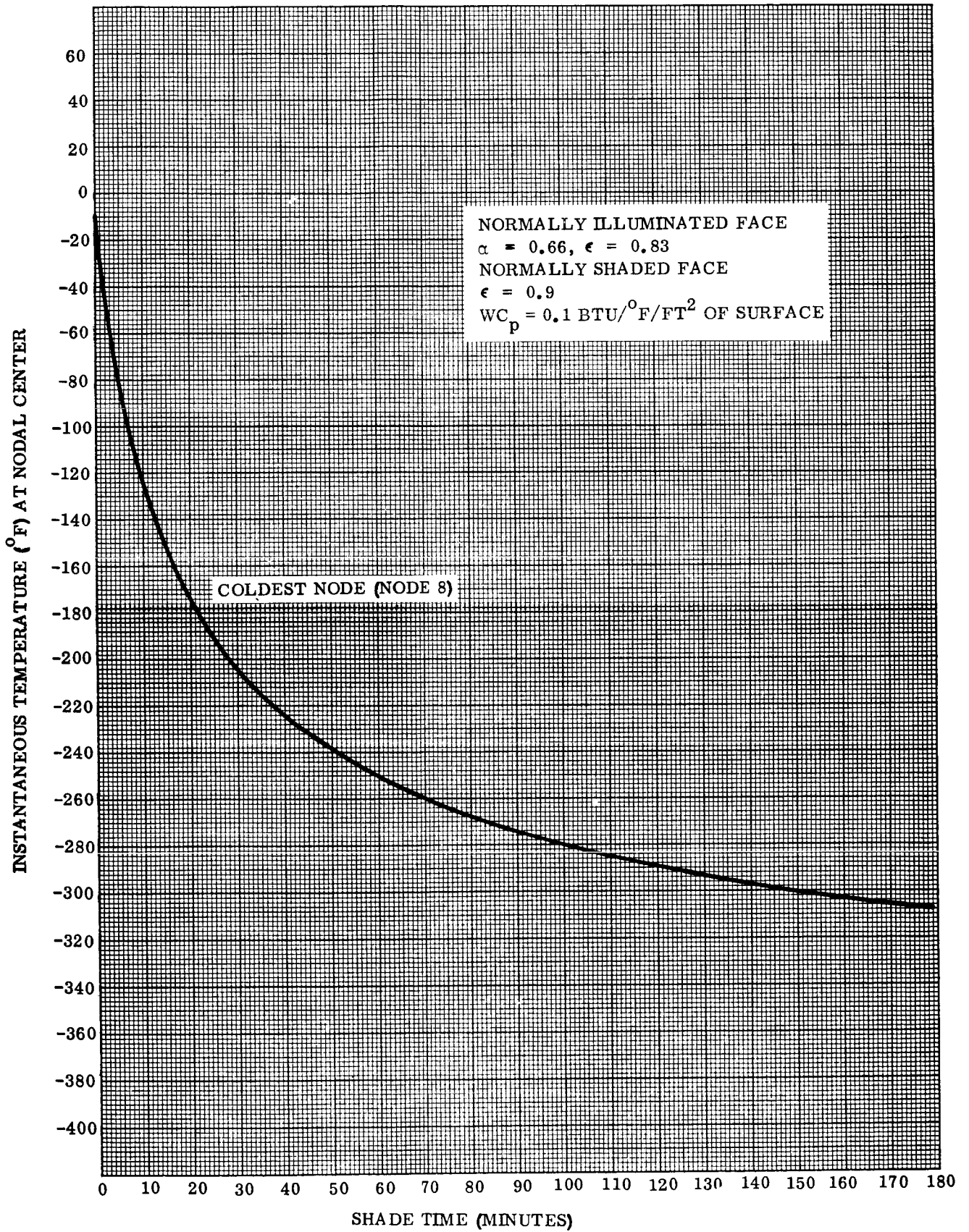


Figure 5-4. Transient Temperature Drop During Mars Shade

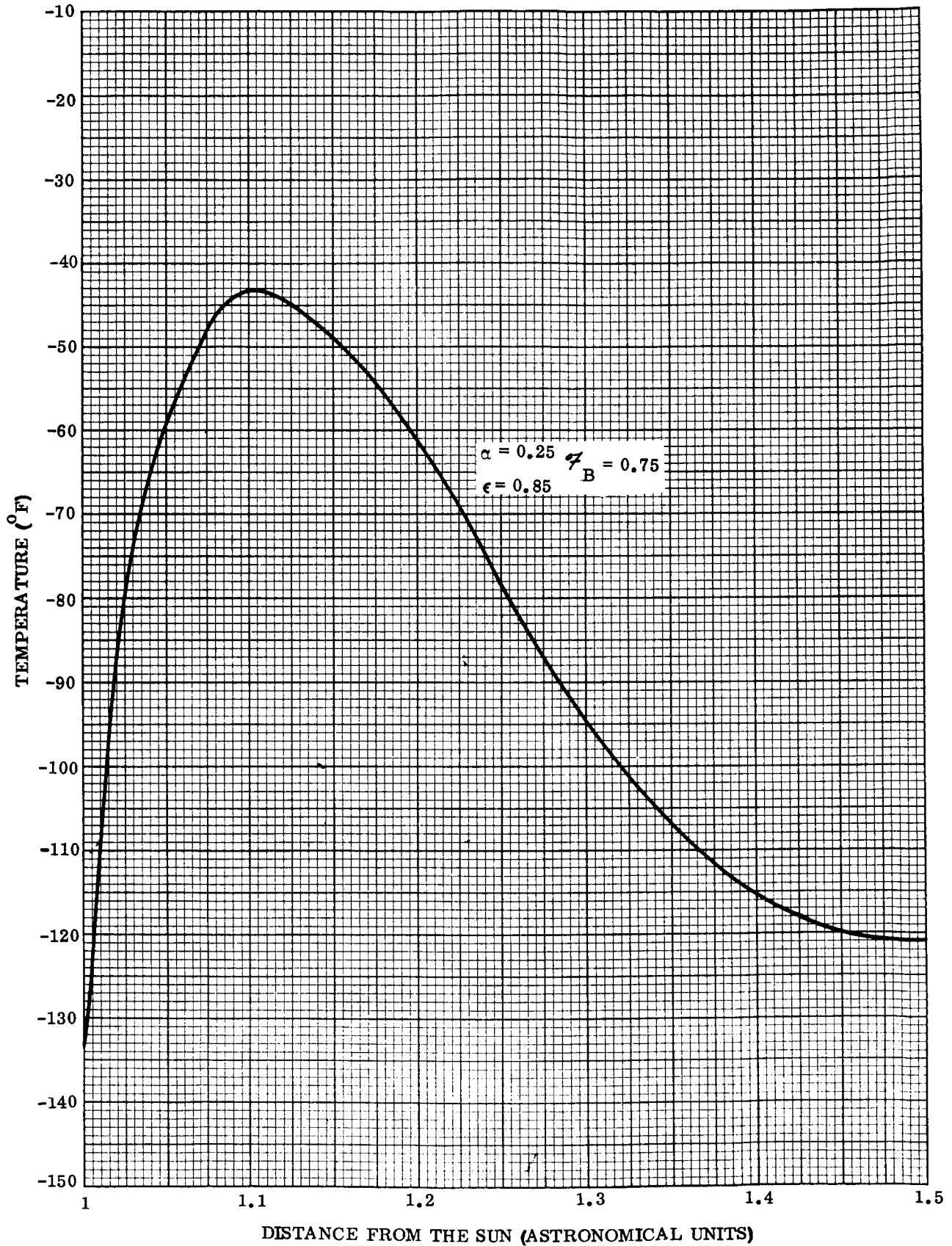


Figure 5-5. Expected Average High Gain Antenna Temperature

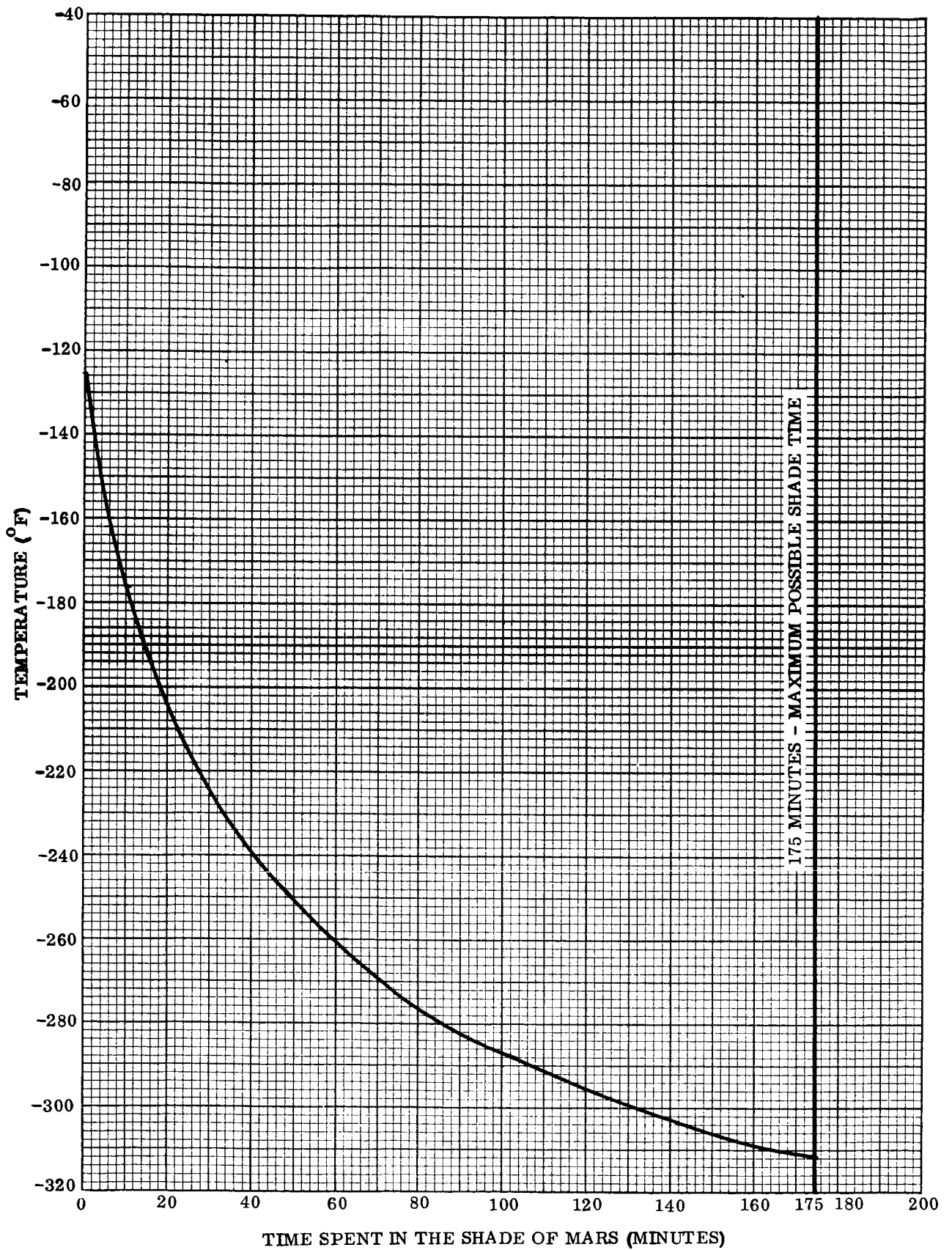


Figure 5-6. Expected High Gain Antenna Transient Temperature during Mars Shade

5.3.3 SHUTTER ACTUATORS

Dual actuators are employed on each shutter assembly to ensure operation in case of pressure loss in one of the actuators. Should both actuators fail (on any given assembly mounting panel) individual return springs will close the shutters. Should this occur in the worst steady state case (Mars orbit) a failed closed shutter assembly will cause a rise of 37°F in the average temperature of the heat rejection surface of the highest dissipating bay (the radio subsystem).

5.3.4 COATING DEGRADATION

5.3.4.1 ROCKET PLUME IMPINGEMENT EFFECTS

Should rocket exhaust particles decrease the $\frac{\alpha}{\epsilon}$ of the normally illuminated superinsulation blanket, the resulting change in heat input to the Bus section can easily be accommodated by the inherent flexibility of the shutter assemblies.

5.3.4.2 NUCLEAR RADIATION EFFECTS

A rise in the value of the solar absorptivity on the Bus section heat rejection surfaces due to exposure to nuclear radiation would cause increased electronic assembly temperatures on the bays exposed to the sun during mid-course or retro maneuvers. However, this is not considered to be serious due to the stability of the Alzac coating.

5.3.5 COMPUTED RELIABILITY

The computed reliability of the temperature control subsystem for the various mission phases is presented in Table 5-3. The reliability analysis (see appendix) is based on the premise that all shutter assemblies and heaters must work properly to ensure mission success. However, if one assembly fails, the heat from that bay could be dissipated to space via its two adjacent bays. Only the failure of three adjacent panels could present a major problem. Using the reliability of one shutter assembly as 0.99808, the probability of three adjacent failures is computed to be less than one in a million. This probability results in a shutter reliability of 0.999999 rather than 0.97922 and raises the temperature control subsystem reliability to 0.99493 rather than 0.97421.

It should be also noted that failure of an individual thermoswitch or heater will probably result in a degradation of some mission function rather than a complete mission failure. Thus the overall subsystem reliability is believed to be conservative.

6.0 PHYSICAL CHARACTERISTICS AND CONSTRAINTS

6.1 THERMAL BALANCE DRAWING

Figure 3-1 is a complete description of the temperature control subsystem. It includes equipment locations, dissipations and temperatures versus mission phase, temperature

TABLE 5-3
TEMPERATURE CONTROL SUBSYSTEM RELIABILITY

Phase #	Mission Event	Reliability
1 and 2	Launch, Cruise mode acquisition, First and second midcourse maneuvers, Pre-encounter checkout, Flight capsule separation.	0.98192
3	Third midcourse maneuver, Mars orbit injection	0.99699
4	Mars orbit	0.99515
	Overall Reliability (all phases)	0.97421

limits, heater requirements and locations, telemetry sensor information, coating requirements, superinsulation blanket locations and compositions, shutter sizes and views of the spacecraft configuration.

6.2 SUPERINSULATION CHARACTERISTICS

The superinsulation blanket covering the normally non-illuminated Bus surfaces consists of a 2 mil outer layer of aluminum foil and 25 layers of 1/4 mil aluminized Mylar in an overall thickness of 1/4 inch. The outer layer is coated with the Fairchild-Hiller MTL-3 alodine process (developed for Pegasus) yielding an $\frac{\alpha}{\epsilon} = 1.0$ with $\epsilon = 0.38$. This ensures that the maximum external surface temperature of the blanket will not exceed 250°F in Earth Parking Orbit.

The normally illuminated surfaces of the superinsulation blanket consist of a three-mil outer layer of dimpled aluminum foil ($\frac{\alpha}{\epsilon}$ about 4.0) followed by eight pairs of two mil Tissuglas/one mil aluminum foil which are followed by 20 layers of 1/4 mil aluminized Mylar in a total thickness of 0.4 inches.

The superinsulation blanket in the immediate vicinity of the midcourse and retro engines consists of a 3 mil outer layer of non-magnetic stainless steel followed by 3 pairs of non-magnetic 1 mil stainless steel foil/0.1 inch Q felt followed by 28 layers of 1/4 mil aluminized Mylar in a total thickness of 0.6 inches.

A typical superinsulation attachment method is illustrated in Figure 6-1. Note that the non-magnetic, low thermal conductivity stainless steel thread is attached to the Velcro tape and not directly to the spacecraft structure, thereby significantly reducing any potential heat leak.

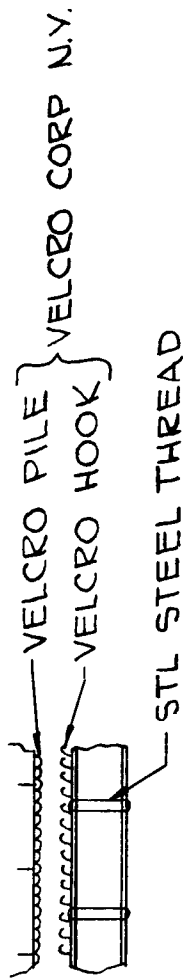
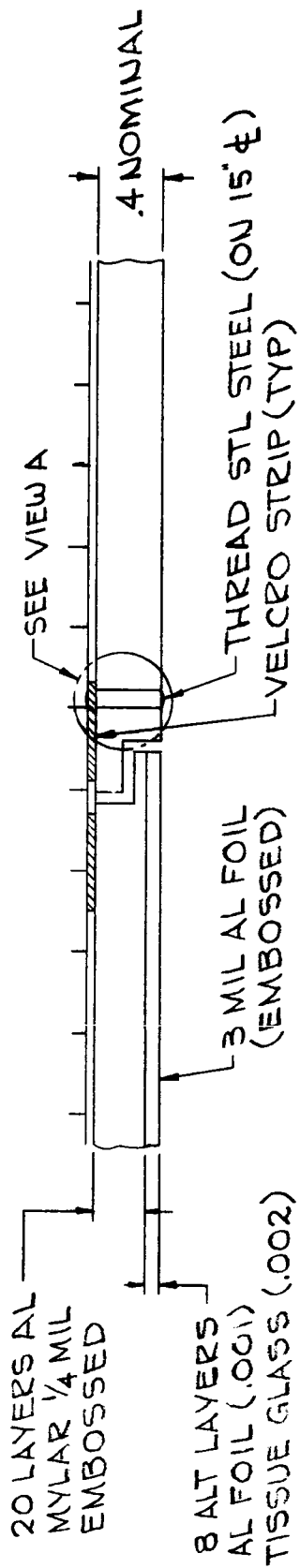
Figure 6-2 shows the method of attaching the high temperature resistant superinsulation blanket around the midcourse engines.

6.3 SHUTTER ASSEMBLY CHARACTERISTICS

The 2 ft² shutter assembly weighs 3 pounds and has three blades each measuring 4 by 20 inches. The 4 ft² shutter assembly weighs 6 pounds and has six 4 by 20 inch blades.

The actuator characteristics are:

Piston face area	1.22 in ²
Maximum piston travel	0.44 in
Return Spring Constant	25.8 lb/in.
$\Delta p / \Delta T$	0.31 psia/°F
Return Spring Force	0.5 lb.
Fluid Pressure	10.8 psia at 40°F
	20 psia at 70°F
	65 psia at 140°F



VIEW A

TYPICAL SUPERINSULATION INSTALLATION FOR NORMALLY SUN ILLUMINATED SURFACES

Figure 6-1. Typical Superinsulation Installation for Normally Sun Illuminated Surfaces

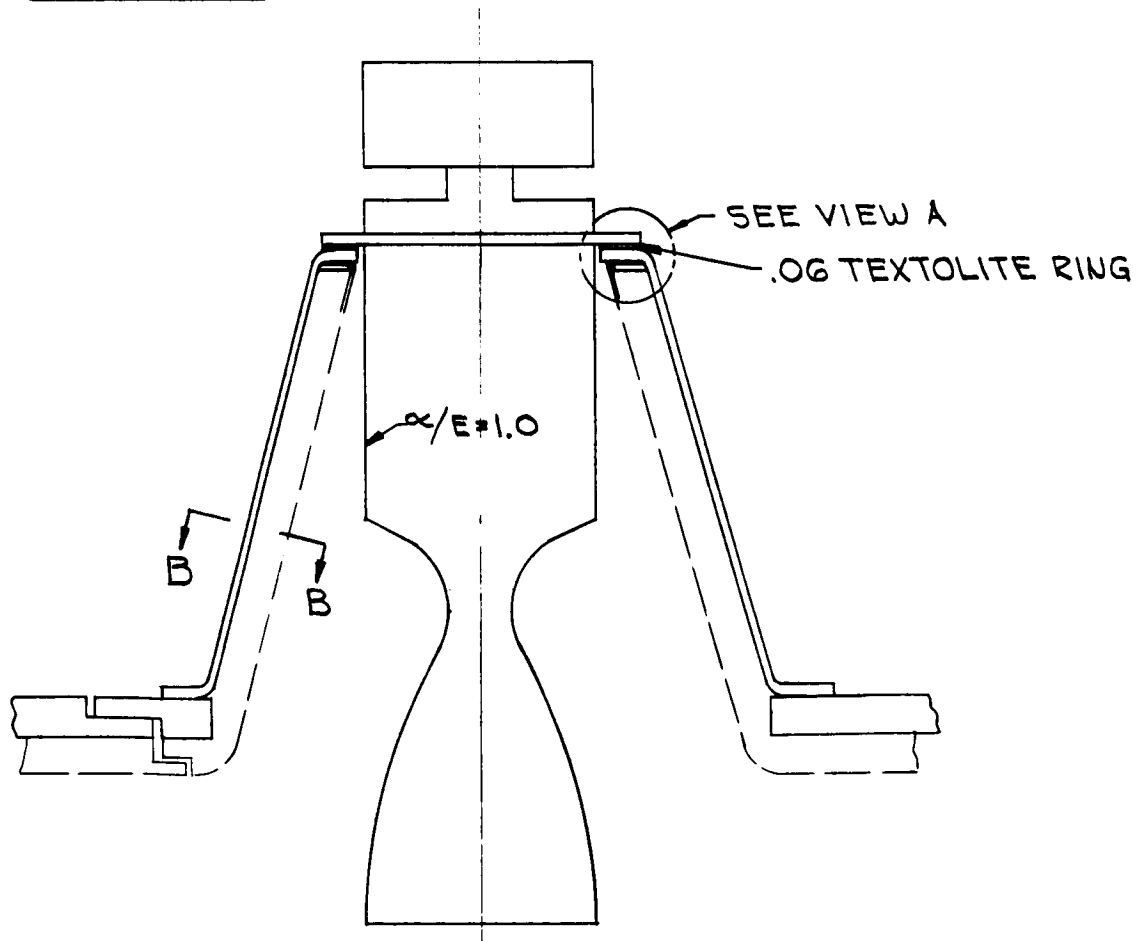
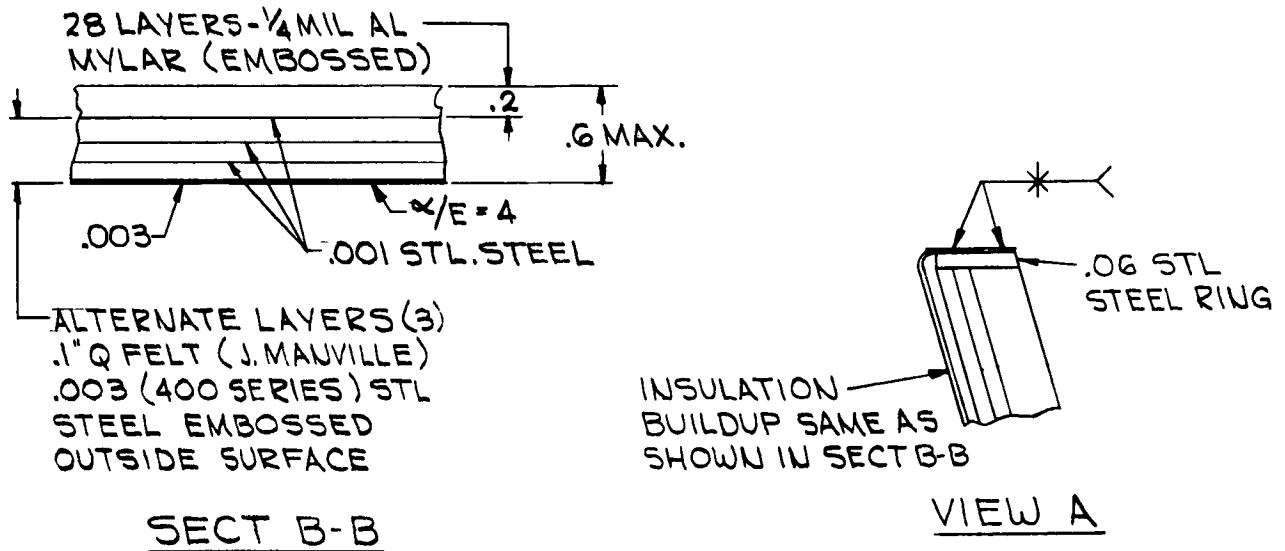


Figure 6-2. Typical Superinsulation Configuration Around Midcourse Engine

6.4 THERMAL SUBSYSTEM CONSTRAINTS

6.4.1 ELECTRONIC ASSEMBLY DISSIPATION LIMIT

The maximum allowable thermal dissipation is 234 watts per assembly.

6.4.2 SHUTTER SUN IMPINGEMENT LIMITATION

The maximum allowable solar energy input to an assembly is 560 Btu/ft² of shutter surface. This is equivalent to direct solar impingement for 1.3 hours near earth and for 2.5 hours at Mars encounter.

6.4.3 EARTH ALTITUDE LIMIT

The minimum allowable circular earth orbit is 90 nautical miles.

7.0 THERMAL SUBSYSTEM SAFETY CONSIDERATIONS

All personnel associated with vehicle handling should exercise caution with respect to the following items:

1. Cleanliness of thermal control coatings
2. Integrity of superinsulation blanket attachments
3. Maintenance of shutter blade alignment
4. The susceptability of the aluminized Mylar superinsulation blankets to temperatures above 300°F

CII - VB235FD101

TEMPERATURE CONTROL SUBSYSTEM

APPENDIX

Index

- 1 Ground Cooling Analysis
- 2 Bus Section Thermal Analysis
- 3 Shutter Analysis
- 4 Mid-Course Engine Analysis
- 5 Solar Array Analysis
- 6 Sizing of Gyro Heaters
- 7 Temperature Predictions for High Gain Antenna
- 8 Reliability Analysis

1.0 GROUND COOLING ANALYSIS

The maximum allowable rise in the cooling air temperature (assuming a 40°F shroud inlet condition) is (60° - 40°F) or 20°F to prevent overheating of the electronic equipment. The thermal dissipations for the 1971 Flight Spacecraft are assumed to be 300W and 150W for the Bus and Flight Capsule, respectively. For the 1973 and subsequent missions a dissipation of 2800 W is considered for the Flight Capsule assuming it contains a radio-isotope thermoelectric generator. From this information the theoretically required air flow rates are:

For 1971 Spacecraft

$$\frac{1530 \text{ Btu/hr}}{0.24 \text{ Btu/lb F} \times 20\text{F}} = 320 \text{ lb/hr} = 5.33 \text{ lb/min.}$$

For 1973 Spacecraft

$$\frac{10,570 \text{ Btu/hr}}{0.24 \text{ Btu/lb F} \times 20\text{F}} = 2200 \text{ lb/hr} = 36.7 \text{ lb/min.}$$

However, to make allowances for inefficiencies in air flow distribution and a small solar load, nominal flow rates of 10 and 50 lbs/min are recommended for the 1971 and 1973 spacecraft, respectively.

2.0 BUS SECTION THERMAL ANALYSIS

2.1 PROBLEM DESCRIPTION

In support of the thermal design of the Bus section, an analog study was performed to predict the gross thermal behavior of the system, to determine the method of temperature control, heat rejection areas, heater power requirements and coating properties. Constraints on the overall system design were also determined. Due to numerous changes in sub-assembly locations and dissipations, it was intended to arrive at a representative approach based on the sub-assembly locations and dissipations as shown in the thermal balance drawing (see Volume A, VB235FD101, Figure 3-1) rather than a firm final design. The results of this study, therefore, demonstrate the capability to devise a suitable control system for a given set of thermal characteristics.

The problem was simulated in an Electronic Associates, Inc. 231R Heat Transfer Analog Computer, employing the Oppenheim radiation network technique. Thirteen computer nodes were allocated as follows: nodes 1-12 corresponding to equipment bays 1-12 which includes the sub-assemblies, mounting panels, and structure; node 13 corresponding to

tankage, structure, propellants, and plumbing centrally located within the Bus section. The analog wiring diagram for solution of the heat balance is shown in Figure A-1.

Figure A-2 is a schematic of the Bus section showing the arrangement of all nodes and the heat paths for three typical nodes. Table A-1 lists the significant properties of each node used in the analog simulation.

2.2 SHUTTER PROPERTIES

Parallel type shutter geometry was employed. All heat rejection surfaces were assumed to be diffuse with an emissivity of 0.9 and a solar absorptivity of 0.3. The effective radiating properties of the shutter system, as predicted by a digital computer program are shown in Figures 3-4 and 3-5 of VB235FD101. The curve for direct sun incidence was selected as the most appropriate for this study because of the narrow range of possible sun incidence angle due to Flight Capsule and solar array shading. Shutters were assumed to be fully opened at 70°F and fully closed at 40°F.

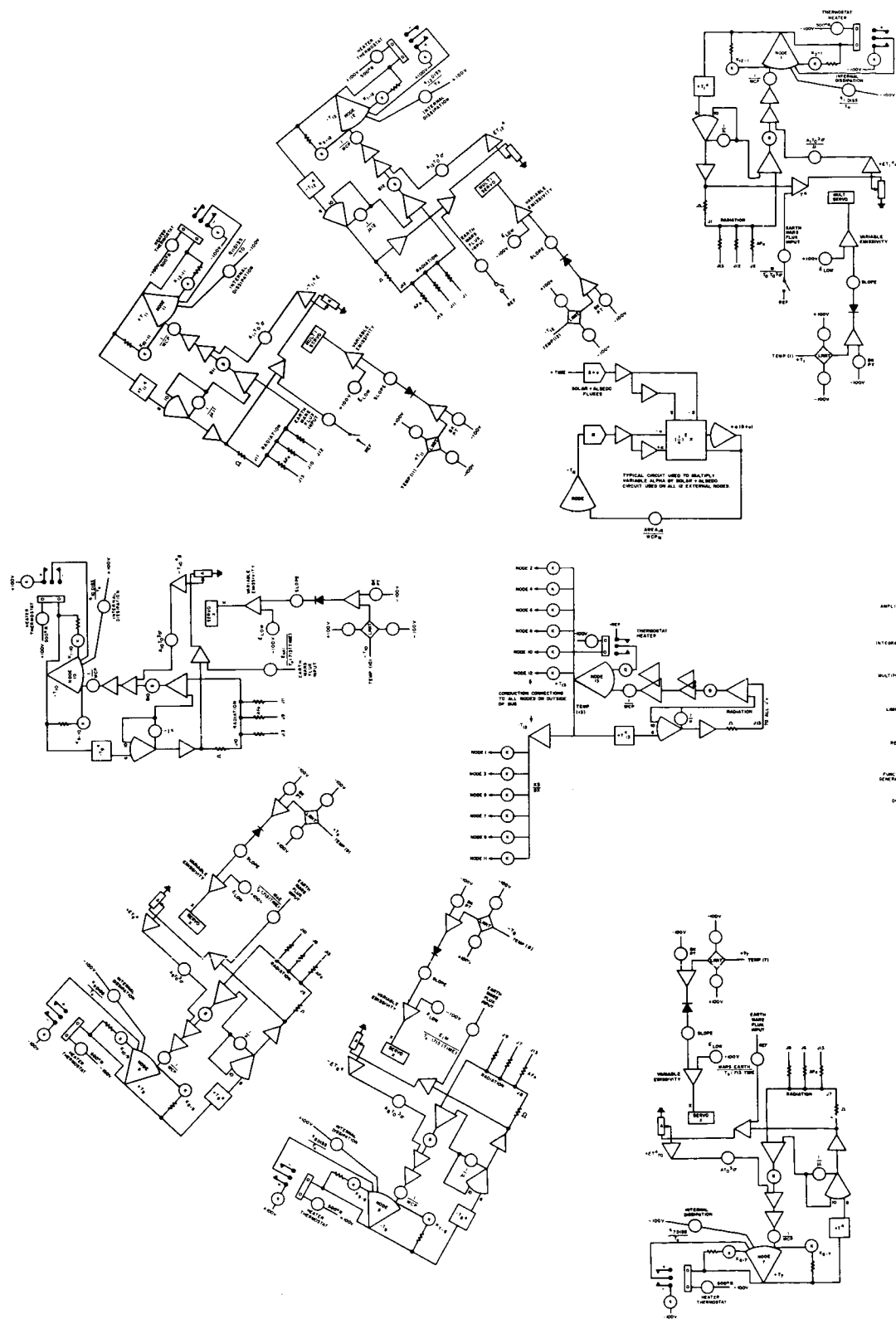
2.3 RADIATION TO SPACE CONSIDERATIONS

Several effects combine to reduce the total effective radiation area to space. Total external surface of each bay is approximately 4.75 ft², but only 4.0 ft² of this area is available for heat rejection due to mechanical considerations. An eighty percent fin effectiveness factor was then applied to this area to account for the distribution of heat from hot spots to the remote areas of the space facing plate (this same factor was applied to all internal radiating areas). Hence, the maximum effective radiating area to space for any bay is 3.2 square feet.

Allowance was made for the effect of the Flight Capsule biological barrier by considering the radiant interchange between the shutter base and a black, adiabatic barrier. It is estimated that five percent of the radiant energy leaving the shutters will return by reflection or reradiation from the biological barrier. Hence, a 0.95 view factor to space is used on all 12 assembly nodes.

Additional external blockages are experienced during various mission phases on bays (nodes) 9, 2, 3 and 4 due to the folded scan package and high gain antenna. The scan package geometry was not defined at the time of the analog study. Therefore, a radiant blockage of fifty percent was assumed for node 9.

During the earth parking orbit, the high gain antenna is folded in front of bays 2, 3, and 4. The extent of this blockage is estimated at 95 percent on bay 3 and 70 percent on bays 2 and 4 (i.e., view factors to space are .05 and .30, respectively).



(5)

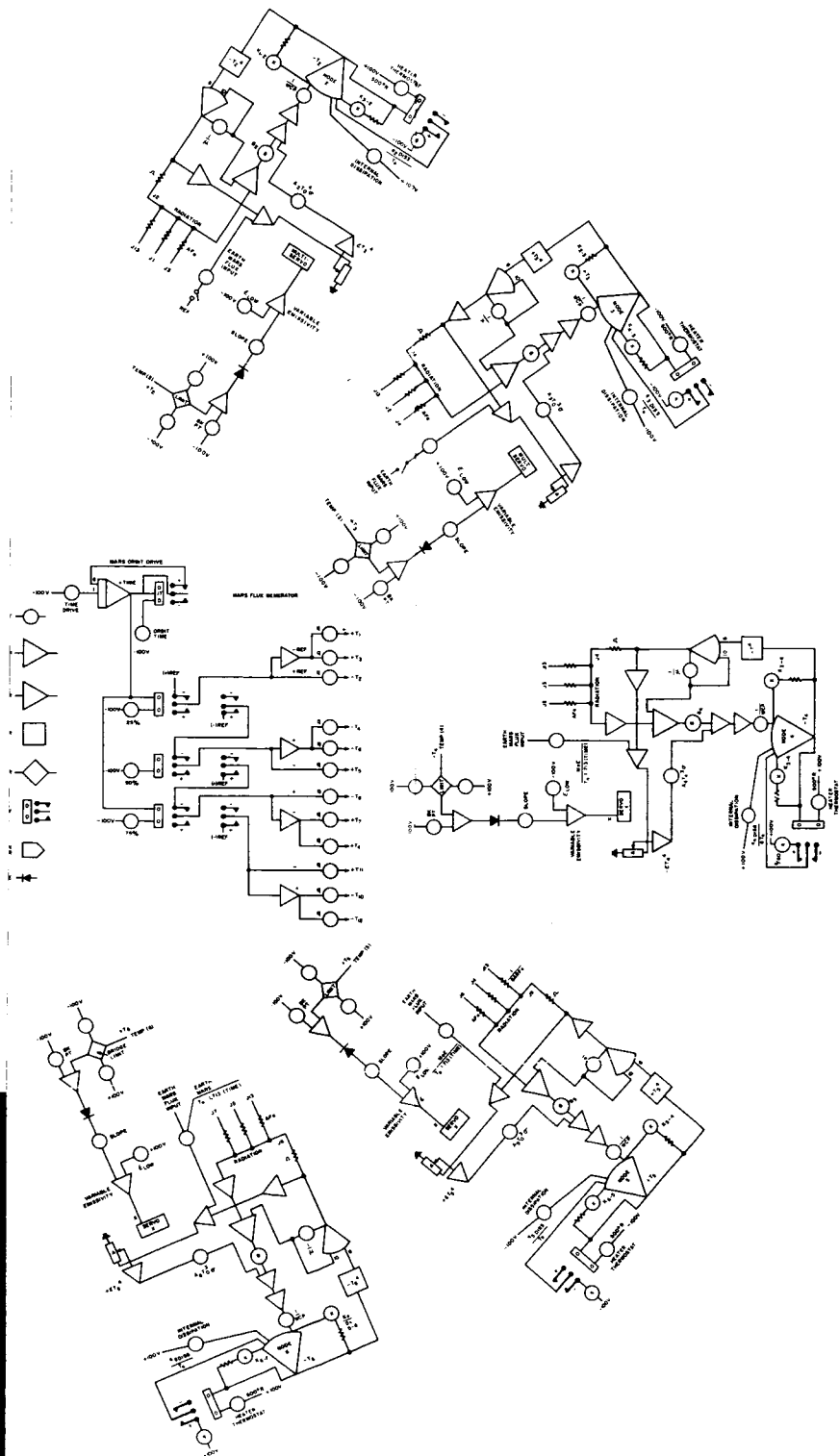
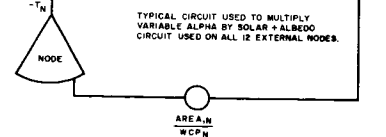
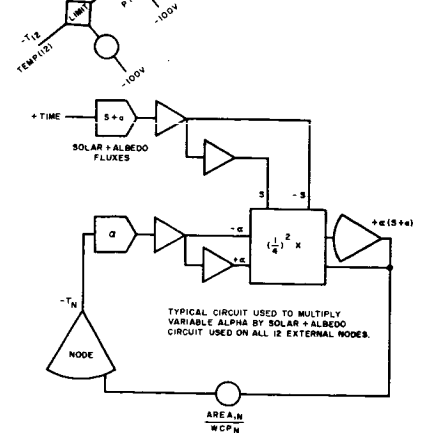
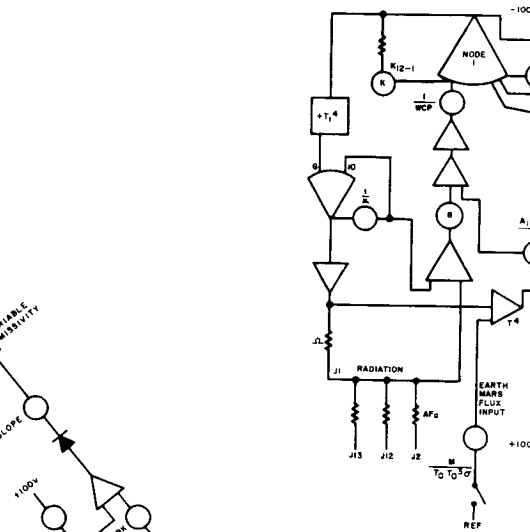
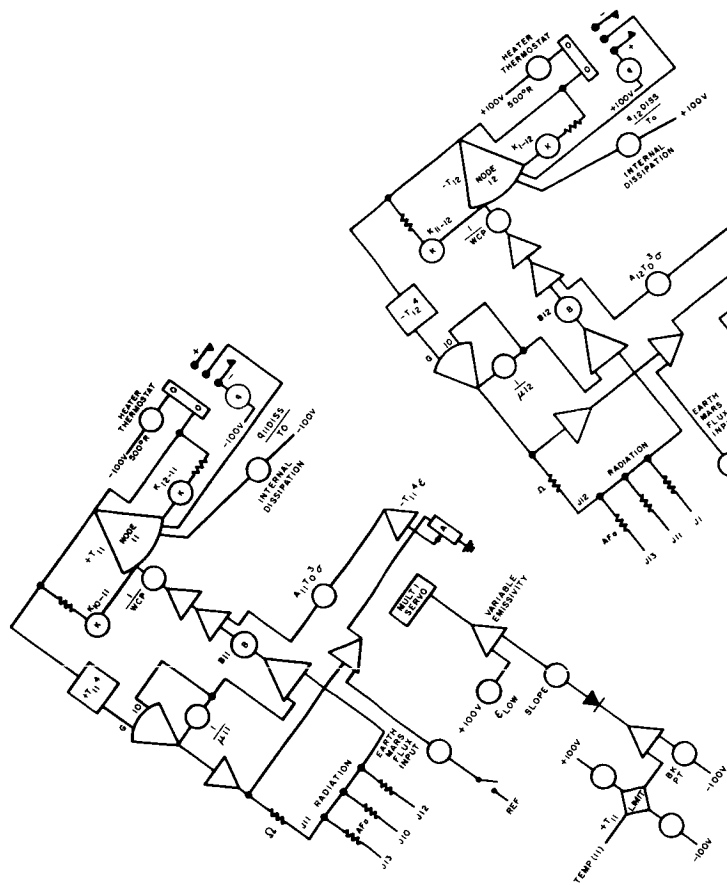


Figure A-1. Voyager Bus Section-Analog Thermal Model (Sheet 1 of 3)



①

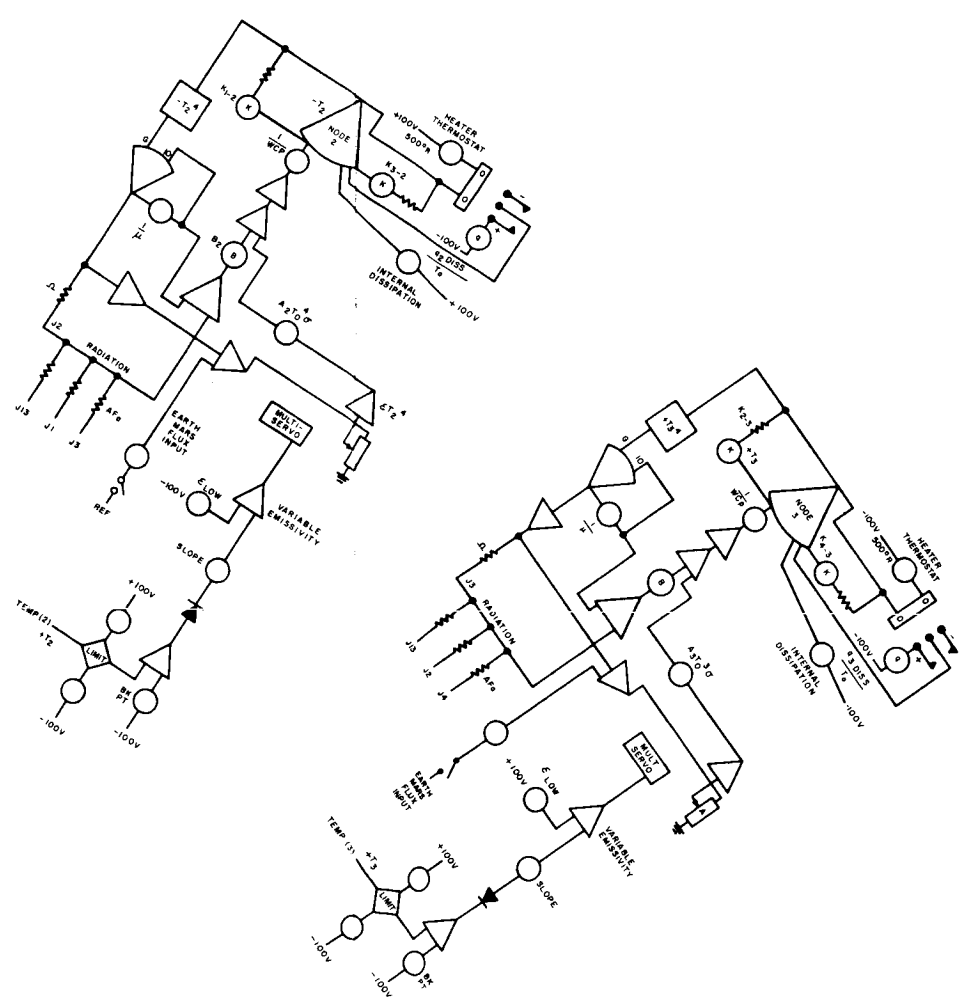
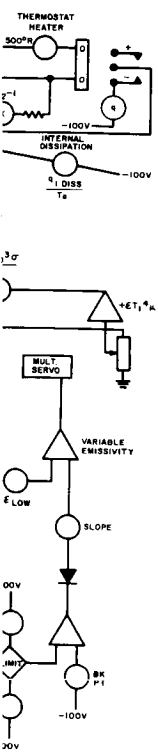
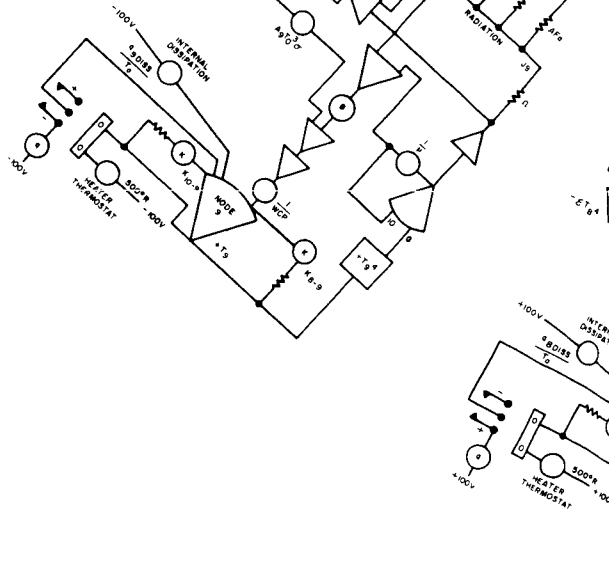
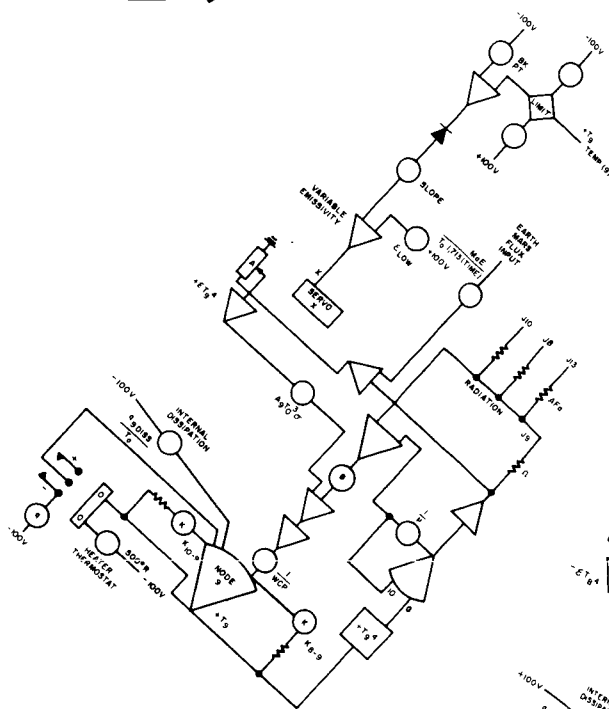
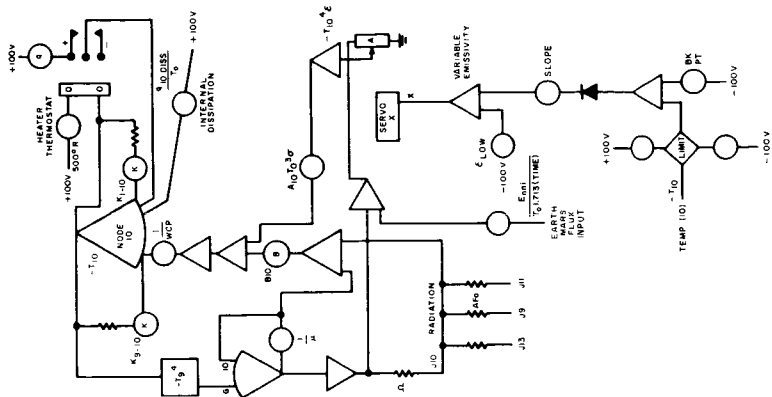
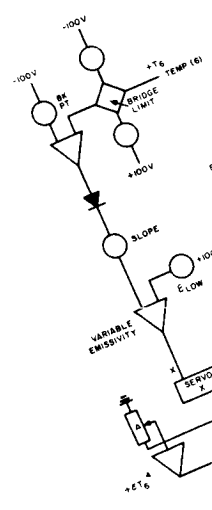
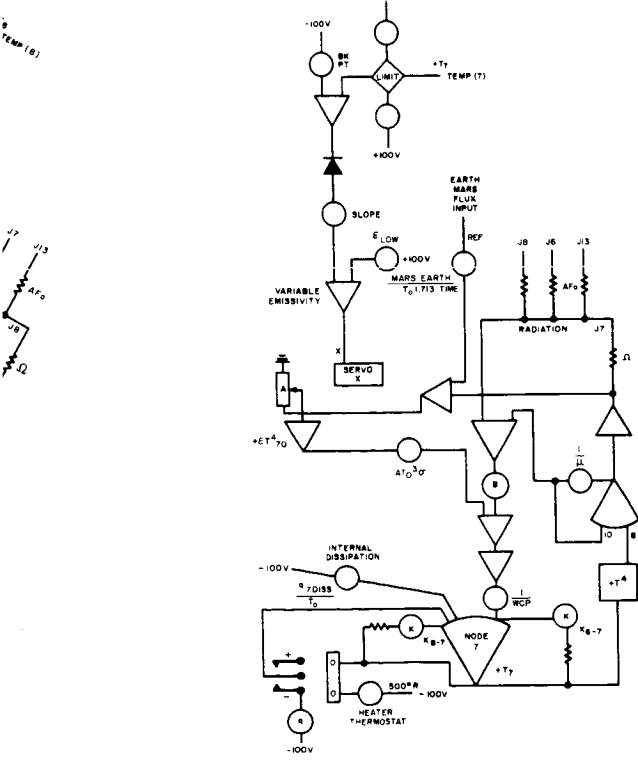
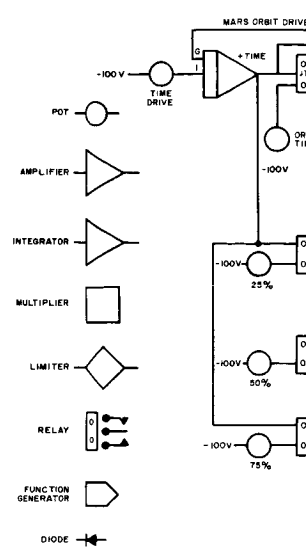
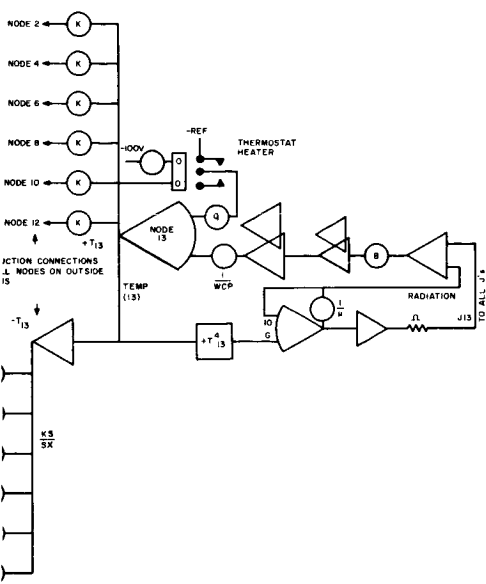


Figure A-1. Voyager Bus Section Analog Thermal Model (Sheet 2 of 3)



- NODE 1 (K)
- NODE 3 (K)
- NODE 5 (K)
- NODE 7 (K)
- NODE 9 (K)
- NODE 11 (K)

100



10(2)

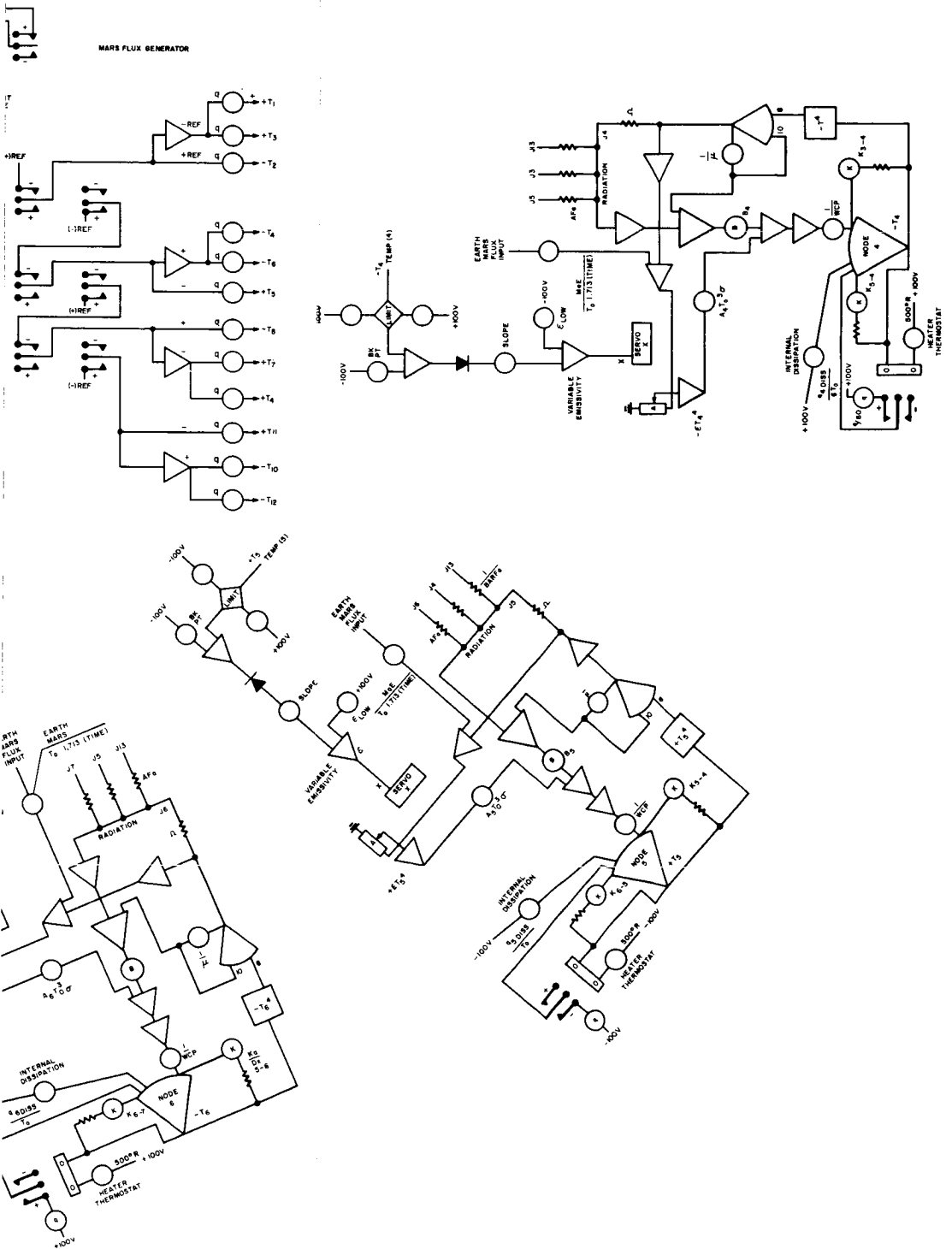
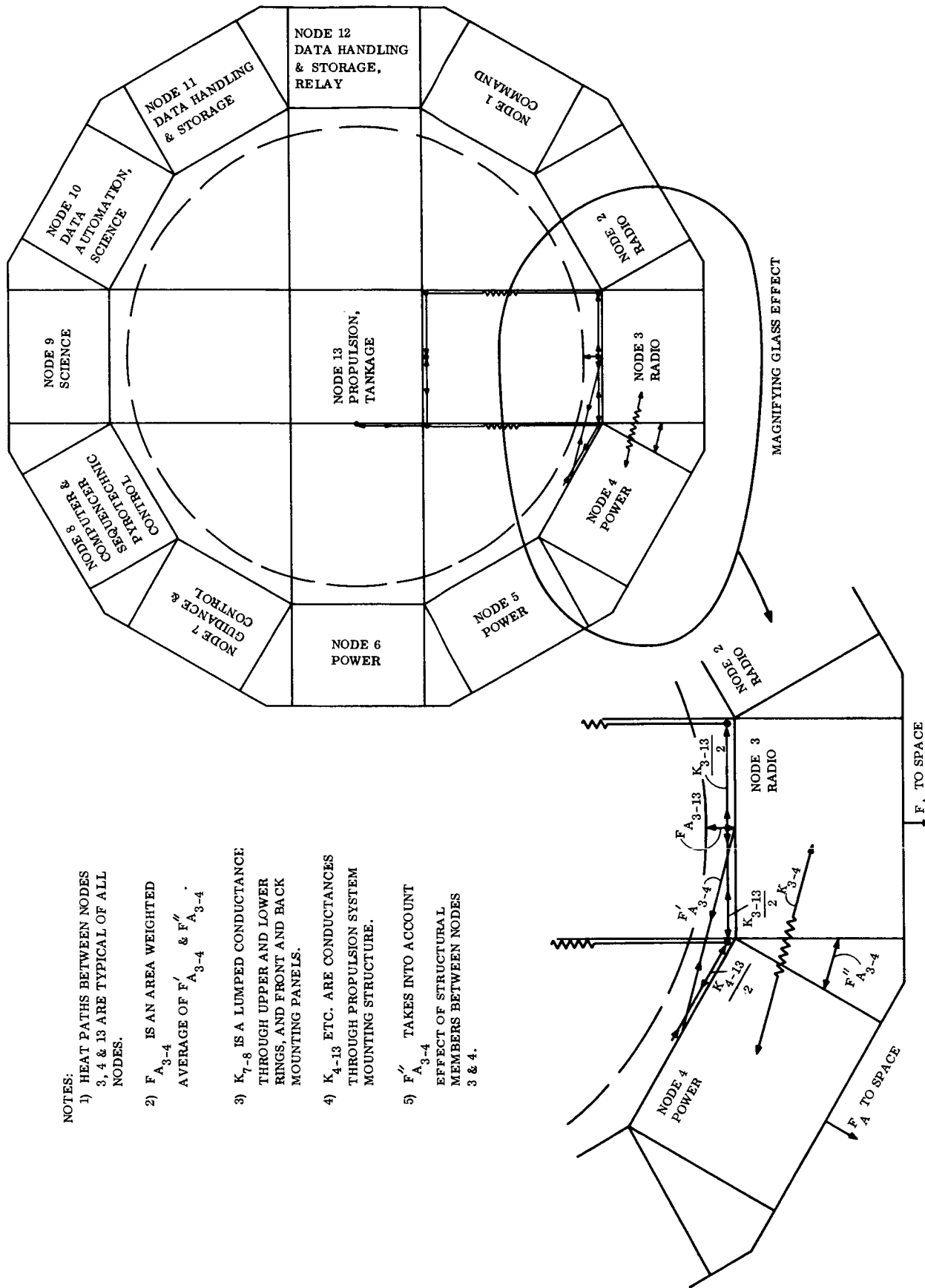


Figure A-1. Voyager Bus Section-Analog Thermal Model (Sheet 3 of 3)

2-1



NOTES:

- 1) HEAT PATHS BETWEEN NODES 3, 4 & 13 ARE TYPICAL OF ALL NODES.
- 2) $F_{A_{3-4}}$ IS AN AREA WEIGHTED AVERAGE OF $F'_{A_{3-4}}$ & $F''_{A_{3-4}}$.
- 3) K_{7-8} IS A LUMPED CONDUCTANCE THROUGH UPPER AND LOWER RINGS, AND FRONT AND BACK MOUNTING PANELS.
- 4) K_{4-13} ETC. ARE CONDUCTANCES THROUGH PROPULSION SYSTEM MOUNTING STRUCTURE.
- 5) $F''_{A_{3-4}}$ TAKES INTO ACCOUNT EFFECT OF STRUCTURAL MEMBERS BETWEEN NODES 3 & 4.

Figure A-2. Voyager Bus Thermal Node Locations

Table A-1. Nodal Properties

Node (i)	Conduc- tance $K_{i,i+1}$ $K_{i,i-1}$ (BTU/ HR-°F)	Conduc- tance $K_{i,i+1}$ $K_{i,i-1}$ (BTU/ HR-°F)	View Factor $F_{A_i, i+1}$ $F_{A_i, i-1}$	View Factor $F_{A_i, i+1}$ $F_{A_i, i-1}$	Internal Area (Ft ²)	View Factor F A to Space	Exter- nal Area (Ft ²)	Thermal Capaci- tance WC (BTU/F)	Park- ing Orbit Thru Acqui- sition	Dissipations (Watts) vs Mission Phase →				
										Transit Max.	Min	Mid- Course Near Earth	Mid- way Mars	Max
9	.784	.378	.082	.646	6.36	.95	4.0	14.1	0.0	17.0	17.0	17.0	47.0	17.0
10	.784	.189	.082	.646	6.36	.95	2.0	15.5	0.0	25.0	25.0	25.0	28.0	28.0
11	.784	.189	.082	.646	6.36	.95	2.0	12.2	8.5	8.5	8.5	8.5	8.5	8.5
12	.784	.378	.082	.646	6.36	.95	2.0	12.7	1.0	1.0	1.0	1.0	25.0	17.0
1	.784	.189	.082	.646	6.36	.95	2.0	13.8	36.6	36.6	36.6	36.6	36.6	36.6
2	.784	.189	.082	.646	6.36	.95	4.0	13.6	40.2	40.2	40.2	40.2	40.2	40.2
3	.784	.378	.082	.646	6.36	.95	4.0	13.9	45.1	86.8	45.1	45.1	86.8	86.8
4	.784	.189	.082	.646	6.36	.95	4.0	21.2	27.9	40.5	36.8	39.8	49.7	46.0
5	.784	.189	.082	.646	6.36	.95	2.0	20.6	20.5	8.1	4.4	25.2	30.8	4.7
6	.784	.378	.082	.646	6.36	.95	4.0	20.5	44.8	66.1	48.6	35.7	68.0	65.8
7	.784	.189	.082	.646	6.36	.95	4.0	15.6	40.4	22.9	9.4	63.8	44.1	13.1
8	.784	.189	.082	.646	6.36	.95	2.0	11.4	20.0	20.0	20.0	20.0	20.0	20.0
13	---	---	---	---	49.52	0	---	1500.0	0.0	0.0	0.0	0.0	0.0	0.0
					(124.0									
					near									
					Mars)									

2.4 SUPERINSULATION HEAT LEAK

All surfaces of the Bus section, except for the heat rejection areas, are covered with superinsulation. It is estimated that a heat leak of approximately 0.5 watts/ft² on non-illuminated superinsulation surface will exist. Working against this heat leak is a conservatively estimated heat input of 0.91 watts/ft² to all superinsulation directly illuminated by sun. The resulting net superinsulation heat leak for the Bus section is about 13 watts. This lost heat tends to lower temperatures in the Bus section. Therefore, during minimum cases, the dissipation in each bay was reduced by 1 watt to account for this loss.

2.5 MISSION PHASES

The Bus analog study considered the following mission phases: 1) Earth parking orbit through acquisition, 2) Transit, 3) Mid-Course maneuver and 4) Mars orbit.

2.5.1 EARTH PARKING ORBIT

The profile assumed for the Earth parking orbit is shown in Figure A-3. Bay 3, containing the highest thermal dissipation, is oriented towards earth, and subsequently towards the sun during acquisition. The Orbital Heat Flux digital computer program was used to calculate the incident fluxes using the following orbit parameters:

- a . Circular 100 nautical mile orbit
- b . Launch at 0600 local time
- c . Inclination = 28.5°
- d . Day 182
- e . Solar constant = 434 Btu/hr-ft², Albedo Factor = 0.38,
Earth flux = 68.2 Btu/hr-ft²
- f . Vehicle path stabilized.

Acquisition was assumed to consist of a 90 degree pitch of the vehicle to bring the roll axis pointing toward the sun in 30 minutes. Because of shading of the solar arrays, the Bus is occulted after 8.3 minutes. This shading effect and that of the Flight Capsule was not considered in the earth orbit portion of this phase. The results then are necessarily conservative. A GE Shaded Orbital Heat Flux program, which is now in the final stages of checkout, could be used in Phase IB to improve the accuracy of this analysis. Figure A-4 shows the simulated fluxes on node 3. This plot is typical of all 12 assembly nodes.

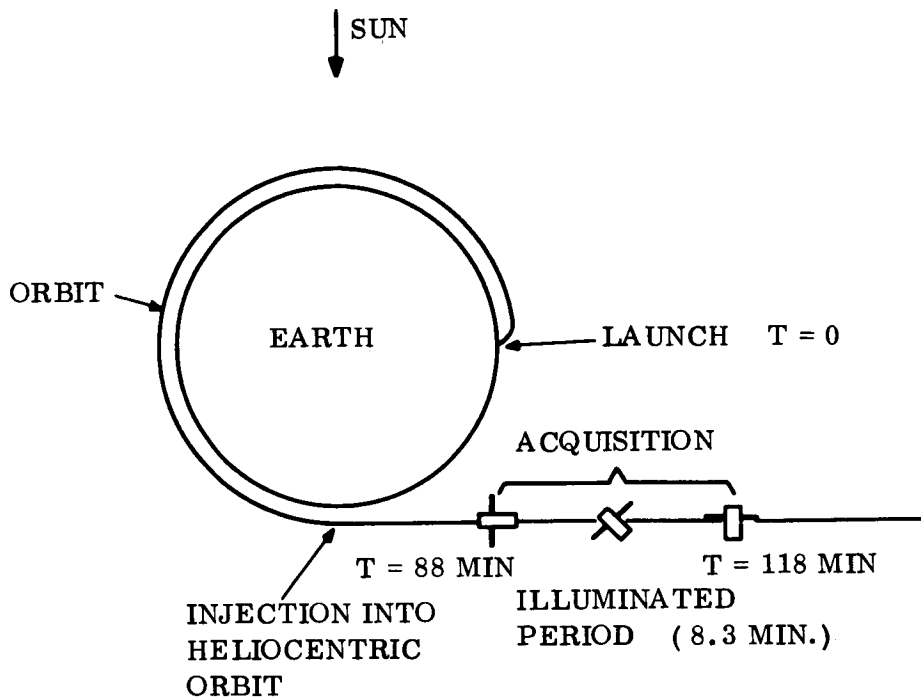


Figure A-3 Earth Orbit Phase Profile

2.5.2 TRANSIT PHASE

The transit phase of the mission is characterized by no external flux impingement. Maximum and minimum dissipations were used in each node. Because of the lack of fluxes and the relatively low minimum dissipations, this case was used for trade-offs requiring a cold case, as well as for heater sizing.

2.5.3 MID-COURSE CORRECTION PHASE

Two mid-course maneuvers were considered in this analysis. The first maneuver will occur between 2 and 10 days from launch, so that a full solar constant (434 btu/hr-ft^2) must be used. However, because of the short communication time at this distance, the total duration of the correction can be limited to one hour. The second maneuver was assumed to occur near the midpoint in the transfer orbit (90 days from launch, 1.25 AU) with a solar constant of 280 btu/hr-ft^2 . The duration of this course correction was assumed to be two hours because of the longer communication time. Because the exact spacecraft orientation, with respect to the sun during the mid-course correction, cannot be predicted, it was assumed that the sun directly impinged on the hottest node (3). A case was also studied for the sun centered about node (5) to input the maximum flux to the critical battery bays. Table A-2 compares the two cases employing maximum dissipations.

In the actual case, the spacecraft rolls at a typical rate of 0.2 degrees per second for a

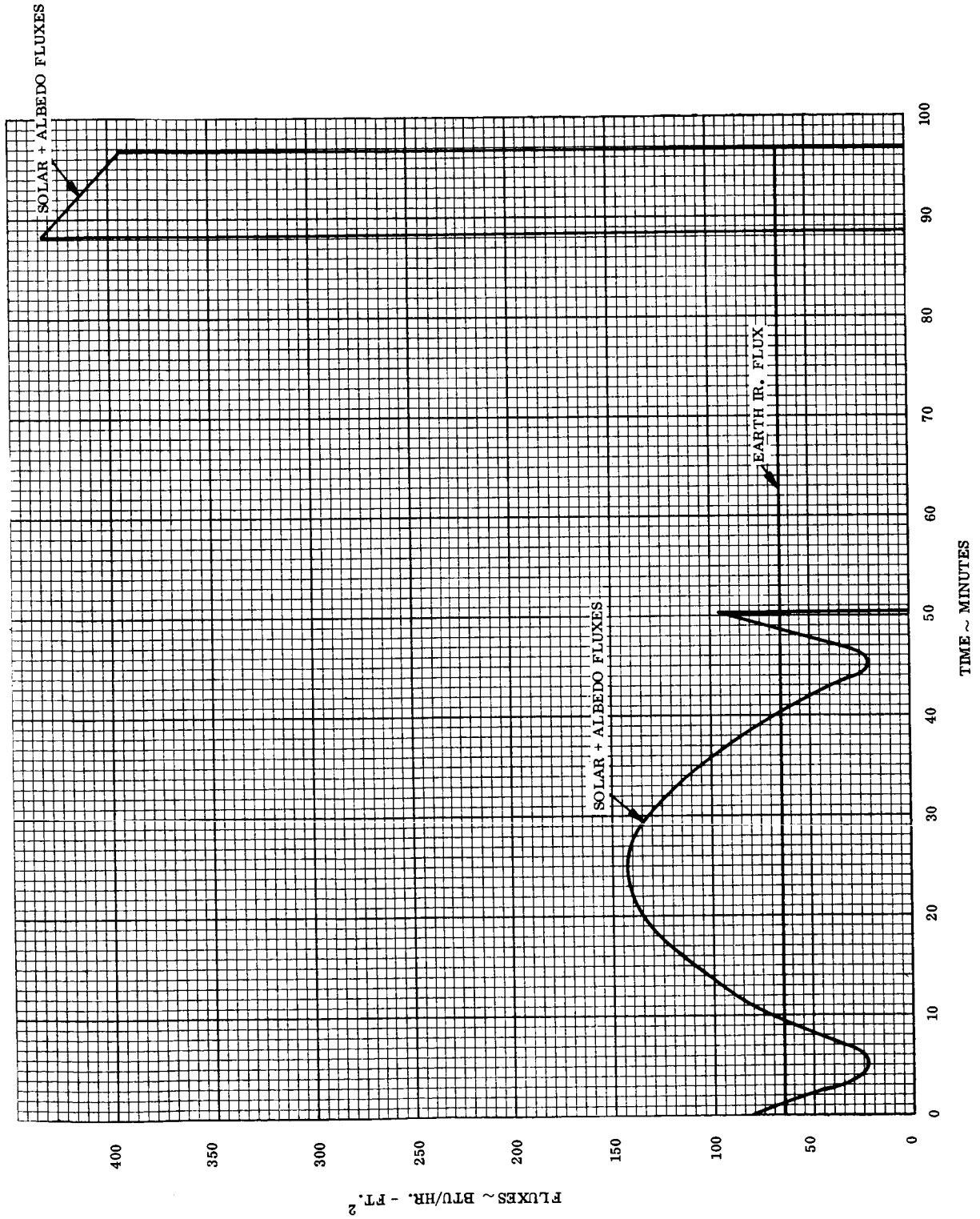


Figure A-4 Typical Earth Orbit Fluxes (Node 3)

total of 90 degrees (worse case). The solar flux incident on a particular sub-assembly mounting panel builds up sinusoidally as the maneuver starts, holds constant for the telecommunications and engine firing, then falls off sinusoidally. However, the solar array shades the Bus until the spacecraft has rolled 65 of the 90 degrees. The remaining 25 degree roll takes only a little more than two minutes, which is negligible as compared to the duration of the maneuver. The solar fluxes during this mission phase were therefore approximated as a square wave pulse.

Table A-2. Maximum Battery Node Temperatures ($^{\circ}$ F) During Mid-Course Maneuver

Battery Node No.	Sun On Nodes <u>1, 2, 3, 4, & 5</u>	Sun On Nodes <u>3, 4, 5, 6, & 7</u>
4	68	63
5	60	65
6	53	59

2.5.4 MARS ORBIT

In the Mars orbit, two distinct cases were considered - maximum and minimum. In the minimum case, no external fluxes were considered and sub-assembly dissipations were at their lowest. The zero external flux case is reasonable considering the high altitude orbits which can be expected (300 x 30,000 Km). A 4000 Km circular orbit with a period of 318 minutes was used for Mars planetary flux of 60 btu/hr-ft². This orbit will provide an average of 4 btu/hr-ft² to every node, with a peak of 12.5 btu/hr-ft². Albedo fluxes for an albedo factor of 0.15, provide only about 0.6 btu/hr-ft² average flux, and can therefore, be neglected. When this maximum case was run, however, it was found that the planetary flux raised the temperature of the hottest node by, at most, 1.5 $^{\circ}$ F. Because of the inconvenience of simulating these fluxes, it was decided to consider them negligible and use the no flux, steady state solution as maximum case. The Mars orbit dissipations are the highest of all the mission phases, so that this case was used for sizing of areas and emissivities.

2.6 EXTERNAL AREA DETERMINATION

The external radiating areas of all nodes were determined in the Mars maximum case with no external fluxes. The heat rejection areas on all nodes were then varied until all temperatures were 70 $^{\circ}$ F. Since all bays were actively controlled, this provided a maximum emissivity to space of 0.53. Actually, this could not be exactly achieved since the maximum area (4 ft²) is not sufficient to dump the high dissipation of node 3. The temperatures of nodes 2 and 4 were kept at 62 and 63 degrees respectively to provide an additional sink for this node 3 heat. Based on the resulting areas, two standard sizes (4 ft² and 2 ft²) were selected, for ease of manufacturing and handling and lower cost. Since all these areas are the same or slightly larger than that required to maintain 70 $^{\circ}$ F, for any particular bay, the

thermal capability of the Bus is greater than the Mars maximum case requires.

2.7 PASSIVE NODE EXTERNAL SURFACE PROPERTIES

Passive thermal control is feasible on nodes 11, 1, 2 and 8 which have constant dissipations throughout the mission. Though the decision has been made to use active control on every node to provide greater flexibility in accommodating design changes, the performance of partial passive control has been studied. The external surface properties of these nodes were determined using Mars maximum dissipations (no external fluxes) and external areas as sized above. The emissivity on each of the passive nodes was then varied until its temperature was 55°F (the midpoint of the desired control band). The solar absorptivity was selected as low as possible (0.15) in anticipation of solar incidence during mid-course maneuver. Table A-3 shows the required emissivities. The thermal performance of the Bus with the four passive nodes is documented throughout this study. The trade-off of active versus passive control is discussed in Volume B (VB235AA101).

Table A-3. Surface Properties of Passive Nodes

<u>Node No.</u>	<u>External Area (ft²)</u>	<u>Emissivity</u>	<u>Solar Absorptivity</u>
11	2.0	0.3	0.15
1	2.0	0.75	0.15
2	4.0	0.5	0.15
8	2.0	0.5	0.15

2.8 FAILURE MODES

Two general types of failure modes were considered in this study -- (1) assembly and (2) shutter failures. There are very few assembly failures which would not be critical to the success of the mission. A partial or complete failure of the science equipment in Bay 9 would not abort this mission since valuable engineering data could still be obtained. This system could also be temporarily turned off during eclipse periods to save battery power. Similarly, the radio subsystem in bays 2 and 3 could be temporarily shut down. No other assembly failures can be considered. When these assemblies are off (nodes 9, 2 and 3), all temperatures in the Bus drop as shown in Table A-4 and 6.2W of heater power is required in node 13. This effect was considered with Transit phase minimum dissipations.

Two types of shutter failures can also be considered - opened or closed. A failed opened shutter has an emissivity of .53 and the temperatures of all nodes are pulled down, with heater power being required in some cases. These cases were run for Transit minimum dissipations. A failed closed shutter has an emissivity of .15 and all Bus section temperatures are increased. Mars orbit maximum dissipations were used for these runs. Shutters were failed one at a time in either position and the effects noted. The results of this analysis and the tradeoffs made as to a preferred position are presented in Volume B (VB235AA101).

Table A-4. Nodal Temperatures - SubAssemblies in Nodes 9, 2 & 3 Off

<u>Node</u>	<u>Temperature (°F)</u>
1	31
2	4
3	23
4	46
5	40
6	50
7	36
8	33
9	30
10	46
11	35
12	31
13	40*

*6.2 watts heater power required

2.9 ASSEMBLY MOUNTING PANEL TEMPERATURE DISTRIBUTIONS

A 90-node two-dimensional steady state digital computer analysis was made on each assembly mounting panel using boundary conditions obtained from the analog computer analysis described previously. Both 30 mil and 60 mil plate thicknesses were used for highest dissipation case (Mars Shade). These temperature distributions (in °F) are shown in Figures A-5 through A-16. The Transit phase results, Figures A-17 through A-28 were determined for the 60 mil plate thickness only. A thermal conductivity of 70 btu/hr-ft °F was assumed for the plates.

3.0 SHUTTER ANALYSIS

3.1 ASSUMPTIONS

- a . Shutter systems are infinitely long
- b . Diffuse surfaces are gray
- c . Specular surfaces are perfectly smooth, perfectly flat and perfectly specular, thus the angle of reflectance equals the angle of incidence.
- d . Specular surfaces radiate (σT^4) according to Lambert's law.
- e . There is no conduction in the system.
- f . Blades are end pivoted.
- g .. The blades have adiabatic back surfaces.

BAY 1 (COMMAND S/S) TEMPERATURE DISTRIBUTION (°F)

MARS SHADE										
(58)	(57)	(56)	(55)	(55)	(55)	(56)	(56)	(56)	(56)	(56)
58	57	56	55	55	55	56	56	56	56	56
(58)	(58)	(56)	(54)	(54)	(54)	(56)	(56)	(57)	(56)	(56)
58	58	56	55	54	54	56	56	56	56	56
(58)	(62)	(55)	(52)	(51)	(52)	(55)	(61)	(57)	(57)	(57)
58	① 60	55	53	53	53	55	59	56	56	56
(59)	(64)	(56)	(52)	(51)	(53)	(55)	(63)	(57)	(57)	(57)
58	② 61	56	53	52	52	55	59	57	57	57
(58)	(61)	(52)	(47)	(46)	(47)	(51)	(60)	(56)	(56)	(56)
58	59	53	50	49	49	52	58	56	56	56
(58)	(59)	(49)	(44)	(42)	(44)	(48)	(58)	(56)	(56)	(56)
58	57	51	48	47	47	50	56	56	56	56
(58)	③ (57)	(46)	(41)	(40)	(41)	(46)	(56)	(56)	(56)	(56)
58	56	50	46	45	46	49	55	56	56	56
(57)	(53)	(42)	(38)	(37)	(38)	(42)	(52)	(56)	(56)	(56)
58	54	47	44	43	44	47	53	55	55	55
(58)	(53)	(48)	(45)	(44)	(45)	(48)	(52)	(56)	(56)	(56)
57	54	51	48	47	47	50	53	55	55	55
(58)	(54)	(51)	(49)	(48)	(48)	(50)	(53)	(56)	(56)	(56)
57	54	52	51	49	49	51	53	55	55	55

COMPONENT	DISSIPATION (WATTS)
① COMMAND DETECTOR	10.0
② COMMAND DECODER	11.0
③ COMMAND POWER SUPPLIES NO. 1, 2	15.4

2 FT² SHUTTER SIZE
 $\epsilon_{\text{EFF}} = 0.57$
 TEMP. IN () ARE FOR 30 MIL PLATE
 OTHER TEMPS. ARE FOR 60 MIL PLATE

Figure A-5. Mars Shade Bay 1 (Command S/S) Temperature Distribution (°F)

BAY 2 (RADIO S/S) TEMPERATURE DISTRIBUTION (°F)

COMPONENT	DISSIPATION (WATTS)
① RCVR & EXC SEL LOGIC	0.01
② EXCITER NO. 1	5.7
③ RCVR NO. 2	5.3
④ T/R NO. 1	6.2
⑤ RCVR NO. 1	5.3
⑥ T/R NO. 3	6.2
⑦ RCVR NO. 3	5.3
⑧ T/R NO. 2	6.2

MARS SHADE

(58)	(44)	(37)	(35)	(36)	(38)	(42)	(49)	(62)
58	49	45	43	44	46	49	54	62
(58)	(45)	(39)	(37)	(39)	(43)	(47)	(52)	(62)
58	50	46	45	46	48	52	56	62
(58)	(46)	(41)	(42)	(47)	(54)	(58)	(61)	(63)
58	51	48	48	51	④ 55	58	61	63
(59)	(49)	(46)	(47)	(54)	(61)	(65)	(66)	(64)
58	53	51	52	56	⑤ 60	63	64	63
(59)	①(55)	(56)	(56)	(59)	(63)	(64)	(64)	(64)
59	57	57	57	60	62	63	64	64
(60)	②(69)	(72)	(73)	(71)	(68)	(68)	(66)	(64)
60	65	67	67	67	66	66	65	64
(61)	③(72)	(76)	(78)	(77)	⑥(76)	(75)	(72)	(64)
61	67	70	70	70	70	70	68	64
(60)	③(64)	(66)	(67)	(67)	⑦(67)	(66)	(65)	(64)
60	63	64	65	65	65	65	65	64
(60)	(60)	(61)	(61)	(61)	(62)	(63)	(59)	(57)
60	60	61	61	62	62	62	63	63
(56)	(56)	(56)	(56)	(57)	(57)	(58)	(58)	(63)
59	58	58	58	59	59	59	60	63

4 FT² SHUTTER SIZE

$\epsilon_{EFF.} = 0.5$

TEMPS. IN () ARE FOR 30 MIL PLATE
OTHER TEMPS. ARE FOR 60 MIL PLATE

Figure A-6. Mars Shade Bay 2 (Radio S/S) Temperature Distribution (°F)

BAY 3 (RADIO S/S) TEMPERATURE DISTRIBUTION (°F)

MARS SHADE

50	37	28	24	21	22	26	35	52
51	39	32	27	24	24	27	36	52
52	① 45	39	35	④ 30	27	29	37	52
53	② 50	47	43	38	32	32	38	52
53	51	49	48	45	38	35	40	53
54	53	54	55	⑤ 62	45	39	41	53
56	64	70	69	62	50	42	43	53
61	92	106	103	⑥ 102	59	47	45	54
69	③ 156	183	177	123	70	51	47	54
64	110	133	139	84	64	50	47	54

COMPONENT	DISSIPATION (WATTS)
① EXCITER NO.3	5.7
② EXCITER NO.2	5.7
③ PA/PS NO.1	75
④ PA SELECT LOGIC	.01
⑤ PA/PS NO.3	OFF
⑥ ANTENNA SELECT LOGIC	.01

4 FT² SHUTTER SIZE
 $\epsilon_{EFF} = 0.65$
 60 MIL PLATE

Figure A-7. Mars Shade Bay 3 (Radio S/S) Temperature Distribution (°F)

BAY 4 (POWER S/S) TEMPERATURE DISTRIBUTION (°F)

MARS SHADE

(60)	(38)	(26)	(20)	(18)	(19)	(24)	(35)	(56)
59	44	36	31	29	30	34	41	54
(60)	(39)	(28)	(23)	(21)	(22)	(26)	(36)	(55)
60	46	37	33	31	32	35	42	54
(61)	(43)	(34)	(29)	(27)	(28)	(32)	(40)	(55)
60	①48	41	37	35	36	39	45	55
(61)	(47)	(40)	(36)	(35)	(35)	(38)	(44)	(56)
61	51	45	41	40	41	44	48	55
(62)	(51)	(45)	(42)	(41)	(42)	(44)	(48)	(56)
61	54	49	47	46	46	47	50	56
(62)	(55)	(52)	(50)	(50)	(50)	(50)	(52)	(56)
62	57	54	53	52	52	52	54	56
(63)	②(64)	(64)	(64)	(63)③	(63)	(63)	(62)	(57)
63	63	62	61	61	60	60	60	57
(63)	(67)	(69)	(69)	(69)	(68)	(67)	(64)	(58)
63	65	65	65	64	64	63	61	58
(63)	(67)	(68)	(68)	(68)	(68)	(66)	(63)	(57)
63	65	65	65	65	64	63	61	58
(63)	(62)	(62)	(62)	(62)	(61)	(60)	(59)	(57)
63	62	62	62	61	61	60	59	57

COMPONENT	DISSIPATION (WATTS)
① BATTERY	12.7
② MAIN BUCK REGULATOR	36.8
③	

4 FT² SHUTTER SIZE
ε_{EFF} = 0.51

TEMPS IN () ARE FOR 30 MIL PLATE
OTHER TEMPS. ARE FOR 60 MIL PLATE

Figure A-8. Mars Shade Bay 4 (Power S/S) Temperature Distribution (°F)

BAY 5 (POWER S/S) TEMPERATURE DISTRIBUTION (°F)

MARS SHADE

(58)	(55)	(53)	(51)	(51)	(54)	(57)	(57)	(60)
58	56	54	53	52	53	55	57	60
(58)	(55)	(51)	(49)	(48)	(49)	(52)	(57)	(60)
58	56	53	51	51	52	54	57	60
(57)	(56)	(47)	(43)	(42)	(43)	(48)	(57)	(61)
58	56	51	48	48	49	52	58	60
(58)	(58)	(48)	(44)	(42)	(44)	(49)	(59)	(61)
58	57	52	49	48	49	53	59	61
(58)	(60)	(61)	(47)	(45)	(47)	(52)	(61)	(61)
58	58	54	51	50	51	54	60	61
(58)	(63)	(55)	(52)	(51)	(52)	(55)	(65)	(61)
58	61	56	54	53	54	57	62	61
(59)	(70)	(64)	(61)	(61)	(62)	(65)	(72)	(62)
59	65	61	60	59	60	63	66	62
(59)	(66)	(61)	(60)	(59)	(60)	(62)	(68)	(62)
59	63	60	60	59	60	61	65	62
(58)	(62)	(61)	(61)	(61)	(61)	(62)	(63)	(61)
58	60	60	60	60	61	61	62	61
(58)	(62)	(63)	(63)	(63)	(64)	(64)	(64)	(61)
58	61	61	61	62	62	62	62	61

COMPONENT	DISSIPATION (WATTS)
① BATTERY	12.7
② DISCHARGE REGULATOR	16.7
③ SINGLE PHASE INVERTER	1.4

2 FT² SHUTTER SIZE

$\epsilon_{EFF} = 0.53$

TEMP. IN () ARE FOR 30 MIL PLATE
OTHER TEMPS. ARE FOR 60 MIL PLATE

Figure A-9. Mars Shade Bay 5 (Power S/S) Temperature Distribution (°F)

BAY 6 (POWER S/S) TEMPERATURE DISTRIBUTION (°F)

MARS SHADE										
(54)	(32)	(20)	(15)	(13)	(15)	(20)	(15)	(20)	(31)	(52)
54	39	30	26	24	26	30	26	30	37	51
(54)	(33)	(22)	(17)	(16)	(17)	(22)	(17)	(22)	(32)	(52)
54	40	32	28	27	38	31	38	31	39	51
(55)	(37)	(28)	(24)	(23)	(24)	(28)	(24)	(28)	(36)	(52)
54	42	36	32	31	32	36	32	36	42	52
(55)	(41)	(34)	(31)	(31)	(33)	(36)	(33)	(36)	(42)	(53)
55	46	40	39	37	45	41	45	41	45	52
(56)	(44)	(39)	(37)	(39)	(42)	(44)	(42)	(44)	(47)	(53)
55	48	44	43	44	46	47	46	47	50	53
(56)	(46)	(43)	(45)	(50)	(56)	(58)	(56)	(58)	(57)	(54)
56	50	48	49	53	56	57	56	57	56	54
(56)	(49)	(49)	(54)	(70)	(84)	(86)	(84)	(86)	(79)	(56)
56	54	55	57	66	73	74	73	74	69	56
(57)	(64)	(69)	(72)	(79)	(84)	(82)	(84)	(82)	(74)	(57)
58	64	68	71	73	74	72	74	72	67	56
(61)	(103)	(116)	(115)	(93)	(70)	(61)	(70)	(61)	(56)	(54)
62	87	97	97	81	67	61	67	61	57	54
(61)	(98)	(111)	(108)	(87)	(63)	(52)	(63)	(52)	(49)	(53)
62	87	98	101	72	61	55	61	55	52	54

COMPONENT	DISSIPATION (WATTS)
① BATTERY	12.7
② 2.4KC INVERTER	30.9
③ POWER SWITCHING & LOGIC	20.0
④ SYNCHRONIZER	30
⑤ 3 PHASE INVERTER	1.4

4FT² SHUTTER SIZE

ε_{EFF} = 0.57

TEMPS. IN () ARE FOR 30 MIL PLATE
OTHER TEMPS. ARE FOR 60 MIL PLATE

Figure A-10. Mars Shade Bay 6 (Power S/S) Temperature Distribution (°F)

BAY 7 (GUIDANCE & CONTROL S/S) TEMPERATURE DISTRIBUTION (°F)

MARS SHADE

(57)	(39)	(29)	(24)	(23)	(24)	(27)	(35)	(51)
56	44	37	33	32	32	35	40	50
(57)	(41)	(32)	(28)	(26)	(27)	(30)	(37)	(51)
57	46	39	36	34	34	36	41	50
(58)	(47)	(40)	(36)	(34)	(35)	(37)	(42)	(51)
57	① 49	44	41	39	39	41	45	51
(58)	(49)	(43)	(39)	(37)	(36)	(37)	(43)	(51)
58	51	46	43	41	40	41	45	51
(58)	(48)	(43)	(39)	(35)	(33)	(33)	(38)	(51)
58	51	48	44	31	39	39	43	51
(59)	(55)	(53)	(49)	(41)	(35)	(33)	(37)	(51)
59	57	55	52	46	41	40	43	51
(61)	(78)	(82)	(77)	(59)	(41)	(35)	(38)	(51)
61	② 70	72	68	57	46	42	43	51
(62)	(95)	(104)	(98)	(73)	(47)	(38)	(40)	(51)
62	81	86	81	65	49	44	44	51
(61)	(83)	(90)	(85)	(67)	(48)	(41)	(42)	(51)
62	③ 75	79	75	62	④ 50	45	46	51
(60)	(63)	(65)	(62)	(54)	(45)	(41)	(43)	(51)
60	64	66	66	52	48	45	46	51

COMPONENT	DISSIPATION (WATTS)
① A/C ELECTRONICS	9.4
② INTEG. GYRO ELEC. & GYRO	31.0
③ ANTENNA CONTROL ELEC.	1.5
④ SCAN PLATFORM ELEC.	2.2

4 FT² SHUTTER SIZE
 $\epsilon_{\text{EFF}} = 0.46$

TEMPS. IN () ARE FOR 30 MIL PLATE
 OTHER TEMPS. ARE FOR 60 MIL PLATE

Figure A-11. Mars Shade Bay 7 (Guidance and Control S/S) Temperature Distribution (°F)

BAY 8 (CENTRAL COMPUTER & PYRO) TEMPERATURE DISTRIBUTION (°F)

MARS SHADE										
(56)	(58)	(59)	(60)	(60)	(60)	(60)	(60)	(60)	(60)	(56)
56	58	59	59	59	59	59	59	59	59	58
(56)	(58)	(59)	(60)	(60)	(60)	(60)	(60)	(60)	(60)	(58)
56	59	59	60	60	60	60	60	60	60	59
(56)	(60)	(60)	(61)	(61)	(61)	(61)	(61)	(61)	(61)	(60)
57	61	61	61	61	61	61	61	61	61	57
(57)	(65)	(64)	(63)	(63)	(63)	(63)	(63)	(63)	(63)	(65)
57	63	62	62	61	63	63	63	63	63	56
(68)	(66)	(65)	(65)	(65)	(65)	(65)	(65)	(65)	(65)	(57)
55	54	53	54	55	57	57	56	56	56	54
(59)	(54)	(52)	(51)	(52)	(54)	(54)	(59)	(59)	(59)	(56)
56	54	50	48	48	48	48	50	50	54	56
(53)	(47)	(44)	(43)	(44)	(47)	(47)	(53)	(53)	(56)	(56)
55	53	48	46	45	46	46	48	48	53	55
(51)	(44)	(40)	(40)	(40)	(44)	(44)	(51)	(51)	(56)	(56)
56	53	51	50	49	49	49	49	49	51	53
(51)	(45)	(42)	(41)	(42)	(45)	(45)	(51)	(51)	(56)	(56)
56	56	54	52	51	50	51	51	51	52	56
(56)	(54)	(51)	(50)	(49)	(50)	(49)	(51)	(51)	(53)	(56)
56	54	52	51	50	51	50	52	52	54	56

COMPONENT
 ① CENTRAL COMPUTER & SEQUENCE
 DISSIPATION (WATTS)
 20.0

2 FT² SHUTTER SIZE
 $\epsilon_{EFF} = 0.5$
 TEMPS. IN () ARE FOR 30 MIL PLATE
 OTHER TEMPS. ARE FOR 60 MIL PLATE

Figure A-12. Mars Shade Bay 8 (Central Computer and Pyro) Temperature Distribution (°F)

BAY 9 (SCIENCE S/S) TEMPERATURE DISTRIBUTION (°F)

MARS SHADE

(54)	(34)	(23)	(17)	(15)	(17)	(22)	(32)	(50)
53	39	31	26	24	25	30	37	50
(54)	(34)	(23)	(17)	(16)	(17)	(22)	(32)	(50)
53	39	31	26	25	26	30	37	50
(54)	(34)	(23)	(18)	(17)	(18)	(23)	(33)	(50)
53	40	31	27	26	27	31	38	50
(54)	(35)	(24)	(20)	(19)	(21)	(26)	(34)	(51)
53	40	32	28	27	29	33	40	50
(54)	(36)	(26)	(23)	(23)	(26)	(31)	(38)	(51)
54	41	34	31	30	32	36	41	50
(54)	(37)	(29)	(27)	(31)	(37)	(41)	(46)	(52)
54	42	36	34	35	39	42	46	51
(55)	(40)	(34)	(32)	(37)	(43)	(47)	(50)	(52)
54	44	39	37	39	43	46	49	52
(55)	(47)	(42)	(40)	(40)	(41)	(43)	(47)	(52)
55	48	44	42	41	42	44	47	51
(55)	(46)	(41)	(39)	(38)	(38)	(40)	(44)	(51)
55	48	44	41	40	40	46	51	54
(55)	(43)	(37)	(34)	(32)	(32)	(34)	(40)	(51)
46	42	39	36	37	39	43	47	51

COMPONENT	DISSIPATION (WATTS)
① MAGNETOMETER ELEC.	5.0
② MICROMET. DET. ELEC.	1.0
③ R.F. OCCULTATION	3.0
④ PART. TELESCOPE ELEC.	3.0
⑤ ENERGETIC PARTICLES ELEC.	1.0
⑥ PLASMA PROBE ELEC.	4.0

4 FT² SHUTTER SIZE

$$\epsilon_{EFF} = 0.43$$

TEMP. IN () IS FOR 30 MIL PLATE

OTHER TEMPS. ARE FOR 60 MIL PLATE

Figure A-13. Mars Shade Bay 9 (Science S/S) Temperature Distribution (°F)

BAY 10 (SCIENCE S/S) TEMPERATURE DISTRIBUTION (°F)

MARS SHADE										
	(56)	(54)	(52)	(51)	(51)	(51)	(51)	(51)	(52)	(55)
56	54	53	52	51	51	51	51	52	53	55
(56)	(54)	(51)	(49)	(48)	(49)	(49)	(49)	(49)	(51)	(55)
56	54	52	51	50	50	50	50	50	52	55
(56)	(55)	(47)	(44)	(43)	(44)	(44)	(44)	(44)	(47)	(55)
56	55	50	48	47	47	48	48	48	50	55
(56)	(58)	(49)	(45)	(44)	(44)	(45)	(45)	(45)	(49)	(55)
56	56	51	48	47	48	48	48	49	51	55
(56)	(59)	(50)	(46)	(45)	(46)	(46)	(46)	(46)	(50)	(55)
56	57	52	49	48	49	49	49	49	51	55
(56)	(60)	(51)	(47)	(46)	(46)	(47)	(47)	(47)	(51)	(55)
56	57	53	50	49	49	50	50	50	52	55
(56)	(61)	(53)	(50)	(49)	(49)	(50)	(50)	(50)	(53)	(56)
56	58	54	52	52	52	52	52	52	54	56
(57)	(62)	(57)	(55)	(54)	(54)	(55)	(55)	(55)	(57)	(56)
60	57	55	55	55	55	56	56	56	59	57
(57)	(64)	(65)	(65)	(65)	(65)	(65)	(65)	(65)	(64)	(57)
61	61	61	61	61	61	61	61	61	61	57
(61)	(63)	(63)	(63)	(63)	(63)	(63)	(63)	(63)	(62)	(56)
59	60	60	60	60	60	60	60	60	59	56

COMPONENT | DISSIPATION (WATTS)

- ① DAS 25.0
- ② R. F. NOISE DETECTOR 3.0

2 FT² SHUTTER SIZE

$\epsilon_{EFF} = 0.51$

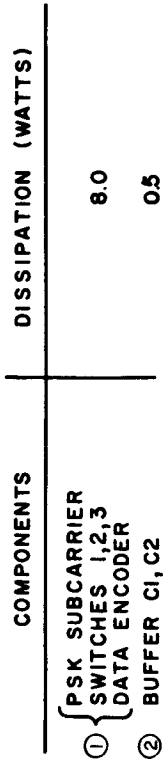
TEMPS. IN () ARE FOR 30 MIL PLATE
OTHER TEMPS. ARE FOR 60 MIL PLATE

Figure A-14. Mars Shade Bay 10 (Science S/S) Temperature Distribution (°F)

BAY 11 (DATA HANDLING & STORAGE S/S)
TEMPERATURE DISTRIBUTION (°F)

MARS SHADE

(58)	(55)	(53)	(51)	(51)	(51)	(53)	(55)	(58)
57	55	54	52	52	52	54	55	57
(58)	(55)	(51)	(49)	(49)	(49)	(51)	(55)	(58)
57	55	53	51	51	51	53	55	57
(58)	(54)	(47)	(44)	(44)	(44)	(47)	(54)	(58)
57	55	50	48	48	48	50	55	57
(58)	(54)	(47)	(43)	(42)	(43)	(46)	(54)	(57)
57	55	50	47	47	47	50	55	57
(58)	(54)	(47)	(43)	(42)	(43)	(47)	(54)	(58)
57	55	50	47	46	47	50	55	57
(58)	(55)	(47)	(43)	(42)	(43)	(47)	(55)	(58)
57	55	50	47	47	47	50	55	57
(58)	(55)	(48)	(44)	(43)	(44)	(48)	(55)	(58)
57	55	51	48	48	48	51	55	57
(58)	(56)	(50)	(47)	(46)	(47)	(50)	(56)	(58)
58	56	52	50	49	50	52	56	58
(58)	(56)	(54)	(52)	(52) ②	(53)	(55)	(57)	(58)
58	56	54	53	53	53	54	56	58
(58)	(56)	(55)	(54)	(53)	(54)	(55)	(57)	(58)
58	56	55	54	54	54	55	56	58



2 FT2 SHUTTER SIZE
ε = 0.3

TEMPS. IN () ARE FOR 30 MIL PLATE
OTHER TEMPS. ARE FOR 60 MIL PLATE

Figure A-15. Mars Shade Bay 11 (Data Handling and Storage S/S) Temperature Distribution (°F)

BAY 12 (RELAY S/S) TEMPERATURE DISTRIBUTION (°F)

MARS SHADE

(54)	(53)	(51)	(49)	(49)	(50)	(52)	(56)	(60)
55	53	51	50	50	51	53	57	60
(55)	(52)	(48)	(46)	(46)	(47)	(50)	(56)	(60)
55	53	50	48	48	50	52	56	60
(55)	(52)	(43)	(39)	(39)	(40)	(45)	(55)	(60)
55	52	47	45	44	46	49	56	60
(55)	(53)	(43)	(39)	(38)	(39)	(45)	(56)	(60)
55	53	47	44	44	45	49	57	60
(55)	(54)	(44)	(39)	(38)	(40)	(46)	(57)	(61)
55	53	48	45	44	46	50	57	60
(55)	(55)	(45)	(41)	(41)	(43)	(58)	(59)	(61)
55	54	49	47	46	48	52	58	60
(55)	(57)	(49)	(46)	(46)	(48)	(53)	(62)	(61)
55	56	52	50	50	52	55	61	61
(56)	(61)	(57)	(60)	(63)	(68)	(62)	(56)	(65)
56	59	56	56	58	60	62	65	62
(67)	(69)	(73)	(77)	(78)	(75)	(62)	(56)	(65)
56	61	62	64	65	70	71	69	62
(69)	(73)	(77)	(81)	(81)	(76)	(81)	(76)	(62)
56	61	63	65	72	73	73	69	62

COMPONENT

- ① TAPE RECORDERS NO'S. 1, 2
- ② RECEIVER (RELAY S/S)
- ③ DETECTOR
- ④ T/R RECEIVER
- ⑤ T/R DETECTOR

DISSIPATION (WATTS)

- 12.0
- 5.3
- 2.5
- 3.7
- 2.5

2 FT² SHUTTER SIZE

ε_{EFF.} = 0.51

TEMPS. IN () ARE FOR 30 MIL PLATE
OTHER TEMPS. ARE FOR 60 MIL PLATE

Figure A-16. Mars Shade Bay 12 (Relay S/S) Temperature Distribution (°F)

BAY 1 (SCIENCE BACKUP & COMMAND S/S) TEMPERATURE DISTRIBUTION (°F)

TRANSIT PHASE										
58	57	56	55	55	55	55	55	56	56	56
58	58	56	55	54	54	55	55	56	56	56
58	60	55	52	51	52	55	55	61		57
58	61	56	63	52	52	55	55	59		57
58	59	53	50	49	49	52	52	58		56
58	57	51	48	47	47	50	50	56		56
58	56	50	46	45	46	49	49	55		56
58	54	47	44	43	44	47	47	53		55
57	54	51	48	47	47	50	50	53		55
57	54	52	51	49	49	51	49	53		55

COMPONENT	DISSIPATION (WATTS)
① COMMAND DETECTOR	10.0
② COMMAND DECODER	11.0
③ COMMAND PWR SUPPLIES NO. 1, 2	15.4

2 FT² SHUTTER SIZE
 $\epsilon_{EFF} = 0.57$
 60 MIL PLATE

Figure A-17. Transit Phase Bay 1 (Science Back Up and Command S/S) Temperature Distribution (°F)

BAY 2 (RADIO S/S) TEMPERATURE DISTRIBUTION (°F)

TRANSIT PHASE

58	49	45	43	44	46	49	54	62
58	50	46	45	46	48	52	56	62
58	51	48	48	51	55	58	61	63
58	53	51	52	56	60	63	64	63
59	57	57	57	60	62	63	64	64
60	65	67	67	67	66	66	65	64
61	67	70	70	70	70	70	68	64
60	63	64	65	65	65	65	65	64
60	60	61	61	62	62	62	63	63
59	58	58	59	59	59	58	60	63

COMPONENT	DISSIPATION (WATTS)
① RCVR & EXC. SEL. LOGIC	0.01
② EXCITER # 1	5.7
③ RCVR # 2	5.3
④ T/R # 1	6.2
⑤ RCVR # 1	5.3
⑥ T/R # 3	6.2
⑦ RCVR # 3	5.3
⑧ T/R # 2	6.2

4 FT² SHUTTER SIZE
 $\epsilon_{EFF} = 0.5$
 60 MIL PLATE

Figure A-18. Transit Phase Bay 2 (Radio S/S) Temperature Distribution (°F)

BAY 3 (RADIO S/S) TEMPERATURE DISTRIBUTION (°F)

TRANSIT PHASE

50	37	28	24	21	22	26	35	52
51	39	32	27	24	24	27	36	52
52	45	39	35	30	27	29	37	52
53	50	47	43	38	32	32	38	52
53	51	49	48	45	38	35	40	53
54	53	54	55	62	45	39	41	53
56	64	70	69	62	50	42	43	53
61	92	106	103	102	59	47	45	54
69	156	183	177	123	70	51	47	54
64	110	133	139	84	64	50	47	54

COMPONENT	DISSIPATION (WATTS)
① EXCITER NO. 3	5.7
② EXCITER NO. 2	5.7
③ PA/PS NO. 1	75 ← ON
④ PA SELECT LOGIC	0.01
⑤ PA/PS NO. 2	33.3 ← OFF
⑥ PA/PS NO. 3	75 ← OFF
⑦ ANTENNA SELECT LOGIC	0.01

4 FT² SHUTTER SIZE
 $\epsilon_{EFF} = 0.65$
 60 MIL PLATE

Figure A-19. Transit Phase Bay 3 (Radio S/S) Temperature Distribution (°F)

BAY 4 (POWER S/S) TEMPERATURE DISTRIBUTION (°F)

TRANSIT PHASE

59	44	36	31	29	30	34	41	54
59	44	36	34	30	34	36	41	54
58	48	41	37	35	36	35	40	54
58	51	41	40	39	38	39	40	54
58	54	49	47	46	46	46	47	54
57	54	49	50	54	54	52	54	56
63	63	62	61	61	60	60	60	57
63	65	65	65	64	64	63	61	58
63	65	65	65	64	64	63	61	58
63	62	62	62	61	61	60	59	57

COMPONENT	DISSIPATION (WATTS)
① BATTERY	3.7
② MAIN BUCK REG.	36.8
③	

4 FT² SHUTTER SIZE
 $\epsilon_{EFF} = 0.39$
 60 MIL PLATE

Figure A-20. Transit Phase Bay 4 (Power S/S) Temperature Distribution (°F)

BAY 5 (POWER S/S) TEMPERATURE DISTRIBUTION (°F)

TRANSIT PHASE									
58	56	54	53	52	53	55	57	60	
	56	54	53	53	53	55	57	60	
57	① 55	49	44	42	44	44	45	59	
58	56	48	44	40	40	44	45	60	
58	55	45	45	45	45	45	48	60	
58	55	49	48	48	48	49	55	60	
58	② 55	55	54	53	54	55	58	60	
59	58	55	54	53	54	55	58	60	
58	60	60	60	60	61	61	62	61	
58	③ 61	61	61	62	62	62	62	61	

COMPONENTS	DISSIPATION (WATTS)
① BATTERY	3.7
② DISCHARGE REG.	3.0
③ SINGLE PHASE INVERT.	1.4

2 FT2 SHUTTER SIZE
 $\epsilon_{EFF} = 0.32$
 60 MIL PLATE

Figure A-21. Transit Phase Bay 5 (Power S/S) Temperature Distribution (°F)

BAY 6 (POWER S/S) TEMPERATURE DISTRIBUTION (°F)

TRANSIT PHASE									
54	38	30	26	24	26	30	37	51	
54	40	32	28	27	38	31	39	51	
54	42	36	32	30	32	36	42	52	
	①								
55	44	38	39	36	36	38	39	52	
55	48	40	40	38	38	40	46	52	
56	50	48	49	53	56	57	56	54	
56	54	55	57	66	73	74	69	56	
				③					
58	60	64	70	70	72	67	64	56	
				④					
60	80	90	90	74	67	61	57	54	
				⑤					
62	70	80	95	72	61	55	52	54	

COMPONENT	DISSIPATION (WATTS)
① BATTERY	3.7
② 2.4 KC INVERTER	24.2
③ PWR. SWITCHING & LOGIC	20.0
④ SYNCHRONIZER	3.0
⑤ 3 PHASE INVERTER	1.4

4 FT² SHUTTER SIZE
 $\epsilon_{\text{EFF.}} = 0.51$
 60 MIL PLATE

Figure A-22. Transit Phase Bay 6 (Power S/S) Temperature Distribution (°F)

BAY 7 (GUIDANCE & CONTROL S/S) TEMPERATURE DISTRIBUTION (°F)

TRANSIT PHASE									
56	44	37	33	32	32	35	40	50	
57	46	39	37	35	34	34	41	50	
57	49	44	41	39	39	41	45	51	
58	51	46	43	41	40	41	45	51	
58	51	46	43	41	41	41	45	51	
58	50	44	40	39	39	41	45	51	
58	50	42	40	37	37	40	46	51	
58	50	40	36	32	36	40	50	51	
58	50	40	35	31	35	40	45	51	
58	50	37	34	31	31	35	40	50	

COMPONENT	DISSIPATION (WATTS)
① A/C ELECTRONICS	9.4
② ANTENNA CONT. ELEC.	1.5

4 FT² SHUTTER SIZE
 $\epsilon_{EFF} = 0.28$
 60 MIL PLATE

Figure A-23. Transit Phase Bay 7 (Guidance and Control S/S) Temperature Distribution (°F)

BAY 8 (CENTRAL COMPUTER & PYRO)
TEMPERATURE DISTRIBUTION (°F)

TRANSIT PHASE

56	58	59	59	59	59	59	59	59	58	56
56	59	59	60	60	60	60	60	60	59	58
57	61	61	61	61	61	61	61	61	60	57
57	63	62	62	61	63	57	56	56	56	57
55	54	53	54	55	57	56	56	56	56	54
56	54	50	48	48	48	50	50	56	56	56
55	53	48	46	45	46	48	48	53	53	55
56	53	51	50	49	49	49	49	51	51	53
56	56	54	52	51	50	51	51	52	52	56
56	54	52	51	50	51	51	52	54	54	56

COMPONENT | DISSIPATION (WATTS)

① CENTRAL COMPUTER & SEQUENCER | 20.0

2 FT² SHUTTER SIZE

$\epsilon_{EFF} = 0.5$

60 MIL PLATE

Figure A-24. Transit Phase Bay 8 (Central Computer and Pyro) Temperature Distribution (°F)

BAY 9 (SCIENCE S/S) TEMPERATURE DISTRIBUTION (°F)

TRANSIT PHASE									
53	39	31	26	24	25	30	37	50	
53	39	31	26	25	26	30	37	50	
53	40	31	27	26	27	31	38	50	
53	40	32	28	27	29	33	40	50	
54	41	34	31	30	32	36	41	50	
54	42	36	34	35	39	42	46	51	
54	44	39	37	39	43	46	49	52	
55	48	44	42	41	42	47	47	51	
55	48	44	41	40	40	46	51	54	
46	42	39	36	37	39	43	47	50	

COMPONENT	DISSIPATION (WATTS)
① MAGNETOMETER ELEC.	5.0
② MICROMET. DET. ELEC.	1.0
③ RF OCCULTATION	3.0
④ PART. TELESCOPE ELEC.	3.0
⑤ ENERGETIC PARTICLES	1.0
⑥ PLASMA PROBE ELEC.	4.0

4 FT² SHUTTER SIZE
 $\epsilon_{\text{EFF.}} = 0.21$
 60 MIL PLATE

Figure A-25. Transit Phase Bay 9 (Science S/S) Temperature Distribution (°F)

BAY 10 (SCIENCE S/S) TEMPERATURE DISTRIBUTION (°F)

		TRANSIT PHASE							
56	55	54	53	52	51	52	53	54	55
56	55	55	52	51	50	50	50	52	55
56	55	55	50	48	47	48	50	54	55
56	56	56	51	48	47	48	51	56	55
56	57	57	52	49	48	49	51	56	55
56	57	57	53	50	49	50	52	57	55
57	59	59	55	51	51	51	55	60	56
55	55	55	54	49	47	50	52	57	55
56	55	55	54	50	50	52	53	56	58
58	57	57	54	50	50	49	57	58	58

COMPONENT	DISSIPATION (WATTS)
① DAS	25.0

2 FT² SHUTTER SIZE
 $\epsilon_{EFF} = 0.39$
 60 MIL PLATE

Figure A-26. Transit Phase Bay 10 (Science S/S) Temperature Distribution (°F)

BAY 11 (DATA HANDLING & STORAGE S/S) TEMPERATURE DISTRIBUTION (°F)

TRANSIT PHASE									
58	54	52	51	52	55	55	55	55	57
57	55	53	51	51	51	51	53	53	57
57	55	50	48	48	48	50	55	55	57
57	55	50	47	47	47	50	55	55	57
57	55	50	47	46	47	50	55	55	57
57	55	50	47	47	47	50	55	55	57
57	55	51	48	48	48	51	55	55	57
58	56	52	50	49	50	52	56	56	58
58	56	54	53	53	53	54	56	56	58
58	56	55	54	54	54	55	56	56	58

COMPONENTS	DISSIPATION (WATTS)
① PSK SUBCARRIER SWITCHES 1, 2, 3 DATA ENCODER	8.0
② BUFFER C1, C2	0.5

2 FT² SHUTTER SIZE
 $\epsilon_{EFF} = .3$
 60 MIL PLATE

Figure A-27. Transit Phase Bay 11 (Data Handling and Storage S/S) Temperature Distribution (°F)

BAY 12 (RELAY S/S) TEMPERATURE DISTRIBUTION (°F)

TRANSIT PHASE									
55	54	53	52	52	53	55	57	60	
54	53	52	51	51	52	54	57	60	
55	52	50	48	48	49	51	56	60	
54	52	48	47	47	48	51	56	60	
54	52	48	48	46	47	50	55	60	
54	52	48	46	46	47	50	55	60	
54	52	48	47	48	51	55	55	60	
54	52	50	48	48	49	52	56	60	
54	53	52	51	51	51	53	57	60	
55	54	53	53	54	54	55	57	60	

COMPONENT

① TAPE RECORDERS 1,2

DISSIPATION (WATTS)

1.0

2 FT² SHUTTER SIZE
 $\epsilon_{\text{EFF}} = 0.19$
 60 MIL PLATE

Figure A-28. Transit Phase Bay 12 (Relay S/S) Temperature Distribution (°F)

3.2 NOMENCLATURE

- G - Total energy incident on a surface (Btu/Hr ft²)
- J - Total energy leaving a surface (radiosity) (Btu/Hr ft²)
- Q Internal - Internally generated heat (Btu/hr ft²)
- T - Surface temperature (°R)
- ε- Surface hemispherical emissivity
- α- Surface solar absorptivity
- ψ- Angle between the normal to the base (assembly mounting panel) and the sun's rays
- F_{ij} - Configuration factor from surface i to surface j
- σ^{ij} Stefan - Boltzmann constant (0.1713 x 10⁻⁸ Btu/hr ft² °R⁴)
- S - Solar constant (Btu / hr ft²)
- S_i - Incident solar energy on surface i (S_i = cos γ; where γ is the angle between the normal to surface i and sun's rays)

Subscripts on symbols

- S - in the solar regime
- 1, 2, etc. - pertaining to surface number 1, 2, etc.

Subscripts on surface numbers (images) (see figure A-29)

- 3 - image of the surface in specular surface 3
- 2 - image of the surface in specular surface 2
- Example 1: 1₃ - The image of surface 1 in surface 3
- Example 2: 1_{3,2} - The image of 1₃ in surface 2

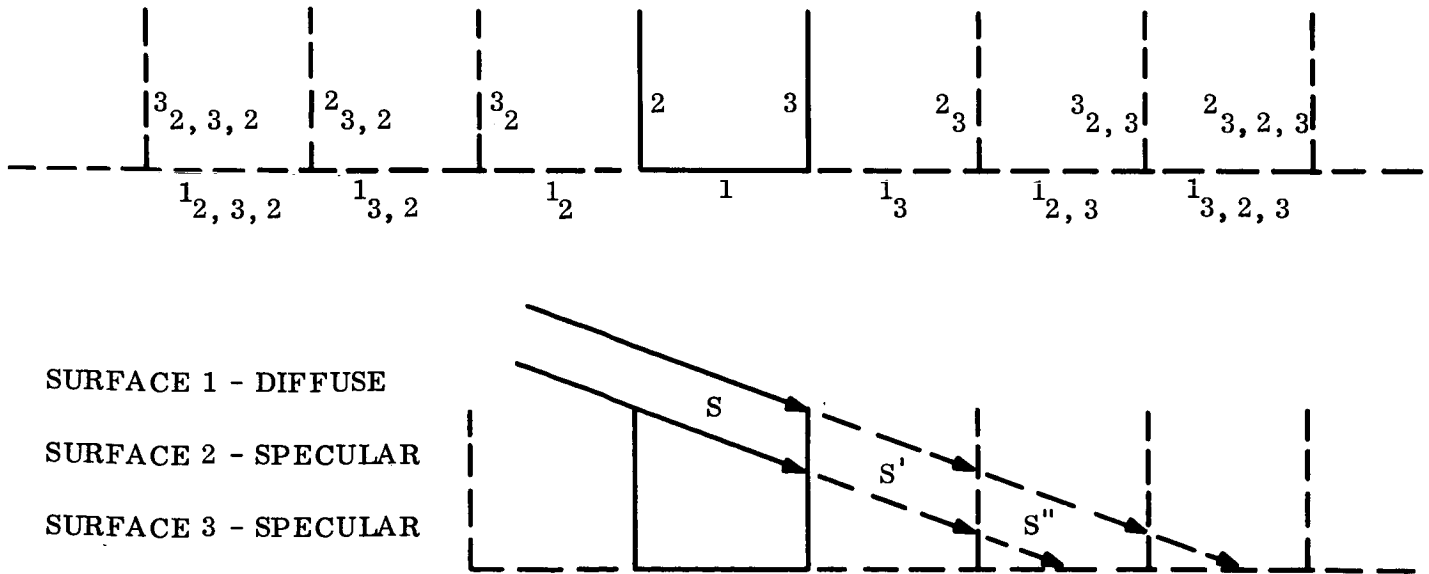


Figure A-29. Specular System in Full Open Position

3.3 ANALYSIS

3.3.1 INTRODUCTION

The following analysis was performed to determine the effective thermal radiative surface properties of three basic types of shutter systems under the influence of incident solar energy so that a choice of one system could be made based on the relative properties of each.

3.3.2 DIFFUSE SYSTEM

In this system, both shutter blades and the base surface are diffuse.

3.3.2.1 SOLAR BALANCE

For each surface:

$$J_{S_i} = (1-\alpha_{S_i}) \left[S_i + \sum_{j=1}^N F_{ij} J_{S_j} \right] \quad (1)$$

The solar radiosity is calculated from the above simultaneous equations. From this, the total incident solar energy on each body is found.

$$G_{S_i} = \frac{J_{S_i}}{(1-\alpha_{S_i})} \quad (2)$$

3.3.2.2 I R BALANCE

Again, for each surface:

$$J_i = Q_i + \sum_{j=1}^N F_{ij} J_j \quad (3)$$

Where:

$$Q_i = G_{S_i} \alpha_{S_i} + Q_{\text{internal}} \quad (3a)$$

(Q Internal = 0 for all surfaces on the shutter blades)

Again, solving the above simultaneous equations, the IR radiosity of each surface is found. Equation (3) is then rewritten as:

$$J_i = \epsilon_i \sigma T_i^4 + (1-\epsilon_i) \sum_{j=1}^N F_{ij} J_j \tag{4}$$

$G_{s_i} A_{s_i}$ in equation (3a) represents the total absorbed solar energy. Since this energy is reradiated in the IR regime, equation (3a) provides a link between the solar and infrared regimes.

Equation (4) is solved for surface temperatures. The temperatures across the base are used in Equation (29) to determine the effective radiative properties of the surfaces. The blade temperatures provide a criterion for the choice of a bonding material used in the shutter blades.

3.3.3 SPECULAR SYSTEM (FIGURE A-29)

3.3.3.1 SOLAR BALANCE

The incident solar energy on each body in the case where both blade surfaces (2 and 3) are specular and the base surface (1) is diffuse, can be determined by a combination of geometric and radiosity calculations. With the shutters in the full open position, where the sun impinges on a specular surface, an equivalent geometric arrangement can be made up of images to trace the solar reflections. Each time the sun is reflected from a surface, it is diminished by the solar absorptivity of that surface. Thus, in Figure A-29

$$S = \text{SOLAR CONSTANT} \tag{5}$$

$$S' = S (1-\alpha_{S_3}) \tag{6}$$

$$S'' = S(1-\alpha_{S_3})(1-\alpha_{S_2}) \tag{7}$$

The incident solar energy is determined by using the appropriate values of S, S' and S'' (the progression continues for successive reflections where the sun angle is greater than that shown in Figure A-29). Since all solar energy reflected from the base will leave the system without being re-reflected to the base,

$$G_{S_1} = S_1 + S'_1 + S''_1 + \dots \tag{8}$$

$$J_{S_1} = (1-\alpha_{S_1})G_{S_1} \tag{9}$$

for all nodes across the base.

The incident solar energy on the blades, however, consists of direct energy and energy reflected from the base. Again using the images to represent successive reflections

$$G_{S_2} = S_2 + S'_2 + S''_2 + \dots + \left[F_{21} + (1-\alpha_{S_3})F_{2(1_3)} + (1-\alpha_{S_2})(1-\alpha_{S_3})F_{2(1_2,3)} + \dots \right] J_{S_1} \tag{10a}$$

G_{S_3} is similarly determined to be:

$$G_{S_3} = S_3 + S'_3 + S''_3 + \dots + \left[F_{31} + (1-\alpha_{S_2})F_{3(1_2)} + (1-\alpha_{S_3})(1-\alpha_{S_2})F_{3(1_3,2)} + \dots \right] J_{S_1} \tag{10b}$$

3.3.3.2 IR BALANCE

The IR radiosity is obtained in a manner similar to that used for the solar energy, except that the blades now contribute to the radiosity of the base by their own radiation ($\epsilon\sigma T^4$)

$$J_1 = Q_1 + \left[F_{13} + (1-\epsilon_2)F_{1(3_2)} + (1-\epsilon_2)(1-\epsilon_3)F_{1(3_2,3)} + \dots \right] J_3 + \left[F_{12} + (1-\epsilon_3)F_{1(2_3)} + (1-\epsilon_2)(1-\epsilon_3)F_{1(2_3,2)} + \dots \right] J_2 \tag{11}$$

$$\text{Where } Q_1 = G_{S_1} \alpha_{S_1} + Q_{\text{internal}} \tag{12}$$

$$J_2 = \epsilon_2 \sigma T_2^4 \tag{13a}$$

$$J_3 = \epsilon_3 \sigma T_3^4 \tag{13b}$$

Since it was assumed that the blades have adiabatic back surfaces, the blade temperatures are solely dependent upon the energy absorbed through their front surfaces. Again, using the images to account for specularly reflected energy:

$$J_2 = \epsilon_2 \sigma T_2^4 = Q_2 + \epsilon_2 \left\{ \begin{aligned} & \left[F_{21} + (1-\epsilon_3)F_{2(1,3)} + (1-\epsilon_2)(1-\epsilon_3)F_{2(1,2,3)} \right. \\ & \left. + \dots \right] J_1 + \left[F_{23} + (1-\epsilon_2)(1-\epsilon_3)F_{2(3,2,3)} + \dots \right] J_3 \\ & \left. + \left[(1-\epsilon_3)F_{2(2,3)} + (1-\epsilon_3)^2(1-\epsilon_2)F_{2(2,3,2,3)} + \dots \right] J_2 \right\} \quad (14)$$

Where: $Q_2 = G S_2 \alpha_{S_2}$ (15)

An equation for J_3 can be set up in the same manner. The radiosities (J) of each body can be determined by solving equations (11), (12) and (14) simultaneously. Knowing the radiosities, the base temperatures can be found by:

$$J_1 = \epsilon_1 \sigma T_1^4 + (1-\epsilon_1) \left\{ \begin{aligned} & \left[F_{13} + (1-\epsilon_2)F_{1(3,2)} + (1-\epsilon_2)(1-\epsilon_3)F_{1(3,2,3)} \right. \\ & \left. + \dots \right] J_3 + \left[F_{12} + (1-\epsilon_3)F_{1(2,3)} + (1-\epsilon_2)(1-\epsilon_3)F_{1(2,3,2)} + \dots \right] J_2 \end{aligned} \right\} \quad (16)$$

These temperatures are used in equation (29) to determine the effective thermal radiative surface properties of the system. The blade temperatures are found using equation (13).

3.3.4 SPECULAR - DIFFUSE SYSTEM (FIGURE A-30)

3.3.4.1 SOLAR BALANCE

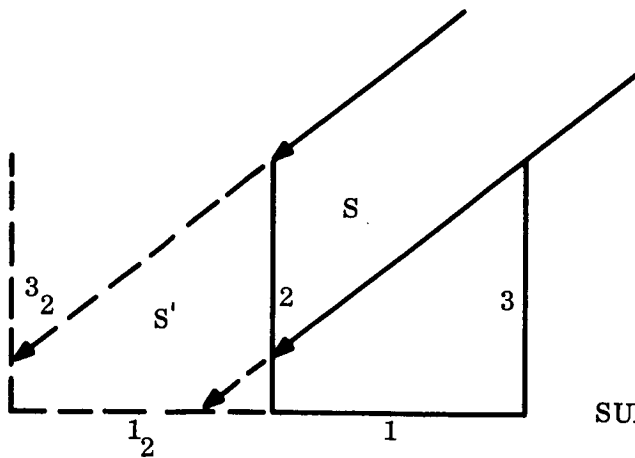
In this system, only one blade surface (2) is specular. All other surfaces (1 and 3) are diffuse. With the shutters in the full open position and the sun incident upon the specular surface:

$$S = \text{Solar Constant} \quad (17)$$

$$S' = S (1 - \alpha_{S_2}) \quad (18)$$

(Equations (19), (20) and (21) are also valid for cases where the sun strikes only the diffuse surface since $S = 0$ in this case).

The Total solar energy leaving each surface is:



SURFACE 1 - DIFFUSE

SURFACE 2 - SPECULAR

SURFACE 3 - DIFFUSE

Figure A-30. Specular-Diffuse System in Full Open Position

$$J_{S_1} = (1-\alpha_{S_1}) \left\{ S_1 + S'_1 + \left[F_{13} + F_{1(3_2)}(1-\alpha_{S_2}) \right] J_{S_3} \right\} \quad (19)$$

$$J_{S_2} = (1-\alpha_{S_2}) \left[S_2 + F_{21} J_{S_1} + F_{23} J_{S_3} \right] \quad (20)$$

$$J_{S_3} = (1-\alpha_{S_3}) \left\{ S_3 + S'_3 + \left[F_{31} + F_{3(1_2)}(1-\alpha_{S_2}) \right] J_{S_1} + (1-\alpha_{S_2}) F_{3(3_2)} J_{S_3} \right\} \quad (21)$$

Equations (19), (20) and (21) are solved simultaneously and the resultant J's are applied to equation (2) to determine the total incident energy.

3.3.4.2 IR BALANCE

The IR radiosity is obtained by using a combination of the methods used to obtain the equations in the diffuse and specular systems

$$J_1 = Q_1 + F_{12} J_2 + \left[F_{13} + (1-\epsilon_2) F_{1(3_2)} \right] J_3 \quad (22)$$

$$J_2 = Q_2 + \epsilon_2 \left[F_{21} J_1 + F_{23} J_3 \right] \quad (23)$$

$$J_3 = Q_3 + \left[F_{31} + F_{3(1_2)}(1-\epsilon_2) \right] J_1 + F_{32} J_2 + (1-\epsilon_2) F_{3(3_2)} J_3 \quad (24)$$

Where: $Q_1 = \alpha_1 G_{S_1} + Q_{\text{internal}}$ (25)

($Q_{\text{internal}} = 0$ for all blade surfaces)

Solving (22), (23) and (24) simultaneously yields the values of J to be used in the following equations to yield the temperature of each body

$$J_1 = \epsilon_1 \sigma T_1^4 + (1-\epsilon_1) \left[F_{12} J_2 + \left[F_{13} + F_{1(3_2)}(1-\epsilon_2) \right] J_3 \right] \quad (26)$$

$$J_2 = \epsilon_2 \sigma T_2^4 \quad (27)$$

$$J_3 = \epsilon_3 \sigma T_3^4 + (1-\epsilon_3) \left\{ \left[F_{31} + F_{3(1_2)}(1-\epsilon_2) \right] J_1 + F_{32} J_2 + (1-\epsilon_2) F_{3(3_2)} J_3 \right\} \quad (28)$$

The temperature of surface 1 is used in equation (29) to determine the effective thermal radiative surface properties. The temperatures of surfaces 2 and 3 are considered in the choice of a bonding material used in the shutter blades.

3.3.5 EFFECTIVE RADIATION SURFACE PROPERTIES

The effective radiation surface properties are defined herein as: The properties which a flat plate would have to possess in order to exhibit the same temperature characteristics as the shutter system under the same conditions of solar energy and internal dissipation. Thus for two levels of internal heat generation:

$$Q_{\text{internal}_1} = \epsilon_{\text{eff}} \sigma T_1^4 - \alpha_{\text{eff}} S \cos \Psi \quad (29a)$$

$$Q_{\text{internal}_2} = \epsilon_{\text{eff}} \sigma T_2^4 - \alpha_{\text{eff}} S \cos \Psi \quad (29b)$$

Having found the temperature distributions at two different values of Q_{internal} , Equations (29a) and (29b) are solved simultaneously for α_{eff} and ϵ_{eff} .

Equations (1) through (29) were programmed for an IBM 7094 computer. Allowance was made to divide the three-surface system into as many as 45 nodes. The configuration factors were calculated by the program using the Hottel method. The results are presented in both the Volume A (VB235FD101) and Volume B (VB235AA101) temperature control subsystem sections.

4.0 MID-COURSE ENGINE ANALYSIS

The effects of four different superinsulation configurations on the steady state and transient cooling temperatures of the midcourse engines are presented in Volume B. The analysis of the preferred superinsulation configuration is shown below.

4.1 STEADY STATE HEAT BALANCE

$$(\epsilon_t A_t + \epsilon_c A_c F_{a \text{ to space}}) \sigma T^4 = \alpha_t A_t S + \alpha_c A_c F_{a \text{ to insulation}} S$$

Where:

ϵ = Surface hemispherical emissivity

α = Surface solar absorptivity

A = Surface area

F = Geometric View Factor

S^a = Solar flux constant

t, c subscripts refer to inside of nozzle, and outside of case, respectively

Assumptions:

- a. α/ϵ of both surfaces is 1.0
- b. $\epsilon_c = 0.8$, $\epsilon_t = 0.85$
- c. Insulation is adiabatic
- d. $S = 228 \text{ Btu/hr} - \text{ft}^2$
- e. Approximate engine geometry by a 3-inch diameter by 9 1/2-inch long cylinder
 $F_{a \text{ from the surface of the cylinder to space}}$ is estimated to be 0.38
 $F_{a \text{ from the surface of the cylinder to the insulation}}$ is estimated to be 0.56. This factor accounts for the angle between the sun's rays and the insulation blanket, and for the portion of the engine which hangs below the blanket. Substitution of the above into the heat balance yields:

$$\sigma T^4 = 320 \text{ Btu/hr-ft}^2 \quad T = 197^\circ \text{F}$$

4.2 TRANSIENT HEAT BALANCE

$$-Wc_p \frac{\Delta T}{\Delta \tau} = (\mathcal{F}_c A_c + \epsilon_t A_t) \sigma T^4$$

Where:

W = weight

c = specific heat

$\Delta \tau$ = time increment

\mathcal{F}_c = total radiant interchange factor between surface of engine and space

Assumptions

a. insulation is very cold ($T \approx 0^\circ \text{R}$)

b. W = 9 pounds

c. c = 0.2 Btu/lb- $^\circ \text{F}$

d. $\epsilon^D = 0.4$ on insulation

The factor \mathcal{F}_c is estimated to be 0.83

Substitution into the heat balance for a two hour time increment yields

After several iterations

$$\Delta T = -137^\circ \text{F}$$

$$T = 60^\circ \text{F after 2 hours}$$

5.0 SOLAR ARRAY ANALYSIS

5.1 RADIAL TEMPERATURE DISTRIBUTION

Steady State Heat Balance

$$(\mathcal{F}_f + \mathcal{F}_b) \sigma T^4 = 0.94 \alpha S \cos \theta$$

Where:

$\mathcal{F}_f, \mathcal{F}_b$ = Net radiant interchange factor to space for front and back faces respectively.

σ = Stefan - Boltzmann Constant (0.1713×10^{-8} Btu/hr-ft 2 - $^\circ \text{R}^4$)

T = Temperature ($^\circ \text{R}$)

- α = front face solar absorptivity
- S = solar constant (BTU/HR FT²)
- θ = angle between surface normal and sun's rays

Assumptions:

- a. Six percent of solar energy is converted to electrical energy, hence 0.94 factor in heat balance
- b. Conduction is negligible in radial direction
- c. Heat interchange between the array and the Bus and between the array and Flight Capsule does not occur. However, these items are considered in calculating geometric view factors to space.
- d. Radiant interchange with the solar array support frame is negligible. The radiant interchange factors were calculated from the following relations:

$$q_f = (F_a)_f \epsilon_f$$

$$q_b = (F_a)_b \epsilon_b$$

Where:

$(F_a)_f$, $(F_b)_b$ are the geometric view factors to space of the front and back faces respectively.

ϵ_f , ϵ_b are the surface emissivities of the front and back faces respectively.

View factors for the back face were calculated using Hamilton and Morgan, "Radiant Interchange Configuration Factors," NACA TN 2836 as follows:

WITH BIO-BARRIER

NODE		$(F_a)_b$
1	(closest to Bus)	0.083
2		0.111
3		0.145
4		0.20
5		0.56
6		0.82
7		0.86
8	(furthest from Bus)	0.88

<u>NODE</u>		<u>(F_a)_b</u>
1	(closest to Bus)	0.60
2		0.74
3		0.80
4		0.83
5		0.87
6		0.90
7		0.93
8	(furthest from Bus)	0.94

Front face surface properties are

$$\epsilon_f = 0.83$$

$$\alpha = 0.66$$

Back face emissivity

$$\epsilon_b = 0.90$$

Temperature curves are shown in Volume A VB235FD101 (Temperature Control Section) for values of the solar constant from 434 Btu/hr-ft² (1.0 AU) to 159 Btu/hr-ft² (1.65 AU) with separation of the bio-barrier occurring at S = 228 Btu/hr-ft² (1.38 AU)

5.2 MARS SHADE COOLING

Transient Heat Balance

$$-\frac{W}{A} c_p \frac{\Delta T}{\Delta \tau} = (\epsilon_f + \epsilon_b) \sigma T^4$$

Where:

$\frac{W}{A}$ = weight per square foot of frontal surface

c_p = specific heat (Btu/lb-°F)

ΔT = temperature increment (°F)

$\Delta \tau$ = time increment (hours)

ϵ_f, ϵ_b = radiant interchange factors to space from front and back faces respectively

σ = Stefan-Boltzmann constant

T = Temperature (°R)

Assumptions:

The same assumptions apply as for the steady state radial distribution analysis

W/A was assumed to be 0.5 lb/ft^2 with a $C_p = 0.2$. Initial temperature was taken as -8°F for the coldest node (node 8) at 1.5 AU

\mathcal{F}_f and \mathcal{F}_b factors were the same as in the steady state analysis

Method:

A finite difference technique was used.

An initial time step of one minute was calculated, until the temperature increment became sufficiently small (after 10 min.)

Then a 5 minute time step was used, again, until a small temperature change was calculated (50 minutes)

Finally, a ten minute time step was used to complete the 180 minutes maximum shade time.

The resulting curve (Volume A, Temperature Control Section VB235FD101) shows a temperature of -308F after three hours in the Mars shade.

6.0 SIZING OF GYRO HEATERS

The gyro/accelerometer assembly dissipates 9 watts at 100°F . Assuming the surroundings to be at 80°F , the thermal resistance between the assembly and its surroundings must be no greater than 2.22°F/Watt .

The thermal capacitance of the gyro/accelerometer assembly is $1.2 \text{ Btu}/^\circ\text{F}$. Any one of the three gyro heaters must have the capacity to raise the temperature of this assembly from 40°F to 100°F in 0.5 hours. Thus, 21 watts are required to take care of increasing the temperature of the thermal mass. To this amount must be added an amount of heat equal to that leaking from the assembly to its surroundings. Based on an average assembly temperature of 70°F during this warm-up period, a surrounding temperature of 40°F and a thermal resistance of 2.22°F/Watt , the leakage heat is 13.5 Watts. Thus, each heater should be capable of producing at least 34.5 Watts.

7.0 TEMPERATURE PREDICTIONS FOR HIGH GAIN ANTENNA

High gain antenna steady state temperatures were predicted with the following:

$$\frac{\alpha}{s} S A_{fp} \cos \phi = \epsilon_f A_{fp} \sigma T^4 + \mathcal{F}_b A_b \sigma T^4$$

The transient temperature drop during Mars shade time was predicted by integrating the following relation:

$$W c_p \frac{dT}{dt} = - (\epsilon_f A_{fp} \sigma T^4 + \alpha_b A_b \sigma T^4)$$

Where:

- S = Solar constant-varying with distance from the sun (Btu/hr-ft²)
- φ = Angle between the sun's rays and the normal to front of the antenna. This angle varies with time in the mission as the antenna turns to face earth.
- α = Solar absorptivity
- ε_f^s = Emissivity of front surface of the antenna
- A_{fp} = Projected area of front of antenna (Ft²)
- A_b = Surface area of back of antenna (Ft²)
- α_b = Radiant interchange factor from back surface to space = product of geometric view factor to space and back surface emissivity
- W = Weight of Antenna (lbs)
- c = Specific heat (Btu/lb-°F)
- t = Time (hours)
- T = Average antenna temperature (°R)
- σ = Stefan - Boltzmann constant (0.1713 x 10⁻⁸ $\frac{\text{Btu}}{\text{Hr} - \text{Ft}^2 - \text{°R}^4}$)

Assumptions:

- a. The effective radiating area of the front of the antenna is equivalent to its projected area.
- b. α_s = 0.25 ε_f = 0.85

Results:

The steady state temperatures are presented in Figure A-31. The Mars shade cooling transients are shown in Figure A-32.

8.0 RELIABILITY ANALYSIS

The reliability analysis of the temperature control subsystem is based on the block diagram shown in Figure A-33. The mathematical reliability model for this subsystem is:

$$R = \left[(1 - [R-R_{1\&2}]^2) \cdot R_3^6 \cdot R_4^6 \cdot R_5^6 \cdot R_6^6 \right]^{11} \cdot [R_7 \cdot R_8]^9 \cdot [R_{7a} \cdot R_{8a}]^4$$

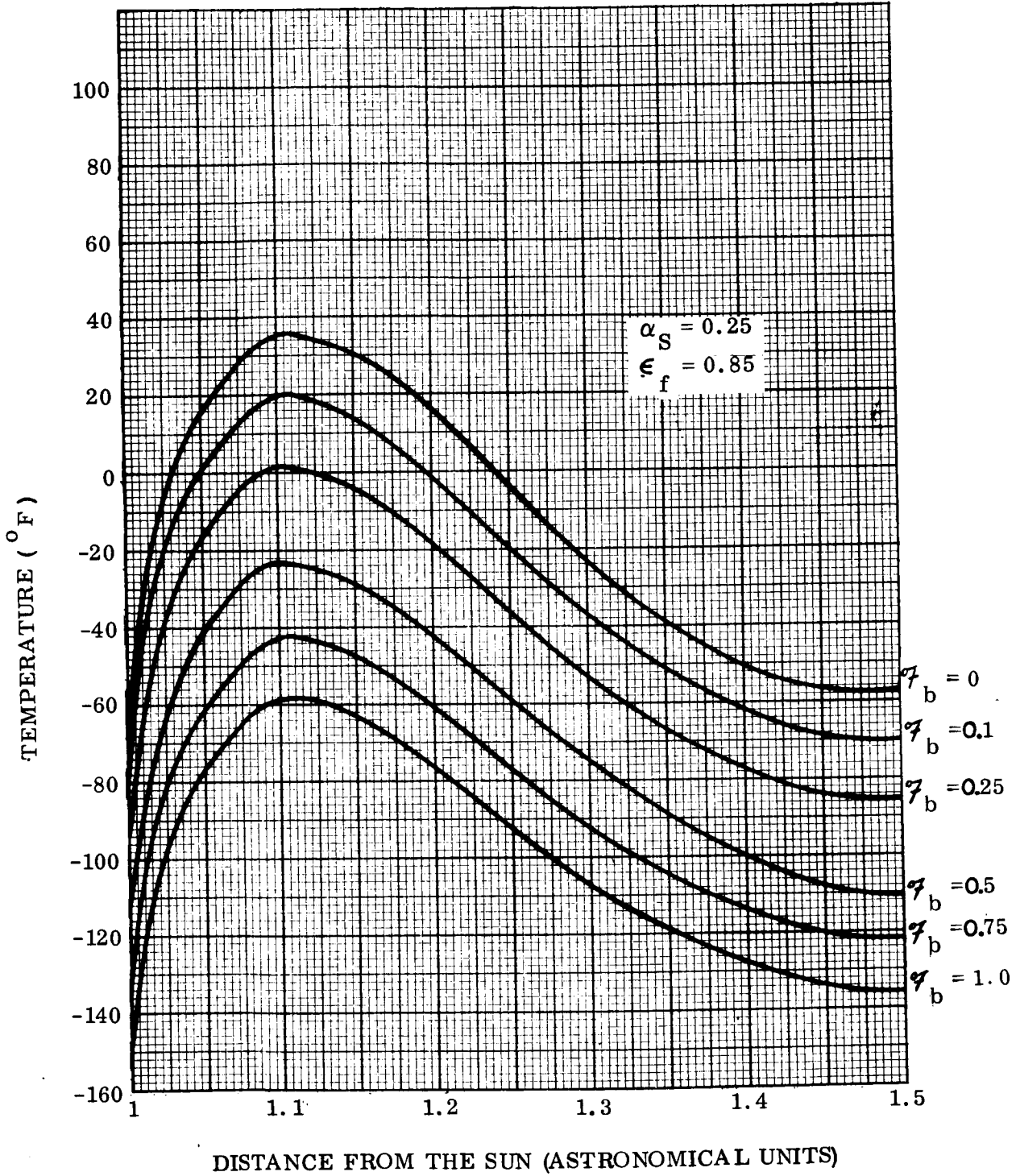


Figure A-31. High Gain Antenna Temperature as a Function of γ_b

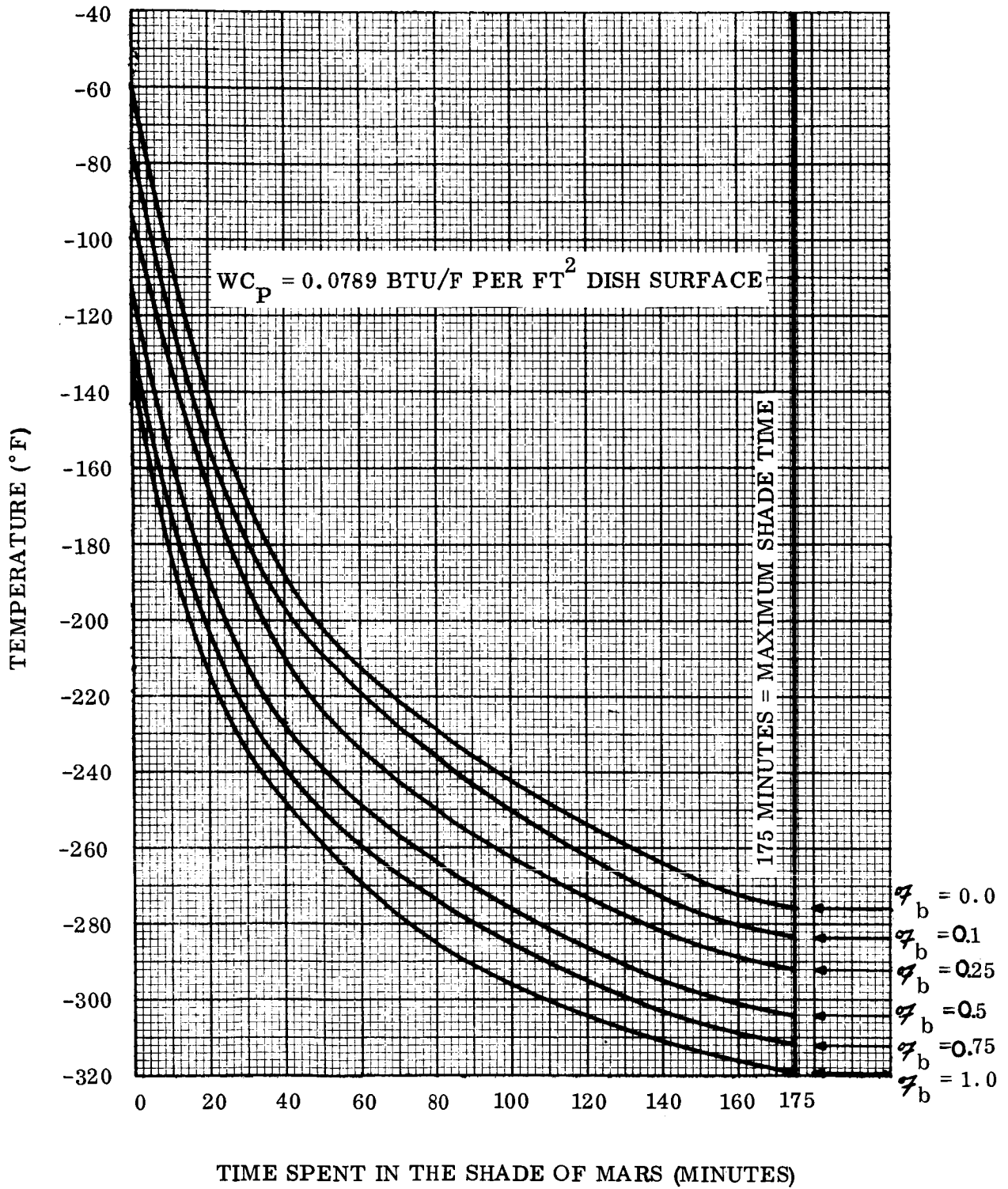


Figure A-32. High Gain Antenna Transient Temperature in the Shade of Mars

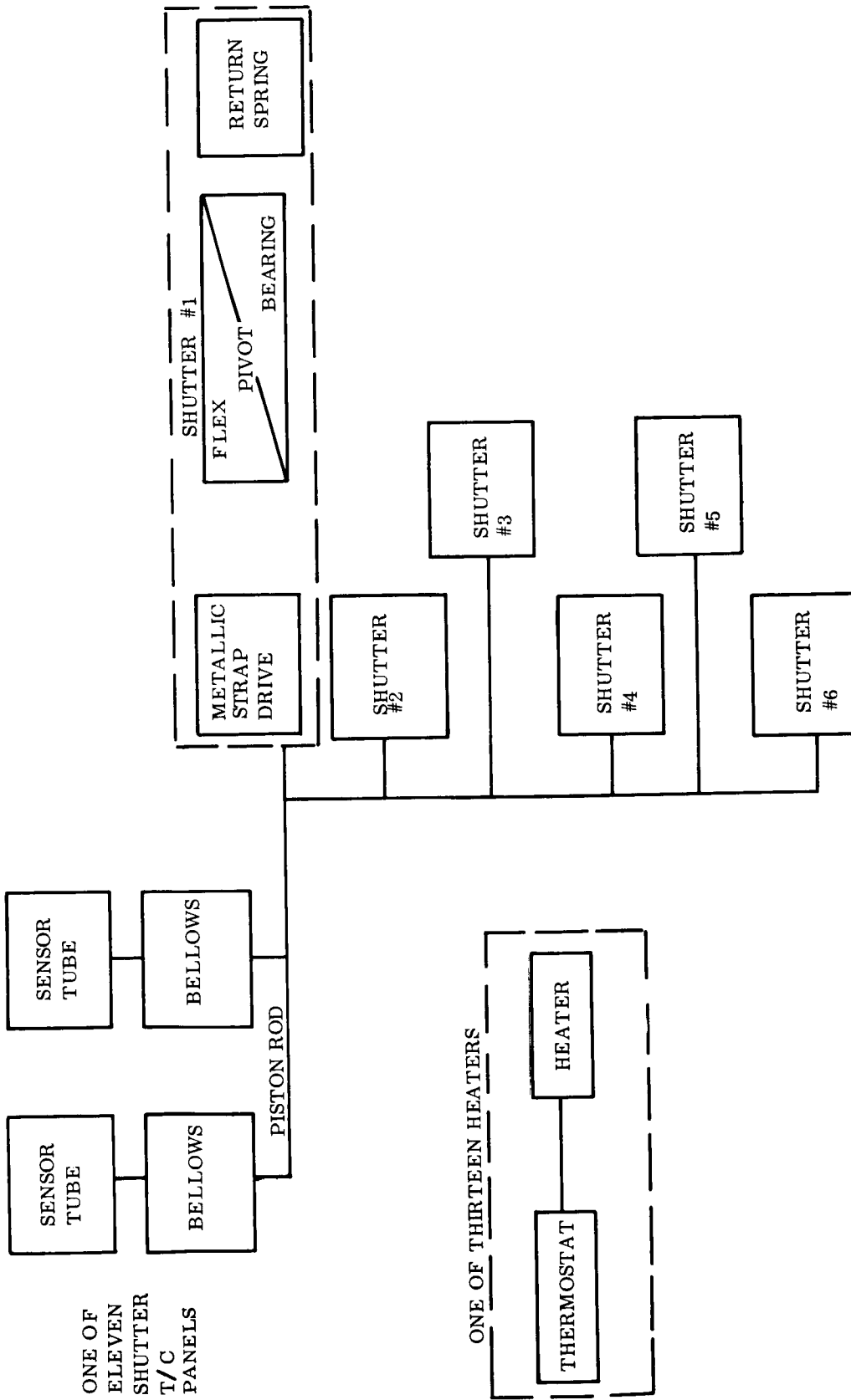


Figure A-33. Thermal Control System Simplified Block Diagram

where the subscripts to each of the "R" factors refer to the component numbers as assigned in Table A-5. The overall subsystem reliability is the product of the individual mission phase reliabilities.

Substitution of the Table A-5 reliability values into the above mathematical model results in the reliability values for the various mission phases as presented in the Volume A temperature control text (VB235FD101).

TABLE A-5
THERMAL CONTROL SUBSYSTEM RELIABILITY DATA

COMPONENTS	QUANTITY	FAILURE RATE* (%/1000 HOURS)	RELIABILITY			
			PHASE 1 & 2	PHASE 3	PHASE 4	
1. Sensor Tube	22	.2237	.99044	.99988	.99838	
2. Bellows						
3. Strap	66	.0001	.99999	.99999	.99999	
4. Flex Pivot	66	.002	.99991	.99999	.99998	
5. Bearing	66	.002	.99991	.99999	.99998	
6. Spring	66	.0001	.99999	.99999	.99999	
7. Thermostat	9	.002	.99991	.99999	.99998	
7a Thermostat (Gyro)	4	.002	.99999	.99999	.99999	
8. Heater	9	.008	.99965	.99999	.99999	
8a Heater (Gyro)	4	.008	.99999	.99999	.99999	

*Based on Advent and Apollo Support Use Data.

CII - VB235FD102

FLIGHT SPACECRAFT STRUCTURE

Index

- 1 **Scope**
- 2 **Applicable Documents**
- 3 **Functional Description**
- 4 **Interfaces**
- 5 **Performance Parameters**
- 6 **Physical Characteristics**
- 7 **Safety Considerations**

1.0 SCOPE

This document describes the complete Flight Spacecraft (FSC) structure which includes the spacecraft (S/C) bus structure, the S/C science payload structure, the S/C retropropulsion structure, and the S/C adapter structure.

2.0 APPLICABLE DOCUMENTATION

VB220SR101	Design Characteristics
VB220SR102	Design Restraints
VB220FD103	Spacecraft Component Design Parameters
VB220FD105	Launch Vehicle Interface
VB220FD106	Capsule Interface
VB235FD103	Structural Design Criteria
VB235FD106	Electronic Packaging

3.0 FUNCTIONAL DESCRIPTION

The FSC structural subsystem serves to support and protect all Voyager system components from the various load environments encountered during the Voyager mission. These include ground handling, transportation, and pre-launch loads, in addition to all launch, boost, transit and orbital loads.

The structure also inherently serves as an integral part of any pointing/aiming alignment system of the various sensing, transmitting, and ejection devices necessary to perform the mission. In addition, the structural subsystem must be an integral part of the thermal control system providing shading, conduction paths and radiation fins as required. Figure 3-1 describes the structural subsystem orientation as part of an overall Voyager functional description. This second level is the starting point for the following functional description of the structural subsystem presented as follows:

3.1 SPACECRAFT BUS STRUCTURE

The primary structure is defined as the structure which provides basic load paths for the introduction of boost loads to the launch vehicle structure.

The secondary structure is the structure which transmits specific component loads to the primary structure; the major design requirement being that allowable component levels for vibration frequency, amplitude, and shock are not exceeded by responses to the launch vehicle environment.

This necessarily includes the effects of the structural stiffness characteristics of the primary structure to which it is attached. Figure 3-2 shows the major components of the S/C primary structure, station locations, and radial element locations used in the text of this functional description. The Voyager Spacecraft Basic Geometry is presented in Figure 3-3. Figure 3-4 shows the Structural General Arrangement.

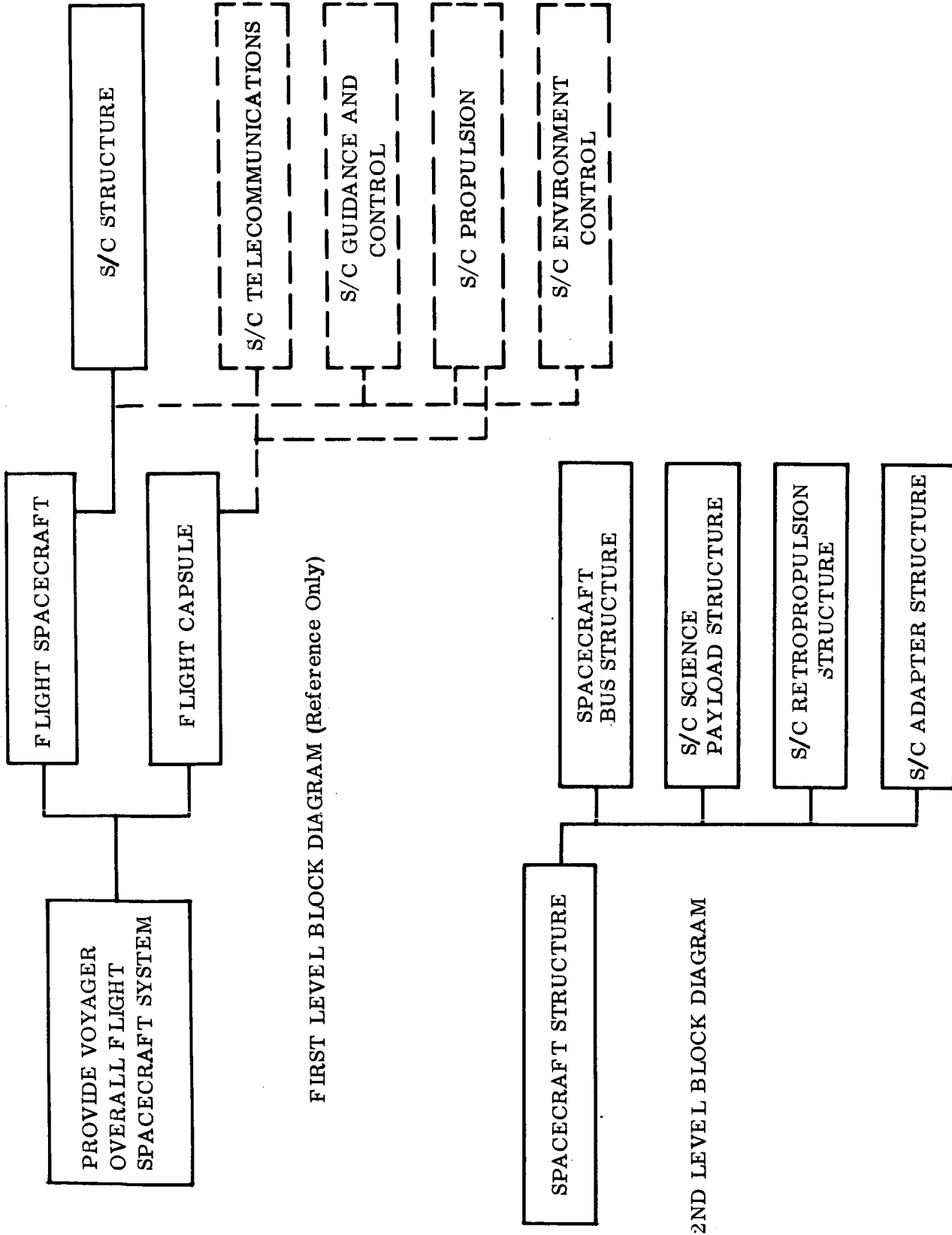


Figure 3-1. Structural Functional Block Diagram

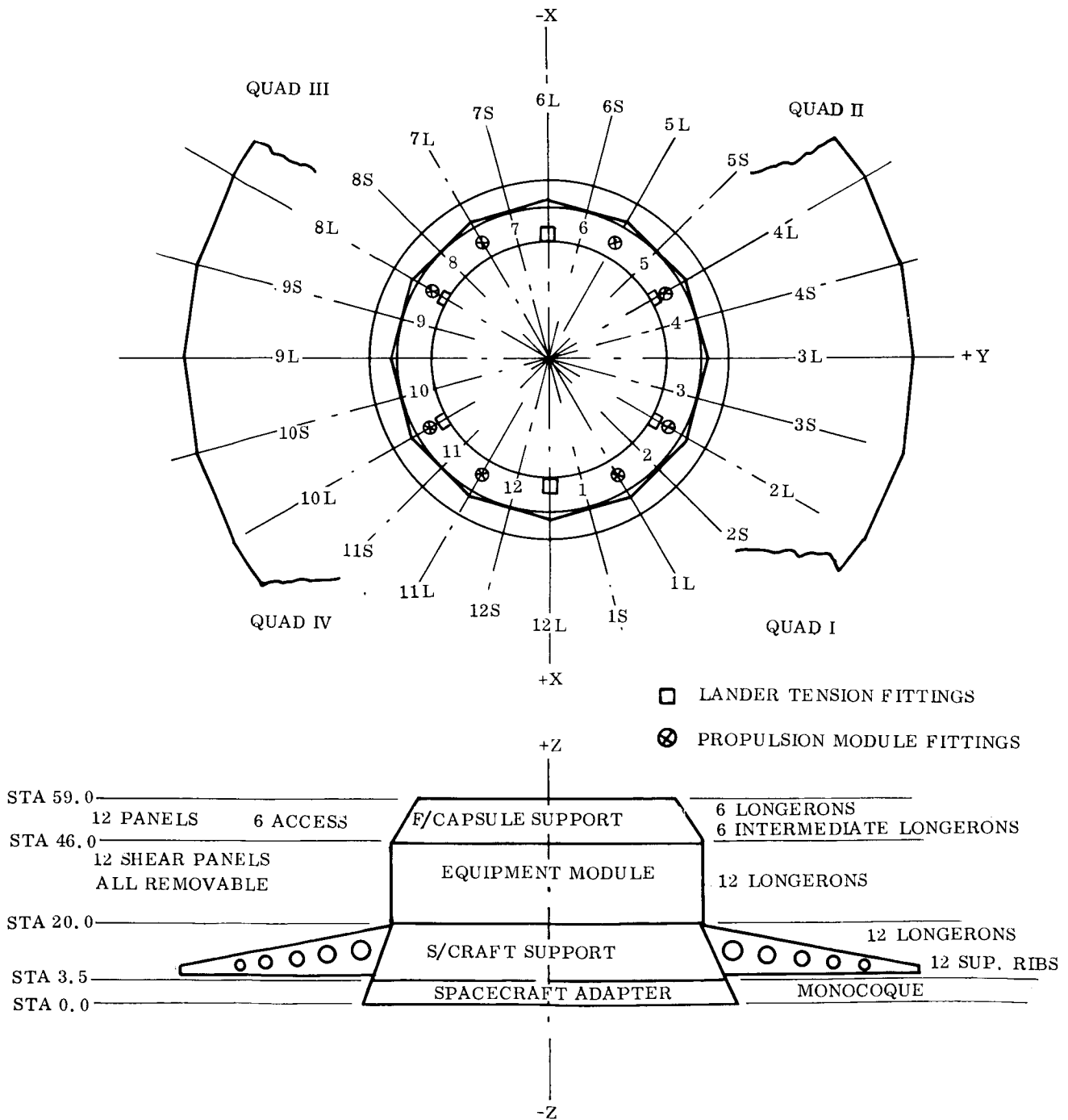
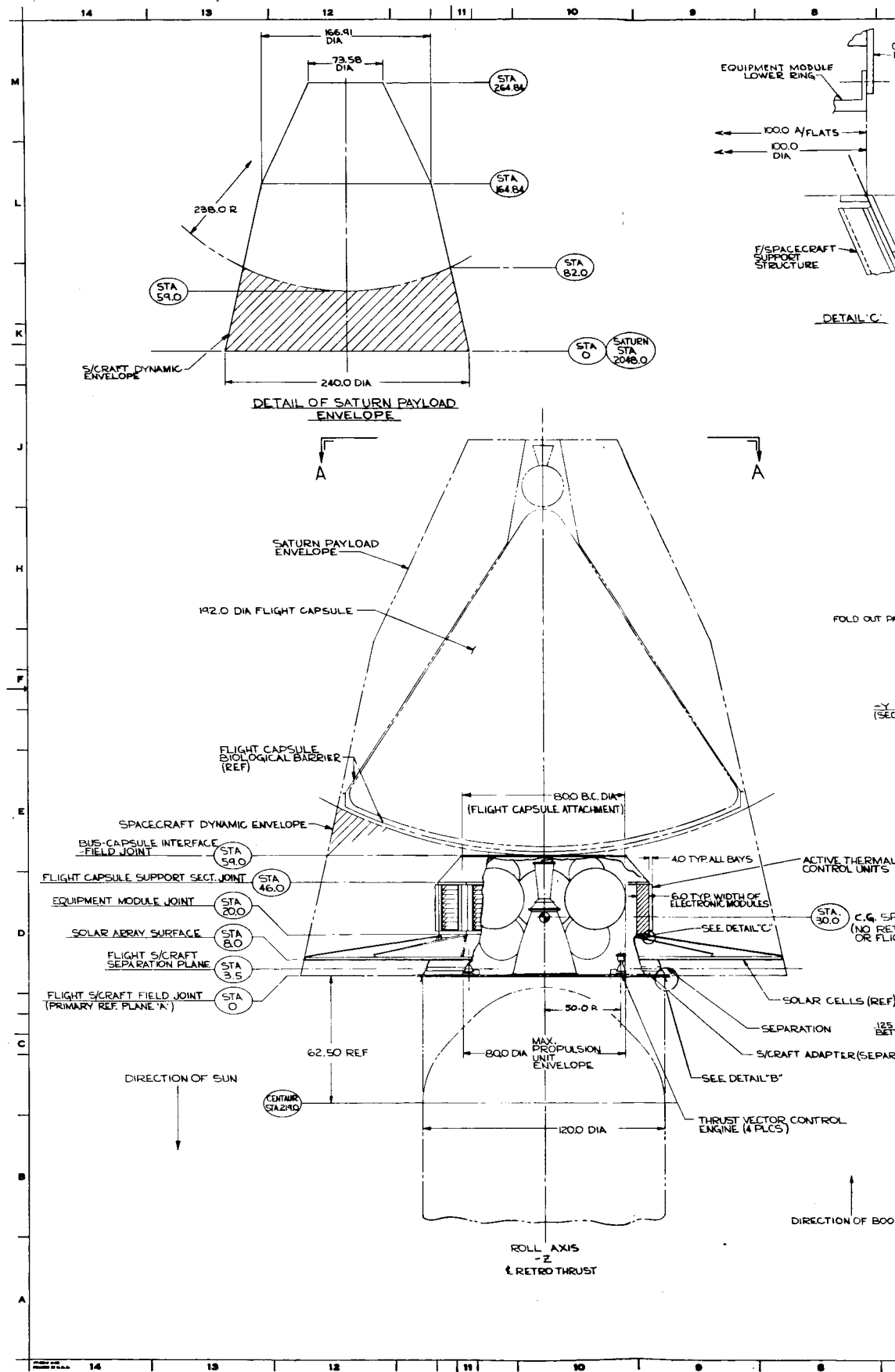


Figure 3-2. Structural Components



(4)

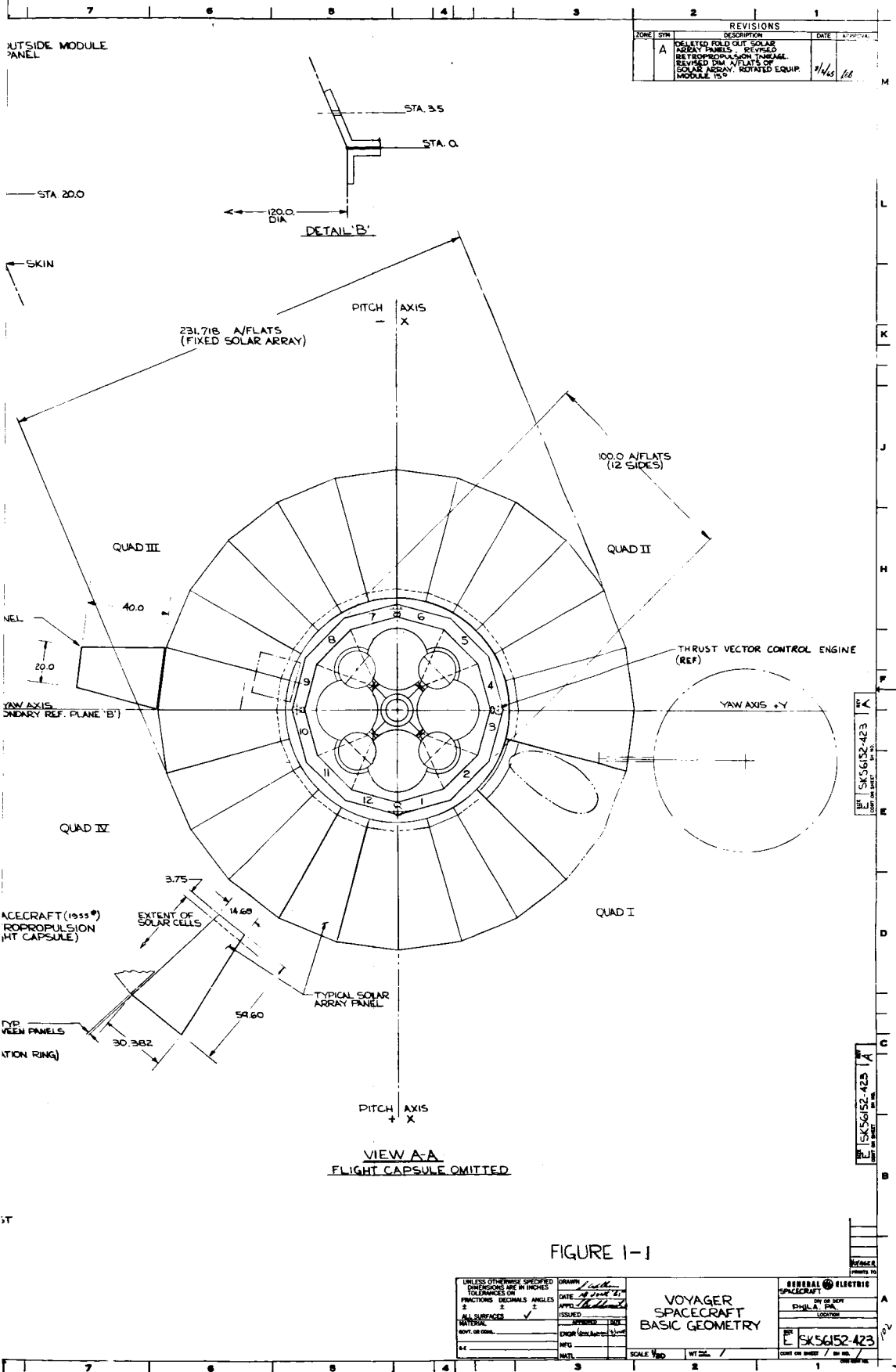
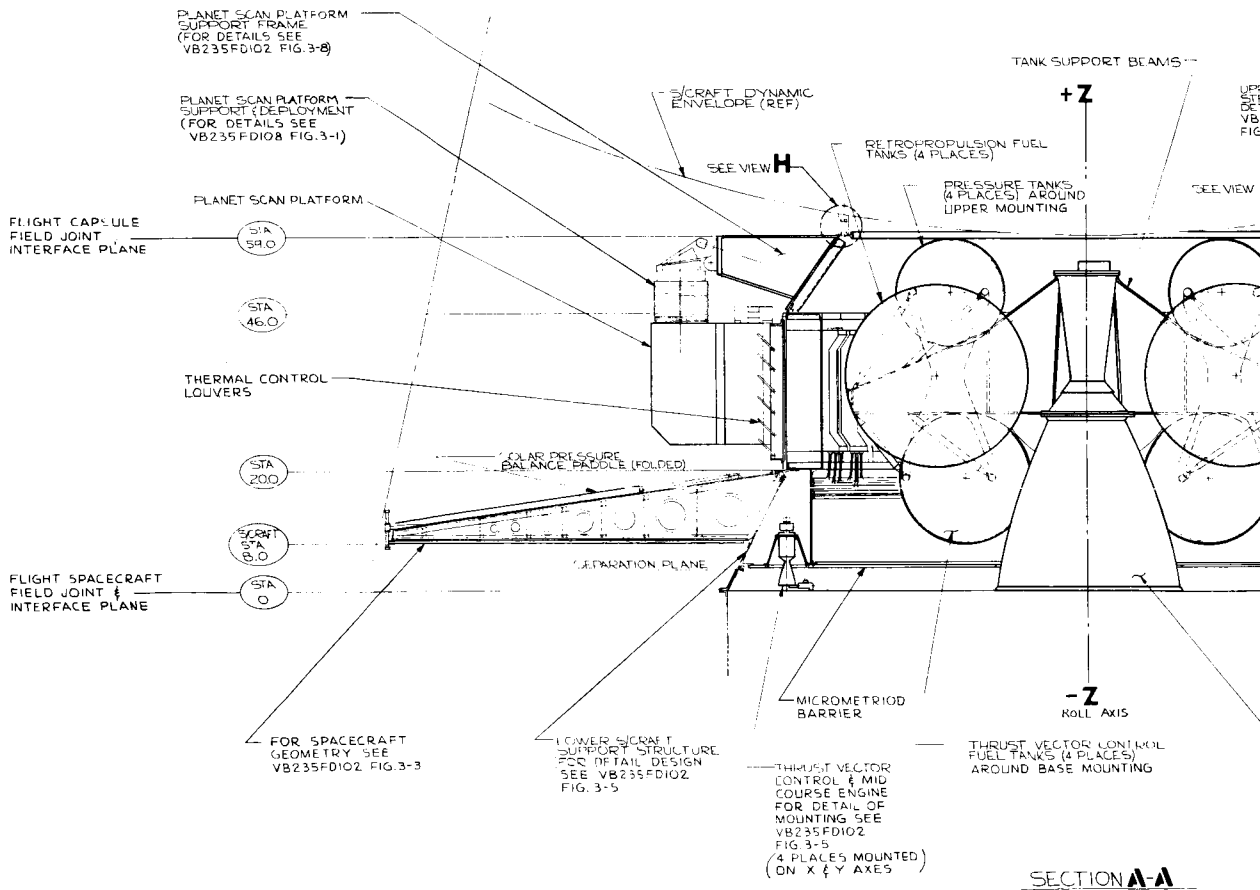
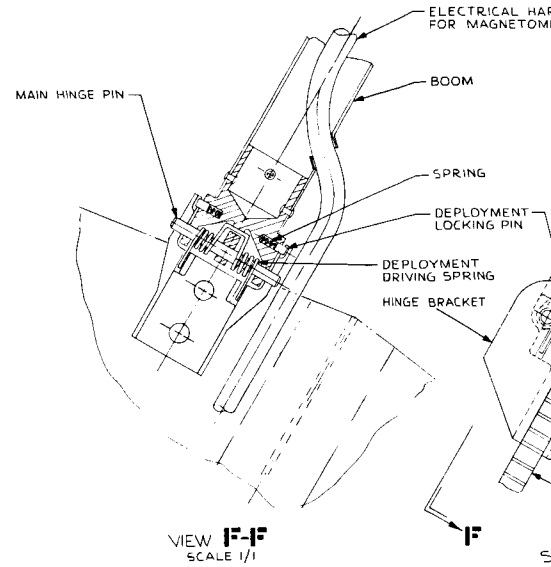
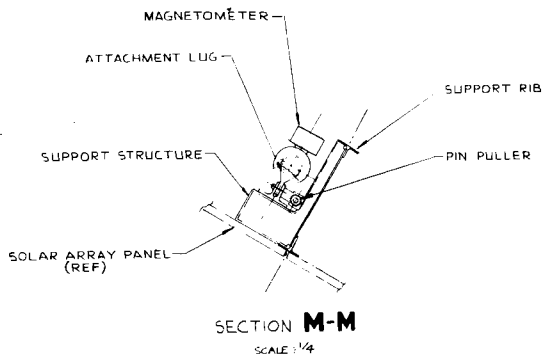
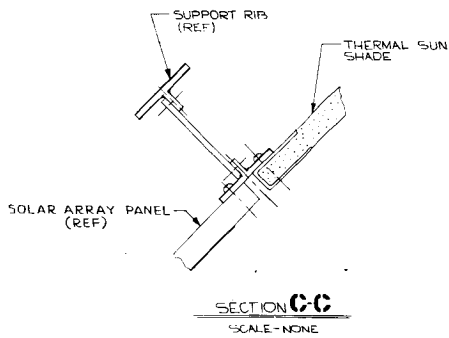
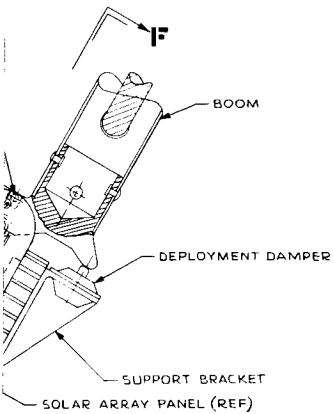


Figure 3-3. Voyager Spacecraft Basic Geometry



80

NESS
ETER



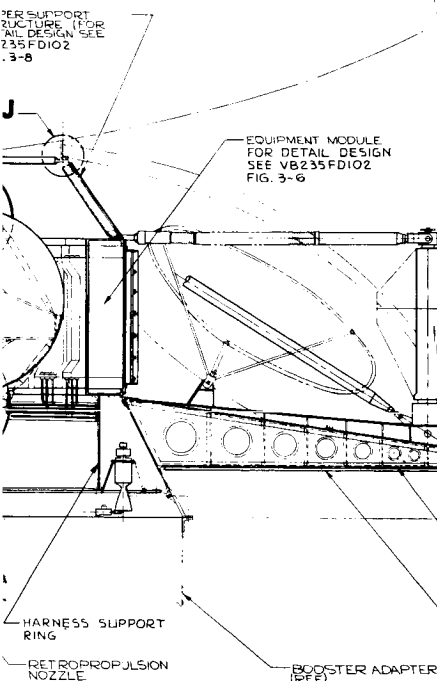
SECTION C-C
SCALE - NONE

QUAD III

PLANET SCAN PLATFORM
FOR DETAILS OF STOWAGE
& DEPLOYMENT SEE
VB235FD-108 FIG. 3-1

APPROACH GUIDANCE
PACKAGE, MOUNTED
TO TOP RING
EQUIPMENT MODULE

SECTION E-E
SCALE 1/1



SOLAR PRESSURE BALANCE VANE
FOR DEPLOYMENT MECHANISM
& STOWAGE SEE VB235FD-110
FIG. 3-2

STOWED POSITION
DEPLOYED POSITION

APPROACH CANOPUS STAR
TRACKER FIELD OF VIEW

SECONDARY LOW
GAIN ANTENNA

HIGH GAIN ANTENNA
SUPPORT (DEPLOYMENT
FOR DETAIL OF
DEPLOYMENT &
MECHANISM
SEE FIG. 3-1)
VB235FD109

ATTITUDE CONTROL
NOZZLES

SOLAR ARRAY
PANELS

SOLAR CELLS ON THIS SIDE

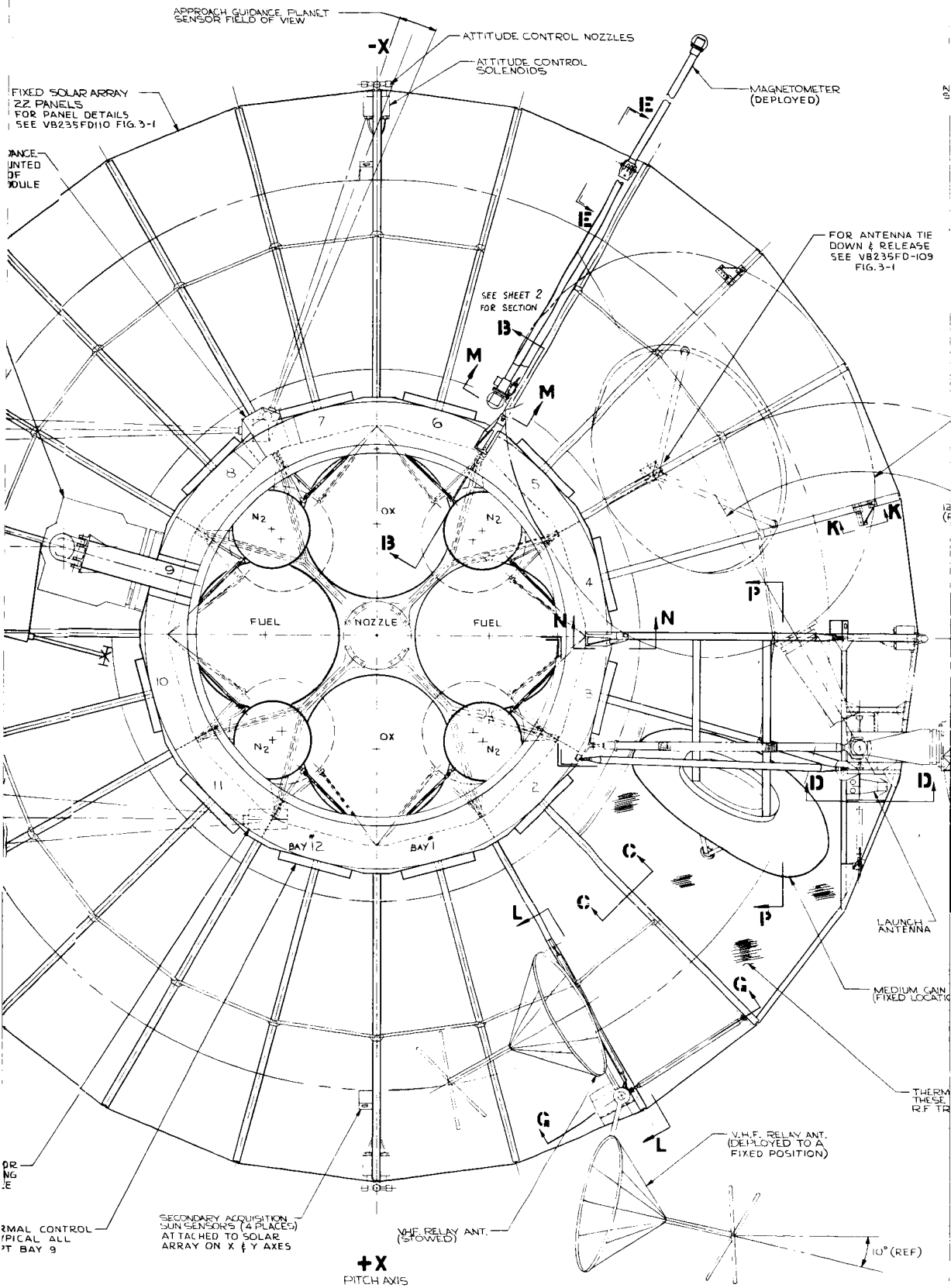
QUAD IV

75 FT DIA. HIGH GAIN
ANTENNA (DEPLOYED POSITION)

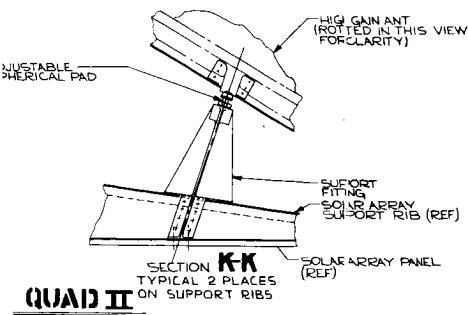
CANOPUS STAR SENSORS
MOUNTED TO TOP RING
OF EQUIPMENT MODULE

ACTIVE THERMAL
LOUVERS TO BE
BAYS EXCEPT

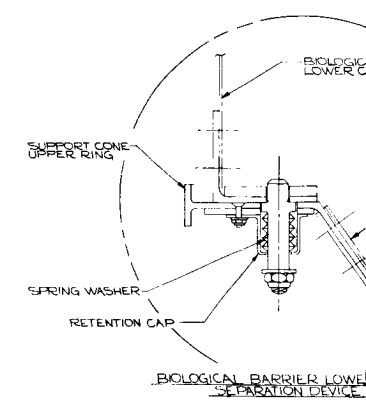
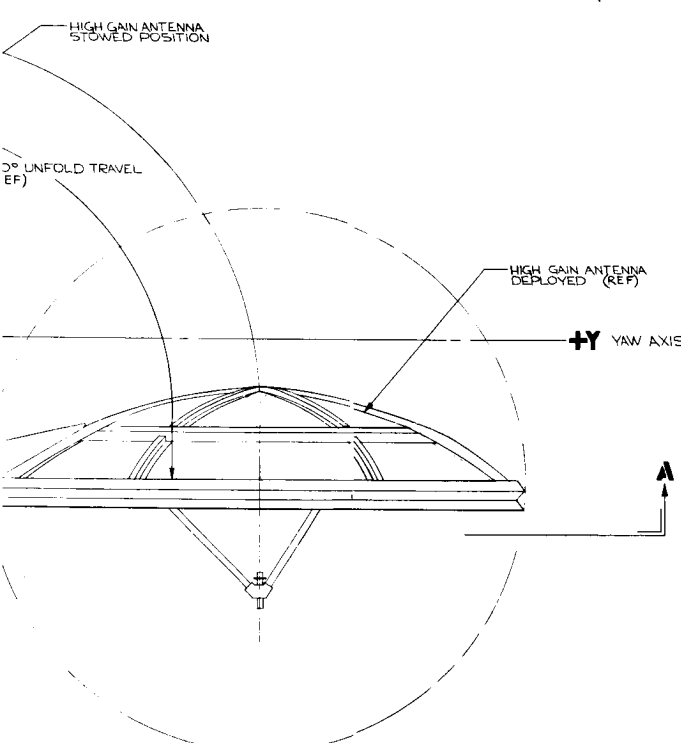
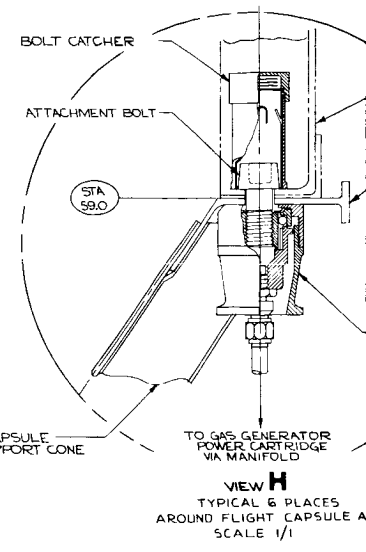
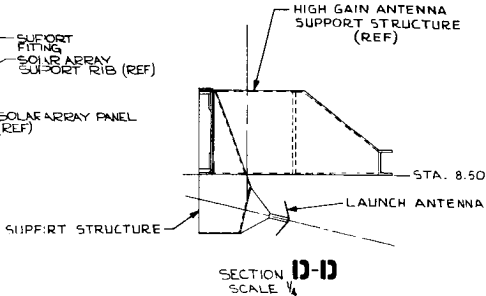
802



83



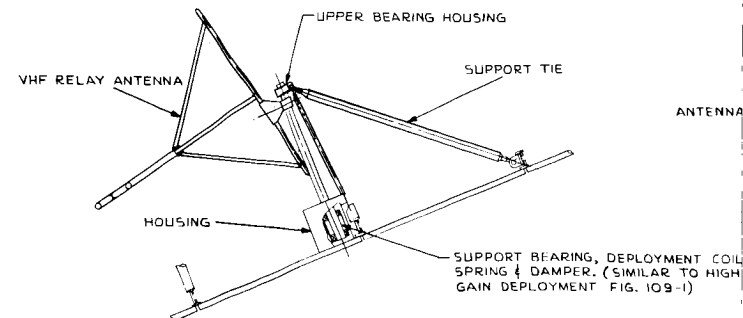
QUAD II



ANT. (N)

QUAD I

ALL SUN SHADE COVER ACROSS TWO BAYS - COVER TO BE TRANSPARENT



VIEW **G-G**
SCALE 1/16

8 (4)

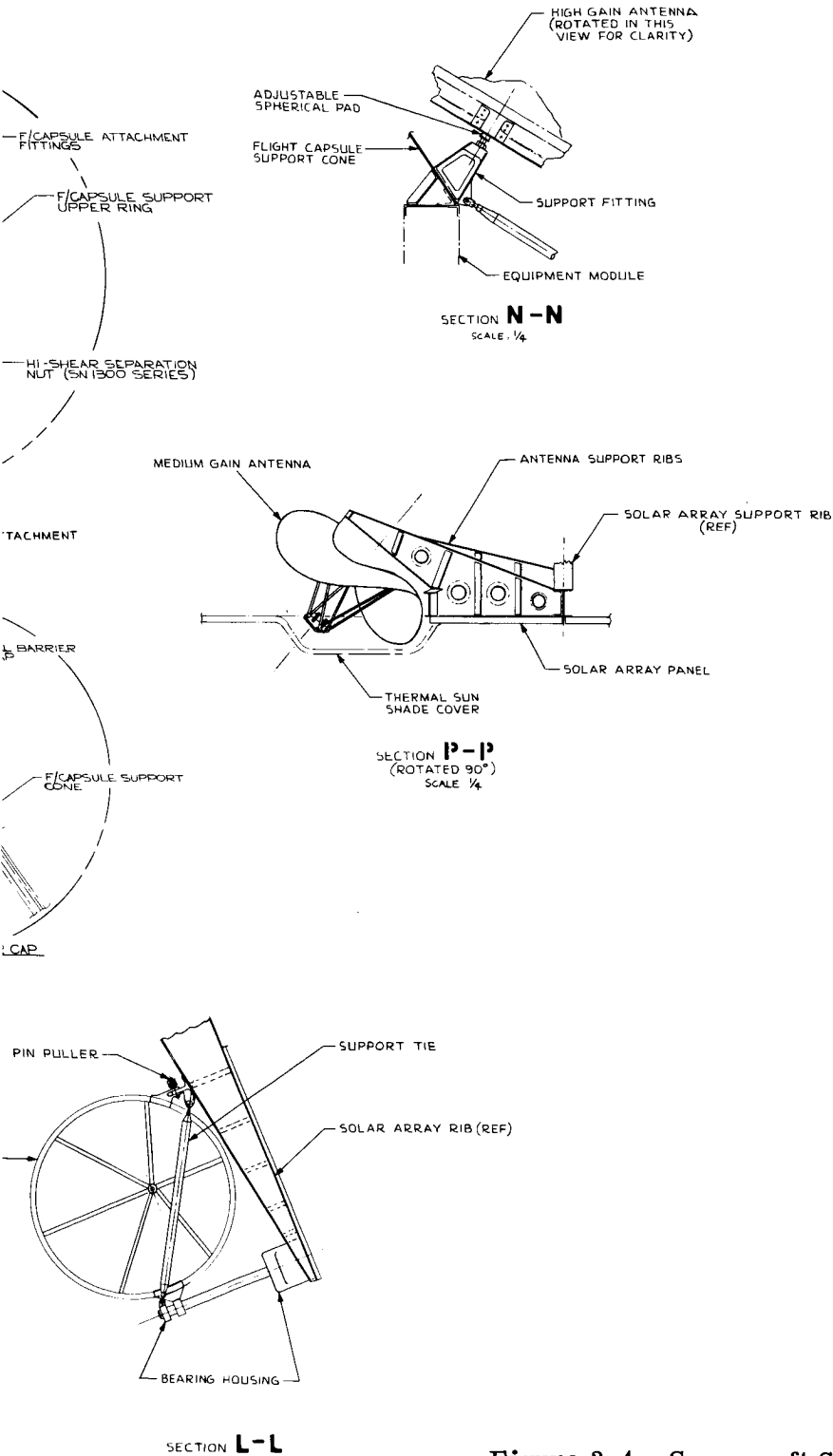
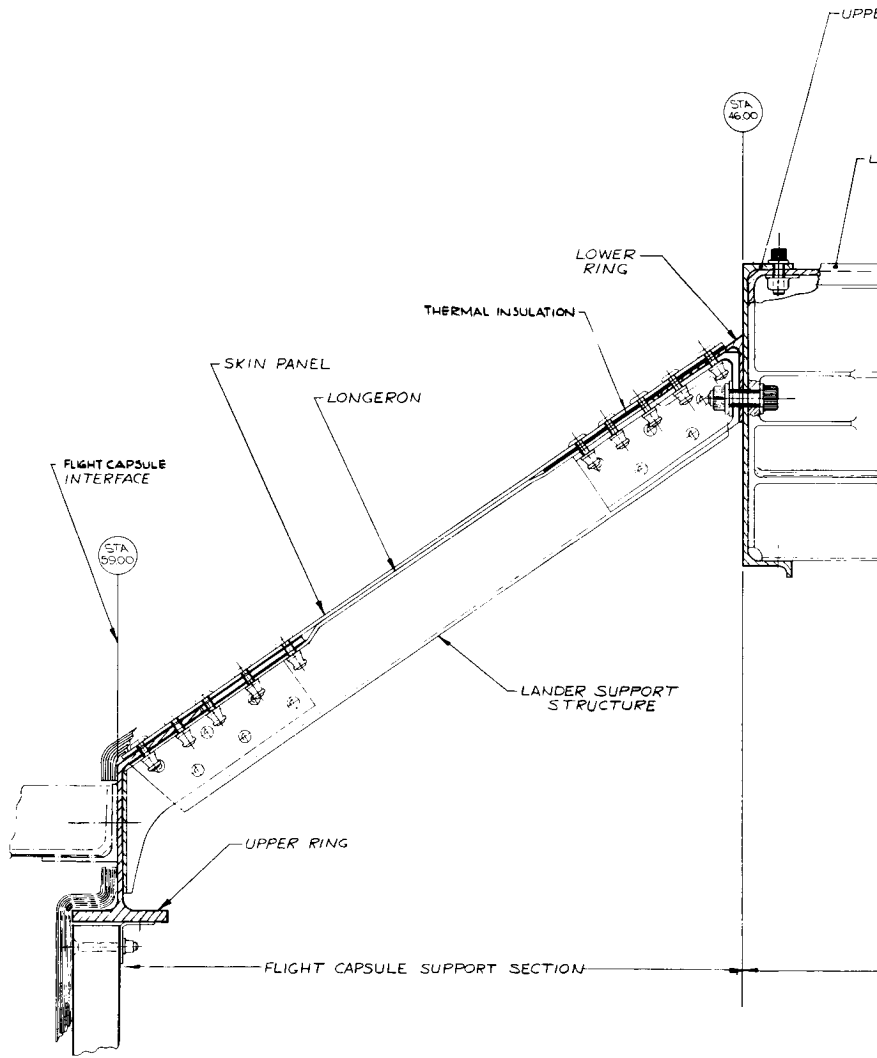
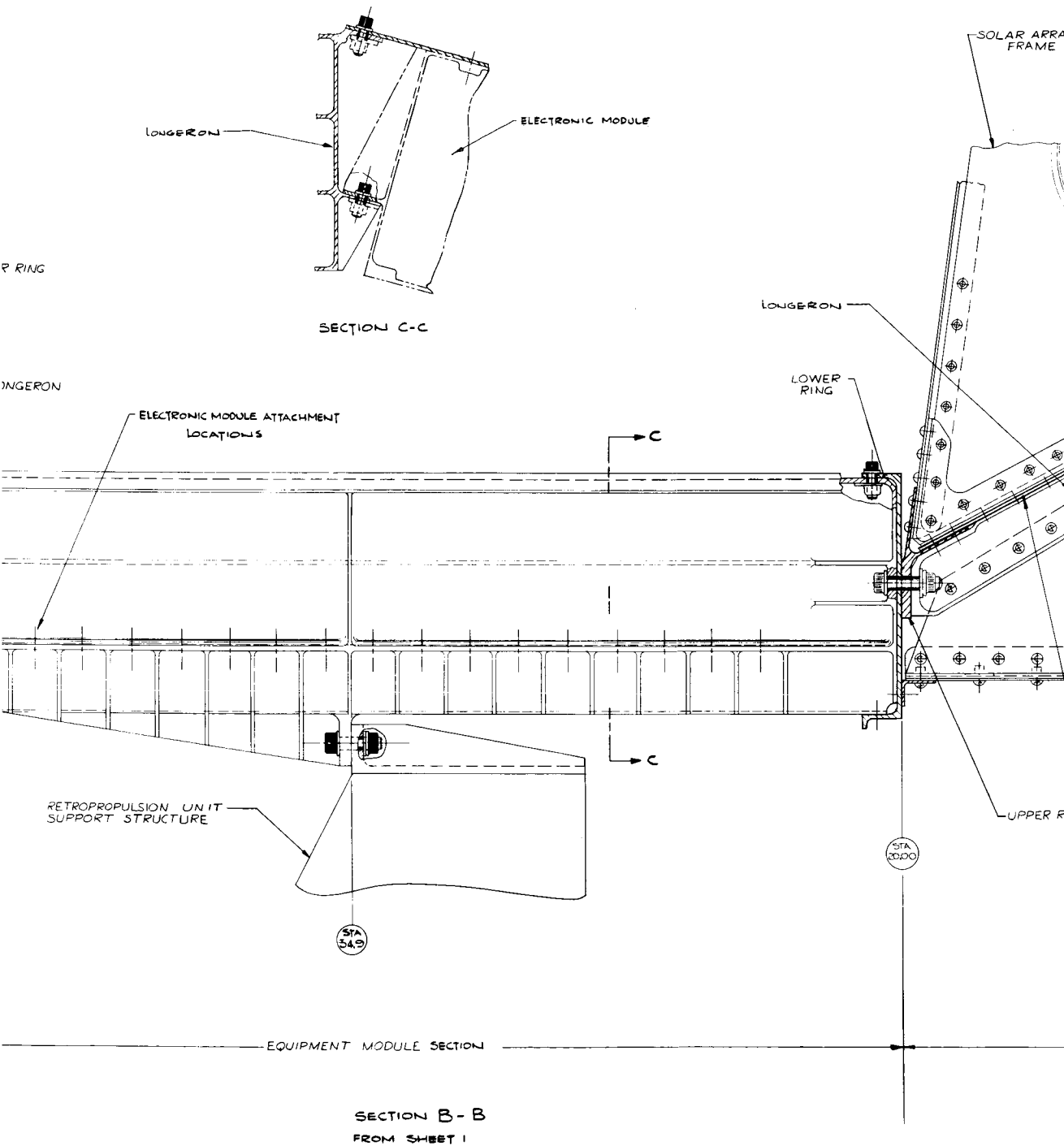


Figure 3-4. Spacecraft Structural General Arrangement/Sheet 1 of 2



100



VB235FD102

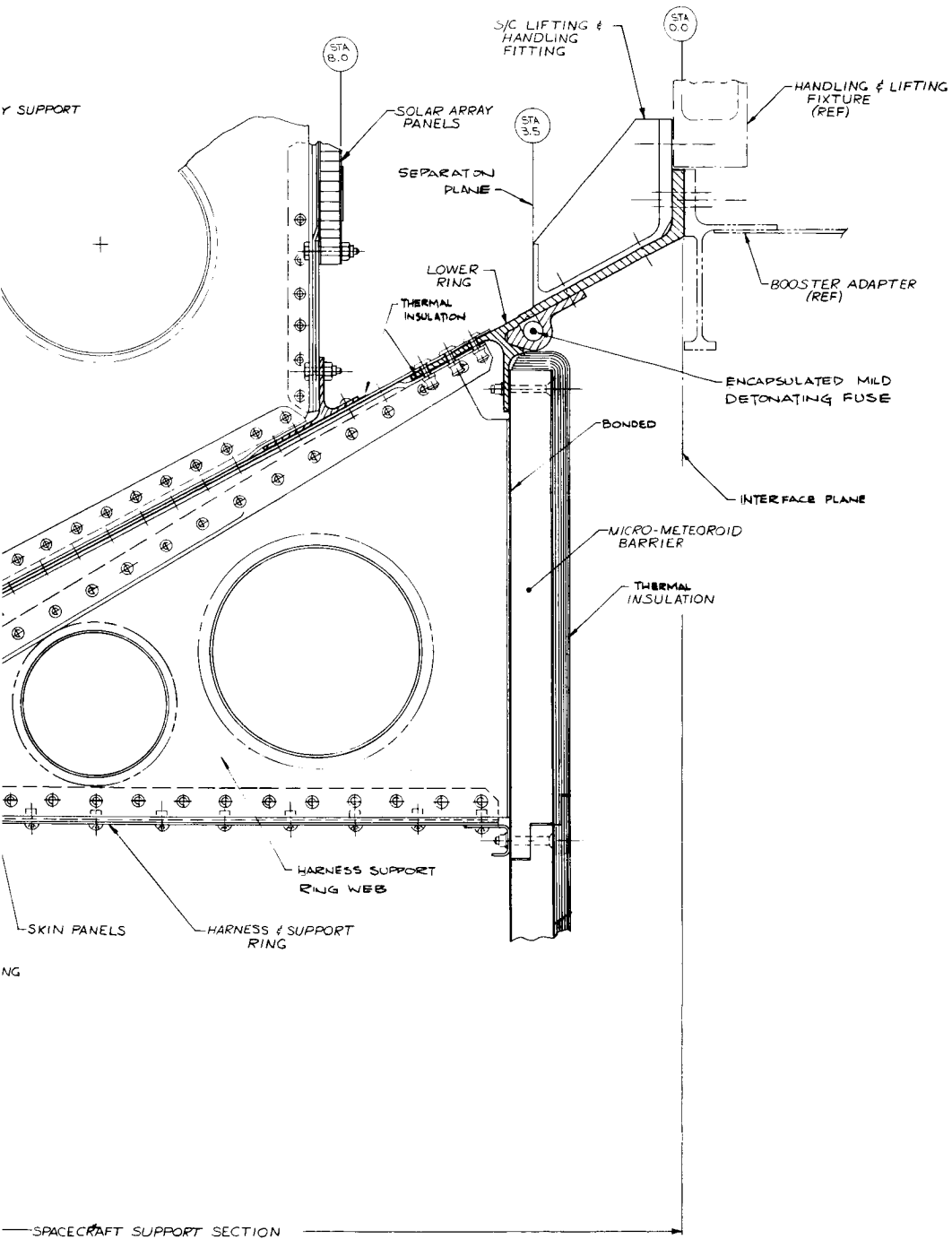


Figure 3-4. Spacecraft Structural General Arrangement/Sheet 2 of 2

3.1.1 CAPSULE SUPPORT STRUCTURE

This structural assembly is presented as Figure 3-5. The primary capsule support structure is a semi-monocoque conical shell which receives loads from the flight capsule at the flight capsule/spacecraft interface at station 59.0 and transmits them to the equipment module at station 46.0. It consists of an interface ring at station 59.0, six primary longerons which pick up the six attachment fittings on the capsule adapter, six intermediate longerons, stiffened skin panels, and a closing ring at station 46.0 which also serves as a manufacturing joint between this structure and the equipment module. The interface ring reacts and re-distributes the radial components of the longerons, in addition to transferring the shear due to lateral and torsion loads into the shell. The primary longerons at locations 2L, 4L, 6L, 8L, 10L & 12L receive axial and bending loads from the flight capsule, the primary load source on this structure. The six intermediate longerons located between the primary longerons pick up approximately 45 percent of these total loads through shear lag of the skin; in this way flight capsule loads are distributed to the twelve longerons in the equipment module.

The stiffened skin is therefore broken up radially into 12 panels, six of which are fixed, and six removable (for access to propulsion components, test harness and sensors). In addition to distributing a proportion of the axial load mentioned above, the skin also serves to react the high shear flow due to load condition 2B (Ref. Table IV of appendix). Secondary structure is provided for the deployed planet scan platform support in the vicinity of Bay 9. It is a short stiff beam mounted off the capsule support structure, affording an aligned, vibration free mounting for the actuation mechanisms which point the scan platform. The requirement for absolute alignment is not particularly critical because the closed loop control system will point the platform as desired. The natural frequency of this structure is such that coupling with the attitude control correction impulse is negligible.

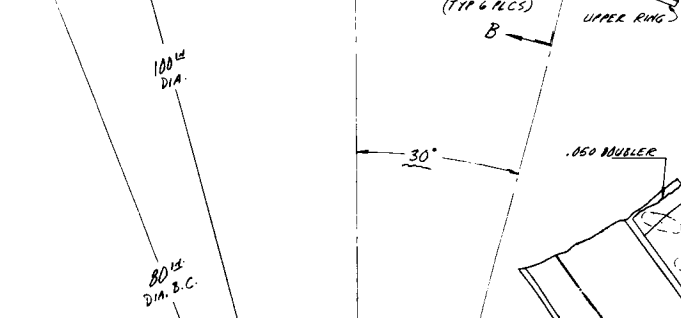
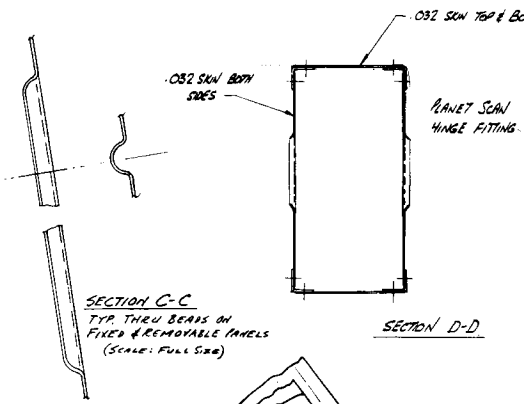
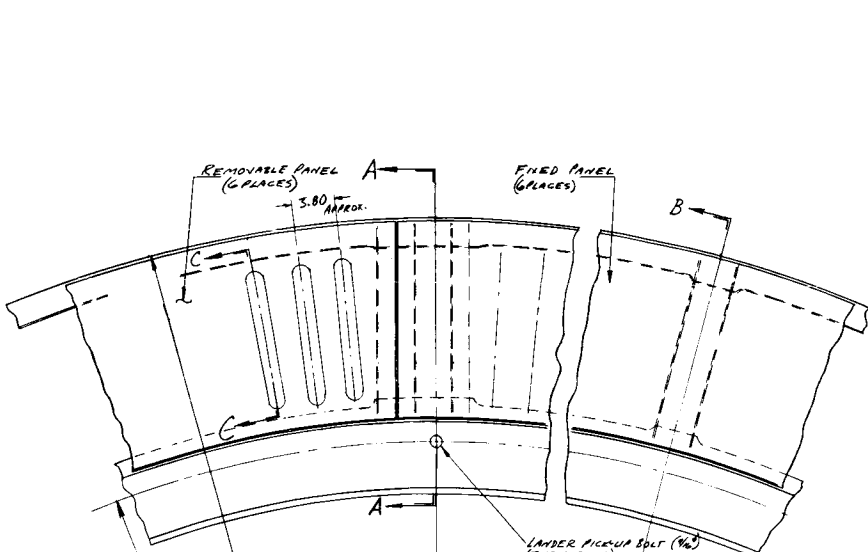
There are two fittings of a flexible organic material located near Station 49.0 in the vicinity of longeron locations 4L, 3L and 5L to act as snubbers for the antenna during flight condition. These snubbers act as end-beam supports for the antenna and are preloaded by the main tiedown fitting at the antenna feed. The preload is sufficient to ensure contact with the snubbers throughout the loading environment.

3.1.2 EQUIPMENT MODULE (E/M) (STATION 20-46)

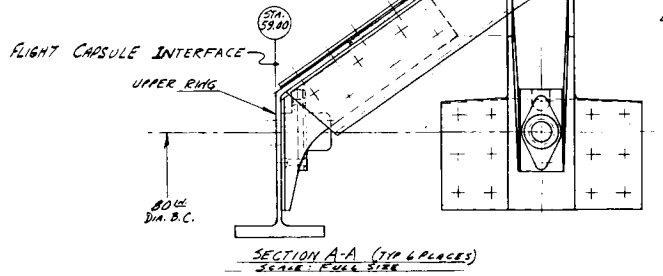
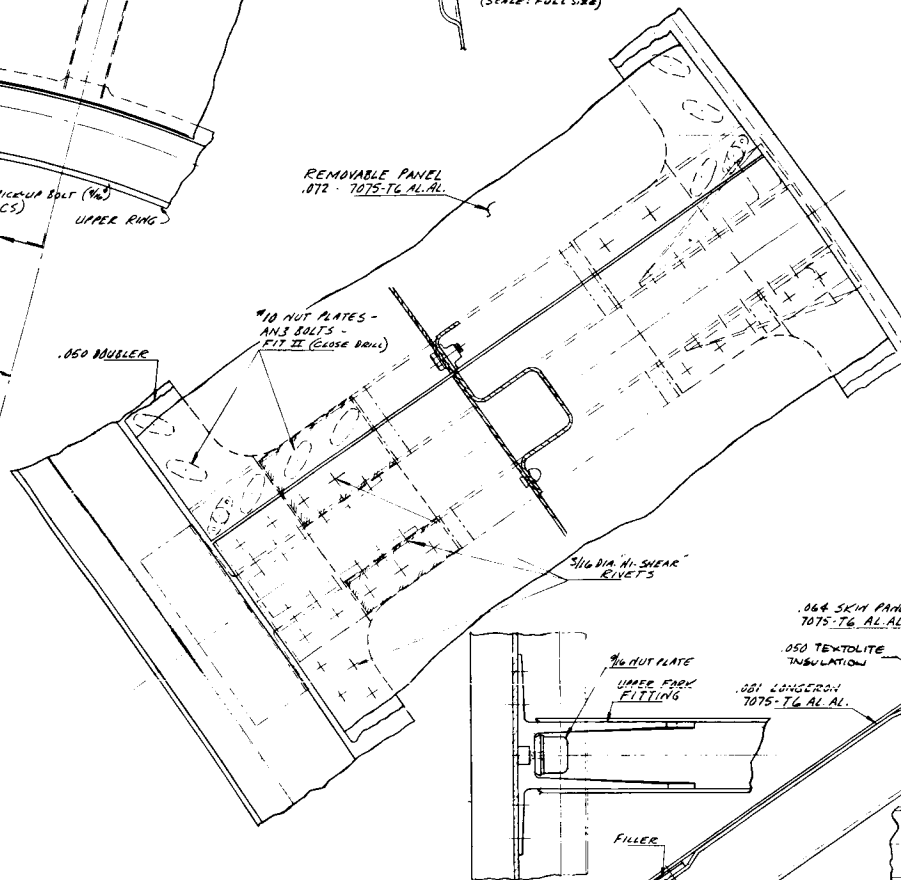
The equipment module shown in Figure 3-6 houses the majority of the S/C electronic equipment, transmits the primary shear, axial, and bending loads and supports the propulsion module.

The basic structure is a framework of two rings, upper and lower, 12 longerons, and 12 shear panels, which pick up secondary loads and transmit primary loads.

The upper ring transmits the shear load from the capsule support to the shear panels of the 12 sided E/M, and reacts the kick loads from the 12 longerons of the capsule support structure. It also serves to transmit the radial loads from the equipment bay modules and Propulsion Module into the basic structure. The lower ring acts similarly to the upper ring except that the shear loads are transmitted from the 12 sided structure to the adjacent space-



PLAN VIEW OF
 CAPSULE SUPPORT
 STRUCTURE
 GEOMETRY
 SCALE: 1/2



13

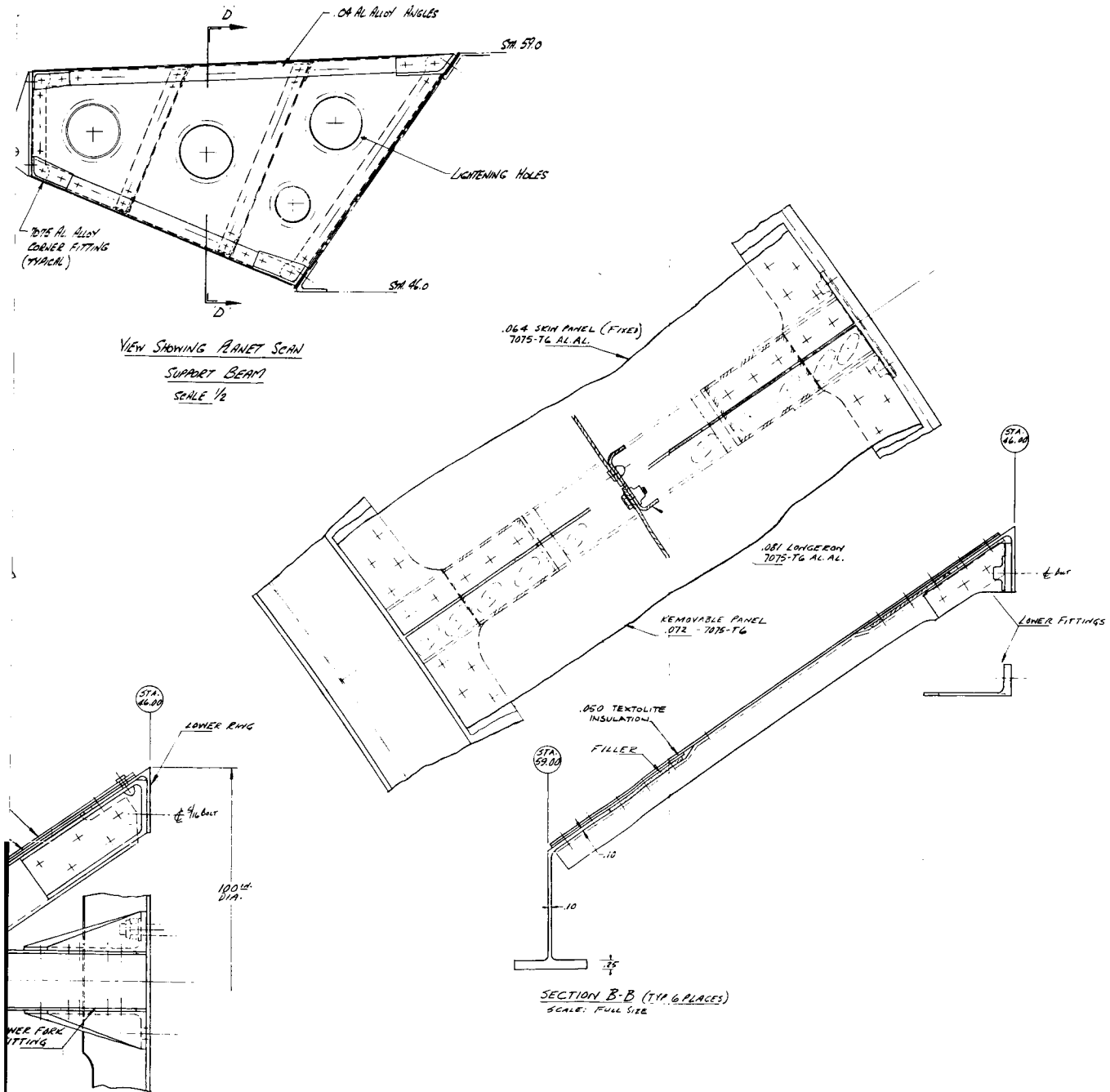
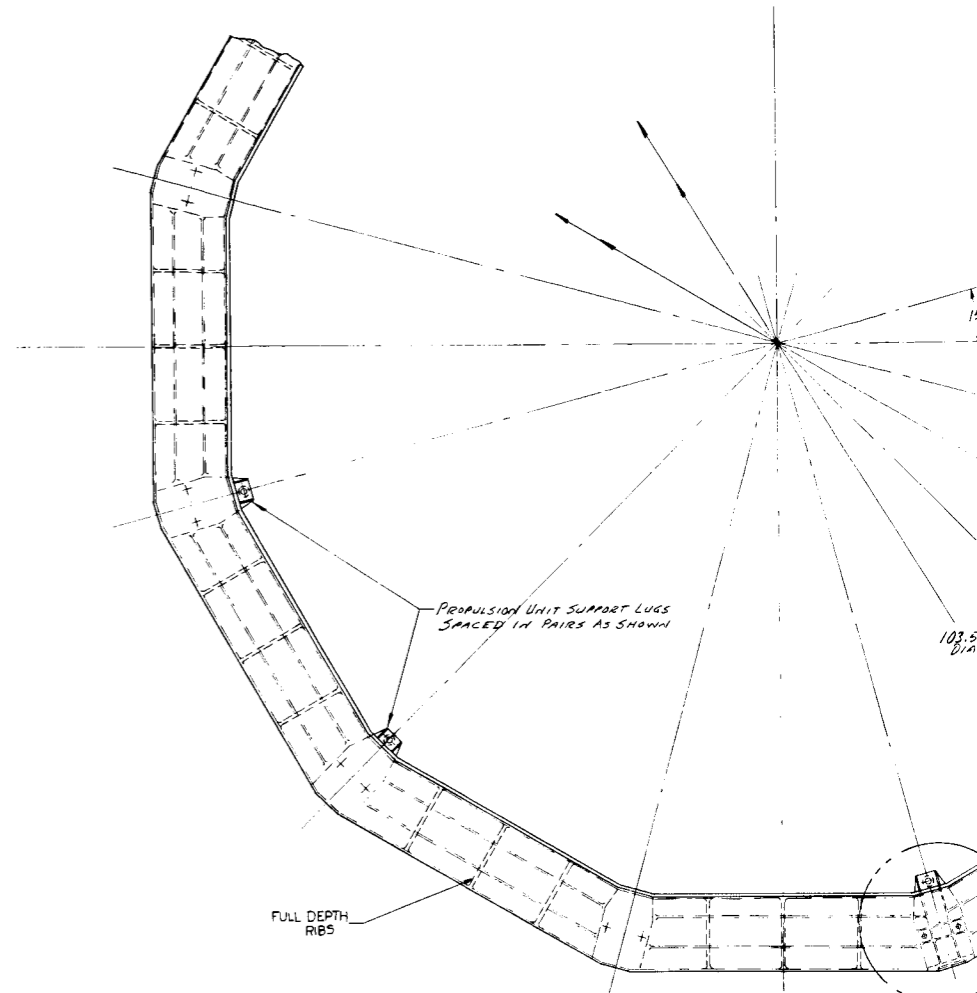
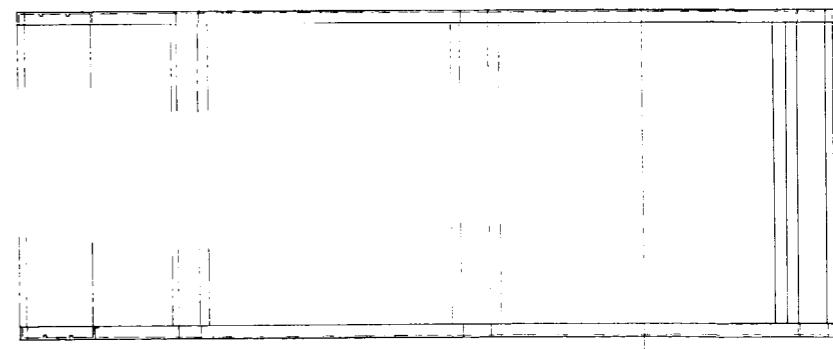


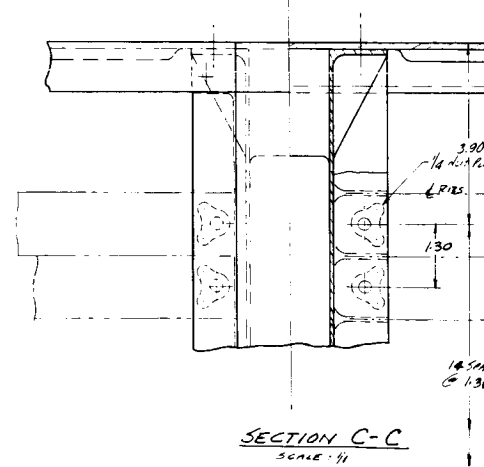
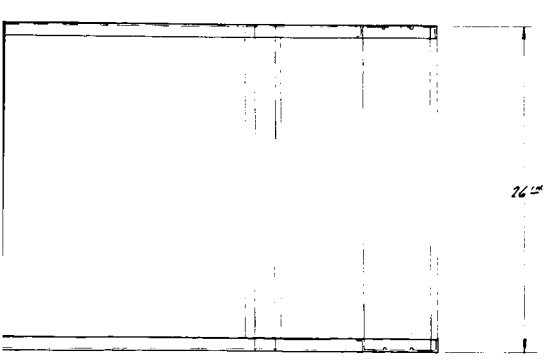
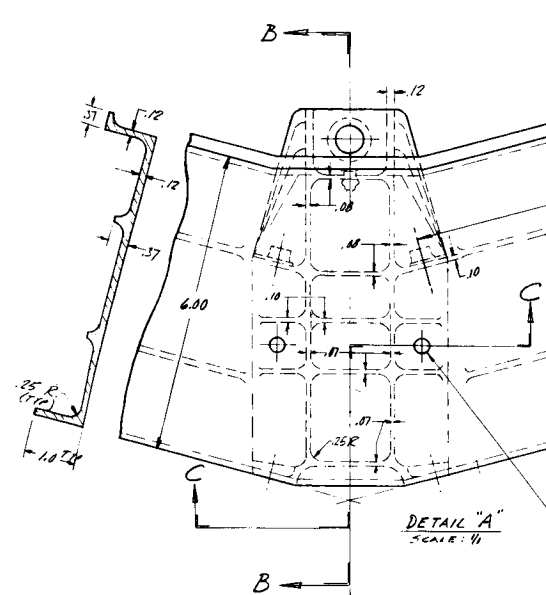
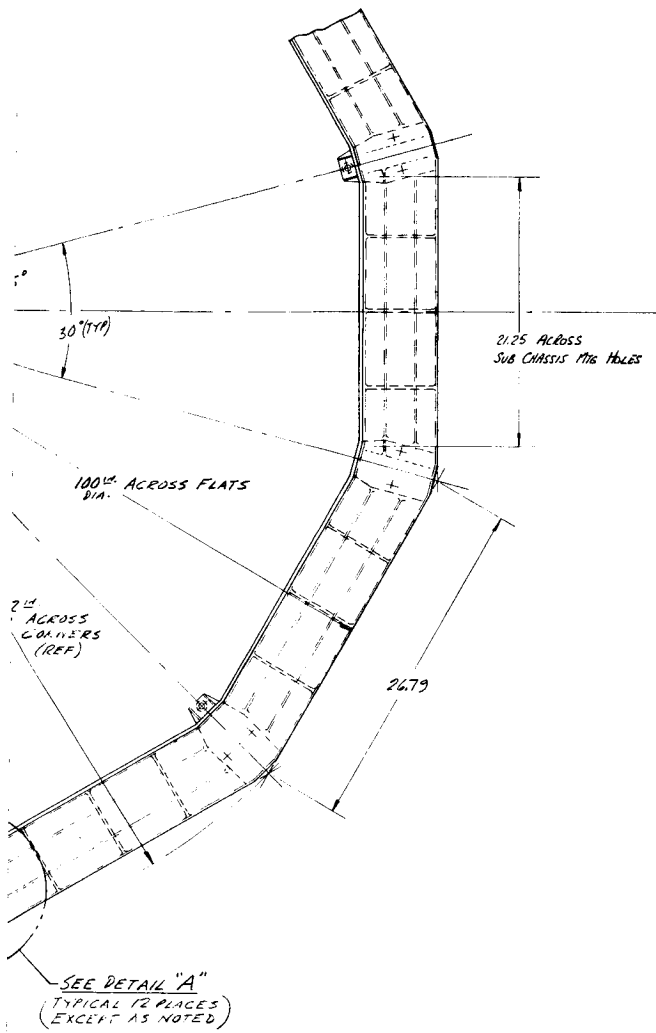
Figure 3-5. Capsule Support Structure

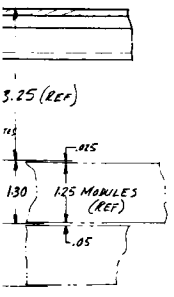
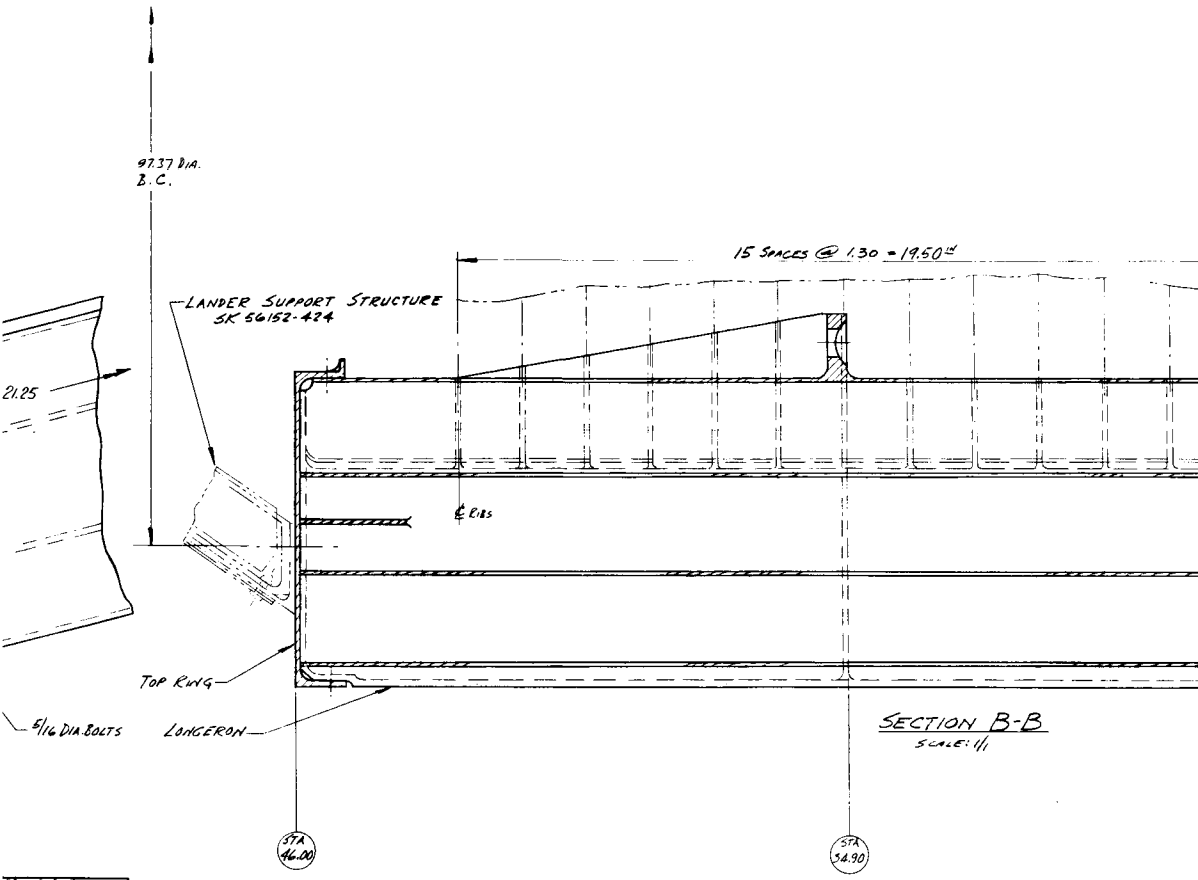


PLAN VIEW OF
EQUIPMENT MODULE
SCALE: 1/4



16 (1)





REF
1-18.20

103

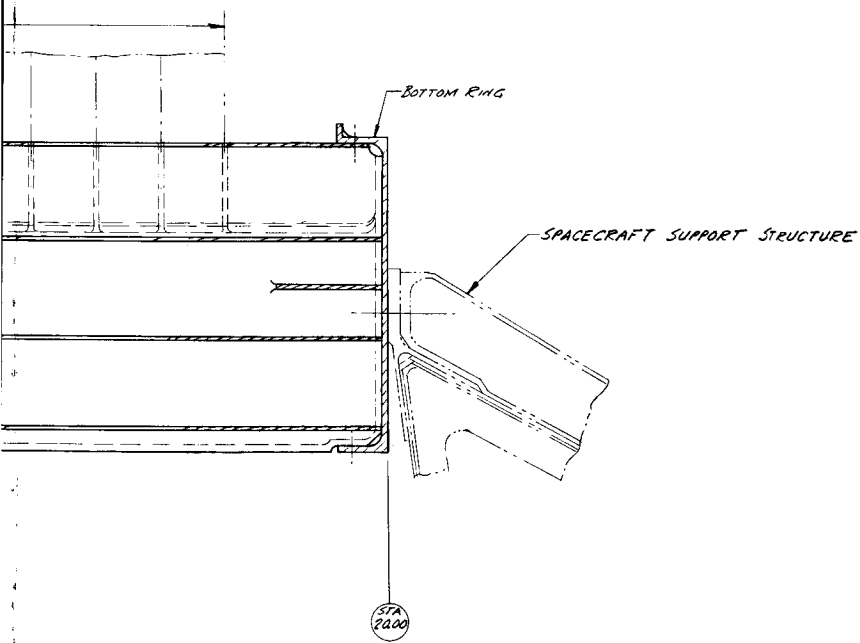


Figure 3-6. Equipment Module

craft support structure. The 12 longerons carry all of the primary axial and bending loads as columns and also serve to introduce the propulsion subsystem loads into the primary structure. In addition the individual electronic submodules are attached directly to the longerons, providing significant stability.

The upper ring of this portion of the structure provides mounting surfaces for the following components:

- 1) Canopus sensor
- 2) Approach Guidance sensor
- 3) Body mounted scientific equipment.

The equipment module front cover plates serve to assemble the individual electronic mounting boxes into a unit by providing a plate to which each box is assembled using seven attachments per submodule. Attachment of the submodules provides a conductance path for the heat loads therein and the panel thus helps to balance the submodule temperature and act as a radiation fin. The last function of these panels is to provide a support base for the thermal shutter assemblies, including the tube required for the liquid-bellows actuation system.

The Propulsion Module attachment structure consists of eight fittings which serve to introduce the loads from the propulsion system into the basic structure at longerons 1L, 2L, 4L, 5L, 7L, 8L, 10L, and 11L at Station 34.90.

The equipment submodule is comprised of a series of separate boxes on which are mounted the cordwood modules and printed circuitry of the electronic assemblies. The boxes provide necessary structural stiffness and thermal conductance to satisfy the operating environment. The loads of each box are directly introduced into the longerons by attaching at either end. This box structure serves a multi-function by stabilizing the outer covers which carry the primary shear load. The potential exists for utilization of these electronic boxes to carry longitudinal loads if required but the existing structural configuration, and necessity for ease of assembly, testing, and maintenance does not require longitudinal load capability. Connector support bracketry includes the submodule inner panels and attached angles. See VB235FD106 for detail discussion. The primary electrical harness extends around the inside circumference of the equipment module on a circular shell, 92.4 inches in diameter, which hangs down 15.8 inches from the lower ring. The harness cabling is distributed on the inner surface of this shell, except that a local tray is provided for harness rerouting at the areas where the attitude control tanks are mounted. This shell introduces the harness loads into the lower ring of the equipment module and is stabilized at the lower end by the meteoroid bumper/thermal shield which also serves to support the midcourse propulsion system engines.

Clevis fittings on the planet scan platform support the science instruments during the boost environment, transmitting loads to longerons 8L & 9L by means of shear pins. Pin pullers are provided at these attachment points for release of the platform. See section 4.5 for the interface of the thermal control louvers with the equipment module.

3.1.3 SPACECRAFT SUPPORT STRUCTURE

This structure shown in Figure 3-7 serves as the transition from the equipment module to the spacecraft adapter and supports the following components: The solar array for the photovoltaic power system, the antennas for the radio system, various sensors and body mounted scientific equipment. Consequently the spacecraft support forms a critical element of the overall spacecraft component support and alignment system.

The primary load carrying semi-monocoque structure consists of upper and lower rings, stiffened skin and twelve tapered longerons which transmit the primary loads to a near uniform distribution at the lower ring in order to comply with the requirement for a fully monocoque structure at the separation joint (due to the usage of the encapsulated Mild Detonating Fuse (MDF) separation device - see VB235FD104).

The upper ring (Station 20) primarily serves to introduce the basic shear loads from the equipment module and the kick loads from the solar array support ribs into the shell, and secondarily helps the equipment module lower ring carry the kick loads introduced by the longerons. The plane defined by the mating surface of this ring with the lower ring of the equipment module serves as the basic alignment reference plane for the spacecraft and is also a manufacturing joint.

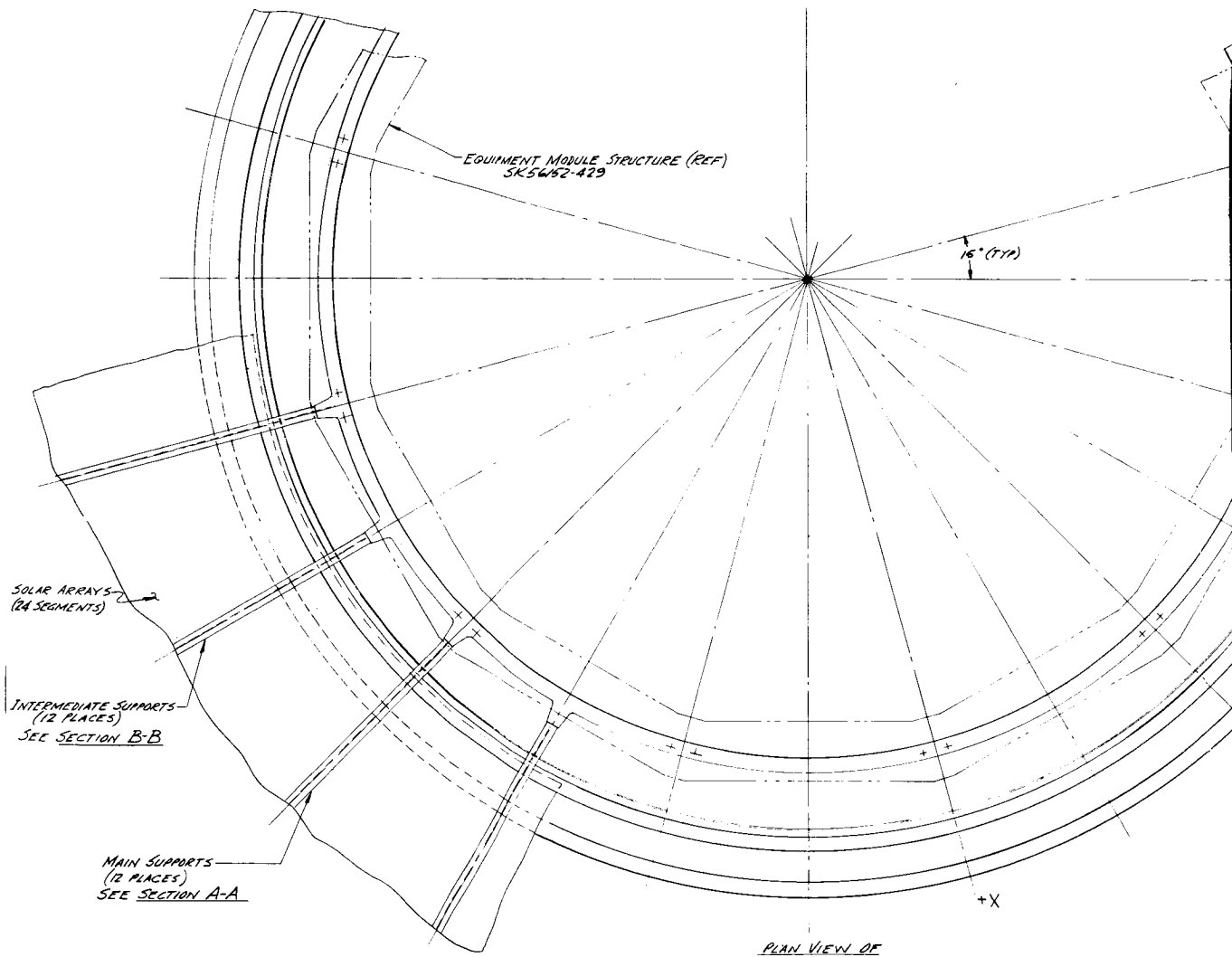
The stiffened skin accommodates the high shear flows of condition 2c (reference Table IV of Appendix) and also functions to distribute the axial load component in the 12 longerons to a more uniform distribution at Station 3.5.

The lower ring at Station 8 serves to react the kick loads from the solar panel support ribs and those from the longeron eccentricity. In addition, tangential loads from the solar panel structure will be introduced uniformly and distributed into the basic shell by the ring.

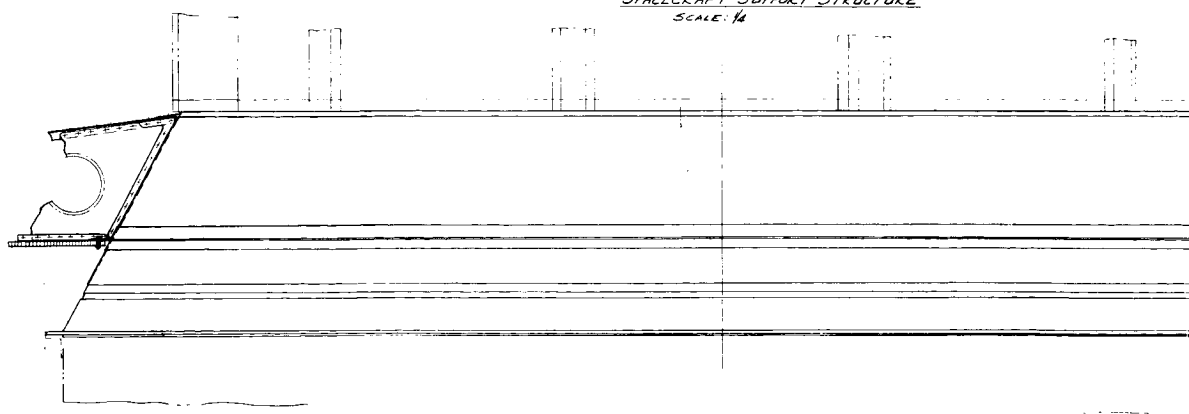
The twelve primary longerons are those receiving the loads from the equipment module at Station 20. Longerons area tapering exists in conjunction with variable thickness skin to force the load to a more uniform distribution at Station 3.5 (separation plane). The intermediate stiffeners serve to introduce the loads from the solar panel support ribs and act as panel breakers for shear buckling requirements.

The solar array structure consists basically of the 22 panels and 23 support ribs, although some of the ribs and panels must be specially designed as support structure for other components. They are designed to support their own weight and that of the components under dynamic boost loads and provide a natural frequency which will prevent coupling with the autopilot system.

The structure of the 22 solar panels is an aluminum alloy honeycomb supporting the silicon solar cells. The solar panel support rib structure is a tapered cantilever rib structure which varies to accommodate the special load requirements in areas such as the antenna supports. Refer to VB235FD110 for more detailed discussion.



PLAN VIEW OF
 SPACECRAFT SUPPORT STRUCTURE
 SCALE: 1/4

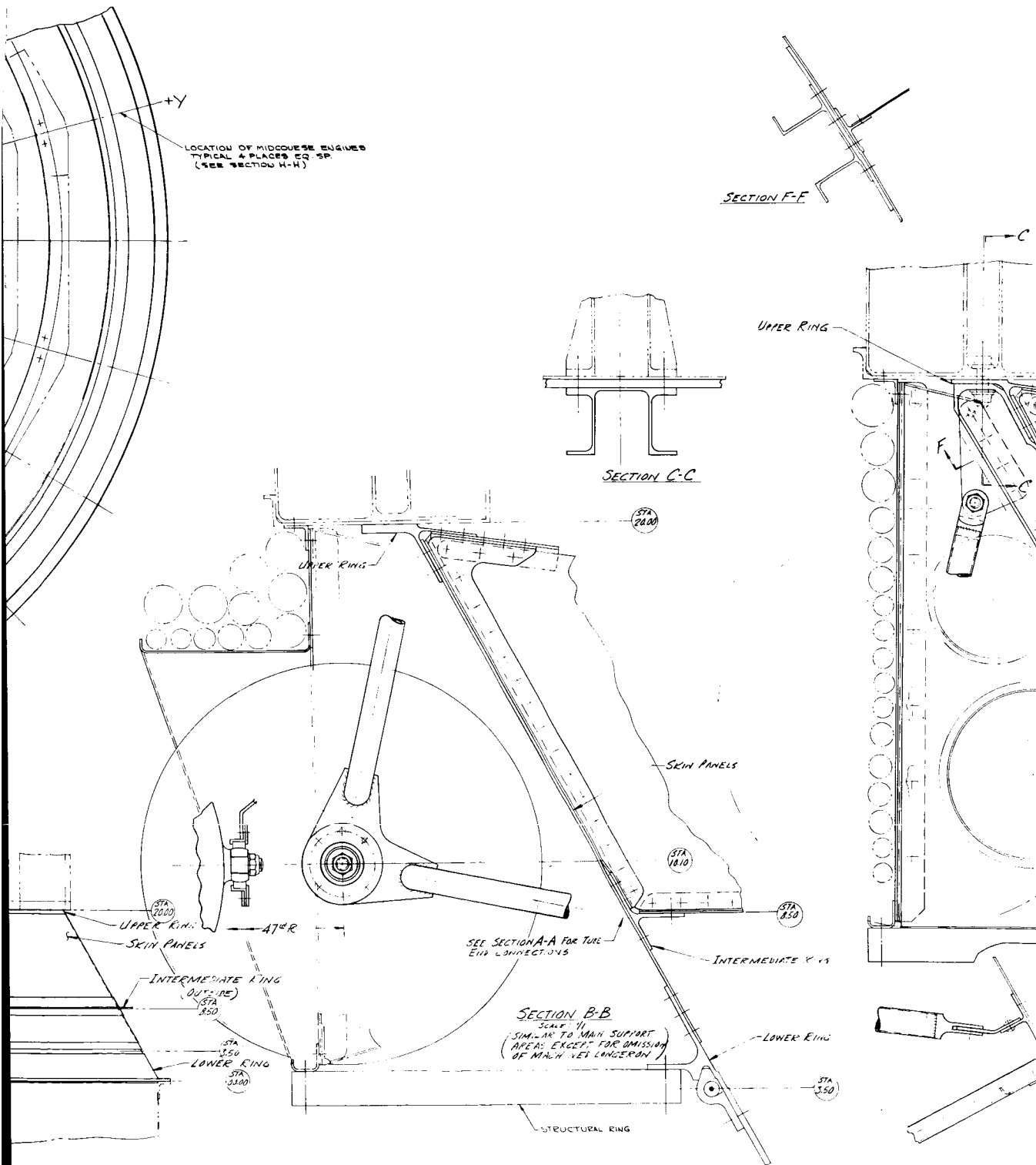


260

LOCATION OF MIDCOURSE ENGINES
TYPICAL PLACES EQ SP.
(SEE SECTION H-H)

SECTION F-F

SECTION C-C



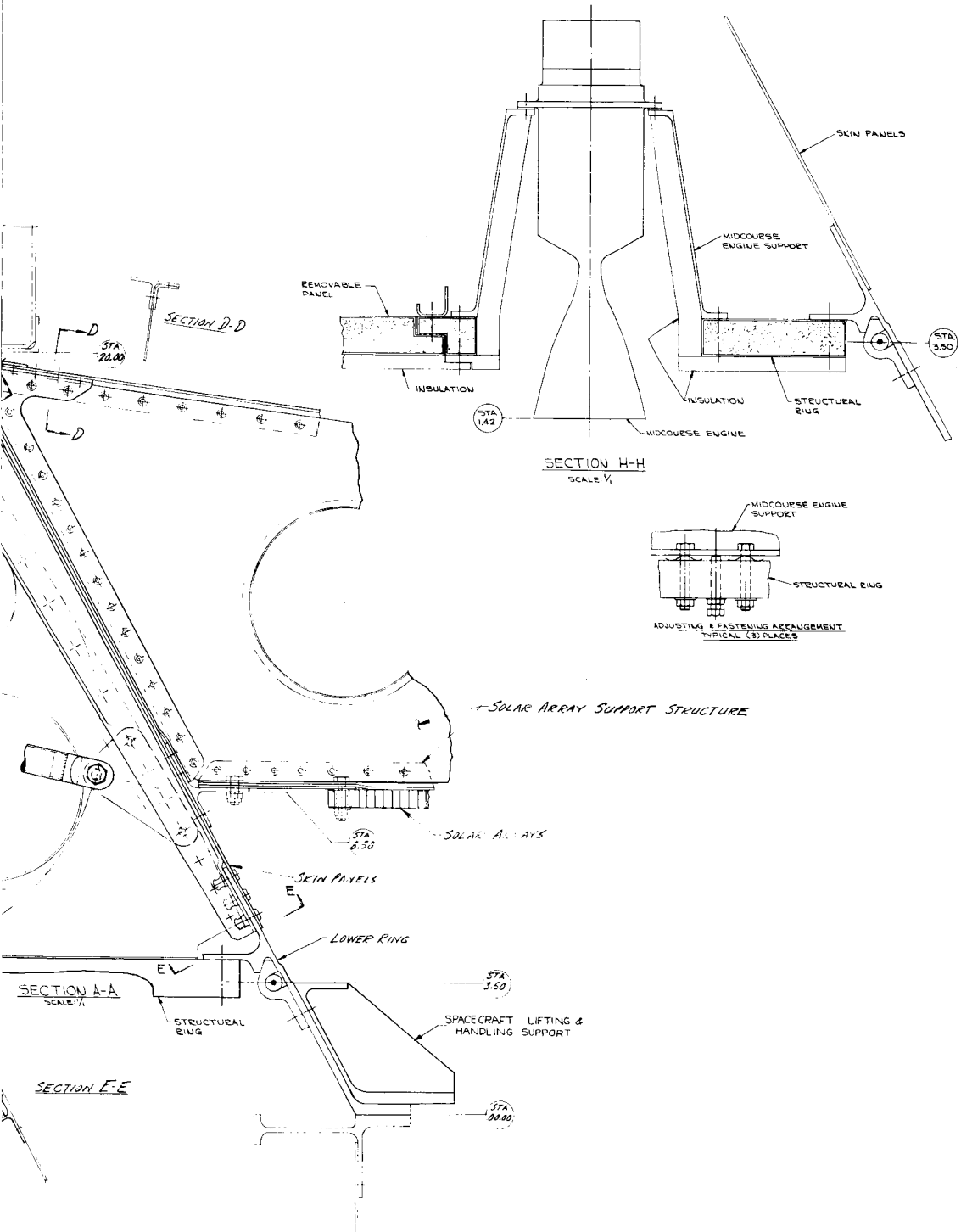


Figure 3-7. Spacecraft Support Structure

The high-gain antenna support rib serves to introduce the antenna inertial loads into the basic structure at stiffener location 3S. Those load components normal to the rib in the X-Y plane will be transferred into the solar panels and the support rib reacts the kick loads produced there in shear. The support ribs are backed up by two tube ties running from the outboard end of the rib to the E/M upper ring.

The medium-gain antenna support structure is a two I-beam cantilever structure bridging across two support ribs as shown in Figure 3-4, and the loads are transferred to the support ribs at locations 3S and 3L.

The primary low-gain antenna is cantilevered from the solar panel support rib at radial element 9S through a cut-out in the solar panel structure.

The secondary low-gain antenna is supported from the side of the solar vane honeycomb panel in Quadrant III, providing necessary antenna alignment.

The VHF relay antenna support structure consists of two fittings attached to the support ribs at 1S and 1L.

The launch antenna is a fixed mount from support rib 3S. There is a tie-down fitting and snubber fitting provided on the support rib at 4L, completing the high-gain antenna tie down.

The magnetometer support is a tubular boom which extends in the X-Y plane of the vehicle and positions the magnetometer 5 feet away from the basic body structure. It mounts into an aluminum alloy tubular support and is deployed with a spring damper system released by a pin-puller. The boom design maintains alignment of one axis of the magnetometer to within 1 degree of the Z axis, and prevents excessive deflection during engine operation.

The attitude control hardware support system includes the control nozzles, plumbing, solenoid valves, initiation squibs, etc. necessary for operation of the attitude control nozzles. The 12 nozzles and associated 24 valves are all permanently affixed to the four support ribs which lie on the X and Y axis. The tanks for the cold gas system are two 12.25-inch diameter titanium tanks containing Freon at 4500 psi. They are trunnion-mounted at two diametrically opposed points which attach to a truss system mounted from the longerons and rings, utilizing intermediate stiffeners and intercostals as required. The two tanks are located diametrically opposite on the S/C to maintain better mass property control.

The meteoroid bumper structure is a multi-functioning structure in that it takes advantage of the attaching thermal super-insulation blanket as an outer bumper. The bumper structure itself is a polystyrene foam-filled aluminum sandwich structure which extends across the lower end of the S/C to protect the propellant tanks from puncture during transit. Thus it is a three layer structure as shown in the following Figure 3-8. An additional function of this bumper is to provide a distortion-free, vibration-free mounting surface for the cruise sun-sensor and the mid-course engines.

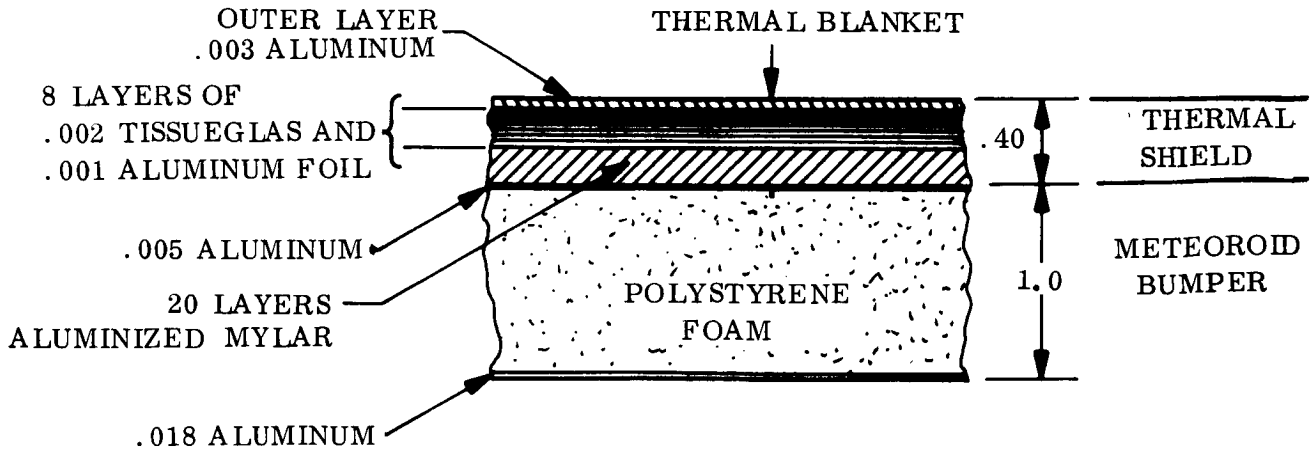


Figure 3-8. Meteoroid Bumper

3.1.4 SPACECRAFT ADAPTER STRUCTURE

This structure serves to transmit all primary loads thru the overall flight spacecraft to the launch vehicle adapter at the field joint at Sta. 0.00. Loads are distributed to this adapter at the spacecraft/launch vehicle separation plane at Station 3.5 in as uniform a manner as possible through the continuation of the support structure skin. This structure is basically a monocoque conical frustrum designed by the high bending load of condition 3b (reference Table IV of Appendix). The aforementioned joint structure contains the expansion of the encapsulated MDF so that the impulse energy severs the skin rather than being dissipated elsewhere. This structure is then an integral and critical part of the separation reliability.

3.2 SPACECRAFT SCIENCE PAYLOAD STRUCTURE

3.2.1 PLANET SCAN PLATFORM

This package is provided as a complete unit, and therefore the primary concern is the interface and provision of rotation mechanism. The package structure itself is designed to be tied down for boost loads and is sufficiently stiff to provide alignment. The rotating interface is similar to that shown for the high-gain antenna.

3.2.2 BODY MOUNTED SCIENTIFIC INSTRUMENTS

Mounting surfaces for any scientific instruments necessary for the Voyager mission are discussed in Section 3.1.2 and Section 3.1.3.

3.3 SPACECRAFT RETROPROPULSION STRUCTURE

The propulsion system is discussed in VB238FD101 and this discussion will be of a preliminary nature. Refer to Figure 3-4 for a sketch of the propulsion unit integration into the spacecraft.

There are 12 spherical tanks which are trunnion-mounted, comprising 4 tanks containing liquid fuel and oxydizer, 4 tanks containing hydrazine for midcourse and thrust vector control, and 4 gas pressurant tanks. These tanks are symmetrically arranged about the roll axis with the engine in the center and its thrust axis coincident with the roll axis. The tanks and engine are joined by a truss and shear beam structure oriented radially at the mid-point of each quadrant. Each of these four members then spreads out to a Y structure (plan view) which picks up the equipment module at eight longerons (longerons 1, 2, 4, 5, 7, 8, 10, 11). At the vicinity of the Y beam the pressurant and monoprellant tanks are located upper and lower and are supported by truss members picking up the trunnion points.

Machined fittings attach to the eight longerons to transfer the primary propulsion module loads to the basic structure. The multi-cell torque box longeron serves to distribute shears and local moments to the rings which serve to react and redistribute these into the basic shell, while the longitudinal loads are transmitted down by the longerons and partially distributed laterally to adjacent longerons less highly loaded.

Mid-Course Engines and Support are located at a radius of 50 inches on the principle spacecraft (X & Y) axes and are mounted on the meteoroid/thermal shield at Station 3.5. The engine mount fitting is a tension cone, (see Figure 3-7) with highly reflective surface insulation on the interior surface. The joint between the mount and the honeycomb is provided with adjustments for aligning the engine thrust axis.

3.4 SEPARATION SYSTEMS (REFERENCE FIGURE 3-4)

The spacecraft Launch Vehicle separation system is an encapsulated mild detonating fuse (MDF) employed at Station 3.5 and provided with two initiators. The fuse is confined between the skin and a segmented ring structure. Upon initiation, the elastomer tube jacket encapsulating the charge transmits the parting and separating force to the skin structure and ruptures the skin where it has been sculptured to control and provide a preferred separation plane. The segmented ring structure which also contains the initiators, remains with the booster.

The spacecraft/flight capsule biological barrier (lower section) separation comprises captive separation units on the six flight capsule attachment bolts, at the interface at Station 59.0. The six units are connected by a manifolded line to a pressurized gas bottle, and actuated by two squibs connected in parallel which release gas pressure to the units (See Figure 3-9). Belleville washers are provided at the separation joint, imparting the required separation velocity.

4.0 INTERFACE DEFINITION

4.1 OPTICAL

The optical interface with the structure is defined as the intersection of the structure with the fields-of-view of the sensors and antennas. (Reference VB220SR102)

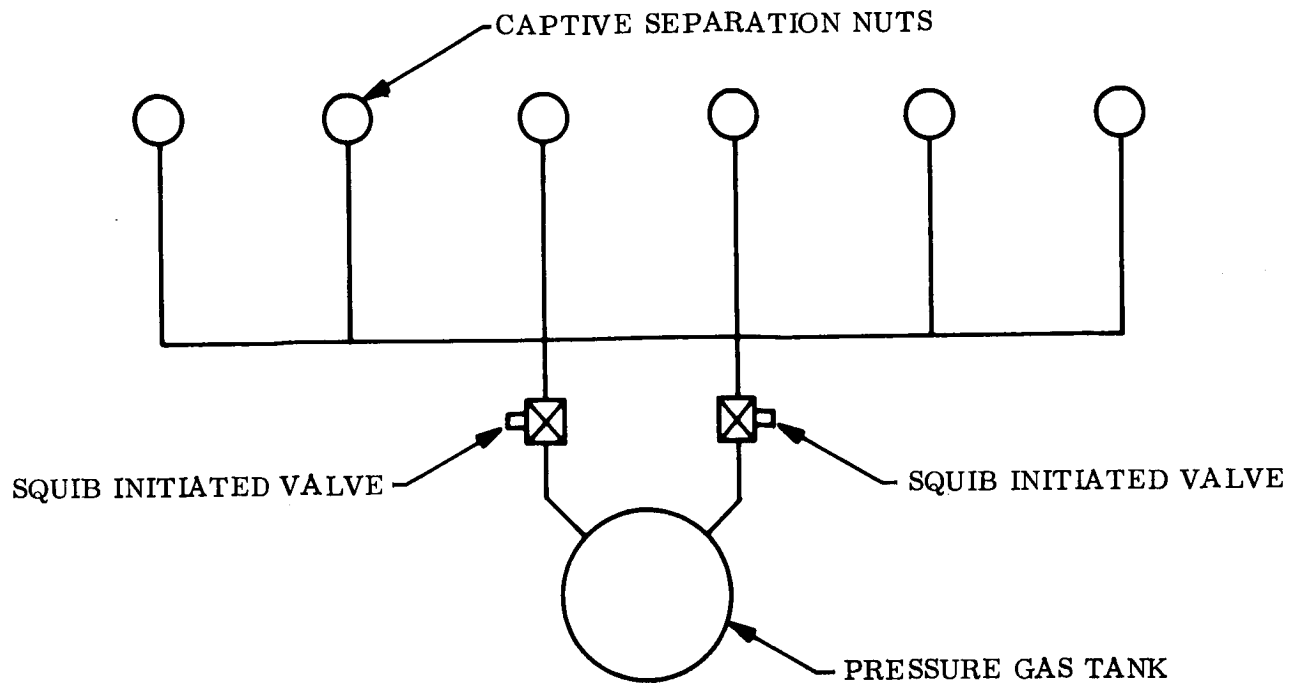


Figure 3-9. Biological Barrier Manifold Separation System Schematic

4.2 MECHANICAL

The mechanical interfaces are located so as to satisfy equipment location requirements and to facilitate manufacture, assembly, and minimum weight design. Some of the mechanical interfaces are defined by VB220SR102, VB220FD105, and VB220FD106. The specific interface location of the structure with a component is described in Section 6.

The structural subsystem includes all of the vehicle structure, except that which is internal to a subsystem component. Every component has a definite interface with the structure, which in most cases will be a mounting surface. The structural subsystem will thus be responsible for introduction of loads to the individual components, and in most cases the component structure will accommodate the imposed load environment. In some cases, the desire to make certain structures be multi-functioning (e.g. the equipment modules, the solar array support, etc.) will make the interface less clear and the structural subsystem then includes the internal structure of these components as they affect overall structural load paths.

4.3 ELECTRICAL

The structural-electrical interface is limited and, in fact, is confined to the measuring devices to determine vibration and acceleration data. These consist of 18 vibration pick-ups and associated wiring to the Centaur T/M system.

4.4 THERMAL CONTROL INTERFACE

This will consist of an attachment system for insulation blankets, thermal shutter support and insulation for portions of the structural system which pierce the insulation blanket.

4.4.1 SHUTTER SUPPORT

This bracket introduces the loads from the thermal shutter system directly into the longeron through nine of the vertical attachments along the edges of the E/M shear panel.

4.4.2 THERMAL INSULATION SUPPORT

The insulation is supported by the basic shell wherever feasible, in which case the support is the attachments which hold the superinsulation blanket. In the instances where the basic shell cannot support the blanket with the necessary spacing of attachment, a separately provided framework supports the blanket during boost load environment and transmits the load to the basic structures. The superinsulation blanket completely encloses the exterior surface of the S/C support cone and will have the 24 support ribs protruding through it. The mating surfaces of the exposed structure and the basic shell are separated by insulation strips of Textolite or Fiberglass and, if necessary, the attachments will also be insulated with non-conductive bushings and washers. This applies to attachment of the support ribs, the Station 20 ring, and the S/C adapter at Station 3.5.

Two solar panels (radial element 2S to 3S in Quadrant I) are removed to accommodate the installation for the intermediate-gain antenna. The surface area of these panels is covered by a fiberglass panel to shade the E/M radiation surface area and flight capsule from sun impingement.

4.5 RADIOACTIVE OR NUCLEAR RADIATION

Applicability to the structural subsystem is limited to the effects on mechanical properties of materials, metals and non-metals. Radiation levels encountered are not sufficient to effect the metals used in S/C construction, but the effect on insulating materials, lubricants, etc., has been investigated in a preliminary nature.

5.0 PERFORMANCE PARAMETERS

The usual performance measuring parameters of a structural subsystem are the weight in relation to the loading index as compared to cost, ease of manufacture, structural integrity (reliability), state-of-the-art, etc. Design constraints such as compatibility of 1971 E/M with the 1969 test shot shroud, number of load introduction points at interfaces, etc. serve to influence the efficiency of a specific structural design and make comparison of one structure to another difficult. An absolute measure of performance is the ratio of operating stress level to material allowable stress which is easily obtained for tensile loadings but much more complex for components critical for stability modes of failure. Another measure of performance is the natural frequency of the final structural design as compared to other designs.

A discussion of the constraints on structural design performance and general philosophy concerning overall structural optimization is presented in Volume B., (VB235AA102), and absolute measurements of performance are evidenced in the supporting structural analysis in the Appendix to Volume A.

6.0 PHYSICAL CHARACTERISTICS

The general structural arrangement is shown as Figure 3-4 (ref). Detailed drawings of the Capsule Support Cone structure, the Equipment Module structure and the S/C Support Cone & Adapter structure, have been shown in Figures 3-5, 3-6, and 3-7, respectively.

A summary of pertinent structural component details such as material, geometry, and method of manufacture along with references to the pertinent text, drawing, or calculations shown elsewhere in the report is presented in Table 6-1.

7.0 SAFETY CONSIDERATIONS

Safety considerations related to the structure include design factors of safety, toxicity of materials, methods of assembly, location of work platforms, eliminating sharp edges and corners, and the like. Design factors of safety have been accounted for in the analysis, and material selection presents no problem to date. The other factors are taken care of with proper attention during detail design.

TABLE 6-1

Functional Description Number and Name	Location		Quad. and/or Rad Element	Figure or sketch Ref. No.	Material	Physical Geometry	Supporting Analysis Reference	Probable Method of Manufacture
	Rad. Dis. From Z Axis	Station						
3.1 Spacecraft Bus Structure		0-59	N/A	3-4	Mostly Alum.	See Separate components		Assembled in master jig
3.1.1 Capsule Support Structure		49-59	N/A	3-5	High Strength Aluminum	Conical Semi-monocoque ($37\frac{1}{2}^{\circ}$ half-angle)		
Basic Structure		49-59				Conical Semi-monocoque ($37\frac{1}{2}^{\circ}$ half-angle)	SA	
Interface Ring	40	59	N/A			Scalloped I-Section approx. $4\frac{1}{2} \times 2 \times 10$	SA	Machined from roll-ring forging
Longerons	N/A	46-59	Eq. Space			.081 Hat Section $1 \times 1.5 \times 1.5 \times 1$	SA	Machined from bar
Skin Panels	N/A	46-59	N/A			.072 (beaded at minimum spacing)	SA	Die formed
Aft Closing Ring	50	46	N/A			.080 Angle 1.5×1.5	SA	Machined
Equipment Support								
Canopus Tracker Mount	48	47	IV; 11L		2024-T3	Flanged open box with single mounting surface		Machined bar
Approach guidance sensors mount	48	47	III; 7L		2219-T87	Flanged open box with two mounting surfaces		Machined weldment
High-gain antenna tie-down	45	49	II; 3L, 5L		Organic	Snubbing blocks preloaded in compression		
Thermal Control Interface								
Insulation Attachment								
Capsule Separation S/C V Motor Support	47	50	1L		2024-T3	4 in. dia. sphere with nozzle		Mounting surface machined from bar
Planet Scar Platform Support	40-64	46-59	III; 9S	3-5	2024-T3	4 in. wide box beam, .040 sheet and $1 \times 1 \times .08$ angle		Extruded caps and sheet riveted
3.1.2 Equipment Module Structure		20-46		3-6				
Basic Structure					7075-T6	12-sided ring, 6" radial depth, 26" long	SA	Assembled in master jig
Rings	47	20-46				$6 \times 1.5 \times .080$ Channel Section	SA	Machined from roll-ring forging
Longerons	49	20-46	Eq. Space			Multicell box section - .060 Wall Thickness	SA	Welded extrusions
Front cover plate	50	20-46	N/A			.058 in. thick	SA	Sheet stock
Propulsion Module Support		34.9			7075-T6	(One bolt bathtub $3" \times 1.5" \times 1.5" \times .15$)	NP	Machined from bar stock
Electronic Package Structure								
Internal Structure	44-50	24-42	N/A		HM21A-T8	Open-Face box $1.09" \text{ deep} \times 6 \times 18 \times .064$	NP	Machined from plate
Inner Panel	44	20-46	N/A		AZ31B	.060" thick	NP	Sheet stock
Electrical Connector Support	46	4.5-20	N/A		AZ31B	.060" thick	NP	Brake-formed sheet
Antenna Actuator Tie-Down	52	46	I, 2L		2024-T3	.10 thick semi-bathtub fitting	NP	Machined from bar
Thermal Control Interface								
Shutter Support	100	21-45	N/A		Fiberglass	.080" $\times 2 \times 1$ angle with gussets		Laminated lay-up
Insulation Support		Entire Surface			N/A	N/A	N/A	-----
Planet Scanner Support	50	20-46	III; 8L-9L	3-6	2024-T3	.080 lug fittings to accommodate shear pins	NP	Machined bar
Electrical Harness Support	46.2	4.2-20	N/A	3-7	AZ31B-H24	.040 skin stiffened by flanged lightening holes	NP	Rolled sheet riveted to end rings
3.1.3 S/C Support Structure								
Basic Structure	N/A	5.7-20	N/A		7075-T6	Semi-Monocoque Cone ($26\frac{1}{2}^{\circ}$ half angle)	SA	
Forward Ring	49	20	N/A			$2 \times 1.5 \times .080$ angle	SA	Machined from roll-ring forging
Conical Shell	--	--	N/A			.064 (beaded at minimum spacing)	SA	Die-formed
Aft Ring	56	--	N/A			$2 \times 1.5 \times .080$ "T" section	NP	Machined from roll-ring forging
Longerons	--	--	Eq. Space			Tapered Channel (Approx. $2 \times 2 \times 2 \times .09$ max)		Machined from bar
Solar Array Structure		8-20	N/A		Aluminum	Disk (10" inner dia. - 18" outer dia) $12"$	SA	-----
Solar Panel Structure	50-117	8.5	N/A		2024-T3 core	.50 in thick honeycomb - fiberglass faces		Bonded sandwich
Solar Panel Support Ribs	50-117	8-20	15° spacing		2024-T3	"T" caps $.70 \times 1.5 \times .06$; .016 in. shear web	SA	Extruded caps riveted to sheet web
High-gain Antenna Support	105	35	I, 3S			6" deep flanged channel	NP	Built-up formed sheet metal
a. Pivot rod support		Same as above.						
b. Boost load support	72	10	II; 4L			Pre-tension mechanism attacks to antenna feed		Machining
Intermed. Gain Antenna Support	83	10	I; 2L-3S			2.5" deep channel beams - mounting ring		Beams are formed sheet metal, and mounting flange is machined
Low-Gain Antenna Support #1	116	8	III; 9S-9L			7" long tube with swaged end fittings		-----
Low-Gain Antenna Support #2	167	8	IV-1			10" long tube with swaged end fittings		-----
V. H. F. Antenna Support	114	10	I; 12L-15			Lug-Type Fitting		Machined from bar
Launch Antenna Support	112	8	I; 3S			Sheet Metal Bracket (.050 in.)		Formed/riveted
Magnetometer Support	115-178	10	II; 5L			2" dia. Tubing 63" long		Tubing with swaged end fittings
Attitude Control Hardware	119	10	X & Y Axes			.060 bracketry		Formed sheet metal
Acquisition Sensor Support (4)	100	10	X & Y Axes	3-7	2024-T3	.060 Box	NP	Built-up formed sheet metal
Solar Vane Support	117	10	III; 9S	3-4	2024-T3	Double hinge bracket	SA	
Guidance and Control Equipment								
Cold Gas System								
a. Tanks	47		I & III; 2S, 8S	3-7	6AL-4VTi-Ann.	12.25 in. dia. spherical trunnion mounted 2 ples	NP	2 machined forging domes (welded)
b. Supports						.060 box with flanged lightening holes	NP	Formed Sheetmetal
Cruise Sun Sensor Mount	53	5	on X axis		2219-T87	Mounting Plate Box with Ribs and Gussets	NP	Machined Weldment
Mid-Course Prop. System Interface	50	10.0	X & Y axes		2024-T3	Conical Structure Attaching to Meteoroid Bumper	NP	Spun Aluminum
Thermal Control Interface								
Thermal Insulation Support								
Heater System	N/A	N/A	N/A		2024-T3	Angle Support Bracketry	--	-----
Meteoroid Bumper	5.8	3.7	N/A		2024-T3 faces	1.0" thick honeycomb with foam core	SA	Bonded sandwich
Spacecraft Adapter Structure								
Forward Joint	55	5.7			7075-T6	2 rows of $3/16"$ hi-shear rivets in .080 sheet		
Basic shell	N/A	0 to 5.7				.072 skin		Machined from roll-ring forging
Aft Field Joint	60	0				.18 in. flange; $(48 \frac{5}{16}"$ bolts)		Machined from roll-ring forging
Separation Joint Structure	58	3.5		3-7	7075-T6	.20 in. thickness		Machined from roll-ring forging
3.2 S/C Science Payload Structure								
See text								
3.3 S/C Propulsion Module Structure				3-4				
Tanks and Support Fittings								
Main Propellant Tanks	24.0	36	X & Y		Titanium	30.25 in. dia. spheres - trunnion mtd.		2 machined forging domes welded
					6AL-4VTi -	two (2) pieces		
					165,000 yield			
Mid-course System Tanks	29.5	18.7	All quads		165,000 yield	18.38 in. dia. spheres - trunnion mtd 2 places		2 machined forging domes welded
Pressurization Tanks	32.0	50	All quads		6AL-4V Ti-Annealed	17.0 in. dia. spheres - trunnion mtd 2 places		2 machined forging domes welded
Main Support Structure					Beryllium	18.7		
Retro Engine and Support		53 (to head end)		3-4	Beryllium	Truss-beams	SA	Welded or brazed
Mid-Course Engines and Support	50"	10.0	X & Y axes			15 in. dia. ring	NP	Machined from forging

NOTES:

1. N/A - Not Applicable
2. NP - Not Provided
3. SA - See Appendix

CII-VB235FD102

SPACECRAFT STRUCTURE

APPENDIX

Index

- I Supporting Structural Analysis
- II Meteoroid Penetration Analysis
- III Structural Dynamics

APPENDIX

I. SUPPORTING STRUCTURAL ANALYSIS

1.0 SCOPE

The analytical substantiation of the structural design of the preferred Voyager 1971 Spacecraft is presented below. The analysis is based on state of the art preliminary design analytical methods and construction practices, and is performed in sufficient detail to size main structural items. Conservative approaches have been taken to allow for a growth potential within the specified weight limitations, and to further emphasize the structural integrity of the design. The structure presented here will serve as a base for the computerized optimization studies which will subsequently be performed.

In order to introduce the basic design philosophy and the analytical approaches, a description of the structure and primary load paths is given.

The meteoroid protection design and analysis and the dynamic analysis are presented as separate entities at the conclusion of the stress analysis.

2.0 BASIC DESIGN PHILOSOPHY

Considerable attention has been devoted toward insuring that the flight capsule loads are carried by the structure and diffused to the base of the spacecraft support structure with the maximum possible efficiency, consistent with a minimum weight design. A major portion of the analysis is to quantitatively evaluate the "shear lag" or load diffusion effect of introducing a concentrated axial load at one or more of the flight capsule support points and determining the resulting load distribution at the spacecraft separation plane. An overall objective is to obtain, within the limits of practicality, a resulting distribution that is uniform for axially applied loads and conforms to elementary theory for bending loads.

The basic philosophy in the load diffusion design was to fully utilize the shear structure required for other loading or thermal conditions. The axial or bending structural configuration was then suitably adjusted to maintain optimum stress levels in the longerons and stringers. In this manner an acceptable load distribution was obtained at the base of the spacecraft support structure with very little weight penalty involved.

The shear structure is designed from considerations of the torsional accelerations (See Table 4-1, Limit Design Loads, design load condition 2c as applied to the 75/77 mission configuration) in conjunction with a "minimum gage" thermal requirement in the equipment module section. The lateral vibration design load condition 3b of the 75/77 mission configuration) is critical for the axial and bending structure and therefore is the only loading condition to be considered in the load diffusion analysis. Only the most severely loaded segment of the structure from the flight capsule interface to the base of the spacecraft support structure has been considered.

3.0 STRUCTURAL DESCRIPTION (REF. FIGURE 3-2)

In order to provide a torsionally shear resistant structure at limit loads and also minimize the structural weight, 7075-T6 aluminum alloy panels, with minimum bead spacing, of gages 0.072 inch and 0.064 inch respectively are required for the flight capsule support structure and for the spacecraft support structure. Thermal conductivity requirements in the equipment module section necessitated the use of 0.055 inch minimum thickness of 7075-T6 aluminum alloy for the outer shear structure. This particular gage and alloy was selected over others suitable for the thermal requirement, because of its superior bearing allowables which minimize the number of attachments required for the removable panels. Functional multiplicity is obtained by utilizing the module subassemblies as panel stiffeners and thereby insuring a shear-resistant structure at ultimate loads.

All structure with major axial load carrying requirements is constructed of closed sections of 7075-T6 aluminum alloy to minimize the effect of flange crippling and thereby permit higher operating stress levels. A beneficial side effect of such construction is the additional edge restraint provided to panels critical from stability considerations. The lesser loaded members in the flight capsule support structure and the spacecraft support structure are constructed of open sections of 7075-T6 aluminum alloy to enhance fabrication.

While it is evident that the optimum structural configuration features direct load paths with full section tension and compression capability, certain deviations from this philosophy were necessitated by the packaging requirements of the equipment module and the overall assembly and access requirements of the three basic sections of the spacecraft.

The change in direction of the axial load originating at the flight capsule interface as it travels thru the spacecraft necessitates the inclusion of kick frames at stations 59, 46, 20 and 0. In keeping with the conservative approach, all frame design is based on elementary theory, i. e. rigid rings loaded via M_c/I and VQ/I distributions. In actuality, ring loading is dependent on the shear lag effects of the structure and the relative stiffnesses of the rings and skins. Inclusion of these refinements will allow further optimization of the sections chosen.

Preliminary analysis has shown that condition 3b of the 1975/1977 mission configuration induces the highest stress resultants in the rings, however, ring design must be consistent with the shear transfer requirements of condition 2c. A frame of 7075-T6 aluminum alloy at station 59 is subjected to a large in-plane kick load at each of the six flight capsule support longerons in addition to in-plane loads at the shear pin locations. The design of this ring will allow yield compression stresses in the inner flange with no crippling or lateral instability of the section. The frame at station "O" is also designed to the same philosophy and benefits from distribution of loads at the base of the spacecraft.

The upper and lower equipment module support frames at stations 46 and 20 are 7075-T6 machined channels. The geometry of the channel has been chosen to be compatible with the electronic packages which provide the restraint against lateral instability. An additional ring is required at the aft support point of the solar panels to absorb the panel kick loads and to serve as shear mounting structure.

4.0 AXIAL LOAD PATHS

In order to fully clarify the assumptions made later in the detailed analysis, a description of the axial load paths is presented.

One of the critical design parameters encountered in the determination of the structural load path is the concept of modularity in the equipment section. This concept is enhanced by minimizing the number of equipment modules within handling and servicing limits. The choice of 12 equipment modules, mounted in twelve bays, allows for axial load to be transferred and diffused only through 12 "hard" points. This is true even on the compression side of the structure due to the required geometric mismatch of the shear panels of the three basic sections. This limits the capability of the shear structure to act as effective axial structure except in the spacecraft support structure where the interface configuration at station O tends to develop the tension and compression capability of the shear panels. The net result of this is that the axial loads applied to the six hard points at the flight capsule interface diffuse slowly through the flight capsule support structure. This rate of diffusion could have been increased by adding additional area to the intermediate stringers, but only at the cost of a considerable weight penalty. The same condition exists in the equipment module section with loads tending to equalize between adjacent longerons. The shear structure between station O and station 20 is effectively used as axial structure resulting in a favorable distribution of loads even though the length of the section is relatively short.

5.0 LIMIT DESIGN LOADS

Limit design loads used to design the structure presented in the preferred 1971 spacecraft configuration are given in this section. Axial tensile and compressive forces, transverse and maximum running skin shears and overturning and torsional moments have been evaluated at discrete vehicle stations. A lumped parameter approach has been taken in that loads from steady state accelerations have been derived with masses for two spacecraft configurations introduced at their respective C.G.'s as shown in Figures 1 and 2 of Table I-1. The most adverse C.G. location has been assumed for the capsule. The dynamic model is more detailed and includes the flexibility of the propulsion unit. Details of the dynamic model and analysis are given in the dynamic analysis section.

The basic environmental conditions are given in the structural design criteria specification VB235FD103. The four design load conditions given in the specification are expanded to nine conditions when the quasi-static and dynamic loads are combined in the required manner. These nine conditions are listed in Table 1-1. All load factors and forces given are limit and are taken in combination.

Given in Table 2-1 are dynamic loads due to a unit sinusoidal vibratory input. These loads are the results of the second iteration analysis of dynamic response as influenced by the stiffness of the support structure. Structural stiffnesses used in this analysis are from structure designed using dynamic responses analytically obtained from a first cut structure.

Good correlation of dynamic loads from the first two analysis was evidenced and the design loads presented here are quite indicative of the loads that will be obtained from more

Table 1-1. Limit Design Load Factors - Inputs at Base

Design Load Condition	Quasi-Static-g's		Vibratory (0 to Peak g's)		
	Longitudinal	Lateral	Longitudinal	Lateral	Torsional
1a	6	1	0.8	0.5	(Radians/Sec ²)
1b	6	1			
2a	2	1	1.2	0.75	60
2b	2	1			
2c	2	1			
3a	1	0	1.6	1.0	60
3b	1	0			
3c	1	0			
4			1.6		

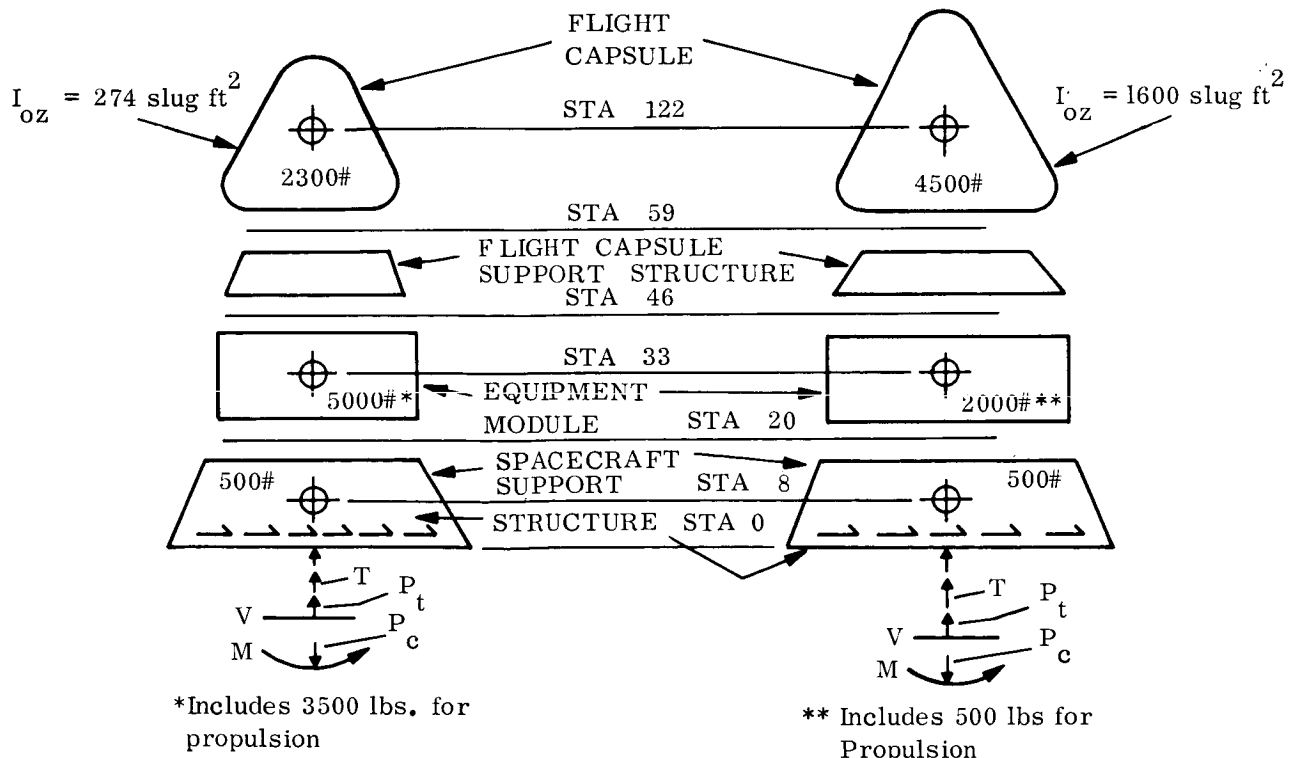


Figure 1. 1971-1973 Mission Configuration

Figure 2. 1975-1977 Mission Configuration

refined analysis. Never the less, a subsequent dynamic analysis has been performed utilizing the structural stiffness of the preferred 1971 design, and is the last iteration performed for this study. These latter dynamic loads given in the dynamic analysis section, which will serve as a basis for initial Phase IB design have not as yet been incorporated into the design.

Loads at two frequencies in each of the torsional and longitudinal modes are given for the 1971/1973 configuration, reflecting the modes governed by the propulsion mass and the lander mass respectively. The highest load at each station from either frequency is taken as the design load. The fundamental system mode is critical for lateral loading at all stations.

Tables 3-1 and 4-1 list the resulting forces at the interfaces. The tensile and compressive axial forces reflect the vibratory nature of the loads and are not taken in combination with each other, but are combined individually with the other forces.

The present design philosophy is to design a single structure compatible with all mission configurations. Therefore, critical loading conditions are obtained from either table and can be intermixed from one station to another.

Table 2-1. Summary of Dynamic Loads Due to Sinusoidal Vibration

A. Axial Vibration - 1g (0 to Peak) Base Excitation

Config- uration	Frequency CPS	Sta. 59	Sta. 46	Sta. 20	Sta. 0	At Propulsion Syst. Supports	Capsule Lander	Propulsion System
		LOADS - lb.					Acceleration - g's	
71/73	30.7	2200	22000	39000	40000	36000	0.97	10.76
	98.8	23000	23000	24000	26000	2500	10.0	.93
75/77	70.3	47000	47000	52000	53000	----	10.57	----

B. Torsional Vibration - 1.0 Radian/sec² (0 to peak) Base Excitation

		TORQUE - in. - lb.					RADIANS/SEC ²	
71/73	35.2	1550	1550	37000	72700	69700	0.47	10.4
	147.2	37500	37500	46000	54800	2600	11.4	0.38
75/77	65.8	200000	200000	206000	212000	1900	10.3	----

C. Lateral Vibration - 1 g (0 to Peak) Base Excitation

		S - SHEAR LBS; M - BENDING MOMENT in. lb.					g's		
71/73	32.2	S	26000	30000	61000	63000	----	11.4	9.0
		M	1800000	2100000	3600000	4800000			
75/77	23.8	S	40000	42000	44000	45000	----	8.95	----
		M	3200000	3800000	4900000	5800000			

Table 3-1. Limit Design Loads 1971/73 Mission Configuration

Vehicle Station	Load Description	Design Load Conditions											
		1a	1b	2a	2b	2c	3a	3b	3c	4			
59	P _c - Longitudinal Compression - lbs.	32200	13800	32200	4600	4600	39100	2300	2300	36800			
	P _T - Longitudinal Tension - lbs.	4600	0	23000	0	0	34500	0	0	36800			
	M - Bending Moment - in.lbs. x 10 ⁻³	144.9	1044.9	144.9	1494.9	144.9	0	1800	0	0			
	V - Lateral Shear - lbs.	2300	15300	2300	21800	2300	0	26000	0	0			
	T - Torsional Moment - in.lbs x 10 ⁻³	0	0	0	0	2225.0	0	0	2225.0	0			
	q - Maximum Skin Shear - lb/in	18.3	121.7	18.3	173.5	229.5	0	206.9	211.2	0			
46	P _c - lbs	32200	13800	32200	4600	4600	39100	2300	2300	36800			
	P _T - lbs	4600	0	23000	0	0	34500	0	0	36800			
	M - in-lbs x 10 ⁻³	174.8	1224.8	174.8	1749.8	174.8	0	2100	0	0			
	V - lbs	2300	17300	2300	24800	2300	0	30000	0	0			
	T - in-lbs x 10 ⁻³	0	0	0	2205.0	2225.0	0	0	2225.0	0			
	q - lb/in	14.6	110.2	14.6	154.2	156.8	0	191.0	141.6	0			
20	P _c - lbs	75000	43800	61400	14600	14600	69700	7300	7300	62400			
	P _T - lbs	-12600	0	32200	0	0	55100	0	0	62400			
	M - in-lbs x 10 ⁻³	299.6	2099.6	299.6	2999.6	299.6	0	3600	0	0			
	V - lbs	7300	37800	7300	53050	7300	0	61000	0	0			
	T - in-lbs x 10 ⁻³	0	0	0	0	2760.0	0	0	2760.0	0			
	q - lb/in	46.5	240.6	46.5	337.7	222.2	0	388.3	175.7	0			
0	P _c - lbs	78800	46800	67600	15600	15600	71800	7800	7800	64000			
	P _T - lbs	14800	0	36400	0	0	56200	0	0	64000			
	M - in-lbs x 10 ⁻³	449.6	2849.6	449.6	4049.6	449.6	0	4800	0	0			
	V - lbs	7800	39300	7800	55050	7800	0	63000	0	0			
	T - in-lbs x 10 ⁻³	0	0	0	0	4362.0	0	0	4362.0	0			
	q - lb/in	41.4	208.4	41.4	292.1	234.2	0	334.2	192.8	0			

Table 4-1. Limit Design Loads 1975/1977 Mission Configuration

Vehicle Station	Load Description	Design Load Conditions									
		1a	1b	2a	2b	2c	3a	3b	3c	4	
59	P ^c - Longitudinal Compression - lbs	64600	27000	65400	9000	9000	79700	4500	4500	75200	
	P ^T - Longitudinal Tension - lbs	10600	0	47400	0	0	70700	0	0	75200	
	M - Bending Moment - in lbs x 10 ⁻³	283.5	1883.5	283.5	2683.5	283.5	0	3200	0	0	
	V - Lateral Shear - lbs	4500	24500	4500	34500	4500	0	40000	0	0	
	T - Torsional Moment - in lbs x 10 ⁻³	0	0	0	0	12000	0	0	12000	0	
	q - Maximum Skin Shear - lb/in	35.8	195.0	35.8	274.6	1175.3	0	318.2	1139.5	0	
46	P ^c - lbs	64600	27000	65400	9000	9000	79700	4500	4500	75200	
	P ^T - lbs	10600	0	47400	0	0	70700	0	0	75200	
	M - in-lbs x 10 ⁻³	342.0	2242	342.0	3192	342.0	0	3800	0	0	
	V - lbs	4500	25500	4500	36000	4500	0	42000	0	0	
	T - in-lbs x 10 ⁻³	0	0	0	0	12000	0	0	12000	0	
	q - lb/in	28.6	162.4	28.6	229.2	792.4	0	267.4	763.8	0	
20	P - lbs	80600	39000	75400	13000	13000	89700	6500	6500	83200	
	P ^c - lbs	2600	0	49400	0	0	76700	0	0	83200	
	M - in-lbs x 10 ⁻³	485.0	2935	485.0	4160	485.0	0	4900	0	0	
	V - lbs	6500	28500	6500	39500	6500	0	44000	0	0	
	T - in-lbs x 10 ⁻³	0	0	0	0	12360	0	0	12360	0	
	q - lb/in	41.4	181.4	41.4	251.5	828.3	0	280.1	786.9	0	
0	P ^c - lbs	84400	42000	77600	14000	14000	91800	7000	7000	84800	
	P ^T - lbs	400	0	49600	0	0	77800	0	0	84800	
	M - in-lbs x 10 ⁻³	619.0	3519	619.0	4969	619.0	0	5800	0	0	
	V - lbs	7000	29500	7000	40750	7000	0	45000	0	0	
	T - in-lbs x 10 ⁻³	0	0	0	0	12720	0	0	12720	0	
	q - lb/in	37.1	156.6	37.1	216.2	599.5	0	238.8	562.4	0	

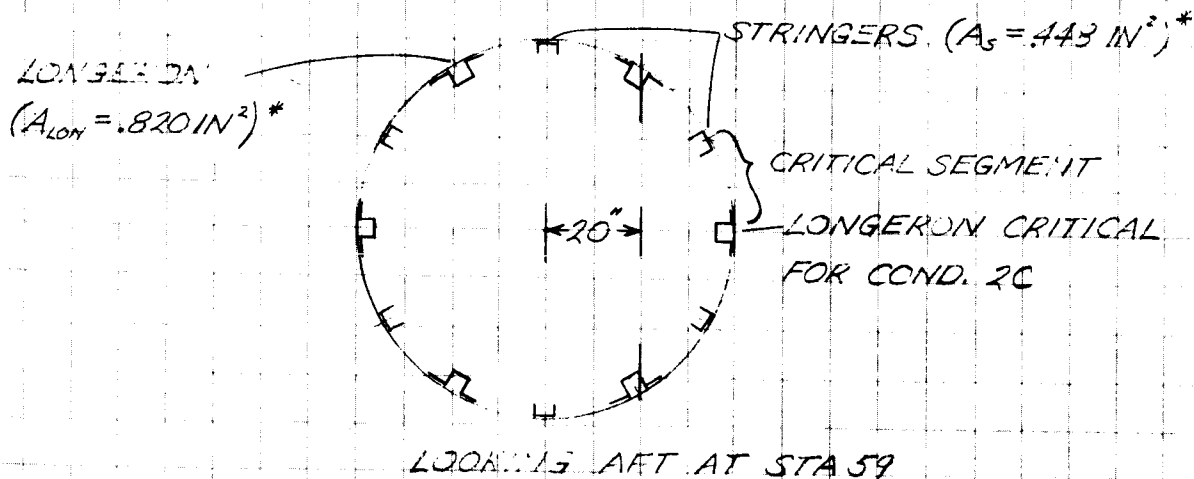
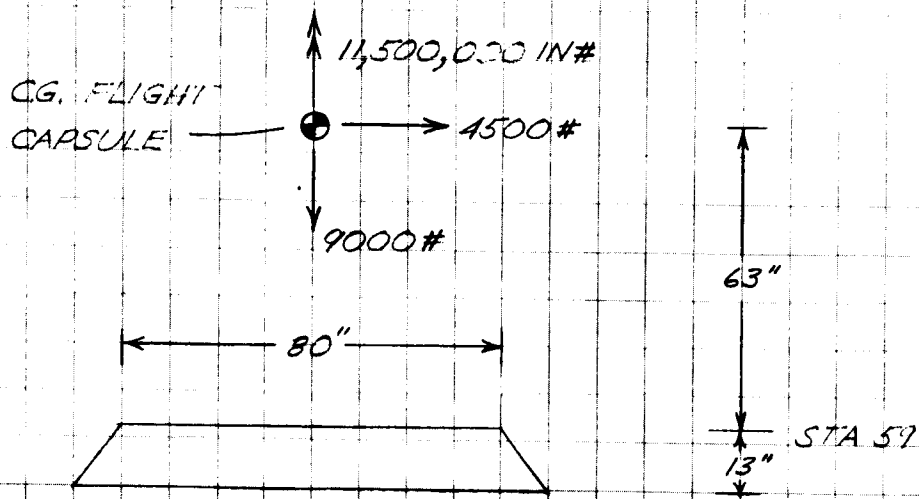
BY
CK
DATE

REV.

GENERAL ELECTRIC

PAGE
MODEL VOYAGER
REPORT

TORSION ANALYSIS - LOAD COND. 2C - '75, '71 CONFIG.
FLIGHT CAPSULE SUPPORT STRUCTURE



* INCLUDING EFFECTIVE SKIN - SEE ANALYSIS FOR LOAD CONDITION 3B WHICH DESIGNS STRINGERS & LONGERONS.

BY
CK.
DATE

GENERAL ELECTRIC

PAGE
MODEL VOYAGER
REPORT

TORSION ANALYSIS

FLIGHT CAPSULE SUPPORT STRUCTURE

AXIAL LOAD AT CRITICAL LONGERON AT STA 59

FOR 9000# AXIAL LOAD

$$P_L = \frac{9000}{6} = 1500 \#$$

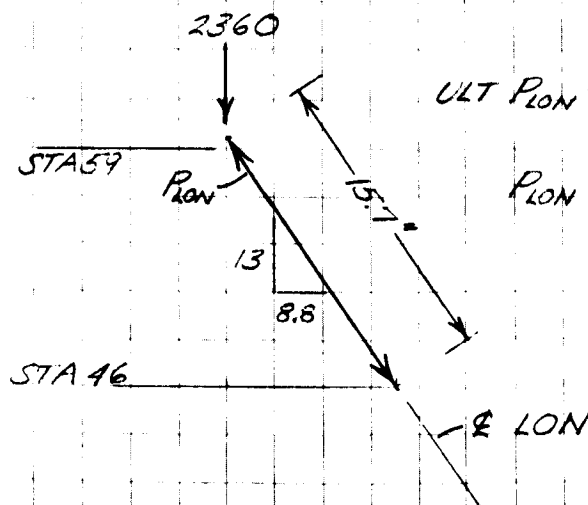
FOR BENDING MOMENT OF 4500×63 IN #, THE LOAD IN THE SIDEWALL LONGERONS IS ONE HALF THE BENDING LOAD IN THE CRITICAL LONGERON.*

EQUATING APPLIED MOMENT TO RESISTING MOMENT

$$4500 \times 63 = 2 \left[P_B \times 40 + 2 \times \frac{1}{2} P_B \times 20 \right] = 120 P_B^{**}$$

$$P_B = \frac{4500 \times 63}{120} = 2360 \#$$

NET AXIAL LOAD ON CRITICAL LONG = 3860 LIMIT



$$ULT P_{LON} = 1.25 \times 3860 \times \frac{15.7}{13}$$

$$P_{LON} = 5830 \# \text{ ULT}$$

* BY ELEMENTARY THEORY

** NO LOAD IN STRINGERS AT STA 59

BY
CK.
DATE

GENERAL ELECTRIC

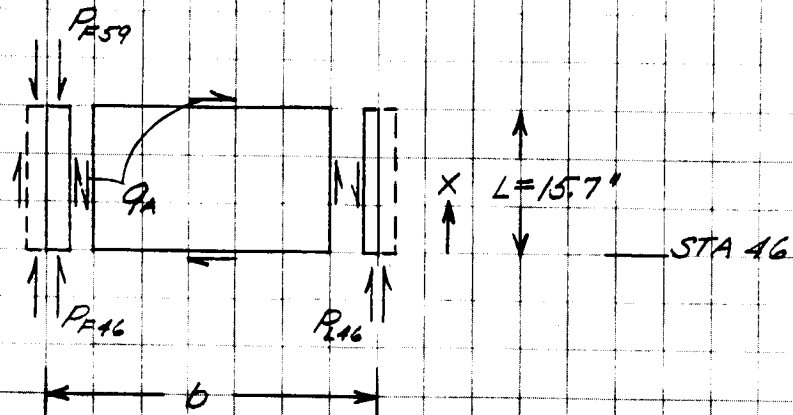
PAGE
MODEL VOYAGER
REPORT

REV.

TORSION ANALYSIS

FLIGHT CAPSULE SUPPORT STRUCTURE

SHEAR LAG ANALYSIS FOR CRITICAL SEGMENT



$$A_F = \frac{1}{2} A_{LON} = .410 \text{ IN}^2$$

$$A_L = \frac{1}{2} A_S = .224 \text{ IN}^2$$

$$b = \frac{2\pi R_{AVG}}{12} = \frac{\pi}{6} \cdot \frac{(40 + 48.9)}{2} = 23.23 \text{ ''}$$

$$A_T = A_L + A_F = .634 \text{ IN}^2$$

$$G_{F46} = \frac{P_{F59}}{A_T} \left(1 + \frac{A_L}{A_F} \frac{\cosh KX}{\cosh KL} \right) \quad \text{REF. 1}$$

WHERE $K^2 = \frac{Gt}{Eb} \left(\frac{1}{A_F} + \frac{1}{A_L} \right)$

t = SHEAR PANEL THICKNESS

BY
CK.
DATE

GENERAL ELECTRIC

PAGE
MODEL VOYAGER
REPORT

TORSION ANALYSIS

FLIGHT CAPSULE SUPPORT STRUCTURE

SHEAR LAG ANALYSIS

ASSUME $t = .072$

ALL MAT'L OF 7075 T6 ALUM. ALLOY

$$G = 3.9 \times 10^6 \text{ PSI}$$

$$E = 10.3 \times 10^6 \text{ PSI}$$

$$K^2 = \frac{3.9 \times 0.72}{10.3 \times 23.23} \left(\frac{1}{.410} + \frac{1}{.224} \right) = .0091$$

$$K = .09$$

$$\text{CORR KL} = 2.1739$$

$$G_{F46} = \frac{2915}{.634} \left(1 + \frac{.224}{.410} \frac{1.000}{2.1739} \right) = 5753 \text{ PSI}$$

$$P_{F46} = 5753 \times .410 = 2357 \#$$

$$P_{L46} = 2915 - 2357 = 558 \#$$

AVERAGE SHEAR FLOW IN THE PANEL

$$q_A = \frac{2915 - 2357}{15.71} = 35.4 \text{ FPI ULT.}$$

BY

GENERAL ELECTRIC

PAGE

CK.

MODEL VOYAGER

DATE

REV.

REPORT

TORSION ANALYSIS

FLIGHT CAPSULE SUPPORT STRUCTURE

SHEAR LAG ANALYSIS

PEAK SHEAR FLOW NEAR LONGERON AT STA 57

$$q_{\max} = \frac{P_{ESR} K_A \sinh KL}{A_T \cosh KL}$$

$$= \frac{3415 \times 0.9 \times 2.24 \times 1.9303}{.634 \times 2.1739} = 82.3 \text{ PPI ULT}$$

ELEMENTARY THEORY SHEAR FLOW DUE TO CHANGE
IN BENDING MOMENT BETWEEN STATIONS 57 + 10MOMENT OF INERTIA OF FULL SECTION AT
STA 46

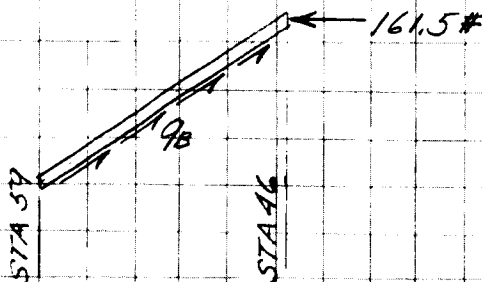
$$I = 2 \cdot 48.3^2 [2 \times 8.20 \times 5^2 + 2 \times 4.50 \times 9.66^2 + 1 \times 3.20 \times 1^2]$$

$$I = 9058.7$$

THE AXIAL COMPONENT OF THE BENDING
LOAD IN THE LONGERON IS

$$P_{BF46} = \frac{1.25 \times 4500 \times 13 \times 48.3 \times 410}{9058.7} = 161.5 \text{ ULT}$$

$$q_B = \frac{161.5}{13} = 12.4 \text{ PPI ULT}$$



BY

GENERAL ELECTRIC

PAGE

6

CK.

MODEL VOYAGER

DATE

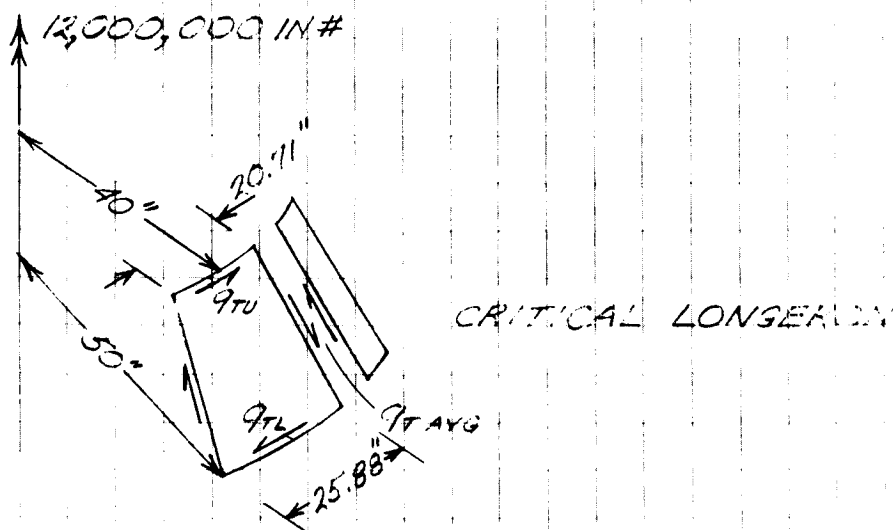
REV.

REPORT

TORSION ANALYSIS

FLIGHT CAPSULE SUPPORT STRUCTURE

ELEMENTARY SHEAR FLOW DUE TO 12,000,000 IN-LB. TORQUE



$$q_{TU} = \frac{1.25 \times 12.0 \times 10^6}{2\pi \cdot 40^2} = 1491 \text{ PPI}$$

$$q_{TL} = \frac{1.25 \times 12.0 \times 10^6}{2\pi \cdot 50^2} = 955 \text{ PPI}$$

$$q_{T \text{ AVG}} = 1491 \times \frac{20.71}{25.88} = 1192 \text{ PPI ULT.}$$

BY

GENERAL ELECTRIC

PAGE

7

CK.

MODEL VOYAGER

DATE

REV.

REPORT

TORSION ANALYSIS

LIGHT CAPSULE SUPPORT STRUCTURE

NEW AVERAGE SHEAR FLOW DUE TO ALL EFFECTS

$$Q_N = 1192 + 35.4 - 12.4 = 1215 \text{ ULT}$$

.072" THICK 7075 T6 MIN. SPACING BEADED PANEL
13.350 IN.

1250 PSI ULT (REF. 2)
1100 PSI LIMIT

$$\text{MIN. MS} = \frac{1250}{1215} - 1 = \underline{\underline{+1.03}}$$

ATTACHMENTS-

PEAK SHEAR FLOW $Q_{MAX} = 1192 + 82.3 - 12.4 = 1262 \text{ PSI (ULT)}$

HAT TO FIXEL PANEL (ALSO REMOVABLE PANEL)

LIMIT

$\frac{3}{16}$ HI-SHEARS (TITAN.) BRG. IN. 072-7075 T6 @ 1.25"
PITCH. ALLOWABLE


$$Q_{AL} = \frac{1350 \times 1.07}{1.25} = 1155$$

$$\text{MS} = \frac{1.25 \times 1155}{1262} - 1 = \underline{\underline{+1.1}}$$

ULT.

$$Q_{AL} = \frac{1350 \times 1.49}{1.25} = 1610$$

$$\text{MS} = \frac{1610}{1262} - 1 = \underline{\underline{+2.8}}$$

BY CK. DATE	GENERAL  ELECTRIC	PAGE 5 MODEL VOYAGER REPORT
DATE REV.		
<p>TORSION ANALYSIS</p> <p>FLIGHT CAROUSEL SUPPORT STRUCTURE</p> <p>ATTACHMENTS</p> <p>INTERFACE RING TO REMOVABLE PANEL</p> <p>$F_{MAX} = 1262 \text{ PSI ULT}$</p> <p>$F_{AL} = 1610 \text{ ULT}, 1155 \text{ LIMIT}$</p> <p>$MIN. MS = \frac{125 \times 1155}{1262} - 1 = \underline{\underline{+1.4 \text{ LIMIT}}}$</p> <p>INTERFACE RING TO FIXED PANEL ATTACHMENTS GIVE BY INSPECTION</p>		

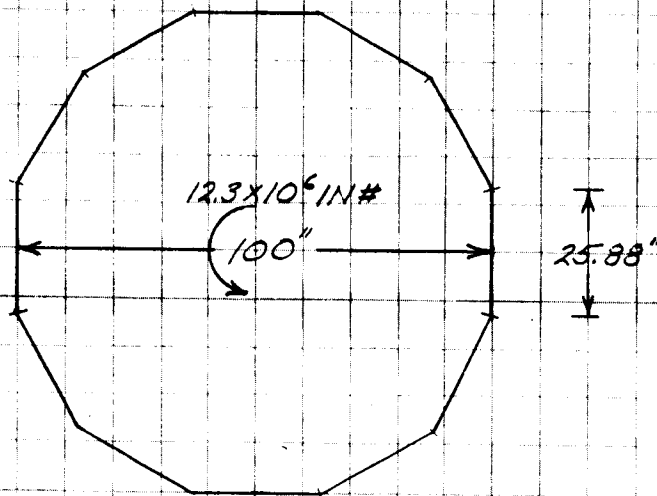
BY
CK.
DATE

GENERAL ELECTRIC

PAGE
MODEL VOYAGER
REPORT

TORSION ANALYSIS - LOAD COND. 20 - '75, '77 COND. 13,
EQUIPMENT MODULE SECTION

ELEMENTARY SHEAR FLOW DUE TO 12,360,000 IN#
TORQUE



$$A = 12 \times \frac{1}{2} \times 50 \times 25.88$$

$$q_T = \frac{1.25 \times 12,360,000}{12 \times 50 \times 25.88} = 995 \text{ PRI ULT}$$

PREVIOUS ANALYSIS OF FLIGHT CAPSULE SUPPORT
STRUCTURE DEMONSTRATES THAT SHEAR FLOWS DUE
TO SHEAR LAG & TRANSVERSE SHEAR TEND TO BE
SELF CANCELLING AND ARE NEGLIBLE.

BY CK. DATE REV.	GENERAL ELECTRIC	PAGE MODEL VOYAGER REPORT
---	-------------------------	---------------------------------

TORSION ANALYSIS

EQUIPMENT MODULE SECTION

FOR THERMAL CONDUCTIVITY PURPOSES

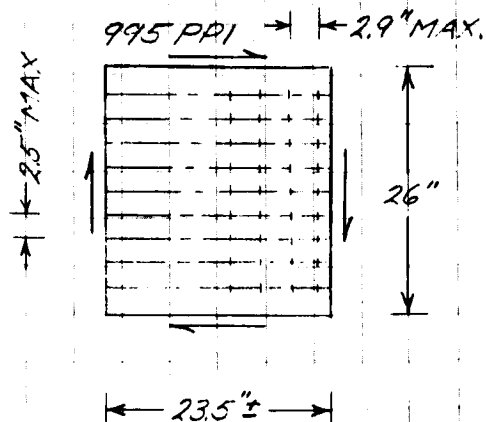
$$kt \geq 4.2 \text{ WHERE}$$

k = THERMAL CONDUCTIVITY OF OUTER SHEAR PANEL
 t = PANEL THICKNESS

7015-16 ALUM. ALLOY WAS SELECTED BECAUSE ITS SUPERIOR BEARING QUALITY WOULD ALLOW FEWER ATTACHMENTS FOR THE REMOVABLE PANELS

$$\text{MIN. } t = \frac{4.2}{76} = .055''$$

THE MODULE TRAYS HAVE AMPLE STIFFNESS TO ACT AS PANEL BREAKERS. THE MAXIMUM SPACING FOR DOUBLE WIDTH TRAYS IS 2.5". THE MAX. SPACING OF SCREENS SECURING TRAYS TO SHEAR PANEL IS 2.9"



TYPICAL OUTER SHEAR PANEL

BY
CK.
DATE

GENERAL ELECTRIC

PAGE
MODEL VOYAGER
REPORT

TORSION ANALYSIS

EQUIPMENT MODULE SECTION

CRITICAL SHEAR STRESS

$$T_{CR} = \frac{\pi^2 K_s E}{12(1-\nu^2)} \left(\frac{t}{b}\right)^2 \quad (\text{REF. 2})$$

$$E = 10.3 \times 10^6 \text{ PSI}$$

$$\nu = 0.3$$

$$t = .055$$

$$a = 26.0$$

$$b = 2.9$$

$$\text{FOR } \frac{a}{b} = 8.96$$

$$K_s = 5.5 \quad (\text{HINGED EDGES})$$

$$T_{CR} = \frac{\pi^2 \times 5.5 \times 10.3 \times 10^6 \times .055^2}{12 \times .91 \times 8.41} = 18,416 \text{ PSI}$$

$$\text{APPLIED } T = \frac{995}{.055} = 18,080 \text{ PSI}$$

$$F_{ST} = 46,000 \text{ PSI}$$

$$MS = \frac{18416}{18080} - 1 = \underline{\underline{+.02}}$$

NOMINAL ALLOWABLE SPACING FOR $\frac{1}{4}$ " EDGE ATTACHMENTS

$$S = \frac{.25 \times .055 \times 10^3 \times .055 \times .25}{995} = 1.85"$$

ALLOWABLE AXIAL LONGERON STRESS FOR INTER-RIVET BUCKLING

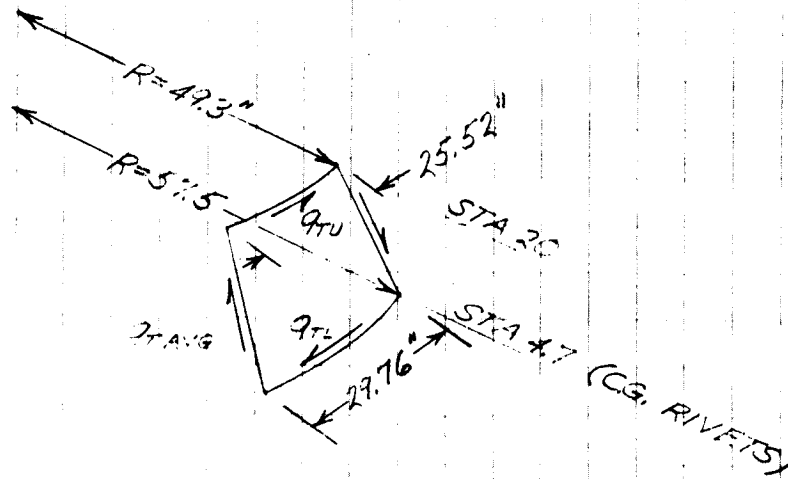
$$F_c = 31,000 \text{ PSI (REF. 3)}$$

BY CK. DATE	REV.	GENERAL ELECTRIC PAGE MODEL VOYAGER REPORT
-------------------	------	---

TORSION ANALYSIS - LOAD COND. 2C-115, 111 CONFIG

SPACECRAFT SUPPORT STRUCTURE

ELEMENTARY SHEAR FLOW DUE TO 12,720,000 IN#
 LOADS



$$q_{TU} = \frac{1.25 \times 12.72 \times 10^6}{271.475^2} = 1041 \text{ PPI. ULT}$$

$$q_{TL} = \frac{1.25 \times 12.72 \times 10^6}{271.475^2} = 765 \text{ PPI. ULT}$$

$$q_{TAVG} = 1041 \times \frac{25.52}{29.76} = 893 \text{ PPI. ULT}$$

0.61" THICK 7075 T6 MIN. SPACING BEARING PANEL IS
 GOOD FOR

1050 PPI. ULT (REF 2)
 ETC ETC ETC

$$\text{MIN. P.S.} = \frac{1050}{893} - 1 = +.18$$

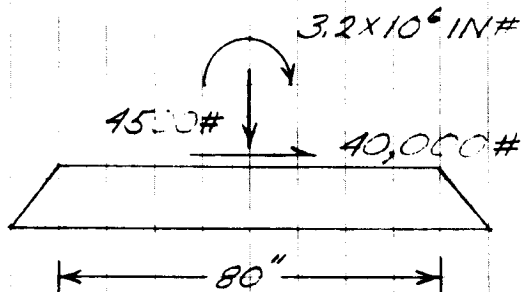
BY
CK.
DATE

GENERAL ELECTRIC

PAGE
MODEL VOYAGER
REPORT

SHEAR LAG ANALYSIS - LOAD COND. 3B-75,77 CONFIG.

FLIGHT CAPSULE SUPPORT STRUCTURE



CALCULATE P_{FC}

FOR 4500# AXIAL LOAD

$$P_A = \frac{4500}{6} = 750 \#$$

FOR 3.2×10^6 IN# MOMENT

$$P_B = \frac{3.2 \times 10^6}{120} = 26,650 \#$$

$$P_{FC} = 34,250 \# \text{ ULT.}$$

$$P_{LON} = 34,250 \times \frac{15.7}{13} = 41,400.$$

BY
CK.
DATE

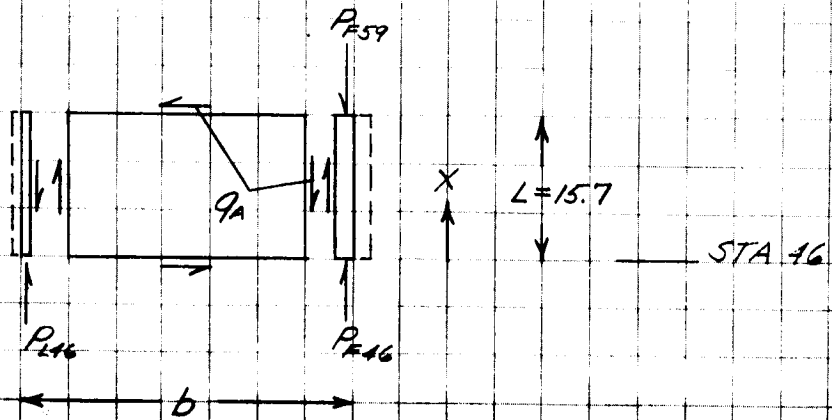
GENERAL ELECTRIC

PAGE
MODEL VOYAGER
REPORT

SHEAR LAG ANALYSIS

FLIGHT CAPSULE SUPPORT STRUCTURE

ANALYSIS FOR CRITICAL SEGMENT



$$G_{F46} = \frac{P_{F59}}{A_T} \left(1 + \frac{A_L \cosh KX}{A_F \cosh KL} \right) \quad (\text{REF 1})$$

$$b = 23.23''$$

$$A_F = \frac{1}{2} A_{LON} = .410 \text{ IN}^2$$

$$A_L = \frac{1}{2} A_S = .224 \text{ IN}^2$$

$$A_T = A_F + A_L = .634 \text{ IN}^2$$

$$P_{F59} = \frac{1}{2} P_{LON} = 20,700$$

BY
CK.
DATE

GENERAL ELECTRIC

PAGE
MODEL VOYAGER
REPORT

SHEAR LAG ANALYSIS

FLIGHT CARCULE SUPPORT STRUCTURE

ANALYSIS FOR CRITICAL SEGMENT

$$K^2 = \frac{Gt}{Eb} \left(\frac{1}{A_f} + \frac{1}{A_L} \right)$$

$$t = .072''$$

$$G = 3.9 \times 10^6 \text{ PSI}$$

$$E = 10.3 \times 10^6 \text{ PSI}$$

THEN $K = .09$, $\cosh KL = 2.1739$

$$P_{FLG} = \frac{20700}{.634} \left(1 + \frac{.224 \cdot 1.000}{.410 \cdot 2.1739} \right) = 40,855$$

$$P_{FLG} = 40,855 \times .410 = 16,750 \# \text{ SHEAR LAG ONLY}$$

$$P_{LAG} = 3750 \# \text{ SHEAR LAG ONLY}$$

$$q_{max} = \frac{P_{FLG} K A_L \sinh KL}{A_f \cosh KL}$$

$$= \frac{20700 \times .09 \times .224 \times 1.9303}{.634 \times 2.1739} = 584 \text{ PSI}$$

BY
CK.
DATE

GENERAL ELECTRIC

PAGE
MODEL VOYAGER
REPORT

SHEAR LAG ANALYSIS

FLIGHT CAPSULE SUPPORT STRUCTURE

THE MEMBER LOADS AT STA 46 DUE TO

TOTAL KICK LOAD AT STA 59

$$V_k = 1.25 \times \frac{8.8}{13} [2 \times 26,650 + 4 \times \frac{1}{4} \times 26,650] = 67,650 \text{ ULT}$$

$$P_{KF46} = \frac{67650 \times 13 \times 48.8 \times 10}{9058.7} \times \frac{15.7}{13} = 2346 \# \text{ TENS}$$

$$P_{KL46} = 1110 \# \text{ TENS}$$

BY CK. DATE REV.	GENERAL ELECTRIC	PAGE MODEL VOYAGER REPORT
---	-------------------------	---------------------------------

SHEAR LAG ANALYSIS

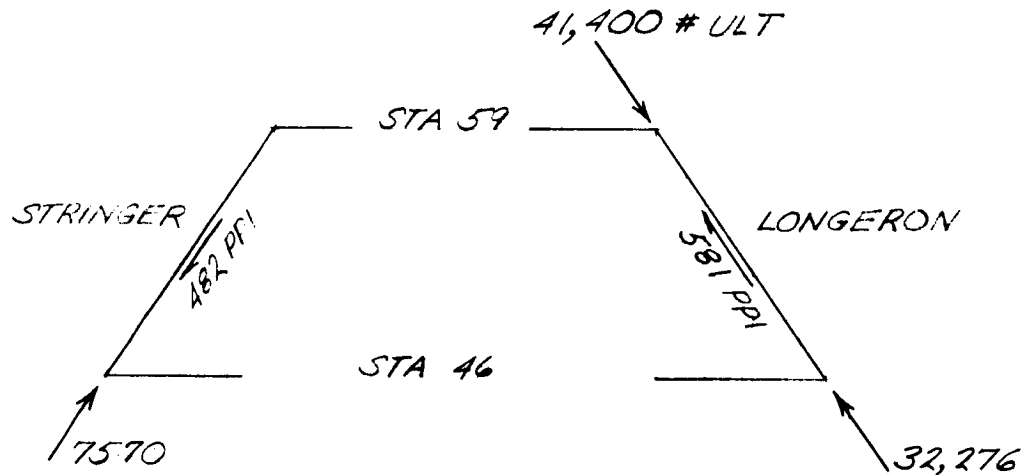
FLIGHT CAPSULE SUPPORT STRUCTURE

ELEMENTARY THEORY BENDING LOAD DUE TO CHANGE IN BENDING MOMENT BETWEEN STATIONS 59 & 46

$$P_{BF46} = \frac{1.25 \times 40,000 \times 13 \times 48.8 \times 410}{9058.7} \times \frac{15.7}{13} = 1734 \# \text{ ULT}$$

$$P_{BL46} = 941 \# \text{ ULT}$$

$$q_B = \frac{1734}{15.7} = 110 \text{ PPI}$$



MEMBER FREE BODIES

BY
CK.
DATE

GENERAL ELECTRIC

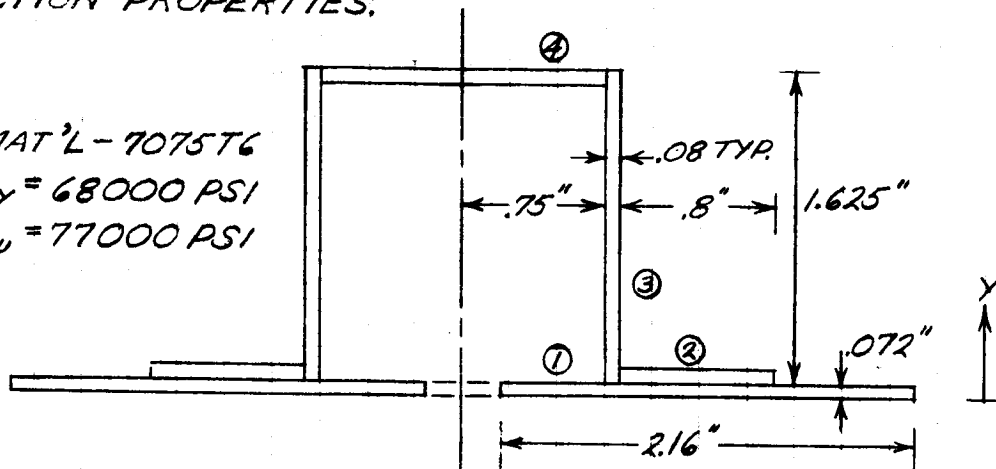
PAGE 18
MODEL VOYAGER
REPORT

SHEAR LAG ANALYSIS

FLIGHT CAPSULE SUPPORT STRUCTURE

SECTION PROPERTIES.

MAT'L - 7075T6
F_{cy} = 68000 PSI
F_{TU} = 77000 PSI



LONGERON

(ASSUME SYMMETRY ABOUT Y)

ELEM	A _F	Y	AY	ΔY	AAY ²	I _c	I/r
1	.1535	.036	.0056	.519	.0419	—	.0419
2	.064	.112	.0072	.443	.0126	—	.0126
3	.130	.8845	.1150	.330	.0142	.0286	.0428
4	.060	1.657	.0994	1.102	.0729	—	.0729

.4095 .5548 .2272 .1702

$$\rho = \left(\frac{.3404}{.819} \right)^{\frac{1}{2}} = .41563^{\frac{1}{2}} = .6447$$

THE CRIPPLING STRESS FOR ELEM 3, F_{cc} = F_{cy} = 68,000 PSI

FOR L/PVC = $\frac{15.7}{.6447} = 24.35$, THE ALLOWABLE COLUMN STRESS

$$F_{col} = 61,200 \text{ (REF 4)}$$

$$G_{AVG} = \frac{11,400 + 32,276}{2 \times .819} = 44,979$$

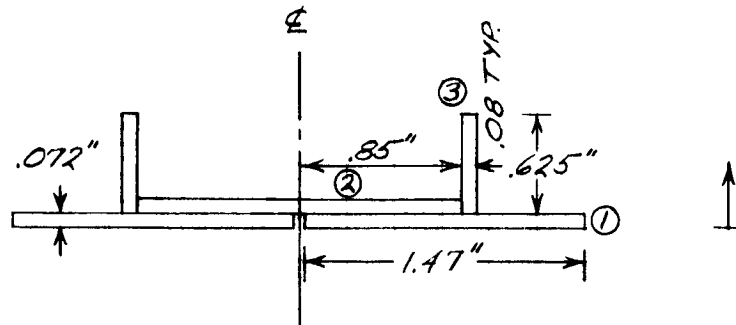
$$MS = \frac{61200}{44979} - 1 = +.36$$

BY	GENERAL ELECTRIC	PAGE
CK.		MODEL VOYAGER
DATE		REV.

SHEAR LAG ANALYSIS

FLIGHT CAPSULE SUPPORT STRUCTURE

SECTION PROPERTIES



MAT'L - 7075 T6
 $F_{cc} = 62,000 \text{ PSI}$
 (REF 4)

STRINGER
 SYMMETRICAL ABOUT Z

ELEM	A_s	y	Ay	Δy	$A\Delta y^2$	I_o	$I/2$
1	.1058	.036	.0038	.1007	.0011	—	.0011
2	.0680	.112	.0076	.0247	—	—	—
3	.0500	.3845	.0192	.2478	.0031	.0016	.0047
	.2238	.1367	.0306				.0058

FOR COLUMN STABILITY

$$9L_{cr} \approx \frac{2\pi^2 EI}{L^2} \quad (\text{REF. 5})$$

$$= 9567$$

$$MS = \frac{9567}{7570} - 1 = +.26$$

BY

GENERAL ELECTRIC

PAGE

CK.

MODEL VOYAGER

DATE

REV.

REPORT

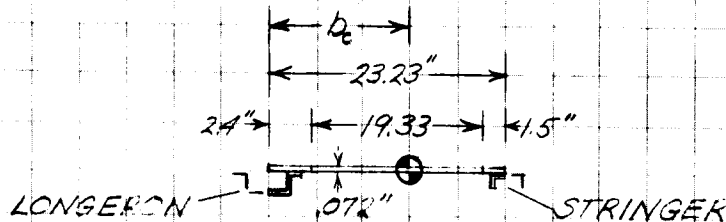
SHEAR LAG ANALYSIS- LOAD CONDITION 3b- '75, '77 CONFIGURATION

Flight Capsule Support Structure

Analysis for critical segment

The member loads and shear flows arrived at on the preceding page reflect the conservative assumption that the effective area of shear panel acting as axial structure is limited due to the bolted connections at station 46 and the geometric mismatch of the shear panels of the flight capsule support structure and the equipment module section. Such a philosophy will be adhered to in determining the overall load distribution at the base of the spacecraft support structure, but will be deviated from to conservatively arrive at the maximum shear flows in the flight capsule support structure. The following analysis will verify the structural integrity of the shear panels.

ASSUME ENTIRE SHEAR PANEL EFFECTIVE

ADDITIONAL EFFECTIVE AREA = $19.33 \times .072 = 1.392$

USING THE SUBSTITUTE STRINGER METHOD (REF 1),
THE DISTANCE TO THE CENTROID OF THE SUBSTITUTE
STRINGER

$$d_c = \frac{.224 \times 23.23 + 1.392 \times 12.065}{.224 + 1.392} = 13.61''$$

$$A_2 = .224 + 1.392 = 1.616$$

BY
CK.
DATE

GENERAL ELECTRIC

PAGE
MODEL VOYAGER
REPORT

SHEAR LAG ANALYSIS

FLIGHT CAPSULE SUPPORT STRUCTURE

ANALYSIS FOR CRITICAL SEGMENT

$$D_s = \left(.65 + \frac{.35}{n^2} \right) D_c$$

$n =$ NUMBER OF STAINGERS $= 2$

$$D_c = 13.61''$$

$$D_s = 10.04$$

$$k = \frac{Gt}{E_b D_s} \left(\frac{1}{A_u} + \frac{1}{A_L} \right) = \frac{3.9 \times 10^7}{10.3 \times 10.04} \left(\frac{1}{.710} + \frac{1}{1.616} \right) = .0083031$$

$$K = .09112$$

$$KL = 1.43$$

$$q_{\max} = \frac{P_{ES9} K A_L \sinh KL}{A_T \cosh KL} = \frac{20,700 \times .09112 \times 1.616 \times 1.9697}{2.026 \times 2.2090}$$

$$q_{\max} = 1340 \text{ PPI ULT.}$$

ATTACHMENTS ARE GOOD FOR 1610 PPI ULT.

$$q_{\text{AVG}} = \frac{20,700 - P_{F16}}{15.1}$$

$$P_{F16} = \frac{A_F P_{ES9}}{A_T} \left(1 + \frac{A_L \cosh Kx}{A_F \cosh KL} \right) = 11,663$$

$$q_{\text{AVG}} = 576 \text{ ULT}$$

DTX BEADED PANEL IS GOOD FOR 1250 PPI ULT (REF. 2)

CONCLUSION: THE PANEL & ATTACHMENTS ARE GOOD FOR THE MOST CONSERVATIVE SHEAR LAG ASSUMPTIONS

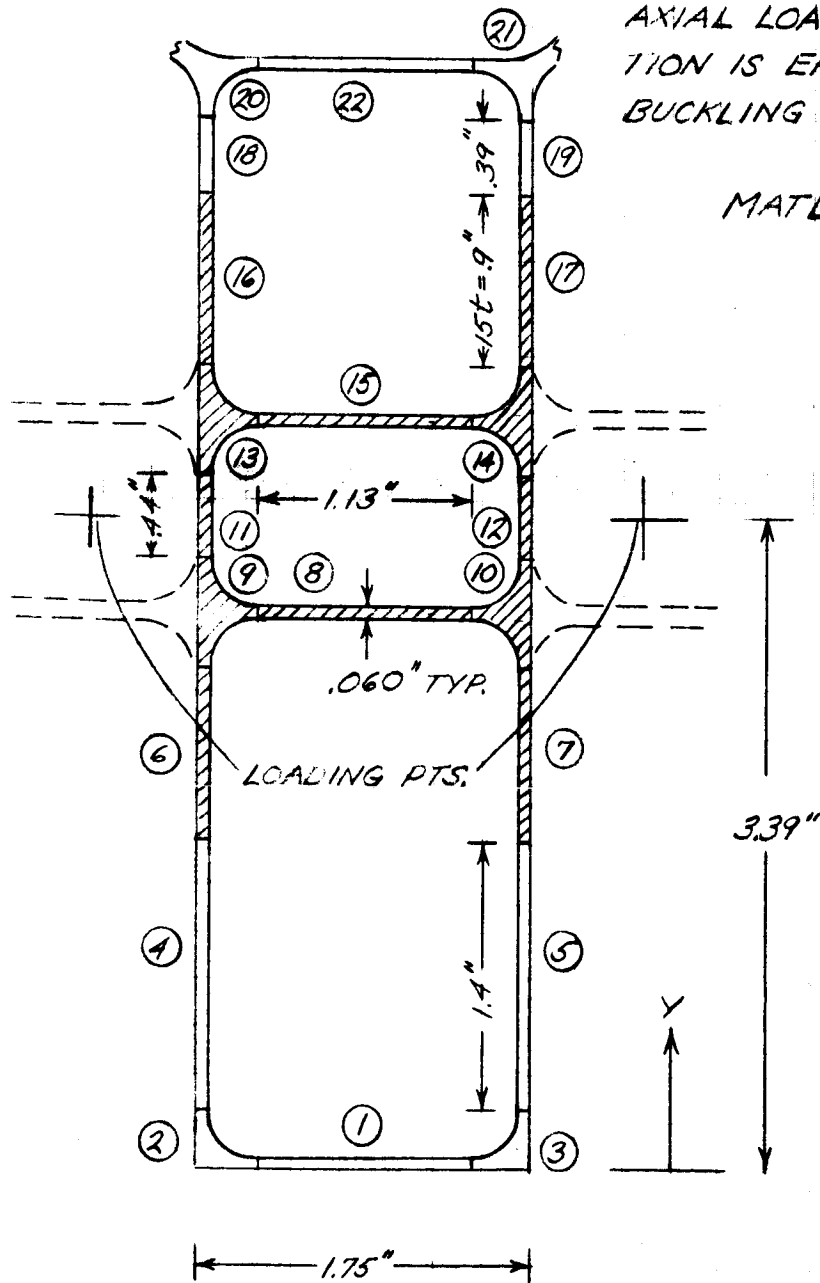
BY CK. DATE	REV.	GENERAL ELECTRIC PAGE MODEL VOYAGER REPORT
-------------------	------	---

SHEAR LAG ANALYSIS - LOAD COND. 3b-'75, '77 CONFIG.

EQUIPMENT MODULE

LONGERON PROPERTIES - DUE TO THE NATURE OF THE LOADING GEOMETRY, ONLY THE SHADED AREA IS EFFECTIVE FOR AXIAL LOADS. THE ENTIRE SECTION IS EFFECTIVE TO PREVENT BUCKLING

MATL ~ 2219
 OR 7075-T6 AL. ALLOY



SECT. STA 46

BY CK. DATE	GENERAL ELECTRIC	PAGE MODEL VOYAGER REPORT
-------------------	-------------------------	---------------------------------

SHEAR LAG ANALYSIS

EQUIPMENT MODULE

LONGERON PROPERTIES

AXIAL EFFECTIVE AREA = .706

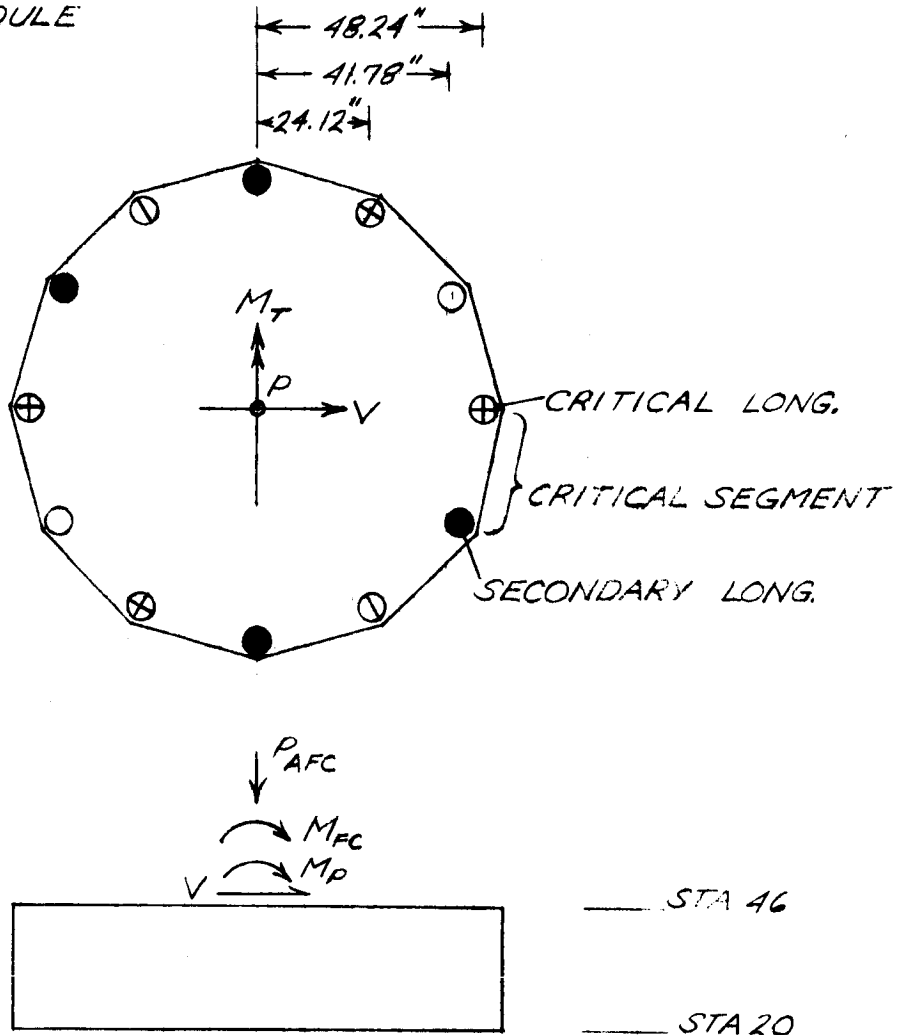
ELEM	A	Y	AY	AY	AAY ²	I.	I
1	.0678	.030	.0020	2.981	.6025	-	.6025
2	.0470	.100	.0047	2.911	.3983	-	.3983
3	.0470	.100	.0047	2.911	.3983	-	.3983
4	.0840	1.010	.0848	2.001	.3363	.0137	.3500
5	.0840	1.010	.0848	2.001	.3363	.0137	.3500
6	.0540	2.160	.1166	.851	.0391	.0036	.0427
7	.0540	2.160	.1166	.851	.0391	.0036	.0427
8	.0678	2.890	.1959	.121	.0010	-	.0010
9	.0754	2.890	.2179	.121	.0011	-	.0011
10	.0754	2.890	.2179	.121	.0011	-	.0011
11	.0264	3.400	.0898	.389	.0040	.0004	.0044
12	.0264	3.400	.0898	.389	.0040	.0004	.0044
13	.0754	3.890	.2933	.879	.0583	-	.0583
14	.0754	3.890	.2933	.879	.0583	-	.0583
15	.0678	3.890	.2637	.879	.0524	-	.0524
16	.0540	4.630	.2500	1.619	.1415	.0036	.1451
17	.0540	4.630	.2500	1.619	.1415	.0036	.1451
18	.0234	5.210	.1233	2.259	.1194	.0003	.1197
19	.0234	5.210	.1233	2.259	.1194	.0003	.1197
20	.0470	5.680	.2670	2.669	.3348	-	.3348
21	.0470	5.680	.2670	2.669	.3348	-	.3348
22	.0678	5.150	.3899	2.139	.5086	-	.5086
	1.2444	3.011	3.7463				4.0733

$$\rho = \sqrt{\frac{I}{A}} = 1.8092 \quad \frac{L}{\rho} = 14.37$$

BY	GENERAL ELECTRIC	PAGE
CK.		MODEL VOYAGER
DATE		REV.

SHEAR LAG ANALYSIS

EQUIPMENT MODULE



AT STA 46

- $P_{afc} = 4500 \#$ (AXIAL LOAD DUE TO FLIGHT CAPSULE)
- $P_{ap} = 2000 \#$ (" " " " PROPULSION EQUIP)
- $M_T = 3.8 \times 10^6 \text{ IN} \#$ (TOTAL MOMENT)
- $M_{fc} = 3.72 \times 10^6 \text{ IN} \#$ (MOMENT DUE TO FLIGHT CAPSULE)
- $M_p = .08 \times 10^6 \text{ IN} \#$ (" " " PROPULSION EQUIP)

LEGEND ~ \odot FLIGHT CAPSULE LOAD PATH
 \bullet PROP. EQUIP. LOAD PATH
 \oplus COMBINED LOAD PATH

BY CK. DATE	REV.	GENERAL ELECTRIC	PAGE MODEL VOYAGER REPORT
-------------------	------	------------------	---------------------------------

SHEAR LAG ANALYSIS

EQUIPMENT MODULE - STA 46

LOAD IN CRITICAL LONGERON DUE TO PROPULSION
EQUIPMENT

FOR 2000# AXIAL LOAD

$$P'_{AP} = \frac{2000}{8} = 250\#$$

FOR THE 80,000 IN# BENDING MOMENT

$$80000 = 2 \left[48.24 P'_{BP} + 41.78 \frac{41.78}{48.24} P'_{BP} + 24.12 \frac{24.12}{48.24} P'_{BP} \right]$$

$$P'_{BP} = 415\#$$

LOAD IN CRITICAL LONGERON DUE TO FLIGHT CASULE

$$P_{FC} = 32,276 \times \frac{13}{15.7} = 26,725 \text{ ULT}$$

NET LOAD IN CRITICAL LONGERON

$$P_{LON} = 26,725 + 1.25(415 + 250) = 27,556 \text{ ULT}$$

LOAD IN SECONDARY LONGERON DUE TO PROP. EQUIP.

$$P'_{AP} = 250\#$$

$$P'_{BP} = 415 \times \frac{41.78}{48.24} = 359$$

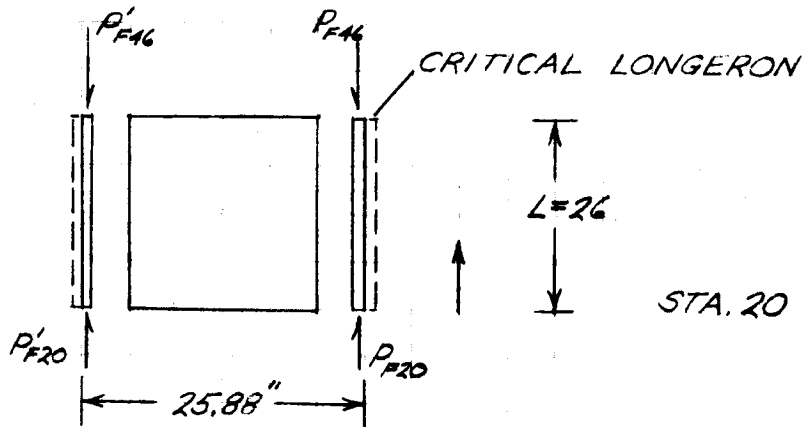
$$P_{FC} = 7570 \times \frac{13}{15.7} = 6268 \text{ ULT}$$

$$P_{LON} = 6268 + 1.25(250 + 359) = 7029 \text{ ULT.}$$

BY	GENERAL ELECTRIC	PAGE
CK.		MODEL VOYAGER
DATE		REV.

SHEAR LAG ANALYSIS

EQUIPMENT MODULE



CASE I (FOR P_{F46})

$$G_{F20} = \frac{P_{F46}}{A_T} \left(1 + \frac{A_L \cosh KX}{A_F \cosh KL} \right) \quad (\text{REF. 1})$$

$$A_F = A_L = \frac{1}{2} \times .706 = .353 \text{ IN}^2$$

$$A_T = .706 \text{ IN}^2$$

$$P_{F46} = \frac{1}{2} P_{LON} = 13,778 \text{ ULT}$$

$$K^2 = \frac{Gt}{Eb} \left(\frac{1}{A_F} + \frac{1}{A_L} \right) \quad 14.57101$$

$$t = .055''$$

$$G = 3.9 \times 10^6 \text{ PSI}$$

$$K^2 = .0045591$$

$$E = 10.3 \times 10^6 \text{ PSI}$$

$$K = .06752$$

$$KL = 1.7555$$

$$\cosh KL = 2.9796$$

$$\sinh KL = 2.8068$$

BY
CK.
DATE

GENERAL ELECTRIC

PAGE
MODEL VOYAGER
REPORT

SHEAR LAG ANALYSIS

EQUIPMENT MODULE

$$G_{F20} = \frac{13,778}{.706} \left(1 + \frac{1.0}{2.9796}\right) = 26,065$$

$$P_{F20} = 9,201$$

$$P'_{F20} = 4577$$

$$q_{AV} = 176 \text{ PPI}$$

$$q_{MAX} = \frac{P_{F46} K_A \text{SINH} KL}{A_T \text{COSH} KL} = \frac{13,778 \times 0.06752 \times 2.8068}{2 \times 2.9796} = 438 \text{ PPI}$$

CASE II (FOR P'_{F46})

$$P'_{F46} = \frac{1}{2} P_{LON} = 3515$$

$$P'_{F20} = 9201 \times \frac{3515}{13,778} = 2347$$

$$P_{F20} = 1168$$

$$q_{AV} = 45 \text{ PPI}$$

$$q_{MAX} = 438 \times \frac{3515}{13,778} = 112 \text{ PPI}$$

BY	GENERAL ELECTRIC	PAGE
CK.		MODEL VOYAGER
DATE		REV.

SHEAR LAG ANALYSIS

EQUIPMENT MODULE

ELEMENTARY THEORY BENDING LOAD DUE TO CHANGE IN BENDING MOMENT BETWEEN STATIONS 46 & 20

$$\Delta M = 4.9 \times 10^6 - 3.8 \times 10^6 = 1.1 \times 10^6$$

$$\Delta M = 2 \left[48.24 P_{BF20} + 2 \times 41.78 \frac{41.78}{48.24} P_{BF20} + 2 \times 24.12 \frac{24.12}{48.24} P_{BF20} \right]$$

$$P_{BF20} = 3800 \# \text{ LIMIT}$$

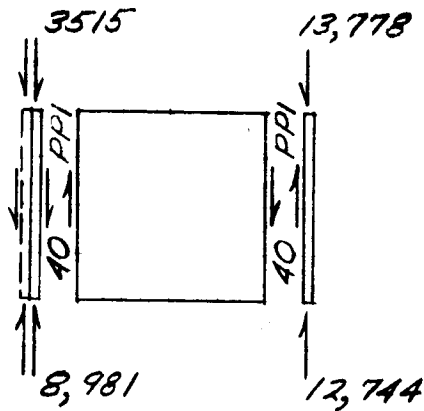
$$P'_{BF20} = 3291 \# \text{ LIMIT}$$

$$\text{NET } P_{F20} = 9,201 + 1168 + 1.25 \times .5 \times 3800 = 12,744$$

$$P_{LON} = 24,934$$

$$\text{NET } P'_{F20} = 4,577 + 2347 + 1.25 \times .5 \times 3291 = 8,981$$

$$P'_{LON} = 17,962$$

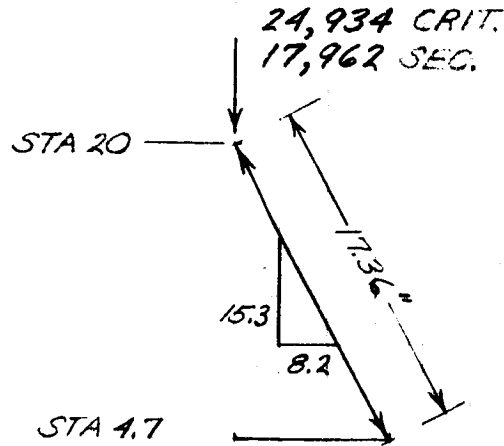


BY CK. DATE	REV.	GENERAL ELECTRIC	PAGE MODEL VOYAGER REPORT
<p>SHEAR LAG ANALYSIS</p> <p>EQUIPMENT MODULE</p> <p>STABILITY OF CRITICAL LONGERON</p> <p>FOR COLUMN BUCKLING</p> $P_{CR} = \frac{\pi^2 EI}{L^2}$ $P_{CR} = 612,000 \#$ $E = 10.3 \times 10^6$ $I = 4.0733$ $L = 26''$ <p>FOR CRIPPLING OF ELEMENTS 8 & 15</p> $\frac{b}{t} = \frac{1.6}{.06} = 26.7$ $F_{cc} = 53,000$ $F_{c \text{ AVG}} = \frac{13,778 + 12,744}{.706} = 37,567$ $\text{CONSERVATIVE M.S.} = \frac{53000}{37567} - 1 = \underline{\underline{1.41}}$			

BY	GENERAL ELECTRIC	PAGE
CK.		MODEL VOYAGER
DATE		REV.

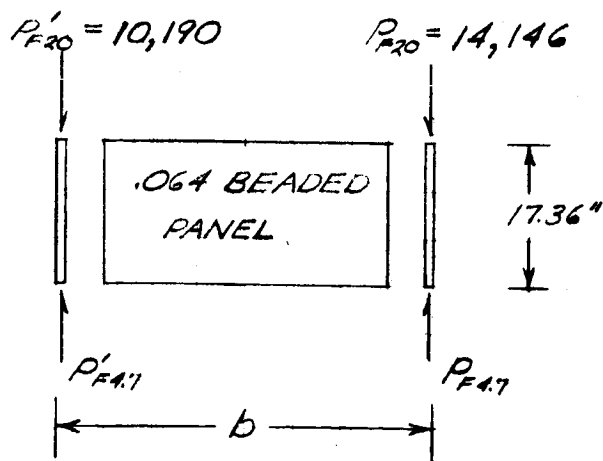
SHEAR LAG ANALYSIS - LOAD COND. 3b-'75,'77 CONFIG.

SPACECRAFT SUPPORT STRUCTURE



$$P_{LON} = 24,934 \times \frac{17.36}{15.30} = 28,291$$

$$P'_{LON} = 17,962 \times \frac{17.36}{15.30} = 20,380$$

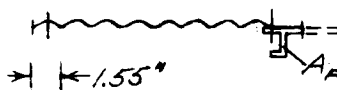
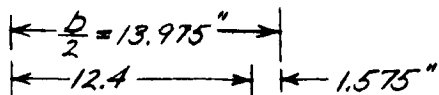


$$b = \frac{R_{AVG} \times 30}{57.3} = \frac{(49.3 + 57.5) 30}{2 \times 57.3} = 27.95"$$

BY	GENERAL ELECTRIC	PAGE
CK.		MODEL <i>VOYAGER</i>
DATE		REV.

SHEAR LAG ANALYSIS

SPACECRAFT SUPPORT STRUCTURE



SECT. THRU CRITICAL PANEL

THE BEADS ACT AS STRINGERS IN A MULTI-STRINGER PANEL AND CAN BE ANALYSED BY THE SUBSTITUTE STRINGER METHOD OF REF 1.

THE AREA OF ONE STRINGER

$$A_s = 1.55 \times .064 = .0992 \text{ IN}^2$$

THE AREA OF THE SUBSTITUTE STRINGER

$$A_L = n A_s = 8 \times .0992 = .7936 \text{ IN}^2$$

THE CENTROID OF THE SUBSTITUTE STRINGER

$$b_c = 1.575 + \frac{12.4}{2} = 7.775 \text{ ''}$$

THE WIDTH OF THE SUB. PANEL

$$b_s = \left(.65 + \frac{35}{n^2} \right) b_c = 5.096 \text{ ''}$$

BY
CK.
DATE

GENERAL ELECTRIC

PAGE
MODEL VOYAGER
REPORT

SHEAR LAG ANALYSIS

SPACECRAFT SUPPORT STRUCTURE

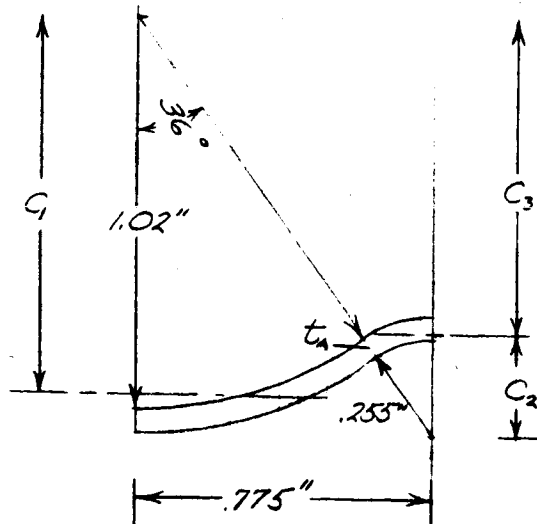
FOR AN OPTIMUM DESIGN IT IS DESIRABLE TO HAVE THE STRESS IN THE SUBSTITUTE STRINGER EQUAL TO THE AXIAL BUCKLING STRESS OF THE BEADED PANEL.

THE BUCKLING STRESS

$$G_{CR} = \frac{.3 E t_e}{R_{AVG}} \quad (\text{CONSERVATIVE}) \quad (\text{REF. 6})$$

WHERE t_e IS THE THICKNESS OF A CURVED PLATE HAVING THE SAME STIFFNESS AS THE BEADED PANEL.

MOMENT OF INERTIA OF ONE HALF BEAD.



$$\begin{aligned} \theta &= 36^\circ \\ &= .62832 \text{ RAD.} \\ \sin \theta &= .58779 \\ \cos \theta &= .80902 \end{aligned}$$

THE ACTUAL THICKNESS AFTER BEADING

$$t_A = \frac{.775 \times .064 \times 57.3}{(1.02 + .03 + .255 + .03) 36} = .059''$$

BY	GENERAL ELECTRIC	PAGE
CK.		MODEL VOYAGER
DATE		REV.

SHEAR LAG ANALYSIS

SPACECRAFT SUPPORT STRUCTURE

$$C_1 = \frac{1.05 \sin \theta}{\theta} = .98226$$

$$C_2 = \frac{.285 \sin \theta}{\theta} = .26661$$

$$I_1 = R^3 t [.55193 - .54987] = .00206 R^3 t = .00238 t$$

$$I_2 = .235^3 \times .00206 t = .00005 t$$

$$C_3 = .80902 (1.02 + .06 + .255) - .26661 = .81343$$

$$\bar{y} = \frac{1.05 \times 6.2832 \times .98226 + .285 \times 6.2832 \times .81343}{1.05 \times 6.2832 + .285 \times 6.2832} = .94622$$

$$I = .00238 t + .00005 t + 1.05 t \times 6.2832 \times .03604^2 + .285 t \times 6.2832 \times .13279^2 = .00644 t = .00038$$

$$t_e^3 = \frac{12 \times .00038}{.775} = .00588$$

$$t_e = .1803$$

$$G_{CR} = \frac{.3 \times 10.3 \times 10^6 \times .1803}{53.4} = 10,433 \text{ PSI}$$

BY	GENERAL ELECTRIC	PAGE
CK.		MODEL VOYAGER
DATE		REV.

SHEAR LAG ANALYSIS

SPACECRAFT SUPPORT STRUCTURE

$$G_{L47} = \frac{P_{F20}}{A_T} \left(1 - \frac{1}{\cosh KL} \right) \leq 10,433 \text{ PSI}$$

FROM TRIAL AND ERROR, LET $A_F = .300 \text{ IN}^2$ (NOMINAL)

$$K^2 = \frac{Gt}{Eb_s} \left(\frac{1}{A_L} + \frac{1}{A_F} \right) = \frac{3.9 \times 0.064}{10.3 \times 5.096} (1.26 + 3.33) = .02184$$

$$K = .1478$$

$$KL = 2.5658$$

$$\cosh KL = 6.5441$$

$$G_{L47} = \frac{14146}{1.0936} (1 - .15281) = 10,959 \text{ CLOSE ENOUGH}$$

(10,433 IS CONSERVATIVE)

$$P_{L47} = .7936 \times 10,959 = 8697$$

$$P_{F47} = 5449$$

$$G_{F47} = 18,163$$

AT STA 20, $A_{F20} = .377$

$$G_{F20} = 37,523$$

IT IS DESIRABLE TO REDUCE A_{F20} TO THE NOMINAL VALUE OF $.30 \text{ IN}^2$ BY TAPERING THE FREE EDGE FLANGE. THE DESIRED STRESS AT THE BREAK POINT IS 25-30,000 PSI.

BY
CK.
DATE

GENERAL ELECTRIC

PAGE
MODEL VOYAGER
REPORT

SHEAR LAG ANALYSIS

SPACECRAFT SUPPORT STRUCTURE

THE DISTANCE "X" TO THE BREAK POINT CAN BE DETERMINED BY THE EXPRESSION

$$\frac{A_{Le}}{A_L} = \frac{1 - e^{-kx}}{1 + A_L/A_F e^{-kx}} \quad (\text{REF. 1})$$

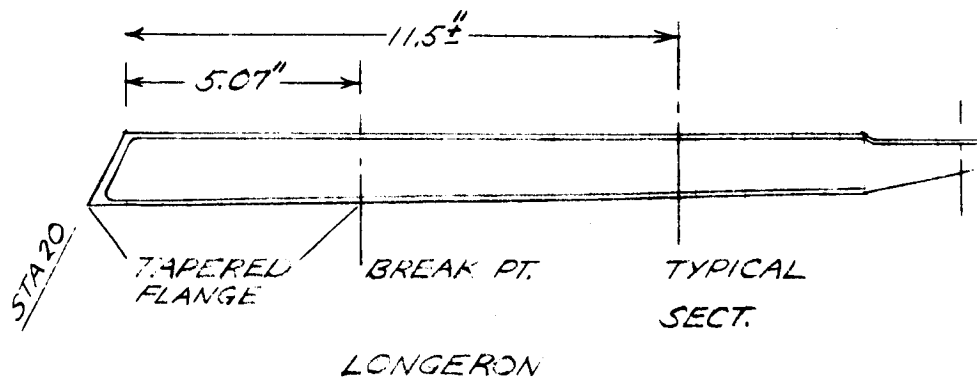
WHERE A_{Le} IS THE EFFECTIVE STRINGER AREA AT A DISTANCE X FROM STA 20

ASSUME $x = 5.07''$

$$e^{-kx} = .47237$$

$$A_{Le} = \frac{1.936 \times 5.2763}{1 + 1.24958} = .1861$$

$$G_F = \frac{14,146}{.34 + .1861} = 29,101 \quad \text{AT THE BREAK POINT}$$



BY	GENERAL ELECTRIC	PAGE
CK.		MODEL VOYAGER
DATE		REV.

SHEAR LAG ANALYSIS

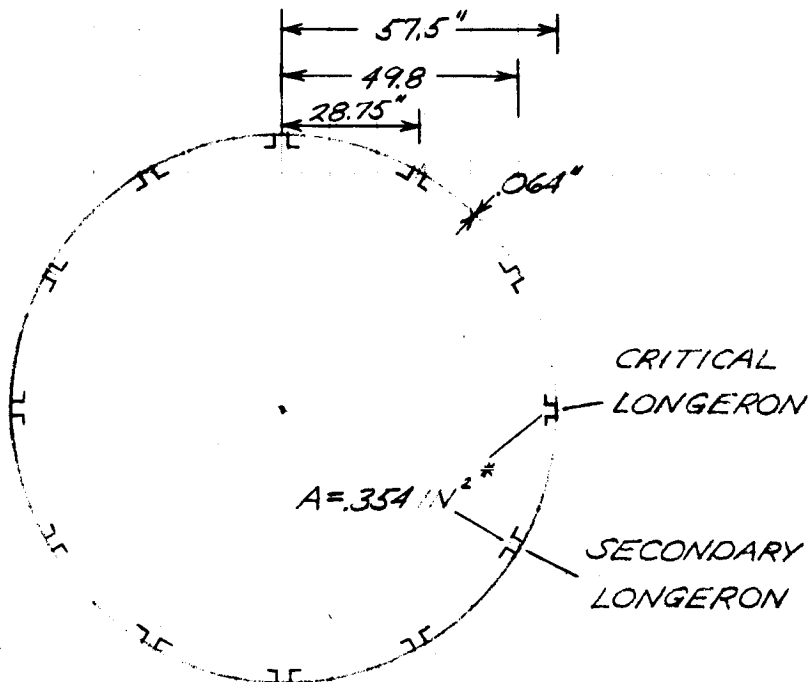
SPACECRAFT SUPPORT STRUCTURE

$$P'_{F4.7} = \frac{10,190}{14,146} P_{F4.7} = 3925$$

$$P'_{L4.7} = 6265$$

ELEMENTARY THEORY BENDING LOAD DUE TO CHANGE IN
BENDING LOAD BETWEEN STATIONS 20 & 4.7

$$\Delta M = 44000(20 - 4.7) = 673,200 \text{ IN}\# \text{ (LIMIT)}$$



FULL SECTION MOMENT OF INERTIA

$$I = \pi 57.5^3 \times 0.64 + 4 \times 0.354 [28.75^2 + 49.8^2] + 2 \times 0.354 \times 57.5^2 = 45,247$$

* NO EFFECTIVE SKIN

BY.
CK.
DATE

GENERAL ELECTRIC

PAGE
MODEL VOYAGER
REPORT

REV.

*SHEAR LAG ANALYSIS**SPACECRAFT SUPPORT STRUCTURE*

$$G_{BF47} = \frac{673,200 \times 57.5 \times 1.25}{45,247} \times \frac{17.36}{15.3} = 1213 \text{ PSI}$$

$$G'_{BF47} = \frac{673,200 \times 49.8 \times 1.25}{45,247} \times \frac{17.36}{15.3} = 1051 \text{ PSI}$$

BY

GENERAL ELECTRIC

PAGE

CK.

MODEL VOYAGER

DATE

REV.

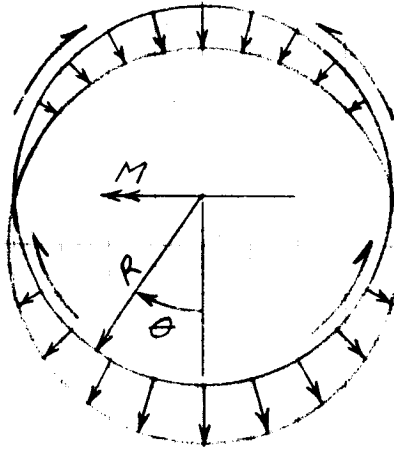
REPORT

SHEAR LAG ANALYSIS

FLIGHT CAPSULE SUPPORT STRUCTURE

THE LOADS AT STA 4.7 ARE REDUCED BY THE MOMENT DUE TO THE KICK LOAD AT STA 20

FOR A UNIFORMLY DISTRIBUTED KICK LOAD



$$M = 1.25 \times 4.9 \times 10^6 \\ = 6.125 \times 10^6 \text{ IN} \cdot \text{#}$$

$$R = 49.3''$$

$$P_{k\theta} = \frac{M \cos \theta}{\pi R^2} \times 8.2$$

$$V_k = 2 \int_0^{\pi} P_{k\theta} \cos \theta ds = \frac{2 \times 8.2 M}{15.3 \pi R} \int_0^{\pi} \cos^2 \theta d\theta = \frac{2 \times 8.2 M}{15.3 \pi R} \left[\frac{\pi}{2} \right]$$

$$= 66,586 \text{ # ULT}$$

$$G_{KFA.7} = \frac{66,586 (20 - 4.7) 57.5}{45,247} \times \frac{17.36}{15.3} = 1469 \text{ PSI TENS.}$$

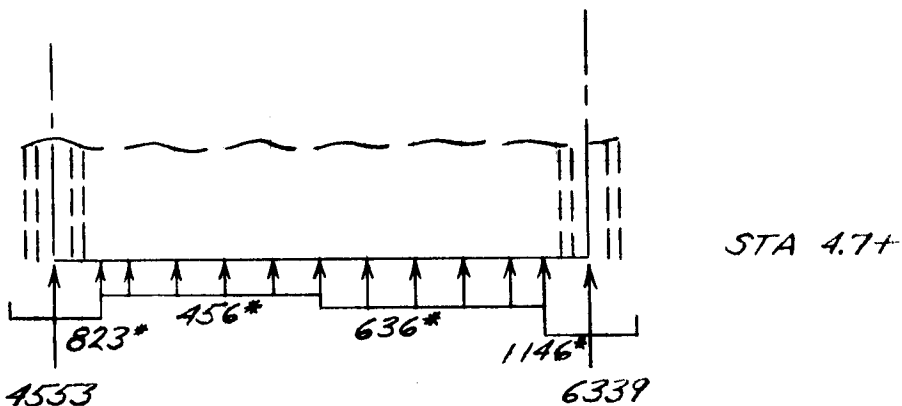
$$G'_{KFA.7} = 1272 \text{ PSI TENS.}$$

BY CK. DATE REV.	GENERAL ELECTRIC	PAGE MODEL <i>VOYAGER</i> REPORT
---	-------------------------	--

SHEAR LAG ANALYSIS

SPACECRAFT SUPPORT STRUCTURE

*NET LOAD DISTRIBUTION ON CRITICAL SEGMENT AT
 LOCATION JUST FWD. OF STA 4.7*



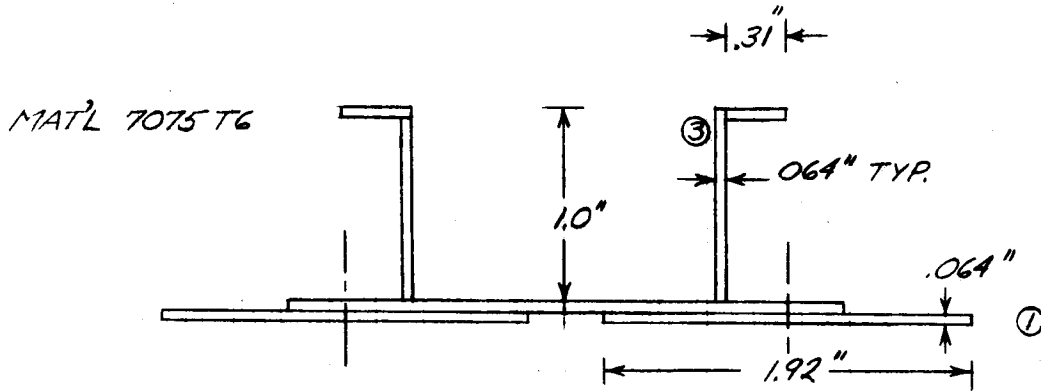
ALL LOADS ULTIMATE

* *AVERAGE SKIN LOAD, PPI*

BY	GENERAL ELECTRIC	PAGE
CK.		MODEL VOYAGER
DATE		REV.

SHEAR LAG ANALYSIS

SPACECRAFT SUPPORT STRUCTURE



TYPICAL SECTION
(NEGLECT SOLAR PANEL STRUCTURE)

ELEM	A	y	Ay	ay	Aay ²	I _o	I/2
1	.123	.032	.0039	.218	.0058	—	.0058
2	.093	.096	.0089	.154	.0022	—	.0022
3	.064	.628	.0402	.378	.0091	.0053	.0144
4	.020	1.096	.0219	.846	.0143	—	.0143
	.300	.250	.0749				.0367

ELEMENT 4 SUFFICIENTLY STIFFENS ELEM. 3
TO OBTAIN FULL EDGE SUPPORT

$$\frac{b}{t} = 15.6 \quad F_{cc} = 68,000 \text{ PSI (REF. 4)}$$

$$\frac{L}{\rho} = \frac{17.36}{.3498} = 49.63$$

ALLOWABLE $F_{COL} = 40,500$ $G_{FAVG} = \frac{14,146 + 5372}{2 \times .3} = 32,530$

$$M.S. = \frac{40500}{32530} - 1 = \underline{\underline{+.25}}$$

BY	GENERAL ELECTRIC	PAGE
CK.		MODEL VOYAGER
DATE		REPORT
REV.		

KICK RING STA 59 - LOAD COND. 3D & 2C, '75, '77 CONFIG.

IN PLANE LOADS DUE TO 4500# AXIAL LOAD

$$\frac{4500}{6} \times \frac{15.7}{13} \times \frac{8.8}{15.7} = 508 \# \text{ LIMIT}$$

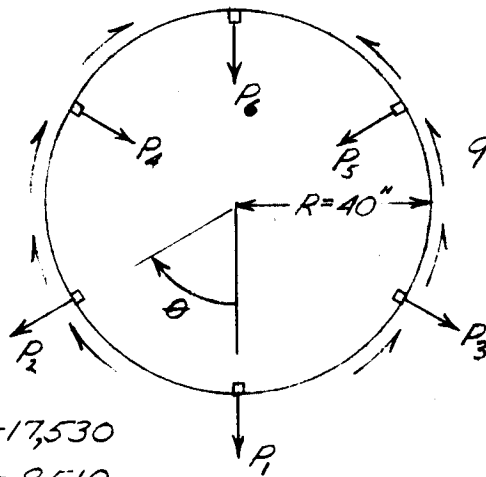
IN PLANE LOADS DUE TO 3.2×10^6 IN# MOMENT
CRITICAL LONGERONS

$$26,650 \times \frac{8.8}{13} = 18,040 \# \text{ LIMIT}$$

SECONDARY LONGERONS

$$\frac{18,040}{2} = 9,020 \text{ LIMIT}$$

IN PLANE LOADS DUE TO 40,000# SHEAR CAN BE
NEGLECTED IN DETERMINING THE RING BENDING
MOMENT & AXIAL LOAD.



$$P_1 = 18040 - 510 = +17530$$

$$P_2 = 9020 - 510 = +8510$$

$$P_3 = 9020 - 510 = +8510$$

$$P_4 = -9020 - 510 = -9530$$

$$P_5 = -9020 - 510 = -9530$$

$$P_6 = -18040 - 510 = -18550$$

$$q = 431 \sin \theta$$

BY	GENERAL ELECTRIC	PAGE
CK.		MODEL VOYAGER
DATE		REV.

KICK RING STASY

RING MOMENT (REF 4) (RIGID RING THEORY)

θ	M_1/R	M_2/R	M_3/R	M_4/R	M_5/R	M_6/R	M(IN#)
0	4184	766	766	210	210	1477	63,800
60	1578	2031	187	858	759	408	30,920
120	386	766	677	2275	210	1670	34,800
180	1395	187	187	858	858	4428	67,640

- MOMENT DENOTES COMP. IN INNER FIBERS

RING AXIAL LOAD (REF 4) (RIGID RING THEORY)

θ	P_1	P_2	P_3	P_4	P_5	P_6	P(LB)
0	4190	3447	3447	238	238	4433	15,041
60	7100	2034	213	3860	2278	464	7,301
120	438	3447	2034	2278	238	7513	8,178
180	4190	213	213	3860	3860	4433	15,917

+ DENOTES TENSION

BY
CK.
DATE

GENERAL ELECTRIC

PAGE
MODEL VOYAGER
REPORT

KICK RING STA 59

THE MIN. WEB GAGE CAN BE ESTIMATED BY CONSIDERATION OF TORSIONAL LOAD COND. 2C

THE SHEAR IN EACH OF THE 36 SHEAR PINS WILL BE

$$V_p = \frac{T}{36R} = \frac{12,000,000}{36 \times 40} = 8333 \# \text{ LIMIT}$$

$\frac{7}{16}$ " GALV TITANIUM SHEAR PINS ARE ADEQUATE

FOR BEARING IN 7075T6 MAT'L WEB

$$\text{MIN. } t = \frac{16 \times 8333}{7 \times 107,000} = .178" \text{ WHICH IS TOO THICK FOR AN EFFICIENT BENDING SECTION.}$$

THEREFORE, USE .2" THICK PAD IN SHEAR PIN AREA & .1" NOMINAL WEB GAGE. THE BASIC DESIGN APPROACH WAS TO SELECT A SECTION IMMUNE TO CRIPPLING & LATERAL BUCKLING WITH A MINIMUM PRODUCT OF INERTIA. THE ADVANTAGE OF SUCH A SECTION IS THAT BENDING DEFLECTIONS ARE IN THE PLANE OF LOADING & THE MODULUS OF RUPTURE CAN BE USED TO DETERMINE ULTIMATE LOADS.

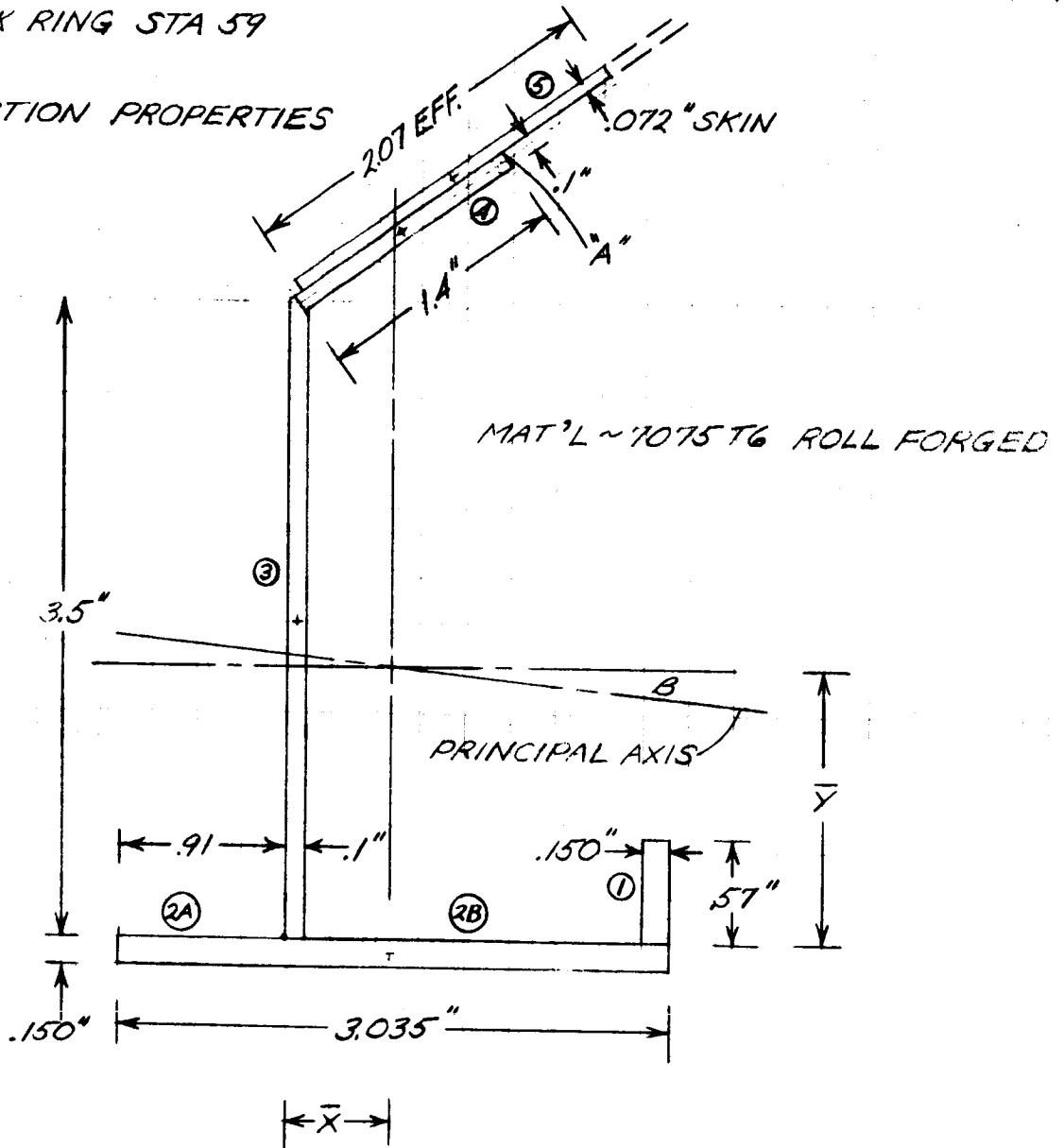
BY
CK.
DATE REV.

GENERAL ELECTRIC

PAGE
MODEL VOYAGER
REPORT

KICK RING STA 59

SECTION PROPERTIES



ELEM	A	Y	AY	AY	AA ²	I _e	I _x
1	.08530	.285	.02437	1.21925	.12710	.00231	.12941
2	.45525	-.075	-.03414	1.57925	1.13541	.00085	1.13626
3	.35000	1.750	.61250	.24575	.02114	.35729	.37843
4	.14000	3.900	.54600	2.39575	.80355	.00760	.81115
5	.14904	4.200	.62597	2.69575	1.08308	.01756	1.10064
	1.17979	1.50425	1.77470				3.55589
		Y					

BY CK. DATE	GENERAL ELECTRIC	PAGE MODEL VOYAGER REPORT
REV.		

KICK RING STA 59

SECTION PROPERTIES

ELEM	A	X	AX	AY	A \bar{X}^2	I _x	I _y
1	.08550	2.050	.17528	1.45631	.18133	.00016	.18149
2	.45525	.6075	.27656	.01381	.00009	.34945	.34954
3	.35000	.0750	.02625	.51869	.09416	.00029	.09445
4	.14000	.6300	.08820	.03631	.00018	.01538	.01601
5	.14904	.9000	.13414	.30631	.01398	.03572	.04970
	1.17979	.59369	.70043				.69119
		\bar{X}					

ELEM	A	AY	AX	I _{xy}
1	.08550	-1.21925	+1.45631	-.15181
2	.45525	-1.57925	+.01381	-.00992
3	.35000	+.24575	-.51869	-.04461
4	.14000	+2.39575	+.03631	+.01218
5	.14904	+2.69575	+.30631	+.12307
				-.07109

$$\tan \beta = \frac{I_{xy}}{I_y} = -.10235$$

$$\beta = -5^{\circ}52'$$

BY
CK.
DATE

GENERAL ELECTRIC

PAGE
MODEL VOYAGER
REPORT

KICK RING STA 59

STRESS ANALYSIS (LIMIT LD.)

AT $\theta = 180^\circ$, PT. "A" IS CRITICAL IN COMPRESSION. ELEMENTS IN THE EFFECTIVE SKIN MORE DISTANT FROM THE PRINCIPAL AXES ARE AT A LOWER STRESS LEVEL DUE TO BUCKLING IN THE SKIN

THE BENDING STRESS AT PT "A"

$$f_b = -\frac{-M_x I_{xy} X}{I_x I_y - I_{xy}^2} - \frac{M_x I_y Y}{I_x I_y - I_{xy}^2} \quad (\text{REF. 7})$$

WHERE

$$M_x = +67640 \text{ LIMIT}$$

$$I_x = 3.55589$$

$$I_y = .69919$$

$$I_{xy} = -.07109$$

$$X = +.58''$$

$$Y = +2.93''$$

$$f_b = -1137 - 53,943 = -55,080 \text{ LIMIT}$$

THE STRESS DUE TO AXIAL LOAD

$$f_a = \frac{-15,917}{1.17979} = -13,491$$

TOTAL $f_t = 68,571$ WHICH IS SLIGHTLY HIGHER THAN THE YIELD STRENGTH OF 7025 T6 ROLL FORGED MATERIAL. THE COMPUTED VALUE FOR f_t IS CONSERVATIVE, HOWEVER, DUE TO THE USE OF RIGID RING COEFFICIENTS IN THE CALCULATION OF THE RING MOMENT & AXIAL LOAD.

BY	GENERAL ELECTRIC	PAGE
CK.		MODEL VOYAGER
DATE		REV.

KICK RING STA 59

STRESS ANALYSIS (ULT. LD.)

$$\text{ULT } f_b = -1.25 \times 55,080 = -68,850$$

FOR A QUICK CHECK OF THE MODULUS OF RUPTURE,
ASSUME A FORM FACTOR OF $K=1.25$.

THE MODULUS OF RUPTURE $f_b \approx 90,000$ (REF. 8)

$$\text{BENDING STRESS RATIO } R_b = \frac{68,850}{90,000} = .765$$

$$\text{THE AXIAL STRESS RATIO } R_a = \frac{1.25 \times 13,491}{73,000} = .231$$

$$\text{CONSERVATIVE } MS = \frac{1}{R_a + R_b} - 1 = \underline{\underline{+1.004}}$$

FLANGE BUCKLING

ELEM 1 & 2A

MAX. ALLOW. b/t TO PREVENT BUCKLING = 6.4 (REF. 4)

$$\text{ELEM 1 } b/t = .645/.150 = 4.3$$

$$\text{ELEM 2A } b/t = .96/.150 = 6.4$$

BUCKLING IS PREVENTED IN ELEM 2B IF ELEM 1 IS
SUFFICIENT TO PROVIDE EDGE SUPPORT

$$b/t_1 = 4.3 \leq .328 \frac{b_{2B}}{t_{2B}} = .328 \frac{2,000}{.150} = 4.37 \text{ (REF. 2)}$$

$$4.3 \leq 4.37 \text{ O.K.}$$

BY CK. DATE	GENERAL ELECTRIC	PAGE MODEL VOYAGER REPORT
REV.		

FRAMES - STATION 46 AND 20

Due to geometry, the frame at Station 46 is subjected to higher loading under condition 3b than the frame at Station 20. This can be readily seen from comparison of the loading parameter $M \tan \phi$ for each ring.

M = applied bending moment

ϕ = angle of inclination of the longerons from vertical

At Station 46

$$M \tan \phi = 3.6 (10)^6 (.675) = 2.43 (10)^6$$

At Station 20

$$M \tan \phi = 4.9 (10)^6 (.4245) = 2.08 (10)^6$$

In consideration of the minimum reasonable machining gages (.07) and the minimum thermal requirement (.055 if 7075-T6 Al alloy is used) both rings are constructed of the same section. Therefore, the frame analysis is performed only for station 46. Torsional loads are higher at Station 20, and consequently this frame is analyzed for condition 2c.

METHOD OF ANALYSIS

As an example of the computerized methods of analysis available, the analysis has been performed using the General Electric Co's MASS computer program. This program is based on the Matrix Force Method of analysis and is readily adaptable to any three dimensional space framework. Additional routines, which permit the introduction of shear panels and bending plates in combination with straight and curved members, can be used to allow a completely computerized analysis of the equipment module and propulsion system support assembly.

The program calculates deflections, loads and stresses in six directions. It includes features for pinned and sliding connections anywhere in the structure, unsymmetrical bending, distributed mass, eccentric connections, shear distortion, variable material properties and loads, and thermal gradients through and along members.

Some simplifying assumptions are made in the analysis, such as

- 1) A constant member section is assumed
- 2) Local loads from planet scanner, canopus tracker and other frame mounted components are neglected.
- 3) Secondary forces from lateral bending and twisting of the equipment modules are neglected.

In view of these assumptions, a cross sectional configuration giving the highest compression strength utilizing the minimum manufacturing gage is chosen for the frames and the resulting margins of safety appear generous.

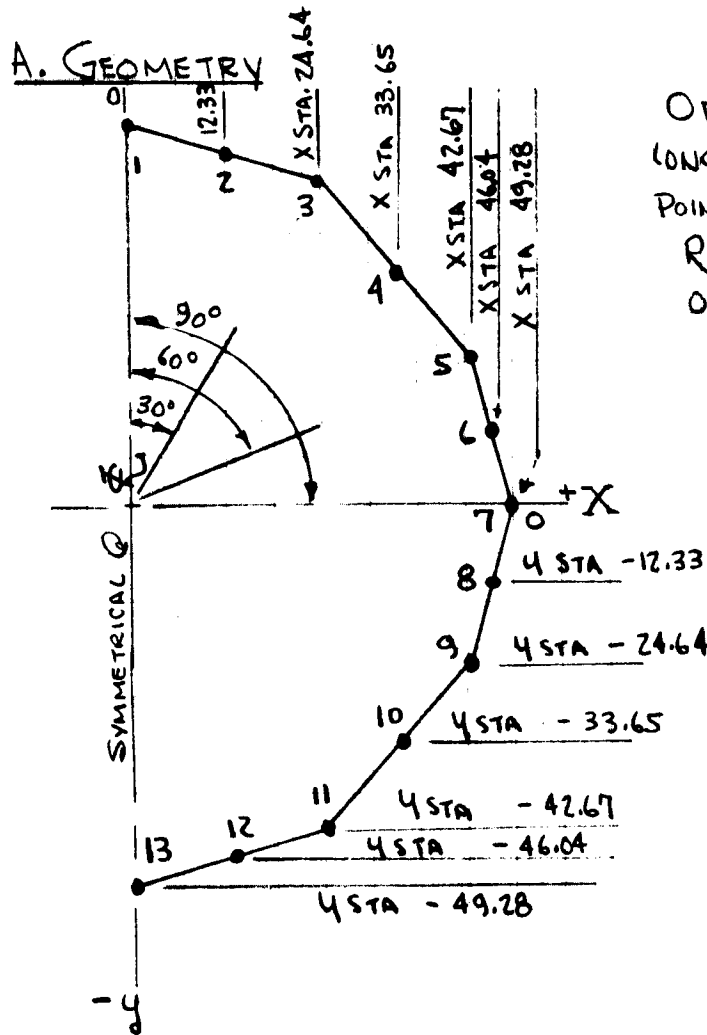
BY
CK.
DATE

GENERAL ELECTRIC

PAGE
MODEL VOYAGER
REPORT

FRAME - STA. 46

PROGRAM INPUTS

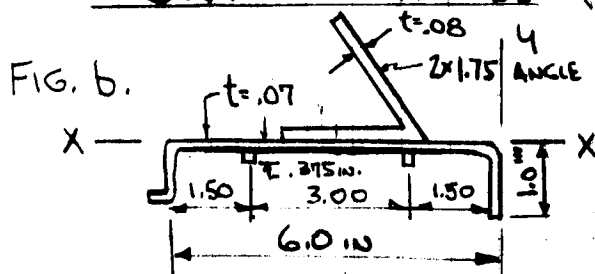


ODD NUMBERED JOINTS ARE LONGERON LOCATIONS AND POINTS OF LOAD APPLICATION
RADIUS FROM ORIGIN TO ODD NUMBERED JOINTS = 49.28 INCHES

EVEN NUMBERED JOINTS ARE MEMBER MIDPOINTS

ALL JOINTS ON RING CENTROID.

B. SECTION PROPERTIES (CONSTANT SECTION MEMBERS ASSUMED)



$I_{OX} = .1749 \text{ in}^4 \quad \bar{X} = 2.8232 \text{ in}$

$I_{OY} = 2.8898 \text{ in}^4 \quad \bar{Y} = .0930 \text{ in.}$
(AT LONGERON LOCATIONS)

$A = .9044 \text{ in}^2$

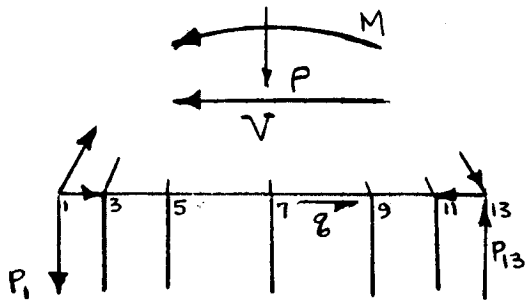
$P_{YY} = 1.7875 \text{ in.}$

MAT: 7075-T6 ALUMINUM

FRAME - STA 46

C. APPLIED LOADS - $\frac{Mc}{I}$, $\frac{VQ}{I}$ & $\frac{P}{A}$ DISTRIBUTION

ASSUME EQUAL LONGERON AREAS



$$c_i = R \cos \theta_i$$

$$I = \sum R^2 \cos^2 \theta_i$$

$$Q = \sum R \cos \theta_i$$

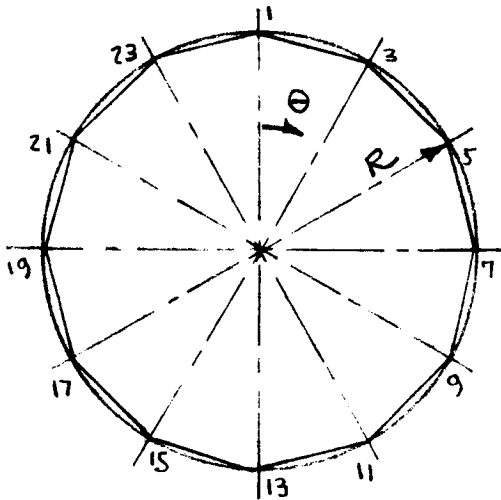
THEN

$$P_i = \frac{P}{A} + \frac{Mc_i}{I} = \frac{MR \cos \theta_i}{\sum R^2 \cos^2 \theta_i} = \frac{M}{R} K_i + \frac{P}{A}$$

WHERE $K_i = \frac{\cos \theta_i}{\sum \cos^2 \theta_i}$

$$Q_i = \frac{VQ}{I} = \frac{V \sum R \cos \theta_i}{\sum R^2 \cos^2 \theta_i} = \frac{V}{R} K_{si}$$

WHERE $K_{si} = \frac{\sum \cos \theta_i}{\sum \cos^2 \theta_i}$



ELEMENT No.	$\cos \theta$	$\cos^2 \theta$	$K_i = \frac{\cos \theta}{\sum \cos^2 \theta}$	SHEET ELEMENT	$\sum \cos \theta_i$	$K_{si} = \frac{\sum \cos \theta_i}{\sum \cos^2 \theta_i}$
1,13	1.00000	1.00000	.16667	1-3	.50000	.08333
3,11,15,23	.86603	.75000	.14434		3-5	1.36603
5,9,17,21	.50000	.25000	.08333	5-7	1.86603	.31100
7,19	0	0	0			

$\sum \cos^2 \theta = 6.00$

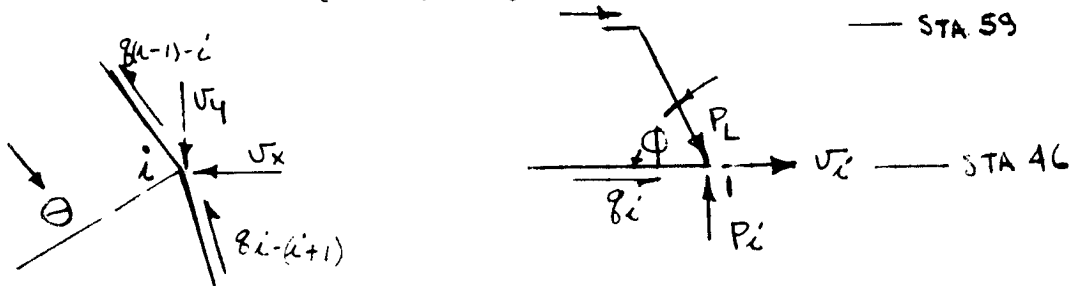
FRAME - STA.46

C. APPLIED LOADS (CONT.)

CONDITION 3b
1975/77 MISSION

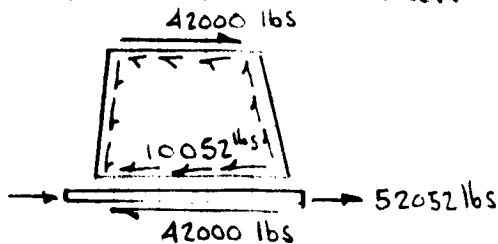
P = 4500 lbs
M = 3800 (10)³ IN-lbs
V = 42000 lbs

CALCULATION OF $\sum X_i$, $\sum Y_i$ & q_i



STA. ①	K_i ②	$\frac{M}{R}$ ③	P_{m_i} ④ ② x ③	$\frac{P}{12}$ ⑤	P_i ⑥ ④ + ⑤	TAN ⑦ Φ	U_i ⑧ ⑥ x ⑦	SIN θ	COS θ	$U_i \sin \theta$ = $\sum X_i$	$U_i \cos \theta$ = $\sum Y_i$
1	.16667	77110	12852	375	13227	.675	8928	0	1.000	0	8928
3	.14434	↑	11130	↑	11505	↑	7766	.500	.866	3883	5726
5	.08333	↑	6426	↑	6801	↑	4591	.866	.5	3976	2296
7	0	↑	0	↑	375	↑	253	1.000	0	253	0
9	-.08333	↓	-6426	↓	-6051	↓	-4084	.866	-.5	-3537	2042
11	-.14434	↓	-11130	↓	-10755	↓	-7260	.5	-.866	-3630	6297
13	-.16667	77110	-12852	375	-12477	.675	-8422	0	-1.000	0	8422
										$\sum U_i (1 \text{ to } 13)$	52052

BALANCING SHEAR FLOW



REACT TOTAL BY $\frac{VQ}{I}$ DISTRIBUTION

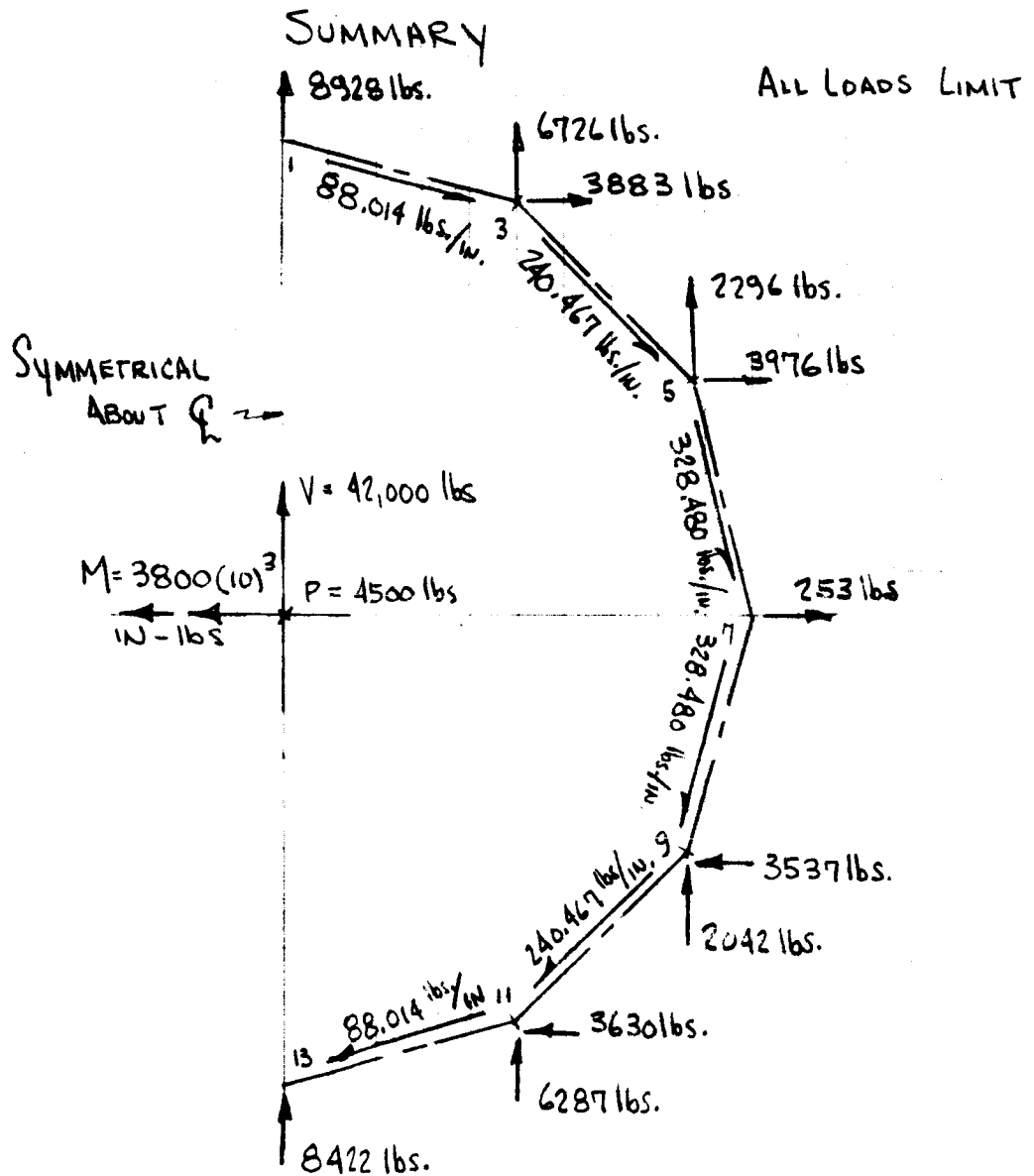
SHEET ELEMENT	$\frac{V}{R}$	K_{sc}	$q_i = K_{sc} \frac{V}{R}$ (#/IN)
1-3	1056.2	.08333	88.014
11-13			
3-5	↑	.22767	240.467
9-11			
5-7	1056.2	.31100	328.480
7-9			

NOTE: 10052 lbs IS TOTAL
OF LONGERON AXIAL LOAD COMPONENT
SKIN SHEAR = 42000 lbs.

BY CK. DATE REV.	GENERAL ELECTRIC	PAGE MODEL VOYAGER REPORT
---	-------------------------	---------------------------------

FRAME - STA. 46

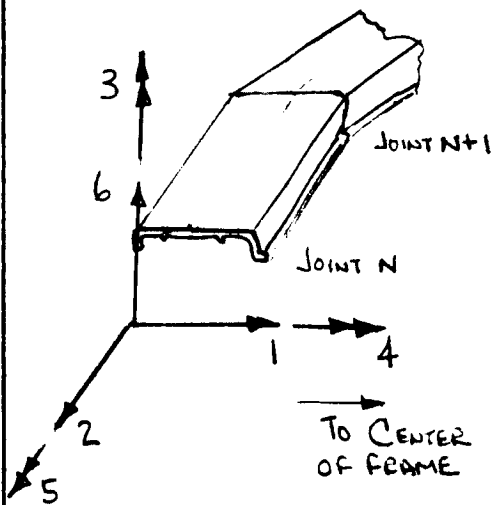
C. APPLIED LOADS (CONT.)



FRAME - STA 46

PROGRAM OUTPUTS -

THE MEMBER LOADS AS CALCULATED ARE SUMMARIZED IN THE TABLE BELOW. THE STRESSES AND DEFLECTIONS OBTAINED ARE NOT REPEATED HERE, SINCE THEY ARE NOT APPLICABLE TO BOTH SECTIONS. THE DIRECTIONS GIVEN REFER TO SIGN CONVENTION SHOWN. ZERO STRESS RESULTANTS ARE OBTAINED FOR DIRECTIONS 4, 5 & 6 SINCE THE FRAME IS RESTRAINED FROM TWISTING BY THE ELECTRONIC MODULES AND AXIAL LOADS ARE TAKEN BY THE LONGERONS.



FRAME IS ORTHOGONAL
 AT EACH JOINT
 POSITIVE SENSE SHOWN

FORCE JOINT	RADIAL SHEAR 1	AXIAL FORCE 2	IN PLANE MOMENT 3
1	-88.4	17230.0	1550.0
2	165.1	16110.0	422.9
3	-82.3	14990.0	1401.5
4	-13.2	11920.0	1329.2
5	-47.6	8865.7	1088.3
6	47.9	4673.8	239.9
7	-4.3	493.1	3.2
8	-37.9	-3694.1	-288.0
9	42.4	-7878.2	-1062.8
10	12.1	-10940.0	-1296.8
11	77.4	-14000.0	-1376.0
12	-155.1	-15130.0	-467.7
13	83.9	-16250.0	-1537.1

BY	GENERAL ELECTRIC	PAGE
CK.		MODEL VOYAGER
DATE		REV.

FRAME - STA 46

STRESS ANALYSIS

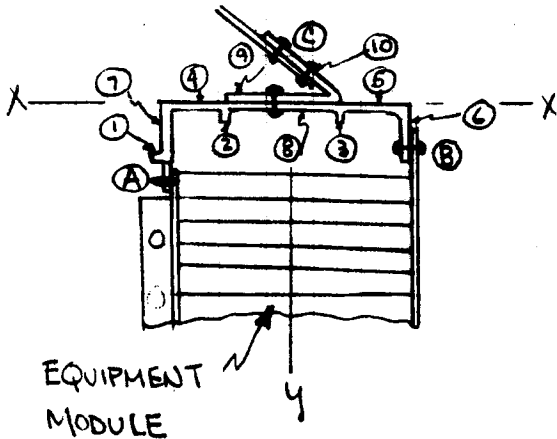


FIG b.

THE SECTION HAS BEEN DESIGNED TO PROVIDE THE MAXIMUM COMPRESSIVE LOAD PATH UTILIZING THE MINIMUM GAGE CONSISTANT WITH THERMAL REQUIREMENTS AND MANUFACTURING RESTRICTIONS.

ATTACHMENTS AT "B" & "C" PROVIDE RESTRAINT AGAINST BUCKLING ABOUT THE X AXIS. TWO SHEAR PINS PER SECTION (A) PROVIDE LATERAL STABILITY UNDER BENDING LOADS TO THE OUTSTANDING FLANGE.

BUCKLING ABOUT AXIS Y

$L = 25.53 \text{ IN.}$

SHORT COLUMN BUCKLING ALLOWABLE

$r_y = 1.7875$

$L' = \frac{L}{C}$ C = FIXITY FACTOR = .75 ASSUMED

PARTIAL FIXITY

$\frac{L'}{r} = 19.2$

$F_{CC} = 60,000 \text{ PSI}$

(REF. 4)

MAXIMUM STRESS AT JOINT 1

$f = \frac{Mc}{I} + \frac{P}{A} = \frac{1550(3.18)}{2.8898} + \frac{17230}{.9044} = 20805 \text{ PSI}$ LIMIT

$M.S. = \frac{60,000}{20805(1.75)} - 1 = \underline{\underline{+1.30}}$

BY CK. DATE REV.	GENERAL ELECTRIC	PAGE MODEL VOYAGER REPORT
<p data-bbox="267 287 592 340"><u>FRAME - STA 46</u></p> <p data-bbox="284 383 625 436"><u>STRESS ANALYSIS</u></p> <p data-bbox="316 478 1096 542">LOCAL CRIPPLING (REF. FIGURES a & b)</p> <p data-bbox="300 585 1437 1032"> THE SECTION IS CRITICAL IN FLANGE AND WEB CRIPPLING. SUPPORT LIPS ①, ② & ③ OF FIGURE b. ARE DESIGNED TO PROVIDE SIMPLE SUPPORT TO REDUCED WEB WIDTHS RESULTING IN A GREATER LOAD CARRYING CAPACITY FOR BOTH AXIAL COMPRESSION AND SHEAR TRANSFER. TO PROVIDE THIS SUPPORT, A LIP MUST HAVE SUFFICIENT STIFFNESS, YET NOT BUCKLE AT A LOWER STRESS THAN THE WEBS. THIS WILL BE ACCOMPLISHED IF THE b/t RATIO OF THE LIP SATISFIES BOTH </p> $.910 \left(\frac{bL}{t}\right)^3 - \frac{bL}{t} = 5 \left(\frac{b}{t}\right)_{\text{WEB}}$ <p data-bbox="397 1159 1331 1266"> AND $\frac{bL}{t} \leq .328 \left(\frac{b}{t}\right)_{\text{WEB}}$ REF <u>2</u> </p> <p data-bbox="397 1287 1388 1393"> For $\left(\frac{b}{t}\right)_{\text{WEB}} = \frac{1.5}{.07} = 21.5$, A .375" by .07" LIP </p> <p data-bbox="852 1404 1128 1447">IS ADEQUATE.</p> <p data-bbox="381 1447 1437 1542"> THE 3.0 INCH WEB IS TREATED AS TWO 1.5" by .07 ONE END FREE ELEMENTS </p>		

BY	GENERAL ELECTRIC	PAGE
CK.		MODEL VOYAGER
DATE		REV.

FRAME - STA 46
CRIPPLING STRENGTH

ELEMENT	b IN.	t IN.	AREA = bt in ²	$\frac{b}{t}$	ENDS FREE	F _{CC} * PSI	P _{CC} lbs	F _{CC} FOR SECTIONS	
1	.375	.07	.026	5.4	ONE	68,000	1768	$F_{CC} = \frac{\sum P_{CC}}{\sum A}$ $= \frac{51424}{.901}$ $= 57000 \text{ psi}$	
2	.375	↓	.026	5.4	ONE	68,000	1768		
3	.375		.026	5.4	ONE	68,000	1768		
4	1.43		.100	20.4	NONE	68,000	6800		
5	1.43		.100	20.4	NONE	68,000	6800		
6	.93		.065	13.3	NONE	68,000	4420		
7	.86		.060	12.3	NONE	68,000	4080		
8 } 8 }	1.46 1.46		.07 ↓	.102 .102	20.6 20.6	ONE ONE	27,000 27,000		2754 2754
9	1.		.08	.134	20.9	NONE	68,000		9112
10			.08	.160	25.0	NONE	47,000		9400

$\sum A = .901$

$\sum P_{CC} = 51424$

* INCLUDES RADII REF. 4

CRIPPLING MARGIN

M.S. = $\frac{57000}{20805(1.25)} - 1 = \underline{\underline{+1.19}}$

IF LIPS ② AND ③ ARE ELIMINATED, ELEMENTS ④, ⑤ AND ⑧ DEVELOP ONLY 6400 lbs. AND THE STRENGTH OF THE SECTION IS GREATLY REDUCED.

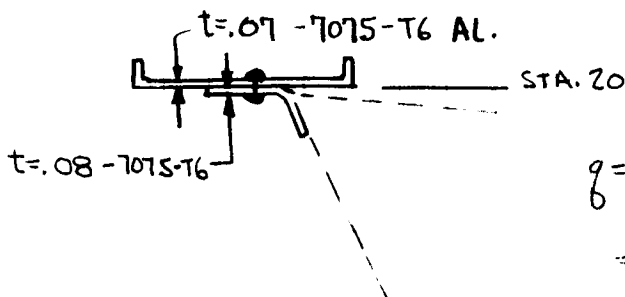
$F_{CC} = 40,000 \text{ PSI}$

$f_c = \sim 24000 \text{ PSI}$

M.S. = $\frac{40,000}{24000(1.25)} - 1 = \underline{\underline{+1.30}}$

FRAME - STA. 20 - SHEAR TRANSFER

THE SHEAR LOADS AT STATION 20, RESULTING FROM CONDITION 2C, ARE LIMITING IN THE DESIGN OF THE BUS ATTACHMENT STRUCTURE.



LOADS
 $q = 828.3 \text{ * / IN}$ LIMIT

$$q = (828.3)(1.15) = 955 \text{ * / IN YIELD}$$

$$= (828.3)(1.25) = 1035 \text{ * / IN ULT.}$$

THE JOINT IS DESIGNED SO THAT IT IS CRITICAL IN SHEET BEARING. HIGH SHEAR TITANIUM - $\frac{1}{4}$ IN. BOLTS ARE USED AT 1.75 IN. PITCH.



$$f_{bry} = \frac{1.75 (955)}{.07 \times .25} = 95600 \text{ psi}$$

$$f_{brv} = 104,000 \text{ psi}$$

$$F_{bry} = 96,000 \text{ psi}$$

$$F_{brv} = 135,000 \text{ psi}$$

$$M.S. = \frac{96,000}{95,600} - 1 = \underline{\underline{+1.005}}$$

BOLT - TITANIUM

$$F_{Su} = 89,000 \text{ psi MIN.}$$

$$\text{SHEAR LOAD / BOLT} = 1.75 (1035) = 1810 \text{ lbs. ULT.}$$

$$P_{ALL} = 80000 (.049) = 3920 \text{ lbs.}$$

$$M.S. = \frac{3920}{1810} - 1 = \underline{\underline{+1.00}}$$

INTERVET BUCKLING IN FLANGE OF SUPPORT RING.

$$f_c = \frac{1810}{.08} = 22650 \text{ psi}$$

$$F_{c12} = 53000 \text{ psi} \left(\frac{S}{t} = \frac{1.75}{.08} = 21.9 \right) \text{ (REF 2)}$$

$$M.S. = \frac{53000}{22650} - 1 = \underline{\underline{+1.33}}$$

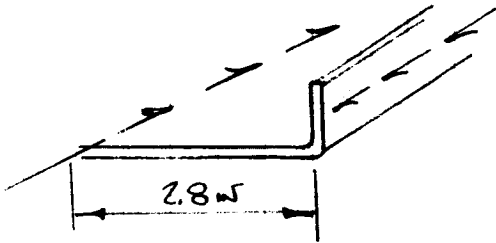
BY
CK.
DATE

GENERAL ELECTRIC

PAGE
MODEL VOYAGER
REPORT

FRAME - STA 20

SHEAR STRESS IN FRAME



$$q = 1035 \text{ lb/in VLT}$$

$$f_s = \frac{1035}{.07} = 14,800 \text{ PSI}$$

$$F_{Sce} = KE \left(\frac{t}{b} \right)^2 = 4.8 (10.5) (10)^6 \left(\frac{.07}{28} \right)^2$$

$$= 31,500 \text{ PSI}$$

$$M.S. = \frac{31500}{14800} - 1 = \underline{\underline{+1.13}}$$

BY

GENERAL ELECTRIC

PAGE

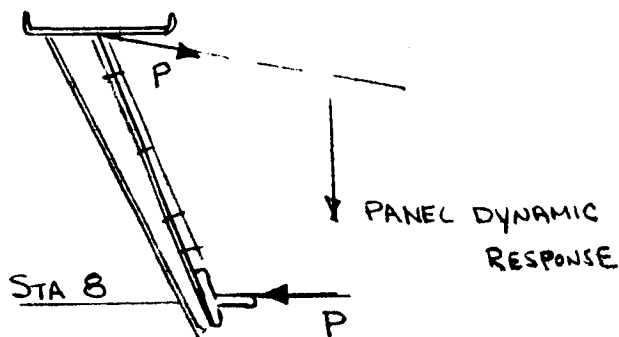
CK.

MODEL VOYAGER

DATE

REV.

REPORT

SOLAR PANEL KICK RING - STA. 8,5

THE TEE RING AT STATION 8 IS DESIGNED TO TAKE THE COUPLE LOADS IN THE PANEL SUPPORT CAPS. THE RESTRAINT OFFERED BY THE LONGERONS AT INTERMEDIATE RIBS IS CONSIDERED ONLY IN BEING SUFFICIENT TO REDUCE THE TWIST IN THE UNSYMMETRICAL TEE TO NEGLIGIBLE PROPORTIONS

FROM THE SOLAR PANEL ANALYSIS

$$P = 1645 \text{ lbs. YIELD } \left(\frac{1.25}{1.15} \right) = 1790 \text{ ULTIMATE}$$

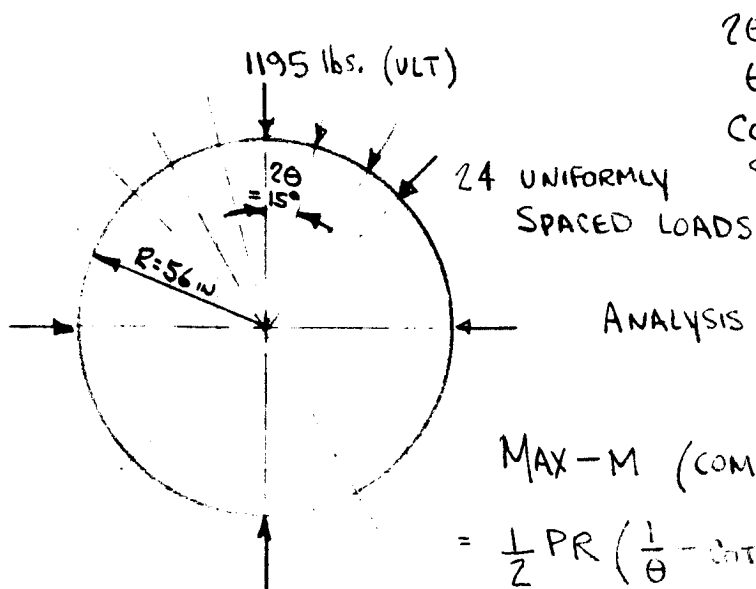
THIS IS BASED ON THE RESPONSE OF THE FIXED PANEL AND A FOLD OUT PANEL. IN CONSIDERATION OF THE PRESENT REQUIREMENT FOR ONLY ONE FOLD OUT PANEL AND OF THE LOCAL LOADS ONLY TWO OPPOSITE RIBS INDUCED BY THE ANTENNA THE ULTIMATE DESIGN LOAD IS TAKEN AS

$$P = \frac{2}{3} (1790) = 1195 \text{ lbs.}$$

WITH LOCAL BUILD-UP ADDED AS REQUIRED.

BY	GENERAL ELECTRIC	PAGE
CK.		MODEL VOYAGER
DATE		REV.

SOLAR PANEL KICK RING - STA 8.5



$$2\theta = 15^\circ$$

$$\theta = 7.5^\circ = .13090 \text{ RADIANS}$$

$$\cot \theta = 7.5958$$

$$\sin \theta = .13053$$

ANALYSIS IS BY REF 9

MAX - M (COMPRESSION ON INNER FLANGE)

$$= \frac{1}{2} PR \left(\frac{1}{\theta} - \cot \theta \right) \text{ AT EACH LOAD POINT}$$

$$= \frac{1}{2} (1195)(56) \left(\frac{1}{.13090} - 7.5958 \right)$$

$$= 1460 \text{ IN-LBS}$$

$$\text{MAX + M} = \frac{1}{2} PR \left(\frac{1}{\sin \theta} - \frac{1}{\theta} \right) \text{ MID POINT BETWEEN LOADS}$$

$$= \frac{1}{2} (1195)(56) \left(\frac{1}{.13053} - \frac{1}{.13090} \right) = 725 \text{ IN-LBS}$$

(COMPRESSION DUE TO AXIAL LOAD)

$$\text{AT LOAD POINTS} \quad T = \frac{1}{2} P \cot \theta = 4530 \text{ lbs}$$

$$\text{AT MID POINTS} \quad T = \frac{1}{2} P \left(\frac{1}{\sin \theta} \right) = 4570 \text{ lbs}$$

SECTION PROPERTIES OF TEE - 2 x 1 x .078 7075-T6 AL ALLOY

$$A = .231 \text{ IN}^2$$

$$I_{xx} = .0171 \text{ IN}^4$$

$$\bar{y} = .194 \text{ IN}$$

ASSUME EFFECTIVE SKIN = 30t (SKINT = .064)

$$\left\{ \begin{array}{l} A = .353 \text{ IN}^2 \\ I_{xx} = .0215 \text{ IN}^4 \\ \bar{y} = .125 \text{ IN} \end{array} \right.$$

BY	GENERAL ELECTRIC	PAGE
CK.		MODEL VOYAGER
DATE		REV.

SOLAR PANEL KICK RING - STA 8.5

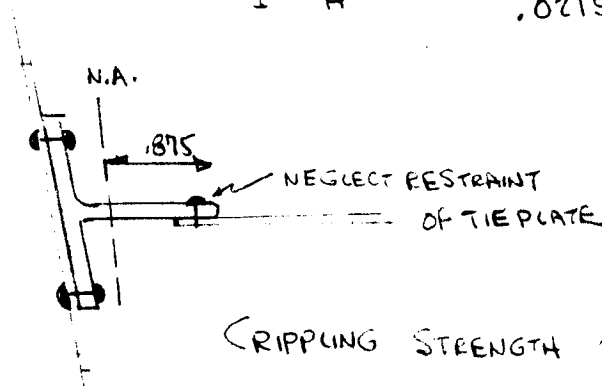
ULT. COMPRESSIVE STRESS

AT LOAD PTS. - INNER FLANGE STRESS

$$f_c = \frac{Mc}{I} + \frac{P}{A} = \frac{1460 (.125)}{.0215} + \frac{4530}{.353} = 20,300 \text{ PSI}$$

AT MID PTS - OUTER WEB STRESS

$$f_c = \frac{Mc}{I} + \frac{P}{A} = \frac{725 (.875)}{.0215} + \frac{4570}{.353} = 42,800 \text{ PSI}$$



CRIPPLING STRENGTH OF WEB

$$\frac{b}{t} = \frac{.875}{.078} = 11.2$$

$$F_{cc} = 45,000 \text{ PSI (REF 4)}$$

(7075 T-6 AL)

$$M.S. = \frac{45,000}{42,800} - 1 = \underline{\underline{+.05}}$$

BY
CK.
DATE

REV.

GENERAL ELECTRIC

PAGE 46
MODEL VOYAGER
REPORT

MONOCOQUE SECTION BETWEEN STA. 0 & STA. 3.5 - COND. 3b.

SHORT CYLINDERS BEHAVE AS FLAT PLATE COLUMNS IN BUCKLING. THE MAX. EDGE LOADING PER INCH IS

$$P = \left[\frac{P_0}{2\pi R} + \frac{M_0}{\pi R^2} \right] \frac{17.36}{15.3} *$$

AT STA 0

$$P_0 = 7000 \# \text{ LIMIT}$$

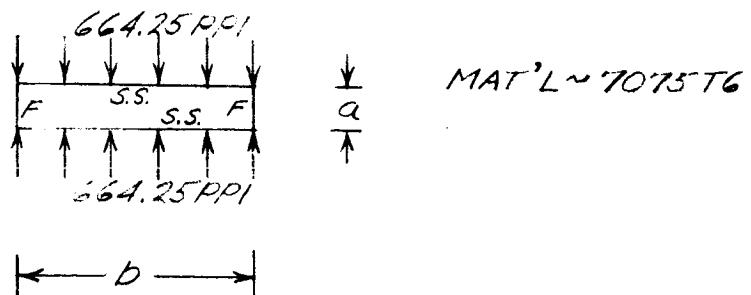
$$M = 5.8 \times 10^4 \text{ IN} \# \text{ LIMIT}$$

$$R = 60''$$

} COND. 3b - '75, '77 CONFIG.

$$P = 18.57 + 512.83 = 531.4 \text{ PPI LIMIT}$$

$$P = 1.25 \times 531.4 = 664.25 \text{ PPI ULT}$$



IDEALIZED STRUCTURE

$$a = 3.5 \times \frac{17.36}{15.3} = 3.97$$

ASSUME b IS THE ARC LENGTH OF A 20° ANGLE

$$b = \frac{20R}{57.295} = 20.94''$$

*
NEGLECT SHEAR LAG EFFECTS

BY	GENERAL ELECTRIC	PAGE
CK.		MODEL VOYAGER
DATE		REV.

STA 0 TO 3.5 - LOAD COND. 3D - '75, '77 CONFIG.

$$\frac{a}{b} \approx .2$$

$$S' = K \frac{E}{(1-\nu^2)} \frac{t^2}{b^2} \quad (\text{REF. 2})$$

FOR SMALL VALUES OF a/b , THE "K" VALUE FOR ALL EDGES SIMPLY SUPPORTED WILL BE EQUAL TO THAT OF THE TWO EDGE FREE PLATE UNDER CONSIDERATION HERE.

$$K = 22.2$$

FOR OPTIMUM DESIGN

$$S't = 664.25 = \frac{KE}{1-\nu^2} \frac{t^3}{b^2}$$

$$t^3 = \frac{b^2(1-\nu^2)664.25}{KE} = \frac{20.94^2 \times .91 \times 664.25}{22.2 \times 10.3 \times 10^6} = 1159 \times 10^{-6}$$

REQ'D $t = .105''$ (USE $t = .110$)

BY CK. DATE	REV.	PAGE MODEL VOYAGER REPORT
-------------------	------	---------------------------------

GENERAL ELECTRIC

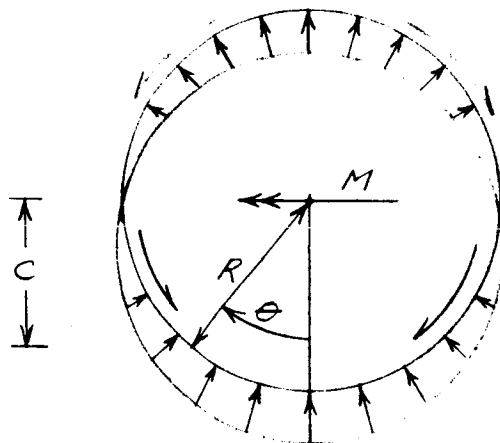
KICK RING STA C - LOAD CONDITION 3b & 2c, '15, '17 CONFIG.

DUE TO THE DISTRIBUTED NATURE OF THE KICK LOADS THAT MUST BE TAKEN BY THE RING AND THE NUMBER OF ATTACHMENTS (48) THAT PROVIDE SHEAR REACTIONS TO THESE LOADS, A SIMPLIFIED APPROACH TO THE PRELIMINARY SIZING OF THIS RING CAN BE TAKEN.

THE IN PLANE LOADS DUE TO THE 7000# AXIAL LOAD

$$P_a = \frac{7000}{2\pi R} \times \frac{17.36}{15.3} \times \frac{8.2}{17.36} = 9.95 \text{ \#/IN RADIALLY OUTWARD}$$

THE IN PLANE LOADS DUE TO THE 5.8×10^6 IN # MOMENT (NEGLECT SMALL KICK LOAD DUE TO BOLT & OFFSET)



$$P_{b\theta} = \frac{Mct}{I} \times \frac{8.2}{15.3} = \frac{M\cancel{R} \cos\theta}{\pi R^3 \cancel{t}} \times \frac{8.2}{15.3} = 274.85 \cos\theta \text{ \#/IN (REF. 4)}$$

BY
CK.
DATE

GENERAL ELECTRIC

PAGE
MODEL VOYAGER
REPORT

KICK RING STA. 0

BY RIGID RING THEORY

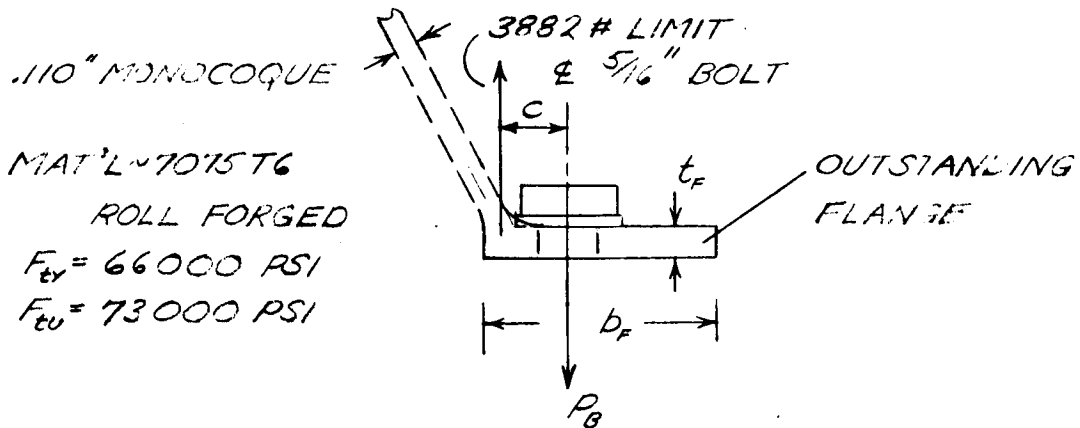
$$M_0 = 0$$

AT $\theta = \pi$

$$P_{MAX} = .5 \times 274.85 \times 60 + .5 \times 9.95 \times 120 = + 8843 \# \text{ LIMIT}$$

ASSUME ALL OF THIS LOAD TAKEN IN OUTSTANDING FLANGE. THE FLANGE MUST ALSO RESIST THE BOLT LOAD PRYING ACTION ON THE TENSION SIDE OF THE SPACECRAFT SUPPORT STRUCTURE.

$$\text{MAX. FLANGE LOAD} = \frac{2\pi R}{48} \left[\frac{M_0}{\pi R^2} - \frac{P_0}{2\pi R} \right] = 3882 \# \text{ LIMIT}$$



BY	GENERAL ELECTRIC	PAGE
CK.		MODEL VOYAGER
DATE	REV.	REPORT

KICK RING STA. 0

FOR AN ECCENTRICITY OF LOADING OF $C = .34"$,
WITH A FLANGE THICKNESS OF $t_f = .220$, THE ULT.
ALLOW. FLANGE LOAD IS 6230# (REF. 3)

$$MS = \frac{6230}{1.25 \times 3882} - 1 = +.28$$

THE MONOCOQUE SECTION IS LESS CRITICAL DUE
TO ITS CURVED PLATE STIFFNESS.

THE REQUIRED NET FLANGE AREA REQUIRED FOR
KICK LOADS

$$\begin{aligned} \text{REQ'D } A_{F \text{ NET}} &= \frac{1.25 \times 8843}{73,000} = .151 \\ &= t_f (b_f - \frac{5}{16}) \end{aligned}$$

$$\text{REQ'D } b_f = .998"$$

$$\text{LET } b_f = 1.2"$$

$$MS = \frac{1.2}{.978} - 1 = \underline{\underline{+.20}}$$

TENSILE BOLT LOAD

$$P_B = 1.25 \times 3882 \frac{b_f}{b_f - C} = 6770 \# \text{ ULT.}$$

$$\text{ALLOWABLE} = .07667 \times 130,000 = 9970$$

$$MS = \frac{9970}{6670} - 1 = \underline{\underline{+.47}}$$

SHEAR BOLT LOAD (COND. 2C)

$$V_B = \frac{T}{48R} = \frac{1.25 \times 12.72 \times 10^6}{48 \times 60} = 5521 \# \text{ ULT.}$$

$$\text{ALLOWABLE} = .07669 \times 80,000 = 6135 \quad MS = \frac{6135}{5521} - 1 = \underline{\underline{+.11}}$$

BY
CK.
DATE

GENERAL ELECTRIC

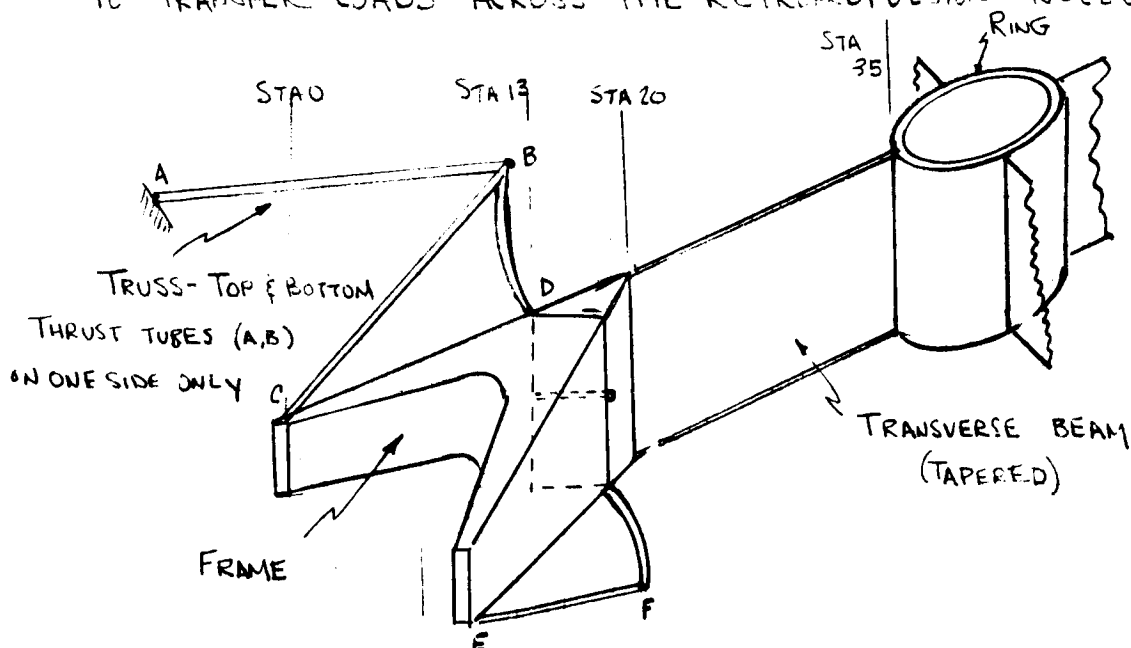
PAGE
MODEL VOYAGER
REPORT

PROPULSION SYSTEM SUPPORT STRUCTURE

THIS ANALYSIS IS PRESENTED TO SUBSTANTIATE A REPRESENTATIVE PROPULSION SYSTEM STRUCTURAL APPROACH. AS SHOWN IN THE FIGURE BELOW, THE BASIC STRUCTURAL ELEMENTS ARE A TRUSS WORK SUPPORTING THE LIGHTER HYDROGEN AND NITROGEN TANKS, AND A MAIN BEAM SUPPORTING THE FUEL AND OXIDIZER TANKS. THIS MAIN BEAM IS A COMPOSITE STRUCTURE, EMPLOYING RIGID FRAMES TO REACT TORSIONAL AND LATERAL LOADS AT THE ENDS AND A DEEP BENDING SECTION AT THE CENTER TO REACT THE BENDING MOMENTS INDUCED BY LONGITUDINAL LOADS.

TO AVOID USING THE TANKS AS TRUSS MEMBERS, AND TO ALLOW TANK GROWTH, ONLY ONE TRUSS UNION PER TANK IS USED THROUGH LOAD CAPABILITY.

THE CENTER SECTION OF THE TRANSVERSE BEAM CONSISTS OF A TOP AND BOTTOM RING FORMING A CYLINDRICAL HOUSING TO TRANSFER LOADS ACROSS THE RETROPROPULSION NOZZLE.

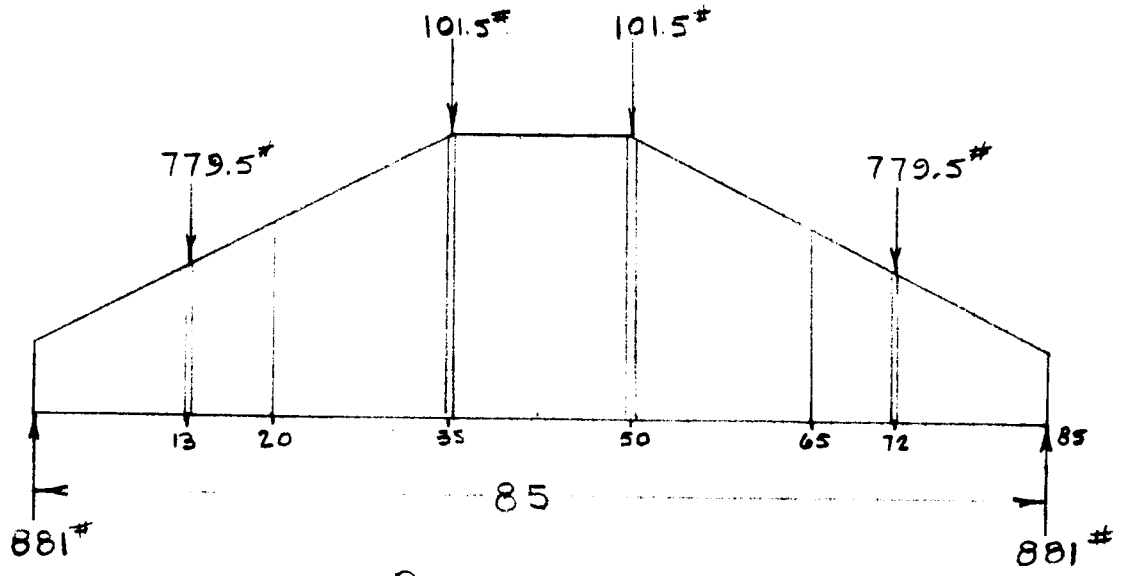


ANALYSIS IS SHOWN FOR SECTION 0-13, 20 TO 35, THE TRUSS TUBES AND THE CENTER RINGS.

BY CK. DATE	REV.	GENERAL ELECTRIC PAGE MODEL VOYAGER REPORT
-------------------	------	---

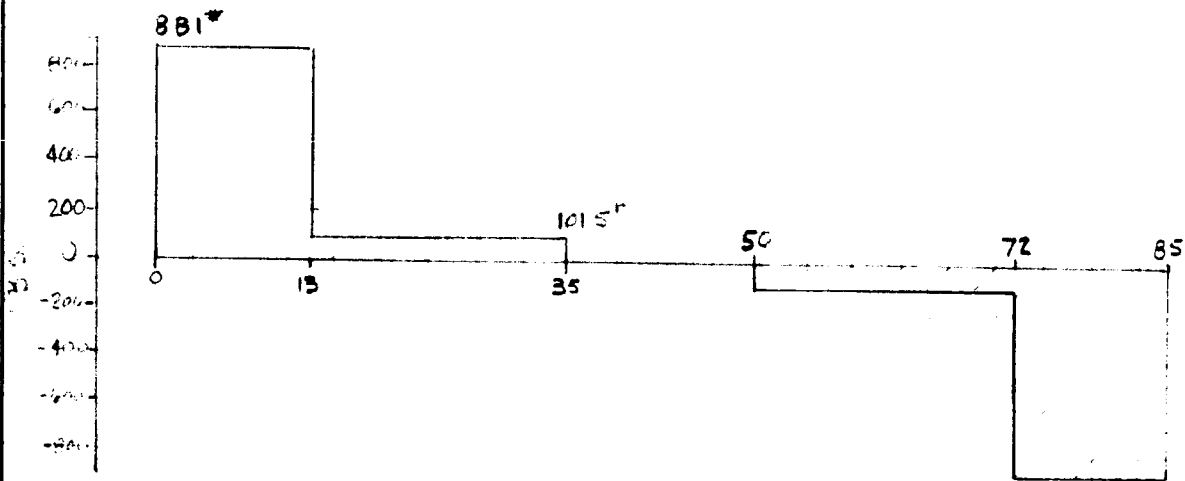
PROPULSION SYSTEM SUPPORT STRUCTURE

TRANSVERSE BEAM ANALYSIS



ONE g LOADING

SHEAR DIAGRAM

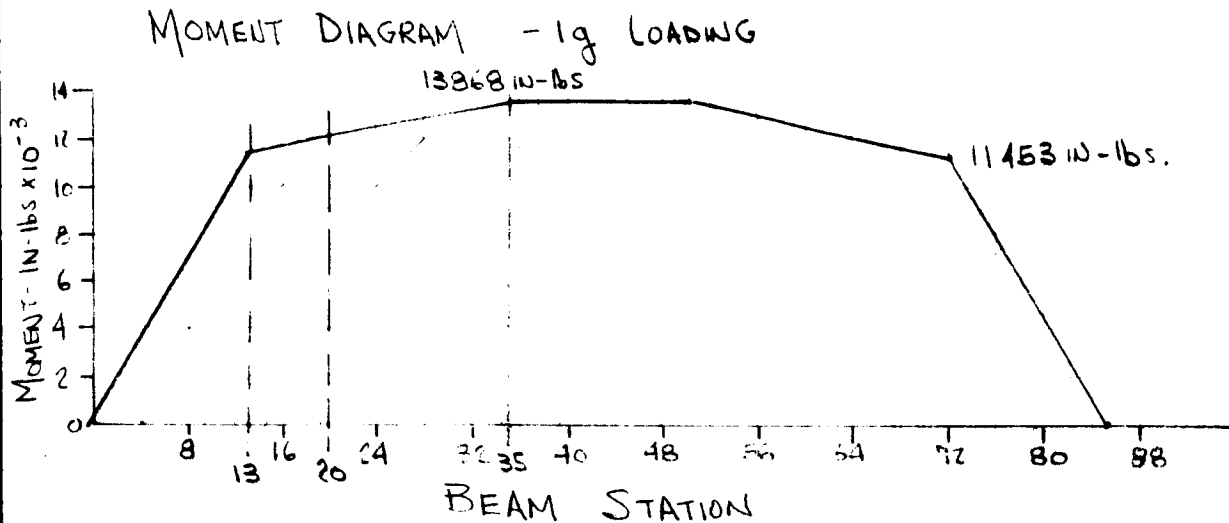


BY
CK.
DATE

GENERAL ELECTRIC

PAGE
MODEL 10YAGER
REPORT

PROPULSION SYSTEM SUPPORT STRUCTURE



DESIGN LOADS

THE CRITICAL LOADING CONDITION IS CONDITION 3a

THE EQUIVALENT STEADY STATE RESPONSE = $1.6 (10.76) = 17.25 \frac{1}{g}$

DESIGN YIELD LOAD FACTOR = $1 + 17.25 = 18.25 \frac{1}{g}$ *

DESIGN ULTIMATE LOAD FACTOR = $18.25 (1.25) = 22.8 \frac{1}{g}$

* THE 1.15 ALIGNMENT FACTOR IS NOT APPLIED TO YIELD LOADS SINCE THE VECTORING CAPABILITIES OF THE SYSTEM ARE DESIGNED TO COMPENSATE FOR MINOR MISALIGNMENTS.

SECTION 20-35

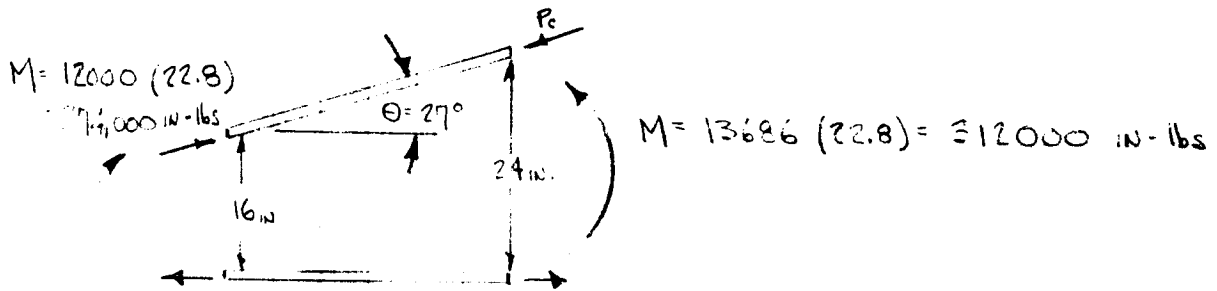
IN THIS SECTION THE WEB IS NOT DESIGNED TO REACT ANY PORTION OF THE MOMENT SINCE A RIGID CYLINDER WOULD BE REQUIRED TO TRANSFER STRESS RESULTANTS ACROSS THE ENGINE. THE WEB IS DESIGNED FOR SHEAR AND THE CAPS REACT THE MOMENT.

BY CK. DATE REV.	GENERAL ELECTRIC	PAGE MODEL VOYAGER REPORT
---	-------------------------	---------------------------------

PROPULSION SYSTEM SUPPORT STRUCTURE

SECTION 20-35

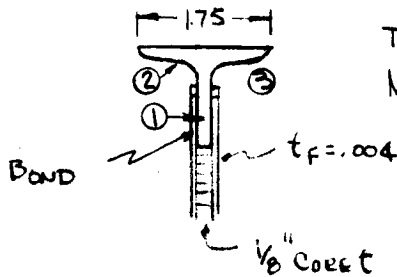
MAXIMUM COMPRESSIVE LOAD IN CAP



At STA 35: $P_c = \frac{312000}{24 \cos 27^\circ} = 14700 \text{ lbs.}$

At STA 20 $P_c = \frac{274,000}{16 \cos 27^\circ} = 19250 \text{ lbs}$

CAP DESIGN



Tee Section 1.75 x .1625 x .125

MATL - 7075-T6

PROPULSION SYSTEM SUPPORT STRUCTURE
 CAP 20-35 - LATERAL STABILITY

$$\frac{L}{\rho} = \frac{15}{.356}$$

$$= 42.1$$

$$F_c = 48,500 \text{ PSI} \quad \text{REF 4}$$

$$f = \frac{19,250}{.405}$$

$$= 47,500 \text{ PSI}$$

$$M.S. = \frac{48,500}{47,500} - 1$$

$$\underline{\underline{M.S. = .02}}$$

CRIPPLING

ITEM	b	t	b/t	F _c	A	F
1	1.562	.125	12.5	68,000	.1950	13300
2	.875	.125	7.0	64,000	.1092	7000
3	.875	.125	7.0	64,000	.1092	7000
Σ					4134	27300

$$F_c = \frac{27300}{.4134}$$

$$= 66,000 \text{ PSI}$$

$$M.S. = \frac{66000}{47500} - 1$$

$$\underline{\underline{M.S. = .39}}$$

BY
CK.
DATE

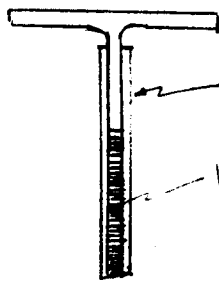
GENERAL ELECTRIC

PAGE
MODEL VOYAGER
REPORT

PROPULSION SYSTEM SUPPORT STRUCTURE

SECTION 20-35

SHEAR WEB DESIGN



FACE $t = .004$ - 7075-6 AL ALLOY.

$1/6$ #/ft. CORE
 $3/16$ \"

NOTE: HIGHER STRENGTH ALUMINUM ALLOYS ARE NOT AVAILABLE IN FOIL GAGES. CHEMICAL MILLING HOWEVER ALLOWS THE USE OF HIGH STRENGTH ALLOYS IN THE FOIL GAGES.

AVERAGE SHEAR STRESS

$$f_s = \frac{101.5(22.8)}{20(.008)} = 14,500 \text{ PSI}$$

ALLOWABLE SHEAR STRESS

INTERCELL BUCKLING - METHOD VIA REFERENCE C

$$\frac{S}{t_f} = \frac{.188}{.004} = 47 \quad \frac{F_{ci}}{n} = 23,000 \quad \frac{F_{si}}{n} = 18,100 \text{ PSI}$$

F_i = STRESS INTENSITY - VON MISES YIELD CRITERIA

$$\frac{F_i}{n} = \sqrt{3}(18,100) = 31,800 \text{ PSI FOR SHEAR}$$

$$\frac{F_{cy}}{F_i} = \frac{67,000}{31,800} = 2.1 \quad F_i' = .47 F_{cy} \text{ FROM CURVE 12.5.2b}$$

$$F_s = \frac{.47(67,000)}{\sqrt{3}} = 18,100 \text{ PSI}$$

$$M.S. = \frac{18,100}{14,500} - 1 = \underline{\underline{+.25}}$$

BY
CK.
DATE

GENERAL ELECTRIC

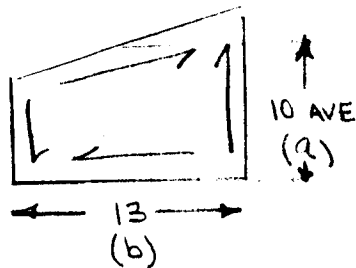
PAGE
MODEL VOYAGER
REPORT

PROPULSION SYSTEM SUPPORT STRUCTURE

SECTION 20-35

OVERALL PANEL SHEAR STABILITY

METHOD VIA REF 10



$$F_{scr} = \frac{\pi^2 G_F D}{a^2 N} K \quad (\text{SIMPLE SUPPORTS})$$

K IS EVALUATED FROM THE PARAMETER

$$V = \frac{\pi^2 D}{a^2 U}$$

$$D = \frac{E F}{12 t_f} [t^3 - t_c^3]$$

$$= \frac{(10.3)(10)^6}{12(.91)} (.133^3 - .125^3)$$

$$= 380 \text{ psi}$$

$$V = \frac{\pi^2 (380)}{100 (1000)} = .0372$$

$$K = \frac{4}{3} \frac{4 + 3 \frac{a^2}{b^2}}{1 + \frac{1}{3} [13 + 9 \frac{a^2}{b^2}]} V = 6.5$$

$$U = G_c t_c = 1000 \text{ psi}$$

($G_c = 8000 \text{ psi}$) REF HEXCELL

$$N = t_f G_F$$

$$F_{scr} = \frac{\pi^2 (3.9)(10)^6 (380)(6.5)}{100 (3.9)(10)^6 (.008)} = 30,800 \text{ psi}$$

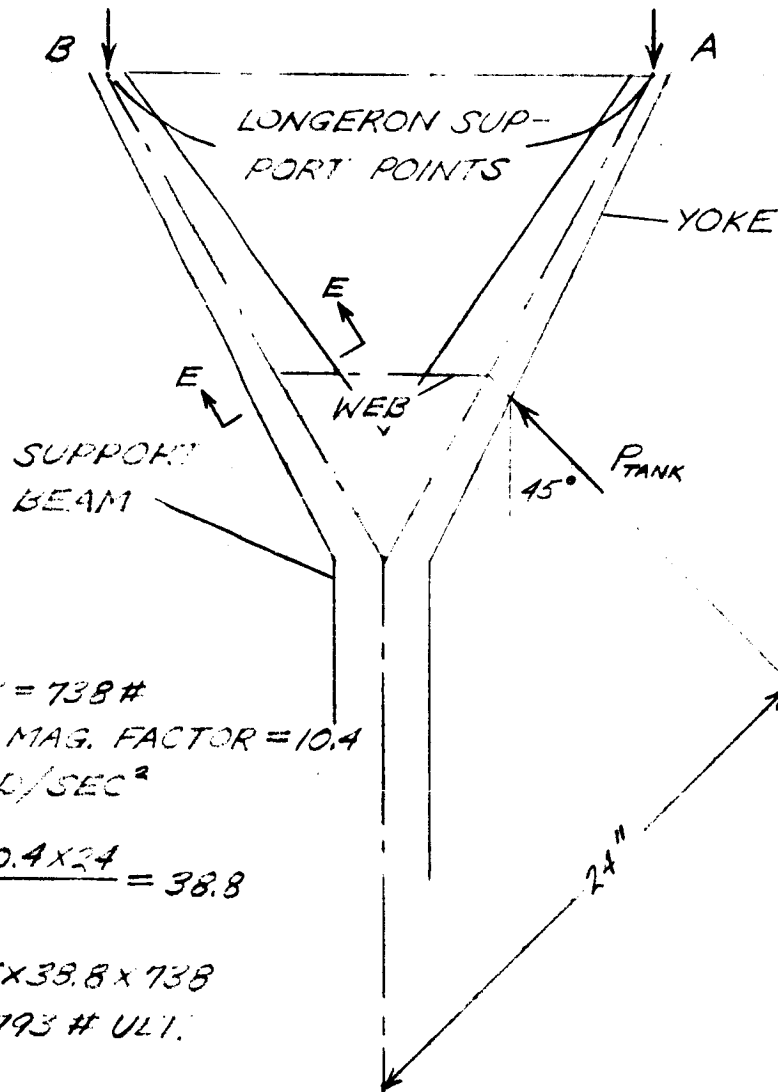
PANEL IS STABLE

(CRITICAL FAILURE MODE IS IN INTERCELL BUCKLING.)

BY	GENERAL ELECTRIC	PAGE
CK.		MODEL VOYAGER
DATE		REV.

PROPELLSION SYSTEM SUPPORT BEAMS - COND. 20-71, 73
 CONFIGURATION - SECTION O-13

FUEL TANK LOADS BEAM AS SHOWN BELOW. THE LOADS OF THE SMALLER TANKS ARE ASSUMED TAKEN DIRECTLY TO THE FRAMES AT STATIONS 20 & 46



WT. TANK = 738 #
 DYNAMIC MAG. FACTOR = 10.4
 $\alpha = 60 \text{ RAD/SEC}^2$

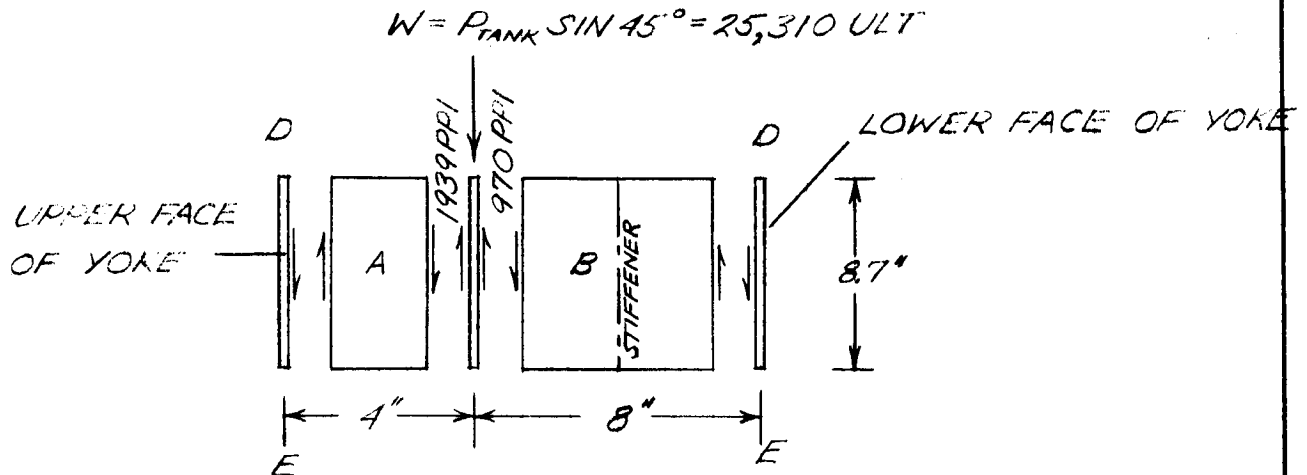
$$g = \frac{60 \times 10.4 \times 24}{386} = 38.8$$

$$P_{TANK} = 1.25 \times 38.8 \times 738 = 35,793 \text{ # U.L.T.}$$

BY	GENERAL ELECTRIC	PAGE
CK.		MODEL <i>VOYAGER</i>
DATE		REV.

PROPULSION SYSTEM SUPPORT BEAMS

TANK LOAD DIST. WEB.



WEB "A" ~ USE 7075 T6 ALUMINUM ALLOY TO PROVIDE FOR SIMPLE RIVETED ATTACHMENTS TO UPPER FACE OF YOKE

FOR A SHEAR RESISTANT PANEL

$$R_{S CR} = t^3 = \frac{12 q_{CR} (1 - \nu^2) b^2}{\pi^2 K_S \times E}$$

$t = .081$

$F_{S CR} = 23,940$

$b = 4"$

$q_{CR} = 1939 \text{ PPI}$

$K_S = 6.3$

$E = 10.3 \times 10^6 \text{ PSI}$

3/16" ATTACHMENTS @ 3/4" PITCH

WEB "B" ~ .081" WEB IS O.K. IF ONE INTERMEDIATE STIFFENER IS PROVIDED (AND 10141-1402)

FOR MEMBER RECEIVING LOAD "W" USE AND 10136-1606 TEE

BY

GENERAL ELECTRIC

PAGE

CK.

MODEL VOYAGER

DATE

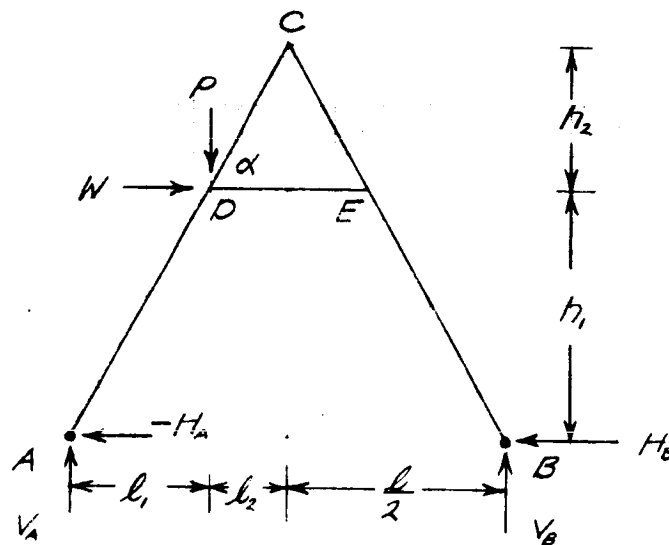
REV.

REPORT

PROPULSION SYSTEM SUPPORT BEAMS

SINCE THE AXIAL STIFFNESS OF THE LEGS OF THE YOKE IS MUCH GREATER THAN THE LATERAL BENDING STIFFNESS OF THE SUPPORT BEAM, THE LOAD CARRYING STRUCTURE MAY BE ANALYSED AS A SIMPLE A-FRAME. ASSUME $\frac{2}{3}$ OF THE TANK LOAD IS SHEARED BY THE WEB TO UPPER FACE OF THE YOKE.

$$P = W = \frac{2}{3} \times 35793 \times .70711 = 16,873 \text{ ULT}$$



$$h = 20.5$$

$$h_1 = 12.75$$

$$h_2 = 7.75$$

$$l = 23.0''$$

$$l_1 = 7.15$$

$$l_2 = 4.35$$

$$\alpha = 60^\circ 43'$$

$$\sin \alpha = .87221$$

$$\cos \alpha = .48913$$

BY	GENERAL ELECTRIC	PAGE
CK.		MODEL VOYAGER
DATE		REV.

PROPULSION SYSTEM SUPPORT BEAMS

$$V_B = \frac{16873 (7.15 + 12.75)}{23.0} = 14,599$$

$$V_A = 16873 - 14,599 = 2274$$

$$H_A = \frac{Pw}{2h} - \frac{W}{2}$$

$$w = \frac{G_1 \cdot r}{h_1} = 11.5$$

$$H_A = \frac{16,873 \times 11.5}{2 \times 20.5} - \frac{16,873}{2} = -3704$$

$$H_B = 13169$$

$$M_D = -M_E - V_B C_2 = 63506 \text{ IN} \cdot \#$$

$$P_{AD} = V_A \sin \alpha + H_A \cos \alpha = 172 \# \text{ COMP}$$

$$P_{DC} = V_B \sin \alpha = 12733 \# \text{ TENS}$$

$$P_{CE} = -P_{CD} = 12733 \# \text{ COMP.}$$

$$F_{DE} = H_B = 13169 \# \text{ COMP.}$$

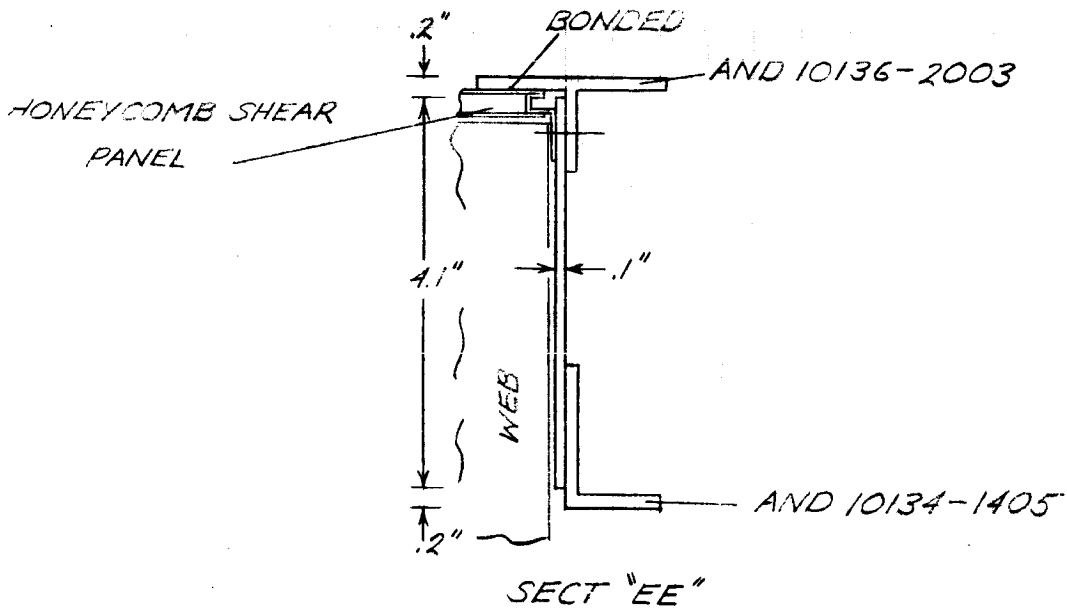
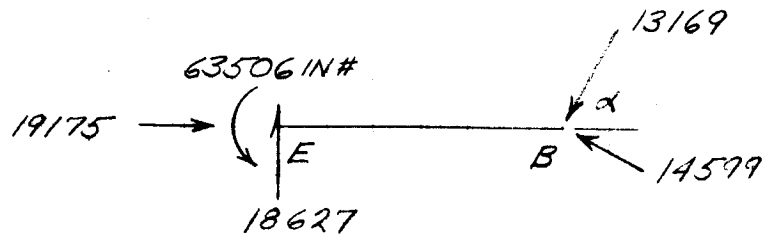
$$P_{BE} = V_B \sin \alpha + H_B \cos \alpha = 19175 \# \text{ COMP.}$$

MEMBER B-E IS CRITICAL WITH AXIAL LOAD OF 19175#
& MOMENT OF 63506 (COMP. ON INNER FLANGE)

BY CK. DATE REV.	GENERAL ELECTRIC	PAGE MODEL VOYAGER REPORT
---	-------------------------	---------------------------------

PROPULSION SYSTEM SUPPORT BEAMS

CRITICAL YOKE MEMBER B-E



THE MAX. STRESS ON INNER FLANGE IS -62,366 PSI

$$F_{cc} = 68,000$$

$$MS = \frac{68,000}{62,366} - 1 = +.09$$

THE SECTION SHOULD BE TAPERED TO A DEPTH OF 2.5" ± AT "B"

BY	GENERAL ELECTRIC	PAGE
CK.		MODEL VOYAGER
DATE		REPORT
REV.		

PROPULSION SYSTEM SUPPORT STRUCTURE

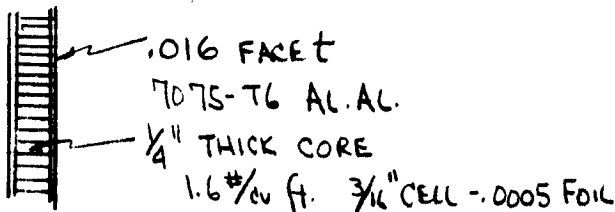
SECTION 0-13 - DESIGN CONDITIONS - 3a

BENDING SECTION IS ADEQUATE WITH CAPS DESIGNED BY COND. 2C

SHEAR WEB

$$q_{AVE} = \frac{881(22.8)}{8(2)} = 1255 \text{ lb./in ULTIMATE}$$

AVERAGE SHEAR STRESS/FACE



$$f_s = \frac{1255}{.032} = 39,200 \text{ PSI}$$

INTERCELL BUCKLING (REF 2)

$$\frac{S}{t_f} = \frac{.188}{.016} = 11.4$$

INTERCELL BUCKLING IS OBVIOUSLY NOT A FAILURE MODE

PANEL STABILITY (REF 10)

$$F_{SCR} = \frac{\pi^2 G_F D}{a^2 N} K$$

$$V = \frac{\pi^2 D}{a^2 U}$$

$$D = \frac{10.3(10)^6 (.782^3 - .75^3)}{12(.91)} = 6494 \text{ PSI}$$

$$\frac{a}{b} = \frac{8}{13}$$

$$K = \frac{1}{V} \text{ if } V > \frac{a^2}{b^2}$$

$$\frac{a^2}{b^2} = .379$$

$$\therefore K = \frac{1}{.482} = 2.07$$

$$V = \frac{\pi^2 (6494)}{(8)^2 (2000)} = .482$$

$$F_{SC} = \frac{\pi^2 (3.9)(10)^6 (6494)(2.07)}{64 (3.9)(10)^6 (.032)} = 54500 \text{ PSI} - \text{PANEL IS STABLE}$$

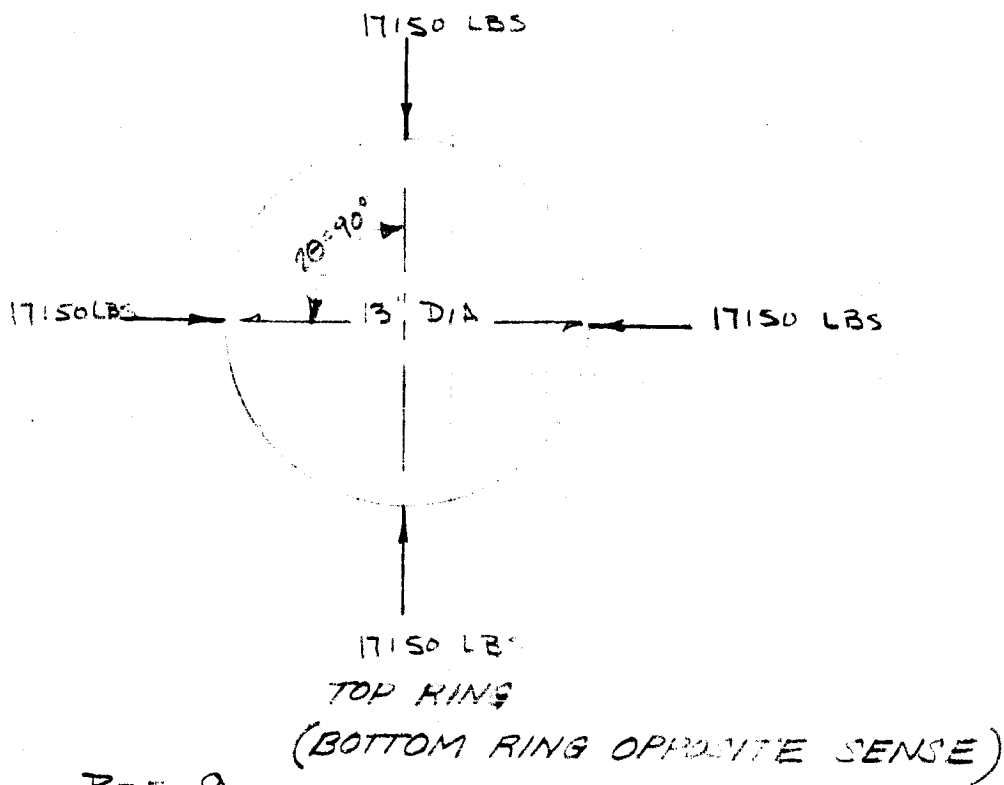
$$F_{SO} - 7075-T6 = 46,000 \text{ PSI}$$

$$M.S. = \frac{46000}{39200} - 1 = \underline{\underline{+.17}}$$

BY	GENERAL ELECTRIC	PAGE
CK.		MODEL VOYAGER
DATE		REV.

PROPULSION SYSTEM - ENGINE SUPPORT RINGS

RINGS ARE ACTUALLY DESIGNED BY ENGINE GIMBALLING AND DYNAMIC RIGIDITY REQUIREMENTS. SECTIONS SHOWN BELOW ARE PRESENTED AS MINIMUM SECTIONS.



REF 9

$$2\theta = 1.5708$$

$$\theta = .7854$$

$$\text{MAX -M} = -\frac{1}{2} WR \left(\frac{1}{3} - \frac{1}{\theta} \right) \quad S = \sin \theta$$

$$= -\frac{1}{2} (17150) (6.5) \left(\frac{1}{.707} - \frac{1}{.7854} \right)$$

$$= -7800 \text{ IN-LBS}$$

BY	GENERAL ELECTRIC	PAGE
CK.		MODEL VOYAGER
DATE		REPORT
REV.		

$$\text{MAX } +M = \frac{1}{2} WR \left(\frac{1}{\theta} - \cot \theta \right)$$

$$= \frac{1}{2} (17150) (6.5) \left(\frac{1}{.7854} - 1 \right)$$

$$= +15000 \text{ IN-LBS (AT LOADS)}$$

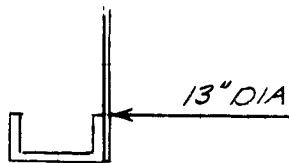
COMP IN OUTER FIBERS (TOP RING)

$$T_{\text{AT LOADS}} = -\frac{1}{2} W \cot \theta$$

$$= -\frac{1}{2} (17150) (1)$$

$$= -8560 \text{ LBS (TOP RING)}$$

BOTTOM RING



AND-10131-2402 7075 T6 AL. ALLOY

MAX TENS IN OUTER FIBERS

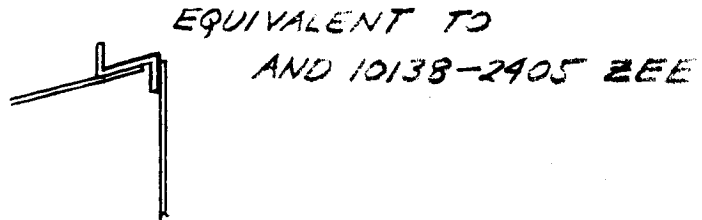
$$S = + \frac{8560}{.531} + \frac{15000 \times 1.25}{.4706} = 56,000$$

$$F_{70} = 75,000$$

$$MS = \frac{75000}{56000} - 1 = +.34$$

BY	GENERAL ELECTRIC	PAGE
CK.		MODEL VOYAGER
DATE		REV.

TOP RING



MAX COMP IN OUTER FIBERS

$$\sigma = -\frac{8560}{.531} - \frac{15,000 \times 1.25}{4706} = 56,000$$

$$\frac{b}{t} = \frac{1.000 - .0625}{.125} = 7.5$$

$$F_{\alpha} = 61,000$$

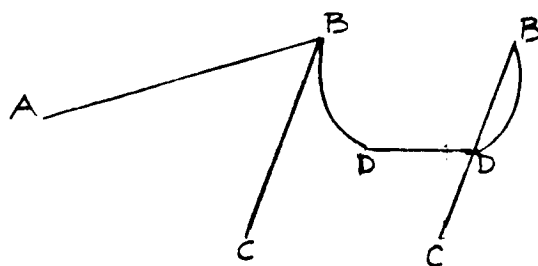
$$MS = \frac{61,000}{56,000} - 1 = +.09$$

BY	GENERAL ELECTRIC	PAGE
CK.		MODEL VOYAGER
DATE		REV.

PROPULSION Sys. TRUSS ANALYSIS

TRANSVERSE AND TORSIONAL LOADS ON THE HYDROZINE AND NITROGEN TANKS WILL BE REACTED BY THE TRUSS WORK AS ILLUSTRATED IN THE SCHEMATIC OF THE SYSTEM. TWO TUBES DESIGNATED AS BC WILL REACT TRANSVERSE LOADS ON THE NITROGEN TANKS AND TUBES EF WILL SUPPORT THE HYDROZINE TANKS IN A SIMILAR MANNER. TORSIONAL LOADS ON THESE TANKS WILL BE REACTED AT THE TRUNIONS. NONE OF THE TORSIONAL OR TRANSVERSE LOADS WILL BE TAKEN IN BENDING BY THE TANK SUPPORT ARMS.

I. UPPER SUPPORT STRUCTURE (NITROGEN TANKS)



BY	GENERAL ELECTRIC	PAGE
CK.		MODEL VOYAGER
DATE		REV.

a. THRUST TUBES BC

DESIGN CONDITION - 3b

$$g \text{ LOAD} = 1(9) = 9$$

$$\text{DESIGN LOAD FACTOR} = 9(1.25) = 11.3$$

EACH TUBE TAKES ONE-HALF THE LOAD
 LATERAL LOAD / TUBE = $\frac{56}{2}(11.3) = 315 \text{ LBS.}$

$$\begin{aligned} \text{COLUMN LOAD / TUBE} &= \frac{315}{(\cos 11^\circ)(\cos 53^\circ)} \\ &= 530 \text{ LBS} \end{aligned}$$

LENGTH OF TUBES = 17.94 IN

USE TUBES $\frac{5}{8}$ DIA - .022 WALL

$$\begin{aligned} \frac{L}{P} &= \frac{17.94}{.2133} \\ &= 84.5 \end{aligned}$$

$$F_c = 14,000 \text{ PSI} \quad \text{REF 4}$$

$$f = \frac{530}{.0417} = 12,700 \text{ PSI}$$

$$M.S. = \frac{14700}{12700} - 1$$

$$M.S. = \underline{\underline{.16}}$$

BY		GENERAL ELECTRIC	PAGE
CK.			MODEL VOYAGER
DATE	REV.		REPORT

b. THRUST TUBE AB

DESIGN CONDITION - 2C OR 3C

$$g \text{ LOAD} = \frac{(10.4)(60)(32)}{386} = 51.5$$

$$\text{DESIGN LOAD FACTOR} = (51.5)(1.25) = 64.5$$

$$\text{FORCE AT TRUNION DUE TO TORSION LOAD} = 56(64.5) = 3620 \text{ LBS.}$$

$$\text{COLUMN LOAD ON TUBE AB} = \frac{3620}{(\cos 2^\circ)(\cos 18.5^\circ)}$$

$$= 3810 \text{ LBS.}$$

LENGTH OF TUBE = 22.86 IN
USE TUBE - 1/8 DIA - .049 WALL

$$\frac{L}{P} = \frac{22.86}{.3808} = 60 \quad F_c = 24,500 \text{ PSI}$$

$$f = \frac{3810}{.1650} = 23,000 \quad (\text{REF 4})$$

$$\text{M.S.} = \frac{24,500}{23,000} - 1$$

$$\underline{\underline{\text{M.S.} = .06}}$$

BY

GENERAL ELECTRIC

PAGE

CK.

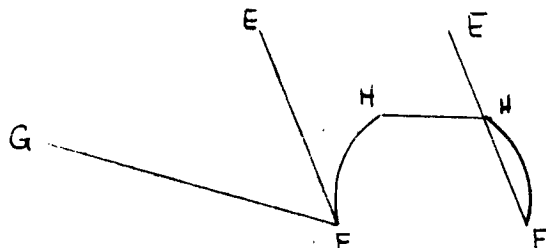
MODEL VOYAGER

DATE

REV.

REPORT

2. LOWER SUPPORT STRUCTURE



a. THRUST TUBES EF

DESIGN CONDITION - 3b

$$g \text{ LOAD} = 1(9) = 9$$

$$\text{DESIGN LOAD FACTOR} = 9(1.25) = 11.3$$

EACH TUBE TAKES ONE-HALF THE LOAD

$$\text{LATERAL LOAD / TUBE} = \frac{119.5}{2} (11.3) = 675 \text{ LBS}$$

$$\text{COLUMN LOAD / TUBE} = \frac{675}{(\cos 20^\circ)(\cos 37.5^\circ)}$$

$$= 850 \text{ LBS.}$$

LENGTH OF TUBES = 16.6 IN

USE TUBE $\frac{11}{16}$ DIA - .022 WALL

$$\frac{L}{P} = \frac{16.6}{.2354} = 70.6$$

$$F_c = 20,000 \text{ PSI (REF 4)}$$

$$f = \frac{850}{.046} = 18500 \text{ PSI}$$

$$\text{M.S.} = \frac{20,000}{18,500} = 1$$

$$\text{M.S.} = .08$$

BY	GENERAL ELECTRIC	PAGE
CK.		MODEL VOYAGER
DATE		REV.

b. THRUST TUBE GF

DESIGN CONDITION - 2C OR 3C

$$g \text{ LOAD} = \frac{(10.4)(60)(29)}{386} = 46.7$$

$$\text{DESIGN LOAD FACTOR} = 46.7(1.25) = 58.5$$

$$\begin{aligned} \text{FORCE AT TRUNION DUE TO TORSION LOAD} &= 58.5(119.5) \\ &= 7000 \text{ LBS} \end{aligned}$$

$$\begin{aligned} \text{COLUMN LOAD} &= \frac{7000}{(\cos 5^\circ)(\cos 35^\circ)} \\ &= 7040 \text{ LBS.} \end{aligned}$$

LENGTH OF TUBE = 1992 IN

USE TUBE 1/4 DIA - .065 WALL

$$\frac{L}{r} = \frac{19.92}{.4196} = 47.5 \quad F_c = 30,000 \text{ PSI (REF. 4)}$$

$$f = \frac{7040}{.242} = 29,100 \text{ PSI}$$

$$M.S. = \frac{30,000}{29,100} - 1$$

$$\underline{M.S. = .03}$$

BY	GENERAL ELECTRIC	PAGE
CK.		MODEL VOYAGER
DATE		REV.

C. TANK SUPPORT ARM

THE TANK SUPPORT ARM WILL BE DESIGNED TO REACT THE TOTAL VERTICAL LOAD.

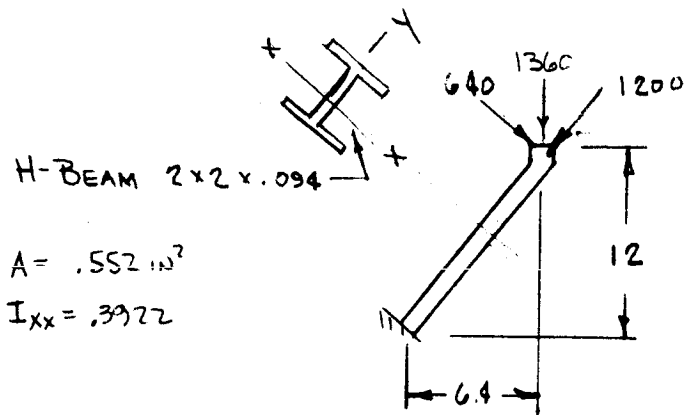
DESIGN CONDITION 3a

$$j \text{ LOAD} = 16(10.76) + 1 = 18.25$$

DESIGN LOAD FACTOR = $(18.25)(1.25) = 22.8$
 EACH TRUSS WILL TAKE ONE HALF THE LOAD.

$$\text{VERTICAL LOAD PER TRUSS} = \frac{(119.5)(22.8)}{2}$$

$$= 1360 \text{ LBS.}$$



H-BEAM 2x2x.094
 $A = .552 \text{ in}^2$
 $I_{xx} = .3922$

BEAM IS SUPPORTED AT TOP BY TRUSS TUBES IN Y DIRECTION

REF (9)

$$\text{MAX } M = -W_j \text{ TAN } U$$

$$U = \frac{1}{J} =$$

$$J = \sqrt{\frac{EI}{P}}$$

$$= \sqrt{\frac{10^7 (.3922)}{1200}}$$

$$= 57.2$$

BY	GENERAL ELECTRIC	PAGE
CK.		MODEL VOYAGER
DATE		REV.

$$J = \frac{13.6}{57.2} = .238$$

$$\text{TAN } U = .236$$

$$\text{Max } M = + 640 (57.2) (.236)$$

$$= + 8650 \text{ in-lbs}$$

$$f = \frac{(8650)(1)}{.3922} + \frac{1200}{.552}$$

$$= 43,800 \text{ PSI}$$

CRIPPLING

$$\frac{b}{t} = \frac{1}{.081} = 12.7$$

$$F_c = 46,300 \text{ PSI}$$

REF 4

$$M.S. = \frac{46,300}{43,800} - 1$$

$$\underline{M.S. = .06}$$

STABILITY

$$L = 13.6 \quad L' = .7(13.6) = 9.5$$

$$\frac{L'}{r} = \frac{9.5}{.463} = 20.6 \quad F_c = 36,500 \text{ PSI} \quad \text{REF 4}$$

BEAM IS CRITICAL IN CRIPPLING

BY CK. DATE	REV.	GENERAL ELECTRIC	PAGE MODEL VOYAGER REPORT
-------------------	------	------------------	---------------------------------

REFERENCES

1. "Stresses in Aircraft & Shell Structures"
Paul Kuhn - McGraw-Hill - 1956
2. "Analysis & Design of Flight Vehicle Structures"
E. F. Bruhn - Tri-State Offset Company - 1965
3. General Electric Structural Data Sheets
4. General Electric Structures Manual
5. Theory of Elastic Stability - S. Timoshenko
6. Aircraft Structures - David J. Peery - McGraw-Hill - 1950
7. Airplane Structures - Niles & Newell - John Wiley - 1954
8. Machine Design - November 14, 1957
9. Formulas for Stress and Strain - Roarke- McGraw-Hill - 1954
10. Sandwich Construction for Aircraft - MIL HDBK 23
11. Theory of Plates & Shells" = Timoshenko, S., and Woinowsky-Krieger, S. - McGraw-Hill, 1959
12. Report 171-48C - Styrofoam, Dow Chemical Company

II METEOROID PENETRATION ANALYSIS

DESIGN PHILOSOPHY

Two sections of the spacecraft that would jeopardize the mission if penetrated by a meteoroid are the Equipment Module and pressure vessels.

1. The electrical components in each bay of the Equipment Module are protected from a radial impact by a double wall of .055 inch thick aluminum and .06 inch thick magnesium. Components are protected from impact along the axial direction by the capsule at the forward end and .06 inch thick aluminum and a foam-filled bumper at the aft end. Since a bumper is being employed, it is assumed there cannot be any penetration through the interior face of the Electronics Module. Shielding from longerons and other built-up areas has been neglected.

A preliminary analysis was performed for the extreme upper limit fluxes. The results were such as to preclude the practicability of protecting against these environments. The reliability against meteoroid penetration is based on upper limit fluxes for a cruise of 180 days and the nominal flux for an elliptical orbit of 30 days, with the consideration that the probability of encountering the extreme upper limit case will be factored into the overall spacecraft reliability analysis on the basis of probability of occurrence. The travel time to escape the Earth's environment is sufficiently small to neglect the near Earth flux. A reliability of .995 against meteoroid penetration is required.

2. The pressure vessels present a special problem when designing against meteoroids because it is not sufficient just to prevent penetration. Impacting particles can produce localized pressure stresses exceeding the design limit of the tank and causing failure.

Since the tanks are to be designed to a 2.2 hazard factor as per VB235FD103 there is some inherent meteoroid protection. The additional thickness required by the load factor will be neglected in designing a main protective wall. It will be assumed that this will be sufficient to withstand any pressure increase and redistribution of stresses that may occur due to spalling or penetration of the bumper.

It is assumed that there cannot be any penetration through the flight capsule or Equipment Module. The only exposed area, therefore, is at the aft end. In orbit, after the lander has been ejected, it is assumed that tanks are no longer pressurized and any penetration will not endanger the orbital mission.

A foam-filled bumper will be employed to ensure a reliability of .995 against meteoroid penetration. The proportions of the bumper chosen are such that it ensures meteoroid protection in addition to providing adequate bending stiffness to support its own weight and the weight of the insulation blanket which is attached to it. A honeycomb core concept has been avoided as it aggravates rather than aids in meteoroid protection.

SUMMARY OF DESIGN CRITERIA AND ASSUMPTIONS

1. Flux - Reference VB235FD103. Assume all hits are normal impacts.
2. Probability of penetration based on Poisson distribution.
 - a. Probability of zero penetrations $P_0 = e^{-NAT}$
 - b. Assume area is total projected area.

3. Herrmann and Jones Logarithmic criteria

$$\frac{P_\infty}{d} = .6 \left(\frac{P_p}{P_t} \right)^{2/3} \ln \left[1 + \frac{\left(\frac{P_p}{P_t} \right)^{2/3} P_t V^2}{4 H_t g} \right]$$

P = Density of meteoroid
 P^p = Density of target
 V^t = Velocity of meteoroid
 H_t = Brinell No. of material

4. Penetration in thin wall material $t = 1.5 P_\infty$

Penetration in 1" deep foam-filled sandwich structure $\bar{t} = .33t = .5P_\infty$
 Reference Frost, V.C. "Recommendations for Revised Meteoroid and Penetration Criterion" - Aerospace Corporation Memorandum. (A complete list of references is given in VB235AA102).

BY
CK.
DATE

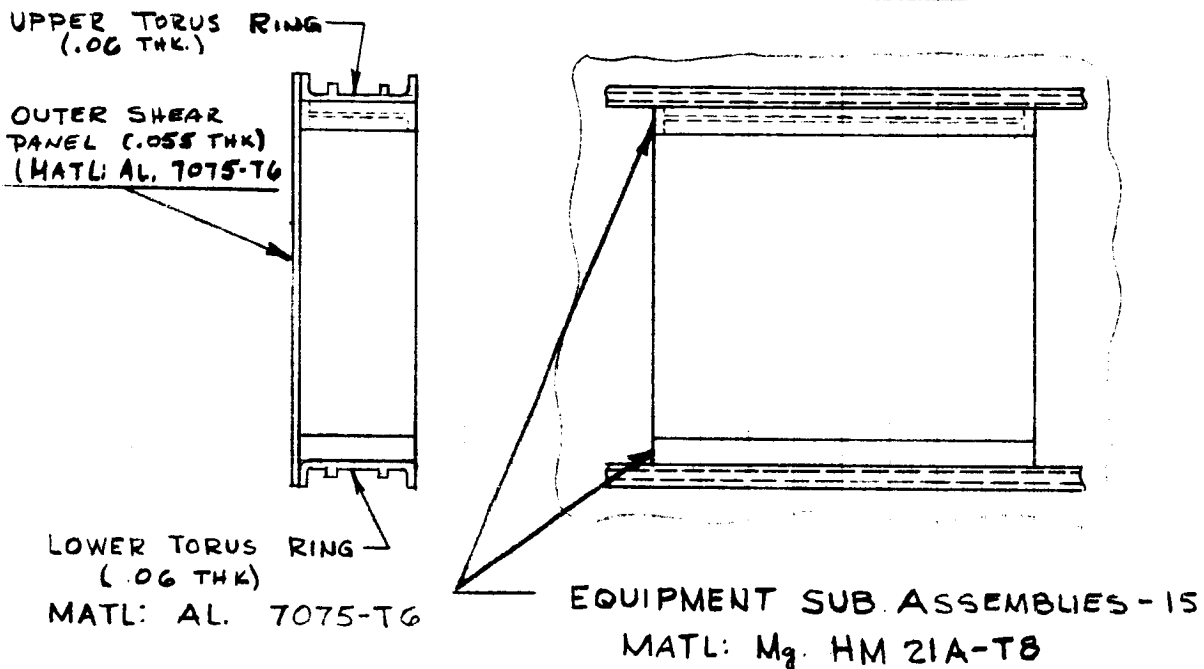
GENERAL ELECTRIC

PAGE
MODEL VOYAGER
REPORT

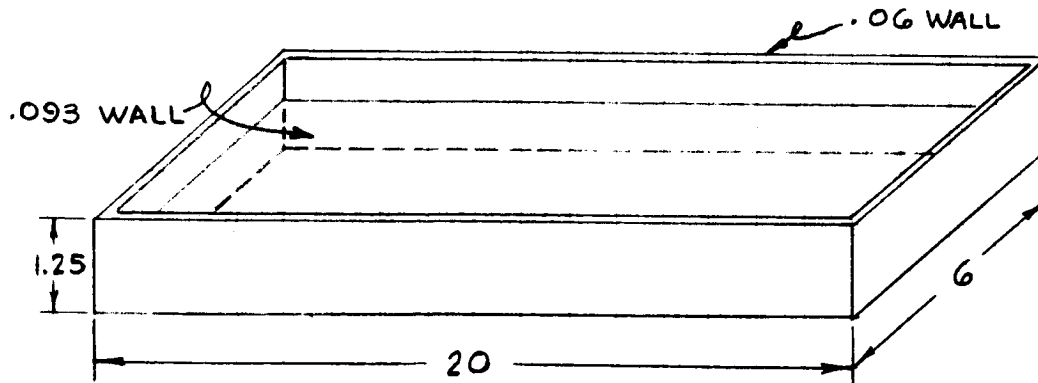
METEOROID PENETRATION ANALYSIS

A. EQUIPMENT MODULE

EQUIPMENT MODULE - 1 BAY



EQUIPMENT TRAY - TYPICAL



BY
CK.
DATE

GENERAL  ELECTRIC

PAGE
MODEL VOYAGER
REPORT

1. AREA ANALYSIS

a. LATERAL AREA EXPOSED TO ENVIRONMENT
(NO HITS ON INTERIOR OF EQUIPMENT MODULE)

$$\text{TOTAL LATERAL AREA/TRAY} = 1.25(20) = 25 \text{ IN}^2$$

UNAVAILABLE AREA

$$2 \text{ WALLS } (.06)(1.25) = .15 \text{ IN}^2$$

$$1 \text{ WEB } (.093)(19.88) = \underline{1.85}$$

$$2.00 \text{ IN}^2$$

$$\text{LATERAL AREA/TRAY AVAILABLE FOR COMPONENTS} = 23 \text{ IN}^2$$

$$\text{ASSUMING } 80\% \text{ PACKING DENSITY} = 18.4 \text{ IN}^2/\text{TRAY}$$

$$(15 \text{ TRAYS/BAY})(12 \text{ BAYS}) = 180 \text{ TRAYS}$$

$$\text{TOTAL COMPONENT AREA (LATERAL)} = 3312 \text{ IN}^2$$

$$= 23 \text{ FT}^2$$

$$= 2.14 \text{ METERS}^2$$

b. BASE AREA EXPOSED TO ENVIRONMENT

ASSUME

1. LANDER CANNOT BE PENETRATED

$$\text{TOTAL BASE AREA} = (9.88)(5.88)(12)(.80) = 1122 \text{ IN}^2$$

$$= 7.8 \text{ FT}^2$$

$$= .725 \text{ M}^2$$

BY
CK.
DATE

GENERAL ELECTRIC

PAGE
MODEL VOYAGER
REPORT

2. WALL THICKNESS ANALYSIS

a. LATERAL AREA

PENETRATION THICKNESS - .055 AL. + .06 Hg.

CHANGE .06 THK Hg TO EQUIVALENT THK OF AL.

$$t_{AL} = \frac{(\rho A t)_{Hg}}{(\rho A)_{AL}} \quad A_{Hg} = A_{AL}$$

$$= \frac{(.0647)(.06)}{.1} = .039 \text{ IN}$$

PENETRATION THICKNESS = .055 + .039 = .094 INCHES
OF AL.

b. BASE AREA

PENETRATION THICKNESS - .06 AL.

3. PENETRATION MECHANICS

a. HERRMANN-JONES LOGARITHMIC CRITERIA

$$\frac{P_{sp}}{d} = .6 \left(\frac{\rho_p}{\rho_t} \right)^{2/3} \ln \left[1 + \frac{\left(\frac{\rho_p}{\rho_t} \right)^{2/3} \rho_t V^2}{4 H_t g} \right]$$

$$= .6 \left(\frac{\rho_p}{\rho_t} \right)^{2/3} \ln \left[1 + 25.5 \left(\frac{\rho_p}{\rho_t} \right)^{2/3} \frac{\rho_t V^2}{H_t} \right]$$

WHERE ρ_t - TARGET DENSITY (GM/CC)
 ρ_p - PROJECTILE DENSITY (GM/CC)
 V - PROJECTILE VELOCITY (KM/SEC)
 H_t - BRINELL HARDNESS OF TARGET (Kg/MM²)

$\rho_t = 2.77$ GMS/CC - 7075-T6
 $\rho_t = 1.77$ GMS/CC - HM 21A-T8
 $H_t = 150$ Kg/MM² - 7075-T6
 $H_t = 56$ Kg/MM² - HM 21A-T8

BY
CK.
DATE

GENERAL ELECTRIC

PAGE
MODEL VOYAGER
REPORT

b. APPLICATION TO ENVIRONMENT

(1) CRUISE

NOMINAL FLUX

$$V = 40 \text{ KM/SEC}$$

$$\rho_p = 0.4 \text{ GMS/CC}$$

PENETRATION IN ALUMINUM

$$\frac{P_{\infty}}{d} = .6 (.274) \ln \left[1 + \frac{25.5 (.274) (2.77) (1600)}{150} \right]$$

$$= 0.875$$

ASSUMING A SPHERICAL PARTICLE

$$d = \left(\frac{6M}{.4\pi} \right)^{1/3} = 1.683 \text{ M}^{1/3} \text{ CM.}$$

(a) PENETRATION IN MAIN WALL

$$t = 15 P_{\infty} = \frac{15 (.875) (.683)}{2.54} \text{ M}^{1/3}$$

$$= 0.872 \text{ M}^{1/3} \text{ INCHES}$$

b) PENETRATION WITH FOAM FILLED BUMPER
1 INCH THICK.

$$\bar{t} = .33 t$$

$$= .29 \text{ M}^{1/3} \text{ INCHES}$$

BY	GENERAL ELECTRIC	PAGE
CK.		MODEL VOYAGER
DATE		REV.

(2) ELLIPTICAL ORBIT

NOMINAL FLUX

$$V = 2.5 \text{ KM/SEC}$$

$$\rho_p = 0.4 \text{ GMS/CC}$$

PENETRATION IN ALUMINUM

$$\frac{P_{\infty}}{d} = .6 (0.274) \ln \left[1 + \frac{25.5 (0.274) (2.77) (6.25)}{150} \right]$$

$$= 0.0975$$

$$d = 1.683 \text{ M}^{1/3} \text{ CM}$$

(a) PENETRATION IN MAIN WALL

$$t = 1.5 P_{\infty} = \frac{1.5 (0.0975) (1.683)}{2.54}$$

$$= 0.0972 \text{ M}^{1/3} \text{ INCHES}$$

(b) PENETRATION WITH FOAM FILLED BUMPER

1 INCH THICK

$$\bar{t} = .33 t$$

$$= .0323 \text{ M}^{1/3} \text{ INCHES}$$

BY CK. DATE	GENERAL ELECTRIC	PAGE MODEL VOYAGER REPORT
REV.		

4 DETERMINATION OF PROBABILITY OF NO PENETRATIONS

a. CRUISE - USE UPPER LIMITS FOR DESIGN CONDITION

1) EARTH TO MID-COURSE FLUX

$$\text{Log } N = -14.43 - 1.34 \text{ Log } M + 2.68 \text{ Log } \left(\frac{.44}{\rho}\right)$$

$\rho = .4 \text{ GMS/CC}$
 $\text{Log } \left(\frac{.44}{.4}\right) = \text{Log } 1.1 = 0.0414$

$$\text{LOG } N = -14.37 - 1.34 \text{ LOG } M$$

2) SHEAR PANELS

$\bar{t} = .872 \text{ m}^{1/3}$ SECTION A.3.b.1.a

$t = .094 \text{ INCHES}$

$M = \left(\frac{.094}{.872}\right)^3 = 1.26 \times 10^{-3} \text{ GMS}$

$\text{Log } N = -14.37 - 1.34 \text{ Log } 1.26 \times 10^{-3}$
 $= -10.48$
 $= 0.52 - 11$

$N = 3.311 \times 10^{-11}$

$NA_{\text{SHEAR PANELS}} = 7.08 \times 10^{-11} \text{ PARTICLES/SEC}$

b) AFT END - FOAM FILLED BUMPER

$\bar{t} = 0.29 \text{ M}^{1/3}$ SECTION A.3.b.1.b

CONSERVATIVE ESTIMATE?
 (NOT CONSIDERING BUMPER THICKNESS)

$t = .06 \text{ INCHES}$
 $M = \left(\frac{.06}{.29}\right)^3 = (.207)^3$
 $= 8.9 \times 10^{-3}$

BY	GENERAL ELECTRIC	PAGE
CK.		MODEL VOYAGER
DATE		REV.

$$\begin{aligned}\log N &= -14.37 - 1.34 \log 8.9 \times 10^{-3} \\ &= -14.37 - 1.34 (7.9494 - 10) \\ &= -11.62 \\ N &= 2.399 \times 10^{-12} \\ NA &= 1.74 \times 10^{-12}\end{aligned}$$

$$\begin{aligned}\text{TOTAL NA} &= (7.08 + .174) \times 10^{-11} \\ &= 7.25 \times 10^{-11}\end{aligned}$$

150 DAY MISSION

EARTH TO MID COURSE - 75 DAYS

$$T = 75(24)(3600) = 6.46 \times 10^6 \text{ SEC}$$

$$\begin{aligned}\mu &= NAT \\ &= 47. \times 10^{-5}\end{aligned}$$

$$P_0 > .999$$

180 DAY MISSION

$$\mu = 564 \times 10^{-5}$$

$$P_0 > .999$$

2) MID-COURSE TO MARS FLUX

$$\begin{aligned}\log N &= -13.98 - 1.34 \log M + 268 \log \left(\frac{14}{R}\right) \\ &= -13.87 - 1.34 \log M\end{aligned}$$

a) SHEAR PANEL

$$M = 1.26 \times 10^{-3} \text{ GMS}$$

$$\log N = -9.98 = 0.02 - 10$$

$$N = 1.047 \times 10^{-10}$$

$$NA = 2.24 \times 10^{-10}$$

BY	GENERAL ELECTRIC	PAGE
CK.		MODEL VOYAGER
DATE		REV.

b) AFT END - FOAM FILLED BUMPER

CONSERVATIVE ESTIMATE
(SEE PAGE 6)

$$M = 8.90 \times 10^{-3} \text{ GMS}$$

$$\begin{aligned} \text{LOG } N &= -13.87 - 1.34 \text{ LOG } 8.90 \times 10^{-3} \\ N &= 7.586 \times 10^{-12} \end{aligned}$$

$$NA = 5.5 \times 10^{-12}$$

$$\begin{aligned} \text{TOTAL } NA &= (2.24 + .055) \times 10^{-10} \\ &= 2.295 \times 10^{-10} \end{aligned}$$

150 DAY MISSION

MID-COURSE TO MARS - 75 DAYS

$$\mu = 14.9 \times 10^{-4}$$

$$P_0 = .9985$$

180 DAY MISSION

$$\mu = 17.9 \times 10^{-4}$$

$$P_0 = .9982$$

b. ELLIPTICAL ORBIT - USE NOMINAL FLUX FOR DESIGN CONDITION

$$\text{LOG } N = -17.20 - 1.7 \text{ LOG } M$$

1) SHEAR PANELS

$$t = 0.0972 \text{ M}^{1/3}$$

$$t = 0.094 \text{ INCHES}$$

$$M = .905 \text{ GMS}$$

BY	GENERAL ELECTRIC	PAGE
CK.		MODEL VOYAGER
DATE		REV.

$$\text{LOG } N = -17.20 - 1.7 \text{ LOG } .905$$

$$N = 7.516 \times 10^{-18}$$

$$NA = 16.1 \times 10^{-18}$$

2) AFT END - FOAM FILLED BUMPER

$$\bar{r} = .0323 M^{1/3} \text{ INCHES}$$

CONSERVATE ESTIMATE $\rightarrow \bar{r} = .06 \text{ INCHES}$

$$M = 6.42 \text{ GMS}$$

$$\text{LOG } N = -17.20 - 1.7 \text{ LOG } 6.42$$

$$= -18.58$$

$$N = 2.63 \times 10^{-19}$$

$$NA = 1.91 \times 10^{-19}$$

$$\text{TOTAL } NA = 16.29 \times 10^{-18}$$

30 DAY ORBIT

$$\mu = 16.29 \times 10^{-18} (30)(24)(3600)$$

$$= 42.4 \times 10^{-12}$$

$$P_0 \gg .999$$

BY
CK.
DATE

GENERAL ELECTRIC

PAGE
MODEL VOYAGER
REPORT

REV.

PRESSURE VESSELS

AREA ANALYSIS

1. OXIDIZER & FUEL TANKS

$$\text{PROJECTED AREA} - 4 \frac{\pi}{4} (30.5)^2 = 2920 \text{ IN}^2$$

2. MONOPROPELLENT TANKS

$$\text{PROJECTED AREA} - 4 \frac{\pi}{4} (22)^2 = \underline{1520 \text{ IN}^2}$$

$$\text{TOTAL PROJECTED AREA} = 4440 \text{ IN}^2$$

$$\text{TOTAL SHIELDED AREA} = \underline{520}$$

$$\begin{aligned} \text{NET PROJECTED AREA} &= 3920 \text{ IN}^2 \\ &= 2.53 \text{ METERS}^2 \end{aligned}$$

PRELIMINARY DESIGN OF PRESSURE VESSELS

MATERIAL: TITANIUM GAL-4V - ANNEALED

REF: MIL HANDBOOK 5

$$F_{tu} = 130,000 \text{ PSI}$$

$$\rho = .16 \text{ LBS/IN}^3$$

$$E = 16 \times 10^6 \text{ PSI}$$

LOAD FACTORS

$$\text{PROOF} - 1.76$$

$$\text{BURST} - 2.2$$

BY	GENERAL ELECTRIC	PAGE
CK.		MODEL VOYAGER
DATE		REV.

1. OXIDIZER & FUEL TANKS

DIAMETER - 30.5 IN.

OPERATING PRESSURE 220 PSI

DESIGN PRESSURE - $220 \times 2.2 = 484$ PSIPROOF PRESSURE - $220 \times 1.76 = 387$ PSI

$$S = \frac{PR}{2t}$$

$$\text{DESIGN THICKNESS} = \frac{PR}{2S} = \frac{(484)(15.25)}{2(130,000)} = .0284 \text{ INCHES}$$

$$\text{THICKNESS FOR OPER. PRESSURE} = \frac{(220)(15.25)}{2(130,000)} = \underline{.0129}$$

INHERENT METEOROID PROTECTION = .0155 INCHES

2. MONOPROPELLANT TANKS

DIAMETER 22 IN.

OPERATING PRESSURE - 285 PSI

DESIGN PRESSURE - $285 \times 2.2 = 627$ PSIPROOF PRESSURE - $285 \times 1.76 = 500$ PSI

$$\text{DESIGN THICKNESS} = \frac{(627)(11)}{2(130,000)} = .0265 \text{ IN.}$$

$$\text{THICKNESS FOR OPER. PRESSURE} = \frac{(285)(11)}{2(130,000)} = \underline{.0120}$$

INHERENT METEOROID PROTECTION = .0145- IN TITANIUM

$$\text{EQUIVALENT THICKNESS OF ALUMINUM} = \frac{.16(.0054)}{.1} = .0087 \text{ IN.}$$

PENETRATING ANALYSIS

CONSIDER CRUISE ENVIRONMENT ONLY

REQUIRE $P_0 = .995$ FOR PRESSURE VESSELSUSE UPPER LIMIT MARS FLUX & DESIGN FOR $P_0 = .997$

USE BUMPER CONCEPT & MAIN WALL OF ALUMINUM

BY
CK.
DATE

GENERAL ELECTRIC

PAGE
MODEL VOYAGER
REPORT

REV.

$$P_0 = e^{-\mu}$$

$$\text{For } P_0 = .997 \quad \mu = .003$$

$$\mu = NAT$$

$$A = 2.53 \text{ METERS}^2$$

$$T = 90(24)(3600) = 7.76 \times 10^6 \text{ SECONDS}$$

$$N = \frac{.003}{(2.53)(7.76 \times 10^6)} = 1.53 \times 10^{-10}$$

UPPER LIMIT MARS FLUX

$$\text{Log } N_M = -13.98 - 1.34 \text{ Log } M + 2.68 \text{ Log} \left(\frac{A}{T} \right)$$

$$\approx -13.87 - 1.34 \text{ Log } M$$

$$\text{Log } 1.53 \times 10^{-10} = 0.1847 - 10 = -9.8153$$

$$\text{Log } M = \frac{-13.87 + 9.8153}{1.34} = -3.02 = 6.98 - 10$$

$$M = 9.55 \times 10^{-4} \text{ GMS}$$

FOAM FILLED BUMPER

$$t = .872 M^{1/3} \text{ INCHES}$$

$$\bar{t} = .33 t$$

$$= 0.29 M^{1/3} \text{ INCHES}$$

$$\bar{t} = 0.29 (9.000955)^{1/3}$$

$$\bar{t} = .0287 \text{ INCHES}$$

UPPER LIMIT EARTH FLUX

$$\text{Log } N = -14.48 - 1.34 \text{ Log } M + 2.68 \text{ Log} \left(\frac{A}{T} \right)$$

$$= -14.48 - 1.34(-3.02) + .11 = -10.32 = 0.68 - 11$$

$$N = 4.786 \times 10^{-11}$$

BY CK. DATE	REV.	GENERAL  ELECTRIC	PAGE MODEL VOYAGER REPORT
-------------------	------	--	---------------------------------

$$u = (4.786 \times 10^{-11})(2.53)(776 \times 10^6)$$

$$= 94 \times 10^{-5}$$

$$P_0 = 0.999$$

SUMMARY

PROBABILITY OF NO PENETRATIONS FOR UPPER LIMIT FLUXES

	EARTH TO MID-COURSE	MID-COURSE TO MARS	ELLIPTICAL ORBIT (30 DAYS)	PROB. OF NO PENETRATION
ELECTRONICS MODULE 180 DAY CRUISE	>.999	.9982	>.999	.9962
PRESSURE VESSELS	.999	.997	—	.996

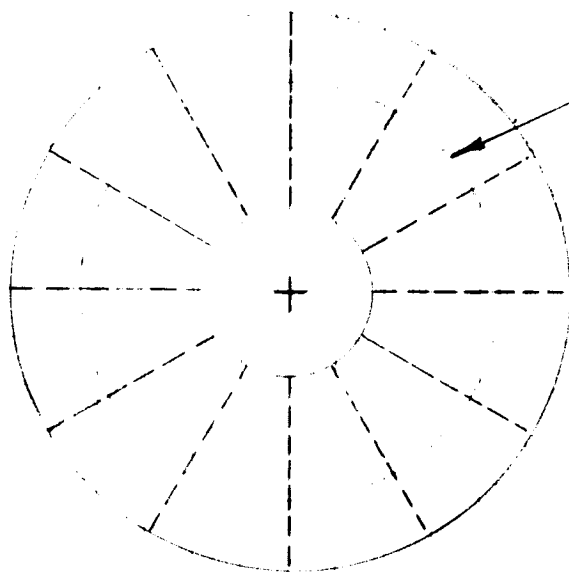
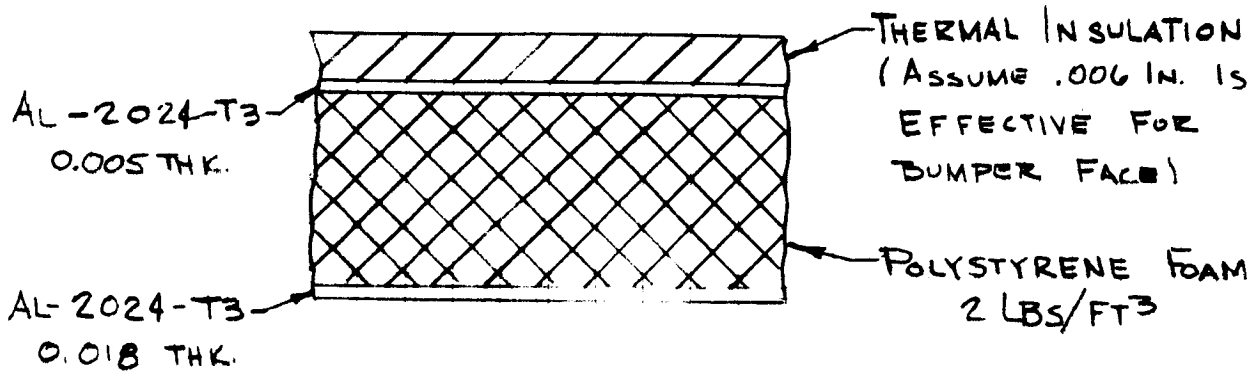
BY
CK.
DATE

GENERAL ELECTRIC

PAGE
MODEL VOYAGER
REPORT

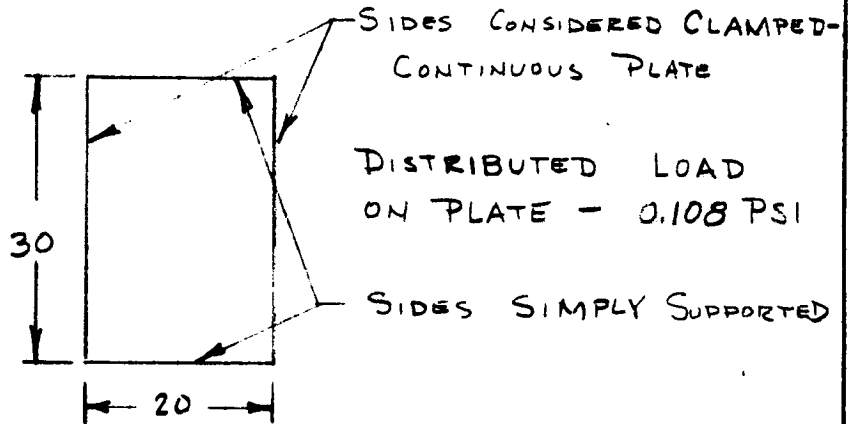
REV.

BUMPER DESIGN



THE PANEL IS
SUPPORTED AS
SHOWN. THE
MAXIMUM BENDING
MOMENTS OCCUR
AT THE CENTERS
OF THE INNER
SEGMENTS

BY	GENERAL ELECTRIC	PAGE
CK.		MODEL VOYAGER
DATE		REV.



$$M_{MAX} = \beta g a^2$$

FOR $b/a = 1.5$

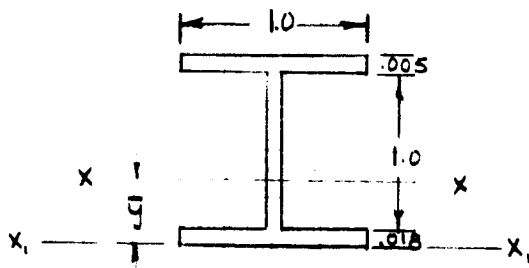
$$M_{Y MAX} = .0514 (.108) (20)^2 = 2.22 \text{ IN-LBS/IN}$$

$$M_{Y MAX} = .046 (.108) (20)^2 = 1.94 \text{ IN-LBS/IN} \quad (\text{REF II})$$

THE MOMENT OF INERTIA OF A 1 INCH WIDE SECTION CAN BE DETERMINED AS FOLLOWS -

EQUATE A 1 INCH WIDE SECTION OF FOAM TO AN EQUIVALENT WIDTH OF ALUMINUM

$$t_e = \frac{E_{FOAM} t_{FOAM}}{E_{ALUM.}} = \frac{(2000)(1)}{10.3 \times 10^6} = .000194 \text{ IN}$$



BY
CK.
DATE

GENERAL ELECTRIC

PAGE
MODEL VOYAGER
REPORT

REV.

$$\bar{y} = \frac{1(.018)(.009) + 1(.000194)(.518) + 1(.005)(1.0205)}{1(.0018 + .000194 + .005)}$$

$$= .231 \text{ IN.}$$

$$I_{xx} = 2 \left[\frac{1}{3} (.4999)(.018)^3 \right] + \frac{1}{3} (.000194)(1.023)^3$$

$$+ 2 \left[\frac{1}{12} (.4999)(.005)^3 + (.4999)(.005)(1.0205)^2 \right]$$

$$= .005274 \text{ IN}^4$$

$$I_{yy} = I_{xx} + A\bar{y}^2$$

$$I_{yy} = .005274 + .02319(.231)^2$$

$$= .004037 \text{ IN}^4$$

STRESSES IN .005 IN. SHEET

$$f_x = \frac{(2.22)(.792)}{.004037}$$

$$= 435 \text{ PSI}$$

$$f_y = \frac{(1.94)(.792)}{.004037}$$

$$= 381 \text{ PSI}$$

THE FOAM MUST HAVE SUFFICIENT SHEAR RIGIDITY TO STABILIZE THE FACE SHEETS.

$$F_{scz} = K_c \left(\frac{t}{b} \right)^2$$

UTILIZING THE METHOD OF REF 10, AN EFFECTIVE $E \& t$ OF THE SANDWICH IS OBTAINED.

BY	GENERAL ELECTRIC	PAGE
CK.		MODEL VOYAGER
DATE		REV.

$$D = EI = 41,500 \text{ PSI} \quad \left(\text{POISSON'S RATIO EFFECT IS SELF CANCELING IN THIS METHOD} \right)$$

$$H = Et_f = (10.3 \times 10^6) (.023) = 237,000$$

$$H = t_e E_e \quad E_e = \frac{H}{2\sqrt{3}\left(\frac{D}{H}\right)} = \frac{237,000}{2\sqrt{3}\left(\frac{41,500}{237,000}\right)}$$

$$= 163,500 \text{ PSI}$$

$$t_e = \frac{237,000}{163,500} = 1.45 \text{ IN}$$

$$F_{cer} = 4.7 (163,500) \left(\frac{1.45}{30}\right)^2$$

$$= 1795 \text{ PSI}$$

VALUES OF F_{cer} OBTAINED THUSLY ARE SOMEWHAT UNCONSERVATIVE. CONSERVATIVE VALUES ARE OBTAINED BY

$$F_{cer,con} = \frac{1}{\frac{1}{F_{cer,unc}} + \frac{1}{G_c}}$$

$$G_c = 1300 \text{ PSI} \quad (\text{REF 12})$$

$$= \frac{1}{\frac{1}{1795} + \frac{1}{1300}}$$

$$F_{cer} = 815 \text{ PSI} \quad - \text{(CONSERVATIVE VALUE)}$$

$$M.S. = \frac{815}{435} - 1 = .88$$

BY CK. DATE	GENERAL ELECTRIC	PAGE MODEL VOYAGER REPORT
REV.		
<p>SHEAR STRESS IN FOAM</p> $\tau_c = \frac{2\gamma g a}{t + t_c}$ $= \frac{2(1.48)(1.108)(20)}{(.023 + 1)}$ $= 2.02 \text{ PSI}$ <p>$\tau_{c \text{ ALLOWABLE}} = 20 \text{ PSI MINIMUM (REF 12)}$</p> $M. S. = \frac{20}{2.02} - 1 = \text{LARGE}$		

APPENDIX

III. STRUCTURAL DYNAMICS

1. SCOPE

The major structural dynamics considerations associated with the design of the preferred 1971 spacecraft are presented in this section. The structural dynamics studies have been carried out in sufficient depth to define the major structural design requirements and provide a basis for more detailed design and analysis.

2. SINUSOIDAL VIBRATION

2.1 MATHEMATICAL MODELS

The basic structure recommended for the 1971 Voyager spacecraft has been designed to withstand the most severe loading condition combinations occurring during any of the 1971 through 1977 missions. Two mathematical models have been derived for use in determining the limiting dynamic loads acting in the structure. One model is representative of the 1971-1973 version and incorporates a 3500-pound propulsion system and a 2300-pound flight capsule. The other model is representative of the 1975-1977 version and incorporates a 500-pound propulsion system and a 4500-pound flight capsule.

One basic spacecraft structure has been assumed for both models. The inertia and stiffness characteristics of the propulsion systems have been based on representative configurations and do not represent precisely any specific propulsion systems shown as typical in other sections of this study.

All appendages have been treated as rigid attachments to the basic structure with the exception of the solar array. The solar array has been represented by an annular ring, concentrated at the radii of gyration and supported by springs which yield a component natural frequency both along the Z axis and about the Y axis equal to the predicted fundamental frequency of the array (approximately 12 cps).

The resulting models, which permit longitudinal vibration along the Z axis, lateral vibration in the X-Y plane and torsional vibration about the Z axis are illustrated by Figure III-1. The corresponding inertial and stiffness coefficient matrices are given in Tables III-1 thru III-4 for the 1971-1973 mission and in Tables III-5 thru III-8 for the 1975-1977 mission.

These models represent the final design iteration of this study and therefore the dynamic loads and characteristics differ slightly from those used in the stress analysis section, which are based on the previous iteration.

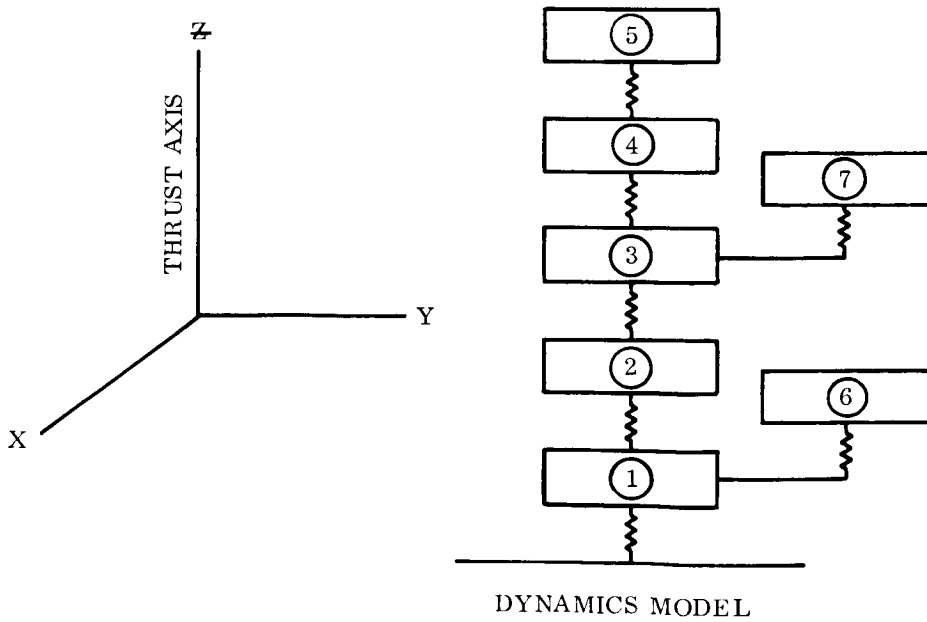
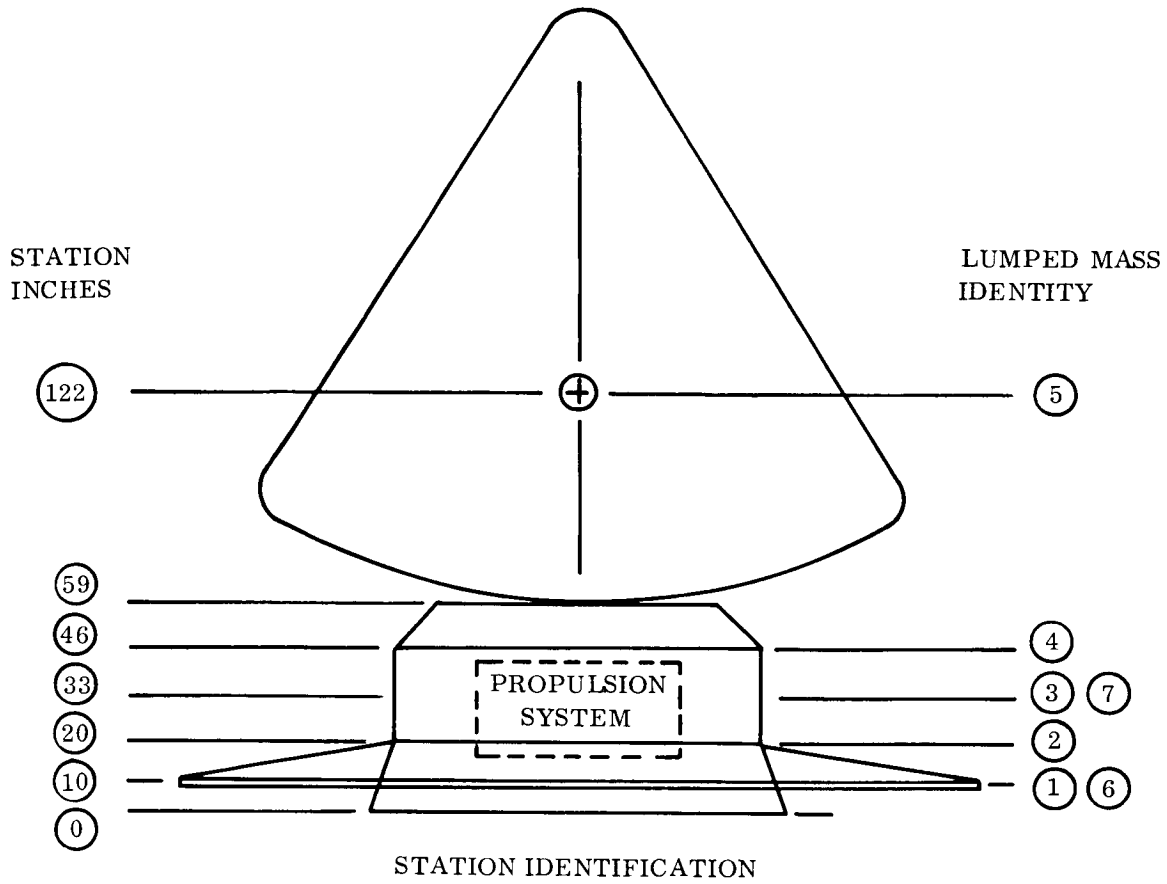


Figure III-1. Dynamics Model Description

2.2 EFFECTS OF TRANSIENT NATURE OF EXCITATION

The resonant response of a structure to a sinusoidal excitation occurring for a specific number of cycles is a function of the level of damping in the structure. Based on the results of vibratory testing of similar structures at GE-MSD, the proposed structure, having numerous removable elements such as doors and equipment modules in parallel with the basic load paths, is anticipated to exhibit a structural damping level of approximately 0.1. An approximation of the ratio of the maximum transient response to the steady state resonant response as a function of the number of cycles of excitation is shown in Figure III-2. The minimum number of cycles of excitation is ten and occurs in torsion in the 40 - 160 cps range⁽¹⁾. As shown in Figure III-2, the resultant maximum response is nearly equal to the steady state response. Therefore, for the purposes of this study, the discrete transient vibration input levels have been treated as steady state levels.

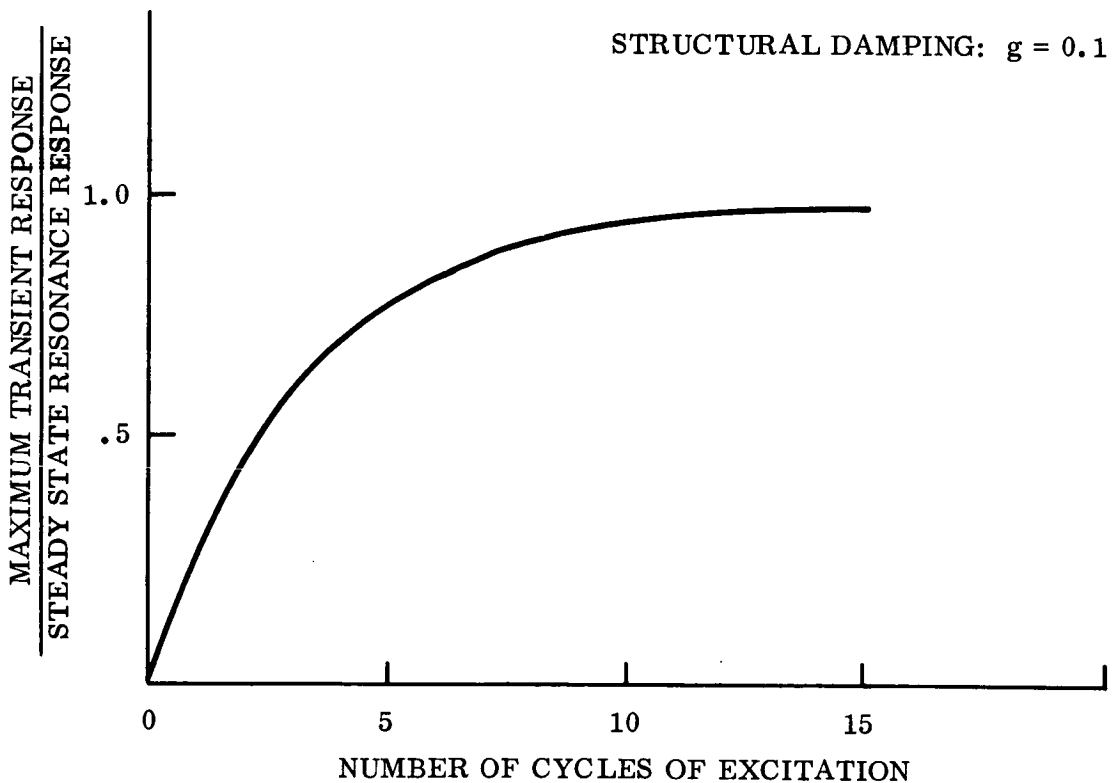


Figure III-2. Maximum Transient Response of System as a Function of the Number of Cycles of Sinusoidal Excitation

(1)Reference Table _____.

2.3 ANALYTICAL APPROACH

The normal modes, natural frequencies and dynamic response of the models have been determined using the modal analysis approach outlined briefly below:

The normal modes and natural frequencies are determined by solution of the standard eigenvalue problem. The dynamic equilibrium equations for free undamped vibration can be expressed:

$$[m] \left\{ \ddot{q} \right\} + k \left\{ q \right\} = 0 \quad (1)$$

m = inertia matrix

k = stiffness matrix

$\left\{ q \right\}$ = displacement vector

Assuming harmonic motion, equation (1) can be written:

$$[A] \left\{ y \right\} = \left\{ y \right\} \lambda \quad (2)$$

where:

$$[A] = [m]^{-1/2} [k] [m]^{-1/2}$$

$$\lambda = \omega^2$$

$$\left\{ q \right\} = [m]^{-1/2} \left\{ y \right\}$$

The application of a diagonalizing technique (the Jacobi Method) to matrix A results in two matrices; one of which is a matrix of normal mode shapes (as columns) and the other a diagonal matrix of the squares of the modal frequencies.

The response to sinusoidal excitation (amplification factors) were determined from solutions of the following equation:

$$[m^*] \left\{ \ddot{\xi} \right\} + [c] \left\{ \dot{\xi} \right\} + [k^*] \left\{ \xi \right\} = \left\{ F^* \right\}$$

where:

$$[m^*] = \phi^T m \phi = \text{Unit Matrix}$$

$$[c^*] = \phi^T C \phi = 2 \xi \left[\lambda^{1/2} \right]$$

$2 \xi = \% \text{ structural damping}$

$$[k^*] = \phi^T K \phi$$

$[\phi] = \text{mode shapes}$

$$[F^*] = \text{Modal forcing function}$$

$$= [\phi^T] \{F\}$$

$\{F\} = \text{Physical forcing function}$

(3)

The solution of Equation (3), assuming harmonic motion, can be written as follows:

$$\text{Total Displacement} = X_{\text{total}} = \sqrt{X_R^2 + X_Q^2}$$

where

$\{X_R\} = \text{Real Displacement}$

$$= [\phi] \left[(\lambda - I \omega^2)^2 + (2\omega)^2 (\xi \lambda^{1/2})^2 \right]^{-1} \left[(\lambda - I \omega^2) F_R^* \right] \quad (4)$$

$X_Q = \text{Quadrature Displacement}$

$$= [\phi] \left[(\lambda - I \omega^2)^2 + (2\omega)^2 (\xi \lambda^{1/2})^2 \right]^{-1} \left[-(2\omega) (\xi \lambda^{1/2}) F_R^* \right] \quad (5)$$

The corresponding load distributions were calculated as follows:

$F_R = \text{Real Forces}$

(6)

$$= [k] \{X_R\}$$

$F_Q = \text{Quadrature Forces}$

(7)

$$= [k] \{X_Q\}$$

Forces = $\left\{ \begin{array}{l} \text{shear \&} \\ \text{moments} \end{array} \right\}$ For the lateral analysis

= Torques for the torsional analysis

The real and quadrature forces were summed by a suitable matrix developed for each model. The total loads are given by the relationship:

$$F_{\text{total}} \Big|_{\text{location}} = \sqrt{(\sum F_R)^2 + (\sum F_Q)^2} \quad (8)$$

2.4 RESULTS OF ANALYSIS

Fixed-free mode shapes, natural frequencies, responses and load distributions are given in Table III-9 for the proposed 1971 total spacecraft. These results are based on sinusoidal excitation of 1g lateral-along X axis, 1g longitudinal-along the Z axis and 1 rad/sec² about the Z axis, input at the launch vehicle - spacecraft interface.

The corresponding results for the model of the 1975-1977 spacecraft, based on the same basic structure, are given in Table III-10.

The sinusoidal excitation specified for preliminary design purposes results in dynamic loads which contribute a major part of the total load distribution in the structure. These loads appear to be overly severe and should be re-evaluated during the next phase of the program. The final structure design loads should be the combined quasi static and dynamic loads derived by "flying" a mathematical model of the spacecraft-launch vehicle total system through the limiting launch environments.

3. RANDOM VIBRATION

The estimated random vibration occurring at the spacecraft-launch vehicle interface during launch, 0.07 g²/cps, is less severe than the sinusoidal vibration design environment and did not influence the preliminary structural design. The effect of the random environment on components requires investigation during phase 1B. It is not anticipated that random vibration will influence the design of the basic structure.

4. SHOCK LOADING INTRODUCED BY PYROTECHNICS

The firing of pyrotechnics to separate the total spacecraft and shroud from the launch vehicle and to separate the biological barrier and flight capsule from the spacecraft will result in high amplitude, high frequency shocks. Test data for shaped charge applications has shown typical shock pulses of several thousand g's amplitude and pulse durations of 0.1 ms in the immediate vicinity of the shaped charge. As the resulting waves travel through the structure, the filtering and attenuation action of the structure results in the waves decreasing in amplitude and increasing in period. The characteristics of the waves are a function of the type of pyrotechnic devices employed.

Past experience has shown that shock loads due to pyrotechnics are not normally limiting for basic structure or component support structure. However, the effects of these shocks on

components containing relays, brittle elements or other highly susceptible parts must be carefully investigated during phase 1B.

Since analytical techniques in this area are still open to question, they must be supplemented by test data. Data is available from similar structures for use in preliminary evaluation during phase 1B.

5. TRANSIENT LOADS ACTING ON DEPLOYED APPENDAGES

Following separation from the launch vehicle, the spacecraft, with deployed appendages, will be subjected to transient loads resulting from operation of the attitude control jets, firing of the midcourse and retro propulsion engines and separation of the biological barrier and flight capsule.

The small accelerations resulting from the attitude control jets will introduce negligible loads in the deployed appendages and the associated supporting structure. The high frequency accelerations due to pyrotechnics will be essentially filtered out by the low frequency deployed appendages.

The simultaneous firing of the midcourse and retro engines will produce a maximum thrust vector of approximately 2200 pounds, resulting in a maximum acceleration of one g for the total spacecraft. It is anticipated that the initial thrust overshoot of these engines will be small. However, because of the short rise time of the thrust, it has been conservatively assumed that a two to one amplification can occur for the deployed appendages. Therefore, all appendages deployed during the firing of these engines have been designed for 2.0 g along the longitudinal axis in the deployed configuration.

6. SERVO-ELASTIC COUPLING BETWEEN AUTO PILOT AND STRUCTURE

To avoid the potential problem of severe servo-elastic coupling between the attitude control system and the low frequency elements of the spacecraft, such as deployed appendages, these elements were designed to have all fundamental frequencies above the control system crossover frequency. An initial target of 10 cps was established to provide a wide margin for preliminary design purposes. However, during the study it was found that several elements could not be designed to meet this target without penalizing the design. The element exhibiting the lowest natural frequency is the high gain antenna which is estimated to have a fundamental frequency of approximately 3.2 cps due to flexibility of the flexible pivots. Analyses of the fundamental frequencies of the planet scan package and the high gain antenna are given following this section.

Further analysis during phase 1B will be carried out to define the interaction of these with the control system.

REFERENCE:

1. H. J. Roberge and J. Rybacki, "Shock Environments Generated by Pyrotechnic Devices," presented to 33rd Symposium on Shock, Vibration and Associated Environments, Washington, D.C. 1963.
2. N.J. Hess, "Separated Clamp Deployment Test" (G.E. Internal Document) Final Report #1140-005. 1964.

Table III-1. 1971-1973 Total Spacecraft

2,300 lb Flight Capsule
 3,500 lb Propulsion System

LATERAL

Mass/Inertia Matrix

Mass - lb-sec²/in.
 Moment of Inertia - lb-in/sec²

.746	\ddot{x}_1
936.	$\ddot{\theta}_{y1}$
.943	\ddot{x}_2
1,180	$\ddot{\theta}_{y2}$
.943	\ddot{x}_3
1,180.	$\ddot{\theta}_{y3}$
1.059	\ddot{x}_4
1,330	$\ddot{\theta}_{y4}$
6.074	\ddot{x}_5
3,460	$\ddot{\theta}_{y5}$
1,970	$\ddot{\theta}_{y6}$
9.065	\ddot{x}_7
4,320	$\ddot{\theta}_{y7}$

= Inertia Forces

Table III-2. 1971-1973 Total Spacecraft

LATERAL

2,300 lb Flight Capsule
3,500 lb Propulsion System

Stiffness Matrix

Translation - lb/in
Rotation - in-lb/rad.

.0133	.4995	-.00637	-.197							X ₁
.4995	55.11	-.260	-23.70							θ y ₁
-.00637	-.260	.00878	.237	-.00244	-.00796					X ₂
-.197	-23.70	.237	37.50	-.0397	-15.2					θ y ₂
		-.00244	-.0397	.00545	.0477	-.00244	-.00796			X ₃
		-.00796	-15.20	.0477	31.05	-.0397	-15.20			θ y ₃
		-.00244	-.0397	.00584	.129	-.00340	.137			X ₄
		-.00796	-15.20	.129	22.16	-.121	2.033			θ y ₄
		-.00340	-.121	-.00340	-.137	.00340	-.137			X ₅
		.137	2.033	-.137	8.395	-.137	8.395			θ y ₅
								.0112		θ y ₆
									.000573	X ₇
										θ y ₇

(10⁹) x

= Spring Forces

TORSIONAL

Table III-4. 1971-1973 Total Spacecraft

2,300 lb Flight Capsule
 3,500 lb Propulsion System

Stiffness Matrix

$$(10^{11}) \begin{bmatrix} .592 & -.256 & & & & & \\ -.256 & .378 & & & & & \\ & & -.122 & & & & \\ & & & .247 & & & \\ & & & & -.122 & & \\ & & & & & .205 & \\ & & & & & & -.0830 \\ & & & & & & & -.0830 \\ & & & & & & & & .0830 \\ & & & & & & & & & -.00337 \\ & & & & & & & & & & .00337 \end{bmatrix} \begin{bmatrix} \theta_{z1} \\ \theta_{z2} \\ \theta_{z3} \\ \theta_{z4} \\ \theta_{z5} \\ \theta_{z7} \end{bmatrix} = \text{Spring Forces}$$

Inertia Matrix

$$(10^4) \begin{bmatrix} .5812 & & & & & & \\ & .2360 & & & & & \\ & & .2360 & & & & \\ & & & .2660 & & & \\ & & & & .3290 & & \\ & & & & & .5950 & \end{bmatrix} \begin{bmatrix} \ddots \\ \theta_{z1} \\ \ddots \\ \theta_{z2} \\ \ddots \\ \theta_{z3} \\ \ddots \\ \theta_{z4} \\ \ddots \\ \theta_{z5} \\ \ddots \\ \theta_{z7} \end{bmatrix} = \text{Inertia Forces}$$

Table III-5. 1975-1977 Total Spacecraft

4,500 lb Flight Capsule
 500 lb Propulsion System

LATERAL

Mass/Inertia Matrix

Mass - lb-Sec/in
 Moment of Inertia - lb-in Sec²

.746		\ddot{X}_1		
936.		\ddot{Y}_1		
.943		\ddot{X}_2		
1,180		\ddot{Y}_2		
.943		\ddot{X}_3		
1,180		\ddot{Y}_3		
1.059		\ddot{X}_4		
1,330		\ddot{Y}_4		
11.77		\ddot{X}_5		
19.200.		\ddot{Y}_5		
1,970.		\ddot{X}_6		
1.295		\ddot{Y}_6		
617.		\ddot{X}_7		
		\ddot{Y}_7		

= Inertia Forces

TORSION

Table III-8. 1975-1977 Total Spacecraft

4,500 lb Flight Capsule
500 lb Propulsion System

Stiffness Matrix

$$(10^{11}) \begin{bmatrix} .592 & -.256 & & & & & \\ -.256 & .378 & -.122 & & & & \\ & -.122 & .245 & -.122 & & & \\ & & -.122 & .205 & -.0830 & & \\ & & & -.0830 & .0830 & & \\ & & & & & & \\ -.000479 & & & & & & .000479 \end{bmatrix} \begin{bmatrix} \theta_{z1} \\ \theta_{z2} \\ \theta_{z3} \\ \theta_{z4} \\ \theta_{z5} \\ \theta_{z7} \end{bmatrix} = \text{Spring Forces}$$

Inertia Matrix

$$(10^4) \begin{bmatrix} .5812 & & & & & & \\ & .2360 & & & & & \\ & & .2360 & & & & \\ & & & .2660 & & & \\ & & & & 1.920 & & \\ & & & & & & \\ & & & & & & .0850 \end{bmatrix} \begin{bmatrix} \ddot{\theta}_{z1} \\ \ddot{\theta}_{z2} \\ \ddot{\theta}_{z3} \\ \ddot{\theta}_{z4} \\ \ddot{\theta}_{z5} \\ \ddot{\theta}_{z7} \end{bmatrix} = \text{Inertia Forces}$$

Lateral
Mode Shapes*

Coordinate	Modal Frequency (cps)				
	11.997	30.36	36.04	45.18	122.3
X ₁	-.000431	.0131	-.0214	-.00298	.132
θ _{y1}	.0000126	.000232	.000463	.000000146	-.00113
X ₂	-.000313	.0308	-.0420	-.00646	.262
θ _{y2}	.0000130	.000477	.00108	.00000845	-.00270
X ₃	-.000133	.0951	-.0442	-.0145	.410
θ _{y3}	.0000135	.000875	.00169	-.00000359	-.00348
X ₄	.0000577	.133	.00745	-.0371	.564
θ _{y4}	.0000138	.00121	.00212	-.000290	-.00458
X ₅	.00114	.283	.242	-.111	.0345
θ _{y5}	.0000144	.00219	.00340	-.00117	-.00997
θ _{y6}	.0225	-.0000429	-.0000578	-.0000000111	.0000110
X ₇	-.000146	.224	-.234	.0527	-.0492
θ _{y7}	.000145	.00160	.00465	.0144	.000550

Locat
1
2
3
4
5

Responses - (Amplification Factors)

Coordinate	Forcing Frequency (cps)				
	11.997	30.36	36.04	45.18	122.3
X ₁	1.014	1.140	.861	.899	1.736
θ _{y1}	.000110	.00912	.00407	.00107	.0126
X ₂	1.031	1.608	.732	.756	2.997
θ _{y2}	.000217	.0187	.00900	.00194	.0299
X ₃	1.079	3.934	.639	.316	4.511
θ _{y3}	.000456	.0345	.0148	.00374	.0383
X ₄	1.104	5.383	.740	.216	6.160
θ _{y4}	.000663	.0476	.0193	.00553	.0502
X ₅	1.189	11.215	2.678	.690	.388
θ _{y5}	.00127	.0367	.0329	.0113	.109
θ _{y6}	.00111	.00169	.000505	.000081	.000122
X ₇	1.185	9.174	3.174	1.088	.543
θ _{y7}	.000489	.0625	.0398	.0374	.00604

* Fixed-free modes normalized to a modal mass of unity.

** Forces and Moments based on 1.g input at base, Torques based on 1.rad./sec² input at base.

138
①

**Lateral
Forces & Moments****

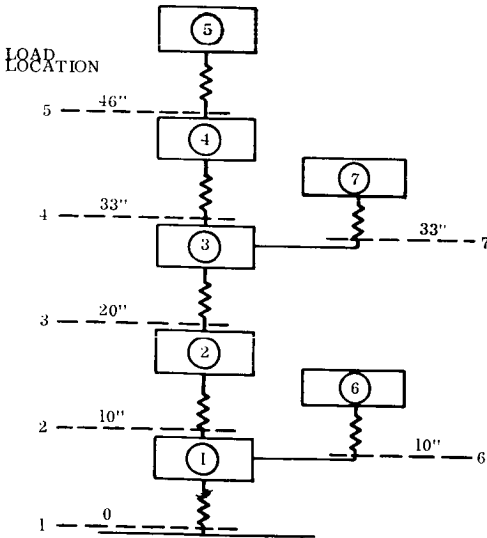
ion	Frequency (cps)					
	11.997		30.36		36.04	
	Shear (#)	Moment (in-#)	Shear (#)	Moment (in-#)	Shear (#)	Moment (in-#)
	9,130	549,780	63,250	4,717,900	14,760	1,053,150
	8,510	454,930	62,740	4,079,600	14,850	931,370
	8,030	368,300	62,280	3,442,800	14,990	812,000
	3,350	262,490	28,630	2,516,960	6,440	610,830
	2,860	218,520	26,400	2,120,400	6,250	517,900

Coordinate	12.003
Z ₁	.000297
Z ₂	.000299
Z ₃	.000302
Z ₄	.000303
Z ₅	.000305
Z ₆	1.119
Z ₇	.000345

Location	Frequency (cps)			
	45.18		122.3	
	Shear (#)	Moment (in-#)	Shear (#)	Moment (in-#)
1	4,710	307,450	4,750	53,330
2	4,920	260,120	4,260	21,310
3	5,180	210,260	3,240	30,490
4	1,650	162,920	3,430	59,980
5	1,640	138,980	920	77,800

Coordinate	Responses
	12.003
Z ₁	1.007
Z ₂	1.013
Z ₃	1.021
Z ₄	1.025
Z ₅	1.031
Z ₆	10.07
Z ₇	1.167

FORCE LOCATION DEFINITION



Location	12.003
1	13,630#
2	8,930
3	8,080
4	3,311
5	2,750
6	3,120
7	4,180

138
2

Table III-9. 1971-1973 Total Spacecraft - Dynamic Analysis Results

Longitudinal Mode Shapes *

Modal Frequency (cps)		
32.55	93.14	349.2
.00789	.0527	.270
.0158	.105	.484
.0264	.172	.601
.0271	.242	.522
.0283	.383	-.125
-.00124	0.000890	-.000320
.331	-.0263	-.00573

Torsion Mode Shapes*

Coordinate	Modal Frequency (cps)	
	36.88	116.98
θ_{z1}	.000135	.00160
θ_{z2}	.000310	.00350
θ_{z3}	.000674	.00712
θ_{z4}	.000692	.0102
θ_{z5}	.000707	.0130
θ_{z7}	.0129	-.000833

Responses - (Amplification Factors)

Forcing Frequency (cps)		
32.55	93.14	349.2
1.032	1.648	2.735
1.124	2.872	4.712
1.320	4.596	5.798
1.355	6.415	5.033
1.423	10.125	1.205
.165	.0288	.0033
10.74	.708	.0555

Responses - (Amplification Factors)

Coordinate	Forcing Frequency (cps)	
	36.88	116.98
θ_{z1}	1.023	1.866
θ_{z2}	1.060	3.583
θ_{z3}	1.189	7.091
θ_{z4}	1.223	10.137
θ_{z5}	1.251	12.882
θ_{z7}	10.894	.833

Forces **

Frequency (cps)		
32.55	93.14	349.2
43,860#	32,400#	9,740#
43,100	31,760	8,920
42,510	30,640	7,190
4,210	26,470	4,880
3,570	23,820	2,820
50	9	1
37,720	2,460	193

Torques**

Location	Frequency (cps)	
	36.88	116.98
1	83,440(#-in)	110,350(#-in)
2	77,500	99,500
3	75,000	91,050
4	7,370	69,350
5	4,110	42,383
7	64,820	4,962

Lateral
Mode Shapes*

Coordinate	Modal Frequency (cps)				
	11.997	22.74	38.60	45.06	68.64
X ₁	-.000431	-.00101	.0142	-.00332	-.0572
θ _{y1}	.0000129	.000311	-.000114	.0000536	.000324
X ₂	-.000312	.000895	.0297	-.00667	-.120
θ _{y2}	.0000136	.000692	-.000291	.000128	.000859
X ₃	-.000100	.0360	.0546	-.00912	-.228
θ _{y3}	.0000145	.00115	-.000402	.000194	.00107
X ₄	.000124	.0765	.0497	-.0114	-.3296
θ _{y4}	.0000151	.00155	-.000491	.00136	.00151
X ₅	.00138	.265	-.00457	-.0119	-.0924
θ _{y5}	.0000171	.00284	-.000888	-.0000506	.00597
θ _{y6}	.0225	-.000120	.0000121	-.00000409	-.0000102
X ₇	-.000110	.0534	.868	.0329	.116
θ _{y7}	.0000156	.00155	-.00149	.0402	-.00821

Location
1
2
3
4
5

Responses - (Amplification Factors)

Coordinate	Forcing Frequency (cps)				
	11.997	22.74	38.60	45.06	68.64
X ₁	1.005	1.030	1.069	1.041	1.375
θ _{y1}	.000350	.0103	.00236	.00154	.00578
X ₂	1.014	1.051	1.153	1.061	2.245
θ _{y2}	.000773	.0229	.00554	.00336	.0151
X ₃	1.067	1.561	1.202	.942	3.971
θ _{y3}	.00134	.0382	.00825	.00524	.0189
X ₄	1.122	2.701	1.075	.901	5.672
θ _{y4}	.00181	.0512	.0107	.00716	.0264
X ₅	1.339	8.765	.255	.00727	1.680
θ _{y5}	.00321	.0940	.0217	.0164	.102
θ _{y6}	.00349	.00395	.000251	.000117	.000181
X ₇	1.173	2.327	10.523	3.161	2.027
θ _{y7}	.00144	.0510	.0292	.0525	.01435

* Fixed-free modes normalized to modal mass of unity.

** Forces and Moments based on 1.g input at base. Torques based on 1. rad/sec² input at base.

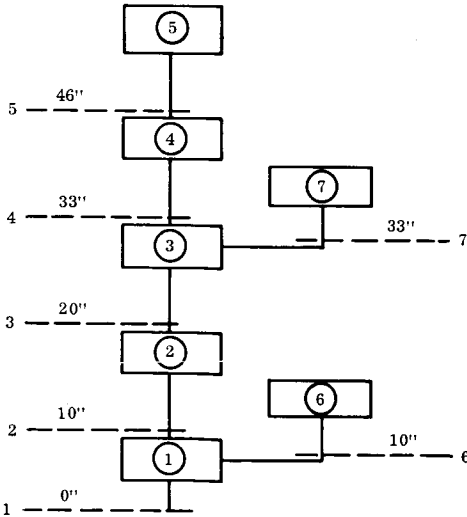
140 (1)

Lateral
Forces & Moments**

Frequency (cps)					
11.997		22.74		38.60	
Shear (#)	Moment (in-#)	Shear (#)	Moment (in-#)	Shear (#)	Moment (in-#)
8,860	857,490	43,530	5,762,900	6,600	284,860
8,240	766,090	43,050	5,321,400	6,280	261,490
7,740	682,260	42,760	4,878,560	6,075	250,300
6,700	580,390	41,200	4,293,340	930	246,100
6,210	492,380	40,080	3,731,770	1,160	232,730

Location	Frequency (cps)			
	45.06		68.64	
	Shear (#)	Moment (in-#)	Shear (#)	Moment (in-#)
1	1,370	162,430	11,650	298,600
2	1,250	156,200	11,230	186,200
3	1,380	147,500	10,490	91,020
4	510	133,770	10,000	80,630
5	400	132,410	7,670	183,630

FORCE LOCATION DEFINITION



Coordinate	12.003
Z ₁	.000297
Z ₂	.000299
Z ₃	.000301
Z ₄	.000303
Z ₅	.000306
Z ₆	1.119
Z ₇	.000344

Responses - (A)

Coordinate	12.003
Z ₁	1.005
Z ₂	1.011
Z ₃	1.018
Z ₄	1.024
Z ₅	1.036
Z ₆	10.06
Z ₇	1.162

Location	12.003
1	12,400#
2	7,730
3	6,880
4	5,700
5	5,150
6	3,110
7	595

140(2)

Table III-10. 1975-1977 Total Spacecraft-Dynamic Analysis Results

Longitudinal Mode Shapes *

Modal Frequency (cps)		
33.75	67.46	336.3
.00347	.0385	.268
.00694	.0766	.484
.0116	.127	.616
.0122	.177	.547
.0135	.283	-.0659
-.000503	-.00126	-.00342
.878	-.0433	-.00635

Amplification Factors

Forcing Frequency (cps)		
33.75	67.46	336.3
1.047	1.670	2.882
1.096	2.928	5.028
1.162	4.731	6.352
1.223	6.539	5.630
1.350	10.418	.679
.152	.0565	.00037
1.64	1.616	.0657

Forces **

Frequency (cps)		
33.75	67.46	336.3
14,305#	54,660#	10,450#
13,600	53,940	9,580
13,106	52,770	7,740
6,800	50,192	5,390
6,260	47,480	3,080
47	20	1
5,840	800	33

Torsion Mode Shapes*

Coordinate	Modal Frequency (cps)	
	37.60	58.60
θ_{z1}	.0000662	.000634
θ_{z2}	.000152	.00145
θ_{z3}	.000331	.00311
θ_{z4}	.000373	.00472
θ_{z5}	.000429	.00687
θ_{z7}	.0342	-.00221

Responses - (Amplification Factors)

Coordinate	Forcing Frequency (cps)	
	37.60	58.60
θ_{z1}	1.078	1.371
θ_{z2}	1.169	2.426
θ_{z3}	1.354	4.932
θ_{z4}	1.527	7.422
θ_{z5}	1.753	10.789
θ_{z7}	13.585	3.508

Torques**

Location	Frequency (cps)	
	37.60	58.60
1	51,090 (in-#)	252,530 (in-#)
2	44,820	244,500
3	42,060	238,840
4	37,710	226,900
5	33,650	207,160
7	1,155	298

3

BY
CK.
DATE

GENERAL ELECTRIC

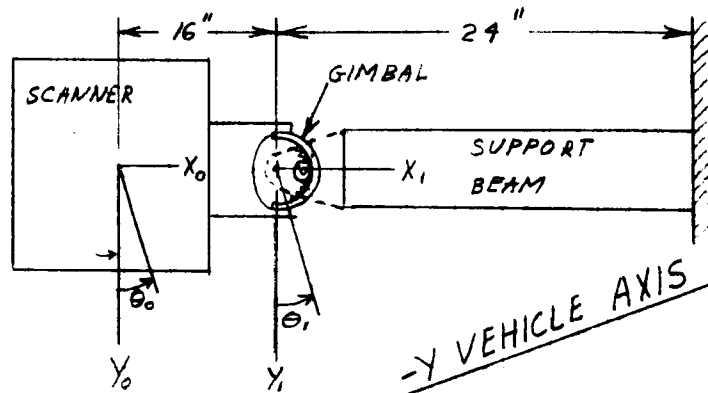
PAGE 1
MODEL VOYAGER
REPORT

PLANET SCAN PACKAGE
FUNDAMENTAL FREQUENCY

THE LOWEST FUNDAMENTAL FREQUENCY WILL OCCUR WHEN THE SCANNER IS ON A RADIAL LINE WITH THE SUPPORT BEAM. MOTION WILL BE IN X-Y PLANE. THE MAJOR FLEXIBILITIES WILL BE DUE TO THE GIMBAL AND THE SUPPORT BEAM.

$$M_0 = .363 \frac{16 \text{ SEC}^2}{\text{IN}}$$

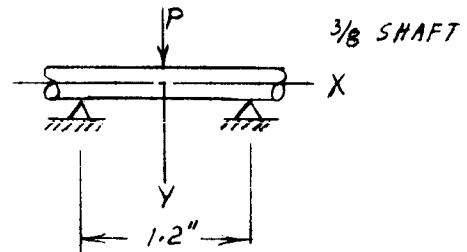
$$I_0 = 29.3 \text{ 16 sec}^2 \text{ IN}$$



MOTOR SHAFT FLEXIBILITY:

$$H_y = \frac{Y}{P} = \frac{l^3}{48EI} = \frac{1.2^3 \times 4}{48 \times 20 \times 10^6 \times \pi \times .187^4}$$

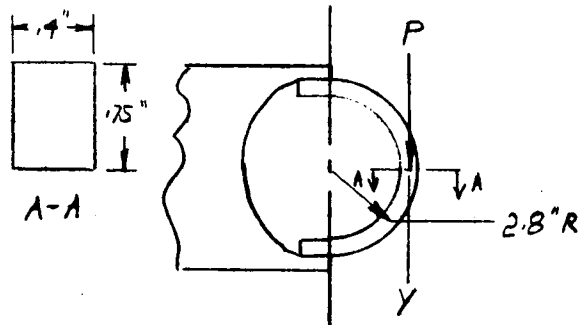
$$= 1.87 \times 10^{-6} \frac{\text{IN}}{16}$$



RING GEAR FLEXIBILITY:

$$H_y = \frac{Y}{P} = .018 \frac{R^3}{EI} = .018 \frac{2.8^3 \times 12}{20 \times 10^6 \times .75 \times .4^3}$$

$$= 0.493 \times 10^{-6} \frac{\text{IN}}{16}$$



BY	GENERAL ELECTRIC	PAGE 2
CK.		MODEL VOYAGER
DATE		REV.

COMBINED SHAFT-GEAR FLEXIBILITY:

$$H_0 = \frac{1.87 \times 10^{-6} + 0.493 \times 10^{-6}}{2.8^2} = 0.87 \times 10^{-6} \frac{\text{RAD}}{\text{IN LB}}$$

SUPPORT BEAM FLEXIBILITY:

$$I_{\text{eff.}} = AR^2 = 2 \times 0.05 \times 10 \times \left(\frac{4.5}{2}\right)^2 = 5.06 \text{ IN}^4$$

$$E = 10 \times 10^6 \text{ PSI}$$

$$\begin{bmatrix} \alpha_{11} & \alpha_{12} \\ \alpha_{21} & \alpha_{22} \end{bmatrix} \begin{bmatrix} F_1 \\ M_1 \end{bmatrix} = \begin{bmatrix} Y_1 \\ \theta_1 \end{bmatrix}$$

WHERE:

$$\alpha_{11} = \frac{l^3}{3EI} = \frac{24^3}{3 \times 10 \times 10^6 \times 5.06} = 91 \times 10^{-6} \frac{\text{IN}}{\text{LB}}$$

$$\alpha_{12} = \alpha_{21} = \frac{l^2}{2EI} = \frac{24^2}{2 \times 10 \times 10^6 \times 5.06} = 5.7 \times 10^{-6} \frac{\text{IN}}{\text{LB}}$$

$$\alpha_{22} = \frac{l}{EI} = \frac{24}{10 \times 10^6 \times 5.06} = 0.475 \times 10^{-6} \frac{\text{IN}}{\text{LB}}$$

COMBINING FLEXIBILITY OF GIMBAL AND BEAM:

$$\alpha'_{22} = 0.475 \times 10^{-6} + 0.87 \times 10^{-6} = 1.345 \times 10^{-6} \frac{\text{IN}}{\text{LB}}$$

INVERTING FLEXIBILITY MATRIX YIELDS:

$$\begin{bmatrix} 14,960 & -63,400 \\ 63,400 & 1,013,180 \end{bmatrix} \begin{bmatrix} Y_1 \\ \theta_1 \end{bmatrix} = \begin{bmatrix} F_1 \\ M_1 \end{bmatrix}$$

$$[H] \begin{bmatrix} Y_1 \\ \theta_1 \end{bmatrix} = \begin{bmatrix} F_1 \\ M_1 \end{bmatrix}$$

BY	GENERAL ELECTRIC	PAGE	3
CK.		MODEL	VOYAGER
DATE		REV.	REPORT

TRANSFORMATION TO COORDINATES OF SCANNER CG. :

$$T = \begin{bmatrix} 1.0 & -16.0 \\ 0 & 1.0 \end{bmatrix}$$

THE SYSTEM STIFFNESS COEFFICIENT MATRIX IS:

$$K = T^T H T$$

$$K = \begin{bmatrix} 14,960 & -302,764 \\ -302,764 & 6,870,810 \end{bmatrix}$$

THE RESULTING EQUATIONS OF DYNAMIC EQUILIBRIUM ARE:

$$[M] \begin{bmatrix} \ddot{Y}_0 \\ \ddot{\Theta}_0 \end{bmatrix} + [K] \begin{bmatrix} Y_0 \\ \Theta_0 \end{bmatrix} = 0$$

OR

$$\begin{bmatrix} 0.363 & \\ & 29.3 \end{bmatrix} \begin{bmatrix} \ddot{Y}_0 \\ \ddot{\Theta}_0 \end{bmatrix} + \begin{bmatrix} 14,960 & -302,764 \\ -302,764 & 6,870,810 \end{bmatrix} \begin{bmatrix} Y_0 \\ \Theta_0 \end{bmatrix} = 0$$

SOLVING FOR EIGENVALUES:

$$\lambda_1 = 3,849$$

$$f_1 = \underline{9.9} \text{ CPS}$$

$$\lambda_2 = 272,528$$

$$f_2 = 82.0 \text{ CPS}$$

THEREFORE, THE FUNDAMENTAL FREQUENCY IS APPROXIMATELY 9.9 CPS

NOTE: THE SUPPORTING STRUCTURE HAS BEEN SIZED BY DYNAMICS CONSIDERATIONS.

BY

GENERAL ELECTRIC

PAGE

4

CK.

MODEL VOYAGER

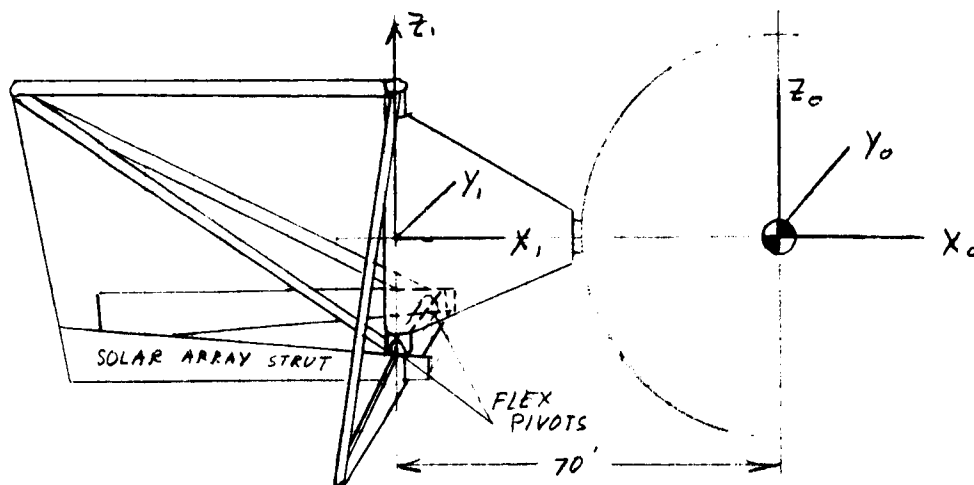
DATE

REV.

REPORT

HIGH GAIN ANTENNA FUNDAMENTAL FREQUENCY

THE MOTION OF THE ANTENNA IN THE FUNDAMENTAL MODE WILL BE ESSENTIALLY IN AN X-Y PLANE OF THE SPACECRAFT



INERTIA PROPERTIES OF ANTENNA:

$$M_0 = .1165 \frac{\text{lb sec}^2}{\text{IN}}$$

$$I_0 = 336.16 \text{ sec}^2 \text{ IN}$$

STIFFNESS COEFFICIENT MATRIX:

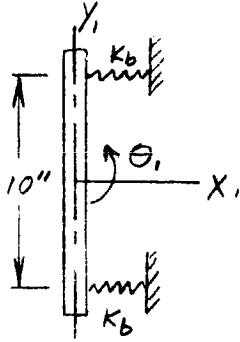
IT HAS BEEN DETERMINED THAT THE SUPPORT STRUCTURE HAS THE FOLLOWING STIFFNESS ALONG THE Y₁ AXIS:

$$K_{y_1} = \frac{F_1}{Y_1} = 1820 \frac{\text{lb}}{\text{IN}}$$

THE FLEXIBILITIES OF THE TRUSS MEMBERS AND SOLAR ARRAY STRUTS ARE INCLUDED IN K_{y₁}.

BY	GENERAL ELECTRIC	PAGE	5
CK.		MODEL	VOYAGER
DATE		REV.	REPORT

THE MAJOR TORSIONAL FLEXIBILITY ABOUT THE Z₁ AXIS IS DUE TO THE FLEX PIVOTS.



$$K_b = 7500 \frac{lb}{IN}$$

BENDIX FLEXIBLE
PIVOT 1" DIA

$$K_{\theta_1} = \frac{K_b l^2}{2}$$

$$= \frac{5650 \times 100}{2} = 282,500 \frac{IN \cdot lb}{RAD}$$

THEN:

$$[H] \begin{bmatrix} Y_1 \\ \theta_1 \end{bmatrix} = \begin{bmatrix} F_1 \\ M_1 \end{bmatrix}$$

$$\begin{bmatrix} 1820 & 0 \\ 0 & 375,000 \end{bmatrix} \begin{bmatrix} Y_1 \\ \theta_1 \end{bmatrix} = \begin{bmatrix} F_1 \\ M_1 \end{bmatrix}$$

TRANSFORMATION TO COORDINATES OF ANTENNA CG. :

$$T = \begin{bmatrix} 1 & -70 \\ 0 & 1 \end{bmatrix}$$

THE SYSTEM STIFFNESS COEFFICIENT MATRIX IS:

$$K = T^T H T$$

$$K = \begin{bmatrix} 1820 & -127,000 \\ -127,000 & 9,275,000 \end{bmatrix}$$

BY
CK.
DATE

GENERAL ELECTRIC

PAGE
MODEL VOYAGER
REPORT

REV.

THE RESULTING EQUATIONS OF DYNAMIC EQUILIBRIUM ARE:

$$[M] \begin{bmatrix} \ddot{Y}_0 \\ \ddot{\theta}_0 \end{bmatrix} + [K] \begin{bmatrix} Y_0 \\ \theta_0 \end{bmatrix} = 0$$

OR

$$\begin{bmatrix} -1165 & \\ & 336 \end{bmatrix} \begin{bmatrix} \ddot{Y}_0 \\ \ddot{\theta}_0 \end{bmatrix} + \begin{bmatrix} 1820 & -127,000 \\ -127,000 & 9,275,000 \end{bmatrix} \begin{bmatrix} Y_0 \\ \theta_0 \end{bmatrix} = 0$$

SOLVING FOR EIGENVALUES:

$$\lambda_1 = 406.4$$

$$f_1 = \underline{\underline{3.2 \text{ cps}}}$$

$$\lambda_2 = 42,820.$$

$$f_2 = 33.0 \text{ cps}$$

THEREFORE, THE FUNDAMENTAL FREQUENCY IS APPROXIMATELY 3.2 CPS

CII-VB235FD103

SUBSYSTEM LEVEL FUNCTIONAL
REQUIREMENTS
ENGINEERING MECHANICS
STRUCTURAL DESIGN CRITERIA

Index

1. Introduction
2. Applicable Documents
3. Definition of Terms
4. Requirements

1.0 INTRODUCTION

This specification presents the basic requirements and environmental conditions deemed significant to the structural design of the flight spacecraft. Its purpose is to insure structural integrity to a uniform degree by providing the design conditions, requirements and objectives.

The emphasis in this document is placed on the detail definition of environmental factors and the strength and stiffness requirements for the primary structural elements. The test conditions, especially as they effect deployed appendages in a one G field and the vibration of small electronic components and system vibration testing are treated in less detail as these conditions constitute specifications of their own.

The most important restriction placed on this document is in its use in subsequent design phases. This specification reflects the data available during the Phase IA study period and the environmental conditions specified by JPL as a design base in Project Document No. 45-Preliminary Voyager 1971 Mission Specification. Much of this data, especially the powered flight environment, will be redefined during Phase IB.

2.0 APPLICABLE DOCUMENTS

The following documents either form a part of this specifications or have been used for background material in its preparations.

a. Specifications

VB220SR101	Design Characteristics
VB220SR102	Design Constraints
VB220SR103	Spacecraft Component Design Parameters
VB220FD105	Launch Vehicle Interface
VB220FD106	Capsule Interface
VB220FD113	Layout and Configuration

b. Drawings

1. General Electric Company

(a) SK56152-423 Voyager Basic Geometry.

2. Military

(a) MIL - HDBK - 5 Metallic materials and elements for flight and vehicular structures - August, 1962; including change notices to May 1, 1964.

(b) MIL - HDBK - 23 Composite Construction for Flight Vehicles - October 1962.

(c) MIL - HDBK - 17 Plastics for Flight Vehicles November 1959.

3. General Dynamics/Astronautics

Report No. GD/A-BTD64-119 Centaur Capability Handbook.

4. General Electric Company

Structures Manual.
Structural Materials Data Handbook.

3.0 DEFINITION OF TERMS

3.1 LOAD DEFINITIONS

3.1.1 LIMIT LOADS

Limit loads are defined as the maximum loads, $+3\sigma$ limits, that the structure is expected to experience under specified conditions of operation, use, and possibly environmental testing. All loads and load factors specified in this document are limit loads unless otherwise specified.

3.1.2 DESIGN LOADS

Design loads are limit loads multiplied by an appropriate design load safety factor.

3.1.2.1 YIELD DESIGN LOADS

The yield design load shall be identical to the limit load with the exception that yield design loads = 1.15 limit loads for structure critical in component alignment.

3.1.2.2 ULTIMATE DESIGN LOADS

The ultimate design loads shall be the limit loads multiplied by the appropriate ultimate load factor. Ultimate design loads = 1.25 limit loads for powered flight and orbit conditions. Ultimate Design Loads = 1.50 limit loads for handling, transportation and other conditions dangerous to personnel.

3.1.3 PRESSURE LOADS

3.1.3.1 OPERATING PRESSURE

The operating pressure is the limit pressure, namely the maximum anticipated pressure including transient peaks and 3σ variations that a vessel will be subjected to.

3.1.3.2 PROOF PRESSURE

Proof pressure is the operating pressure multiplied by an appropriate hazard factor. It is applied to a pressure vessel as a test at room temperature as evidence of satisfactory workmanship and quantity.

3.1.3.3 BURST PRESSURE

Burst pressure is the pressure which the vessel must sustain, as a singular load condition, without rupture. It is analogous to the Ultimate Design Load and is obtained by multiplying the operating pressure by an appropriate hazard factor.

3.1.4 ALLOWABLE LOAD (OR STRESS)

The allowable load (or stress) is defined as the maximum load that a particular element can withstand and still perform its intended function.

3.2 ALLOWABLE STRESS DATA AND MATERIAL PROPERTIES

The allowable stress values and material properties used to substantiate the structural integrity of the spacecraft shall be obtained from:

- a. MIL - HDBK - 5 Metallic Materials and Elements for Flight Vehicle Structures.
- b. General Electric Co. Structural Materials Data Handbook. If necessary, reference may be made to other approved sources listing verified test results. Values used must consider temperature and instability effects.

3.3 MARGINS OF SAFETY

Margins of safety are defined as $M.S. = \frac{\text{Allowable Stress (or Load)}}{\text{Design Stress (or Load)}} - 1$

Margins of safety may also be based on specified deflection limits or stiffness characteristics as determined by alignment and dynamic characteristics. Margins of safety shall be investigated at both yield and ultimate load conditions. A negative margin of safety shall be deemed indicative of a structural failure; i.e. the structural element is not considered capable of performing its intended function.

3.4 COORDINATE AXES

The load factors given in this specification are oriented in respect to the axis shown in Figure 3-1.

3.5 MASS DISTRIBUTION

The overall mass distribution for the various missions has been specified in the Voyager mission specification. Detail mass distributions and CG locations shall be obtained from the Voyager Weight Specification VB220FD113.

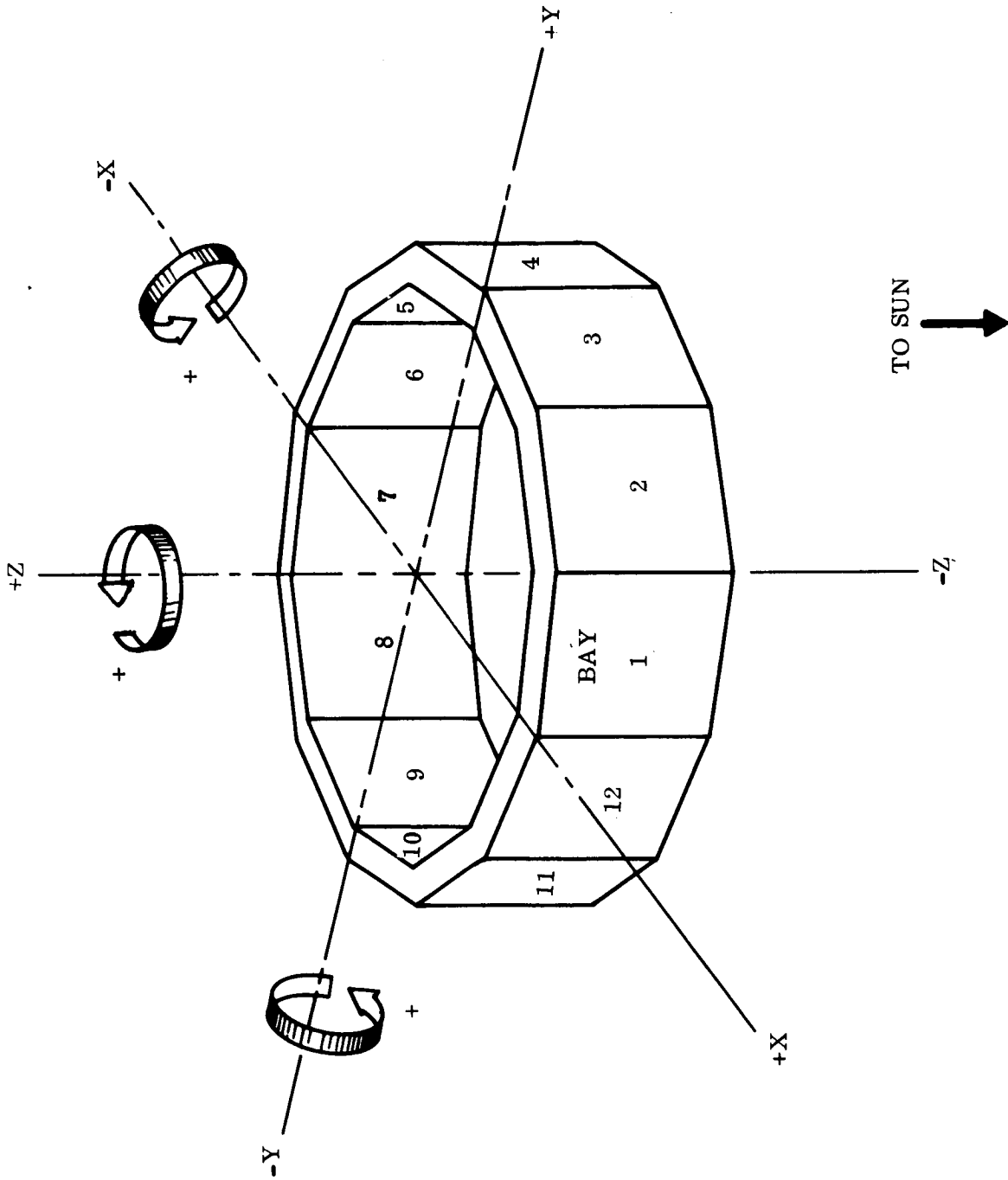


Figure 3-1. Coordinate Axes Orientation

4.0 REQUIREMENTS

4.1 GENERAL DESIGN PHILOSOPHY

It is required that the structure shall possess sufficient strength, rigidity and other physical characteristics necessary to insure that it survive the environmental and loading conditions that occur during the mission in a manner such that the probability of successful completion of the mission is not reduced. Consistent with the above, the structure shall also be designed to achieve minimum weight wherever practical.

The structural design shall reach the upper limits of but not exceed the current state of the art. Reliability will be enhanced by the use of familiar design approaches, materials and fabrication methods, substantiated by proven and accepted analytical approaches. Cost, safety, human factors, accessibility, cleanliness, manufacturing and inspection ease shall be considered during design selection studies.

The structural efficiency, as measured against the critical flight and orbital conditions, will not be compromised for pre-flight environments such as assembly, handling, and transportation. The influence of these environments shall be limited by the specification of appropriate fixturing, packaging, and handling techniques. The structural efficiency of the spacecraft must be measured against the design objective of utilizing one basic structure for all mission opportunities encompassing various landers and propulsion system configurations.

4.1.1 YIELD STRENGTH

The stress in any element of the structure shall not exceed the allowable yield stress when subjected to the yield design load. The entire structure shall be capable of withstanding the yield design load without significant permanent deformation.

4.1.2 ULTIMATE STRENGTH

The stress in any element, when subjected to an ultimate design load, shall not exceed the allowable ultimate stress. The entire structure shall be capable of withstanding the ultimate design load without failure by rupture or instability, and without loss of mission functional capability.

4.1.3 DEFLECTION AND STIFFNESS CRITERIA

The structure shall possess sufficient rigidity to permit successful performance and fulfillment of the mission objectives without jeopardy from excessive deflections.

Deflections shall be considered excessive if they result in:

- a. Significant unintentional contact between various spacecraft components
- b. Excursions which exceed the limitations of the specified dynamic envelope.
- c. Misalignment of structure and components such to affect performance accuracy.

4.1.4 PRESSURE VESSEL CRITERIA

In the interest of safety, a hazard factor shall be used in the design of vessels pressurized in the vicinity of personnel.

For Design: Proof Pressure = 1.76 Operating Pressure
Burst Pressure = 2.20 Operating Pressure

An additional requirement is that Ti-6AL-4V Titanium alloy in the annealed condition is specified as the material to be used for above designed tanks.

4.1.5 SPECIFIED MINIMUM MARGINS OF SAFETY

In keeping with the emphasis on high reliability, specific minimum margins of safety are designated for structural elements known to be susceptible to random type failures because of manufacturing and load distribution inconsistencies.

These are:

	<u>Structural Element</u>	<u>Required M. S.</u>
a.	Fasteners in shear	+.15 (Ultimate only)
b.	Bolts in tension (Eccentric load only)	+.50 (Ultimate only)
c.	Fittings	+.15
d.	Lugs	+.25
e.	Welds - Electron Beam	+.15
f.	Other welds	+.50
g.	Bonded Joints	+.50

4.1.6 METEOROID PROTECTION CRITERIA

The governing criteria for evaluating the adequacy of the structural design for the meteoroid environment shall be a specified probability of zero penetration (P_0) for structure-enclosing components whose failure through meteoroid puncture will jeopardize mission success.

Until the effect of this requirement on the overall mission reliability is assessed,

$(P_0) = 0.995$ for electronics and propulsion tankage.

4.2 DESIGN CONSIDERATIONS

Details of the mission associated environmental loads are given in subsequent paragraphs. The interpretation of these loads in formulating design parameters should include the following considerations.

4.2.1 QUASI-STATIC LOADS

All quasi-static loads and the particular attitude of components at the time of their occurrence must be considered. This includes both Saturn and Centaur thrust and flight maneuver loads, spacecraft attitude and control thrusts, main orbit injection engine firing loads, and all static tie down preloads.

4.2.2 DYNAMIC LOADS

Analysis of the dynamic loads of the spacecraft shall consider the loads induced by the elastic response of the entire flight vehicle in addition to the rigid body response to excitation.

The coupling of structural modes during launch, midcourse, and retropropulsion sequences must be considered. During launch it is necessary to consider the dynamic structural interaction of the launch vehicle and the flight spacecraft. During midcourse and retropropulsion sequences it is necessary to consider the dynamic structural interaction of the flight spacecraft with its autopilot system.

4.2.2.1 TRANSIENT LOADS

The effects of all loads of a transient nature shall be considered. Included shall be suddenly applied forces, acoustics, separation forces, and engine starting and cutoff transients. For example the use of brittle materials and shock susceptible design concepts shall be avoided.

4.2.2.2 VIBRATION LOADS

All aspects of the flight spacecraft design must consider the requirements which will arise from vibratory environmental forces prevalent during the mission.

4.2.3 FATIGUE CONSIDERATIONS

Consideration shall be given in the design of spacecraft structure towards obtaining a good fatigue design. Materials utilized shall exhibit satisfactory fatigue characteristics and care shall be exercised to avoid excessive residual stresses and stress concentrations, and poor surface finishes. Areas particularly susceptible to fatigue failure are components subjected to repeated stress reversals such as may be induced by pressure cycling, sinusoidal, random and acoustical vibration excitation and possibly thermal cycling.

4.2.4 THERMAL CONSIDERATIONS

The degrading of material properties, the buildup of thermal stresses in restrained sections and the adverse effects of thermal distortions shall be considered at each point in mission time. Mating of dissimilar materials with widely varying coefficients of expansion in locations susceptible to high temperature variations will be restricted.

4.2.5 PRESSURE DIFFERENTIAL

Consideration shall be given to the sudden pressure drop occurring during the launch phase of the flight due to change in ambient pressure. Adequate venting provisions shall be included. Inadequately vented structure must be designed for internal pressure.

4.2.6 AUTOPILOT COUPLING

Of particular importance in the design is the avoidance of adverse servoelastic coupling of structural elements with the autopilot system. To avoid degradation of the autopilot system performance natural frequency requirements of space deployed booms and components will be specified.

4.2.7 STRUCTURAL NON-LINEARITIES

The Voyager structure shall possess "linearity" to a degree which will allow accurate prediction of its behavior at any time. Important types of nonlinearities which should be avoided are adverse nonlinearities in energy dissipating mechanisms, mechanical backlash, and to a certain degree, elastic shear buckling in structural elements.

The separation joints shall be designed so that mating surfaces will remain in contact during the application of the highest separation loads.

4.2.8 METEOROIDS

The possibility of hypervelocity impact of meteoroids on the spacecraft will be considered. It shall be a requirement of the primary structural elements, augmented as necessary with additional bumpers, to provide the necessary protection to sensitive electronics, mechanisms, and propulsion tankage.

4.2.9 STERILIZATION

It is not a requirement to sterilize the flight spacecraft; however, the influence of the capsule sterilization requirements on the adapter interface design shall be considered. For example, the use of materials compatible with ethylene oxide is mandatory in the design of the capsule-spacecraft adapter, since an ETO purging operation can be expected.

4.2.10 MATERIAL COMPATIBILITY

The materials of construction will be carefully chosen for compatibility with the mission environment. Materials with low levels of outgassing as demonstrated by laboratory tests

and analytical studies will be used. These materials will not suffer intolerable degradation such as to jeopardize the mission, nor evolve fractions which could interface with sensors, experiments or thermal control surfaces. In addition, the materials selected will have the lowest possible magnetic permeability consistent with functional requirements.

Resistance to terrestrial environments will also be incorporated into the design. Materials which are corrosion resistant or have corrosion resistant finishes will be used. Recommended practice for prevention of galvanic corrosion between dissimilar metals will be followed.

4.3 LOAD FACTORS AND ENVIRONMENTAL DATA

The following load factors and environmental data shall be used to design the Voyager flight spacecraft structure. The weight of the structural elements themselves shall be included in all analysis.

4.3.1 PRE-LAUNCH (SHIPPING, HANDLING, AND STORAGE)

The limiting conditions on the design of the spacecraft shall be the actual flight environments. Pre-flight environments, such as assembly, handling, transportation, storage and mating should not influence the structural weight of the flight spacecraft, but be used as a base for the design of special handling fixtures and procedures that will insure structural loadings that are less severe than flight loads. In most cases the environmental factors specified below are **not applicable to the entire spacecraft but only to discreet subsystem structural components.**

4.3.1.1 STEADY STATE ACCELERATIONS

- | | N_z | N_x | N_y |
|---|----------------|------------------|------------|
| a. Hoist & Booster-Spacecraft Mating | -3.0 ± 0.5 | ± 0.5 | ± 0.5 |
| b. Air Transportation | ----- | -3.62 ± 1.82 | ± 3.62 |
| c. Ground Transportation - Special handling procedures will be adhered to so that above factors are not exceeded. | | | |

Note: The spacecraft is not complete when shipped (i.e., lander is shipped separately, fuel tanks empty, etc.) load factors are taken in combination.

4.3.1.2 SHOCK

Shock loading transmitted to the spacecraft from the shipping container shall be attenuated such that the loads in the vehicle structure do not exceed the powered flight loads.

A free drop of 1/2 inch maximum can be expected on the complete spacecraft under "normal" handling conditions. Precautions must be taken during the mating procedure to limit free drop to a minimum.

4.3.1.3 VIBRATION

Vibration loads will be attenuated by the shipping container so that the structural member loads do not exceed those experienced under the launch load conditions.

4.3.1.4 TEMPERATURE

Temperature extremes of -80° to 125° F are to be expected during all phases of shipping, handling, and storage. For the specific components that cannot withstand this environment, special handling techniques and packaging specifications that limit the temperature will be specified.

4.3.1.5 PRESSURE

Items may be stored in containers at 2.5 psig and 5 percent relative humidity referred to 70° F. Other items may be subjected to pressures of 15.4 to 10.2 psia (0-10,000 ft.) and 10.2 to 1.69 psia (10,000-50,000 ft.) during storage and air transportation.

4.3.2 LAUNCH VEHICLE BOOST FLIGHT

4.3.2.1 STEADY STATE AND SINUSOIDAL VIBRATIONS

Table 4-1 lists the load factors designated in the mission specification as a design base at the start of Phase IA. These loads will be continually upgraded as composite launch vehicle-payload trajectory analyses are performed.

The loads are applicable only during the boost phase of the mission, while the vehicle is complete, mounted on the launch vehicle adapter and shrouded for protection against aerodynamic loadings. All appendages are in folded or tied down attitudes.

4.3.2.2 RANDOM VIBRATIONS

The significance of the random vibration environment is usually limited to fatigue considerations. As a consequence, the following random environment shall be considered applicable, but not to the extent that it is additive to peak sinusoidal G's. The omnidirectional input at the spacecraft adapter-launch vehicle adapter mechanical interface is:

- a. Power spectral density peaks of $0.07 \text{ g}^2/\text{cps}$ ranging from 100 to 1500 cps with a 6 db rolloff in the envelope defining peaks below and above these frequencies.
- b. Maximum total time is 60 seconds.

Table 4-1. Steady State and Sinusoidal Vibration Loads

DESIGN LOADING CONDITIONS	STEADY STATE		SINUSOIDAL VIBRATION		
	Longitudinal (-Z axis)	Lateral (XY Plane)	Longitudinal 0 to Peak g's (± Z axis)	Lateral 0 to Peak g's (XY Plane)	Torsional 0 to Peak Radians/sec ² (about Z axis)
	g	g			
1	6	1	0.8	0.5	0
2	2	1	1.2	0.75	60
3	1	0	1.6	1.0	60
4	0	0	1.6	0	0

NOTES:

1. The combined longitudinal and lateral steady state loads are to be combined with the sinusoidal vibration acting in one most critical direction.
2. Lateral loads are considered acting along any vector in the XY plane.
3. Torsional loads are considered to act about the Z axis.
4. Loads are considered acting at the spacecraft adapter-launch vehicle adapter mechanical interface.
5. Vibration inputs shall be considered as discrete transients which may occur at any frequency for the duration as indicated in Table 4-2.

Table 4-2. Length of Vibration Transient

DIRECTION	VIBRATION FREQUENCY RANGE (cps)		
	2.5 -10	10 - 40	40 - 60
Longitudinal	40 cycles	30 cycles	0.5 sec
Lateral	40 cycles	30 cycles	0.5 sec
Torsional	20 cycles	20 cycles	0.25 sec

NOTE: In addition to the above strength requirements, it is desirable to design a relatively rigid payload structure.
A recommended lowest cantilever resonant frequency is 20 cps.

4.3.2.3 COMPONENT VIBRATION LOADS

Vibration loads experienced by spacecraft mounted components during the mission will be governed by the resonance to excitation of the mounting structure. It shall be a requirement of the structure to limit dynamic inputs to mounted components to levels such that the response of the component at system resonance does not exceed the maximum resonance the component experiences during its qualification testing.

The dynamic envelope of Centaur and Saturn component qualification levels is shown in Figure 4-1 as an indication of typical component test levels.

4.3.2.4 SYSTEM VIBRATION TESTING

Details of system vibration testing will be given in the appropriate test specification. Flight acceptance testing will be performed at the 95th percentile predicted flight environment and type approval testing at 5 db above the FA level.

4.3.2.5 SYSTEM SHOCK LOADING

The significant shock loading expected in the Centaur environment is the separation charge shock at such times as insulation panel and nose fairing jettison, or spacecraft separation. Generally, the shock loading can be represented by a half wave length sinusoidal shock of 1000 g's amplitude and 0.4×10^{-3} seconds duration. This shock can be experienced along any axis at the point of application.

While a basic design goal shall be to minimize explosive devices, the Voyager Spacecraft design may incorporate pyrotechnic devices for ejecting the support structure containing the lander, the biological barrier, and the lander itself. The high frequency impulse data given above can be taken as representative; however, detail investigations must be performed to determine the extent and effect, if any, of low frequency impulses.

4.3.2.6 ACOUSTICAL NOISE

While operating, vehicle borne equipment will be subjected to a maximum, broadband, random incidence, sound pressure field composed of the following levels, within an overall sound pressure level of 142 decibels (decibels referenced to $2(10)^{-5}$ N/mtr²):

- a. SPL of 133.5 db/third octave from 85 to 250 cps
- b. Rolloff at 11 db/octave below 85 cps
- c. Rolloff at 5 db/octave above 250 cps

Total duration is about two (2) minutes.

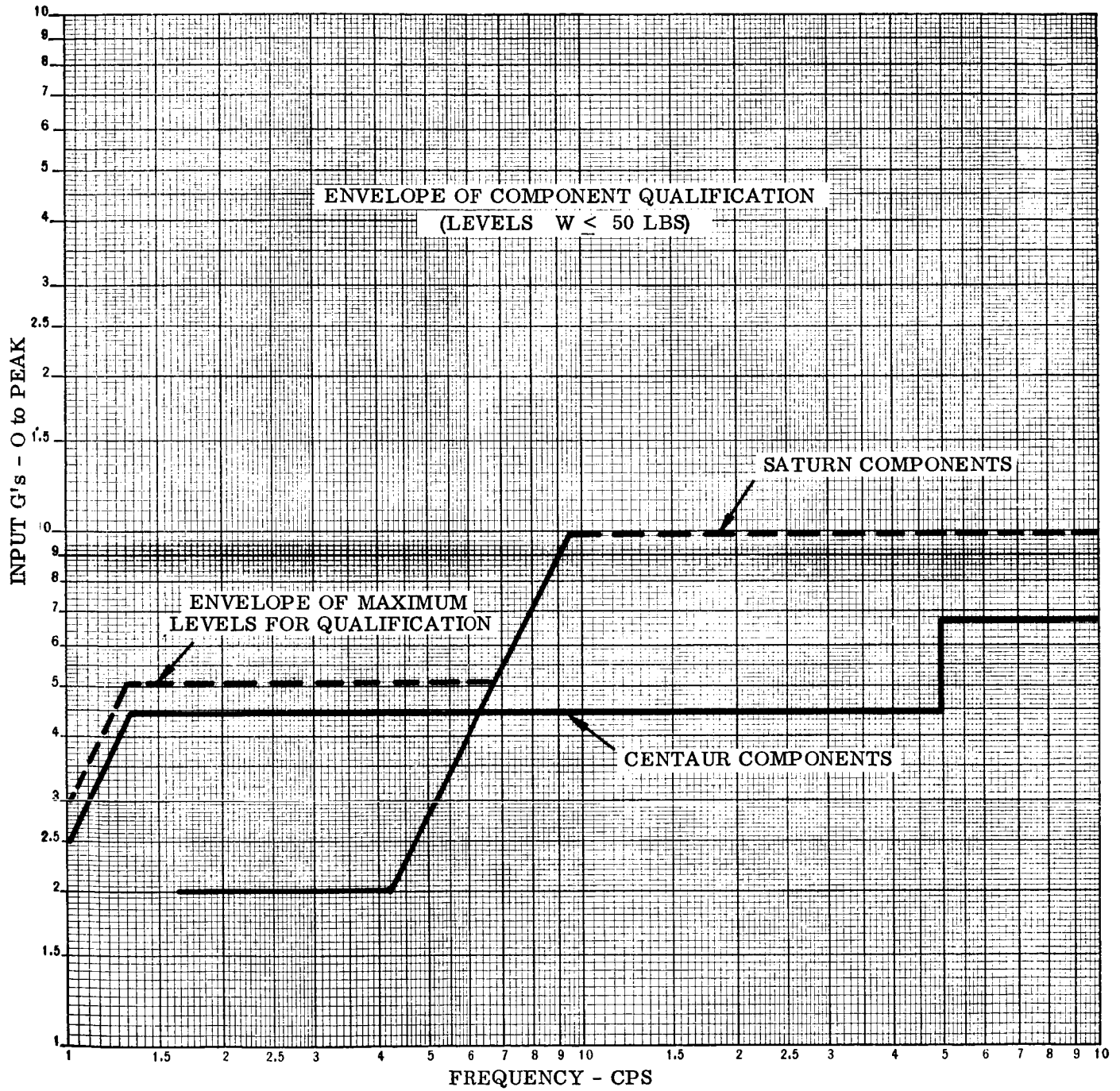


Figure 4-1. Envelope of Component Qualification Levels
($W \leq 50$ lbs)

4.3.2.7 PRESSURE

- a. Aerodynamic pressure at max q (estimated at 975 lb/ft.^2) will be taken by the shroud and is not applicable for spacecraft design.
- b. Table 4-3 gives the assumed nominal environment.

Table 4-3. Time of Flight versus Ambient Pressure

Time of Flight (sec)	Ambient Pressure (psia)
0	14.5
10	14.0
20	13.2
30	11.8
40	9.5
50	6.6
60	4.3
70	2.5
80	1.4
90	0.7
100	0.4

4.3.2.8 TEMPERATURE

The temperature profile during the launch flight phase is not usually significant to structural design. In consideration of the adverse effects of differential expansions on mutually moving parts and the degradation of material properties, critical areas will be checked on an individual basis with temperatures determined from the thermal analysis.

Factors affecting temperature distributions are:

- a. Effect of thermal control devices
- b. Aerodynamic heating and radiation from walls of shroud
- c. Internal power dissipation
- d. Thermal capacitance.

4.3.3 PLANETARY TRANSIT AND ORBIT

4.3.3.1 STEADY STATE ACCELERATION, VIBRATORY AND SHOCK LOADS AND ORBIT RETROPROPULSION ROCKET FIRING

Minor vibrations and accelerations as excited during attitude and control and mid-course engine firing and orientation of deployed appendages will be encountered. While load levels

are low, structural frequencies must be such that severe servo-elastic coupling between the attitude control system and the appendages can be avoided.

For initial design of deployment structure and support booms, a minimum fundamental resonant frequency of 10 cps for motion about the spacecraft X and Y axis and 5 cps for motion about the spacecraft Z axis is specified. This requirement will be modified as further iterative analyses are performed.

Loads resulting from four mid-course engines of 40 pounds \pm 15 pounds thrust, diametrically located in the XY plane at a radial distance of 38.5 inches from the Z axis shall be considered in the design.

During rocket firing, a thrust of 2200 pounds will be applied along the Z axis in the positive sense. Lateral loading in the XY plane is negligible, however, the vectoring effects of simultaneous control jet firings must be considered in the design of deployed appendages.

Shock and vibration loads on primary structures will in general be much less severe than those encountered during boost flight. These loads may be limiting on deployed appendages.

4.3.3.2 TEMPERATURE

Component thermal environment will be passively and actively controlled to maintain temperatures within specified design limits.

Extremes of 200^o to -310^oF can be expected on structural items. Actual temperature distributions will be a function of:

- a. Spacecraft orientation
- b. Solar irradiation
- c. Planetary flux
- d. Planetary albedo
- e. Internal power dissipation
- f. Thermal radiation to cold walls and free space
- g. Retro-Rocket exhaust plume radiation
- h. Inter radiation and conduction among components
- i. Solar absorptivity and emissivity.

4.3.3.3 VACUUM

The spacecraft will be designed to operate at ambient pressures less than 10^{-10} mm Hg.

4.3.3.4 RADIATION

Charged particles, resultant X-rays and gamma rays associated with artificial and natural belt radiation and solar flares will be encountered. The environmental criteria given in the JPL Mission Specification is noted as being applicable and part of this document, and to be used in the design of such structural shielding as is found necessary.

4.3.3.5 METEOROIDS

The meteoroid flux to be used for design purposes is given below. Also listed are extreme upper limits of particle fluxes based on Kessler's equation for asteroidal debris. Design will be based on the normally expected fluxes. The influence of the extreme upper limits of particle flux will be factored into the reliability analysis on the basis of probability of occurrence. At the present time it is assumed that this upper limit is a $+3\sigma$ extreme.

a. Flux Near Earth

1. Particle flux $\log N = -17.0 - 1.70 \log M$

N = number of particles/ (m^2 - sec) of mass M and greater.

2. Velocity of Particles ≈ 0 to 10 km/sec.

3. Average density of particles ≈ 0.4 gm/cm³.

b. Cruise

1. Particle $\log N_E = -13.80 - \log M + 2 \log \frac{0.44}{\rho}$

to

$-14.48 - 1.34 \log M + 2.68 \log \frac{0.44}{\rho}$

$\log N_M \lesssim -13.30 - \log M + 2 \log \frac{0.44}{\rho}$

to

$-13.98 - 1.34 \log M +$

$+2.68 \log \frac{0.44}{\rho}$

N_E = number of particles/ m^2 - sec of mass M and greater and of density ρ in the vicinity of the Earth; N_M is the particle flux in the vicinity of Mars.

2. Velocity of particles

$\approx 10 - 70$ km/sec (Average ≈ 40 km/sec).

3. Average density of particles ≈ 0.4 gm/cm³. An extreme upper limit for N_M (on the basis of Kessler's equation for asteroidal debres);

$$\log N_{AM} = -12.83 - \log M$$

N_{AM} = number of micrometeorite particles/(m² - sec) in vicinity of Mars of Mass M and greater.

Velocity of particles $\approx 20 - 40$ km/sec.

Average density of particles ≈ 4.37 gm/cm³.

c. Elliptic Orbit

1. Particle flux

$$\log N \approx -17.20 - 1.70 \log M$$

N = number of particles/(m² - sec) of mass M and greater.

2. Velocity of particles

≈ 0 to 5 km/sec.

3. Average density of particles

≈ 0.4 gm/cm³

4. Extreme upper limit

$$\log N_A \approx -10.13 - 1.70 \log M$$

N_A = number of micrometeorite particles/(m² - sec) of mass M and greater.

Velocity of particles ≈ 0 to 5 km/sec

Average density of particles ≈ 4.37 gm/cm³.

CII-VB235FD104

FUNCTIONAL DESCRIPTION

PYROTECHNIC SUBSYSTEM

Index

- 1 Scope
- 2 Applicable Documentation
- 3 Functional Description
- 4 Interface Definition
- 5 Performance Parameters
- 6 Physical Characteristics

1.0 SCOPE

This document describes the functional performance of a Pyrotechnic Subsystem for the Voyager Space Vehicle, intended to accomplish nonrepetitive mechanical actions by explosive means; and the peculiar design, fabrication, installation, and test requirements for the following parts and components required for safe and reliable control of explosive type charges:

- a. Parallel redundant Separation Switches are used as positive lockout devices to safe the subsystem and inhibit the Controller and Sequencer during pad and prelaunch checkout and powered flight, and to arm the subsystem, Controller and Sequencer, and the Guidance and Control Subsystem cold gas system upon physical separation from the launch vehicle.
- b. A Pyrotechnic Controller which transforms low level electrical command signals into high energy pulses.
- c. Electroexplosive Devices which generate a controlled explosive force when electrically initiated.
- d. Pin Pullers, Explosive Nuts, an Electrical Disconnect, and a Separation Joint as the mechanical devices which are activated by the generated force when electroexplosive devices are initiated.
- e. All harness and electrical connections between the safe and arm devices, the Pyrotechnic Controller, and the electroexplosive devices, cabled and installed as separate cables.

2.0 APPLICABLE DOCUMENTATION

Applicable documents are AFMTC 80-2 Range Safety Manual, Interstate Commerce Commission regulations, and

VB235FD101	Temperature Control Subsystem
VB235FD103	Structural Design Criteria
VB220SR101	Design Characteristics
VB220SR102	Design Restraints

3.0 FUNCTIONAL DESCRIPTION

The Pyrotechnic Subsystem is shown in block diagram form in Figure 3-1. The Pyrotechnic Controller receives 2400 cycle square wave ac power thru a parallel/redundant connection of two electromechanical safe and arm devices both of which are positively locked out for pad safety, but which are activated upon separation of the spacecraft from the launch vehicle. Separation Switch No. 1 provides immediate electrical continuity from the Electric Power Subsystem to the Pyrotechnic Controller and enables the Controller and Sequencer and the Guidance and Control Subsystem cold gas system. These functions are provided by the closure of normally open electrical contacts which carry signal lines from the Controller and Sequencer and the Guidance and Control Subsystem.

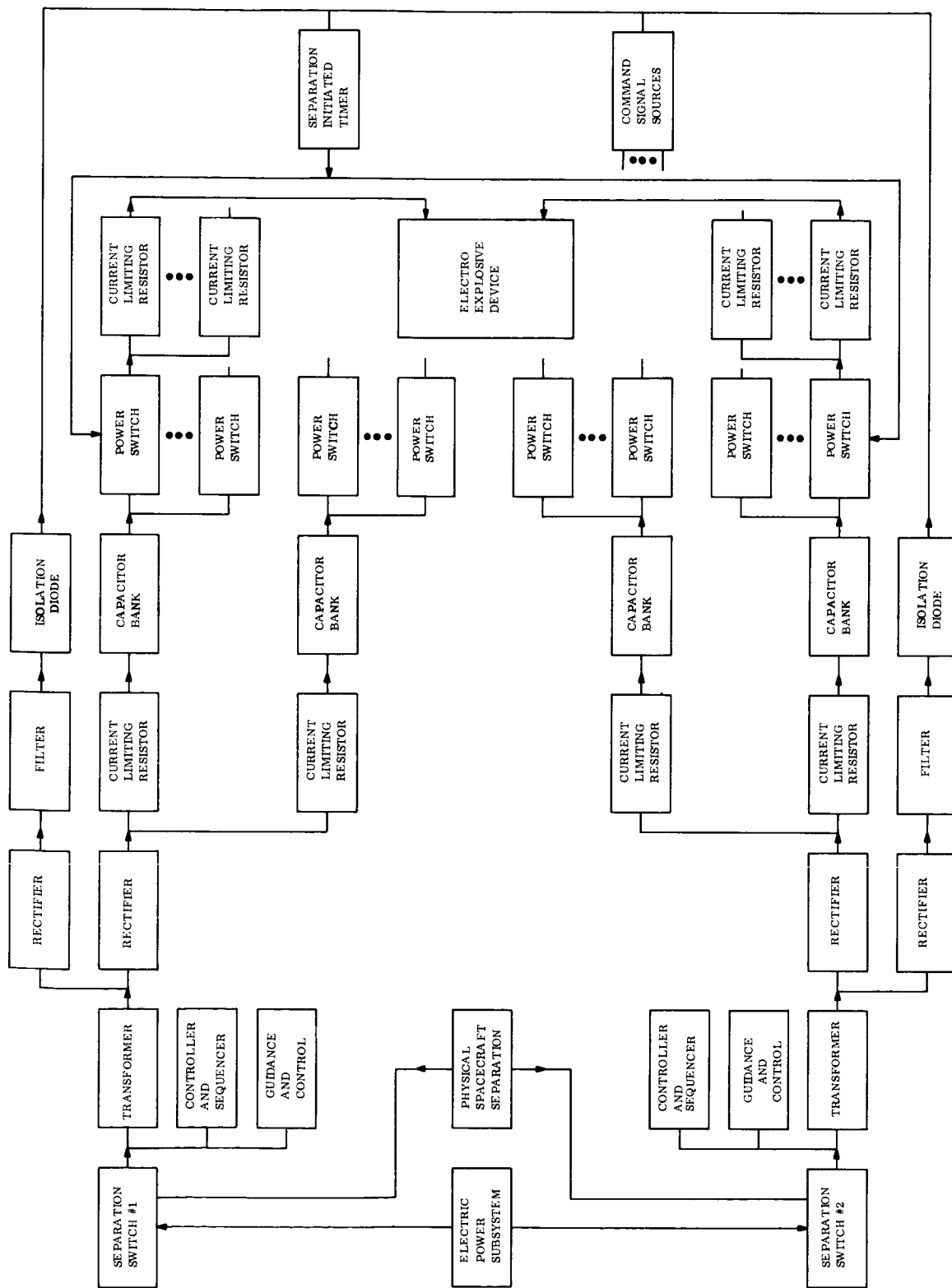


Figure 3-1. Pyrotechnic Subsystem Block Diagram

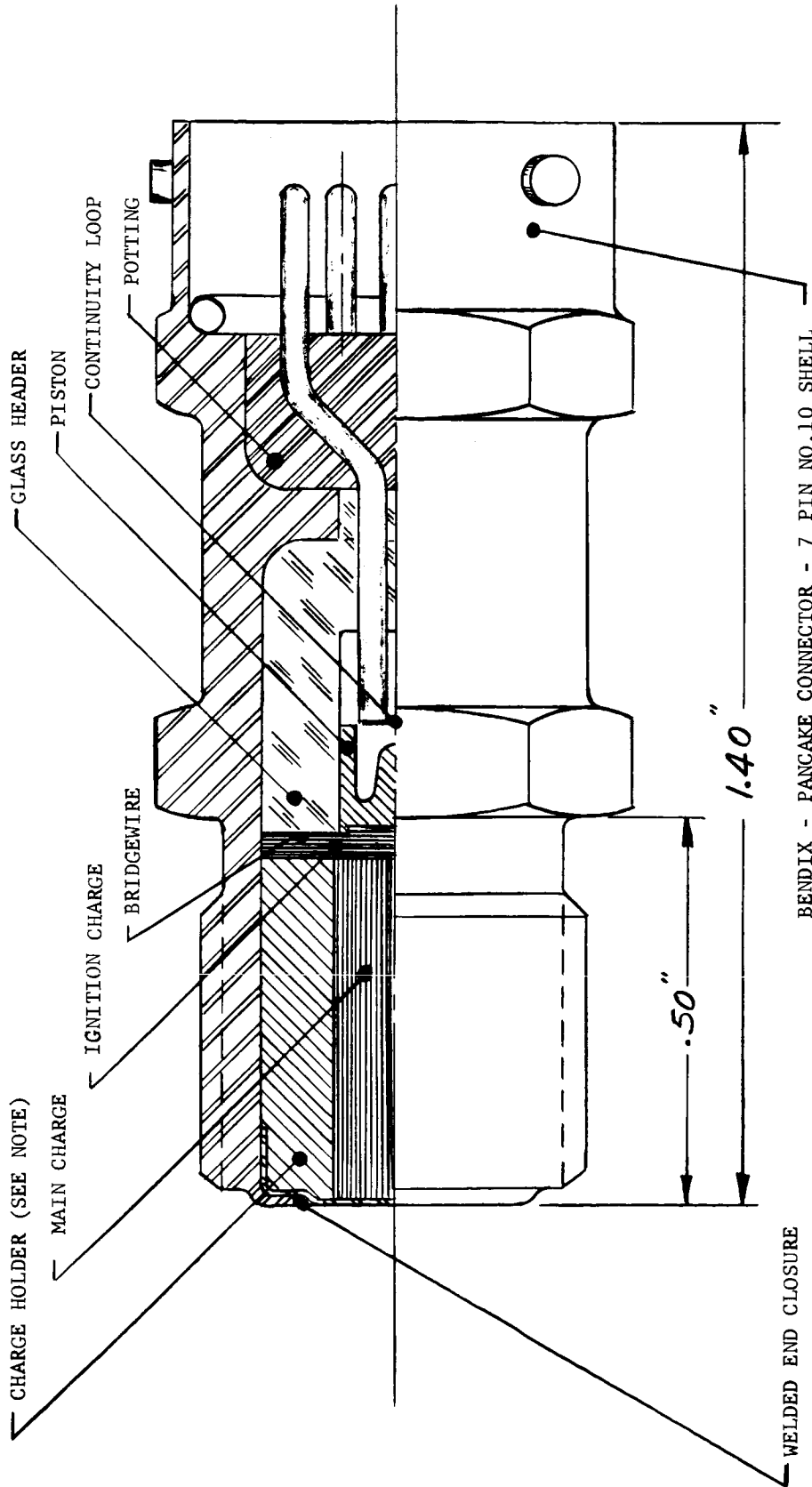
Separation Switch No. 2 also enables the Pyrotechnic Controller and the Guidance and Control Subsystem cold gas system. Separation Switch closure initiates a three minute electronic timer in the Pyrotechnic Controller. At time-out, a power pulse is given to fire the pyrotechnics to deploy the Antennas, enabling the RF link through low gain antenna No. 2.

Arming of the Pyrotechnic Controller energizes redundant transformer rectifier power supplies which transform down the ac voltage, rectify it, and charge capacitor banks thru current limiting resistors. These resistors prevent the initial current drain of the uncharged capacitors from loading down the transformer. Electrical isolation is provided between the primary and the secondary of each transformer. Command signals received after a pre-determined time from Pyrotechnic Controller arming can turn on discrete semiconductor power switches in the required sequence to accomplish pyrotechnic events. Each semiconductor switch is a silicon controlled rectifier, selected as being ideally suited to this application. It is made conductive by a low level gate signal. The magnitude of controlled current is not dependent on the gate signal amplitude over the minimum amount necessary to fire the silicon controlled rectifier, and current can continue to flow after the gate signal is removed. Current flow continues until the capacitor bank is discharged, or until the bridgewire burns open, at which time the silicon controlled rectifier returns to its nonconducting state. The current limiting resistor to charge the capacitor bank must furnish less current than the minimum holding current for the silicon controlled rectifier to insure turnoff in the event that a bridgewire fails to open completely.

Each semiconductor switch delivers electrical energy pulses thru a parallel connection of from one to six current limiting resistors, each of which has a series connected electroexplosive device. The bridgewire in the electroexplosive device burns open in less than three milliseconds, effectively opening the circuit. In the event of a malfunctioning bridgewire, the capacitor would discharge completely, cutting off the semiconductor switch, and allowing the capacitor bank to recharge for subsequent events. Spurious command signals received simultaneous with the arm signal as a result of mechanical disturbances associated with separation are ineffective to cause pyro events, since the capacitors will have accumulated insufficient energy to initiate the electroexplosive device.

The major elements of a standardized electroexplosive device are shown in Figure 3-2. This device is designed to meet all requirements of the national ranges, and is used for operation of Pin Pullers, Explosive Nuts, an Electrical Disconnect, Propulsion Valves, and as detonators for initiating the spacecraft Separation Joint. All electroexplosive devices have various pyrotechnic compounds but have identical electrical characteristics, and are capable of being initiated from a common switching circuit in the Pyrotechnic Controller. These electroexplosive devices use a common cartridge envelope and match head configuration with pressure cartridge mixes to provide either 3, 5, or 8 thousand pounds per square inch pressure, and detonator cartridge mixes to provide one of two different pulses to meet all anticipated Voyager requirements.

Pin Pullers are used as locking devices. Gas pressure released on command by an electroexplosive device retracts the piston and releases the locked device for deployment. The Pin Pullers are capable of functioning with single or redundant electroexplosive devices without release of damaging gases or fragmentation of parts. Pistons are locked in the extended position by shear pins or shear rings to prevent premature retraction of the piston.



NOTE
 INSIDE DIAMETER OF CHARGE HOLDER IS VARIABLE TO
 ACCEPT DIFFERENT TYPES AND WEIGHTS OF MAIN CHARGE



WIRING DIAGRAM

~ BRIDGEWIRES

⌞ CONTINUITY LOOP (NORMALLY CLOSED)
 OPENS WHEN CARTRIDGE IS FIRED

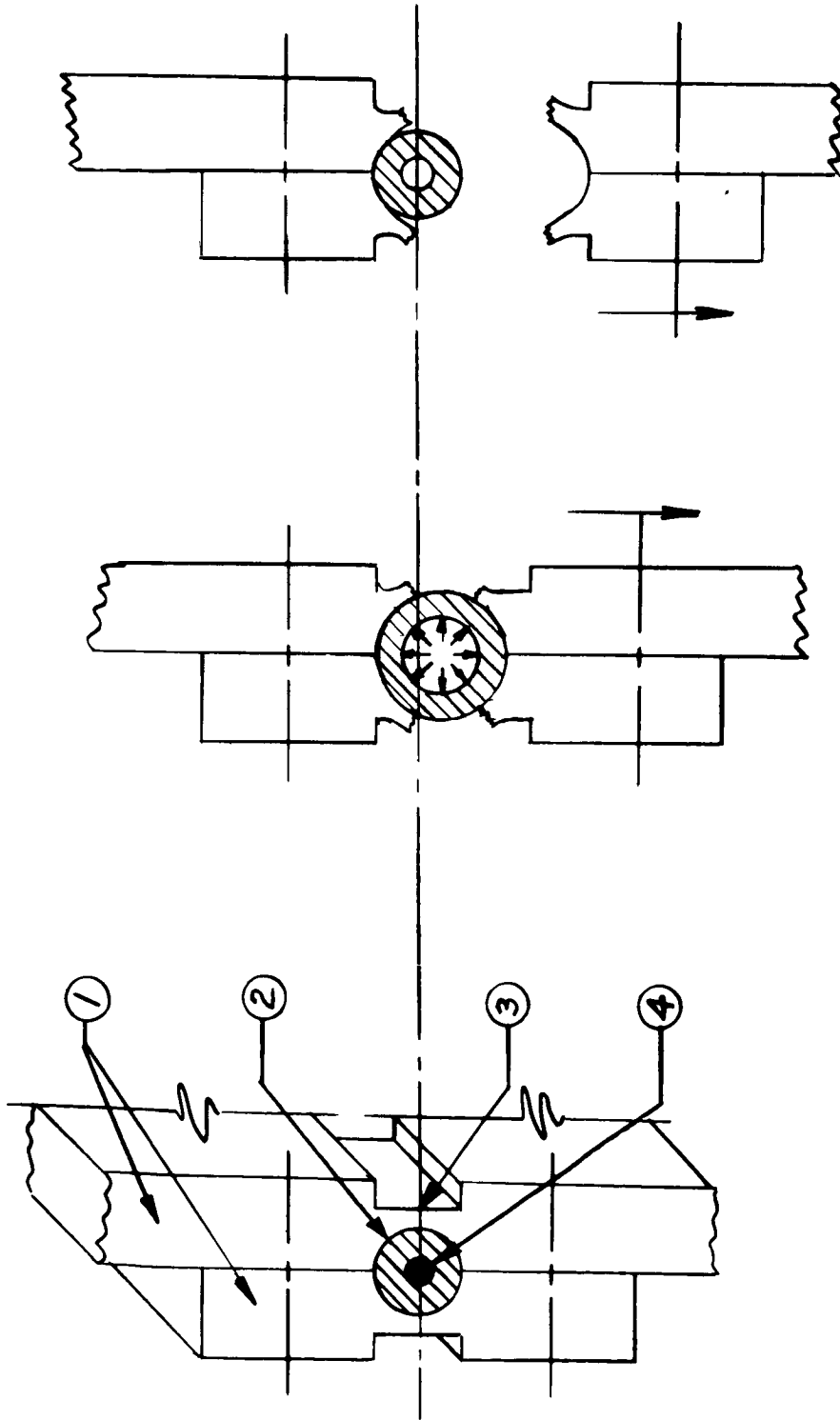
Figure 3-2. Envelope Drawing Standardized Electroexplosive Cartridge Device

The spacecraft Separation Joint, as shown in Figure 3-3, will use a Sealed Explosive Application for Linear Separation (SEALS) that was developed by the Spacecraft Department of the General Electric Company and which employs a mild detonating fuze encapsulated in an elastomer tube jacket. The elastomer tube jacket ruggedizes and protects the explosive core against the detrimental effects of handling, installation, and flight environments. This design concept will part a structural ring between the launch vehicle and the spacecraft circumferentially.

Pneumatic Valves are furnished with the midcourse and retrorocket equipment and are fully described under the Propulsion Subsystem.

Events such as the release of the magnetometer boom and the unlatching of the scan platform will be sensed as having been accomplished by one or more plunger actuated, miniature switches. These switches are constructed almost entirely of non-magnetic materials. Stainless steels of numbers 310 or higher are used in place of the more common, but potentially more magnetic, 302, 303, and 304 stainless steels. The switches are bushing mounted to permit fine adjustment of the height of the switch, and the mounting nuts are safety wired. The switching chambers are evacuated and filled with an inert gas.

The Pyrotechnic Subsystem is completely redundant, including power supply, energy storage, arming device, wiring from the Electric Power Subsystem to the Pyrotechnic Controller, and by dual harness segments downstream of the Pyrotechnic Controller. Two capacitor banks are discharged into the two bridgewires furnished for each event. Failure of either bridgewire or either capacitor bank will not prevent the event from occurring. Either harness segment with its associated electroexplosive device is capable of performing the required functions.



View 1
Before Explosion

View 2
During Explosion

View 3
After Explosion

- (1) Primary Structure to be separated
- (2) Elastomer tube jacket used to seal explosive charge, transmit parting and separating force, and to confine by-products of explosion.
- (3) Structure sculptured to control and provide a preferred separation plane.
- (4) Explosive charge, (linear detonating cord) which on explosion subjects the structure to a parting force transmitted thru the elastomer jacket and traveling in the direction of the detonating wave front.

Figure 3-3. Schematic Diagram - Confined Linear Delineation Cord Separation

4.0 INTERFACE DEFINITION

4.1 COMMAND SIGNALS

All command signals shall be supplied to the Pyrotechnic Controller. The commands are identified as follows:

Number	Phase	Description	Source	Back-up	BW	Actuator	Event
EC 57	1	Deploy Solar Pressure Balance Vane, Antennas (2), and Magnetometer	Pyro-technic Timer	CD	6	3	PP
EC 65	2	Remove Science Covers	C&S	CD	6	3	PP
EC 38	2	Initiate Mono-Propellant pressurization Pyro #1	C&S	CD	2	1	NCV
EC 46	2	Open Mono-Propellant Flow Valve #1	C&S	CD	2	1	NCV
EC 39	2	Initiate Mono-Propellant Isolation Pyro #1	C&S	CD	2	1	NOV
EC 47	2	Close Mono-Propellant Flow Valve #1	C&S	CD	2	1	NOV
EC 40	2	Initiate Mono-Propellant Pressurization Pyro #2	C&S	CD	2	1	NCV
EC 48	2	Open Mono-Propellant Flow Valve #2	C&S	CD	2	1	NCV
EC 41	2	Initiate Mono-Propellant Isolation Pyro #2	C&S	CD	2	1	NOV
EC 49	2	Close Mono-Propellant Flow Valve #2	C&S	CD	2	1	NOV
EC 61	2	Separate Capsule	C&S	CD	12	6	EN
EC 60	2	Initiate Lower Bio-Barrier Electrical Disconnect	C&S	CD	2	1	ED
EC 67	2	Initiate Cold Gas Separation Velocity Increment Pyro	C&S	CD	2	2	NCV
EC 68	2	Jettison Lower Bio-Barrier	C&S	CD	2	2	EN
EC 42	3	Initiate Mono-Propellant Pressurization Pyro #3	C&S	CD	2	1	NCV

VB235FD104

Number	Phase	Source	Back-up	Actu-		Event	
				BW	ator		
EC 50	3	Open Mono-Propellant Flow Valve #3	C&S	CD	2	1	NCV
EC 58	3	Pressurize Bi-Propellant	C&S	CD	2	2	NCV
	3	Start Bi-Propellant Engine	Auto-Pilot	---	4	4	NCV
SC 31	3	Initiate Bi-Propellant Engine Upstream Stop Pyro	Auto-Pilot	C&S	4	2	NOV
EC 54	3	Initiate Bi-Propellant Engine Downstream Stop Pyro	C&S	CD	4	2	NOV
EC 43	3	Initiate Mono-Propellant Isolation Pyro #3	C&S	CD	2	1	NOV
EC 51	3	Close Mono-Propellant Flow Valve #3	C&S	CD	2	1	NOV
EC 56	3	Unlatch Planet Scanner Platform	C&S	CD	2	1	PP
EC 66	3	Jettison Approach Guidance Covers	C&S	CD	4	2	PP
DC 25	*	Initiate Backup Mono-Propellant Regulator Pyro	Prop	CD	2	1	3WV
EC 59	4	Remove Instrument Covers	C&S	CD	6	3	PP
EC 44	4	Initiate Mono-Propellant Pressurization Pyro #4	C&S	CD	2	1	NCV
EC 52	4	Open Mono-Propellant Flow Valve #4	C&S	CD	2	1	NCV
EC 45	4	Initiate Mono-Propellant Isolation Pyro #4	C&S	CD	2	1	NOV
EC 53	4	Close Mono-Propellant Flow Valve #4	C&S	CD	2	1	NOV

ABBREVIATIONS

BW	Bridgewire	EN	Explosive Nut
CD	Command Decoder	NOV	Normally Open Valve
C&S	Controller and Sequencer	NCV	Normally Closed Valve
DC	Discrete Command	SC	Stored Command
EC	Either Command	3WV	Three Way Valve
ED	Electrical Disconnect		

4.2 INPUT POWER

The only Electric Power Subsystem interface is the 2400 cycle per second square wave ac power lines to the safe and arm devices.

4.3 OUTPUT POWER PULSES

Receipt of a command signal causes an output power pulse to appear on the number of bridge-wire electroexplosive device lines shown in the command list.

4.4 THERMAL

Normal thermal dissipation of the Pyrotechnic Controller is two watts continuous. The thermal dissipation of all other components and parts in the Pyrotechnic Subsystem is essentially zero because of the low duty cycle.

4.5 MECHANICAL

The mechanical interface is the Pin Puller, Nut, Plug, or Valve actuated by the electrical pulse initiating the electroexplosive device bridgewire listed in the command list. Vehicle packaging must provide accessibility for inspection of shear pins just prior to fairing installation, and mandatory isolation of the piston from disturbance is necessary during the assembly sequence following inspection.

4.6 TELEMETRY

The Pyrotechnic Controller requires four voltage monitors to determine the condition of the capacitor banks, and an event counter on each capacitor bank capable of advancing its count for each occurrence of the 30 events during the phases indicated in the command list.

4.7 RF INTERFERENCE

The pulse power characteristic of the capacitor discharge may be a noise source.

4.8 UMBILICAL OSE TEST POINTS

The condition of each safe and arm device and the total bridgewire continuity loop is brought out on the umbilical.

4.9 DIRECT ACCESS OSE TEST POINTS

Each of the 90 bridgewire points with a nominally 500,000 ohm resistance is brought out to permit monitoring the power pulse delivered to the squib simulator. Each of four capacitor bank voltages is also monitored, as well as the command power voltage level, and the ac input voltage level.

4.10 LAUNCH VEHICLE

No direct electrical interface with the launch vehicle is necessary, but the launch vehicle is expected to furnish the electrical energy at the proper time to initiate the Separation Joint explosive by energizing the electroexplosive devices. The electrical connections for the Separation Joint are located on the launch vehicle side.

5.0 PERFORMANCE PARAMETERS

5.1 SIMULTANEOUS EVENTS

A maximum of six events can be electroexplosively initiated simultaneously, with a maximum of two bridgewires for each event.

5.2 SEQUENCE

A maximum of two events may constitute a sequence, with no time limit on the time between commands.

5.3 REPETITION RATE

The maximum sequence repetition rate is one per three minutes, with at least a three-minute delay following the initial arming of the Separation Switches.

5.4 SENSITIVITY

A command signal of nominally 15 volts dc is applied simultaneously to resistor and capacitor networks connected gate to cathode of the silicon controlled rectifier switches feeding the desired event. The voltage at this gate capacitor must rise above 0.25 volts before the silicon controlled rectifier can conduct. At worse case, as much as 3.0 volts may be required. The gate voltage must be kept below ten volts. This provides ample delay to insure that the silicon controlled rectifier will not fire on expected noise signals. The Pyrotechnic Controller is designed so it will not respond to a command signal for at least one millisecond after the signal has reached 90 percent of its nominal value. The command signal is provided from a direct current two wire floating system which must be kept isolated from all other circuitry external to the Pyrotechnic Controller.

5.5 ELECTROEXPLOSIVE DEVICE SENSITIVITY

Both bridgewires are capable of withstanding simultaneously one ampere/one watt at 120° F for a period of five minutes without degradation and without firing, but each bridgewire ignites and burns clear within three milliseconds and the actuator completes its function within twenty milliseconds of application of a 3.2 ampere direct current pulse or a 0.10 joule pulse from a capacitor. The one ampere no-fire and the all-fire characteristics have a 0.999 probability of occurrence with a 95 percent confidence level.

5.6 OUTPUT PULSES

Receipt of a command signal causes an output power pulse of 0.2 joules minimum per device to appear within fifty milliseconds at the number of electroexplosive device bridgewires indicated in the command list. The electroexplosive device power leads are capable of transmitting the pulse to arrive at the electroexplosive device with at least the all-fire energy.

5.7 INITIATION TIMER

A single operation unijunction oscillator provides a three minute delay between the arming of the Pyrotechnic Controller and the initiation of the first event to deploy antennas for the RF link.

5.8 BRIDGEWIRE RESISTANCE

The bridgewire resistance is 0.9 ohm minimum to 1.1 ohms maximum. Current limiting resistors are provided in the Pyrotechnic Controller to permit OSE monitoring of energy pulses to simulators and to insure current sharing to simultaneous events.

5.9 RELIABILITY ASSESSMENT OF THE PYROTECHNIC NETWORK

A reliability assessment of the preferred design of the Pyrotechnic Controller circuitry shown in Figure 5-1 indicates a reliability of 0.999 for the complete mission. To assist in the analysis, the complete mission has been divided into four mission phases defined in the Preliminary Voyager 1971 Mission Specification, JPL Project Document No. 45. The four phases are defined as launch, cruise, orbit injection, and Mars orbit.

The mathematical model given below is based on the functional block diagram of Figure 3-1 and the data given in Table 5-1.

$$R_{\text{(Pyrotechnic Controller)}} = \left[1 - \left[1 - R_{\text{(Pyrotechnic Control Circuit)}} \right]^2 \right] \times R_{\text{(Timer)}}$$

Entering the reliability values tabulated in Table 5-1 into the mathematical model gives the estimated reliability of the Pyrotechnic Controller for each mission phase. These estimates are also tabulated in Table 5-1.

The reliability estimate for the Pyrotechnic Controller for the complete mission is:

$$\begin{aligned}
 R_{\text{(Pyrotechnic Controller)}} &= R_{\text{(Phase 1)}} \cdot R_{\text{(Phase 2)}} \cdot R_{\text{(Phase 3)}} \cdot R_{\text{(Phase 4)}} \\
 &= (.9999) (.9999) (.9999) (.9999) \\
 &= .999
 \end{aligned}$$

TABLE 5-1
PYROTECHNIC CONTROLLER RELIABILITY DATA

Mission Phase	Pyrotechnic Control Circuit	TIMER	Complete Pyrotechnic Controller
1	.9999	.9999	.999
2	.9991	Not Req'd.	.999
3	.9996	" "	.999
4	.9996	" "	.999

The proposed Pyrotechnic Controller has been designed to achieve an inherently high level of reliability. The Pyrotechnic Controller circuitry is made completely redundant. The timer circuit is active for one event only and is backed up by a ground command. Thus, the basic techniques of circuit simplicity and redundancy are utilized to obtain a highly reliable design.

6.0 PHYSICAL CHARACTERISTICS AND CONSTRAINTS

6.1 WEIGHT

The weight of the Pyrotechnic Controller is 7.5 pounds. The weight of Pin Pullers, the Separation Joint, and all valves are charged against the respective subsystems requiring the actuation. Each event switch weighs two ounces. The weight of the complete Pyrotechnic Harness is four pounds.

6.2 VOLUME

The volume of the Pyrotechnic Controller is five hundred cubic inches. Each event switch is one half inch in diameter and two inches high.

6.3 POWER CONSUMPTION

The peak power demand on the ac power supply is ten watts decaying to two watts within one minute following each arming or command initiation. The average power drain is two watts over the entire mission.

6.4 ENVIRONMENTAL AND OPERATING CONDITIONS

Environmental conditions are as defined in the following documents:

VB235FD101 Temperature Control Subsystem
VB235FD103 Structural Design Criteria

6.5 SEPARATION JOINT

The design of the Separation Joint insures confinement of all explosive by-products and a controllable shock pulse into the spacecraft structure. Minimum weight of explosive core load is used since the total energy available in the explosive core is directed toward accomplishing the separation function.

7.0 SAFETY CONSIDERATIONS

The requirements of AFMTC 80-2 and ICC regulations must be complied with during all activities of transportation, storage, handling, installation, checkout, and range safety.

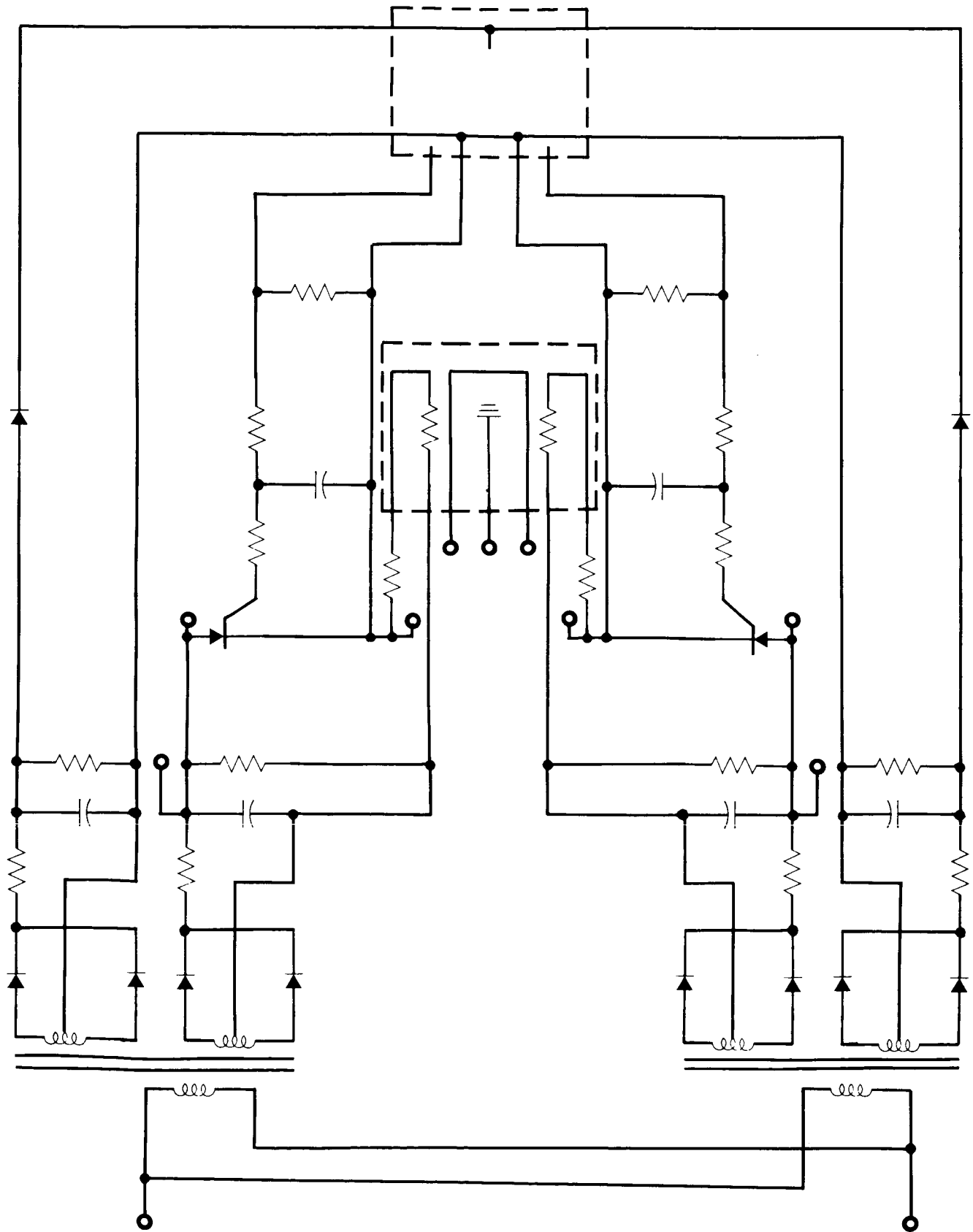


Figure 5-1. Typical Pyrotechnic Switching Circuit

CII- VB235FD105

FUNCTIONAL SPECIFICATION
VOYAGER 71 DETERMINATION OF WEIGHT,
CENTER-OF-GRAVITY, MOMENTS OF INERTIA,
AND PRODUCTS OF INERTIA

Index

- 1 Scope**
- 2 Applicable Documents**
- 3 Functional Description**

1.0 SCOPE

This specification covers the following items:

Functional requirements for design control of rigid-body mass properties of Voyager 71.

General methods for determination of mass properties of each flight article.

2.0 APPLICABLE DOCUMENTS

The following documents form a part of this specification:

SPECIFICATIONS:

General Electric:

VB220SR101	Design Characteristics
VB220SR102	Design Restraints
VB220FD103	Spacecraft Component Design Parameters
VB220FD113	Layout and Configuration, Voyager 71

NASA:

M-DE-8000.006	Mass Properties Standard - reference only
---------------	---

3.0 FUNCTIONAL DESCRIPTION

3.1 GENERAL

Spacecraft weight control during design is essential to the realization and potential up-grading of mission objectives. Accurate knowledge of the actual weight of each flight article is essential to mission operations analysis.

The requirements for spacecraft attitude control, in general, and for guidance and control during maneuvers, in particular, impose design constraints upon center-of-gravity location and upon mass products of inertia in relation to corresponding moments of inertia.

In the launch configuration a knowledge of mass parameters, to an accuracy commensurate with stated requirements, is necessary to an evaluation of dynamic loads within the spacecraft and to dynamic loads imposed on the launch vehicle.

This specification defines the detailed requirements for mass parameter control and determination.

3.2 PRIMARY REQUIREMENTS

3.2.1 WEIGHT

The weight of each Voyager 71 spacecraft shall be determined by components, computationally, empirically, or experimentally during design and fabrication as an adjunct to V Weight Control (Reference VB110VP003 Design and Development Plan, Paragraph 2.3):

- a. Structure and Harness - All structure and harness drawings will be computed utilizing standard calculation procedures. Calculation will be confirmed by actual measurement of piece parts during assembly.
- b. Components - Component weight will be determined empirically and computationally utilizing specifications, drawings and functional descriptions. These weights will be confirmed by actual measurements of the completed unit following assembly.

The final weight of each flight article, complete and after final inspection, shall be determined experimentally to an accuracy of 0.1 percent. An error analysis of the chosen weighing method shall accompany the test results.

The spacecraft weight shall be determined with the propellant and gas tanks empty, and with inert pyrotechnics installed. Propellant loadings will be determined at the launch complex by using a linear, sensitive and stable force sensor, (or load cell) and its associated electronics. The load cell readout is given a resolution of approximately .01 percent of fuel load with an electronics counter. The counter reading would be repeated on digital tape for verification record. The gas weight will be calculated based on temperature and pressure of the gases going into a predetermined volume (by calibration tests) of the pressurant and attitude control tanks. This information will then be analytically assembled to the flight spacecraft dry weight (Reference VB2080FD109 Propellant and Gas Loading Equipment).

3.2.2 CENTER OF GRAVITY DETERMINATIONS

3.2.2.1 Launch Configuration

The spacecraft cg in the launch configuration shall be determined by components computationally during design and fabrication to assure compliance with launch vehicle requirements. Actual centers of gravity will be determined for each subassembly during the actual weight measurements as described in paragraph 3.2.1. These will confirm the computations made during spacecraft design. Actual centers of gravity will be separately determined for the spacecraft and capsule in the launch configuration with propellants and gases removed and inert pyrotechnics installed. Propellant loadings effect on center of gravity will be computed using the procedure in paragraph 3.2.1.

3.2.2.2. Cruise Configurations

Spacecraft Assembly - "C.G. envelopes" defining c.g. migrations as appropriate functions of variable geometrics shall be determined computationally during design and fabrication as an adjunct to c.g. control to assure compliance with guidance and control. Additionally, the c.g. location of each flight spacecraft shall be determined experimentally for each configuration shown by computation to be marginal in terms of the requirements.

CG shifts due to antenna and scan platform deployment will be determined by actual measurement of the spacecraft without antenna and scan platform and analytically adding the actual measurements of the antenna and scan platform in the stowed and deployed positions.

3.2.3 CENTROIDAL MOMENTS OF INERTIA

3.2.3.1 Launch Configuration

Centroidal moments of inertia of each flight spacecraft about axes parallel to the basic reference axes shall be determined computationally during design to the accuracy required for dynamic loads analysis.

3.2.3.2 Cruise Configuration

Centroidal moments of inertia of each flight spacecraft about axes parallel to the basic reference axes shall be determined computationally during design and fabrication to an accuracy of ± 5.0 percent for each basic cruise configuration. Additionally, the centroidal moments of inertia of each flight spacecraft shall be determined experimentally if it is shown by computation to be marginal in terms of the guidance and control requirements. All computations and required measurements will consider deployment of antennas and scientific experiments. All measurements will be made with the propellant tanks empty and pyrotechnics removed. Effect of these items will be computed. Moment of inertia computations will utilize spacecraft component and subsystem actual weight and center of gravity measurements.

3.2.4 CENTROIDAL PRODUCTS OF INERTIA

3.2.4.1 Launch Configuration

Centroidal products of inertia about axes parallel to the basic reference axes shall be determined computationally during design to the accuracy required for dynamic loads analysis.

3.2.4.2 Cruise Configuration

Centroidal products of inertia of each flight spacecraft for each basic cruise configuration shall be determined computationally during design and fabrication. Additionally the centroidal products of inertia shall be determined experimentally if it is shown by computation to be marginal in terms of the guidance and control requirements.

The vehicle centroidal product of inertia will be determined computationally to an accuracy ± 7.0 percent for each basic cruise configuration. Product of inertia computation will utilize spacecraft component and subassembly actual weight and center of gravity measurements.

3.3 SECONDARY REQUIREMENTS

Computational and experimental methods employed in determination of spacecraft cg coordinates, moments of inertia, and products of inertia shall be documented. Additionally, an error analysis shall accompany all test results.

All actual measurements will be performed on standard industry equipment where possible. This equipment will include a three scale measurement fixture for weight and center of gravity determination. A torsional and bifilar pendulum will be utilized for moment and product of inertia measurements unless accuracy requirements of guidance and control dictate a more sophisticated approach.

CH-VB235FD106

ELECTRONIC PACKAGING

Index

- 1 **Scope**
- 2 **Applicable Documents**
- 3 **Functional Description**
- 4 **Performance Parameters**
- 5 **Interfaces**
- 6 **Physical Characteristics and Restraints**
- 7 **Safety**

1.0 SCOPE

This section describes the packaging techniques used in the assembly of the electronic equipment in the Flight spacecraft.

2.0 APPLICABLE DOCUMENTS

2.1 GOVERNMENT

MIL-STD-275A	Printed Wiring for Electronic Equipment
MIL-C-26482	Connectors, Electric, Circular Miniature Quick Disconnect
MIL-W-16878	Wire, Electrical, Insulated, High Temperature
MIL-S-7742	Screw Threads, Standard Aeronautical

2.2 GENERAL ELECTRIC

S-30000	MSD Design Requirements for Electronic Modules
S-30023	Cross Wire Resistance Welding Process
S-30100	MSD Design Requirements for the Soldering of Electrical Connections
VB220SR101	Design Characteristics
VB220SR102	Design Restraints
VB220FD113	Layout & Configuration

3.0 FUNCTIONAL DESCRIPTION

3.1 GENERAL

The principal restraints governing the packaging design are 1) a lightweight, flexible and compact configuration for the spacecraft electronic equipment; 2) mounting and inter-connection for electronic parts so that they will perform reliably and efficiently during launch and long-time exposure to space environment, and 3) use of standardization to the greatest possible extent, to allow parallel development of electronics and vehicle structure.

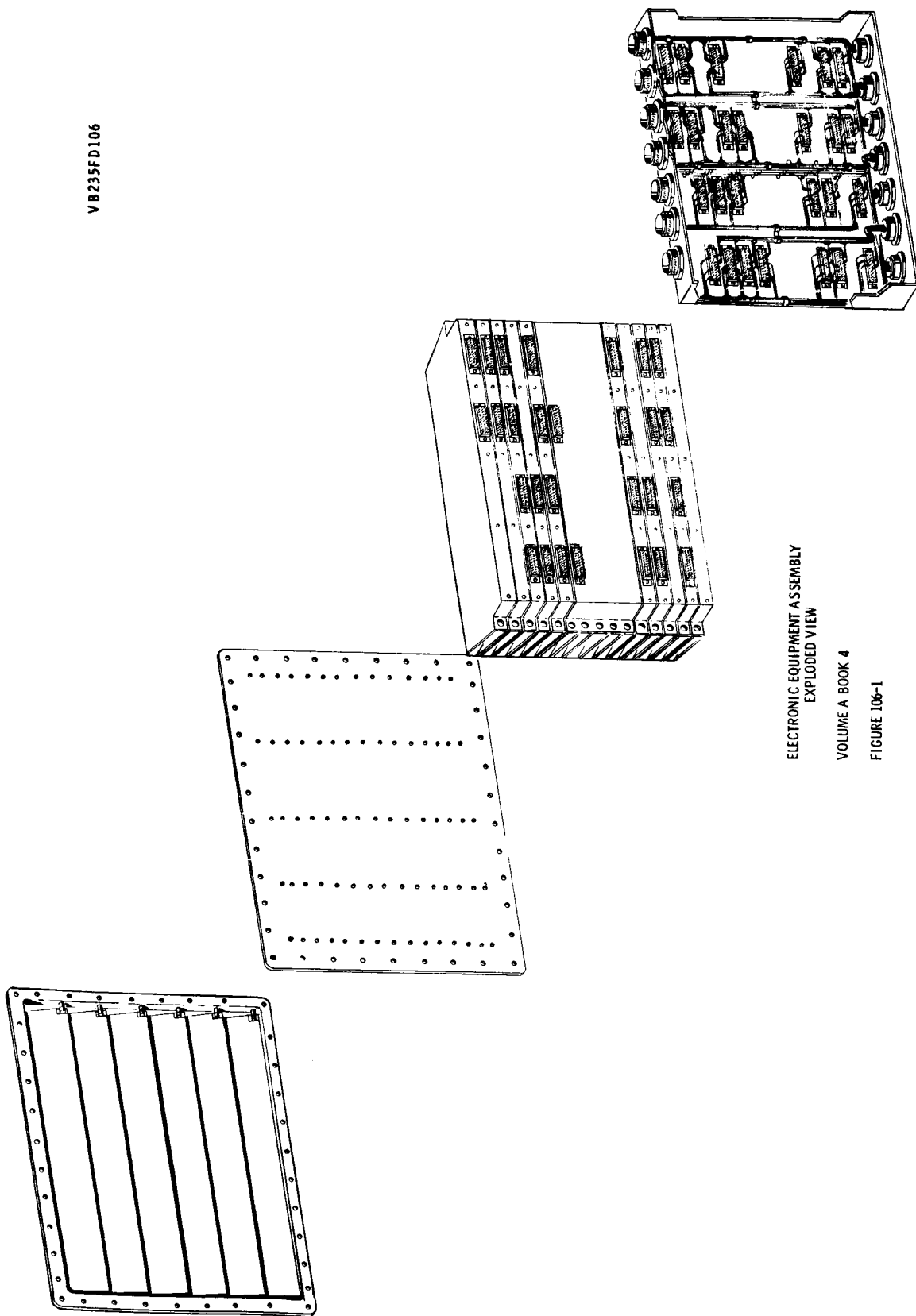
The concept of structural integration, used on Ranger and Mariner has been actively pursued and adapted to the needs of the Voyager Spacecraft.

3.2 DESCRIPTION

The spacecraft electronic equipment is packaged in the 12 bays of the Spacecraft Bus, in modular assemblies of standard size and shape (See Figure 3-1). When assembled, these integrated packages give rigid support to the electronic components, stabilize the equipment module structure against dynamic and static loads, and provide conductive heat paths from the dissipating parts to the thermal radiating surface.

VB235FD106

VB235FD106



ELECTRONIC EQUIPMENT ASSEMBLY
EXPLODED VIEW
VOLUME A BOOK 4
FIGURE 106-1

Figure 3-1 Electronic Equipment Assembly-Exploded View

A preferred, standard approach is specified with the provision that non-standard solutions to accommodate special problems may be used with proper approvals. The standard design involves three levels of interconnections, as defined below:

- Level I - A functional grouping of parts interconnected and encapsulated to form a module.
- Level II - A subassembly of parts and modules in a machined housing of standard profile.
- Level III - An assembly of subchassis and plates mounted to, and made integral with, the vehicle structure.

3.2.1 ASSEMBLY

The assembly package consists of up to 15 level II subassemblies sandwiched between two plates as shown in Figure 3-2. The inner plate, in the form of a shallow tray, provides a mounting base for the subassemblies as well as a supporting structure for the assembly harness and connectors. This harness tray is a magnesium structure, 20 by 20 by 3.5 inches, which provides locations for 60 float mounted subassembly connectors and 14 system connectors. The upper seven locations have been designated for test harness connections, and the lower seven reserved for mating with the spacecraft ring harness. In total, provision is made for 854 connections into and out of each standard assembly; and 3000 pins can be made available for subassembly interwiring.

The outer plate, stabilized by the subassembly chassis, is the shear panel of the equipment module structure. It also acts as a radiating surface for heat rejection to space. See Figure 3-3.

3.2.2 SUBASSEMBLY

The electronic subchassis is of standard profile. Two dimensional standards are specified; 10.0 by 6.0 by 1.25 inches and 20.0 by 6.0 by 1.25 inches. The 10-inch subassemblies are used in pairs, locked and bolted together to satisfy the structural requirements. An offset web of 0.062-inch section, rib stiffened, is included, pre-drilled with a 0.100 staggered grid hole pattern. See Figure 3-4. The subchassis is a machined housing of HM21A-T8 magnesium, suitably finished for chemical compatibility and thermal control. The housing contains integral bathtub fittings at each end for mounting into the vehicle longerons. Non-magnetic attachments are used to mount the subchassis to the harness tray and shear panel. They are located in a standard pattern on each side of the housing. These attachments are spaced on 2.9 inch centers to provide the required stabilization to the shear panel.

Each 20-inch subchassis has four standard mounting locations for 50 pin, Cannon Golden D connectors. A 10-inch subchassis has 2 connector locations. Electrical continuity from the subassembly circuitry to the assembly harness is accomplished by a connector module. See Figure 3-5. The connector modules contain guide pins for alignment with the mating

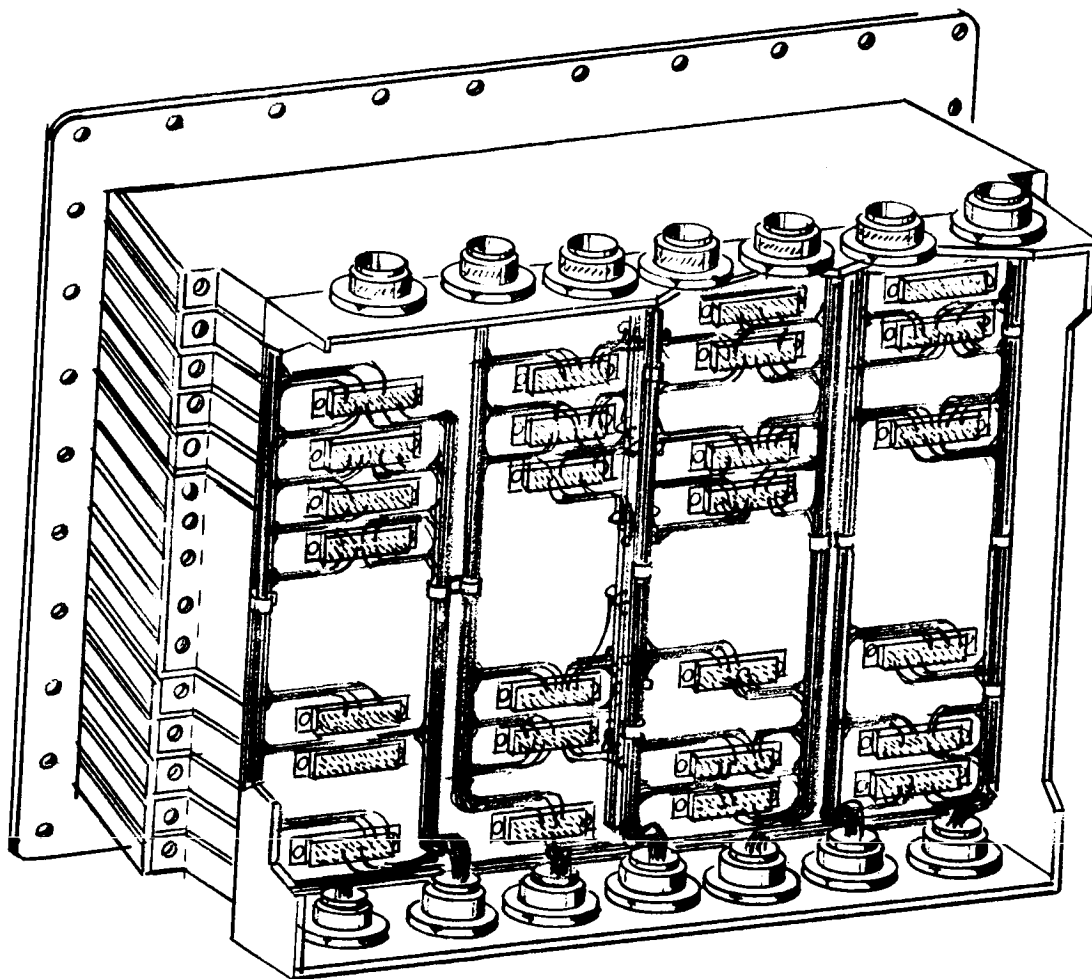


Figure 3-2 Electronic Equipment Assembly

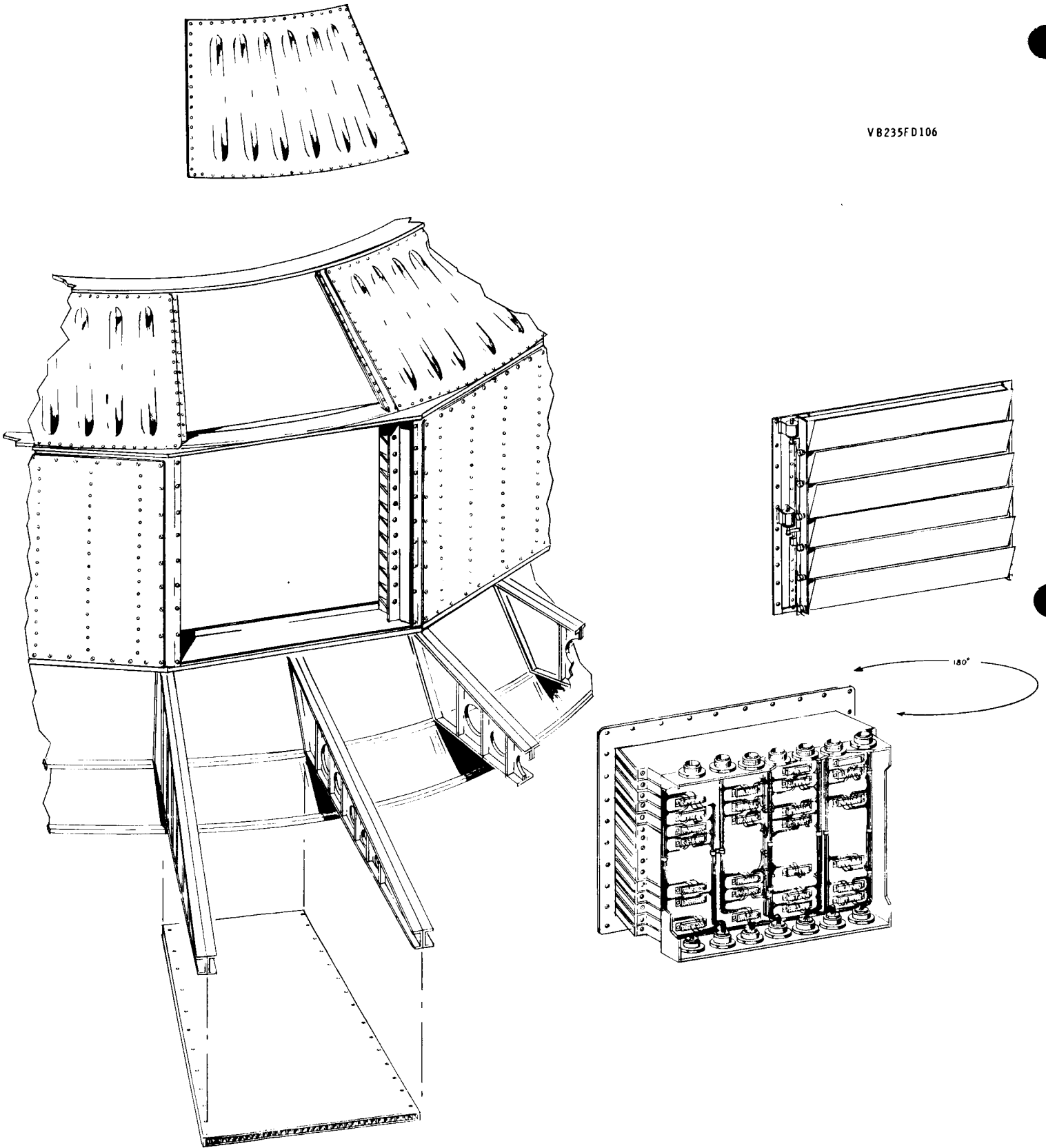


Figure 3-3. Installation of Electronic Equipment Assembly

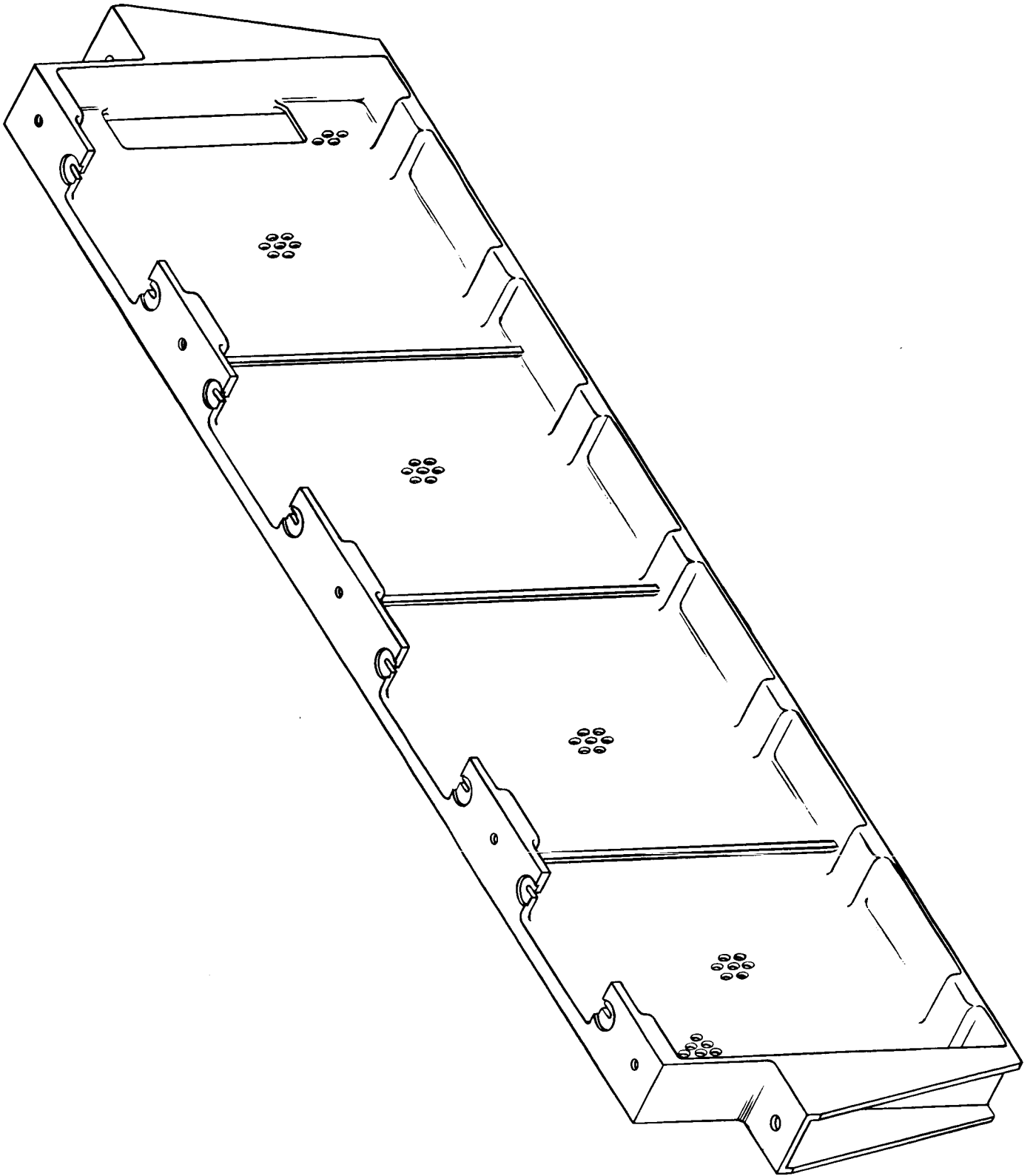


Figure 3-4 Electronic Subchassis

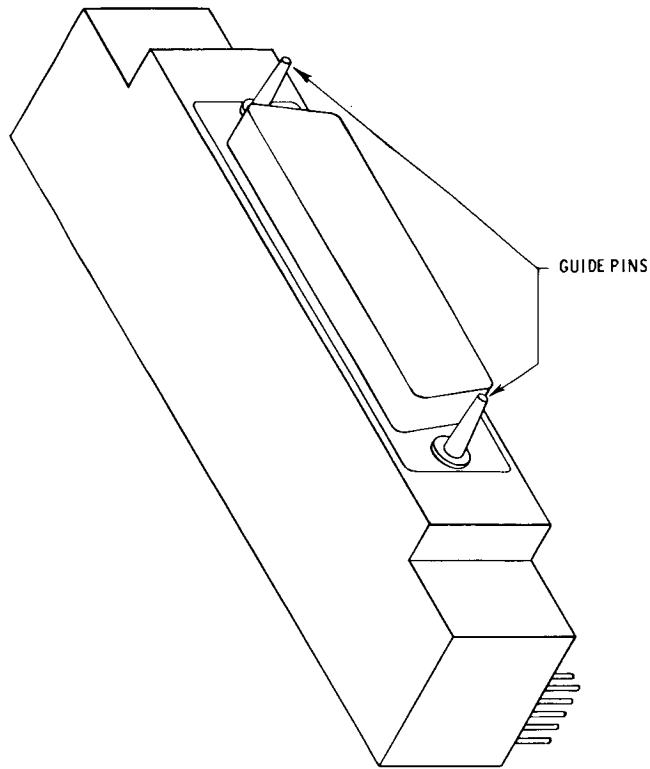


Figure 3-5 Connector Module

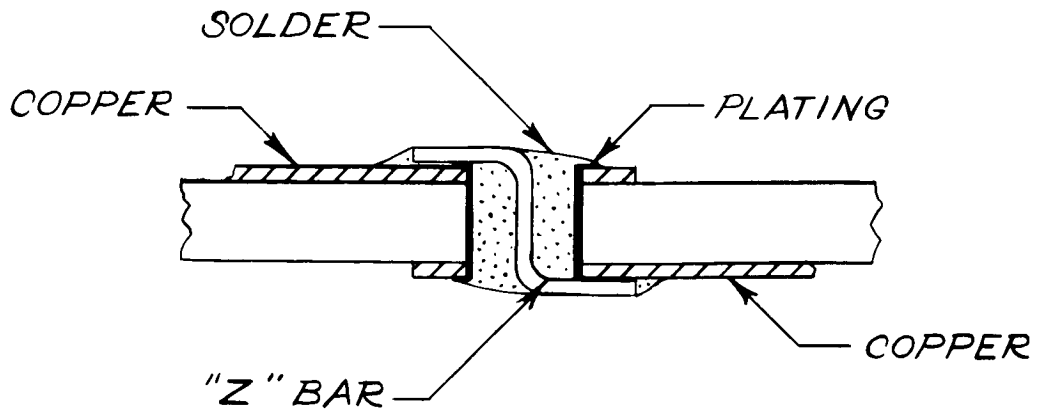


Figure 3-6 Printed Wiring Through Connection

connectors which are float mounted in the assembly harness tray. This technique provides for straight, in-line engagement and disengagement of connectors to reduce the possibility of bending connector pins.

Interconnection of modules in the subassemblies is accomplished by a double sided printed wiring board. The connection between the two circuit patterns is effected by a plated-through hole and a "Z" bar connection. See Figure 3-6. Indexing of the subassemblies is accomplished by varying the orientation of the "D" shape of the Cannon connector 180 degrees. Since there are four connector locations on each subchassis, there are 16 possible keyed positions.

3.2.3 MODULES

Discreet part circuits are packaged into encapsulated cordwood modules consistent with circuit performance requirements. The module dimensions are standardized to assure maximum utilization of the given subchassis area without sacrificing flexibility. In conformity with the principle of minimizing techniques and materials, the design and fabrication of the cordwood modules will be in accordance with GE specification S-30002, or approved alternative. The encapsulated design provides protection against shock and vibration environments and adequate thermal conductivity to insure component operating temperature within acceptable limits. Buffer coatings are specified to guarantee compatibility of the encapsulating compound with fragile parts.

The packaging of microelectronics is limited to the use of planar construction, using parallel gap welding on double sided printed wiring boards; or 3-Dimensional construction of flat packages in special welded modules. See Figure 3-7.

4.0 PERFORMANCE PARAMETERS

4.1 DYNAMIC RESPONSE

The electronic subassemblies, housed in a rib stiffened machined chassis and assembled as shown in Figure 4-1 are designed for a composite response of 400 cps or higher.

4.2 THERMAL PERFORMANCE

The longest conductive thermal path from a dissipating part to the radiating panel is six inches. Series thermal joints are limited to three: part to module encapsulating material; module to subassembly web; and subassembly to radiating panel.

In the event of temperature control shutter failure, thermal contact maintained between the subassembly and the harness assembly tray, provides a secondary heat rejection path by radiation exchange within the spacecraft.

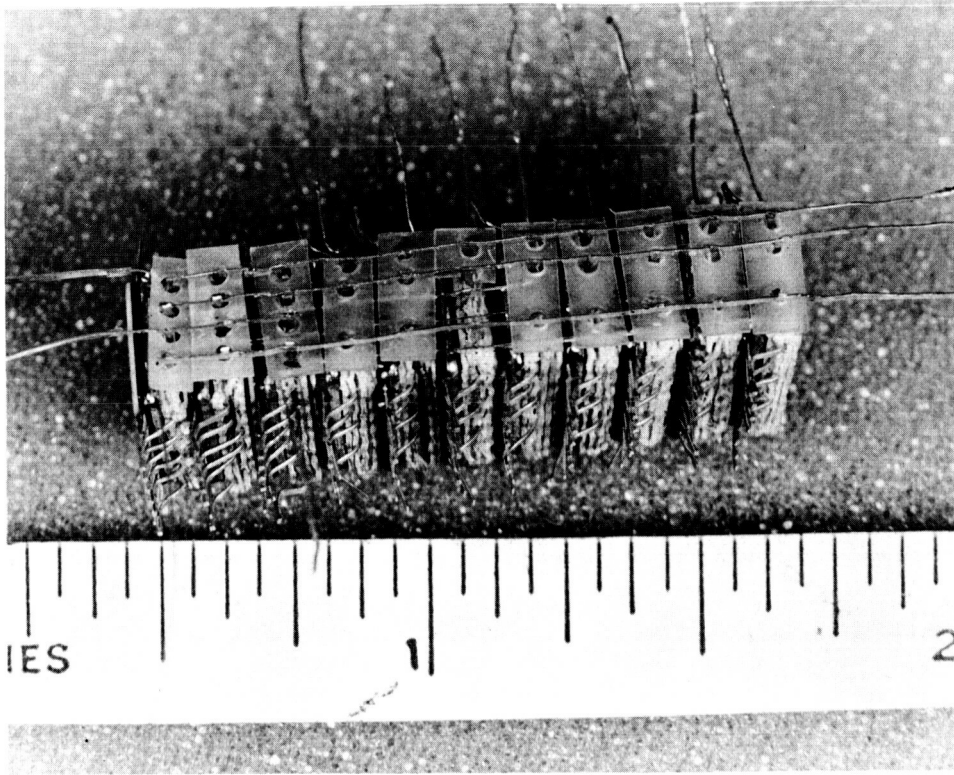


Figure 3-7. Microelectronic Module

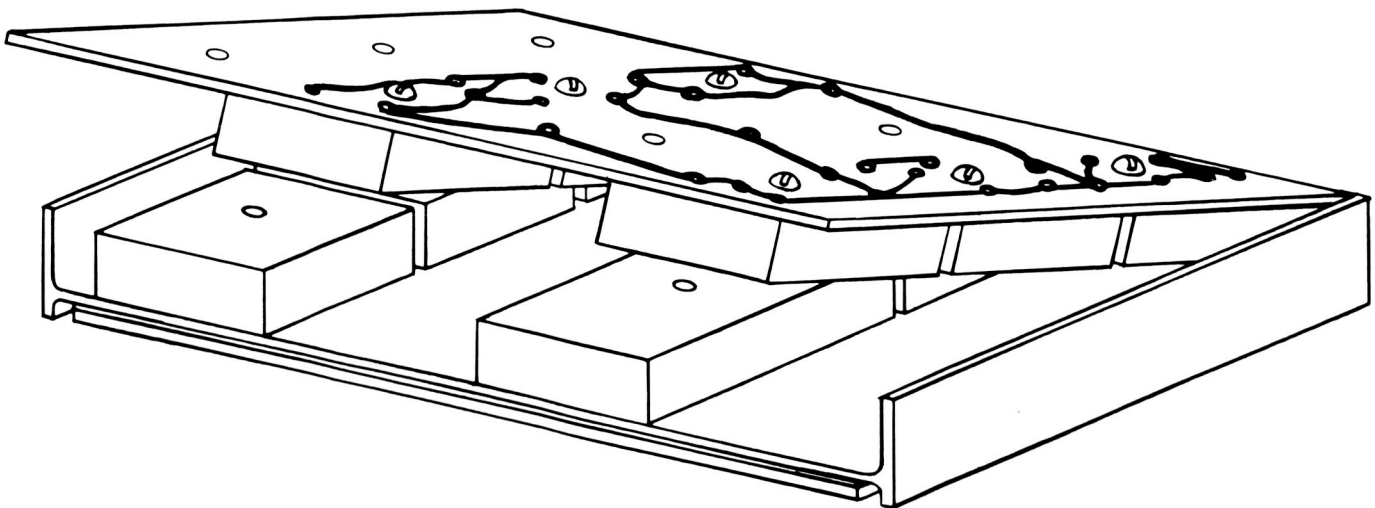


Figure 4-1. Electronic Subassembly Sandwich Construction

4.3 ENVIRONMENTAL PROTECTION

Encapsulated construction and conformal coating is used to assure protection of the parts against handling, dirt, humidity and corrosive atmospheres.

4.4 MAINTAINABILITY

The modular packaging design facilitates repair and revision of electronic assemblies. It is possible to replace any subassembly without mechanically or electrically disturbing any other subassembly.

5.0 INTERFACES

5.1 MECHANICAL

The electronic mounting assembly, consisting of the subassemblies mounted to the harness tray, (See Figure 3-3) is attached to the vehicle structural longerons by means of bolts passed through integral bathtub fittings on the individual subassemblies. After the mounting assembly is in place, the thermal control shear panel is bolted to the subassemblies and the spacecraft structure, completing the load and thermal paths to the spacecraft frame. The outer panel need not be attached until after the system checkout is complete. This facilitates removal and replacement of assemblies as required during testing.

5.2 ELECTRICAL

The electronic assemblies are joined to the system harness through a series of system interface connectors, located at upper and lower ends of the harness tray. Each assembly is provided with 7 upper and 7 lower positions, in which system or test connectors may be mounted. After the assembly is mounted to the spacecraft, the system (lower) connectors are mated by means of flexible pigtails in the vehicle ring harness. Mismatching is prevented by the use of indexed connectors. Pigtails from an external test harness are mated to the test (upper) connectors through access panels in the lander support cone.

5.3 EMI

In the event of electrostatic interference problems, shielding is applied at the subassembly level, in the form of RF-tight covers. Back panel wiring geometry is designed to minimize interference and pickup. (See VB235FD107, Electrical Harnessing)

5.4 MAGNETIC CLEANLINESS

Considerations of magnetic cleanliness are extended down to the module level through specification of non-magnetic part lead materials, interconnections and hardware. Deviations from this requirement will be allowed only if it can be shown that the substitution of paramagnetic materials is necessary to assure proper performance and/or reliability of the unit.

6.0 PHYSICAL CHARACTERISTICS AND RESTRAINTS

A level III assembly occupies 2.2 cubic feet and may contain from 40 to 80 pounds of electronic equipment. A drawing of a typical assembly is shown in Figure 3-1. It is comprised of three sections, as shown, a) the thermal control/shear panel, b) a group of electronic subassemblies and c) the harness subassembly.

When the subassembly chasses are bolted to the harness tray, a mounting assembly is formed which can be transported, tested and assembled into the vehicle as a unit.

In order that the electronic assemblies act efficiently in stabilizing the equipment module structure, it is necessary that the level II chassis span the 20 inch width between longerons.

In applications where a subchassis width of less than the 20-inch is desired, two 10-inch subassemblies are bolted and locked together to form a 20-inch overall dimension so that the structural integrity of the assembly is maintained. (See Figure 6-1)

It is necessary for prevention of shear buckling in the thermal control/shear plate that the level II chassis be attached at a bolt spacing of 2.9 inches thus requiring that no more than a single 1.25-inch space be left vacant between any two subassemblies. Where electronic equipment does not fill a panel to this extent, structural stiffeners are substituted for the chasses.

To accommodate bulky, non-standard components such as transformers, filter chokes and capacitors, gyros, tape recorders and radio equipment, the standard profile subchassis is allowed to vary in integral multiples of its unit thickness maintaining standard connector and mounting insert locations. High thermal dissipating parts or modules are located near the edge of the subassembly that is adjacent to the temperature control/shear plate. Thermal loading of subassemblies is controlled to insure that part operating temperatures are within the limits for which they have been qualified.

Subassemblies are functional and testable units of the subsystem. The sandwich design of the subassemblies provides adequate stiffness to insure that components, modules and printed wiring boards are not damaged from deflections caused by shock and vibration.

All connections between the outgoing module terminals and the printed wiring board is done only on the exposed side of the board to allow visual verification of the connections. The module terminal clearance hole through the web is provided with annular insulation in the form of an injection molded insert.

Subassemblies containing repetitive circuits requiring more than two layers of interconnections are packaged in a sandwich configuration. See Figure 4-1. Two double sided printed wiring boards are used to obtain four layers of wiring. Encapsulated cordwood modules are assembled between a top wiring board and the offset web. Alternate rows of modules are reversed to mate into their respective wiring boards. Titanium fasteners are used to seat all modules firmly against the web for maximum heat transfer and to secure the printed wiring boards. Interconnections between the boards is accomplished by flat cables, soldered

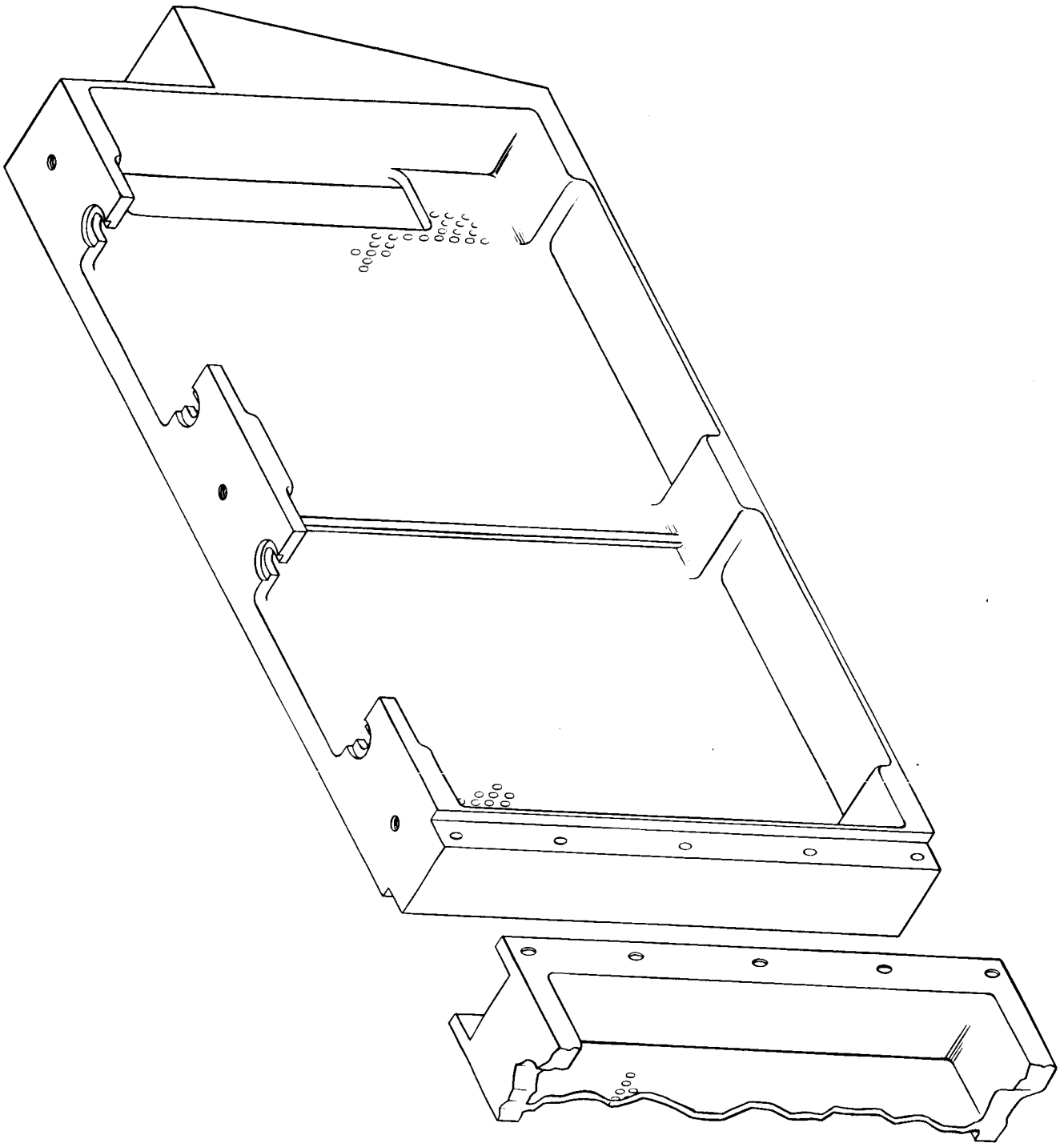


Figure 6-1. Ten-Inch Subchassis Lock Design

to terminals, electrically and mechanically secured to the boards. A photograph of a typical working subassembly built to the above criteria is shown in Figure 6-2. Subassemblies containing large variations in part sizes, or requiring part value changes for tuning and adjustment, are packaged in a flat layout. Those circuits which are not part of the tuning and adjustment are packaged in cordwood modules. The tuning and/or select-at-test parts are mounted to the printed wiring boards, through a cutout in the web, with their leads wired to terminals mounted on the boards. See Figure 6-3. In the event that any of these parts have high thermal dissipations, they will be mounted on the web with their leads wired to insulated terminals passing through the web and into the printed wiring board.

7.0 SAFETY

Handling - A set of special fixtures will be provided for assistance in handling and positioning the electronic assemblies, as their weight (40 to 80 pounds) exceeds allowable limits for safe manual handling by an individual.

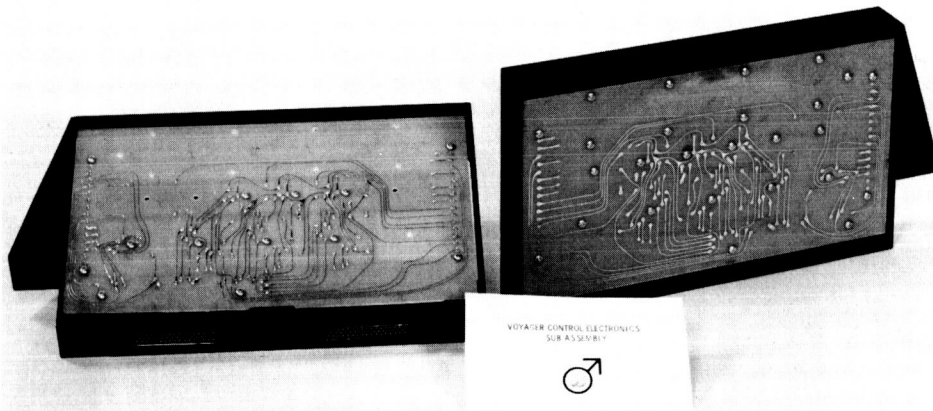


Figure 6-2. Attitude Control Component in Standard Subassembly

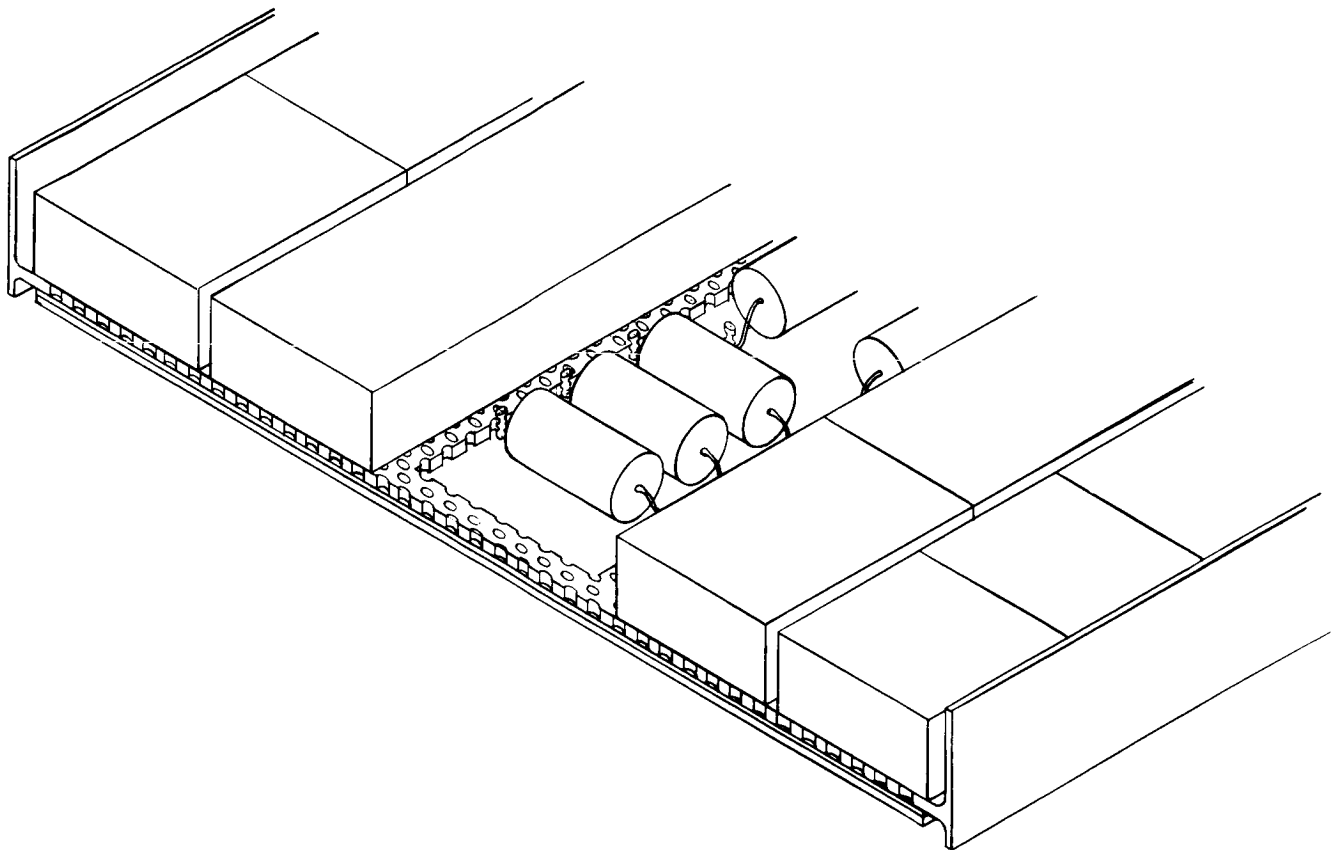
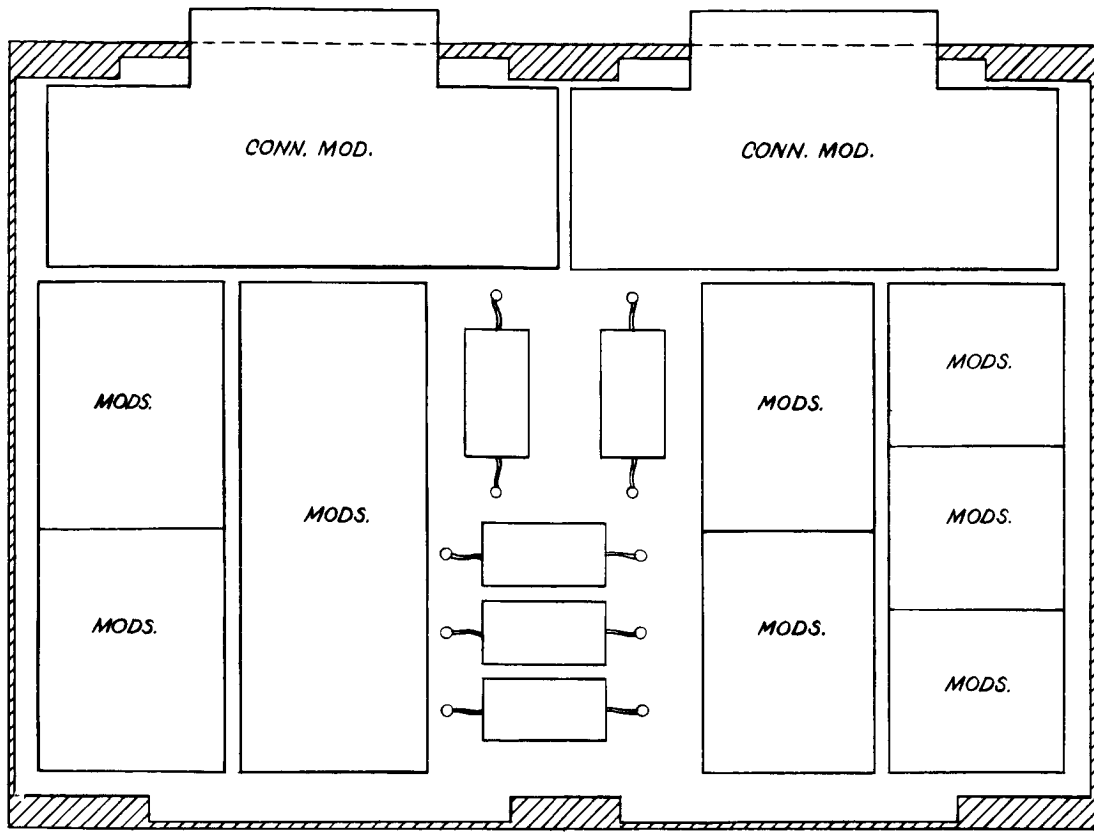


Figure 6-3. Standard Subassembly with Board Mounted Parts

APPENDIX

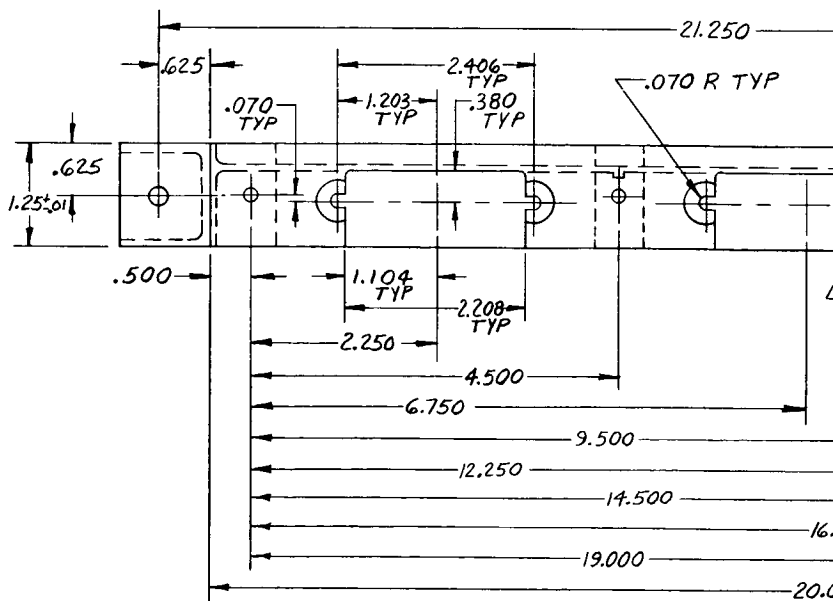
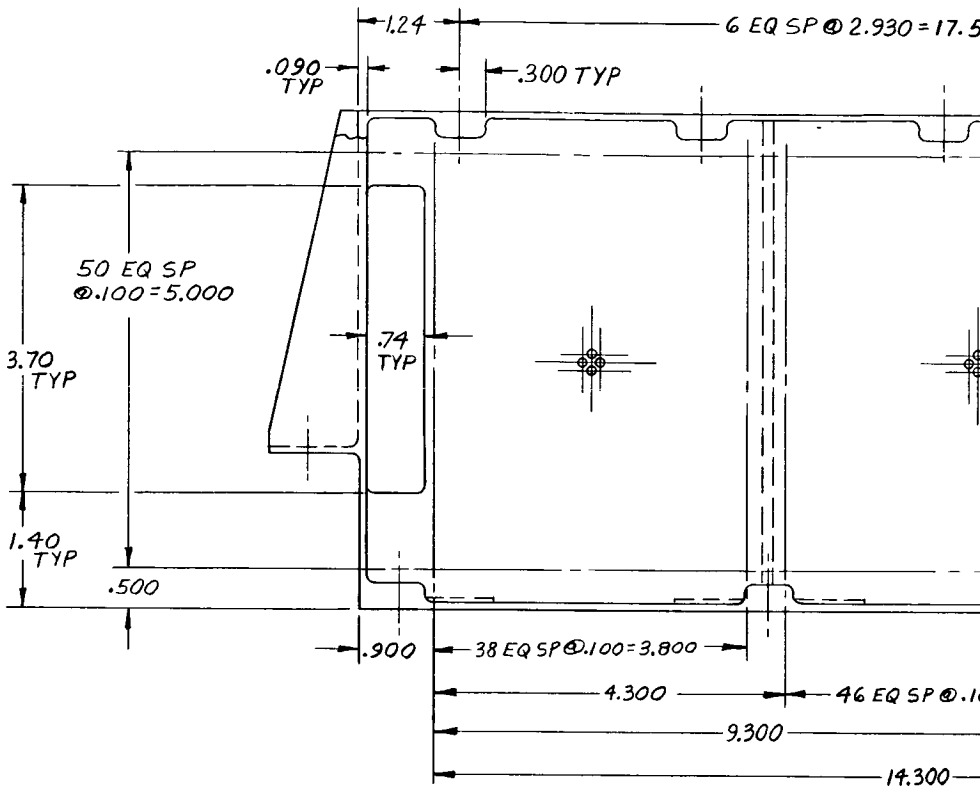
The drawings reproduced below are representative of the details required to implement the standard packaging design described in VB235FD106.

Drawings

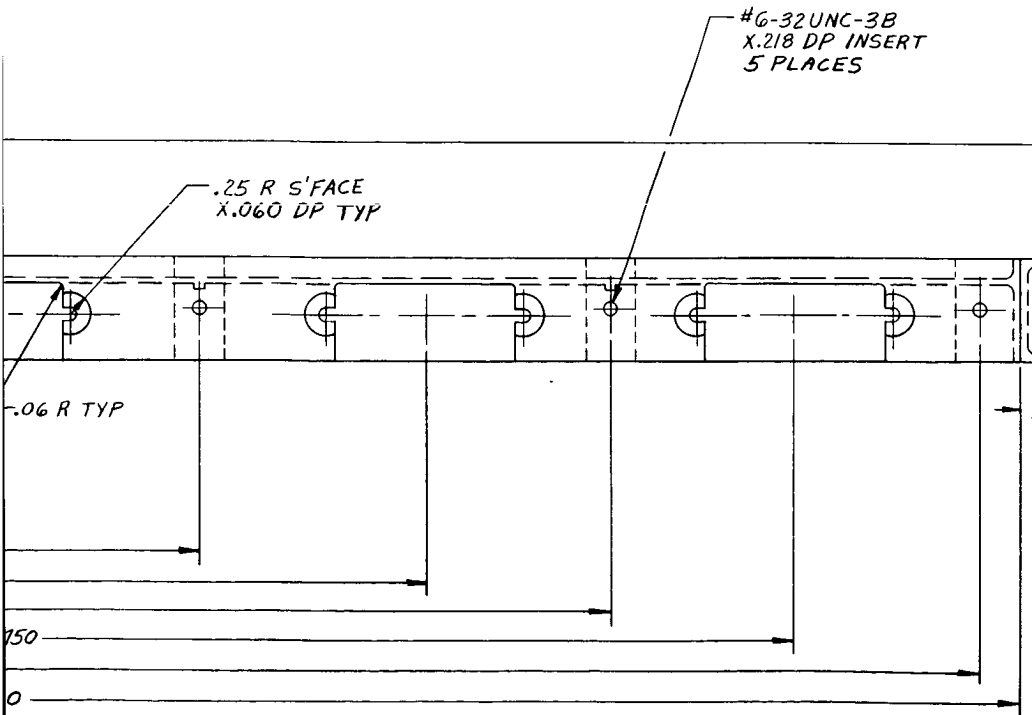
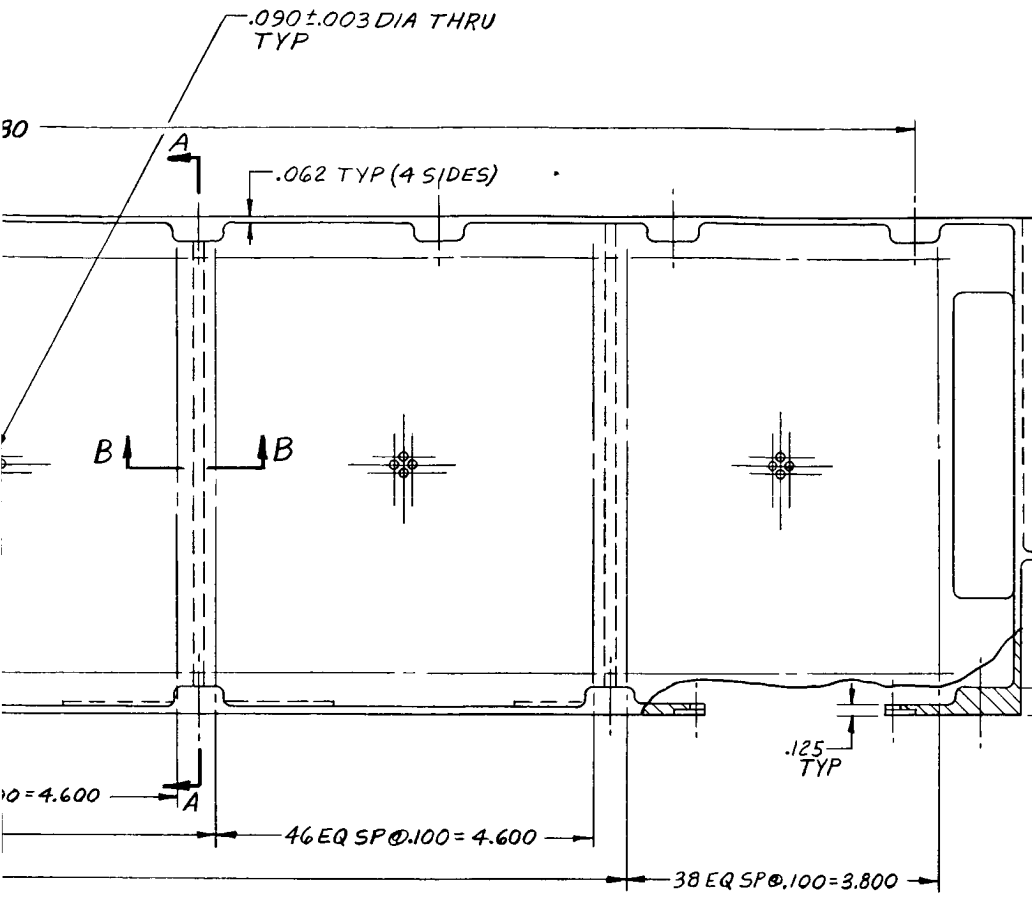
- I SK56152-436 - 20" X 1.25" Subchassis, Four Connector
- II SK56152-434 - 20" X 1.09" Subchassis, Four Connector
- III SK56152-562 - 10" Subchassis, Interlocking
- IV SK56152-437 - Harness Tray
- V SK56152-553 - Temperature Control/Shear Panel
- VI SK56152-551 - Stiffener, Bracket
- VII SK56152-564 - Level III Assembly

Photos

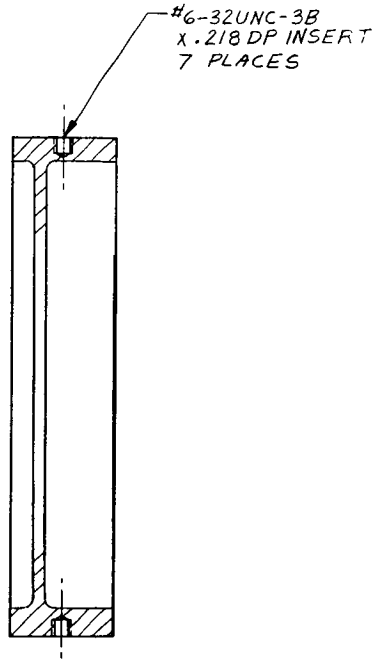
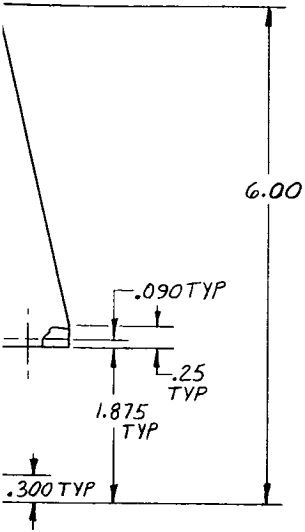
- VIII 10" Subchassis
- IX Hybrid Cordwood Module - Instrumented
- X Hybrid Cordwood Module Incorporating Microelectronics
- XI 10" Subassembly - Sandwich Construction
- XII 10" Subassemblies - Interlocked Design



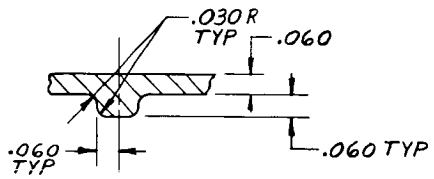
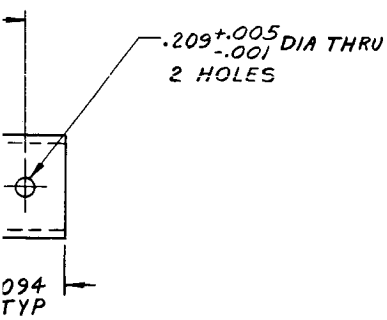
40



4 (2)



SECTION A-A

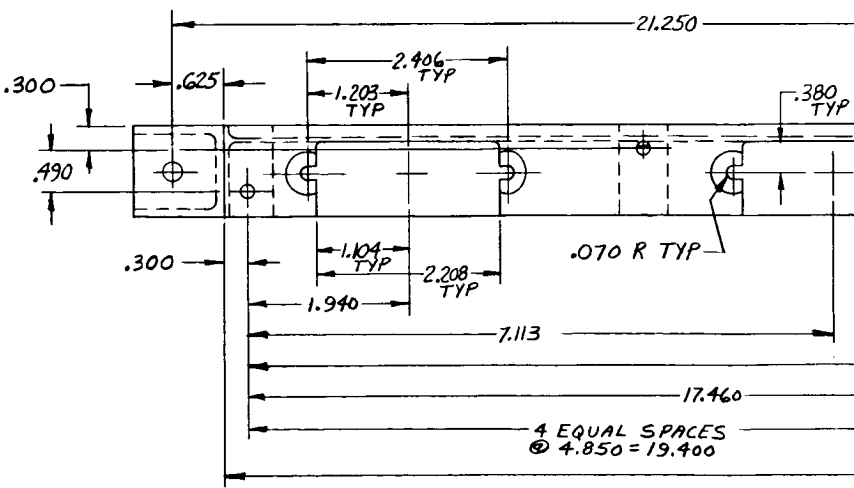
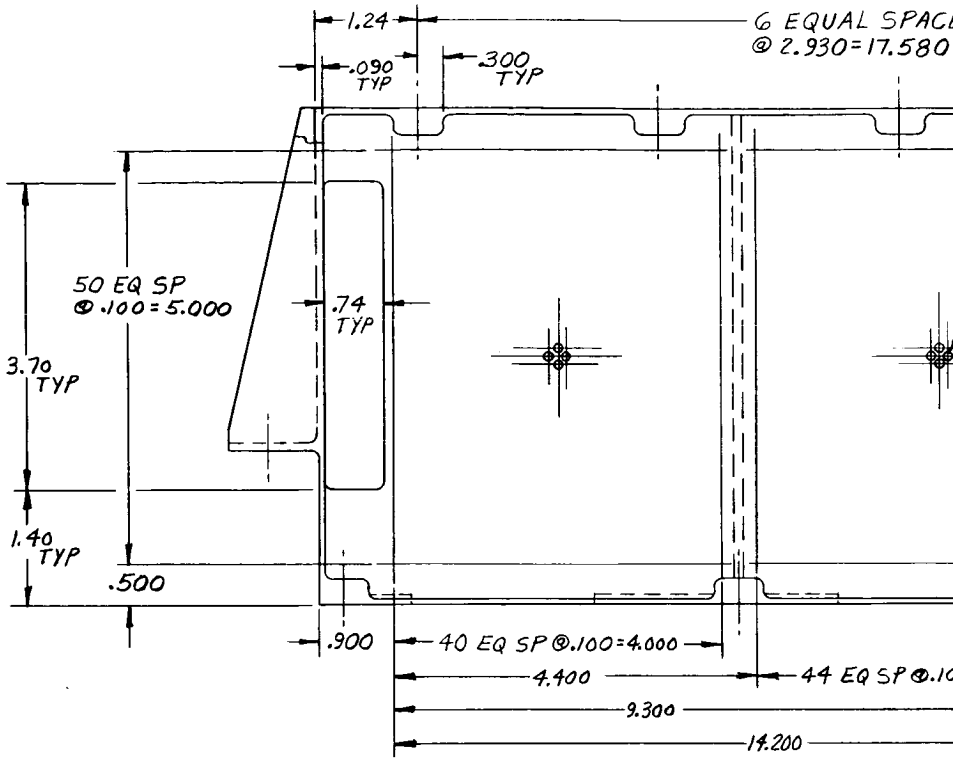


SECTION B-B
 TYP 3 PLACES
 SCALE: 4/1

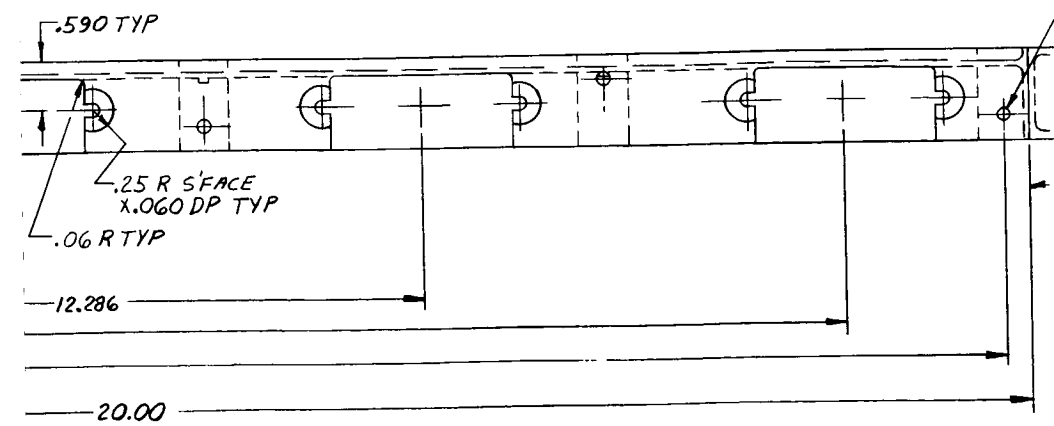
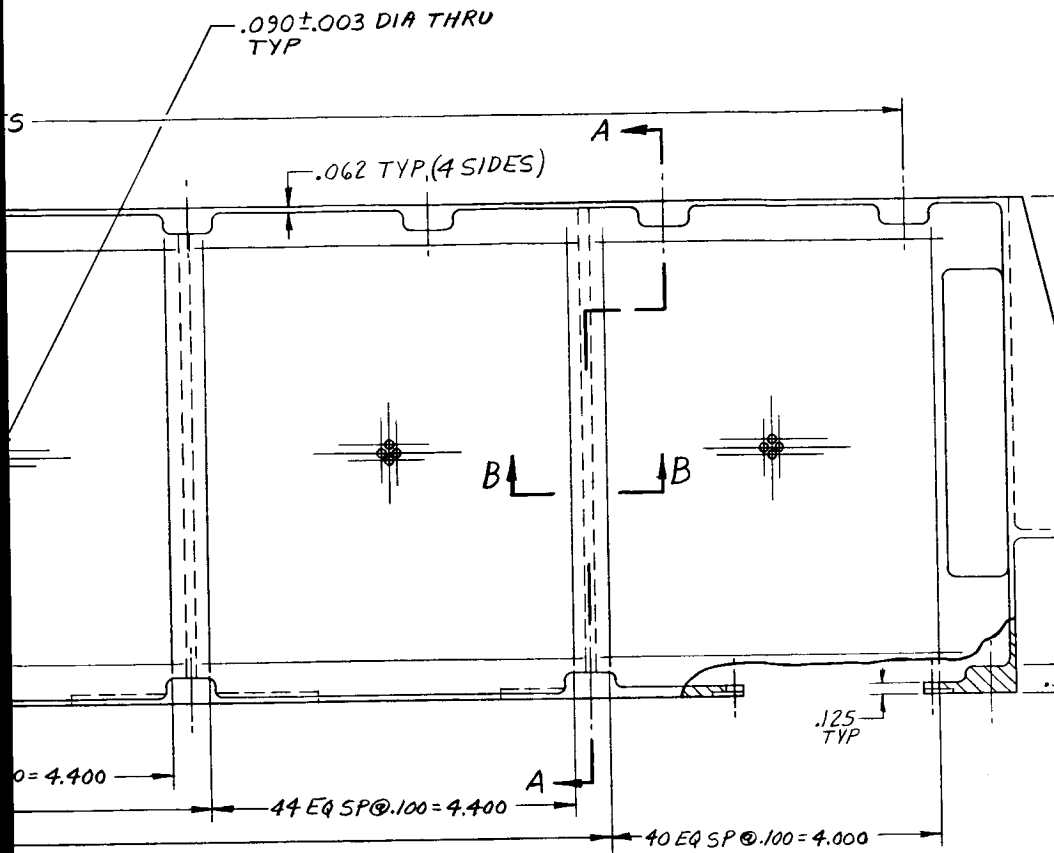
NOTE:

ALL RADII .09 ± .03 UNLESS NOTED
 TOL: 3 PLACE DEC. ± .005
 2 " " ± .02

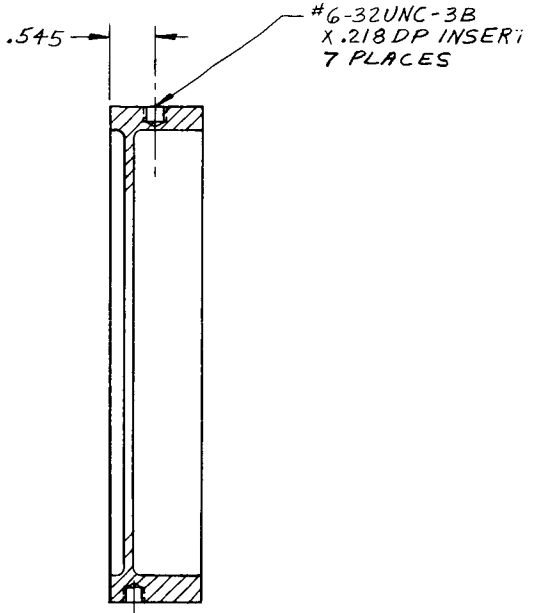
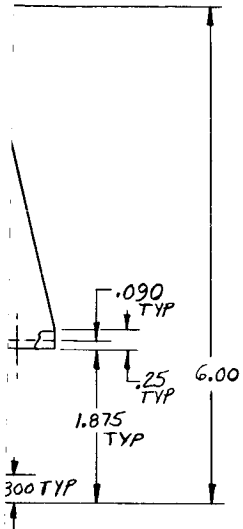
Figure I. SK56152-436 - 20" X 1.25"
 Subchassis, Four Connector



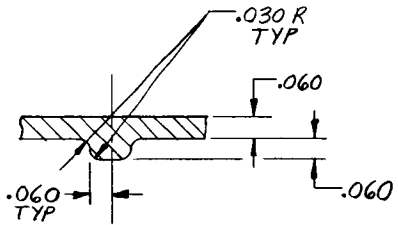
60



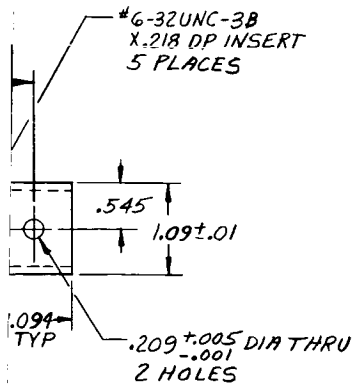
62



SECTION A-A



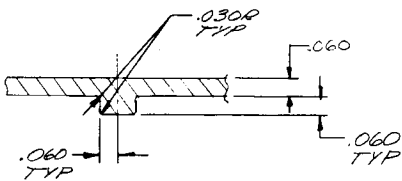
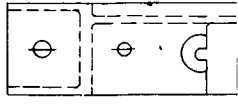
SECTION B-B
SCALE: 4/1
TYP 3 PLACES



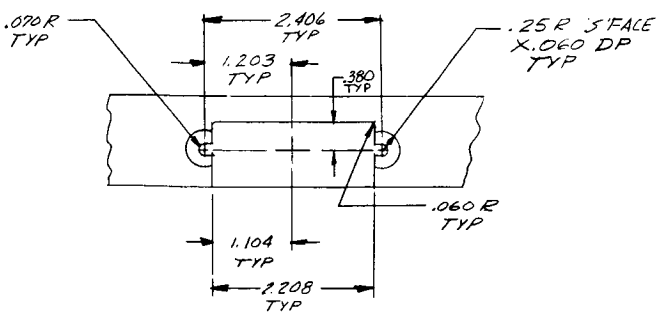
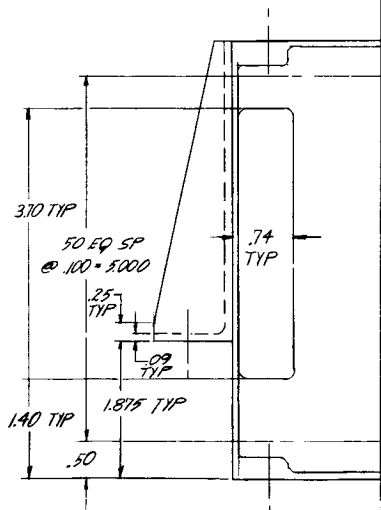
NOTE:
ALL RADII .09 ± .03 UNLESS NOTED
TOL: 3 PLACE DEC. ± .005
2 " " ± .02

Figure II. SK56152-434 - 20" X 1.09"
Subchassis, Four Connector

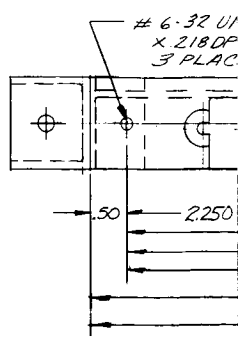
①



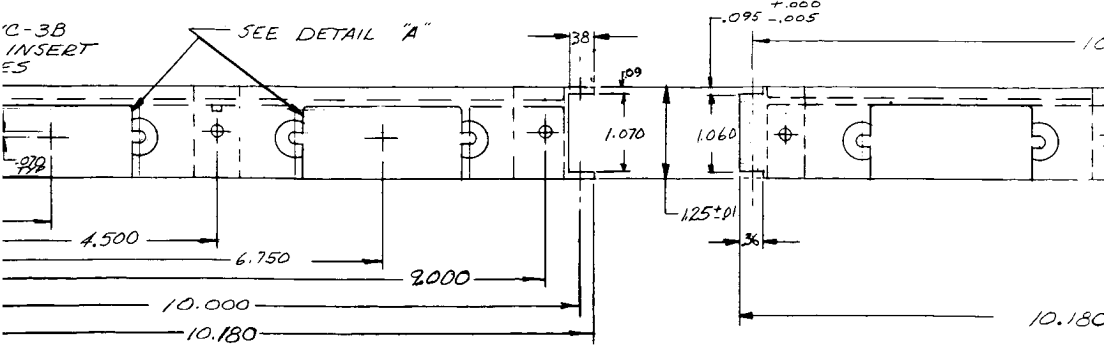
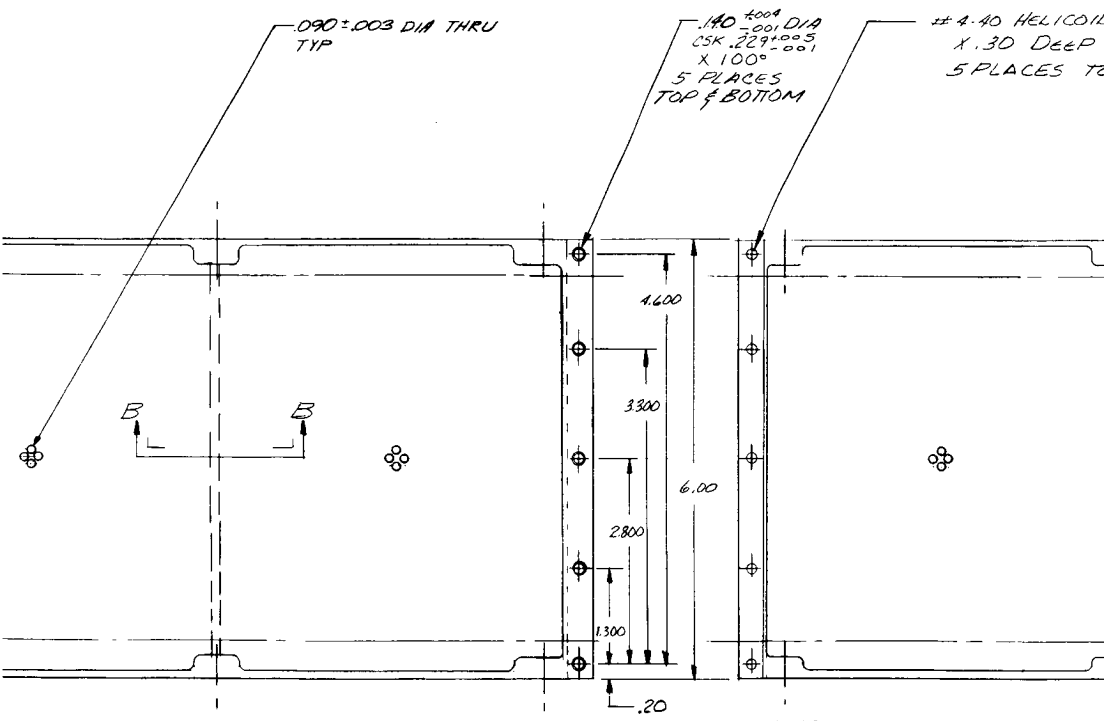
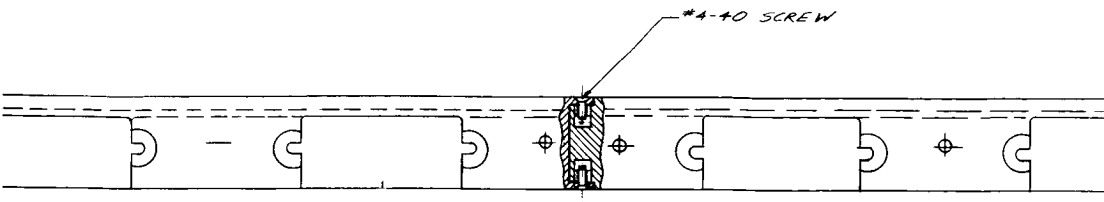
SECTION B-B
NO SCALE



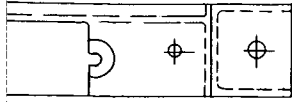
DETAIL "A"



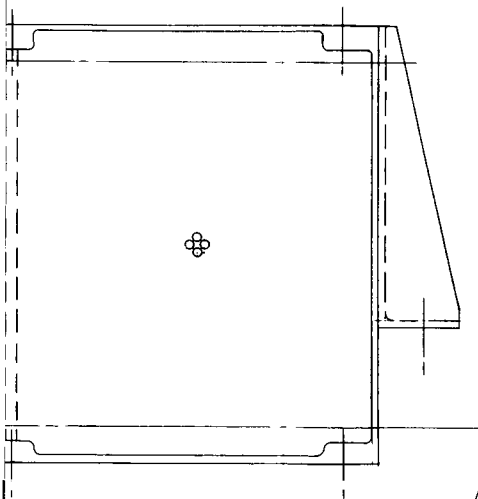
80



82

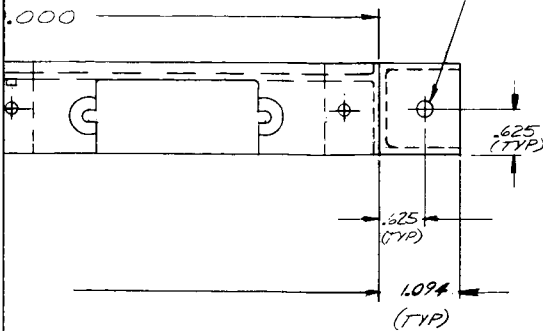


REF BOTTOM



NOTES

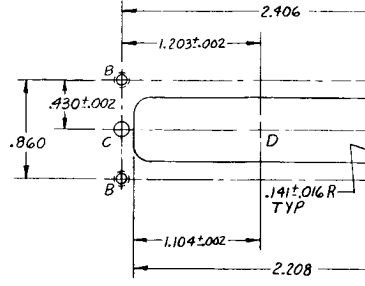
- 1 ALL RADII $.09 \pm .03$
UNLESS OTHERWISE SPECIFIED.
- 2 TOL ARE $.XX \pm .01$
 $.XXX \pm .005$
UNLESS OTHERWISE SPECIFIED



VOYAGER

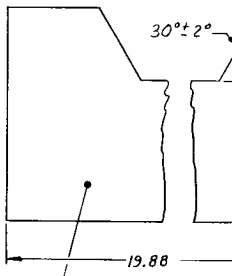
Figure III. SK56152-562 -
10" Subchassis, Interlocking

HOLE NO.	DIM. X	DIM. Y	HOLE CODE	CENTERLINE OF CONN.	DIM. X	DIM. Y	HOLE CODE
1	0,000	0,000	A	A	2,250	-0,070	D
2	4,500	0,000	A	B	6,750	-0,070	D
3	9,500	0,000	A	C	12,250	-0,070	D
4	14,500	0,000	A	D	16,750	-0,070	D
5	19,000	0,000	A	E	2,250	1,230	D
6	0,000	1,300	A	F	6,750	1,230	D
7	4,500	1,300	A	G	12,250	1,230	D
8	9,500	1,300	A	H	16,750	1,230	D
9	14,500	1,300	A	J	2,250	2,530	D
10	19,000	1,300	A	K	6,750	2,530	D
11	0,000	2,600	A	L	12,250	2,530	D
12	4,500	2,600	A	M	16,750	2,530	D
13	9,500	2,600	A	N	2,250	3,830	D
14	14,500	2,600	A	P	6,750	3,830	D
15	19,000	2,600	A	R	12,250	3,830	D
16	0,000	3,900	A	S	16,750	3,830	D
17	4,500	3,900	A	T	2,250	5,130	D
18	9,500	3,900	A	U	6,750	5,130	D
19	14,500	3,900	A	V	12,250	5,130	D
20	19,000	3,900	A	W	16,750	5,130	D
21	0,000	5,200	A	Y	2,250	6,430	D
22	4,000	5,200	A	Z	6,750	6,430	D
23	9,500	5,200	A	AA	12,250	6,430	D
24	14,500	5,200	A	AB	16,750	6,430	D
25	19,000	5,200	A	AC	2,250	7,730	D
26	0,000	6,500	A	AD	6,750	7,730	D
27	4,500	6,500	A	AE	12,250	7,730	D
28	9,500	6,500	A	AF	16,750	7,730	D
29	14,500	6,500	A	AG	2,250	9,030	D
30	19,000	6,500	A	AH	6,750	9,030	D
31	0,000	7,800	A	AJ	12,250	9,030	D
32	4,500	7,800	A	AK	16,750	9,030	D
33	9,500	7,800	A	AL	2,250	10,330	D
34	14,500	7,800	A	AM	6,750	10,330	D
35	19,000	7,800	A	AN	12,250	10,330	D
36	0,000	9,100	A	AP	16,750	10,330	D
37	4,500	9,100	A	AR	2,250	11,630	D
38	9,500	9,100	A	AS	6,750	11,630	D
39	14,500	9,100	A	AT	12,250	11,630	D
40	19,000	9,100	A	AU	16,750	11,630	D
41	0,000	10,400	A	AV	2,250	12,930	D
42	4,500	10,400	A	AW	6,750	12,930	D
43	9,500	10,400	A	AY	12,250	12,930	D
44	14,500	10,400	A	AZ	16,750	12,930	D
45	19,000	10,400	A	BA	2,250	14,230	D
46	0,000	11,700	A	BB	6,750	14,230	D
47	4,500	11,700	A	BC	12,250	14,230	D
48	9,500	11,700	A	BD	16,750	14,230	D
49	14,500	11,700	A	BE	2,250	15,530	D
50	19,000	11,700	A	BF	6,750	15,530	D
51	0,000	13,000	A	BG	12,250	15,530	D
52	4,500	13,000	A	BH	16,750	15,530	D
53	9,500	13,000	A	BJ	2,250	16,830	D
54	14,500	13,000	A	BK	6,750	16,830	D
55	19,000	13,000	A	BL	12,250	16,830	D
56	0,000	14,300	A	BM	16,750	16,830	D
57	4,500	14,300	A	BN	2,250	18,130	D
58	9,500	14,300	A	BP	6,750	18,130	D
59	14,500	14,300	A	BR	12,250	18,130	D
60	19,000	14,300	A	BS	16,750	18,130	D
61	0,000	15,600	A				
62	4,500	15,600	A				
63	9,500	15,600	A				
64	14,500	15,600	A				
65	19,000	15,600	A				
66	0,000	16,900	A				
67	4,500	16,900	A				
68	9,500	16,900	A				
69	14,500	16,900	A				
70	19,000	16,900	A				
71	0,000	18,200	A				
72	4,500	18,200	A				
73	9,500	18,200	A				
74	14,500	18,200	A				
75	19,000	18,200	A				



DETAIL E
SCALE: 2/1

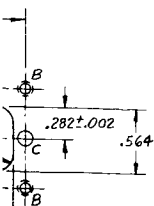
HOLE CHART	
HOLE CODE	SIZE
A	.169±.005 DIA THRU -.001
B	CSK .284±.005 DIA X -.001
C	#2-56UNC-3B THRU
D	.128±.005 DIA THRU -.001
D	SEE DETAIL E



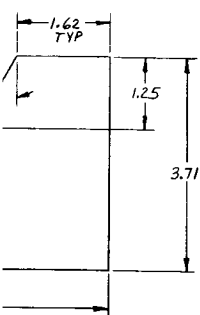
SIDE PLATE;.062
TYP 2 PLACES

DETAIL G
ROTATED APPROX.

10 0

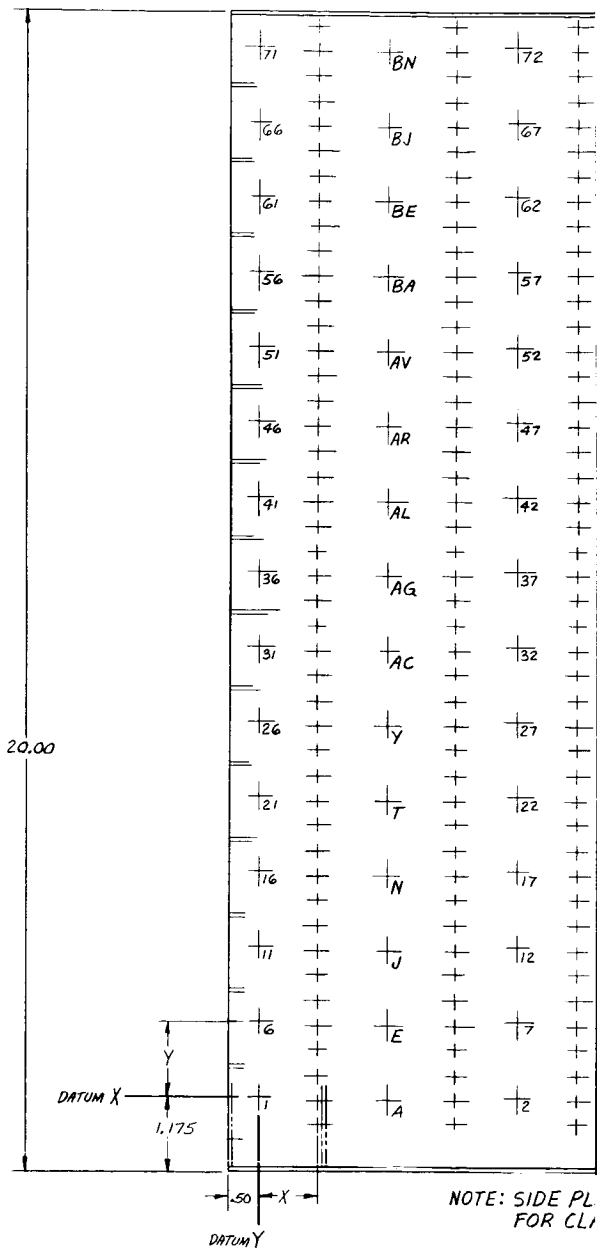


	QTY
20°	75
	240
	120
	60

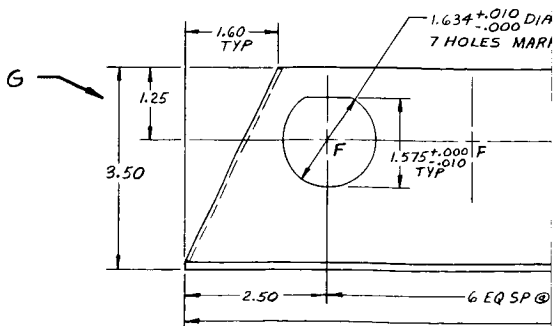


STOCK

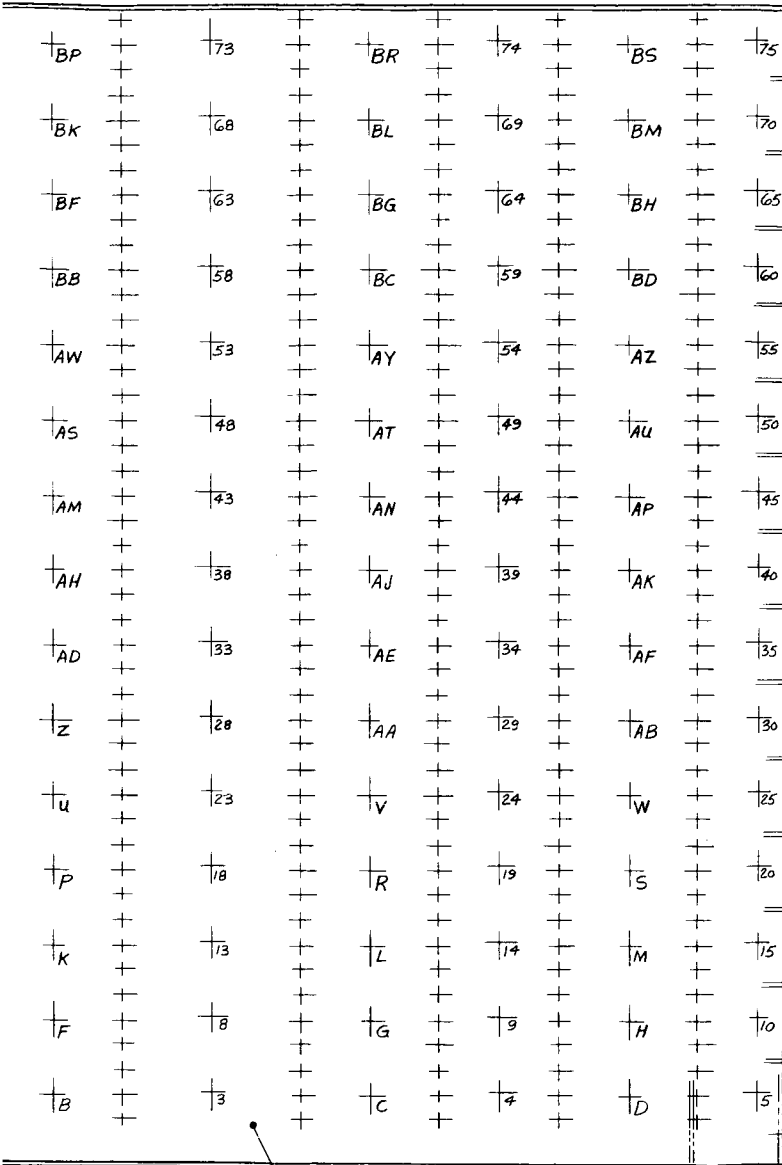
26°



NOTE: SIDE PL FOR CL



102



DATE OMITTED
 VARIETY THIS VIEW

BASE PLATE; .125 STOCK

NOTE:
 TOL: 2 PLACE DEC. ±.02
 3 " " ±.005

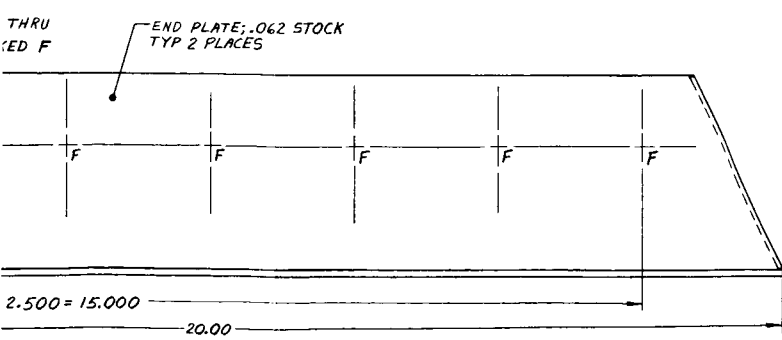


Figure IV. SK56152-437 -
 Harness Tray

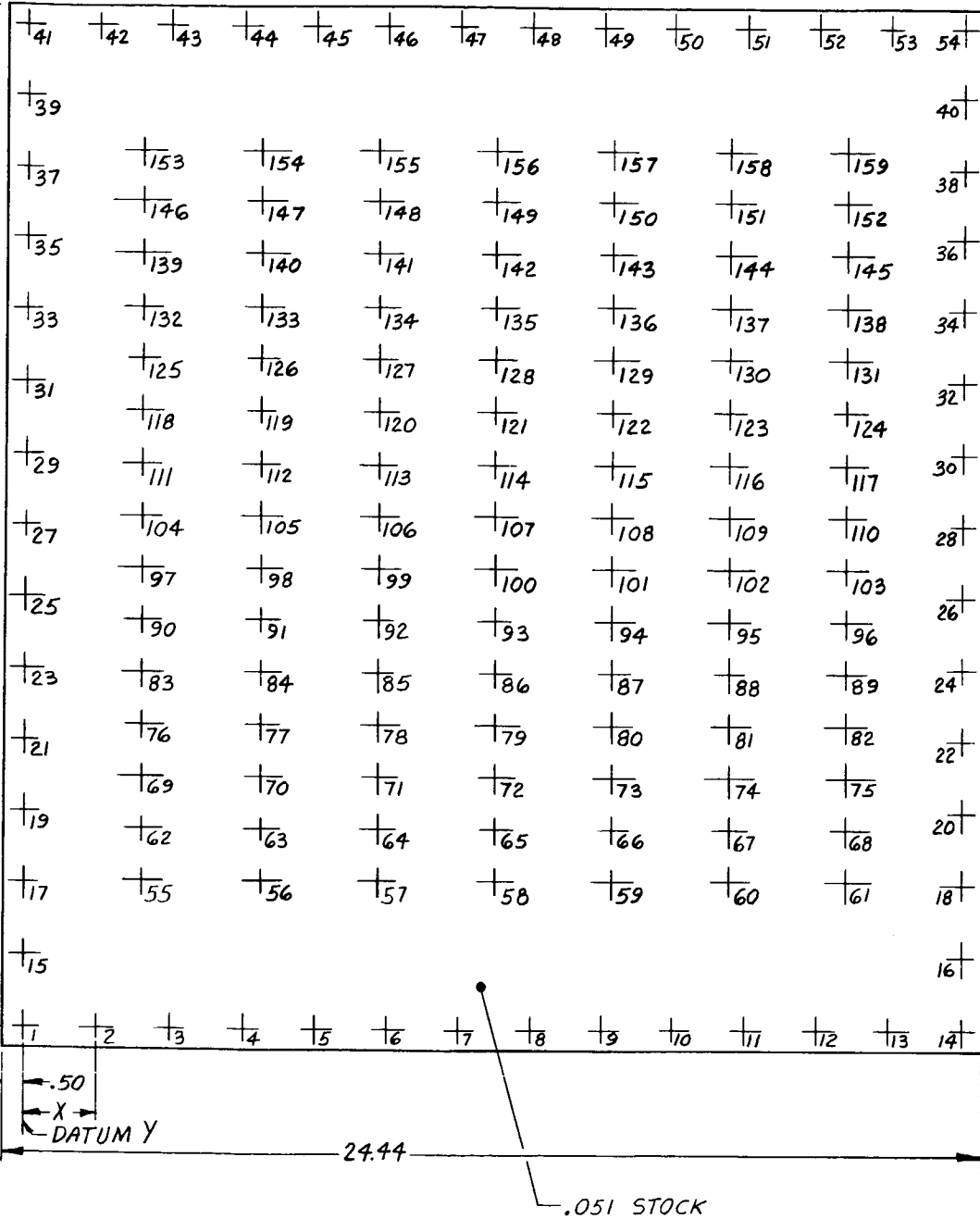
3

HOLE NO.	DIM. X	DIM. Y	HOLE CODE	HOLE NO.	DIM. X	DIM. Y	HOLE CODE
1	0.000	0.000	A	81	17.580	7.575	B
2	1.803	0.000	A	82	20.510	7.575	B
3	3.606	0.000	A	83	2.930	8.875	B
4	5.409	0.000	A	84	5.860	8.875	B
5	7.212	0.000	A	85	8.790	8.875	B
6	9.016	0.000	A	86	11.720	8.875	B
7	10.819	0.000	A	87	14.650	8.875	B
8	12.622	0.000	A	88	17.580	8.875	B
9	14.425	0.000	A	89	20.510	8.875	B
10	16.228	0.000	A	90	2.930	10.175	B
11	18.031	0.000	A	91	5.860	10.175	B
12	19.834	0.000	A	92	8.790	10.175	B
13	21.637	0.000	A	93	11.720	10.175	B
14	23.440	0.000	A	94	14.650	10.175	B
15	0.000	1.786	A	95	17.580	10.175	B
16	23.440	1.786	A	96	20.510	10.175	B
17	0.000	3.571	A	97	2.930	11.475	B
18	23.440	3.571	A	98	5.860	11.475	B
19	0.000	5.357	A	99	8.790	11.475	B
20	23.440	5.357	A	100	11.720	11.475	B
21	0.000	7.143	A	101	14.650	11.475	B
22	23.440	7.143	A	102	17.580	11.475	B
23	0.000	8.929	A	103	20.510	11.475	B
24	23.440	8.929	A	104	2.930	12.775	B
25	0.000	10.714	A	105	5.860	12.775	B
26	23.440	10.714	A	106	8.790	12.775	B
27	0.000	12.500	A	107	11.720	12.775	B
28	23.440	12.500	A	108	14.650	12.775	B
29	0.000	14.286	A	109	17.580	12.775	B
30	23.440	14.286	A	110	20.510	12.775	B
31	0.000	16.071	A	111	2.930	14.075	B
32	23.440	16.071	A	112	5.860	14.075	B
33	0.000	17.857	A	113	8.790	14.075	B
34	23.440	17.857	A	114	11.720	14.075	B
35	0.000	19.643	A	115	14.650	14.075	B
36	23.440	19.643	A	116	17.580	14.075	B
37	0.000	21.429	A	117	20.510	14.075	B
38	23.440	21.429	A	118	2.930	15.375	B
39	0.000	23.214	A	119	5.860	15.375	B
40	23.440	23.214	A	120	8.790	15.375	B
41	0.000	25.000	A	121	11.720	15.375	B
42	1.803	25.000	A	122	14.650	15.375	B
43	3.606	25.000	A	123	17.580	15.375	B
44	5.409	25.000	A	124	20.510	15.375	B
45	7.212	25.000	A	125	2.930	16.675	B
46	9.016	25.000	A	126	5.860	16.675	B
47	10.819	25.000	A	127	8.790	16.675	B
48	12.622	25.000	A	128	11.720	16.675	B
49	14.425	25.000	A	129	14.650	16.675	B
50	16.228	25.000	A	130	17.580	16.675	B
51	18.031	25.000	A	131	20.510	16.675	B
52	19.834	25.000	A	132	2.930	17.975	B
53	21.637	25.000	A	133	5.860	17.975	B
54	23.440	25.000	A	134	8.790	17.975	B
55	2.930	3.675	B	135	11.720	17.975	B
56	5.860	3.675	B	136	14.650	17.975	B
57	8.790	3.675	B	137	17.580	17.975	B
58	11.720	3.675	B	138	20.510	17.975	B
59	14.650	3.675	B	139	2.930	19.275	B
60	17.580	3.675	B	140	5.860	19.275	B
61	20.510	3.675	B	141	8.790	19.275	B
62	2.930	4.975	B	142	11.720	19.275	B
63	5.860	4.975	B	143	14.650	19.275	B
64	8.790	4.975	B	144	17.580	19.275	B
65	11.720	4.975	B	145	20.510	19.275	B
66	14.650	4.975	B	146	2.930	20.575	B
67	17.580	4.975	B	147	5.860	20.575	B
68	20.510	4.975	B	148	8.790	20.575	B
69	2.930	6.275	B	149	11.720	20.575	B
70	5.860	6.275	B	150	14.650	20.575	B
71	8.790	6.275	B	151	17.580	20.575	B
72	11.720	6.275	B	152	20.510	20.575	B
73	14.650	6.275	B	153	2.930	21.875	B
74	17.580	6.275	B	154	5.860	21.875	B
75	20.510	6.275	B	155	8.790	21.875	B
76	2.930	7.575	B	156	11.720	21.875	B
77	5.860	7.575	B	157	14.650	21.875	B
78	8.790	7.575	B	158	17.580	21.875	B
79	11.720	7.575	B	159	20.510	21.875	B
80	14.650	7.575	B				

26.00

DATUM X $\begin{matrix} \uparrow \\ Y \\ \downarrow \end{matrix}$.50

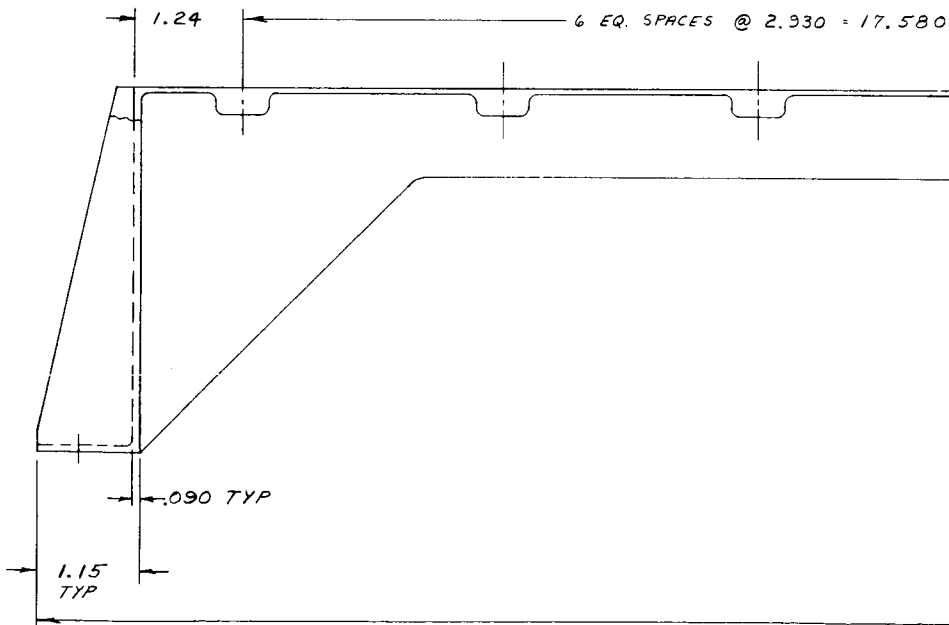
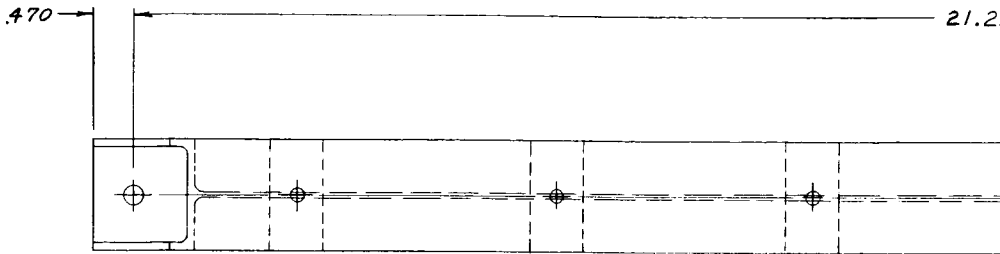
17



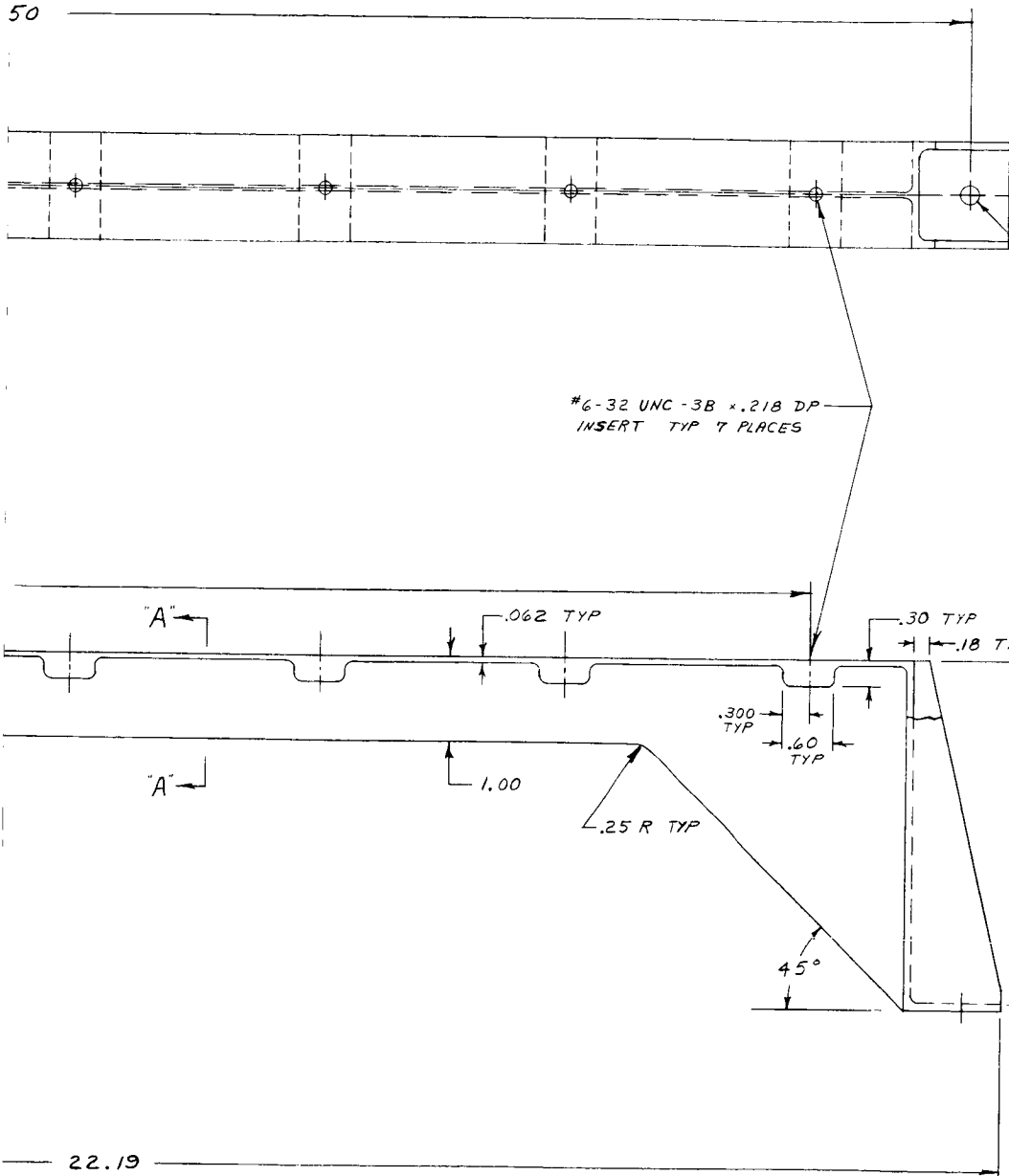
HOLE CHART		
HOLE CODE	SIZE	QTY
A	.2505 \pm .0010 -.0000 DIA THRU	54
B	.169 \pm .005 -.001 DIA THRU	105

NOTE:
TOL: 3 PLACE DEC. \pm .005
2 " " \pm .02

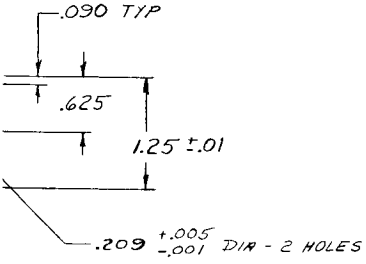
Figure V. SK56152-553 - Temperature Control/Shear Panel



140



142



NOTES:

1. DWG. TERMS & TOL. PER GE 118A1669
2. MARK PART "GE SK-56152-551 P1 PER GE 118A1526 CLASS 21
3. MAT'L TO BE - MAG. HM21A-T8
4. ALL RADII TO BE $.09 \pm .03$ UNLESS OTHERWISE NOTED
5. TOL UNLESS OTHERWISE NOTED ARE:
 - .XX $\pm .02$
 - .XXX $\pm .005$

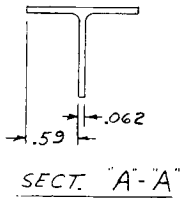
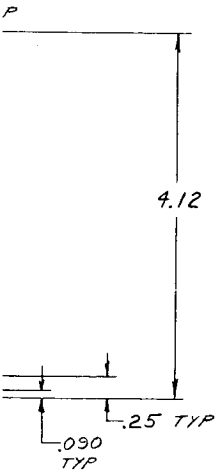
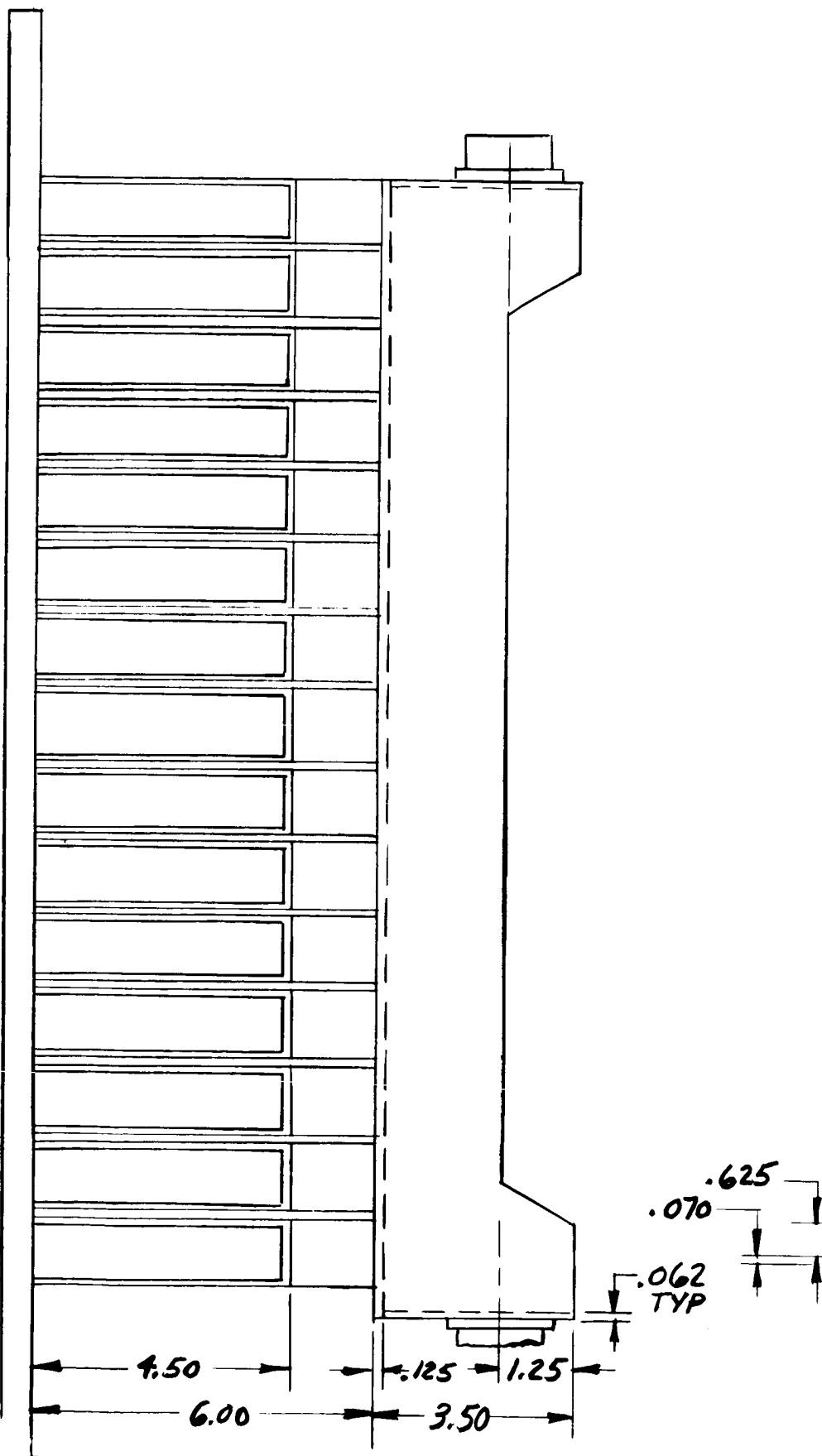
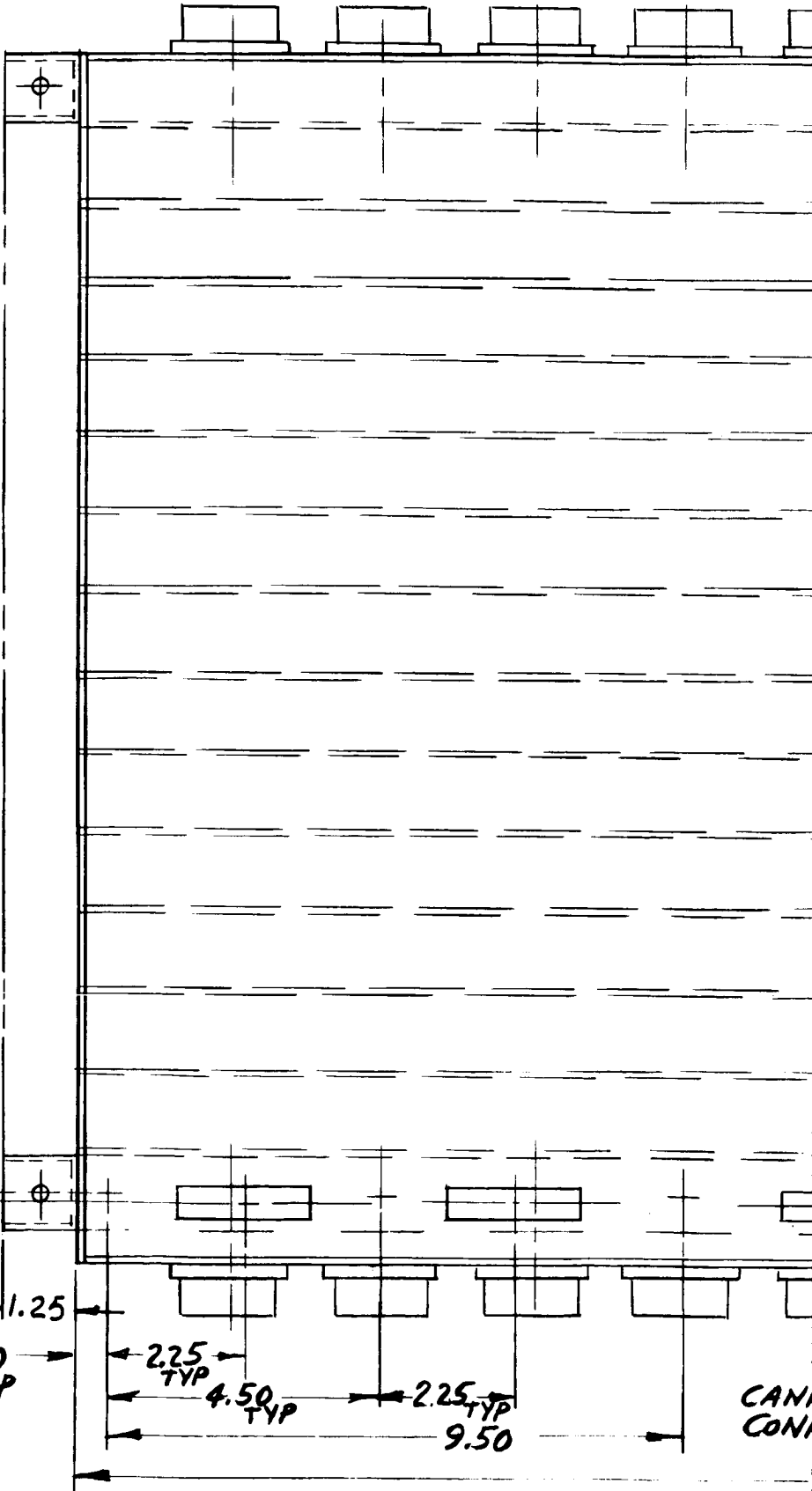


Figure VI. SK56152-551 -
Stiffener, Bracket

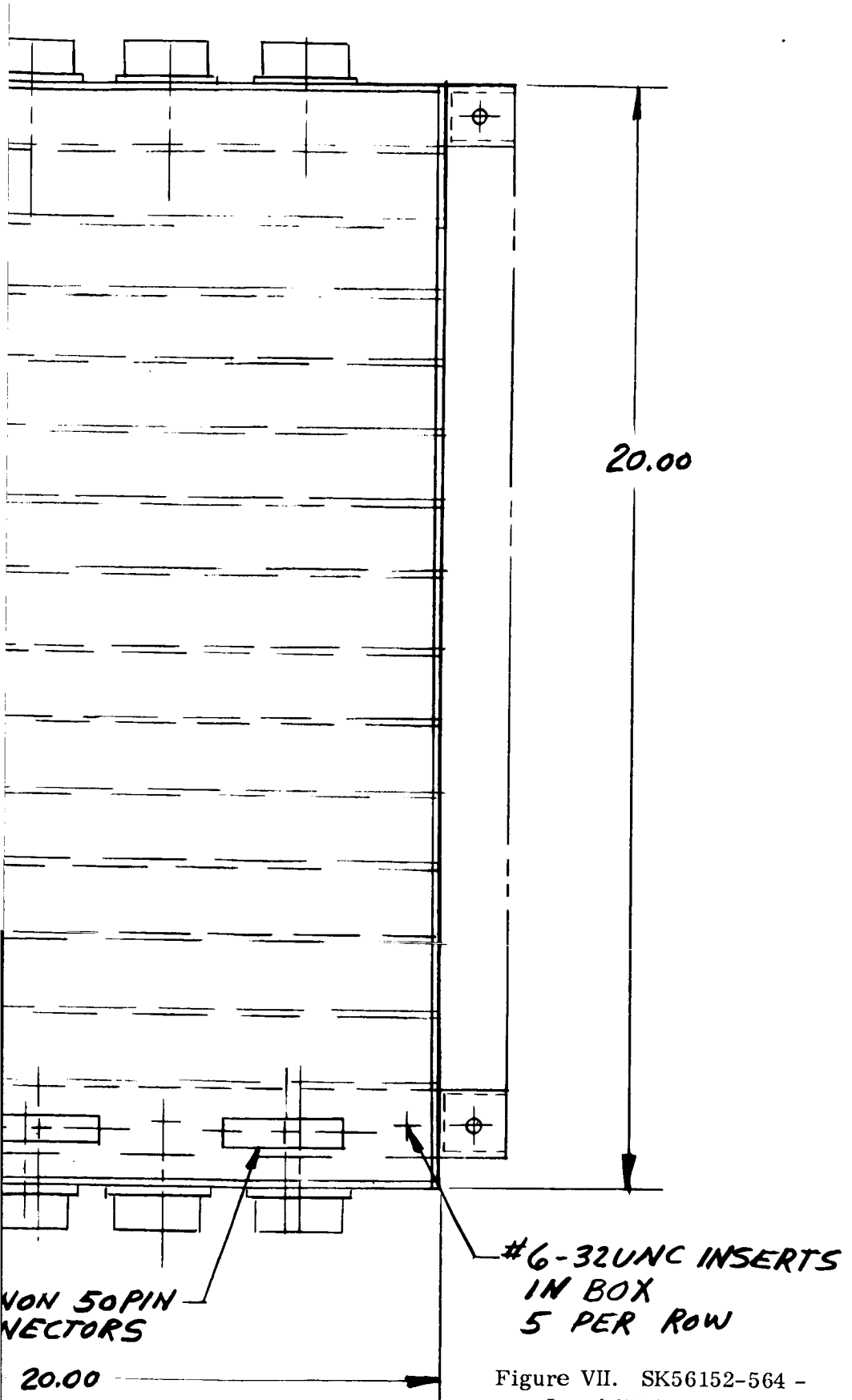


16 (1)



CANI
CONI

1100



#6-32UNC INSERTS
IN BOX
5 PER ROW

NON 50PIN
CONNECTORS

Figure VII. SK56152-564 -
Level III Assembly

(3)



Figure VIII. 10" Subchassis

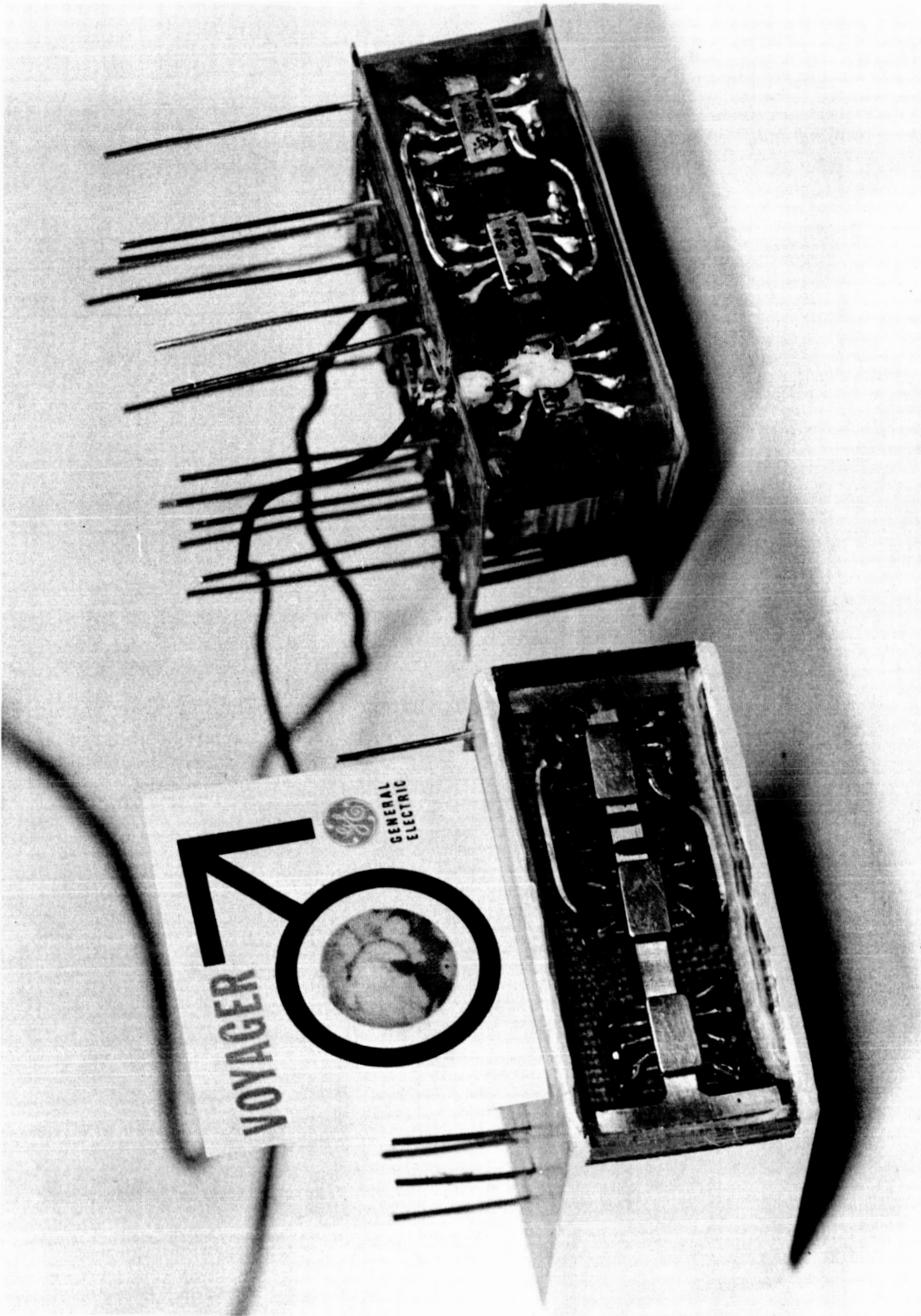


Figure IX. Hybrid Cordwood Module - Instrumented

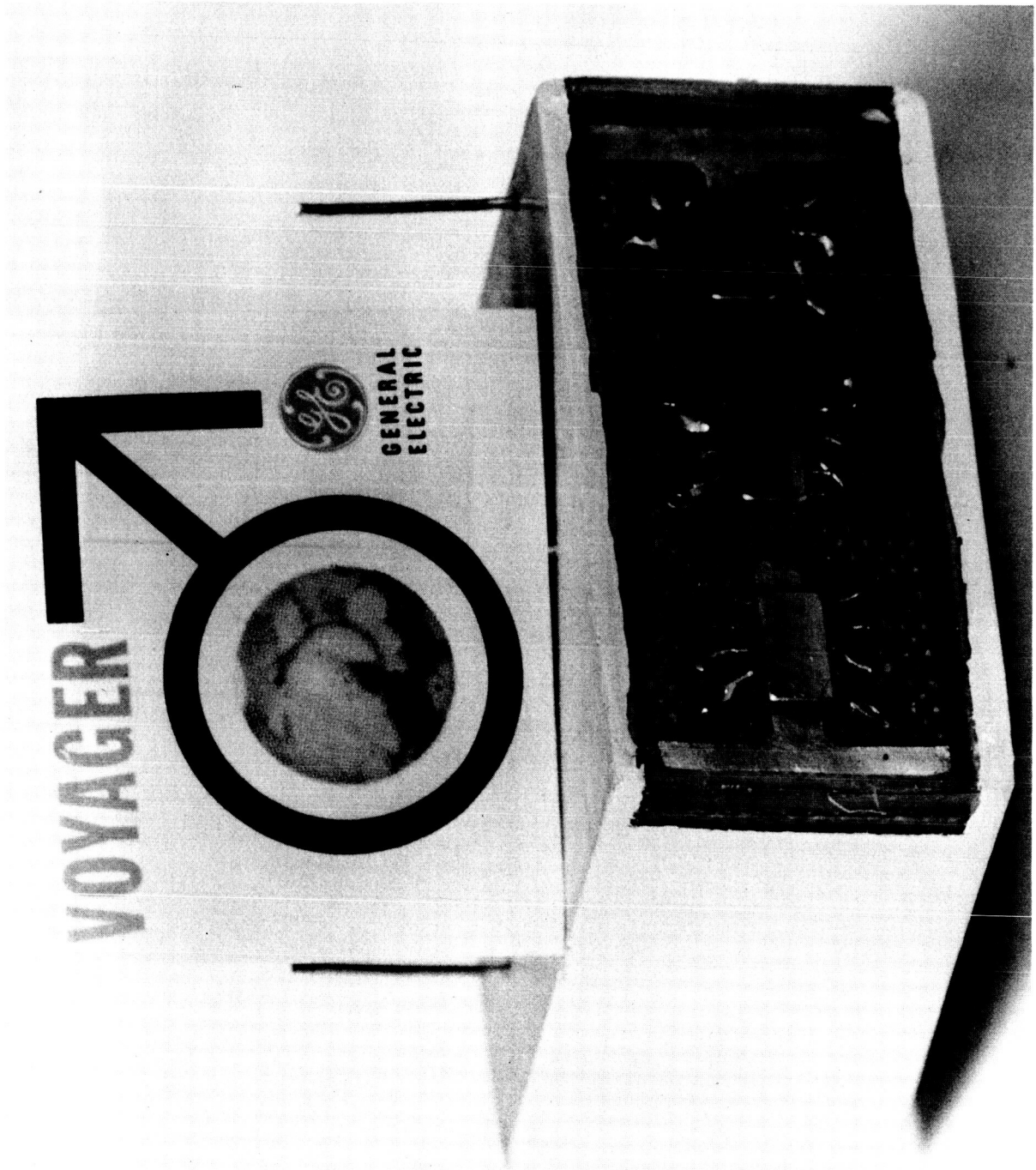


Figure X. Hybrid Cordwood Module Incorporating Microelectronics

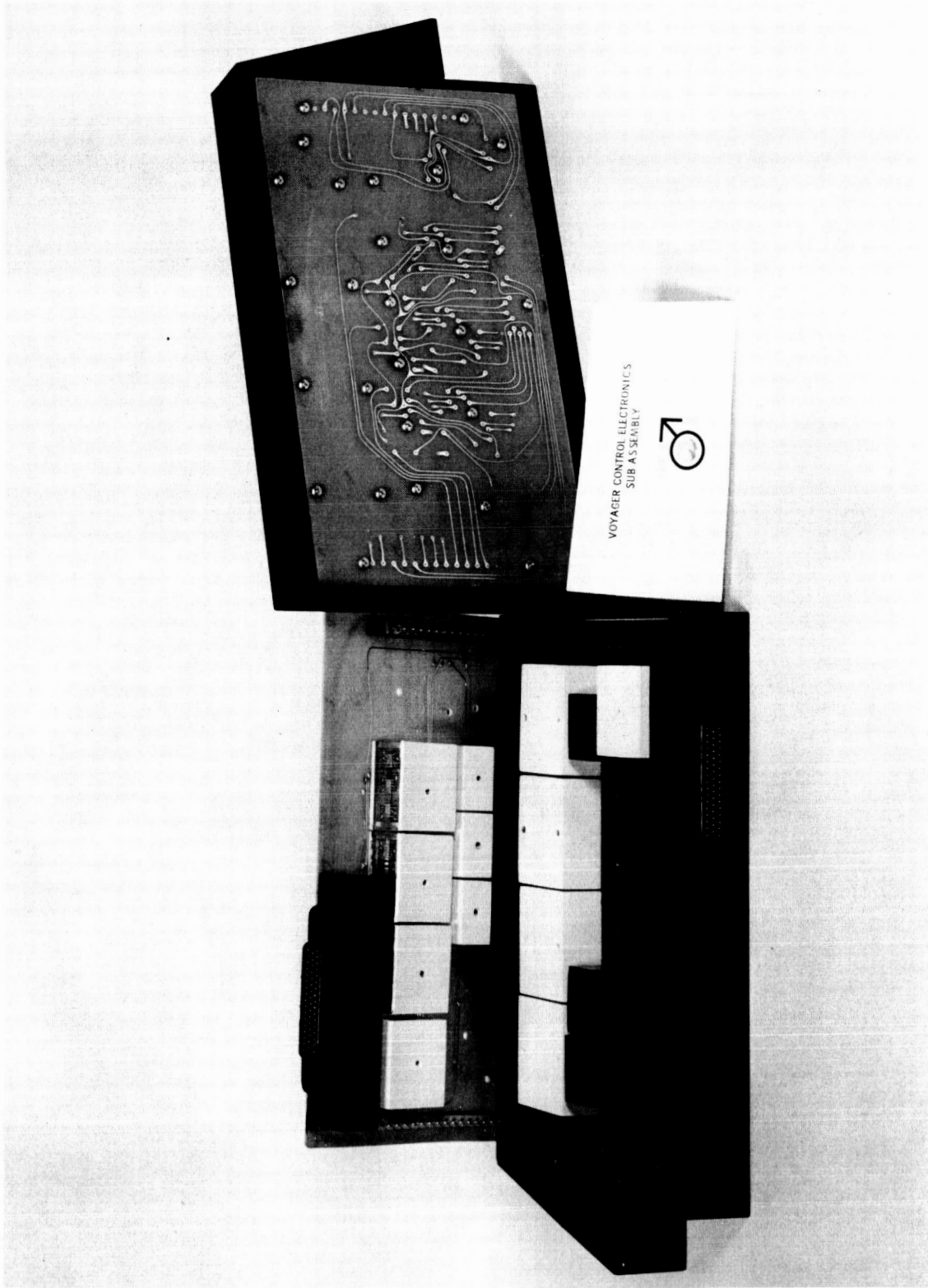


Figure XI. 10" Subassembly - Sandwich Construction

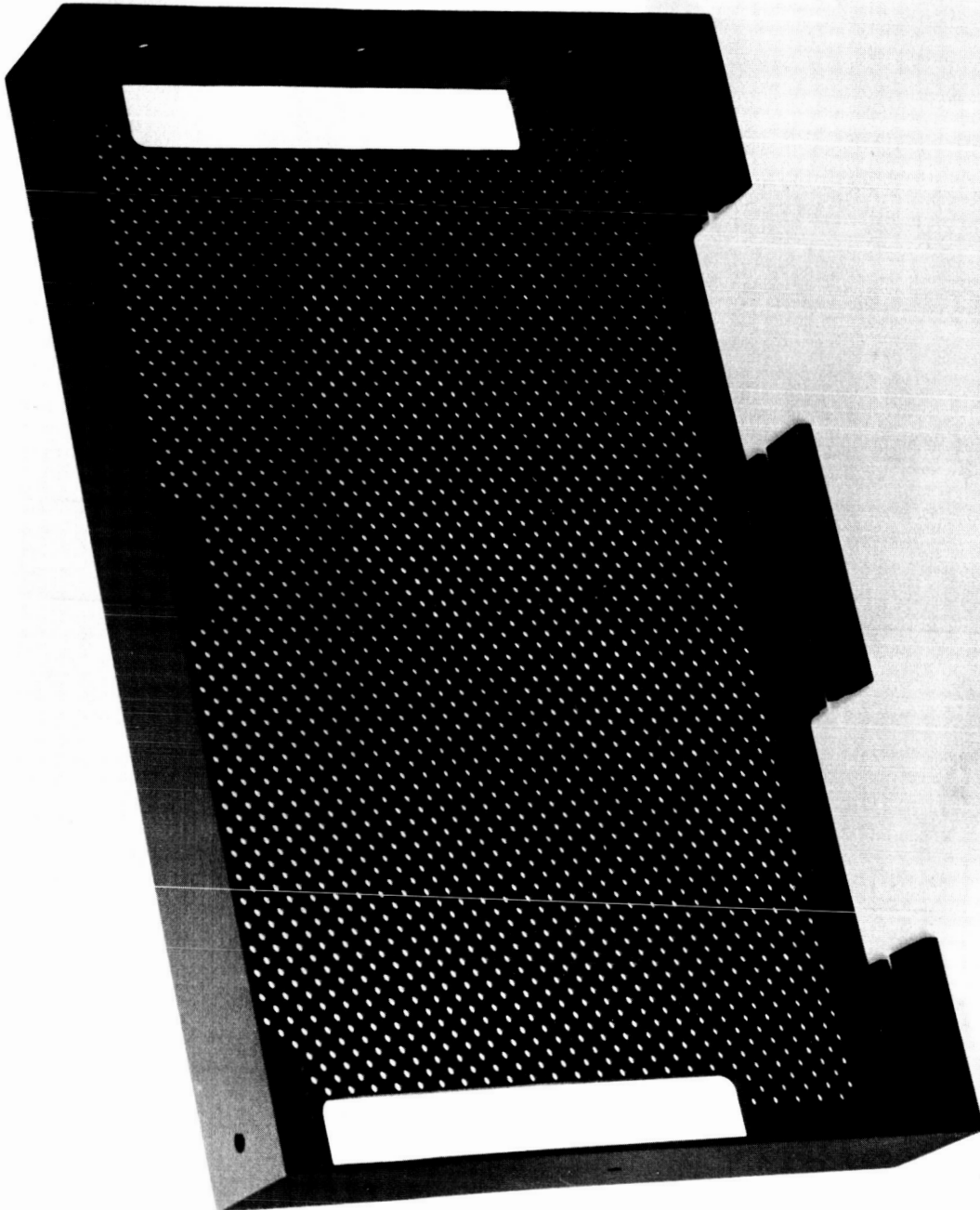


Figure XII. 10" Subassemblies - Interlocked Design

51

CII-VB235FD106

APPENDIX

II TYPICAL ELECTRONIC ASSEMBLY

This section shows photographic views of a typical Electronic Assembly as described in VB235FD106 Electronic Packaging.

Figure II-1 depicts the Harness Tray Assembly, showing standard connector and insert locations.

Figure II-2 shows a pair of standard 10-inch subassemblies mated to the Harness Tray Assembly. The unit shown is an operational Attitude Control Component.

Figure II-3 represents a completed Electronic Mounting Assembly, ready for installation into the Equipment Module Structure. Note that the Assembly can be handled, mounted and tested prior to the attachment of the thermal control/shear panel.

Figure II-4 is a view of the inner side of the Harness Tray, showing the subassembly interwiring and cable runs to the system and test connectors mounted at each end of the Tray.

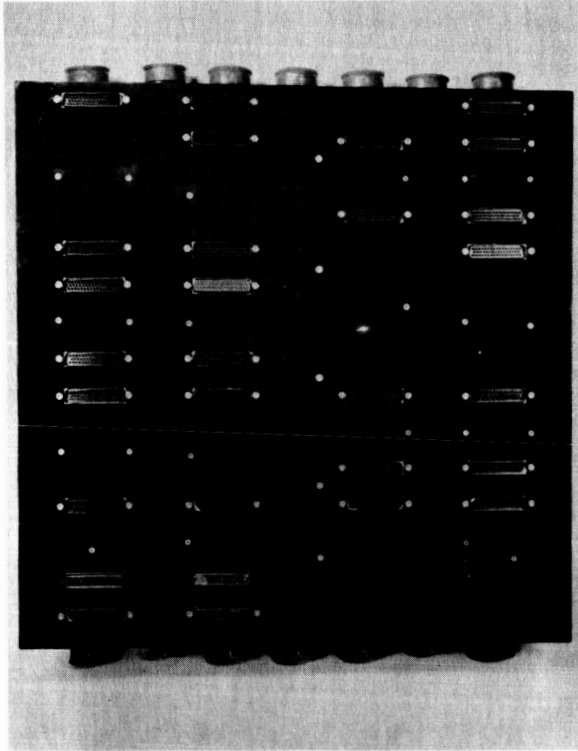


Figure II-1. Subsystem Baseplate

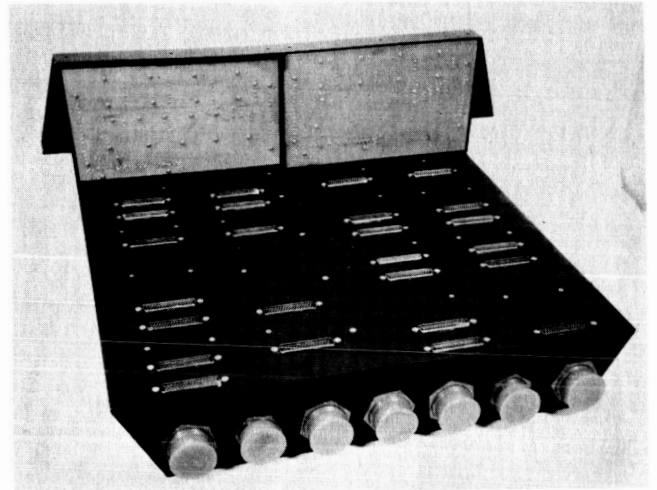


Figure II-2. Subsystem Baseplate with Control Electronics

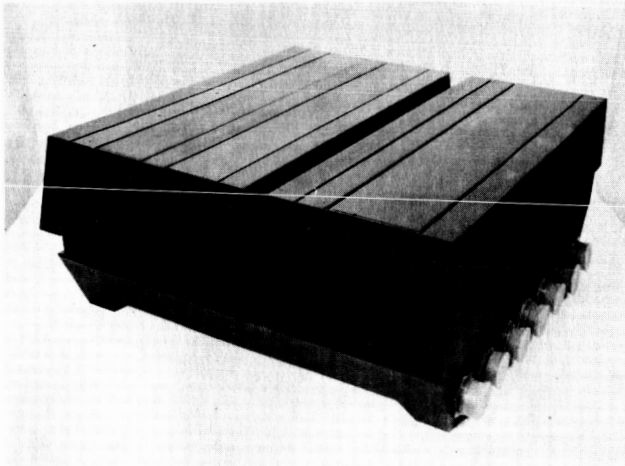


Figure II-3. Subsystem Assembly

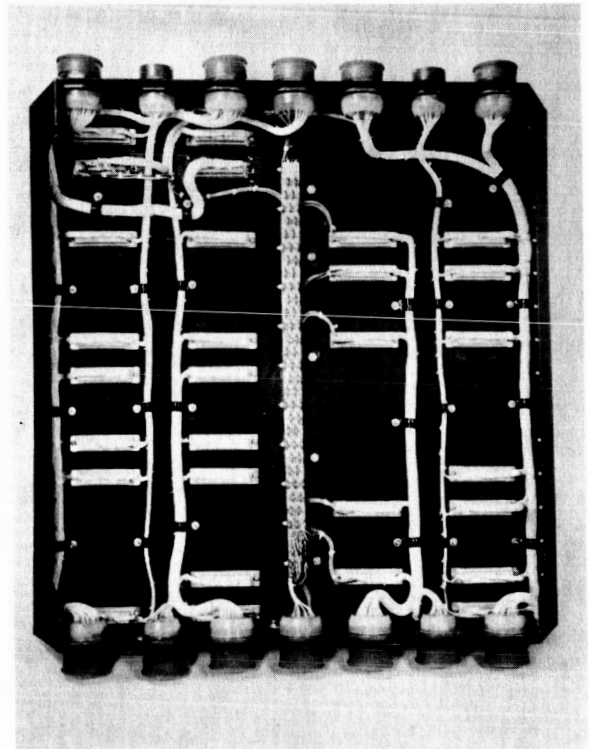


Figure II-4. Subsystem Harness

CII - VB235FD107

FUNCTIONAL DESCRIPTION

ELECTRICAL HARNESSING

Index

1. **Scope**
2. **Applicable Documents**
3. **Functional Description**
4. **Interfaces**
5. **Physical Characteristics**
6. **Safety**

1.0 SCOPE

This section describes the electrical harnessing and cables for the 1971 Voyager Flight Spacecraft.

2.0 APPLICABLE DOCUMENTS

- VB220SR101 Design Characteristics
- VB220SR102 Design Restraints
- VB220FD105 Launch Vehicle Interface
- VB220FD106 Capsule Interface
- VB220FD113 Layout and Configuration

Specifications and Standards

General Electric

- S30109 Harness Design Requirements Standard
- S30028 Wiring Harness Fabrication and Installation Standard
- S30011 Acceptance Criteria for Soldered Corrections
- S30100 MSD Design Requirements for the Soldering of Electrical Corrections
- S30027 Soldered Corrections, Shielding Terminations, and Wire Dress - Requirements for
- 118A1526 Identification Marking

NASA

- NPC 200-4 Quality requirements for Hand Soldering of Electrical Connections

3.0 FUNCTIONAL DESCRIPTION

3.1 GENERAL

The electrical harnesses for the Voyager Spacecraft Bus consists of a main ring harness assembly of many individual cables, six separate system interconnecting cables not part of the main harness, individual bay harnesses for each of the eleven electronics assemblies, and in-flight disconnecting cables to the Launch Vehicle and Flight Capsule.

The harnesses are composed of one or more cables of insulated and twisted wires, either shielded or unshielded, bundled together and terminated at the ends by connectors.

The primary objective of the Voyager system interconnections is reliability of operation i. e. , the transportation of electrical energy without degradation, through test and launch and throughout the mission lifetime in space.

3.2 MAIN SYSTEM HARNESS

The main system harness is made up of a ring of individual cables, each capable of independent definition, fabrication, test and installation.

The harness is pre-assembled into a ring-type supporting structure to mount into the spacecraft below the electronic bays.

The installed structure is used to provide additional support for other spacecraft items such as pneumatic lines and tank cradles.

The design of the harness support structure spacecraft provides sufficient access for reworking or removing individual cables without removing the entire harness assembly.

Breakouts of pigtails from the harness mate to hard mounted connectors at the bottom of each electronic assembly (bay).

3.3 UPPER SYSTEM CABLES

Individual cables connect the Canopus Sensor, Planet Scan Platform and Capsule to the system via connectors at the top of the associated bays. The flexible cable to the Scan Platform accommodates the position changes of this unit through deployment and throughout the required scan angles in operation. Refer to VB235FD108, Planet Scan Platform for details of this cable.

3.4 ASSEMBLY HARNESS

The harness for each electronic assembly is composed of separated signal, command, telemetry and power bundles from the module connectors to the respective signal connectors and insulated copper bus bars. Interconnections between subassemblies generally follow the bundle groupings with short direct connections routed to cross the bundles at right angles.

All connectors are hard mounted. Float is provided in the subassembly connector mounting to minimize alignment problems. (Reference - VB235FD106).

Most of the system interface connectors are mounted at the bottom of the bay (towards the S/C booster). Located at the top are the test connectors and those connectors interfacing with the components at the top of the spacecraft.

3.5 IN-FLIGHT DISCONNECTS

The cables to the Launch Vehicle and Capsule interfaces are each terminated in connectors which form part of an in-flight disconnecting device at the separation joints. The Launch Vehicle cable forms part of the main ring harness and the Capsule cable, one of the individual cables at the top of the spacecraft.

4.0 INTERFACES

4.1 ELECTRICAL

4.1.1 SYSTEM HARNESS

The system harness electrically interconnects the various subsystem and peripheral components and provide the connections to the Launch Vehicle and Capsule. (See Figure 4-1 for the various functional cable interfaces).

Cables are segregated into logical groups to reduce complexity, to control electrostatic and electromagnetic interference and to increase reliability. The basis for segregation is the destination, characteristics of the current flow and possibility of crosstalk.

System IR drops and power losses are minimized by the use of adequate wire size and judicious routing of cables to reduce wire runs and series-connections.

4.1.2 ELECTRONIC ASSEMBLY HARNESS

The individual electronic assembly harness interconnects the subassemblies in each bay to each other and to the system interface and test connectors. (See Figure 3-2 for a typical bay harness).

Control of electrostatic interference and electromagnetic fields is accomplished by segregating the bay harness into functional cable runs, and the signal cables further segregated on the basis of the characteristics of the current flowing into high and low level and/or sensitive and noisy signals.

To minimize power losses and IR drops, to reduce complexity of wiring, and provide the equivalent of a unipoint ground within the assembly, insulated bus bars distribute power and collect grounds for each subassembly in the more densely packed bays. Where the density or power distribution does not warrant power busses, only insulated ground busses are used to reduce wiring complexity.

All test points are brought out to the test connectors.

4.2 TEST HARNESS

No system test harness is designed into the vehicle. Instead external OSE test harnesses will be provided for system and subsystem test purposes. These harnesses will be supported by an external duct or other support temporarily fastened to the vehicle just above the electronic assembly module, and mate with the test connectors at the top of the bays through removable access panels. Upon completion of tests, the connectors will be demated, the test connectors capped, and the entire test assembly detached and removed from the vehicle.

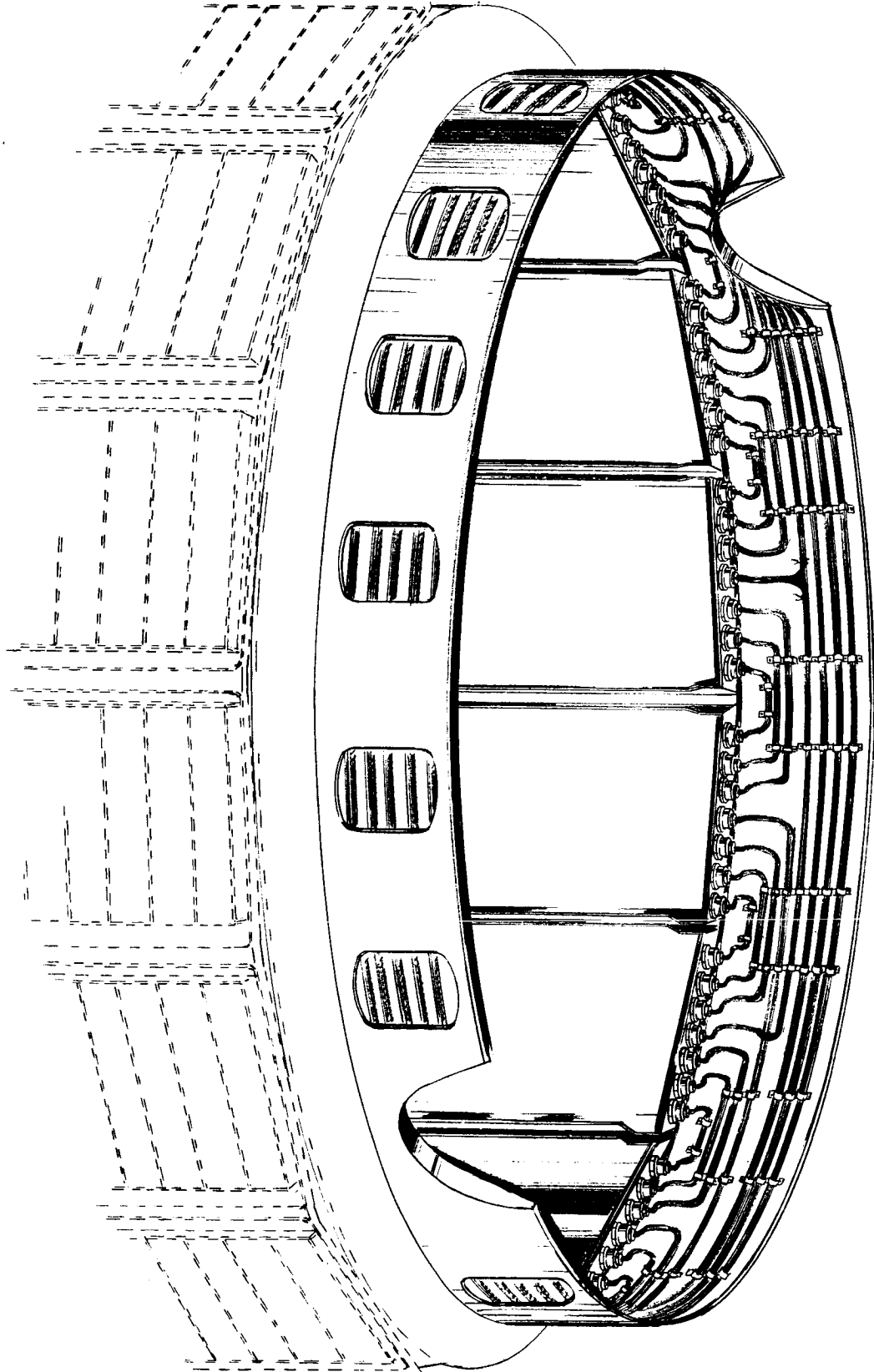


Figure 3-1. Main System Harness

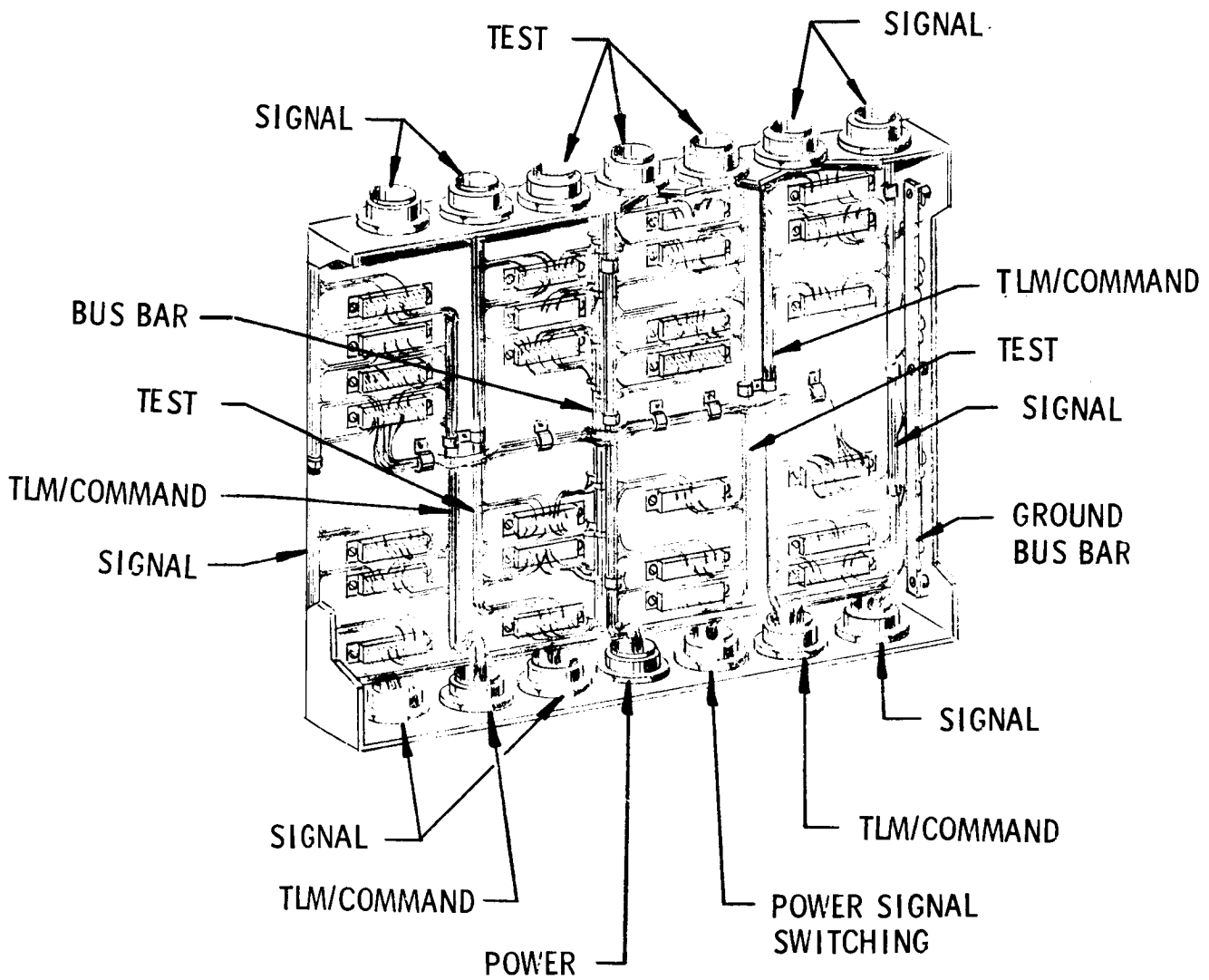


Figure 3-2. Typical Electronic Assembly Harness

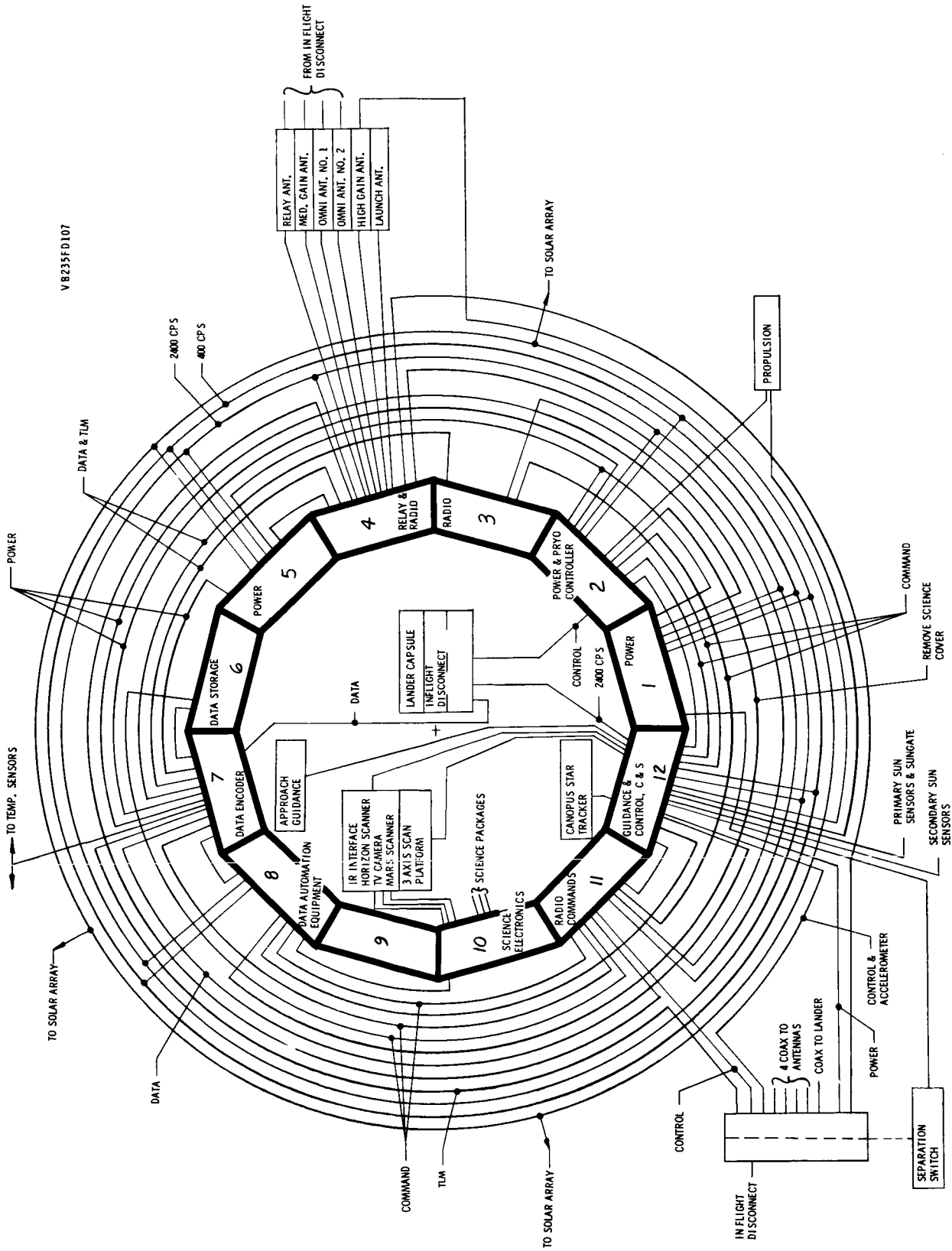


Figure 4-1. Voyager System Harness Schematic

4.3 CAPSULE INTERFACE

The Capsule interface cable feeds telemetry data, commands, both stored and ground transmitted, power and on-pad test signals to the Capsule through the Capsule/Bus in-flight-disconnect connector.

4.4 LAUNCH VEHICLE INTERFACE

The Launch Vehicle Spacecraft interface physically consists of a cable to the in-flight disconnect connector. The cable carries Launch Complex DC power, launch control and monitor signals from the pad umbilical through the field connection to the Spacecraft. In addition, on-pad RF signals are interconnected to the Spacecraft and Capsule via coaxial cables and coaxial inserts in the in-flight disconnect.

5.0 PHYSICAL CHARACTERISTICS

5.1 PHYSICAL CONSTRAINTS

The physical constraints determining the harness design are:

- a. Minimum weight and size compatible with the reliability and life objectives
- b. Layout of the spacecraft structure, and location of the interconnected assemblies
- c. Restricted areas and clearances necessary for optical, rf, radiation and magnetic particle devices, attitude control and thrust jets or nozzles and articulating members
- d. Flexibility and access for rework, adjustment and test without damage to the harness, spacecraft or personnel
- e. Capability for accommodating system and subsystem perturbations which result in interconnection changes
- f. Protection from heat, vibration and other environmental stresses
- g. Quality of interconnected assemblies and connectors

5.2 ELECTRICAL CONSTRAINTS

The electrical constraints include:

- a. The multiplicity and characteristics of the signal being routed
- b. The possible degradation of these signals by inductive, capacitive and resistive effects
- c. Control of magnetic and electro-static interference (EMI). See VB220SR102 for specific details of design practices to be followed to control EMI and prevent signal degradation due to inductive and capacitive effects.

5.3 RELIABILITY, MATERIALS AND PARTS

The design of the electrical harnesses and cables is based on the same care, consideration and regard for reliability as any other electronic component or unit. Only parts and materials proven for their reliability in the pre-space and space environment are used together with fabrication and handling techniques which do not degrade but rather enhance the reliability of the installed harnesses.

5.3.1

Materials and parts used in the design, fabrication and assembly of cables and harnesses, such as wire, insulation, sleeving, connectors, terminal blocks, grounding device, clamps, and terminals are selected from approved parts and material lists.

5.3.2

Size 24 AWG wire is listed for most signal leads and where potential drop and heat dissipation are not critical; size 22 and 20 AWG wire, where these factors are critical. Current carrying capacity, as specified in military wire tables, shall be derated fifty percent.

5.3.3

Only non-magnetic materials shall be specified for connectors and hardware.

5.4 SYSTEM HARNESS DESIGN

Lower Ring Harness - The basic system harness assembly consists of a ring of cables clamped and supported by a ring structure of 0.04 thick magnesium. Individual cables or cable break-outs (pigtailed) connect to the bottom system-interface connectors on the 11 equipment bays. Breaking out from the ring are cables to the solar array connectors, antenna connectors, propulsion and pneumatic subsystem connectors, Launch Vehicle in-flight disconnect, and all other subsystem connectors located at the bottom of the spacecraft. The support ring bolts to the bottom of the bays and to 24 magnesium brackets riveted to the lower longerons. (Reference - VB220FD102).

Upper Cables - Individual cables for the G & C and science subsystems and Capsule interface run from the top connectors on bays 7, 8, 11 and 12 and from a power bay to the Canopus Sensor, the Approach Guidance Sensor, the Planet Scan Platform and to the Capsule in-flight disconnect Connector. These cables are locally supported on top of the bays and upper spacecraft structure.

Routing

Routing problems are minimized on interbay wiring by the relatively large supporting structure and number of connector location available at the bays which allows for individual cables.

Those bays which functionally form an interconnection nucleus to many subsystems and subassemblies such as bay #12 (Guidance and Control, Controller and Sequencer) employ additional routing measures. Several cables or bundles may be routed through one connector. However these are categorized as to their destinations. Wires are grouped and separated by controlled pin assignments in the connector by cable and further by shielded groups.

In general, maximum use is made of the existing structural members which support peripheral equipment to support the cables to this equipment. However, it is necessary in some cases to avoid interference with intermediate obstructions, to simplify routing and/or minimize cable lengths by providing additional local support for cables running between members where direct structure does not presently exist.

In all cases cables are routed and protected to avoid contact with rough or irregular surfaces or sharp edges of structure and hardware. Cables passing through holes in the structure are protected by sleeving and/or grommets or bushing of approved materials.

Cables are routed around or behind intermediate structure to avoid interference with antenna patterns, sensors, jets, nozzles or articulating members and/or minimize heat effects from exhausts or other thermal sources. Additional measures to take care of thermal effects on cables subject to flexing during flight include derating, inclusion of heaters and application of insulation.

6.0 SAFETY

The harness and cables in themselves do not constitute a hazard to personnel either in the pre-assembly or assembled stage. Sufficient access exists for personnel to work on the installed harness providing reasonable care is exercised to prevent damage to propulsion lines and other equipment in the immediate area of the harness. The harness support ring design incorporates protective shrouds over the two 12-inch diameter tanks directly underneath.

VB235FD108

FUNCTIONAL DESCRIPTION
PLANET SCAN PLATFORM
DEPLOYMENT AND GIMBALING

Index

- 1 **Scope**
- 2 **Applicable Documents**
- 3 **Functional Description**
- 4 **Interface Description**
- 5 **Performance Parameters**
- 6 **Physical Characteristics**

1 0 SCOPE

This specification describes the actuation mechanism and structure needed to provide support and orientation capability for the planetary surface observation instruments.

2.0 APPLICABLE DOCUMENTS

VB220SR101 Design Characteristics
 VB220SR102 Design Restraints
 VB220FD113 Layout and Configuration
 VB220FD101 Standard Trajectories
 VB234FD108 Articulation Subsystem

3.0 FUNCTIONAL DESCRIPTION

Science instruments will be located in a planet scan platform structure which is in a stowed position during launch, transit and orbit injection, and in a deployed position oriented to the planet during Mars orbit. Three degrees of freedom are provided by the scan platform actuators and gimbals. Motion about axes "C" and "D" will erect a perpendicular to the orbit plane. Motion about Axis "E" rotates the scan platform in the orbit plane as well as providing an initial rotational motion to position the scan platform in a nominal operating position.

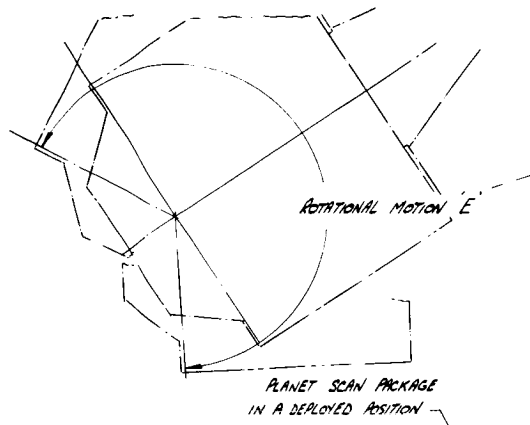
The initial deployment of this scanner to a deployed position is done by a separate linear actuator and hinge. Retraction of the linear activator rotates the planet scan platform including axes C, D and E and locks it into the deployed position as indicated in Figure 3-1.

3 1 STOWED POSITION

The stowed position of the scan platform is such that boost loads are not transmitted into the actuation mechanism. The scanner is mounted to the basic structure of the equipment module at bay 9 with support brackets attached to four points, two upper and two lower. The brackets mate with similar supports on the scan platform structure to provide firm support during boost.

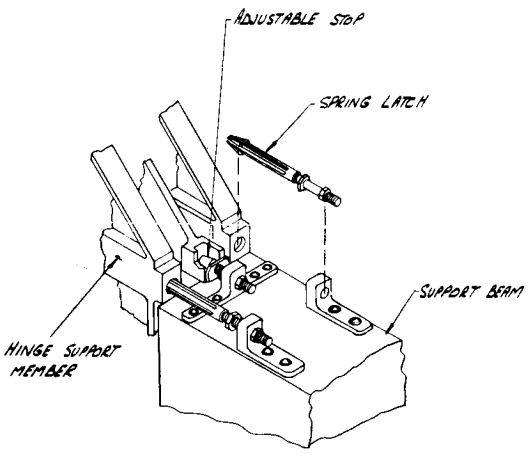
The outer surface of bay 9, will be covered with an insulation blanket (Reference VB235FD101) and appropriate lens covers. In the stowed position the instrument face of the planet scanner is oriented so that the instruments are located against the lens covers, thus providing a "fixed in place" cover for the instruments.

Motion of the planet scanner for deployment will be away from the support points so that there is no requirement for deployment of instrument covers. The insulation acts both as a cover and as thermal control for bay 9.



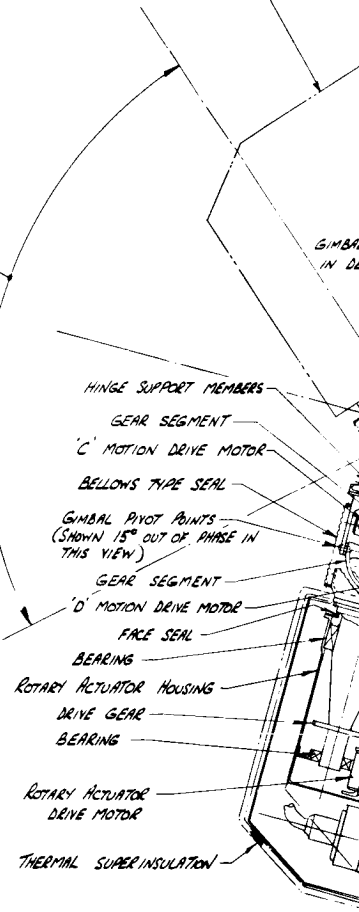
ANGULAR MOTION 'D'
ABOUT 'X' AXIS

GIMBAL
IN DE



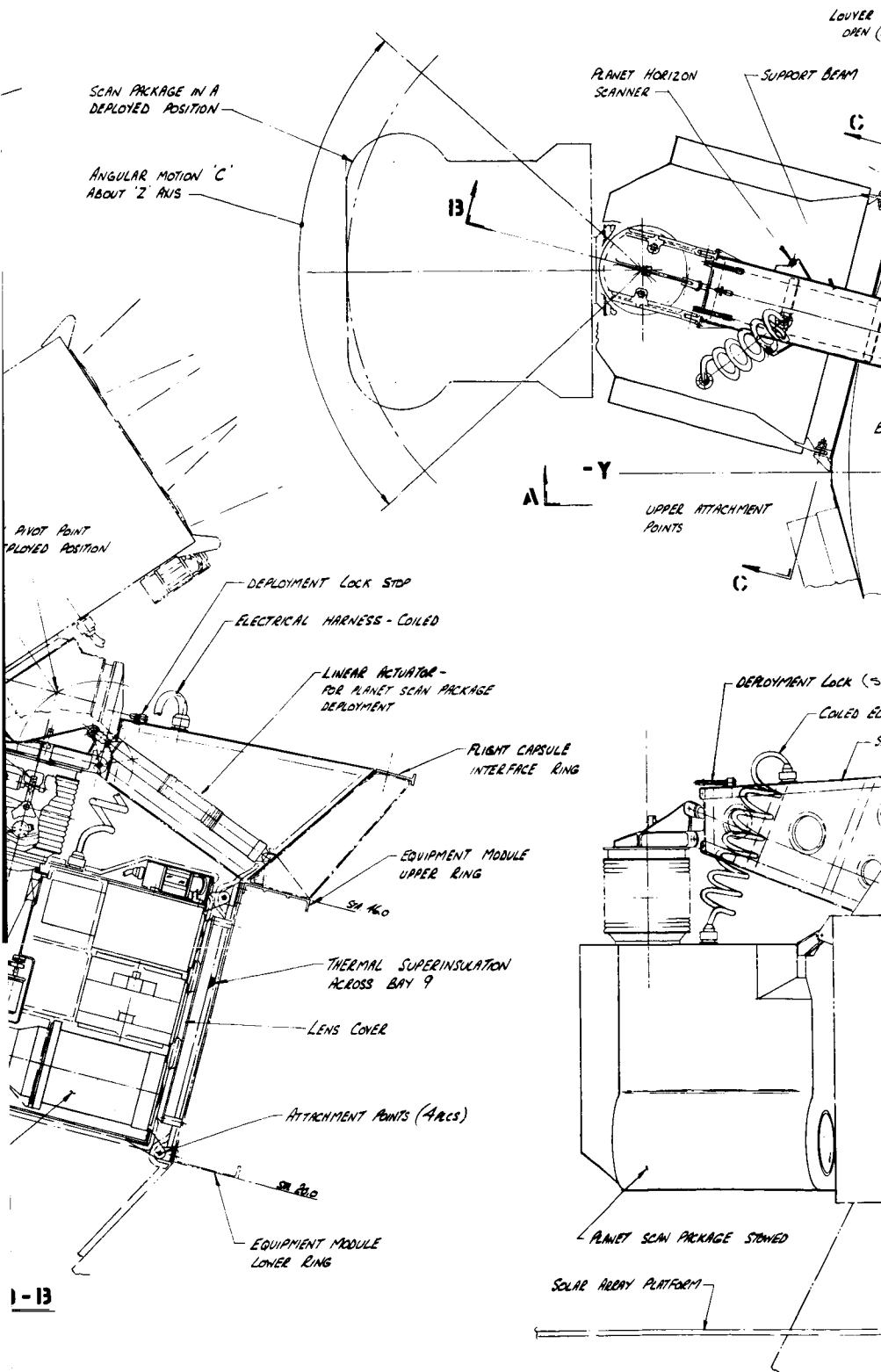
PROPOSED PLANET SCANNER
DEPLOYMENT LOCK

VIEW F



SCIENTIFIC SCANNING
EQUIPMENT (REF)

SECTION I



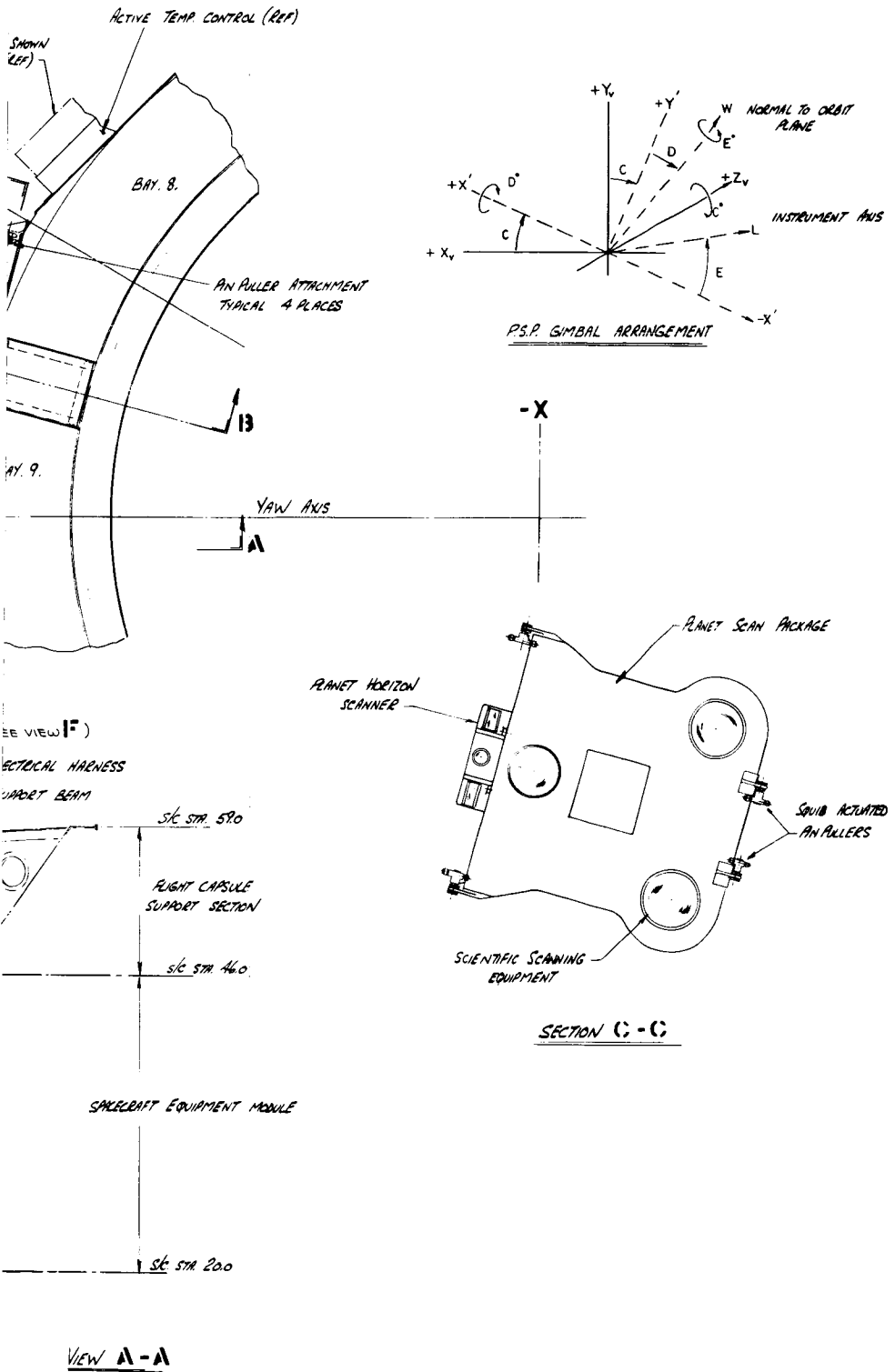


Figure 3-1. Planetary Scan Platform

③

3.2 DEPLOYMENT

Deployment of the planet scanner will be by means of a linear actuator and separate hinge as shown on Figure 3-1. The deployment will be a "one shot" system arranged so that the planet scanner locks into the deployed position.

The separate hinge for deployment was selected so that the actuation mechanism could remain sealed and pressurized.

After the squibs of the pin pullers located at the four support points are actuated (Reference VB235FD104), the linear actuator retracts and locks the planet scanner into the deployed position. The locking device is a spring loaded male fitting which is mounted on the cantilever beams extending from the capsule support structures and is inserted into a female fitting mounted on the planet scan platform. This mechanism was originally designed and tested for the Advent program and is shown in Figure 3-2.

The linear actuator shown in Figure 3-3 is composed of a DC Servo motor, similar to a Globe type BL-8, a torque multiplying gear train, and a ball nut-shaft assembly which converts the rotary torque to a linear force and a structural telescoping housing, with attachment fittings, sealed with a flexible metal bellows.

The stroke of this actuator is 4.5 inches and contains adjustable limit switches so that the current will be interrupted at the completion of the desired stroke. The gear reduction is 337 revolutions of the motor per inch of travel so that 9 seconds are taken for one complete stroke.

The motor output is fed through a spur gear reduction using staddle-mounted spur gears supported on ball bearings. Translation of rotary to linear motion is provided thru the use of a re-circulating - ball nut - lead screw combination.

Sealing of the actuator will be accomplished thru the use of a flexible bellows attached to the two major telescoping tubes in such a manner as to permit their required relative motion while preventing leakage through the gap between them.

The ends of the actuator tubes are welded to the attachment fitting providing a hermetic seal. The electrical leads are also provided with a hermetic sealed electrical connector.

Ball bearings will be lubricated with a proven low vapor pressure grease (GE Versilube G 300) throughout the sealed actuator.

The internal pressure will be reduced to one-half atmosphere to reduce the differential pressure loads generated during both ground testing and actual use, while still providing a pressure to limit lubricant evaporation.

The bearings on which the planet scanner rotates during deployment as well as the exposed bearings of the deployment actuator will be self-aligning spherical bearings of "DU material" (lead-teflon impregnated sintered bronze) which require no other lubrication. All machined

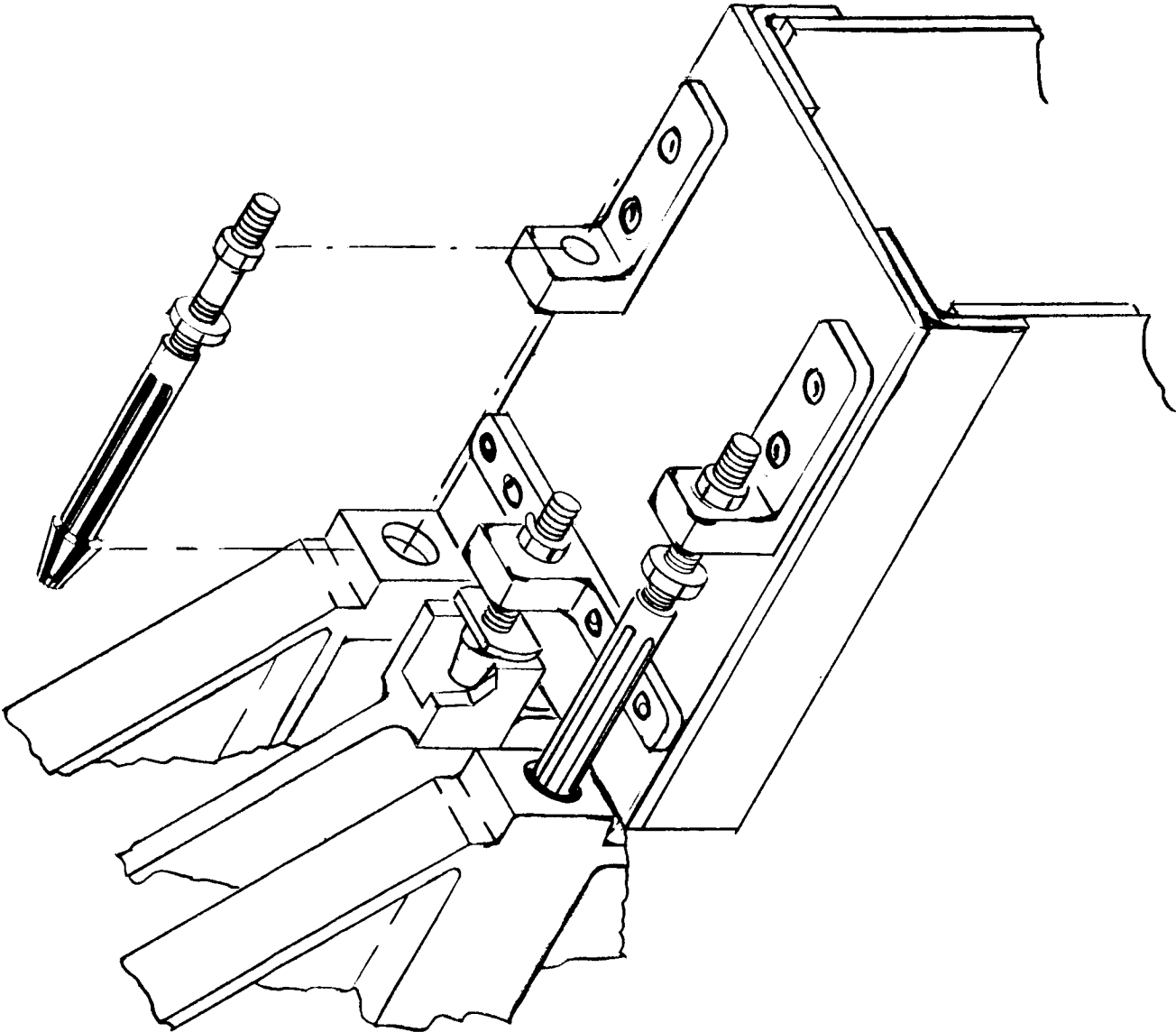


Figure 3-2. Platform Lacking Device

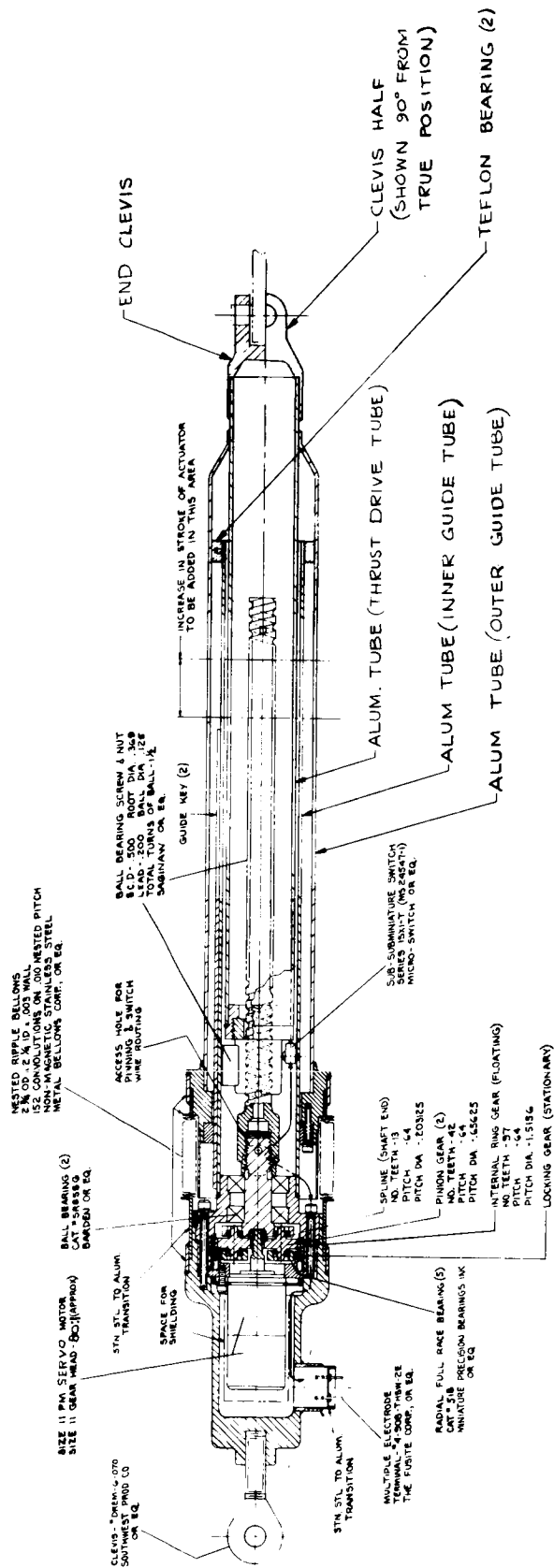


Figure 3-3. Linear Actuator

faces in this area, including the latching mechanism, will be hard anodized and sealed to prevent cold welding.

3.3 ACTUATION

In the deployed position, the actuation mechanism locates the planet scanner so that the instruments view the planet. The required view angles, actuation motors, and their control are defined in VB238FD108. Three axes of freedom are provided by gimbals C, D, and E. Rotation about axes C and D will erect a normal to the orbit plane, and rotation about E provides rotation of the scan package in the orbit plane.

The gimbals and actuators required to supply rotation about axis "C" and "D" are positioned within a sealed pressurized structure. Pressurization is maintained by means of a metallic bellows which is fitted around the gimbals and actuators as shown in Figure 3-1. Motions of the planet scanner about axis "C" and "D" flex the bellows. Pressurization is maintained at 1/2 psi.

The gimbal structure is the connecting link between the rotary actuator in the scan package and the supporting structure. This gimbal provides for rotation about the C and D axis. The gimbals are driven by two IMC 020-800 stepper motor prime movers, each driving a torque multiplying gear train, each gear train engaging internal sector gears secured to a spider on the C and D axis. Limit switches for both axes of freedom, stepper sensors for each motor, a temperature indicator for each motor, and a pressure sensor to sense internal pressure are provided. The area between the fixed face and the moveable face will be enclosed within a metallic flexible bellows that provides a hermetic seal.

Each motor output shaft will be fed through a spur gear reduction using straddle mounted gears supported on ball bearings. The total reduction of each gear train is 720 to 1 resulting in a one-fourth degree rotation of the gimbal moveable face for two 90-degree steps of the stepper motor. Low vapor pressure grease lubrication (G300) will be provided.

The step sensors will be mounted on the end of the stepper motor opposite the output shaft end. The limit switches will be mounted on the sector gears.

The rotary actuator for Gimbal E serves as the structural link between the gimbal output shaft and the planet scan platform. The rotary actuators outer housing being hard mounted to the planet scan platform, and the actuator output shaft with integral mounting flange being hard mounted onto the moveable face of the gimbal structure.

After the linear actuator has completed its operation of positioning and locking the planet scanner in place, the rotary actuator rotates the scan package from its stowed position of -90 degrees to its neutral position of 0 degrees at which time the limit switches will become effective limiting the subsequent motion of this actuator to -10 and +190 degrees.

The actuator is composed of a prime mover, an IMC 020-800 stepper motor, a torque multiplying gear train, a bell shaped output shaft and mounting flange, limit switches and stepper sensors mounted in a structural housing and sealed with a Nylon M₀S₂ seal rotating on a hard anodized and sealed aluminum face.

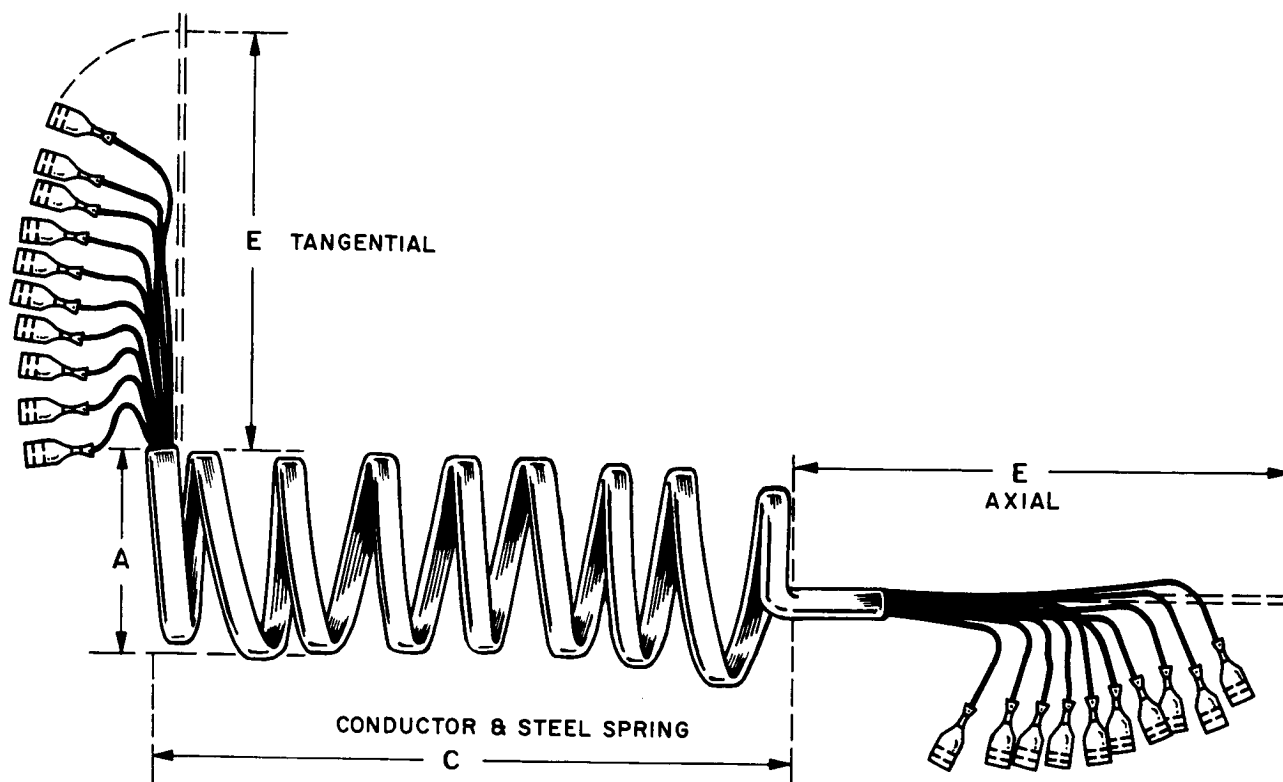


Figure 4-1. Flexible Hard-wire Conductor

The motor output will be fed through a spur gear reduction using straddle mounted gears supported on ball bearings utilizing gear material which have been proven in space. The total reduction is 720 to 1 resulting in a one-fourth degree rotation of the output shaft for two 90-degree steps of the stepper motor.

G300 low vapor pressure grease used in the other gears and bearings is also used in this location. The step sensor will be mounted on the end of the stepper motor opposite the output shaft end. The limit sensors will be incorporated in the final drive. Motor temperature and an internal pressure sensor will be provided.

4.0 INTERFACE DEFINITION

Transmission of data and power from the planet scanner to the spacecraft and return is by means of hard-wire with flexing provisions incorporated to accommodate the movement of the planet scanner. Figure 4-1 shows the required type of flexing. Heater wires are incorporated into the cable and the complete assembly is wrapped in super insulation.

A horizon scanner is mounted on the planet scan package structure and provides outputs for control of the scan platform about axis E. (Reference VB234FD108)

All science instruments located within the planet scan platform are provided with a cover, as previously described, to provide for lens and instrument protection during launch and transit.

5.0 PERFORMANCE PARAMETERS

Angle	Motion	Actual Rate
C	+53	.25°/sec
	-23	
D	+6	.25°/sec
	-57	
E	+190	.25°/sec
	-10	

The actuation and deployment system operational components are shown in the simplified block diagram (Figure 5-1) to provide a basis for the reliability analysis.

The mathematical model for the Planet Scan Platform Gimbal system is

$$R_{(PSP)} = R_{(Gimbal\ C\ \&\ D)} R_{(Gimbal\ "E")}\ R^4_{(pin\ puller)}\ R_{(linear\ actuator)}\ R^3_{(bearings)}$$

Where the mathematical models for the gimbal units are given by

$$R_{CD} = R_1^4 \cdot R_2^8 \cdot R_3 \quad (C\ \&\ D\ combined)$$

$$R_E = R_1^2 \cdot R_2^4 \cdot R_3$$

Entering the proper component reliability values tabulated in Table 5-1 into the above mathematical models results in a reliability prediction of .99605 for one month in orbit.

Table 5-1

Components	Quantity	Failure Rate (% per 1000 hrs)
1 Gear	4	.001
2 Bearing	15	.002
3 Seal C&D)	1	.030
Seal (E)	1	.070
4 Pin Puller	4	4 x 10 ⁻⁴ per hour .001 x 10 ⁻⁵ per hour
5 Linear Actuator	1	1 x 10 ⁻³ per cycle .100 x 10 ⁻⁶ per hour

METALLIC BELLOWS

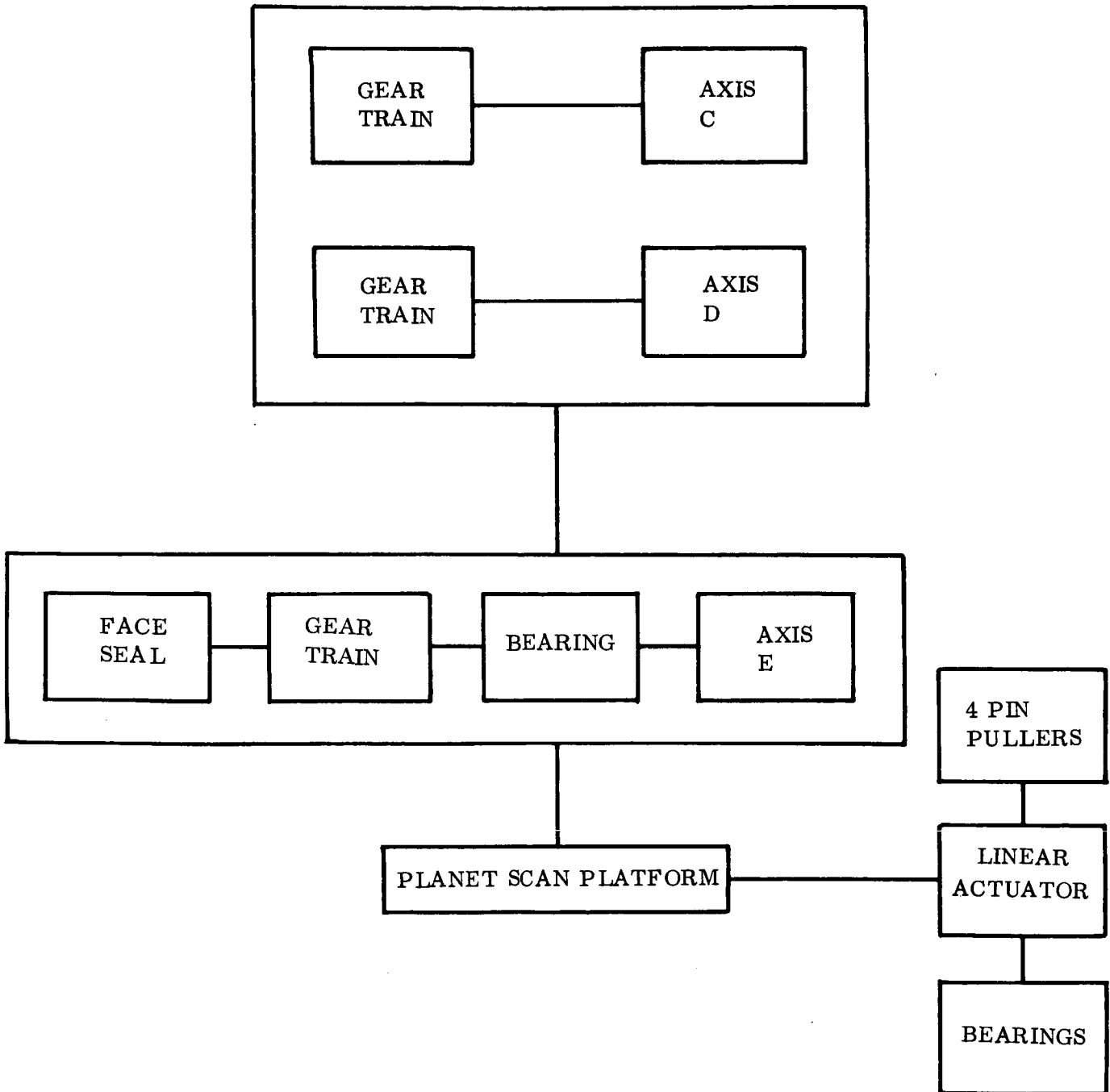


Figure 5-1. Simplified Block Diagram

6.0 PHYSICAL CHARACTERISTICS AND CONSTRAINTS

The planet scan platform will be structured to efficiently house and support the required instrumentation.

This scan platform will be latched down to provide rigid support to the equipment during the time from lift-off until after orbit injection and will provide protection to the instruments optics during this period.

In order to provide for proper deployment and actuation of the planet scan package, this lower portion of the biological barrier must be removed from the spacecraft. This operation will be performed prior to retropropulsion firing.

The weight of this scan platform, and gimbal structure is 50 pounds with a minimum volume of 5.0 cubic feet being available for science instrumentation.

CII-VB235FD109

HIGH GAIN ANTENNA
DEPLOYMENT AND GIMBAL MECHANISM

Index

1. Scope
2. Applicable Documents
3. Functional Description
4. Interface Definition
5. Performance Parameters
6. Physical Characteristics
7. Safety Consideration

1.0 SCOPE

This document describes the high gain antenna deployment mechanism, the gimbal mechanism, and the structure required to provide the antenna with the capability to be accurately pointed toward Earth during cruise, interplanetary or Mars orbit, and with the spacecraft in a maneuver attitude.

2.0 APPLICABLE DOCUMENTS

VB220SR101 - Design Characteristics

VB220SR102 - Design Restraints

VB220FD113 - Layout and Configuration

VB220FD101 - Standard Trajectories

VB234FD108 - Articulation Subsystem

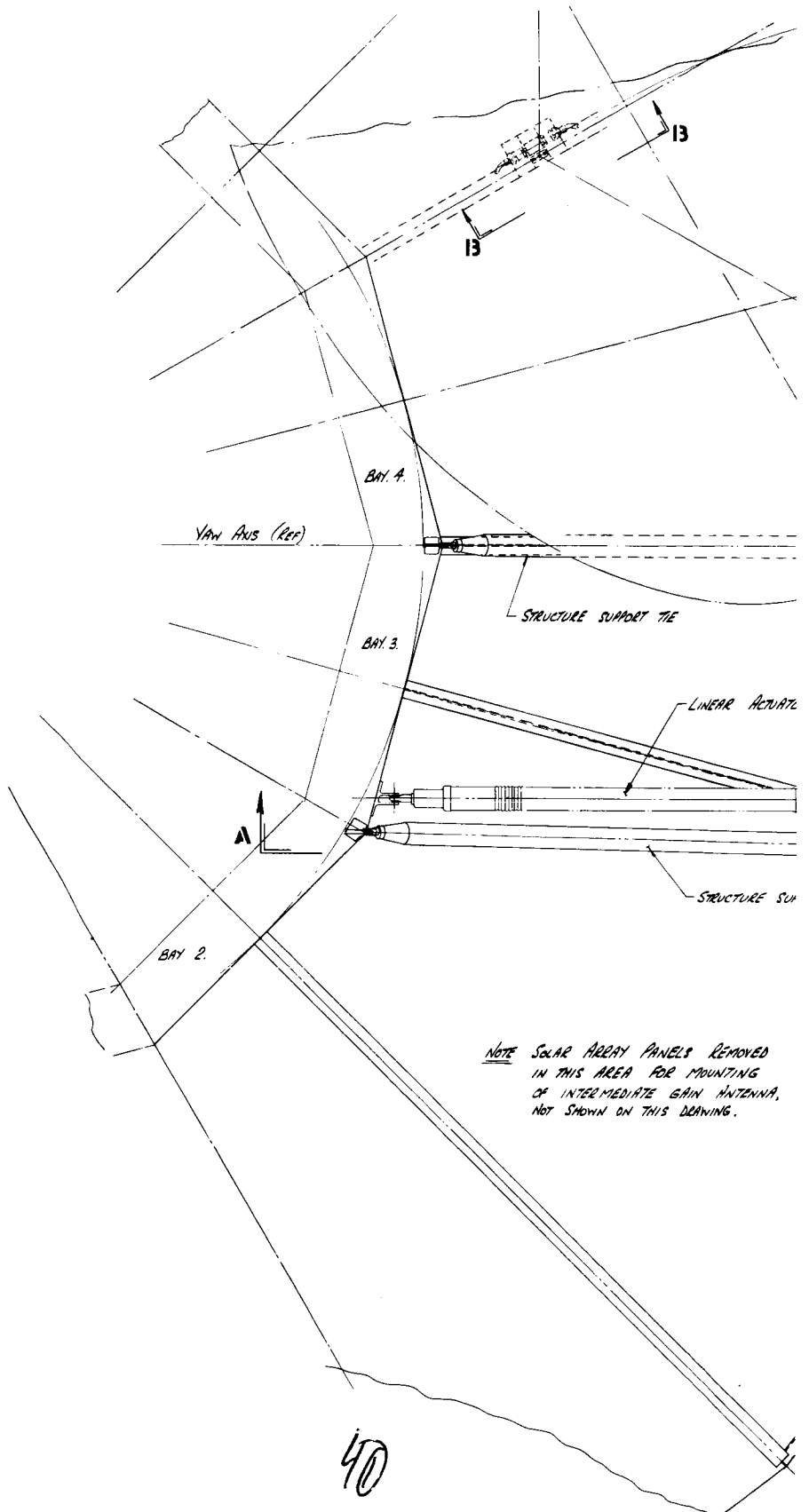
3.0 FUNCTIONAL DESCRIPTION

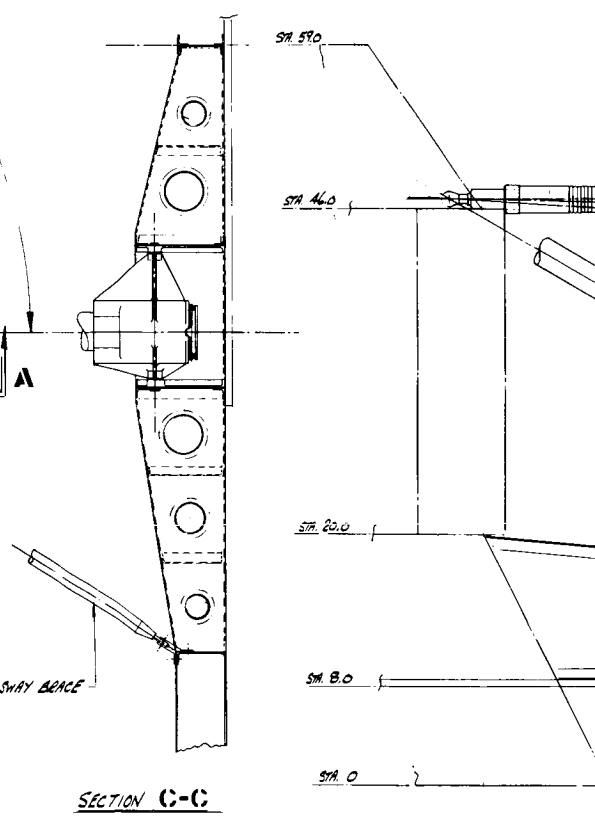
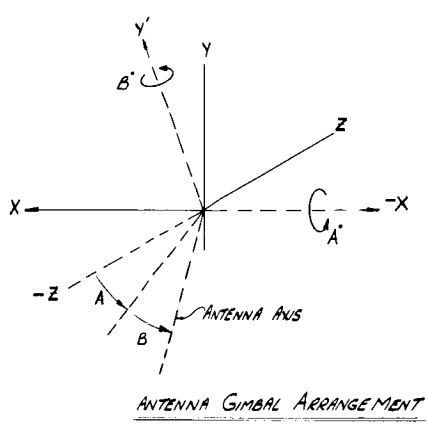
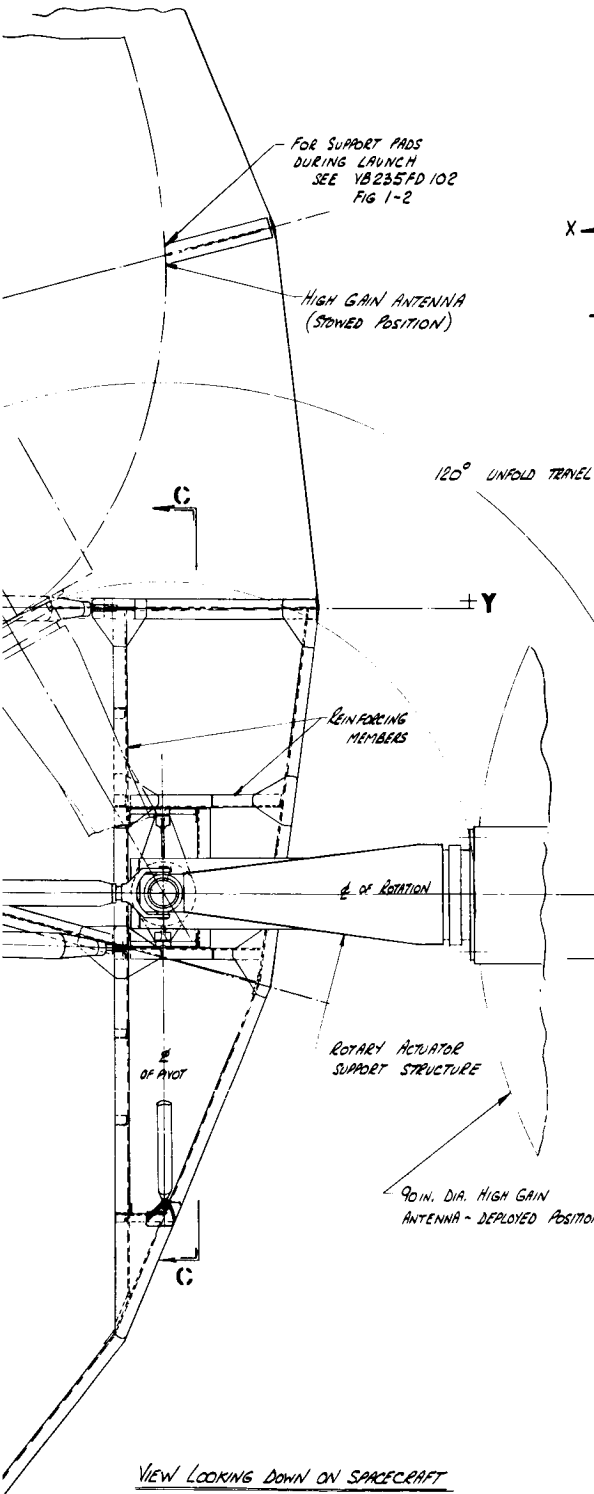
A 90-inch diameter parabolic reflector antenna is mounted on a structure capable of pointing the antenna toward Earth for the useful life of the Voyager spacecraft. There is a stowed position and a deployed position of the antenna pointing mechanism. The stowed position is such that the antenna lies within the aerodynamic shroud and is supported primarily by the spars of the solar array structure. The launch loads imposed on the antenna are therefore not transmitted into the antenna actuating mechanism. In the deployed position, the antenna extends beyond the solar panels. Acceleration loads generated during propulsion operations are carried through the antenna support and actuating structure.

Two degrees of freedom are provided by the gimbal mechanism. This mechanism, with the antenna in the deployed position, will be capable of rotating the antenna +15 to -25 degrees about an axis parallel to the spacecraft X axis herein referred to as the "A" axis, and to rotate the antenna 256 degrees (+206 to -50 degrees) about the antenna support axis, called the "B" axis (see Figure 3-1).

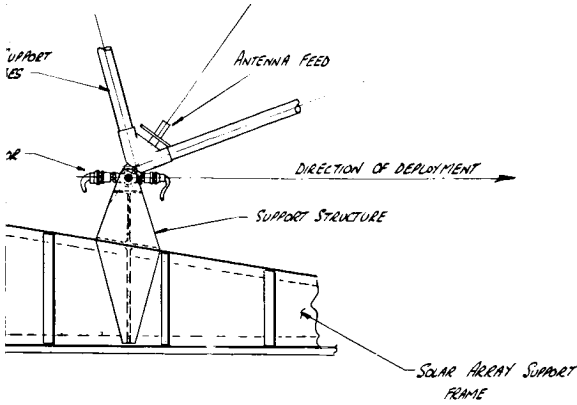
The antenna support structure includes upper and lower trunnions, diagonal supports, vertical members which house the rotary actuator, and gimbal mechanism used to rotate the antenna about the "A" axis. This structure is located outboard of the equipment module (Bay 3). Figure 3-1 shows this support structure and mechanism in relation to the spacecraft in the deployed condition and references the stowed position.

The antenna is bolted to a circular mounting flange 10.5 inches in diameter with a bolt circle of 9.5 inches. During launch the antenna is restrained by a release mechanism which consists of a pyrotechnic pin puller mounted on the solar array support between Bay 4 and Bay 5. The latching and release mechanism is secured to the antenna feed structure. Launch loads

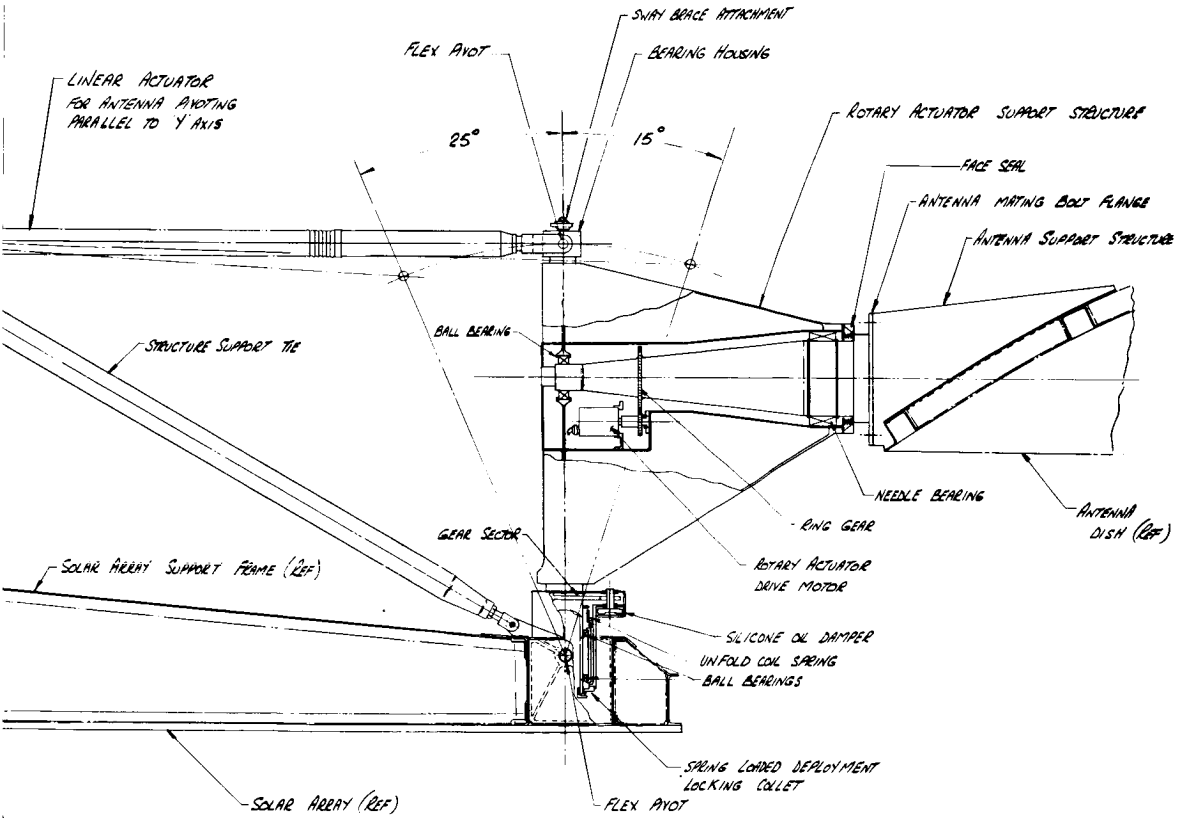




412



SECTION 13-13
 SHOWING ANTENNA TIE DOWN POINT
 (VIEW ROTATED)



SECTION A-A

Figure 3-1. High Gain Antenna Deployment Mechanism

3

are carried as axial loads through the feed support tubes. Four compression support pads are provided at the outer edge of the antenna. These pads are adjusted to provide a support against the antenna in order to minimize deflections during launch.

3.1 DEPLOYMENT MECHANISM

After separation of the spacecraft from the launch vehicle, a signal is given to deploy the antenna, and the pin puller releases the antenna feed structure from the spacecraft structure allowing the spring located in the lower trunnion to rotate the antenna system into its deployed position. The rate at which the antenna system rotates is controlled throughout its entire travel by a viscous rotary damper. After deployment is complete, a mechanical lock engages providing maximum stiffness to the structure.

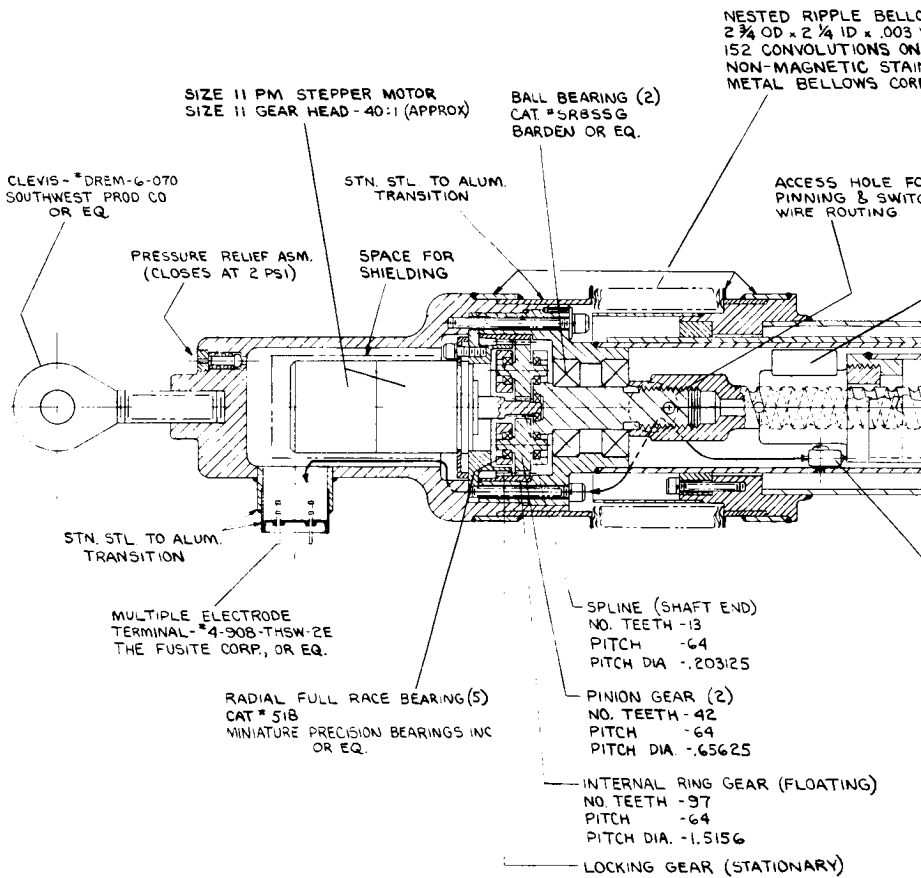
The damper provided to control the deployment spring is of the disc type. The disc type was selected because it is not limited in amount of motion and need not contain a large reservoir to contain oil that is used only once per stroke in passing around a piston. The locking mechanism consists of spring loaded locking lugs which mate with machined recesses in the lower trunnion structure. Engagement of the lugs into the machined recess effectively latches the high gain antenna into the deployed position.

Ball bearings in both the upper and lower trunnions are shielded precision bearings. These bearings, before assembly into the trunnion, are subjected to a short run-in period using light lubricating oil, then ultrasonically cleaned and packed with GE Versilube (G300) grease. Although it is not required that the bearings operate after antenna deployment, these precautions are taken to insure deployment even if the deployment is subjected to an unexpected time delay. G300 is a low vapor pressure grease capable of operating for long periods of time at high rotational speeds in a vacuum.

3.2 LINEAR ACTUATOR

The linear actuator (Figure 3-2) serves as a structural connecting link between the upper trunnion and the spacecraft and provides the antenna with its required rotation about the "A" axis. This is accomplished by extending or retracting the sealed actuator a total of 23 inches. The actuator is supported at the trunnion with two 3/4-inch "Bendix Flexural pivots," and to the spacecraft with a self-aligning spherical bearing made from "DU-material," a lead Teflon in sintered bronze. "DU-material" is a self-lubricating bearing material suitable for use in space, and requires no other form of lubrication. Tests were conducted on "DU-material" (20 percent Pb, TFE in porous bronze on steel) for 1000 hours without excessive wear at contact pressures ranging between 10 and 1,500 PSI. Teflon in porous bronze on steel wore 0.005-inch after 213 hours and graphite and lead bronze wore 0.010-inch after 158 hours under the same test conditions. Data obtained from Space Material Handbook ML-TDR-C4-40 March 1964.

The actuating mechanism is comprised of a stepping motor prime mover (IMC 020-800), a torque multiplying gear reduction, a linear ball screw which provides an axial force to rotate the antenna, limit switches, stepper sensor, motor temperature indicator and an internal pressure sensor. This mechanism is enclosed in a telescoping structural housing sealed



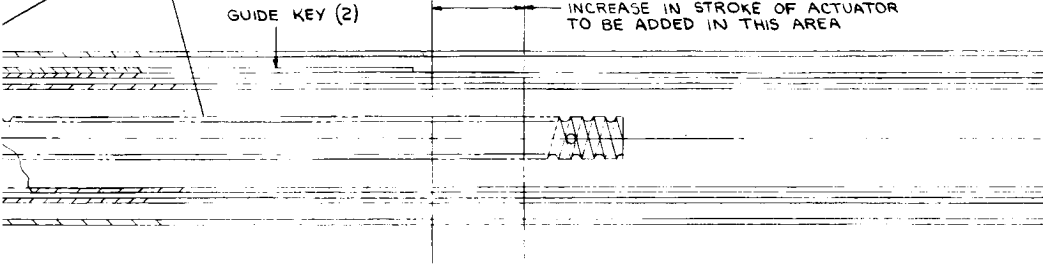
80

VS
ALL
.010 NESTED PITCH
LESS STEEL
, OR EQ.

BALL BEARING SCREW & NUT
B.C.D. .500 ROOT DIA. .369
LEAD .200 BALL DIA. .125
TOTAL TURNS OF BALL-1 1/2
SAGINAW OR EQ.

GUIDE KEY (2)

INCREASE IN STROKE OF ACTUATOR
TO BE ADDED IN THIS AREA



SUB-SUBMINIATURE SWITCH
SERIES ISXI-T (MS 24547-1)
MICRO-SWITCH OR EQ.

82

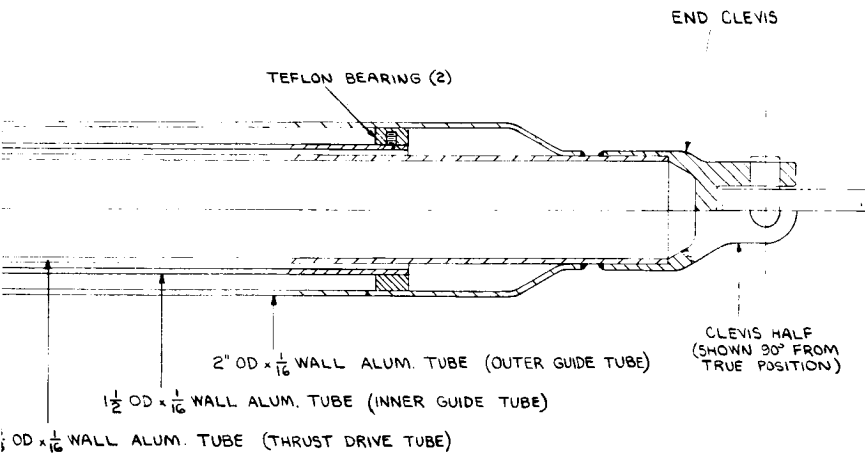


Figure 3-2. Linear Actuator

③

with a flexible metal bellows.

The stepper motor output which is applied in 90-degree impulses, is fed through a spur gear reduction using straddle mounted spur gears supported by ball bearings. The translation from rotary motion to linear motion is accomplished with a recirculating-ballnut-lead screw combination which incorporates the final reduction stage. Reduction is 2880 to 1 so that eight 90-degree pulses of the stepper motor produce a 0.25 degree rotation of the antenna about the "A" axis. Sealing of the actuator is accomplished through the use of a flexible bellows attached to the two major telescoping tubes in such a manner as to permit the required relative motion without leakage. Stepper sensors are mounted on the motor shaft opposite the power take off. A motor temperature sensor and an internal pressure sensor are also provided. The limit switches are mounted at the ends of the leadscrew.

Lubrication is provided by a low vapor pressure grease consisting of a chlorophenyl methyl silicone oil in a lithium soap thickener (General Electric Versilube G300). During retro-fire the stepper motors will be put in the stall condition to prevent movement of the antenna.

3.3 ROTARY ACTUATION

The rotary actuator serves as the connecting member between the support structures and the antenna. The actuator output shaft is an integral part of the antenna mounting flange and provides rotation about the "B" axis. The non-rotating section of the actuator is hard mounted to the vertical member which provides the nodding motion (axis A) of the antenna.

The actuator is comprised of a stepping motor prime mover (EMC 020-800) a torque multiplying gear reduction with a cone shaped output shaft, a set of limit switches, a stepper sensor, motor temperature sensor and an internal pressure sensor. This mechanism is assembled in a structural housing containing a Nylon - MoS₂ rotary seal. The stepper motor output, which is applied in 90-degree impulses, is fed through a spur gear reduction system using straddle mounted spur gears supported by ball bearings. The final reduction being a four to one drive of the output shaft. The total reduction is 720 to one resulting in a one-fourth degree output shaft rotation for two 90-degree steps of the driving motor. The output shaft is supported on the outboard end with a Torrington needle bearing HJ-9612040 or equivalent, which has an inside diameter of six inches, and is located adjacent to the Nylon-MoS₂ seal. The Nylon-MoS₂ seal rotates on a hard anodized and sealed aluminum surface, and is spring loaded to compensate for wear or differential expansion thereby approaching the effectiveness of a hermetic seal. The actuator housing also provides for the attachment of the stepper sensor and the limit sensors which limit the rotation to 256 degrees. The stepper sensor is mounted on the output shaft of the stepper motor opposite the power takeoff. All electrical connections are made through a hermetically sealed connector. Lubrication is provided by a low vapor pressure grease, G300. The structure that provides for mounting of the rotary actuator is a triangular shaped box section of varying thickness which transfers the antenna loads to the upper and lower trunnions through the ball bearings that provide for antennas deployment as discussed earlier.

3.4 SUPPORT STRUCTURE

The support structure shown in Figure 3-1 includes the vertical member providing attachment for the rotary actuator and the diagonal braces giving rigidity to the vertical member. The linear actuator also serves as part of the support structure .

Two diagonal members or supports extend from the spacecraft structure to the ends of the structural members in the solar array and provide the mounting structure for the lower trunnion. The support ties provide a rigid support for the lower support structure. However, the lower trunnion which is connected to this support by means of two 3/4-inch Bendix Flexure pivots does not maintain this rigidity. This loss in rigidity is counteracted by one additional diagonal member extending from the solar array structure to the upper trunnion, so that both the upper and lower trunnions are supported by rigid members at two points. Flexure pivots are used in order to eliminate the need for lubrication.

The diagonal extending from the solar array to the upper trunnion is required to move when the antenna is rotated around its "A" axis. To allow this movement, the diagonal member is equipped at each end with a self-aligning spherical bearing made of "DU-material" (lead Teflon in a porous bronze). No lubricant is required under the conditions expected on the Voyager.

4.0 INTERFACE DEFINITION

Power will be carried through flexible leads between the antenna gimbaling mechanisms and the spacecraft. Provisions are made to support the flexible leads in such a manner as to prevent bending stress from reducing the expected life of the leads. RF current is carried by a one-half inch diameter co-axial cable. This cable requires the use of a hermetically sealed coax connector to allow the cable to pass through the "B" axis of the rotating mechanism. The small degree of bending required of the co-axial cable to allow for the rotation about the "A" axis can be tolerated without flexible or rotary joints.

5.0 PERFORMANCE PARAMETERS

For proper orientation of the antenna, it is necessary that the rate of motion be compatible with the antenna control system. The rate of control is as follows:

<u>Angle</u>	<u>Motion-degrees</u>	<u>Rate</u>
A	-25° to +15°	0.25°/sec.
B	-50° to +206°	0.25°/sec.

The high gain antenna is capable of pointing to the earth for the useful life of the spacecraft. The minimum correction angle is 0.25 degrees with a maximum incorrect angle of 0.125 degrees around the A and B axis.

The high gain antenna will be deployed following separation of the spacecraft from the launch vehicle and will operate during all maneuvers, the transit period after reaching 15 million km from earth, and the entire orbital period. The deployment system and the operational gimbal system reliability are shown in simplified block diagrams in Figure 5-1 and 5-2.

Mathematical Model and Reliability Computation

The mathematical model for the high gain antenna positioning system during any mission phase is:

$$R_{(HGA)} = R_{\text{Deployment System}} \cdot R_{\text{Gimbal A}} \cdot R_{\text{Gimbal B}}$$

The mathematical model for deployment is:

$$R_{(\text{Deployment})} = R_1 \cdot R_2 \cdot R_3 \cdot (R_4)^5 \cdot (R_5)^4$$

where the above subscripts refer to the component numbers assigned to each of the components as indicated below. Substituting the proper reliability values tabulated for each component into the mathematical model results in the following reliability:

$$R_{\text{High Gain Antenna}} = 0.99868$$

HIGH GAIN ANTENNA DEPLOYMENT SYSTEM

<u>Components</u>	<u>Quantity</u>
1 pin puller	1
2 Spring	1
3 Damper	1
4 Bearings	5
5 Gears	4

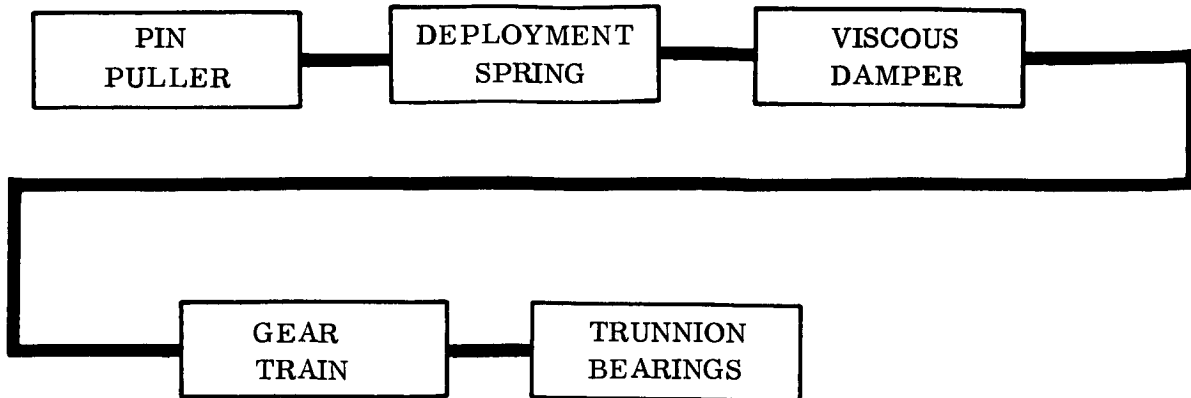


Figure 5-1. High Gain Antenna Deployment System Block Diagram

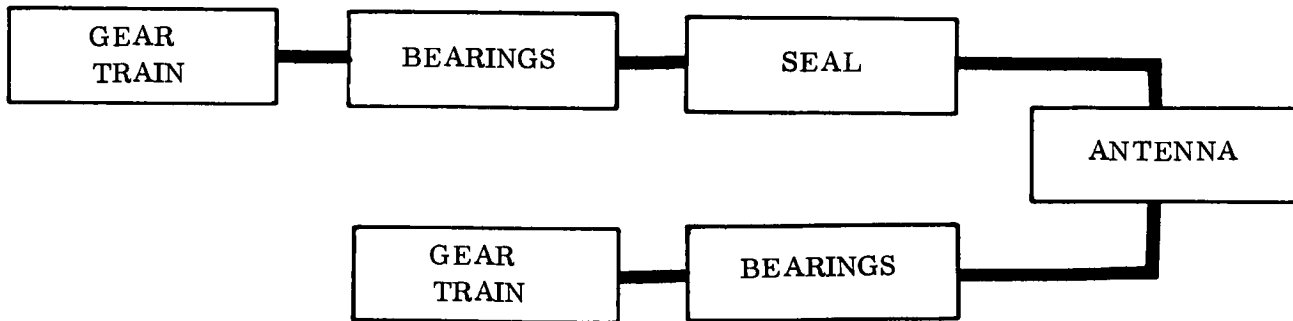


Figure 5-2. High Gain Antenna Operational Gimbal System Block Diagram

HIGH GAIN ANTENNA OPERATIONAL SYSTEM

<u>Components</u>	<u>Quantity</u>	<u>(% per 1000 hrs.)</u>
6 Gear	8	.001
7 Bearings	6	.002
8 { Seal ("A")	1	.070
Seal ("B")	1	.030

7.0 PHYSICAL CHARACTERISTICS

The weight of the antenna deployment and gimbal mechanism is 22.9 pounds.


8.0 SAFETY CONSIDERATION

The viscous damper controls the rate of deployment at all times and prevents damage to equipment and personnel in case of inadvertent deployment during test.

All springs are suitably protected so that they cannot be inadvertently released.

CII-VB235FD110

APPROVED:


Ryan Engineering

SUBSYSTEM LEVEL FUNCTIONAL
REQUIREMENTS
ENGINEERING MECHANICS
SOLAR ARRAY STRUCTURE

Index

- 1 Scope
- 2 Applicable Documents
- 3 Description of Solar Array
- 4 Interfaces
- 5 Performance Parameters
- 6 Constraints

Prepared by Ryan Aeronautical Company
for
General Electric Missile and Space Division

1.0 SCOPE

This document describes the mechanical and functional characteristics of the preferred design configuration of the 1971 Flight Spacecraft Solar Array Structure. The solar panels provide 197 square feet of effective area for mounting photovoltaic solar cells which furnish the primary electrical power for the over-all Spacecraft System.

2.0 APPLICABLE DOCUMENTS

The following documents apply to this description

VB220SR101	Design Characteristics
VB220SR102	Design Restraints
VB235FD103	Spacecraft Design Criteria
VB220FD113	Layout and Configuration

3.0 DESCRIPTION OF SOLAR ARRAY

3.1 GENERAL

The electrical power for the spacecraft is provided by an array of solar cells mounted on 22 geometrically identical panels. These panels are arranged in 15 degree segments around the bus with a space of 30 degrees (2 panels) left clear for mounting a fixed antenna. Fixed panels are supported by tapered spars extending radially outboard from the spacecraft interface. One fold-out panel is employed to compensate for solar pressure on the high gain antenna and does not require solar cells.

3.2 STRUCTURE

Trapezoidally shaped panels of honeycomb construction are used on both fixed and foldout panels. Details of construction for foldout and fixed panels and also support spar structure are included in this section. The fixed panel is securely held along two sides at all times in contrast to the foldout panel which must survive a 1.13 g (0-peak) retro-rocket excitation vibration load when extended and supported by two corners only. The balance of many factors such as temperature drop, fabrication problems, interchangeability, cost, etc. were, of course, all used in the selection of panel structure. These will be explored in detail in Volume VB235AA110.

3.2.1 FIXED PANELS (Figure 3-1)

Length along Centerline	55.88 in.
Width at Wide End	30.38 in.
Width at Narrow End	15.67 in.
Panel Thickness	0.50 in.
Included Angle	15 ⁰

The core selected for the panel is 3/16 inch Hex aluminum honeycomb (vented) with a density of 1.6 lb/ft³. The cell side of the panel is fabricated from two layers of fiberglass cloth which sandwich a thin layer of expanded silver mesh used for cancellation of magnetic fields. (Inner skin 1 ply 0.0055 thick #1557 fiberglass-epoxy sheet, 0.002 silver mesh; outer skin 1 ply 0.002 thick #108 fiberglass-epoxy sheet.) This composite skin is bonded to the honeycomb core using a film type adhesive (FM-1000). The same adhesive is used for attaching the skin to the opposite core face (back skin). This back skin is fabricated from 1 ply 0.0055 thick #1557 fiberglass-epoxy sheet, since there is no requirement for expanded mesh on this side.

All panel edges are enclosed by 0.012 aluminum channels 1/2 x 0.16 inch. The legs of the channels extend outward to enable tooling to locate and support the channels during pressure curing. Machined aluminum fittings are bonded inside the structure to react the loads at attachment points and to spread these loads to the core and skins.

The top fiberglass layer of the front skin is cut out in a pattern at the end of each cell group to allow electrical connection to the imbedded mesh layer mentioned previously. Electrical feed-through terminals are provided as required along one side of the panel for transfer of electrical power from the cell side to a wire harness which connects the various cell groups and routes the power to the spacecraft. Six terminals are provided at the small end of the panel for conveyance of harness termination and blocking diode provisions. A bracket to support a connector plug is also provided. A doubler with threaded inserts is mounted on the back of the panel to accommodate a diode package. No mounting provisions for additional equipment or device are anticipated at this time, but additional mount plates, clips, doublers, etc. could be easily incorporated if required.

Breather holes 3/16 inch in diameter are spaced at 4-inch intervals through all edge closure channels. This provision is expected to allow for pressure changes to be encountered. Additional holes may be added to the back skin if tests indicate a need.

3.2.2 FOLD-OUT PANEL (Figure 3-1)

The basic geometry of the foldout panel is similar to the fixed panels. The core remains unchanged as do the closeout channels. Aluminum alloy skins are used in place of the fiberglass skins because of the difference in the method of support during the time of critical load. The skins (both sides) are fabricated from 0.0041 aluminum alloy.

Mounting differences require a change in the internal spacer fittings. The general type of fitting is the same, but the detail parts change in the area of the hinge and latch fittings to provide additional attach holes and to spread the load more effectively.

3.2.3 SUPPORT STRUCTURE (Figure 3-2)

The 22 fixed panels as well as the foldout panel are supported by tapered spar sections 63 inches in length, 11.3-inch deep at the root and tapering to 1.25 inch at the tip. The basic construction is an 0.016 sheet metal web containing various size lightening holes and

web stiffening angles. The top and bottom caps of the spar are extruded "T" sections 1-1/2" in width. The bottom "T" section mounts the nut plates for attaching fixed panels. The top cap supports the damper pads and panel latch which, in turn, support the foldout panel. The inboard end of the spar contains a hole pattern for attachment to the spacecraft. The outboard end contains a hole pattern for attaching the hinge fittings and cruise dampers. No provisions are shown at present for auxiliary equipment mounting to spars, but the structure is readily adaptable to this eventuality.

3.3 DEPLOYMENT SYSTEM (Reference 8)

The foldout panel is attached by two hinge brackets at the wide end. This arrangement allows the panel to swing outboard approximately 180 degrees to the deployed position. The force which causes this movement is provided by two torsion springs (one at each hinge attachment). The springs are similar in design to those used on Mariner C, however the spring rate is lower because of a lower mass moment of inertia about the hinge line.

The panel is secured in the stowed position by explosive pin puller latches. An electrical impulse to the latches detonates the explosive and pulls a pin from two brackets mounted at each side of the foldout panel. This action allows the torsion springs to rotate the panel to the deployed position.

A damper at the tip of each of the two tapered spars which support the foldout panel absorbs the energy at the end of the travel and also latches the panel in the deployed position. These dampers are capable of reacting loads in two directions and, therefore, are used as cruise dampers to provide damping for load inputs during midcourse corrections. The dampers will "bottom out" to react retro-rocket loads.

4.0 INTERFACES

4.1 GENERAL

The major interface areas for solar array attachment to spacecraft are as follows: A machined ring will provide the attach flange for the panel support spar lower cap attachment. A structural bulkhead frame approximately 11.5 inches from the base ring provides a surface for attaching the top cap of the spar. The sheet metal cone connecting these two rings is used for attaching the web of the spar.

Maximum solar array deflection is in the longitudinal direction with reference to spacecraft centerline. Since deflection is small, the total dynamic envelope was used for array design.

4.1.1 STRUCTURE

The support for the solar panels is provided by the tapered spars previously described. These spars carry the load induced by the solar panels. The alternating tension and compression spar cap loads are transferred to the spacecraft frames by the use of 3/16-

inch diameter bolts in shear at the bottom cap and in tension at the top cap. Spar shear loads are taken out by an angle stiffener bolted to spacecraft stringers.

4.1.2 ELECTRICAL

The electrical power is routed from the individual panels to the spacecraft by wire harnesses. Mounting brackets for connector plugs are provided on each panel for termination of panel wiring and connection of harnesses.

4.1.3 DEPLOYMENT

The outer tip of the panel support spar provides for attaching a hinge fitting for mounting adjacent corners of two panels. The foldout panel is mounted in this location by simply inserting a 5/16-inch bolt at each corner and tightening a lock nut. The panel latch is mounted on the top cap of the spar approximately at 2/3 of the panel length inboard. This latch assembly is designed to slide outboard to allow the foldout panel latch brackets to move into a clevis. The latch is then moved inboard to lock the brackets in place and is secured by an Allen screw thus restricting latch movement. The latch pin at this point is loaded in double shear to react rubber damper preload forces and panel dynamic loads.

5.0 PERFORMANCE PARAMETERS

The solar array has been designed to survive the various environmental conditions encountered from fabrication to mission orbit. Simplicity in the design of assemblies, deployment system and installation of all components was a major goal in the creation of a design which would be highly reliable in fulfilling the various performance parameters.

5.1 DESIGN CRITERIA

Design criteria are given in Reference Volume VB235FD103.

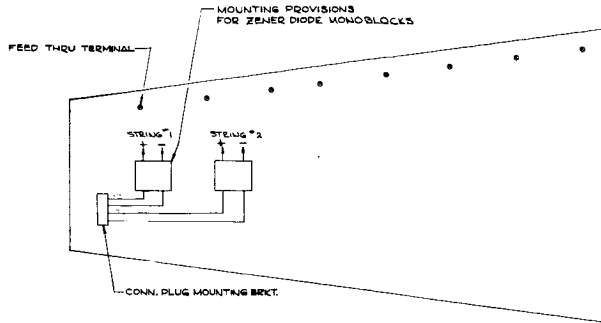
5.2 DEPLOYMENT SYSTEM (Figure 3-2)

The basic requirement of the deployment system is to extend the foldout panel to the deployed position at a rate acceptable to the structure and stabilization system. This problem is resolved by mounting a torsion spring at each hinge axis to provide the moving force. One spring will provide this movement, however, complete redundancy is provided by having two springs. The two other basic elements of this system are: (1) A latch to restrain the panel during boost and release it at the proper time, (2) a damper to absorb the energy at the end of travel and provide damping during maneuvers.

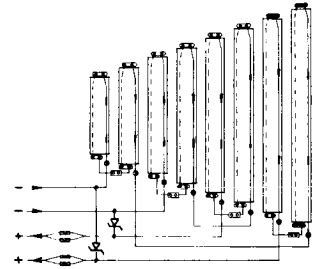
The requirement for extending the panel in a specified time lapse is not critical if the system fulfills its other requirements. The approximate time for deployment is estimated to be six seconds. This rate may fall within a range of 10 degrees/sec. to 40 degrees/sec., depending on the final design and if one or two springs are used, i. e., the system must function acceptably with either one or two springs if the redundancy is to be demonstrated.

6.0 CONSTRAINTS

1. The solar panel dynamic envelope is given in Section VB220FD113.
2. Overall panel flatness to be within ± 0.06 . Local depressions should not exceed ± 0.010 within an area of one square inch. (See Reference 7.)
3. Array location with respect to the spacecraft booster interface is given in Section VB220FD113. Dynamic excitation levels at the solar array support are affected by the location and any deviation would change solar panel design loads.
4. Solar array weight shall be minimum compatible with intended mission design requirements.

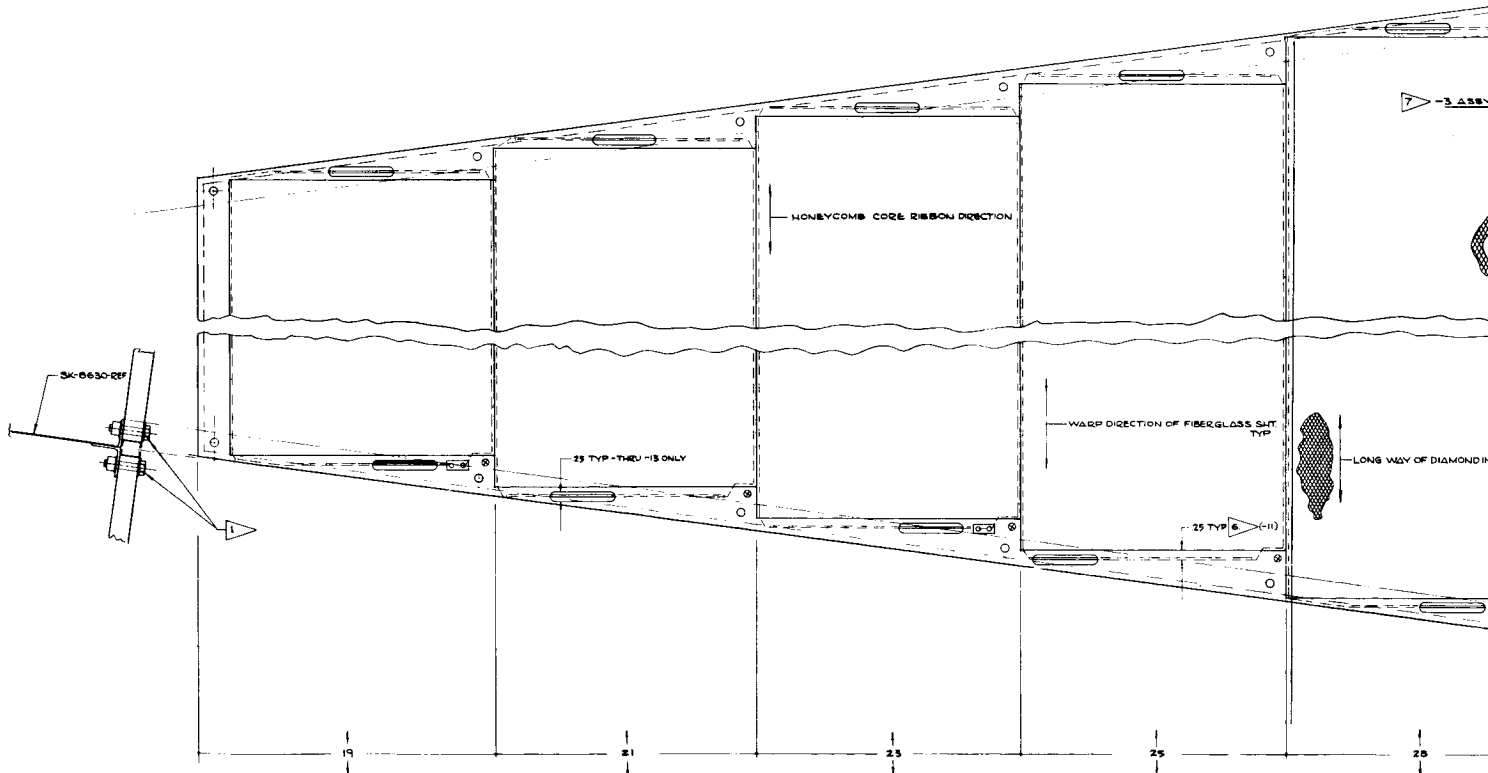


VIEW OF BACK SIDE OF PANEL SHOWING ELECTRICAL PROVISIONS
SCALE: NONE



ELECTRICAL SCHEMATIC

LEG
 ⊗ FE
 ⊙ ME
 ⊕ CE
 ⊖ BU
 ⊚ ZE

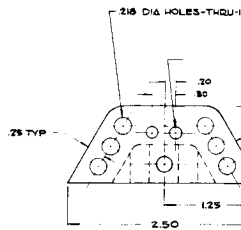


VIEW OF FRONT FACE OF PANEL SHOWING CELL LAYOUT & ELECTRICAL
SCALE: 1/4"

80

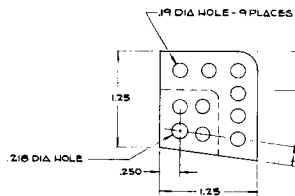
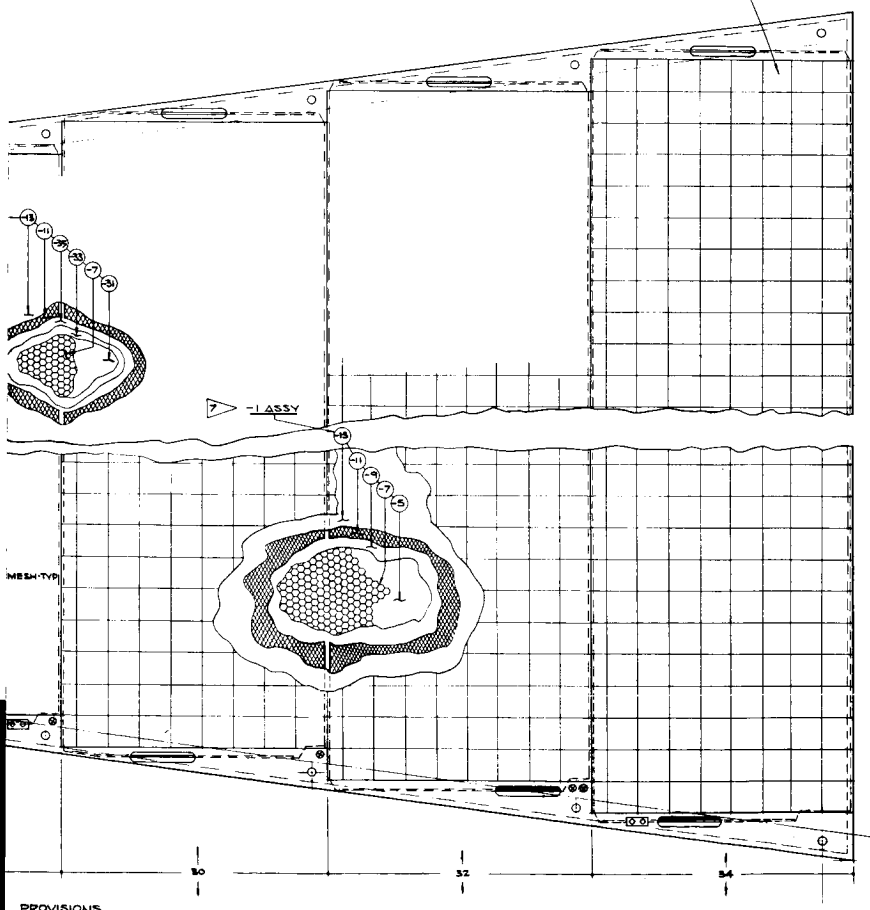
END
 ID THRU TERMINAL
 M CONN. BLOCK
 L ATTACH TO MESH
 KUNG DIODE
 R REGULATOR

34	30
32	28
21	25
18	23
106	106

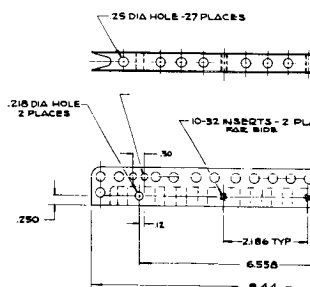


DETAIL OF -25 F
 SCALE 2/1

SOLAR CELLS SHOWN FOR REFERENCE

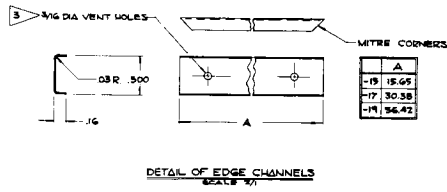
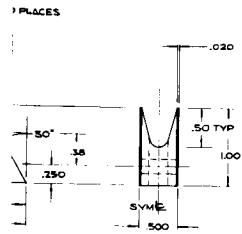


DETAIL OF -25 F
 SCALE 2/1

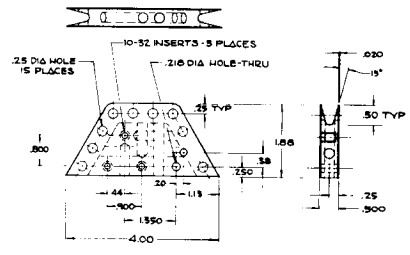
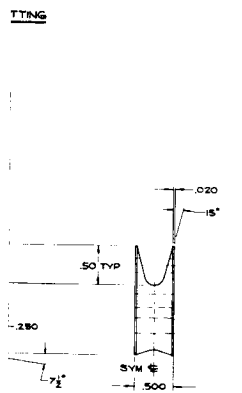


DETAIL OF -27 F
 SCALE 1/1

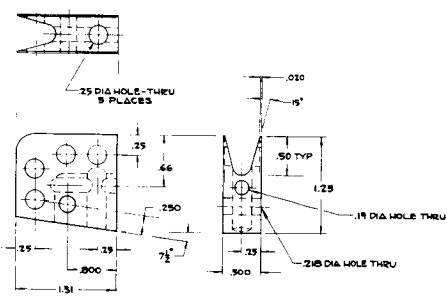
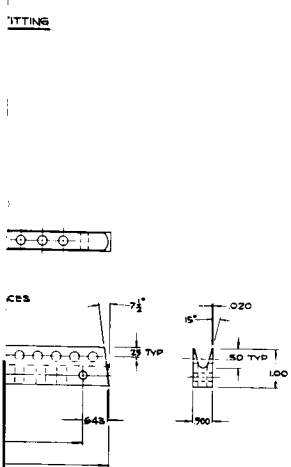
82



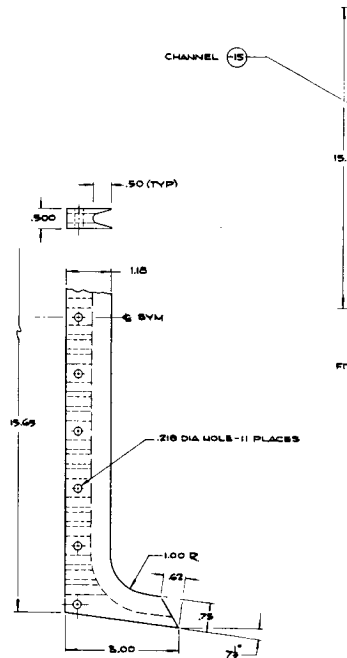
DETAIL OF EDGE CHANNELS
SCALE 1/1



DETAIL OF -29 FITTING - 80 OPP
SCALE 1/1

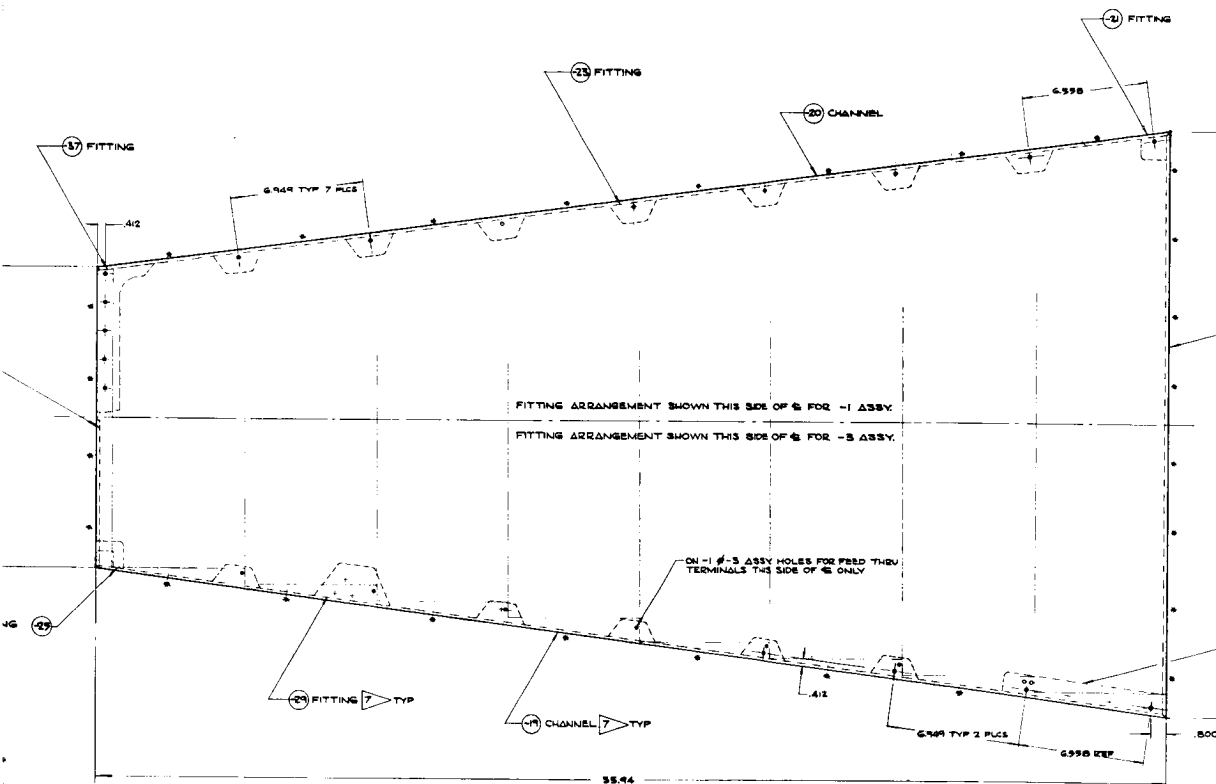


DETAIL OF -21 FITTING
SCALE 1/1



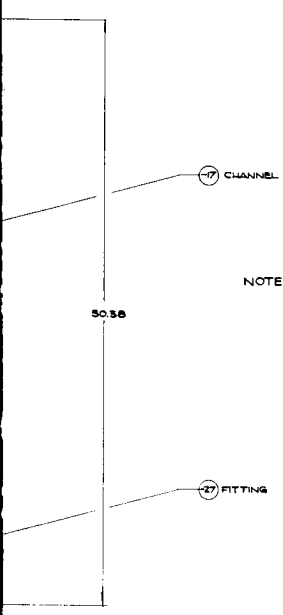
DETAIL OF -37 FITTING
SCALE 1/1

83



PLAN VIEW - CELL SIDE

84



NOTES:

- 1 PANEL ASSEMBLY ATTACH HOLE PATTERN TO BE INTER-CHANGEABLE ON -1 AND -3 ASSY
- 2 OVERALL PANEL FLATNESS TO BE WITHIN ± .06-LOCAL DEPRESSIONS SHOULD NOT EXCEED ±.010 WITHIN AN AREA 1" x 1"
- 3 LOCATE 3/16 DIA VENT HOLES AT LOCATIONS MARKED *
- 4 PANEL SIDE OPPOSITE CELLS TO RECEIVE AN EMISSIVITY COATING .0012 TO .0025 THICK USING A-4823 WHITE PAINT-COLOR NO SA-9185 (ANDREW BROWN OR EQUIV)
- 5 SHEET TOLERANCE +.0005/- .0000

FIGURE 110-3-1

QTY REQD PER ASSY	PART NUMBER	DESCRIPTION	STOCK SIZE	MATERIAL	SPECIFICATION	FINISH	REF TO CODE
1	-37	FITTING		AL ALY-7075-T6			
1	-38	SKIN		AL ALY-2024-T8-0041			
1	-31	SKIN		AL ALY-2024-T8-0041			
1	-29	FITTING		AL ALY-7075-T6			
2	-27	FITTING					
2	-29	FITTING					
7	-28	FITTING					
2	-21	FITTING		AL ALY-7075-T6			
1	-19	CHANNEL		AL ALY-2024-T8-012			
1	-17	CHANNEL					
1	-19	CHANNEL		AL ALY-2024-T8-012			
1	-1	SKIN		FIBERGLASS EPOXY SHEET ONE PLY STYLE 1557-0095			
1	-7	CORE		ALUMINUM HONEYCOMB CORE HEATED 800 THICK 159713-516 REC-0009 EOL			
1	-5	SKIN		FIBERGLASS EPOXY SHEET ONE PLY STYLE 1557-0095			
-	-3	ASSY - DEPLOYABLE PANEL					
-	-1	ASSY - FIXED PANEL					

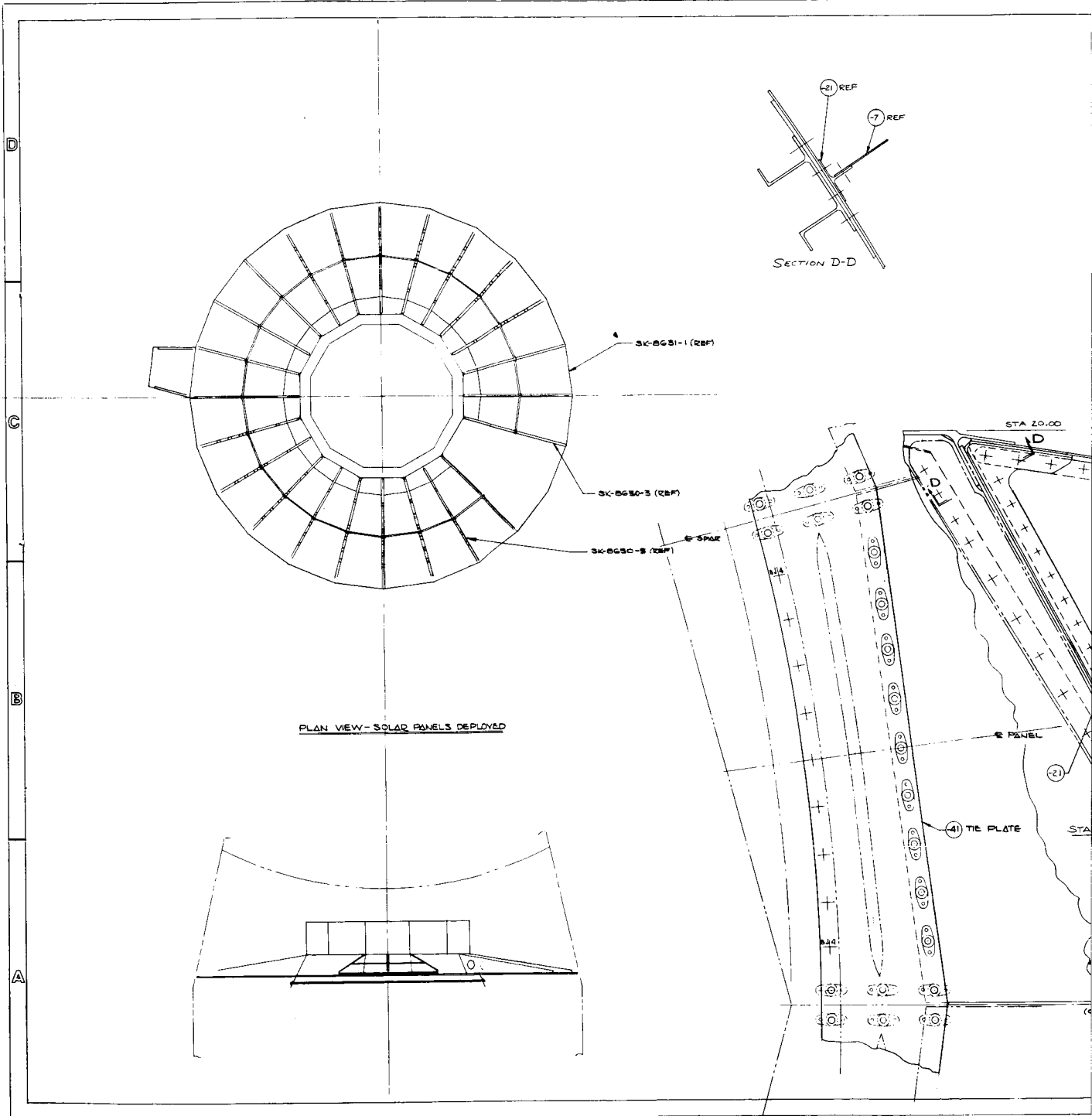
RELEASE & DATE	QTY REQD PER ASSY	PART NUMBER	DESCRIPTION	STOCK SIZE	MATERIAL	SPECIFICATION	FINISH	REF TO CODE

UNLESS OTHERWISE SPECIFIED		CONTRACT NUMBER	REV A
DIMENSIONS ARE IN INCHES AND INCLUDE DIM APPLIED ON PLATED PARTS			
TOLERANCES	DATE	DESIGNED BY	DATE
LINEAR	ANGULAR	BY	DATE
± .010	± .005	CHKD	DATE
± .005	± .002	APP'D	DATE
± .002	± .001	DR	DATE
± .001	± .0005	DESIGNED BY	DATE
± .0005	± .0002	CHKD	DATE
± .0002	± .0001	APP'D	DATE
± .0001	± .00005	DR	DATE

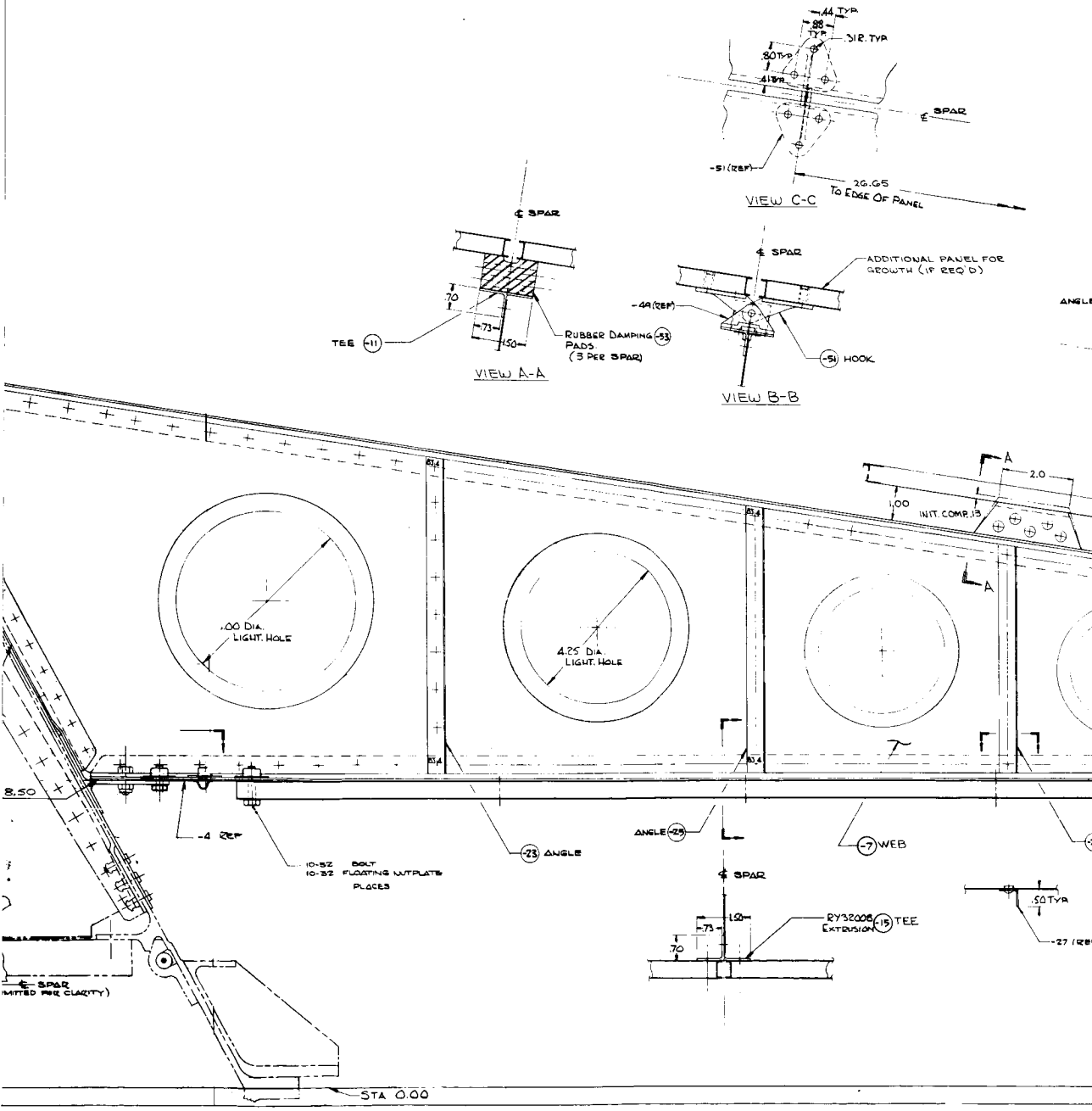
PARTS TO BE FREE OF BURS AND SHARP EDGES		DESIGN ACTIVITY APPROVAL	SIZE
MANUFACTURING RESIDUE REMOVE PER FIG 5B1		DESIGN APPROVAL	TORQUE REQD PER DRAWING
STANDARDS INCLUDE:			78022
PRN ASSY: M07 ASSY	NEST USED ON		SK-8631
QTY REQUIRED	APPLICATION		SCALE: 1" = 1" WEIGHT

Figure 3-1. Solar Panel Assembly

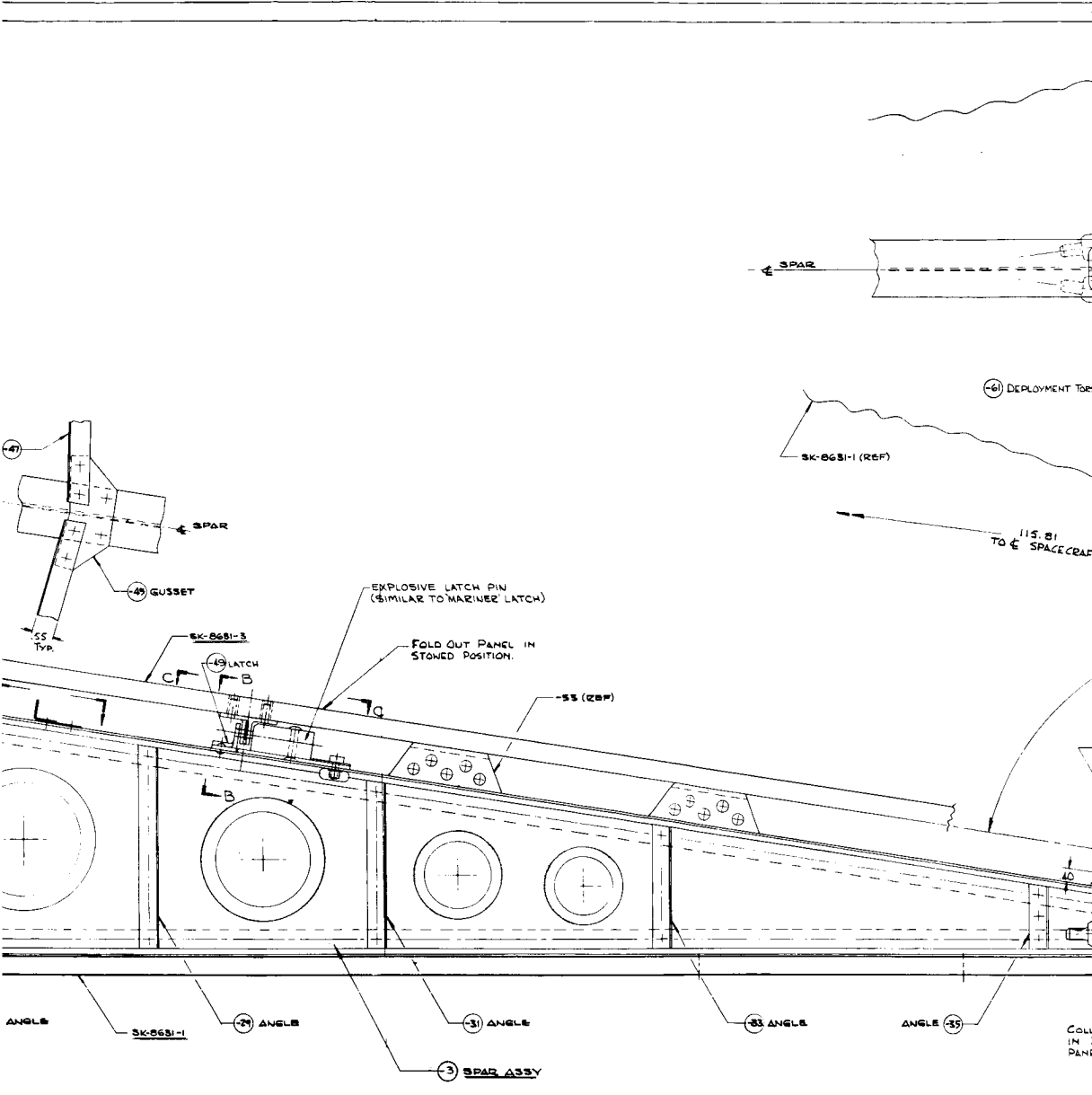




10①

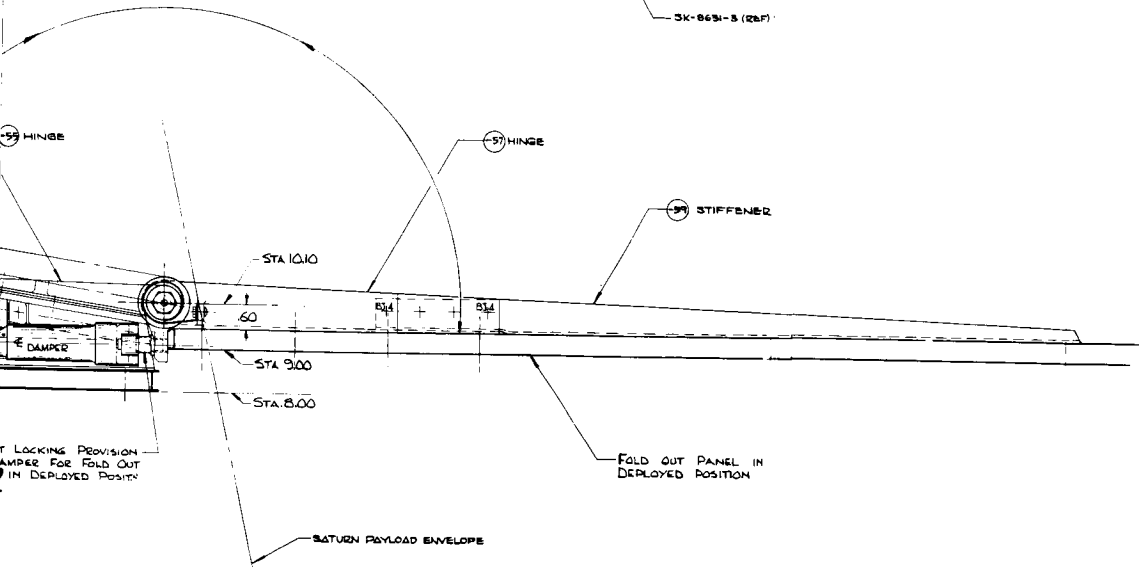
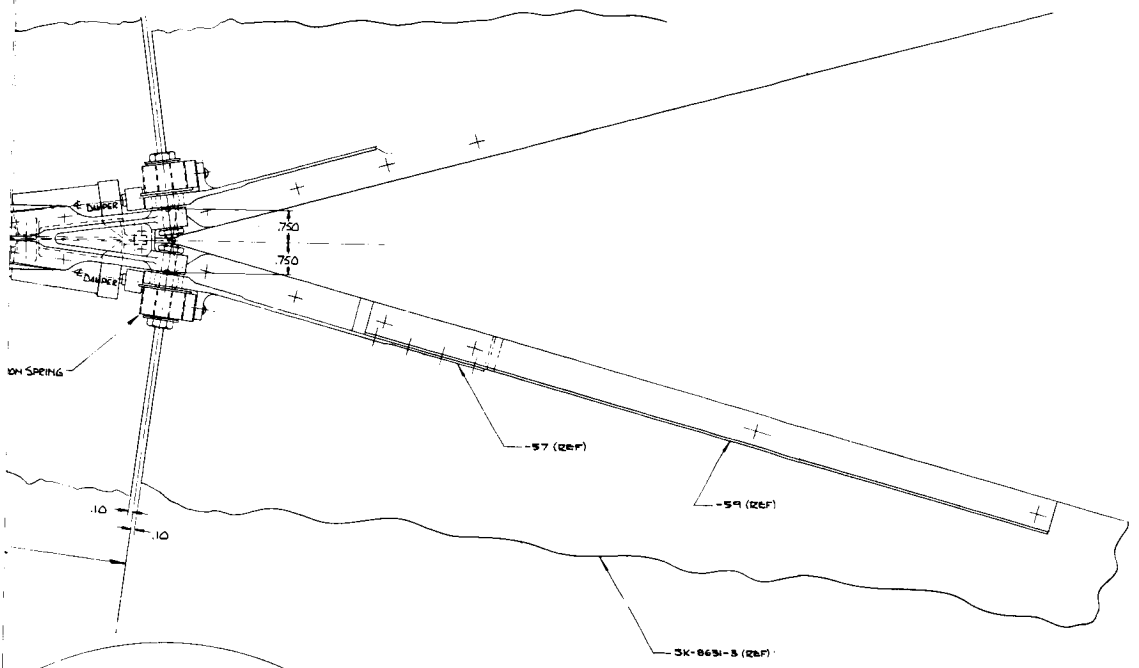


10(2)



(-1) SOLAR PANEL INSTALLATION

10 (B)



AT LOCKING PROVISION
 DAMPER FOR FOLD OUT
 IN DEPLOYED POSITION

10 (4)

2		1											
		REVISIONS											
		LIT	EFF. ON	DESCRIPTION	DATE APPROVED								
12	SK-8631-3	DEPLOYABLE PANEL											
21	SK-8631-1	FIXED PANEL											
378	10-32	BOLT											
18484	10-32	NUTPLATE FLOATING-NON MAGNETIC											
14		EXPLOSIVE LATCH (SIMILAR TO 410-0314-2-MARINER B)											
24		DAMPER ASSY (SIMILAR TO 410-160-MARINER C)											
24	-G1	TORSION SPRING ASSY (SIMILAR TO 410-1700-MARINER C)											
12	-60	-58	STIFFENER								AL ALY	D60	2024-T3
12	-58	-57	HINGE								AL ALY		2024-T3
14	-55		HINGE								AL ALY		2024-T3
G	-53		PAD								RUBBER		
24	-51		HOOK								AL ALY		2024-T3
14	-49		LATCH								AL ALY		2024-T3
21	-47		ANGLE								AL ALY	040	2024-T3
11	-45		GUSSET								AL ALY	040	2024-T3
11	-35		ANGLE										
11	-33												
11	-31												
11	-29										AL ALY 032		2024-T3
11	-27												
11	-25												
11	-23										AL ALY 040		2024-T3
11	-21		ANGLE								AL ALY 040		2024-T3
11	-19		TEE								MAKE FROM AL ALY EXTRUSION-2024 BY 51008.T		
11	-11		TEE										
11	-7		WEB								AL ALY 020-2024-T3		
-11	-3		SPAR ASSY										
-	-1		INSTALLATION										

-5-3-1	COOK	PART NUMBER	DESCRIPTION	STOCK	MATERIAL	SPECIFICATION	RYAN	ITEM
QTY REQD	IDENT			SIZE			MATL CODE	NO
PER ASSY								

RELEASE & DATE		LIST OF MATERIAL	
	UNLESS OTHERWISE SPECIFIED DIMENSIONS ARE IN INCHES AND INCLUDE DIM APPLIED OR PLATED FINISHES	CONTRACT NUMBER	RYAN A N RYAN AERONAUTICAL COMPANY SAN DIEGO, CALIFORNIA 92112
	TOLERANCES		
	LINEAR .010 ANGULAR .010		
	X .1 (EXCL OF SHEET METAL)		
	XX .005 (EXCL OF SHEET METAL)		
	XXX .002 (EXCL OF SHEET METAL)		
	JOCK .010 (EXCL OF SHEET METAL)		
	PARTS TO BE FREE OF BURRS AND SHARP EDGES MANUFACTURING REQUIRE- MENTS PER RYAN MFG STANDARD NO. 110.		
	DESIGN APPROVAL		
		DATE	COOK IDENT NO
		E 78022	SK-8630
		SCALE	REV
			SYM

VB235 FD110

FIGURE 3-2

Figure 3-2. Solar Panel Installation

5

CII-VB235FD110

VOLUME A
SUBSYSTEM LEVEL FUNCTIONAL
REQUIREMENTS
APPENDIX I

Index

- 1 Stress Analysis
- 2 Weight Analysis
- 3 Dynamic Analysis
- 4 Thermal Analysis
- 5 List of References

This section contains supporting analysis for the selected concept. Analysis for the fold-out panel is based on a panel equivalent in size to the fixed panel. Justification of this approach is as follows: In the event that fold-out panels are required for additional solar cell mounting area it is desirable, for standardization of the solar cell arrangement, to use the same size established for the fixed panels. The analysis presented for the fold-out panel is considered conservative based on a more critically loaded, 55.9 inch long panel, rather than the shortened 40-inch panel required for this configuration.

1.0 STRESS ANALYSIS

Dynamic loads are treated as static loads in this analysis. Only critical loading conditions are considered for analysis. Elastic buckling of the solar cell mounting surface is considered a design ultimate to prevent loading the solar cells.

$$\text{Yield Design Loads} = 1.15 \times \text{Limit}$$

$$\text{Ult Design Loads} = 1.25 \times \text{Limit}$$

1.1 FIXED PANEL-TRANSVERSE VIBRATION MODE

Figures 3-2 through 3-5 (Volume VB235AA110) show that the lightest substrate configuration results using honeycomb core with fiberglass skins. Critical load conditions occur during launch if the solar panel substrate is excited at its natural vibration frequency. Temperature levels are at room temperature.

Analysis presented is conservative when noting that the attachment of the substrate to the longitudinal spars provides a small amount of moment restraint which has been neglected. The effect is to increase the indicated natural frequency (36 cps for a section with 0.5-inch thick honeycomb core) and decrease the dynamic amplification factor. An amplification factor of 16.7 at maximum deflection point based on a structural damping ratio of 0.03 and applied to the 3.2 g excitation level was used for determining the load distribution. A static 1 g load occurring simultaneously is insignificant and, therefore, neglected. The 0.5-inch thick section was selected to give a reasonable skin thickness for surface flatness. The substrate is designed based on the maximum transverse span, resulting in a slight conservatism as the panel width decreases.

From Figure 3-5 (Volume VB235AA110), cross section requirements for a section with 0.5 inch thick core (h) are:

$$\text{Substrate unit weight} = 0.226 \text{ lbs/ft}^2$$

$$I = 6.4 \times 10^{-4} \text{ in}^4/\text{in of cross section}$$

then,

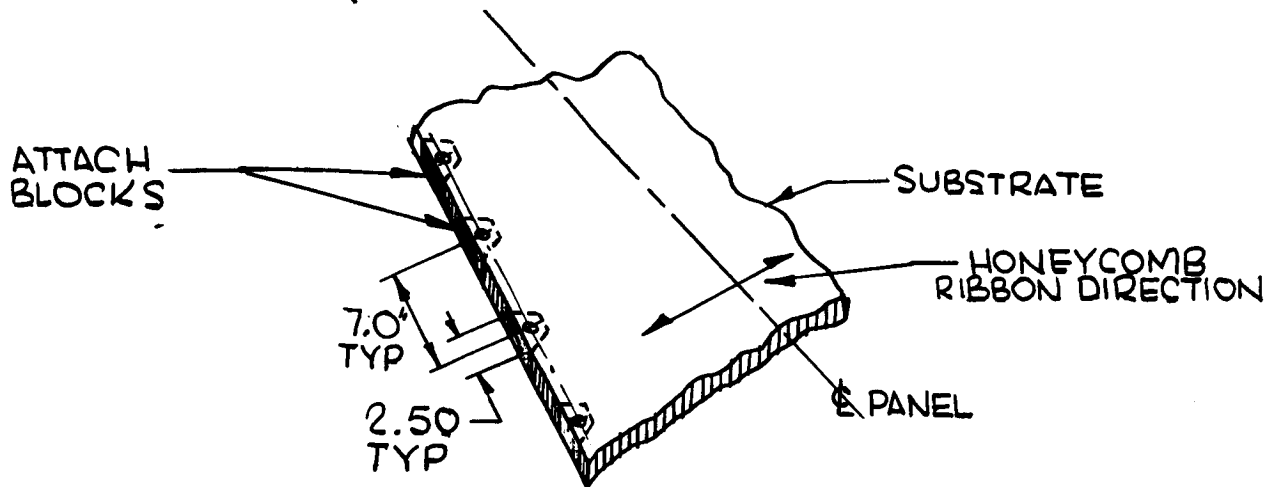
$$\text{Unit weight} = 133.33 \times 10^{-3} h + 288 t + (0.050 + 0.016)$$

$$t = \frac{\text{unit weight} - 133.33 \times 10^{-3} h - (0.050 + 0.016)}{288 \rho}$$

$$= \frac{0.226 - 133.33 \times 10^{-3} \times 0.5 - (0.050 + 0.016)}{288 \times 0.065} = \underline{\underline{0.005 \text{ in.}}}$$

let $t = 0.0055 \text{ in.}$ using one layer 1557 Epoxy impregnated glass cloth. (See Table 3-7, Volume VB235 AA110.)

Shear is transferred from the honeycomb core and skin-core adhesive into panel edge attach blocks into which the core is sandwiched and bonded.



Assuming the shear to be entirely concentrated at the attach blocks:

$$\text{Core shear} = 2.06 \times \left(\frac{7}{2.5 \times 0.5} \right) = 11.5 \text{ psi Ult.}$$

Core shear allowable (Ref. 9) = 56 psi Min.

M.S. HIGH

Skin-core Adhesive

$$\text{Shear} = \frac{(V) (Q)}{(I) \left(\frac{\text{shear}}{\text{area}} \right)} = \frac{\left(\frac{2.06 \times 7}{2.5} \right) (0.0055 \times 0.2528)}{(7.03 \times 10^{-4}) (0.00925)} = 1232 \text{ psi Ult.}$$

Adhesive shear allowable = 4000 psi for FM-1000 (0.025 lbs/ft²) at room temperature (Reference 10).

$$M.S. = \frac{4000}{1232} - 1 = \underline{\underline{+2.25}}$$

$$M = \frac{F_c \cdot I}{\left(\frac{h+t}{2}\right)}$$

$$F_c = 2 \cdot \frac{E_c}{(1-\mu^2)} \left(\frac{t}{s}\right)^2 = 2 \times \frac{5 \times 10^6}{1-0.25^2} \left(\frac{0.0055}{0.1875}\right)^2 = 9176 \text{ psi}$$

$$I = 2t \left(\frac{h+t}{2}\right)^2 = 2 \times 0.0055 \left(\frac{0.5+0.0055}{2}\right)^2 = 7.03 \times 10^{-4} \text{ in}^4/\text{in}$$

$$M = \frac{9176 \times 7.03 \times 10^{-4}}{\left(\frac{0.5+0.0055}{2}\right)} = 25.52 \text{ in-lbs/in}$$

$$m = \frac{1}{12} (\text{wg}) \ell^2$$

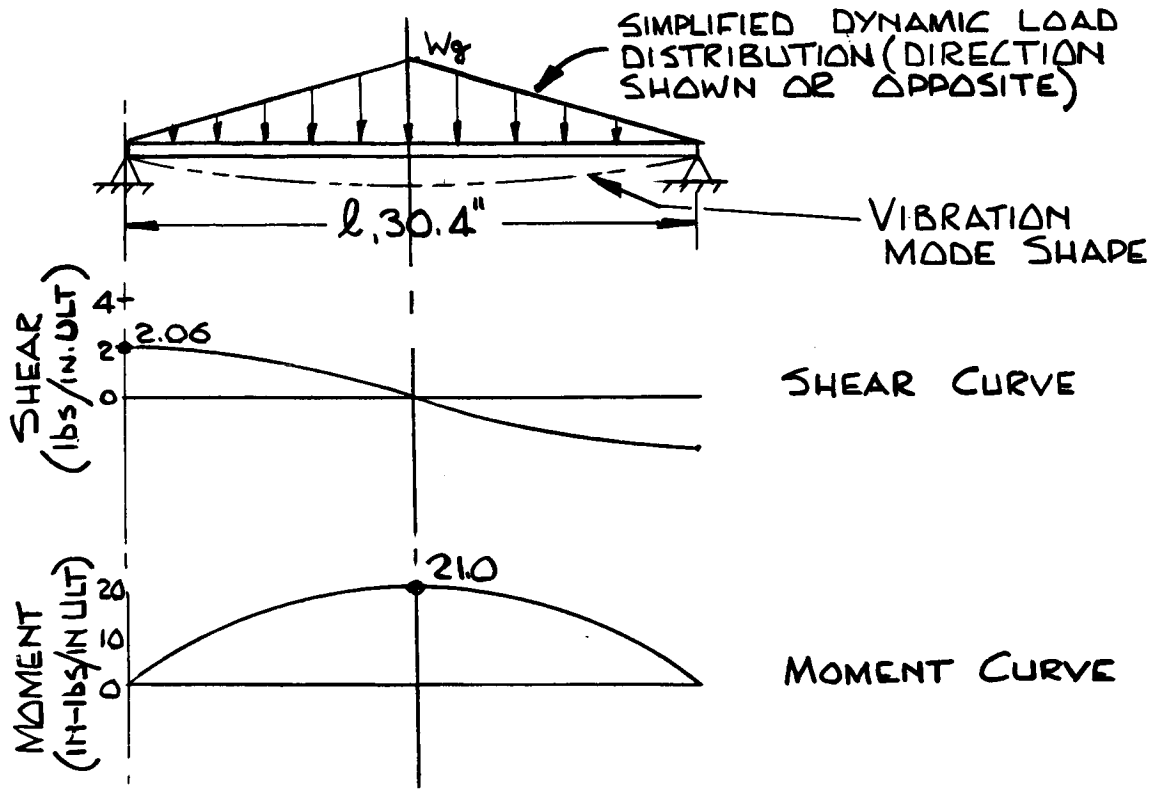
$$w = (\text{substrate}) + (\text{installed solar cell unit weights})$$

$$= (133.33 \times 10^{-3} \times 0.5 + 288 \times 0.065 \times 0.0055 + 0.050 + 0.016) + (0.34)$$

$$= 0.575 \text{ lbs/ft}^2 = 0.004 \text{ lbs/in}^2$$

$$m = \frac{1}{12} (0.004 \times 16.7 \times 1.6 \times 2 \times 1.25) 30.4^2 = 21.0 \text{ in-lbs/in. Ult.}$$

$$M.S. = \frac{M}{m} - 1 = \frac{25.52}{21.0} - 1 = \underline{\underline{+0.22}}$$



Maximum transverse panel deflection for sinusoidal vibration is calculated as:

$$\delta = \frac{386 (g)}{(2 \pi f_n)^2}$$

g = output acceleration
 f_n = natural frequency, cps
 δ = single amplitude, in.

$$\delta = \frac{386 (16.7 \times 1.6 \times 2)}{(2 \pi \times 36)^2} = \underline{\underline{0.4 \text{ in.}}}$$

1.2 FOLD-OUT SOLAR PANEL - TRANSFERSE VIBRATION MODE

Fiberglass is not considered for honeycomb skins due to its low modulus of elasticity normal to fiber warp, making the section incompatible with vibration loading conditions during retro-rocket firing. Figure 3-4 Volume VB235AA110 shows the following requirements for an aluminum skinned honeycomb section with 0.5 inch thick core. Design considerations are similar to that for the fixed panel.

$$\text{Substrate unit weight} = 0.28 \text{ lbs/ft}^2$$

then,

$$t = \frac{\text{unit weight} - 133.33 \times 10^{-3} h - 95 \times 10^{-3}}{288 \rho}$$

$$t = \frac{0.28 - 133.33 \times 10^{-3} \times 0.5 - 95 \times 10^{-3}}{288 \times 0.1} = \underline{\underline{0.0041 \text{ in.}}}$$

Bending in hinge areas

$$M = \frac{F_c \cdot I}{\left(\frac{h+t}{2}\right)}$$

$$I = 2t \left(\frac{h+t}{2}\right)^2 = 2 \times 0.0041 \left(\frac{0.5+0.0041}{2}\right)^2 = 5.21 \times 10^{-4} \text{ in}^4/\text{in}$$

$$F_c = 2 \cdot \frac{E_c}{(1-\mu^2)} \left(\frac{t}{s}\right)^2 = 2 \times \frac{10 \times 10^6}{(1-0.32^2)} \left(\frac{0.0041}{0.1875}\right)^2 = 10647 \text{ psi}$$

$$M = \frac{10647 \times 5.21 \times 10^{-4}}{\left(\frac{0.5+0.0041}{2}\right)} = 22 \text{ in-lbs/in}$$

$$m = \frac{1}{12} (\text{wg}) \ell^2$$

$$w = (\text{substrate}) + (\text{installed solar cell unit weights})$$

$$w = (0.28) + (0.34) = 0.62 \text{ lbs/ft}^2 = 0.0043 \text{ lbs/in}^2$$

$$m = \frac{1}{12} (0.0043 \times 16.7 \times 1.6 \times 2 \times 1.25) 30.4^2 = 22 \text{ in-lbs/in Ult.}$$

M.S. 0

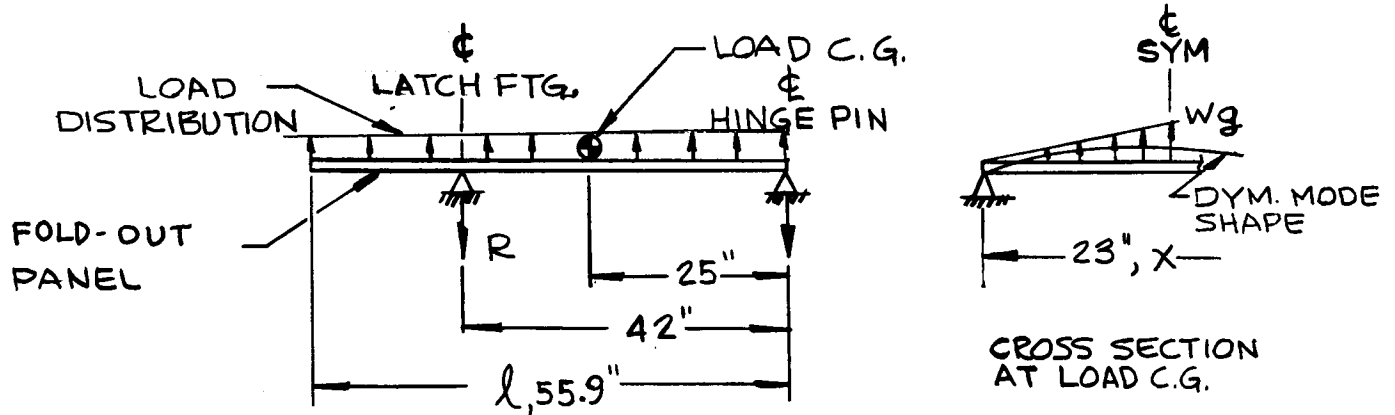
Maximum transverse panel deflection for sinusoidal vibration is calculated as:

$$\delta = \frac{386 (g)}{(2\pi f_n)^2}$$

g = output acceleration
 f_n = natural frequency, cps
 δ = single amplitude, in.

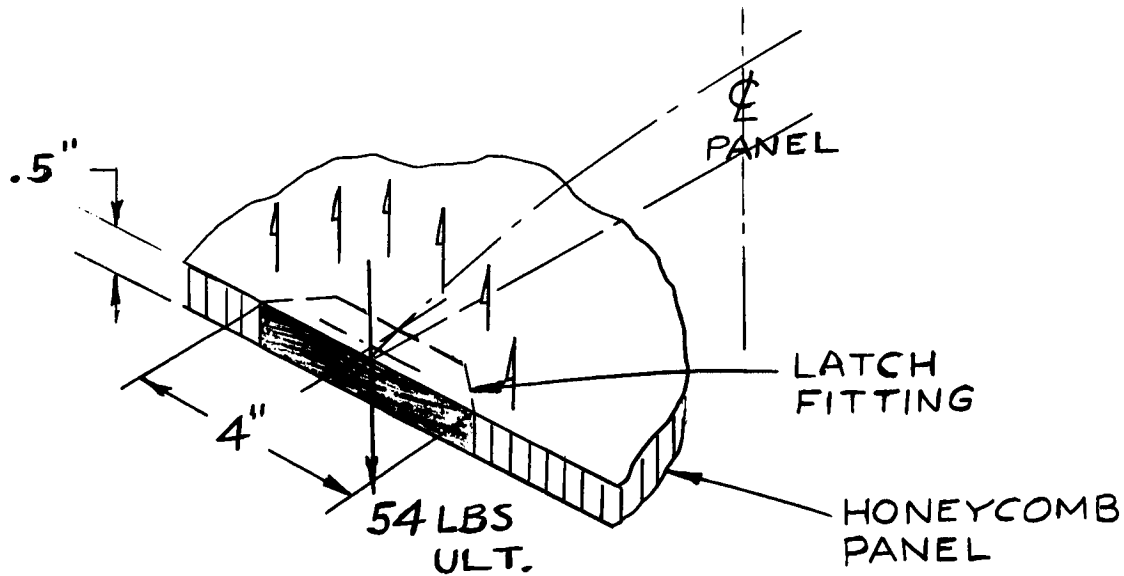
$$\delta = \frac{386 (16.7 \times 1.6 \times 2)}{(2\pi \times 38)^2} = \underline{\underline{0.36 \text{ in.}}}$$

Shear Concentration at Latch Fitting —



$$R = (wg) \frac{x}{4} \cdot l \left(\frac{25}{42} \right) = (0.0043 \times 16.7 \times 1.6 \times 2 \times 1.25) \times \frac{23}{4} \times 55.9 \left(\frac{25}{42} \right)$$

$$R = \underline{\underline{54 \text{ lbs Ult.}}}$$



Skin-Core Adhesive

$$\text{Shear} = \frac{(V) (Q)}{(I) \left(\frac{\text{shear}}{\text{area}} \right)}$$

$$V = \frac{54}{4} = 13.5 \text{ lbs/in Ult.}$$

$$\text{Adhesive shear} = \frac{(13.5) (0.0041 \times 0.252)}{(5.2 \times 10^{-4}) (0.00925)} = 2897 \text{ psi Ult.}$$

Adhesive shear allow. = 4000 psi for FM-1000 (0.025 lbs/ft²) at room temperature (Reference 10)

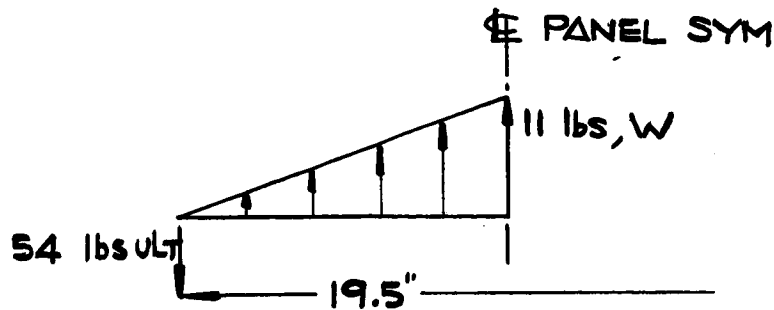
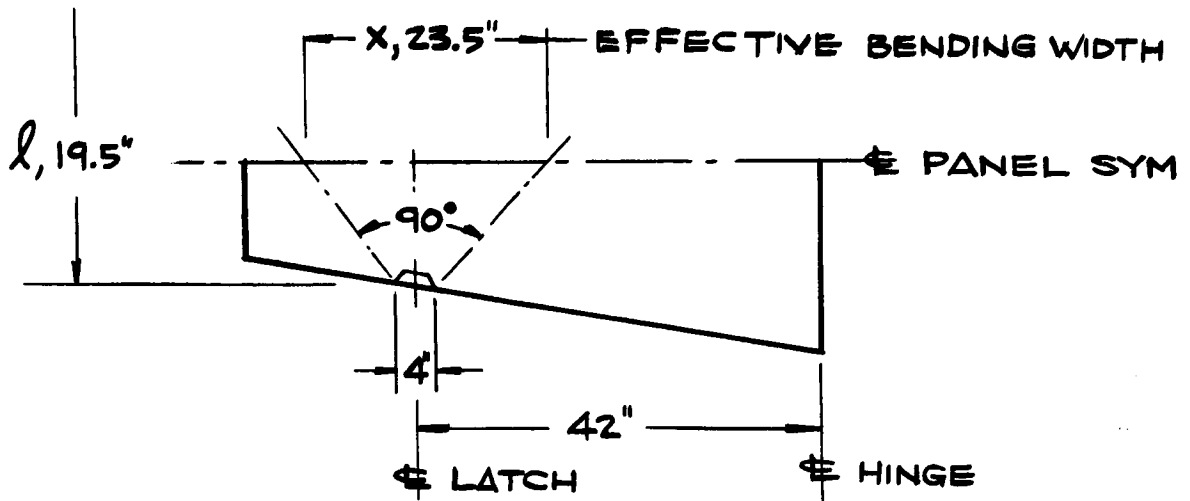
$$\text{M.S.} = \frac{4000}{2897} - 1 = \underline{\underline{+0.38}}$$

$$\text{Core shear, } V = \frac{R}{\text{Area}} = \frac{54}{4 \times 0.5} = 27 \text{ psi Ult.}$$

Core shear allowable = 56 psi min. (Reference 9)

$$\text{M.S.} = \frac{56}{27} - 1 = \underline{\underline{+1.07}}$$

Transverse bending at the panel G_L is spread over a width compatible with the magnitude of the bending moment.



DYNAMIC LOAD DISTRIBUTION AT LATCH

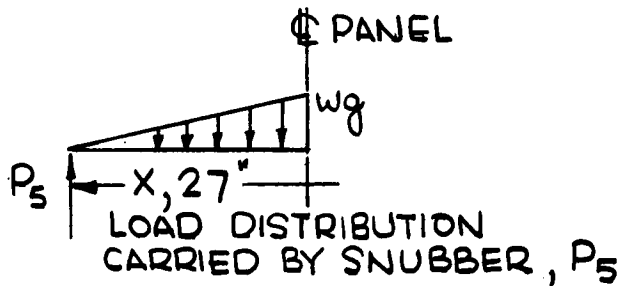
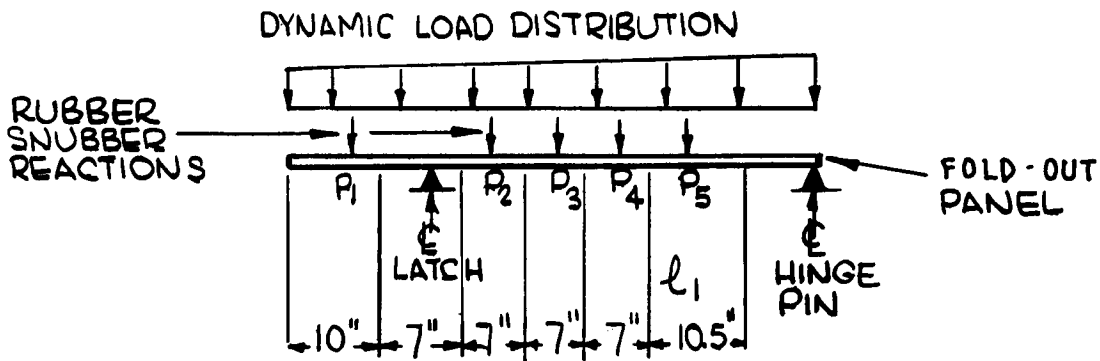
$$m = \left[\frac{1}{12} (w) (\ell)^2 \right] \frac{1}{x} = \left[\frac{1}{12} (11) (19.5)^2 \right] \frac{1}{23.5} = 14.8 \text{ in-lbs/in Ult.}$$

$$M = 22 \text{ in-lbs/in}$$

$$M.S. = \frac{M}{m} - 1 = \frac{22}{14.8} - 1 = \underline{\underline{+0.49}}$$

Compression in Snubbers —

Maximum compression occurs at Snubber P₅.



$$P_5 = (wg) \frac{x}{4} \cdot \ell = (0.0043 \times 16.7 \times 1.6 \times 2) \times \frac{27}{4} \times 10.5$$

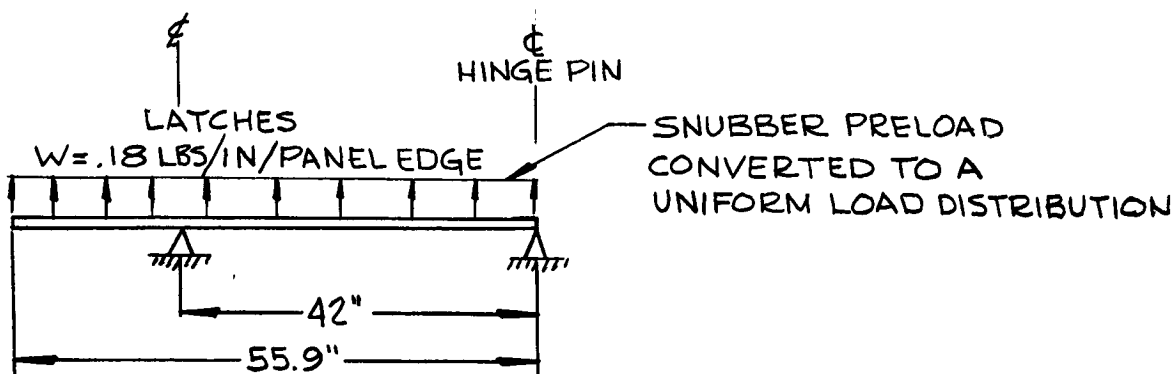
$$P_5 = 16 \text{ lbs Limit}$$

A static deflection of approximately 0.25 in. is suggested.

$$\text{Spring constant required} = \frac{P_5}{\delta} = \frac{16}{0.25} = \underline{\underline{64}} \text{ psi/in}$$

1.2.1 EDGE SNUBBER PRE-LOAD ON FOLD-OUT PANEL

A preload of approximately 0.125 RMS (0.18 inch maximum) in rubber snubbers along the panel edges is required to eliminate a longitudinal vibration bending mode with the panel in the launch position. A preload of 2 pounds per snubber for a load area of 1 in.² is suggested.

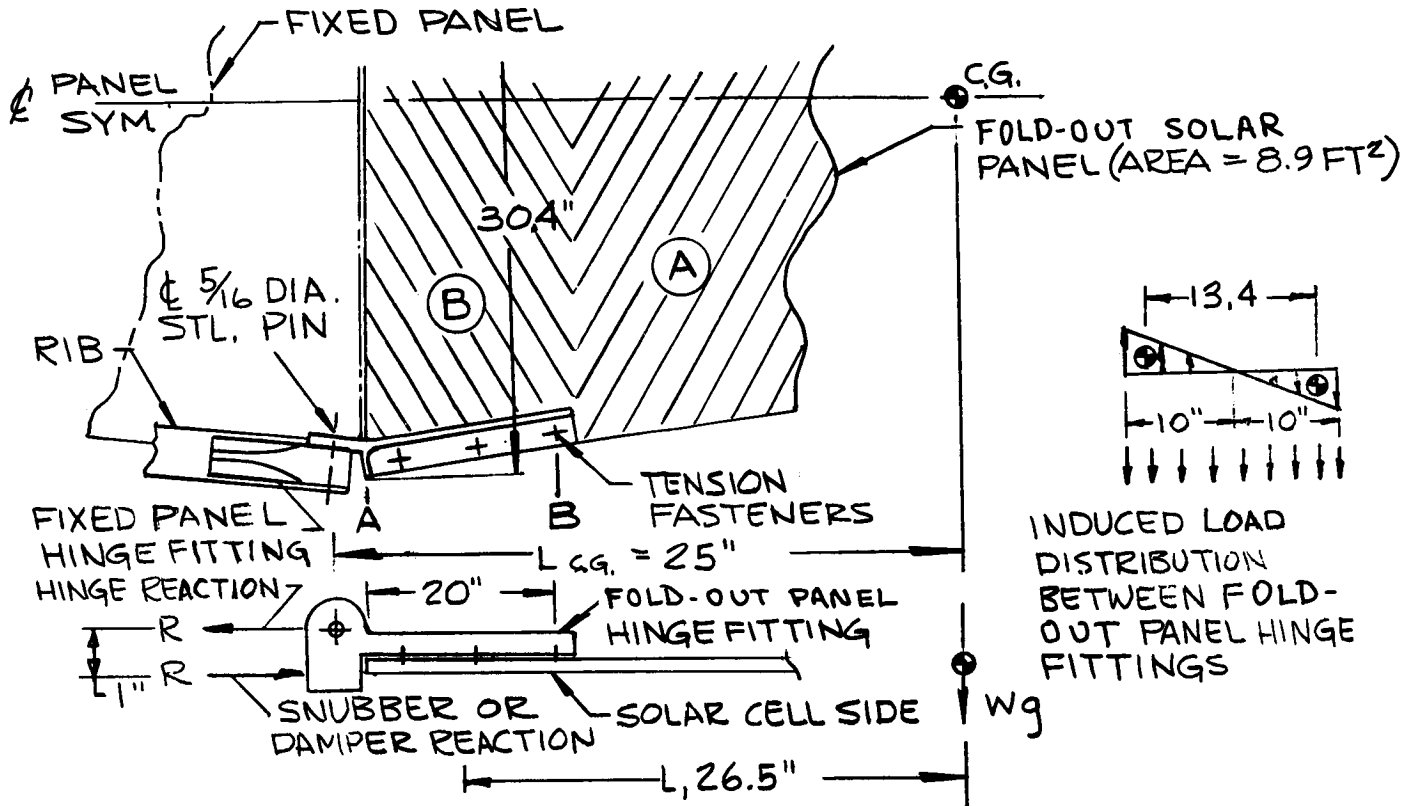


$$\text{Spring constant required} = \frac{\text{preload}}{\text{deflection}} = \frac{2}{0.125} = 16 \text{ psi/in}$$

1.2.2 RETRO-ROCKET "G" EFFECTS ON FOLD-OUT PANEL

The fold-out panel is extended and the spacecraft in the vicinity of Mars when the retro-rocket is fired. Panel temperatures are considered no greater than room temperature (see Figure I-1). A 3 g limit steady state acceleration in the negative thrust direction is considered for design (per amendment Page 9 of Reference 11). Bending and shear are transferred into both spars of the fixed panel for greater effectiveness. Whether snubbers or cruise dampers are used is not considered to affect this analysis. Uncertainties and unknowns of dynamic vibration levels during retro-rocket firing and during mid-course maneuvers suggest a conservative analysis based on minimum deflections.

Transverse bending loads are induced in the fold-out panel between the panel hinge fittings which are treated as rigid beams.

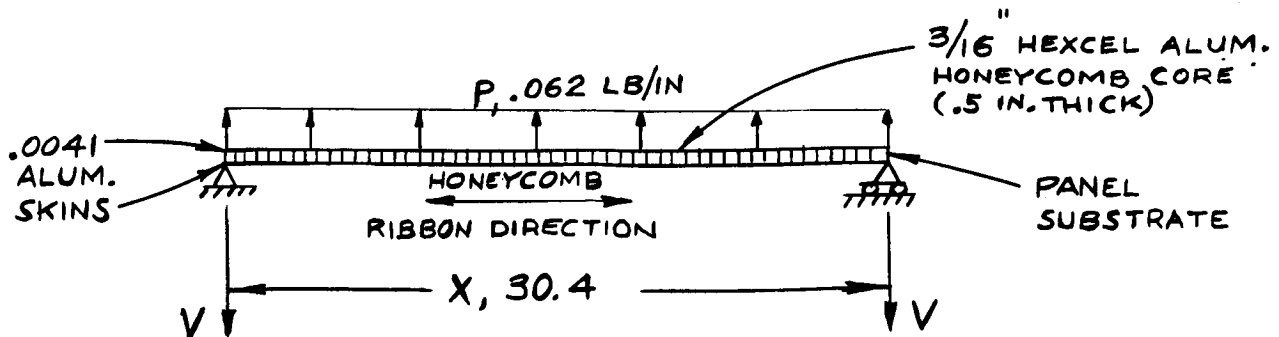


Bending at Station A:

$$P = \left[\frac{(\text{Weight}_A) \times g}{10} \left(\frac{l}{13.4} \right) \times 1.3 - \frac{(\text{Weight}_A) \times g}{20} - \frac{(\text{Weight}_B) \times g}{20} \right] \frac{1}{30.4}$$

$$= \left[\frac{(3.1) \times 3 \times 1.25}{10} \left(\frac{26.5}{13.4} \right) 1.3 - \frac{(3.1) \times 3 \times 1.25}{20} - \frac{(2.4) \times 3 \times 1.25}{20} \right] \frac{1}{30.4}$$

$$P = [3.0 - 0.6 - 0.5] \frac{1}{30.4} = [1.9] \frac{1}{30.4} = 0.062 \text{ lbs/in Ult.}$$



$$\text{Core shear} = \frac{P}{0.5} \cdot \left(\frac{x}{2}\right) = \frac{0.062}{0.5} \left(\frac{30.4}{2}\right) = 1.9 \text{ psi Ult.}$$

Core shear allowable = 56 psi Min. (Reference 9)

$$\text{M.S.} = \frac{\text{HIGH}}{\underline{\underline{\hspace{1cm}}}}$$

Skin-Core Adhesive

$$\text{Shear} = \frac{V(Q)}{I \cdot \left(\frac{\text{shear}}{\text{area}}\right)} = \frac{3.8 (0.0041 \times 0.252)}{5.2 \times 10^{-4} (0.00925)} = 811 \text{ psi Ult.}$$

Adhesive shear allowable = 4000 psi for FM-1000 (0.025 lbs/ft²) at room temperature (Reference 10).

$$\text{M.S.} = \frac{4000}{811} - 1 = \underline{\underline{+3.9}}$$

$$f_{bc}(\text{skin}) = \frac{Mc}{I}$$

$$M = \frac{P(x)^2}{8} = \frac{0.062 (30.4)^2}{8} = 7.2 \text{ in-lbs. Ult.}$$

$$f_{bc}(\text{skin}) = \frac{7.2 \times 0.252}{5 \times 10^{-4}} = 3629 \text{ psi Ult.}$$

$$F_c(\text{skin}) = \frac{2 \cdot E_c}{(1 - \mu^2)} \left(\frac{t}{s}\right)^2 \quad (\text{Reference 21})$$

$$F_c(\text{skin}) = \frac{2 \times 10^7}{(1 - 0.32^2)} \left(\frac{0.0041}{0.1875}\right)^2 = 10647 \text{ psi}$$

$$\text{M.S.} = \frac{F_c}{f_{bc}} - 1 = \frac{10647}{3629} - 1 = \underline{\underline{+1.93}}$$

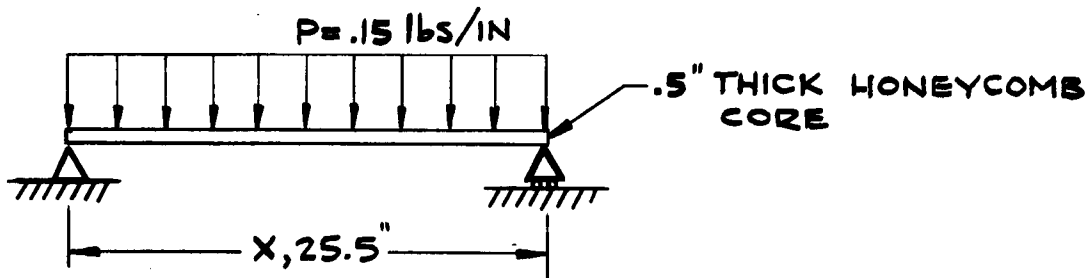
Transverse Deflection,

$$\delta_{(Max)} = \frac{5}{384} \cdot \frac{P(x)^4}{E(I)} = \frac{5}{384} \times \frac{0.062 (30.4)^4}{(10^7) (5 \times 10^{-4})} = 0.14 \text{ in.}$$

Bending at Station B:

$$P = \left[\frac{(\text{Weight}_A) \times g}{10} \left(\frac{\ell}{13.4} \right) \times 1.3 + \frac{(\text{Weight}_A) \times g}{20} + \frac{(\text{Weight}_B) \times g}{20} \right] \frac{1}{25.5}$$

$$P = [3.8] \frac{1}{25.5} = 0.15 \text{ lbs/in Ult.}$$



$$\text{Core shear} = \frac{P}{0.5} \left(\frac{x}{2} \right) = \frac{0.15}{0.5} \left(\frac{25.5}{2} \right) = 3.8 \text{ psi Ult.}$$

M.S. → HIGH

Skin-Core Adhesive

$$\text{Shear} = \frac{V(Q)}{I \left(\frac{\text{shear area}}{\text{area}} \right)} = \frac{7.6 (0.0041 \times 0.252)}{5.2 \times 10^{-4} (0.00925)} = 1633 \text{ psi Ult.}$$

$$\text{M.S.} = \frac{4000}{1633} - 1 = \underline{\underline{+1.45}}$$

$$f_{bc}(\text{skin}) = \frac{MC}{I}$$

$$M = \frac{P(x)^2}{8} = \frac{0.15 (25.5)^2}{8} = 12 \text{ in-lbs Ult.}$$

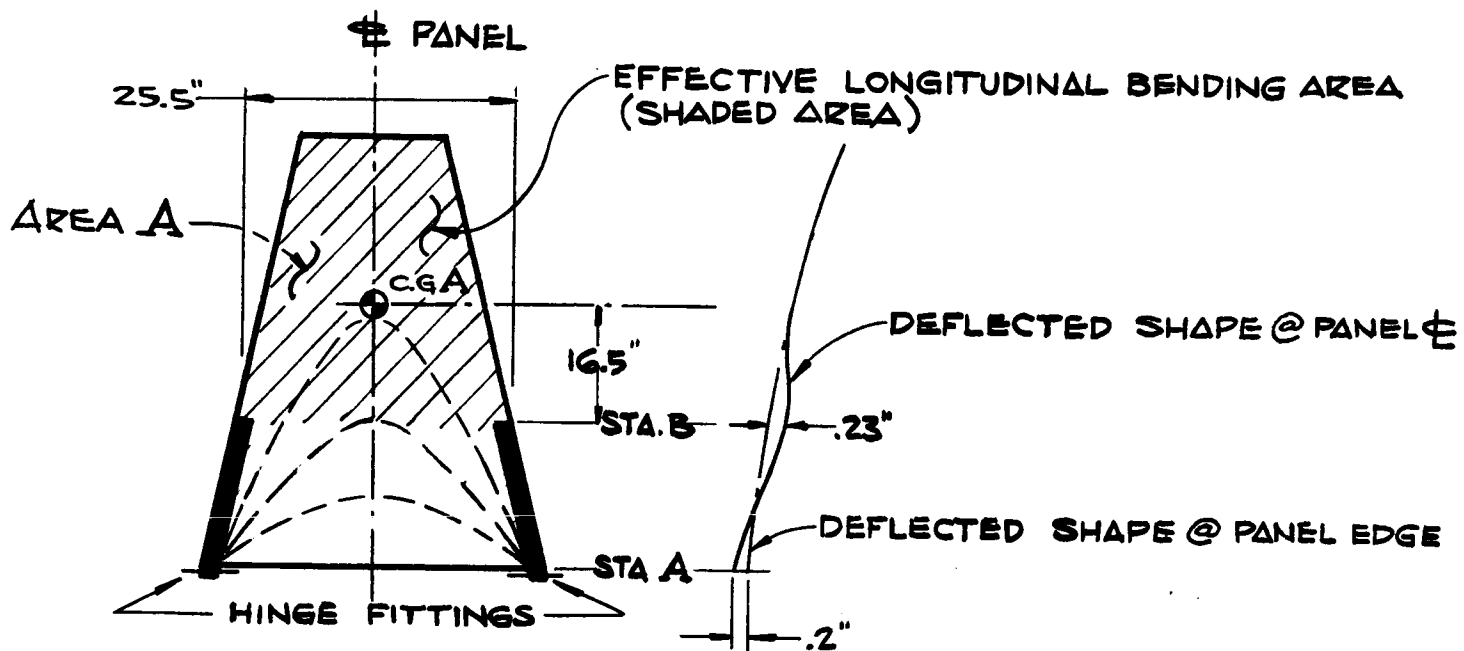
$$f_{bc(\text{skin})} = \frac{12 \times 0.252}{5.2 \times 10^{-4}} = 5815 \text{ psi Ult.}$$

$$\text{M.S.} = \frac{F_c}{f_{bc}} - 1 = \frac{10647}{5815} - 1 = \underline{\underline{+0.83}}$$

Transverse Deflection,

$$\delta_{(\text{Max})} = \frac{5}{384} \cdot \frac{P(x)^4}{(E)(I)} = \frac{5}{384} \times \frac{0.15 (25.5)^4}{(10^7) (5.2 \times 10^{-4})} = \underline{\underline{0.16 \text{ in.}}}$$

Longitudinal Bending —



The full panel width is considered effective in bending at Station B:

$$\text{Core Shear} = \frac{(\text{Weight}_A) \times g}{25.5 \times 0.5} = \frac{(3.1) \times 3 \times 1.25}{25.5 \times 0.5} = 0.91 \text{ psi Ult.}$$

Core Shear Allowable = 32 psi Min. (Reference 9)

M.S. HIGH

Skin-Core Adhesive

$$\text{Shear} = \frac{V(Q)}{I \left(\frac{\text{shear}}{\text{area}} \right)} = \frac{1.82 (0.0041 \times 0.252)}{5.2 \times 10^{-4} (0.00925)} = 389 \text{ psi Ult.}$$

M.S. → HIGH

$$f_{bc}(\text{skin}) = \frac{Mc}{I}$$

$$M = \frac{(\text{Weight}_A) \times g \times 16.5}{25.5} = \frac{(3.1) \times 3 \times 1.25 \times 16.5}{25.5} = 7.5 \text{ in-lb/in Ult.}$$

$$f_{bc}(\text{skin}) = \frac{7.5 \times 0.252}{5.2 \times 10^{-4}} = 3635 \text{ psi Ult.}$$

$$\text{M.S.} = \frac{Fc}{f_{bc}} - 1 = \frac{10647}{3635} - 1 = \underline{\underline{+1.93}}$$

Hinge and Cruise Damper Reactions —

$$R = \left[\frac{(\text{Weight}_{A+B}) \times g \times l_{c.g.}}{1} \right] \frac{1}{2}$$

$$= \left[\frac{(5.5) \times 3 \times 1.25 \times 25}{1} \right] \frac{1}{2} = \underline{\underline{258}} \text{ lb Ult.}$$

Bending in Hinge Pin (0.156 inch radius Stl. Pin) —

This is due to a 0.2 inch offset of the Q_L of the ball support bearing in the fold-out panel hinge fitting with respect to the bearing edge of the fixed panel hinge fitting.

$$M = 258 \times 0.2 = 52 \text{ in-lb Ult.}$$

$$f_b = \frac{Mr}{(I)} = \frac{Mr}{\frac{(\pi r^4)}{4}} = \frac{4M}{\pi r^3} = \frac{4 \times 52}{\pi (0.156)^3} = 17422 \text{ psi Ult.}$$

M.S. → HIGH

Shear in Hinge Pin,

$$\text{Shear} = \frac{R}{\pi r^2} = \frac{258}{\pi (0.156)^2} = 3380 \text{ psi Ult.}$$

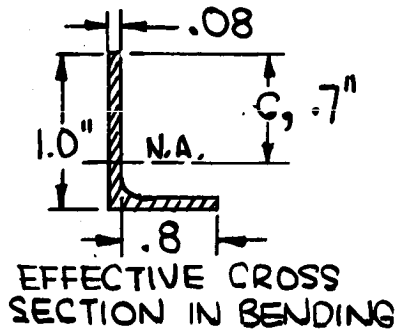
M.S. → HIGH

Bending in Fold-Out Panel Hinge Fitting —

Stiffness is a prime requirement here and M.S. should be high.

$$M_{(\text{Max})} = \left[(\text{Weight}_{A+B}) \times g \times l_{\text{c.g.}} \right] \frac{1}{2} = \left[(5.5) \times 3 \times 1.15 \times 25 \right] \frac{1}{2}$$

$$= 237 \text{ in-lb. yield}$$



$$I_{N.A.} = .0142 \text{ IN}^4$$

$$f_{bt} = \frac{Mc}{I} = \frac{237 \times 0.7}{0.0142} = 11682 \text{ psi yield}$$

$$F_{tu} = 42000 \text{ psi for 2024-T3 Aluminum (Reference 12, Page 43)}$$

M.S. → HIGH

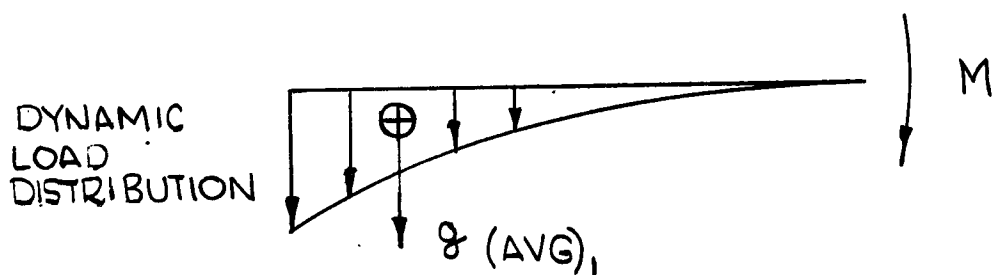
1.2.3 CRUISE DAMPER EFFECTS ON FOLD-OUT PANEL DESIGN

Reference 1 suggests a sinusoidal excitation level of 1.13 g (0-Peak) in the 2-20 cps frequency range during retro-rocket firing. Longitudinal bending of the foldout panel is calculated:

- a. Assuming that cruise dampers are not used

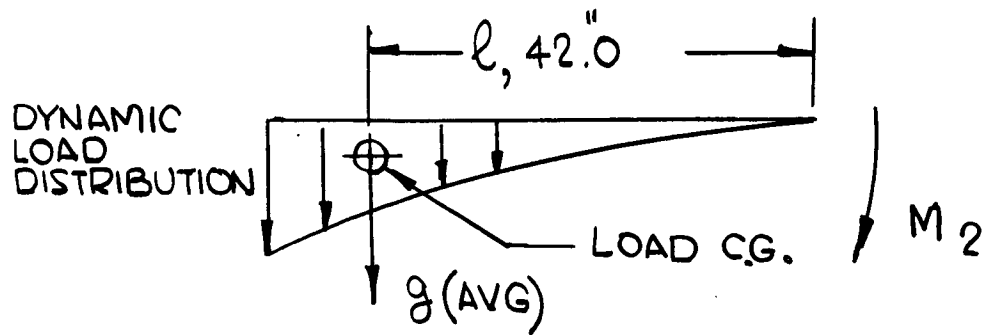
$$g_{(Avg)_1} = \left[g_{(in)} \times \text{Dyn. Amp. Factor} \right] \frac{1}{3} = \left[1.13 \times 16.7 \right] \times \frac{1}{3}$$

$$g_{(Avg)_1} = \underline{6.3} \text{ g Limit}$$



- b. Assuming that cruise dampers are used and provide a dynamic damping ratio equal to that of rubber mounted structure:

$$\text{Dynamic Ampl. Factor} = \frac{\sqrt{1 + 2 (c/c_c)^2}}{2 \times c/c_c} = \frac{\sqrt{1 + 2 (0.1)^2}}{2 \times 0.1} = \underline{5} \text{ g}$$



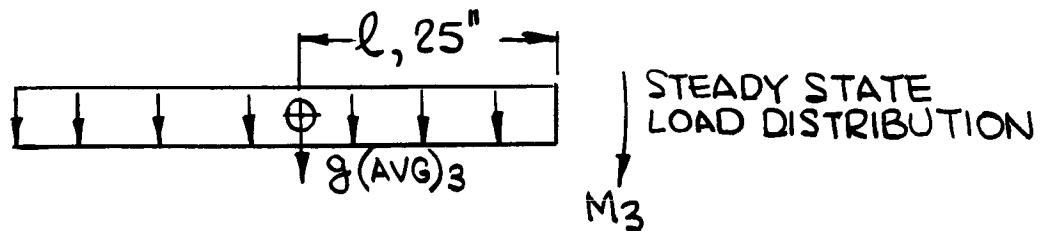
$$g_{(Avg)_2} = \left[g_{(in)} \times \text{Dyn. Amp. Factor} \right] \frac{1}{3} = \left[1.13 \times 5 \right] \frac{1}{3} = \underline{1.9} \text{ Limit}$$

Relative longitudinal dynamic bending moment in the panel using cruise dampers:

$$M_2 = g_{(Avg)_2} \times l$$

$$= 1.9 \times 42 = \underline{80} \text{ in-lb Limit}$$

Relative bending moment in substrate based on a 3 "g" steady state retro-rocket limit level:



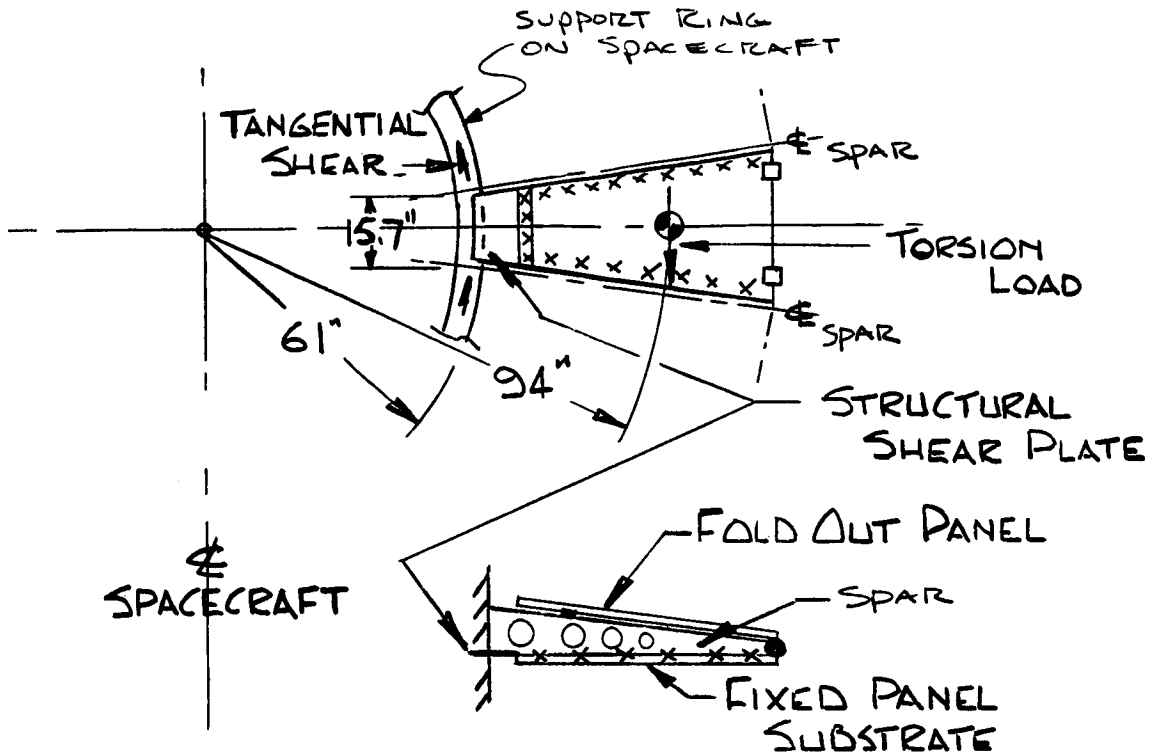
$$M_3 = g_{(Avg)_3} \times L_{cg} = 3 \times 25 = \underline{75} \text{ in-lb Limit}$$

Therefore, the resulting dynamic bending using cruise dampers is comparable to the steady state bending due to retro-rocket firing.

1.2.4 EFFECTS OF IN-PLANE TORSION VIBRATION

This condition occurs during launch in the plane of the fixed array. A complete modal analysis is not available at this time. Therefore, the mode for this analysis will be considered as one which acts as a concentric one-plane rigid body disc about the support ring on the spacecraft. The sinusoidal excitation level of 60 radians/sec² at the spacecraft

booster interface is amplified by a factor of two for use as a (0-peak) limit input level to the solar panels. Torsion loads are carried in the plane of the fixed panel and transferred to the lower support ring on the spacecraft. Loads are conservative based on the assumption that a fold-out panel with solar cells is used.



Tangential shear at lower support ring,

$$q = \left[I_{\text{Mass (Solar Panel)}} \times \text{Torsion Acceleration} \right] \frac{1}{61} \times \frac{1}{15.7}$$

$$q = \left[\frac{13(94)^2}{386.4} \times 60 \times 2 \times 1.25 \right] \frac{1}{61} \times \frac{1}{15.7} = 47 \text{ lb/in Ult.}$$

The in-plane shear is transferred to the spacecraft support ring by both skins of the fixed panel.

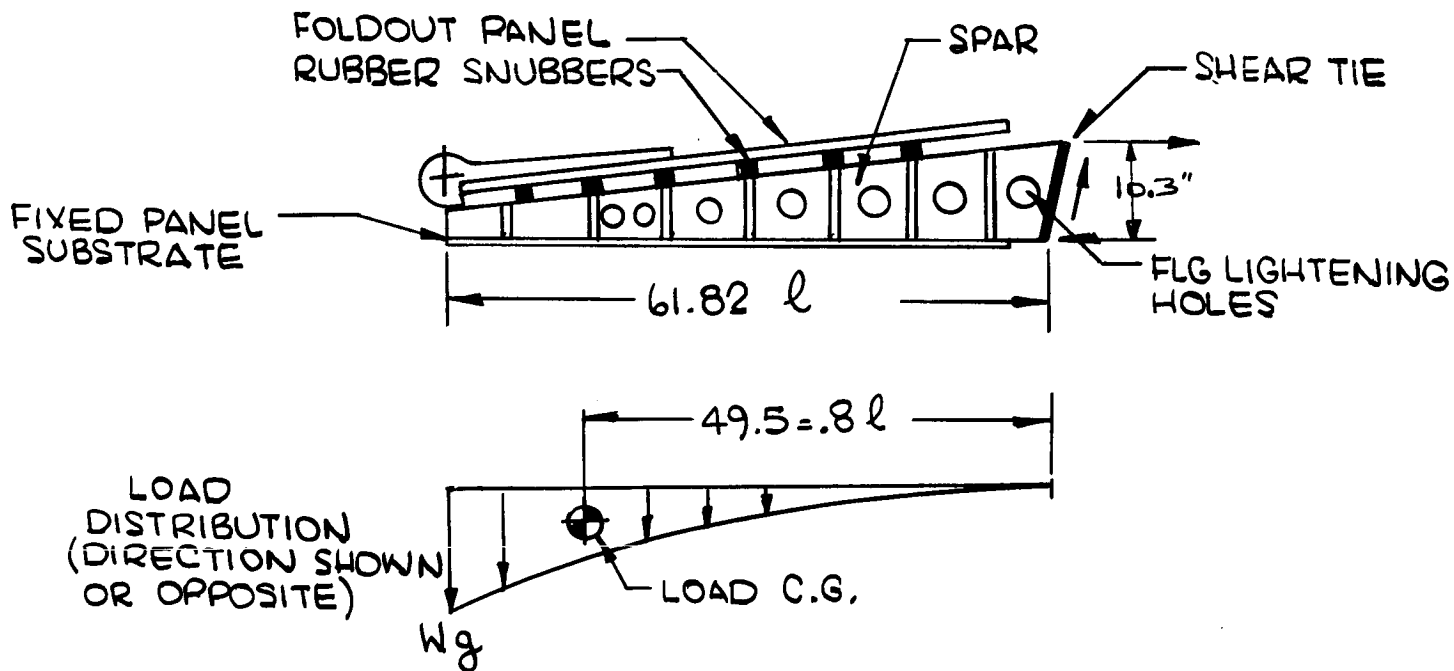
$$f_s = \frac{q}{2t} = \frac{47}{2 \times 0.0055} = 4273 \text{ psi Ult.}$$

$F_s = 7400$ psi min. for 1557 epoxy impregnated glass cloth at room temperature
(based on 143 glass cloth, Reference 17, Page 110)

$$M.S. = \frac{F_s}{f_s} - 1 = \frac{7400}{4273} - 1 = \underline{\underline{+0.73}}$$

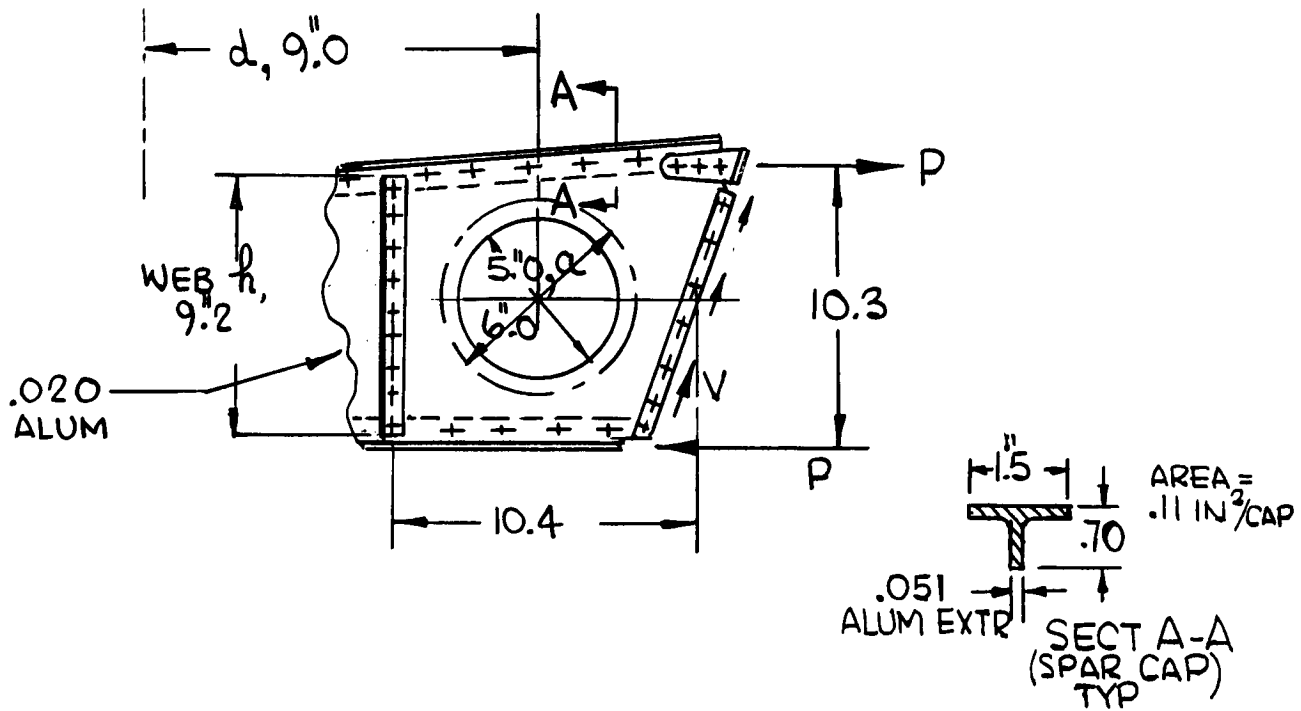
1.2.5 SPAR ANALYSIS - LONGITUDINAL VIBRATION MODE

This loading condition is used for spar design. The condition could occur if the panel were excited in a cantilevered mode of vibration during launch. Temperatures are considered no greater than 75° F. Stiffness contributed by the attached substrate affects over-all stiffness negligibly and is, therefore, disregarded. A dynamic amplification factor of 16.7 at maximum deflection point, based on a structural damping ratio of 0.03, and applied to the 3.2 g excitation level was used for determining the load distribution. Loads are conservative based on the assumption that a fold-out panel with solar cells is used.



Spar Web Shear in Critical Bay -

Analysis is presented for only the critical bay of the spar, i.e., at spar root.



$$V = \frac{1}{3} (W)(g) \times l_1$$

Let W = Weight of 1 in. wide strip at load c.g. \approx .27 lb.

$$V = \frac{1}{3} (.27) (1.6 \times 2 \times 16.7 \times 1.25) \times 61.82 = 372 \text{ lb. Ult.}$$

$$q_{(Avg)} = \frac{V}{9.2} = \frac{372}{9.2} = 40 \text{ lb/in. Ult.}$$

$$f_s_{(Avg)} = \frac{q}{t} = \frac{40}{.020} = 2000 \text{ psi Ult.}$$

Note that the objective of the vertical web stiffeners is to increase lateral vibration frequencies of the webs for decoupling with respect to the cantilever spar mode. The minimum web thickness chosen was considered to be elastically stable under the shear loads, not requiring vertical stiffeners for tension field purposes. If the vertical stiffener effects are neglected, (Section 5.3 of Reference 20)

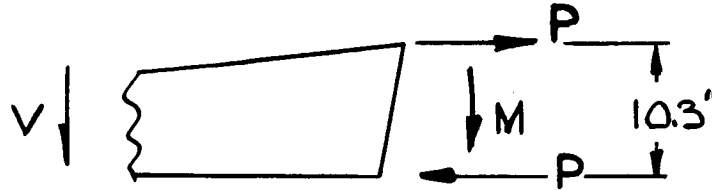
$$q_{(Allow)} = \frac{900000(t)^2}{d}$$

$$q_{(Allow)} = \frac{900000(.020)^2}{9.0} = 40 \text{ lbs/in. for elastic buckling}$$

$$M.S. = \frac{q_{(Allow)}}{q_{Actual}} - 1 = \underline{\underline{0}}$$

Bending --

Bending is considered carried as an alternating compression-tension couple by the spar caps.



Cap load, P

$$= \frac{M}{10.3} = \frac{V (.8l)}{10.3} = \frac{372 (49.5)}{10.3} \left(\frac{1.15}{1.25}\right) = 1645 \text{ lb. yield}$$

$$f_c (\text{cap}) = \frac{P}{A} = \frac{1645}{0.11} = 14955 \text{ psi yield}$$

$F_{c_y} = 38000$ psi for 2024-T4 aluminum extrusion at room temperature (Reference 12, Pg. 50)

$$\text{M.S.} = \frac{F_c}{f_c} - 1 = \frac{38000}{14955} - 1 = +1.54$$

Spar Deflection --

Dynamic deflection at the array periphery is calculated as:

$$\delta = \frac{386(g)}{(2\pi f_n)^2} \quad g = \text{output acceleration}$$

f_n = natural frequency

δ = single amplitude

$$f_n = 3.89 \sqrt{\frac{1}{\text{Tip Deflection (lg)}}}$$

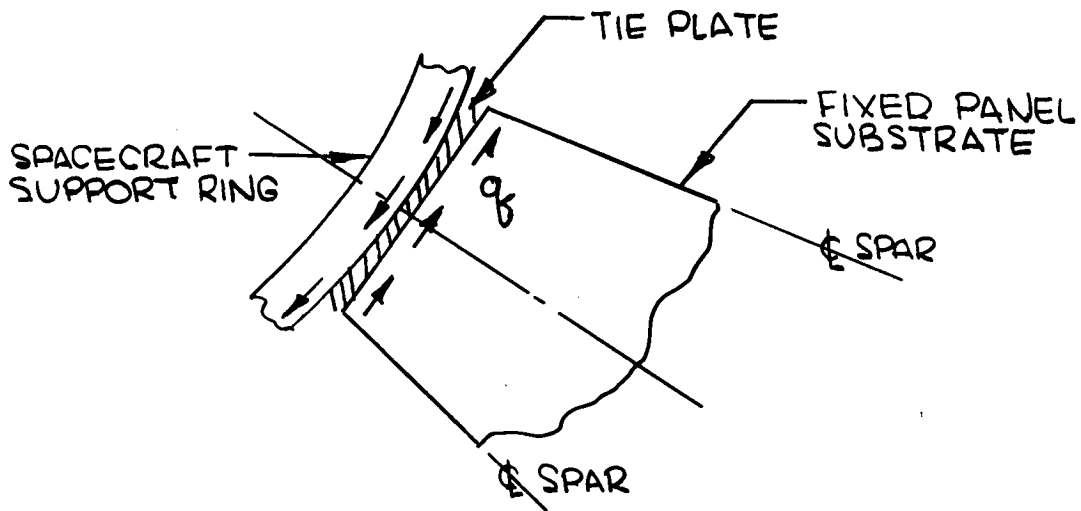
Where tip deflection_(lg) for the tapered cantilever spar is based on spar weight properties at the C.G. of the dynamic load distribution, and an average stiffness property,

$$\begin{aligned} \text{Tip Deflection (lg)} &= \frac{W l^4}{8E(I)} \\ &= \frac{.27 (61.82)^4}{8 \times 10^7 (2 \times .11 \times 2.75^2)} = .03 \text{ in.} \end{aligned}$$

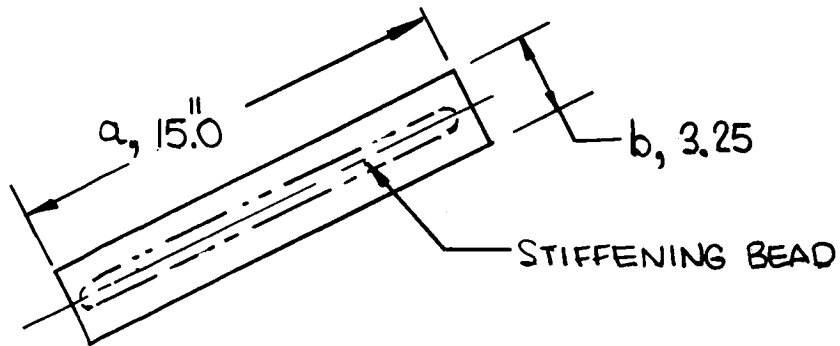
$$f_n = 3.89 \sqrt{\frac{1}{.03}} = 23 \text{ cps}$$

$$\delta = \frac{386(16.7 \times 1.6 \times 2)}{(2 \pi \times 23)^2} = \underline{\underline{1.0 \text{ in.}}}$$

Shear in Fixed Panel Tie-Plate



Calculations are based on average dimensions of the tie-plate,



$$q_{(\text{Allow})} = K E_c \cdot \frac{(t)^3}{(b)^2} \cdot \frac{\pi^2}{12 (1-\mu^2)} \quad \mu = .32$$

$$K = 5.35 \text{ for simply supported edges}$$

$$E_c = 10^7 \text{ psi for aluminum at room temperature}$$

$$= 5.35 \times 10^7 \cdot \frac{(.020)^3}{\left(\frac{3.25}{2}\right)^2} \cdot \frac{\pi^2}{12 (1-.32^2)}$$

$$= 148 \text{ lb/in Ult.}$$

$$q_{(\text{Actual})} = 47 \text{ lb/in Ult. (See effects of in-plane torsion vibration)}$$

$$\text{M. S.} = \frac{q_{(\text{Allow})}}{q_{(\text{Actual})}} - 1 = \frac{148}{47} - 1 = \underline{\underline{+2.15}}$$

As noted in previous paragraphs, analysis affecting both the fixed panels and the spars were based on the use of active fold-out solar panels to provide capability for growth in the event that this becomes a requirement. However, since this is not an immediate requirement the following corrections are presented for the analysis affecting the spar caps and spar shear web. The two spars, which in addition support the existing fold-out panel, will require a bonded doubler on each spar cap of aluminum alloy .010" thick.

Effects on Spar Caps

By eliminating 1/2 the load,

$$f_{c \text{ cap}} = \frac{P}{A}$$

$$A_{(\text{req'd})} = \frac{P}{f_c} = \frac{\left(\frac{1645}{2}\right)}{38000} = .022 \text{ in.}^2$$

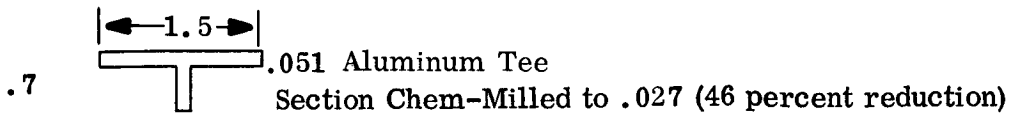
$$\text{Reduction} = \frac{.11 - .022}{.11} = 80 \text{ percent}$$

Assume Load Reduction of 50 percent,

$$\text{Tip Deflection (lg)} = \frac{w l^4}{8 E(I)} = \frac{.27 (61.82)^4}{8 \times 10^7 (2 \times .055 \times 2.75)}$$

$$= \frac{.27 (61.82)^4}{6.65 \times 10^7} = .06 \text{ in.}$$

$$f_n = 3.89 \sqrt{\frac{1}{.06}} = 15.9 \text{ cps}$$



$$F_c = KE \left(\frac{t}{b}\right)^2 = 1.2 \times 10^7 \left(\frac{.027}{.75}\right)^2 = 15552 \text{ psi.}$$

$$f_{bc} = \frac{[M]}{10.3 A} = \frac{\left[\left(\frac{372}{2}\right) \times 49.5\right]}{10.3 \times .059} = 15153 \text{ psi. Ult.}$$

$$\text{M. S.} = \frac{F_c}{f_{bc}} - 1 = \frac{15552}{15153} - 1 = \underline{\underline{+.02}}$$

Effects on Spar Webs

Assume 20 percent thickness reduction, and 50 percent load reduction,

$$q_{(\text{Allow})} = \frac{900000 (.016)^2}{9.0} = 26 \text{ lb/in.}$$

$$q_{(\text{Actual})} = \frac{\left(\frac{372}{2}\right)}{9.2} = 20 \text{ lb/in.}$$

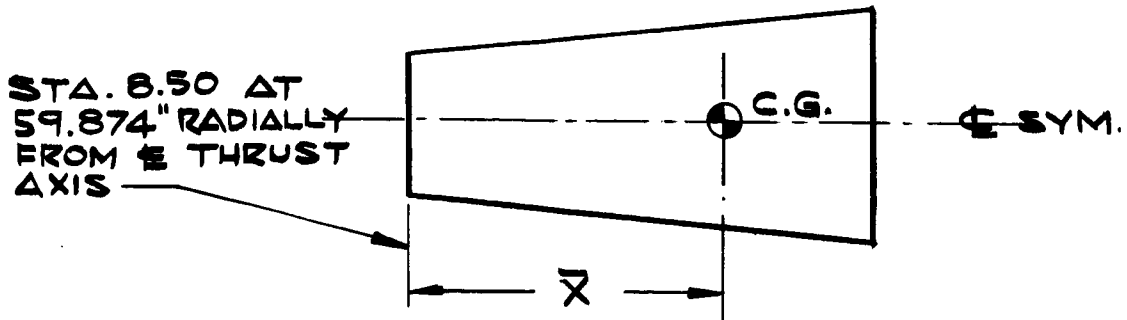
$$\text{M. S.} = \frac{26}{20} - 1 = \underline{\underline{+.30}}$$

2.0 WEIGHT ANALYSIS

All weights calculated are considered nominal. A deviation of $\pm 4\%$ from nominal is reasonable based on Ryan experience with solar panel fabrication.

2.1 FIXED PANEL

Items included are considered a part of the structure of the fixed panel.



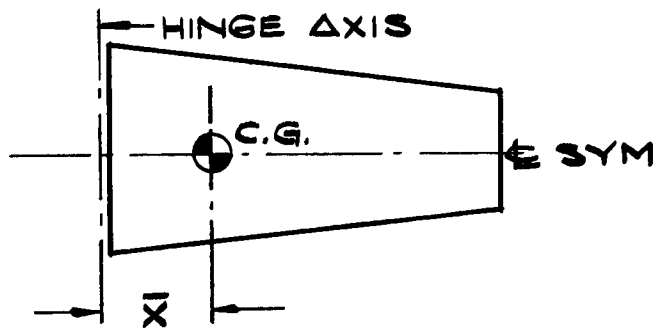
Ryan Dwg. Dash No.	Item	1 X, in.	2 Weight, lb	1 x 2
	Reference Figure 3-1			
	Paint	30.95	0.141	4.36
-5 & 9	Skins (2)	↕	0.901	27.89
-11	Mesh (Exmet Corp.)		0.265	8.20
-13	Dielectric		0.167	5.17
	Skin Adhesive (2)		0.447	13.83
-7	Honeycomb Core		0.596	18.45
	Dielectric Adhesive		0.112	3.466
	Mesh Adhesive	30.95	0.112	3.466
-17	Channel	55.94	0.029	1.62
-19 & 20	Channels (2)	27.97	0.108	3.02
-21	Fittings (2)	55.14	0.074	4.08
-23	Fittings (14)	27.97	0.601	16.81
-37	Fitting	1.00	0.686	0.69
	Sub-Total (Substrate)		4.239	111.05
Ryan Dwg. Dash No.	Reference Figure 3-2 Item	1 X, in.	2 Weight, lb	1 x 2
	Reference Figure 3-2			
	Nut Plates and Screws (18)	27.97	0.227	6.35
Avg. of -9 & -7	Spar Web	15.26	0.475	7.24
	Web Angles	15.26	0.189	2.88
	2 Spar Caps (Tee)	25.80	0.733	18.9
-39	Fitting	-6.20	0.036	-0.22
-45	Gusset	25.70	0.012	0.31
-47	Angle	25.70	0.101	2.60
	Total (Fixed Panel)		6.012	149.11

$$\text{Structure Unit Weight} = \frac{\Sigma 2}{\text{Substrate Area/Panel}} = \frac{6.012}{8.94} = \underline{.67} \text{ lb/ft}^2$$

$$\text{Fixed Panel C.G.} = \frac{\Sigma 1 \times 2}{\Sigma 2} = \frac{149.11}{6.012} = \underline{24.8} \text{ in.}$$

2.2 FOLDOUT PANEL

Items included are considered a necessary part of the structure of the foldout panel. This includes all hinge fittings, cruise dampers, latches, and snubber pads. C.G. analysis is for cruise position.



Ryan Dwg. Dash No.	Item	1 X, in.	2 Weight, lb	1 x 2
	Reference Figure 3-1			
	Paint	19.3	0.103	1.99
-31 & 33	Skins (2)	19.3	0.818	15.80
	Skin Adhesive (2)	19.3	0.326	6.30
-7	Honeycomb Core	19.3	0.435	8.49
-17	Channel	0.10	0.029	0.00
-19 & 20	Channels (2)	20.10	0.078	1.57
-15	Channel	40.10	0.015	0.60
-23	Fittings (6)	22.00	0.257	5.65
-25	Fittings (2)	39.50	0.074	2.93
-27	Fittings (2)	4.22	0.546	2.30
-29 & 30	Fittings (2)	26.65	0.404	10.80

Ryan Dwg. Dash No.	Item	1 X, in.	2 Weight, lb	1 x 2
	Reference Figure 3-2			
	Cruise Dampers	-2.60	0.170	-0.44
-61	Torsion Springs (2)	0	0.375	0
	Hinge Pins (2)	0	0.122	0
-57 & 58	Hinges (2)	3.00	0.174	0.52
-59 & 60	Stiffeners (2)	10.25	0.274	2.81
-55	Hinge	-1.70	0.066	-0.11
-53	Snubber Pads (3)	-24.00	0.052	-1.25
-49	Latch	-26.65	0.015	-0.40
	Explosive Latch Pin	-26.65	0.078	-2.08
-51	Hooks (2)	-26.65	0.041	-1.09
	Total (Foldout Panel)		4.452	54.39

$$\text{Structure Unit Weight} = \frac{\sum 2}{\text{Substrate Area/Panel}} = \frac{4.452}{6.52} = \underline{0.69} \text{ lbs/ft}^2$$

$$\text{C. G.} = \frac{\sum 1 \times 2}{\sum 2} = \frac{54.39}{4.452} = \underline{12.2} \text{ in.}$$

3.0 DYNAMICS ANALYSIS

Analysis for the fold-out panel is based on a panel equivalent in size to that of the fixed panel. The justification for this approach is as follows; in the event that fold-out panels are required to provide additional solar-cell mounting area, it is desirable for standardization of solar cell arrangement, to use the same size as is established for the fixed panels. Frequencies for the existing fold-out panel should be increased by approximately the following percentages.

Stowed,	1st plate bending	41%
Deployed,	1st cantilever bending	180%
Deployed,	1st torsion	180%

The result is that frequencies are above the desired minimum of 10 cps which will prevent dynamic coupling with the auto pilot system.

3.1 SUMMARY OF PRELIMINARY NATURAL FREQUENCY ESTIMATES:

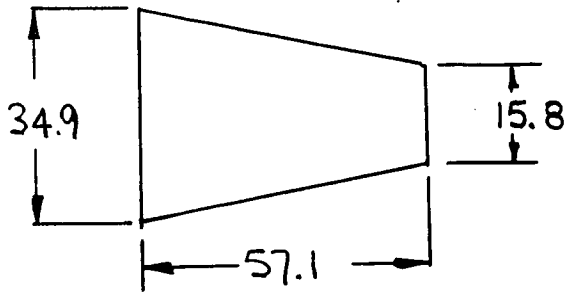
Foldout Panel

Stowed, 1st plate Bending	15.6 cps
Deployed, 1st Cantilever Bending	4.8 cps
Deployed, 1st Torsion	20.1 cps

Fixed Panel

1st Plate Bending	13.1 cps
Spar Web, 1st Transverse Bending	45.6 cps

3.1.1 FOLDED PANEL - STOWED CONFIGURATION, FUNDAMENTAL PLATE BENDING MODE



The panel is assumed pinned on all four edges, and an equivalent rectangular panel of the same planform area and length as the actual panel is also assumed.

$$\text{Width of equivalent rectangular panel} = \frac{30.9 + 15.8}{2} = 23.35 \text{ in.}$$

The frequency of a pin supported uniform rectangular plate is given by Reference 18, Eq. 2, Page 371, with $m = 1$, $n = 1$ (Fundamental Mode):

$$\omega = c^2 \pi^2 \left(\frac{1}{a^2} + \frac{1}{b^2} \right) \text{ (rad/sec)} \tag{Eq. 1}$$

$$\text{where } c^4 = \frac{Eh^2}{3\rho(1-\mu^2)} \text{ (in}^4 \text{ sec}^{-2}\text{)} \tag{Eq. 2}$$

ω = circular natural frequency, rad/sec.

a = length of shorter side = 23.35 in.

b = length of longer side = 55.9 in.

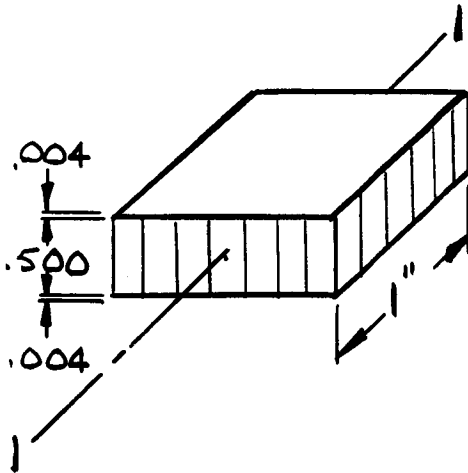
E = modulus of elasticity = 10.5×10^6 #/in² (Al. alloy)

h = effective thickness of solid plate, in. (see below)

ρ = mass density, # sec² in⁻⁴ (see below)

μ = Poisson's Ratio, a value of 1/3 is assumed for μ

Effective thickness h



For a 1" wide piece of sandwich used for the foldout panel

$$I_{1-1} = 2(.004)(1)(.252)^2 = 5.080 \times 10^{-4} \text{ in}^4$$

$$EI_{1-1} = 10.5 \times 10^6 \times 5.080 \times 10^{-4} = 5334 \text{ #in}^2$$

For a 1" wide piece of solid plate

$$I_{1-1} = \frac{1(h^3)}{12} \text{ (in}^4)$$

Equating I_{1-1} 's and solving for h,

$$h = 0.1827 \text{ in.}$$

Mass density ρ

$$\begin{aligned} \text{wt/ft}^2, \text{ sandwich} &= 0.28 \text{ (substrate)} + 0.34 \text{ (cells and wiring)} \\ &= 0.62 \text{ lb/ft}^2 \end{aligned}$$

$$\text{wt/in}^2, \text{ sandwich} = \frac{0.62}{144} = 0.004306 \text{ lb/in}^2$$

$$\text{Effective wt/in}^3, \text{ solid plate} = \frac{.004306}{.1827} = .02357 \text{ lb/in}^3$$

$$\rho = \frac{.02357}{g} = \frac{.02357}{386.04} = 6.106 \cdot 10^{-5} \text{ lb/sec}^2 \text{ in}^{-4}$$

substituting E, h, ρ and μ in Equation 2) and solving for c^2 gives

$$c^2 = 4.640 \times 10^4 \text{ in}^2/\text{sec}$$

Substitution of c^2 , a and b in Equation 1 gives

$$\omega = 98.05 \text{ rad/sec}$$

$$f = \frac{\omega}{2\pi} = 15.61 \text{ cps (Fundamental Mode)}$$

3.1.2 FOLDOUT PANEL - DEPLOYED CONFIGURATION, FUNDAMENTAL CANTILEVER BENDING MODE

Distributed mass m (per inch of span)

$$\text{Weight} = .004306 \text{ lb/in}^2$$

$$\text{At root, Wt.} = .004306 \times 30.9 = .1331 \text{ lb/in}$$

$$m = \frac{.1331}{g} = \frac{.1331}{386.04} = 3.447 \times 10^{-4} \text{ lb sec}^2 \text{ in}^{-2}$$

$$\text{At tip, Wt.} = .004306 \times 15.8 = .06803 \text{ lb/in}$$

$$m = \frac{.06803}{386.04} = 1.762 \times 10^{-4} \text{ lb sec}^2 \text{ in}^{-2}$$

Since m is linear with span

$$m = a_1 + a_2 X \text{ where } a_1 = 3.447 \times 10^{-4} \text{ lb sec}^2 \text{ in}^{-2}$$

$$\text{and } a_2 = -2.9510 \times 10^{-6} \text{ lb sec}^2 \text{ in}^{-3}$$

Stiffness EI

$$\text{At root, } EI = 10.5 \times 10^6 \times 5.080 \times 10^{-4} = 30.9 = 1.6482 \times 10^5 \text{ lb in}^2$$

$$\text{At tip, } EI = 10.5 \times 10^6 \times 5.080 \times 10^{-4} \times 15.8 = 0.8428 \times 10^5 \text{ lb in}^2$$

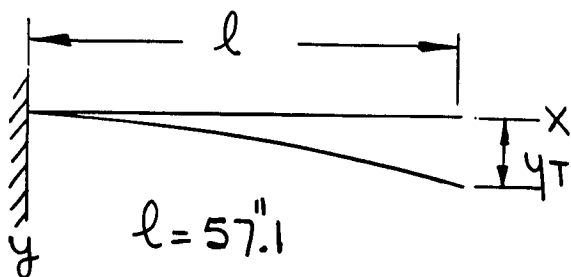
Since EI is linear with span,

$$EI = a_3 + a_4 x \text{ where } a_3 = 1.6482 \times 10^5 \text{ lb in}^2$$

$$\text{and } a_4 = -1410.5 \text{ lb in}$$

The method of analysis is the Rayleigh method

Assumed mode shape: $y = y_T (1 - \cos \frac{x}{2 \ell})$



$$\frac{dy}{dx} = y_T \frac{\pi}{2 \ell} \cdot \sin \frac{\pi x}{2 \ell}$$

$$\frac{d^2y}{dx^2} = y_T \frac{\pi^2}{4 \ell^2} \cdot \cos \frac{\pi x}{2 \ell}$$

Note that the assumed mode shape meets the necessary boundary conditions:

$$y_{x=0} = 0, \quad y_{x=l} = y_T$$

$$\left(\frac{dy}{dx}\right)_{x=0} = 0, \quad \left(\frac{d^2y}{dx^2}\right)_{x=l} = 0$$

$$\text{Maximum Kinetic Energy} = \frac{1}{2} \omega^2 \int_0^l m y^2 dx$$

Upon substitution of m and y functions of x in the integrand and integrating the expression over the indicated limits, the result is

$$\begin{aligned} \text{Maximum Kinetic Energy} &= \frac{1}{2} \omega^2 y_T^2 l \left[a_1 \left(\frac{3}{2} - \frac{4}{\pi} \right) + a_2 l \left(\frac{3}{4} + \frac{7}{\pi^2} - \frac{2}{\pi} \right) \right] \\ \text{Maximum Potential Energy} &= \frac{1}{2} \int_0^l EI \left(\frac{d^2y}{dx^2} \right)^2 dx \end{aligned} \quad \text{Eq. 3}$$

Upon substitution of EI and $\frac{d^2y}{dx^2}$ functions of x in the integrand and integrating the expression over the indicated limits, the result is

$$\text{Maximum Potential Energy} = \frac{1}{2} \frac{\pi^4}{32 l^4} \cdot y_T^2 l \left[a_3 + a_4 \left(\frac{1}{2} - \frac{2}{\pi^2} \right) \right]$$

Equating Maximum Kinetic Energy to Maximum Potential Energy (the heart of the Rayleigh method), and dividing through by $\frac{1}{2} y_T^2 l$, one obtains

$$\omega^2 \left[a_1 \left(\frac{3}{2} - \frac{4}{\pi} \right) + a_2 l \left(\frac{3}{4} + \frac{7}{\pi^2} - \frac{2}{\pi} \right) \right] = \frac{\pi^4}{32 l^4} \left[a_3 + a_4 l \left(\frac{1}{2} - \frac{2}{\pi^2} \right) \right]$$

Putting in numbers for a_1, a_2, a_3, a_4 and the result is:

$$\omega^2 \times .00007818 \text{ lb sec}^2 \text{ in}^{-2} = .04654 \text{ lb in}^{-2} \quad \text{(Basic Panel)} \quad \text{Eq. 4}$$

The presence of side members, tapered angles, on the foldout panel in the root area requires modification of Eq. 4 .

It is assumed that the Kinetic Energy due to effects of increased mass in the root area is increased by 10 percent. The KE term, the left hand side of Eq. 4 , then becomes

$$\text{LHS} = 1.10 \omega^2 \times .00007818 = \omega^2 \times .00008600 \text{ lb in}^{-2}$$

The Potential Energy increase is assumed that of twice the EI of the basic panel (each angle has an EI approximately equal to the EI of the basic panel). The angles extend over the first 20 inches of panel. Let this distance be b. Integrating the maximum Potential Integral (Eq. 3) over the limit 0 to b, and multiplying by two, the result is:

$$\Delta \text{ Max. PE} = \frac{1}{2} \frac{\pi^4}{16\ell^4} \cdot y_T^2 \ell \left\{ 2a_3 \left(\frac{b}{2\ell} + \frac{1}{2\pi} \sin \frac{\pi b}{\ell} \right) + 2a_4 \left[\frac{b^2}{4\ell} + \frac{b}{2\pi} \sin \frac{\pi b}{\ell} + \frac{\ell}{2\pi^2} \left(\cos \frac{\pi b}{\ell} - 1 \right) \right] \right\}$$

Dividing this expression by $\frac{1}{2} y_T^2 \ell$ and substituting numbers for a_3 , a_4 , b and ℓ , one obtains for the increase in the right hand side of Eq. 4 ,

$$\Delta \text{ RHS} = .03235 \text{ lb in}^{-2}$$

and the corrected right side of Eq. 4) is:

$$\text{RHS} = .04654 + .03235 = .07889 \text{ lb in}^{-2}$$

Thus, Eq. 4) corrected, becomes

$$\omega^2 \times .00008600 = .07889 \text{ lb in}^{-2} \text{ (Panel plus Angles)}$$

Solving for ω , the result is

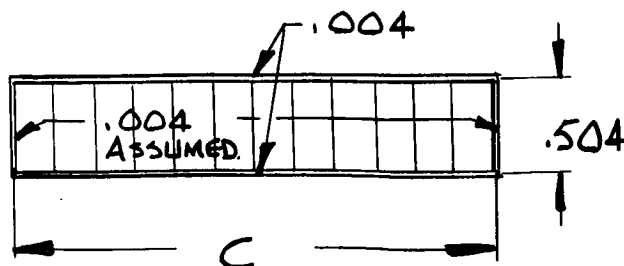
$$\omega = 30.29 \text{ rad/sec}$$

$$f = \frac{\omega}{2\pi} = 4.82 \text{ cps}$$

3.1.3 FOLDOUT PANEL - DEPLOYED CONFIGURATION, FUNDAMENTAL TORSION MODE

Stiffness distribution GJ_p

It is assumed that the sandwich substrate can be represented torsionally by a single cell torque box as shown. The width c is the actual width of the panel.



Measuring spanwise distance x , in inches, from the root

at $x = 0$, $c = 30.9$ in, and at $x = \ell = 57.1$ in, $c = 15.8$ in.

Thus,

$$c = -0.2644x + 30.9 \text{ or } x = -3.781c + 116.8 \text{ (in)}$$

The method of analysis is the Rayleigh method.

Assumed mode shape: $\phi = \phi_T \cdot \frac{x}{\ell} = \frac{\phi_T}{\ell} (-3.781c + 116.8)$

where ϕ = twist angle at Station x (rad), and ϕ_T = twist angle at tip (rad). Note that the assumed mode shape meets the necessary boundary condition: $\phi_{x=0} = 0$

$$\text{Maximum KE} = \frac{1}{2} \omega^2 \int_0^{\ell} \gamma \phi^2 dx$$

We change the variable of integration from x to c for convenience. At $x = 0$,

$c = 30.9$; at $x = \ell$, $c = 15.1$, $\gamma = 1.292 \times 10^{-6} c^3$, $\phi^2 = \frac{\phi_T^2}{\ell^2} (14.29c^2 - 883.2c + 13.642)$, and $dx = -3.781 dc$. Substitution gives,

$$\text{Maximum KE} = \frac{1}{2} \omega^2 \frac{\phi_T^2}{\ell^2} \times 1.292 \times 10^{-6} (-3.781) \int_{30.9}^{15.1} (14.29c^5 - 883.2c^4 + 13.642c^3) dc$$

Integrating this expression over the indicated limits, the result is

$$\text{Maximum KE} = \frac{1}{2} \omega^2 \frac{\phi_T^2}{\ell^2} \times 682.0 \text{ lb in}$$

$$\text{Maximum PE} = \frac{1}{2} \int_0^{\ell} GJ \left(\frac{d\theta}{dx} \right)^2 dx$$

Changing the variable of integration from x to c again for convenience,

with $\frac{d\phi}{dx} = \frac{\phi_T}{\ell}$ and $GJ = 7925c$,

$$\begin{aligned} \text{Maximum PE} &= \frac{1}{2} \frac{\phi_T^2}{2\ell^2} \times 7925 (-3.781) \int_{30.9}^{15.1} c dc \\ &= \frac{1}{2} \frac{\phi_T^2}{\ell^2} \times 1.089 \times 10^7 \text{ lb in} \end{aligned}$$

Equating Maximum KE to Maximum PE and dividing through by $\frac{1}{2} \frac{\phi T^2}{l^2}$, the result is

$$\omega^2 \times 682.0 = 1.089 \times 10^7 \text{ lb in}^{-2} \text{ (Basic Panel)}$$

It is assumed that, due to the side members (angles) in the root area, any small increase in KE from mass moment of inertia increase is balanced by a corresponding small increase in PE from differential bending stiffness of the angles. Thus, the relationship just obtained stands, without modification.

Solving for ω , the result is:

$$\omega = 126.4 \text{ rad/sec}$$

$$f = \frac{\omega}{2\pi} = 20.12 \text{ cps}$$

3.1.4 FIXED PANEL - FUNDAMENTAL PLATE BENDING MODE

The panel is assumed pinned on all four edges, and an equivalent rectangular panel of the same planform area and length as the actual panel is assumed. The geometry and analysis is precisely that for the fundamental plate bending mode of the foldout panel, with the exception that the .004 aluminum alloy sandwich faces are replaced by .0055 fiberglass faces.

$$I_{1-1} = 2(.0055)(1)(.25275)^2 = 7.027 \times 10^{-4} \text{ in}^4$$

$$EI_{1-1} = 5 \times 10^6 \times 7.027 \times 10^{-4} = 3514 \text{ lb in}^2 \text{ versus } 5334 \text{ lb in}^2$$

for the 0.004 aluminum alloy faced sandwich (per inch of width).

$$\text{wt/ft}^2 = .226 + .340 = .566 \text{ lb/ft}^2 \text{ versus } 0.620 \text{ lb/ft}^2 \text{ for the .004 aluminum}$$

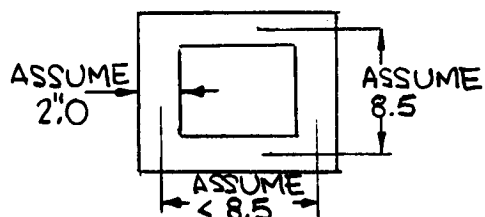
alloy faced sandwich (substrate plus cells and wiring).

Examination of the frequency equation (Eq. 1) or, for that matter, the frequency equation for any structural system with distributed mass and stiffness, the frequency varies directly as the square root of stiffness (EI_{1-1} in the case at hand) and inversely as the square root of mass (which is directly related to wt/ft^2 in the present case). Thus, correcting the frequency obtained for the .004 aluminum alloy faced sandwich panel, the result is, for the present panel.

$$f = 15.66 \sqrt{\frac{3514}{5334} \times \frac{.620}{.566}} = 13.16 \text{ cps}$$

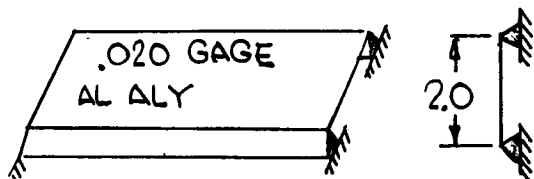
3.1.5 SPAR WEB, FUNDAMENTAL TRANSVERSE BENDING

The analysis made herein of the spar web must be considered highly approximate because of the questionable nature of the assumptions made. Verification by test is strongly indicated.



The largest bay (actually the bay is trapezoidal, with a large circular flanged lightning hole) is assumed as shown in the figures to the left.

The mass m , per inch of space along the 2nd side, is



$$m = \frac{0.1 \times 0.020 \times 8.5}{386.04} = 4.4037 \times 10^{-5} \text{ lb sec}^2 \text{ in}^{-2}$$

Assume .020 x 2 x 8.5 effective, pinned along edges, free on short edges, 2 inch long beam on simple supports, 8.5 inches wide.

$$EI = 10.5 \times 10^6 \times \frac{8.5 \cdot (.020)^3}{12} = 59.50 \text{ c in}^2$$

$$l = 2.00, \quad l^4 = 16.00$$

Referring to Reference 19 (Eq. 21, Page 459), the frequency of a simply supported uniform beam is given by

$$\omega = \pi^2 \sqrt{\frac{EI}{m l^4}} \text{ rad/sec}$$

Substitution of the indicated values for EI , m and l^4 ($\pi^2 = 9.870$) in this equation gives

$$\omega = 286.8 \text{ rad/sec}$$

$$f = \frac{\omega}{2 \pi} = 45.64 \text{ cps}$$

3.2 SUMMARY OF OVER-ALL DYNAMICS PROBLEMS

The primary problem, of course, is to ensure that the array will pass its qualification tests with regard to sinusoidal and random vibration inputs, shock inputs and acoustical noise.

Considerable analysis and test will be required to determine, for the complete array, magnification factors, which are functions of structural damping mode shapes and frequencies, and which determine dynamic loads. This program would necessarily be a quite comprehensive and detailed one. It is outlined subsequently.

In comparison to other arrays with which Ryan has had experience, the sinusoidal inputs in the 5-50 cps range (where major resonances occur) and in the 50-150 cps range are rather moderate. In the 150-2000 cps range, where fairly large sinusoidal inputs are encountered, responses are expected to be small, and local. Further analysis in the 5-150 cps range is indicated.

In regard to random vibration input for qualification tests, again, the region of high level input, over the 100-1000 cps band, is outside the region of major resonances. The steep skirts of the specified power spectral density curve outside the 100-1000 cps band (6 db/octave is specified) leads to the conclusion that the important 5-50 cps band inputs will be quite small, e.g. at 50 cps, roll-off gives a P.S.D. of $0.0175 \text{ g}^2/\text{cps}$ as compared with 0.07 specified at 100 cps. The $.0175 \text{ g}^2/\text{cps}$ value is equivalent to $\sqrt{0.0175 \times 50} = 0.935 \text{ g RMS}$ input at 50 cps as compared to 1.875 g RMS sinusoidal input specified at 50 cps. The random inputs at frequency samples less than 50 cps are sharply reduced to even smaller values due to roll-off. It is expected that response to random inputs will be negligible compared to sinusoidal inputs, in the fundamental modes. Response in higher modes, and in local modes, requires further analysis and test support.

The effects of shock input also must await further analysis. A 200 g terminal peak sawtooth input is specified, with 1.0 millisecond maximum rise time. Assuming an array weight of 216 lbs, 200 g is 43,200 lbs peak applied to the array (assumed in the stowed configuration). The impulse is $1/2 \times 43,200 \times .001 = 21.6 \text{ lb sec}$ total, or 0.65 lb sec per panel (23 panels total, 22 fixed and 1 foldout).

Just to get a feel for the response, in an undamped single degree of freedom case, the response to a Dirac spike (infinite amplitude with infinitesimally small base time, but with impulse I) is $\frac{I}{m\omega}$ where $\omega = \sqrt{\frac{K}{m}}$. If I is 0.003 lb sec and $m = \frac{.707 \times 6.0}{386.04} = .0110$ $\text{lb sec}^2 \text{ in}^{-1}$ (assumes a generalized, i.e., effective mass, of .707 the actual mass -- with a panel weight of 6.0 lb, and $\omega = 98.05 \text{ rad/sec}$ (foldout panel, stowed configuration, 1st plate bending mode) then the maximum deflection is

$$y_{\max} = \frac{.60}{.0110 \times 98.05} = 0.647 \text{ inch}$$

which is not small and not large. The conclusion is made that the 200 g shock input may present a problem. It needs further study.

A launch primary problem is determining the limiting of the response to safe levels for the so-called torsion input (sinusoidal, $\pm 60 \text{ rad/sec}^2$ amplitude, about the longitudinal axis, x axis - assumed at major resonances). The fixed part of the array is excited in its plane, and will present large stiffness in this loading configuration. However, the masses whose locations are displaced in the x direction from the plane of the fixed part of the array (these displaced masses are the planet scanner, foldout antenna, and the one foldout panel) present, under the torsional input, inertia moments about radial axes which will cause the fixed portion, especially along the outer rim, to weave. The analysis can be set up as one phase of the over-all array analysis mentioned previously. This detailed and comprehensive work would logically be accomplished in the Phase II effort.

The response to acoustical noise is a problem less amenable to analysis than to a test program. Such things as fatigue failure in bonded joints and local oil canning are best solved in the sound chamber, and a strong test program, possibly with structural samples as well as full scale hardware, is indicated. The specified sound pressure levels (137 db max. in the band 600 to 1200 cps) are levels typical of previous Ryan solar panel experience, and should present no large difficulties. However, a strong test program is almost mandatory to ensure structural integrity, including detection and correction of design deficiencies, if any, with regard to acoustical noise.

A secondary over-all problem, in addition to meeting qualification test specifications, in the realm of dynamics performance, is that the fundamental guidance system natural frequency and any of the structural frequencies must be de-coupled so as to prevent structural feed-back which might cause a serious system instability or performance degradation. The fundamental frequency for the complete array (which should be around 5 cps on the basis of the lowest uncoupled frequency obtained in the present analysis) is the important one. Most guidance resonance frequencies are in the range 1/2 to 2 cps. The degree of de-coupling necessary is a function of many guidance system parameters and requires detailed study on the part of specialists in that area before structural isolation requirements can be laid down.

4.0 THERMAL ANALYSIS

Figures I-1 and I-2 are present best estimates of temperature distributions and Mars sun occultation transients for the selected configuration. These figures assume the back of the panel to have the radiative surface properties of a selected white paint (0.9 emissivity). If the panel back mosaic pattern (described in Thermodynamic Parametric Studies section) were used, the presented figures would change as follows:

- Figure A1 Temperatures from distances 6 to 116 inches would be approximately the temperatures indicated at a distance of six inches from bus.
- Figure A2 Initial temperature would be approximately 75°F and the time to reach temperatures in the range of -180°F or -200°F would increase 25 percent for the fixed panels and 60 percent for the foldout panel sections.

Further assumptions and presentation of values of thermal properties and equations used are presented later in this section.

It is noted that both surfaces and temperature distributions presented for Figure A1 (on the figure and verbally for the mosaic above) are amenable to the requirements of References 8 and 11. If -180°F is considered to be the minimum allowable temperature, Figure A2 indicates this temperature is reached in 53 minutes for the fixed panel, and 28 minutes for the foldout panel. Use of the mosaic pattern concept would increase these times to 66 and 46 minutes for the fixed and foldout panel respectively.

4.1 TEMPERATURE DISTRIBUTION

S (Incident Thermal Flux)	
Solar Cell Assembly Including Filter, Adhesives, Insulation, etc.	0
Panel Facing (Front)	1
Panel Core	2
Panel Facing (Back)	3
Paint	4
	5

The equations below are assumed to govern the heat transfer in the direction normal to the planes of the figure above in the absence of heat transfer in any other direction.*

a. Heat transfer through surfaces 0 and 5:

Cell filter -- space plane (surface 0)

$$(Q/A)_0 = \alpha_{s0} S - \sigma \epsilon_0 F_0 T_0^4$$

Panel back (painted) -- space plane (surface 5)

$$(Q/A)_5 = \sigma \epsilon_5 F_5 T_5^4$$

Where

- Q/A = heat flux per surface area
- S = incident (solar flux)
- σ = Stefan-Boltzmann constant
- ϵ = emissivity
- F = view factor of surface to space
- T = absolute temperature

* This is a conservative assumption tending to increase the severity of the maximum temperature gradients within the planes (1, 2, 3, etc.) of the figure and in the direction of the heat transfer considered.

b. Heat transfer through panel core (surface 2 to surface 3):

$$(Q/A)_{2-3} = \frac{k_{2-3} (Ax/A_{2-3})}{L_{2-3}} = (T_2 - T_3) + F_e T_2^4 - T_3^4 \sigma$$

where

The first term on the left side of the equation represents the flux conducted through the core and the second the radiative flux.

F_e = emissivity-view factor product between surfaces 2 and 3

k_{2-3} = thermal conductivity of metal in core

A_x = cross-sectional area of metal in core

L_{2-3} = distance between surfaces 2 and 3

$\frac{k_{2-3} (Ax/A_{2-3})}{L_{2-3}}$ = conductance of panel core which can be determined from a gradient versus flux plot (such as Figure 3-11 Vol VB235AA110 if the second term of the above equation is known.

c. Heat transfer through panel facing (surface 1 to 2 only for a corrugated panel core) or facings (surface 1 to 2 and 3 to 4 for a honeycomb with front and back skins):

$$(Q/A)_{1-2} = \frac{k_{1-2}}{L_{1-2}} (T_1 - T_2)$$

$$(Q/A)_{3-4} = \frac{k_{3-4}}{L_{3-4}} (T_3 - T_4)$$

d. Temperature gradients through solar cell assembly (surface 0 to 1) and through paint (surface 4 to 5) are considered negligible in comparison to other gradients so that

$$T_0 = T_1 \text{ and } T_4 = T_5.$$

Figure 3-12 Volume VB235AA110 has been generated to illustrate the effect of choice of panel back side properties upon the temperature level of the solar panel. The following method and assumption were used:

$$(1) (Q/A)_0 = (Q/A)_5$$

$$(2) T_0 = T_5$$

- (3) $S = 440 \text{ Btu/hr-ft}^2$ (Earth), 195 BTU/hr-ft^2 (Mars)
- (4) $\alpha_{so} = 0.81, \epsilon_o = 0.84$ (solar cell and filter)
- (5) $F_o = 1$
- (6) $\epsilon_5 F_5$ varied (abscissa of figure)

Figure A-1 has been generated as a best estimate of the temperature distribution to be expected for the selected solar panel design. The following method and assumptions were used:

- (1) $(Q/A)_o = (Q/A)_{1-2} = (Q/A)_{2-3} = (Q/A)_{3-4} = (Q/A)_5$
- (2) $S = 440 \text{ Btu hr-ft}^2$ (Earth), 195 Btu hr-ft^2 (Mars)
- (3) $\alpha_{so} = 0.81, \epsilon_o = 0.84$
- (4) $\epsilon_5 = 0.9$ (selected white paint, Reference 14)
- (5) F_5 and F_o (functions of distance from bus, d)

<u>d (inches)</u>	<u>F_o</u>	<u>F₅</u>
3.6	0.85	0.39
10.8	0.97	0.43
18.0	0.99	0.47
25.2	1.	0.52
32.4	1.	0.58
39.6	1.	0.65
46.8	1.	0.71
54.	1.	0.75
83.	1.	0.89
112.	1.	0.94

Reference 15 used with an approximation of the geometry of Reference 16.

$$(6) \frac{k_{2-3} (Ax/A_{2-3})}{L_{2-3}} = 9.47 \text{ Btu hr-ft}^2 \text{ } ^\circ\text{F}$$

(slope of gradient-flux curve, Figure 3-11, Volume VB235AA110)

- (7) $F_e = 0.65$ (parallel plates, fiberglass skin emissivity of approximately 0.79)
- (8) $k_{1-2} = k_{3-4} = 0.89 \text{ Btu-in/hr-ft}^2 \text{ } ^\circ\text{F}$ (fiberglass skins)
- $L_{1-2} = L_{3-4} = 0.0055 \text{ inch}$

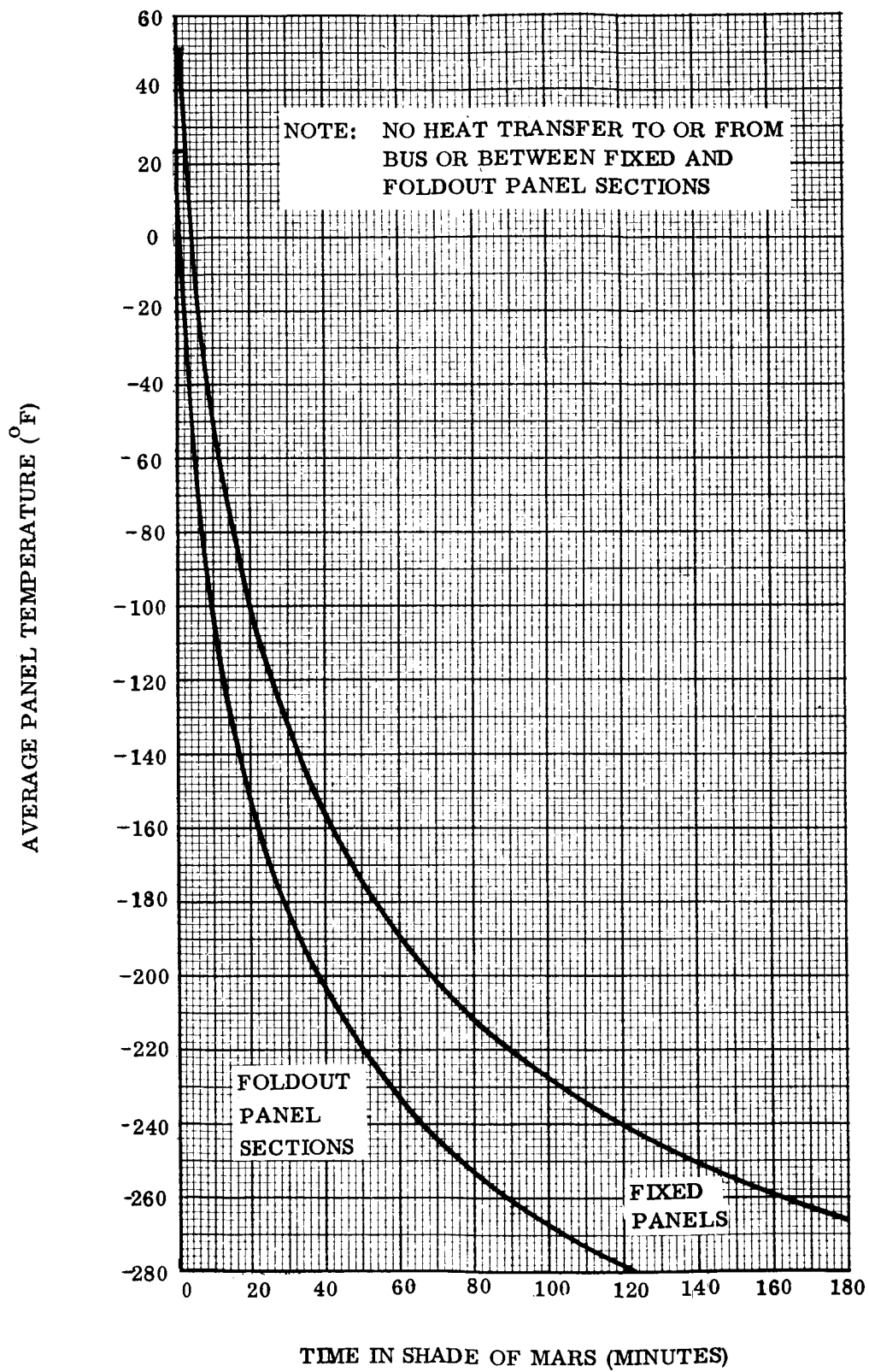


Figure I-1. Solar Panel Temperature Distribution

4.2 TRANSIENTS

Transients for the condition of sun occultation (absence of all exterior heat sources) can be generated for a unit area of solar panel by equating the change in heat content to the radiative heat loss:

$$\frac{\rho VC}{A} \left(\frac{dT}{dt} \right) = -\sigma (\epsilon_o F_o + \epsilon_5 F_5) T^4$$

After separating variables and integrating over a finite time interval this yields:

$$\Delta t = \frac{\rho VC/A}{3\sigma (\epsilon_o F_o + \epsilon_5 F_5)} \left[\frac{1}{(T_{\text{final}})^3} - \frac{1}{(T_{\text{initial}})^3} \right]$$

where

Δt = finite time increment

σ , ϵ_o , ϵ_5 , F_o , F_5 and T have been identified in previous paragraphs.

$\rho V/A$ = weight per unit area

= C specific heat

Figure 3-13, Volume VB235AA110 has been generated using the above equation with the following values:

- (1) $\epsilon_o = 0.84$, $F_o = 1$
- (2) $\epsilon_5 F_5 = 0.25, 0.5, 0.75$
- (3) $\rho VC/A = 0.1, 0.2, 0.3 \text{ Btu/}^\circ\text{F-ft}^2$
- (4) T_{initial} = from Figure 3-12, Volume VB235AA110, Mars vicinity, emissivity-view factor product of $\epsilon_5 F_5$
- (5) T_{final} = ordinate, Δt = abscissa

For Figure A-2 (the transient for the selected panel design) the equation is used with the following values:

Fixed panel section

- (1) $\epsilon_o = 0.84$, $F_o = 0.976$ (average)

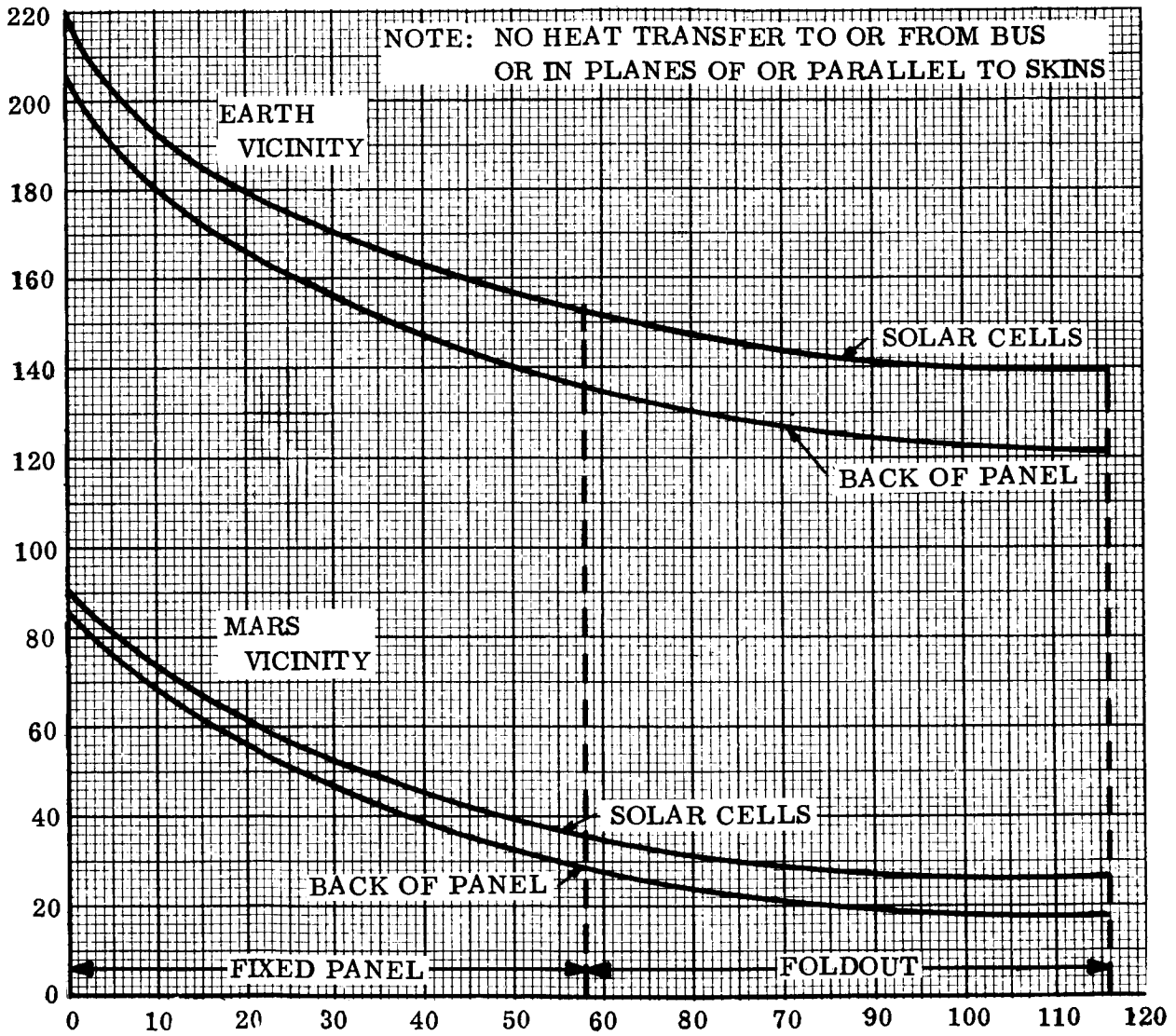


Figure I-2. Mars-Sun Occultation Cool-Down Transient

- (2) $\epsilon_5 = 0.9$, $F_5 = 0.563$ (average)
- (3) $\rho VC/A = 0.16 \text{ Btu}/^\circ\text{F-ft}^2$
- (4) $T_{\text{initial}} = 511^\circ\text{F}$ (per unit area average of Figure A-1, Mars vicinity)

Foldout panel section

- (1) $\epsilon_0 = 0.84$, $F_0 = 1$
- (2) $\epsilon_5 = 0.9$, $F_5 = 0.915$ (average)
- (3) $\rho VC/A = 0.11 \text{ Btu}/^\circ\text{F-ft}^2$
- (4) $T_{\text{initial}} = 485^\circ\text{F}$ (per unit area average of Figure A-1, Mars vicinity)

5.0 LIST OF REFERENCES

1. Ryan Contract with JPL for Development, Design and Fabrication of a Prototype Deployable Large Area Solar Array Supporting Structure, Ryan Report No. 20869-1.
2. Environmental Test Specification, Mariner C, Flight Equipment Type Approval Requirements, Power Subsystem, Solar Panel, JPL Specification MCP-31584-TAT.
3. Qualification Test Report for Mariner C Solar Panels and Thermal Test Specimens, Ryan Report No. 63B133.
4. JPL Test Report "Mariner Mars 1964 Solar Panel Deployment System", Test Report No. 176.
5. Phase I Report to GSFC on the Development of Deployable Solar Arrays, Ryan Report No. 64B119.
6. AIAA Paper No. 64-740.
7. JPL Mariner C Design Specification No. 31169A, Paragraph 3.4.2.
8. Preliminary Voyager 1971 Mission Specification, May 1, 1965, JPL Project Document No. 45-V-MA-004-001-14-03.
9. "Honeycomb Sandwich Structures", Design News, March 31, 1965.
10. Ryan Materials and Processes Laboratory Test Data.
11. "Preliminary Structural Design Criteria - Voyager", General Electric Specification No. 4145-VR350PM002.

12. Alcoa Structural Handbook.
13. "Design and Analysis of Rigid Mechanically-Folded Solar Energy Collector", Ryan Report No. V16-0203, May 1965.
14. T. F. Vajta, "Thermal Control Materials", Space Materials Handbook, Wright-Patterson AFB, ML-TDR-64-40, January 1965.
15. D. C. Hamilton and W. R. Morgan, "Radiant-Interchange Configuration Factors", Purdue University, NACA TN 2836, December 1952.
16. General Electric Drawing SK 56152-402, "Voyager Spacecraft Configuration No. 1", 26 May 1965.
17. MIL-HDBK-17, Plastics for Flight Vehicles, Part I.
18. Rayleigh Theory of Sound, Volume I.
19. Dan Hartog, Mechanical Vibrations, Third Edition.
20. Glenn L. Martin "Structures Design Manual"
21. MIL-HDBK-23, Part III.

VB236FD101

**POWER SUBSYSTEM
FUNCTIONAL DESCRIPTION**

Index

- 1 Scope**
- 2 Applicable Documents**
- 3 Functional Description**
- 4 Interface Definition**
- 5 Performance Parameters**
- 6 Physical Characteristics**
- 7 Safety Considerations**

1.0 SCOPE

This functional description pertains to the Voyager spacecraft power subsystem.

2.0 APPLICABLE DOCUMENTS

VB220SR101	Design Characteristics
VB220SR102	Design Restraints
VB220FD101	Standard Trajectories
VB220FD112	Flight Sequence
VB220FD113	Layout & Configuration
VB220FD103	Spacecraft Component Design Parameters
VB235FD110	Solar Panels

3.0 FUNCTIONAL DESCRIPTION

3.1 REQUIREMENTS

The power subsystem supplies electrical power to the flight spacecraft from launch through all mission phases. It also supplies raw power to the flight capsule during periods of solar array illumination up to the time of capsule separation. Estimates of the average load requirements for each mission phase are presented in Table 3-1 and Figure 3-1.

3.2 POWER FLOW

The power system block diagram is shown in Figure 3-2. Primary power is derived from the solar array consisting of 22 fixed panels forming a flat annular ring about the spacecraft. Each panel contains two solar cell strings which are diode-isolated and have their own zener regulators which limit maximum array output voltage to 55 volts. Array output is fed to the raw array/battery bus and each of three battery charge regulators through an array enabling switch, SW-1, which is closed by the Launch Complex Equipment prior to launch.

Power may also be fed to the raw array/battery bus by three diode-isolated silver-cadmium batteries, depending on relative array power capability and load requirements. Battery power is transferred through the prelaunch-actuated enabling switch SW-1. The range of voltage at the raw array/battery bus is 30 to 55 volts, corresponding to the lower level of battery discharge and the zener regulator cutoff voltage respectively.

The batteries also provide power to a raw battery bus for peak short-term loads. The range of this bus is 30 to 44 volts, with the latter value corresponding to battery charging voltage.

Table 3-1. Voyager 1971 Load Profile (in watts)

	Launch to Acquisition		Cruise (143-182 days)		All Maneuvers	Approach Guidance	MARS Orbit		Spacecraft Eclipse
	Launch to Solar Panel Deployment	Solar Panel Deployment to Cruise	First	After			Spacecraft Day (5 months)	Other Times	
Duration	26-46 min.	995-1065 min.	38-64 days	105-118 days	110-171 min.	11 days	Full Science	3 hours max.	
Power Source	Batteries	Solar Array	Solar Array	Solar Array	Batteries & Array	Solar Array	Solar Array	Batteries	
Capsule Unreg. DC	-----	-----	*200.0	*200.0	-----	until sep 200.0	-----	-----	-----
Science 2.4 Kcs 400 CPS 3φ	-----	-----	* 25.0	* 25.0	-----	*	94.0	30.0	30.0
Pyrotechnic 2.4 Kcs	2.0	2.0	2.0	2.0	2.0	2.0	2.0	2.0	2.0
Environmental 2.4 Kcs	-----	-----	15.0	15.0	15.0	15.0	15.0	15.0	15.0
Radio 2.4 Kcs Unreg. DC	29.8 -----	29.8 145.0	29.8 145.0	29.8 57.0	29.8 145.0/57.0	29.8 57.0	29.8 145.0	29.8 145.0	29.8 57.0
Relay Radio 2.4 Kcs	-----	-----	-----	** 11.2	** 11.2	**	-----	-----	-----
Data Handling 2.4 Kcs 400 CPS 3φ	22.5 -----	13.5 -----	13.5 -----	13.5 -----	13.5 -----	13.5 -----	16.5 5.0	16.5 -----	16.5 -----
Command 2.4 Kcs	20.2	20.2	20.2	20.2	20.2	20.2	20.2	20.2	20.2
G&C 2.4 Kcs 400 CPS 3φ Unreg. DC	17.6 9.0 6.0	17.6 9.0 6.0	9.6 -----	10.9 -----	29.8 9.0 6.0#	30.9 -----	16.2 -----	16.2 -----	24.2 9.0 6.0
C&S 2.4 Kcs	20.0	20.0	20.0	20.0	20.0	20.0	20.0	20.0	20.0

* Off during maneuvers
 ** Relay receiver operates from capsule separation to orbit insertion
 # Plus 78 watts during engine fire periods (6 min.)

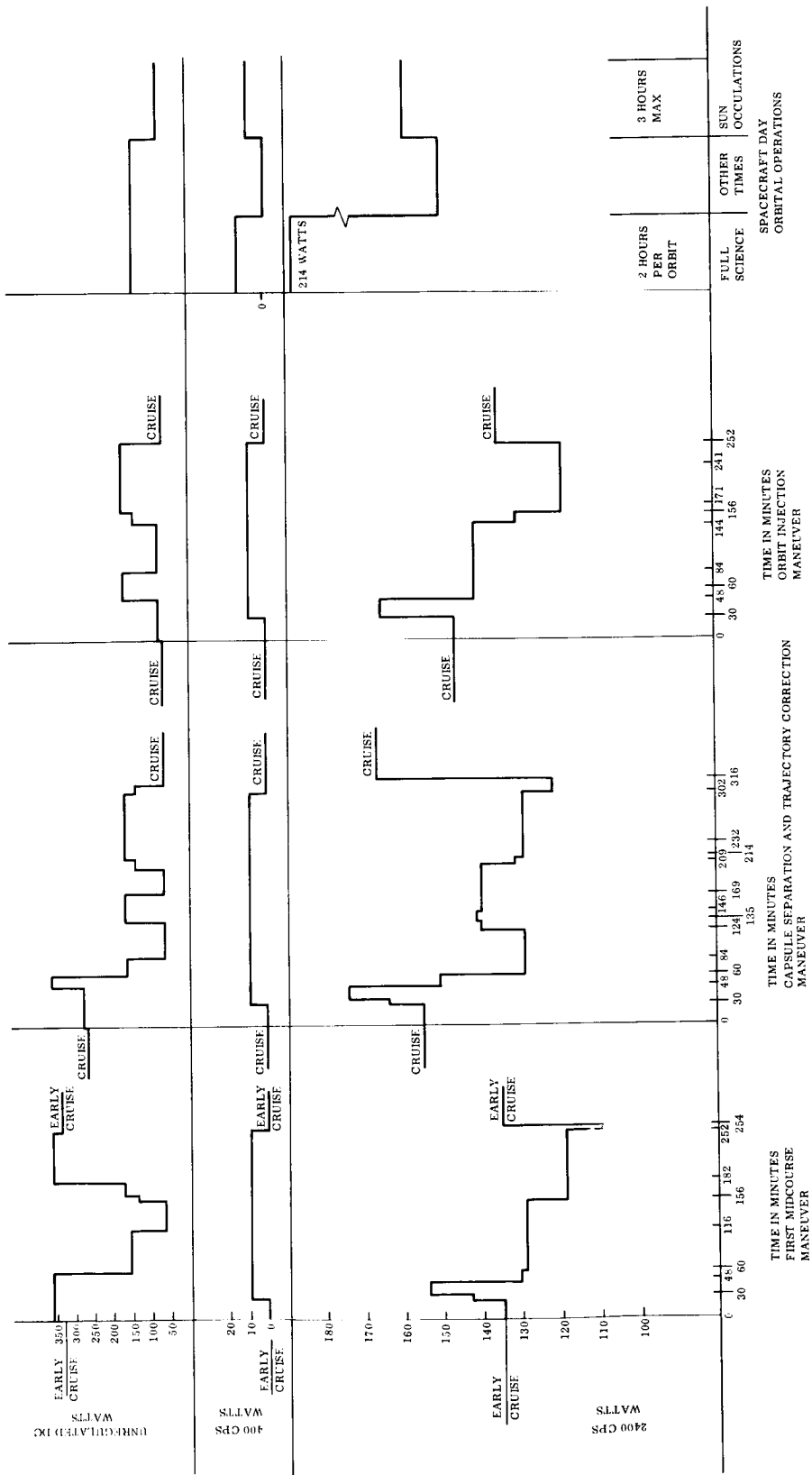


Figure 3-1. Voyager Load Profile

VB236FD101

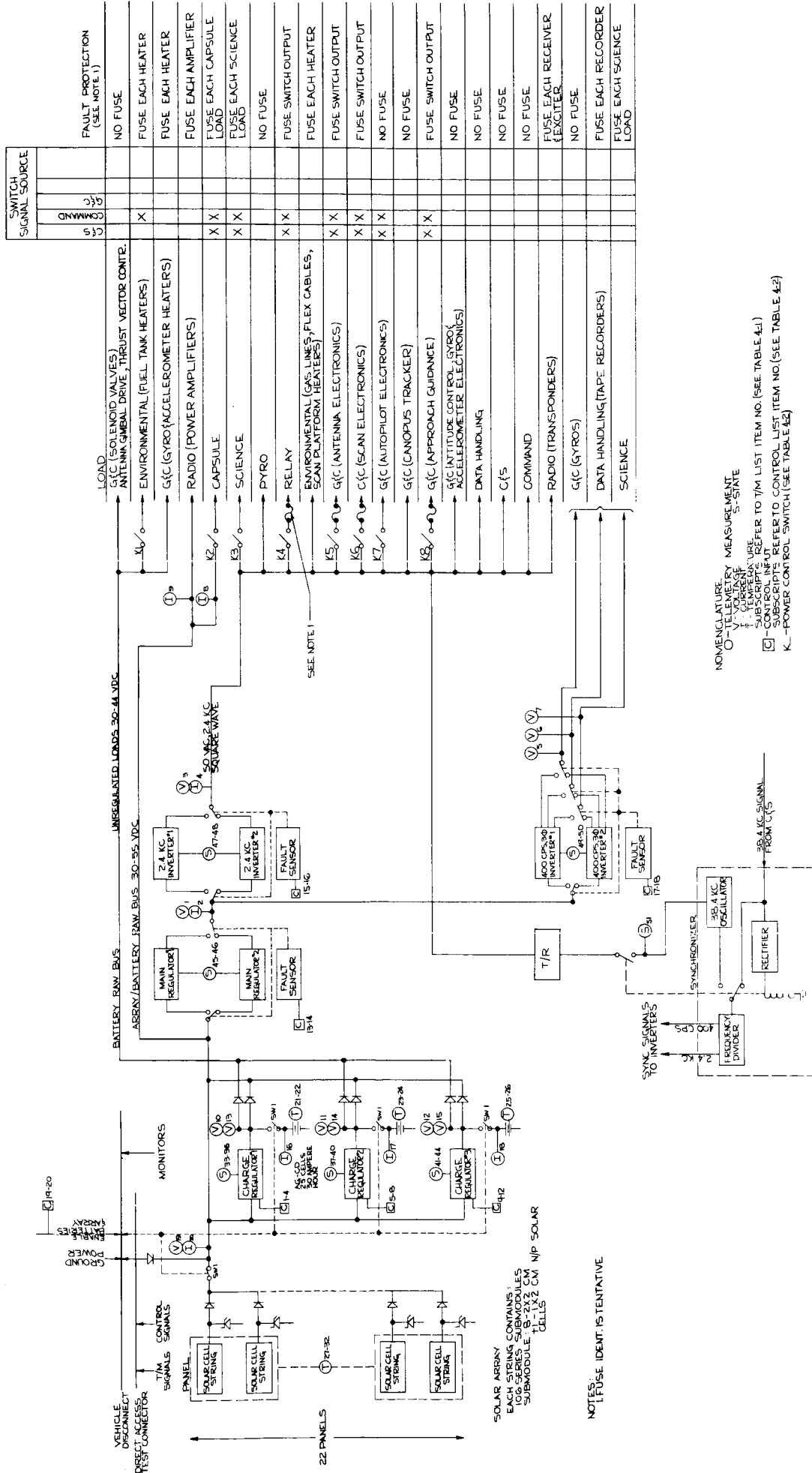


Figure 3-2. Functional Block Diagram

Power from the raw array/battery bus is fed directly to the radio system, the flight capsule, and the main regulator. This regulator is a series-switching type which converts higher input voltages to a lower regulated output level of 28 vdc at one percent regulation. This output is directed to a 2400 cps, 50 volt AC square wave inverter, which supplies AC power to the majority of the user subsystems. Transformer-rectifier units located at the various points of use convert the AC power to desired DC levels.

The 28 vdc main regulator output is also directed to a 400 cps 3 phase, stepped square wave inverter for supplying power to the gyros, tape recorder motors, and to Science payloads, if desired.

Both the 2.4 kc and 400 cps inverters are frequency-controlled by a synchronizer, which receives a clock signal of $38.4 \text{ kc} \pm .01$ percent from the C&S subsystem.

3.3 BATTERY CHARGING

The battery charge regulators are of the series-dissipative type in which the regulator impedance is varied to limit battery charging voltage and current. With all three charge regulators in operation, each regulator limits the charging current into its associated battery to a nominal one ampere. This value is the highest recharge requirement of the overall mission, which occurs during occulted Martian orbits. See Appendix B for the specific calculations leading to this value. If faulty battery operation is detected through telemetry information it is possible, by command, to remove charging power to the particular battery. Under this condition the current limit to the remaining two batteries is automatically increased by 50 percent to 1.5 amperes, thus maintaining a total charging current of 3 amperes. Similarly, with two faulty batteries, the current limit is automatically increased to 3 amperes on the one remaining battery with removal of charge from the second regulator. By the above means it is possible to maintain the original load profile, though greater depths of discharge are experienced with the use of fewer batteries. With all batteries operational the maximum depth of discharge is 56 percent occurring during a Martian orbit with an occultation time of 3 hours. With a nominal capacity of 25 ampere-hours for each battery, maximum charging occurs at the 8.3 hour rate with one regulator set at the 3 ampere limit. The charge regulators also provide upper voltage limits for battery charging. One of three limit levels may be selected by command for each regulator:

Voltage Limit A : 44.2 volts

Voltage Limit B : 42.65 volts

Voltage Limit C : 41.1 volts

This adjustability is included to accommodate the possibility of battery performance variations, such as partial cell shorting.

The information required for modifying the regulator setting is derived from battery voltage, current and temperature telemetry information. Possible abnormal operating conditions may be deduced from the following:

- a. Uneven sharing of the load during battery discharge cycles. The battery(s) with partially or fully shorted cells will initially provide a small percentage of the load current and assume a greater percentage at deep discharges of the remaining good battery(s).
- b. Excessive battery temperature
- c. Discrepancy between the ampere-hours removed during discharge periods and re-stored during recharge periods. The ampere-hour efficiency of silver-cadmium batteries is on the order of 98 percent over wide ranges of charge and discharge rates and therefore the restored ampere-hour charge is slightly greater than the removed ampere-hours. Under normal conditions the regulator voltage limit provides the means by which charging current is reduced to zero as the battery approaches full charge. With shorted cells the voltage limit cannot perform this function and the battery may be excessively charged. The accounting of ampere-hours in and out of the battery is required as a function of the operational support during flight in order to forestall the overcharge possibility.

A decrease in the voltage limit, by command, removes the potential danger of overcharge although the condition described in (2) above will not necessarily be relieved. Unequal battery sharing, per se, is not considered serious as long as end of discharge voltages are above specified limits.

3.4 DISTRIBUTION

Power is distributed to the various loads through switching devices located at the user subsystems or in the Power Switching and Logic (PS&L) Unit of the Power System. Those located in the PS&L derive their switching signals externally to the user subsystem, whereas those located at the user subsystems derive their signals from internal logic.

The functional block diagram, Figure 3-2 shows those switching elements assigned to the PS&L along with the driving signal sources.

3.5 FAULT PROTECTION

The potential use of fuses are shown in Figure 3-2 and are identified with loads whose loss are not catastrophic to the mission. The actual use of such protective devices must be determined from reliability trade studies carried out at a system level.

Where identified as part of the power system, these devices are located within the PS&L unit.

3.6 REDUNDANCY

Redundant units along with appropriate fault sensing and switchover circuitry are provided for the following units:

- a. Main Regulator - Fault criterion is based on under- or over-voltage at regulator output sustained for a period greater than three seconds.
- b. 2.4 kc Inverter - Fault criterion is based on exceeding the tolerance limit of the output-to-input voltage ratio. Signal rectification of the AC output is required for this purpose.
- c. 400 cps Inverter - Fault criterion is based on exceeding the tolerance limit of the output-to-input voltage ratio of any phase of the output. Signal rectification of the three output phases is required for this purpose.
- d. Synchronizer - The scheme used is identical to that used in the Mariner IV spacecraft. A 38.4 kc timing signal from C&S drives a frequency divider providing synchronizing signals to the 2.4 kc and 400 cps inverters. Loss of the C&S results in switchover to a 38.4 kc oscillator internal to the power system. Loss of this backup results in a free-running mode of the 2.4 kc inverter, but not for the 400 cps inverter which would be rendered inoperative.

3.7 OPERATIONAL MODES

The principal operational modes of the power system are described below:

3.7.1 PRE-LAUNCH

The sequence of events from hangar checkout to on-pad operations are:

- a. The Overall Flight Spacecraft is transferred to the launch pad. The power subsystem is inoperative, with all contacts of switch SW-1 open.
- b. Subsequent to on-pad mating, ground power is gradually applied through the umbilical disconnect and raised to a level of 45 to 55 volts DC. The battery charge regulators are turned off.
- c. Switch SW-1 is closed through umbilical signal leads only after proper ground power voltages have been established. This sequence prevents arcing across the switch contacts by eliminating the possibility of large battery currents during switch closure.

- d. Battery charging is initiated, to the degree required, by selection, through the command link, of proper charge regulator settings. Normal on-pad checkout of the power system may now proceed.
- e. Subsequent to removal of the umbilical, just prior to launch, the batteries supply all power at a discharge voltage in the range of 32 to 37 volts DC.

3.7.2 LAUNCH PHASE

The batteries continue to supply power. Loads are supplied through load control switches receiving signal inputs external to the power system.

3.7.3 ACQUISITION

With solar acquisition, the solar array output is established and the conditions of operation are shown in Figure 3-3. The excess array capability in near-earth operation eliminates the possibility of an array-battery load sharing mode. Equilibrium conditions between array output and load and zener regulator demand occur at point A. The battery discharge diodes are back-biased and charging commences through the charge regulators at a current limit of 1 ampere. The capsule load of 200 watts is introduced by command or sequence logic and has the effect of shifting the load characteristic line to the right. The higher demand is still significantly less than the array capability and no danger of load sharing exists. The main regulator receives input power at the array output voltage and converts it to 28 volts \pm 1 percent for further processing by the inventor. Raw battery power may be periodically demanded by heater elements or solenoid valves. The charge regulators will supply this power up to the limit of three amperes, which is far greater than the anticipated heater and solenoid loads, and therefore no battery discharge is expected.

3.7.4 CRUISE

Cruise operation is identical to that described above. The batteries will have achieved full charge and charging current reduced to very small values by the action of the charge regulator voltage limit. During long periods without battery use the charge regulator voltage limit will be reduced to its lowest setting to minimize the effect of silver migration into the cell separator materials. Some period prior to planned maneuvers the highest setting would be used to assure maximum battery capability.

3.7.5 MID-COURSE AND RETRO-MANEUVERS

The batteries supply full or partial power depending on the degree of array orientation. Periods between maneuvers are sufficiently long to permit battery recharge. To obviate the possibility of array-battery load sharing the capsule load is switched on after full solar acquisition.

3.7.6 MARS ORBITAL OPERATION

Operation is similar to cruise. Array power capability decreases with time because of the increasing sun-spacecraft distance. After two or three months of orbital operation sun occultations may occur and the load-sharing problem may be critical. The conditions of operation are shown in Figure 3-4. Loads are reduced during occultations until array output is established upon emergence, thus avoiding the possibility of load sharing. If large loads in excess of array output are introduced during non-occulted periods, again load-sharing can be a problem and it would be necessary to temporarily interrupt some of the loads. So far no such case has been identified.

3.8 HARDWARE DESCRIPTION

3.8.1 SOLAR ARRAY

The solar array consists of 22 trapezoidal solar panels separately fastened to a framework formed around the periphery of the vehicle.

The panel substrates consist of honeycomb with fiberglass face sheets. The details of this construction along with the structural framework are discussed in VB235FD110.

Mounted on each panel are eight rows of solar cells as shown in Figure 3-5. Properly interconnected these rows form two identical solar cell strings: the two shortest and the two longest rows form one string; the remaining four rows form the second string.

Each string contains 106 submodule elements in series. Each submodule contains eight 2 x 2 centimeter and one 1 x 2 centimeter cells in parallel.

Each panel contains the equivalent of 1802 2 x 2 centimeter cells. The total array contains the equivalent of 39,644 2 x 2 centimeter cells.

Solar cell characteristics are as follows:

Type:	N/P, silicon
Dimension:	1 x 2 and 2 x 2 centimeters, 13 mil thickness
Effective cell area:	95 percent
Contacts:	Sintered titanium - silver, solder-free, standard top and bottom contact configuration.
Bare cell efficiency:	11.0 percent at zero air-mass at mean earth-sun distance, cell temperature 28 ^o C.

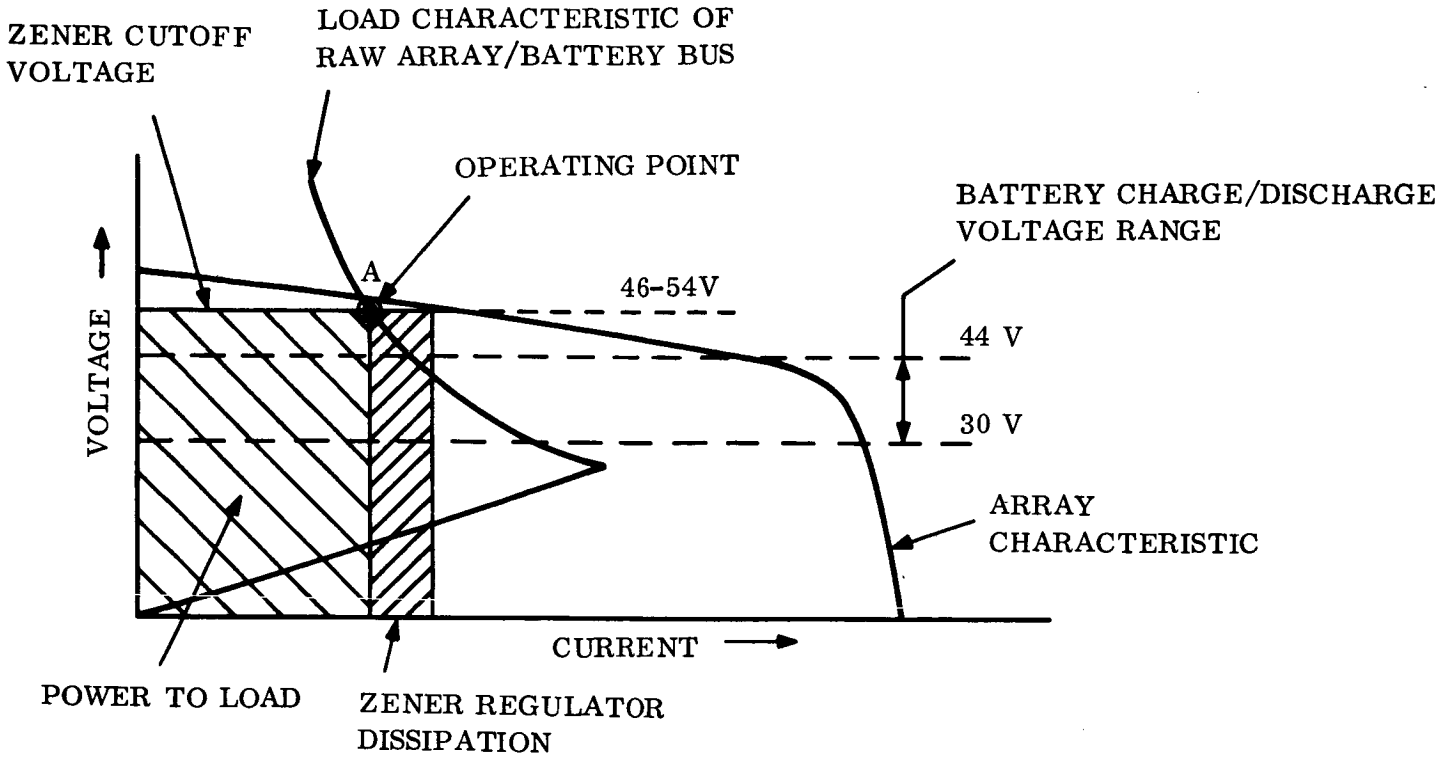


Figure 3-3. Near-Earth V-I Characteristics

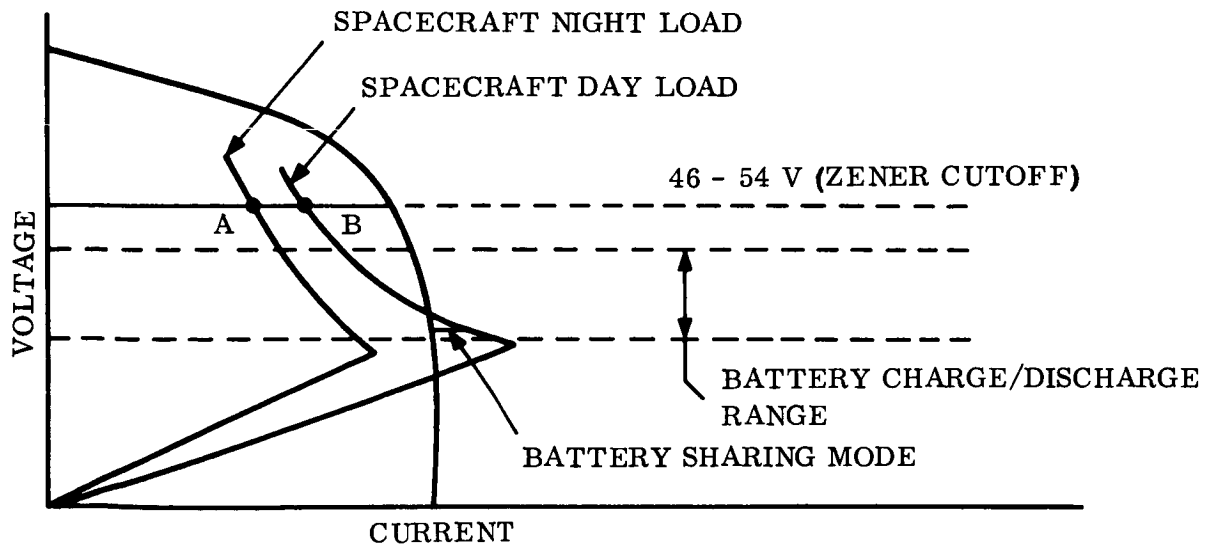
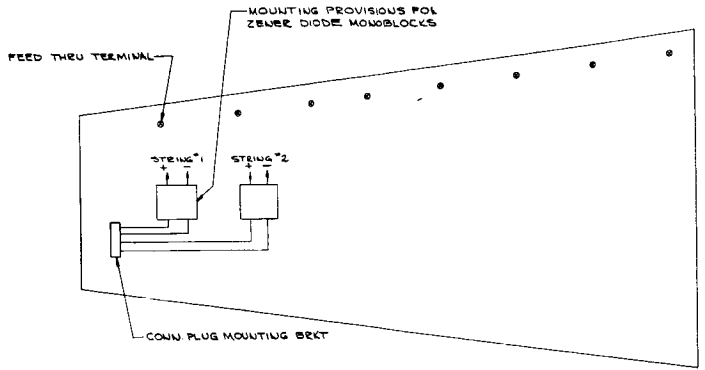
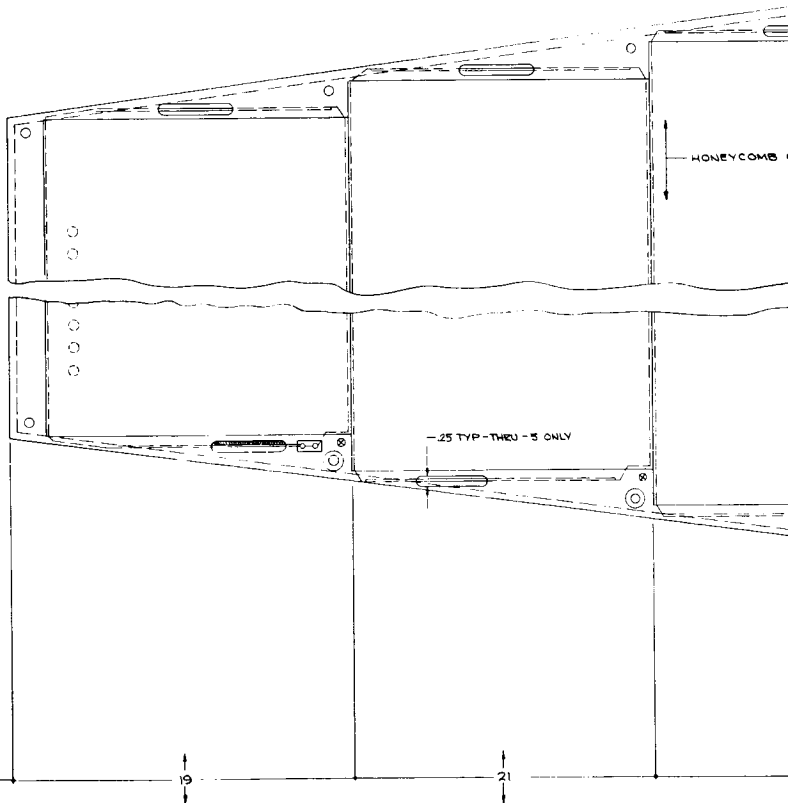


Figure 3-4. Orbital V-I Characteristics

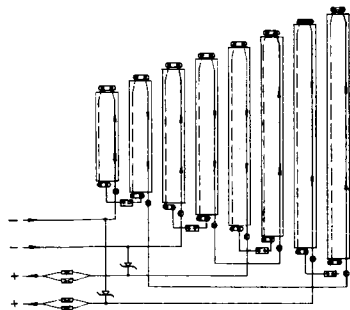


VIEW OF BACK SIDE OF PANEL SHOWING ELECTRICAL PROVISIONS
SCALE: NONE



NUMBER OF
SUBMODULES
PER ROW

140

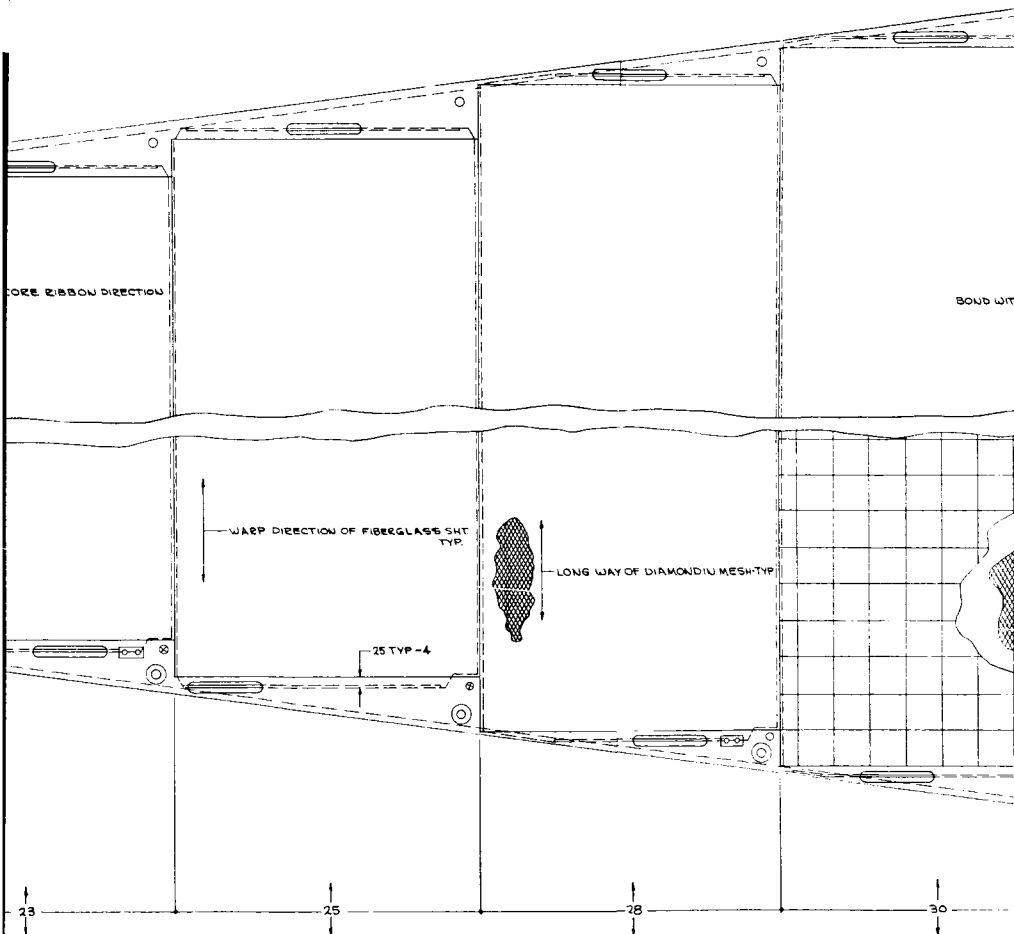


ELECTRICAL SCHEMATIC

LEGEND

- ⊗ FEED THRU TERMINAL
- ⊠ MESH CONN. BLOCK
- ⊡ CELL ATTACH TO MESH
- ⊞ BLOCKING DIODE
- ⊟ ZENER REGULATOR

STEELING	1
SUBMO	32
WEE	32
	21
	18
TOTAL	102



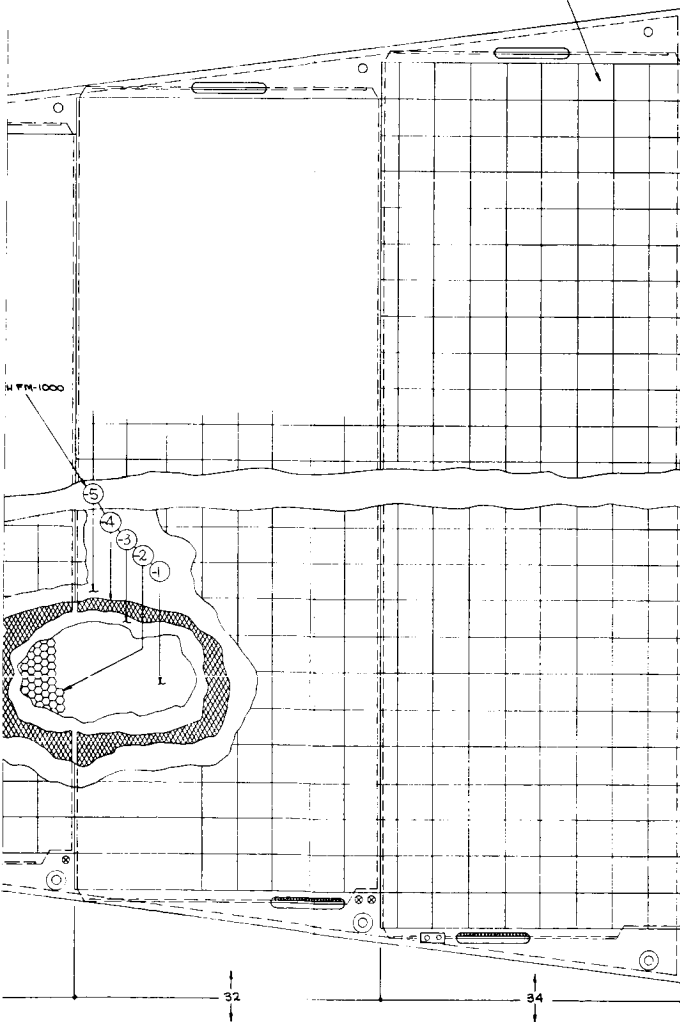
VIEW OF FRONT FACE OF PANEL SHOWING CELL LAYOUT & ELECTRICAL PROVISIONS

SCALE: 1/4"

14 (2)

NO	2
SUN	100
NO	30
NO	28
NO	26
NO	24
NO	100

SOLAR CELL SUBMODULE 24x2 CM PLUS 1-1x2 CM CELLS IN PARALLEL



-5	SKIN	FIBERGLASS EPOXY SHEET ONE PLY STYLE 108-002
-4	MESH	FINE EXPANDED SILVER MESH PLATTED & ANNEALED 24 T. 2/0E
-3	SKIN	FIBERGLASS EPOXY SHEET ONE PLY STYLE 108-002S
-2	CORE	ALUMINUM HONEYCOMB CORE-VENTED 300 THICK-1/4" DIA. HEN-0005 POL
-1	SKIN	FIBERGLASS EPOXY SHEET ONE PLY STYLE 557-005S
PART NO	DESC	MATERIAL

Figure 3-5. Solar Panel

5

Prospective Vendors: RCA, Semiconductor Division
 Texas Instruments
 Heliotek, Division of Textron, Inc.
 Hoffman Electronics
 International Rectifier Corp.

Protective solar cell cover windows are bonded to each solar cell. Characteristics are:

Material: Fused silica, Corning #7940

Filter: Blue, .41 micron cut-on frequency,
 deposited on solar cell side of window,
 anti-reflection coating on opposite face.

Thickness: 6 mils

The window to cell bond is GE clear silicone rubber RTV-602.

Cells are interconnected by means of 3 mil expandable strips of the type shown on Figure 3-6. Material selection for this strip is not resolved, but the principal contenders are molybdenum and tantalum.

The submodule elements are bonded to the honeycomb substrate using GE silicone rubber RTV-560.

To minimize the generation of induced magnetic fields the return current path of each submodule row is through a silver mesh imbedded between layers of the top fiberglass facesheets of the honeycomb.

3.8.2 ZENER REGULATOR

The Zener Regulator module for each array string consists of three parallel strings of seven diodes each, and two isolation diodes in parallel as shown in Figure 3-7. The Zener diodes are 7.0 volt breakdown devices manufactured by Unitorde Transistor Products Incorporated, Waltham, Mass.

The diodes are encapsulated in a resilient, thermally conductive, electrical insulator in cylindrical holes in an aluminum monoblock that measures approximately 1 inch x 3 inch by one-quarter inch high and weighs approximately 35 grams. The monoblock is capable of thermal cycling from -260°F to $+200^{\circ}\text{F}$ and is capable of dissipating fifty watts through a dry interface into an infinite heat sink, maintained at $+100^{\circ}\text{F}$ maximum.

The module must be capable of regulating the voltage from a 12 ohm source variable from 30 volts to 90 volts and current limited to 0.84 ampere to hold 50 volts \pm 4 volts at its input terminals over the temperature range from -170° to $+100^{\circ}\text{F}$.

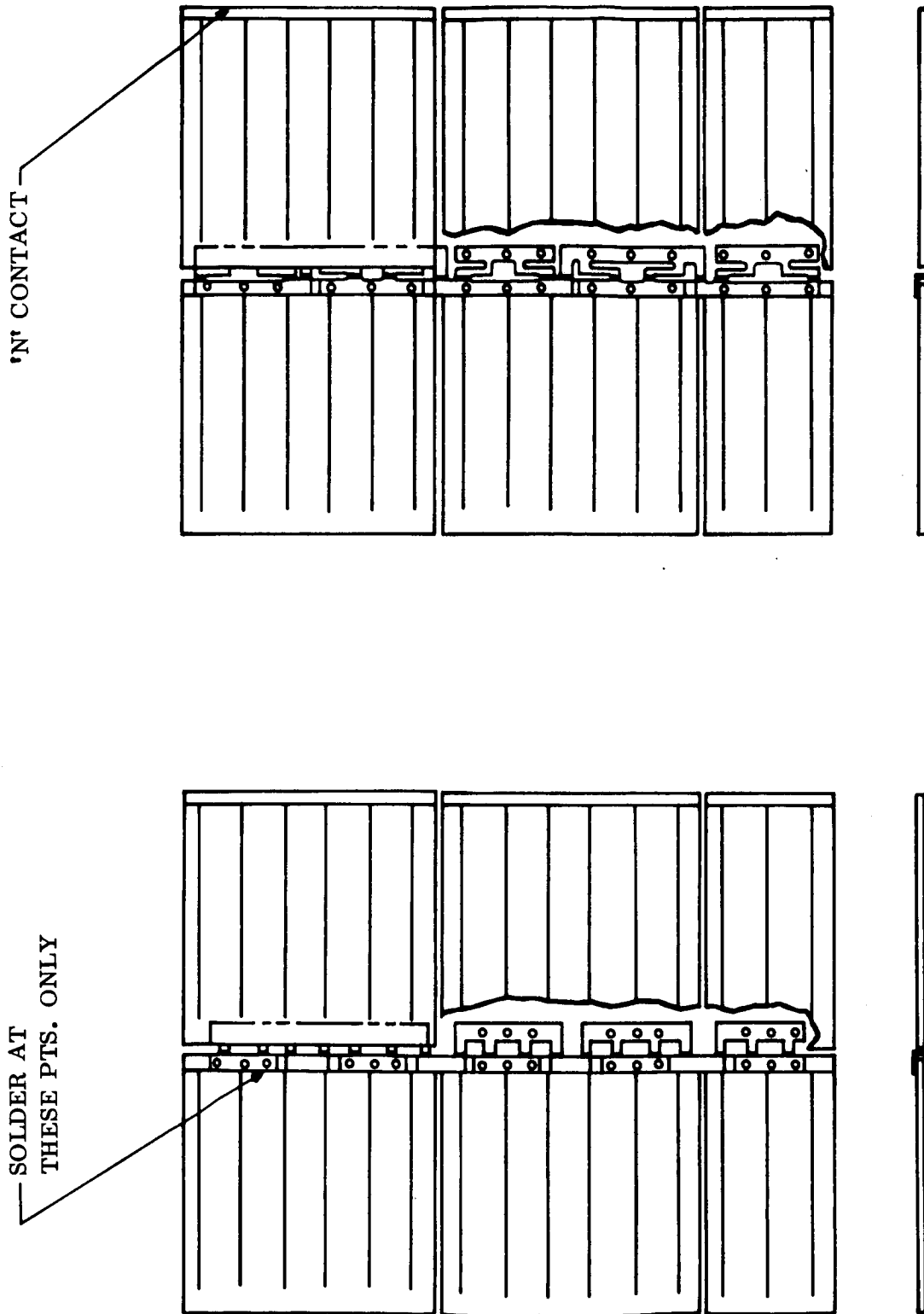


Figure 3-6. Solar Cell Interconnection

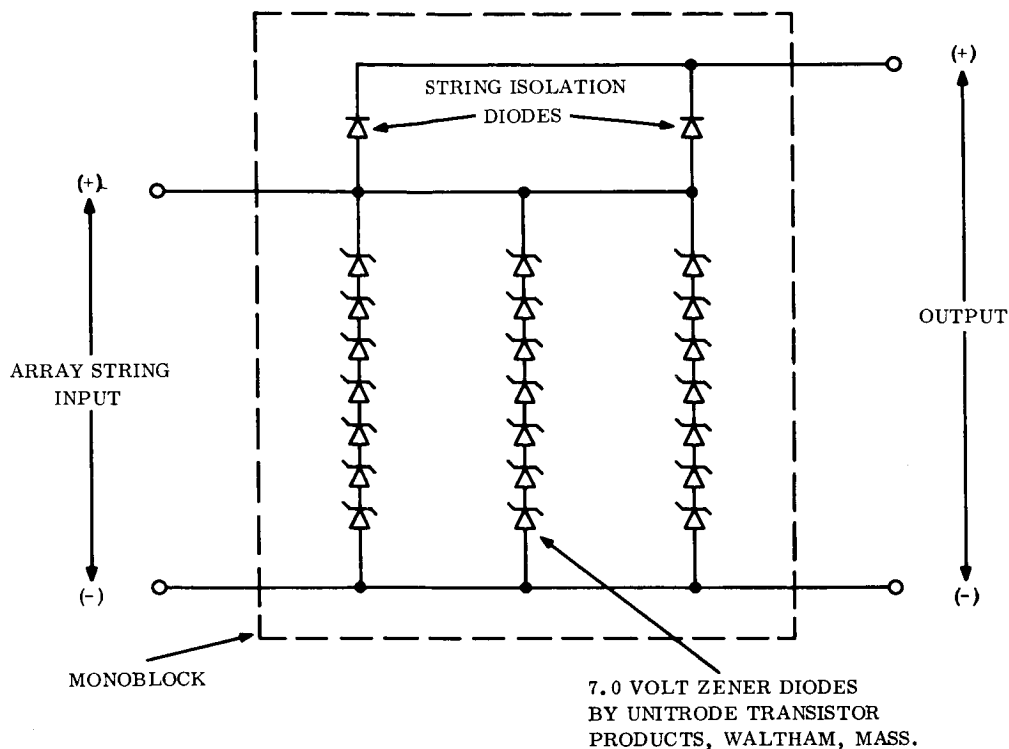


Figure 3-7. Zener Regulator Schematic

3.8.3 BATTERIES

The battery system consists of three independently controlled and identical battery assemblies. The characteristics of each battery assembly are:

- a. Type: Silver - cadmium, sealed cells
- b. Rated Capacity: 25 ampere - hours
- c. Number of series cells: 29
- d. Schematic: See Figure 3-8.

Each battery assembly is non-magnetic and capable of functioning as a sealed unit for a period in excess of two years.

Silver cadmium cells of standard design encased in non-magnetic stainless steel are used. Each cell contains ceramic hermetic seals at each terminal. A safety vent, which is set at 200 psig, is provided with each cell in the event of overcharge.

Internal cell separators are designed for the required life while introducing the least possible internal resistance. Separator material properties are chiefly responsible for restricting battery operating temperatures to 40 to 80° F.

The positive plates consist of finely divided sintered silver securely attached to a silver mesh grid. The negative plates consist of a blend of cadmium oxide deposited onto a silver mesh grid. Active material thicknesses are controlled to ± 0.003 inch.

The electrolyte consists of potassium hydroxide in distilled water with concentration established by the desired operating temperature range.

An anti-polar mass is added to the positive active material to serve as protection against over-discharge. This permits up to 2-3 ampere-hours of reverse charge if, as a result of extensive ground testing, the battery cells become unbalanced and are totally discharged.

In addition to the above precaution, a special access connector is provided to permit discharge of each cell individually prior to its installation in the spacecraft. This permits all cells to be charged to a uniform capacity level.

The cells are packaged in a magnesium case and interconnected in a figure "8" arrangement to maintain magnetic cleanliness.

3.8.4 CHARGE REGULATOR

The charge regulator maintains the charging current into the battery at a preset current until the battery terminal voltage reaches a preset voltage. At this point the regulator maintains constant terminal voltage by controlling the current flow. In no case will the current exceed 3 amperes, the maximum preset value.

The charge regulator circuit is a dissipative series regulator which is current limited at a preset current, and voltage regulated at all lower currents. The regulation voltage is determined by three "on" commands which set the regulated level at 44.2, 42.65, and 41.1 volts. A fourth command shuts the regulator "Off" by grounding the reference voltage. When all three charge regulators are operating, each one is current limited to 1 ampere. If one is shut off, the remaining two are current limited to 1.5 amperes. If two are shut off, the last one will current limit at 3 amperes. The charge regulator control circuits set the voltage levels by command and set the current levels automatically when any regulators are turned off by command.

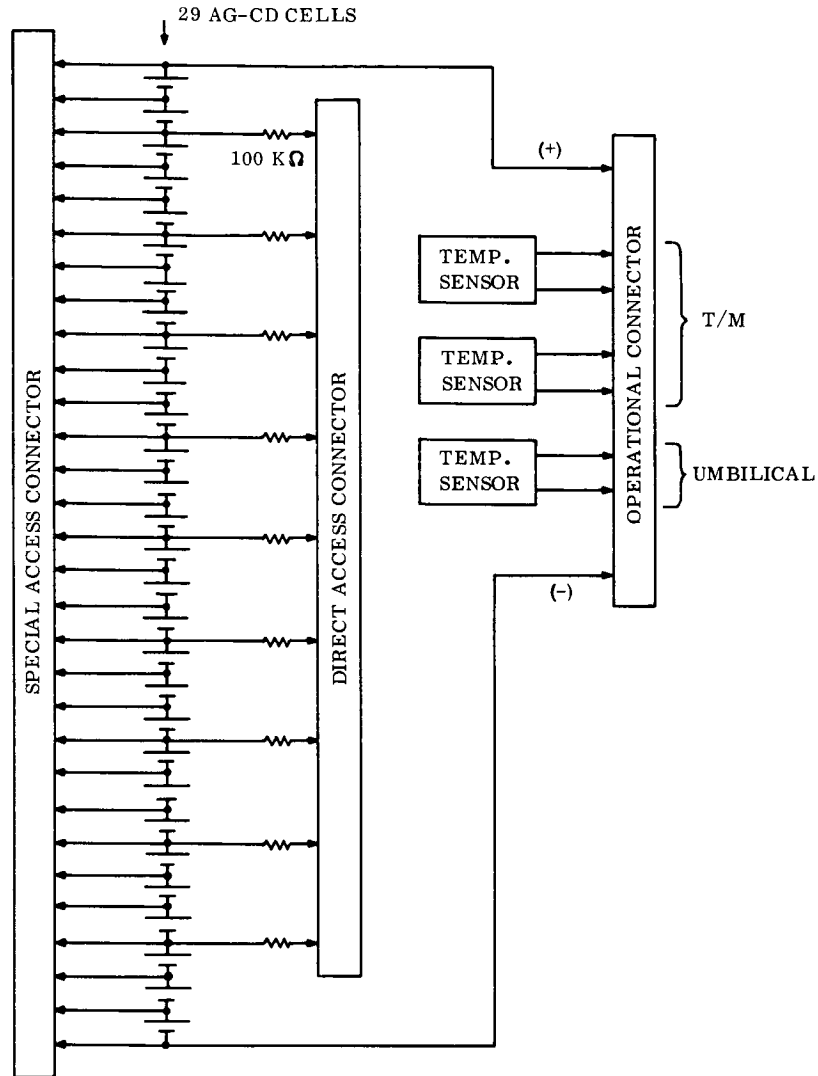


Figure 3-8. Battery Schematic

The series regulating transistors consist of an NPN compound transistor driven by a PNP transistor. These are identified as Q2 and Q3 in Figure 3-9. These are connected to behave like a single PNP transistor with current gain equal to the product of the three individual gains. The series regulator current is controlled by Q1's collector 2 current. For low battery voltage this current is constant and the regulator current is fixed. As the battery voltage rises to the voltage regulating level, section 1 of Q1 comes on and collector 2 current will start to reduce and will continue to reduce as necessary to prevent the battery voltage from exceeding the regulating level.

The charge control circuit consists of four multivibrators which are set by command. (See Figure 3-10.) These are interconnected so that a set command to any one will automatically reset all others. Three of the multivibrators control shunts from base 1 of Q1 in the

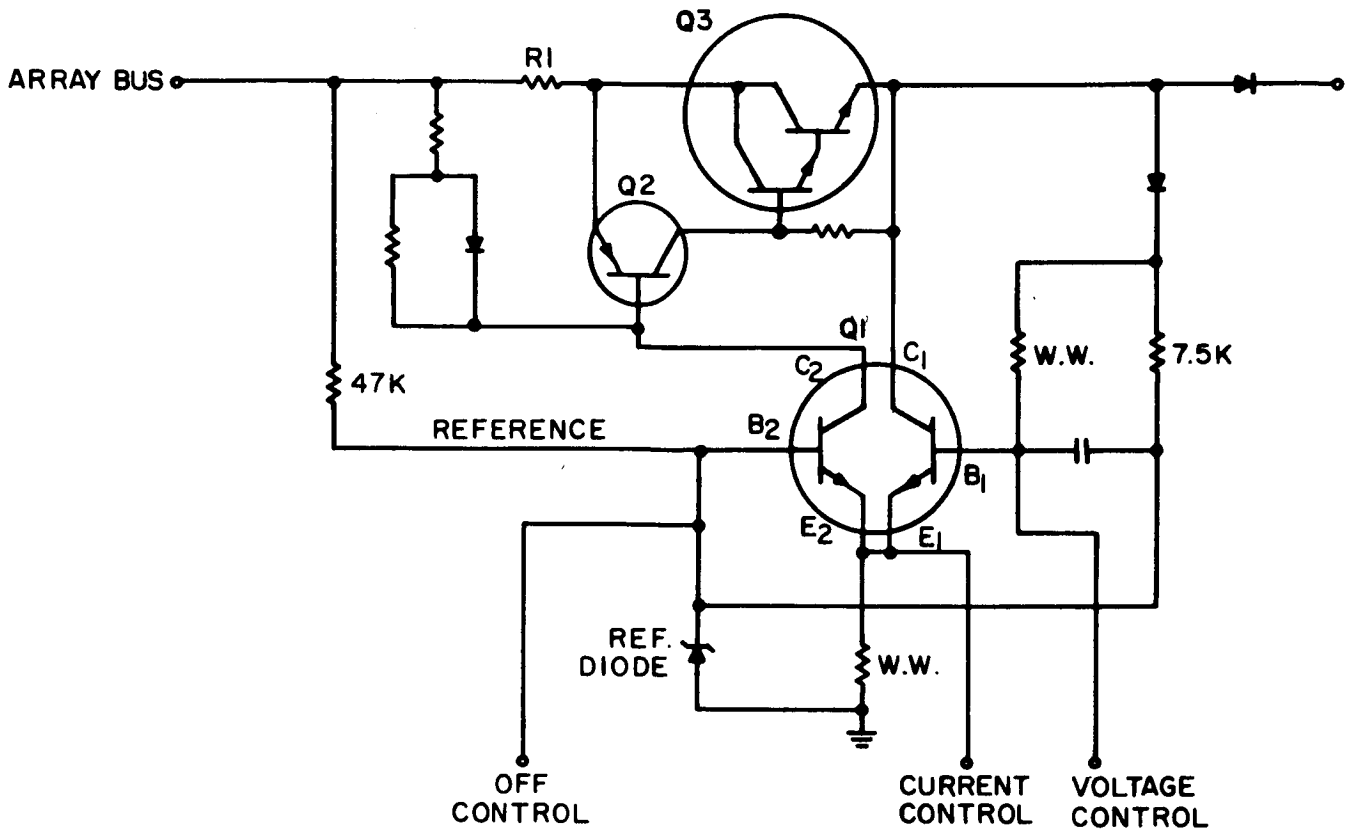


Figure 3-9. Charge Regulator Schematic

regulator and thereby set the regulator voltage to any one of three levels. The fourth multivibrator grounds the reference voltage which reduces the charging current to zero thereby turning off the charger when "off" is commanded.

A current is taken from each multivibrator and is used to furnish T/M information on the state of the charge control circuit. Current control logic is used to change the preset current limit in the charge regulator and this level is determined by sensing if one or both of the other regulators are off. This logic is as follows:

Current level for Regulator No. 1

$$1 \text{ amp} = 2 \cdot 3$$

$$1.5 \text{ amp} = \bar{2} + \bar{3}$$

$$3 \text{ amp} = \bar{2} \cdot \bar{3}$$

Current level for Regulator No. 2

$$1 \text{ amp} = 1 \cdot 3$$

$$1.5 \text{ amp} = \bar{1} + \bar{3}$$

$$3 \text{ amp} = \bar{1} \cdot \bar{3}$$

VB236FD101

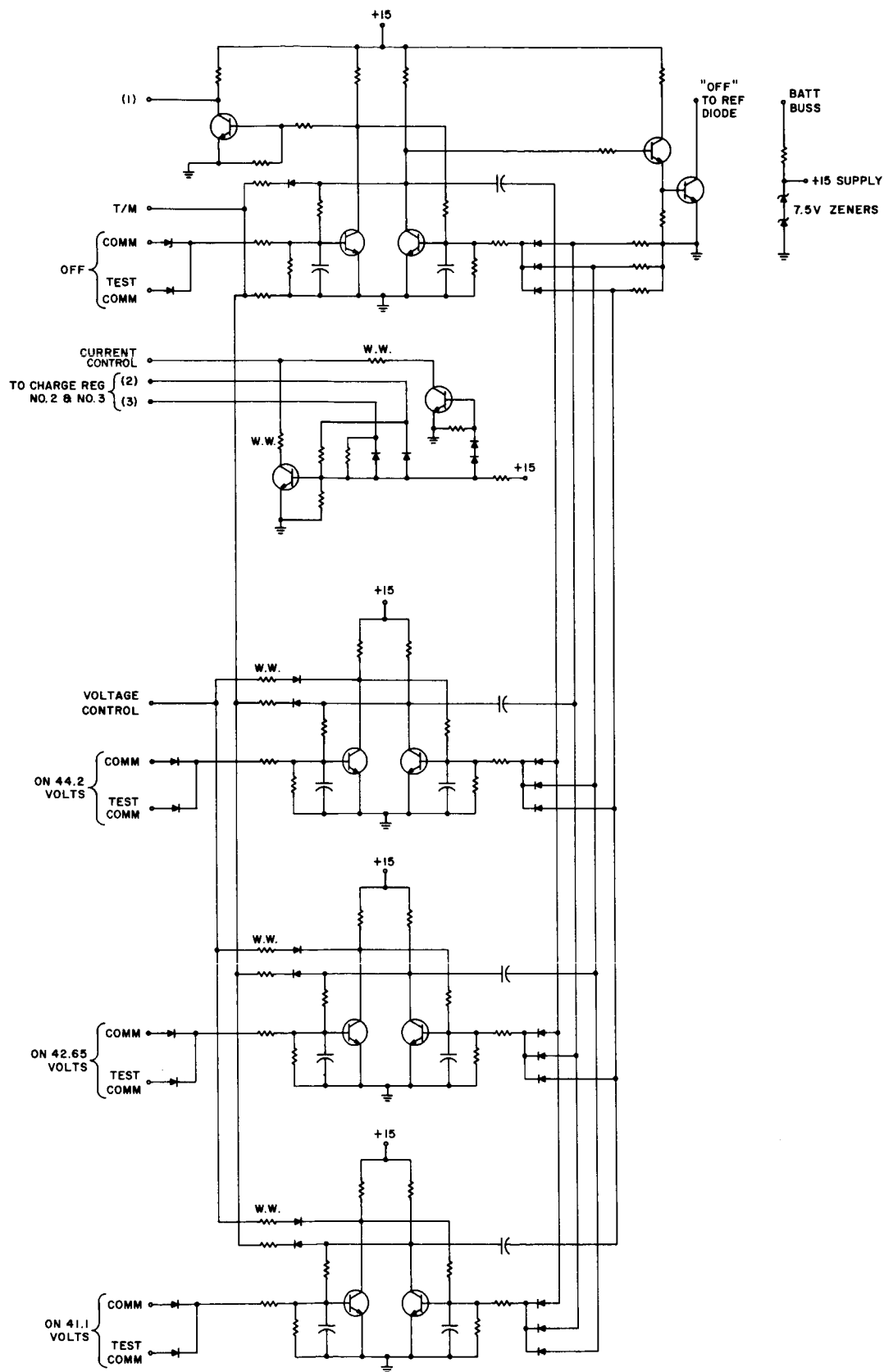


Figure 3-10. Charge Regulator Control

Current level for Regulator No. 3

$$1 \text{ amp} = \bar{1} \cdot \bar{2}$$

$$1.5 \text{ amp} = \bar{1} + \bar{2}$$

$$3 \text{ amp} = \bar{1} \cdot \bar{2}$$

3.8.5 MAIN REGULATOR

The main regulator reduces the unregulated bus voltage to + 28 vdc and maintains this level independent of load and input voltage variations. In addition, the regulator maintains a very low +28 volt line impedance, which provides isolation between users at regulated voltage, even those using inverter voltages. Active regulation with input and output filters provide effective isolation of the regulated lines from battery and solar array disturbances.

The main regulator is of the high efficiency time-ratio-control type, preset for a fixed output and with a self contained inverter and dc power supply. Reduction of the unregulated bus voltage is accomplished by **not** connecting it to the output bus all the time. This may be illustrated by assuming the unregulated output is + 56 volts. By connecting the unregulated bus to the regulated bus 50 percent of the time, the average output voltage is 1/2 the input voltage of +56 volts or +28 volts. To regulate or maintain +28 volts out as the input voltage reduces, it is necessary to increase the 50 percent on time to total time. This changing of the on time to total time ratio identifies this regulating method as time ratio control.

The switch which connects the unregulated bus to the regulated output is transistor Q1 of Figure 3-11. It is driven on and off by Q2 and Q3 which are in turn switched on and off by Q4, the time ratio control transistor. The on-off periods occur at a kilocycle rate established by the inverter consisting of Q6, Q7 and saturable reactor SR-1. The square wave at the secondary S1 of SR-1 is made roughly triangular by an RC network, and amplified by Q5. The triangular output of Q5 is summed with a current from the control circuit and turns A4 on and off. With no current from the control circuit the equal (+) and (-) currents of the triangular waveform will turn Q4 on and off with a 50 percent duty cycle. A (+) current from the control will increase the duty cycle by holding Q4 on longer. If the (+) control current equals the peak (-) triangular current Q4 will remain on all the time.

This would connect the unregulated bus to the regulated bus 100 percent of the time and is the limit of the regulation capability. Similarly, if the control current is (-) and equal to the (+) peak of the triangular wave Q4 will remain off and there will be no output voltage. This point however is not practical for regulation and could only be used to shut off the regulator.

The control circuit is a two stage feedback amplifier consisting of Q8 and Q9. Hence the regulated voltage is divided down and compared to the reference at Q8 base. Any error is amplified and causes sufficient swing of Q9 emitter to vary the control current. The

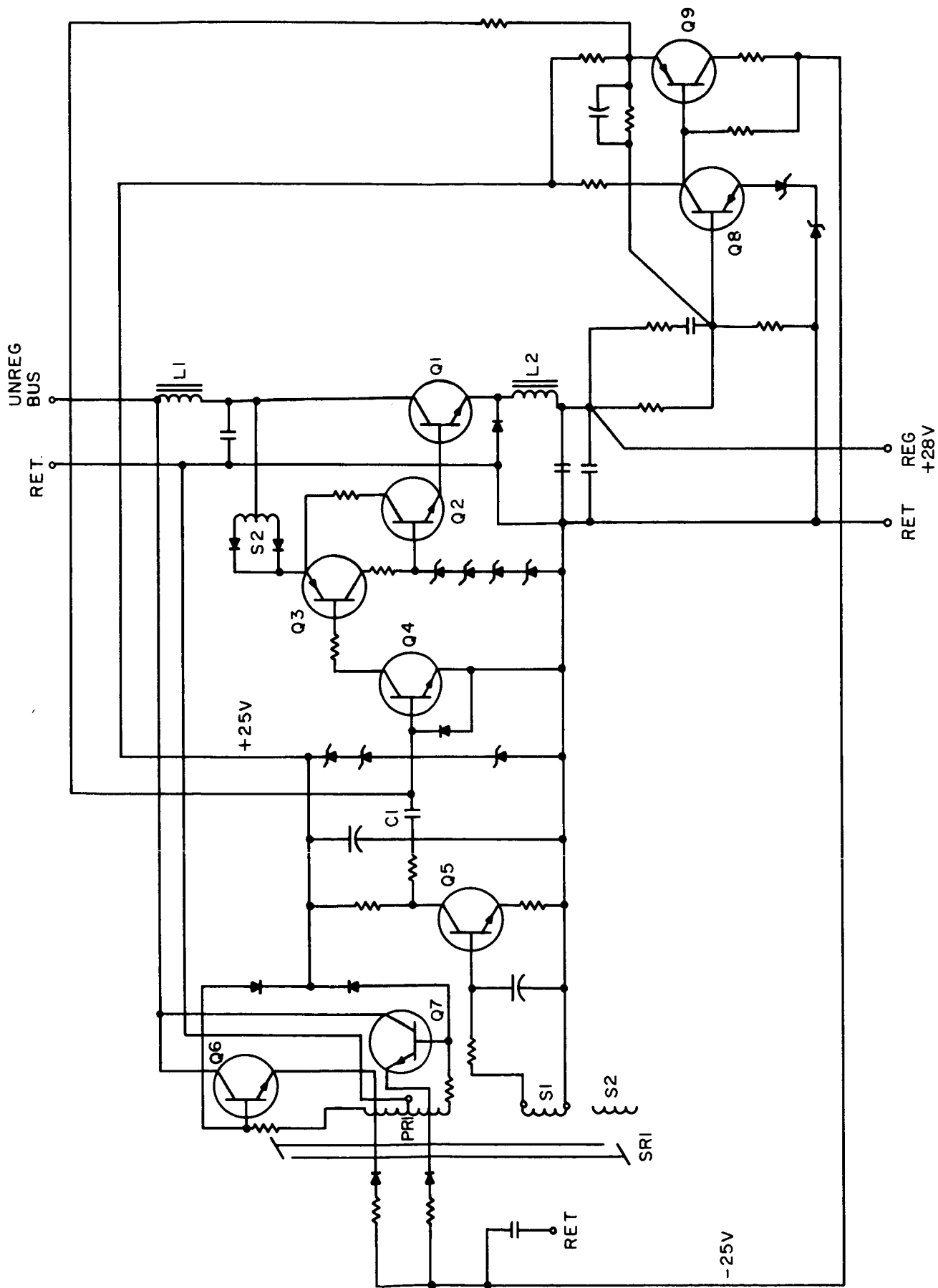


Figure 3-11. Main Regulator Schematic

The gain is such that no more than ± 0.5 percent at the regulated bus is required to turn the regulator completely off. Because this control circuit input is sampled at the filter output a low regulated bus impedance is assured, even at the resonance frequency of the filter.

3.8.6. 2.4 kc Inverter

The 2.4 kc inverter (see Figure 3-12) transforms the regulated +28 vdc to regulated 50⁰ vac at 2.4 kc. This ac is distributed to the various subsystems where it is transformed and rectified locally to regulated dc for powering electronic circuits. This inverter is the same as the Mariner C inverter but scaled for higher power.

The 2.4 kc inverter consists of a small 2.4 kc oscillating inverter and a switching power stage. The small internal inverter drives the output stage and is synchronized but will run freely. The design uses three transformers; one feedback, one interstage, and one output. The input to the inverter is LC filtered to protect the +28 vdc bus from current and voltage spikes generated by the switching transistors.

3.8.7 400 CPS THREE-PHASE INVERTER

The 400 cps three-phase inverter (see Figure 3-13) transforms the +28 vdc bus voltage to three-phase ac at 26 vac rms with a stepped waveform. This inverter needs three properly timed drive signals which come from the synchronizer. This inverter is identical to the Mariner C design.

The three phase inverter consists of three separate switching power amplifiers, each operating 120 degrees apart. The three outputs are interconnected so that the line-to-line waveform is a stepped square wave. This circuit uses three drive transformers, three output transformers with three secondaries each, and a filter choke in the input line. The choke and a capacitor at the input protect the +28 vdc regulated line from switching transients originating in the switching power amplifiers.

3.8.8 FAULT SENSORS AND REDUNDANCY SWITCHING

3.8.8.1 Main Regulator Fault Sensor

The buck regulator fault sensor must detect an output voltage which is significantly higher or lower than +28 vdc and, if this condition is maintained for 3 seconds nominal, it must switch out the regulator No. 1 and switch in regulator No. 2. The fault sensor cannot switch back to regulator No. 1 but either No. 1 or No. 2 can be switched in by command. (See Figure 3-14 .)

The trigger device in the sensor is a unijunction transistor. This drives a transistor which operates the "set" coil of a latching relay. This relay is a double pole double throw unit which switches both the input and output lines thereby isolating the defective regulator.

VB236FD101

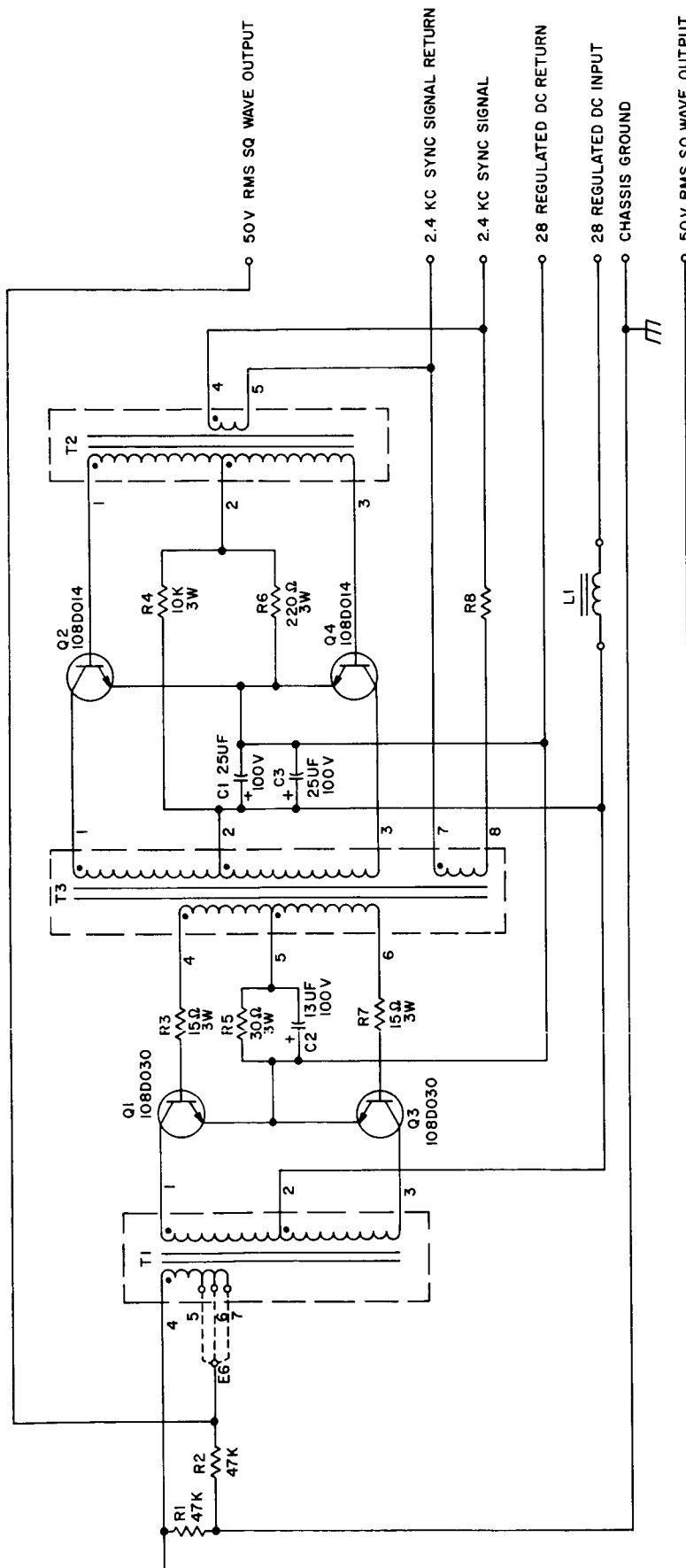


Figure 3-12. 2.4 KC Inverter Schematic

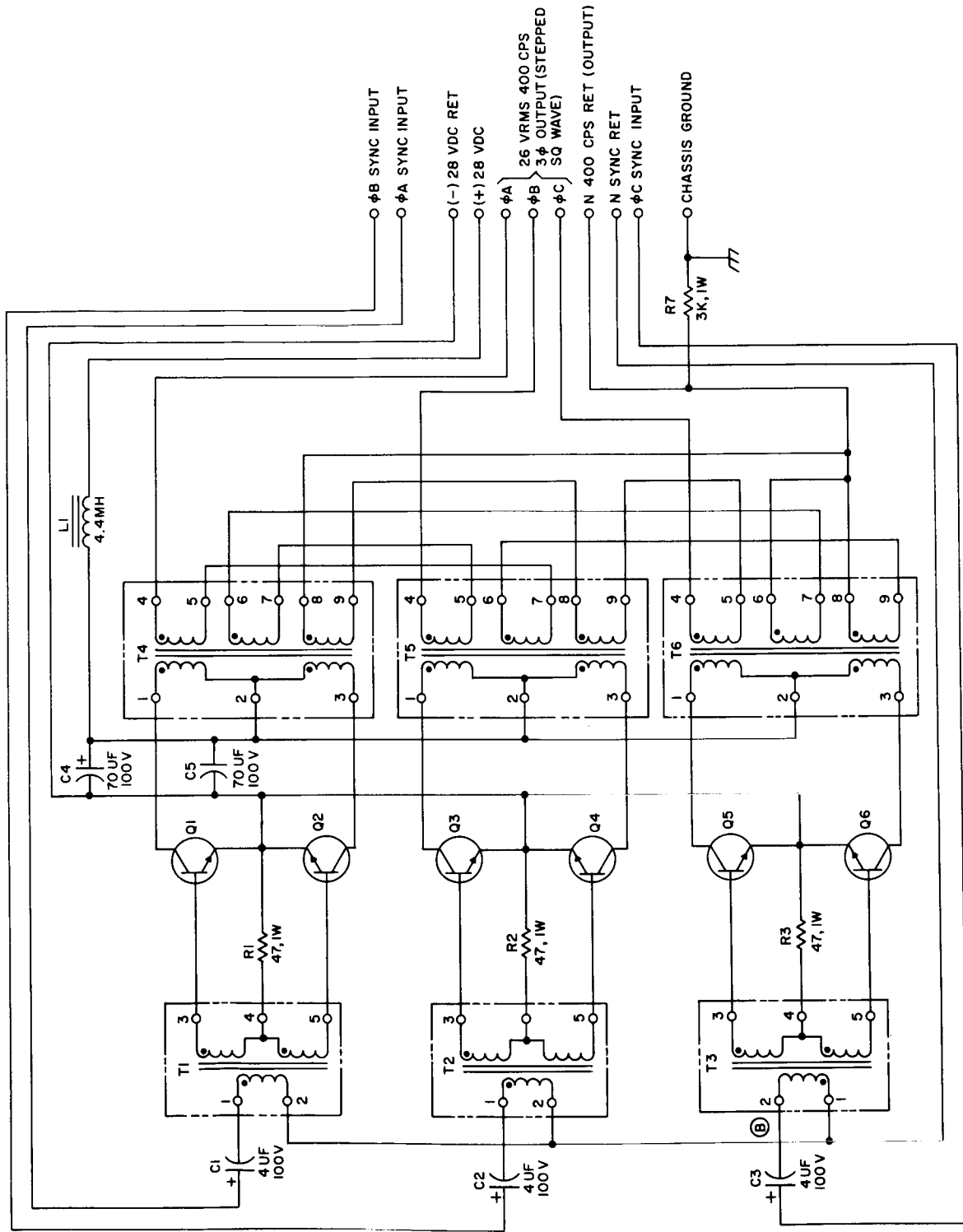


Figure 3-13. 400 cps Inverter Schematic

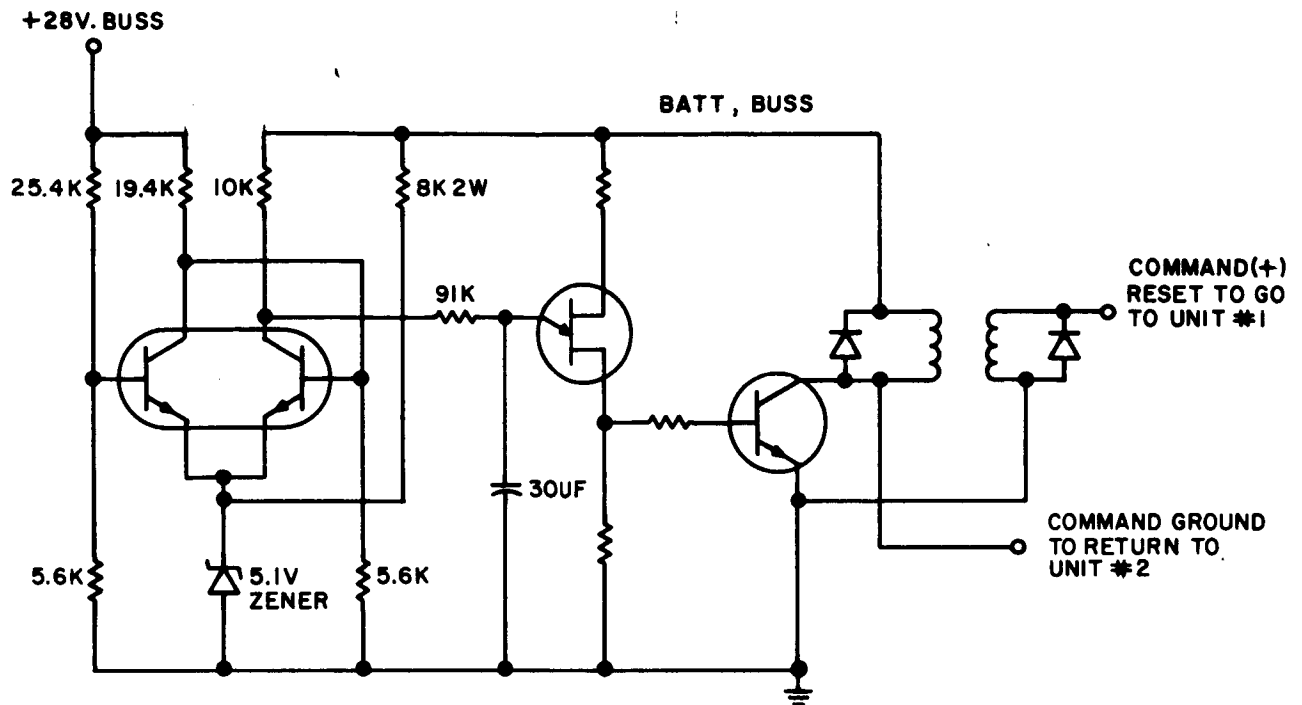


Figure 3-14. Main Regulator Fault Sensor

Both the "set" and "reset" coils may be operated by command. Generation of the unijunction trigger circuit is controlled by two transistors, one to sense under voltage and one to sense over voltage on the regulated bus. The sensor is powered by the batteries through isolation diodes.

3.8.8.2 2.4 kc and 400 CPS, 3 ϕ Inverter Fault Sensors

The inverter fault sensor must switch over from inverter No. 1 to No. 2 in the event the output goes significantly below nominal for a period of 3 seconds while the regulated bus is normal. If the regulated bus is significantly below normal when the output drops (fault in buck regulator but not the inverter) the fault sensor does not switch the inverters. The fault sensor cannot switch back to inverter No. 1 but either No. 1 or No. 2 can be switched in by command. (See Figure 3-15.)

The circuit consists of a transistor inhibit, a unijunction trigger generator, a transistor amplifier and a latching relay. The presence of a normal output voltage maintains the inhibit transistor saturated sufficiently to prevent the unijunction trigger circuit from generating.

If the output drops significantly, the inhibit transistor remains off and the trigger circuit starts charging. After 3 seconds a trigger is generated and the latching relay changes inverters. However if the input regulated bus is below normal, there is not enough pulse

VB236FD101

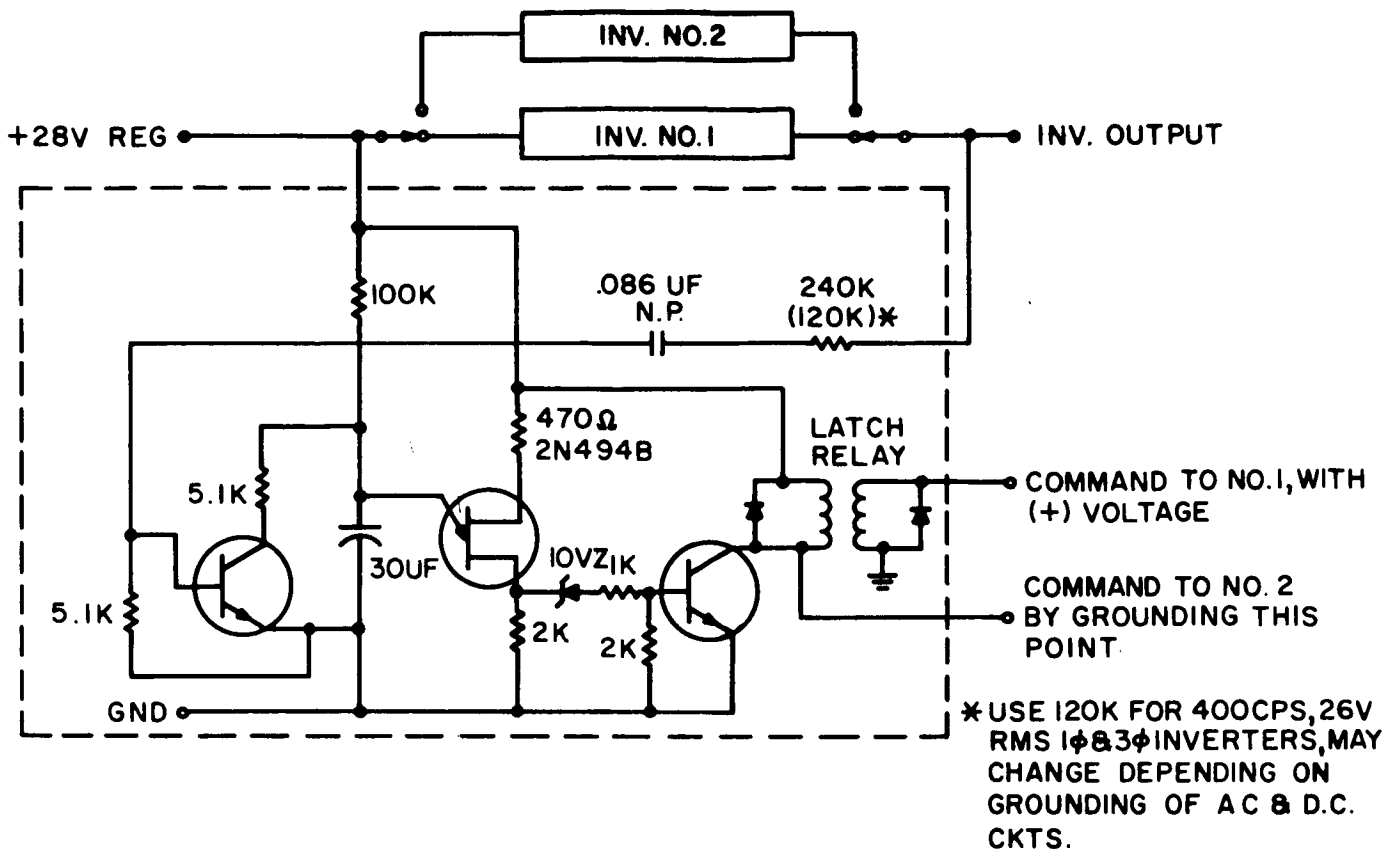


Figure 3-15. Inverter

amplitude to generate the amplifier due to a zener in series with the amplifier input. This feature prevents switchover of inverters when there is loss of regulation on the main bus.

3.8.9 SYNCHRONIZER

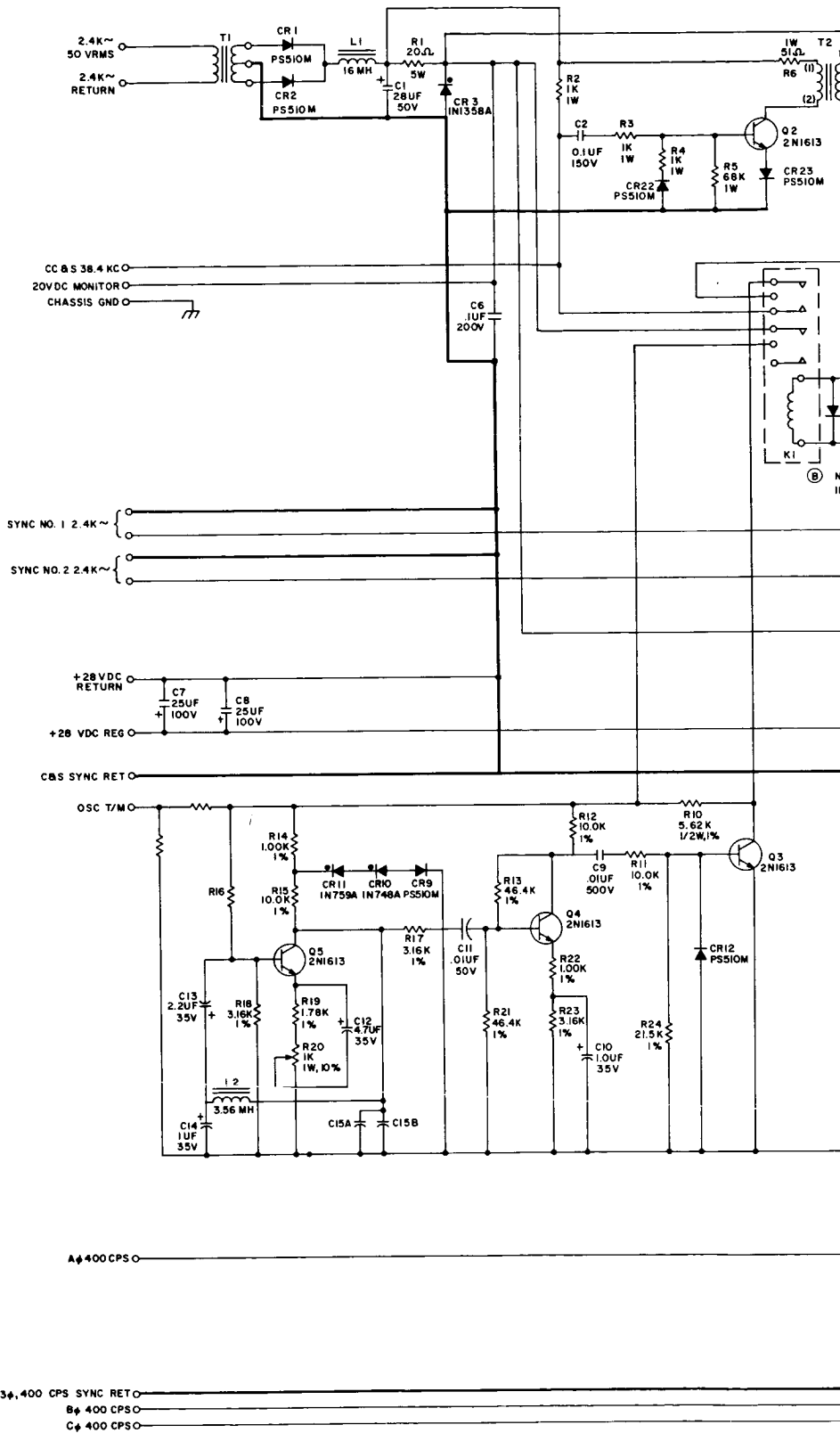
The synchronizer provides sync signals for the 2.4 kc inverters and 400 cps inverters. These sync signals are timed by a 38.4 kc signal from the C&S clock. The synchronizer has its own 38.4 kc oscillator which is switched in if the clock 38.4 kc is missing. (See Figure 3-16.) This synchronizer is identical to the Mariner C design.

The input 38.4 kc signal is divided by 16, the resulting 2.4 kc signal is divided by 2 and the 1.2 kc signal produced drives a two flip-flop chain. By proper interconnection this produces the three 400 cps signals 120 degrees apart which drive the two 400 cps 3 phase inverters.

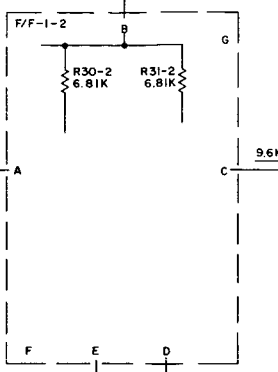
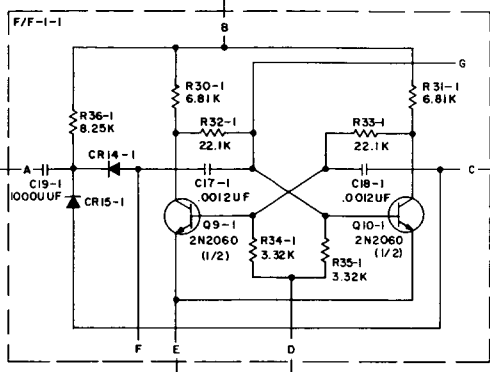
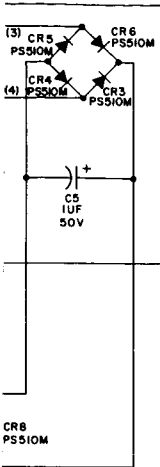
3.8.10 POWER SWITCHING AND LOGIC UNIT

The PS&L unit contains:

- a. Load control switching devices
- b. Switch buffer circuits



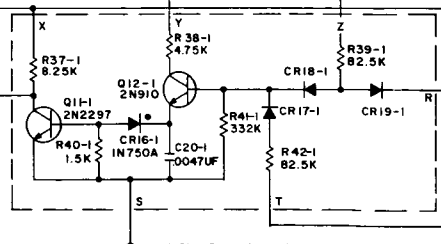
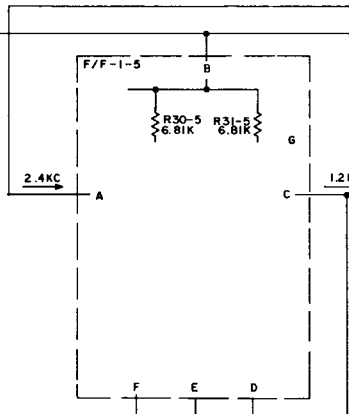
300



NOTE: RELAY SHOWN
 IN ENERGIZED POSITION

R29
 22.1Ω

C16
 10UF 15V



30

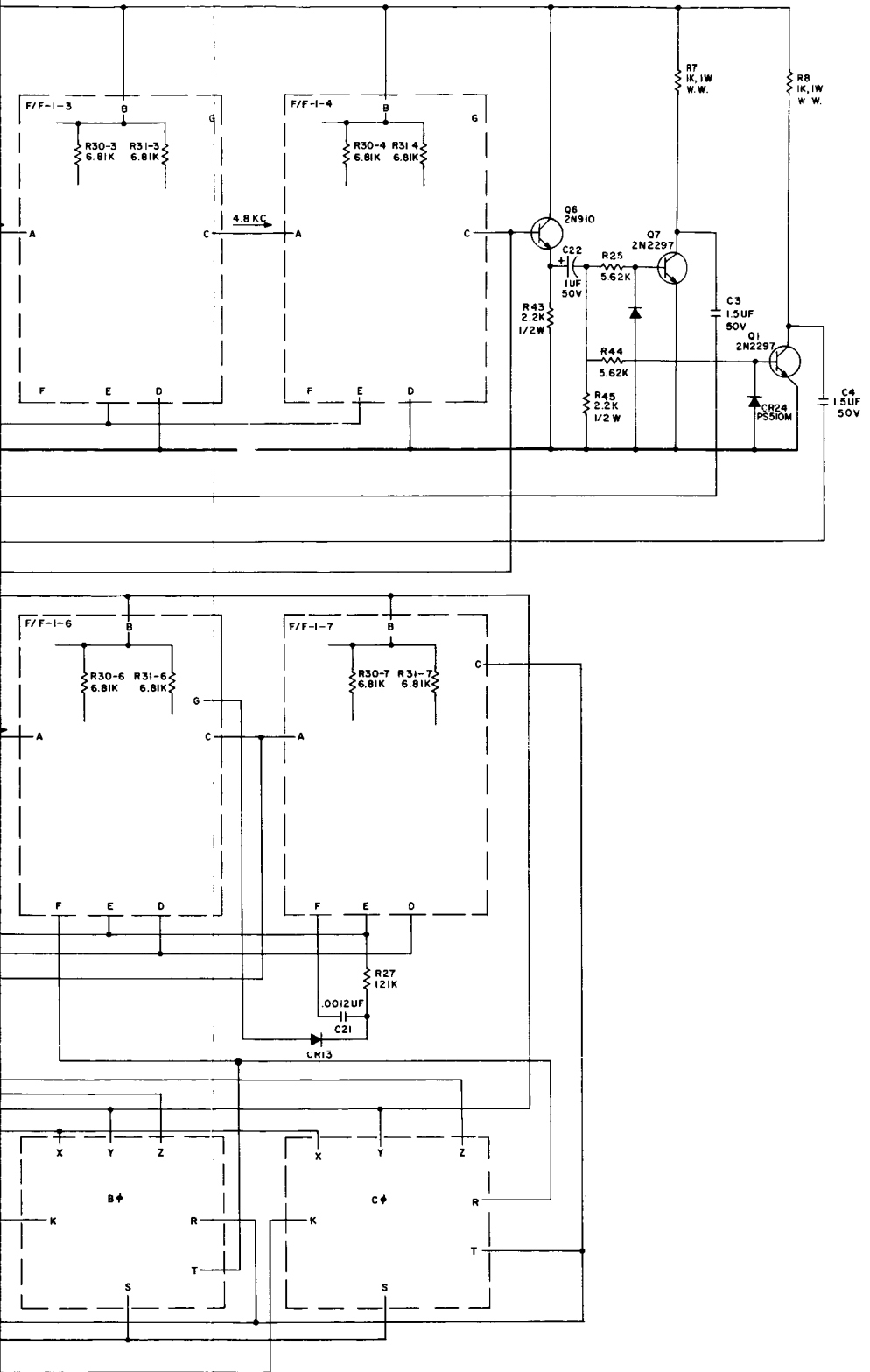


Figure 3-16. Synchronizer Schematic

- c. Fault protection devices
- d. Array/battery enabling switch SW-1
- e. Telemetry monitor circuits used for general subsystem measurements such as bus voltage and current output.

3.8.11 MISCELLANEOUS CIRCUIT ELEMENTS

Each of the functions described above contain circuit elements required for telemetry, command, and direct access test purposes. Among the more significant circuit elements are the following:

a. Current T/M Sensors

The sensors used to measure dc current for telemetering are magnetic amplifiers with the current being monitored flowing through the control winding. The output current is passed through a feedback winding to cancel the effect of the line current, hence, the output current by the degenerative feedback is proportioned to the line current (See Figure 3-17). An inverter, Figure 3-18 is provided to furnish excitation for all the dc current sensors. Output voltage is limited between 0 and +3.2 volts.

Sensors for ac currents are in reality current transformers, the low secondary currents being rectified and passed through a T/M load resistor (see Figure 3-19). The drop across this resistor is proportional to current and is sampled for telemetering. Both ac and dc T/M current sensors are fully isolated. Output voltage is limited between 0 and +3.2 volts.

b. Voltage T/M Circuit

Figure 3-20 illustrates the voltage T/M circuit used for all dc battery and bus voltages, and when used with a half-wave rectifier, all ac inverter voltages. It is very flexible and can be used to accurately monitor a narrow portion of a relatively high voltage. The output voltage excursion is limited to 0 at the low end and +3.2 volts at the high end.

4.0 INTERFACE DEFINITION

4.1 TELEMETRY MEASUREMENTS

Telemetry measurement requirements for in-flight evaluation of the power system are listed on Table 4-1.

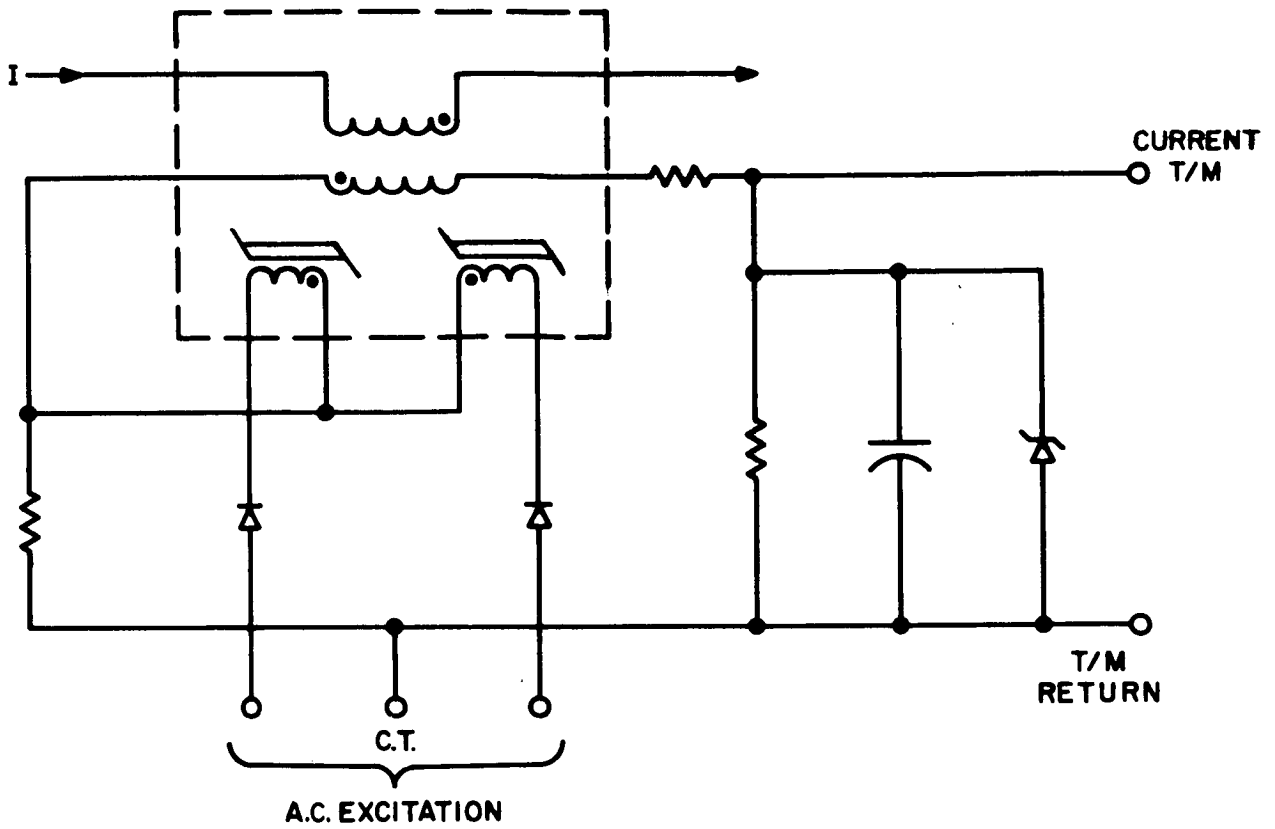


Figure 3-17. DC Current T/M Sensor

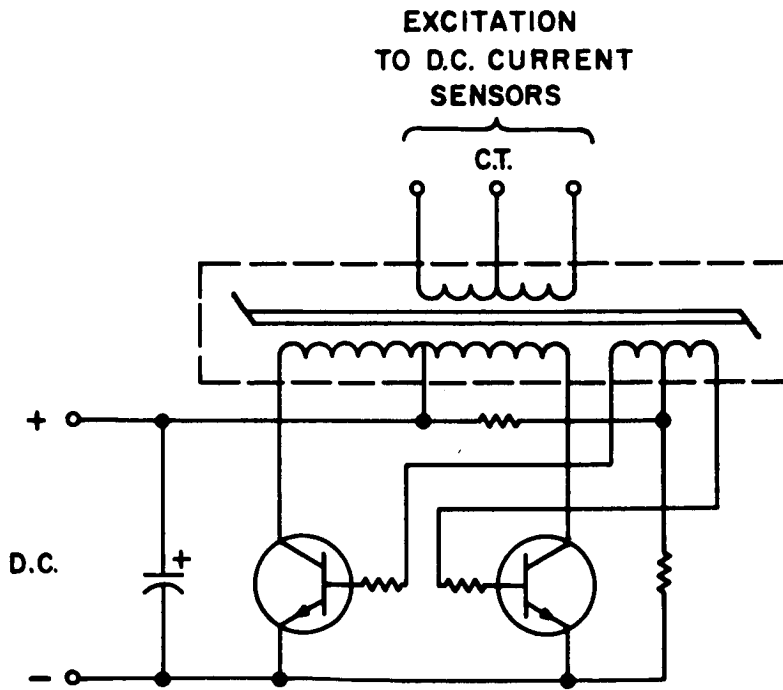


Figure 3-18. DC Current T/M Inverter

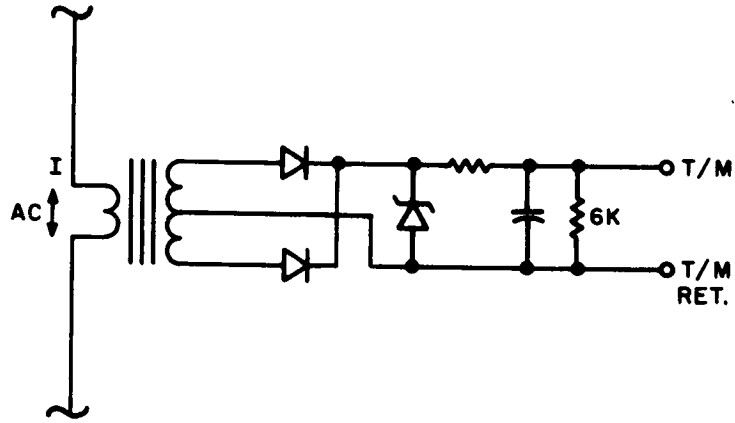


Figure 3-19. AC Current T/M Sensor

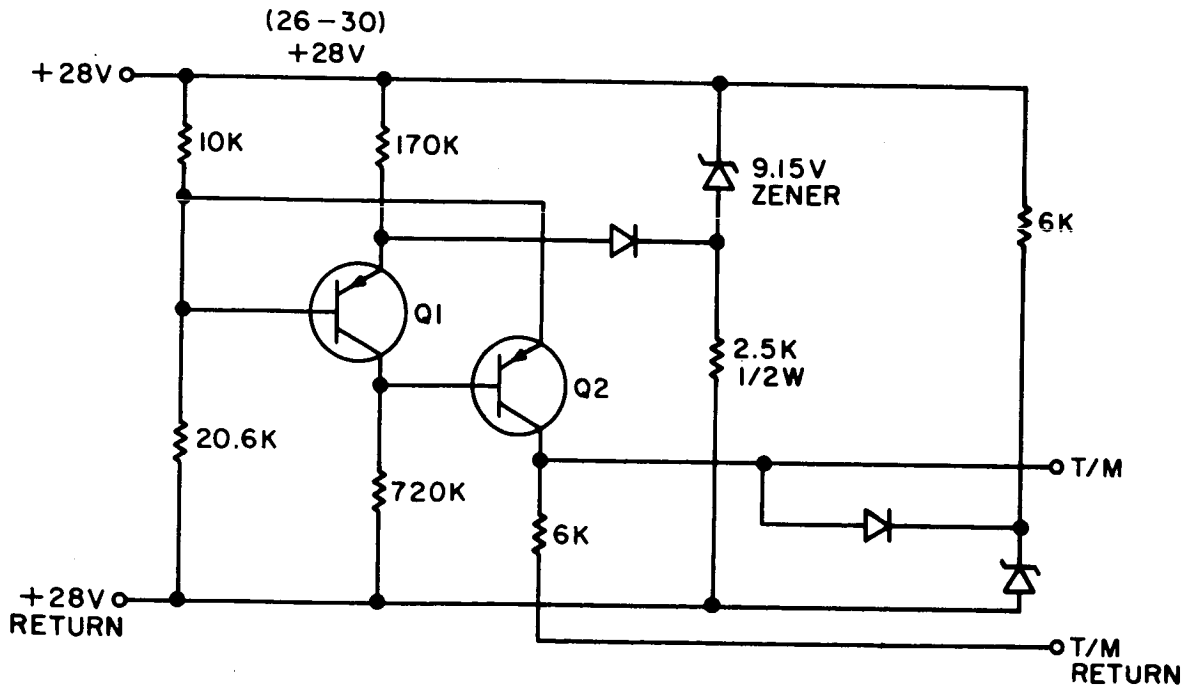


Figure 3-20. AC Voltage T/M Inverter

Table 4-1. Power System Telemetry Requirements

Item No.*	Measurement	Sensor Output	Volts	% Error Full Scale	Eng'r. Units
1	Regulated Bus Voltage	0-3.2	↓	3	26 to 30V
2	Regulated Bus Current	0-3.2		3	0 to 15A
3	2.4 KC Bus Voltage	0-3.2		3	45 to 55 VAC
4	2.4 KC Bus Current	0-3.2		3	0 to 6A
5, 6, 7	400 CPS 3 phase Voltage	0-3.2		3	22 to 30 VAC
8	Capsule Current	0-3.2		3	0 to 7A
9	XMTR Current	0-3.2		3	0 to 6A
10	Battery 1 Voltage Coarse	0-3.2		3	25 to 45V
11	Battery 2 Voltage Coarse	0-3.2		3	25 to 45V
12	Battery 3 Voltage Coarse	0-3.2		3	25 to 45V
13	Battery 1 Voltage Fine	0-3.2		3	40 to 45V
14	Battery 2 Voltage Fine	0-3.2		3	40 to 45V
15	Battery 3 Voltage Fine	0-3.2		3	40 to 45V
16	Battery 1 Current	0-3.2		3	-7 to +25A
17	Battery 2 Current	0-3.2		5	-7 to +25A
18	Battery 3 Current	0-3.2		5	-7 to +25A
19	Power Bus Voltage	0-3.2		5	30 to 60V
20	Array Current	0-3.2		5	0 to 25A
21	Battery No. 1 Temp.	0 - 100		5	0 to +130°F
22	Battery No. 1 Temp.	0 - 100		5	0 to +130°F
23	Battery No. 2 Temp.	0 - 100		5	0 to +130°F
24	Battery No. 2 Temp.	0 - 100		5	0 to +130°F
25	Battery No. 3 Temp.	0 - 100		5	0 to +130°F
26	Battery No. 3 Temp.	0 - 100		5	0 to +130°F

Table 4-1. Power System Telemetry Requirements (Cont)

27-30	Solar Array Temp.	0 - 100 mv	5	-100 to +250 ^o F
31-32	Solar Array Temp.	0 - 100 mv	5	-350 to +100 ^o F
33-36	Charge Reg. No. 1 State	Digital		
37-40	Charge Reg. No. 2 State	Digital		
41-44	Charge Reg. No. 3 State	Digital		
45-46	Main Regulator in use	Digital		
47-48	2400 cps inverter in use	Digital		
49-50	3 ϕ inverter in use	Digital		
51	Inverter Back-up oscillator	Digital		

* Item No. refers to subscript shown on Figure 3-2.

4.2 COMMAND REQUIREMENTS

External stimuli for power system and load control are required as follows on Table 4-2.

Item No.*	Function	Signal Source
1	Turn off charge Regulator No. 1	CD
2	Setting A - charge Regulator No. 1	CD
3	Setting B - charge Regulator No. 1	CD
4	Setting C - charge Regulator No. 1	CD
5	Turn off - charge Regulator No. 2	CD
6	Setting A - charge Regulator No. 2	CD
7	Setting B - charge Regulator No. 2	CD
8	Setting C - charge Regulator No. 2	CD
9	Turn off - charge Regulator No. 3	CD
10	Setting A - charge Regulator No. 3	CD
11	Setting B - charge Regulator No. 3	CD
12	Setting C - charge Regulator No. 3	CD
13	Switch to Main Regulator No. 1	CD
14	Switch to Main Regulator No. 2	CD
15	Switch to 2.4 kc inverter No. 1	CD
16	Switch to 2.4 kc inverter No. 2	CD
17	Switch to 400 cps inverter No. 1	CD
18	Switch to 400 cps inverter No. 2	CD
19	Enable array and batteries - SW - 1	LCE
20	Disable array and batteries - SW - 1	LCE

Relay No.

K1	on - Power to Fuel Tank Heaters
K1	off - Power to Fuel Tank Heaters
K2	on - Power to Capsule
K2	off - Power to Capsule
K3	on - Power to Science
K3	off - Power to Science
K4	on - Power to Relay
K4	off - Power to Relay
K5	on - Power to Antenna Electronics
K5	off - Power to Antenna Electronics
K6	on - Power to Scan Electronics
K6	off - Power to Scan Electronics
K7	on - Power to Autopilot Electronics
K7	off - Power to Autopilot Electronics
K8	on - Power to Approach Guidance
K8	off - Power to Approach Guidance

* Item No. refers to command subscripts in Figure 3-2.

4.3 UMBILICAL DISCONNECT REQUIREMENTS

Item No.	Function
1	Array/Battery Bus Voltage
2	Array Enable Switch SW-1 Monitor
3	Turn-on Enable Switch, SW-1
4	Turn-off Enable Switch, SW-1
5	Enable Switch, SW-1, return
6	External power, 44-55 vdc, 15 amps.
7	External power return
8	Battery No. 1 Voltage
9	Battery No. 2 Voltage
10	Battery No. 3 Voltage
11	Battery No. 1 Temperature
12	Battery No. 2 Temperature
13	Battery No. 3 Temperature
14	Battery Temperature Sensor Return
15	400 cps, ϕ 1 voltage
16	400 cps, ϕ 2 voltage
17	400 cps, ϕ 3 voltage
18	2.4 kc voltage
19	2.4 kc voltage return
20	Raw Battery Bus Voltage

4.4 DIRECT ACCESS REQUIREMENTS

Item No.	Function
1	Main Regulator Voltage
2	Main Regulator Current
3	2.4 KC Bus Current
4	Capsule Current
5	XMTR Current
6	Battery No. 1 Current
7	Battery No. 2 Current
8	Battery No. 3 Current
9	Array Current
10	Charge Reg. No. 1 - off, A, B, or C Setting
11	Charge Reg. No. 2 - off, A, B, or C Setting
12	Charge Reg. No. 3 - off, A, B, or C Setting
13	Main Regulator No. 1 on/off
14	Main Regulator No. 2 on/off
15	2.4 kc Inverter No. 1 on/off
16	2.4 kc Inverter No. 2 on/off
17	400 cps Inverter No. 1 on/off

Item No.	Function
18	400 cps Inverter No. 2 on/off
19	Backup Oscillator Input Voltage
20	Stimulate Fault Sensor - Main Regulator
21	Stimulate Fault Sensor - 2.4 kc Inverter
22	Stimulate Fault Sensor - 400 cps Inverter
23	K1 Switch Monitor
24	K2 Switch Monitor
25	K3 Switch Monitor
26	K4 Switch Monitor
27	K5 Switch Monitor
28	K6 Switch Monitor
29	K7 Switch Monitor
30	K8 Switch Monitor
31-57	Battery cell voltage monitors (3 batteries) Cells 3, 6, 9, 12, 15, 18, 21, 24, 27

4.5 SPECIAL ACCESS REQUIREMENTS

- a. Battery - Special access to each intercell connection will be available for uniformly discharging each cell prior to installment in the spacecraft. These access points will be located directly on a connector at the battery case and will not be available for subsystem or system test.
- b. Solar Array - Special access connectors will be provided for testing each solar panel. These connectors will be located ahead of each isolation diode.

4.6 THERMAL INTERFACE REQUIREMENTS

Battery operating temperatures must be limited to 40 to 80° F.

4.7 RETRO-PROPULSION

The plume of the retro-propulsion engine shall not cause more than one percent output degradation of the solar array.

5.0 PERFORMANCE PARAMETER

5.1 SIZING CRITERIA

Table 5-1 shows the calculation procedures for the sizing determination of the power system components.

Table 5-1. Energy Balance Table

Mission Phase	Launch to Solar Acquisition	Early Cruise	Late Cruise	Mid-Course Maneuver	Approach Guidance (β days)	Capsule Separation Maneuver	Post Separation Cruise	Orbit Insertion	Spacecraft		Spacecraft Eclipse	Alternate Mode Full Science (*Differences)
									Full Sci. (hours)	Day Other Times		
2400 cps Inverter Loads:												
Science (including platform scan)		25.0	25.0		25.0		25.0			94.0	20.0	94.0
Radio	29.8	29.8	29.8	29.8	29.8	29.8	29.8	29.8		29.8	29.8	29.8
Capsule Relay						11.2	11.2	11.2				
Data Handling	22.5	13.5	13.5	13.5	13.5	13.5	13.5	13.5		16.5	16.5	16.5
Guidance & Control	17.6	9.6	10.9	29.8	30.9	29.8	10.9	29.8		16.2	24.2	*24.2
Command	20.2	20.2	20.2	20.2	20.2	20.2	20.2	20.2		20.2	20.2	20.2
Controller & Sequencer	20.0	20.0	20.0	20.0	20.0	20.0	20.0	20.0		20.0	20.0	20.0
Pyrotechnic Control	2.0	2.0	2.0	2.0	2.0	2.0	2.0	2.0		2.0	2.0	2.0
Power Synchronizer	5.0	5.0	5.0	5.0	5.0	5.0	5.0	5.0		5.0	5.0	5.0
Thermal Control		15.0	15.0	15.0	15.0	15.0	15.0	15.0		15.0	15.0	15.0
Inverter Load Sub-total	117.1	140.1	141.4	135.3	161.4	146.5	152.6	146.5		218.7	162.7	226.7
Harness Loss	1.2	1.4	1.4	1.4	1.6	1.5	1.6	1.5		2.2	1.6	2.3
Total Inverter Output Efficiency	118.3	141.5	142.8	136.7	163.0	148.0	154.2	148.0		220.9	164.3	229.0
Thermal Loss	.86	.87	.87	.87	.88	.88	.88	.88		.90	.88	.90
Total 2400 cps Inverter Input	19.3	20.6	20.7	20.3	21.8	21.0	21.3	21.0		25.1	21.4	25.5
400 cps, 3φ Inverter Loads:	137.6	162.1	163.5	157.0	184.8	169.0	175.5	169.0		246.0	177.7	254.5
Guidance & Control				9.0		9.0		9.0			9.0	*9.0
Data Handling										5.0		5.0
Science										6.0		6.0
Inverter Load Sub-total	9.0			9.0		9.0		9.0		11.0	9.0	20.0
Harness Loss	0.1			0.1		0.1		0.1		0.1	0.1	0.2
Total Inverter Output Efficiency	9.1			9.1		9.1		9.1		11.1	9.1	20.2
Thermal Loss	.72			.72		.72		.72		.74	.72	.80
	12.7	2.5	2.5	3.6	2.5	3.6	2.5	3.6		3.9	2.5	5.0
	12.7	2.5	2.5	19.7	2.5	12.7	2.5	12.7		15.0	2.5	12.7

Inverter Input	150.3	164.6	166.0	169.7	187.3	181.7	178.0	181.7	261.0	180.2	198.9	279.7
Total Buck Regulator Output	.86	.87	.87	.87	.88	.88	.88	.88	.90	.88	.89	.90
Thermal Loss	23.9	24.6	24.8	25.0	25.9	25.2	25.4	25.2	30.1	25.5	26.6	31.1
Total Buck Regulator Input	174.2	189.2	190.8	194.7	213.2	206.9	203.4	206.9	291.1	205.7	225.5	310.8
Unregulated D. C. Loads:												
Radio (**Maximum)	145.0	145.0	57.0	***145.0	57.0	***145.0	57.0	***145.0	145.0	145.0	57.0	145.0
Capsule		200.0	200.0		200.0							
Unreg. D. C. Load Subtotal	145.0	345.0	257.0	145.0	257.0	145.0	57.0	145.0	145.0	145.0	57.0	145.0
Harness Loss	1.5	3.5	2.6	1.5	2.6	1.5	0.6	1.5	1.5	1.5	0.6	1.5
Unregulated D. C. Loads	146.5	348.5	259.6	146.5	259.6	146.5	57.6	146.5	146.5	146.5	57.6	146.5
Unregulated D. C. Bus Req't	320.7	537.7	450.4	341.2	472.8	353.4	261.0	353.4	437.6	352.2	283.1	457.3
Unregulated Battery Loads:												
Buck Reg. Fault Det.	1.0	1.0	1.0	1.0	1.0	1.0	1.0	1.0	1.0	1.0	1.0	1.0
Gyro Heaters (Avg.)	6.0			6.0		6.0		6.0		(1 hr) 6.0	6.0	*6.0
Thrust Vector Control Engine Controls				18.0		18.0		18.0				
Antenna Gymbal Drive				60.0		60.0		60.0				
Unreg. Battery Load Subtotal	7.0	1.0	1.0	85.0	1.0	85.0	1.0	85.0	1.0	7.0	7.0	7.0
Thermal Loss	327.7			431.5		438.4		438.4			290.1	
Battery Output	3.3			4.4		4.4		4.4			2.9	
Battery	331.0			435.9		442.8		442.8			293.0	
Thermal Loss	28.0	0- 9.4	0- 9.4	36.0	0- 9.4	37.0	9.4	37.0	0- 3.1	0- 9.4	25.0	3.7
Battery Input		0-121.2	0-121.2		0-121.2		121.2		0- 39.1	0-121.2		22.1
Charger Output		1.0-122.2	1.0-122.2		1.0-122.2		122.2		1.0- 40.1	1.0-122.2		40.1
Charger Efficiency		44.2/46.0	44.2/46.0		44.2/46.0		44.2/46.0		44.2/46.0	44.2/46.0		22.4/46.0
Thermal Loss		1.0- 5.0	1.0- 5.0		1.0- 5.0		5.0		1.0- 1.7	1.0- 5.0		1.0
Charger Input		1.0-127.2	2.0-127.2		2.0-127.2		127.2		2.0- 41.8	2.0-127.2		41.8
Array Bus Power		539.7-664.9	452.4-577.6		474.8-600.0		388.2		439.6-479.4	354.2-479.4		499.1
Harness Loss		5.4- 6.7	4.5- 5.8		4.8- 6.1		3.9		4.4- 4.8	3.6- 4.8		5.0
Thermal Loss		9.5- 11.7	7.9- 10.1		8.3- 10.5		6.9		7.7- 8.4	6.2- 8.4		8.8
Array Power Output Requirement		554.6-684.2	464.8-593.5		487.9-616.6		399.0		451.7-492.6	364.0-492.6		512.9
Array Power Available		862	743		725		725		572	572		572

5.2 SOLAR ARRAY CAPABILITY

Usable power from the solar array is shown on Figure 5-1 as a function of mission time. Usable power is defined as the power availability at 46 volts or greater which is the minimum required for battery charging. This restriction accounts for the apparent lower power at the start of the mission though, in fact, greater power is available at lower voltages. See Appendix A for further analysis. The net array requirements based on the calculations of Table 5-1 is shown for comparative purposes. The limitation imposed by the possibility of battery load-sharing is shown as well as potential array degradation from potential Martian radiation belts 10^4 times greater than earth radiation belts. In the latter case sufficient power is available for up to 36 days after encounter. Partial operation is possible thereafter.

5.3 BATTERY CAPABILITY

The installed battery capacity is 2280 watt-hours. It is estimated that the capacity will be reduced by 30 percent to result in an end-of-life capability of 1600 watt-hours.

Figure 5-2 shows the energy removed for different mission phases and the time required for recharging. See Appendix II for further analysis. Figures 5-3 and 5-4 show charge-discharge characteristics and discharge temperature characteristics respectively.

5.4 REGULATION

Estimates of voltage source regulation are presented below on Table 5-2.

Table 5-2

Voltage Source	Steady-state Regulation	Transient Regulation	Frequency Stability		
			C&S Sync Signal	Back-up Oscillator	Free-running
2.4 kc 50 volt RMS	± 2%	± 5%	± .01%	± 2%	± 5%
400 cps, 3 phase, 26 volt RMS	± 5%	± 10%	± .01%	± 2%	—
30-55 VDC	—	—	—	—	—
30-44 VDC	—	—	—	—	—

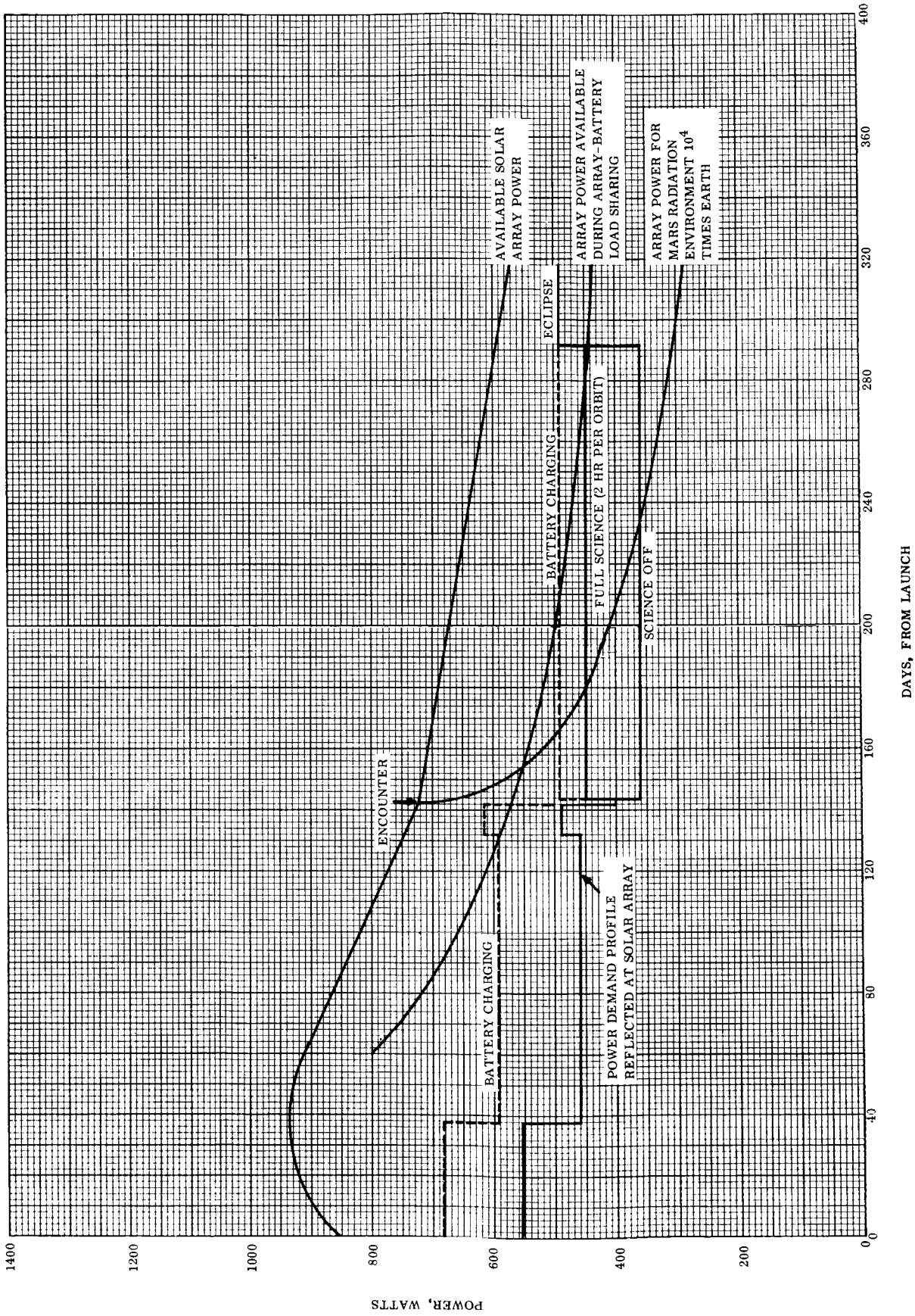
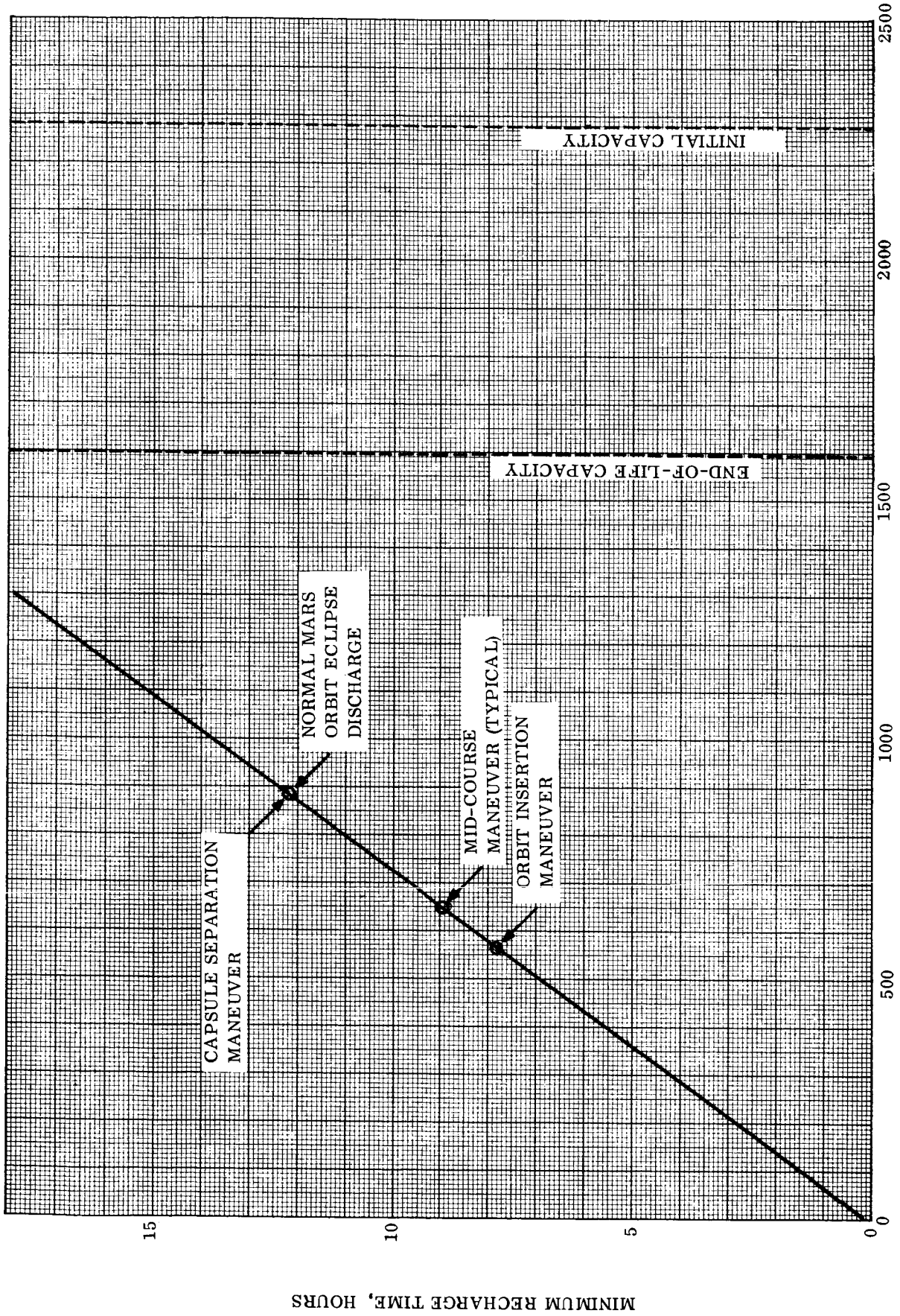


Figure 5-1. Array Output vs Time

DAYS, FROM LAUNCH

POWER, WATTS



BATTERY ENERGY REMOVED, WATT-HOURS

Figure 5-2. Battery Usage vs Charge Time

MINIMUM RECHARGE TIME, HOURS

VOYAGER BATTERY CHARGE - DISCHARGE DATA

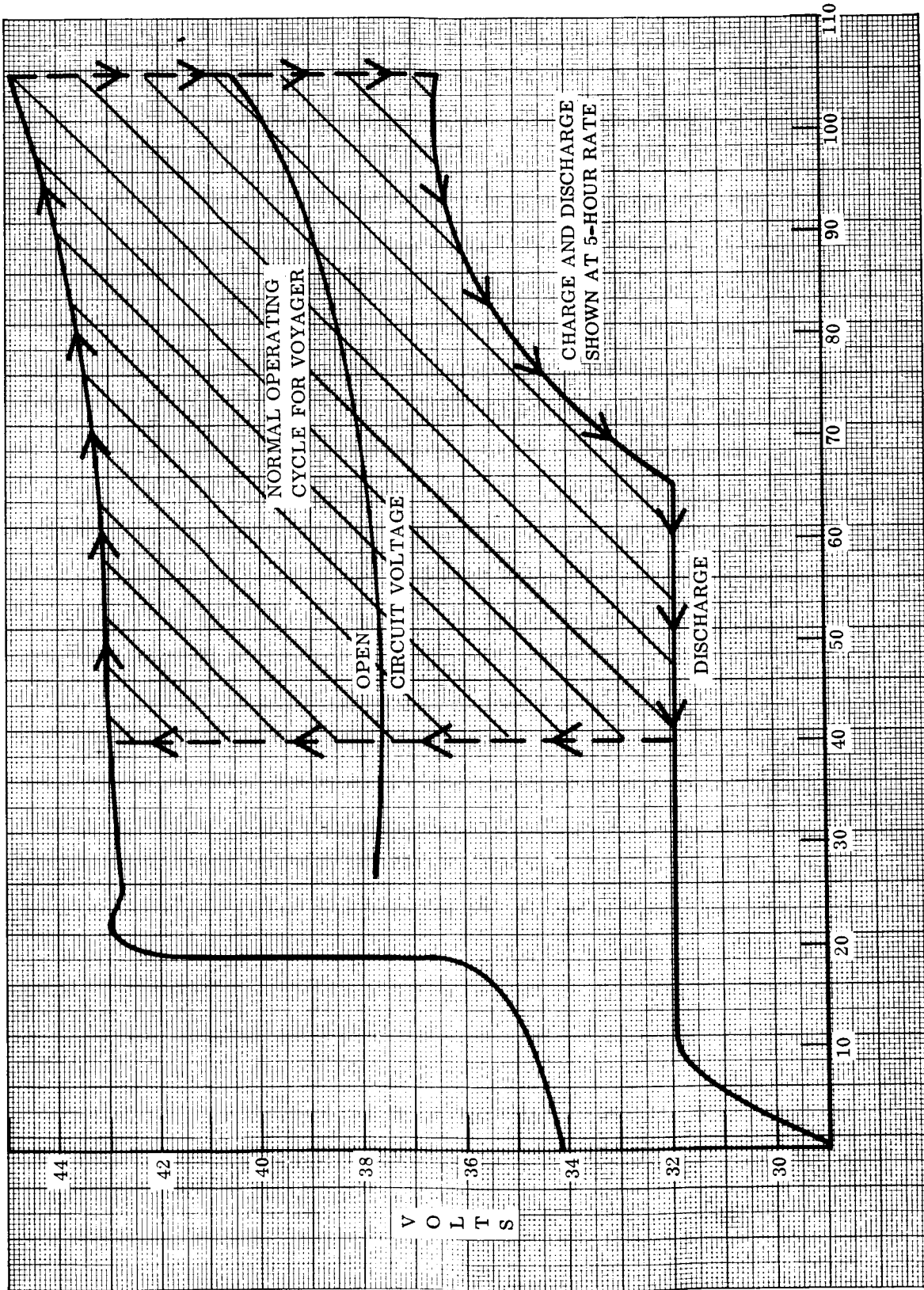


Figure 5-3. Voyager Battery Charge-Discharge Data

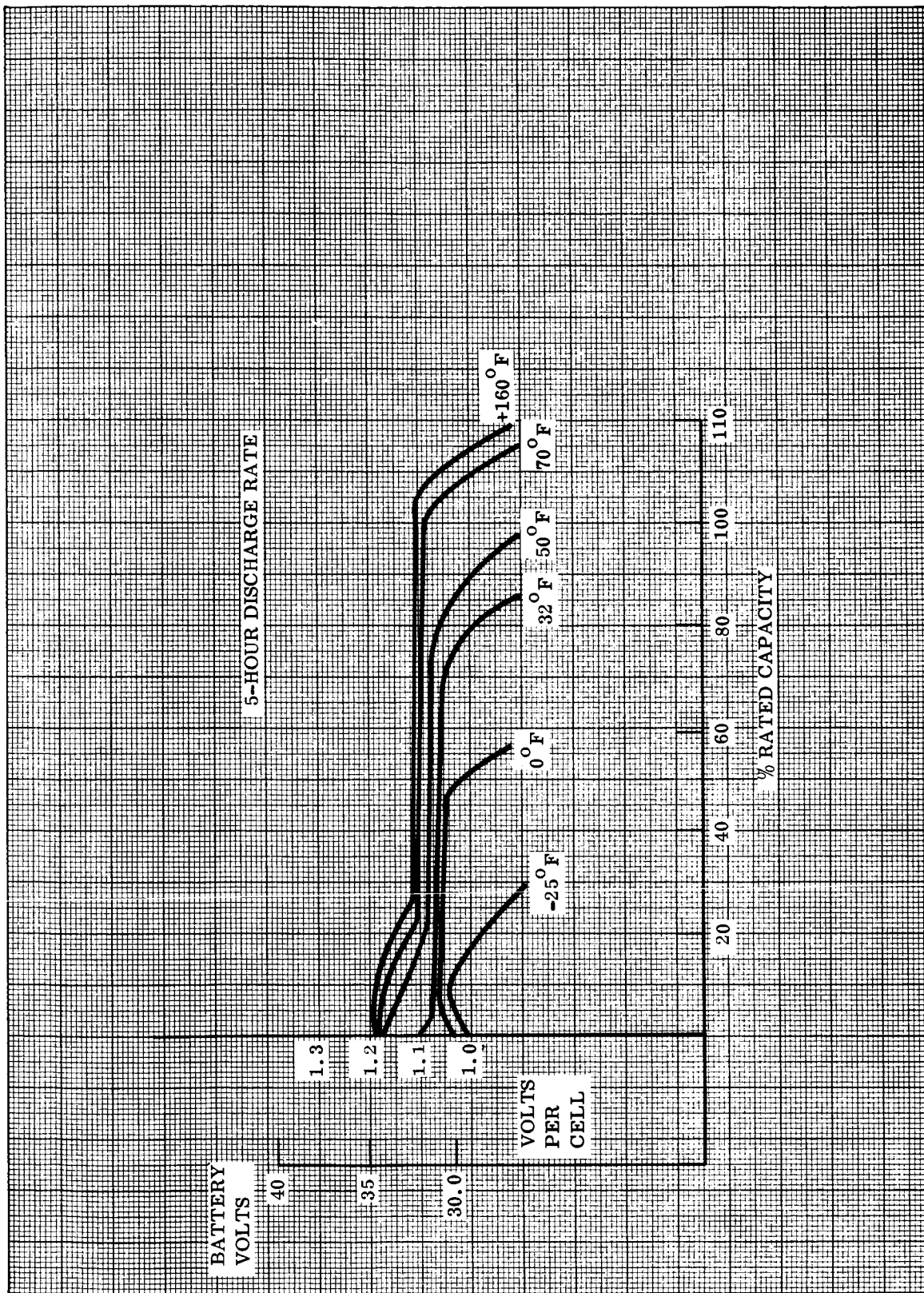


Figure 5-4. Voyager Battery Discharge Temperature Characteristics

5.5 LIMITS OF CAPABILITY

Approximate power magnitude limits for each voltage source are listed below on Table 5-3.

Table 5-3

Voltage Source	Power Limit
2.4 KC 50 volt RMS	300 watts
400 cps, 3 phase, 26 volt RMS	25 watts
30-55 volts DC	1 kw - occultation 1.5 kw - Mars day
30-44 volts DC	1 kw

5.6 RELIABILITY

The reliability of the power system is estimated to be 0.991 up to one month after encounter. See Appendix III for the analysis.

6.0 PHYSICAL CHARACTERISTICS

6.1 SOLAR ARRAY

The principal physical characteristics are described below:

- a. Form -22 separate & identical honeycomb panels forming an annular ring about the spacecraft
- b. Panel configuration and cell layout - See Figure 3-5
- c. Total array area - 196.6 square feet
- d. Effective cell area - 162.1 square feet
- e. Solar Cell Packing Factor-82.5 percent

f. Weight

Solar Panels and Support Structure*	178.5 lbs.
Harness	25.0 lbs.
Zener Regulator	<u>15.0 lbs.</u>
Total	218.5 lbs

*Breakdown of weight per square foot based on total area:

Item	<u>Weight, lb/ft²</u>
6-mil cover glass	.057
Cover glass	.013
Cells, solder-free, 12-mil	.136
Cell interconnection strips and solder	.025
Cell-to-substrate bond, 5 mils	.031
Terminals, diodes, wire, etc.	.018
Panel substrate and support structure	<u>.628</u>
Total	.908 lbs/ft ²

- g. Attachment - By means of screw fasteners
- h. Electrical Mating - Separate operational and direct access connectors
- i. Zener regulators - Consists of 1/4 x 1 x 3 inch monoblocks mounted on back panel face. Two such monoblocks are required - one for each of two solar cell strings on each panel assembly.

6.2 ELECTRONIC ASSEMBLY EQUIPMENT

Power system equipment, aside from the solar array, is mounted in Electronic Assembly Bays 1, 2 and 5. The allocation of equipment for each bay is shown on Figures 6-1, 6-2, and 6-3.

Weight and volume characteristics for each bay are listed in Table 6-1.

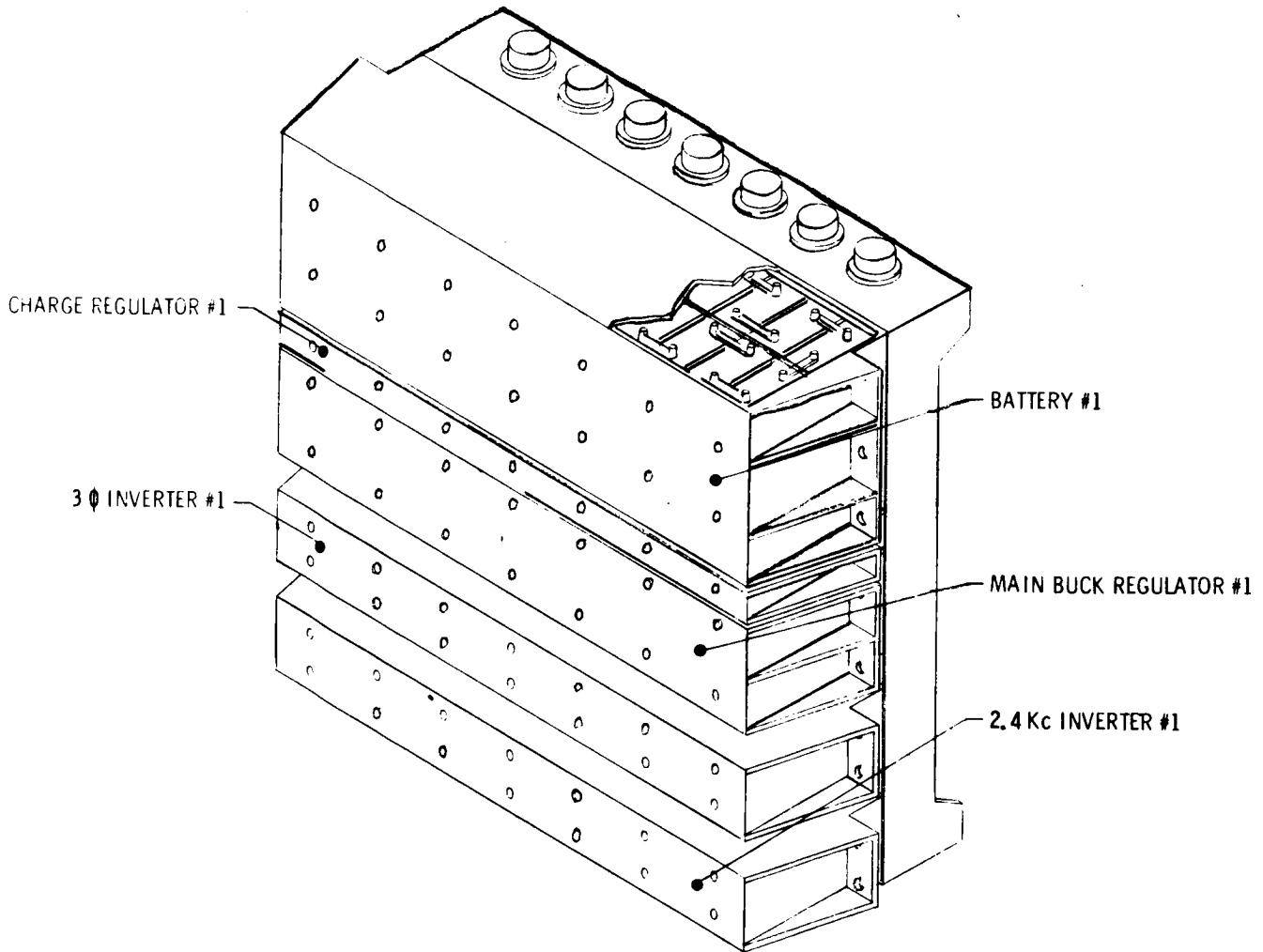


Figure 6-1. Bay No. 1 Equipment

VB236FD101

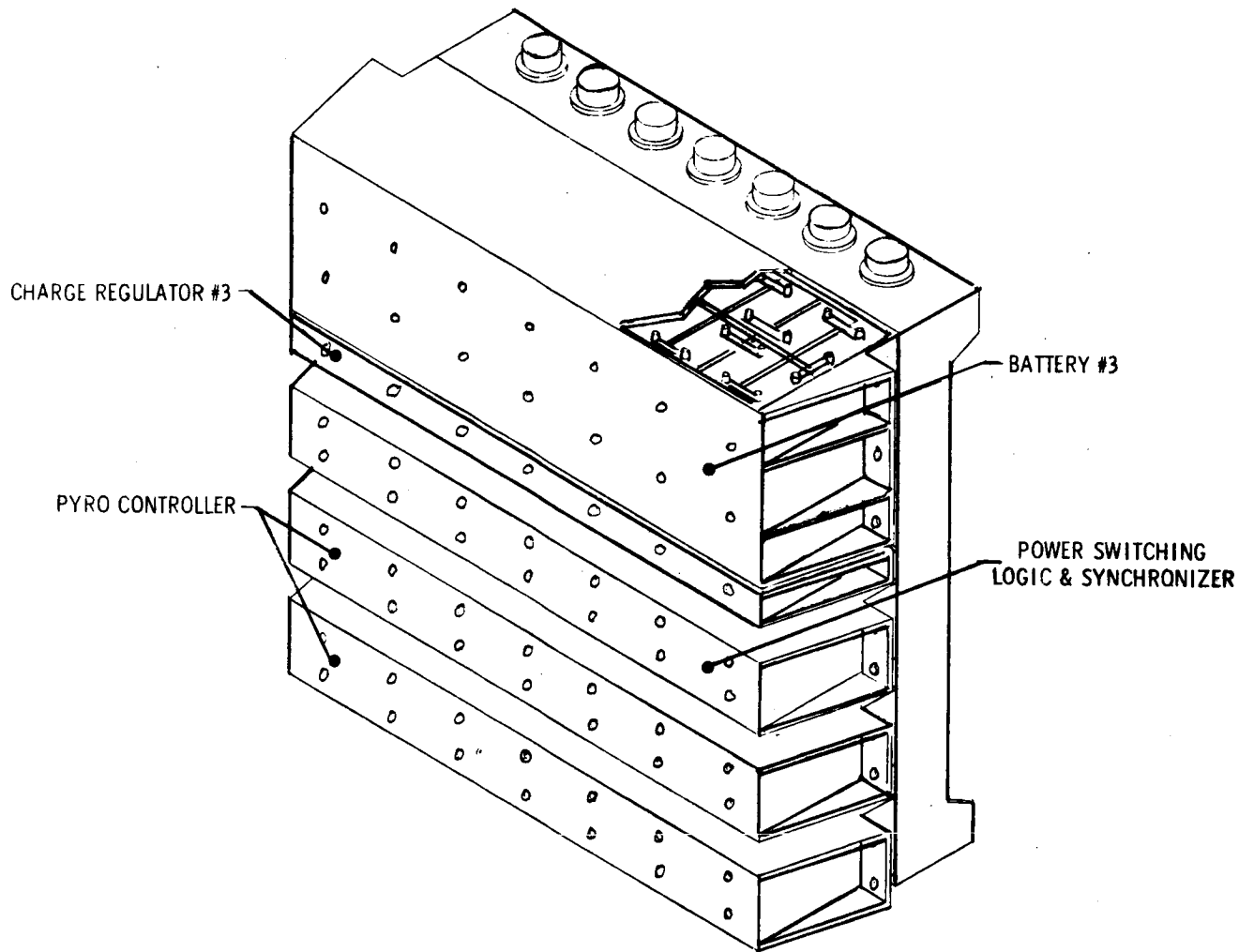


Figure 6-2. Bay No. 2 Equipment

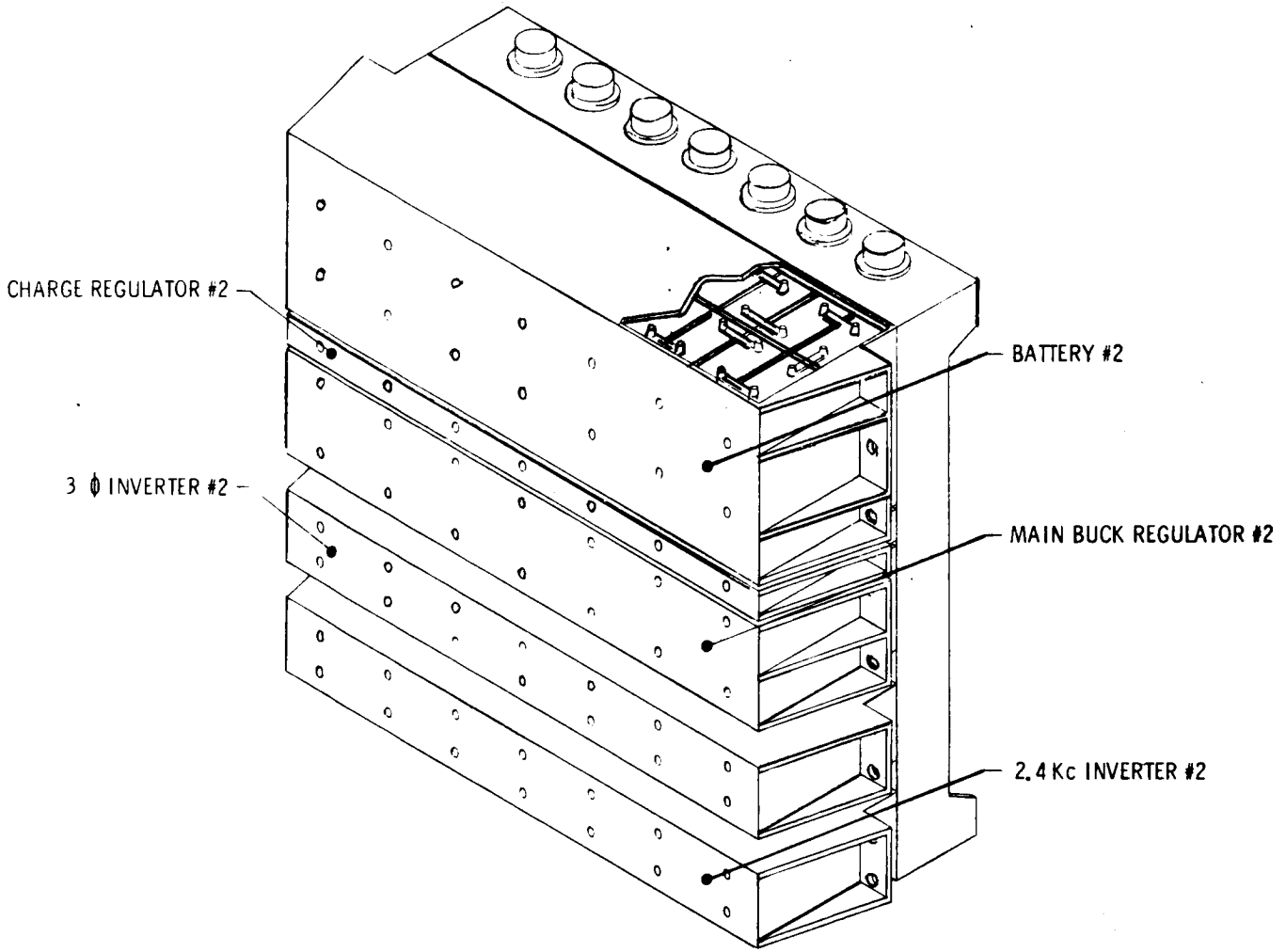


Figure 6-3. Bay No. 5 Equipment

Table 6-1. Power System Electronics Assembly Equipment

Assembly	Weight, lbs.	Volume, cu. ft.
<u>Bay No. 1</u>		
Battery No. 1	39.0	.35
Main Regulator No. 1	11.5	.22
Charge Regulator No. 1	1.5	.03
Inverter, 400 cps, 3 phase, No. 2	3.5	.06
Inverter, 2400 cps, No. 2	4.5	.08
Power Harness	3.0	.03
Chassis	3.8	-
Miscellaneous	<u>1.5</u>	-
Total	68.3	
<u>Bay No. 2</u>		
Battery No. 3	39.0	.35
Charge Regulator No. 3	1.5	.03
Synchronizer	1.6	.03
Power Switching and Logic	5.5	.10
Pyrotechnic Controller*	7.5	.13
Power and Pyrotechnic Harness	2.5	.03
Chassis	3.8	-
Miscellaneous	<u>1.5</u>	-
Total	62.9	
*Included in bay but not part of power system		
<u>Bay No. 5</u>		
Battery No. 2	39.0	.35
Main Regulator No. 2	11.5	.22
Charge Regulator No. 2	1.5	.03
Inverter, 400 cps, 3 phase, No. 1	3.5	.06
Inverter, 2400 cps, No. 1	4.5	.08
Power Harness	3.0	.03
Chassis	3.8	-
Miscellaneous	<u>1.5</u>	-
Total	68.3	

7.0 SAFETY CONSIDERATIONS

Precaution must be exercised in handling the batteries for the following dangers:

- a. The batteries are high energy, low impedance devices, and inadvertent shorting of the output terminals can cause personal or equipment injuries.
- b. Pressure buildup due to overcharge can result in a battery rupture by explosion.
- c. Minor seal or case rupture may permit the leakage of potassium hydroxide electrolyte, which is a strong alkali capable of causing serious burns.

CII-VB236FD101

APPENDIX I

SOLAR ARRAY PERFORMANCE

Index

- 1 Computer Analysis of Solar Array
- 2 Solar Array Power Output
- 3 Solar Cell Characteristics
- 4 Filter Selection
- 5 Solar Cell Radiation Damage
- 6 Cover Thickness Analysis
- 7 Thermal Analysis

APPENDIX I

SOLAR ARRAY PERFORMANCE

1.0 COMPUTER ANALYSIS OF SOLAR ARRAY

A computer analysis was performed to determine the power output of the Voyager solar array as a function of sun-spacecraft distance. As solar intensity decreases, the power output of a solar array also decreases, but the accompanying decrease in array temperature increases the voltage at which this power is available. Thus, consideration of the interactions of array temperature and solar intensity is essential in determining the proper voltage match between the array, the spacecraft loads, and the battery.

The array output computer program calculates the total current and power output of a solar array taking into account the following parameters:

- a. Solar intensity
- b. Temperature
- c. Angle of solar incidence
- d. Number of cells in series in a series string
- e. Number of cells in parallel in a series string
- f. Number of series strings
- g. Basic cell characteristics (efficiency, base resistivity)
- h. Losses and uncertainties

The output of the program is a listing, for each set of input parameters, of:

Voltage vs 1. Total current

2. Power

The program calculates the array output based on the characteristics of a single solar cell, multiplying the voltages and currents by the number of cells in series and parallel, respectively, to obtain the voltage-current characteristics of the total array.

The voltage-current characteristics of a single solar cell are represented by the following relation:

$$I = I_{sc} - \frac{V}{R_p} - I_o \left[e^{K(V+R_s I)} - 1 \right]$$

where the variables are:

- I = Cell current output
- V = Voltage on solar cell

and the coefficients are:

- I_{sc} = Illumination current (virtually equal to short circuit current)
- R_p = Shunt resistance of the cell
- I_o = Reverse saturation current of the ideal diode characteristic
- K = Coefficient of the exponential
- R_s = Series resistance of the cell

The coefficients are further treated as functions of cell temperature, using sixth-degree polynomial approximations, to more accurately reflect changes in cell characteristics with temperature. The coefficients in the cell characteristic equation were derived from the basic cell V-I curves given in Section 3.1 of this appendix, adjusted to represent 11 percent efficient cells.

Correction coefficients are added to the above relation to account for various operating and loss factors, and uncertainties. These are:

CDEG = Short Circuit Current Degradation Factor, containing

Loss factors:

Variations in solar intensity, which term is equal to (AU) ⁻²	
Filter transmission loss	0.94
Micrometeoroid effects and random cell failures	0.95
Radiation degradation effect on current	0.845
	0.9265
Uncertainties whose rms effect is	
Mismatch and manufacturing	2%
Measurement uncertainties	5%
Ultraviolet effects	5%

VDEG = Voltage Degradation Factor, containing

Radiation degradation effect on voltage	0.975
---	-------

β = Correction for angle of solar incidence (not used for Voyager studies since the solar array will be pointed to the sun with an angular error of less than 1 degree).

The value of CDEG for a sun-spacecraft distance of 1 AU is 0.6992. The above loss coefficients are discussed in detail in Section 3.3 of this Appendix.

The resulting cell current-voltage equation appears as:

$$I = \text{CDEG} (\beta) I_{sc} - \frac{V}{R_p} - I_o \left[e^{K(V + R_s I + V_{oc}(1 - \text{VDEG}))} - 1 \right]$$

where

V_{oc} = Open circuit voltage (also a sixth-degree polynomial function of temperature).

The computer program also takes into account the voltage drop due to the blocking diode associated with each series string, and the effects of blocking diode temperature (assumed to be the same as solar panel temperature).

2.0 SOLAR ARRAY POWER OUTPUT

The calculated solar array voltage-current characteristics are shown in Figure I-1 and the voltage-power characteristics in Figure I-2. These curves were based on an array of 22 solar cell panels, each containing two series strings of 106 series by 8 1/2 parallel 2 cm x 2 cm solar cells.

The curves show that adequate array power is available at 48 volts for the entire range of sun-spacecraft distances to be encountered during the 1971 flight. In fact, even though the maximum power voltage at 1.62 AU is approximately 49 volts, power can be extracted at 46 volts with less than 2 percent penalty. Thus, it will be possible to treat the array as having a constant range of source voltage characteristics.

Figure I-3 shows the array power output as a function of sun-spacecraft distance. The curve marked "Power Available at 46 Volts" is the power which can be extracted from the array at 46 volts. For the portion of the "Maximum Power" curve to the left of the point of tangency (approximately 1.4 AU) the maximum power can be obtained only at less than 46 volts. Because a buck regulator is to be used for voltage regulation, the array power actually available will follow the "46 Volt" curve to the left of the point of tangency, and the "Maximum Power" curve to the right.

A problem of some interest is the load-sharing condition, where both the array and the battery supply power to the load, and the array voltage is drawn down to the battery discharge voltage. Under this condition, the array will produce less than its design power capability and could possibly "lock" in this condition, permitting battery discharge when the array itself is fully capable of supplying the required power. The power supply can be brought out of this condition by a momentary interruption of the load to reduce the loads to less than the "load-sharing" array power output; i. e., to "turn off" the battery. A knowledge of the value of this load-sharing array power will indicate the mission time and power levels at which the load-sharing lock-in might become a problem, and the loads can be programmed to avoid the condition.

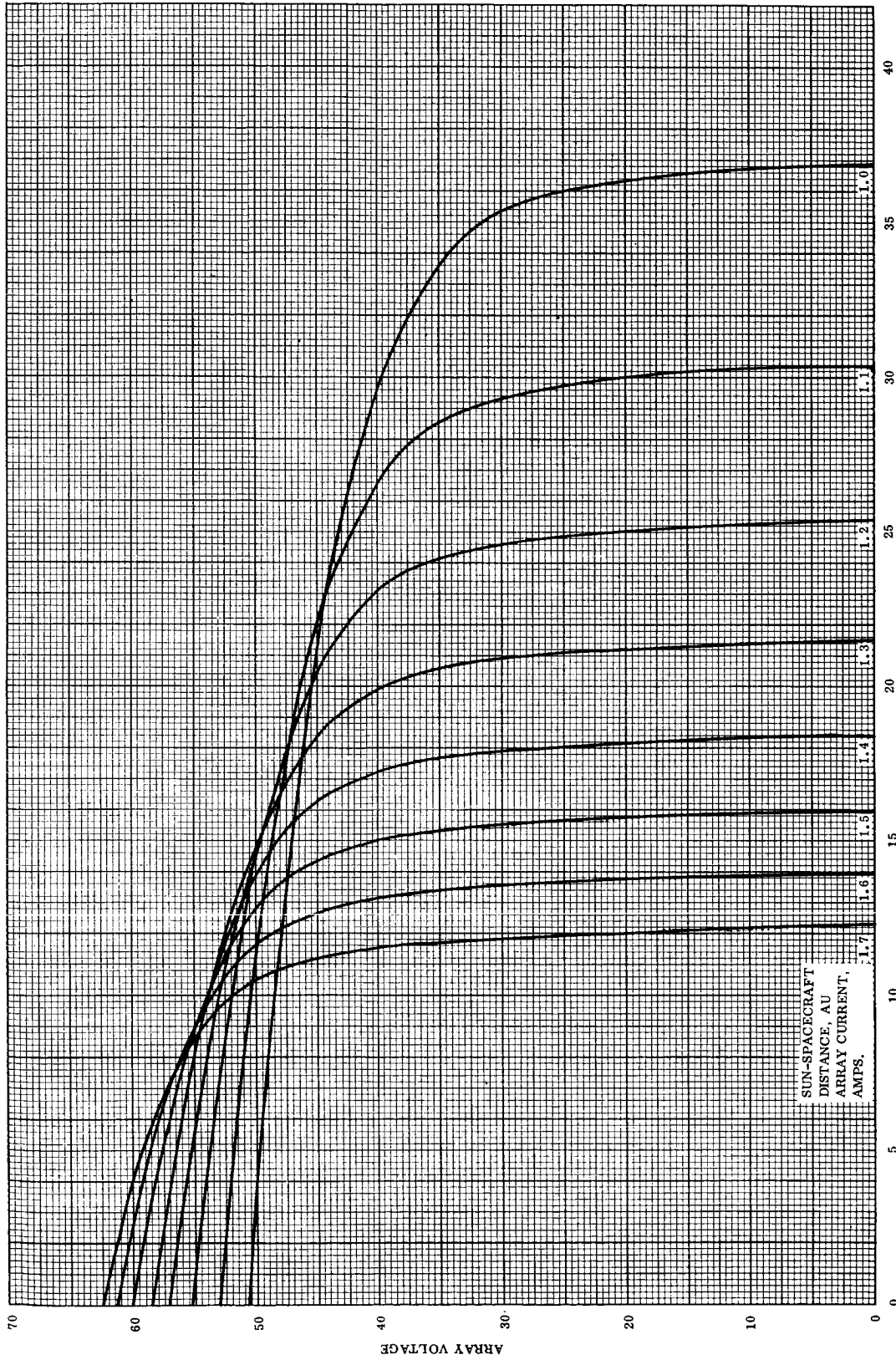


Figure I-1. Solar Array Voltage-Current Characteristics

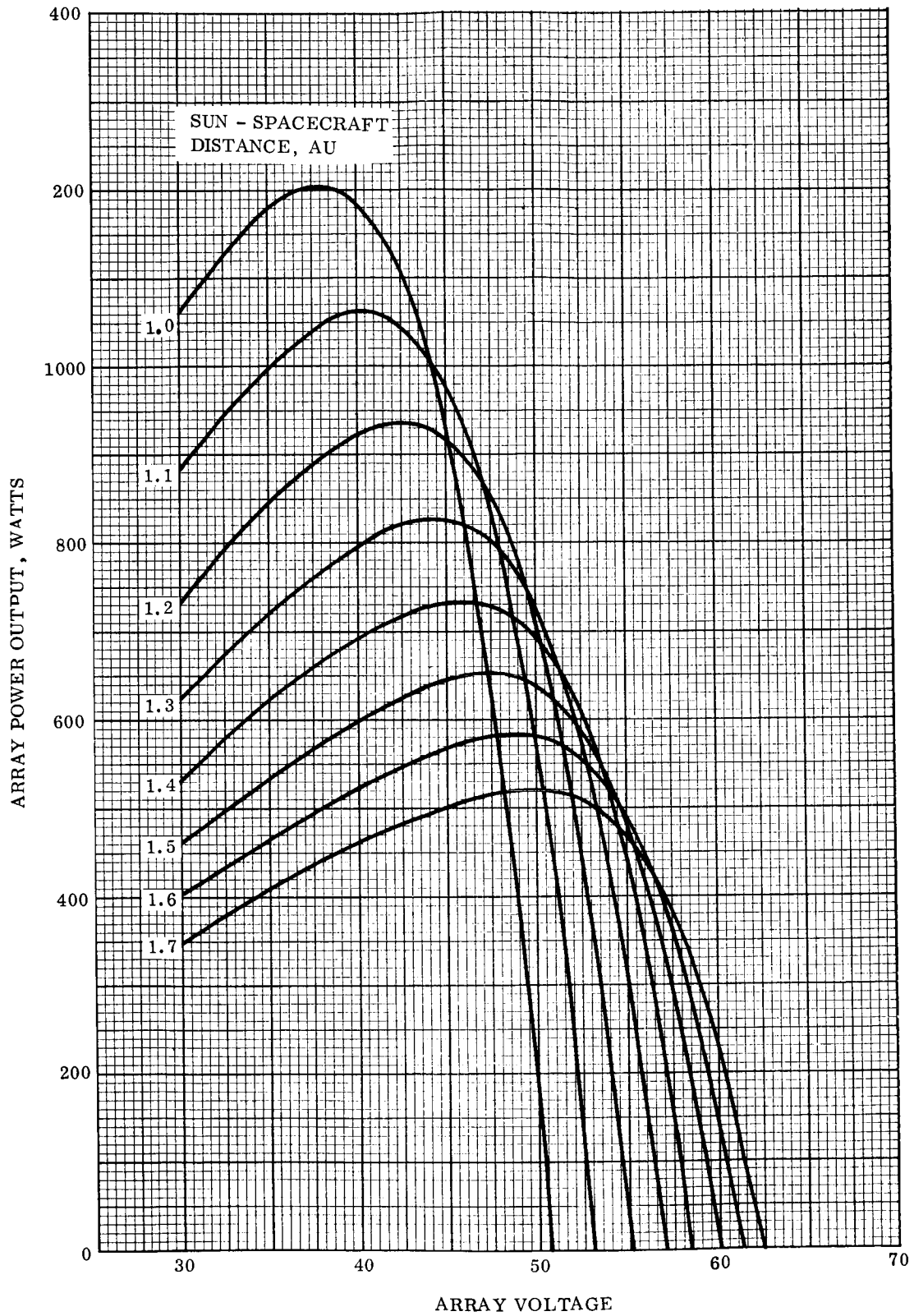
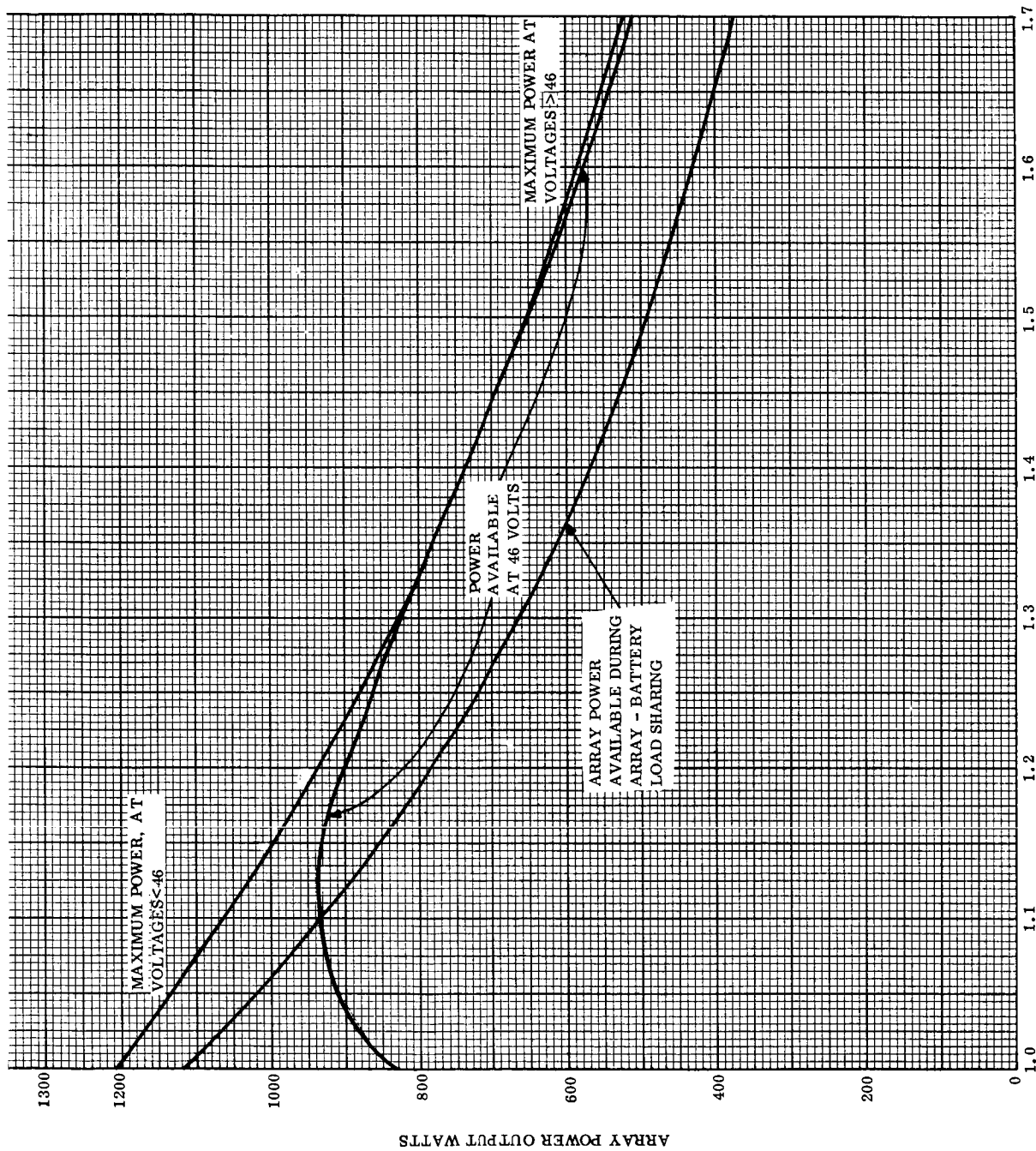


Figure I-2. Solar Array Voltage-Power Characteristics



SUN-SPACECRAFT DISTANCE, A.U.

Figure I-3. Solar Array Power Output

The predicted sun-spacecraft distance is shown in Figure I-4 as a function of time since launch for the extremes in launch date. Factoring this time-distance data into the distance - power data in Figure I-3 yields, for the latest launch date, the array power output as a function of time in Figure I-5. Superimposed on this is the power profile. The solid lines in the power profile represent the power requirements most likely expected. The dashed lines indicate the increased power required for battery charging, as for several hours after maneuvers, or during those orbits experiencing solar occultation. Also shown in this figure is the load-sharing array power output, indicating the load-sharing problem is largely confined to the last stages of the mission.

Another curve included in Figure I-5 shows the decay of solar array power in Mars orbit for the case where the Mars "Van Allen" radiation is 10^4 times greater than that at the earth. This curve includes the effects of both the radiation and also the increasing sun-spacecraft distance as functions of time. The power available decreases very rapidly the first few days in Mars orbit, but sufficient power will be available to operate the spacecraft and complete science payload for 36 days without requiring the use of the battery and with no degradation of spacecraft performance. After this, the full science payload may be operated for its required 2 hours per orbit for up to an additional 30 to 40 days, depending on the orbit period, by cycling the batteries. The science payload may be operated for at least part of each orbit for up to 87 days from orbit injection, providing there is no eclipse in the orbit. Thus, the effects of an unexpectedly high radiation environment will be to reduce the performance in the latter portion of the Mars orbit phase, when such reduction in performance will have the least effect on overall mission value.

3.0 SOLAR CELL CHARACTERISTICS

3.1 BASIC CELL V-I CHARACTERISTICS

The voltage-current characteristics used as the basis for predicting the solar array output were derived from V-I measurements made under simulated air mass zero solar illumination over a range of temperatures (-200F to +200F) on a group of RCA 1 ohm-cm 10.5 percent efficient N/P silicon solar cells. The averaged (in current, since the cells will be used connected in parallel) V-I curves for these cells are shown as a function of cell temperature in Figure I-6. Since cells are presently being delivered for another program with efficiencies averaging in excess of 11 percent, the V-I curves were adjusted upward in current to represent 11 percent efficient cells at 85°F. The general temperature-efficiency coefficient for these cells is - 0.26 percent/°F (referred to 85°F).

3.2 INTENSITY DEPENDENCE

As the solar intensity decreases, the solar cell short circuit current decreases, and in the normal range of solar intensity, the decrease in short circuit current is proportional to the decrease in solar intensity.

The characteristics of the solar cell are such that a decrease in short circuit current causes a linear shift of the V-I curve to lower current values; i. e., a differential current is subtracted from the entire V-I curve. Thus, because of the shape of the V-I curve, the power

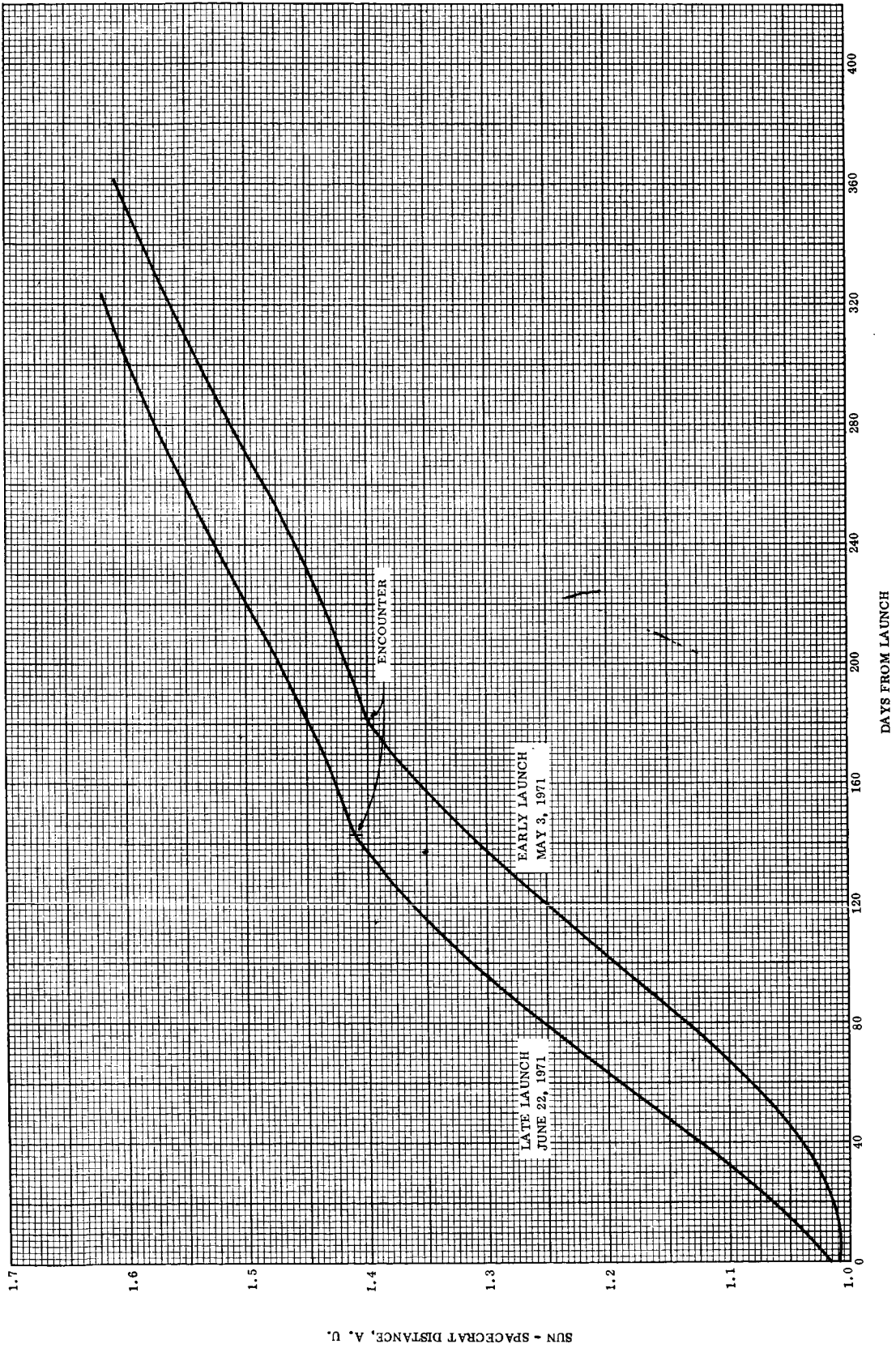


Figure I-4. Sun-Spacecraft Distance

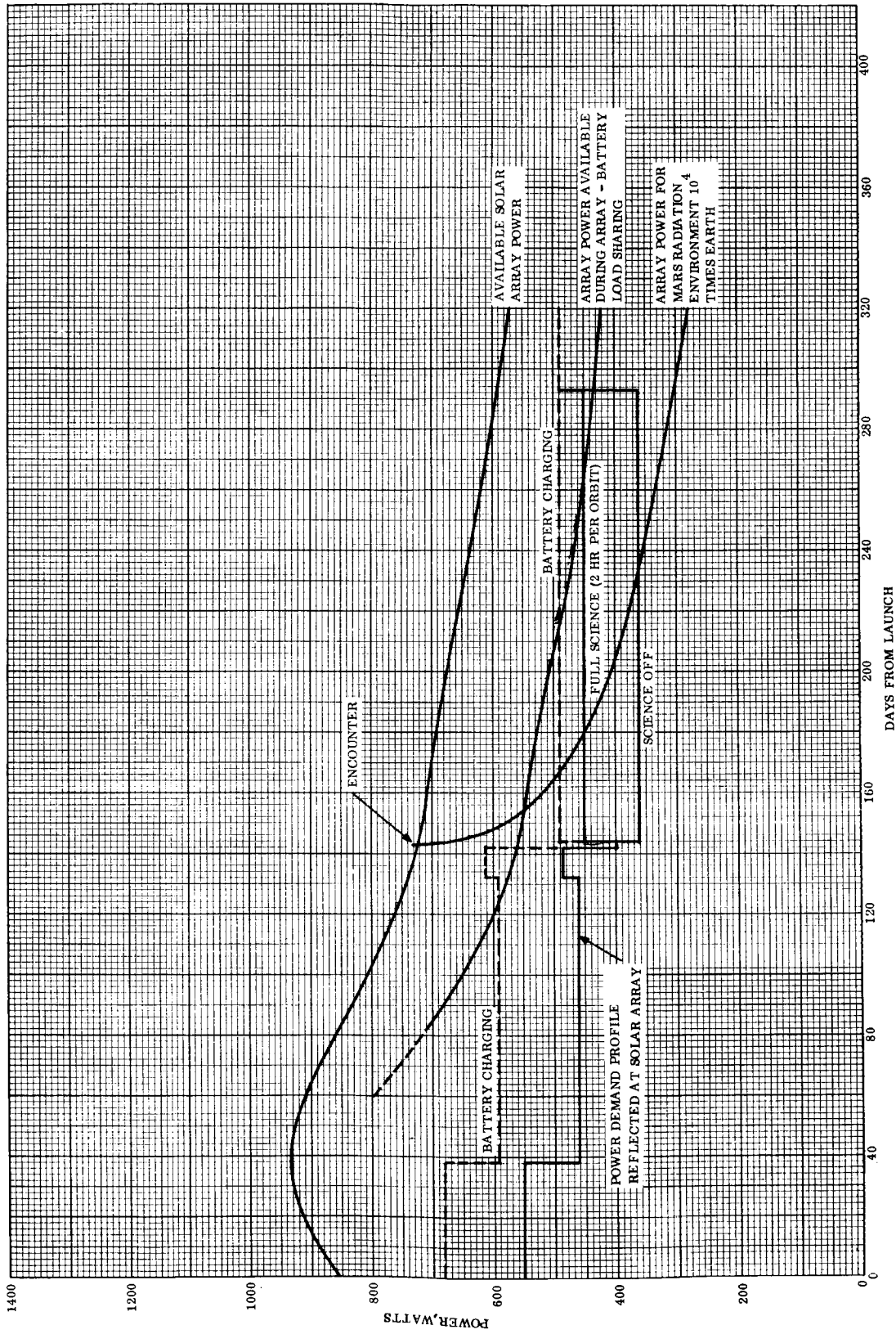


Figure I-5. Available Solar Array Power

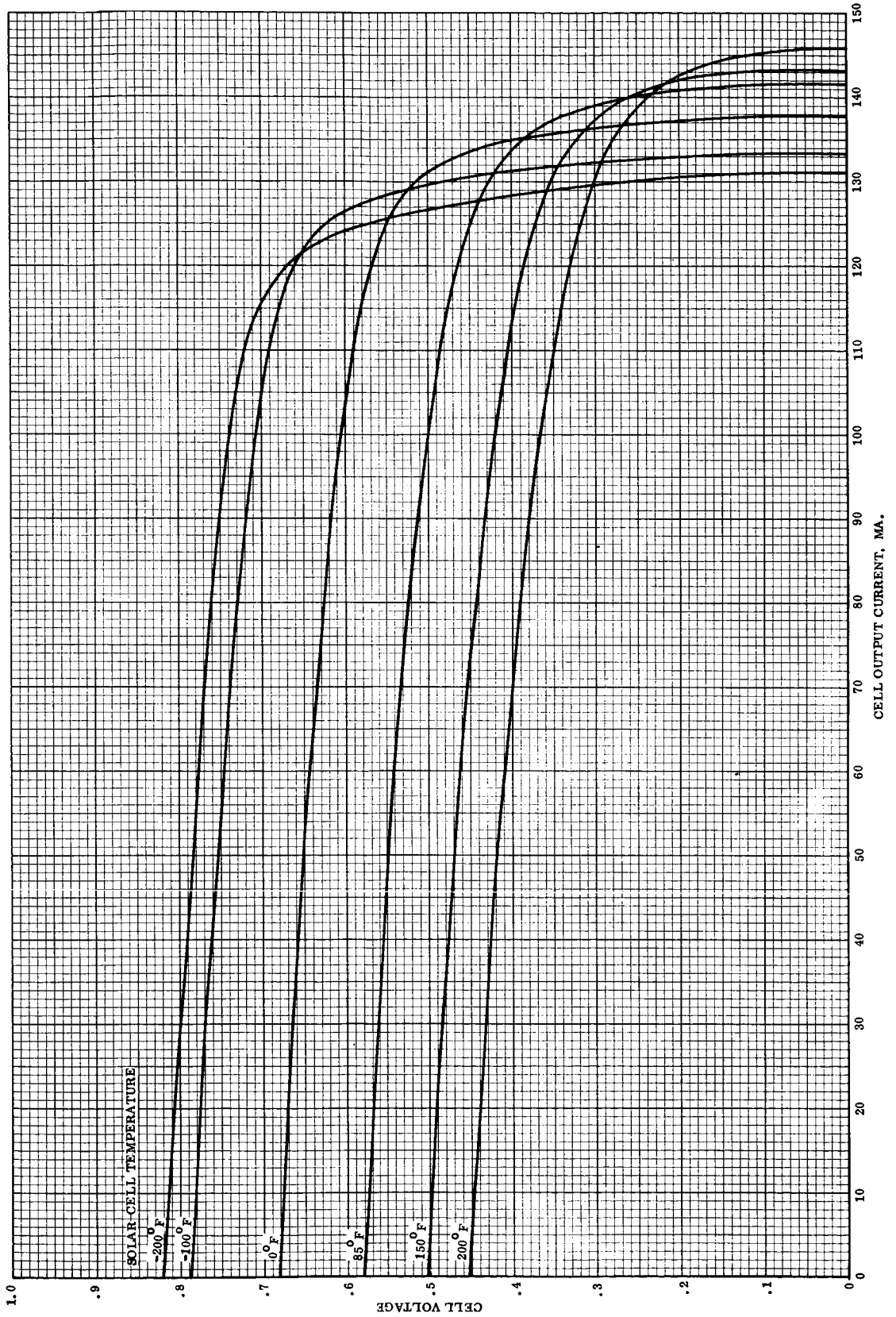


Figure I-6. Voltage-Current Characteristics of 1-Ohm-cm N/P Solar Cells

output of the solar array at a fixed voltage will decrease faster than the solar intensity (at a constant temperature). A second effect must also be included -- because of the series resistance of the solar cell, a small increase in the voltage values of the V-I curve will accompany the decrease in cell output current. The computer program takes both these effects into account.

3.3 LOSS ANALYSIS

In determining the solar array output, certain losses and output uncertainties must be accounted for. These factors are summarized below:

Losses

Filter transmission loss factor (affects cell current)	0.94
Micrometeoroid effects and random cell failures (current)	0.95
Radiation degradation - effect on current	0.845
- effect on voltage	0.975
Uncertainties, with a total rms effect on current of	0.9265
Mismatch and manufacturing	2%
Measurement uncertainties	5%
Ultraviolet effects	5%

A discussion of each of these loss factors follows.

3.3.1 FILTER TRANSMISSION LOSS

When solar cell covers with filters are bonded to solar cells, a loss in cell current output occurs due to the imperfect transmission of the filter. It is estimated that this loss will be less than six percent. The exact amount will depend on the spectral reflectance and index of refraction of the solar cell anti-reflection coating, and the index of refraction of the organic coverglass bond. Average values less than one percent loss have been reported by others for filters on polished N/P cells.

3.3.2 MICROMETEOROID EFFECTS AND RANDOM CELL FAILURES

Measurements made at MSD on solar cell-filter composites indicate the maximum power degradation from micrometeoroid erosion to be five percent, for the case of complete surface "sandblasting." There are large uncertainties in the micrometeoroid environment, but the fraction of surface area erosion is expected to be much less than 100 percent. Also, there will be random failures of individual cells both from meteoroid punctures and from solar cell contact and wiring failures due to thermal cycling. A degradation factor of 0.95 was used to allow for erosion, puncture, and random cell failures.

3.3.3 RADIATION DEGRADATION

The analysis of the radiation degradation of solar cell output is detailed in Section 5.0. The optimum fused silica cover thickness was determined on the weight trade-off between radiation degradation and array unit weight, and six mils was selected to be the cover thickness. Thus, the radiation degradation factor used in sizing the array, expressed as the fraction of original power remaining at the end of the mission, was 0.80. Separation of the effects of radiation damage on cell short circuit current and open circuit voltage shows the two terms to be:

$$\text{Residual } I_{sc} = 0.845$$

$$\text{Residual } V_{oc} = 0.948$$

Examining the effects of the reduction in short circuit current on open circuit voltage shows that the I_{sc} reduction indicated will result in a V_{oc} reduction of about 0.97 just due to the V-I characteristics of the cell. Thus, the reduction in cell voltage characteristics due to radiation will be 0.975, and the two radiation damage V-I coefficients are

Current Coefficient 0.845

Voltage Coefficient 0.975

3.3.4 MANUFACTURING AND CELL MISMATCH

Cell to cell V-I differences result in a net V-I characteristic which may be slightly penalized. These differences exist initially and may be increased with soldering operations. A two percent allowance is made for this factor.

3.3.5 MEASUREMENT UNCERTAINTY

The mean solar radiation external to the earth's atmosphere has been determined by deductions based primarily on earth surface observations. Many values of the solar constant have been reported by different investigators, the values reported having an aggregate 3σ tolerance of ± 3 percent about a nominal 140 mw/cm^2 . The tolerance accounts for the uncertainty in the actual value of the solar constant due to measurement limitations.

Measurements of solar cell output on earth are subject to many errors -- uncertainty in establishing the spectrum and intensity of the light sources used during testing, instrumentation errors, tolerance due to thermal fluctuations, etc.

For sizing calculations a five percent allowance (rms) is made for "measurement uncertainty," which includes the uncertainty in the solar constant as well as the instrumentation errors associated with solar cell measurements.

3.3.6 ULTRAVIOLET EFFECTS

Extensive testing on composite assemblies of filters, fused silica covers, organic bonds, and silicon solar cells has led to confidence in the use of organic cover glass bonds. The

filter (blue or blue-red) reduces the damaging ultraviolet radiation impinging on the organic bond so that it does not experience discoloration and reduced transmission. However, past experimental results have indicated that there is an initial decrease of about five percent in the transmission properties of the filter itself due to the exposure to ultraviolet. Subsequent work has cast some doubt on these original findings. Until this question is fully resolved a five percent allowance is made for this factor.

4.0 FILTER SELECTION

A blue filter will be used with the solar cells for the Voyager power supply.

Previous studies have shown that, for P/N cells, using the best extrapolated properties of blue and blue-red filters, the optimum cover for panel-mounted solar cells at Mars is an unfiltered cover. The power output of P/N solar cells with plain covers was predicted to be 0.8 percent greater than for cells with the optimum blue-red filter, and 2.8 percent greater than for cells with optimum blue filters.

Polished N/P solar cells have a higher surface reflectance than P/N cells, particularly in the near infrared, where the specular reflectance rises rapidly to values of 60 to 80 percent in the wavelength region beyond 1.1 microns. This built-in filter effect reduces further the value of bandpass filters (so much so that the measured weighted solar absorptance for filter - N/P cell composites is the same within measurement error for blue and blue-red filters with the same blue cut-on wavelength, apparently eliminating the need for blue-red filters even in earth orbit, since their thermal advantage no longer exists with N/P cells). Thus, the power output advantage of using unfiltered covers will be even greater for N/P cells than for P/N cells.

However, the organic adhesives used to bond the covers onto the solar cells are susceptible to darkening by ultraviolet radiation, and a blue filter will be required to protect the adhesive. The blue filter cut-on wavelength will be selected as low as possible to minimize the transmission loss to the solar cell, consistent with the required reduction in transmission in the U-V region to protect the adhesive.

5.0 SOLAR CELL RADIATION DAMAGE

5.1 BACKGROUND

The general effect of energetic particles in solar cells is to cause disordering of the atoms in the crystal structure of the cells. The high efficiency silicon solar cell in use today is made from single crystal material and its energy conversion capability is very dependent on the highly ordered arrangement of the crystal lattice. The disordering caused by charged particles, such as that found in space, creates defects in the crystal lattice which in turn serve as trapping centers for the carriers (electrons or holes) created by the absorption of light energy. Thus, these carriers are absorbed in the solar cell and never appear as electrical output of the cell. The type of defect formed is very dependent upon the type and energy of the incident radiation causing the damage.

However, insofar as the effect on the electrical output of a cell is concerned, the damage caused by one type of monoenergetic particle (say 0.5 Mev electrons) differs from that caused by another type of monoenergetic particle (say 20 Mev protons) by a constant factor relating the total dose of each type of radiation that causes equal damage to the cell. This has been shown by experiments conducted in many laboratories (1)*, (2). This implies that one can determine the flux of radiation of a given type and energy (here called the equivalent flux) that will cause the same damage to the electrical output of a cell as that due to a complex radiation environment. Also, for cell types that depend upon minority carrier diffusion for the majority of their power output, this equivalence can be established between different cell types. P/N and N/P silicon cells are of this type. An example of this is shown in Figure I-7. Here the effects of 1 Mev electrons in N/P cells (the actual data is given in Figure I-8) is multiplied by the specified constants and plotted over the effects of 0.5 Mev electrons in P/N cells.

These curves show the decrease in cell short circuit current and open circuit voltage. This cell data is representative of cell degradation under space sun illumination. The P/N data was taken under a carbon arc solar simulator (1). The N/P data was derived by a technique which is equivalent to solar illumination (2). This is a very important point to consider if one desires the absolute value of radiation flux for a given decrease in a cell electrical parameter when the cell is to be used in space. The silicon cell is a selective absorber of light energy. The power conversion capability of these cells for incident light in the wavelength region from ~ 0.7 to 1.1 microns is affected more so by the radiation encountered in space than the wavelength region below ~ 0.7 microns. Therefore, the degradation of the electrical output of the cell for a given dose of radiation will be dependent upon the type of light source used to illuminate it for power output measurements. For example, the radiation dose required to decrease the cell short circuit current by 25 percent under space illumination is approximately twice that required under 2800^oK tungsten light (3). Therefore, in order to calculate the effects of radiation on satellite photovoltaic power systems, all laboratory measurements must ultimately be referred back to the measurement of the power output of the cell under space illumination.

It has further been shown by extensive laboratory work performed at General Electric (1) that the radiation effect on the voltage-current characteristic of a cell can be defined by a degradation of the cell short circuit current and open circuit voltage, at least for radiation doses up to where the cells are rendered useless for most applications. Therefore, the essence of the radiation effects due to a complex radiation environment on the electrical output of a solar cell of a given type is to calculate the equivalent flux of a reference radiation in some reference type cell. When this is done for both the short circuit current and open circuit voltage, the entire voltage-current characteristic can be defined. Here the equivalent flux is taken as 0.50 Mev electrons, the reference cell type is the standard P/N silicon cell, space efficiency > 9 percent. The effect of 0.5 Mev electrons on P/N silicon cells is shown in Figure I-7 for a cell temperature of 85^oF. This is taken as the reference decay curve in the general solar cell radiation damage computer program, and all radiation-effects data due to electrons and protons in P/N and N/P silicon cells is referred to this curve. Since the present system design uses the N/P silicon cell, only the calculational procedure and experimental data for these devices will be discussed.

*See References in Section 5.6.

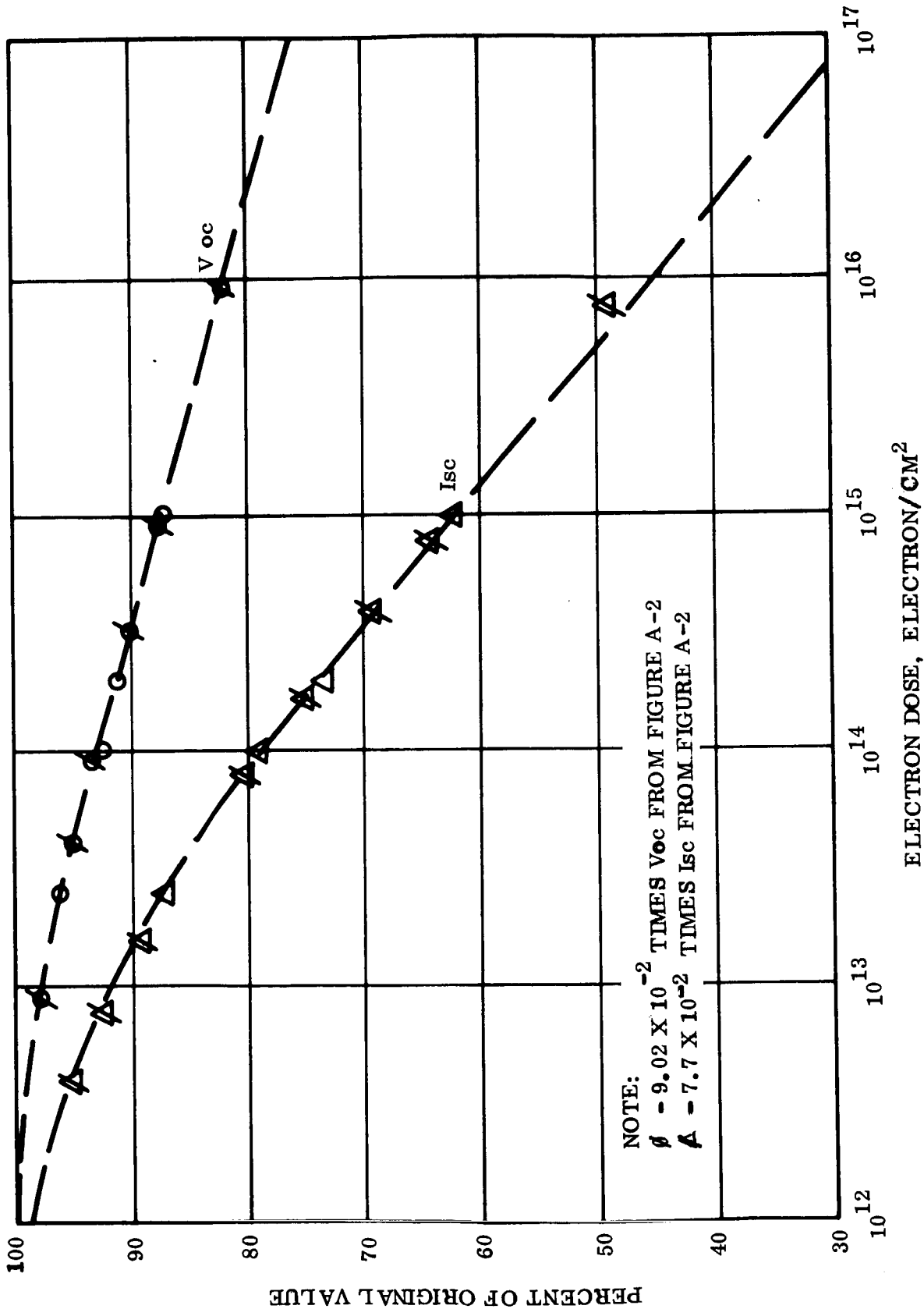


Figure I-7. P/N Solar Cell Characteristics Under 0.5 Mev Electrons

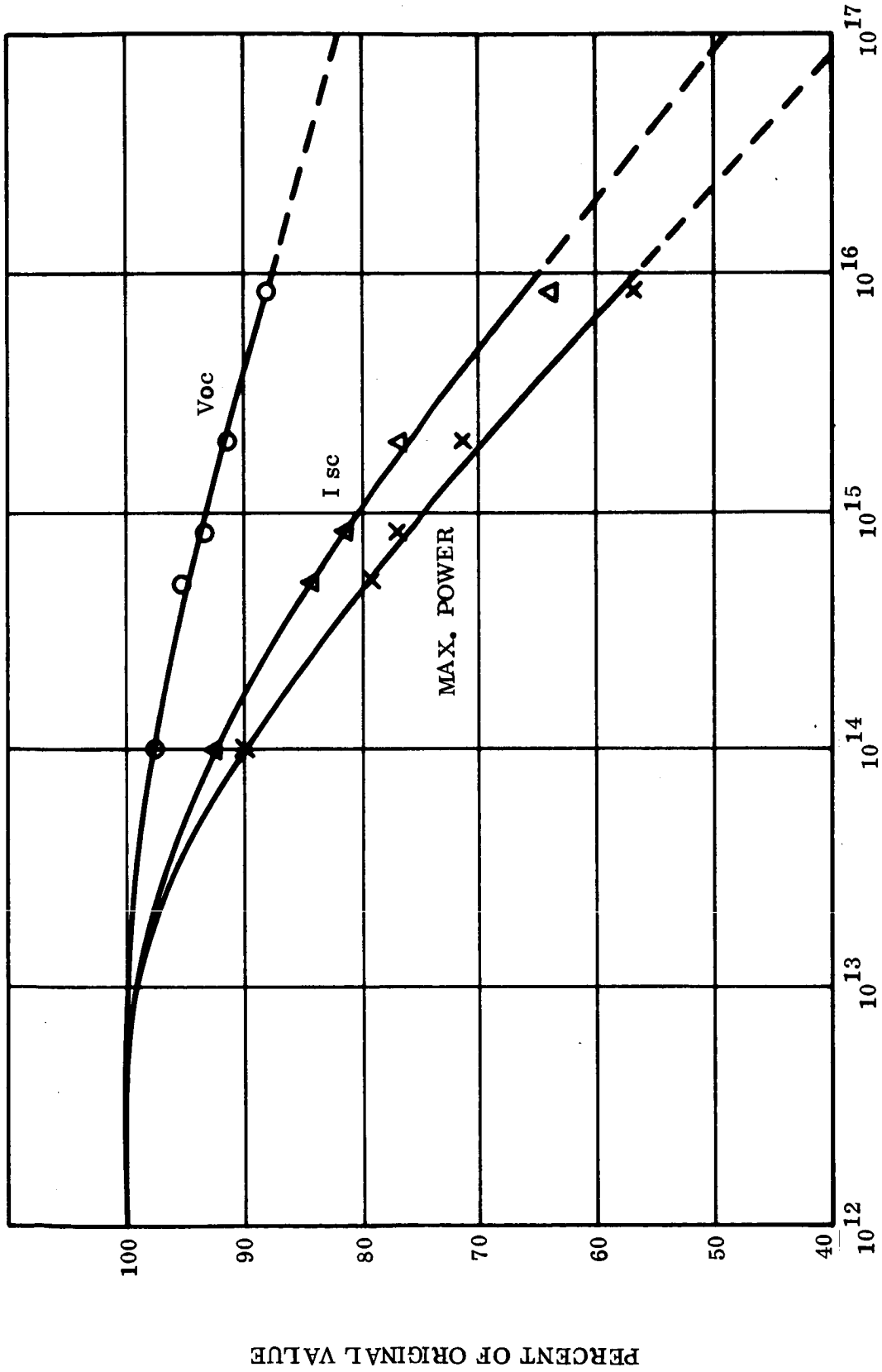


Figure I-8. N/P Solar Cell Characteristics Under 1.0 Mev Electrons

ELECTRON DOSE, ELECTRON/CM²

PERCENT OF ORIGINAL VALUE

The effect of temperature on the damage rate is not considered here, mainly due to lack of data. Some work has been done at General Electric (1) on the damage rate of electrons in P/N cells as a function of temperature. This work indicates that over a temperature range of $\pm 150^{\circ}\text{F}$ the equivalent fluxes would not vary more than ± 20 percent from that at 85°F . This variation would result in a very small error in the cell damage estimate. The Voyager solar cell damage estimates are given in Section E following a discussion of damage calculational procedure.

5.2 DEFINITION OF EQUIVALENT FLUXES - N/P CELLS

The equivalent fluxes can be stated mathematically as follows:

$$\Phi_{in} = \iint_{tE} \phi_p(E, t) D_{pin}(E) dEdt + \iint_{tE} \phi_e(E, t) D_{ein}(E) dEdt \tag{1}$$

$$\Phi_{vn} = \iint_{tE} \phi_p(E, t) D_{pvn}(E) dEdt + \iint_{tE} \phi_e(E, t) D_{evn}(E) dEdt \tag{2}$$

where the foregoing symbols have the following meanings:

- D_{pin} = short circuit current proton damage constant
- D_{ein} = short circuit current electron damage constant
- D_{pvn} = open circuit voltage proton damage constant
- D_{evn} = open circuit voltage electron damage constant
- Φ_{in} = short circuit current equivalent flux
- Φ_{vn} = open circuit voltage equivalent flux

The units of the equivalent fluxes are electrons (0.5 Mev)/cm²/unit time.

Once the equivalent fluxes are determined for each radiation component in the environment, the total is found by the summation of the components:

$$\Phi_{i \text{ Total}} = \sum_j \Phi_{ij}$$

$$\Phi_{v \text{ Total}} = \sum_j \Phi_{vj}$$

The damage is found by determining the decay of the short circuit current and open circuit voltage from Figure I-7, based on the total equivalent fluxes. It can further be shown that the maximum power point of the cell voltage-current curve is equal to (1):

$$P = I*V*$$

where:

P = fraction of original power remaining

I* = fraction of original short circuit current remaining

V* = fraction of original open circuit voltage remaining

The damage constants defined above are experimentally-determined functions and are described in detail in Section 5.3 below. The differential flux spectra are those incident perpendicular on the cell surface. When a shield material is used, the effect of this shield on the incident spectrum must be taken into account. Also, when the incident particle spectrum is isotropic, the effect of the isotropy must be considered.

5.3 THE DAMAGE CONSTANTS

Specifically, the damage constants are defined as $\Phi_{xyz} = D_{xyz}(E) \phi_x(E)$. That is, if $\phi_x(E)$ is the incident dose of radiation "X" of energy "E" on cell type "Z" and Φ_{yz} is the dose of 0.50 Mev electrons that will cause equal damage to cell parameter "Y" in P/N cells as $\phi_x(E)$ causes in cell parameter "Y" in cell type "Z", then $D_{xyz}(E)$ is the ratio of these two fluxes. The following describes the damage constants for electrons and protons in N/P silicon cells. All temperatures are 85° F.

5.3.1 PROTONS

The damage constants for protons are based on the decrease of the minority carrier diffusion length (L) in the cell base region as a function of dose. This follows a well-established relation:

$$\frac{1}{L^2} = \frac{1}{L_o^2} + K \phi \quad \text{for monoenergetic particles.} \quad (3)$$

or

$$\frac{1}{L^2} = \frac{1}{L_o^2} + \int K(E) \phi(E) dE \quad \text{for a spectrum of energies.} \quad (4)$$

This relation holds as long as the fraction of the total collected current coming from the cell surface layer is negligible since the diffusion length, and therefore K, are determined by measuring the current output of the cell under electron bombardment (4). The collection of carriers from the surface layer is not primarily by diffusion, but rather due to electric field considerations. The above relation holds for either electrons or protons.

For 1 Mev electrons in N/P cells the value of K is 1.7×10^{-10} (2); therefore,

$$\frac{1}{L^2} = \frac{1}{L_o^2} + 1.7 \times 10^{-10} \phi \quad (5)$$

where ϕ is the dose of 1 Mev electrons in electrons/cm².

Similarly, if the degradation of L is caused by spectrum of protons one can define an equivalent 1 Mev electron flux, from equation (5) as

$$\phi_{(1 \text{ mev}) \text{ eq}} = \left[\frac{1}{L^2} - \frac{1}{L_o^2} \right] \times \frac{10^{10}}{1.7}$$

Using equation (4), this becomes

$$\phi_{(1 \text{ mev}) \text{ eq}} = \frac{10^{10}}{1.7} \int K(E) \phi(E) dE \quad (6)$$

The utility of these relations is the well-known fact that cells with equal diffusion lengths will have the same output regardless of what type of radiation affected the diffusion length. Therefore, if the incident radiation is a spectrum of protons, Equation (6) will define an equivalent 1 Mev electron flux in N/P cells where K(E) is the proper function for protons and $\phi(E)$ is the incident proton spectrum. The function K(E) for protons in N/P cells is taken from Reference 2 and is given in Figure I-9. This function is approximated by the following equations for the specified energy intervals:

$$K(E) = 3.53 \times 10^{-6}, \quad E < 1 \text{ Mev} \quad (7)$$

$$K(E) = 3.53 \times 10^{-6} E^{-0.778}, \quad 1 < E < 10 \quad (8)$$

$$K(E) = 5.88 \times 10^{-7}, \quad 10 < E < 50 \quad (9)$$

$$K(E) = 2.25 \times 10^{-5} E^{-0.914}, \quad 50 < E \quad (10)$$

The value below 1.0 Mev is assumed constant since there is no data below this point. It is difficult to say how K(E) would vary at these low energies since these particles are being absorbed in the first few microns of the cell surface. Recent experiments with low energy protons ($E < 1.0$ Mev) indicate that the open circuit voltage is more drastically affected than the short circuit current, implying greater junction damage. This problem is somewhat lessened as long as there is some shield material on the cell surface. This would tend to harden the incident spectrum.

Equation (6) can be referred back to the reference decay curve by multiplying Equation (6) by the previously determined constants relating 1 Mev N/P data to the reference curve.

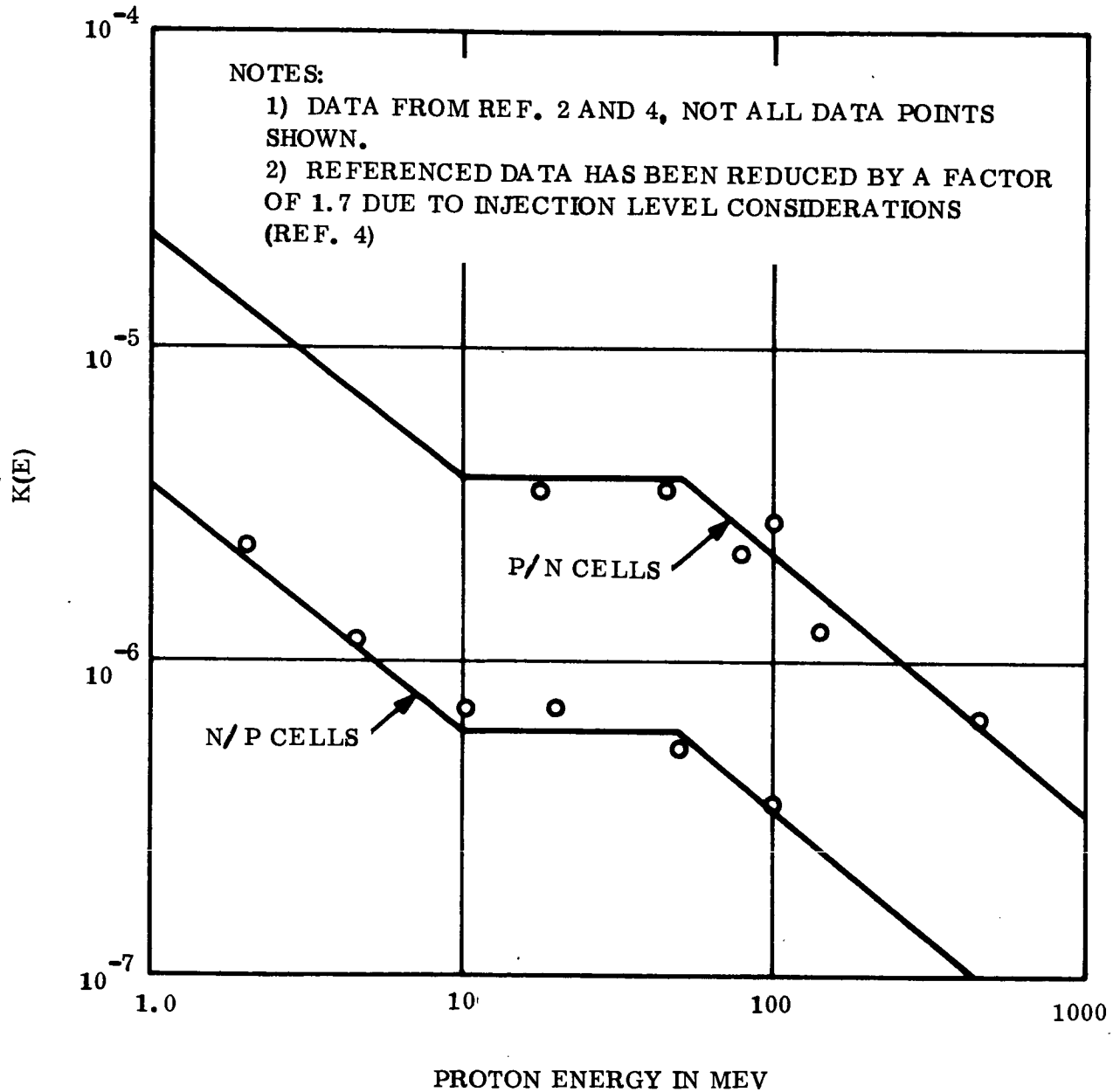


Figure I-9. Degradation Constants for Protons

These are 0.077 for short circuit current and 0.0902 for open circuit voltage. Therefore, the desired damage constants as defined in Equations (1) and (2) are:

$$\begin{aligned}
 D_{pin} &= 1.6 \times 10^3, E < 1 \text{ Mev} & (11) \\
 &= 1.6 \times 10^3 E^{-0.778}, 1 < E < 10 \\
 &= 2.67 \times 10^2, 10 < E < 50 \\
 &= 1.02 \times 10^4 E^{-0.914}, 50 < E
 \end{aligned}$$

and

$$\begin{aligned}
 D_{pvn} &= 1.87 \times 10^3, E < 1 & (12) \\
 &= 1.87 \times 10^3 E^{-0.778}, 1 < E < 10 \\
 &= 3.12 \times 10^2, 10 < E < 50 \\
 &= 1.19 \times 10^4 E^{-0.914}, 50 < E
 \end{aligned}$$

5.3.2 ELECTRONS

The electron damage constants D_{ein} and D_{evn} are derived in a similar fashion as the proton damage constants. Figure I-10 shows the electron damage function versus energy, normalized to 1 Mev. This data is obtained from references (5) and (6). The damage constants D_{ein} and D_{evn} are then obtained by referring this relative damage function back to the reference decay curves of Figure I-7 by multiplying this function by the constant 0.077 to obtain D_{ein} and by 0.0902 to obtain D_{evn} . The final values for D_{ein} and D_{evn} are shown in Figure I-11.

5.4 SHIELDING EFFECTS

The previous section defined the damage rate in silicon solar cells in terms of the dose of radiation incident perpendicular to the cell surface. When one has shield material surrounding the solar cell, the change in the radiation spectrum as it passes through the shield and the effect of isotropy (as is usually assumed for space radiation) must be properly taken into account in order to apply the previously derived equations. For a given incident isotropic spectrum, one must calculate an equivalent normal spectrum incident on the cell surface that would cause the same cell damage as the isotropic spectrum.

5.4.1 ELECTRONS

Neglect, for the moment, the effect of isotropy and assume all particles are incident normal to the cell and shield.

The residual spectrum of electrons that emerges from the under surface of the shield material can be estimated using range-energy data for aluminum. This method is only an approximate method and ignores the straggling effect of the electrons. However, for thin shields the net effect of this will be quite small.

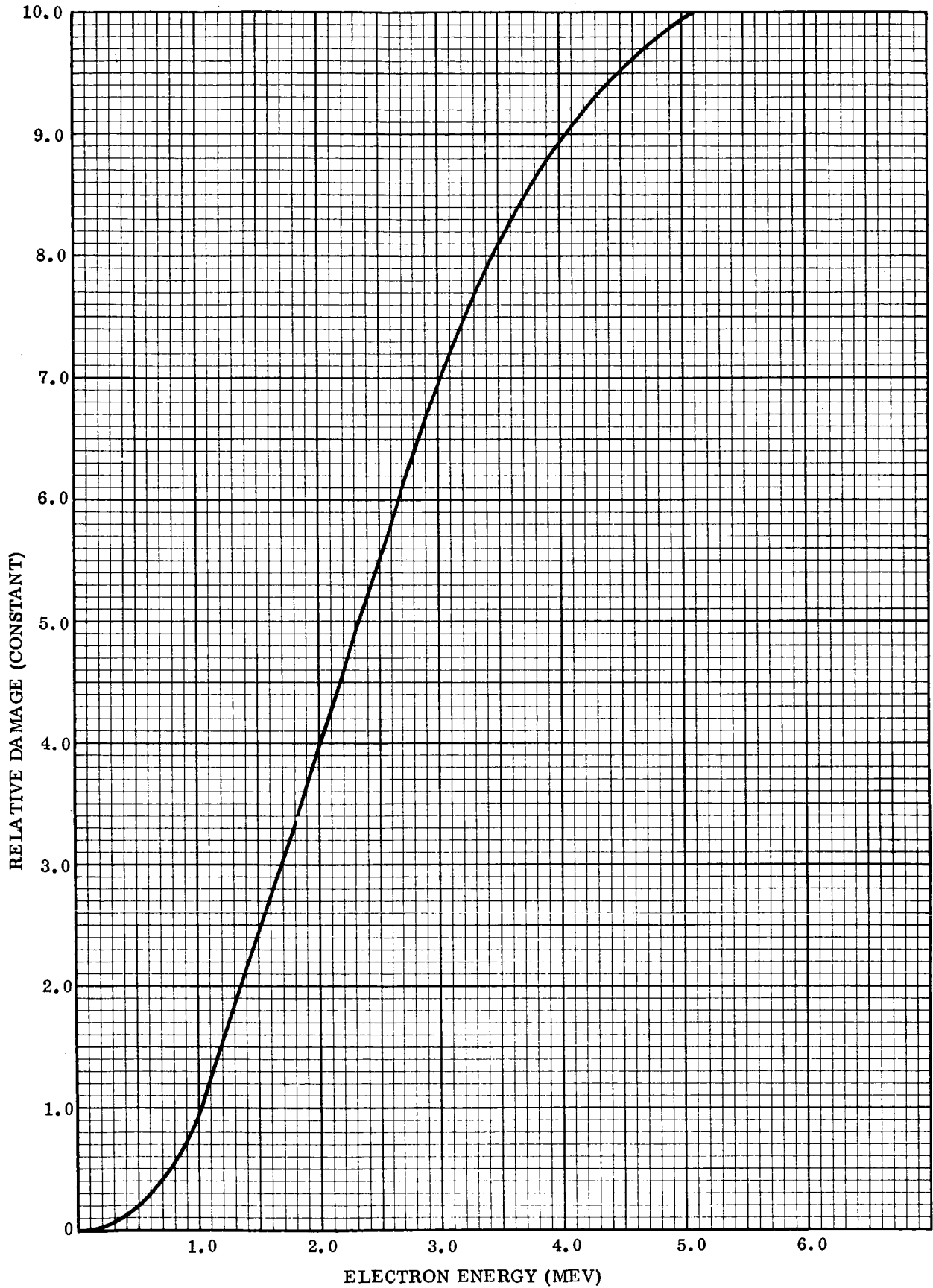


Figure I-10. Relative N/P Damage Constants - Electrons

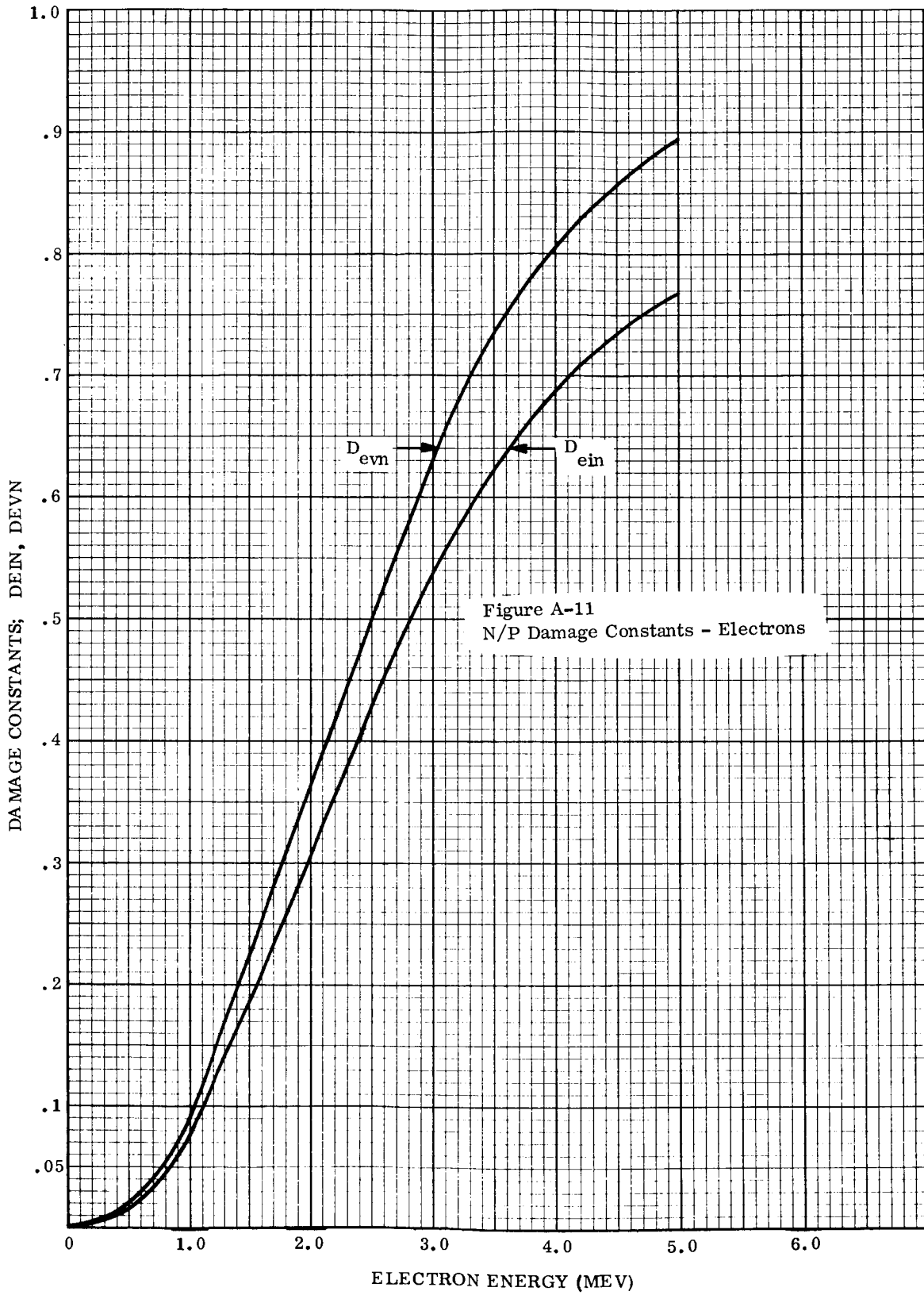


Figure I-11. N/P Damage Constants - Electrons

The range-energy data is taken from Katz and Penfold (7). The range curve for energies less than several Mev can be defined by

$$R_o \text{ (gms/cm}^2\text{)} = 0.412 E_o^{1.4} \tag{13}$$

Now the residual range of an electron (i.e. its energy) after it traverses a given thickness of material is

$$R_r = R_o - R_s \tag{14}$$

where

R_r = residual range of the electron corresponding to its residual energy, E_r

R_o = initial range of the electron corresponding to its initial energy, E_o

R_s = thickness of shield in gms/cm²

When applying range-energy data to a continuous spectrum one must work in a step-wise fashion. For instance, it is assumed that electrons having average intensity ϕ_o and average energy E_o within an energy interval ΔE_o will emerge (providing E_o is larger than the cutoff energy corresponding to R_s) from the other side of the material with intensity ϕ_r , energy E_r and contained within the energy interval ΔE_r .

Now assuming no absorption of these particles as they traverse the shield, then it follows that:

$$\phi_o \Delta E_o = \phi_r \Delta E_r \tag{15}$$

or

$$\phi_r = \phi_o \frac{dE_o}{dE_r} \tag{16}$$

where ϕ represents the electrons/cm²/Mev so that Equation (15) is the total electrons in the energy interval.

Using Equation (13) and (14), Equation (16) becomes

$$\phi_r = \phi_o \left[\frac{E_r}{E_o} \right]^{0.4} \tag{17}$$

Now the energy that a particle loses in traversing a thickness is

$$E_{\text{loss}} = \int_{R_0 - R_s}^{R_0} \left[\frac{dE}{dR} \right] dR$$

$$= E_0 - 1.885 \left[0.412 E_0^{1.4} - R_s \right]^{0.714}$$

The residual energy is then

$$E_r = E_0 - E_{\text{loss}} = E_0 \left(1 - \frac{2.43 R_s}{E_0^{1.4}} \right)^{0.714} \tag{18}$$

Therefore, using Equations (17) and (18) in stepwise fashion from the maximum energy in the spectrum to the cutoff energy, one can calculate the residual spectrum for a shield thickness R_s , where

$$R_s = \rho T, \quad \text{where } \rho = \text{gms/cc} \tag{19}$$

$T = \text{thickness (cm)}$

The cutoff energy for electrons is

$$E_c = 1.885 R_s^{0.714} \tag{20}$$

The above discussion does not take into account the effect of isotropy. Consider the diagram in Figure I-12. Here the number of electrons/cm²/sec/Mev incident on the shield and contained between the two cones of semi-aperture θ and $\theta + d\theta$ is equal to

$$\phi_0(E_0) \frac{d\omega}{2\pi},$$

where $d\omega = 2\pi \sin \theta d\theta$ is the solid angle and $\phi_0(E_0)$ is equal to 1/4 the total isotropic flux. The electrons contained in this cone will pass through a distance $R_s/\cos \theta$ in traveling through the shield. Therefore, the energy loss for these particles, using equation (18) is

$$E_r(\theta) = E_0 \left[1 - \frac{2.43 R_s / \cos \theta}{E_0^{1.4}} \right]^{0.714} \tag{21}$$

Similarly, these same particles will enter the cell at the same angle θ , assuming the electron path has not deviated appreciably from a straight line. If the particle range, $R(E_r)$, after it passes through the shield is greater than the thickness of the active region of the cell, it will cause more damage than a normally incident particle of the same energy. If the damage is assumed to be proportional to the path length through the active region and this is assumed to be a thickness equal to bulk diffusion length, L , then a particle entering at an angle θ will cause $1/\cos \theta$ times more damage than a normally incident particle of the same energy.

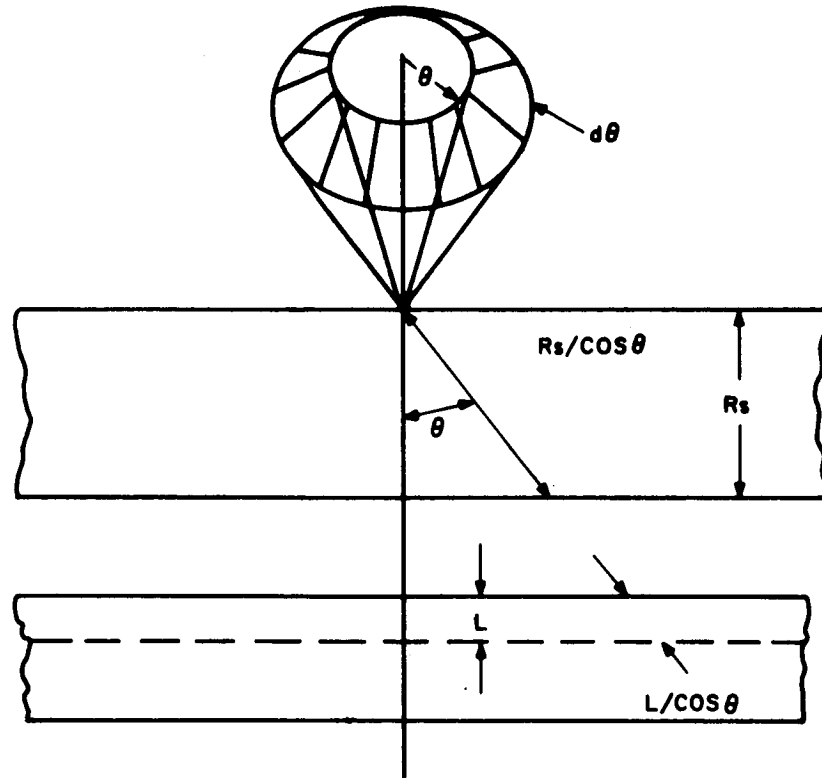


Figure I-12. Geometry for Isotropic Flux

However, the dose received at the cell surface in particles/cm²/sec is reduced to $\phi \cos \theta$ where ϕ is the particles/cm²/sec normal to the direction of the incident particles. Therefore, for particles whose residual range, $R(E_r)$, exceeds the path length through the cell, $L/\cos \theta$, for a given incidence angle, θ , the net effect in the cell is the same as particles entering normal to the cell surface having intensity, ϕ , and energy, E_r , since the damage is proportional to the surface dose times the path length. This has been shown experimentally using 1 Mev electrons where the cell damage was found to be independent of angle of incidence when the damage is referred to the incident beam intensity (8).

However, when the angle of incidence and the residual range are such that $R(E_r) < L/\cos \theta$, the damage becomes proportional to $\phi \cos \theta \times R(E_r)/L$ relative to a particle entering normal with range $R(E_r)$. Further, if the incident particles have a residual range which is less than L , the incident particles will have the same range in the cell independent of the angle of incidence. Therefore, the damage when referred to the cell surface dose should decrease with $\cos \theta$.

Based on the preceding remarks an isotropy-damage function, $\sigma(E_r, \theta)$, can be defined which relates the cell damage for isotropic incidence to cell damage due to normal incidence. If $\phi(E_r, \theta)$ is the particle flux measured normal to the direction of the particle direction then the equivalent normal flux, $\bar{\phi}(E_r, \theta)$, which will cause the same cell damage is $\bar{\phi}(E_r, \theta) = \sigma(E_r, \theta) \phi(E_r, \theta)$, where $\sigma(E_r, \theta)$ is defined as follows:

$$R(E_r) < L, \sigma(E_r, \theta) = \cos \theta$$

$$R(E_r) < L/\cos \theta, \sigma(E_r, \theta) = \frac{R(E_r)}{L} \cos \theta \tag{22}$$

$$R(E_r) > L/\cos \theta, \sigma(E_r, \theta) = 1.0$$

The total equivalent-normal flux of energy, E_r , is then, using Equation (17)

$$\Phi(E_r) = \int_0^{\pi/2} \phi(E_o) \left(\frac{E_r}{E_o}\right)^{0.4} \sigma(E_r, \theta) \sin \theta d\theta \tag{23}$$

Further, letting $\mu = \cos \theta$, $d\mu = -\sin \theta d\theta$, and using Equation (21),

$$\Phi(E_r) = \int_0^1 \phi(E_o) \left[\frac{E_r}{E_r^{1.4} + \frac{2.43 R_s}{\mu}} \right]^{0.4} \sigma(E_r, \mu) d\mu \tag{24}$$

where $\sigma(E_r, \mu)$ is:

$$R(E_r) < L, \sigma = \mu$$

$$R(E_r) < L/\mu, \sigma = \frac{R(E_r)}{L} \mu \tag{25}$$

$$R(E_r) > L/\mu, \sigma = 1.0$$

If it is also assumed that the environment $\phi(E_o)$ can be defined by a number of line segments of the form $\phi(E_o) = G E_o^{-H}$, where G and H are constants over a specified interval of E_o , then using equation (21) to define E_o as a function of E_r , Equation (24) becomes

$$\Phi(E_r) = \int_0^1 \frac{G E_r^{0.4} \sigma(E_r, \mu) d\mu}{\left(E_r^{1.4} + \frac{2.43 R_s}{\mu}\right)^{0.714 (H + 0.4)}} \tag{26}$$

and $\sigma(E_r, \mu)$ is defined by Equation (25) for each value of E_r and μ .

5.4.2 PROTONS

Identical considerations are used to calculate the equivalent-normal residual proton spectrum as was used for the electrons. The range-energy data is taken from Reference 9. This is approximated by:

$$R \text{ (gms/cm}^2\text{)} = 0.00334 E^{1.73}, E = \text{mev} \tag{27}$$

The resultant equivalent-normal residual proton spectrum is

$$\Phi(E_r) = \int_0^1 \frac{G_p E_r^{0.73} \sigma(E_r, \mu) d\mu}{\left(E_r^{1.73} + \frac{300 R_s}{\mu} \right) 0.578 (H_p + 0.73)} \tag{28}$$

Here $\sigma(E_r, \mu)$ has the same definition as given by equation (25) except the range, $R(E_r)$, now applies to protons in silicon, which is calculated in the same units as the diffusion length, L .

The differential proton spectrum is also assumed to be defined as, $\phi_p(E_o) = G_p E_o^{-H_p}$, where G_p and H_p are constants.

Both the electron and proton differential spectra are defined in particles/cm²/mev/unit time and represent the dose received per unit time on one side of a flat surface. Therefore, these spectra are equal to 1/4 the total intensity of the isotropic spectra. The equations give the value of flux for a given value of E_r . By repetitively applying these equations for different values of E_r , one can calculate as many points as desired on the residual spectrum.

5.5 SOLAR CELL DAMAGE ESTIMATES

The specified radiation environments for the Voyager 1969 and 1971 missions were given in the Preliminary Mission Specification, JPL Doc. No. 45. These environments were used to calculate the N/P, one ohm-cm, silicon solar cell degradations by the methods described above. Of course, as a result of the recent Mariner 4 experiment, the intensity of the Martian radiation belt may be negligible.

In any case, parametric calculations have been performed for various assumptions on the Martian belt. These results are shown in Figure I-13 as a function of front shield thickness. The back shielding for the cells in all cases is assumed to be 0.2 gm/cm², equivalent to approximately 35 mils of aluminum.

Included here are the effects of the solar flare protons for both the cruise and orbit phases of the mission along with the various assumptions on the intensity of the Martian belt for the elliptical orbit mission. The Martian environment calculations for the elliptical orbit are

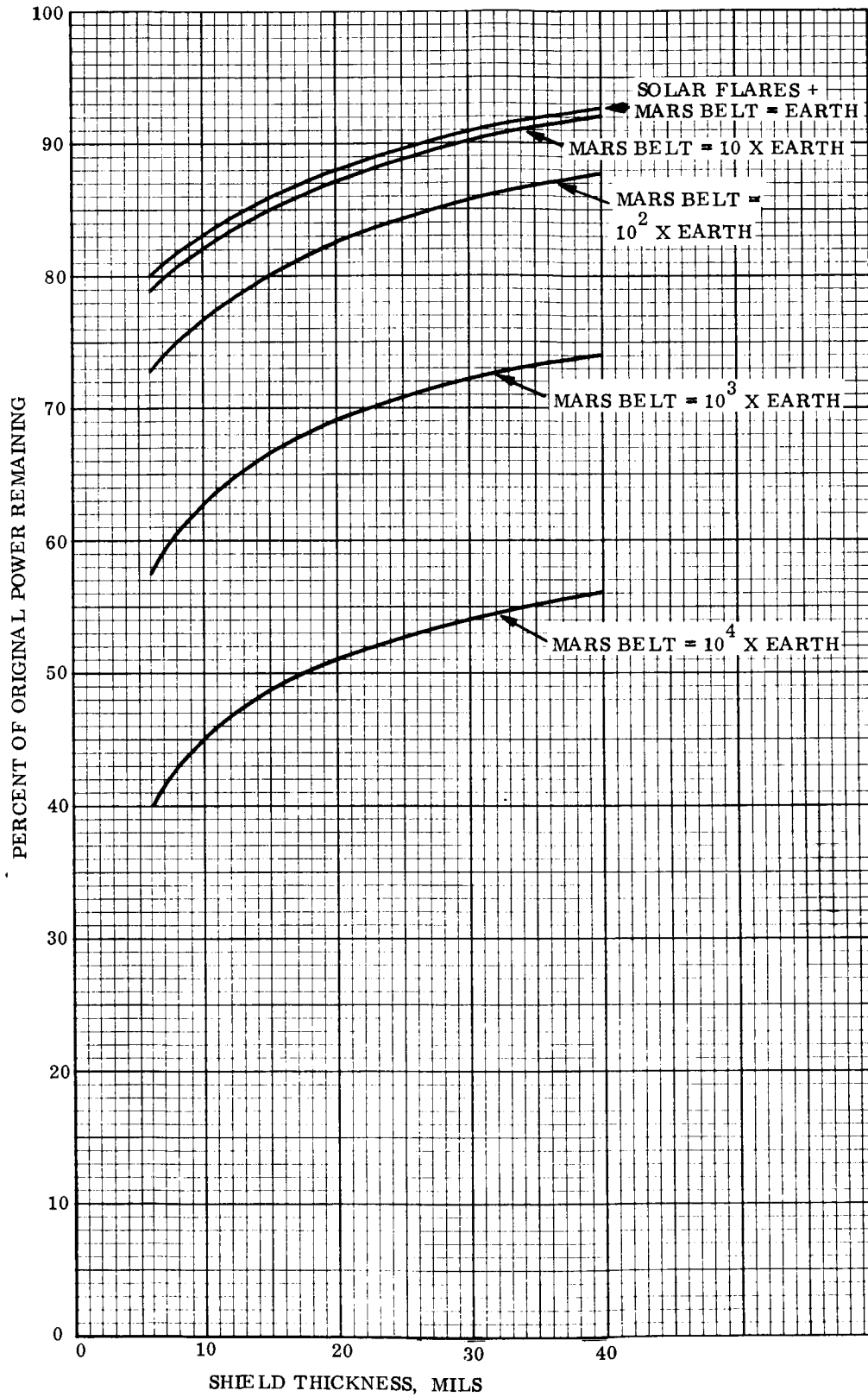


Figure I-13. Solar Cell Damage Estimates, 1971 Mission

based on the assumption that the Martian belt is identical to the Earth's belt in terms of spatial distribution relative to the planet size.

The curves of Figure I-13 show the expected degradation of the solar cells at the end of the entire mission, six months cruise plus six months Mars orbit, for the case where the Mars belt is equal in intensity to the Earth's belt and for the cases where the Mars belt is various orders of magnitude higher than the Earth's belt up to a maximum of 10^4 times the Earth's belt.

For the case where the Mars belt is equal to the Earth's belt, the degradation is almost entirely due to the solar protons. Even for the case where the Mars belt is ten times the Earth's belt, the solar protons are still the predominant environmental component. For higher assumptions on the Martian intensity, however, the Martian belt becomes the predominant component.

Figure I-14 shows similar degradation curves for the 1969 mission. The curves show the degradation at the end of the two-month Earth orbital phase and also the degradation at the end of the cruise phase. As can be seen, most of the degradation occurs in the Earth orbit phase.

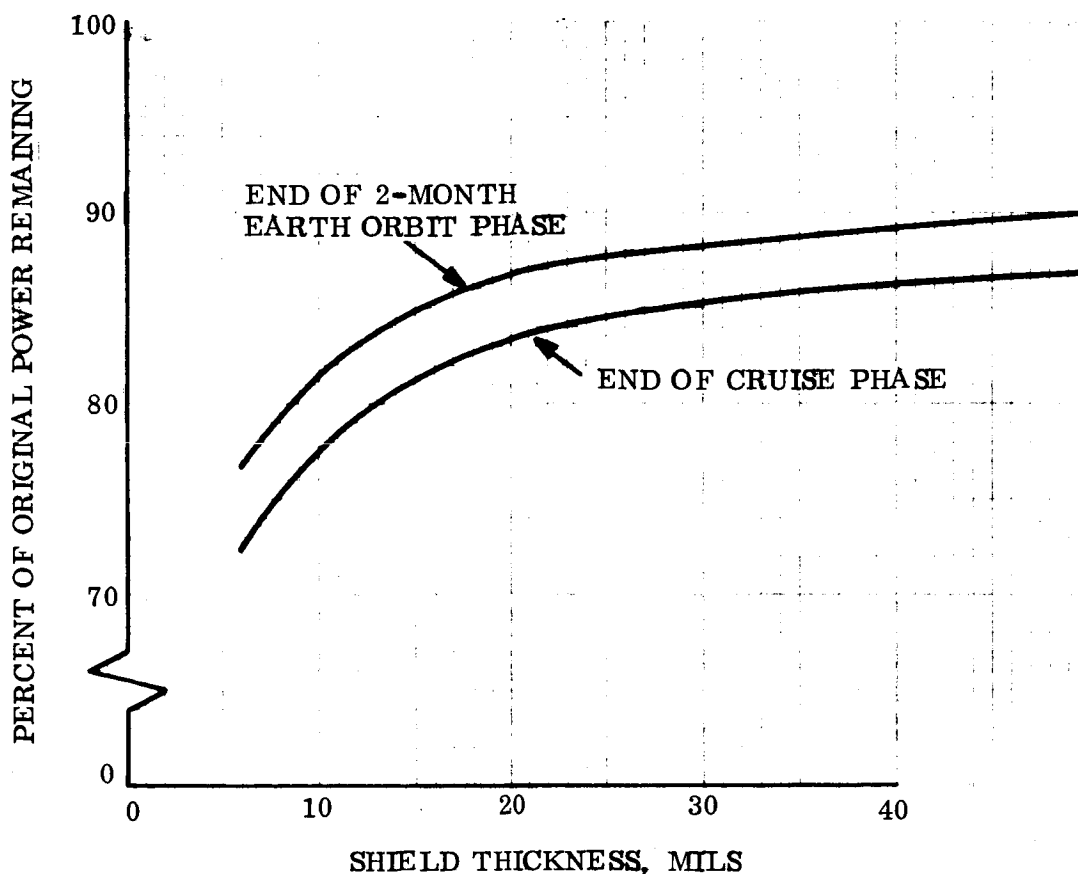


Figure I-14. Solar Cell Damage Estimates, 1969 Mission

5.6 REFERENCES

1. R. Bobone, B. W. Merchant, Predicting Damage to Silicon Solar Cells Subject to Complex Radiation Spectra, General Electric Company, AIEE Conference Paper CP-62-1279, AIEE Conference - Denver 1962.
2. F. M. Smits, The Degradation of Solar Cells Under Van Allen Radiation, IEEE Transactions on Nuclear Science, Volume NS-10, No. 1, Jan. 1963.
3. J. M. Denny, R. G. Downing, Charged Particle Radiation Damage in Semiconductors, I: Experimental Proton Irradiation of Solar Cells, Space Technology Laboratories, Inc., Doc. No. 8987-0001-RU-000, Sept. 15, 1961.
4. F. M. Smits, et al, Report of Solar Cell Work at Bell Telephone Laboratories, Proceedings of the Solar Working Group Conference, Interagency Advanced Power Group, PIC-SOL 209/2, Vol. I, April, 1962.
5. W. Rosenzweig, Radiation Damage Effects, IEEE Photovoltaic Specialists Conference Washington, D.C., April 10-11, 1963.
6. W. Cooley, and R. Janda, Handbook of Space Radiation Effects On Solar Cell Power Systems, NASA SP-3003, 1963.
7. Katz and Penfold, Rev. Mod. Phys., 24, 28 (1952).
8. F. M. Smits, Sandia Corporation, Private Communication.
9. R. M. Sternheimer, Phys. Rev., 115, 137 (1959).

6.0 COVER THICKNESS ANALYSIS

The coverglass thickness is determined by a weight tradeoff. As the coverglass thickness is increased, the radiation damage is decreased and the required array area is decreased, but the unit area weight of the array is increased. The optimum coverglass thickness is theoretically at the point where the resultant weight is at a minimum. The following table outlines the calculation steps taken to determine the optimum glass thickness. The residual power fractions are those derived in Section 5.0 for 1 ohm-cm N/P solar cells.

Table I-1. Relative Specific Weight vs. Coverglass Thickness

Glass Thickness mils	Parametric Solar Panel Weight, lb/ft ²	Residual Power Fraction	Relative Specific Weight (Arbitrary Units)
6	.95	.80	1.188
10	.99	.83	1.192
20	1.09	.88	1.24
30	1.19	.905	1.32

It should be noted that the unit area weights are based on gross array area, and were derived from approximate array sizing exercises. While an actual design is necessary to determine the panel weights for a particular design, the parametric weights given are close enough to correctly indicate the optimum glass thickness. In this case the optimum thickness occurs at about 6 mils, and since 6 mils is the minimum practical thickness for handling and manufacturing, it was selected.

7.0 THERMAL ANALYSIS

In designing a solar array, the array temperature and temperature distribution must be taken into account, since the temperature of a solar cell determines its voltage characteristics. The dependence of cell voltage characteristics on temperature was indicated by the V-I curves shown in Figure I-6. From this data a prime design parameter can be derived -- the voltage at which maximum power can be extracted from a solar cell. The variation of this maximum power point voltage with cell temperature is shown in Figure I-15.

A thermal analysis reported in VB235FD101-Appendix yielded the solar panel temperature profiles shown in Figure I-16. Because the panels are not at a uniform temperature, it is necessary to balance the number of cells in each series string and select their locations on the panel so that a reasonably uniform voltage characteristic is obtained for all series strings. As a result, since two series strings are to be placed on each panel, part of one string will be mounted on the high-temperature end of the panel near the spacecraft body, and the remainder of the string on the cooler outboard end. The second string will be mounted at the center of the panel. The resultant maximum power voltages for the two strings are derived in Table I-2. The temperatures on which the calculation is based are those occurring at Mars encounter with the bio-barrier in place, since this results in the worst thermal gradient at the lowest power output capability at which the barrier will be in place.

Table I-2. Voltage Match Between Series Strings

Cell Row (Thermal Node)	No. of Cells in Series	Cell Temp. °F	Cell Voltage at Maximum Power	Cell Row Power Voltage
1	19	90	.446	8.47
2	21	86	.451	9.47
3	23	82	.455	10.46
4	25	74	.465	11.62
5	28	39	.507	14.19
6	30	19	.531	15.93
7	32	16	.535	17.11
8	34	15	.536	18.22

Rows 1, 2, 7 and 8 are connected in series to form one series string, and rows 3 through 6 to form the other. Thus, the two string voltages are 53.2 and 52.2 respectively, and are within 1 percent of a median value.

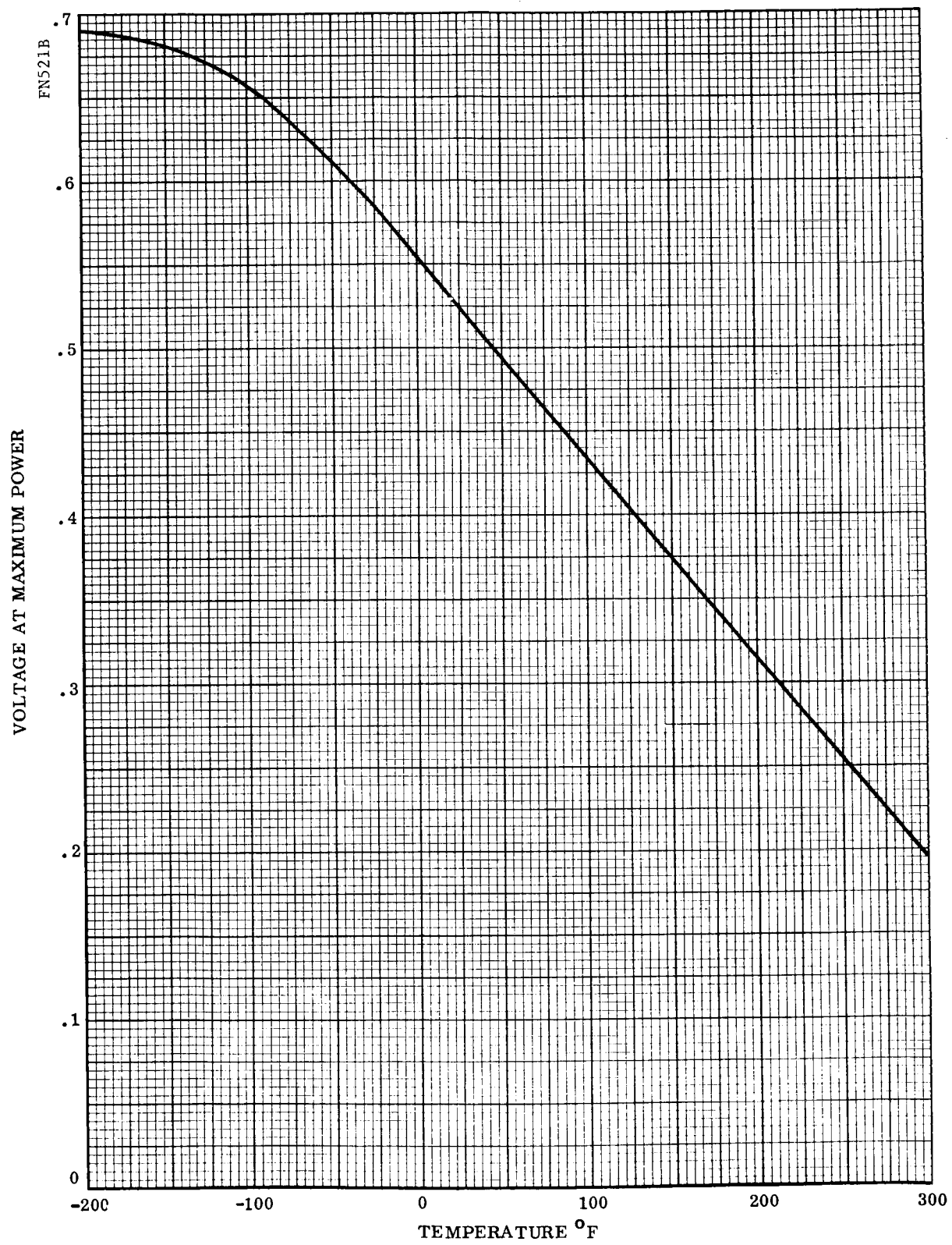


Figure I-15. Voltage at Maximum Power

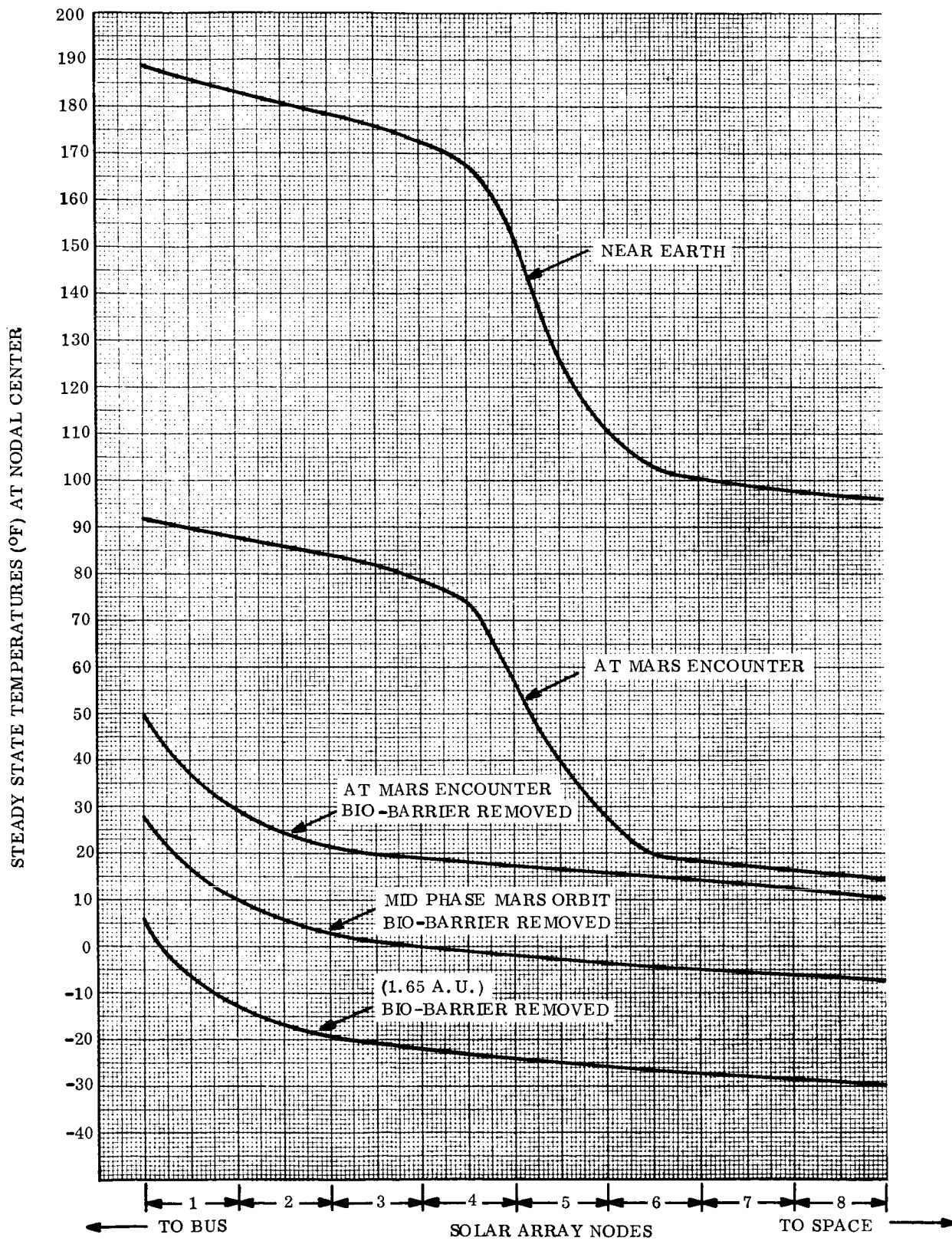


Figure I-16. Fixed Solar Array Radial Temperature Distribution

A second problem of some concern is the effect of a large temperature gradient across a single row of solar cells. The largest gradient occurs across Node 5, and amounts to 29 degrees F. The highest temperature is 56°F, the average 39°F, and the lowest 27°F. The cell power point voltages corresponding to the highest, average, and lowest temperatures are .486, .507, and .522 volts, respectively. The difference between the power point voltages in cells connected in parallel will cause a mismatch loss. This loss can be estimated through the use of the normalized cell power voltage data in Figure I-17. In this graph, the raw solar cell V-I data from Figure I-6 has been normalized to the maximum power point at each temperature, showing the cell power output loss as the output voltage deviates from the maximum power voltage. In the case under consideration, the normalized cell voltages at which power is removed from the "hot" and "cold" cells are $.507/.486 = 1.043$ and $.507/.522 = .972$, respectively. Thus, using the data in Figure I-17, the relative power losses will be .02 and .005 at the extremes of the cell row. Assuming a parabolic shape for the loss curve gives an average power loss of 0.4 percent in that cell row, which appears to be the worst of the lot. Examination of the mismatch curve indicates that the temperature gradient-voltage mismatch effect is approximately proportional to the square of the temperature gradient, thus the effects of the temperature gradient on the power output of the other cell rows will be even less than the 0.4 percent. This loss is so small as to be swamped by the uncertainties in predicting solar array output, and was ignored.

For predicting the power output of the solar array, an average solar panel temperature was determined by weighting the temperature of each panel thermal node by the number of solar cells in that node. The resultant weighted average effective solar panel temperature at 1 AU is 135°F. The panel temperatures at other sun-spacecraft distances were determined using a temperature-distance relationship of $(\text{Distance})^{-1/2}$, which assumes only solar heat input to the panels.

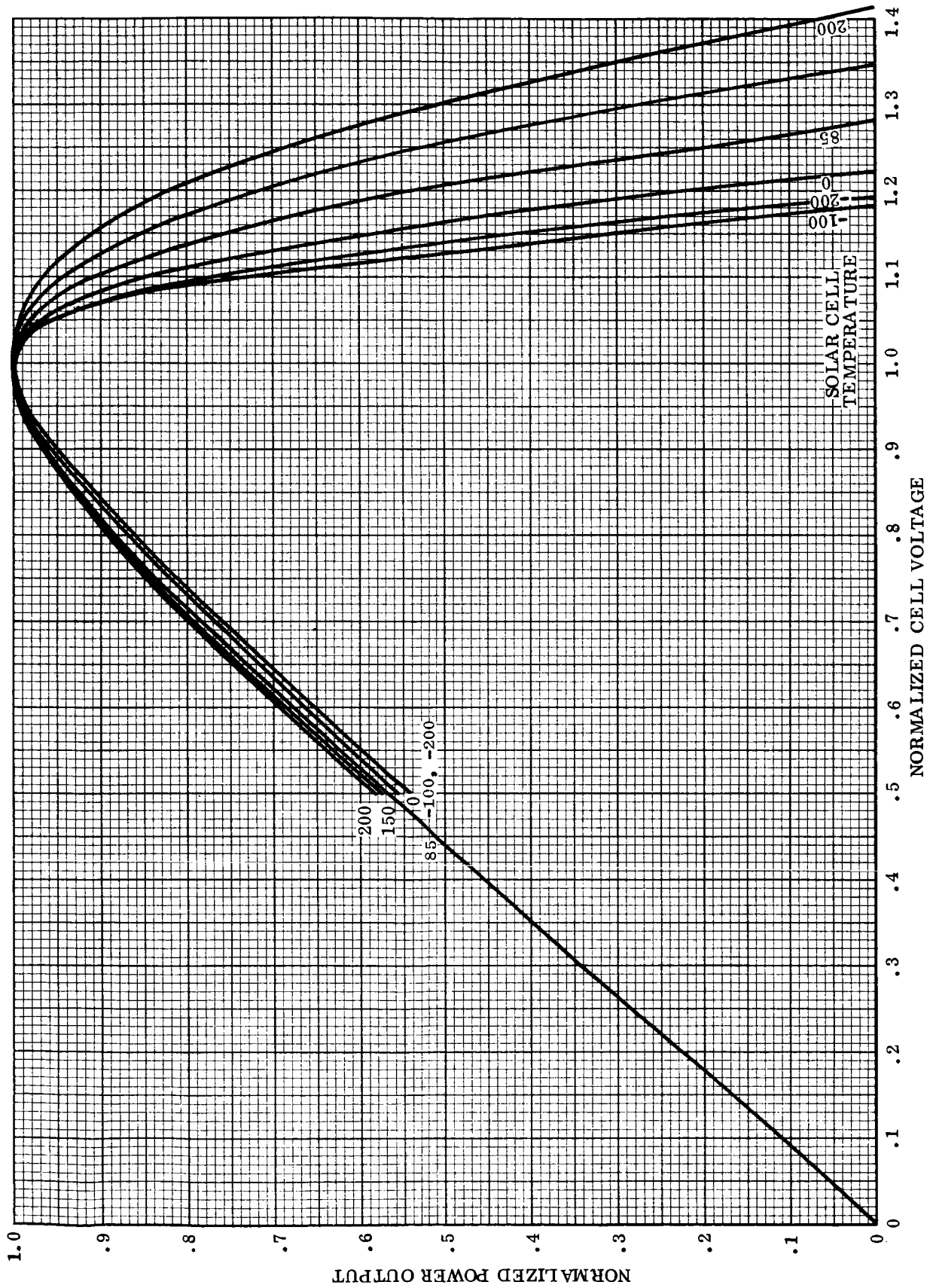


Figure I-17. Solar Cell Voltage Mismatch Characteristics

CII-VB236FD101

APPENDIX II
SIZING ANALYSIS

Index

1 Sizing Analysis

APPENDIX II

1.0 SIZING ANALYSIS

The solar array and battery size requirements were determined with the aid of the Energy Balance Table in Table II-1. The electrical loads are summarized in the table, and the accounting of the loads includes the various power subsystem losses and is extended to determine the loads directly at the solar array and the battery.

The following loss and efficiency relationships were used in the load analysis:

Harness Loss - The power loss in the power distribution harness was assumed to be 1 percent for all loads, both AC and unregulated DC.

2400 cps Inverter Efficiency - The main inverter was taken to be 90 percent efficient at full load, and the no-load loss to be one-half the full-load loss. The inverter thermal loss at intermediate power output levels was assumed to vary linearly between the two defined end points.

400 cps Three Phase Inverter - The thermal loss was assumed to vary similarly to the 2400 cps inverter, with a full load efficiency of 80 percent.

Regulator Efficiency - The regulator efficiency was also taken to be 90 percent at full load, with a variation in thermal loss similar to the main inverter.

Battery Diode - The battery diode voltage drop was taken to be 0.3 volts (germanium diode), resulting in an efficiency of 99 percent.

Battery Charger - The efficiency of the battery charger will be proportional to the output/input voltage ratio, since the charger is a series regulating voltage and current limiter. In the Energy Balance Table the battery charger efficiency and thermal loss (both indicated by **) are based on an input voltage (solar array voltage) of 46 volts. For sizing purposes, this corresponds to the worst case, when minimum array power is available at 46 volts. In actuality, the available array power will be greater than the minimum required power, and the charger input voltage will be higher than 46 volts, thus, the thermal loss in the chargers will be higher, ranging up to a maximum steady-state value of 25 watts.

The worst case for battery charging power is the shortest orbit (12 hours) since the higher science power requirements occur a relatively fixed 2 hours per orbit, thus a higher percentage of the shorter orbit.

The battery charging power was determined based on the following data and assumptions:

- Maximum Mars orbit eclipse will be 15 percent of the orbit period or 3 hours, whichever is less.

Regulator	24.6	24.8	25.0	25.2	25.4	25.2	30.1	25.5	26.6	31.1
Thermal Loss	174.2	189.2	190.8	194.7	203.4	206.9	291.1	205.7	225.5	310.8
Total Buck Regulator Input	145.0	145.0	57.0	***145.0	57.0	***145.0	145.0	145.0	57.0	145.0
Unregulated D.C. Loads:	200.0	200.0	200.0	200.0	200.0	200.0				
Radio (**Maximum)	145.0	145.0	57.0	***145.0	57.0	***145.0	145.0	145.0	57.0	145.0
Capsule	145.0	345.0	257.0	145.0	57.0	145.0	145.0	145.0	57.0	145.0
Unreg. D.C. Load Subtotal	1.5	3.5	2.6	1.5	0.6	1.5	1.5	1.5	0.6	1.5
Harness Loss	146.5	348.5	259.6	146.5	57.6	146.5	146.5	146.5	57.6	146.5
Unregulated D.C. Loads	320.7	537.7	450.4	341.2	472.8	353.4	437.6	352.2	283.1	457.3
Unregulated D.C. Bus Req't										
Unregulated Battery Loads:	1.0	1.0	1.0	1.0	1.0	1.0	1.0	1.0	1.0	1.0
Buck Reg. Fault Det.	6.0			6.0		6.0				6.0
Gyro Heaters (Avg.)				18.0		18.0				
Thrust Vector Control Engine Controls				60.0		60.0				
Antenna Gymbal Drive	7.0	1.0	1.0	85.0	1.0	85.0	1.0	7.0	7.0	7.0
Unreg. Battery Load Subtotal	327.7			431.5		438.4			290.1	
Thermal Loss	3.3			4.4		4.4			2.9	
Battery Output	331.0			435.9		442.8			293.0	
Thermal Loss	28.0	0- 9.4	0- 9.4	36.0	0- 9.4	37.0	0- 3.1	0- 9.4	25.0	3.7
Battery Input		0-121.2	0-121.2	0-121.2	121.2	121.2	0- 39.1	0-121.2		22.1
Charger Output		1.0-122.2	1.0-122.2	1.0-122.2	122.2	122.2	1.0- 40.1	1.0-122.2		40.1
Efficiency		44.2/46.0	44.2/46.0	44.2/46.0	44.2/46.0	44.2/46.0	44.2/46.0	44.2/46.0		22.4/46.0
Thermal Loss		1.0- 5.0	1.0- 5.0	1.0- 5.0	5.0	5.0	1.0- 1.7	1.0- 5.0		1.0
Charger Input		1.0-127.2	2.0-127.2	2.0-127.2	127.2	127.2	2.0- 41.8	2.0-127.2		41.8
Array Bus Power		539.7-564.9	452.4-577.6	474.8-600.0	388.2	388.2	439.6-479.4	354.2-479.4		499.1
Harness Loss		5.4- 6.7	4.5- 5.8	4.8- 6.1	3.9	3.9	4.4- 4.8	3.6- 4.8		5.0
Thermal Loss		9.5- 11.7	7.9- 10.1	8.3- 10.5	6.9	6.9	7.7- 8.4	6.2- 8.4		8.8
Array Power Output Requirement		554.6-684.2	464.8-593.5	487.9-616.6	399.0	399.0	451.7-492.6	364.0-492.6		512.9
Array Power Available		862	743		725	725	572	572		572

- Mars orbit period will range from 12 to 24 hours.
- Silver-cadmium battery effective watt-hour charging efficiency when new is 60 percent based on voltage ratio and allowing for current tapering at the end of the charging period.
- A silver-cadmium battery will require approximately 15 percent current over-charge when old.

The energy which must be returned to the battery is

$$E_{ch} = \frac{293. \text{ w (1.8 hr) (1.15)}}{.60} = 1011 \text{ w-hr.}$$

To this must be added energy for the gyro heaters (contingency) and the buck regulator fault detector during the sunlit portion of the orbit, since this energy passes through the battery chargers.

$$\text{Batt. Ch. } E_{out} = 1011 + 10.2 (7) = 1082 \text{ w-hr.}$$

Accounting for the battery charger inefficiency yields:

$$\text{Batt. Ch. } E_{in} = 1082 \frac{(46)}{(44.2)} = 1126 \text{ w-hr.}$$

Because the full science payload draws 85.4 more watts at the unregulated bus for two hours per orbit, the charge power is reduced during the full science period. The charging power may be obtained using:

$$2 (P - 85.4) + 8.2 (P) = 1126 \text{ w-hr.}$$

The gross battery charging power, $P = 127.2$ watts. Deducting for the battery bus loads leaves a charging current of 0.87 amps per battery, or a nominal 1 ampere.

The idle thermal loss in the battery chargers was taken to be one watt.

The battery charger current limit was sized large enough to provide heater power to the gyros during the entire sunlit portion of the occulted orbits, as well as the eclipsed portion. It is expected that the residual vehicle angular rates on entering the shadow of Mars will be low enough so that gyro operation will not be required to maintain reasonable vehicle attitudes on emergency into the sunlight, and the normal mode of operation will be not to use the gyros once the Mars orbit has been established. However, if angular rates are higher than anticipated, gyros may be required for stabilization during spacecraft eclipse. It is not necessary to operate the gyros during the sunlit portion of the orbit, but if extra array power is available, continuous operation of the gyros will permit more reliable, drift-free performance. Thus, the charge current limit was set high enough to permit gyro operation not only

during eclipse, but full time. The alternate Mode Full Science column, marked with an asterisk, outlines the power accounting for full time gyro operation, and indicates that an additional 20.5 watts would be required.

The battery capacity is determined by the power requirements during Mars orbit eclipse. The maximum eclipse time will be 3 hours, and the power required at the battery, from the Energy Balance Table, will be 294 watts. The working energy storage required will be 882 watt-hours. If the desirable maximum depth of discharge of a silver-cadmium battery is about 65 percent, and a silver-cadmium battery degrades about 30 percent in capacity in a year, the battery capacity must be 1940 watt-hours. The capacity provided is 75 ampere-hours at a discharge voltage of 30.4 volts, or 2280 watt-hours.

The maneuvers are of shorter duration, and the imposed energy storage requirements less than for the orbit eclipse. The energy requirements will be 640, 881, and 563 watt-hours for the mid-course, capsule separation, and orbit insertion maneuvers, respectively.

The relation between battery energy capacity, maneuver and eclipse loads, and battery recharge time is indicated in Figure II-1. This data shows that at least 9 hours are required between consecutive midcourse maneuvers to allow the battery to recharge.

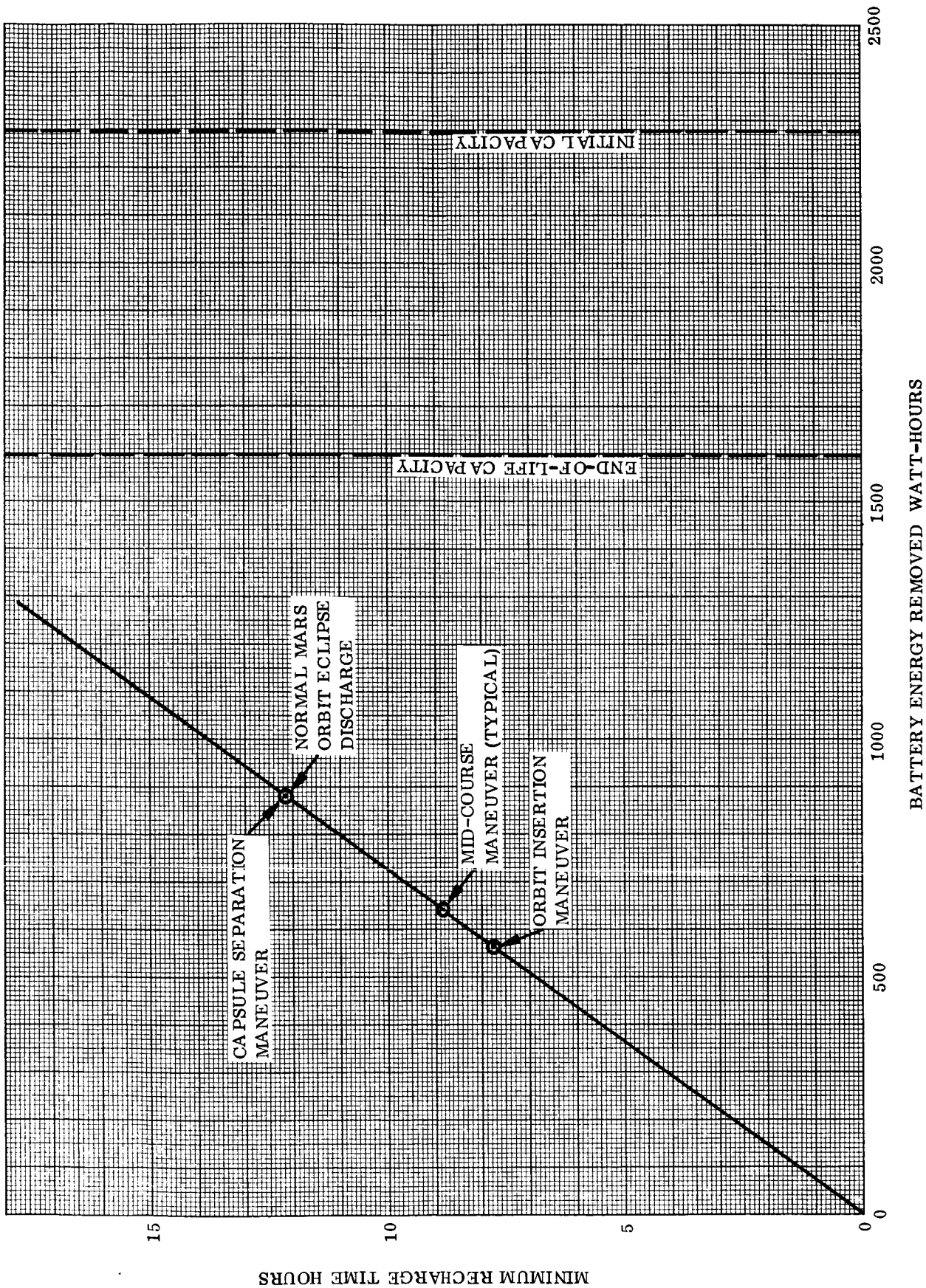


Figure II-1. Battery Energy Utilization

CII-VB236FD101

CII-VB236FD101

APPENDIX III

POWER SUBSYSTEM RELIABILITY ANALYSIS

Index

- 1 Summary
- 2 Mathematical Mode IV and Reliability Computation

1.0 SUMMARY

A reliability assessment of the preferred design of the Power Subsystem which is shown in Figure 3-2 indicates a reliability of 0.991 for a total mission of launch, transit to Mars, and orbiting Mars for a period of one month. This reliability assessment is slightly above the value of 0.989 which was apportioned to this subsystem.

To assist in the analysis, the complete mission has been divided into the four mission phases defined in the Preliminary Voyager 1971 Mission Specification (JPL Project Document #45).

2.0 MATHEMATICAL MODEL AND RELIABILITY COMPUTATION

The mathematical model which defines the backup capability and the interaction of all the components in the subsystem is:

$$R_{\text{(power s/s)}} = R_{\text{(solar array)}} \cdot R_{\text{(charge Reg. \& Batt. package)}} \cdot R_{\text{(main Reg. Pack)}} \cdot R_{\text{(2.4 KC Inverter Pack)}} \cdot R_{\text{(400 cps Inverter Pack.)}} \cdot R_{\text{(Synchronizer)}}$$

where:

$$R_{\text{(charge Reg. \& Batt. Pack.)}} = \sum_{S=2}^{\eta=3} \binom{\eta}{S} R_1^S (1-R_1)^{\eta-S}$$

$$\text{and } R_1 = R_{\text{(charge Reg.)}} \cdot R_{\text{(controls)}} \cdot R_{\text{(diodes)}} \cdot R_{\text{(Battery)}}$$

$$R_{\text{(main Reg. Pack.)}} = \left[R_{\text{(Reg.)}} \cdot R_{\text{(Controls)}} \right] + \left[R_{\text{(fault Sensor)}} \right] \left[R_{\text{(Reg.)}} \cdot R_{\text{(controls)}} \right] \left[\lambda_{\text{(Reg. \& Contr.)}} t \right]$$

$$R_{\text{(2.4 KC Inverter Pack.)}} = \left[R_{\text{(2.4 KC Inverter)}} \right] + \left[R_{\text{(fault sensor)}} \right] \left[R_{\text{(Inverter)}} \right] \left[\lambda_{\text{(Inverter)}} t \right]$$

$$R_{\substack{(400 \text{ cps Inverter} \\ \text{Pack.})}} = \left[R_{(400 \text{ cps Inv.})} \right] + \left[R_{(\text{fault sens.})} \right] \left[R_{(\text{Inv.})} \right] \left[\lambda (\text{Inverter})^t \right]$$

Entering the component reliability values tabulated in Table III-1 into the mathematical model gives the estimated reliability of the Power subsystem as follows:

$$R_{(\text{Phase 1})} = (1) (1) (.99999) (.99999) (.99999) (.99997) = .99993$$

$$R_{(\text{Phase 2})} = (1) (.99963) (.99988) (.99997) (.99999) (.99272) = .99219$$

$$R_{(\text{Phase 3})} = (1) (.99999) (.99999) (.99999) (.99999) (.99991) = .99987$$

$$R_{(\text{Phase 4})} = (1) (.99999) (.99999) (.99999) (.99999) (.99877) = .99873$$

For complete mission,

$$R_{(\text{Power S/S})} = R_{(\text{Phase 1})} \cdot R_{(\text{Phase 2})} \cdot R_{(\text{Phase 3})} \cdot R_{(\text{Phase 4})}$$

$$= (.99993) (.99219) (.99987) (.99873)$$

$$= .991$$

TABLE III-1 POWER SUBSYSTEM RELIABILITY DATA

COMP. NO.	COMPONENTS	RELIABILITY BY MISSION PHASE			
		Phase 1	Phase 2	Phase 3	Phase 4
1	Solar Array	1.0	1.0	1.0	1.0
2	Charge Regulator	.99999	.99805	.99998	.99967
3	Charge Reg. Controls	.99998	.99234	.99991	.99871
4	Battery	.99974	.99848	.99987	.99976
5	Main Regulator	.99997	.99102	.99990	.99849
6	Main Reg. Controls	.99999	.99846	.99998	.99974
7	Reg. Fault Sensor	.99999	.99820	.99998	.99970
8	2.4 KC Inverter	.99999	.99498	.99998	.99915
9	Inverter Fault Sensor	.99999	.99823	.99998	.99970
10	400 CPS Inverter	.99996	.98660	.99985	.99773
11	Synchronizer	.99997	.99272	.99991	.99877

Note -- Due to the short time periods involved in mission phases 1, 3 and 4, the reliability estimates are taken to five decimal places in order to show the differences in the distinct mission phases.

CII-VB238FD101

PROPULSION SUBSYSTEM

Index

- 1 Scope
- 2 Applicable Documentation
- 3 Functional Description
- 4 Interface Definition
- 5 Performance Parameters
- 6 Physical Characteristics and Constraints
- 7 Safety Considerations

1.0 SCOPE

This section describes the preferred Propulsion Subsystem for the Voyager Spacecraft. The subsystem provides for midcourse velocity increments of 75 meters/second and an orbit insertion maneuver of 1360 meters/second. Fuel not used for midcourse corrections may be utilized for orbit adjust maneuvers.

2.0 APPLICABLE DOCUMENTATION

VR211SR101 Mission Objectives and Design Criteria
VB220SR101 Design Characteristics
VB220SR102 Design Restraints
VB220FD111 Maneuver Execution Accuracy
VB234FD105 Autopilot Subsystem
VB235FD103 Structural Design Criteria

3.0 FUNCTIONAL DESCRIPTION

The preferred propulsion system for the Voyager spacecraft consists of a monopropellant hydrazine system for midcourse maneuvers and a liquid bipropellant system for the orbit insertion maneuver. The monopropellant system has four thrust chambers which are throttled for thrust vector control in the pitch and yaw planes during all maneuvers including orbit insertion. Roll control is achieved through the use of a single jet vane in each monopropellant thrust chamber. No additional thrust vectoring capability is incorporated in the bipropellant orbit insertion system. Total impulse capability of the system is approximately 789,000 lb -secs.

3.1 MONOPROPELLANT PROPULSION SUBSYSTEM

3.1.1 SUBSYSTEM DESCRIPTION

A schematic of the Voyager Monopropellant Propulsion Subsystem is presented in Figure 3-1. It is a regulated-gas-pressure-fed system utilizing anhydrous hydrazine (N_2H_4) as the monopropellant. Helium gas, stored at 3500 psia, is used as the pressurant. The four thrust chamber assemblies are designed to operate over a thrust range of 25 to 55 pounds to meet all thrust vectoring requirements.

Insofar as possible, components are grouped together and connections are welded to eliminate external leakage. Different functional groups are joined by field brazed joints where welding is not practical. Squib valves are used, where feasible, to eliminate solenoid-operated valves and thus assure higher system reliability. Each of the major functional groups (pressurization, propellant feed and thrust chambers) is described in the following paragraphs.

VB238FD101

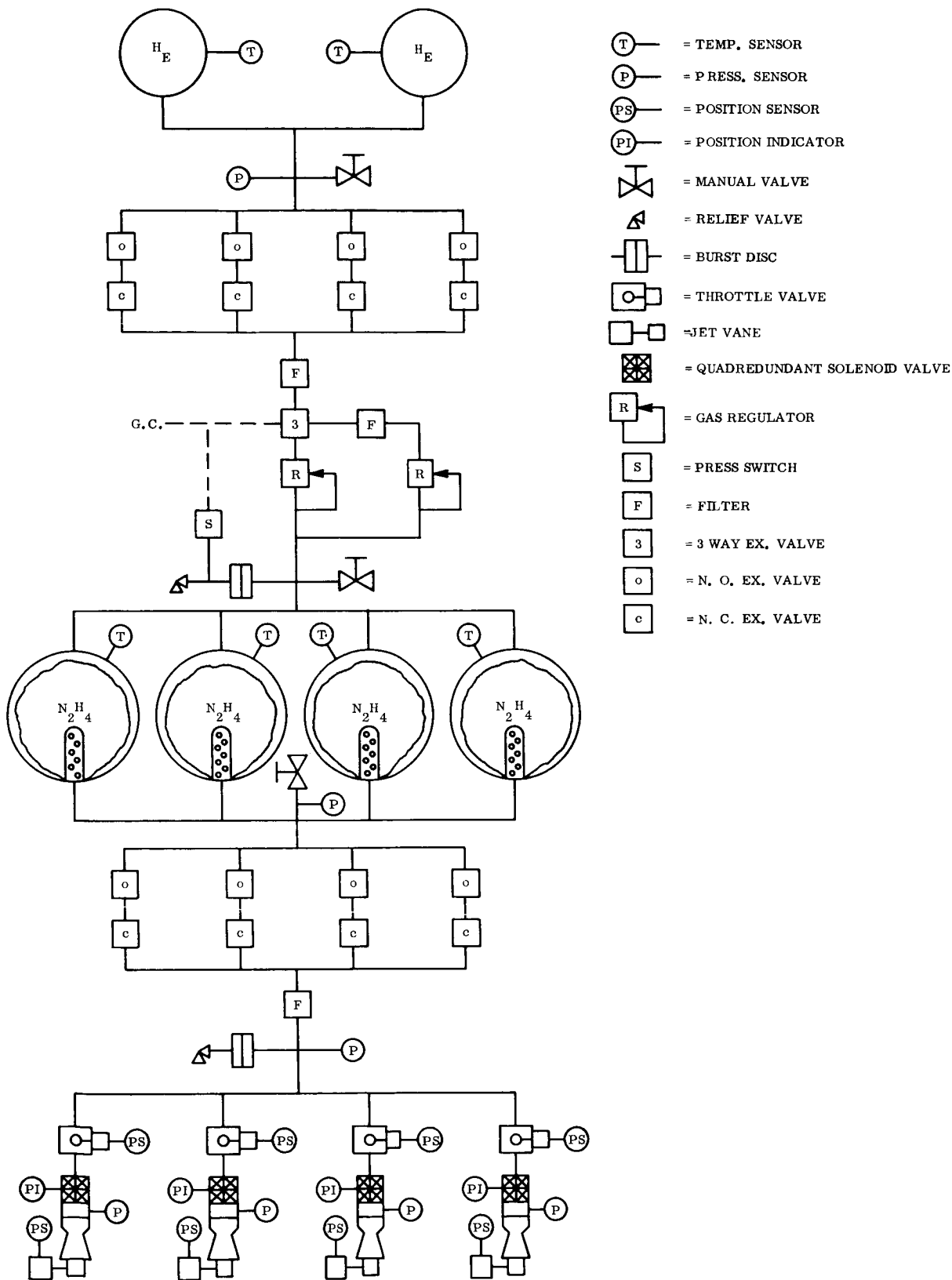


Figure 3-1. Monopropellant Propulsion Subsystem

3.1.2 PRESSURIZATION SYSTEM

The helium gas is stored in two 17-inch diameter titanium tanks which are joined to a bank of squib operated gas pressurization and shut-off valves. This bank of valves has four parallel legs with a normally open and a normally closed valve in series in each leg. Between these valves and the tanks is a manually operated fill valve.

Immediately downstream of the squib valves is a filter to remove any particles which might be generated by the squib valve actuation. A three-way squib-operated valve below the filter feeds high pressure gas through a normally open port to the primary regulator. This regulator provides regulated gas at a pressure of 285 psia directly to the four propellant storage tanks. To protect the propellant tanks from overpressurization, a burst disc-relief valve unit is installed downstream of the regulator. Because of the long-life operational requirements, a redundant filter and regulator leg is provided in the event of failure of the primary regulator. A malfunction signal to the three-way squib valve causes a switchover to the second regulator. For filling and venting of the tanks a manual fill valve is provided in the propellant tank pressurization line. The final component is a pressure switch downstream of the burst disc to sense primary regulator failure in a high pressure mode and to actuate the three-way squib valve. All of the pressurization components, except the tanks, are tray mounted as a single all-welded unit.

3.1.3 PROPELLANT FEED SYSTEM

All four propellant tanks are identical. They are fabricated from titanium alloy and contain butyl rubber bladders which collapse, when pressurized, around a standpipe to assure positive expulsion. All tank discharge lines feed to a common squib valve manifold. A manually operated fill and drain valve is located in the common line. The bank of squib valves is similar to the pressurization system in that there are four parallel legs with a normally open and a normally closed squib valve in series in each leg. Downstream of the squib valves is a filter to trap particles generated by squib valve action. A burst disc and relief valve assembly is provided between the squib valves and thrust chamber assemblies since liquid will be trapped in the lines subsequent to the first midcourse correction. All of these valves and the filter are again tray mounted and welded together to minimize leakage.

3.1.4 THRUST CHAMBER ASSEMBLIES

The four thrust chambers are identical units. Each chamber operates over a chamber pressure range of 75-165 psia and a thrust range of 25-55 pounds. Decomposition of the hydrazine is accomplished in a catalyst bed made from Shell 405 catalyst. Decomposed hydrazine at a temperature of approximately 1800° F discharges through the 50 to 1 expansion ratio nozzle to provide the desired thrust. A single torque-motor-operated jet vane in each exhaust jet provides roll control. Although roll requirements do not require more than one jet vane, the additional vanes permit a single basic thrust chamber configuration and higher reliability through redundant components.

Thrust chamber operation is initiated and terminated by quad-redundant solenoid valves mounted directly on each chamber. Immediately upstream of each quad-redundant valve is a throttling valve capable of modulating the output of each chamber from 25 to 55 pounds.

3.1.5 COMPONENT DESCRIPTION

The Voyager propulsion system utilizes, where possible, materials and manufacturing methods that have demonstrated successful performance on other space programs with mission and duty cycles comparable to that assigned to Voyager. Components with previously acquired qualification records were selected to assure adequacy and maximum confidence to meet mission functional and schedule requirements.

3.1.5.1 PRESSURANT TANK

The use of a pressure regulated propellant feed system requires a high pressure gas source. The midcourse propulsion system is pressure fed from two 3500 psi pressure spheres. Each tank is 17-inches in diameter and is designed to hold 6 pounds of helium at 3500 psi and 40°F. Proof and burst pressures are 6750 and 9000 psig respectively. The demonstrated leakage rate will be less than 10^{-8} scc/sec of helium at the operating pressure. The tanks are fabricated from fully annealed 6Al 4V titanium alloy. Each tank is made of two die-formed hemispheres. Each unit is machined to the required thickness $\pm .002$ inch maximum tolerance and the hemispheres joined by fusion welding. Final heat treatment and finish machining are performed to bring the tank to desired dimensional limits and to a fully annealed condition. Filling and discharge requirements of the tank are facilitated by a tube extension welded to the tank shell. Experience in fabrication of tanks of this configuration is currently "state-of-the-art" and has been proven in many space applications. Airite Corporation is currently active in fabrication of tanks that would satisfy Voyager needs.

3.1.5.2 PROPELLANT TANKS

Because of the requirement of the propulsion system to function in a zero gravity state, positive expulsion propellant tanks are required. The tanks and the expulsion system must provide storage of anhydrous hydrazine for a minimum 300-day period, and provide gas-free propellant to the engines during midcourse maneuver functions.

The selected propellant tank assembly consists of four tanks of 18.38-inch diameter, containing a total of 444 pounds of anhydrous hydrazine. Each tank consists of, the tank shell, inlet and outlet ports, Butyl expulsion bladder, standpipe (to prevent entrapment of fluid during bladder collapse) and mounts. The tanks are fabricated from 6Al 4V titanium in hemispherical sections of 0.035 wall thickness. The hemispheres are joined by welding and finish machined to requirements. Nominal tank working pressure is 285 psi. The design safety factor exceeds 1.50 and 2.2 times working pressure for proof and burst since a minimum gage of .035 inch is used.

The expulsion bladders are made from butyl rubber with a wall thickness of 0.040 inch. Bladder outlet wall thickness is increased to 0.1 inch and formed to provide bladder retention and a seal integral with the propellant tank. The standpipe (perforated tube) is integral with

the discharge port assembly and is bolted to the tank assembly. The tank assembly is proof and leak tested as an integral unit. Leakage shall be less than 10^{-8} scc/sec of helium at operating pressure. Airite Corporation has manufactured tanks of this configuration for other space programs.

3.1.5.3 FILL AND VENT VALVES

The fill and vent valves are required to service the propellant and pressurization system. These valves are designed to provide a safe, leak-tight means of filling, venting, purging and unloading the pressurization and propellant system.

The selected unit is a manually operated poppet valve which provides redundant seals in the poppet stem and inlet assemblies for positive sealing against propellant or gas leakage. The valve inlet will contain a built-in 10 micron wire cloth filter element to provide final filtering between spacecraft and OSE equipment. The proposed fill and drain valves have been successfully used on Rocketdyne propulsion systems on various space applications, the latest being the SE5 program. Valve operating characteristics are:

Operating Pressure	4500 psi
Leakage	10^{-5} scc/sec
Inlet and Outlet Size	1/4" gas, 1/2 " liquid
Life	1000 repeated open and close cycles
Seals	Teflon

3.1.5.4 SQUIB ACTUATED ISOLATION VALVES

Isolation valves are used in the pressurization and propellant control modules for system lockup during various propulsion system coast periods. Each module contains four normally closed and four normally open valves manifolded together in a welded unit. The control modules provide four parallel flow paths each containing a normally open and closed valve in series. The individual normally open and closed valves are explosively actuated shear seal design valves to provide positive sealing of the propellant and pressurization feed systems. A single squib cartridge with dual bridgewires is provided for each valve. The squib provides the force to drive a plunger to shear the end caps and allow for a normally closed valve. Normally open valves are closed by a plunger that shears the flow tube and blocks the flow path. Captive cavities are provided within the body of the valves to contain the sheared fragments. Both Pyronetics and Conax corporations are currently producing these valves.

3.1.5.5 RELIEF VALVES

To protect the propellant tanks from possible overpressurization, a relief valve is used in the regulated pressure line of the propellant pressurization system. Since this valve is not normally required to operate, the prime design consideration is long term storage.

The selected valve incorporates an inverted seal design to maintain narrow limits between cracking, reset and full flow pressure. The inverted valves also provide superior sealing capabilities and valve seal life. For minimum leak considerations during long storage periods a burst disc and filter screen are provided between the valve and the gas pressure. Valves of this configuration are available from Marotta Valve Corporation. This valve is similar to relief valves qualified for use in the Gemini, Transtage and Saturn space programs.

The inverted valve design allows the seat and poppet assembly to move against the spring force until the desired relief pressure is attained. At this preset position, the poppet is stopped by a retainer. Additional pressure separates the seat from the poppet allowing relief of the system.

3.1.5.6 REGULATOR

Pressure regulation of the propellant tanks is accomplished through redundant regulators. The pressure regulators are mounted in parallel with the primary regulator open to the pressure loop. Activation of the secondary regulator is accomplished automatically by a pressure switch which fires a three-way explosive valve to seal off the primary regulator and supply pressure to the secondary unit. The pressure switch will activate the secondary regulator when the regulated pressure exceeds 335 psi and breaks the burst diaphragm. Since leakage and failure in the open position are the primary failure modes for the regulators, (which cause overpressure) underpressure will not be sensed.

The selected regulator is constructed of annealed stainless steel and is satisfactory for 4500 psi operation. A single stage, dome-loaded, spring-referenced, pilot-operated regulating principle was selected to provide simple, reliable operation. The regulator functions from a discharge pressure sensor which positions a diaphragm-actuated, flow-balanced throttle valve. The position of the throttle valve regulates the pressure drop across the valve to maintain the desired propellant system working pressure as the supply pressure decays. A filter is provided upstream of the valve to minimize failure due to contamination. Hardware design will feature metallic hard seats, metallic bellows sensing element, low stress reference spring, bellows contained reference spring assembly, and welded inlet and outlet stems.

Regulator operating parameters are as shown below.

Inlet Pressure	4500 psi max.
Regulated Pressure	250 psi \pm 5 psi
Internal Leakage	100 scc/hr. max.
Proof Pressure	
Inlet	6750 psig
Outlet	660
External Leakage	10^{-8} cc/hr.
Temperature Range	120°F to -200°F
Flow Rate	40 SCFM Nominal
Min. differential Pressure	200 psi

A regulator for Voyager requirements will require minimum development since the basic design concepts have extensive background and significant reliability data has been accumulated. The National Water Lift Co. has qualified similar regulators on the Rocketdyne SE5 program.

3.1.5.7 THREE-WAY SQUIB VALVE

A three-way two-position squib actuated valve is located upstream of the redundant pressure regulators to switch flow from the primary to secondary regulator. The valve is connected electrically to a pressure switch. In the normal position, the open flow path is to the primary regulator. Should a regulator failure occur, the pressure switch will provide the electrical signal to ignite the squib of the three-way valve to position the flow path to the secondary regulator.

The three-way valve selected is a patented design by SieBelAir Inc. The valve selects the flow path by positioning a spool that isolates the primary flow path while uncovering the secondary flow path in a single motion. Tight seals are provided by using a spool with an interference fit to the valve body (ballizing principal). This design appears suitable for Voyager application. Since these valves have not been qualified on previous space programs, a thorough development program will be required.

3.1.5.8 FILTERS

Filters are utilized throughout the pressurization and propellant feed systems. They are located at strategic points to minimize contamination caused by actuation of squib valves and contamination occurring in filling and draining of the propellant and pressurization system.

The selected filters will be of the inline type with a woven metal screen of a nominal 10 micron filtration rating. The filters will fall into two categories,

1. High Pressure Gas
2. Low Pressure Gas, and Liquid

The high pressure gas filters will be designed to function at 4500 psi. The internal screen assembly will be structurally supported to prevent collapse upon sudden pressure surges. The filter body will be constructed from annealed stainless steel with monel wire cloth screens. Total ΔP at operating flow rates will not exceed 10 psi. Filters of this type are available from Wintec Corporation.

Low pressure gas and liquid filters are designed for operation to 500 psi. The design is similar to the high pressure filters. The material used is compatible with both helium and anhydrous hydrazine. Sizes are selected to provide less than 10 psi ΔP during full flow conditions.

3.1.5.9 QUAD-REDUNDANT SOLENOID VALVES

A quad-redundant solenoid actuated propellant valve is used to control the initiation and termination of propellant flow to each engine in the monopropellant system. The valve package is bolted directly to each of the thrust chamber injector assemblies. The quad-redundant solenoid valves are arranged to provide a series-parallel flow path to the engine. The parallel valve arrangement provides redundancy in the engine startup mode, while the series arrangement provides redundancy in the engine shutdown mode. The quad-redundant valve assembly is a completely welded unit consisting of four solenoid valves internally manifolded to provide the series-parallel flow path. Each valve consists of a normally closed single coil solenoid valve utilizing a direct acting poppet. A Teflon insert contained in the end of the poppet is semi-edged loaded by a metal seat on the valve body to provide a seal-on closure. The valve incorporates a fail-safe design (fail in the closed position) by providing a compression spring acting on the back of the plunger (poppet) to close the valve on power failure. The valve is fabricated from 304 stainless steel with exception of the solenoid and poppet assembly. The solenoids are designed to have low current drain and to maintain the lines of magnetic flux within the solenoid for magnetic cleanliness. Additional shielding can be added if necessary to meet mission magnetic goals.

Valves of this configuration are currently being manufactured by the Valcor Corp. for use in the SIVB attitude control system. Minor changes would be required to the Valcor valve to handle Voyager flow requirements and mounting configuration. Valve operating characteristics are as follows.

Operating Voltage	30 to 44
Current at 26 VDC	1.3 amps initial, 0.13 holding
Response Time	
Close to Open	.022
Open to Close	.011
Internal Leakage	.01 ₇ cc/hr. at 300 psi
External Leakage	10 ⁻⁷ SCC/sec helium at 300 psi
Pressure drop	7 ± 1 psi at rated flow
Weight	5 lb

3.1.5.10 THRUST CHAMBERS

The thrust chambers for the Voyager Monopropellant Propulsion Subsystem are based upon the proven Ranger 50 pound thrust hydrazine units. Modifications will include the elimination of the Ranger N₂O₄ injection port and the change of the catalyst bed to use Shell 405 spontaneous catalyst. The optimum bed configuration must be determined experimentally. Operational margins of the chamber, quad-redundant solenoid valves and the throttle valve combination will be ascertained to assure that subsystem requirements can be met. The throttling of hydrazine decomposers is an established technique although no known flight data exists for this type of system. Recent static tests by TRW Inc., Redondo Beach, Calif. have demonstrated the operation and throtteability of a basic 50-pound thrust chamber over a chamber pressure range of 82 to 247 psia.

Verification of the Shell 405 catalyst operation under space vacuum conditions will be required before it can be flown on the Voyager spacecraft. It is anticipated that programs already underway at Rocket Research will provide this information in ample time.

3.1.5.11 TUBING AND FITTINGS

The Monopropellant Propulsion Subsystems will utilize packaging of hardware groups into functional modules. The functional modules are:

1. Pressurant tank module
2. Pressure control module
3. Propellant tank modules
4. Propellant control modules
5. Engine (thrust chamber) modules.

The pressurization and propellant feed and manifolding lines of the individual hardware components of each functional group are welded together to form a module. This modular concept facilitates assembly, disassembly, and testing of the propulsion systems. Each module is connected to its appropriate functional module within the spacecraft by brazed joints to form the entire propulsion subsystem.

Welded and brazed joints were selected due to their demonstrated capability to maintain a leak-tight system on the Mariner program.

The braze fittings selected are of sleeve design manufactured by Aeroquip Corp. (Aeroquip Spacecraft Fittings). Each sleeve fitting contains the brazing material within the sleeve. Joints are made by inserting the tube into the fitting and heating the fitting with an induction heater tool until bonding is complete.

This type of joint has the advantage of ease of installation, less magnetic prone parts, low temperature fusion and ease of maintenance, over the mechanical or welded joints.

The brazing material will be a nickel gold alloy. Tubing selected to interconnect and manifold the hardware elements will be fabricated from 321 Stainless Steel. Quarter-inch tubing will be used in the gas system and 3/8" for the liquid systems.

3.1.5.12 PRESSURE SWITCH

A pressure switch is located in the propellant tank pressurization circuit to detect out-of-tolerance propellant tank pressurization. The selected switch is a hermetically sealed, snap-action unit employing redundant switching elements. Linear motion is transmitted by a piston into a snap-action Belville spring. The piston snaps through when the preset load on the Belville spring is reached. The snap-through allows the piston to activate the electrical contacts which provides the power to the three-way valve.

The switch will be set to actuate at 100 psia \pm 2 percent. The switch will be constructed of 316

stainless steel and welded into the regulated pressure module.

3.1.5.13 JET VANES

The jet vanes are identical to existing Ranger jet vanes except that only one is used with each thrust chamber. Jet Vane actuators are discussed under Autopilot Section VB234FD105.

3.1.5.14 THROTTLE VALVES

Final selection of a throttle valve has not been made. A first analysis of the requirements indicates that a variable area cavitating venturi type of valve will be employed. This type permits a bellows seal and thus eliminates the many seal problems associated with rotating shafts of butterfly or ball type valves. Valve actuator requirements are discussed in Autopilot Section BV234FD105.

3.1.6 SUBSYSTEM OPERATION (FLIGHT)

Following launch and prior to the first operational cycle, the thrust chamber quad-redundant valves will be opened and closed to permit air trapped in the propellant lines to be vented. Timing for this operation is not critical. It may be accomplished hours or days before the first maneuvering operation. The Monopropellant Propulsion Subsystem is prepared for the first midcourse maneuvering operation by simultaneously supplying power to one of the normally closed valves in both the pressurization system and the propellant feed system (See Figure 3-1). This will allow high pressure gas to flow through the filter, the three way squib valve and the primary regulator up to each of the main propellant tanks. Fluid pressure will force propellant through the propellant line filter up to each of the quad-redundant main propellant valves.

Again, the timing for this operation is not critical. It may be made several hours or several days prior to execution of the anticipated maneuver. One advantage of preparing the system well in advance of the actual maneuvering time is to permit verification of system readiness through telemetry indications.

All tank temperatures (two pressurant and four propellant), pressurant tank pressure, propellant tank outlet pressure, and thrust chamber feed line pressure will be monitored on a periodic basis. All squib valves will have an event indication circuit which will verify firing of the squib. With this information, readiness of the system for making a maneuver may be verified prior to the command for execution.

Upon the maneuver command (with the spacecraft properly oriented), the four quad-redundant valves open with the four throttling valves in minimum thrust position permitting propellant flow to the thrust chambers. Thrust vectoring is accomplished by modulation of these four throttling valves as signalled by the guidance and control subsystem.

Upon signal to terminate thrust, the four quad-redundant valves will close, shutting off propellant flow to the chambers. The system may now be maintained in the ready condition for

an indefinite period. If another maneuver is anticipated within a few days or even a few weeks, the system will be ready at all times for the maneuver command. If no further maneuvers are anticipated until the Mars encounter phase (six months later), the system will be sealed off by firing the normally open squib valves in the active legs of the pressurant and propellant supply lines. While this does not necessarily relieve pressures throughout the system, it will prevent catastrophic losses due to small leaks in tank pressurizing line joints or through the main quad-redundant propellant valves.

Position indicators (open and closed) will be incorporated in each valve. These will serve for diagnostic purposes only and will not be used for failure sensing. Failure of the monopropellant system would be sensed by the guidance and control system and shutdown of the system initiated only when thrust vector control of the spacecraft cannot be maintained.

With four engines firing during all maneuvers, roll moments may be introduced due to variations in thrust vector alignment. The jet vanes in each chamber (operating in parallel) will correct for any roll moments so induced. Position sensors on each jet vane actuator will permit the telemetry data of vane position to be examined for indications of system readiness or for post maneuver diagnosis as required. Position sensors on the throttling valves will serve in the same fashion.

Because of the extended period over which the monopropellant system must operate, a second gas regulator is provided. The failure mode of the primary regulator is assumed to be leakage through the regulator seat to give excess propellant tank pressure. If this occurs the burst disc will fail at 335 psi. A pressure switch, which may be set at a relatively low pressure (100 psi) will be actuated and will fire the three-way solenoid to divert high pressure gas to the secondary pressure regulator. Failure of the primary regulator to open will be sensed by ground diagnosis and a ground command will be required to actuate the three-way solenoid. Difficulties in detecting and evaluating low pressure indications and the lesser likelihood of this failure mode favor ground diagnosis over on-board diagnosis.

Subsequent maneuvers will follow the same operating sequence required for the first mid-course maneuvers. The system is placed in readiness, checked and operated. In the Mars encounter phase there may be one or two course corrections, a firing for propellant acquisition and thrust vector control during retropropulsion, and a possible orbit adjust maneuver all within a few weeks period. Provision has been made to reseal the system by squib valve actuation at this point. Additional legs in the squib valve banks are provided for redundancy in the event of failure of one of the required legs to open when commanded.

Since all pressurant and propellant tanks of the monopropellant system are mounted symmetrically about the roll axis, lateral center of gravity shift should, in theory, be zero during maneuvers. The only shift would be along the roll or thrust axis. Minor differences in fabrication, line pressure drops or characteristics of the individual bladders could affect discharge from the individual tanks to give small lateral cg variations. However, the use of throttling for TVC makes such small variations insignificant in comparison with the available correcting forces from the four thrust chambers. Sloshing of fuel in the hydrazine tanks will be minimized by using a standpipe (inside its bladder) anchored to both ends of

the tank. This will restrain motion of the bladder and tend to damp out any oscillatory motions.

3.2 RETROPROPULSION SUBSYSTEM

3.2.1 SUBSYSTEM DESCRIPTION

A schematic of the Voyager Retropropulsion Subsystem is shown in Figure 3-2. As with the monopropellant system previously discussed it is a regulated-gas-pressure-fed system utilizing helium gas, stored at 3500 psia, as the pressurant. Propellants are nitrogen tetroxide (N_2O_4) as the oxidizer and a blend of 50% hydrazine (N_2H_4) and 50% unsymmetrical dimethyl hydrazine ($(CH_3)_2N_2H_2$) as the fuel. The thrust chamber is a fixed (no TVC) installation using an all ablative construction. Thrust is 2200 pounds at a chamber pressure of 100 psia.

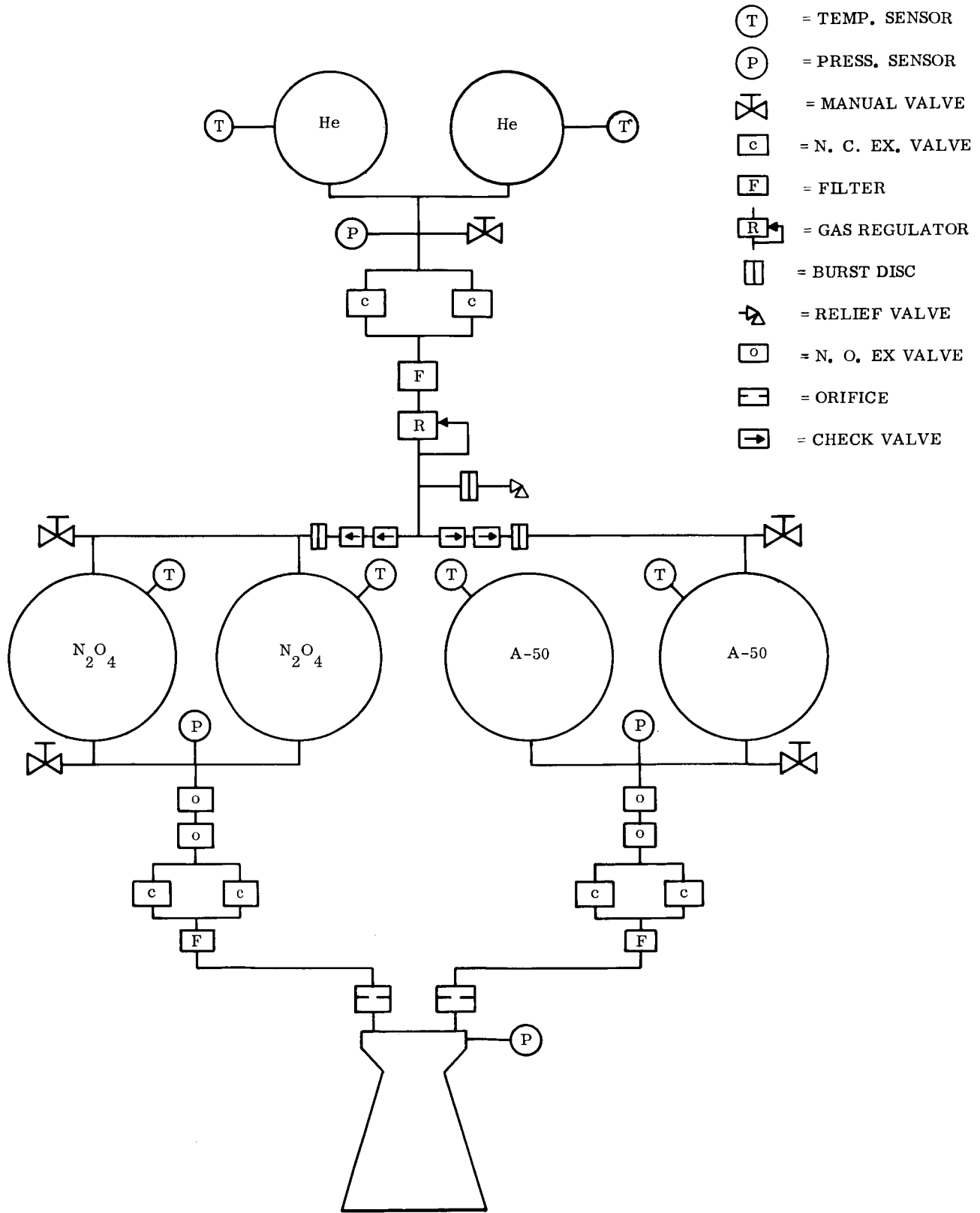
The relative simplicity of the design permits the mounting of components into welded functional groups to eliminate external leakage. Functional groups are joined by field brazed joints. Squib valves are used throughout to assure the highest reliability. Following is a description of the major functional groups.

3.2.2 PRESSURIZATION SYSTEM

Helium gas is stored in two 18.7-inch diameter titanium tanks joined by a common manifold to two normally closed squib valves in parallel. Between the tanks and the squib valves is a manually operated fill valve. Downstream of the squib valves is a filter to remove all particles which may be generated by squib actuation. Below the filter a single stage regulator supplies helium gas at 220 psia to each of the main propellant tanks. A burst disc and relief valve in series are installed downstream of the regulator to protect the system from leakage through the regulator which would over-pressurize the propellant tanks. Burst discs are also provided in both the oxidizer and fuel legs of the pressurization system to keep the propellant vapors from mixing or contaminating the regulator, during the 9 months storage period. These burst discs will have a 110 psi breaking pressure. As further protection during and subsequent to the operational period, two check valves in series are installed in each pressurization leg. All of the foregoing valves, filter, regulator and burst discs are tray mounted and welded together to eliminate leakage. A manually operated vent valve is provided in each pressurization leg to aid in filling and emptying of the tanks as required during ground checkout cycles.

3.2.3 PROPELLANT FEED SYSTEM

Identical spherical tanks fabricated from titanium alloy are used for the oxidizer and the fuel. Since propellant settling and acquisition are achieved by firing the Monopropellant Propulsion Subsystem, no positive expulsion devices are required for these tanks. Each pair of tanks (oxidizer and fuel) are joined by a common discharge manifold. A manually operated fill or drain valve connects to each manifold. Both manifolds connect in turn to a redundant squib network for starting and shutting down of the retropropulsion thrust chamber. Two normally open squib valves in series are followed by two normally closed valves in parallel in each propellant leg. A filter downstream of each squib valve leg protects the injector from all



- (T) = TEMP. SENSOR
- (P) = PRESS. SENSOR
- ⊗ = MANUAL VALVE
- c = N. C. EX. VALVE
- F = FILTER
- R = GAS REGULATOR
- || = BURST DISC
- ↗ = RELIEF VALVE
- o = N. O. EX VALVE
- = ORIFICE
- = CHECK VALVE

Figure 3-2. Retropropulsion Subsystem

upstream contamination sources. Orifices in each side of the injector are used to calibrate all thrust chamber assemblies to identical pressure drops to assure interchangeability. All of these valves, filters and orifices are mounted directly on the thrust chamber and welded together to eliminate leakage problems.

3.2.4 THRUST CHAMBER ASSEMBLY

The selected thrust chamber is an all ablative chamber with an expansion ratio of 60:1. The injector is fabricated from aluminum and uses a conventional doublet impinging injection pattern. Since the required burn time is less than 400 seconds, the design is well within the present state-of-the-art and thus provides a high reliability potential. Lack of TVC requirements with no need for gimbals, actuators and flexible lines, further enhances the reliability of the unit.

3.2.5 COMPONENT DESCRIPTION

Components used in the Retropropulsion Subsystem will, in most cases, be similar to those described for the Monopropellant Subsystem except for size. Those components used only in the Retropropulsion Subsystem are described in the following paragraphs.

3.2.5.1 BURST DIAPHRAGM ASSEMBLY

Two burst diaphragm assemblies are used on the propellant pressurizing lines to isolate the fuel pressurization from the oxidizer pressurization during the cruise phase. The burst discs are ruptured when the pressurization system is activated. The burst disc is designed to rupture at approximately 30 percent of the operating pressure. The burst disc assembly will also contain a downstream filter element for containing the particles generated during diaphragm rupture. Burst diaphragms of this configuration manufactured by Del Mfg Co have been qualified and flight proven for GE Spacecraft Dept.

3.2.5.2 ABLATIVE THRUST CHAMBER ASSEMBLIES

The 2200-pound thrust all-ablative chamber selected for the preferred Propulsion Subsystem is derived directly from thrust chambers developed on the Saint and Apollo Sub-Scale programs. No particular Propulsion Supplier is favored at this time for this component. Those working on the above programs have all demonstrated adequate performance and long life with their respective designs. It must be remembered, however, that any ablative thrust chamber design is of necessity a blend of injector characteristics, ablative material properties and ablative material fabrication techniques. That is, an injector which works successfully with one suppliers chamber, might destroy another suppliers proven chamber in a very short period. Thus the injector-chamber combinations are in general inseparable and must be procured as a unit. The major change for the Voyager program is an all ablative expansion section rather than a radiatively cooled skirt. This adds to the weight of the thrust chamber but minimizes the need for shielding and insulation in the engine compartment. To keep this weight at a minimum, and yet realize high performance, an 80 percent bell contour is specified.

3.2.5.3 PROPELLANT TANKS

The propellant tanks for the Retropropulsion Subsystem are similar to the monopropellant tanks except that no positive expulsion devices are needed. These tanks will be fabricated with 0.035 inch thick walls as previously described. Tank diameter will be 30.25 inches and working pressure 220 psia.

One area which is not felt to be a problem but which cannot be properly evaluated analytically is the discharge characteristics of parallel propellant tanks. To maintain C.G. location within specified limits, the discharge from the two tanks must be relatively equal at all times. Therefore some experimental work must be carried out early in the program to determine how much variation can exist between tanks as the propellant is discharged. If excessive variations are noted some form of flow equalization device may be required to minimize cg uncertainties.

3.2.6 SUBSYSTEM OPERATION (FLIGHT)

The Retropropulsion Subsystem may be prepared for operation at any time prior to firing command. Preferably this should be several hours prior to the anticipated command to permit verification of total propulsion subsystem readiness for the maneuver. To prepare the Retropropulsion Subsystem, the command will fire both normally closed squib valves in the pressurization system line. This will permit high pressure helium gas to flow to the gas regulator. Regulated gas will then flow down each pressurization leg, break the two burst discs and apply full tank pressure to each of the four propellant tanks.

Verification of the ready condition may now be made through telemetry monitoring of all tank temperatures, helium tank pressure and the two propellant line pressures. Event indicators in the squib valves will also permit verification of squib actuation.

Five seconds prior to the firing command for the Retropropulsion Subsystem, the Monopropellant Propulsion System will begin firing to settle the propellants in the bipropellant system tanks and thus assure propellant acquisition.

Upon firing command to the Retropropulsion Subsystem the four normally closed squib valves in the propellant feed lines (two in each leg) are fired. This permits flow of propellants to the thrust chamber for the planned duration of the maneuver. The monopropellant engine will fire continuously during the maneuver to provide thrust vector control.

Shutdown of the Retropropulsion Subsystem is accomplished by firing the upstream normally open squib valve in each propellant feed line. The second set of normally open squib valves may be fired anytime after three seconds to secure the system.

Shutdown of the monopropellant system will follow that of the Retropropulsion Subsystem by five seconds to eliminate potential transient side forces induced in high expansion ratio nozzles during thrust termination (even under vacuum conditions).

The only failure mode provided for in the system (other than by redundancy of components) is overpressurization of the propellant tanks by leakage through the regulator. This will cause rupture of the burst disc and bleeding of excess pressure through the relief valve. Because of the short operational cycle a redundant regulator does not contribute significantly to overall system reliability.

4 INTERFACE DEFINITION

Following are the interfaces between the Propulsion Subsystem and the indicated subsystems.

4.1 SPACECRAFT BUS SUBSYSTEM

4.1.1 MECHANICAL INTERFACE

Attachment points between Propulsion Subsystem structure and bus structure.

4.1.2 MECHANICAL INTERFACE

Electrical harness connectors to bus connectors

4.2 TEMPERATURE CONTROL SUBSYSTEM

4.2.1 MECHANICAL INTERFACE

Monopropellant tank heaters and thermostatic controls

4.2.2 MECHANICAL INTERFACE

Insulation and radiation shielding for maintaining the temperature of the Propulsion Subsystem between +40° and +80° F

4.3 PYRO SUBSYSTEM

4.3.1 ELECTRICAL INTERFACE

Commands to squib valve

4.3.1.1 MONOPROPELLANT SYSTEM

Prepare system - 2 squib valves
Secure system - 2 squib valves
Repeat above 3 more times
Switch to back up regulator - 1 squib valve

4.3.1.2 RETROPROPULSION SYSTEM

Prepare system - 2 squib valves
Start maneuver - 4 squib valves
Stop maneuver - 2 squib valves
Secure system - 2 squib valves

4.4 CONTROLLER AND SEQUENCER SUBSYSTEM

4.4.1 ELECTRICAL INTERFACE COMMANDS TO SOLENOID VALVES (MONOPROPELLANT SUBSYSTEM)

4.4.1.1 START MANEUVER-OPEN 4 QUADREDUNDANT VALVES

4.4.1.2 STOP MANEUVER - CLOSE 4 QUADREDUNDANT VALVES

4.4.1.3 REPEAT START AND SHUTDOWN MANEUVERS AS REQUIRED

4.5 AUTOPILOT SUBSYSTEM

4.5.1 ELECTRICAL INTERFACE - COMMANDS FOR THRUST VECTORING

1. Signals to 4 throttle valves

4.5.2 ELECTRICAL INTERFACE-COMMANDS FOR ROLL CONTROL CORRECTION

1. Signals to 4 jet vane actuators

4.6 DATA HANDLING AND STORAGE SUBSYSTEM

4.6.1 ELECTRICAL INTERFACE

Monopropellant Subsystem sends signals from

4.6.1.1 7 PRESSURE TRANSDUCERS

4.6.1.2 6 TEMPERATURE SENSORS

4.6.1.3 17 EVENTS INDICATORS (SQUIB VALVES)

4.6.1.4 16 SOLENOID VALVE OPEN INDICATORS

4.6.1.5 16 SOLENOID VALVE CLOSE INDICATORS

4.6.2.6 4 THROTTLE VALVE POSITION INDICATORS

4.6.3.7 4 JET VANE POSITION INDICATORS

4.6.2 ELECTRICAL INTERFACE

Retropropulsion Subsystem sends signals from

4.6.2.1 4 PRESSURE TRANSDUCERS

4.6.2.2 6 TEMPERATURE SENSORS

4.6.2.3 10 EVENT INDICATORS (SQUIB VALVES)

4.7 OPERATIONAL SERVICE EQUIPMENT

4.7.1 MECHANICAL INTERFACE

Provide hardpoints for support and handling fixtures

4.7.2 MECHANICAL INTERFACE

Provide adjustment for aligning thrust vectors relative to vehicle C.G.

4.7.3 MECHANICAL INTERFACE

Provide fill and drain points as follows

4.7.3.1 MONOPROPELLANT SUBSYSTEM

Helium Tank Fill Valve
Hydrazine Tank Fill Valve
Hydrazine Tank Vent Valve

4.7.3.2 RETROPROPULSION SUBSYSTEM

Helium Tank Fill Valve
Oxidizer Tank Fill Valve
Oxidizer Tank Vent Valve
Fuel Tank Fill Valve
Fuel Tank Vent Valve

4.7.4 ELECTRICAL-MECHANICAL INTERFACE

Harness for connecting subsystem valves and actuators to checkout and monitoring equipment

4.7.5 MECHANICAL INTERFACE

Provide access points to subsystem piping for leak check requirements (to be established

during final design).

5. PERFORMANCE PARAMETERS

The performance parameters for the Propulsion Subsystem are listed in Table 5-1

TABLE 5-1

PROPULSION SUBSYSTEM PERFORMANCE PARAMETERS

Monopropellant Subsystem (4 thrust chambers)

Delivered Specific Impulse, secs.	230
Thrust (minimum per chamber), pounds	25
Thrust (maximum per chamber), pounds	55
Chamber pressure range, psia	75-165
Total Deliverable Impulse, lb-secs.	99,000

Retropropulsion Subsystem

Delivered Specific Impulse, secs.	307
Thrust, pounds	2200
Chamber pressure, psia	100
Total Deliverable Impulse, lb-secs.	690,000
Burn Time, seconds (max.)	316

6. PHYSICAL CHARACTERISTICS AND CONSTRAINTS

Major characteristics of the Propulsion Subsystem are presented in Table 6-1.

Constraints placed upon the propulsion system shall be as follows.

- 6.1 The propulsion subsystem shall be designed to be installed and removed as a unit from the spacecraft.
- 6.2 The propulsion subsystem when loaded with propellant and with the pressurant tanks charged to 3500 psia shall be safe for personnel to work around at temperatures up to 80° F.
- 6.3 The propulsion subsystem shall not require the use of liquid or gas umbilicals.
- 6.4 The effective thrust vectors for all thrust chambers shall be predictable to within ± 0.25 degrees and $\pm .060$ inches measured at the mounting plane for each type of chamber.
- 6.5 Both the retropropulsion and monopropellant thrust chambers shall provide adjustments for aligning the thrust vectors with the spacecraft capable of an angular adjustment of $\pm 2^\circ$ and a position adjustment of ± 0.25 inches from the nominal.

- 6.6 The Monopropellant Propulsion Subsystem (MPS) must be capable of imparting a total impulse of 99,000 lb.-secs. to the spacecraft in a total of 5 operating periods (max.).
- 6.7 The MPS shall be capable of imparting a minimum midcourse correction velocity increment of $0.1 \pm .007$ meters/sec. to a 7800 pound spacecraft.
- 6.8 The Propulsion Subsystem (RPS) shall be capable of imparting a velocity increment of 1860 meters/second to a 5550 pound spacecraft.
- 6.9 The propulsion subsystem must ignite and operate in a vacuum environment.
- 6.10 The MPS must ignite in a zero-g environment.
- 6.11 The propulsion subsystem temperature limits from the time of loading propellants through termination of the flight shall be $+40^{\circ}\text{F}$ to $+80^{\circ}\text{F}$.
- 6.12 The propulsion subsystem must be capable of vacuum environment storage in excess of 290 days without detrimental effects on ignition or performance.
- 6.13 Thrust vector control during both midcourse, retrofire and orbit adjust shall be achieved by utilizing four thrust chambers in the MPS and throttling each engine as required to provide control in the pitch and yaw plane.
- 6.14 The volume within the spacecraft available to the propulsion subsystem shall be a cylinder 80 inches in diameter by 59 inches high.
- 6.15 The loads imposed by the Retropropulsion Subsystem on the spacecraft shall not exceed 4 g's with lower values desirable.

TABLE 6-1

PROPULSION SUBSYSTEM CHARACTERISTICS

Monopropellant Subsystem

<u>General</u>	
Propellant	N_2H_4
Pressurant	Helium
Gross Weight, pounds	677
Burnout Weight, pounds	246
Dry Weight, pounds	227
<u>Thrust Chamber (4)</u>	
Type	Radiatively cooled
Catalyst	Shell 405
Expansion Area Ratio	50
Throat Area, sq. inches	0.19
Throat Diameter, inches	0.491
Exit Diameter, inches	3.480
<u>Propellant System</u>	
Total Loaded Propellant Weight, pounds	444
Usable Propellant Weight, pounds	431
Propellant Tank Pressure, psia	285
<u>Pressurant System</u>	
Pressurant Weight, pounds	6

Initial Storage Pressure, psia	3500
<u>Reliability</u>	
Probability of Mission Success	.966962

Retropropulsion Subsystem

General

Propellants - Oxidizer	N ₂ O ₄
Fuel	N ₂ H ₄ /UDMH (50-50)
Pressurant	Helium
Gross Weight, pounds	2799
Burnout Weight, pounds	531
Dry Weight, pounds	455
<u>Thrust Chamber</u>	
Type	All Ablative
Expansion Area Ratio	60:1
Throat Area, Square inches	12.0
Exit Diameter, inches	30.3
Throat Diameter, inches	3.91
<u>Propellant System</u>	
Total Loaded Propellant Weight, pounds	2328
Usable Propellant Weight, pounds	2260
Propellant Tank Pressure	220
<u>Pressurant System</u>	
Pressurant Weight, pounds	8
Initial Storage Pressure, psia	3500
<u>Reliability</u>	
Probability of Mission Success	.989216

7. SAFETY CONSIDERATIONS

In formulating operational procedures for the propulsion subsystem, the following factors will be considered:

1. Transfer and storage of high pressure gases
2. Toxicity of nitrogen tetroxide and hydrazine compounds
3. Fire hazards of hydrazine compounds and their vapors in air
4. Explosive and fire hazards associated with mixing of oxidizer and fuel vapors
5. Decontamination of propellant spills
6. Unloading procedures and disposal of propellants
7. Conformity of design limits with AFETR requirements.

Safety and operational considerations for squib valves are discussed in VB235FD104 Pyrotechnics Subsystem.

CII-VB238FD101

APPENDIX

PROPULSION SUBSYSTEM DESIGN

Index

- 1 Reliability
- 2 Systems Performance Calculations
- 3 Component Weight and Volume Estimates

1.0 RELIABILITY

The reliability of the propulsion subsystem recommended for Voyager has been estimated in detail. This was accomplished by estimating the probability of success in the various phases of the mission for each engine. These probabilities were combined to arrive at an estimate of the overall propulsion system probability of success.

1.1 MISSION

The primary mission Voyager as defined in the Preliminary Voyager 1971 Mission Specification ends 30 days after injection into Mars orbit. This will occur at a maximum of 210 days after launch. The reliability apportionment has been made on the basis of this maximum 210 day mission. The propulsion system must have a longer functional capability than 210 days since it may provide an additional orbit adjust 270 days after launch. This requires two sets of mission reliability estimates for the propulsion system.

1.1.1 SUBCONTRACTOR ANALYSES

An apparent anomaly with respect to mission definition will become apparent on review of the various subcontractor inputs included with this report. The mission durations used in the estimates are longer than the 270 days. Further, the vendor orbit injections occur 200 to 220 days after launch. This variation in mission definition came about because of the necessity of providing preliminary information to the subcontractors early in the program.

1.1.2 PROPULSION SUBSYSTEM FUNCTION DURING PRIMARY MISSION

During the primary mission, the propulsion subsystem performs up to four trajectory corrections, injection into Mars orbit, and one orbit adjust.

1.1.3 PROPULSION SUBSYSTEM COMPLETE FUNCTION

The propulsion subsystem overall mission consists of the primary mission described in 1.1.2 above followed by an additional coast period and a possible additional orbit adjust at the end of the 60 days.

1.2 RELIABILITY ESTIMATE

1.2.1 PROBABILITY OF SUCCESS

Table 1-1 is a summary of the mission phases, time durations and estimated probabilities of success. The details of the calculations for these phases are contained in Section 6.

1.2.2 FAILURE RATE SOURCE

In making these estimates, most of the generic failure rates for parts were based on information taken from a report entitled "Reliability Physics (The Physics of Failure)" by

TABLE 1-1. PROPULSION SYSTEM MISSION PHASES, TIME DURATIONS AND PROBABILITIES OF SUCCESS

MISSION PHASE	TIME DURATION	PROBABILITY OF SUCCESS***	
		CORRECTION ENGINE	INJECTION ENGINE
1. Launch	.683 hours	.999845	.999888
2. First Cruise Period	47.300 "	.999791	.999888
3. First Trajectory Correction	.067 "	.999190	.999995
4. Second Cruise Period	432.000 "	.998120	.998970
5. Second Trajectory Correction	.014 "	.999830	.999999
6. Third Cruise Period	3790.000 "	.983300	.991020
7. Third Trajectory Correction	.014 "	.999827	.999999
8. Fourth Cruise Period	24.000 "	.999894	.999943
9. Fourth Trajectory Correction*	.014 "	.999831	.999999
10. Fifth Cruise Period	24.000 "	.999894	.999943
11. Orbit Injection			
11.1 Correction Engine Operation	.104 "	.997490**	--
11.2 Injection Engine Operation	.101 "	--	.999672
12. First Orbiting Period	48.000 "	.999788	≈ 1.
13. First Orbit Adjust	.021 "	.999742	≈ 1.
14. Second Orbiting Period	2110.000 "	.990690	≈ 1.
15. Second Orbit Adjust	.021 "	.999730	≈ 1.
Engine Cumulative Probabilities of Mission Success		.966962	.989316
Propulsion System probability of Mission Success		.956278	

* For this analysis it is assumed the four corrections may be required.

** In making this calculation it was assumed injection engine was firing for full .104 hr.

*** Estimates approximated using $P = 1 - \lambda t$. The error using this approximation will not exceed .03% in these estimates and only effect the 4th or 5th significant figures in some of the estimates. These errors have been ignored and all numbers carried so that the critical reliability phases could be easily identified.

D. R. Earles and M. F. Eddins as published in the "Proceedings of the Ninth National Symposium on Reliability and Quality Control". The selection of this source of failure rates was made on the following basis: 1. A broad spectrum of part types are presented including most of those used in propulsion systems. 2. The failure rates were established from a quantity of data per component. This is apparent from the fact that a lower limit, a mean and an upper limit are presented for most components. 3. The source is unbiased with respect to Voyager i.e. in making a selection of the optimum approach to performing the propulsion function the data supplied by proponents of particular techniques may possibly be optimistic in favor of these techniques.

In using this data, the lower limit failure rate value was used in all cases. These are probably applicable to Voyager because of the stringent part program to be followed, including part and vendor selection, part testing, vendor control and complete inspection and quality control.

1.2.3 STATE OF THE ART "K" FACTOR

The failure rates described above were published and updated by D. R. Earles in 1963. To bring these in line with the current state of the art a "K" factor as described on page 2-4 of GE Reliability Manual TRA-873-74 was used.

1.2.4 ENVIRONMENTAL "K" FACTOR

An environmental "K" factor was applied in the analysis. This factor is defined on page 2-5 of the GE Reliability Manual. The environmental factor failure rate modifiers selected for use in the various phases of the propulsion system mission are presented in Table 1-2. These K_e values were selected on the basis of an estimate of the anticipated stress levels during the mission and a comparison with those presented on page 2-5 of the GE Reliability Manual. The basic part reliability numerics used in analyzing the propulsion system are presented in Table 1-3.

1.3 COMPARISON OF THE RELIABILITY ESTIMATE TO THE RELIABILITY GOAL

The reliability requirement defined in the Preliminary Voyager 1971 Mission Specification for the primary mission was analyzed at a system level and apportioned as a reliability goal to each of the various subsystems on the basis of the subsystem functional contribution to overall system performance and the degree of interfacing the subsystem has with the other Voyager subsystems. The primary mission ends, as previously mentioned, after one month of orbit, which is 210 days after launch. This is a shorter mission than is covered in Table 1-1 and terminates after 28 days of the second orbiting period. The estimate of probability of success of the propulsion subsystem performing this primary mission is .9626 which indicates the propulsion and system reliability will more than meet the allotted goal.

TABLE 1-2. ENVIRONMENTAL FACTOR FAILURE RATE MODIFIERS, K_e

MODIFIER VALUE	MISSION PHASE	PARTS TO WHICH MODIFIER IS APPLICABLE
$K_{e1} = 900$	LAUNCH	High pressurized parts
$K_{e2} = 90$	LAUNCH	Low pressurized parts
$K_{e3} = 5$	LAUNCH	Non-functioning parts
$K_{e3} = 5$	CRUISE	All pressurized parts
$K_{e4} = 50$	TRAJEC. CORREC.	All propellant engine parts
$K_{e5} = 1$	CRUISE	Operational parts
$K_{e6} = .1$	CRUISE	Non-operational parts
$K_{e7} = 100$	ORBIT INJECTION	All propellant engine parts

TABLE I-3. PROPULSION SYSTEMS PART FAILURE RATES OR PROBABILITIES OF OPERATION

	(1) FAILURES PER HOUR $\times 10^6$	(2) (1) $\times K_i$	(3)	(4)	(5)	(6)	(7)	(8)	(9)
			$K_{e1} = 900$ (2) $\times K_{e1}$	$K_{e2} = 90$ (2) $\times K_{e2}$	$K_{e3} = 5$ (2) $\times K_{e3}$	$K_{e4} = 50$ (2) $\times K_{e4}$	$K_{e5} = 1$ (2) $\times K_{e5}$	$K_{e6} = .1$ (2) $\times K_{e6}$	$K_{e7} = 100.$ (2) $\times K_{e7}$
1. Helium Pressurant Tank	.039	.026	23.	---	.13	1.3	---	---	2.6
2. Fill Valve	.100	.066	59.	5.9	.33	3.3	---	---	6.6
3. Explosive Squib Valve	.999	---	---	---	---	.999	.999	---	.999
4. Filter	.011	.0073	6.3	---	.037	0.37	.0073	.00073	.73
5. Pneumatic Regulator	.77	.51	460.	---	2.6	26.	.77	---	51
6. Pressure Switch	.970*	---	---	---	---	---	---	---	---
7. Burst Diaphragm	.100	.066	---	5.9	.33	3.3	.066	.0066	6.6
8. Relief Valve	.224	.150	---	---	.75	---	.75	.0224	15.
9. Propellant Outer Tank	.083	.054	---	4.9	.27	2.7	---	.0054	5.4
10. Propellant Inner Tank	.100	.066	---	5.9	.33	3.3	---	---	6.6
11. Manual Valve	.112	.074	---	6.7	.37	3.7	---	.0112	7.4
12. Servo Motor	.101	.067	---	---	.34	3.4	.067	.0067	6.8
13. Solenoid Valve	2.27	1.50	---	---	.75	7.5	2.27	---	15.
14. Thrust Chamber	3000.	---	---	---	---	3000.	---	---	3000.
15. Fittings	.04	.026	23.	2.3	.13	1.3	.026	.0026	2.6
16. Lines	.05	.033	30.	3.0	.17	1.7	.033	.0033	3.3
17. Check Valves	.112	.074	---	---	.37	3.7	.074	---	7.4
18. Fixed Orifice	.100	.066	---	5.9	.33	3.3	.066	.0066	6.6

* Failure rate assumed negligible when not performing its intended function.

1.4 FAILURE MODES AND THEIR EFFECT ON DESIGN

Table 1-4 lists the potential part failure modes and suggestions for alleviating them. Many of the features have been incorporated into the preferred propulsion subsystem.

1.5 RELIABILITY IMPROVEMENT OF DESIGN CONCEPT

The schedule requirements for this phase of the Voyager study program preclude the possibility of analyzing further reliability improvement in the preferred propulsion system design concept at this time. Presented below is a review of the reliability analysis included in Section 6 to illustrate the potential reliability improvement that is possible in the propulsion subsystem design concept.

1.5.1 MIDCOURSE CORRECTION SUBSYSTEM UNRELIABILITY REDUCTION

Mission Phase ranked in inverse order of reliability (from Table 1-1).

RANK	MISSION PHASE	RELIABILITY, P _S	UNRELIABILITY, Q
1	6. Third Cruise Period	.983300	.016700
2	14. Second Orbiting Period	.990690	.009310
3	11. Orbit Injection Period	.997490	.002510
4	4. Second Cruise Period	.998120	.001880
			TOTAL .030400

$$\text{Corr. Eng. total } \frac{Q}{Q} = \frac{.030400}{.033038} = 92\%$$

92% of correction engine unreliability is in the above 4 mission phases.

The ranking was stopped at 4. since these 4 of the 15 phases are responsible for 92% of the unreliability. Further evaluation of these 4 phases are made below.

1.5.1.1 PHASE 6. THIRD CRUISE PERIOD

Parts used in this phase are ranked in inverse order of failure rate contribution (partial list only).

Rank	Item	Total Failure Rate F/H x 10 ⁶	Recommendation
1	10. Propellant Inner Tank	1.32	Redundancy (see 1. below)
2	9. Propellant Outer Tank	1.08	Redundancy (see 1. below)
3	2. Fill Valve	0.99	Redundancy (see 2. below)
Total		3.39	

1. One solution may be to increase tank size to a point where one of 4 tanks can be redundant.
2. Add check valves in series with each fill valve or cap off after filling.

Estimate of Q reduction (phase duration = 3790 hours)

$$Q = \lambda t = 3.39 \times 10^{-6} \times 3790 = 1.29 \times 10^{-2}$$

$$= 0.01290$$

$$\frac{Q}{\text{Corr. Eng. total } Q} = \frac{0.01290}{0.033038} = 39\%$$

TABLE 1-4. PART FAILURE MODE ANALYSIS

ITEM	FAILURE MODE	POTENTIAL PREVENTATIVE MEASURES
1. Helium Pressurant Tank	Leakage or rupture	Conservative design, pressure testing, inclusion of pressurant reserve, if possible and necessary redundant tanks.
2. Fill valve	Leakage	Adding series check valve, sealing after filling, pressurant reserve
3. Explosive Squib Valve	Failure of squib to fire, failure to open, failure to close	Addition of redundant squibs, or redundant valves in series or parallel
4. Filter	Leakage, failure to filter large particles	Leak testing, filters in series, pressurant reserve
5. Pneumatic Regulator	High downstream pressure	Redundant regulators and bypass provisions
6. Pressure Switch	Failure to close	Provide means to activate valve from ground
7. Burst diaphragm	Leakage, early burst	Provide redundant burst disks or a backup provision
8. Relief Valve	Leakage	Back up with burst diaphragm, pressurant reserve

TABLE 1-4. PART FAILURE MODE ANALYSIS (Cont'd)

ITEM	FAILURE MODE	POTENTIAL PREVENTIVE MEASURES
9. Propellant Outer Tank	External leakage, rupture	Conservative design, pressure testing, fuel reserve, redundant tank
10. Propellant Inner Tank (bladder)	Rupture, leakage	Inspection, testing and conservative design, fuel reserve, redundant tank
11. Manual valve	Leakage	Adding series check valve, sealing after filling fuel reserve
12. Servo Motor	Shorted rotor winding or field coil, bearing failure, brush wear	Selection of insulation, electrical derating of motor, derating or bearings, sealing bearings
13. Solenoid Valve	Leakage, failure to open	Redundancy in series combined with redundancy in parallel.
14. Thrust Chamber	Burn through walls of chamber, rupture of weld	Design with safety margin, inspection of welds and ablative material
15. Fittings	Leakage	Selection or design of leak resistant fitting, proper assembly procedure, pre-launch inspection, pressurant reserve
16. Lines	Rupture	Conservative design, control of handling techniques.
17. Check Valve	Leakage	Use series arrangement of valves, pressurant reserve
18. Fixed Orifice	Clogging	Proper filtering

1.5.1.2 PHASE 14. SECOND ORBITING PERIOD

The same part ranking and recommendations as in 1.5.1.1 are applicable here. Estimate of Q reduction (phase duration 2110 hours)

$$\begin{aligned}
 Q &= \lambda t = 3.39 \times 10^{-6} \times 2110 = 0.715 \times 10^{-2} \\
 &= 0.00715
 \end{aligned}$$

$$\frac{Q}{\text{Corr. Eng. total } Q} = \frac{0.00125}{0.0330038} = 3.8\%$$

1.5.1.3 PHASE 11. ORBIT INJECTION PERIOD

Parts used in this phase are ranked in inverse order of failure rate contribution (partial listing only)

Rank	Item	Total Failure Rate F/H x 10 ⁶	Recommendation
1	14. Thrust Chamber	12,000	Redundancy (see 1 below)
2	12. Servo Motor	27.2	No change

- Four thrust chambers are now used. If possible make two chambers capable of providing required thrust vector and make the other 2 redundant.

Estimate of Q reduction (phase duration 0.104 hours)

$$Q \approx \lambda t = 1200. \times 10^{-6} \times 0.104 = 1.25 \times 10^{-3}$$

$$= 0.00125$$

$$\frac{Q}{\text{Corr. Eng. Total } Q} = \frac{0.00125}{0.33038} = 3.8\%$$

1.5.1.4 PHASE 4. SECOND CRUISE PERIOD

The same part ranking and recommendations as in 1.5.1.1 are applicable here.

Estimate of Q reduction (phase duration 432 hours)

$$Q = \lambda t = 3.39 \times 10^{-6} \times 432 = 1.465 \times 10^{-3}$$

$$= 0.00147$$

$$\frac{Q}{\text{Corr. Eng. Total } Q} = \frac{0.00147}{0.033038} = 4.4\%$$

1.5.2 SUMMARY

The three modifications could boost the correction engine cumulative probability of mission success estimate from 0.966962 to a value of 0.989732. This is a decrease in unreliability of 69%.

The purpose of this analysis is to illustrate an approach to reliability improvement, and not to imply that the recommended modifications are possible or feasible. Before such modifications can be incorporated further study will be required of such factors as weight, space,

configuration, power consumption, effect on other subsystems, etc. The same approach to reliability improvement will also be applicable to the retro engine.

PROPULSION SYSTEM

1.6 RELIABILITY CALCULATIONS

The information used in these analyses was taken from the system schematics included in Section 3.3.1 and 3.2, and tables 1-1, 1-2 and 1-3 herein. Where the reliability ≈ 1.0 the calculations have been excluded.

1.6.1 PHASE 1, LAUNCH, TIME = 0.683

1.6.1.1 MIDCOURSE CORRECTION ENGINE SERIES ITEMS

Value of K_E	Item	Quan.	$\lambda \times 10^6$	$\Sigma \lambda \times 10^{-6}$	
900	1	2	23.0	46.0	$P = e^{-\lambda t} \approx 1 - \lambda t^*$
900	2	1	59.0	59.0	
900	15	1 set	23.0	23.0	$P = 1 - 227.0 \times 10^{-6} \times 0.683$
900	16	1 set	30.0	30.0	
90	2	2	5.9	11.8	$= 1 - 1.55 \times 10^{-4}$
90	7	1	5.9	5.9	
90	9	4	4.9	19.6	$= 1 - 0.000155$
90	10	4	5.9	23.6	
90	15	1 set	2.3	2.3	$= 0.999845$
90	16	1 set	3.0	3.0	
5	4	2	0.037	0.074	*This approximation is used in all applicable calculations below.
5	12	8	0.34	2.72	
				226.994	

1.6.1.2 RETRO ENGINE SERIES ITEMS

Value of K_E	Item	Quan.	$\lambda \times 10^6$	$\Sigma \lambda \times 10^{-6}$	
900	1	2	23.0	46.0	$P = 1 - \lambda t$
900	2	1	59.0	59.0	
900	15	1 set	23.0	23.0	$= 1 - 163.9 \times 10^{-6} \times 0.683$
900	16	1 set	30.0	30.0	
5	7	1	0.33	0.33	$= 1 - 1.12 \times 10^{-4}$
5	2	4	0.33	1.32	
5	9	4	0.27	1.08	$= 1 - 0.000112$
5	15	1 set	0.13	0.13	
5	16	1 set	0.17	0.17	$= 1 - 0.999888$
5	4	3	0.037	0.111	
5	7	2	0.33	0.66	
5	18	2	0.33	0.66	
5	17	4	0.37	1.48	
				163.941	

1.6.2 PHASE 2, FIRST CRUISE PERIOD, TIME = 47.3 HOURS

1.6.2.1 MID-COURSE CORRECTION ENGINE SERIES ITEMS

Value of K_E	Item	Quan.	$\lambda \times 10^{-6}$	$\Sigma \lambda \times 10^{-6}$	
5	1	2	0.13	0.26	$P = 1 - \lambda t$
5	2	3	0.33	0.99	
5	7	1	0.33	0.33	$= 1 - 4.41 \times 10^{-6} \times 47.3$
5	9	4	0.27	1.08	
5	10	4	0.33	1.32	$= 1 - 2.09 \times 10^{-4}$
5	15	1 set	0.13	0.13	
5	16	1 set	0.13	0.13	$= 1 - 0.000209$
1.0	4	1	0.0073	0.0073	
1	15	1 set	0.026	0.026	$= 0.999791$
1	16	1 set	0.033	0.033	
0.1	8	2	0.0224	0.0448	
0.1	4	1	0.00073	0.00073	
0.1	7	1	0.0063	0.0063	
0.1	12	8	0.0067	0.0563	
				4.41173	

1.6.2.2 RETRO ENGINE SERIES ITEMS

Value of K_E	Item	Quan.	$\lambda \times 10^{-6}$	$\Sigma \lambda \times 10^{-6}$	
5	1	2	0.13	0.26	$P = 1 - \lambda t$
5	2	5	0.33	1.65	
0.1	9	4	0.0054	0.0216	$P = 1 - 2.37 \times 10^{-6} \times 47.3$
5	15	1 set	0.13	0.13	
5	16	1 set	0.17	0.17	$= 1 - 1.123 \times 10^{-4} \times 1 - 0.000123$
0.1	4	1	0.00073	0.00073	
0.1	5	1	0.007	0.077	$= 0.999888$
0.1	17	4	0.0074	0.0296	
0.1	7	2	0.0066	0.0123	
0.1	15	1 set	0.0026	0.0026	
0.1	16	1 set	0.0033	0.0033	
0.1	4	2	0.00073	0.00146	
0.1	18	2	0.0066	0.0132	
				2.37269	

1.6.3 PHASE 3, FIRST TRAJECTORY CORRECTION, TIME = 0.067 HOURS

1.6.3.1 MID-COURSE CORRECTION ENGINE P = 0.999190

1.6.3.1.1 FIRE SQUIB VALVES OPEN

$$P = 2 (0.999) - (0.999)^2$$

$$= 0.999999$$

for 2 sets P = 0.999998

1.6.3.1.2 OPERATION SERIES ITEMS

Value of K_E	Item	Quan.	$\lambda \times 10^{-6}$	$\Sigma \lambda \times 10^{-6}$	
50	1	2	1.3	2.6	$P = 1 - \lambda t$
50	2	3	3.3	9.9	
50	4	2	0.37	0.74	$P = 1 - 12067 \times 10^{-6} \times 0.067$
50	9	4	2.7	10.8	
50	10	4	3.3	13.2	$= 1 - 8.08 \times 10^{-4} = 1 - 0.000808$
50	15	1 set	1.3	1.3	
50	16	1 set	1.7	1.7	$= .999192$
50	12	8	3.4	27.2	
50	14	4	3000.	12000.	
				12067.44	

1.6.3.2 RETRO ENGINE SERIES ITEMS

Value of K_E	Item	Quan.	$\lambda \times 10^{-6}$	$\Sigma \lambda \times 10^{-6}$	
50	1	2	1.3	2.6	$P = 1 - \lambda t$
50	2	5	3.3	16.5	
50	4	3	0.37	1.11	$P = 1 - 81.41 \times 10^{-6} \times 0.067$
50	5	1	26.0	26.0	
50	17	4	3.7	14.8	$= 1 - 5.4 \times 10^{-6} = 1 - 0.0000054$
50	7	2	3.3	6.6	
50	9	4	2.7	10.8	$= 0.9999946$
50	15	1 set	1.3	1.3	
50	16	1 set	1.7	1.7	
				81.41	

1.6.4 PHASE 4, SECOND CRUISE PERIOD, TIME 432, HOURS

1.6.4.1 MID-COURSE CORRECTION ENGINE SERIES ITEMS

$$\begin{aligned}
 P &= 1 - \lambda t \\
 &= 1 - 4.41 \times 10^{-6} \times 432. = 1 - 1.88 \times 10^{-3} = 1 - 0.00188 \\
 &= 0.998120
 \end{aligned}$$

1.6.4.2 RETRO ENGINE SERIES ITEMS

$$\begin{aligned}
 P &= 1 - \lambda t \\
 &= 1 - 2.37 \times 10^{-6} \times 432. = 1 - 1.03 \times 10^{-3} = 1 - 0.00103 \\
 &= 0.998970
 \end{aligned}$$

1.6.5 PHASE 5, SECOND TRAJECTORY CORRECTION, TIME = 0.014 HOURS

1.6.5.1 MID-COURSE CORRECTION ENGINE P = 0.999830

1.6.5.1.1 OPERATION SERIES ITEMS

$$\begin{aligned}
 P &= 1 - \lambda t \\
 &= 1 - 12067.0 \times 10^{-6} \times 0.014 = 1 - 1.69 \times 10^{-4} = 1 - 0.000169 \\
 &= 0.999831
 \end{aligned}$$

1.6.5.1.2 FIRE SQUIB VALVES CLOSED

$$\begin{aligned}
 P &= 2(0.999) - (0.999)^2 \\
 P &= 0.999999
 \end{aligned}$$

1.6.5.2 RETRO ENGINE SERIES ITEMS

$$\begin{aligned}
 P &= 1 - \lambda t \\
 &= 1 - 81.41 \times 10^{-6} \times 0.014 = 1 - 1.13 \times 10^{-6} = 1 - 0.00000113 \\
 &= 0.999999
 \end{aligned}$$

1.6.6 PHASE 6, THIRD CRUISE PERIOD, TIME = 3790 HOURS

1.6.6.1 CORRECTION ENGINE SERIES ITEMS

$$\begin{aligned}
 P &= e^{-\lambda t} \approx 1 - \lambda t \\
 &= 1 - 4.41 \times 10^{-6} \times 3790 = 1 - 1.67 \times 10^{-2} = 1 - 0.0167 \\
 &= 0.9833
 \end{aligned}$$

1.6.6.2 RETRO ENGINE SERIES ITEMS

$$\begin{aligned}
 P &= 1 - \lambda t \\
 &= 1 - 2.37 \times 10^{-6} \times 3790 = 1 - 0.898 \times 10^{-2} = 1 - 0.00898 \\
 P &= 0.99102
 \end{aligned}$$

1.6.7. PHASE 7, THIRD TRAJECTORY CORRECTION, TIME = 0.014

1.6.7.1 MID-COURSE CORRECTION ENGINE P = 0.999827

1.6.7.1.1 FIRE SQUIB VALVES OPEN

$$\begin{aligned}
 P &= 0.999998 \text{ degraded because only 1 backup in system; for 2 sets} \\
 P &= 0.999996
 \end{aligned}$$

1.6.7.1.2 OPERATION P = 0.999831

1.6.7.2 RETRO ENGINE SERIES ITEMS

$$P = 0.999999$$

1.6.8 PHASE 8, FOURTH CRUISE PERIOD, TIME = 24.0 HOURS

1.6.8.1 MID-COURSE CORRECTION ENGINE SERIES ITEMS

$$\begin{aligned}
 P &= 1 - \lambda t \\
 &= 1 - 4.41 \times 10^{-6} \times 24.0 = 1 - 1.06 \times 10^{-4} = 1 - 0.000106 \\
 &= 0.999894
 \end{aligned}$$

1.6.8.2 RETRO ENGINE SERIES ITEMS

$$\begin{aligned}
 P &= 1 - \lambda t \\
 &= 1 - 2.37 \times 10^{-6} \times 24.0 = 1 - 0.570 \times 10^{-4} = 1 - 0.000057 \\
 &= 0.999943
 \end{aligned}$$

1.6.9 PHASE 9, FOURTH TRAJECTORY CORRECTION, TIME = 0.014 HOURS

1.6.9.1 MID-COURSE CORRECTION ENGINE OPERATION

$$P = 0.999831$$

1.6.9.2 RETRO ENGINE

$$P = 0.999999$$

1.6.10 PHASE 10, FIFTH CRUISE PERIOD, TIME = 24.0 HOURS

1.6.10.1 MID-COURSE CORRECTION ENGINE P = 0.999894

1.6.10.2 RETRO ENGINE P = 0.999943

1.6.11 PHASE 11, ORBIT INJECTION

1.6.11.1 MID-COURSE CORRECTION ENGINE, TIME = 0.104 HOURS

Series items $K_E = 100$ instead of $K_E = 50$ therefore λ are double

$$\lambda = 2 \times 12067 \times 10^{-6} = 24134 \times 10^{-6}$$

$$P = 1 - \lambda t$$

$$= 1 - 24134 \times 10^{-6} \times 0.104 = 1 - 2.510 \times 10^{-3} = 1 - 0.00251$$

$$= 0.99749$$

1.6.11.2 RETRO ENGINE, TIME = 0.101 HOURS P = 0.999672

1.6.11.2.1 FIRE SQUIB VALVES OPEN

1 set P = 0.999999

3 sets P = 0.999997

1.6.11.2.2 OPERATION SERIES ITEMS

Value of K_E	Item	Quan	$\lambda \times 10^{-6}$	$\Sigma \lambda \times 10^{-6}$	
100	1	2	2.6	5.20	$\lambda = 3187.0 \times 10^{-6}$
100	2	5	6.6	33.00	
100	4	3	0.73	2.19	$P = 1 - \lambda t = 1 - 3187 \times 10^{-6} \times 0.101$
100	5	1	51.0	51.00	
100	17	4	7.4	29.60	$= 1 - 3.22 \times 10^{-4} = 1 - 0.000322$
100	18	18	6.6	13.20	$= 0.999678$
100	7	7	6.6	13.20	
100	9	4	5.4	21.60	
100	14	1	3000.0	3000.00	
100	15	3 sets	2.6	7.80	
100	16	3 sets	3.3	9.90	
		Total		3186.69	

1.6.11.2.3 FIRE SQUIB VALVES CLOSED $P = 0.999997$

1.6.12 PHASE 12, FIRST ORBITING PERIOD, TIME = 48 HOURS

1.6.12.1 MID-COURSE CORRECTION ENGINE

$$P = 1 - \lambda t = 1 - 4.41 \times 10^{-6} \times 48 = 1 - 2.12 \times 10^{-4} = 1 - 0.000212$$

$$P = 0.999788$$

1.6.12.2 RETRO ENGINE

A catastrophic failure would occur if N_2O_4 became combined with A-50; this would occur if 2 check valves or one of 2 tanks opened on one side at the same time that 2 check valves or one of 2 tanks opened on the other side.

1.6.12.2.1 CHECK VALVE PROBABILITY TIME = 48 HOURS

$$K_{E3} = 5 \quad \lambda = 0.37 \times 10^{-6}$$

$$P = 1 - \lambda t = 1 - 0.37 \times 10^{-6} \times 48 = 1 - 0.18 \times 10^{-4} = 1 - 0.000018$$

$$P = 0.999982$$

Probability of 2 check valves failing together ≈ 0

1.6.12.2.2 TANK PROBABILITY TIME 48 HOURS

$$= (0.27 \times 10^{-6})^2 \text{ tanks}$$

Probability of 2 tanks failing together ≈ 0

1.6.13 PHASE 13, FIRST ORBIT ADJUST TIME 0.021 HOURS

1.6.13.1 MID-COURSE CORRECTION ENGINE $P = 0.999742$

1.6.13.1.1 SERIES ITEMS

$$P = 1 - \lambda t = 1 - 12067 \times 10^{-6} \times 0.021 = 1 - 2.54 \times 10^{-4}$$

$$P = 1 - 0.000254 = 0.999746$$

1.6.13.1.2 FIRE SQUIB VALVES CLOSED

$$P = 0.999996 \text{ see 7.1.1}$$

1.6.14 PHASE 14, SECOND ORBITING PERIOD, TIME = 2110 HOURS

1.6.14.1 MID-COURSE CORRECTION ENGINE SERIES ITEMS

$$P = 1 - \lambda t = 1 - 4.41 \times 10^{-6} \times 2110 = 1 - 9.31 \times 10^{-3}$$

$$= 1 - .00931 = .99069$$

1.6.14.2.1 CHECK VALVE PROBABILITY TIME 2110 HOURS

$$P = 1 - \lambda t = 1 - .37 \times 10^{-6} \times 2110 = 1 - 7.81 \times 10^{-4} = 1 - .000781$$

$$P = .999219$$

$$\text{Probability of either check valve working} = 2(.99922) - (.99922)^2$$

$$P = .9999994$$

This probability is high enough to be ignored

1.6.14.2.2 TANK PROBABILITY $P \approx 1$

1.6.15 PHASE 15, SECOND ORBIT ADJUST, TIME = .021

1.6.15.1 MID-COURSE CORRECTION ENGINE P = .999730

1.6.15.1.1 FIRE SQUIB VALVES OPEN

P = .999997 degraded from 7.1.1 because only 1 back up in system; for 2 sets

$$P = .999994$$

1.6.15.1.2 SERIES ITEMS P = .999742 (See 13.1.1)

1.6.15.1.3 FIRE SQUIB VALVES CLOSED

$$P = .999994 \text{ (See 15.1.1)}$$

2.0 SYSTEM PERFORMANCE CALCULATIONS

Propulsion requirements for the Voyager spacecraft are predicated upon a requirement of 1860 meters/second (6100 fps) for orbit insertion, 75 meters/second (246 fps) for mid-course maneuvers and a desired capability of 100 meters/second for orbit adjust maneuvers. A 3500 pound weight allocation has been made for the complete loaded propulsion system.

Since total maneuvering requirements may not be compatible with the weight limitation, a first approximation is made by assuming that the first two maneuvering requirements will be met and by solving for total system loaded weight as various amounts of hydrazine are carried into orbit. The following values are assumed constant in all cases.

Initial Weight of Over-all Flight Spacecraft	7800 lb
Flight Spacecraft (less propulsion)	2000 lb
Specific Impulse Monopropellant System (I_{SM})	230 sec
Specific Impulse Retropropulsion System (I_{SR})	307 sec

For a small maneuver where the propellant usage is small compared to the vehicle weight, the propellant requirement can be estimated conservatively by equating momentum change to total impulse. Thus, for the midcourse correction of 75 meters/second (246 fps), the hydrazine requirement (W_H) is

$$W_H I_{SM} = \Delta VM \text{ where } M \text{ is the mass of the Over-all Flight Spacecraft}$$

$$W_H \times 230 = 246 \times 7800/32.2$$

$$W_H = 259 \text{ lbs.}$$

For the large retropropulsion maneuver the familiar equation

$$\Delta V = V_{\text{eff}} \ln \frac{\text{INITIAL WEIGHT } (W_I)}{\text{FINAL WEIGHT } (W_{BO})}$$

will be used. However, there are a number of items to be evaluated in this equation and certain estimates must be made. First is the effective specific impulse during the retropropulsion maneuver. Since both propulsion systems are operating during this time, the effective specific impulse must be a weighted average based on the relative flow of the two propellants. The flow rate of the main retropropulsion subsystem is fixed at 2200/307 = 7.15 lb/sec. However since burn time (B_T) is unknown, the average flow rate of the mono-propellant system is unknown. An estimation for the burn time of 300 seconds permits a first approximation of

$$W_M = \frac{4 \times 25}{230} + \frac{25}{300} = .52 \text{ lb /sec}$$

where 25 pounds of hydrazine is the propellant required for TVC .

$$W_T = W_M + W_R = .52 + 7.15 = 7.67 \text{ lb/sec}$$

$$I_{SM} (\text{eff}) = .52 \times 230/7.67 + 7.15 \times 307/7.67$$

$$= 301.5 \text{ seconds}$$

$$V_{\text{eff}} = I_{SM} \times g = 301.5 \times 32.2 = 9700 \text{ fps}$$

The initial and burnout weights may be broken down as follows

$$W_I = 1.03 W_P + W_{BUS} + W_{RP} + W_M + W_H$$

$$W_{BO} = .03 W_P + W_{BUS} + W_{RP} + W_M + W_H$$

where

$$W_P = \text{Propellant used by main retro engine}$$

- 1.03 W_p = Propellant Loaded (3% Outage)
- W_{BUS} = 2000 lbs.
- W_{RP} = Weight of Retropropulsion inert components
- W_M = Weight of monopropellant inert components
- W_H = initial hydrazine loaded
- W'_H = hydrazine carried into orbit

By substituting in the general equation and using various values of W'_H a curve of Total Propulsion Subsystem Weight versus Hydrazine carried into orbit (W'_H) was derived (Figure 2-1). It is immediately obvious that with a 3500 pound system limit, no appreciable quantity of hydrazine can be carried into orbit. To complete an orbit adjust maneuver of 100 meters/second requires slightly more than 100 pounds of hydrazine. This would bring the total propulsion weight to nearly 3700 pounds. Because of this excess weight the propulsion system has been sized without allowing for orbit adjust propellants.

From the previous computations burn time for the retropropulsion system was also derived and is indicated in Figure 2-1.

A three percent allowance on total hydrazine is about 13 pounds (as indicated by the foregoing calculations) which would be carried into orbit. Burntime for this value is approximately 316 seconds.

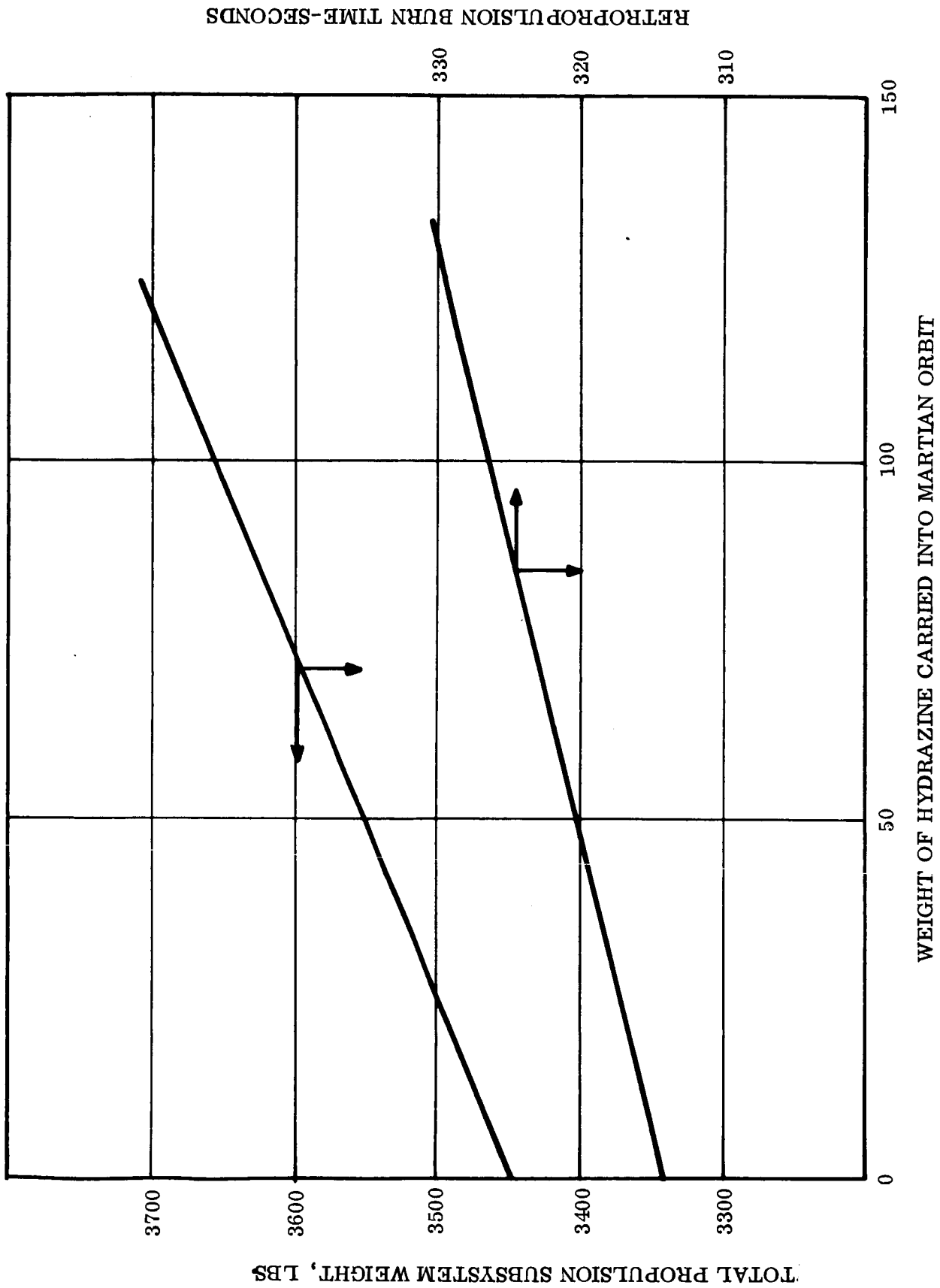
Recalculation of retropropulsion propellant requirements based on the above burn time and a detailed weight breakdown (See following section) gives the following propellant figures.

TABLE 2-1. PROPULSION SUBSYSTEM WEIGHTS

Retropropellant Tanked	2328 lbs.
Retropropellant Used	2260 lbs
Monopropellant Tanked	444 lbs.
Monopropellant Used	431 lbs.

Subsystem Weights are then

Retropropulsion Dry Weight	455
Pressurant	8
Propellant	<u>2328</u>
	2791
Midcourse Correction Propulsion Dry Weight	227
Pressurant	6



RETROPULSION BURN TIME-SECONDS

TOTAL PROPULSION SUBSYSTEM WEIGHT, LBS

Figure 2-1. Total Propulsion Subsystem Weight and Retropulsion Subsystem Burn Time versus Weight of Hydrazine Carried into Martian Orbit

Propellant	<u>444</u>
	677
Total Propulsion Weight	3468 lbs.

3.0 COMPONENT WEIGHT AND VOLUME ESTIMATES

3.1 TANKS

Propellant and pressurant tanks are designed to the 2.2 safety factor requirement or to a minimum gage of .035, whichever governs. All tanks are fabricated from 6Al-4V Titanium and are spherically shaped. Propellant volumes and tank characteristics are shown in Table 3-1. A 3 percent ullage volume is provided in the propellant tanks.

3.2 COMPLETE PROPULSION SUBSYSTEM

Estimated weight breakdowns for the Monopropellant and Retropropulsion Subsystems are shown in Table 3-2.

TABLE 3-1. TANK CHARACTERISTICS

Tank	No Req.	Total Fluid Weight-Lbs.	Total Fluid Vol. -Ft. ³	Unit		Tank O.D. -In.	Tank Oper. Press-PSIA	Tank Wall-In	Tank Wt.-Lbs.
				Tank Vol. Ft. ³	Tank				
Monopropellant N ₂ H ₄	4	444	7.1	1.86*	18.38	285	.035	7	
Monopropellant Pressurant	2	6	---	1.37	17	3500	.235	41	
Retropropulsion Propellant	4	2328	32.2	8.30	30.25	220	.035	22	
Retropropulsion Pressurant	2	8	---	1.84	18.7	3500	.252	52	

*Allowance is made for bladder

TABLE 3-2. PROPULSION SUBSYSTEM
ESTIMATED WEIGHT BREAKDOWN

Midcourse Propulsion Subsystem		277 lbs.
Thrust Chamber w/quad valves (4)	47.2	
Jet Vanes and Actuators (4)	8	
Propellant Tanks w/bladders (4)	34	
Throttle Valves (4)	6	
Pressurant Tanks (2)	82	
Valves and Piping	30.8	
Support Structure	19	
Retropropulsion Subsystem		455 lbs.
Thrust Chamber (1)	156	
Propellant Tanks (4)	88	
Pressurant Tanks (2)	104	
Valves and Piping	31	
Support Structure	76	

TOTAL PROPULSION SUBSYSTEM DRY WEIGHT 682 lbs.

VOLUME A

BOOK 3

CHVB234FD105

1. Page 5 of 14, Top part of diagram: Insert division line in all four transfer function.
2. Page 5 of 14: Velocimeter disable signal feeds a flip-flop.
3. Page 5 of 14, bottom of diagram: Change No. 1-4 start indication to engine No. 1-4 start indication.

CHVB235FD102

1. Page 3 of 28, figure 3-1: Remove dotted line extending from fight capsule block of first level block diagram.
2. Page 11/12 of 28, second paragraph, Line 4: Change 2B (Ref. Table IV of appendix) "to 2C (Ref. Table 4-1)"
3. Page 10 of 28, fourth paragraph, Line 1: Change "Table IV of appendix I" to Table 4-1 of Appendix I.
4. Page 18 of 28, first paragraph, Line 1: Change is an aluminum alloy honeycomb to is a Fiberglas honeycomb.
5. Page 27/28 of 146: Add title to Table 6-1 Structural Component Details.
6. Page 123 of 146, foot note: Insert in Reference _____, Table 4-2 of VB235FD105 .
7. Page 124 of 146, first equation: Change to
$$\begin{bmatrix} m \end{bmatrix} \begin{Bmatrix} \ddot{q} \end{Bmatrix} + \begin{bmatrix} K \end{bmatrix} \begin{Bmatrix} g \end{Bmatrix} = 0$$
8. Page 121 of 146, Section 2-1, fourth paragraph, Line 2: Change "X-Y plane" to "X-Z plane".
9. Page 125 of 146, first equation: Change
$$\begin{bmatrix} C^* \end{bmatrix} = \phi^T C \phi = \zeta 2 \begin{bmatrix} 2\frac{1}{2} \end{bmatrix}$$
 to
$$\begin{bmatrix} C \end{bmatrix} = \phi^T C \phi = 2\zeta \begin{bmatrix} 2\frac{1}{2} \end{bmatrix}$$
10. Page 125 of 146, Line 2: Change $2\zeta = \% \text{ structural damping}$ to $2\zeta = \% \text{ structural damping}$
100
11. Page 125 of 146, Line 2: Change XQ = Quadrature Displacement to Xys = Quadrature Displacement.

CHVB235FD103

1. Page 17 of 20, paragraph 3, Line 2: Change 38.5 inches to 50.0 inches.

CIIVB235FD105

1. Page 3 of 6, paragraph 3.2.1, Line 2: Delete V.
2. Page 3 of 6, paragraph 3.2.1, Line 3: Change 2.3 to 1.4.

CIIVB235FD108

1. Page 5 of 12, tenth paragraph, line 1: Change one-half atmosphere to one-half psia.
2. Page 8 of 12, paragraph 3.3, Line 3: Change VB238FD108 to VB234FD108.

CIIVB235FD109

1. Page 4 of 10 of 102: Battery charger efficiency on last column should read "44.2/46.0" instead of "22.4/46.0".
2. Page 4 of 102, paragraph 5.2, Line 5: Change "Appendix A" to Appendix I.
3. Page 5 of 102, first equation: Exponent of e requires additional closing parenthesis after VDEG.
4. Page 57 of 102: Abcissa of Figure I-1 should be labelled. "Array current, amps". Delete this from curve parameter identification.

CIIVB235FD109

1. Page 6 of 22, paragraph 3.1.5.4, sixth sentence: Delete sixth sentence and substitute "Normally closed valves are opened by a plunger that shears the flow tube and caps to allow a flow path".
2. Page 7 of 22, paragraph 3.1.5.6, Line 20: Regulator pressure should be "235" instead of "250".
3. Page 8 of 22, paragraph 3.1.5.8, Line 10: Change "monel" to "stainless steel".
4. Page 12 of 22, fourth paragraph from top, Line 8: Change "three-way solenoid" to "three-way squib valve".
5. Page 14 of 22, Figure 3-2: A line should be added to connect fuel tank to pressurant manifold.